Towards Earth Independence – Tradespace Exploration of Long-Duration Crewed Mars Surface System Architectures

by

Sydney Do

B.E. (Hons. 1 & Univ. Medal), Aeronautical (Space), University of Sydney (2008)
S.M., Aeronautics and Astronautics, Massachusetts Institute of Technology (2011)

Submitted to the Department of Aeronautics and Astronautics
in partial fulfillment of the requirements for the degree of

Doctor of Philosophy

at the

MASSACHUSETTS INSTITUTE OF TECHNOLOGY

June 2016

Author……
Department of Aeronautics and Astronautics
May 9, 2016

Certified by…….
Olivier L. de Weck
Professor of Aeronautics and Astronautics and Engineering Systems
Thesis Supervisor

Certified by…….
Jeffrey A. Hoffman
Professor of the Practice, Department of Aeronautics and Astronautics
Thesis Committee Member

Certified by…….
Charles J. Camarda
Senior Advisor for Engineering Development, NASA Langley Research Center
Thesis Committee Member

Accepted by…….....
Paulo C. Lozano
Associate Professor of Aeronautics and Astronautics
Chair, Graduate Program Committee

Towards Earth Independence – Tradespace Exploration of Long-Duration Crewed Mars Surface System Architectures

by

Sydney Do

Submitted to the Department of Aeronautics and Astronautics
on May 19, 2016 in partial fulfillment of the
requirements for the degree of
Doctor of Philosophy

Abstract

In recent years, an unprecedented level of interest has grown around the prospect of sending humans to Mars for the exploration and eventual settlement of that planet. With the signing of the 2010 NASA Authorization Act, this goal became the official policy of the United States and consequently, has become the long-term objective of NASA's human spaceflight activities.

A review of past Mars mission planning efforts, however, reveals that while numerous analyses have studied the challenges of transporting people to the red planet, relatively little analyses have been performed in characterizing the challenges of sustaining humans upon arrival. In light of this observation, this thesis develops HabNet – an integrated Habitation, Environmental Control and Life Support (ECLS), In-Situ Resource Utilization (ISRU), and Supportability analysis framework – and applies it to three different Mars mission scenarios to analyze the impacts of different system architectures on the costs of deploying and sustaining a continuous human presence on the surface of Mars.

Through these case studies, a number of new insights on the mass-optimality of Mars surface system architectures are derived. The most significant of these is the finding that ECLS architecture mass-optimality is strongly dependent on the cost of ISRU – where open-loop ECLS architectures become mass-optimal when the cost of ISRU is low, and ECLS architectures with higher levels of resource recycling become mass-optimal when the cost of ISRU is high. For the Martian surface, the relative abundance of resources equates to a low cost of ISRU, which results in an open-loop ECLS system supplemented with ISRU becoming an attractive, if not dominant surface system architecture, over a range of mission scenarios and ISRU performance levels.

This result, along with the others made in this thesis, demonstrates the large potential of integrated system analyses in uncovering previously unseen trends within the Mars mission architecture tradespace. By integrating multiple traditionally disparate spaceflight disciplines into a unified analysis framework, this thesis attempts to make the first steps towards codifying the human spaceflight mission architecting process, with the ultimate goal of enabling the efficient evaluation of the architectural decisions that will shape humanity's expansion into the cosmos.

Thesis Supervisor: Olivier L. de Weck
Title: Professor of Aeronautics and Astronautics and Engineering Systems

Financial support for this research was provided by the NASA Office of the Chief Engineer for the NASA Innovative Mars Habitat Design Concepts Project under Award number 020758-001, the NASA Human Exploration and Operations Mission Directorate for the NASA / Launch.org Initiative, the 2012 MIT Alumni Class Funds, the MIT Department of Aeronautics and Astronautics John (1943) and Irene M Goldsmith Scholarship, the MIT Office of the Dean for Graduate Education Jonathon Whitney Fund, the 2014-2015 AIAA John Leland Atwood Graduate Award, and the Josephine de Karman Fellowship Trust

Acknowledgments

What a ride…

This thesis is the culmination of an eight year rollercoaster ride that took me to the highest of heights, dropped me down to the lowest of lows, and threw at me everything else in between. Throughout this ride, a number of important people have helped to create the highs, while providing me with the strength to keep marching on through the lows. It is these people whom I would like to express my gratitude towards here. In particular, I would like to thank:

Professor Olivier "Oli" de Weck – my research advisor for almost a decade. I'd be nowhere near the researcher I am today without him. It was through his vision, guidance, and belief in me, that I was able to follow my passion and pursue research in human spaceflight. Every day I am in awe by the very notion that I have the privilege of working in a field that truly endeavors to advance the human experience.

Dr. Charlie Camarda – the most down-to-Earth astronaut I've ever met! In addition to being a valuable member of my doctoral committee, Charlie has been a part of every step of my MIT graduate school experience – from being the biggest supporter of the "personal airbag system" that I developed during my Master's thesis, to hosting me at NASA Johnson Space Center at the beginning of my PhD, to reviewing this very thesis and signing the front page.

Professor Jeff Hoffman – the third member of my doctoral committee, who went out of his way to periodically check up on me during my first few turbulent months at MIT, and was always willing to provide me with support, both in terms of feedback on my research, and in providing connections to other scholars in the field.

My thesis readers: Prof Sheila Widnall, and Dr. Robert Shishko, for taking time out of their busy schedules to review what ended up being quite the long thesis! Their support throughout the final phases of this thesis journey have been invaluable.

The many professors at MIT, who have taught me so much about framing, decomposing and solving tough problems across a wide array of disciplines, including Professors Dave Miller, Ed Crawley, Dava Newman, Annalisa Weigel, Bryan Mosur, and Karen Willcox.

Dean Christine Ortiz, for supporting me through one of the more stressful periods of my MIT experience, and for providing me with a last minute fellowship that not only reinvigorated this research from its difficult beginnings, but also gave me the confidence and self-belief that fueled the completion of this thesis.

Julie Finn, Beth Marois, Bill Litant, and the other administrators, officers, and assistants at MIT, who took care of the multitude of administrative and logistical challenges that inevitably arose, allowing myself and others to focus on performing and presenting research both at MIT and at conferences and meetings across the world.

My fellow human spaceflight researchers in the MIT HabNet and Mars One analysis teams: Andrew Owens, Koki Ho, Sam Schreiner, Lukas Schrenk, Margaret Shaw, and Ioana Josan-Drinceanu, for helping to mold and advance the field of integrated space systems architecting through your ideas, and knowledge of your respective fields of expertise. It has been a pleasure

to work with you all towards our collective goal of architecting efficient solutions to addressing the numerous technical and economic challenges of advancing and sustaining human presence beyond Earth orbit.

My fellow lab mates and friends from SERG, 33-409, across the AeroAstro Department and the greater MIT community, for your everlasting support and friendship, during both the highs and the lows. You helped me settle into a new country and built a community around me that truly made Boston feel like home. Special thanks go to Narek, Andrew, Demetris, Lukas, Marc, Sam, Veronica, Tak, Bianca, MJ, and Phil, who got me through the final stages of this thesis, as well as Mody, Hemant, Jon, Russ, and Hiten, who helped me navigate life as a new grad student during my early years at MIT.

Rebecca Chung, for her rides to the weekly group meditation sessions that helped me recharge for another week of focused research, and for her constant support throughout the past eight years.

My friends from back home in Australia, for helping me to define my identity and to set goals in life, as we all grew up together in the immigrant neighborhoods of southwestern Sydney. I never would have gotten to this point in life without your never-ending friendship. I always look forward to my annual trip home to celebrate the beginning of the New Year with you all, under the glow of fireworks above Sydney's summer skyline.

My mother, for her love, courage, and all the sacrifices that she has made for me to pursue my dreams. From her, I learned the value of hard work, and perseverance through tough circumstances. Every day, I am inspired by her journey from war-torn Vietnam, across the pirate-infested waters of the South China Sea in an unseaworthy boat, to a refugee camp on a remote Malaysian island, and finally to a new foreign land, where she rebuilt her life and provided her son with everything that he needed to reach for the stars.

And finally, to Vivian, my partner and best friend, who came into my life during some of its toughest moments, and helped me to re-find myself when I thought that all was lost. I've loved every moment of our adventure together. You have been a constant source of happiness for me, through the good times and the bad. It is only through your unconditional love and support that this thesis exists today.

Contents

List of Figures

List of Tables

Nomenclature

Abbreviations

AC	Assembly Complete
ACS	Atmosphere Control and Supply
ADG	Architecture Decision Graph
ALSSAT	Advanced Life Support Sizing and Analysis Tool
AP	Atmospheric Processor
AR	Atmosphere Revitalization
ARC	Ames Research Center
ARFTA	Advanced Recycle Filter Tank Assembly
ASV	Air Selector Valve
BCF	Biomass Carbon Fraction
BIO-Plex	Bioregenerative Planetary Life Support System Test Complex
BMS	Bed Molecular Sieve
BPC	Biomass Production Chamber
BPS	Biomass Production System
BVAD	Baseline Values and Assumptions Document
CCAA	Common Cabin Air Assembly
CCC	Contaminant Control Cartridge
CDF	Cumulative Distribution Function
CDRA	Carbon Dioxide Removal Assembly
CDT	Central Daylight Time
CEEF	Closed Ecology Experiment Facilities
CHX	Condensing Heat eXchanger
CM	Command Module
CONOPS	Concept of Operations
CPS	Cabin Pressure Sensor

CQY	Canopy Quantum Yield
CRS	Carbon Dioxide Reduction System
CSA	Canadian Space Agency
CUE	Carbon Use Efficiency
CWC	Contingency Water Container
DA	Distillation Assembly
DAB	Desiccant/Adsorbent Bed
DCG	Daily Carbon Gain
DLR	Deutsches Zentrum für Luft- und Raumfahrt (German Aerospace Center
DMSD	dimethylsilanediol
DRA	Design Reference Architecture
DRM	Design Reference Mission
DSH	Deep Space Habitat
DSM	Design Structure Matrix
EAWG	Exploration Atmospheres Working Group
ECLS	Environmental Control and Life Support
ECLSS	Environmental Control and Life Support System
EDB-Y	Russian Urine Tank
EDL	Entry Descent and Landing
EDO	Extended Duration Orbiter
EIB	Electronic Interface Box
ELISSA	Environment for Life Support Systems Simulation and Analysis
EMAT	Exploration Maintainability Analysis Tool
EMC	Evolvable Mars Campaign
EMU	Extravehicular Mobility Unit
EOL	End Of Life
ESA	European Space Agency
ESM	Equivalent System Mass
ETHOS	Environment and Thermal Operating Systems
EVA	Extravehicular Activity
EZ	Exploration Zone
FCPA	Fluids Control and Pump Assembly
FDS	Fire Detection and Suppression

FOM	Figure of Merit
FY	Fiscal Year
GLS	Growth Lighting System
GPL3.0	General Public License 3.0
GRS	Gamma Ray Spectrometer
HEFT	Human Exploration Framework Team
HIDH	Human Integration Design Handbook
HPGT	High Pressure Gas Tank
HVAC	Humidity Ventilation and Air Conditioning
HX	Heat Exchanger
IMLEO	Initial Mass to Low Earth Orbit
IMV	Intermodule Ventilation
ISPP	In-Situ Propellant Production
ISRU	In-Situ Resource Utilization
ISS	International Space Station
IVA	Intravehicular Activity
JSC	Johnson Space Center
KSC	Kennedy Space Center
LED	Light Emitting Diode
LMLSTP	Lunar-Mars Life Support Test Project
LOC	Loss Of Crew
LOR	Lunar Orbit Rendezvous
MAG	Maximum Absorbency Garment
MAV	Mars Ascent Vehicle
MARCO-POLO	Mars Atmosphere and Regolith Collector/PrOcessor for Lander Operations
MATLAB	Matrix Laboratory
MCC	Mission Control Center
MEC	Modified Energy Cascade
MEL	Master Equipment List
METOX	Metal Oxide
MF	Multifiltration
MFB	Multifiltration Bed
MIP	Mars ISPP Precursor

MIT	Massachusetts Institute of Technology
MLS	Mostly Liquid Separator
MOLA	Mars Orbiter Laser Altimeter
MOR	Mars Orbit Rendezvous
MOXIE	Mars Oxygen ISRU Experiment
MRF	Microbial Removal Filter
MRO	Mars Reconnaissance Orbiter
MSFC	Marshall Space Flight Center
MTBF	Mean Time Between Failure
MTTR	Mean Time To Repair
MTV	Mars Transit Vehicle
NASA	National Aeronautics and Space Administration
NFT	Nutrient Film Technique
NIV	Nitrogen Interface Valve
NORCAT	Northern Centre for Advanced Technology
OGA	Oxygen Generation Assembly
OGS	Oxygen Generation System
OIV	Oxygen Interface Valve
OPD	Object Process Diagram
OPL	Object Process Language
OPM	Object Process Methodology
ORA	Oxygen Removal Assembly
ORU	Orbital Replacement Unit
PC	Personal Computer
PCA	Pressure Control Assembly
PCM	Pressurized Core Module
PCPA	Pressure Control and Pump Assembly
PDAM	Predetermined Debris Avoidance Maneuver
PDF	Probability Distribution Function
PDISRU	Pre-Deploy In-Situ Resource Utilization
PDMS	polydimethylsiloxane
PEM	Proton Exchange Membrane
PGA	Pressure Garment Assembly

PILOT	Precursor ISRU Lunar Oxygen Testbed
PLM	Pressurized Logistics Module
PLOC	Probability of Loss of Crew
PLOM	Probability of Loss of Mission
PLSS	Portable Life Support System
PMF	Probability Mass Function
PMM	Permanent Multipurpose Module
PNNL	Pacific Northwest National Laboratory
PPF	Photosynthetic Photon Flux
ppm	parts per million
PPRV	Positive Pressure Relief Valve
PWD	Potable Water Dispensor
R&R	Remove and Replace
RCA	Rapid Cycle Amine
RESOLVE	Regolith & Environment Science and Oxygen & Lunar Volatile Extraction
RH	Relative Humidity
RO	Reverse Osmosis
ROI	Region of Interest
RP	Resource Prospector
RPCM	Remote Power Control Module
RPM	Revolutions Per Minute
RS	Russian Segment (of the International Space Station)
RSA	Rotary / Separator Accumulator
RWGS	Reverse Water Gas Shift
SCUBA	Self-Contained Underwater Breathing Apparatus
SDTTR	Standard Deviation in Time To Repair
SF	Stored Food
SFWE	Static Feed Water Electrolysis
SMP	Semi-Markov Process
SOCE	Solid Oxide CO2 Electrolysis
SPWE	Solid Polymer Water Electrolysis
SSF	Space Station Freedom
STS	Space Transportation System

SWME	Spacesuit Water Membrane Evaporator
TCC	Trace Contaminant Control
TCCV	Temperature Control Check Valve
THC	Temperature and Humidity Control
TIMES	Thermoelectric Integrated Membrane Evaporation System
TOC	Total Organic Carbon
TRL	Technology Readiness Level
UCTA	Urine Collection and Transfer Assembly
UI	User Interface
ULD	Ultrasonic Leakage Detector
UPA	Urine Processor Assembly
URL	Uniform Resource Locator
US	United States
USOS	United States Orbital Segment
UTC	Universal Coordinated Time
VCD	Vapor Compression Distillation
VRCV	Vent and Relief Control Valve
VRIV	Vent and Relief Isolation Valve
VS	Vacuum Systems
WEH	Water Equivalent Hydrogen
WHC	Waste and Hygiene Compartment
WM	Waste Management
WPA	Water Processor Assembly
WRM	Water Recovery and Management
WRS	Water Recovery System
WSTA	Wastewater Storage Tank Assembly
XRD	X-Ray Diffraction
XRF	X-Ray Fluorescence
YSZ	yttrium-stabilized-zirconia

Roman Symbols

a	Base length (m)
A	Area (m^2)

Ar	Argon
b	Backup soil level in ISRU hopper
c	carbohydrate fraction of crop dry mass
C	Carbon; Cooling requirement (kW)
d	Diameter (m)
E	Expected value; Mass equivalency used in ESM calculations; Energy (J)
f	fat fraction of crop dry mass; fill factor (%)
F	Probability Density Function
g	PDF of first passage time; Inequality constraints
G	CDF of first passage time
H	Hydrogen; Unconditional waiting time density matrix; height (m)
I	Identity Matrix; System current (Amperes)
k	Counter for the number of times a system has entered an SMP state
J	Objective function
L	Length (m)
m	Mass of individual item (kg)
M	Mass of system (kg)
n	number of spares required; number of moles; number of items
N	Nitrogen; Number of items
O	Oxygen
p	protein fraction of crop dry mass
P	Pressure (kPa); Probability; Power (kW); Pitch (m)
Q	Kernel Matrix
r	Crop static growth rates ($g/m^2/day$); radius (m)
R	Universal Gas Constant; Resource production rate (kg/h); Radius (m)
S	Laplace domain coordinate; Safety margin
t	Time domain coordinate (s); Thickness (mm)
T	Time (h); Temperature (K)
U	Electrolysis cell voltage (Volts)
v	Volume of individual item (m^3)
V	Markov renewal process probability; Volume of system (m^3)
w	Weighting value (from 0 to 1)
x	Generic variable

y	Generic variable

Greek Symbols

η	Efficiency
ϕ	Time-dependent state probability
μ	Log-scale parameter
ρ	Mass density (kg/m^3); Current density (kA/m^2)
σ	Shape parameter; standard deviation; Stefan-Boltzmann Constant

Subscripts

auger	Auger
B	Batch
c	Container
cond	Condensing
cool	Cooling
D	Daylight
env	Ambient environment
E	Electrical; Eclipse
fail	Component failure
h	Heating; Heating rod
i	Generic index
j	Generic index
p	Piping
PI	Active ECLS systems installed in spacecraft racks
PS	Consumables and systems stored within a pressurized environment
rep	Component repair
resub	Resublimation
s	Soil; Sieve
SA	Solar Array
t	Time domain coordinate (s)
TA	Tube Assembly
U	Consumables and systems stored within an unpressurized environment

Chapter 1

Introduction

1.1 Background and Motivation

Since the dawn of the space age, humanity has aspired towards traveling to and settling distant worlds. These goals have been motivated by curiosity, the desire for exploration, and the promise of new knowledge and discoveries [1]. Of all the possible destinations within our local planetary neighborhood, Mars has time and time again been identified as the horizon goal for human spaceflight – the guiding destination for long-range programmatic planning, and the next major waypoint in humanity's expansion into the cosmos [1,2].

Given these enduring aspirations, it is not surprising that over the past sixty years, numerous Mars mission design studies have been undertaken, each exploring various options for transporting humans to and from the red planet (see Figure 1-1).

While these studies have provided great insight into addressing the challenges of transporting people to the surface of Mars, relatively little research has been done in addressing the challenges of sustaining them once they get there, particularly for durations greater than those of the traditional 30 day short- and 500 day long-stay sortie missions. Recently however, research in the domain of long-duration space habitation has gained increasing importance. This originated with President Obama's signing of the 2010 NASA Authorization Act, which for the first time, declared that:

> *"The long term goal of the human space flight and exploration efforts of NASA shall be to expand permanent human presence beyond low-Earth orbit"* [3]

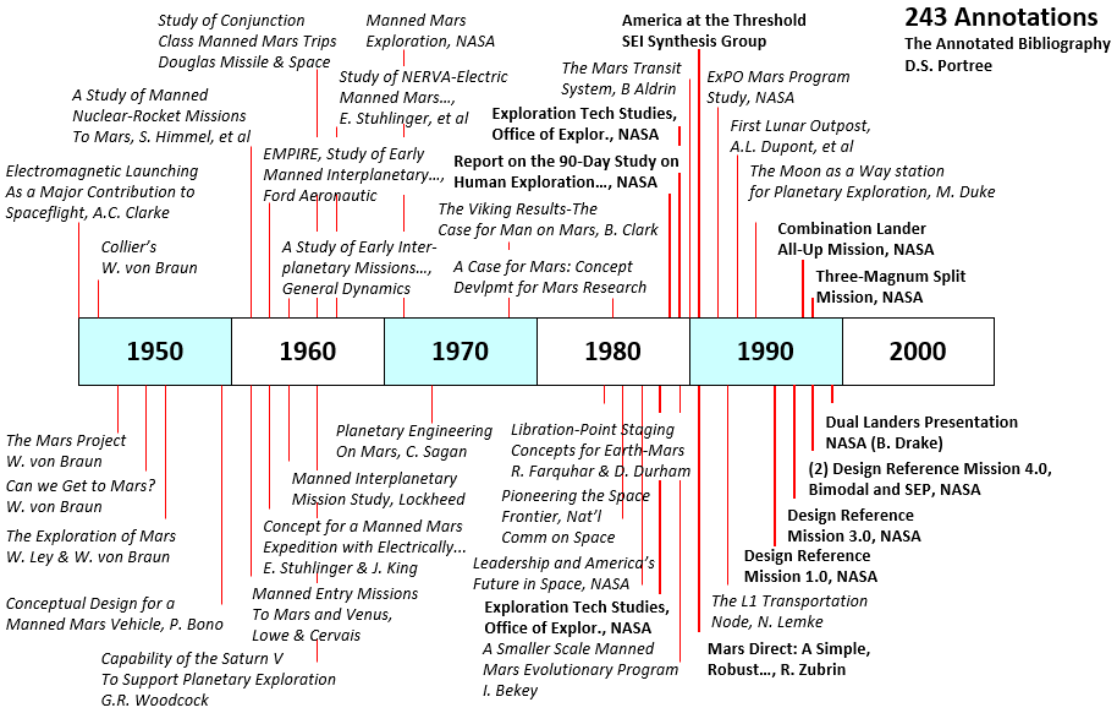

Figure 1-1: Summary of the Major Mars Mission Transportation Studies from 1950 to 2000 [4]

This goal was reaffirmed in the 2015 NASA Authorization Act, with the statement that:

> *"Human exploration deeper into the Solar System shall be a core mission of the Administration. It is the policy of the United States that the goal of the Administration's exploration program shall be to successfully conduct a crewed mission to the surface of Mars to begin human exploration of that planet."* [5]

In response to this mandate, NASA began conducting a series of studies in 2014 entitled the "Evolvable Mars Campaign" (EMC) [6] with the intent of identifying and developing a better understanding of the technological and programmatic challenges of developing a permanent human presence on Mars. An important outcome of this effort has been the division of the agency's crewed Mars exploration program into three distinct phases, each mapping directly to a particular region of space between Earth and Mars [7]. As shown in Figure 1-2, these phases are:

- The Earth Reliant Phase, which revolves around research and technology demonstrations onboard the International Space Station (ISS)
- The Proving Ground Phase, which is based on testing in-space propulsion, and deep space habitation and operations within cislunar space; and
- The Earth Independent Phase, where humans visit locations within the Martian system, and validate, deploy, and operate orbital and ground infrastructure that will enable repeated crewed expeditions to the surface of Mars.

As the name of the final phase suggests, the ultimate objective of this program is to develop the capability for people to live and work on the surface of Mars in a self-reliant manner – one that is independent from periodic resupply from Earth. As of late 2015 however, most major results published by the EMC effort have revolved around decisions related to propulsive elements and staging locations for the transportation of crew and cargo to the Martian system [8].

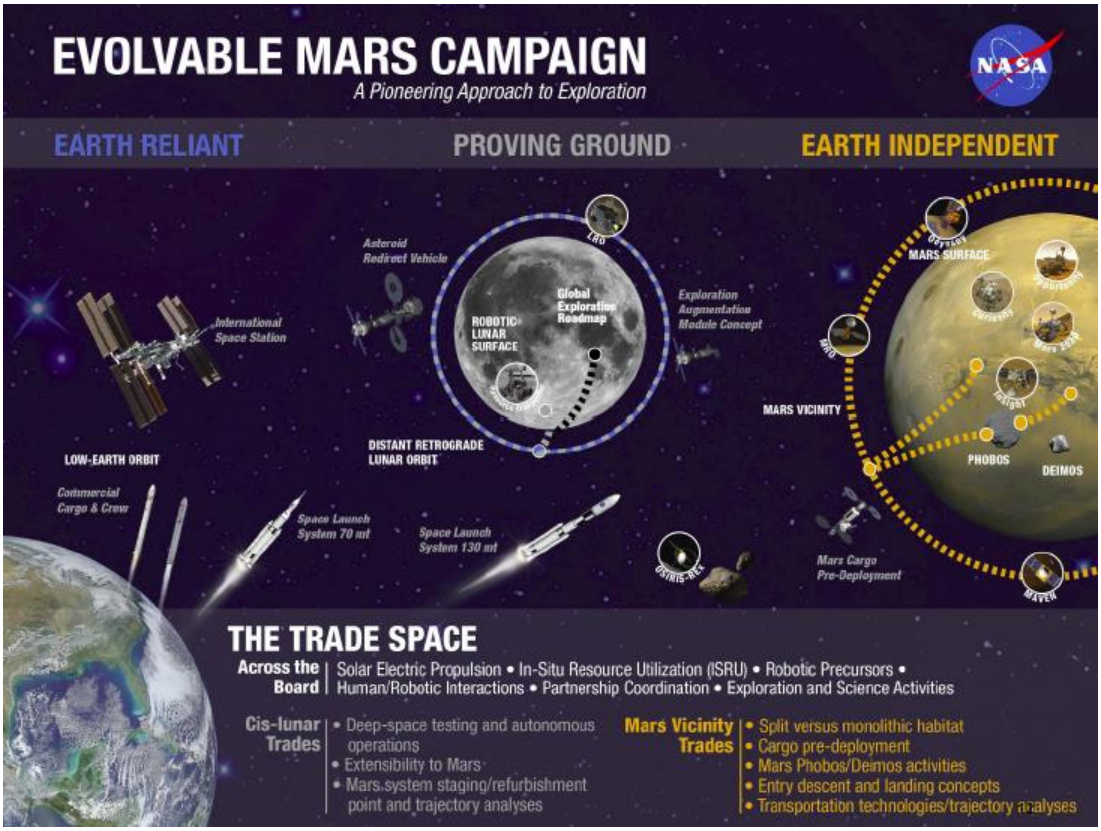

Figure 1-2: Summary of the NASA Evolvable Mars Campaign [8]

In parallel to NASA's efforts, a number of individuals and private organizations have also recently expressed interest in developing systems that would enable the rapid settlement and expansion of humans on Mars. These include proposals from Space Exploration Technologies Corporation (SpaceX) for a "Mars Colonial Transporter" capable of delivering people to the surface of Mars by the mid-2020s [9], Dr. Buzz Aldrin's plan for attaining human "permanence" on Mars based on the use of reusable Earth-Mars "cycler" spacecraft as a low-cost means of transporting crew and cargo through interplanetary space [10], as well as a proposal by the Dutch organization, Mars One, to rapidly colonize Mars via a series of consecutive one-way missions, each delivering four people to the surface of the planet [11].

As is the case with the majority of the past mission studies summarized in Figure 1-1, these alternative mission proposals have primarily focused on developing solutions to addressing the challenges of mass transportation to the Martian system – little detail has been presented on strategies for addressing the long-term demands of sustaining humans on the Martian surface.

Thus, the traditional mode of human Mars mission architecting can be characterized as one that mainly focuses on the **transportation** segment of missions, and invests less effort in characterizing the **habitation** segment of missions. Expressed another way, most previous mission studies have focused on the challenges of **supplying** crew and cargo to different mission destinations, but have not dedicated as much effort in characterizing the **demands** of this crew and cargo once they intend to establish a sustained presence at the final intended destination.

This trend overlooks the past 15 years of operational experience in sustaining a continuous crewed presence onboard the International Space Station (ISS), where we have observed the significant impact of mission support and logistics on program lifecycle cost and sustainability, especially as the duration of the program has increased [12]. As future missions venture further away from Earth and their frequency of mission abort opportunities decreases, it is expected that the demands of the crew, and the lifecycle properties of the systems needed to sustain them, will increasingly impact program lifecycle costs [7,12].

Motivated by these observations, this thesis develops an integrated habitation analysis tool to quantitatively evaluate the impact of technology choices and operational strategies on the sustainability and lifecycle costs of future long-duration planetary habitation systems. This tool, entitled HabNet, is then applied to a range of "permanent presence" mission scenarios, with the objective of identifying enabling and/or dominant technologies and architectures that are worthy of further research and development.

This goal is based on the premise that understanding the impact of system architecture decisions on the demands generated by long duration habitation scenarios and their operational costs will better inform near term decisions regarding mission sequencing, operational strategies, and technology investment and roadmapping [13].

1.2 Framing the Challenge of Sustaining Continuous Human Presence on the Surface of Mars

1.2.1 The Evolution of Mars Mission Design and Systems Architecting Methodologies

Fundamentally, space mission design is a systems architecting problem – that is, one that involves defining a set of technologies, supporting systems, and operational strategies to accomplish a set of functions that together, deliver value to the system's stakeholders.

As a result of this underlying problem structure, all previous Mars mission studies have employed systems architecting techniques to some degree of formality. Early Mars mission concepts developed during the 1950s and 1960s (see Figure 1-1) were in large part based on the experience of the system architect. This tended to result in a rapid convergence on system concepts, from which mass and cost estimates were calculated. As the body of knowledge surrounding human spaceflight and planetary science grew, space mission architecting began to adopt the process of enumerating operational and technological options based on expert knowledge, then performing comparative analyses of the costs of feasible combinations of selected options. This trend was influenced by the post-World War II birth of systems thinking [14], and enabled a deeper understanding of the impact of each component of a spaceflight system on its performance as a whole. These architectural options tended to cover major in-space transportation variables such as the type of trajectories employed, the location at which in-space propulsion and habitation elements are aggregated, and the types of propulsion systems utilized. Indeed, it was these same variables that characterized the "mission mode" discussions that led to the selection of the lunar orbit rendezvous profile for the Apollo program.

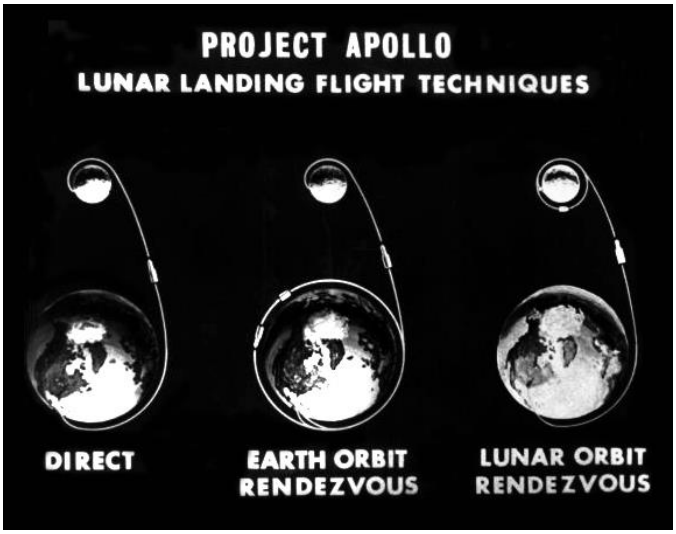

Figure 1-3: The Apollo Mission Mode Decision that shaped the transportation architecture that was adopted by the Apollo Program to transport humans to and from the lunar surface [15]

In 1978, two years after the Viking landers began taking measurements from the Martian surface, Ash et al. [16] published a seminal study that introduced the concept of generating rocket propellant from the Martian environment as a means of reducing the total mass of human missions to Mars. This study represented the first analysis of In-Situ Resource Utilization (ISRU) – the concept of employing locally-derived resources to produce useful consumables for a human crew. Shortly thereafter, ISRU became increasingly incorporated in mission concepts proposed within the Mars exploration community, frequently appearing in presentations given at the "Case for Mars" conferences held throughout the 1980s [17].

In 1990, ISRU gained further recognition when Baker and Zubrin published their "Mars Direct" mission concept [18]. Similar to that proposed by Ash et al., this concept revolved around the production of Mars ascent vehicle propellant by reacting Earth-delivered hydrogen with carbon dioxide derived from the Martian atmosphere. This plan later evolved to become the first NASA Mars Design Reference Mission (DRM1.0) in 1993 [17,19], which has since been iterated upon on multiple occasions with increasingly higher fidelity analysis to form the current NASA Design Reference Architecture 5.0 (DRA5.0) [20,21].

The introduction of the concept of ISRU added another decision variable to the traditional Mars mission architecture tradespace that simultaneously increased its complexity and provided potential for more attractive solutions. To structure the analysis of this tradespace, NASA began to use decision trees during their DRA5.0 activities. This approach consisted of enumerating all conceivable high level architectural options, which in turn allowed individual

architectures to be selected, analyzed in-depth, and compared with the performance of other previously assessed architectures. Figure 1-4 shows the top-level decision tree developed during the NASA DRA5.0 efforts, summarizing key transportation architecture decisions along with the architectures assessed during the prior major Mars mission studies.

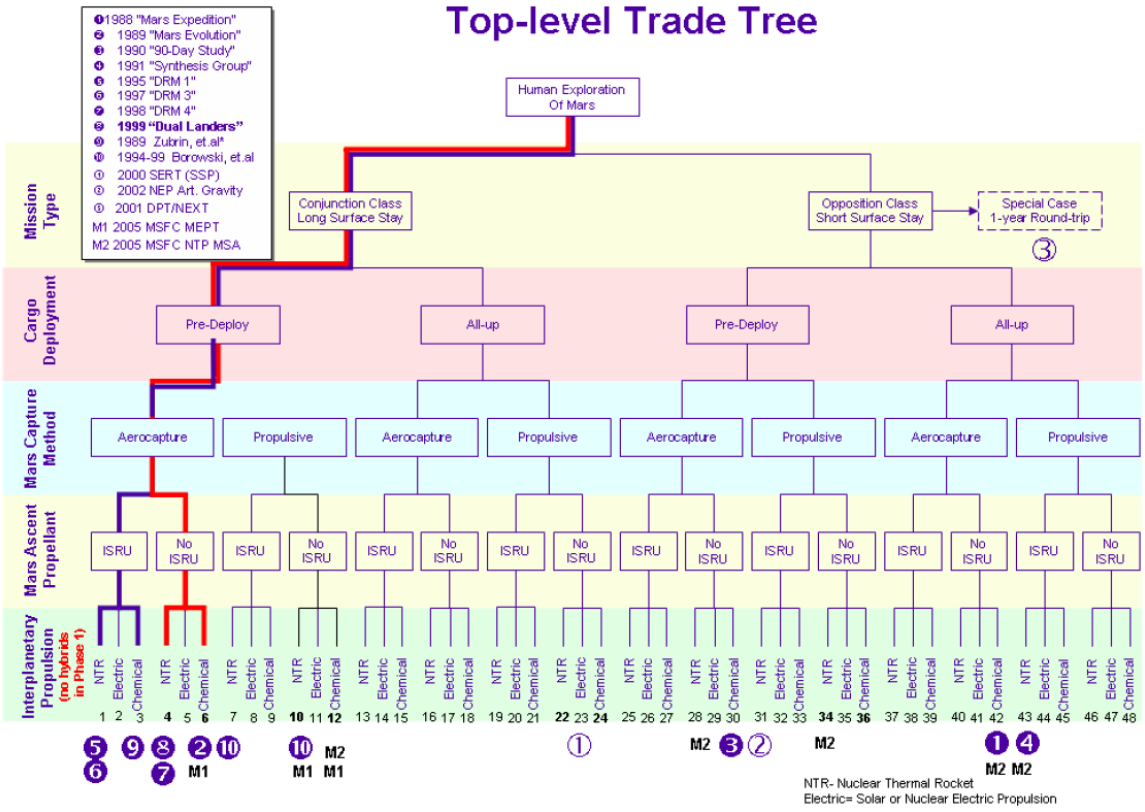

Figure 1-4: NASA DRA5.0 Top Level Architectural Trade Tree [20,21]

In this same period, researchers at MIT began to develop more formal approaches to structuring and exploring the Mars mission architecture tradespace. Instead of the traditional NASA and industry approach of using expert opinion to select a branch of a decision tree and analyzing it in great detail, these researchers proposed algorithms that: (1) structured architectural decisions as networks based on their inherent dependency on one another, (2) searched for all feasible combinations of architectural decisions from this network structure; and (3) evaluated feasible architectures at low- to mid- fidelity to characterize and analyze the entire tradespace.

One of the key ideas that developed during this period was the notion that systems architecting is fundamentally a decision-making process [22,23]. Decisions can be classified as those that differentiate architectures, and those that do not. Thus, the process of systems architecting was formulated as one that focuses on how *architecturally distinguishing decisions* affect the performance of an architecture. To structure these decisions, Simmons [22] developed a representation scheme called the Architecture Decision Graph (ADG) – a network graph that depicts the key architecturally distinguishing decisions that characterize a particular architecture, the constraints between these decisions, and the metrics for evaluating the architecture that emerges when these decisions are made.

An example of an ADG for the Apollo mission architecting problem is shown in Figure 1-5. As can be seen in this figure, the ADG can generally be thought of as a suppressed decision tree (see Figure 1-4), in that the types of decisions are shown, but not the options for each decision. The advantage of this representation is that coupling and feedback between decisions are explicitly represented – a feature not captured in the serial structure of decision trees.

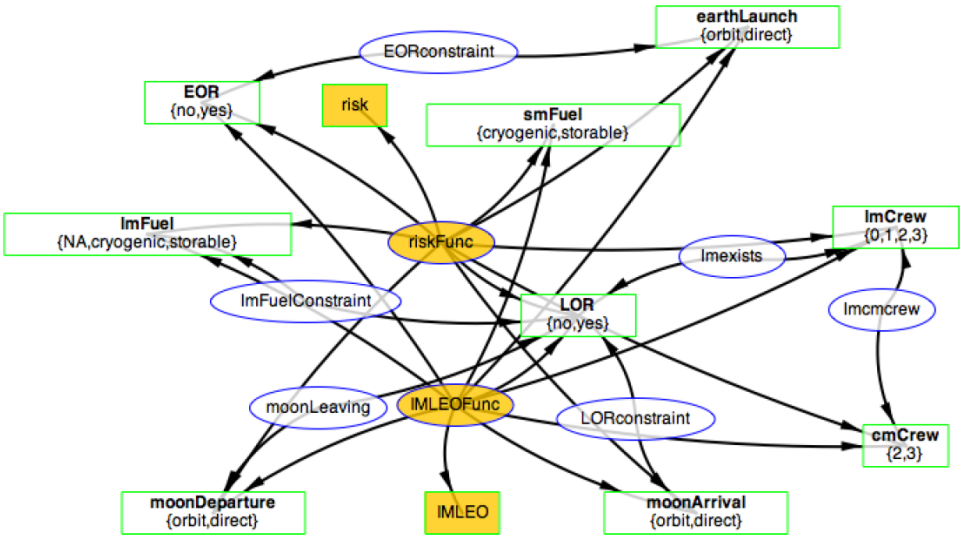

Figure 1-5: Architecture Decision Graph of the Apollo mission mode decision [22] (sm: service module, lm: lunar module, EOR: Earth Orbit Rendezvous, LOR: Lunar Orbit Rendezvous, IMLEO: Initial Mass to Low Earth Orbit)

Since its introduction, the ADG-approach has been used in concert with morphological matrices to study a variety of space systems architecting problems related to human spaceflight. Such examples include the architecting of evolvable heavy lift launch vehicle families [24],

and the high level architecting of vehicle elements for crewed interplanetary transportation systems [25].

More recently, systems architecting research has expanded beyond the traditional analysis scope of sortie-class space missions based on single-use systems, to the analysis of campaigns of multiple missions that rely on reusable, multipurpose systems visiting multiple mission locations. This increase in scope was motivated by the emerging field of space logistics, defined as "the theory and practice of driving space system design for operability, and of managing the flow of materiel, services, and information needed throughout the space system lifecycle."[26]. One of the key outcomes of this research was the use of graph theory to formulate and analyze space mission campaigns as a network problem, where nodes represent physical locations within a space transportation network, and arcs connecting these nodes represent possible transportation links between two adjacent locations [27,28]. Solutions to this class of problem consist of the identification of a network of vehicles, propellant production and storage infrastructure, and intermediate destinations that best satisfy mission objectives at minimal system mass. Figure 1-6 depicts an example of an Earth-Moon-Mars logistics network, including representative nodes in the cislunar and Martian systems.

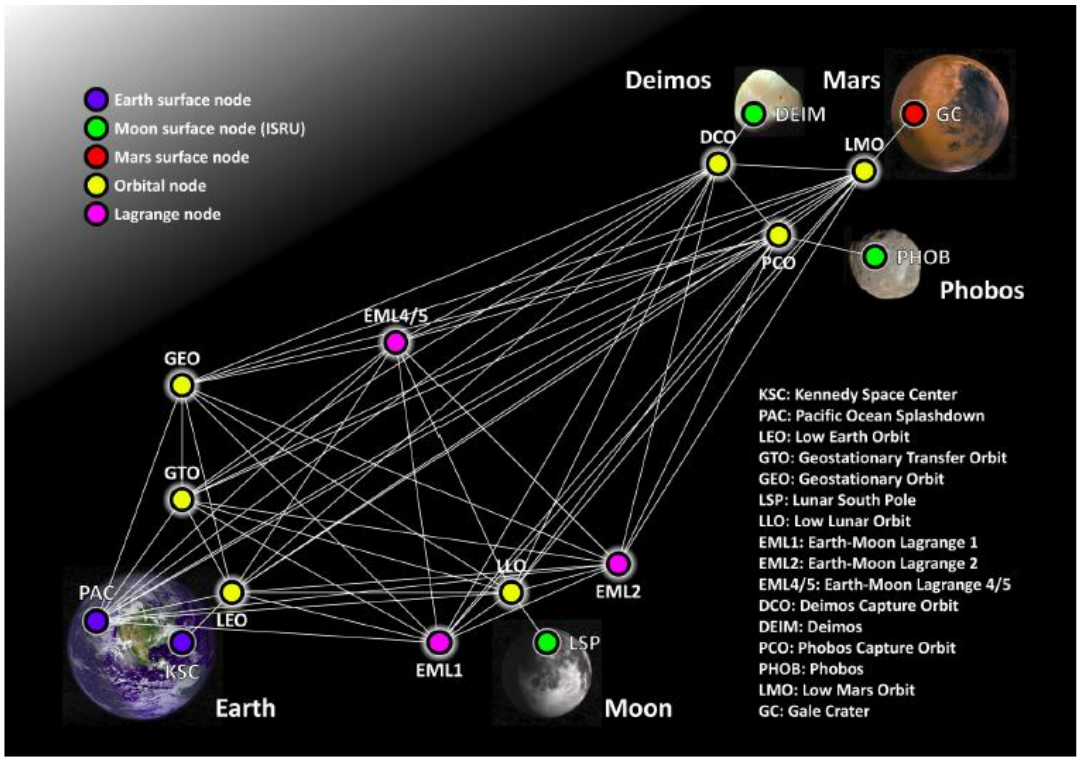

Figure 1-6: Node-Arc Formulation for an Earth-Moon-Mars logistics network [27]

While these recently developed systems architecting methodologies have advanced the breadth and efficiency of exploration of the space transportation architecture tradespace, they have yet to be applied to the problem of space habitation systems architecting – defined in the NASA Space Technology Roadmap as the selection of "capabilities with the optimal combination of mass, size, reliability, logistics, and loop closure characteristics that will best support the given mission scenario." [29]

Moreover, in almost all of the space transportation system studies discussed above, the demands for consumables such as food, gases, and water by the crew at each exploration destination were based on fixed assumptions on the habitation system architecture – no analysis of habitation system architectural decisions on mission-wide cost and performance was performed [27,28].

As a result, this thesis aims to apply and refine contemporary systems architecting methodologies to analyze continuously crewed Mars habitation scenarios, in line with NASA's planned "Earth Independent" exploration phase. As part of this effort, this thesis develops a modeling and simulation environment that predicts crew demands for consumables and spare parts as a function of the key architecturally distinguishing decisions that characterize Mars habitation systems. This simulation environment is intended to facilitate both the exploration of the Mars habitation architecture tradespace, as well as the prediction of crew demands for integration with the network-based space transportation architecture frameworks described above. Moreover, this modeling and simulation environment will also be developed with the capability to perform analyses of habitation systems at other destinations in addition to Mars. These include the Earth's moon, near Earth objects, Earth-based habitats, and beyond.

1.2.2 The Challenge of Developing a Sustained Human Presence in Space

As a first step towards characterizing the challenges of developing a sustained human presence on the surface of Mars, we briefly review humanity's past space habitation accomplishments. Figure 1-7 depicts a log-log plot of the endurance, a term we define as the maximum time that a habitat can sustain a given number of crew before needing to be resupplied with resources derived from Earth; versus the population of the major space habitats that have been flown to date.

From Figure 1-7, we observe the steady evolution of our space habitation capabilities, beginning with the early crewed capsules of the 1960s, through to the era of three-person long duration Earth orbiting space stations that were operated from the mid-1970s through to the mid-1990s. In 1995, the initiation of the Shuttle-Mir Program led to the temporary creation of large space habitats capable of sustaining up to ten people over short durations. The 1997 docking of Space Shuttle Atlantis to Space Station Mir during STS-86 formed the highest capacity space habitat created at the time, supporting 10 people over a period of almost six days, and weighing approximately 200 metric tons [30] (see Figure 1-8(a)).

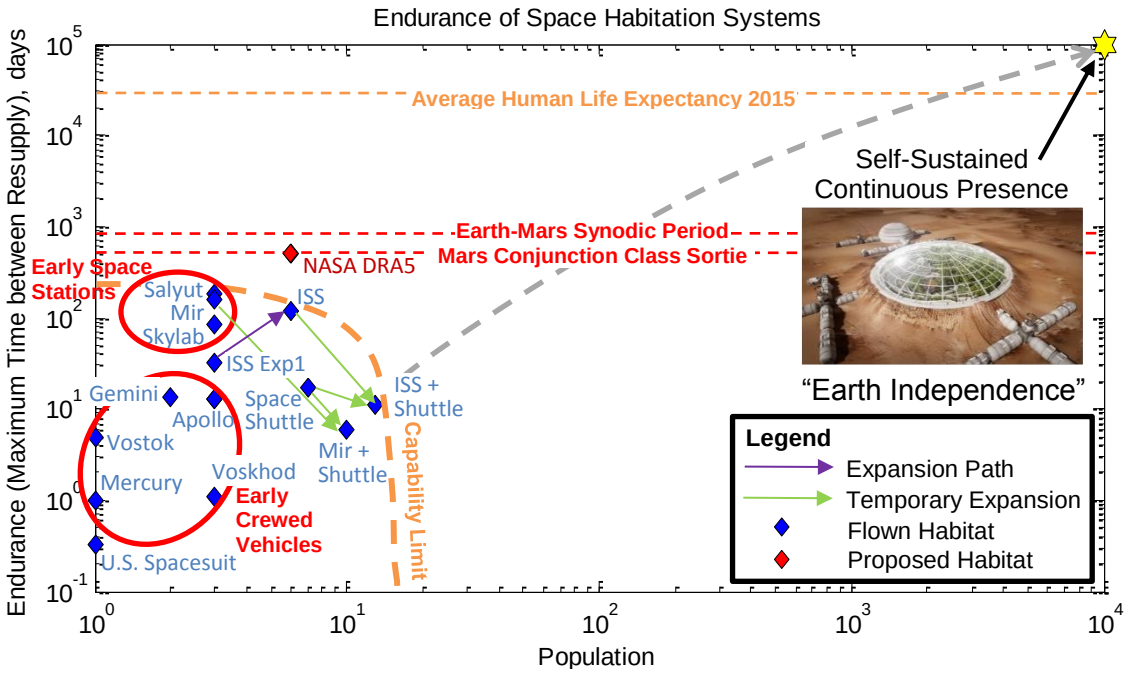

Figure 1-7: Evolution of Space Habitation Capabilities

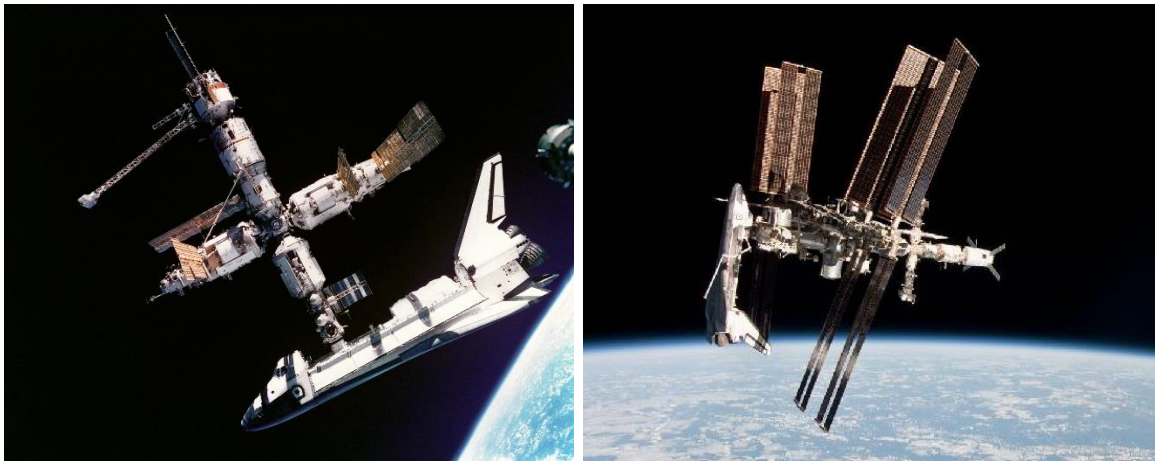

Figure 1-8: High Population Space Habitats (a). Space Shuttle – Mir Stack [31] (b). Space Shuttle Docked to the International Space Station [32]

Currently, the only space habitat in operation is the International Space Station (ISS), which has been continuously crewed since November 2001. The ISS nominally accommodates a crew of six, and requires the resupply of consumables and spare parts approximately every 30 to 90 days [33] to maintain continuous operations. On three separate occasions during its construction however, the combined population of the Space Shuttle and ISS stack accommodated a total of 13 crewmembers for a period of up to 10 days [34–37] (see Figure 1-8(b)). These values comprise the best habitation performance values that have been attained to date in space and as such, the ISS can be considered to be the state of the art in our space habitation capabilities.

In contrast, current plans for long-stay sortie missions to Mars require habitation systems that are capable of sustaining four to six people for periods of up to 540 days on the Martian surface without resupply from Earth [20]. As can be seen by the line labeled "Mars Conjunction Class Sortie" in Figure 1-7, this duration far exceeds that of any previously developed space habitat.

To bridge this capability gap, mission architects have over the past 30 years developed mission concepts that increasingly rely on ISRU. By generating resources locally rather than relying on their delivery from Earth, ISRU has been adopted with the primary goal of increasing the endurance of a habitation system by replacing the requirement for resupply with systems that extract and produce required materiel locally. The effectiveness of ISRU however, is dependent on: (1). the original availability of resources at the exploration destination; and (2). the ease at which these resources can be converted into useful products and stored in a stable manner. As a consequence, the use of ISRU to reduce the burden of resupply is typically only considered for planetary surface missions, as compared to deep space or orbital habitats, where in-situ resources are scarcer.

This suggests that the lifecycle costs of sustaining any Mars habitation system of a predetermined endurance and population will be primarily dependent on the selection of the:

- Environmental Control and Life Support (ECLS) system architecture, as these systems create the habitable environment initially required to sustain a given population
- In-Situ Resource Utilization (ISRU) architecture, which can provide some proportion of the required resupply mass in-situ, thereby influencing the endurance of the habitation system; and the

- Surface mission operational strategy, which imposes consumables demands on both ECLS and ISRU systems

In addition to the functional performance of ECLS and ISRU systems, their supportability attributes are also a critical driver of habitat lifecycle costs. The term supportability encompasses considerations related to system reliability, maintainability, reparability, redundancy, and sparing philosophy [12] – attributes that influence the resupply requirements and hence endurance of habitation systems.

Thus, each point on the comparative habitat performance chart shown in Figure 1-7 can be framed as the result of the combined selection of ECLS, ISRU, and supportability architectures, as well as the choice of mission operational strategy. Moreover, NASA's long-term goal of expanding "permanent human presence beyond low-Earth orbit" [3] can be thought of as pushing the current state of the art in habitation capabilities, as indicated by the dashed orange "capability limit" depicted in Figure 1-7, towards the top right hand corner, where habitats are capable of sustaining large populations in an "Earth Independent", self-sustaining mode. This thesis aims to inform the various architectural pathways between our current habitation capabilities and this "utopian" point by analyzing the lifecycle impacts of habitation scenarios at various points beyond the capability limit in the endurance-population space represented in Figure 1-7. For the purposes of depicting self-sustaining habitats in this figure, we define an "Earth Independent" habitat as one with an endurance that is longer than the span of an average human life – approximately 79 years or 29,000 days for an average American living in 2013 [38]. At these levels of endurance and beyond, it may be more instructive to adopt the term "carrying capacity" to characterize habitation systems – a term used in the field of ecology to describe the maximum population of a biological species that an environment or habitation system can sustain indefinitely [39].

1.2.3 Endurance Levels Required for Mars Mission Habitats

For habitation systems on the surface of Mars, the frequency of resupply is constrained by the relative orbital mechanics of Earth and Mars. Assuming that all crew and cargo delivery missions adopt the NASA DRA5.0 recommendation of using conjunction class long-stay missions [20] (see Figure 1-9b), the minimum period between resupply of a continuously

crewed Mars habitation system, and hence its minimum endurance, is approximately 26 months – the synodic period of the Earth and Mars about the Sun.

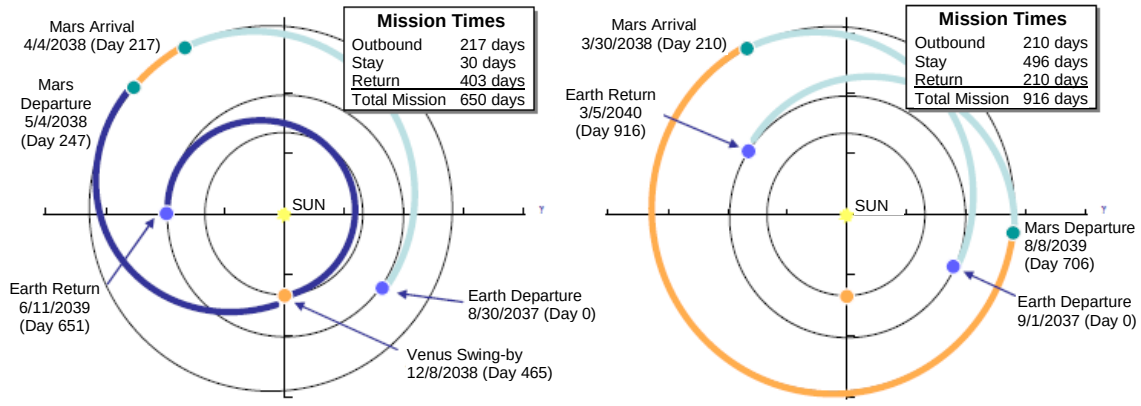

Figure 1-9: Representative Mars mission profiles (a). Opposition-class, where the crew spends 30-60 days on the Martian surface (b). Conjunction-class, where the crew spends up to 540 days on the Martian surface [20]

As shown in Figure 1-10, this 26-month constraint affects the profile by which a Mars surface habitat is populated. For a scenario where multiple crews make consecutive sortie missions to the same surface habitat, a conjunction-class mission implies that the habitat will be crewed for up to 540 days, and left in a dormant state for approximately 250 days until the next crew arrives, 26 months or approximately 790 days after the previous crew landed (Figure 1-10(a)). If a continuous human presence is desired, some portion of the crew is required to remain on the Martian surface for approximately 790+540 = 1330 days to bridge the 250 day dormancy gap between the first and second crews, and to wait for Earth and Mars to align for their return trip back to Earth. As shown in Figure 1-10(b), this would result in a non-uniform population profile where the population periodically increases during crew changeover periods in a manner similar to that currently observed on the ISS. We note that this expedition length could be reduced to approximately 790+60 = 850 days if an opposition class return trajectory were chosen (see Figure 1-9(b)). This shorter mission duration option, however, would require a fly-by of Venus by the in-space transit vehicle on either the outbound or inbound legs from Mars, necessitating additional mass for thermal systems to manage the increased heat load as the spacecraft moves through the vicinity of Venus [21].

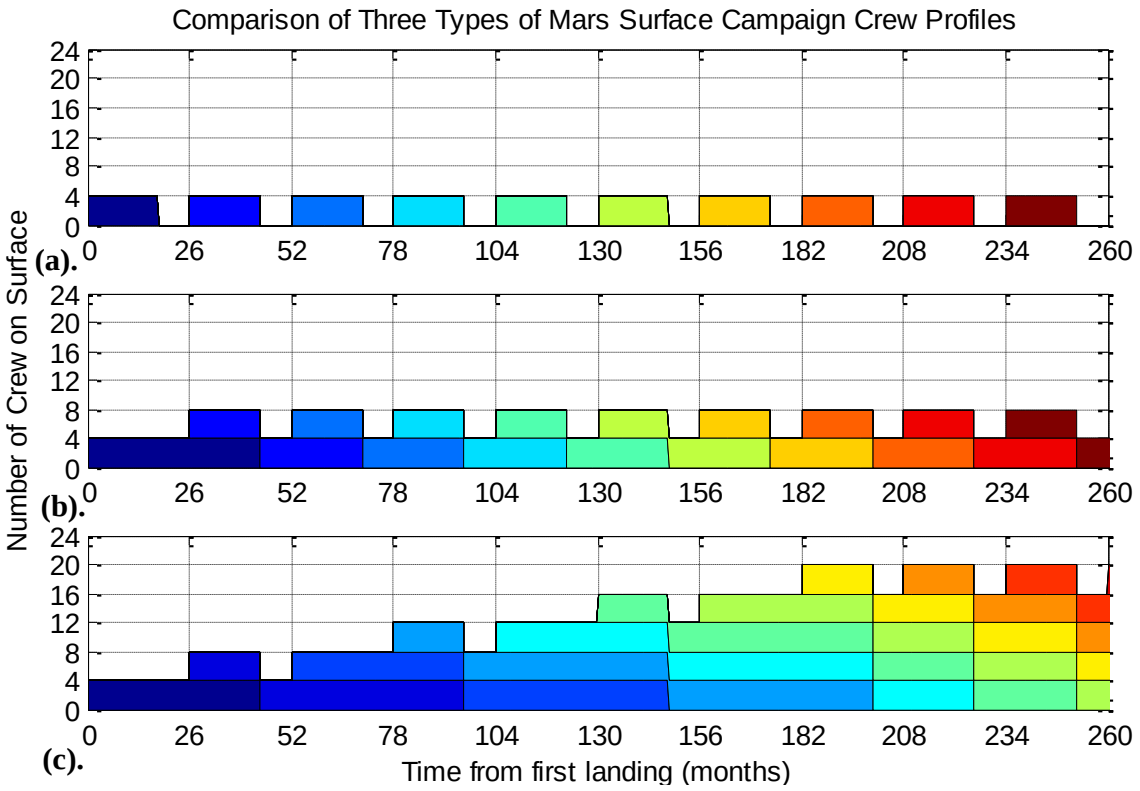

Figure 1-10: Crew Population Profiles for Three Types of Mars Surface Campaigns. Here, each expedition (the members of a crew for a particular mission) is represented by a different colored cell. Here, it is assumed that only four crew can be delivered to Mars at any one time (a). A string of conjunction-class sortie missions (b). A minimum continuous presence profile, where successive four-person crews spend 1330 days (44 months) on Mars and overlap for 540 days (18 months) for every 26 month period (c). A gradual population ramp up profile, where each successive four-person crew stays for an additional 26-month period on the surface of Mars, so that the total surface population increases over time

Finally, in the extreme case where an increasing and continuous crewed presence is desired, each successive crew is required to remain on the Martian surface for progressively longer durations until the desired steady state population is attained. Figure 1-10(c) depicts one example of this scenario, where the surface population is ramped up to a steady state value of 24 crew members after the 7^{th} crew is sent to the surface. Here, the n^{th} crew remains on the surface for 790n+540 days until the 7^{th} crew arrives, after which all subsequent crews remain at Mars for this same duration of 790×7+540 = 6070 days (≈16.6 years) in order to maintain the surface population. We note that the long surface stay time in this example is based on the assumption that each mission is constrained to deliver four crewmembers to the Martian surface via a conjunction class mission trajectory, and that over the multi-decadal duration of

the campaign depicted, the crew does not procreate on the surface. It is likely that a crew ramp up can be obtained with lower surface stays if these constraints are relaxed (by for example, adopting an opposition class trajectory).

These three mission scenarios assumed that crewmembers would be returned to Earth after spending some extended period of time on the Martian surface. In recent years however, the concept of rapidly settling the surface of Mars via one-way missions has gained increasing recognition. In these one-way mission scenarios, crewmembers live out the rest of their lives upon landing on the surface of Mars. This can result in durations upwards of 50 years that a habitation system is required to sustain a one-way crew – a capability level that is even further beyond those summarized in Figure 1-10.

These large mission stay times illustrate the magnitude of the capability gap between the current state of the art in space habitation and the goal of developing a sustained human presence on the surface of Mars. Bridging this gap will entail transitioning from current ISS operations towards the three general habitation scenarios depicted in Figure 1-10 – namely from a sequence of initial sortie missions where there are gaps in human presence between missions, followed by a continuously crewed habitat with a minimum crew size, and finally to a population ramp-up to some sustainable population.

While sequences of sortie missions have been studied in detail over the past few decades by NASA and other organizations [21], little attention has been given to the continuous-presence mission scenarios depicted in Figures 1-10(b) and 1-10(c), and the transition towards and between them. As a result of this trend, this thesis aims to make the first steps towards analyzing these latter two habitation scenarios in further detail to inform the decisions that will dictate the architecture of the first missions that will establish a human presence on the surface of Mars.

1.3 Thesis Statement

In light of the previously discussed challenges associated with developing a continuously crewed Mars habitation system, we pose the following guiding question for this thesis:

What is the optimal set of coupled technologies and operational strategies required to develop a sustained human presence on the surface of Mars?

This question was formulated with the intent of building upon the high level goals of the Evolvable Mars Campaign (EMC) studies that NASA is currently undertaking. The main differences between this work and that encompassed by the EMC are the scope of the missions explored, and the methodology employed. As discussed earlier in Section 1.2.1, this thesis aims to explore "permanent presence" mission scenarios beyond the conjunction-class sortie missions currently being studied by NASA. This includes mission scenarios with both fixed and expanding population profiles. In addition, as has been discussed throughout this chapter, this thesis is primarily interested in the **habitation** segment of Mars mission architecting – that is, the surface infrastructure required to sustain human life, and how architectural decisions related to these systems affect their long-term sustainability. Finally, since the habitation segment of Mars mission architecting has in the past received relatively little focus, this thesis addresses this guiding question through the development of an integrated habitation framework to increase the fidelity and scope of traditional habitation analysis approaches.

1.3.1 Goal Statement

With the overarching research question and scope of this thesis now established, we define specific objectives for this work. This is encapsulated within the following goal statement:

To quantify and compare the requirements for emplacing, maintaining, and resupplying the various systems required to enable the range of "permanent presence" mission scenarios assessed, in order to identify architecturally distinguishing technologies and operational strategies worthy of further research and development, **by:**

- Combining the key habitat endurance-influencing disciplines of mission operations, life support, in-situ resource utilization, and system supportability (see Section 1.2.2) to develop HabNet – a single unified habitation analysis tool designed to predict the costs of deploying and sustaining continuously crewed habitation systems on the surface of Mars
- Developing and/or integrating existing technology performance and sizing models pertinent to each of the aforementioned disciplines into a model library to enable comparative architecture assessments by the integrated habitation analysis tool

- Applying the developed analysis tool to a series of "permanent presence" mission case studies, including one way and return trip mission scenarios involving the sustainment of both a fixed and growing crew size.

Using the Architecture Decision Graph approach developed in the field of systems architecting

1.3.2 Case Studies

This thesis will explore the technological and operational requirements of sustaining a continuous human presence on the surface of Mars with various population profiles by performing three major case studies. These include:

- A **Validation Case Study** based on the Deep Space Habitat concept developed during the NASA Human Exploration Framework Team (HEFT) Phase 2 activities [40]. This habitat is intended to sustain a 4-person crew on sortie missions in deep space lasting one year. While this habitation scenario does not aim to achieve "permanent presence", it is well documented and studied, and provides a dataset from which the HabNet environment can be validated.
- **Case Study 1: The Mars One Mission Plan** – a highly publicized mission that proposes to begin colonizing Mars in 2025 using a series of one-way 4-person crewed missions to the Martian surface [11]. While this plan is not the first to propose the adoption of one-way missions as a means of accelerating the first landing of humans on Mars [41], the fact that: (1) it is the most documented one-way mission proposal that has been publicly announced; (2) as of this writing, no technical analyses of the sustainability of the plan have been published in the technical literature by proponents of the plan; and (3) it is indeed a "permanent presence" Mars mission scenario with the added attribute of a rapid population ramp-up profile; make it an ideal case study for the independent analysis of the technological and operational implications of one-way variants of "permanent presence" Mars mission scenarios.
- **Case Study 2**: **Continuously Crewed Mars Surface Field Station** – this case study builds on a concept recently developed during the NASA EMC studies for a field or experiment station on the surface of Mars [42]. This field station is intended to facilitate in-situ research and development on approaches to living and working in the Martian environment for

progressively longer mission durations and at increasing levels of logistics independence from Earth (i.e. increasing levels of habitat endurance). The experimental nature of this mission scenario means that multiple crews will visit and return from the station on a number of expeditions, in a manner similar to the current operation of the International Space Station. After a number of preliminary 540-day sortie missions, the surface habitat will transition to supporting continuous human presence in a manner similar to that depicted in Figures 1-10(b) and 1-10(c). This case study will investigate the technologies required to support this field station during the first two mission scenarios, where a "String of Sorties" is first undertaken (Figure 1-10(a)), before a transition to "Minimum Continuous Presence" (Figure 1-10(b)) is undertaken. The analysis of the ramp-up mission scenario depicted in Figure 1-10(c) is left for future work.

These case studies are depicted in an updated version of the Endurance-Population chart, shown below:

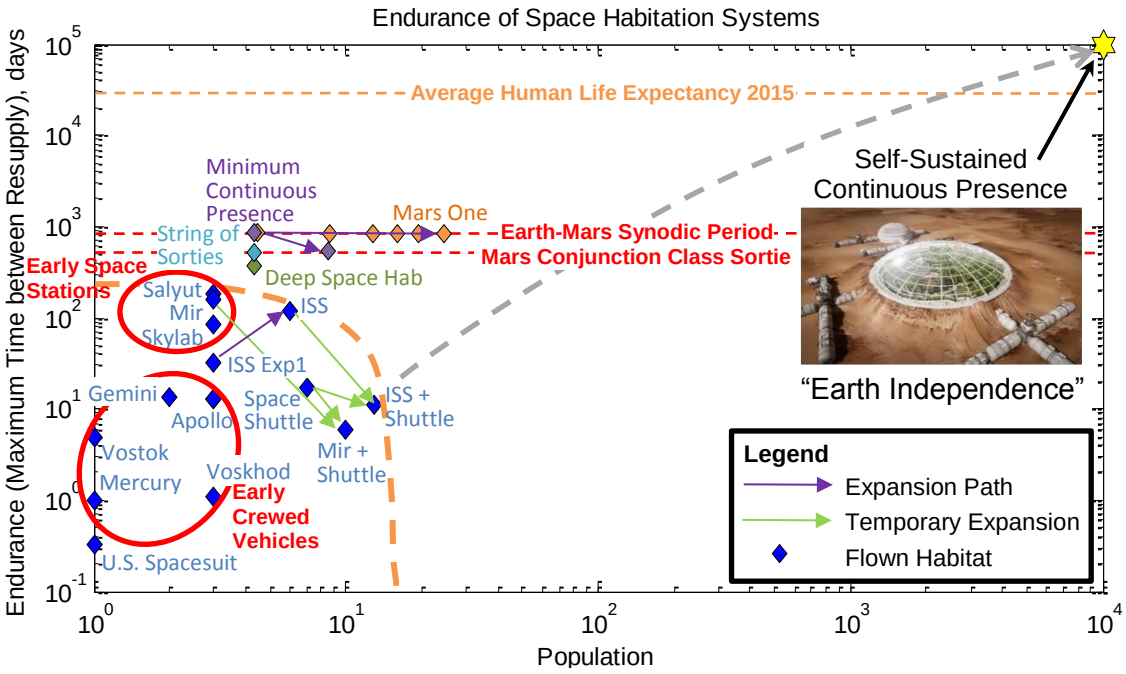

Figure 1-11: Evolution of Space Habitation Capabilities including Case Studies performed in this thesis

1.4 Thesis Outline

In order to present each of the major stages in the evolution of this work, the remainder of this thesis is organized as follows.

Chapter 2 provides a historical overview of the development of ECLS and ISRU technologies, as well as a summary of more recent studies on the impact of supportability on future, long duration mission scenarios beyond low Earth orbit. Through this, we gather insights into the design philosophies that drove the architecture of the current systems operating onboard the International Space Station, as well as the philosophies that influence current thinking on the drivers of long-endurance Mars surface system architectures.

Chapter 3 combines relevant features of the analysis approaches reviewed in Chapter 2, along with contemporary systems architecting methodologies to develop the HabNet framework. This chapter commences with the development of an Architecture Decision Graph to identify the interactions between the key architectural decisions that shape a human spaceflight system. This graph is then used to formulate the high level HabNet framework, from which individual modules are identified and further developed.

In Chapter 4, we validate both the dynamic simulation and sizing capabilities of HabNet. This commences with the comparison of system dynamic behaviors predicted by HabNet with those obtained from the open-source BioSim software package at varying levels of system complexity. Following this, the dynamic behavior of each of the HabNet ECLS technology models is validated against operational data from the corresponding ISS technology. With a reliable dynamic prediction capability established, a validation case study is then performed with HabNet where its sizing capability is compared with results previously published from an analysis performed on a one-year deep space habitat mission scenario.

Chapter 5 presents the first of the two major case studies performed within this thesis, focusing on the "Mars to Stay" class of Mars mission architectures. These are characterized by campaigns of one-way crewed missions to the surface of Mars that are periodically supported by cargo delivery missions. Over time, these plans propose the buildup of infrastructure on the Martian surface, ultimately leading towards self-sustainability. In this chapter, we provide a brief historical overview of "Mars to Stay" class missions prior to performing a feasibility analysis on the most publicized variants of these – the Mars One mission plan. Here, we use HabNet to perform an iterative analysis of the Mars One mission plan based on statements and assumptions made publically by the organization. Through this, we identify challenges

associated with providing the logistics required to sustain a one-way growing colony, and identify technologies and operational approaches that may mitigate some of these challenges.

Chapter 6 then explores campaigns of Mars surface missions based on return-trip missions, where crews periodically switch out with other crews after some extended period of time spent on the Martian surface. This chapter commences with an analysis on the impacts of varying levels of crop growth on the architecture of a surface habitat, before performing a larger trade study to analyze the impacts of ECLS and food growth architectures on total ISRU and lifecycle logistics mass. These results are then used to assess the total mass that must be emplaced and delivered to the Martian base over time for two mission scenarios – the "String of (conjunction-class) Sorties" (Figure 1-10(a)), and the "Minimum Continuous Presence" (Figure 1-10(b)). Through this, we identify the key architectural drivers of campaign sustainability based on the insights obtained.

Finally, in Chapter 7, we conclude this work by summarizing the major contributions and findings of this thesis. Based on these findings, we describe the future work required to continue to further evolve both the HabNet capability developed here, as well as our collective understanding of the requirements for developing a sustained human presence on the surface of Mars.

Chapter 2

Literature Review

In the previous chapter, we reviewed the evolution of Mars mission design and identified the main drivers of habitat endurance as being the Environmental Control and Life Support (ECLS) system architecture, the In-Situ Resource Utilization (ISRU) architecture, and the supportability strategy adopted for these two systems. This chapter explores the development and operational history of these systems, as well as recent analyses into system-wide considerations related to their supportability. From this review, we gather observations and lessons learned to develop high-level requirements for the development of HabNet.

2.1 Historical Review of Environmental Control and Life Support Systems

2.1.1 Basics of Spacecraft Environmental Control and Life Support

As the name suggests, the role of Environmental Control and Life Support (ECLS) systems is to provide an environment that can sustain human life. Although we explore it in the context of spacecraft in this thesis, it can be interpreted as a general term that refers to any system in any context that keeps people comfortable by controlling their immediate environment. Such examples range from the combination of Heating, Ventilation, and Air Conditioning (HVAC) and plumbing systems of a modern building, to the cabin of an aircraft, to SCUBA diving equipment [5]. As a result of this, the origins of ECLS can be thought of as extending back to the time when humans first found solutions to survival, either by finding a means to shelter from the elements, or by discovering ways to obtain and manage the resources necessary for survival. Additionally, the Earth's biosphere can be thought of as a natural ECLS system, a

notion that has gained increasing public awareness in recent years due to the growing threat of climate change.

With regard to crewed spacecraft, ECLS is defined as a system of technologies and processes that accomplish a set of functions. These functions are derived from the basic human needs of maintaining a comfortable atmosphere, providing potable water and food, and managing metabolic waste. Other functions are also included in the definition of ECLS systems, and are usually derived from the context in which the aforementioned high level functions are accomplished. Table 2.1 lists all of the functions typically considered under the purview of spacecraft ECLS. These particular functions were developed for the International Space Station program. It is interesting to note that U.S. and Russian ECLS system designers typically categorize these functions into different systems. This was an important factor to account for during the development and construction of the ISS [43]. These approaches to ECLS function categorization are also listed in Table 2.1.

Table 2.1: ECLS Functions and Subfunctions (Adapted from [43,44])

Function (with sub-functions bulleted)	**U.S. Categorization**	**Russian Categorization**
Atmosphere Revitalization (AR) • CO_2 Removal • CO_2 Reduction • O_2 Generation/Supply • Trace Contaminant Monitoring and Control • Microorganism Control	ECLS	ECLS
Atmosphere Control and Supply (ACS) • Major Constituents Monitoring • Atmosphere Composition Control • Atmosphere Constituents Storage • Pressure Control	ECLS	ECLS
Temperature and Humidity Control (THC) • Temperature Control • Humidity Control • Ventilation • Equipment Cooling	ECLS	Thermal Control System
Water Recovery and Management (WRM) • Water Storage and Distribution • Water Recovery	ECLS	ECLS

• Water Quality Monitoring and Control		
Waste Management (WM) • Metabolic Waste Management • Other Solid Waste Management • Liquid/Gaseous Waste Management	ECLS	ECLS
Fire Detection and Suppression (FDS) • Detection of Incipient Fires • Suppression of Fires • Cleanup After a Fire	ECLS	ECLS
Vacuum System (VS) For scientific payloads	ECLS	Not Applicable
Food Storage and Preparation[1]	CHeCS[2]	ECLS
Thermally Conditioned Storage (Refrigeration and Freezers)	CHeCS[2]	ECLS
Wholebody Cleaning	CHeCS[2]	ECLS
Housekeeping	CHeCS[2]	ECLS

[1]Food production is also a CHeCS function, but is not considered in the International Space Station Program. Rather, it is a function being investigated under the ISS Program Science Office.
[2]CHeCS refers to Crew Health Care System

Traditionally, architecting ECLS systems involves first heuristically selecting a subset of the above functions based primarily on the number of "person-days" that the system is required to support – that is, the product of the number of crewmembers, and the duration over which they will inhabit a particular spacecraft [43]. This is typically informed by a predefined mission profile, based on a preselected mission destination. Once the ECLS functions are chosen, technologies are selected and developed to accomplish the set of functions. These technologies are then connected with the appropriate input/output structure to form an ECLS architecture.

Generally, as the number of person-days increases, more of the above ECLS functions are selected in an attempt to increase the amount of "mass loop closure" targeted for the system. The mass loop closure, also referred to as the "loop closure rate", is defined as the extent of resource reclamation within the system. A higher mass loop closure has traditionally been chosen for longer, more distant missions. This has been based on the notion that the high costs of Earth-to-space transportation impose significant limitations in the mass and volume of resources such as oxygen, potable water, and food that can be carried along with the crew. By including more resource recycling functions such as CO_2 reduction and water recovery, less of

the same resources are required to be initially transported with the crew, which potentially leads to a lower overall system mass.

As will be seen in Sections 2.1.3 and 2.3, this view has been challenged more recently, when issues of system reliability and supportability have been factored into the system analysis. These analyses have revealed that the appropriate level of resource loop closure for long duration missions is influenced by more factors than just the allocated number of person-days for the mission, and still remains an open question. This question will be revisited and explored throughout the case studies performed in this thesis.

Table 2.2 categorizes the US-defined ECLS functions listed in Table 2.1 by their typical inclusion within a mass loop closure approach. Approaches for technology selection in relation to the mission duration and level of loop closure are also listed.

Table 2.2: Levels of Mass Loop Closure and their Corresponding Functions and Typical Technology Selection Approaches (Adapted from [43] and [45])

Level of Closure	**ECLS Functions Addressed**	**Description of Technology Selection Approach**	**Mission Duration (Example Scenarios)**
Completely Open, Using Nonregenerable Techniques	• CO_2 Removal • O_2 Supply • Trace Contaminant Control • Atmosphere Constituents Storage • Pressure Control • Temperature and Humidity Control • Water Storage and Distribution • Metabolic Waste Collection • Other Waste Management • Fire Detection and Suppression	All consumables mass is brought along, or resupplied with no reuse. Waste is either vented or stored. All treatment agents are expendable	Days (Examples: Mercury, Gemini, Apollo, and the Space Shuttle Orbiter)
Completely Open, Using Regenerable Techniques	Same as above	Reduced use of expendables in treatment agents. E.g. using a molecular sieve	Months (Examples: Skylab)

		instead of LiOH for CO_2 removal	
Water Recycling	All of the above plus: • Water Recovery • Water Quality Monitoring and Control • Liquid Waste Management	Water is recovered for reuse. Typical sources for recovery are cabin humidity condensate and urine	Years (Examples: Mir, ISS)
O_2 Recycling	All of the above plus: • CO_2 Reduction • O_2 Generation • Trace Contaminant Monitoring • Microorganism Control • Major Constituents Monitoring • Atmosphere Composition Control • Gaseous Waste Management	O_2 is recovered for reuse, typically by the electrolysis of recycled water, or by the reduction of collected CO_2	Years (Examples: Mir, ISS)
Food Production	All of the above plus some fresh food grown to supplement stored food	Currently, some fresh vegetables are grown on the Russian Segment of the ISS for both scientific research and food supplementation purposes [10]	Years (Examples: ISS)
Solid Waste Recycling	All of the above plus a solid waste recovery system	One example of solid waste recovery is through the use of a composter to generate fertilizer from organic waste to support plant growth	Decades (Examples: Lunar base, Mars base)
Totally Closed	All of the above	An entirely closed system except for losses due to leaks, etc. Biological life support technologies are a common candidate for such systems	Permanent and Self-Sustainable (Examples: Lunar colony, Mars colony)

As indicated in the last column of Table 2.2, spacecraft life support technologies and systems have evolved since the early days of spaceflight in the 1960s in synchronization with growing mission durations and crew sizes. The general trend has been a gradual increase in loop closure rates, through an evolutionary development path heavily influenced by legacy technologies. Tables 2.3 and 2.4 summarize this evolution for both U.S. and Russian spacecraft ECLS, from the early 1960s to present day. Here, the font color of the listed technology choices represents the program from which the choice was originally chosen, and hence, where it obtained its heritage (as indicated by the font colors of the spacecraft listed in the first row of each table).

Table 2.3: Evolution of ECLS Technologies used in U.S. Spacecraft (compiled from data from [15,44–49])

	Mercury	**Gemini**	**Apollo CM**	**Skylab**	**Orbiter**	**ISS USOS**
Atmosphere	100% O_2 @5psi	100% O_2 @5psi	100% O_2 @5psi (60% O_2 / 40% N_2 at launch)	72%O_2/ 28%N_2 @5psi	21.5%O_2/ 78.5%N_2 @14.7psi	21.5%O_2/ 78.5%N_2 @14.7psi
Gas Storage	High Press. Tanks	Supercritical Storage	Supercritical Storage	High Press. Tanks	High Press. Tanks (N_2) Supercritical Storage (O_2)	High Press. Tanks
O_2 Generation	None	None	None	None	None	Solid Polymer Water Electrolysis
CO_2 Removal	LiOH	LiOH	LiOH	Molecular Sieve (Zeolite5A)	LiOH (EDO:Amine swing bed)	Molecular Sieve (Zeolite5A)
Gas Recovery	None	None	None	None	None	Sabatier Reactor
TCC	Activated Carbon & Filters	Activated Carbon & Filters	Activated Carbon & Filters	Activated Carbon & Filters, Venting Atmosphere	Activated Carbon & Filters & Catalytic Oxidizer	Activated Carbon & Filters & Catalytic Oxidizer
Water Supply	Bladder Tanks	Bladder Tanks	H2-O2 Fuel Cells	Bellows Tanks	H2-O2 Fuel Cells	Bellows Tanks
Water Processing	None	None	None	None	None	Vapor Compression Distillation & Multifiltration
Waste Processing	Stored until end of mission	Stored until end of mission	Feces Stored & Urine Vented	Stored and Returned	Feces Stored & Urine Vented	Water recovered from urine via VCD. Feces and brine disposed in Progress

Table 2.4: Evolution of ECLS Technologies used in Russian Spacecraft (compiled from data from [45,50–52])

	Vostok	**Voskhod**	**Soyuz**	**Salyut**	**Mir**	**ISS Russian Segment**
Atmosphere	21.5%O_2/ 78.5%N_2 @14.7psi	21.5%O_2/ 78.5%N_2 @14.7psi	21.5%O_2/ 78.5%N_2 @14.7psi	21.5%O_2/ 78.5%N_2 @14.7psi	21.5%O_2/ 78.5%N_2 @14.7psi	21.5%O_2/ 78.5%N_2 @14.7psi
Gas Storage	High Press. Tanks (as backup)	High Press. Tanks (as backup)	No additional supply besides KO_2 cartridges	High Press. Tanks (as backup)	High Press. Tanks (as backup)	No onboard storage. High Press. Storage on Progress
O_2 Generation	KO_2 cartridges	KO_2 cartridges	KO_2 cartridges	KO_2 cartridges	Water electrolysis, Lithium Perchlorate cartridges (backup)	Water electrolysis, Lithium Perchlorate cartridges (backup)
CO_2 Removal	KO_2 cartridges	KO_2 cartridges	KO_2 cartridges & LiOH	KO_2 cartridges & LiOH	Molecular Sieve (Amines), LiOH (backup)	Molecular Sieve (Amines), LiOH (backup)
Gas Recovery	KO_2 cartridges	KO_2 cartridges	KO_2 cartridges	KO_2 cartridges	None	None
TCC	Activated Carbon	Activated Carbon	Activated Carbon	Activated Carbon & Filters	Activated Carbon, Filters & Catalytic Oxidizer	Activated Carbon, Filters & Catalytic Oxidizer
Water Supply	Polyethylene container	Polyethylene container	Polyethylene container	Bladder Tanks	Bladder Tanks	Bladder Tanks
Water Processing	None	None	None	Ion Exchange Resins & Multifiltration for humidity condensate recovery	Ion Exchange Resins & Multifiltration for humidity condensate recovery, Vapor Diffusion Distillation to recover water from urine, which was then used for electrolysis	Ion Exchange Resins & Multifiltration for humidity condensate recovery, Urine processed by VCD on USOS
Waste Processing	Stored until end of mission	Stored until end of mission	Stored until end of mission	Stored and ejected into space, Disposed of in Progress	Disposed of in Progress	Disposed of in Progress

Comparing Tables 2.3 and 2.4, it can be observed that the current Russian ECLS architecture has evolved from the extensive experience gathered through its early space station programs. Starting with the long duration Salyut missions, new technologies for water and waste processing were introduced. As space station Mir was brought online, it added new oxygen generation and regenerable CO_2 techniques to the baseline Salyut architecture. The Russian segment of the International Space Station has further built upon this, taking advantage of the Progress logistics spacecraft for gas storage and the United States Orbital Segment (USOS) Vapor Compression Distillation (VCD) unit for urine processing.

Contrastingly, U.S. ECLS architectures have gone through a combination of evolutionary and clean-sheet development. During the Space Race, new ECLS technologies were successively phased into the Mercury, Gemini, and Apollo spacecraft in an evolutionary manner. The longer duration flights planned for Skylab drove the decision to move to a different atmospheric composition, due to concerns related to the effects of oxygen toxicity over long exposure periods, and science requirements for the mission [53]. Skylab also introduced the molecular sieve for CO_2 removal, a technology which would ultimately be deployed on the U.S. segment of the ISS. Other than these changes, most of the Skylab ECLS architecture mirrored that of its predecessor spacecraft, due to its origins with the Apollo Applications Program, and the heavy-lift availability of the Saturn V launch vehicle, which made an open loop air and water architecture feasible [54].

The development of the Space Shuttle Orbiter further introduced new ECLS architecture decisions due to spacecraft reusability and science requirements [55]. These came primarily in the form of the selection of an Earth-like operating atmosphere (that lowered to 70.3kPa prior to EVA to reduce pre-breathe requirements) and the introduction of a catalytic oxidizer, to reduce organic trace contaminants into CO_2 and water, where it could be further processed [45,56]. The subsequent ECLS development would occur for the International Space Station, where lessons learned from the Shuttle-Mir program were employed, especially in designing systems for maintainability [44] and providing adequate volume for the stowage of equipment [57]. As can be seen in Table 2.3, several new ECLS technologies were developed for the ISS USOS [55], including the Solid Polymer Water Electrolysis (SPWE) unit, the Sabatier reactor, and the Urine Processor Assembly (UPA), which is based on the Vapor Compression Distillation (VCD) process. Moreover, the two bed molecular sieve used during Skylab was upgraded to a four-bed variant for the ISS, and forms the Carbon Dioxide Removal Assembly (CDRA) located in Node 3.

Since the ISS represents the first phase in NASA's current development path towards the Earth-Independent human exploration of Mars (see Section 1.1), and given that the ISS ECLS architecture has been baselined for the first habitats to be emplaced by NASA on the Martian surface [58], it is instructive to review the numerous lessons that have been learned over the past 15 years of continuous ISS operations as well as the design philosophies and processes that occurred throughout the early-1980s to early-1990s that led to the current ISS architecture.

2.1.2 Selection of the ISS ECLS Architecture

The original selection of the ISS life support technologies can be traced back to Phase B of development for the Space Station Freedom program that occurred throughout the 1980s [59,60]. At the time, the general consensus within the spaceflight community was that life support systems for long duration space habitats should be designed with the maximum level of resource recycling and the minimum level of required expendables as possible [43]. This philosophy was based on the high cost of transporting consumables and equipment to low-Earth orbit. Figure 2-1 presents a sample of some of the results of the trade studies conducted at the time that led to this conclusion.

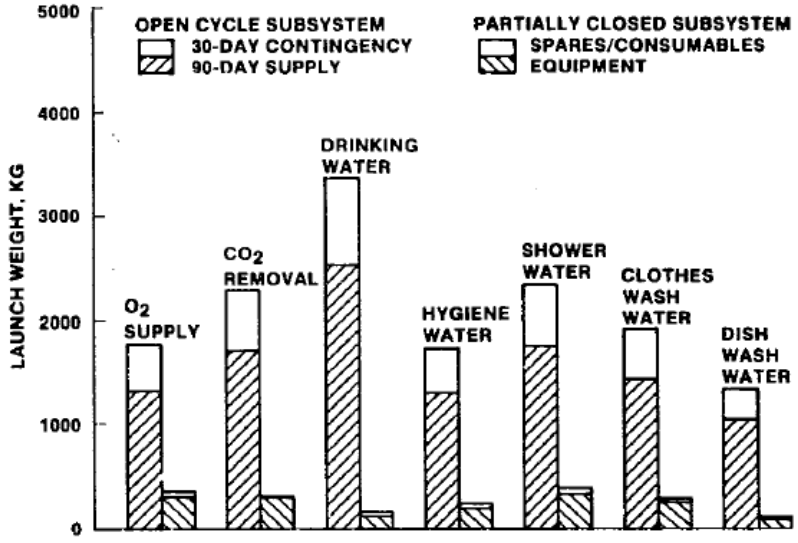

Figure 2-1: Results of a Trade Study Comparing the Launch Requirements for Open-Cycle and Partially Closed ECLS systems for Space Station Freedom published by Lin and Meyer in 1983 [61]. Here, the left bar of each cluster represents an Open-Cycle ECLS subsystem, while the right bar of each cluster represents a Partially Closed ECLS subsystem. The authors conclude that "The study strongly suggests that a partially closed cycle ECLSS using state-of-the-art regenerative life support technology is the optimal option for cycle closure"

As a result, the baseline architecture was defined such that water would be recycled as much as possible, carbon dioxide expended by the crew was removed primarily with regenerable technologies, and oxygen was partially recovered through the reduction of extracted carbon dioxide and the electrolysis of the resulting product water [43]. In fact, by 1982, this architectural definition had become codified within the set of requirements for the Space Station Freedom ECLS System. Figure 2-2 summarizes a subset of these requirements while Figure 2-3 presents a high-level overview of the resource flows that characterized the baseline Space Station Freedom architecture.

Space Station Program Regenerative ECLS Functional Requirements (Nov. 1982)

1. The cabin oxygen shall be supplied by electrolysis of water.
2. A regenerative CO_2 removal subsystem, which concentrates the CO_2 for further processing, shall be provided to maintain the habitat module CO_2 partial pressure under 400 N/m^2(3.0 mmHg) in nominal operation.
3. The humidity condensate collected in the CO_2 reduction and other air-revitalization processes shall be used first to produce potable quality water with chemical and physical treatments to satisfy potability requirements.
4. Urine and expended hygiene water shall be processed by a concept incorporating a phase change and posttreatment & to produce potable quality water that is acceptable for water electrolysis and other ECLSS uses.

Figure 2-2: Subset of Space Station Freedom ECLS Requirements published by in the Space Station Program Description Document (Book 3, First Edition) by NASA Johnson Space Center in November 1982 [61,62]

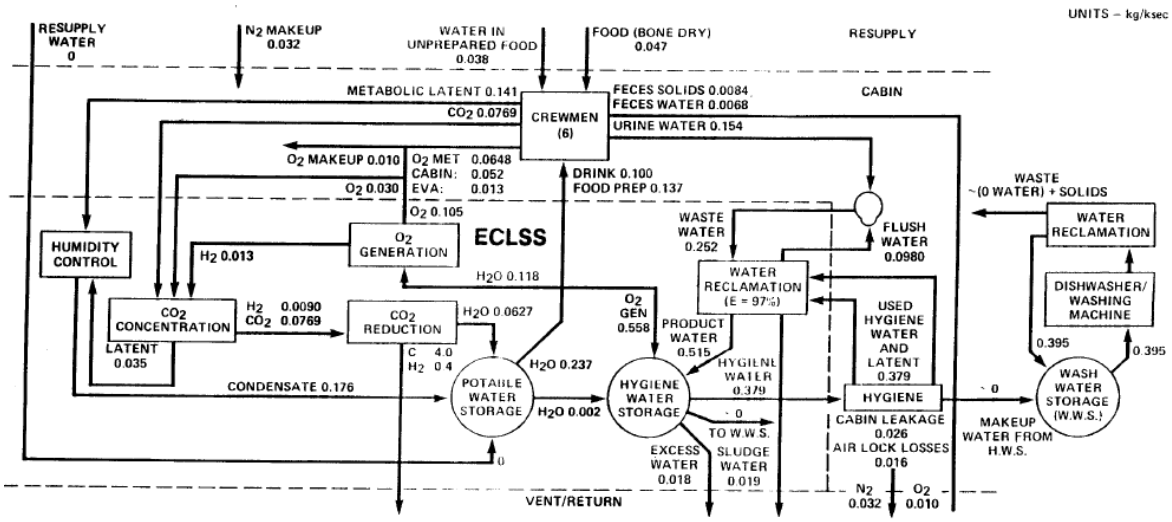

Figure 2-3: Overview of the Space Station Freedom ECLS Architecture [63]

In addition, schedule and budgetary constraints imposed on the Space Station Freedom program led to a strong preference for technologies with a high level of technological maturity. At the time, NASA had developed a number of experimental water processing, oxygen generation, and carbon reduction technologies, but had not yet gained experience in operating these technologies in space (see Table 2.3). As a result of these two facts, the ECLS technology selection process involved firstly narrowing the pool of candidate technologies to only those that were sufficiently mature to meet the schedule of the Space Station Freedom program [59,60]. Following this initial downselection, quantitative trade studies were performed on the remaining set of technologies to assess their launch and resupply mass and volume requirements, as well as their on-orbit power and thermal requirements. Furthermore, qualitative assessments were performed to assess a number of lifecycle and performance properties, including system safety, maintainability, reliability, complexity, technical maturity, and microgravity sensitivity [59]. The result of this process was a set of baseline and alternative candidate technologies for Space Station Freedom, which were ultimately prototyped and comparatively tested at NASA Marshall Space Flight Center between 1990 and 1992 [59] (see Figure 2-4). Table 2.5 summarizes the original set of candidate technologies along with the final technology selected after the Comparative Test Program. We note here that Molecular Sieve technology was selected as the baseline carbon dioxide removal technology without an alternative option based on its previous operational experience onboard Skylab [59,62].

Table 2.5: Summary of the original set of candidate ECLS technologies evaluated during the Comparative Test Program [59]. Further details on each of these technologies are discussed in Appendix D.

ECLS Function	**Candidate Technologies Prior to Comparative Testing**		**SSF Selected Technology**	**Rationale for Selected Technology**
	Original Baseline	**Original Alternative**		
CO_2 Reduction	Bosch Reactor $CO_2 + 2H_2 \xrightarrow{\text{Catalyst}} C + 2H_2O + \text{Heat}$	Sabatier Reactor $CO_2 + 4H_2 \xrightarrow{\text{Catalyst}} CH_4 + 2H_2O + \text{Heat}$	Sabatier Reactor $CO_2 + 4H_2 \xrightarrow{\text{Catalyst}} CH_4 + 2H_2O + \text{Heat}$	The Sabatier reactor was found to have a substantially lower on-orbit mass, volume, and power requirement, while having a higher technological maturity. Challenges were also observed in packaging the Bosch subsystem into the volume of the Air Revitalization rack allocated for the space station
O_2 Generation	Static Feed Water Electrolysis (SFWE) $2H_2O + \text{Energy} \longrightarrow 2H_2 + O_2 + \text{Heat}$	Solid Polymer Water Electrolysis (SPWE) $2H_2O + \text{Energy} \longrightarrow 2H_2 + O_2 + \text{Heat}$	Static Feed Water Electrolysis (SFWE) $2H_2O + \text{Energy} \longrightarrow 2H_2 + O_2 + \text{Heat}$	Multiple failures experienced during subsystem startup for the SPWE during checkout testing meant that comparative testing could not take place and no useful data was recorded. Conversely, the SFWE system was successfully operated for 667 hours with input water at two different test compositions.
Potable Water Processing	Multifiltration Greywater $\longrightarrow$ Potable Water + Contaminants	Reverse Osmosis Greywater $\longrightarrow$ Potable Water + Contaminants	Multifiltration Greywater $\longrightarrow$ Potable Water + Contaminants	Multifiltration was found to be significantly less complex than reverse osmosis (a single-pass design as compared to a recycle loop), and hence more reliable and easier to integrate into the larger ECLS system
Hygiene Water Processing	Reverse Osmosis Urine condensate + Wash Water $\longrightarrow$ Hygiene water + Contaminants	Multifiltration Urine condensate + Wash Water $\longrightarrow$ Hygiene water + Contaminants	Multifiltration Urine condensate + Wash Water $\longrightarrow$ Hygiene water + Contaminants	Testing found the multifiltration system to be significantly more reliable than the reverse osmosis system. In addition, multifiltration was found to be more capable of handling a wider range of input water quality than reverse osmosis
Urine Processing	Thermoelectric Integrated Membrane Evaporation System (TIMES) Urine $\longrightarrow$ Urine Condensate + Brine	Vapor Compression Distillation (VCD) Urine $\longrightarrow$ Urine Condensate + Brine	Vapor Compression Distillation (VCD) Urine $\longrightarrow$ Urine Condensate + Brine	During testing, it was found that VCD was able to meet the urine processing rate requirement of 3.5lb/hr while TIMES had difficulty meeting this requirement. In addition VCD was found to have lower power requirements and a higher level of technology maturity compared to TIMES

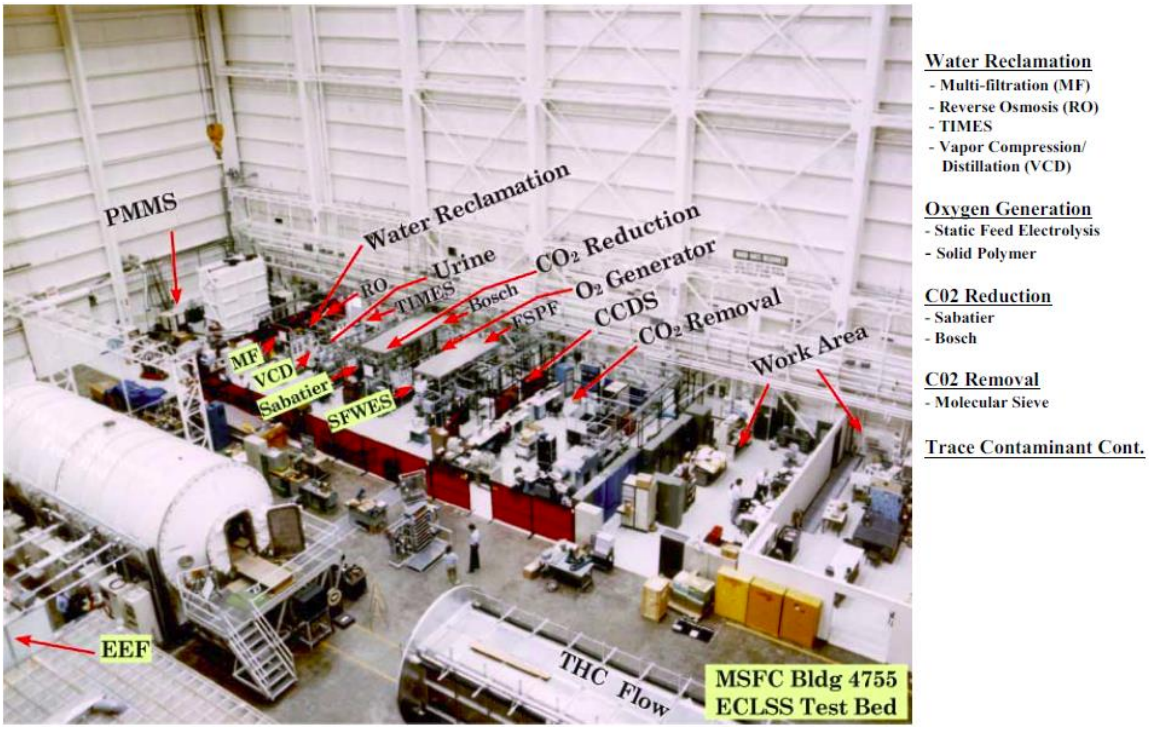

Figure 2-4: Photo of the ECLS Test Facility in the North Bay of Building 4755 at NASA Marshall Space Flight Center taken during the Comparative Testing of ECLS Technologies for Space Station Freedom (circa 1990-1992) [64]

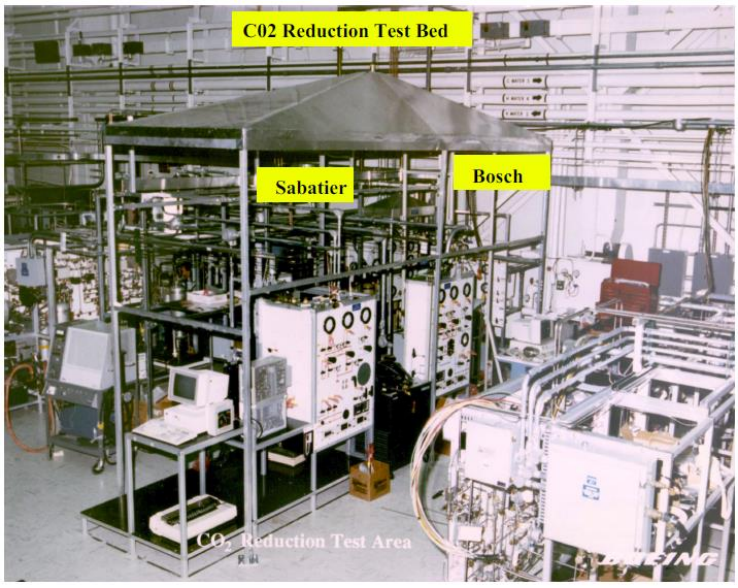

Figure 2-5: Setup for the Comparative Testing of Carbon Dioxide Reduction Technologies [64]

Approximately one year after the completion of the ECLS Comparative Test Project, President Clinton directed NASA to begin incorporating Russia's Mir-2 project into the space

station program in an attempt to enhance the capabilities of the station, reduce its programmatic cost, increase research opportunities, and provide additional means for accessing the station [65]. This coincided with a series of high level negotiations that led to a formal cooperative agreement between the United States and Russia in human spaceflight. By November 1993, these two efforts led to the restructuring of the Space Station Freedom program to form the current International Space Station (ISS) Program.

One of the outcomes of this restructuring was the redesign of the SSF ECLS system to meet the updated requirements of the ISS. In order to accomplish this goal while remaining within cost and schedule constraints, the program issued the following guidelines for the ISS ECLS architecture [66]:

- Utilize the U.S. Space Station Freedom hardware to the maximum extent possible
- Combine U.S. and Russian Segment (RS) functionalities for shared failure tolerance to reduce costs
- Utilize Russian experience and hardware to achieve early permanent human presence (achieved on the third assembly flight for a three person crew), while building the U.S. and RS capabilities during assembly to support a six person crew at Assembly Complete (AC)
- Maintain a U.S. ECLS "fallback" capability to support the Space Station assembly and operation in case of loss of the RS at any point in the program

As a result of these guidelines, almost all of the technologies selected from the SSF Comparative Test Program were baselined and further developed for the ISS. The only exception to this trend was the decision to adopt Solid Polymer Water Electrolysis (SPWE) for oxygen generation rather than the originally selected Static Feed Water Electrolysis (SFWE) concept. This decision was based on a redesigned SPWE concept that overcame the startup issues observed during comparative testing for SSF (see Table 2.5) and was found to perform more reliably than the SFWE concept [67].

In addition, the ECLS redesign process led to the simplification of the water processing architecture through the combination of the originally separated potable and hygiene water loops into a single combined loop for water reclamation. This modification is depicted in Figure 2-6.

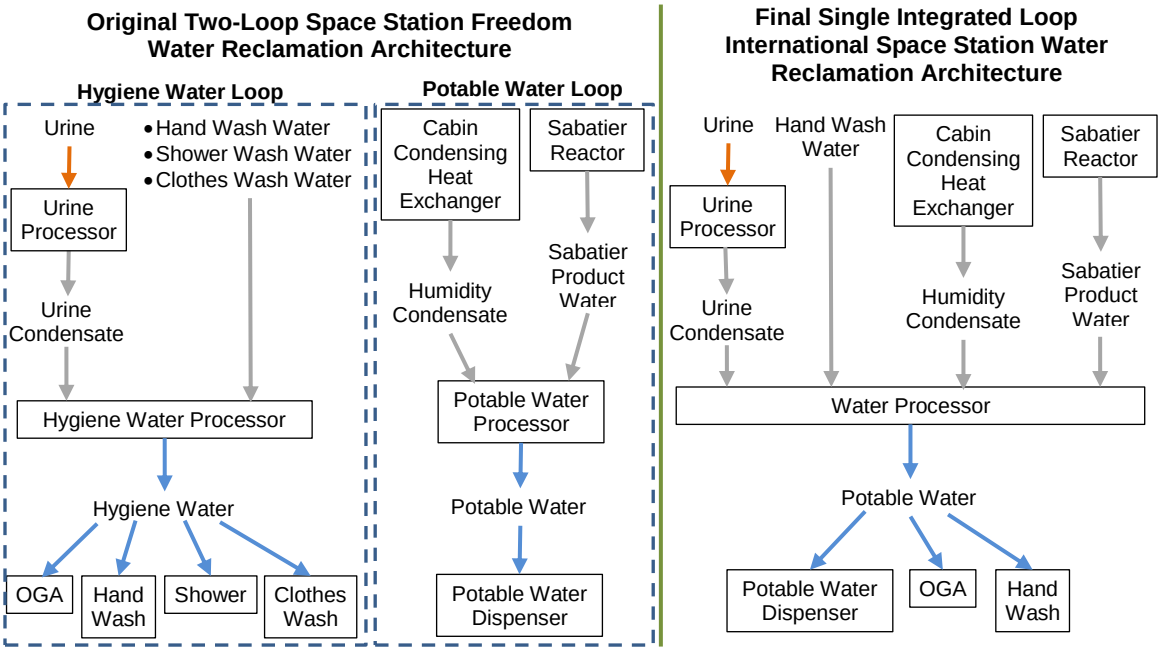

Figure 2-6: Comparison between Original Space Station Freedom and Final International Space Station Water Reclamation Architectures (OGA: Oxygen Generation Assembly that generates oxygen through the electrolysis of water)

Following this restructuring, several more ground-based test campaigns were performed to better characterize and mature the ECLS system at increasingly higher levels of flight fidelity and system integrality. In parallel, a number of flight tests were performed on various subsystems including a full-size demonstration of the ISS Urine Processor Assembly (UPA) on STS-107, and experiments with the Volatile Removal Assembly used in the ISS Water Processor Assembly on missions STS-89 [68] and STS-96 [64]. Figure 2-7 summarizes the SSF and ISS ECLS development and test program while Table 2.3 compares the final set of technologies that were developed for the ISS in context to earlier ECLS development programs.

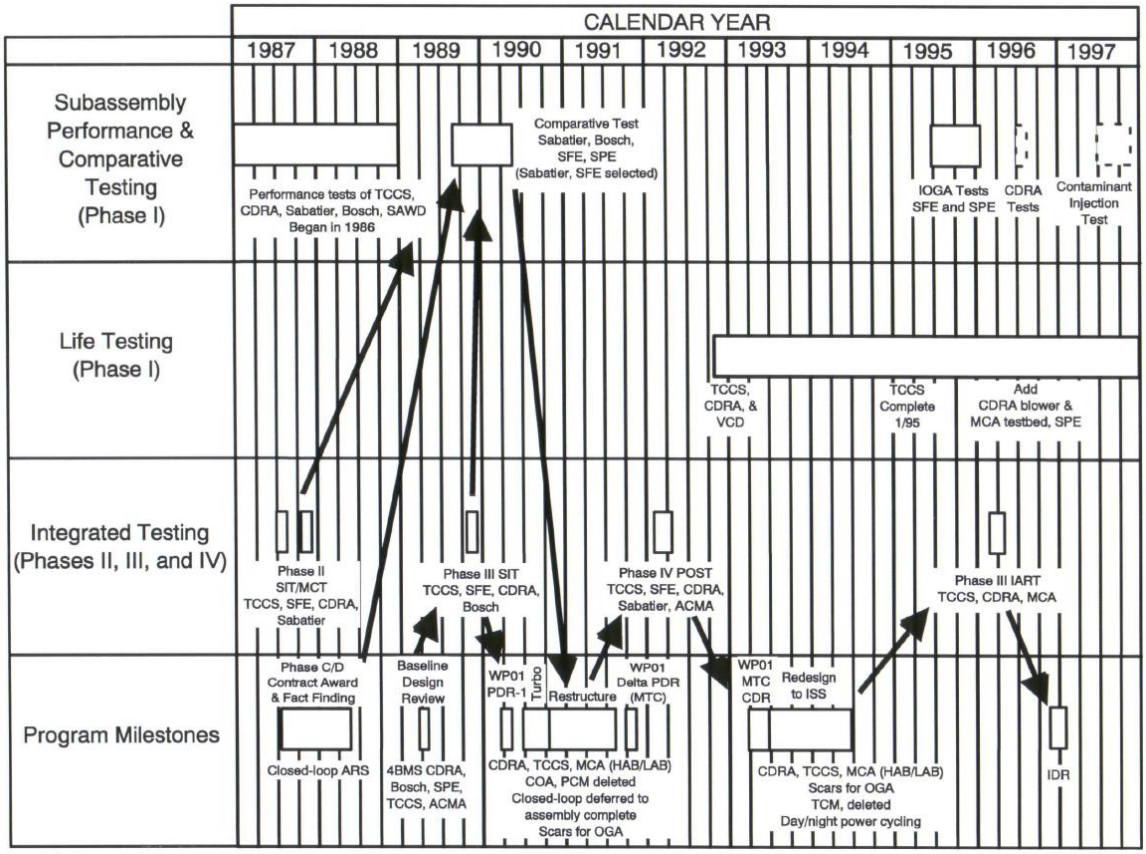

Figure 2-7: Summary of the SSF and ISS ECLS development and test program [64]

2.1.3 Operational Experience with the ISS ECLS System

Construction of the International Space Station commenced in November 1998 with the launch of the Russian-built Functional Cargo Block (Zarya) and concluded in March 2011 with the installation of the Permanent Multipurpose Module (PMM). Over this 12.25 year period, a permanent human presence was established initially for three people, and eventually expanded to the current population of six people. This was accomplished through the gradual deployment and installation of addition modules and supporting systems, and the periodic resupply of consumables and spare parts.

Throughout this assembly period and through to the current utilization period, many challenges have been experienced in the deployment, operations, and sustainment of the life support systems onboard the station. These challenges have been experienced with almost all of the regenerative life support systems flown, and have required some combination of the development of on-orbit procedures to bypass the problems experienced at the cost of degraded

performance, a redesign of some component of the system in question, or the reliance on redundant Russian systems or contingency resources. Figure 2-8 shows the final distribution of ECLS technologies across the ISS while Table 2.6 summarizes the major life support systems challenges experienced and life support lessons learned on ISS since permanent human presence was established in November 2000. Note that this table focuses exclusively on life support technologies on the United States Orbital Segment (USOS) of the ISS. While challenges experienced with some Russian ECLS technologies have been described at a high level in the literature [69], little detail has been published on the root causes of these challenges.

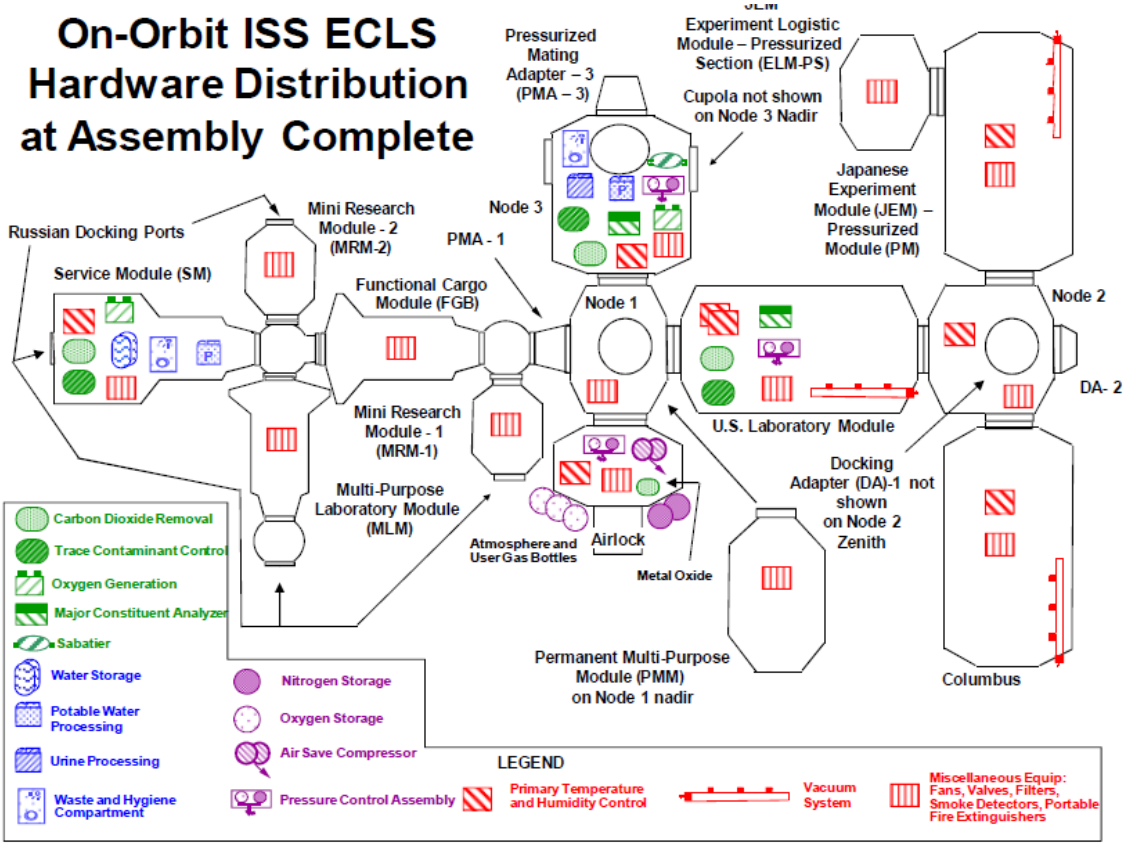

Figure 2-8: Distribution of ECLS Hardware on the ISS at Assembly Complete [49]

Table 2.6: Summary of the Major Operational Challenges Experienced with the ISS ECLS System (see Appendix D for further details on each of the ISS ECLS technologies described)

ISS ECLS Technology	Major Challenge(s) Experienced and Lessons Learned
Carbon Dioxide Removal Assembly (CDRA) **Baseline Technology:** Four Bed Molecular Sieve **Launched:** February 2001 (STS-98)	• During initial installation and checkout on STS-98, the air-save pump within CDRA failed to activate, preventing the CDRA from starting up. A replacement pump, motor controller and interface cable were delivered and installed on the next shuttle mission (STS-102) [70] • After the air-save pump was replaced and successful system startup was achieved, problems were observed in the first CO_2 bed in pumping down to vacuum during its desorption cycle. This was attributed to a check valve within one of the Desiccant/ Adsorbent Beds (DABs) being stuck open. A software procedure was implemented to route airflow around this failed DAB during its desorption half-cycle. This allowed the CDRA to operate at a half its design capacity [70,71] • Further analysis since the problems experienced on STS-102 revealed that loose sorbent pellets tended to escape from their sorbent beds, obstructing and damaging the check valves within the DABs. This led to the redesign of the DAB to include sorbent and desiccant material containment systems [71] • The redesigned DAB (referred to as the "-2" configuration) addressed the pellet containment problems but resulted in the unintended consequence of trapping sorbent dust in the containment screens, eventually obstructing flow through the system to a level that prevented proper system function. As a result, another redesign effort was undertaken to allow the crew to remove the adsorbent containment screen on-orbit and clean it of accumulated sorbent dust [69,72]. This resulted in a "-4" DAB configuration, which also included a different sorbent material (zeolite RK-38) that was observed to be more resilient to dusting than the original material. (Note that the "-3" DAB was an interim system implemented before the -4 DAB design update was complete [72]) • After a year of on-orbit operations, it was found that the -4 DAB required significantly more frequent maintenance than originally expected due to higher than anticipated dusting of the newly installed RK-38 zeolite sorbent. This was attributed to possible water carrying over from the desiccant bed and adversely reacting with the RK-38. This resulted in the development of a "-5" version of the DAB where the RK-38 sorbent was replaced with the original ASRT zeolite sorbent after testing revealed that ASRT performed better under wetter conditions. The -5 DAB has been operating on-orbit as of May 2015 [72]
Oxygen Generation Assembly (OGA) **Baseline Technology:** Solid Polymer Water Electrolysis (SPWE) **Launched:** July 2006 (STS-121)	• On July 5th 2010, after 231 days of operation onboard the ISS, the Hydrogen Orbital Replacement Unit (ORU) within the OGA experienced a sudden high-voltage shutdown. At the time, the rated life of this ORU was five years [73]. The failed unit was replaced with an on-orbit spare and was returned to the ground in March 2011 for further inspection and analysis. After six months of detailed investigations, it was found that under nominal operating conditions, chemical degradation of the cell membranes occurred, forming hydrofluoric and sulfuric acid as degradation byproducts. These byproducts lowered the pH of the water loop to a level where metallic hardware within the loop began to corrode, producing a source of cations that contaminated the cell membranes, which in turn reduced water transport and proton conductivity of the membranes, and catalyzed further reactions that accelerated the rate of membrane degradation. This combination of events led to a rapid increase of cell resistance, resulting in a rise in voltage above the shutdown limit [73,74]. To mitigate these phenomena, a mixed resin deionization bed was installed within the recirculation loop in May 2011 to remove hydrofluoric and sulfuric acid degradation products from the water loop, thereby preventing the follow-on degradation events previously observed [73]

	• The hydrogen sensors used in the OGA to detect potential hydrogen leaks have been found to experience significant drift in signal output, so much so, that on a number of occasions, an inhibit command has had to be sent from the ground to prevent system shutdown. This drift results in each sensor having a relatively short calibration life of 150 days. After this period, the sensor is removed and returned to the ground for recalibration [73]. Since the activation of the OGA, the periodic replacement of hydrogen sensors has consumed the largest proportion of total crew time spent on maintaining the OGA [75]
Water Processor Assembly (WPA) **Baseline Technology:** Multifiltration **Launched:** November 2008 (STS-126)	• A process pump within the WPA failed in October 2012 after 970 days of operation, preventing the WPA from beginning its process cycle. This failure was attributed to be the wear of a key that maintains gear position on the pump shaft. The material of this key has since been changed to a harder material to prevent future failures of this nature [76] • In May 2010, the Total Organic Carbon (TOC) content within the WPA product water began to increase continuously until October 2010, when it abruptly dropped back down to a nominal level [77]. This trend was observed again in 2012, 2013, and 2014, within one to two months after the periodic replacement of the WPA multifiltration beds (MFBs) [76]. Ground testing of water samples indicated that the source of this TOC increase was dimethylsilanediol (DMSD), a degradation byproduct of polydimethylsiloxane (PDMS) compounds that are known to off-gas from various products used on the ISS, including lubricants, caulks, adhesives, and hygiene products. Further ground analysis revealed that DMSD had been present in water collected by the condensing heat exchangers since WPA operations began, and that DMSD is likely formed from the reaction of PDMS and the hydrophilic coating used on the condensing heat exchanger used to collect cabin humidity condensate. Because DMSD is small in size, highly soluble in water, and primarily neutral in charge, the multifiltration, catalytic oxidizer and ion exchange beds within the WPA have been found to be limited in their capability in removing it from the process water stream [77]. It was found that while new MFBs are initially capable of removing some DMSD, their adsorbent and ion exchange resins eventually become saturated, rendering the beds prematurely ineffective at their intended function of removing ionic constituents. Analyses of MFBs returned to the ground found that up to 40% of unused resin capacity remained in the beds due to DMSD saturation [75]. Following DMSD breakthrough of the MFBs, the process water stream passes through a catalytic reactor, which was found to oxidize approximately 78% of the DMSD [77]. The reactor effluent is then flowed to an ion exchange bed, which like the MFBs, is initially capable of removing DMSD but after some time, becomes saturated, resulting in a breakthrough that leads to the TOC trends observed [76] (see Figure 2-9). As of July 2015, research into methods for removing DMSD from the WPA process stream is ongoing [76,78] • In June 2009, a higher than expected pressure drop was observed between the WPA wastewater (input) tank and the Mostly Liquid Separator (MLS) system used to separate gas from the incoming water stream. By September 2009, this pressure drop had increased to a point where it prohibited the incoming water stream from reaching the WPA system pump. To maintain continued operations, the WPA was programmed to operate in a degraded mode, where the incoming flow rate was reduced to allow for more time for the MLS to fill prior to the system continuing to process incoming wastewater. This allowed the WPA to continue operating until January 2010, when the entire system shutdown due to near zero flow between the MLS and the WPA pump. In response to this failure, these two systems were removed, replaced, and returned to the ground for further inspection. This inspection found that the cause of the observed pressure drop was significant blockage of the MLS inlet solenoid valve with accumulated biomass growth [79]. To mitigate this problem, additional filters were installed within the system and a new operational concept was implemented, whereby the WPA wastewater tank bellows are cycled every month to prevent

	biomass growth, and the wastewater filter and MLS inlet are flushed with iodinated water at the end of each process cycle [76]. These modifications appear to have resolved this problem. • Leakage in the WPA catalytic reactor due to degradation of o-rings has been a recurring problem since March 2010. The first instance of leakage was found to be a combination of o-ring degradation resulting from prolonged exposure to the operating temperature of the reactor and o-ring compression set that allowed leakage to occur. To mitigate this problem, the catalytic reactor was redesigned with different o-ring materials that were more tolerant to compression set. On March 2014, less than two years after this updated reactor was implemented, another leak was found in the reactor (note that the intended operating life for the reactor is five years). Upon further inspection and analysis, it was found that all seals within the system had significant leaks and that the seal material chosen is incompatible with the high process temperatures of the reactor. In response to this finding, the standby temperature of the reactor has been lowered from 131°C to 93°C in an attempt to improve seal life. As of May 2015, the effectiveness of this operational change was still being evaluated.
Urine Processor Assembly (UPA) **Baseline Technology:** Vapor Compression Distillation **Launched:** November 2008 (STS-126)	• Since it was first operated on the ISS, the UPA has experienced a number of challenges with its Distillation Assembly (DA) – a rotating centrifuge that performs the core function of evaporating the incoming waste urine stream to recover condensate for further processing by the WPA into water. In December 2008, shortly after initial activation of the UPA, the DA failed due to a high current fault within the DA motor. Upon subsequent investigation, it was found that this fault was the result of mechanical interference between a speed sensor and the centrifuge body caused by a structural failure in the bearings of the pinion driving the main shaft of the centrifuge. To prevent future occurrences of this structural failure, these bearings were replaced with bearings made of a harder material [79]. • In October 2010, another high current fault was experienced with the updated DA. On this occasion, it was observed that the UPA was delivering significantly less condensate to the WPA wastewater tank than was expected. After several unsuccessful troubleshooting efforts on-orbit, the DA was removed and returned to the ground for further investigation. This investigation found that calcium sulfate had accumulated on the wall of the DA, blocking the flow of brine out of the system and causing the DA to flood. Further analysis concluded that this calcium sulfate was formed from a reaction between higher than anticipated calcium levels within the crew's urine caused by bone demineralization in microgravity, and the sulfuric acid used to pretreat urine before distillation. During its development, testing of the UPA with ground-based urine proved that the system could easily recover 85% of water from pretreated urine. However, the high concentration of calcium present in on-orbit urine meant that operating the UPA at an 85% recovery level would result in calcium sulfate exceeding its solubility limit and therefore precipitating within the DA. In response to this, the UPA has been operated at a degraded recovery level of 70% to 75% since early 2010 [76,79]. In addition, the crew has been instructed to increase their water intake to both improve general health, as well as to reduce the calcium concentration within their urine. Efforts to recover the UPA to its nominal 85% recovery level are ongoing [76]. • Similar to the DA, the UPA Fluids Control and Pump Assembly (FCPA) has also experienced recurring failures throughout its operational life. The FCPA is a four-tube peristaltic pump that transports input wastewater to the DA. In September 2011, an FCPA failed due to insufficient lubrication of the pump motor bearing at the manufacturer. One year later, a refurbished FCPA experienced a failure due to the misalignment of the motor adapter to the motor shaft on the FCPA. This was attributed to improper assembly of the system at the manufacturer. In March 2013, a third FCPA failed due to a misalignment of the harmonic drive and an interfering snap ring groove. This was also attributed to an error at the manufacturer. This same error caused the failure of another two FCPA units before it was identified. Finally, a failure was

	experienced with a seventh FCPA in February 2015 after seven months of operation, resulting in the leakage of pretreated urine. As of July 2015, the investigation of this failure is still underway. The recurrence of these failures has prompted NASA to begin the development of an upgraded and more reliable FCPA design that would be better suited for future exploration missions [76].

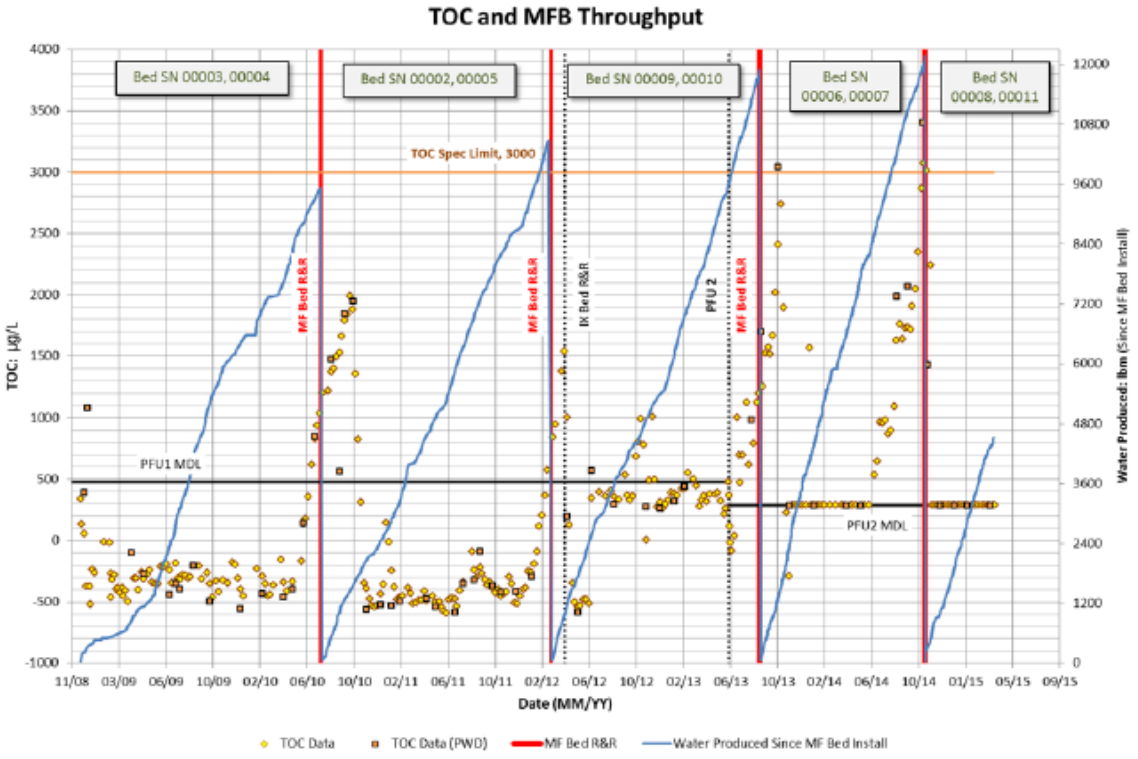

Figure 2-9: Comparison between ISS Product Water Total Organic Carbon (TOC) Level and WPA Multifiltration Bed (MFB) throughput, indicating the breakthrough of DMSD (as indicated by the sharp increase in TOC level) prior to a new MFB installation and a sharp drop in TOC after MFB installation [76]

As can be seen from Table 2.6, the challenges experienced with ECLS technologies have been persistent throughout the ISS program. Even with these challenges, however, the ISS has been able to sustain a continued presence on-orbit for over fifteen years. This has been enabled by the short travel times to the ISS, relatively frequent resupply opportunities, and capability to return hardware to the ground for troubleshooting, inspection, and refurbishment. As the ISS moves into its final decade of operations, this continued transfer of materiel to and from the space station is expected to continue, even as its systems mature and less redesign cycles are needed. Figure 2-10 depicts the predicted annual requirements for up and down mass of equipment and consumables to support preventative and corrective maintenance of the ISS systems from the period spanning 2012 through to 2020.

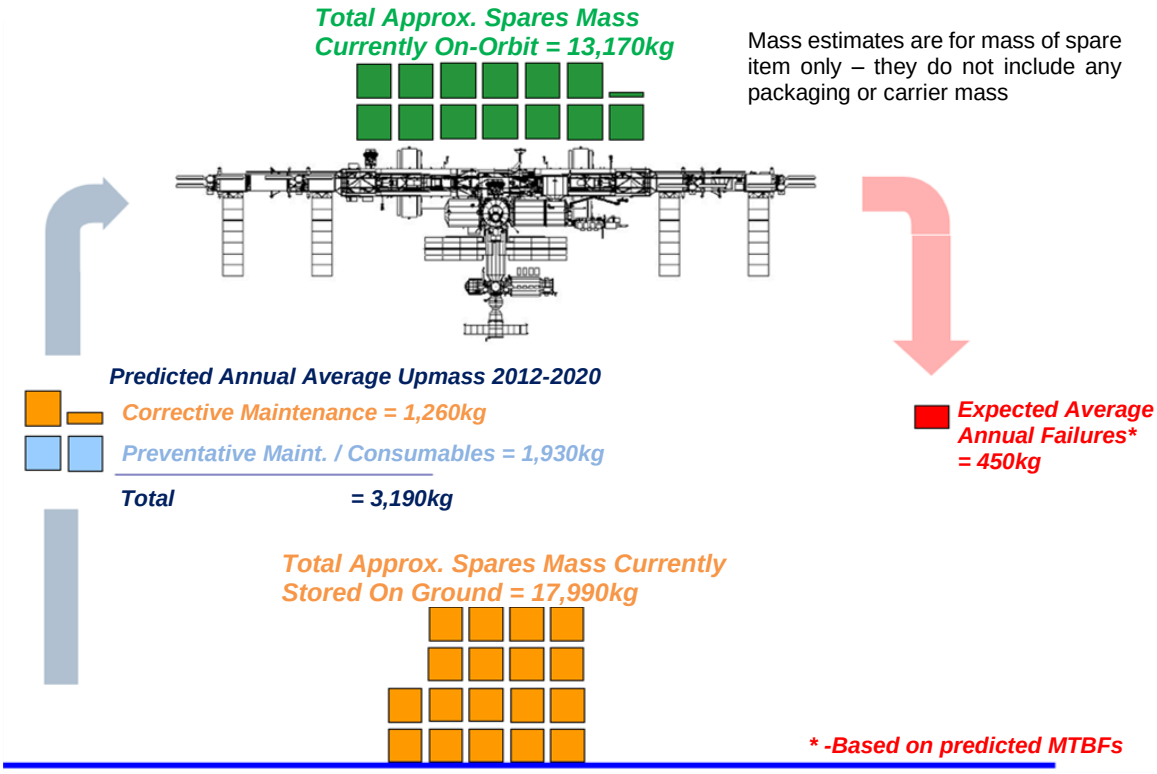

Figure 2-10: Predicted annual ISS logistics requirements from 2012 to 2020 [80]

From Figure 2-10, we observe that annually, 450kg of equipment is expected to experience some form of failure on the ISS. To recover from this failure however, 13,170kg of spare parts have been pre-positioned on-orbit. A large contributor to this spare parts pool was the conscious decision to pre-emplace large components prior to the ending of the Space Shuttle program, after which, the capability to transport large spare parts to orbit would be lost for some unknown period of time [81]. Currently, this pool of spares is supplemented by an annual average upmass of 3,190kg via a fleet of smaller government and commercial cargo transportation spacecraft, and is supported by a ground inventory of 17,990kg of equipment. The large discrepancy between the expected mass of failed hardware and the on-orbit spare parts inventory arises from the fact that critical failure modes are present within the system that require near immediate access to a spare part to manage. In these cases, there is insufficient time to wait for the required spare parts and tooling to be delivered from the ground to the ISS before the appropriate repair actions need to be initiated. Therefore, the equipment required to manage these failure modes is pre-positioned onboard the station. This requirement becomes

even more critical when limits in transportation capacity are imposed, as was the case with the ending of the Space Shuttle program [81]. Moreover, because of the inherent uncertainty associated with knowing a priori what equipment will fail, sparing is based on the number of components that potentially *could* fail, rather than what components *will* fail [80]. This results in a substantially higher mass of pre-positioned spare parts than the mass of equipment that will actually fail.

Thus, we observe from the experiences gained from operating the ISS that the total mass of pre-positioned spare parts required to sustain a habitation system is driven by a combination of factors, including the endurance required by the system (i.e. the time between resupply), the complexity of the system, the system architecture, and the supportability considerations described earlier (see Section 1.2.2).

2.2 Historical Review of In-Situ Resource Utilization (ISRU)

Over the past three decades, interest has been growing in understanding the impacts of In-Situ Resource Utilization (ISRU) technologies on mission architectures, due to its significant potential in reducing the total mass of equipment and consumables needed to be transported from Earth. ISRU refers to the concept of converting locally available materials at the exploration destination into useful resources for use by the crew. In this section, we review the history of mission studies incorporating ISRU, and summarize ongoing technology development efforts in this area.

2.2.1 Early ISRU Studies and their Evolution within NASA's Mars Mission Planning

The concept of adopting ISRU as an approach to reducing the logistics demands of Mars missions can be traced back to the late 1960s [82], where it was first proposed as an option for generating life support consumables to support conjunction-class missions to the Martian surface [17]. Since data on the type and availability of in-situ Mars resources was limited at the time, ISRU was discussed only in broad terms, and was mainly used as a motivator for precursor missions that would characterize the Martian environment [17].

It was not until over a decade later that ISRU concepts were developed in greater detail. This was enabled by the Viking 1 and 2 missions, which began returning their first set of in-situ surface data in mid-1976. Two years later, Ash et al. [16] published the first study to explore the technical feasibility of producing different rocket propellants using Martian in-situ resources. Based on the availability of resources on Mars, the maturity of technology, and preliminary sizing estimates, this study proposed powering a Mars ascent vehicle with liquid methane and oxygen produced from a reaction between atmospheric carbon dioxide (CO_2) and hydrogen obtained from the electrolysis of extracted soil-bound water (see Equations (2.1) and (2.2)). It was found that implementing an in-situ propellant manufacturing system could yield mass savings as much as half of the baseline concept of delivering ascent vehicle fuel to the Martian surface. Figure 2-11 summarizes the ISRU architecture proposed in this study.

$$CO_2 + 4H_2 \xrightarrow{\text{Catalyst}} CH_4 + 2H_2O \tag{2.1}$$

and

$$2H_2O + 2H_2O \xrightarrow{\text{Electrolysis}} 4H_2 + 2O_2 \tag{2.2}$$

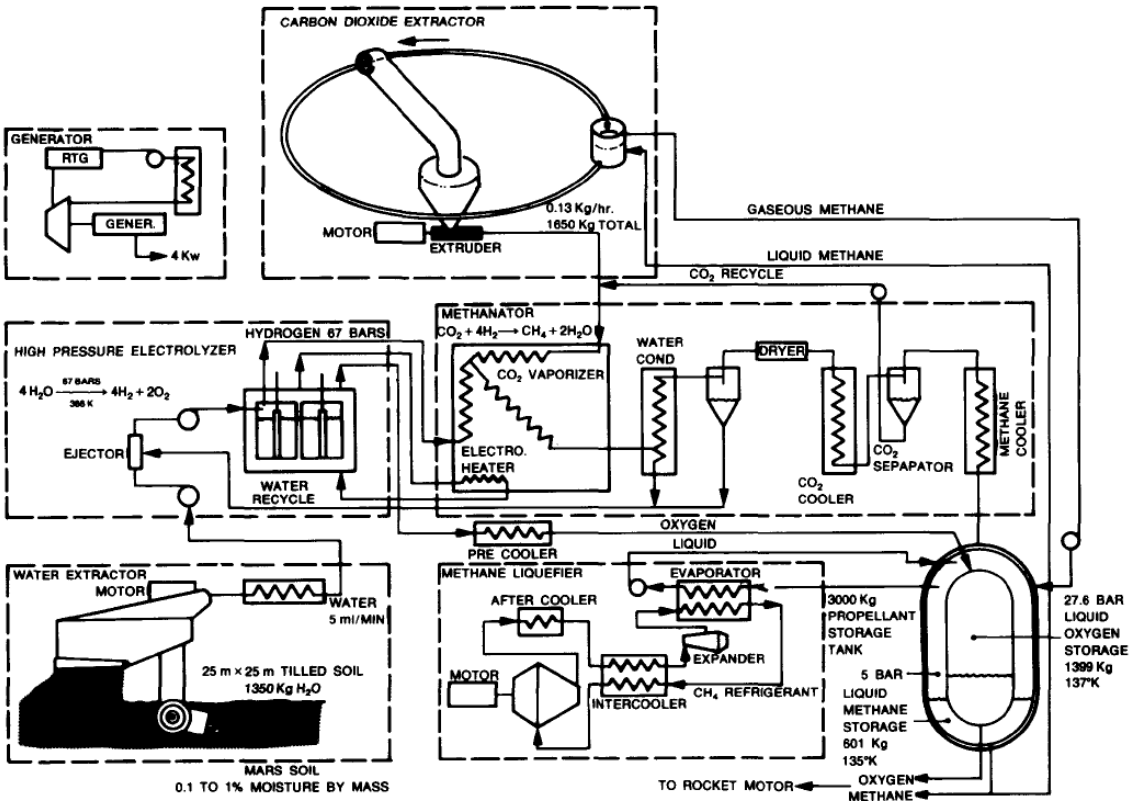

Figure 2-11: Mars In-Situ Propellant Production (ISPP) Architecture proposed by Ash et al. [16]

The concept of using ISRU-derived propellants to reduce mission mass gained further recognition in 1990, when Baker and Zubrin published their "Mars Direct" mission concept. This plan exploited the same Sabatier process proposed by Ash et al. [16] to produce liquid methane and oxygen, but differed slightly in its approach to initiating the propellant production process. Instead of processing Martian soil to obtain hydrogen, the Mars Direct plan relied on carrying 5.8 tonnes of liquid hydrogen from Earth to initiate the Sabatier reaction. This deviation from the Ash et al. concept was based on the uncertainty in the availability of water on Mars at the time. The resulting product water was then electrolyzed to produce additional hydrogen to maintain the reaction [18]. Through this process, a total of 107 tonnes of methane and oxygen propellant would be produced, 11 of which would be reserved for powering two pressurized surface rovers. In addition, the direct electrolysis of atmospheric CO_2 was included to produce additional oxygen to supplement the oxidizer requirements of the ascent vehicle.

The Mars Direct ISRU concept formed the basis of the first NASA Mars Design Reference Mission (DRM 1.0) published in 1993 [17,19]. In addition to producing only ascent vehicle propellants, DRM 1.0 also proposed using ISRU to generate a reserve supply of life support consumables, including water, breathing oxygen, and nitrogen and argon as atmospheric diluent gases. Water and oxygen would be generated by the same ISRU processes proposed by Baker and Zubrin, and the diluent gases would be obtained from thermal swing adsorption of the Martian atmosphere [19].

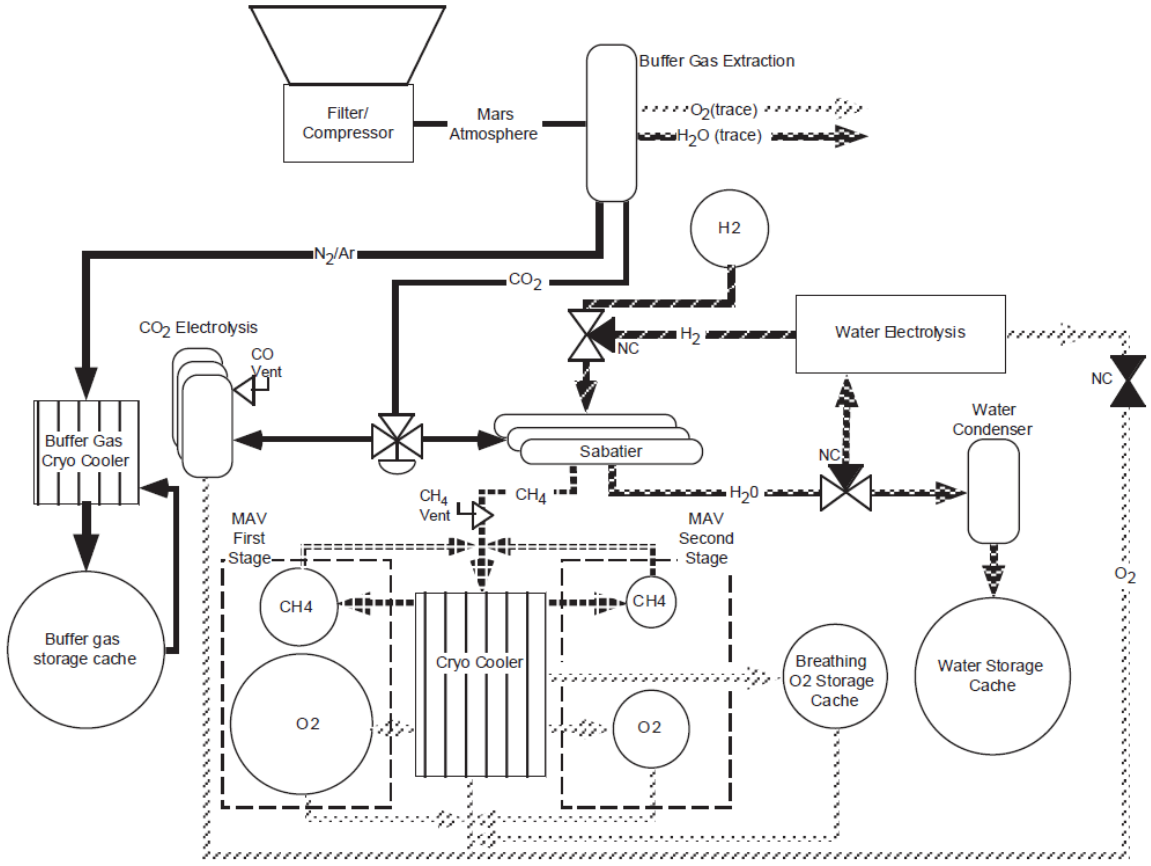

Figure 2-12: NASA Design Reference Mission 1.0 ISRU Concept [19]

The DRM 1.0 ISRU concept was adopted by all subsequent NASA mission plans until Design Reference Architecture 5.0 (DRA 5.0) analyses were performed in 2007 [20]. A few years prior to this period, science data obtained by the Mars Odyssey orbiter and the Mars Exploration Rovers revealed that water is globally available in Martian soil at varying concentrations and depths [20]. As a result, the use of Mars water as an ISRU resource for the production of propellant and life support consumables was revisited and traded against other architecture options including atmospheric-based ISRU. Figure 2-13 summarizes the various ISRU options studied, as well as the final ISRU concept baselined for DRA 5.0. Here, each branch of the "trade tree" corresponds to a particular architecture.

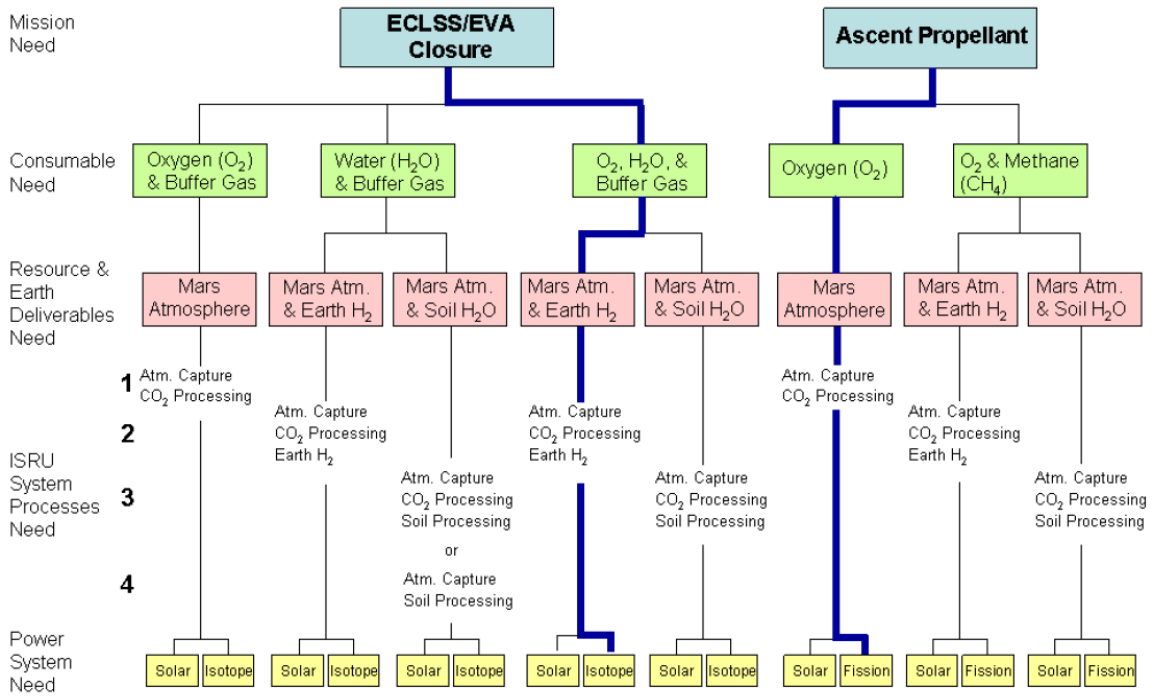

Figure 3-49. Selected branches of the in-situ resource utilization trade tree.

Figure 2-13: ISRU Concepts Evaluated as part of the NASA Design Reference Architecture 5.0 Analysis Activities. The architecture highlighted by the blue line represents the final architecture selected [83]

As can be seen in Figure 2-13, DRA 5.0 baselined an ISRU concept consisting of processing Martian atmosphere to obtain oxygen and atmospheric buffer gases (argon and nitrogen), and delivering hydrogen from Earth to generate water for life support needs. Here, the Solid Oxide CO_2 Electrolysis (SOCE) process was chosen to extract oxygen from Martian atmospheric CO_2 collected by a microchannel adsorption pump. Water for life support and extravehicular activities (EVAs) was to be obtained by reacting SOCE-generated oxygen with hydrogen delivered from Earth [20].

For the Mars ascent vehicle, DRA 5.0 system architects chose to deliver methane from Earth, rather than produce it in-situ. Oxygen required by the ascent vehicle was to be provided by the same SOCE-based atmospheric processor system used to generate breathing oxygen for life support. This decision was based on the finding that using ISRU to produce oxygen alone would still yield mass savings of greater than 25t as compared to mission architectures that relied on delivering ascent vehicle oxidizer directly to the Martian surface [83]. Figure 2-14 depicts a flowsheet of the ISRU architecture chosen for Mars DRA 5.0.

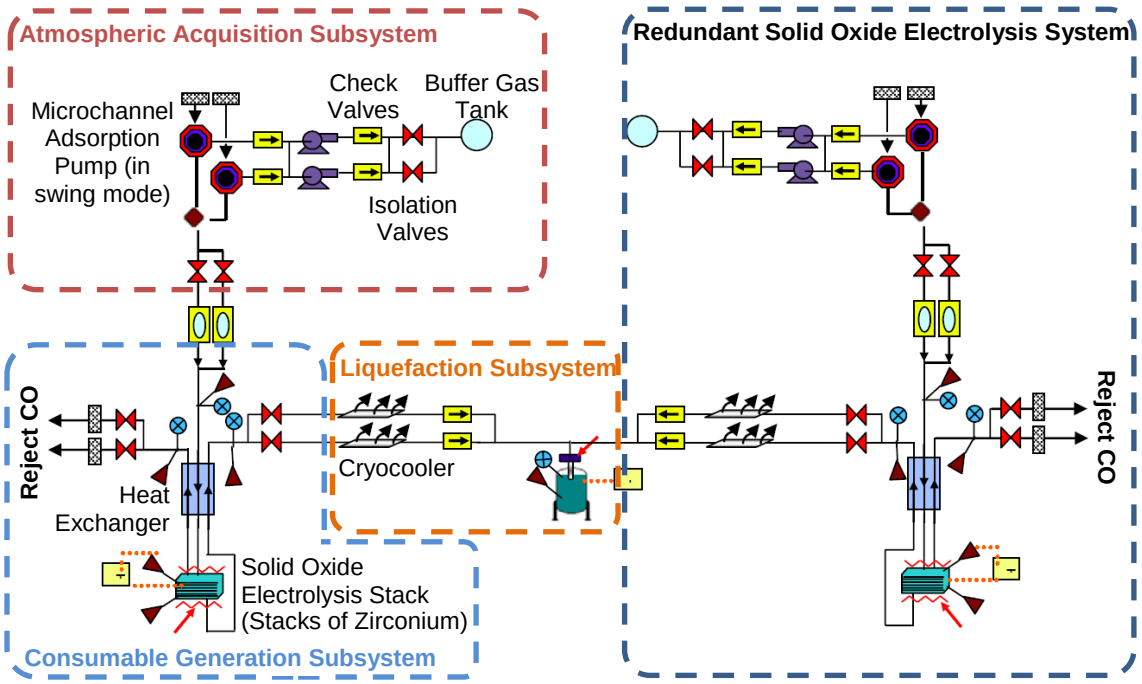

Figure 2-14: The ISRU architecture selected for NASA DRA5.0. Here the ISRU system is divided into an Atmospheric Acquisition Subsystem, a Consumable Generation Subsystem, and a Liquefaction Subsystem, as indicated above. A redundant copy of the system is incorporated to ensure that the system is single-fault tolerant, with each subsystem sized to generate the oxygen needs for the entire mission [83]

This architecture represents a departure from the Sabatier-based concepts proposed in previous studies, and was the result of the finding that delivering sufficient hydrogen from Earth to produce the required amount of ascent vehicle fuel would require over three times the volume of delivering the methane fuel alone. Although delivering hydrogen is more mass efficient than delivering methane, its large storage requirements would require a larger entry, descent and landing (EDL) system, which would result in a larger required Initial Mass to Low Earth Orbit (IMLEO).

In addition, the DRA 5.0 study concluded that the additional complexity of excavating, transporting and processing soil, combined with the uncertainties in Mars surface water properties and distribution, meant that it could not be baselined without further investigation and technology development. As a result, the study recommended that research continue in further characterizing these uncertainties to better understand the infrastructure required to extract and utilize Martian water with an electrolyzer/Sabatier reactor system.

2.2.2 Mars ISRU Technology Development Programs from the 1990s through to the Early 2000s

In parallel to the mission studies discussed in the previous section, several ISRU technology development programs have been undertaken since the early 1990s, with a number of these maturing to subscale prototypes that have been tested in laboratory and analog environments. Originally, these development efforts focused on technologies required for Mars atmospheric resource collection and processing, in support of the development of a Mars Sample Return Mission based on In-Situ Propellant Production (ISPP) [83]. These technologies included:

- Micro-channel adsorption pumps developed by Pacific Northwest National Laboratory (PNNL) to extract and pressurize Mars atmospheric CO_2 in a mass and volume efficient manner (see Figure 2-15(a)). This technology is based on the rapid adsorption and desorption of CO_2 using a series of eight relatively small sorbent beds
- CO_2 solidification pumps developed by Lockheed Martin as an alternative means of separating CO_2 from the Martian atmosphere by using a cryocooler to solidify gaseous CO_2 out of an incoming airstream (see Figure 2-15(b)).
- A Solid Oxide Carbon Dioxide Electrolysis (SOCE) unit developed at the University of Arizona to generate oxygen through the dissociation of CO_2 via electrolysis with electrodes made of yttria-stabilized Zirconia (YSZ) (see Figure 2-15(c)).
- A Sabatier reactor testbed developed at NASA Johnson Space Center (JSC) to evaluate the production of methane at production rates required for a Mars robotic sample return mission (see Figure 2-15(d)).
- A Reverse Water Gas Shift (RWGS) reactor testbed developed by Pioneer Astronautics and NASA Kennedy Space Center (KSC) as an alternative approach to the Sabatier and SOCE reactions for obtaining oxygen from Mars atmospheric CO_2 (see Figure 2-15(e)). This testbed was used to characterize the reaction kinetics of the RWGS reaction; and
- Water electrolysis systems developed at NASA JSC for integrated testing with the Sabatier and RWGS reactor testbeds (see Figure 2-15(f))

Figure 2-15 depicts a sample of these technologies. Further details on these technologies are described in the Addendum document to NASA DRA 5.0 [83].

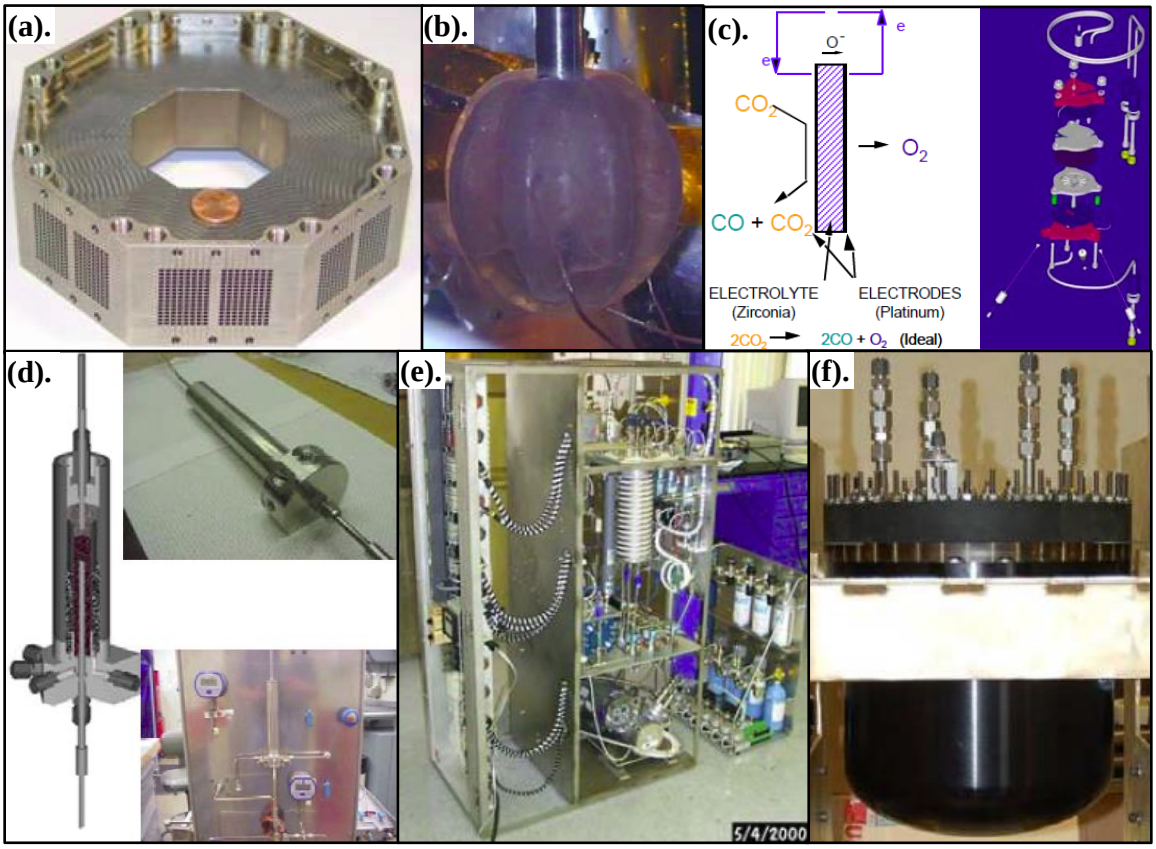

Figure 2-15: Summary of ISRU technology development efforts from the 1990s through to the early 2000s (a). Eight-cell Microchannel adsorption pump developed by Pacific Northwest National Laboratories (b). Solid CO_2 growth on a copper heat exchanger within a CO_2 solidification pump developed by Lockheed Martin (c). Single-cell SOCE unit developed by the University of Arizona for the Mars In-Situ Propellant Production Precursor flight experiment (d). ISRU Sabatier reactor developed at NASA JSC (e). Reverse Water Gas Shift reactor testbed co-developed by Pioneer Astronautics and NASA KSC (f). Water electrolysis developed at NASA JSC for oxygen generation

From 1995 to 2001, a number of these efforts were conducted as part of the development of the Mars ISPP Precursor (MIP) flight demonstration unit that was to be flown on the 2001 Mars Surveyor Lander. In addition to gathering data on Mars atmospheric dust and temperature data, this unit aimed to characterize the performance of CO_2 adsorption pump and solid oxide electrolysis technologies in the Martian environment [84,85]. These efforts, however, were canceled after the failure of the Mars 98 Surveyor lander.

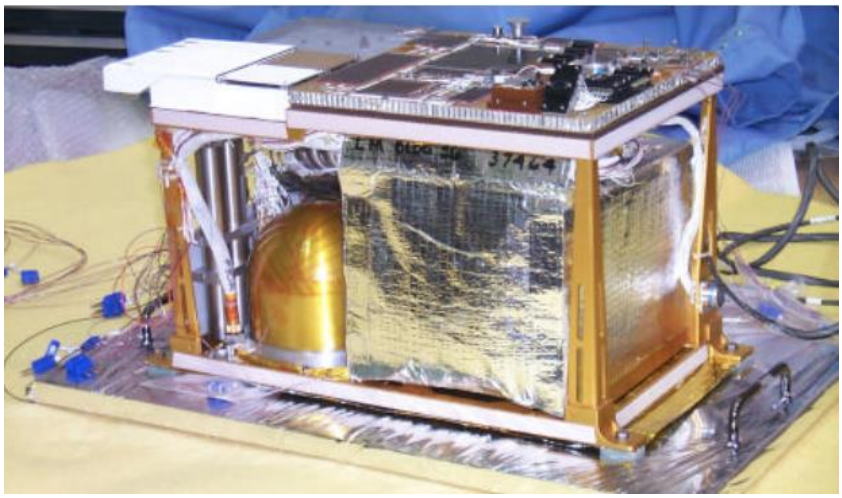

Figure 2-16: Mars ISPP Precursor (MIP) Engineering Development Unit [85]

2.2.3 The Constellation Program and Lunar ISRU

In 2004, shortly after the Vision for Space Exploration was announced, ISRU research shifted towards lunar applications to support the Constellation Program. This led to an intense development period from 2005 to 2011 that resulted in a number of soil extraction and processing technologies that were field tested in Hawaii over three separate campaigns conducted between 2008 and 2012. The goal of these tests was to evaluate the individual and integrated performance of all systems involved in the "Space ISRU Mining Cycle". As shown in Figure 2-17, this cycle consists of firstly prospecting for valuable in-situ resources at a variety of length scales, followed by site preparation and the emplacement of required infrastructure, mining, beneficiation of raw materials, processing of raw materials to extract useful resources, product storage and utilization, and remediation of waste materials.

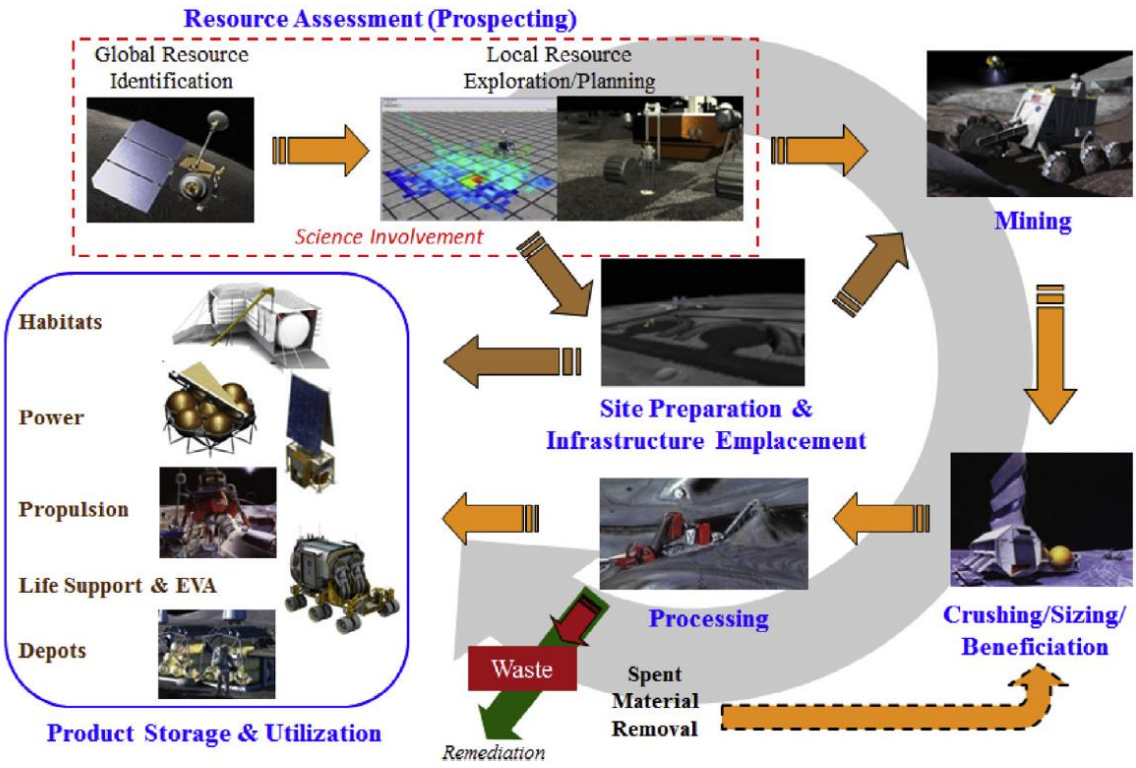

Figure 2-17: The Space ISRU Mining Cycle [86]

Through this effort, the following technologies were developed and successfully demonstrated within the analog operating environment [86]:

- A variety of small robotic excavation rovers of different architectures that were comparatively tested. These included the Cratos rover developed by NASA which was based on a center-scoop design, the bucket drum soil excavator developed by Lockheed Martin [87]), and the Load-Haul-Dump excavation unit developed by the Northern Centre for Advanced Technology (NORCAT) (see Figure 2-15(a) to Figure 2-15(c).)
- The NASA-developed Regolith & Environment Science and Oxygen & Lunar Volatile Extraction (RESOLVE) integrated payload for characterization and extraction of resources from lunar regolith (see Figure 2-15(d)). RESOLVE consisted of a one meter coring drill to acquire subsurface regolith, a gas chromatograph to analyze collected materials for volatiles, and a hydrogen (H_2) reduction reactor to extract oxygen from regolith (see below for further details on the H_2 reduction process)
- The Regolith-Oxygen (ROxygen) system developed by NASA (see Figure 2-15(e)) and the Precursor ISRU Lunar Oxygen Testbed (PILOT) (see Figure 2-15(f)) developed by Lockheed Martin – both of which adopt different system architectures to extract oxygen

from regolith via the hydrogen reduction process. This involves mixing hydrogen gas with regolith heated to between 800 and 1000°C. This process reduces iron oxide-bearing minerals and glasses within the regolith to water vapor, which is then collected and electrolyzed to produce hydrogen and oxygen. The oxygen is collected while the hydrogen is recycled back into the reactor for further processing. During testing, both systems were able to produce water from the local Hawaiian volcanic tephra material. The PILOT system performed particularly well, producing 1000mL of water.

- An integrated carbothermal reduction reactor and water processing and electrolysis unit co-developed by Orbitec and NASA as an alternative process for extracting oxygen from regolith (see Figure 2-15(g)). This process involves firstly flowing methane over regolith that has been heated to between 1650 and 1800°C. Upon contact with the molten regolith, the methane cracks into hydrogen and carbon, the latter of which reacts with the iron and silicon oxides within the regolith to produce carbon monoxide. This carbon monoxide is then reacted with hydrogen gas in a separate reactor to form methane and water. The methane is recycled into the carbothermal reduction reactor while the water is electrolyzed to produce oxygen. During testing, this system successfully produced 28 grams of oxygen, which was subsequently liquefied in-situ and used to fire a liquid oxygen/methane thruster, thereby demonstrating the entire cycle from “Dust to Thrust”.
- A number of sensors for mineral evaluation, including a Mossbauer spectrometer developed by the German Aerospace Center (DLR), the NASA Mini Chemistry & Mineralogy (CheMin) X-Ray Diffraction/X-Ray Fluorescence (XRD/XRF) Instrument, and Raman spectrometers developed by the Canadian Space Agency (CSA). All sensors were successfully demonstrated during testing, each providing useful data during resource prospecting activities.

Figure 2-18 depicts some of the technologies developed.

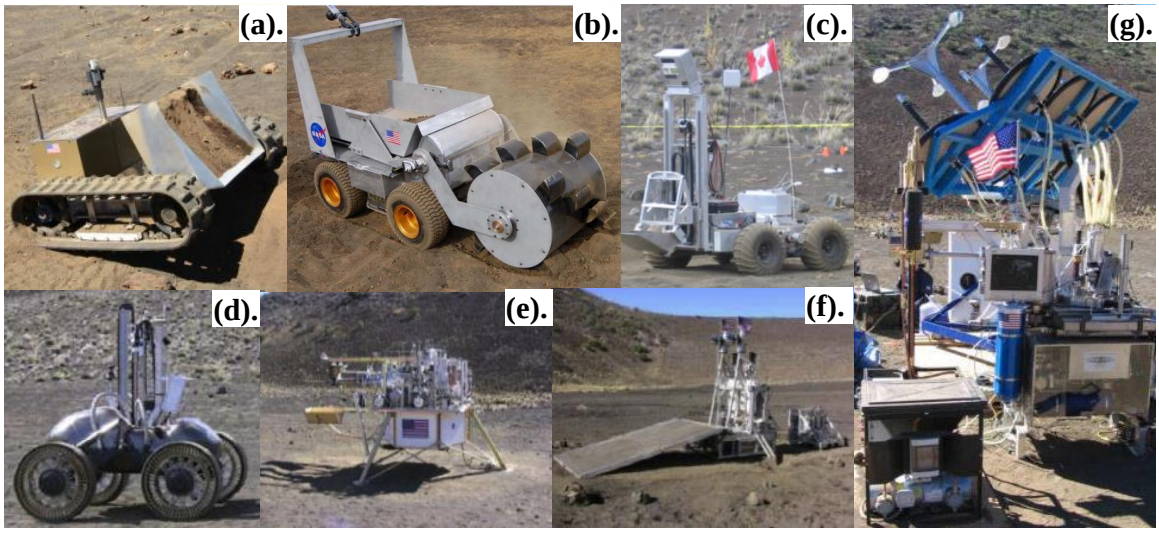

Figure 2-18: ISRU Systems Field Tested during Campaigns conducted between 2008 and 2012 in Hawaii [86] (a). NASA developed Cratos rover [88] (b). Lockheed Martin Bucket Drum Soil Excavator [87] (c). NORCAT Load-Haul-Dump Excavation Unit [89] (d). The NASA Regolith & Environment Science and Oxygen & Lunar Volatile Extraction (RESOLVE) integrated payload (e). The Regolith-Oxygen (ROxygen) system developed by NASA (f). The Precursor ISRU Lunar Oxygen Testbed (PILOT) developed by Lockheed Martin (g). Carbothermal reduction reactor and water processing and electrolysis unit co-developed by Orbitec and NASA [90]

During the third and final ISRU test campaign, an end-to-end simulation of a robotic lunar resource prospecting mission was conducted with an updated version of the RESOLVE payload. The simulation involved the mapping of hydrogen and lunar volatiles to depths of up to 1m over traverses of up to 500m in length, the collection and processing of several core samples, and the evaluation of various mineral and resource characterization payloads. In addition, to better simulate an actual flight mission, all operations were performed remotely by a combination of test engineers located at nearby support facilities and personnel located at control centers at NASA JSC, KSC, ARC, and the Canadian Space Agency. This final test campaign generated a number of lessons that have since been used to develop the Resource Prospector mission currently planned for launch in 2020. This mission has adopted the same objectives as those evaluated during the third ISRU test campaign and will be based on an upgraded version of the RESOLVE payload [91,92].

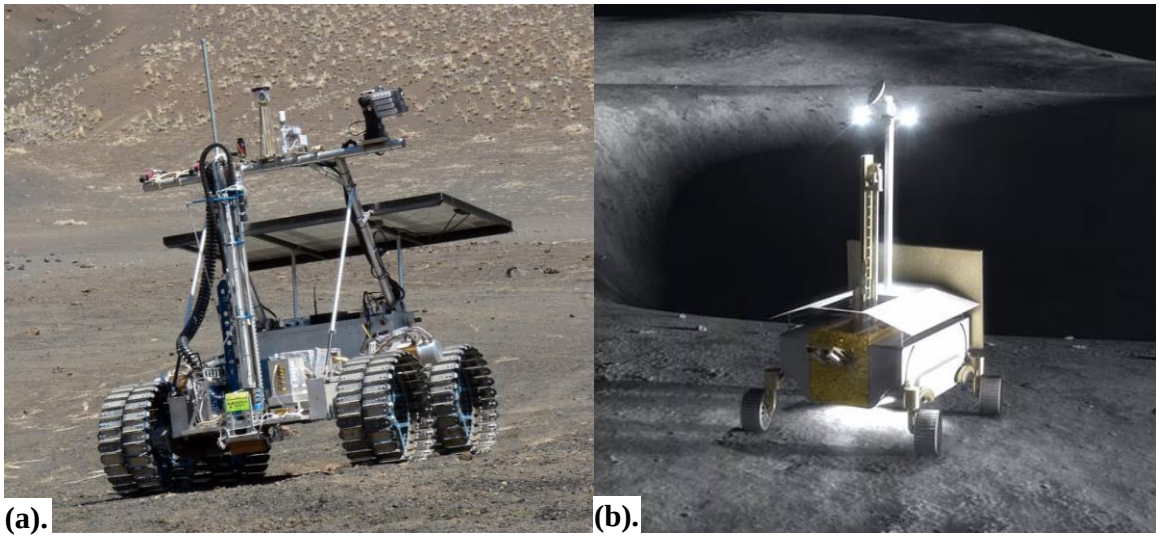

(a). **(b).**

Figure 2-19: The RESOLVE Payload (a). Integrated on the Artemis Jr. Rover provided by the Canadian Space Agency for a field test during the third ISRU test campaign in 2012 [93] (b). An artist's depiction of the NASA Resource Prospector Mission, consisting of the RESOLVE payload being carried on a custom-built lunar rover [92]

2.2.4 Mars ISRU Technology Development Post-Constellation

While much of the focus of ISRU technology development over the early part of this decade revolved around lunar applications, the significant commonality in regolith processing technologies and operations across the lunar and Martian environments have enabled the straightforward transfer of technologies and experiences from the Hawaiian ISRU Test Campaigns to Mars mission development efforts [94]. In fact, many of the sizing models used to estimate the mass, power, and volume of Mars regolith processing systems studies in the NASA DRA 5.0 study were based on those developed in support of lunar ISRU activities [20]. Since this period, a number of major ISRU activities focused on Martian applications have been undertaken.

In 2011, the development of the Mars Atmosphere and Regolith Collector/PrOcessor for Lander Operations (MARCO POLO) project commenced at NASA JSC and KSC. This project was initiated in direct response to the recommendation of the DRA 5.0 study to further investigate electrolyzer/Sabatier reactor-based ISRU concepts, and aims to develop the first ever integrated Mars ISRU atmospheric and soil-processing system for producing propellants at scales comparable to that needed for a Mars sample return mission based on ISPP. The ultimate goal of the project is to field test the system at an analog mission site under realistic

mission conditions. These conditions include limiting the available power to that expected during the mission, and remotely collecting and storing generated propellants for eventual firing of a liquid oxygen/methane thruster [95].

MARCO POLO consists of a number of modules that when operated together, enable the system to produce methane, water, oxygen, and power from in-situ resources. As can be seen in Figure 2-20, these include: (1) an Atmospheric Processing Module that utilizes cryocoolers to capture atmospheric CO_2 for use in a Sabatier reactor; (2) a Soil Processing Module that uses a heater and sweep gas to evaporate water out of collected regolith; (3) a Water Cleanup Module that removes perchlorates and other contaminants from water extracted by the Soil Processing Module; (4) a Water Processor Module that electrolyzes clean water into hydrogen for the Sabatier reactor and oxygen for use as either a life support consumable or an oxidizer; and (5) a Power Production Module based on a hydrogen fuel cell to generate power from gaseous hydrogen and oxygen produced within the system [95]. As of September 2015, all of the major MARCO POLO systems had been built and were undergoing testing and integration [94].

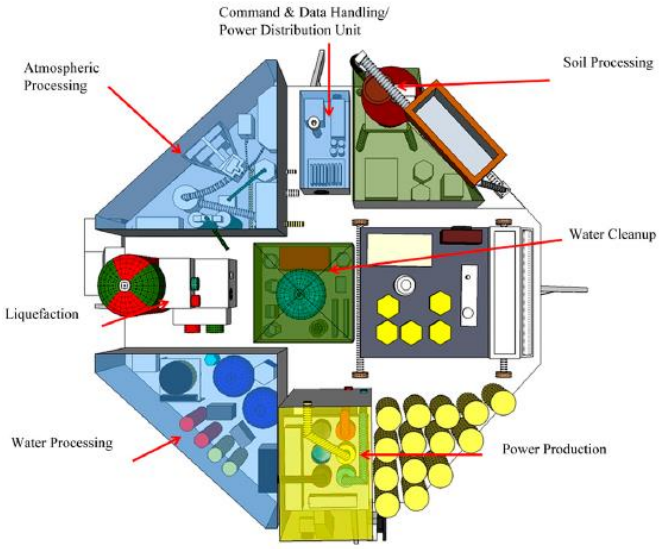

Figure 2-20: The MARCO POLO ISRU System [94]

Furthermore, in July 2014, the Mars Oxygen ISRU Experiment (MOXIE) was selected by NASA as a payload for the Mars 2020 rover mission [94]. This payload will employ the Solid Oxide CO_2 Electrolysis (SOCE) process recommended by NASA DRA 5.0 and investigated as part of the MIP payload development (see Section 2.2.2) to produce oxygen from CO_2 on the surface of Mars at a rate of up to 20g/hr – a value equivalent to approximately 1% of that

required by a crewed Mars Ascent Vehicle. In addition to validating the SOCE process within the Martian environment, the MOXIE experiment also aims to collect data on the health and degradation of the electrolysis unit and its supporting systems in order to inform approaches to scaling up SOCE technologies and operations to support human-class missions. As of September 2015, development of MOXIE is ongoing at MIT and its partner institutions. Figure 2-21 depicts a prototype of the SOCE assembly, as well as flowsheet of the MOXIE architecture.

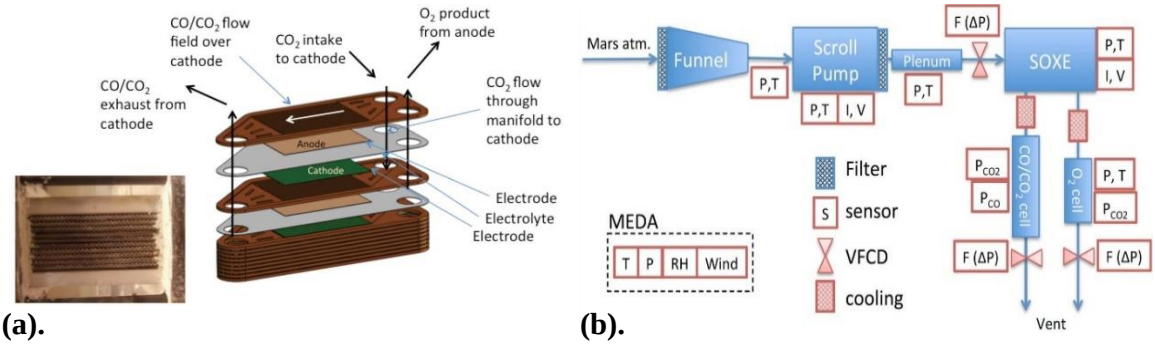

(a). **(b).**

Figure 2-21: The MOXIE Payload (a). The MOXIE Solid Oxide Electrolysis Cell Stack (b). Flowsheet of the MOXIE architecture [96] (VFCD: Viscous Flow Control Devices)

2.3 Recent Analyses on the Supportability of Long-Duration Space Habitation Systems

2.3.1 Impacts of Supportability at the Campaign and Mission Levels

In light of the challenges experienced throughout the operation of the ISS, system analysts have over the past decade become increasingly interested in understanding the effects of system reliability and supportability on future human spaceflight mission scenarios beyond Earth orbit. This trend was particularly evident during the 2006-2008 period, when large-scale studies were performed across NASA to define the Constellation Program architecture that would best accomplish its goal of establishing a permanently occupied outpost at the Lunar South Pole [97,98]. These studies explored a broad range of aspects related to the supportability of a lunar outpost, including its logistics requirements, parts cannibalization and consumables scavenging from spent systems, and commonality across the system architecture. The results of these analyses were then used to inform the sizing of the transportation vehicles intended to

deliver these systems and their logistics to the Moon, as well as to estimate the cost and other figures of merit for the lunar campaign [80,98].

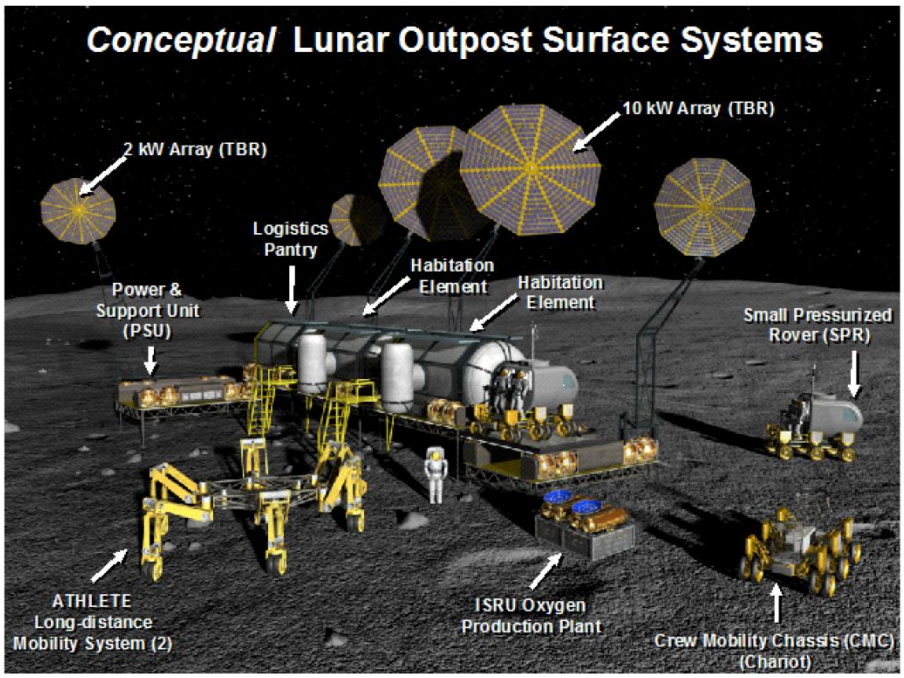

Figure 2-22: Conceptual Design of the Constellation Program Lunar Outpost [98]

To initiate an analysis, a potential campaign of missions was first defined. This included the definition of the number of crew delivered to the lunar surface over time, the duration that each crew spends at the lunar surface, the capacity of the transportation systems planned to deliver crew and cargo to the lunar surface, and the specific payloads delivered [99] (we note that this campaign definition is very similar to the habitat population profiles described in Section 1.2.3 and depicted in Figure 1-10). From this input, logistics requirements were estimated by subject matter experts. This in turn produced a manifest of equipment, which was then distributed among the in-space transportation vehicles assigned to each mission within the campaign. This last step typically required some intermediate analysis iterations to ensure that all manifested equipment could fit within the pressurized and unpressurized mass and volume constraints of the available in-space transportation vehicles. Once this manifesting process was successfully complete, campaign figures of merit (FOMs) were calculated, and sensitivities of these FOMs to variations in the input assumptions were performed.

Cirillo et al. [99] developed and applied this process to a series of decade-long lunar outpost buildup campaigns based on launching a mission to the moon every six months. Four-person

crews would visit the outpost initially for 7-day sorties. As the outpost grew with successive missions, the crew-stay time would gradually ramp up to 180 days. One instance of the campaign architectures evaluated during this series of analyses is summarized in Figure 2-23.

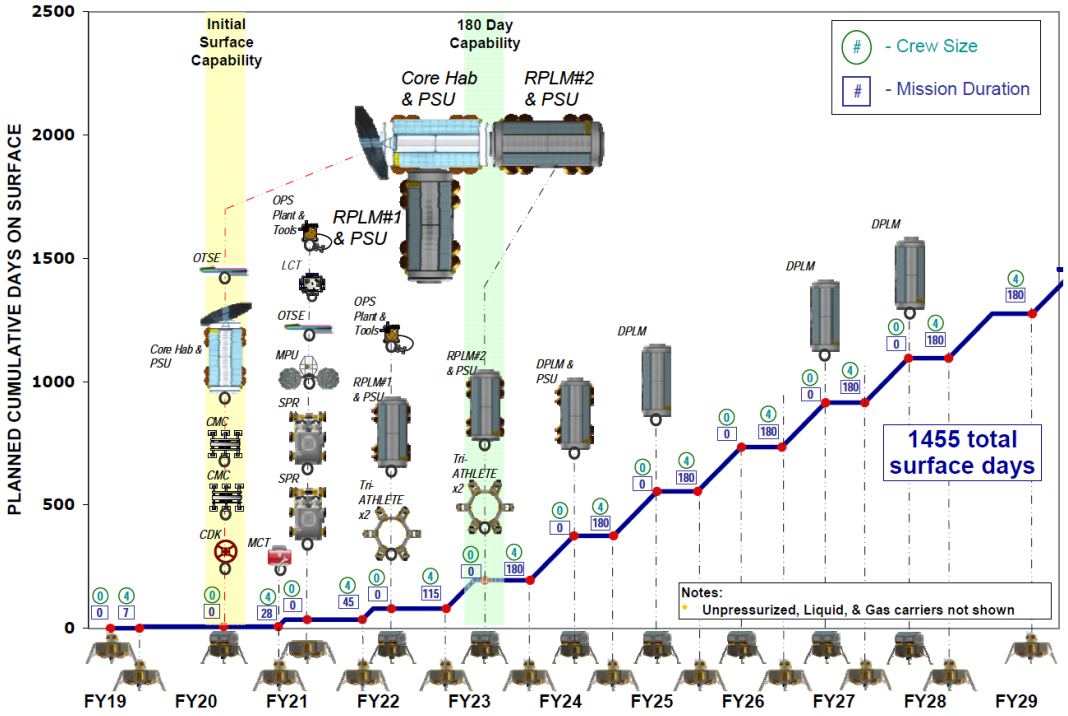

Figure 2-23: Lunar Mission Campaign evaluated by Cirillo et al. [99]

A key finding of this study was that "logistics are a major campaign driver. The variability in logistics requirements and strategies remain a first order driver to campaign performance" [99]. This was based on a sensitivity analysis (see Figure 2-24) that found that a reduction in spares and maintenance mass led to slight increases in available person-days (due to the reduction in time required to perform maintenance and cargo transfer activities) and a significant increase in payload mass available onboard the delivery spacecraft. Conversely, increases in spares and maintenance requirements led to medium to large losses in available crew days and significant losses in available payload mass.

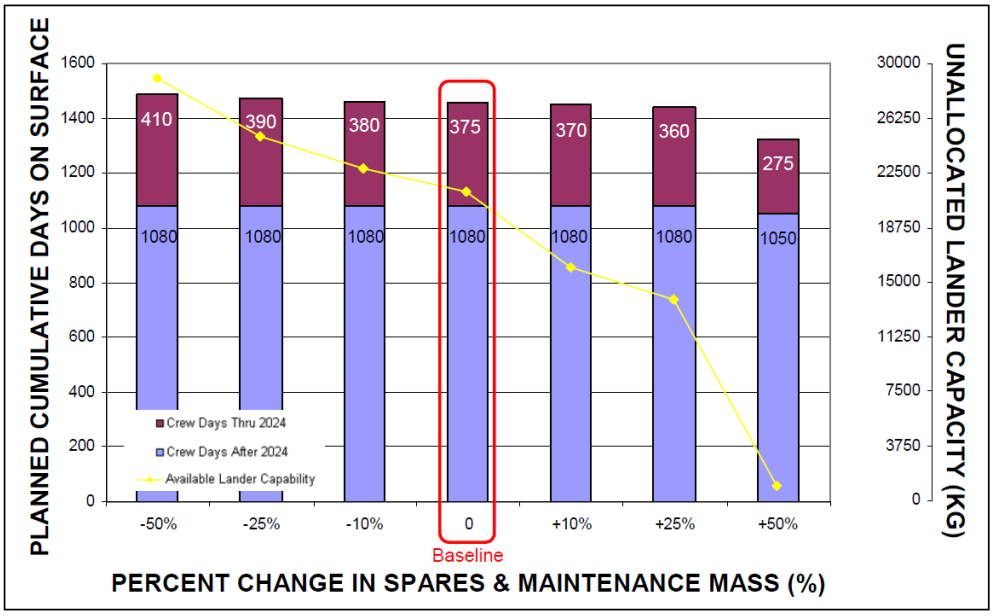

Figure 2-24: Sensitivity Analysis of Cumulative Crew Days on Surface and Available Lander Payload Mass to Variation in Spares and Maintenance Mass

In a complimentary study, Green et al. [98] performed a first-order prediction of the average annual resupply spares demand for eight of the Constellation Lunar Outpost's major subsystems. This was based on using reliability and maintenance data at the lowest component level available to estimate the number of maintenance actions required per year for each component, and multiplying this estimate by the unit mass of the component being evaluated. This calculation is summarized in Equation (2.3), below:

Maintenance Actions/Year = (Quantity x Duty Cycle x K-Factor x 8760 hours)/ MTBF

Where:

- *Quantity = number of ORUs*
- *Duty Cycle = Active duty cycle (dormant factor applied for uncrewed period)*
- *K-Factor = multiplier to account for induced failures, assumed to be 1.2*
- *MTBF = Mean Time Between Failure, estimated through numerous sources*

(2.3)

*Mass of Spare Parts for Component i per Year = Maintenance Actions / Year * Mass of Component i*

In instances where required data was not available, data from analogous systems operated onboard the ISS were adopted. This analysis concluded that of the eight major subsystems examined, the life support system has by far the largest spare parts demand, comprising approximately 70% of the total average annual spare parts resupply requirements (see Figure

2-25). Furthermore, it was found that 91% of the spare parts required by the life support system were derived from two subsystems: the Air Revitalization System (54%), and the Water Management System (37%) – both of which require regular preventative maintenance. Such maintenance actions include the replacement of filters and other life limited items before they are either saturated or fail. This in turn requires replacement parts and thus a higher spares demand.

TS1 Pressurized Module Average Annual Spares		
	Mass/Year (kg)	Volume/Year (m^3)
Life Support	288.9	1.183
Mechanisms	70.2	0.150
Thermal	27.9	0.158
Outfitting	12.3	0.013
Power	9.7	0.029
Avionics	3.1	0.004
TOTAL	**412**	**1.54**

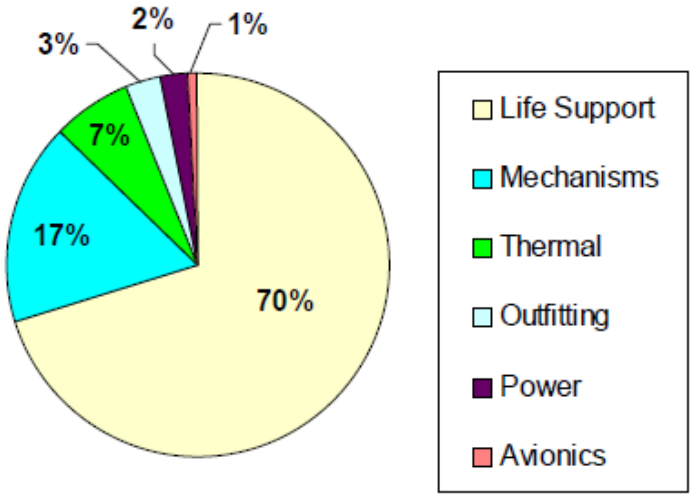

Figure 2-25: Average annual resupply spares demand estimate for the Constellation Lunar Outpost [98]

A more recent study by Stromgren et al. [100] developed and applied a Monte Carlo based tool called the Exploration Maintainability Analysis Tool (EMAT) to study the spare parts requirements for a representative one-year long Near-Earth asteroid deep space vehicle. This tool simulates the day-to-day operations of a mission over a predefined mission timeline, stochastically invoking component failures, implementing corresponding repair actions, and tracking the number of spare parts required to perform each repair. The dependency and propagation of failures is based on a network diagram representing the functional connectivity between all components within the system, as well as reliability, mass, and repair time data on each component. In addition, each component modeled within the system carries two states that are monitored throughout the simulation to enable the tracking of spare parts demands. These states are: (1) whether or not a component is currently functional; and (2) whether or not a component is operational (note that it is possible for a component to be functional but not operational due to failures of connected components located elsewhere in the system, or due to a component being deliberately placed in a dormant or standby mode).

A Monte Carlo engine repeats this simulation process several times, with each run invoking its own independent set of stochastic failures, until statistical convergence in the results is obtained. These results are then post-processed to produce estimates on the required mass of spares as a function of a target probability of loss of mission (PLOM) and probability of loss of crew (PLOC)

Figure 2-26 summarizes the results that were obtained when EMAT was applied to the deep space vehicle mission scenario. The PLOC vs Spares Mass graph depicted in Figure 2-26(a) indicates that without manifested spare parts, the probability of loss of crew is near certain, at a value of 99%. Increasing the mass of manifested spare parts reduces the PLOC in a non-linear fashion, due to the discrete nature in which individual parts are manifested. In addition, obtaining low PLOC values in the sub-5% range requires manifesting progressively larger spare parts, thereby increasing the total required spares mass at a higher rate as compared to reducing the PLOC from higher initial levels.

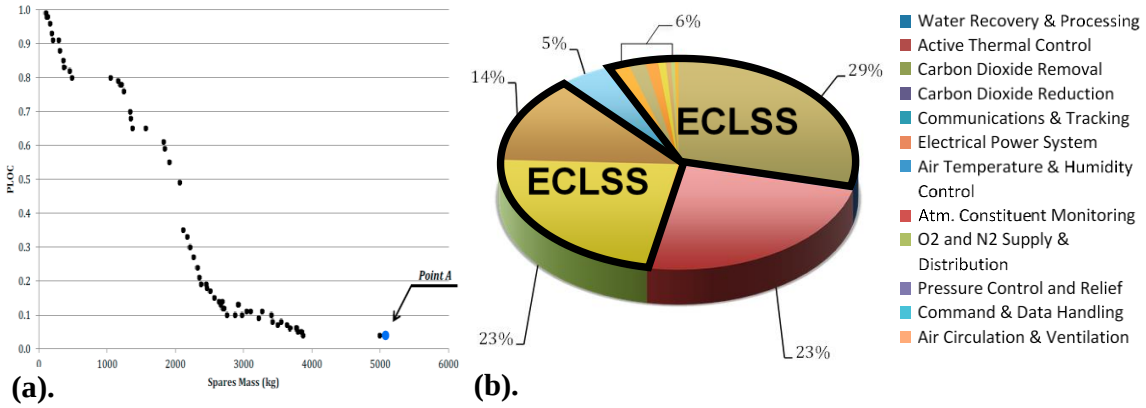

Figure 2-26: Spare parts requirements calculated for a representative one-year long Near-Earth asteroid deep space vehicle (a). PLOC vs Spares Mass (b). Breakdown of the spare parts requirements by subsystem for a target PLOC of 4% [100]

Figure 2-26(b) shows a breakdown of the spare parts requirements by subsystem for a target PLOC of 4% (represented by Point A in Figure 2-26(a)). It is interesting to note that when all ECLS spares are aggregated, their total contribution equates to 72% – a value very similar to that obtained in the lunar outpost study described earlier.

2.3.2 Impacts of Supportability on Life Support System Architectures

In parallel to supportability analyses at the mission and campaign level, analysts from within the life support community have also begun to factor supportability considerations into their analyses. This has been especially motivated by the dominant contribution of life support spares on total logistics requirements observed both in ISS operations and predicted in mission level studies such as those discussed above.

Recent studies by Lange et al. [101] and Jones [102] independently found that when system reliability is accounted for, the heuristic adopted during the Space Station Freedom era that more materially closed ECLS architectures are more mass-efficient at increasing mission durations (see Section 2.1.2) does not necessarily hold. This is because technologies that enable recycling functions are typically much more complex than those used in open loop systems. These recycling technologies generally contain a larger number of moving parts such as pumps, blowers, and motors that are subjected to wider temperature ranges – attributes that make them more susceptible to failure than the simpler storage and distribution based systems characteristic of open loop technologies. A consequence of this is that to maintain the same system availability, more spares are typically required for recycling technologies. In some cases, this can offset the mass savings obtained from recycling consumables and increasing loop closure.

In both of these studies, an Equivalent System Mass (ESM) (see Section 4.4.5 for further details) analysis was performed to investigate the impacts of different levels of ECLS loop closure, sparing and redundancy on meeting a target system reliability of 0.999. Jones [102] found that for missions lasting up to 1000 days, only architectures employing either six redundant copies of existing regenerative ECLS technologies, or a hybrid combination of an open-loop gas supply and partial closure of the water system, could meet the predefined 0.999 reliability target. Here, total system reliability was increased by either increasing the amount of resources carried along (essentially increasing tank sizes), or including additional copies of existing systems.

Similarly, Lange et al. [101] investigated ten different ECLS architectures of increasing resource loop closure for a four person deep space habitat on a one year mission. Using a reliability block diagram approach, the reliability of each architectural option was quantified and increased until the target reliability level of 0.999 was met. In this case, reliability was

increased by adding redundant systems for atmospheric management systems (considered to be more time-critical in the case of a failure) and spare parts at the Orbital Replacement Unit (ORU) level for the remaining systems. Through this analysis, it was found that for a fixed reliability level, a partially closed system consisting of water and urine processing technologies and an open loop oxygen supply was the most mass efficient. Figure 2-27 summarizes the results of these two studies.

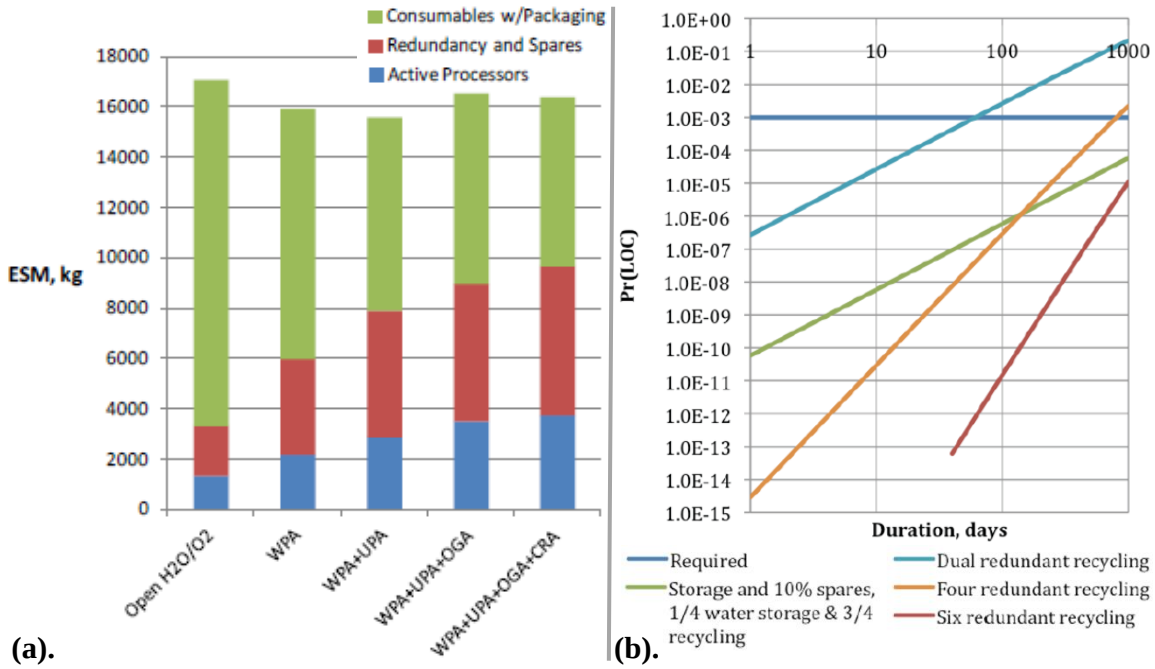

Figure 2-27: Recent analyses investigating the impact of spare parts requirements on total ECLS system mass (a). Analysis results from Lange et al. [101] (b). Analysis results from Jones [102]

In related work, researchers at the Charles Stark Draper Laboratory surveyed a wide range of avionics and control hardware for lunar surface habitat systems to relate subsystem components of varying complexity and reliability to their cost [103]. Through this, an exponential relationship was observed, whereby the cost of a subsystem grows asymptotically as its reliability is increased. In addition, the rate of this cost growth was observed to increase with the level of complexity within the system, as approximated by the number of parts within the system. These trends were correlated with earlier work by Metta [104], who proposed an analytical expression for this relationship based on the observations that: (1) It is typically easier to incrementally improve the reliability of systems that have an initial low level of

reliability; and (2) Beyond a certain capability and reliability level, limits in technology cause the cost of improving the reliability of a system to rapidly increase. This correlation is shown in Figure 2-28.

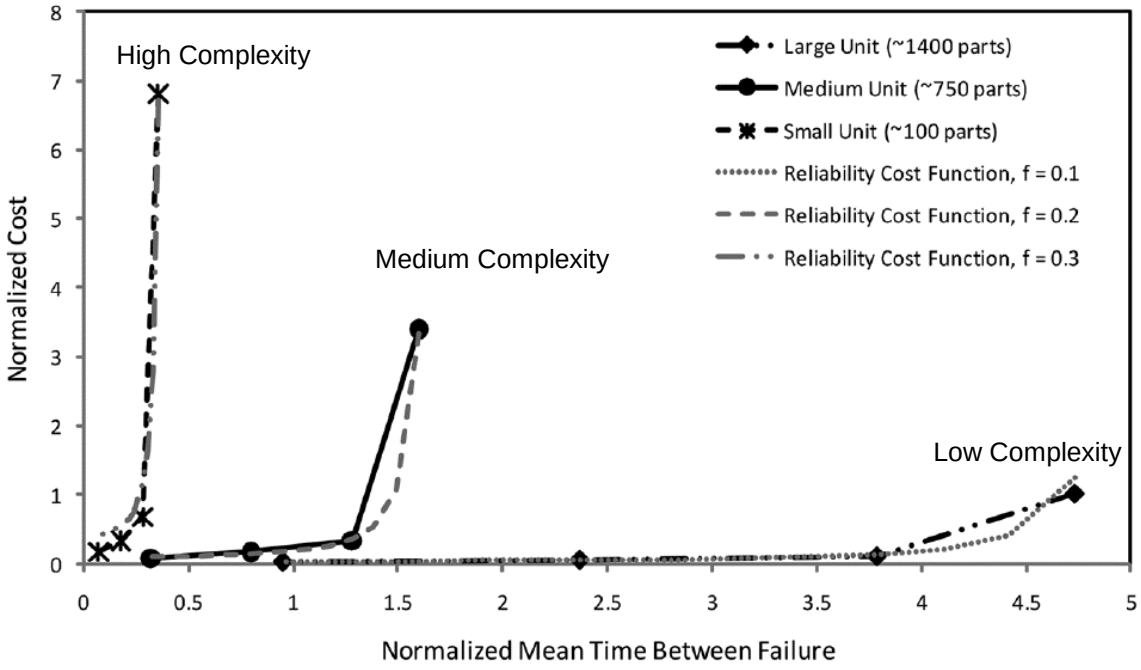

Figure 2-28: Correlation between Cost vs Reliability (measured by Mean Time Between Failure) for surveyed space-rated avionics and control systems, and general trends predicted by Metta [103]

Since ECLS technologies consist of a number of space-rated avionics and control systems similar to those considered in the Draper study, this result implies that the cost of improving the reliability of existing ECLS technologies will likely be high. This is especially the case for ISS ECLS technologies, since their regenerative nature makes them significantly more complex than ECLS systems flown on earlier spacecraft (see Table 2.3). This finding further suggests that increasing system reliability may not be the most effective approach to reducing the high spare parts requirements of regenerative ECLS technologies observed in contemporary system analyses.

2.3.3 Impacts of Supportability on In-Situ Resource Utilization Technologies

In comparison to life support systems, relatively little analysis on the supportability of ISRU technologies has been performed, primarily due to their developmental nature and their lack of operational experience. The majority of knowledge in this domain was obtained during the Hawaiian Analog Field Test Campaigns discussed in Section 2.2.3. While these tests were able to demonstrate the basic performance of ISRU technologies, they also revealed reliability challenges that could only be uncovered while operating within the intended mission environment. These challenges most commonly occurred in the form of component failures that arose due to some combination of thermal cycling, windy and dusty conditions, and unanticipated surface properties [86].

More specifically, temperature cycling and humidity were observed to cause cold solder joint and other unanticipated electrical failures, while fine blowing dust caused intermittent problems with drill electronics. Dust intrusion was also found to have caused excessive wear in gears and motors of several of the excavators that were tested, causing their complete shutdown. In addition, the softer than expected tephra material that made up the analog site prevented some rovers from traversing across the analog site while at the same time creating difficulties in excavation and materials handling for other test vehicles [86].

These experiences illustrate the significant impact that uncertainty in environmental conditions have on the reliability of hardware expected to operate within the given environment. Contrasting to life support technologies which typically operate in controlled pressurized environments, ISRU technologies are expected to operate continuously for long periods of time within the exploration environment, where they can directly interact with in-situ resources. As a consequence, ISRU technologies are exposed to a wider range of environmental conditions that can impact their reliability in unexpected ways. This in turn, makes the prediction of logistics requirements for ISRU technologies especially difficult.

As an example, a study by Woldman et al. [105] attempting to predict the expected mean time between failure (MTBF) of sprocket wheels on infantry military vehicles operating within sandy environments found that even with detailed information on terrain and soil properties, physics-based analyses could only predict the MTBF to an accuracy of within an order of magnitude of the MTBF actually experienced. In another study, Treichel et al. [106] performed a series of experiments on two types of motorized electric fans operating in a simulated dusty

lunar environment (using JSC-1AF Lunar Mare Regolith Simulant) to determine their rate of performance degradation. This study revealed that while both fans have an expected operating life of greater than 50,000 hours under typical indoor use, the performance obtained for the same fans operating under various simulated lunar conditions ranged from 88 hours to 1150 hours. This wide-ranging and high level of degradation may potentially be even more significant within the Martian environment, given that Mars surface soil is substantially more oxidizing and reactive than lunar dust [107].

Given the difficulty in predicting the reliability of systems operating within extreme dusty environments, it is not surprising that there is currently little data available on the reliability of ISRU technologies. In fact, to better inform future reliability analyses, one of the primary objectives of the MOXIE mission (see Section 2.2.4) is to collect data on how the instrument degrades over time within the Martian environment [96]. For the purposes of analyzing ISRU logistics requirements within this thesis, reliability data of analogous technologies at the component level will be taken as an upper bound, and sensitivity analyses will be conducted to assess how variations in ISRU component level reliability affect system level logistics requirements.

2.4 Chapter Summary

Throughout this chapter, we reviewed the history of ECLS and ISRU technologies and their supportability challenges in an attempt to gain insight into the requirements of HabNet – the integrated habitation analysis tool that we intend to develop to analyze and compare future "permanent presence" Mars mission scenarios. One of the major observations made from this review was the importance of incorporating supportability considerations into early system conceptual design. This was particularly evidenced by the reliability and manifesting challenges that have been experienced throughout the past 15+ years of ISS operational experience, and the multiple recent analyses on long duration ECLS systems finding that maximizing loop closure is not necessarily the optimal architectural solution, especially when factors related to reliability and supportability are included. This is a particularly important consideration given recent findings that ECLS technologies will likely make up the majority of the spare parts demands of future long duration missions beyond Earth orbit.

From the review of ISRU technologies, we learned that while much technology has been developed and tested in analog environments, little system level analyses has been performed on the supportability requirements of ISRU systems and their impact on mission lifecycle cost. This is partly a result of the large uncertainty in the characteristics of the operating environment, and the impact of these environmental conditions on ISRU component reliability. Given that ISRU has been a critical component of all Mars mission plans since the early 1990s, it is important to factor in the supporting systems required to sustain their continued operation when performing system architecting activities.

Interestingly, when comparing these reviews in the context of past mission and campaign level supportability studies, it was found that little analysis had been previously performed on the interactions between the mass closure and hence architecture of life support systems, the implications of this on ISRU system architecture and sizing, and the supportability requirements of both. Rather, recent mission studies have instead been based on either: (1) combining the results of subsystem-specific studies performed within their respective communities, to make first-order static estimates of architecture level behavior; or (2) performing Monte Carlo analyses on detailed subsystem level reliability block diagrams to make probabilistic estimates of sparing requirements

While the first approach enables the determination of quick first-order results, it does not capture the dynamic complexities within crewed spaceflight systems that are required to understand their supportability requirements. Conversely, while the second approach does indeed capture the complexities of nonlinear system dynamics, it requires numerous simulation runs that are computationally expensive, which can in turn limit the number of architectural options that can be explored.

From the perspective of developing a capability to perform integrated architectural studies on a broad range of mission scenarios, this observation implies that a balance is required between being able to model a broad range of system architectures, while at the same time capturing their dynamic complexity to allow for the computation of supportability requirements. This is especially important for missions with long time scales, like those of the "permanent presence" Mars missions that will be explored later in this thesis. In the next chapter, we attempt to achieve this balance by combining architecting and analysis methodologies from multiple disciplines to develop the HabNet habitation analysis environment.

Chapter 3

HabNet Development

In this chapter, we describe the development of HabNet – an integrated habitation and supportability architecting and analysis environment. Named in reference to the network of systems required to enable continued habitation in extreme and remote environments, HabNet will be applied to a range of long-duration continuously crewed Mars mission scenarios to characterize the drivers of their sustainability. We commence the development of HabNet by firstly building an Architecture Decision Graph (ADG) (see Section 1.2.1) of human spaceflight systems, in order to develop an understanding of both the key decisions that shape the architecture of space habitation systems in general, as well as the surrounding ecosystem of decisions that constrain them. Following this, we perform a functional decomposition of the decisions that directly influence the habitation architecting process to a level where they map to technology choices that can be dynamically modeled. This process allows us to derive an overall module structure for the HabNet environment, from which we base the development of a library of models and simulation routines. The selection of a particular set of models corresponds to the choice of a particular set of architectural decisions. Thus, when the outcome of all architecturally distinguishing decisions and their corresponding models are combined, a habitation architecture is synthesized and modeled, which can in turn be simulated and further analyzed. Each of the major steps in this development process are further discussed throughout the following sections.

3.1 Developing the HabNet Framework

3.1.1 Constructing the Human Spaceflight System Architecture Decision Graph

As was discussed in Section 1.2.1, an Architecture Decision Graph (ADG) is essentially a graph that depicts both the major architecturally distinguishing decisions that need to be made to architect a given system, as well as the dependency between these decisions. In this section, we reference the mission architecting processes adopted during the Apollo program and in more recent Mars mission planning activities to identify key architecturally distinguishing decisions from which we can construct a human spaceflight system ADG. This ADG is intended to capture the set of decisions that dictate the set of system architectures that transport human crews to and from an exploration destination, as well as the system architectures that sustain these crews for the duration of their mission.

We commence the ADG development process by first reviewing what it means to define the goals for a human space exploration program. Here, we refer to one of the first, and perhaps most succinct declarations of a human spaceflight endeavor: President Kennedy's 1961 announcement of the Apollo Program. During a special joint session of Congress convened seven weeks after Yuri Gagarin's historic first spaceflight, President Kennedy announced that:

"*this nation should commit itself to achieving the goal, before this decade is out, of landing a man on the moon and returning him safely to Earth*" [108]

With this statement, he outlined the high level decisions that defined the Apollo Program. Here, he defined the **mission destination** and **timeline**, and the high level **crew task** – to operate on the lunar surface. Earlier in this same speech, he explained the **goal** of restoring national prestige and global leadership as being the key motivation for this project:

"*…if we are to win the battle for men's minds, the dramatic achievements in space which occurred in recent weeks* (referring to Yuri Gagarin's orbital flight) *should have made clear to us all as did Sputnik in 1957, the impact of this adventure on the minds of men everywhere who are attempting to make a determination of which road they should take"* [108]

The four key elements used by President Kennedy to define the scope of the Apollo program: the **Program Goals**, **Mission Destination**, **Mission Timeline**, and the Crew Tasks (or **Concept of Operations**); correspond to the first four key decisions that shape the architecture of a human spaceflight system. These are encapsulated within our initial ADG, as depicted in Figure 3-1 below. Here, we note that the selection of the overarching **Program Goals** dictates the selection of the **Mission Destination** and **Timeline**, as well as the **Crew Concept of Operations**. These are indicated by the red connecting arrows within Figure 3-1.

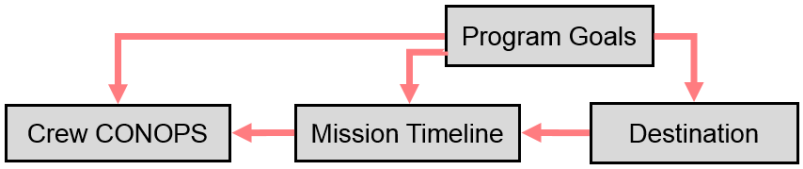

Figure 3-1: Initial ADG – The selection of the overarching Program Goals dictates the selection of the Mission Destination and Timeline, as well as the Crew Concept of Operations (CONOPS)

The next tier of architecturally distinguishing decisions can be derived from examining the mission planning activities that occurred across NASA in the 18 months immediately following the Apollo announcement. During this period, a series of NASA-wide studies were undertaken to determine the "mission-mode" – the combination of habitation elements, propulsive elements, and transportation staging locations that would best meet the objectives of landing humans on the moon within the shortest period of time possible.

At the time, it was widely recognized that the choice of mission mode would dictate the architecture of the launch vehicle, the lunar lander, the crew operations, as well as the cost and schedule of the program (see Figure 3-2). In fact, it was the November 1962 selection of lunar orbit rendezvous (LOR) as the Apollo mission mode that was later identified as being one of the most critical and influential factors in determining the success of the Apollo program [109].

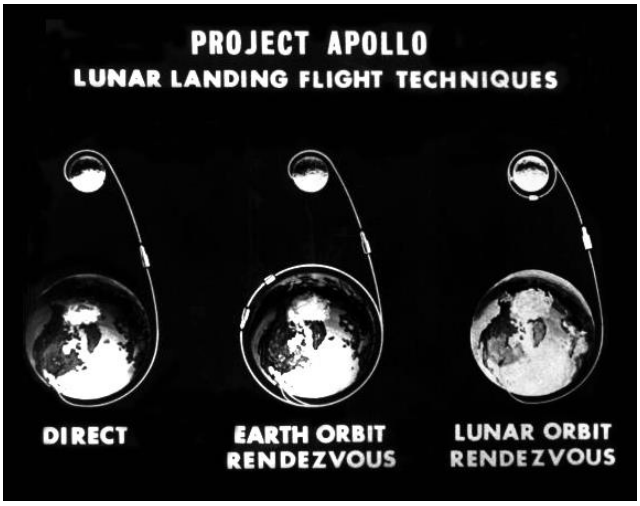

Figure 3-2: The Apollo Mission Mode Decision [15]

It is interesting to note that this mission-mode decision has also been a key point of discussion in the Mars mission planning community. The use of nuclear thermal rockets and the division of the lander and transit vehicles adopted by the current NASA Design Reference Architecture 5.0 (DRA) (see Section 1.2.1) can be traced back to the "Mars Orbit Rendezvous" (MOR) architectures studied by researchers at NASA Lewis Research Center in November 1957 [17]. Thus, the prevalence of the coupled decisions that form the mission-mode decision: the distribution of **Habitation Elements** and **Propulsive Elements**, as well as the **Transportation Staging Strategy**; make them the key elements of the next tier of decisions within our ADG, as depicted below in Figure 3-3.

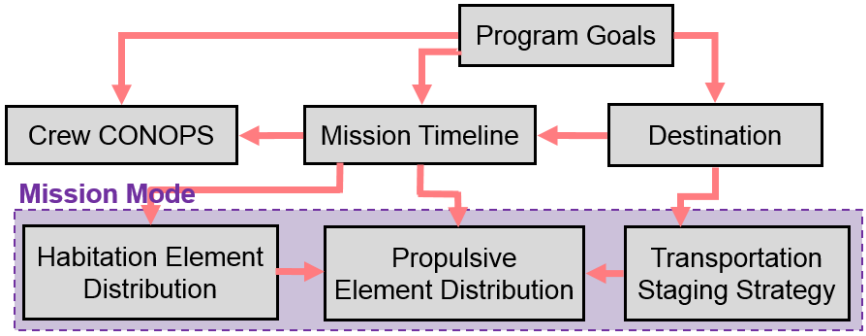

Figure 3-3: ADG Updated with Decisions Related to the "Mission Mode"

From Figure 3-3, we observe that decisions related to the **Mission Destination** and **Mission Timeline** both constrain the **Transportation Staging Strategy** (including the

corresponding set of feasible trajectories), which in turn influences the **Propulsive Element Distribution** – or the number, type, and allocation of propulsive elements. At the same time, the **Mission Timeline** and **Crew CONOPS** influences the **Habitation Element Distribution**, which in turn affects the distribution of propulsive elements required to transport them.

Since we are ultimately interested in the decisions that affect "permanent presence" mission scenarios, we continue the development of this ADG by looking towards more recent human spaceflight experience and mission concepts, where the increase in mission duration has introduced the need for additional system capabilities. In Section 1.2.2, after reviewing the evolution of space habitation development and Mars mission planning, we identified the main drivers of habitat endurance as being the **ECLS Architecture**, the **ISRU Architecture**, and the **Supportability Strategy** adopted for the mission. The influence of these drivers was reaffirmed throughout Chapter 2, when a more detailed review was conducted.

The identification of these factors was based on the assumption that the **Habitation Architecture** was already specified. This refers to considerations related to the internal volume and layout of a habitat, and its ability to facilitate an effective space for living, working, and the storage of equipment [110]. Since the beginning of long duration spaceflight in the 1970s (see Section 1.2.2), it has become increasingly understood that as mission durations increase, the number of psychological stressors that can affect a crew also increases. These stressors include feelings of social and sensory deprivation and monotony that can arise from spending several months to years in a closed environment with the same crew [111]. While some of these stressors can be overcome through appropriate crew selection, a large portion of these can only be managed through proper habitat volume selection and layout design. It is well-known that as mission durations increase, the required habitable volume per person, as well as the requirement to manage habitat layout and zoning also increases [110,111]; primarily due to the need to minimize the impact of the aforementioned psychological stressors.

The long-term influence of these four decisions: the **Habitation Architecture**, the **ECLS Architecture**, the **ISRU Strategy**, and the **Supportability Strategy**; justify their inclusion as the last layer of our ADG. This final ADG, including all major connections between each of the identified architecturally distinguishing decisions, is depicted below in Figure 3-4. In addition, Table 3.1 lists a selection of example options for each of the architectural decisions shown here.

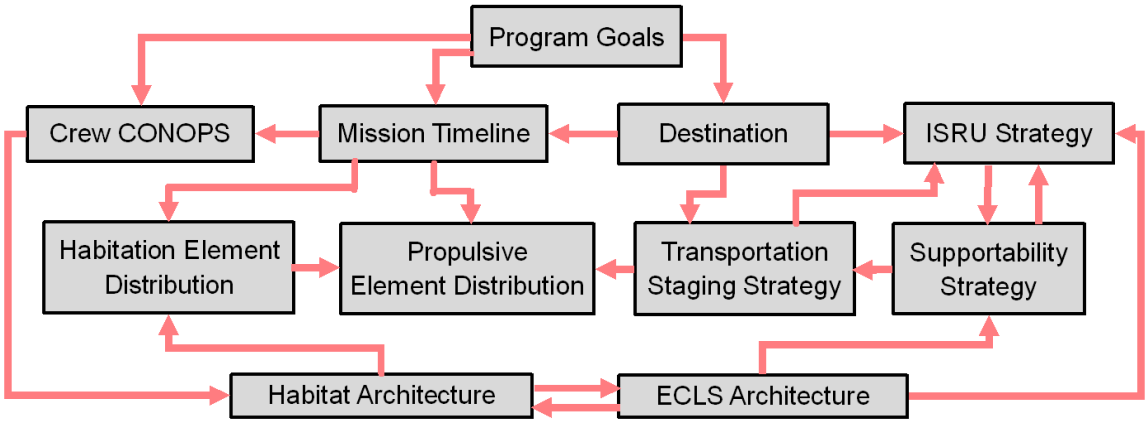

Figure 3-4: The final integrated ADG. The inclusion of the Habitation Architecture, ECLS Architecture, ISRU Architecture, and Supportability Strategy decision sets represent the factors that drive long term sustainability of a human spaceflight system.

In the final integrated ADG shown in Figure 3-4, we observe several connections between the final set of "permanent presence" related decisions and those that define the human space exploration program and the mission mode. Specifically, decisions related to the **Supportability Strategy** influence the **Transportation Staging Strategy** throughout the mission campaign, are influenced by decisions related to the **ECLS architecture**, and have a two way coupling with the **ISRU Strategy**. The dependencies to and from the **Supportability Strategy** primarily arise from the impact of system spare parts resupply demands and ISRU-derived products on space logistics throughout the mission campaign. The availability of ISRU-derived products is a result of the **ISRU Strategy**, which is driven by the choice of mission **Destination**, which constrains the type and quantity of resources that are locally available.

In addition, we note a two-way coupling between the **Habitation** and **ECLS Architecture** decisions, as well as dependencies from the **Crew CONOPS** and dependencies to decisions related to the **Habitation Element Distribution**, the **Supportability Strategy**, and the **ISRU Strategy**. As discussed earlier, the **Habitat Architecture** refers to the functional zones and elements within a habitat, while the **Habitation Element Distribution** refers to the allocation of these functional zones to physical volumes. That is, whether these functional zones are contained within a single monolithic habitat, or whether they are distributed across multiple small habitats. The required functional zones and their associated coupling is driven by the **Crew CONOPS** (i.e. the crew activities), which is in turn driven by the **Mission Timeline**.

Moreover, the consumables and sparing requirements of the selected **ECLS Architecture** drive **Supportability** and **ISRU Strategy** decisions.

Table 3.1: Example Options for each of the architectural decisions depicted in the integrated Human Spaceflight System ADG shown in Figure 3-4.

Architectural Decision	**Example Option 1**	**Example Option 2**	**Example Option 3**
Program Goals	National Prestige	Exploration	Engineering Qualification
Crew CONOPS	No EVA	5 EVAs per week	Two week Mars surface expeditions in pressurized rovers every month
Mission Timeline	30-day opposition class Mars sortie mission	500-day conjunction-class Mars sortie mission	Continuous human presence on Mars supported by resupply missions every 26 months (corresponding to the Earth-Mars synodic period)
Destination	Mars orbit	Phobos	Mars Surface
ISRU Strategy	None	Use Mars atmospheric ISRU only to generate O_2	Use both Mars atmospheric and soil-based ISRU to generate water and O_2
Habitation Element Distribution	Monolithic habitat	Multiple modules connected via node elements	Multiple modules periodically expanded with the permanent addition of visiting logistics carriers
Propulsive Element Distributions	One propulsive element per habitation module for in-space transit (e.g. Lunar Orbit Rendezvous – see Figure 3-2)	One propulsive element for all habitation modules for in-space transit (e.g. Direct Ascent – see Figure 3-2)	Multi-stage propulsion for Mars ascent
Transportation Staging Strategy	Assemble trans-Mars injection stack in an Earth parking orbit	Assemble trans-Mars injecton stack in lunar distant retrograde orbit	Direct injection from Earth surface to Mars
Supportability Strategy	Maximize system reliability and include two fault-tolerant systems	Reparable single fault-tolerant systems with spare parts carried along	Reparable systems with on-demand in-situ parts manufacturing to produce required spare parts
Habitat Architecture	Minimal volume - single open multifunctional space (analogous to a studio apartment)	Separation of work and living spaces; dedicated private quarters for each crewmember (typical for crew sizes of 4 to 8)	Separated exercise areas, shared sleeping and bathroom areas, dedicated laboratory and work spaces, and dedicated mess hall (analogous to Antarctic research stations with dozens to hundreds of people)
ECLS Architecture	Open loop – all water, food and gases supplied directly from tanks	ISS-based – partially closed water and oxygen loops with prepackaged food	Bioregenerative with large scale crop growth, integrated with oxygen generation and CO_2 removal systems. Water is supplied from in-situ resources

Finally, we note that in this version of our guiding ADG, we have omitted decisions related to supporting systems such as power systems, thermal management, and communications architecture. While these are clearly important, they are not architecturally distinguishing – that is, the choice of technological architectures for each of these decisions has converged to a single option. For example, it is widely agreed upon that a Martian outpost will be nuclear-powered due to its greater mass efficiency, resilience to dusty environments, and flexibility in maintaining a continuous power output as compared to solar-powered alternatives [21].

3.1.2 Mapping Previous Research to the Human Spaceflight System Architecture Decision Graph

In addition to identifying the key decisions that shape the architecture of a human spaceflight system, the newly developed ADG also provides us with a common framework to represent the scope of this current research effort with respect to previous mission planning and research efforts. As will be seen in the discussion below, the general trend has been that over time, as more knowledge and experience is gained from operating progressively longer duration and higher endurance human spaceflight systems, more decision sets have been incorporated into mission architecting analyses.

We begin this analysis by first reviewing the decision sets examined in the traditional transportation-centric Mars mission architecting studies summarized in Figure 1-1. As discussed in Section 1.1, these studies typically focused on analyzing the mission-mode set of coupled decisions and their impact on the ISRU strategy for sortie-class missions to the Martian system. This traditional decision set is depicted by the elements enclosed within the yellow polygon drawn in Figure 3-5.

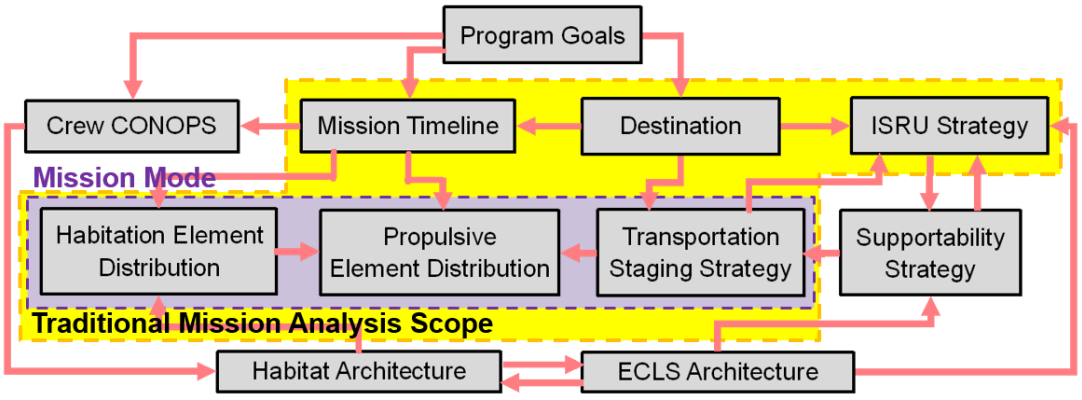

Figure 3-5: Set of transportation-centric architectural decisions traditionally analyzed in Mars mission architecting studies

As the field of space logistics matured and its methods began to be applied to mission campaign studies, considerations related to the Supportability Strategy began to be incorporated into the space of decisions analyzed. This evolution in the scope of mission architecting is depicted by the elements within the green polygon drawn in Figure 3-6.

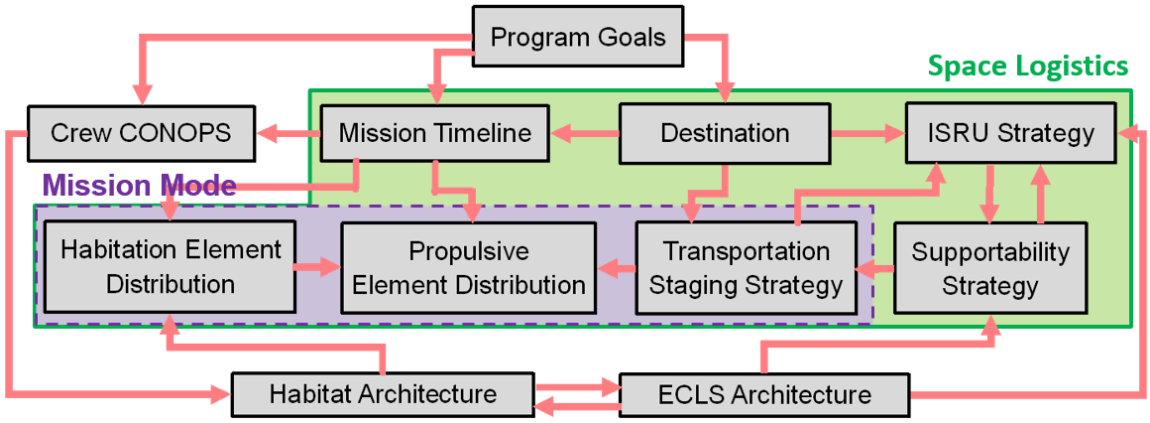

Figure 3-6: Set of architectural decisions within the scope of modern space logistics analyses

Finally, within the past decade, it has become increasingly understood that: (1) as mission durations increase, logistics demands become increasing drivers of operation cost; and (2) the largest contributors to logistics demands of long duration spaceflight missions are derived from crew and life support systems (see Section 2.3.1). Through the development and demonstration of HabNet, this research aims to explore the impact of these lower level habitation and life support decisions on space logistics requirements and the resulting operational cost, thereby integrating these architectural decisions into the traditional mission architecting decision space. Specifically, HabNet targets the elements enclosed within the blue polygon depicted in the ADG in Figure 3-7. In Section 3.2, we formulate the high level structure for HabNet based on this final set of HabNet-specific decisions.

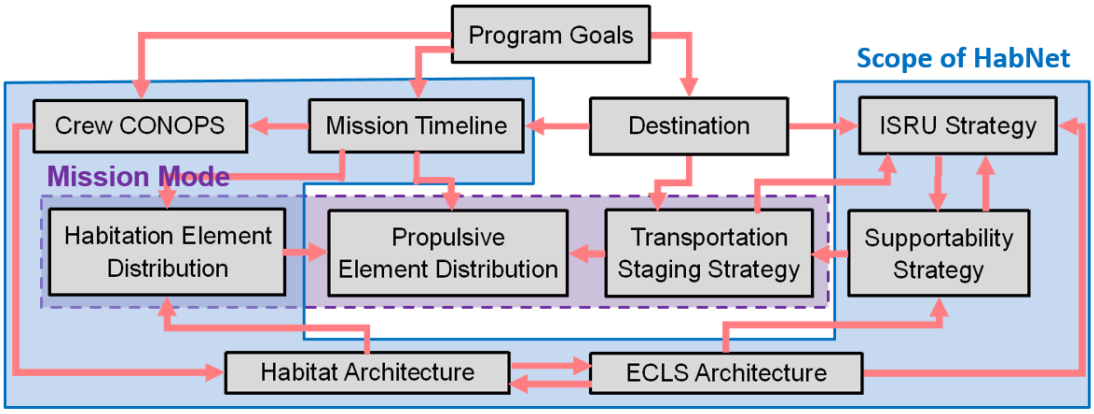

Figure 3-7: Set of architectural decisions targeted by HabNet

3.1.3 The Four Classes of Space Habitation

In addition to gaining insight into key architecturally distinguishing decisions and their relative dependencies, analyzing the process of human spaceflight system architecting from the perspective of a decision making problem also allows us to derive new classification schemes for the various types of human spaceflight activities that are currently being pursued. In Section 1.2.2 we classified space habitation systems by their endurance and population. From the ADG depicted in Figure 3-7, we observe that decisions regarding the Habitat Architecture are directly influenced by decisions related to the Crew Concept of Operations (CONOPS). In this section, we use this observation to derive an alternative classification to space habitation systems and by extension, human spaceflight missions.

Two key decisions that constitute the selection of a Crew CONOPS include: (1) whether or not extravehicular activities (EVAs) are performed, and (2) whether the crew is sent on a sortie-type mission or an outpost development and utilization type mission. Sortie-type missions are characterized by single visits to a predefined location, as was the case with the Apollo lunar missions. Contrastingly, outpost development type missions consist of repeated visits to the same exploration site with the intent of expanding infrastructure at that location over time. These two sub-decisions are considered to be architecturally distinguishing as they directly affect decisions related to the habitat architecture.

Specifically, facilitating frequent EVA requires the appropriate selection of the total pressure and composition of the operating atmosphere for the habitat in order to manage crew pre-breathing times prior to EVA [112]. This in turn affects fire safety risk, as well as structural mass of the habitat pressure vessel, both in terms of withstanding the hoop stress imposed by the atmosphere on the habitat as well as the mass of an airlock or other system for facilitating the transfer of crew into and out of the habitat (e.g. suitlocks or suitports) [110].

Additionally, the mission-type influences the internal layout of the habitat as well as the modularity and expandability of its architecture. In particular, a habitat designed for a sortie-class mission would likely have a more integrated and compact layout due to the overriding need to minimize mass. Conversely, a habitat deployed for an outpost would have mechanical interfaces in the form of either nodes or docking ports to allow for the delivery of logistics modules and the expansion of pressurized volume over time – in a manner similar to that of the International Space Station. As the outpost grows in volume, the internal layout will

become more clearly delineated into functional zones [113] (such as work and living spaces) to increase the habitability and operational efficiency of the outpost.

The significant impact of these two sub-decisions on habitat architecture provide a basis from which we can develop a classification scheme for space habitats, and the human spaceflight missions that they are intended to support. Figure 3-8 depicts the resulting classification matrix, where each quadrant of the two-by-two matrix represents a category of spaceflight mission. Within each of these quadrants, an image of a recently proposed mission concept that matches with the given category has been included as a representative example.

From Figure 3-8, it can be seen that the proposed space mission classification scheme captures the majority of the types of missions that have been proposed within recent years, ranging from the fly-by type missions typified by Dennis Tito's Inspiration Mars proposal [114], to the space hotel concepts proposed since the late 1960s [115,116] . In addition to these proposed commercial space ventures, mission concepts developed by government agencies are also captured, including the exploration missions developed within the NASA Mars Design Reference Missions, and the Permanent Presence class missions that have recently been proposed.

Within this classification matrix, each quadrant represents a "mode" of habitation and by extension, a "mode" of human spaceflight. As was the case with the evolution of human spaceflight in near Earth space (from Alan Shepard's initial sub-orbital "fly-bys" to the sorties of the Space Shuttle era and to our current era of sustained presence onboard the ISS); achieving the ultimate goal of developing a continuous human presence on the surface of Mars will require transitioning through some subset of the spaceflight modes depicted in Figure 3-8 towards the Permanent Presence Mode in the lower right hand quadrant. While the case studies examined in this thesis will focus exclusively on Permanent Presence Mode habitation scenarios, HabNet will be developed with the intention of being generalizable across all of the habitation modes classified in Figure 3-8, in order to facilitate future analyses of the architectural implications of transitioning between various habitation modes. This will be accomplished by mapping the structure of HabNet to the generalized ADG for human spaceflight developed in Section 3.1.1.

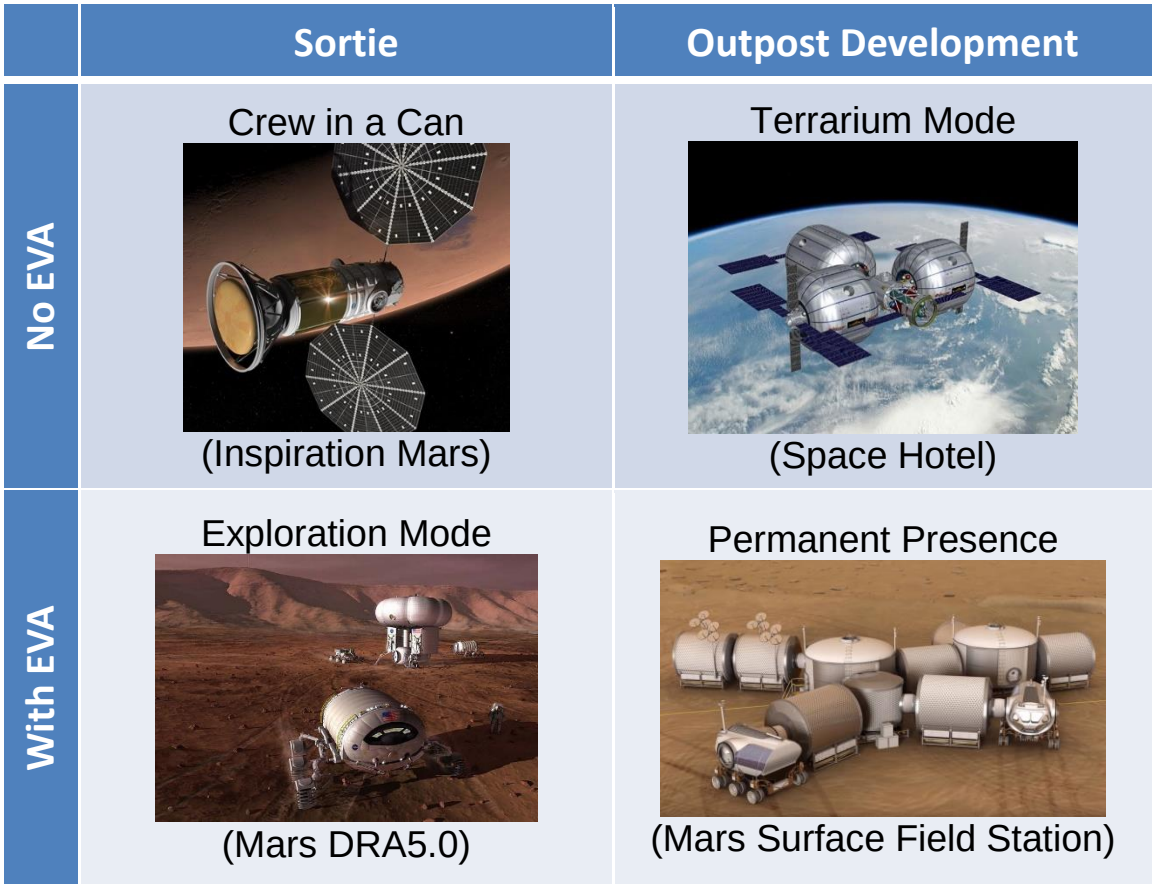

Figure 3-8: The Four Classes of Space Habitation (clockwise from top left): (1). Crew in a Can: Inspiration Mars is a Mars flyby mission proposed by Dennis Tito in 2013 [114]. (2). Terrarium Mode: Space Hotels have been proposed for a number of years. Bigelow Aerospace has proposed the development of commercial space stations in Low Earth Orbit [117]. Potential applications include space hotels [115,116]. (3). Exploration Mode represents the typical class of sortie mission to an exploration destination mission, such as the opposition and conjunction class missions to Mars [20] (4). Permanent Presence missions are those that involve the investment of infrastructure at one long location over a campaign of missions with the ultimate goal of supporting the continuous presence of humans at that location [42]

3.2 Formulating the High Level HabNet Structure

With an Architecture Decision Graph for Human Spaceflight Systems established, we now formulate the high level structure of HabNet. This is performed by extracting the HabNet-specific decision sets identified in Section 3.1.2, along with the dependencies between them, and further decomposing them to a level where decisions can be parameterized and assigned with quantitative values. This process is depicted in Figure 3-9, where each colored line linking

the ADG to the block diagram represents a direct connection between an architectural decision and an input parameter defined for HabNet.

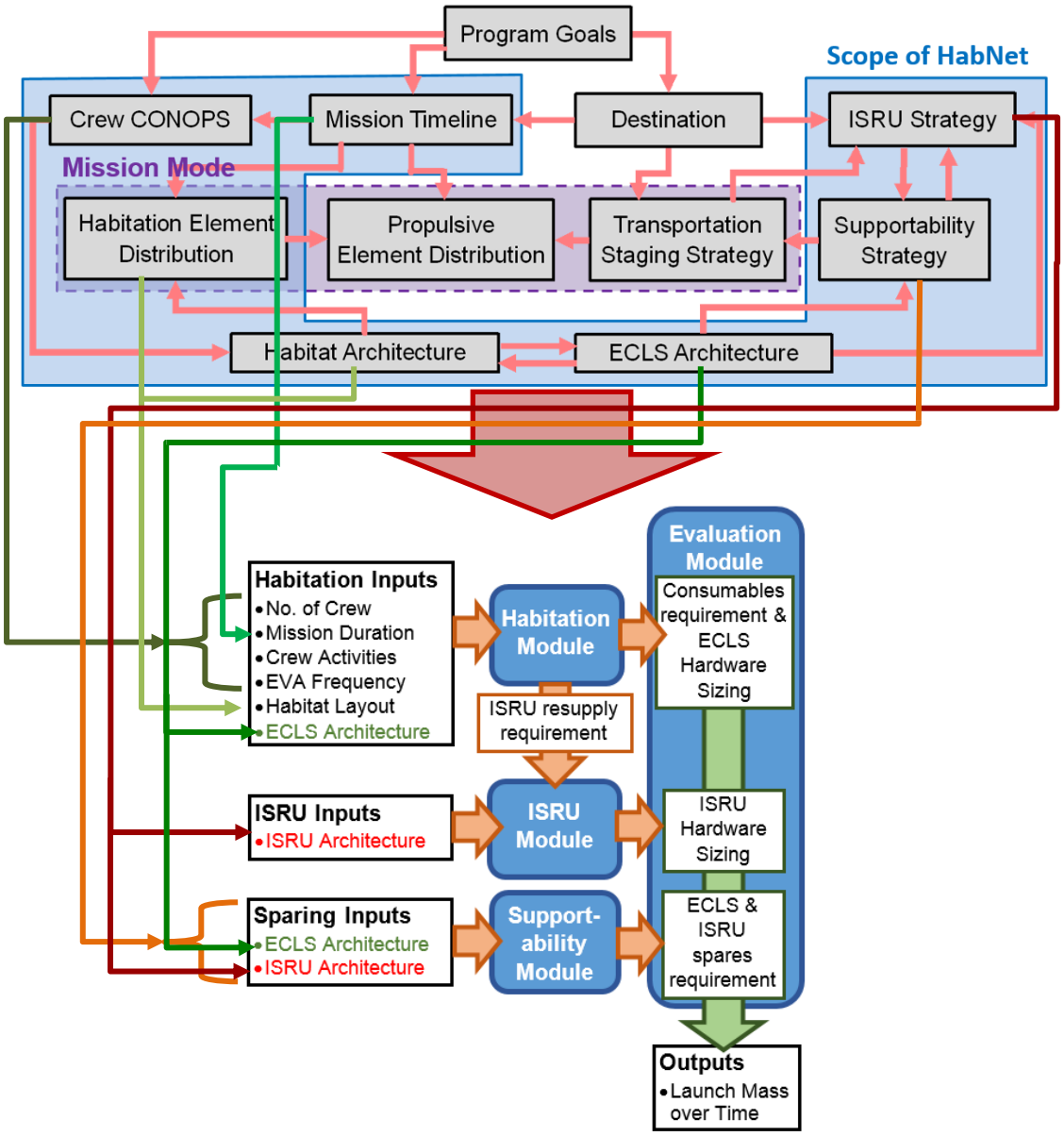

Figure 3-9: Derivation of the High Level HabNet structure from the Human Spaceflight ADG

As can be seen in the lower half of Figure 3-9, this process has resulted in four major modules that together, make up HabNet. Here, decisions related to the Mission Timeline, Crew CONOPS, Habitat Architecture, and the ECLS Architecture have been combined to form the Habitation Module of HabNet. Conversely, the remaining decisions related to the ISRU and

Supportability Strategies have been assigned their own modules, due to their lower level of coupling with other architecturally distinguishing decisions.

To model a particular mission scenario, these three modules are initialized by inputting values corresponding to each of the key architectural decisions that they represent. Specifically, the Habitation Module takes in key mission parameters related to the Crew CONOPS and Habitat and ECLS Architectures as its inputs, and outputs the consumables requirement and the sizing for the ECLS hardware used. Additionally, the Habitation Module feeds an ISRU resupply requirement to the ISRU Module, which combines this information with the selected ISRU architecture to predict the mass and volume of the required ISRU hardware. In parallel, the Supportability Module takes reliability, maintenance, and repair information regarding the selected ECLS and ISRU architectures and outputs the number and type of spares required for both systems. Finally, the remaining module, entitled the "Evaluation Module", integrates the information outputted by the three pre-processing models to predict the required mass delivered to the exploration site over time to sustain the habitation system being assessed. This final module represents the remaining transportation-related decisions within the greater human spaceflight ADG. In a typical end to end mission analysis, this mass delivery profile would be fed into an analysis of the in-space transportation architecture and used to size the transportation systems required to accommodate this profile. An example of such an analysis is presented in Chapter 5.

3.3 Modeling the Systems Architecting Process as a Technology Selection Problem

In the previous section, we defined the initial inputs to HabNet as being the choice of ECLS and ISRU architecture. As was discussed in Section 2.1.1, the definition of an ECLS architecture entails the selection of a set of technologies to serve the long-duration ECLS functions listed in Table 2.1. Similarly, the definition of an ISRU architecture consists of selecting technologies based on known chemical reactions to convert locally available resources into required consumables (or perhaps even building materials and feedstock for local manufacturing, which are not considered in this thesis). As a result of these observations, we conclude that from the standpoint of identifying input parameters for the construction and simulation of proposed habitation architectures, the architecture definition process can be

modeled as a technology selection process. In the following sections, we further explore the implications of this observation from the perspective of classifying the types of technology selection problems that might be encountered when performing systems architecture studies with HabNet, as well as the software implementation of the technology selection process in a scalable and evolvable manner.

3.3.1 Categorization of Technology Selection Problems

An interesting outcome of formulating the architecture definition process as a technology selection problem is the ability to now categorize the problem being addressed by the specific decisions that need to be made. Based on a review of the different types of studies that have been performed to evaluate technologies and architectures in various space mission contexts, we have formulated the following classification for the different types of technology selection problems. We refer to this classification as: "The Four Classes of the Technology Selection Problem". As depicted in Figure 3-10, this classification is performed along two dimensions: the feasibility vs sensitivity dimension, and the forward vs reverse dimension.

The feasibility versus sensitivity dimension distinguishes between instances when either an architecture (or a set of technologies) is being investigated, or whether the impact of the introduction of a single technology on an architecture is being studied. Contrastingly, the forward versus reverse dimension differentiates between whether the goal of the analysis is to find a solution that either best meets some objective, or seeks to satisfy some predefined constraint.

	Forward	**Reverse**
Feasibility	**Forward Problem** *Feasibility Testing* Can a set of technology options meet system requirements?	**Reverse Problem** *Isoperformance Analysis* What are all the sets of technologies that can meet a given set of system requirements?
Sensitivity	**Sensitivity Problem** *Technology Impact Assessment* What is the impact of introducing a new technology on the overall system performance?	**Reverse Sensitivity Problem** *Technology Development Guidance* What are the requirements for a specific technological concept to meet a given level of system performance?

Figure 3-10: The Four Classes of the Technology Selection Problem

We further expand on each of these four classes as follows:

- The Forward Problem: The objective of this type of problem is to test the feasibility of a preselected system architecture. A typical example of a forward problem would be when an ECLS architecture for say, a lunar surface habitat, has been proposed [118]. Here, the architecture is sized such that it can meet mission objectives (e.g. sustain a given crew size over a predefined period of time). From this, the resulting Equivalent System Mass (ESM) is calculated
- The Reverse Problem: This problem typically arises when some sort of budget has been assigned to a particular system. That is, the development of a system might need to meet a certain predefined mass, volume, and power budget. One such example is the development of a crew return vehicle such that its mass and outer mold line fit within the constraints imposed on it by the payload capacity of a given launch vehicle and its fairing geometry [119]
- The Sensitivity Problem: This problem assumes that a preexisting, well established architecture exists. The goal of this class of problem is to investigate the impacts on the performance of the preexisting system when a new technology is introduced. One such example might be a study on the impact of introducing a Cascade Distillation System-based Urine Processor Assembly unit [120,121] on the ISS water balance. This type of problem is sometimes referred to as a technology infusion problem [122]
- The Reverse Sensitivity Problem: This class of problem is essentially a reframing of the Sensitivity Problem, whereby the goal is to characterize the top level requirements for a yet-to-be-developed technology to meet prespecified requirements for an existing, well-established architecture. One such example might be the development of requirements for a laundering machine for the ISS such that its overall ESM is less than that of the current open-loop clothing system [123]

As can be seen from the above examples, the type of problem classification is dependent on the specific proportion of well-established versus newly-developed elements incorporated into the proposed system architecture. Current proposals for Mars surface architectures involve ECLS technologies that are largely based on the ISS ECLS architecture [58], with ISRU technologies that are still very much in development. As a result, the case studies explored in this thesis will be based on the forward class of problems when investigating ECLS architectures, and the reverse class of problems when evaluating ISRU architectures. As more

technological concepts are matured in the future, it is anticipated that a larger variety of problems that span the four classes described above will become more prevalent.

3.3.2 Object Oriented Programming and the Technology Concept Template

Earlier in this section, we observed that the architecture definition process could be modeled as a technology selection process. In HabNet, this process is implemented through the development of libraries of ECLS and ISRU technology models from which proposed system architectures are built and simulated. As more data becomes available on evolving ECLS, ISRU and other surface habitation and exploration technologies over time, it is expected that these technology libraries within HabNet will evolve and expand accordingly. Consequently, to streamline the input and management of these technology libraries, we have developed a generalized, common representation scheme for all technologies based on the syntax and rules of the Object Process Methodology (OPM) [124] – a generalized system architecture description language that explicitly represents system function and form (see Appendix A for a summary of the main constructs within OPM).

This representation scheme is referred to as the Technology Concept Template, and is built upon the basic notion that all technologies can be represented in the same manner at some level of abstraction. This level of abstraction is the level at which an engineering concept is selected – that is, when some decision is made to accomplish some defined function with some form of engineering system. In OPM, a function is represented as a process acting on an object to change its state [124], as indicated in the light-orange labeled box within Figure 3-11(b). This state-changing object is sometimes referred to as the operand, as it is changes in this specific class of object that yield value to the beneficiary. One such example of an operand is the atmosphere within an enclosed habitat. Value is generated when the process of CO_2 removing is performed on the atmosphere to change its state from having a high partial pressure of CO_2, to a state in which its CO_2 partial pressure is low. This example is depicted in Figure 3-11(c).

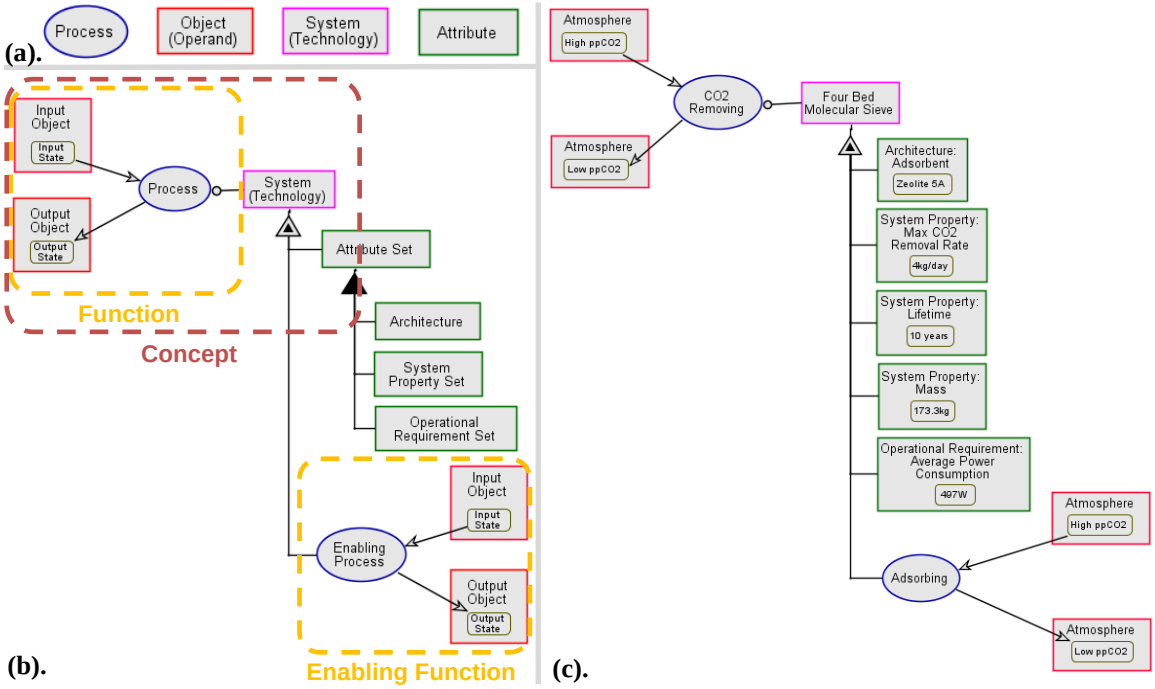

Figure 3-11: (a). The Elements of the Technology Concept Template (b). The Technology Concept Template (c). A simplified Technology Map corresponding simplified representation of a Four Bed Molecular Sieve (4BMS) (data here was obtained from Wieland et al. [44]. See Appendix A for a summary of the main elements of OPM)

Once a function is identified, a technology (either existing or yet-to-be-developed), is selected to satisfy it. This selection process is indicated by the "lollipop" symbol connecting the process symbol (blue ellipse) and the system symbol (pink rectangle) in Figure 3-11(b). Each technology has a set of attributes, and performs some operation, or enabling function(s), that allows it to accomplish the original function for which it was selected. These attributes can be classified as either its architecture, its system properties, or its operational requirements.

Architectural attributes are those that the designer has control over, such as the sizing of its geometry. These can be thought of as the elements of the system's design vector. System properties are those that emerge from the selection of architectural attributes, such as its performance and its operational lifetime. Finally, operational requirements represent the operational conditions that need to be maintained in order for the system to operate. Examples of these include power and thermal control requirements. This specific class of attributes typically requires some derived process to maintain their value, hence allowing the system to operate within a safe envelope. Examples of derived processes include the provision of power, thermal control and structural support.

In addition to exhibiting attributes, a technology also performs some operation to enable it to meet the function for which it was originally intended. In physicochemical ECLS and ISRU technologies, these operations tend to be reactions or separations that either generate useful products, or remove undesired components from some waste stream. These operations commonly require other operands in order to enable the system to perform its original functions. Such operands can be considered as consumables that a technology might require. In some cases, this operation is the same as the function that the system was chosen for. We explicitly represent both the original and the enabling functions, since the former represents the original requirement, while the latter represents the manner in which the original requirement is met through the selection of a particular system. When combined together, each of the aforementioned elements forms the Technology Concept Template, shown in Figure 3-11(b). When the Technology Concept Template is applied to a particular technology, the result is referred to as a Technology Map. Figure 3-11(c) presents a simplified example of the Technology Map of a Four Bed Molecular Sieve – a system intended to remove CO_2 from the atmosphere of a pressurized habitat.

With the Technology Concept Template now established as a common representation scheme for all elements within the HabNet technology library, we now derive an equivalent software structure to digitally store all information represented within instances of the technologies represented by the template.

The process of selecting and instantiating multiple instances of various classes of technology from a model library naturally lends itself to an object-oriented programming framework. As a result, we adopt this object-oriented framework for HabNet, and structure the class definitions of the software objects within HabNet to coincide with the information fields of the Technology Concept Template. Figure 3-12 depicts the direct mapping between the Technology Concept Template and the basic class definition that has been developed for a software object within HabNet's technology library.

In general, a software object consists of a set of properties that store information that is unique to that object, and a set of methods that perform functions on the stored properties. From the pseudocode for the software object in Figure 3-12, it can be observed that all operands (red boxed elements) from the Technology Concept Template have been stored within the (public) properties field of the software object, while all Technology Concept Template

attributes (green boxed elements) have been stored in a private properties field within the software object.

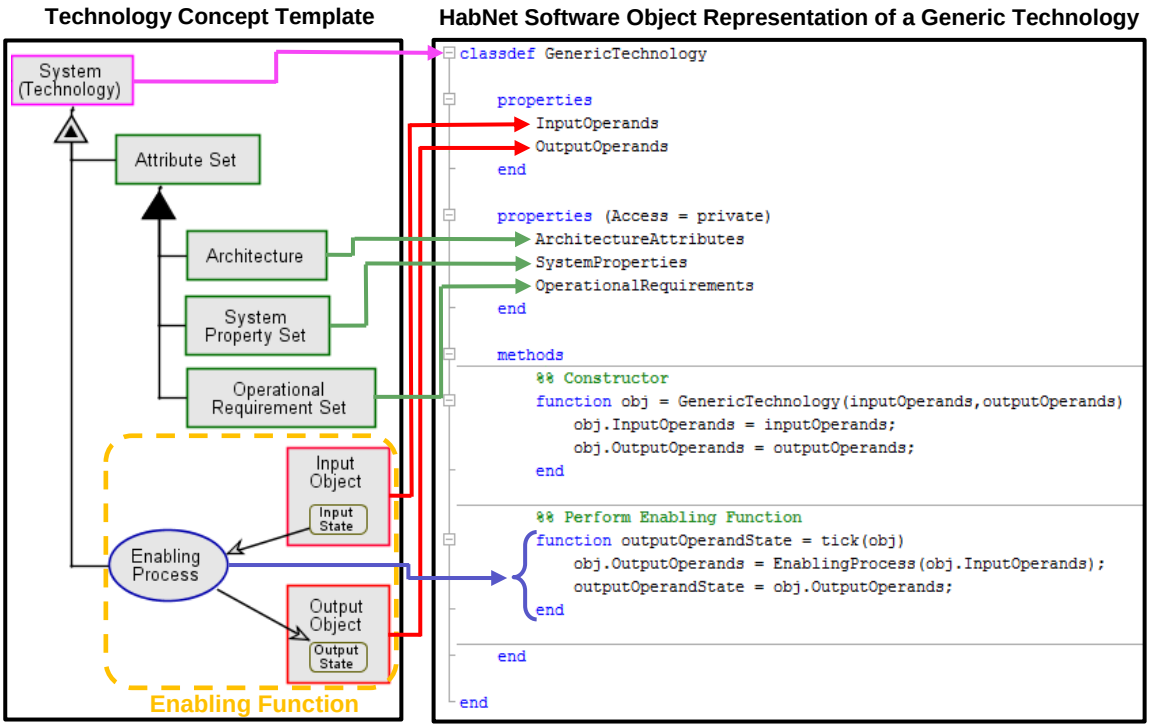

Figure 3-12: Mapping from the Technology Concept Template to an Object-Oriented Programming Object

This allocation is based on the fact that operands are typically manipulated by multiple technologies, and are therefore required to be accessible by software objects other than the software object in which the operand is stored. Conversely, information related to the attributes of a technology (the green boxed elements of the Technology Concept Template) are unique to that technology and should only be accessible from within that technology. Thus, they have been stored within a private properties field within the software object.

In addition, we observe from Figure 3-12 that the enabling process of the technology is modeled as a method entitled “tick” within the software object. During the simulation of a technology, the tick method is called to activate its enabling process in order for it to serve its required function. In a dynamic simulation, this method is called every time step. Moreover, to simulate control logic embedded within a technology, logical conditions can be incorporated within the tick method to manipulate the states of the output operands based on variations in the states of the input operands.

Thus, in order to build the HabNet technology library, information regarding each technology is first extracted and placed into the Technology Concept Template. From this, the equivalent software object is developed for the technology based on the mapping scheme depicted in Figure 3-12. When defining an architecture, this software object is accessed from the HabNet technology library and an instance of the object is created. Finally, during the simulation of an architecture, the "tick" methods of each software object are accessed to simulate the execution of the enabling function(s) of each technology. The development of the HabNet ECLS and ISRU technology libraries are further discussed in Appendices B to F.

3.3.3 The Fundamental Functions

In the previous section, we defined a function as a process acting on an object to change its state. We also discussed how at the abstract level of generic functions and systems, all technologies could be represented in the same manner. Recent insights into the nature of engineering systems have postulated that at this abstract level, the set of all possible objects and processes may be classified into five distinct categories [125]. These categories, and examples of systems that accomplish the resulting function, are listed in Table 3.2.

Table 3.2: Fundamental Object and Process Set adapted from de Weck et al. [125]. The first row lists the classes of fundamental objects and the first column lists the classes of fundamental processes. Elements listed within the table are examples of systems that accomplish the functions derived from combining object-process pairs

Objects / Processes	Living Organisms	Matter	Energy	Information	Money
Transforming	Hospital	Blast furnace	Engine, electric motor	Analytical engine, calculator	Bureau of Printing and Engraving
Transporting	Car, airplane, train	Truck, train, car, airplane	Electricity grid	Cables, radio, telephone, Internet	Banking Fedwire and SWIFT transfer systems
Storing	Farm, apartment complex	Warehouse	Battery, flywheel, capacitor	Magnetic tape and disk, book	US Bullion Repository (Fort Knox)
Exchanging	Plant Swap	eBay trading system	Energy market	World Wide Web, Wikipedia	London Stock Exchange
Controlling	US Constitution and laws	Hoover Dam	Nuclear Regulatory Commission	Internet Engineering Task Force	United States Federal Reserve

The fact that all possible functions can be limited to a finite set of 25 possibilities (the product of five objects and five processes) has significant implications on the use of the Technology Concept Template. This is because a finite set of objects and processes results in a finite set of entries into the template, resulting in a finite set of abstracted technology concepts. This finite space of concepts consequently makes the problem of exploring all feasible architectural solutions for a given problem more tractable. Unambiguous rules can be written to dictate connections between specific classes of technology concepts, thereby allowing for architectures to be computationally synthesized.

An illustrative analogy for this scenario is the written English language. Written language is composed of a finite set of letters, which form the alphabet. This set is analogous to the individual elements of OPM – the objects, processes, and states. Through a set of spelling rules, letters are combined to form words, as our technology template is used to combine OPM elements to form technologies. Now, words can be classified as articles, nouns, verbs, adjectives, and so on. In the same way, the fundamental set of functions can be used to classify technologies into either "Living Organism Transformers" (element (1,1) of Table 3.2), "Energy Storers" (element (3,3) of Table 3.2), or any of the others listed in Table 3.2. Different classes of words can then be used to form sentences with the aid of grammatical rules. Similarly, with the aid of an analogous "architectural grammar", different classes of technologies can be connected with each other to automatically synthesize architectures. While the development of this "architectural grammar" is beyond the scope of this thesis, the adoption of the Technology Concept Template as a common means to represent and model technologies provides an avenue for the future addition of this capability to the current HabNet architecture.

3.4 HabNet Module Development

In Section 3.2 we derived the high level structure for HabNet (see Figure 3-13 below) based on the Human Spaceflight Systems Architecture Decision Graph developed in Section 3.1.1, and described the high level interaction between the four main modules of this structure. In the following sections, we describe each of the components of these four modules in further detail. Specific details regarding the implementation of these modules are described in Appendices B to F.

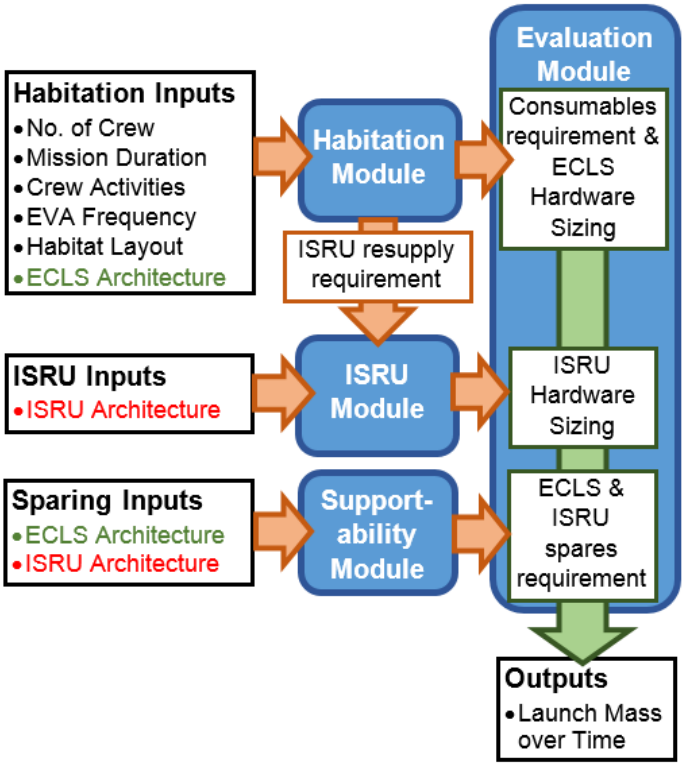

Figure 3-13: The High Level HabNet Structure

3.4.1 Habitation Module

One of the main conclusions drawn from the literature review conducted in Chapter 2 was that an integrated architectural analysis of long-duration mission scenarios requires a balance between being able to model a broad range of architectural options, while simultaneously being capable of capturing the dynamic complexity inherent within human spaceflight systems.

These requirements arise from the fact that supportability analysis is fundamentally based on understanding the impacts of system degradation and failure over time, so that mitigation and recovery strategies can be determined. In spaceflight systems, hazardous conditions arise from unanticipated dynamic interactions between the spacecraft, the internal and external environment, and the crew. Moreover, these interactions typically occur over short time scales, on the order of minutes to hours. Consequently, a modeling capability that captures dynamic behavior at time scales of minutes to hours is required to facilitate combined operations and supportability analysis.

In addition, the large combinatorial space of architectural and operational decisions required to define a spaceflight architecture (see ADG in Figure 3-4) suggests that a fast

simulation execution time is required to explore the impact of the numerous architectural options. Due to limitations in computational speed, this equates to some sacrifice in modeling fidelity, which for our purposes, is acceptable since we are primarily interested in understanding the high level system impacts of key architectural decisions.

In this section, we develop the HabNet Habitation Module based on these requirements. As was described in Section 3.2, the main role of the Habitation Module is to predict the requirements for both Earth-derived and ISRU-derived consumables based on architectural decisions related to the Mission Timeline, Crew CONOPS, Habitat Architecture, and ECLS Architecture. These consumables requirements are then used by other HabNet modules to size the required ISRU systems and to compute lifecycle logistics resupply or pre-positioning requirements.

We begin this development process by surveying the existing habitation and life support modeling and sizing tools. Here, we are particularly interested in understanding how the currently available analysis tools perform in terms of the two requirements specified above – that is, their modeling fidelity and computational speed. Table 3.3 summarizes the findings of this survey.

The results in Table 3.3 reveal that there are currently only a handful of existing habitation and life support modeling and sizing tools. Of these, even fewer meet the aforementioned requirements for a fast, dynamic simulation environment. Here, it can be observed that most existing habitation and life support tools sit on either extreme of the fidelity/speed spectrum. They are either fast, steady state, and relatively low-fidelity flowsheeting tools intended for preliminary analysis and sizing; or high fidelity, dynamic simulators intended for detailed controls and operations studies of one particular ECLS architecture. In some cases, these dynamic simulators can take up to a few weeks to produce results, and are hence not suited for systems-level analyses.

The one exception to these observations is BioSim [126], an open-source software package that was originally developed in the early 2000s at NASA Johnson Space Center to support integrated ECLS controls research. As can be seen in Table 3.3, BioSim is a mid-fidelity dynamic simulator with execution times on the order of tens of seconds. This relatively fast execution time is enabled by employing a simple Euler time stepping scheme to model system dynamics, and by making the simplifying assumption that all processes are isothermal, such that only mass balance calculations are required.

Table 3.3: A Survey of Existing Habitation and Life Support Modeling and Sizing Tools

Modeling Tool (Software Language)	**Year of First Publication**	**Summary**	**Steady State or Dynamic Analysis?**	**Modeling Fidelity**	**Function Evaluation Time (for a 90 day mission)**
Target for HabNet	2015	For tradespace exploration	Dynamic	Medium	O(10 seconds - minutes)
ALSSAT (Microsoft Excel) [127]	1998	NASA Standard Tool. Spreadsheet-based. Contains a database of NASA ECLS technology that is regularly updated	Steady State	Low-Medium	O(1 second) *"tens of thousands of life support configurations in a matter of hours"*[128]
EcoSimPro (Custom Environment) [129]	2003	ESA Standard Tool, used for ISS Columbus Module. Commercially available. Intended for detailed ECLS controls and operations analysis.	Dynamic	High	O(weeks) *"the ratio between CPU time consumed and total simulated time, has been around 17%."* [130]
BioSim (Java) [131]	2003	Developed by TracLabs (NASA JSC Contractor) exclusively for integrated ECLS controls research	Dynamic	Medium	O(10 seconds) *"approximately 200 simulation hours per second on a single PC"* [131]
V-Hab (MATLAB) [132]	2006	Developed at TU Munich. Includes detailed human model. Intended for detailed ECLS operations analysis	Dynamic	High	O(1 week) *"2 hours of simulated time takes about 10 minutes to simulate"* [133]
ELISSA (LabView) [134–136]	2001	Developed at Univ. Stuttgart as a preliminary ECLS sizing tool. Built in LabVIEW	Dynamic	Medium-High	O(1 hour) *"approximately 1 minute for each simulated day"* [137]

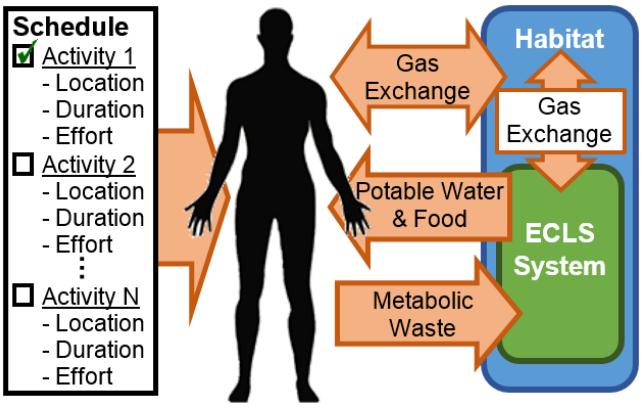

Figure 3-14: Data flow within the Habitation Module

Given the similarity between BioSim's attributes and our own modeling requirements (listed in the green row in Table 3.3), and the fact that it is freely available under the GPL3.0

open source license, we have chosen to use BioSim's software architecture as the basis of the habitation modeling portion of HabNet. Specifically, we have tuned the suite of BioSim technologies to behave in the same manner as the set of currently existing ISS life support technologies and ported the BioSim architecture into the MATLAB environment so that other HabNet modules depicted in Figure 3-13 can be integrated. A high level summary of the data flow within the Habitation Module is presented in Figure 3-14.

As can be seen in Figure 3-14, the first input to the Habitation Module is the assignment of a schedule to each crewmember (i.e., the Crew CONOPS). The schedule consists of a set of activities, each with its own location, duration, and effort level. Here, the minimum duration of an activity is fixed to one hour – a value that corresponds to the simulation time step adopted within the HabNet Habitation Module, and one that is within the same order of magnitude as the time scale of the dynamic interactions described earlier. Here, the fixed time step length of one hour was chosen as a compromise between capturing the major dynamics of metabolic resource exchanges within the operation of a habitat over the course of a mission, and the computational cost of simulating these dynamic interactions.

As the simulation propagates forward in time, each crewmember progresses through their own schedule, expending varying levels of effort, which in turn varies their resource consumption and metabolic exchange rates with the habitat. Here, the model developed by Goudarzi and Ting [138] is used to determine crew resource demands based on their activity level and their basal metabolic rate, which is driven by their gender, age, and body mass. The implementation of this model is described in further detail in Appendix C.3. In the case of multi-module habitats (see Appendix B.2 for a discussion on how these are modeled within HabNet), activities can be allocated to individual locations, thus allowing the crew to move throughout the habitat as they work through their activity list. Through the introduction of varying effort levels and activity locations, transient behavior is introduced into the habitation simulation environment.

Predefined ECLS technologies modeled within this module act to manage this transient behavior by controlling resource consumption and production to the levels appropriate for maintaining crew health. The user allocates these ECLS technologies to different modules within the habitat, which in turn, handle varying crew metabolic waste loads as each crewmember moves through a given habitat module. Table 3.4 summarizes the ECLS technologies currently modeled within HabNet, and the sections in this thesis where their implementation within HabNet is further detailed.

Table 3.4: Summary of the ECLS Technologies Currently Modeled within HabNet

ECLS Function	Technology	Based On	HabNet Class Name	For details see:
Resource Storage				
Resource Containment	Tanks (both rigid and soft goods)	ISS Resource Containers, including High Pressure Gas Tanks (HPGTs), Contingency Water Containers (CWC), and Advanced Recycle Filter Tank Assemblies (ARFTAs)	Store	Appendix D.1
Atmosphere Revitalization (AR)				
Carbon Dioxide Removal	Four Bed Molecular Sieve (CO_2 Adsorption with Zeolites)	ISS Carbon Dioxide Removal Assembly (CDRA)	ISSVCCRLinear	Appendix D.4
Oxygen Generation	Solid Polymer Water Electrolysis	ISS Oxygen Generation Assembly (OGA)	ISSOGA	Appendix D.5
Carbon Dioxide Reduction	Sabatier Reactor	ISS Carbon Dioxide Reduction System (CRS)	ISSCRS	Appendix D.7
Atmosphere Control and Supply (ACS)				
Atmospheric Pressure Containment	Habitat Modules	Rigid Space-rated Habitable Pressure Vessels	SimEnvironment	Appendix B.1
Pressure Control	Pressure Control Venting and Relief Valves fed by High Pressure Gas Tanks	ISS Pressure Control Assembly (PCA)	ISSInjector	Appendix D.2
Temperature and Humidity Control (THC)				
Humidity Control	Intramodule Fans and Condensing Heat Exchangers	ISS Common Cabin Air Assembly (CCAA)	ISSDehumidifier	Appendix D.3
Ventilation	Intermodule Ventilation Fans	ISS Intermodule Ventilation (IMV) Fans	ISSFan	Appendix B.3
Water Recovery and Management (WRM)				
Water Processing	Multifiltration, Catalytic Oxidation, Ion Exchange	ISS Water Processor Assembly (WPA)	ISSWaterRSLinear	Appendix D.6
Urine Processing	Vapor Compression Distillation	ISS Urine Processor Assembly (UPA)	ISSWaterRSLinear	Appendix D.6
Food Storage and Preparation				
Biomass Production	Hydroponics under Artificial Lighting	NASA BIO-Plex Food Growth Chamber	ShelfImpl	Appendix D.8

Once running, one of two conditions terminates the simulation. The first is if one of the pre-specified failure conditions is met, while the second occurs when the simulation uneventfully reaches the end of the specified simulation time horizon without meeting any of these failure conditions. In the former case, a failure occurs due to the depletion of one or more resource stores, which in turn leads to insufficient resources available for crew consumption. In addition to the resource consumption rates of the crew, this resource management is strongly influenced by the control logic encoded into each of the modeled ECLS technologies (see Appendix D for details).

Furthermore, the amount of simulated time that passes before the onset of a failure informs the actions that are taken to rectify the experienced failure. In the case that the failure occurs early in the simulation, an architectural change for the ECLS system is typically required. Conversely, failures that occur later in the simulation time horizon are typically rectified by introducing some source of additional resources. These can come from either an ISRU technology, from a logistics resupply source, or by increasing the initial amount of resource carried. The failure conditions employed within the Habitation Module are summarized in Table 3.5.

Table 3.5: Failure Conditions Employed within the HabNet Habitation Module

Failure Condition	**Model Implementation**
Crew starvation	When a predefined aggregate caloric deficit (the difference between crew caloric consumption requirements and calories available within the food store) is reached. The default value assumed within HabNet is 180,000 kilocalories. This value can be changed accordingly to match the gender, body weight, and other attributes of the simulated crew
Crew dehydration	Crew water requirement is greater than potable water available within potable water store
Crew hypoxia	Partial pressure of oxygen within crew environment is less than 15.168kPa [139]
Crew hyperoxia	Molar fraction of oxygen within crew environment exceeds 50% (for a 70.3kPa atmosphere) [139]
Crew CO_2 poisoning	Partial pressure of CO2 within crew environment is greater than 0.482kPa (0.07psi) [139]
Cabin underpressure condition	Total cabin pressure is less than 20.7kPa (3psi) [139]
High Fire Risk	Molar fraction of oxygen within crew environment exceeds 30% [140]
Crop Death	CO_2 concentration within plant growth environment reduces below 150 parts per million (ppm) [141,142]. When crop death occurs, the crew consumes food from the prepackaged food store until crop growth can be recovered.

3.4.2 In-Situ Resource Utilization (ISRU) Module

To estimate the size of the ISRU technologies needed to satisfy the consumables demands predicted by the Habitation Module, an ISRU sizing model library was developed and integrated into the HabNet framework. As was mentioned in Section 3.2, this ISRU Module receives information regarding the ISRU architecture (i.e. the selection of ISRU technologies) and the consumables production rate requirement from the Habitation Module. From this input, the ISRU module predicts the mass, power, and volume requirements for the chosen ISRU technologies so that their contribution to the emplacement and sustainment cost of a campaign of missions can be evaluated.

The HabNet ISRU Module was initially developed by Schreiner [143], and later extended by Schrenk [144] to encompass a broader range of ISRU technologies. Currently, the model library within the ISRU Module consists of only Mars-based ISRU technologies. Here, only technologies related to resource processing are modeled. Technologies related to other parts of the "Space ISRU Mining Cycle" discussed in Section 2.2.3, such as resource mining, transportation, and beneficiation are not currently included. Table 3.6 summarizes the technologies currently modeled within the ISRU Module.

Table 3.6: Summary of Technologies Currently Modeled within the HabNet ISRU Module

ISRU Function	**ISRU Technology**	**Governing Reaction**
Water Extraction / Production	Soil Processor	Hydrated Soil → H_2O + Dehydrated Soil
	Sabatier Reactor	$CO_2 + 4H_2 \rightarrow CH_4 + 2H_2O$
	Reverse Water Gas Shift Reactor	$CO_2 + H_2 \rightleftharpoons CO + H_2O$
CO_2 Extraction	CO_2 Cryocooler	Mars Atmosphere → CO_2 + N_2 + Ar + Unused Products
Inert Gas Extraction	Atmospheric Processor	
Oxygen Production	Water Electrolyzer	$2H_2O \rightarrow 2H_2 + O_2$
	Solid Oxide CO_2 Electrolyzer	$2CO_2 \rightarrow 2CO + O_2$

The technology models listed in Table 3.6 were derived from first-order process flowsheets developed for each technology. These describe the components and the component interactions that enable each of the unit operations required to convert the input reactants into the desired

output products. Once all components were identified within a technology, their operational and sizing requirements were estimated using a combination of physics-based equations, and sizing by analogy to similar systems. The resulting sizing equations were then compared to sizing estimates of corresponding technologies within the literature, and correction factors were developed and applied to account for any observed discrepancies. The development and correlation of the sizing equations for each of the technologies listed in Table 3.6 are described in detail by Schrenk [144], and are summarized in Appendix F.

In addition to these equations, the ISRU Module also contains an optimizer that automatically searches and generates feasible ISRU system architectures based on a set of input resource demands. This optimizer was also developed by Schrenk [144], and is based on the application of the Design Structure Matrix (DSM) methodology to the chemical reactions that govern each of the ISRU technologies listed in Table 3.6. Once all feasible ISRU system architectures are generated, the user has the option of executing an additional optimizer that exhaustively searches through the feasible set of architectures for the architecture with the minimum total system mass, and the minimum number of system elements. Figure 3-15 depicts the feasible connections that are present within the set of ISRU technologies modeled. Here an architecture is defined as the activation of a subset of these connections and an assignment of resource flowrates through them, based on an input vector of resource demands.

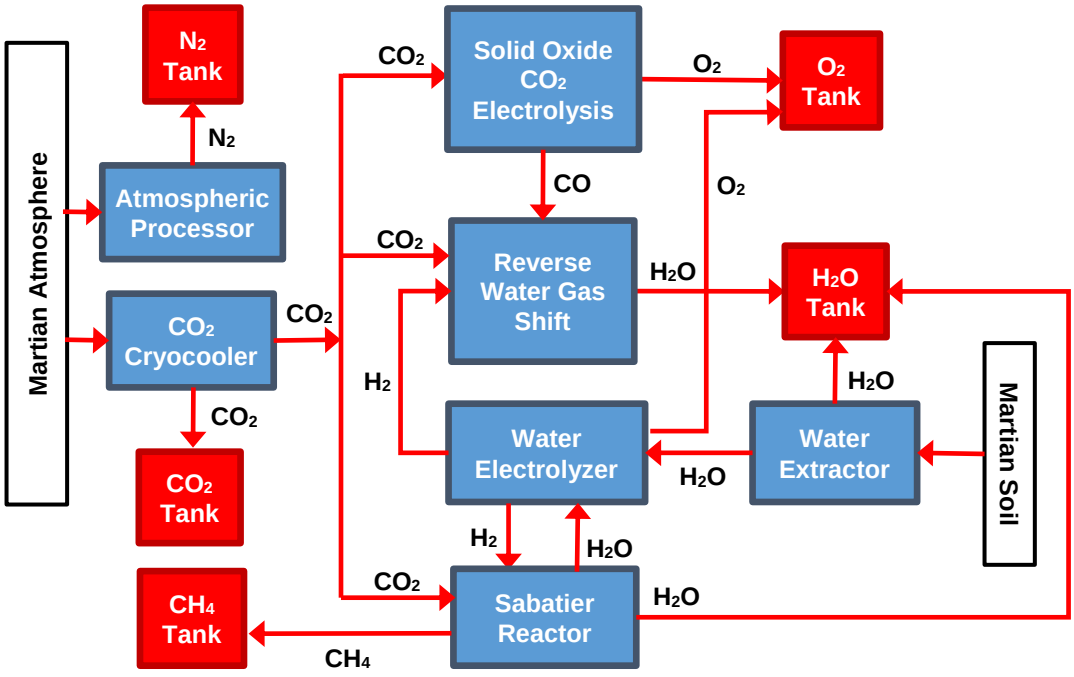

Figure 3-15: Feasible connections between the technologies currently modeled within the HabNet ISRU Module [144]

Finally, since the scale of ISRU technologies required to generate a given amount of resources is strongly dependent on the availability of resources at the operational site, the HabNet ISRU Module contains an internal map of resources on Mars. This map relates a particular location on the planet, as measured by its longitude, latitude, and altitude, to the water content, heat capacity and density of the local soil, as well as the ambient atmospheric temperature and pressure. Also developed by Schrenk [144] for incorporation within the HabNet ISRU Module, this resource map is based on a combination of:

- Mars Orbiter Laser Altimeter (MOLA) data for elevation information [145]
- Mean annual surface temperature predictions derived by Mellon et al. [146]
- Regolith property distribution data based on surveys performed by Mellon et al. [146] and Grott et al. [147]; and
- Multi-depth water equivalent hydrogen (WEH) data based on the analysis of data from the Gamma Ray Spectrometer (GRS) suite onboard the Mars Odyssey orbiter by Mitrofanov et al. [148], Maurice et al. [149] and Feldman et al. [150].

Figures 3-16 to 3-19 depict some of the data used in the construction of this resource map while Table 3.7 lists the uniform global Martian atmospheric composition assumed within the ISRU Module. For more details on the development of this resource map, the reader is referred to Schrenk [144].

Table 3.7: Martian Atmospheric Composition assumed in the ISRU Module (based on ISRU studies performed by Muscatello et al. [151])

Atmospheric Species	**Mass Fraction (%)**
Carbon Dioxide (CO_2)	95.32
Nitrogen (N_2)	2.7
Argon (Ar)	1.6
Oxygen (O_2)	0.13
Carbon Monoxide (CO)	0.07

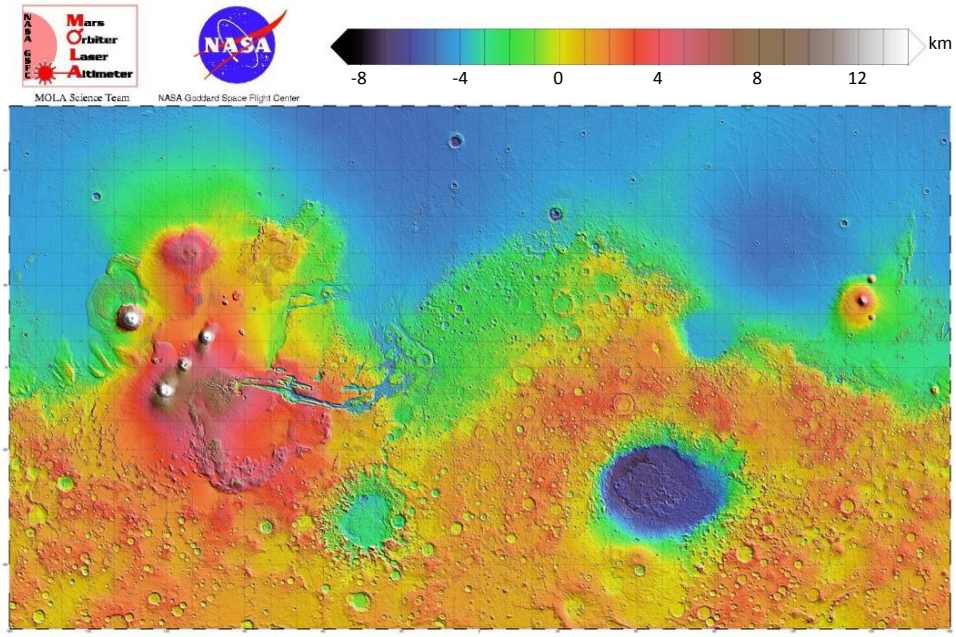

Figure 3-16: Mars Orbiter Laser Altimeter (MOLA) map [145]

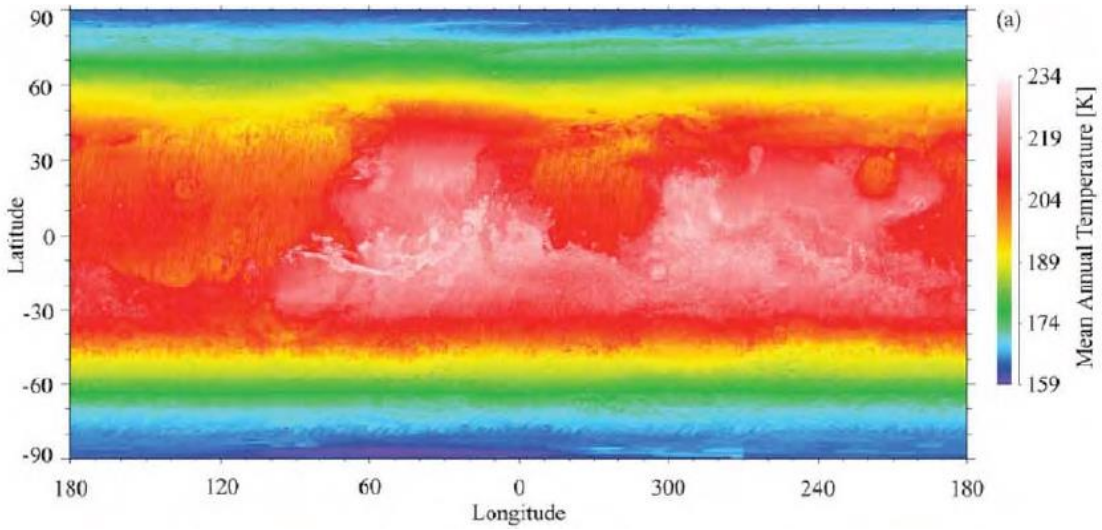

Figure 3-17: Mean annual temperature on Mars surface, from Mellon et al. [146]

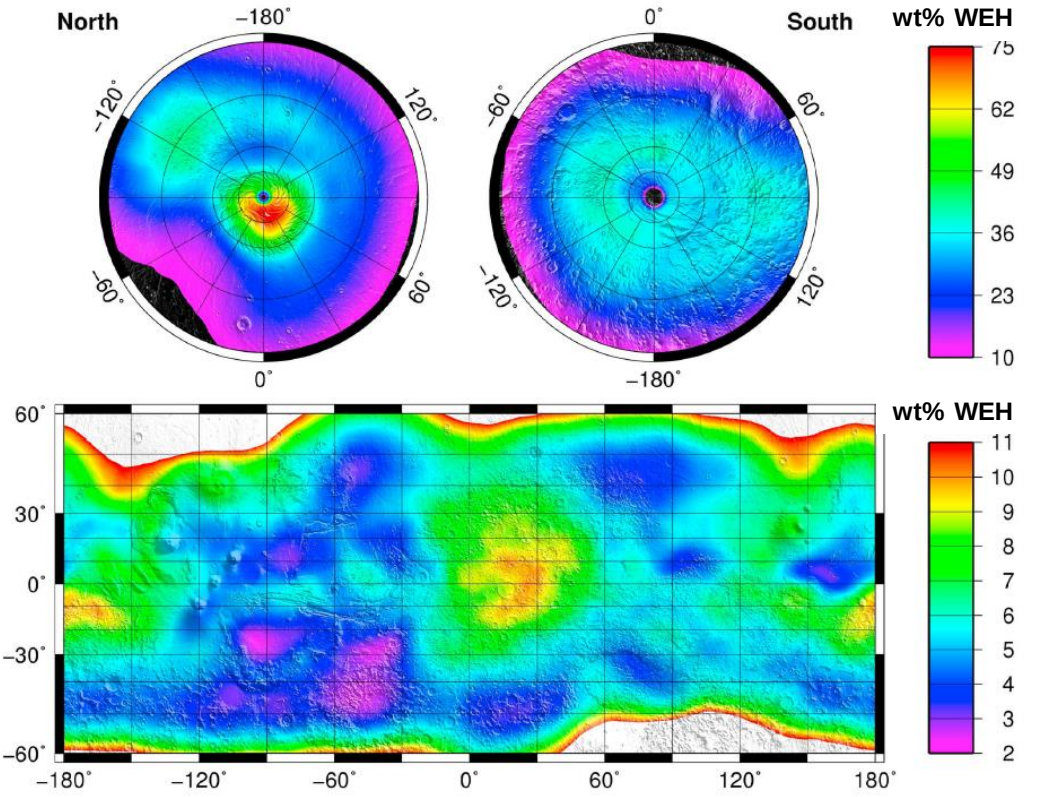

Figure 3-18: WEH estimation, using a one layer model, adapted by Schrenk [144] from Maurice et al. [149]

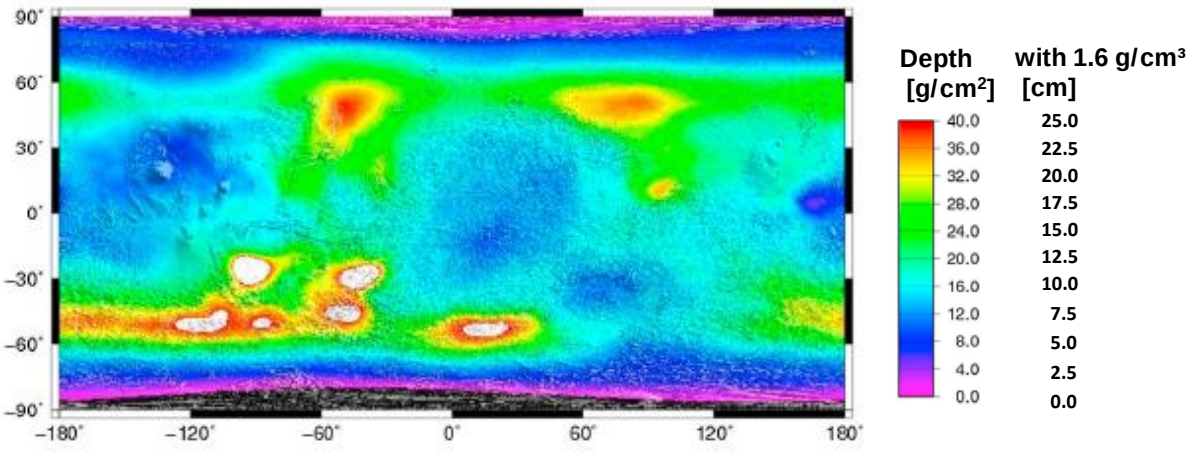

Figure 3-19: Burial depth D estimation for the lower soil layer W_{dn}, adapted from Maurice et al. [149]. The upper layer WEH content is 2% by weight

3.4.3 Supportability Module

The HabNet Supportability Module predicts spare parts requirements for the selected ECLS and ISRU systems using the Semi-Markov Process (SMP)-based algorithm developed by Owens [152,153]. In this section, we provide a brief summary of this algorithm and its implementation within HabNet.

As was discussed in Section 3.2, the Supportability Module uses information related to the component reliability, repair and maintenance strategy, and the system structure to estimate the number of spare parts needed to ensure that some pre-specified probability of continuous system operation over a predetermined mission duration is met. Across all analyses performed in this thesis, components are assumed to be spared at the lowest level of detail at which data is available. For ECLS technologies, this corresponds to the component breakdowns adopted on the ISS, as described throughout Appendix D. Similarly, ISRU technologies are spared at the level at which components are sized in Appendix F. This implementation is intended to balance the analysis objectives of minimizing total spare parts mass over the lifecycle of a campaign of missions, while incorporating the most up-to-date data available on the lifecycle properties of each of the selected systems.

At a high level, the Owens approach [152,153] computes spare parts requirements by performing two separate calculations and comparing the two to determine the required number of spares for each component. These two calculations evaluate: (1) the number of spare parts required to repair components that have experienced random failure over the course of the mission; and (2) the number of spare parts required to support scheduled maintenance activities over the length of a mission. Once these two calculations are performed, the larger of the two is selected as the spare parts requirement. This approach implicitly assumes that one of the two mechanisms: random failure or scheduled repair, dominates the spare parts requirements. Moreover, it is important to note that the approach adopted here predicts spare parts requirements analytically, based on reliability data for each component within a modeled system, rather than explicitly simulating the dynamics of component failure, as is the case in other approaches such as EMAT (see Section 2.3.1). The following sections summarize the spares predictions methods adopted here.

3.4.3.1 Estimating the Number of Spare Parts Required to Support Random Failure

Predicting the number of spare parts needed to manage random failure is inherently an uncertain process, since the probabilistic nature of random failure means that one cannot predict a priori the precise time at which each component within a system will fail. To address this uncertainty, Owens [152,153] adopted the Semi-Markov Process (SMP) structure to calculate the likelihood that each component within a system will enter a failed state throughout a mission and the number of corrective actions required to recover from these failed states. As shown in the examples in Figure 3-20, SMPs are probabilistic, network-based representations of system states and the transitions between them. Here, each transition is defined by a probability density function (PDF) that represents the time at which the transition is initiated after the system enters its current state.

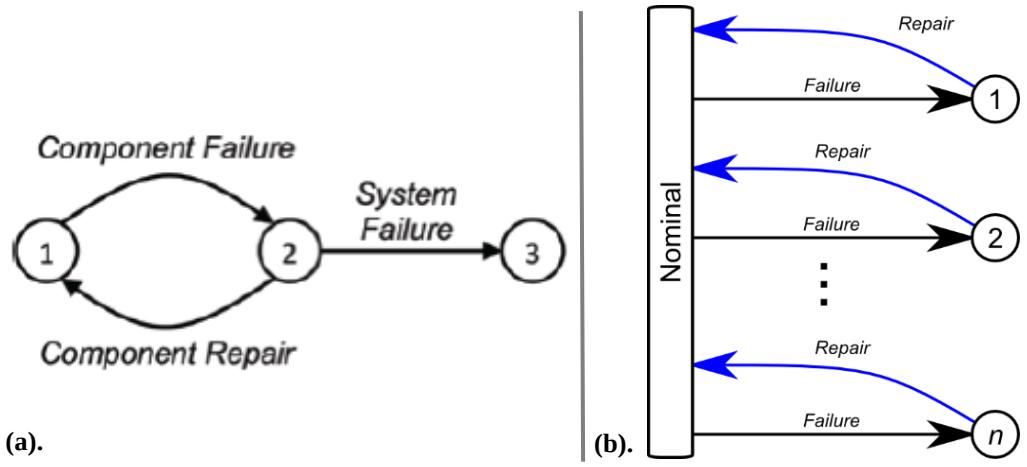

Figure 3-20: (a). An SMP network showing operational, degraded, and failed states of a system and the potential transitions between them (b). An SMP diagram for a one-failure-at-a-time scenario, showing cycles of failure and repair for n components [143,153]

With respect to spaceflight hardware, the Owens approach [152,153] assumes that all components can be in one of three states at any one time: (1) a nominal, operational state (2) an offline, but recoverable state; and (3) a failed and irrecoverable state. As shown in the SMP depicted in Figure 3-20(a), the combination of these three states and the transitions between them comprise a simplified representation of all the major operational scenarios that a system might experience over the course of a mission. That is, a system can initially operate in a nominal state (1) until a random failure occurs, causing it to transition into a degraded state (2). From here, the system can either be repaired with the use of a spare part, thereby returning

it back its nominal state (1); or left to fail, which would cause it to transition into an irreparably failed state (3).

In order to estimate the number of spare parts required, the SMP structure depicted in Figure 3-20(b) is adopted, whereby the transition from a degraded state to an irreparably failed state is removed to enforce the immediate repair of a system. This formulation assumes that:

- All failures are assumed to be diagnosed and acted upon as soon as they occur
- All repairs are assumed to follow the remove and replace strategy currently in use on the ISS; and
- All repairs are assumed to bring the system back to a good-as-new condition

Thus, every time a transition occurs from a nominal state to a degraded state, a spare part is required. Because the number of transitions is a probabilistic value, the number of spares is based on cumulative distribution functions that are obtained from solving the SMP (discussed further below). These represent the probability that the system has entered a degraded state (and therefore requires a spare part) a given number of times (or less) over the planned system operational duration.

Within the Owens approach [152,153], transitions from a nominal to a degraded state (i.e. random failure events) for each component are assumed to follow an exponential distribution shaped by their Mean Time Between Failure (MTBF). This commonly used first-order component failure model is represented by the following probability density function (PDF), which describes the time to failure for a given component:

$$f_{fail}(t) = \frac{1}{MTBF} e^{\frac{-1}{MTBF}t} \tag{3.1}$$

Conversely, transitions from a degraded state back to a nominal state (representing repair actions) are modeled with a log-normal distribution, which is typically used for corrective repair processes [154,155]. As a simplifying assumption, all components are assumed to have a Mean Time To Repair (MTTR) of 12 hours, with a standard deviation of one hour. The resulting PDF of the repair time is given by:

$$f_{rep}(t) = \frac{1}{t\sqrt{2\pi}\sigma} e^{\frac{-(\ln(t)-\mu)^2}{2\sigma^2}} \tag{3.2}$$

Where σ is the shape parameter and μ is the log-scale parameter, both of which are functions of the MTTR and standard deviation in time to repair (SDTTR), as seen in the following equations:

$$\sigma = \sqrt{\ln\left(1 + \frac{SDTTR^2}{MTTR^2}\right)} \tag{3.3}$$

$$\mu = \ln(MTTR) - \frac{1}{2}\sigma^2 \tag{3.4}$$

Thus, to estimate the number of spare parts required to mitigate system down time due to random failure, an SMP network is first developed based on the inherent structure of the system, and PDFs (*f(t)*) representing random failure and repair actions are derived for all transitions within the SMP. Using these PDFs, two matrices are developed that mathematically describe the SMP. These are the Kernel Matrix (*Q(t)*), and the Unconditional Waiting Time Density Matrix (*H(t)*). The Kernel Matrix represents the PDFs defining the time until a transition occurs from one state to each known subsequent state at time t, while the Unconditional Waiting Time Density Matrix contains PDFs defining the time spent in each state since the last transition into that state occurred. Equations for the entries of each of these matrices are listed below. Here, the subscript *i,j* indicates the transition from state i to state j.

$$Q_{i,j}(t) = f_{i,j}(t)\prod_{n \neq j}\left(1 - \int_0^t f_{i,j}(t)dt\right) \tag{3.5}$$

$$H_{i,j}(t) = \sum_j Q_{i,j}(t) \tag{3.6}$$

Once these matrices are formulated, they are transformed into the Laplace domain and used to calculate five metrics that characterize the probabilistic behavior of the system. These are then numerically transformed back into the time domain and analyzed to determine probabilistic values for spare parts requirements. These metrics are summarized in Table 3.8 below:

Table 3.8: Symbols, names, descriptions, and equations used in the Owens SMP Approach to predict the spare parts requirements needed to manage random component failure [153].

Symbol	Name	Description	Equation (Laplace Domain)
$\phi_{i,j}(t)$	Time-dependent state probability	Probability that the system will be in state *j* at time *t*	$\tilde{\phi}(s) = \frac{1}{s}\left(I - \tilde{Q}(s)\right)^{-1}\left(I - \tilde{H}(s)\right)$
$E_{i,j}(t)$	Expected time spent in state	Expected amount of time that the system will have spent in state *j* up to time *t*	$\tilde{E}(s) = \frac{1}{s}\tilde{\phi}(s)$
$g_{i,j}(t)$	PDF of first passage time	PDF describing the time taken to reach state *j*	$\tilde{g}(s) = \tilde{Q}(s)\left(I - \tilde{Q}(s)\right)^{-1}\left[I \circ \left(I - \tilde{Q}(s)\right)^{-1}\right]^{-1}$
$G_{i,j}(t)$	CDF of first passage time	CDF giving the probability that the system has reached state *j* by time *t*	$\tilde{G}(s) = \frac{1}{s}\tilde{g}(s)$
$V_{i,j}(k,t)$	Markov renewal process probability	CDF giving the probability that the system has reached state *j* a total of *k* or fewer times by time *t*	$\tilde{V}(k,s) = \frac{1}{s}\left(1 - \tilde{g}(s) \circ \left[1\left(I \circ \tilde{g}(s)\right)^{k}\right]\right)$

Of the five metrics listed in Table 3.8, the Markov renewal process probability ($V_{i,j}(k,t)$) is of most interest with respect to the determination of spare parts. When applied to nodes that represent degraded system states in an SMP network, the Markov renewal probability provides a cumulative distribution of the probability that the system has reached that particular degraded state *k* or fewer times. To determine the number of spares required, this calculation is repeated with increasing integer values of *k* (representing the number of times the state is visited and hence the number of spare parts required), and are discretely differentiated to generate probability mass functions (PMFs) of the probability that the degraded state has been visited exactly *k* times. These PMFs are then convolved and numerically integrated to yield a CDF of the probability of needing *k* spares to manage random system failure over the predefined mission time horizon. Figure 3-21 provides an example of a typical CDF resulting from this calculation:

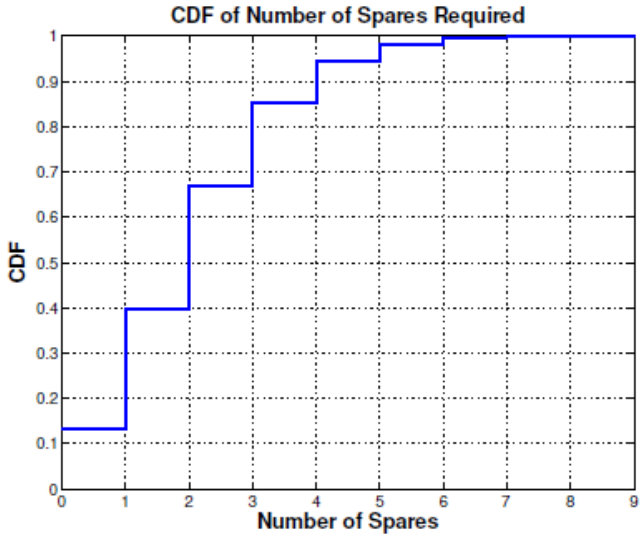

Figure 3-21: A sample CDF solution obtained from solving the set of equations in Table 3.8

As can be seen from Figure 3-21, the number of spare parts required to manage random failure is a probabilistic value. In order to select a specific quantity of spare parts, a desired probability threshold of having sufficient spare parts needs to be specified. For example, if an 80% likelihood of having sufficient spares is desired, three spare parts would be required for the system represented in Figure 3-21. Adding another spare part increases this likelihood of having sufficient spares to approximately 95%, and an additional spare part after that increases this value to 98%. This diminishing rate of return is an important trend that is typical of spare parts analysis for random failure – that is, after a certain threshold probability is obtained through the allocation of a given number of spares, every additional spare contributes progressively less to the overall probability of having sufficient spares. It is important to note here that this calculation assumes that all repairs are successfully performed and that common cause failures do not occur - hence the repeated reference to this result being a "probability of having sufficient spares" rather than a "system reliability". This quantity can therefore be considered to be a lower bound on the total system reliability. For the case studies examined in this thesis, a threshold probability of sufficient total spares for the entire system is assumed to be either 0.99 or 0.999, depending on the context of the analysis being performed.

3.4.3.2 Estimating the Number of Spare Parts Required to Support Scheduled Maintenance

In contrast to the probabilistic calculation of the number of spare parts needed to support random failure, the determination of the number of spare parts needed to support scheduled

maintenance involves a simple deterministic calculation based on the designed life limit of each component. Here, the spare parts required for each component is calculated as the rounded down integer of the ratio of the planned total component operational time and the life limit of the component:

$$n_{repair} = \left\lfloor \frac{t_{\text{Total Operational}}}{\text{Life Limit}} \right\rfloor \tag{3.7}$$

3.4.4 Evaluation Module

The HabNet Evaluation Module integrates the outputs of the Habitation, ISRU, and Supportability Modules to estimate the total system mass required to be delivered to the exploration site over time. As was mentioned in Section 3.2, this value is a key initial input to any subsequent space mission transportation analysis that might occur after all surface infrastructure has been architected and sized.

Moreover, it is important to note that while cost (in dollars) is the ultimate value of interest to decision makers, total system mass has been adopted here. This is due to the significant uncertainties inherent in predicting the costs of developing and sustaining the types of technologies that are typical of human spaceflight missions. These include those that have traditionally been developed as one-off items for a specific purpose that is not necessarily applicable to the mission context being analyzed, and those that are at such an early stage of maturity that significant research is still required to bring it to a mission-ready level. Estimating the development costs of such systems would require an estimate of the total time and resources required to mature the state of knowledge for each system to a level where it would be ready to fly on a mission to Mars. Similarly estimating their sustainment costs requires estimates of the infrastructure and the size of the "standing army" required to support the operations, maintenance, replacement, and upgrade of each system once they are deployed on a mission. Methods for estimating these quantities are still very much within the domain of ongoing research and as such, are considered to be beyond the scope of this thesis.

Contrastingly, system mass is a parameter that can be decomposed and traced to some combination of a first principles, physics-based calculation, or a property of an analogous, previously flown system. As a result, total system mass is adopted within the case studies performed in this thesis as a proxy to dollar cost. Within the Evaluation Module, this is

calculated as the sum of the mass of the habitation, ECLS and ISRU systems required to sustain a crew at a mission site over some mission duration (as computed by the Habitation and ISRU modules), and the total mass of the spare parts and consumables resupply required to sustain these systems (as computed by the Supportability Module). The first component of this total mass is referred to as the "emplaced mass", while the second component is referred to as the "resupply mass".

With respect to the various components of dollar cost described above, the emplaced mass can be considered as representative of the development cost, since this mass encapsulates the architecture of the systems that were chosen to serve the functions required to carry out the proposed mission. Here, each of the elements of the selected architecture requires its own development program to be realized and integrated into the system. By extension, the number of different types of technologies present in the selected architecture is an indicator of the number of unique development programs required, which in turn affects the development cost. These two parameters: the emplaced mass and the number of unique technologies; are thus considered to be qualitative measures of development.

Similarly, the resupply mass can be considered as a proxy for sustainment cost, or the cost of maintaining the selected architecture over its program lifecycle. When examining the lifecycle impacts of various system architectures within this thesis, trends in the total mass of resupply over time will be used as an indicator of program sustainability.

Finally, when applicable, the mass of the systems needed to support the operation of the emplaced technologies (habitation, ECLS, and ISRU systems) is also calculated. These supporting systems typically consist of additional structural, power, and thermal management systems to respectively accommodate the volumetric impacts, and power and cooling demands of each emplaced technology. The calculation of the mass of these systems is typically based on "equivalency factors" that are derived from data on the sizing and performance of space-rated instances of the technologies being sized. The summation of the "equivalent mass" of these supporting systems with the raw mass of the selected technologies results in a quantity referred to as the "Equivalent System Mass" (ESM). The definition of this metric varies from case to case, based on the scope of the analysis, and will therefore be explicitly defined for each case study in which it is adopted as a figure of merit.

3.5 Chapter Summary

Over the course of this chapter, the development of the HabNet framework and its modules was presented. This commenced with the derivation of a high level Architecture Decision Graph (ADG) representing the key decisions that shape the architecture of a human spaceflight system. From this ADG, the scope of HabNet with respect to traditional mission architecture and space logistics analyses was identified, based on the sets of decisions that they encompassed. This set of coupled decisions was then used to form the high level HabNet framework, consisting of four interconnected modules – the Habitation Module, the ISRU Module, the Supportability Module, and the Evaluation Module.

With this high level framework established, the software implementation of HabNet was explored. Based on an analysis of the decision-making processes involved in architecting a human spaceflight system, it was observed that the space systems architecting process can be modeled as a technology selection process. This insight led to the development of a categorization scheme for different technology selection problems, as well as the development of the Technology Concept Template, which was subsequently combined with an object oriented programming framework to structure all technology model libraries implemented within the HabNet modules. These model libraries are described in greater detail in Appendices B to F.

This chapter concluded with a discussion on the implementation of each of the four major modules of HabNet. Here, the dynamic simulation capability of the BioSim software package was updated with ISS-based technology models to build the Habitation Module. This was combined with the ISRU technology library model developed by Schrenk [144] and the SMP-based sparing algorithm developed by Owens [152,153], to form the main computational engine for HabNet. The output of these modules was connected to the Evaluation Module, which generates predictions for the emplaced and lifecycle resupply mass of the space habitation architecture defined by the previous HabNet modules.

With the HabNet modules defined, developed and integrated, end-to-end space habitation analyses can now be performed. These analyses will be performed via a series of case studies presented in the following chapters, where HabNet will be used to examine increasingly complex space habitation scenarios.

Chapter 4

HabNet Validation

In the previous chapter, the HabNet framework and its individual modules were developed. Together, these modules simulate the dynamics of crew activities and their impact on resource consumption within a habitation system, as well as size the systems required to sustain the crew. In this chapter, the dynamic simulation and sizing capabilities of HabNet will both be compared and validated against external data. As was mentioned in Section 3.4.1, all dynamic simulations within HabNet are performed within the Habitation Module, whose framework was based on that of the open-source BioSim software package developed for NASA Johnson Space Center. As a result, all validation efforts related to HabNet's dynamic modeling and simulation capabilities will be focused on the Habitation Module. This will involve firstly comparing the outputs of the Habitation Module with those of BioSim for increasingly complex habitation scenarios to establish that the underlying modeling framework has been correctly implemented. Following this, each of the major ECLS technologies modeled within the Habitation Module will be validated against operational data obtained for the corresponding technology currently operating onboard the International Space Station. Once the HabNet dynamic simulation capability is validated, the accuracy of its sizing estimates will be examined via a validation case study based on the analysis of Lange and Anderson [101] described in Section 2.3.2. Here, an end-to-end analysis of the impacts of different ECLS architectures on the total ECLS mass required to sustain a one year crewed deep space mission is performed with HabNet, and the results are compared with those published by Lange and Anderson [101]. In addition to enabling the assessment of the accuracy HabNet's sizing predictions, this validation case study also provides a means for illustrating the key steps

involved in performing lifecycle analyses of space habitation scenarios with HabNet. Each of these validation studies is detailed in the following subsections.

4.1 Validation of the HabNet Dynamic Simulation Capability with BioSim

In Section 3.4.1., a survey of existing habitation and life support modeling capabilities was performed as a first step in the development of the HabNet Habitation Module. From this, it was observed that of all the modeling environments examined, the BioSim open-source software package had the most suitable balance of simulation execution time and modeling fidelity relative to the requirements derived for HabNet.

BioSim is an integrated mid-fidelity ECLS simulator that was developed at NASA Johnson Space Center to investigate the impact of integrated control strategies on the consumables demands of ECLS systems [131]. Since its first release in the early 2000s, it has been used by a number of researchers to study a range of lunar habitation architectures. These range from analyses examining the consumables demands of 90-day lunar habitat ECLS architectures with different levels and implementations of food production [156], to studies investigating the impact of varying habitat volumes on system resilience and reliability [157].

As a consequence of its prevalence within the life support literature and the similarity between its attributes and those required for HabNet, the BioSim software architecture was adopted for the HabNet Habitation Module. This involved first porting the BioSim code from its native Java programming language into the MATLAB modeling and simulation environment so that it could be integrated with the other HabNet Modules (see Section 3.4.1 for details). Following this, each of the individual technology models within the MATLAB-based version of BioSim were modified to match the operational behavior of the ECLS technologies currently operating onboard the ISS (see Appendix D). The resulting product formed what has since been referred to as the HabNet Habitation Module.

As part of the preliminary porting process, a series of validation studies was performed to ensure that the output of the MATLAB-ported version of BioSim matched that of the native Java-based version of BioSim. This involved simulating habitation scenarios of increasing complexity in both the Java and MATLAB implementations of BioSim and comparing the resulting output to verify the successful transfer of the BioSim software architecture into the MATLAB environment. Here, each mission was set to run for up to 19000 simulated hours

(equivalent to approximately 26 months) and had a habitat with an initial total pressure and composition of 55kPa, at 65.9% N_2, 33% O_2, 1% H_2O, 0% CO_2, and 0.1% Other Trace Elements. In addition, the initial resource tank levels and crew hazardous conditions were set to the default values used in BioSim. These initial resource levels include an initial water supply of 1000L and an initial food supply of 1000kg of wheat. With regards to BioSim-specific crew hazardous conditions, the default lower ambient oxygen concentration limit of 10% was used for this validation study – a value that differs from that baselined in the Habitation Module and published in the literature (see Section 3.4.1). Table 4.1 summarizes the habitation scenarios that were simulated and their corresponding results, while Figures 4-1 and 4-2 depict selected results from this validation exercise. As can be seen in the fourth column of Table 4.1, each simulation either ended when a hazardous condition was entered, or when the predefined simulation time horizon was reached. For a complete catalog of all results obtained from this validation exercise, the reader is referred to Appendix G.

Table 4.1: Summary of Habitation Scenarios Compared between BioSim and HabNet

Simulation Case	**Habitation Scenario**	**Simulation Goal**	**Simulation Result**	**For results see:**
1. Open loop ECLS	One 35 year old 75kg male in a single 2700m^3 habitat with an open-loop water supply (1000L) food store (10000kg of wheat). No CO_2 removal system is included. Crew Daily Schedule: 12h IVA, 8h sleep, 2h exercise, 2h EVA	Validate crew model implementation	Crew CO_2 poisoning threshold is exceeded after 524 hours (~22 days)	Appendix G.1
2.Open loop ECLS with a CDRA	Same as Simulation Case 1 but with a CO_2 Removal Assembly (CDRA) installed that removes CO_2 and vents it overboard	Validate CDRA model implementation	Potable water store emptied on mission day 251, causing a crew dehydration risk	Appendix G.2
3.Partially Closed H_2O cycle (with WRS and CDRA)	Same as Simulation Case 2 but with Water Recovery System (WRS) installed that processes collected urine into potable water	Validate WRS model implementation	Atmospheric oxygen decreased beneath the hypoxic threshold on mission day 473, causing a crew suffocation hazard	Appendix G.3
4.Partially Closed H_2O cycle (with WRS and CDRA). O_2 supplied by an OGA	Same as Simulation Case 3 but with an Oxygen Generation Assembly (OGA) installed to provide additional O_2 to the crew via the electrolysis of potable water. Here the simulation time horizon was reduced to 10000h	Validate OGA model implementation	Although the potable water store emptied at day 72, the crewmember survived until the end of the simulated mission, because the WRS was able to generate drinking water at a rate required to sustain the crewmember	Appendix G.4

5. Mostly Closed O_2 and Semi-Closed H_2O Loops	Same as Simulation Case 4 but with a CO_2 Reduction System (CRS) that uses the Sabatier reaction to produce water from CO_2 that will eventually be electrolyzed to recover O_2. Here the simulation time horizon has been reduced to 6000h	Validate CRS model implementation	Similar to Case 4: the water store is emptied (on day 77 here), but the crewmember still survives until the end of the mission due to the water production capacity of the WRS and the CRS	Appendix G.5
6.Mostly Closed O_2 and H_2O Loops (ISS-based ECLS)	Same as Simulation Case 5 but with a condensing heat exchanger included to extract humidity condensate from the environment for subsequent processing into potable water	Validate the Dehumidifier implementation	Similar to Cases 4 and 5, the water store is emptied (on day 81 here), but the crewmember still survives until the end of the mission due to the water production capacity of the WRS and the CRS	Appendix G.6
7.Four-module Habitat with Four Crew (Default BioSim case)	Four crewmembers inhabit a four-module habitat (Two 2700m^3 living modules, one 1900m^3 lab module, and a 19m^3 service module with the ECLS systems). The crew consists of two males and two females who all follow the same crew schedule. The ECLS architecture is the same as Simulation Case 6, with fans now included to ensure intermodule ventilation between modules.	Validate the capability to simulate multiple crewmembers within a multi-module habitat (including intermodule ventilation)	The crew survives to the end of the simulated mission (set to 250 days for this simulation case)	Appendix G.7

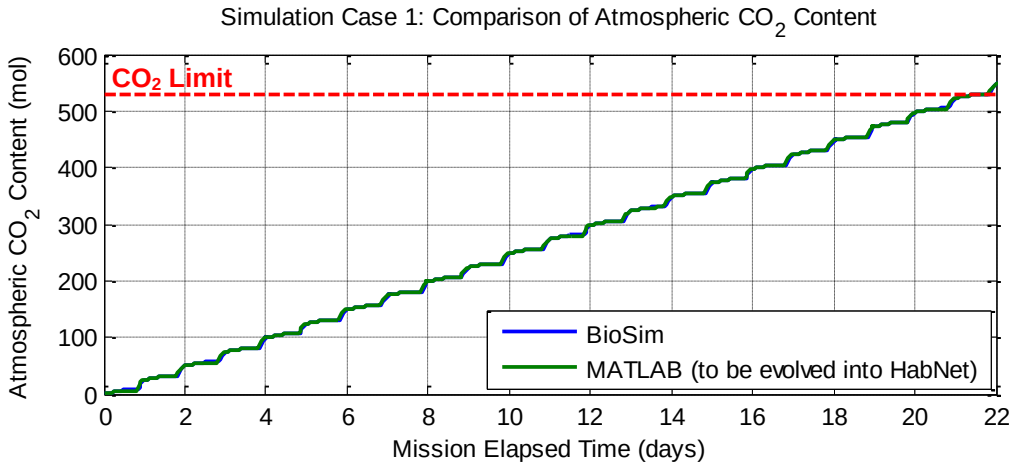

Figure 4-1: Sample validation plot of Simulation Case 1 (see Table 4.1) comparing the BioSim and MATLAB implementation of a single crew, single module habitation scenario with an open-loop ECLS system. Here, the atmospheric CO_2 content is compared, indicating that in both implementations, the CO_2 poisoning limit is exceeded on mission day 21.

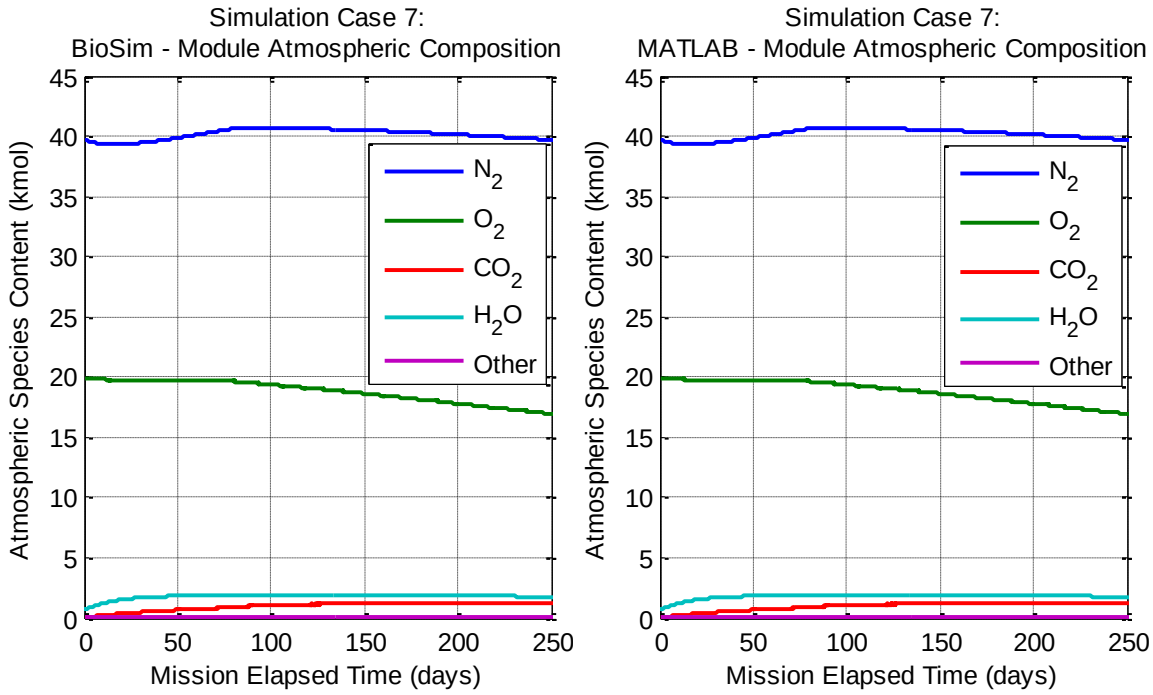

Figure 4-2: Sample validation plot of Simulation Case 7 (see Table 4.1) comparing the BioSim and MATLAB implementation of a four crew, four module habitation scenario with an ISS-based ECLS architecture. Here, the atmospheric composition is compared. Decreases in O_2 over time indicate the need for makeup O_2 to be provided for the crew.

As can be seen in Figures 4-1 and 4-2, as well as the figures cataloged in Appendix G, a complete agreement between the native Java version of BioSim and its MATLAB-ported version was achieved. The fact that the same results were produced in both the Java-based and MATLAB versions of BioSim for each of the simulation cases listed in Table 4.1 indicates that both the implementation of the BioSim architecture within MATLAB, as well as the implementation of each the individual BioSim-modeled technologies, have been validated.

4.2 Validation of the HabNet ECLS Models with ISS ECLS Technologies

With the BioSim software architecture successfully ported into MATLAB, each of the original BioSim ECLS models was rewritten to match the behavior of the ECLS technologies currently operating onboard the International Space Station. This resulted in the ECLS Technology Model Library that was introduced in Section 3.3.2 and is described in Appendices B to

D. During a typical execution of the HabNet Habitation Module, this library is accessed to define and simulate the desired ECLS architecture.

As is discussed throughout Appendix D, the behavior of each of these ECLS technologies has been modeled with a series of linear equations that become active under various predefined operational conditions. These equations typically model resource processing rates and reaction stoichiometry, and have been tuned to match the attributes of their corresponding ISS ECLS technologies. Moreover, as was mentioned in Section 3.4.1, all atmospheric processes have been assumed to be isothermal, so that only mass balance calculations are required, thereby increasing the speed of simulation by reducing the number of equations that need to be solved. This isothermal assumption means that the operation of passive and active thermal control systems in response to environmental and internal thermal loads on a simulated habitat are not modeled.

In this section, we evaluate the suitability of both of these modeling assumptions by comparing the dynamic behavior predicted by each of the major regenerative ECLS technologies modeled within the ECLS Technology Model Library with the behavior of its corresponding ISS ECLS technology. Table 4.2 summarizes each of the technology models investigated, along with the corresponding ISS technology that each model was baselined against.

Table 4.2: HabNet ECLS Models compared against their ISS Counterparts

ECLS Function	**HabNet Class**	**ISS Regenerative ECLS Technology**	**For technology summary and model discussion, see:**	**For model comparison see:**
Urine Processing	ISSWaterRSLinear	Urine Processor Assembly (UPA)	Appendix D.6.1	Section 4.2.3
Water Processing	ISSWaterRSLinear	Water Processor Assembly (WPA)	Appendix D.6.2	Section 4.2.4
Oxygen Generation	ISSOGA	Oxygen Generation Assembly (OGA)	Appendix D.5	Section 4.2.5
CO_2 Removal	ISSVCCRLinearImpl	Carbon Dioxide Removal Assembly (CDRA)	Appendix D.4	Section 4.2.6
CO_2 Reduction	ISSCRS	CO_2 Reduction System (CRS)	Appendix D.7	Section 4.2.7

4.2.1 Obtaining ISS ECLS Technology Data

In order to obtain a "truth" data set from which the HabNet ECLS models could be validated, a "data stream client" application was commissioned to record live ISS telemetry data from the NASA "ISS Live!" website [158]. The "ISS Live!" project was initiated as part of NASA's Open Government Initiative in 2011 to provide live ISS data feeds to the public [159]. As can be seen in the screenshot in Figure 4-3, the project's website displays near real-time information about the status of the ISS and the activities of the crew. This data is obtained from a server located at the NASA Mission Control Center (MCC) that receives data downlinked directly from the ISS.

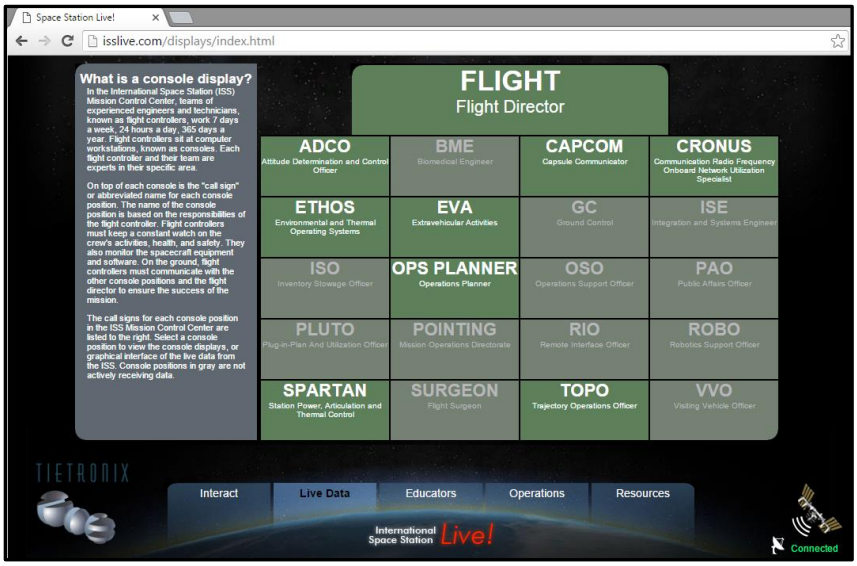

Figure 4-3: Screenshot of the Console Display Summary on the ISS Live! Website [160]

For this validation exercise, data from the Environmental and Thermal Operating Systems (ETHOS) console display was recorded. This console corresponds to the first element in the second row of the console display summary shown in Figure 4-3. As can be seen in Figures 4-3 and 4-4, the ETHOS console displays information regarding the atmospheric pressure, composition, and temperature of each of the modules within the ISS USOS, as well as the status of the major regenerative ECLS technologies and the capacities of their resource tanks.

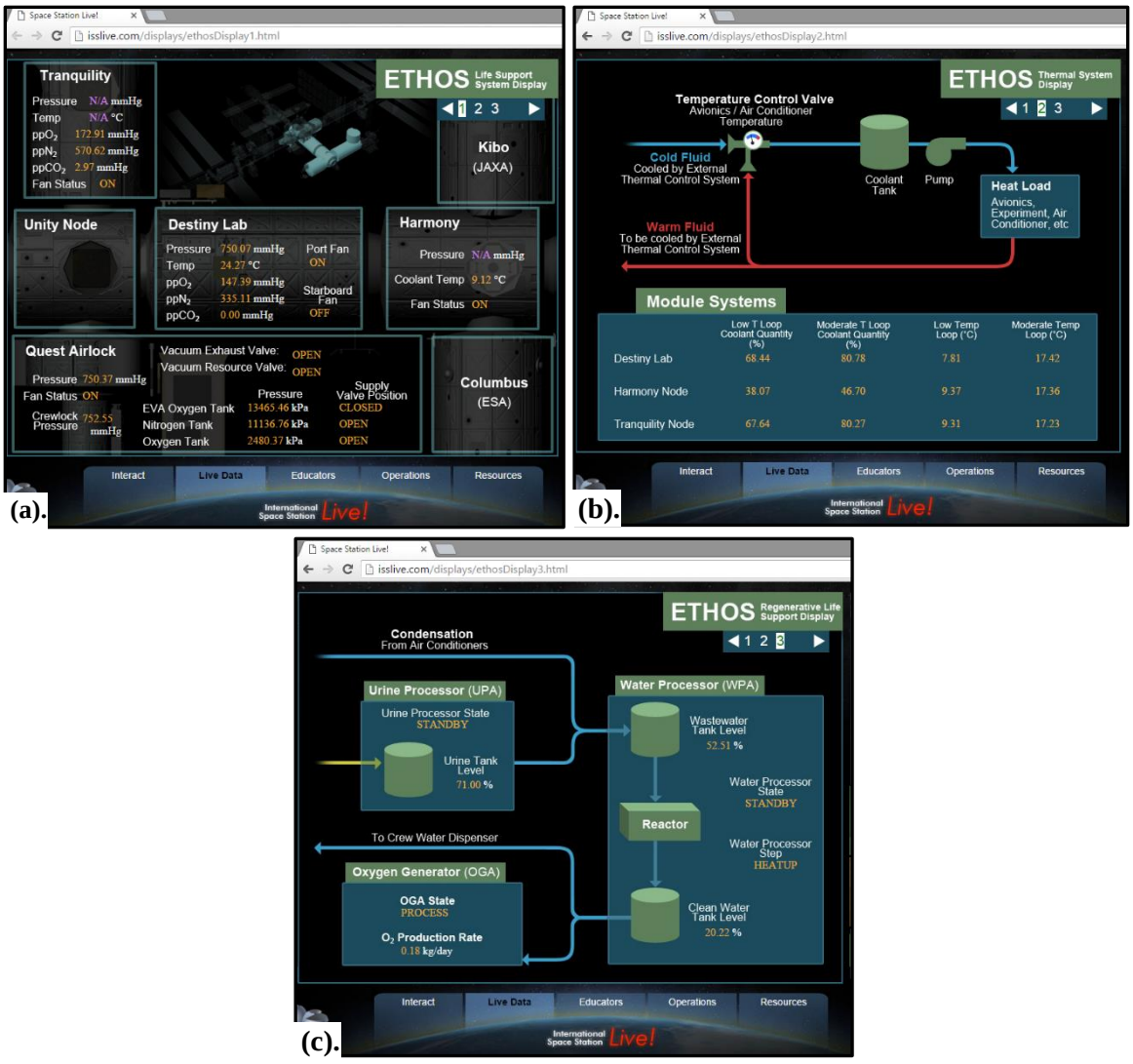

Figure 4-4: The three ETHOS console displays [160] (a). Atmospheric pressure, temperature, and composition within the ISS USOS (b). ISS USOS Active Thermal Control System (c). ISS USOS Regenerative ECLS Technologies

To record this ETHOS console data, a "data stream client" script developed by the Syntelos open source project [161] was modified and compiled within the Node.js runtime environment [158] to create a server and socket to connect to the same NASA MCC server accessed by the "ISS Live!" website. To obtain a data packet from the MCC server, the data stream client script makes three requests to the MCC server, from which a unique response is provided. These are:

- A request to create a session with the MCC server, from which a session identification number is returned

- A request on what specific telemetry data is desired, from which a confirmation of receipt of the request is returned; and
- A request to download the data packet, from which a socket is opened and a stream of data corresponding to the requested telemetry is sent.

Once the data packet is received, the three requests are repeated to ensure a near-continuous downlink from the server. On average, it was found that the delay in reconnecting to the server between data packet downloads was less than one second. In addition, it was observed that while the data stream client was continuously connected to the MCC server, gaps were present in the downloaded ISS telemetry data due to communications gaps between the ISS and the MCC server (as will be seen in the results presented in Sections 4.2.2 to 4.2.6).

As a final step in the data collection process, all received data is recorded in an online mongoDB database, where it is periodically exported to a comma-separated value (.csv) file and downloaded for subsequent data processing. Figure 4-5 summarizes this data recording process.

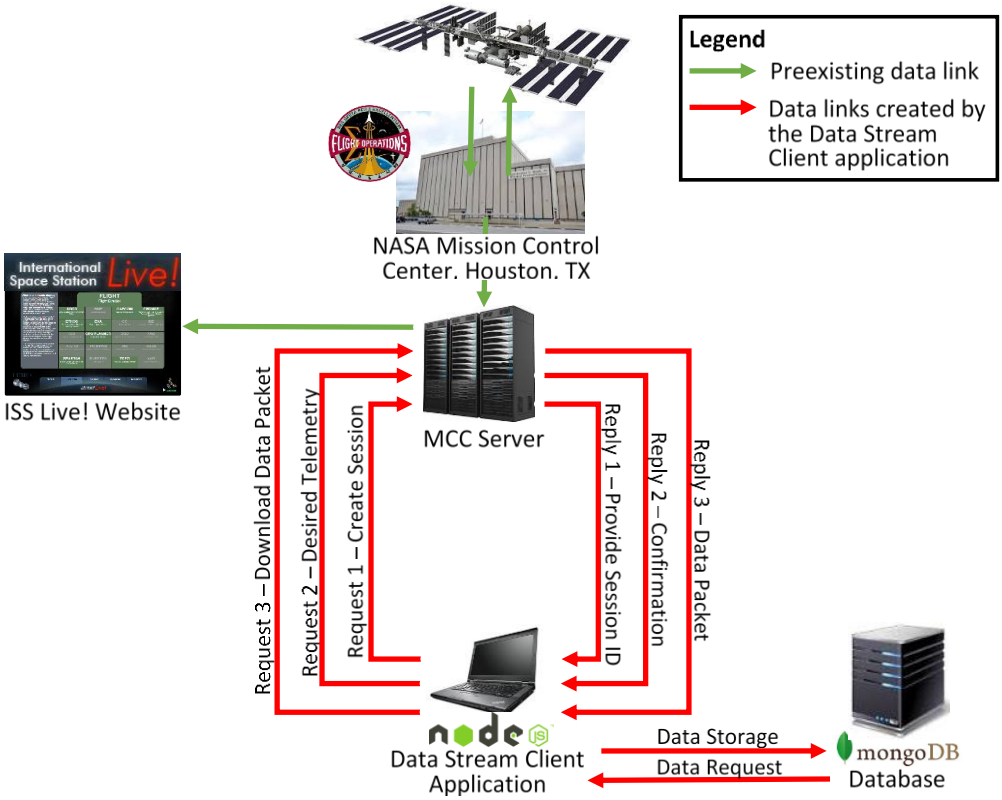

Figure 4-5: The Data Stream Client ISS Data Recording Process

In total, data from 43 data channels was recorded over the periods spanning from July 14th, 2015 to August 4th, 2015 and from February 9th, 2016 to February 29th, 2016. In some cases,

over 60,000 unique data points were recorded per channel. To contextualize this raw data, daily ISS operations logs published on the NASA website were reviewed for every day that data was collected, and events that could potentially affect the station's ECLS systems were recorded. These events are summarized below in Tables 4.3 and 4.4.

Table 4.3: Major ISS and ISS ECLS related activities on the ISS from July 14th, 2015 to August 4th, 2015 [162]

Date (hours since 00:00 1/1/2015)	**Major ISS Event and/or ISS ECLS Event**
Tues 7/14/2015 (hours 4656-4680)	Node 3 CDRA was successfully activated after a fault in the Air Selector Valve (ASV) 104 was discovered the previous day
Weds 7/15/2015 (hours 4680-4704)	Node 3 CDRA was commanded to standby in preparation for tomorrow's maintenance to recover the Air Selector Valve (ASV) 104. After the ASV 104 R&R, the crew will conduct additional Node 3 CDRA Leak Check steps.
Thu 7/16/2015 (hours 4707-4728)	Late Notice Conjunction: A late notice conjunction was experienced early this morning with insufficient time to execute a Predetermined Debris Avoidance Maneuver (PDAM). The ISS crew was directed to safe the ISS and shelter in place in the Soyuz. The conjunction passed without incident and the crew re-ingressed the ISS.
Fri 7/17/2015 (hours 4728-4752)	WRS – ARFTA Tank Fill
Mon 7/20/2015 (hours 4800-4824)	The Node 3 CDRA Air Selector Valve (ASV) 104 was replaced and successfully checked out by the ground. Reactivation of the Node 3 CDRA was performed through the night.
Tues 7/21/2015 (hours 4824-4848)	A likely source of leaking in the Node 3 CDRA was found during inspection with Ultrasonic Leak Detector (ULD). Ground teams will be reviewing the data and developing a leak repair task for the crew to perform in the future. Overnight, the Node 3 CDRA was activated and operated nominally following the replacement of Air Selector Valve (ASV) 104, and it is actively scrubbing Carbon Dioxide.
Thurs 7/23/2015 (hours 4872-4896)	Soyuz 43S launched at 4:02 PM CDT and docked at 9:46 PM CDT
Fri 7/24/2015 (hours 4896-4920)	The Remote Power Control Module (RPCM) that powers the Lab CDRA Air Selector Valves (ASVs) 1-6 has experienced trips since early 2014. Data analysis indicates a true overcurrent event signifying a fault downstream of the RPCMs. The RPCMs were removed and replaced to eliminate it as the source of the trips and attempt to restore reliable power to the ASVs
Sat 7/25/2015 (hours 4920-4944)	The ISS performed a Pre-determined Debris Avoidance Maneuver (PDAM) using Progress 58 R&D thrusters. This was the result of a late notification conjunction. Delta-V was 0.50 meters/second (m/s); burn duration was 4 minutes, 12 seconds.
Tues 7/28/2015 (hours 4992-5016)	Condensate tank offloaded to CWCs
Thurs 7/30/2015 (hours 5040-5064)	Wastewater bus connected to the Lab Condensate Tank and disconnected from the WPA
Fri 7/31/2015 (hours 5064-5088)	WRS – ARFTA Tank Fill
Mon 8/3/2015 (hours 5136-5160)	Condensate transfer from condensate tank to CWC WRS – ARFTA Tank Fill
Tues 8/4/2015 (hours 5160- 5184)	WRS – ARFTA Tank Fill

Table 4.4: Major ISS and ISS ECLS related activities on the ISS from February 9th to 29th, 2016 [162]

Date (hours since 00:00 1/1/2016)	Major ISS Event and/or ISS ECLS Event
Tues 2/9/2016 (hours 936-960)	WRS Maintenance
Fri 2/12/2016 (hours 984-1008)	WPA process cycles were suspended and manual water operations mandated until the WPA catalytic reactor replacement planned for February 23rd. The catalytic reactor has been suspected of leaking since November, and has shown signs of increased leakage since Monday. Yesterday, the crew reported an "offgassing" smell coming from the rack that houses the WPA.
Tues 2/16/2016 (hours 1104-1128)	WRS Waste Water Tank Drain Transfer of water to the water storage tank via the microbial removal filter (MRF)
Weds 2/17/2016 (hours 1128-1152)	ISS Reboost: The ISS successfully performed a reboost using the Progress 61 thrusters. The burn duration was 11 minutes long in order to achieve a delta-V of 1.05 meters per second.
Thurs 2/18/2016 (hours 1152-1176)	WRS – ARFTA Tank Drain and Fill
Fri 2/19/2016 (hours 1176-1200)	Cygnus departed after being berthed to the ISS for 72 days. WRS Waste Water Tank Drain
Sun 2/21/2016 (hours 1224-1248)	The UPA faulted out due to belt slippage between the distillation assembly and its motor. After faulting out 3 times, the ground team stood down from additional process attempts and directed the crew to configure the Waste and Hygiene Compartment (WHC) to store urine via internal tank [EDB-Y]. Ground teams are currently assessing a forward troubleshooting plan.
Mon 2/22/2016 (hours 1248-1272)	Equipment and tools were gathered in preparation for the WPA Catalytic Reactor R&R activity scheduled for tomorrow. The WPA Catalytic Reactor has been suspected of leaking since November, and has shown signs of increased leakage the past few weeks.
Tues 2/23/2016 (hours 1272-1296)	WPA Catalytic Reactor removed and replaced, a filter kit was installed in the WPA, and an inspection on the failed Catalytic Reactor was performed. Ground teams activated the WPA and performed a series of checks on the system.
Weds 2/24/2016 (hours 1296-1320)	Following yesterday's WPA Catalytic Reactor replacement, the WPA successfully completed a process cycle and is working nominally.
Thurs 2/25/2016 (hours 1320-1344)	Water Recovery and Management - Configure condensate collection connections
Fri 2/26/2016 (hours 1344-1368)	UPA transitioned from shutdown to standby in order to prepare for purge and recovery
Mon 2/29/2016 (hours 1416-1440)	Change of Command Ceremony from Expedition 46 Commander Scott Kelly to Expedition 47 Commander Tim Kopra

4.2.2 Validating the Isothermal Atmospheric Process Assumption

As was mentioned earlier, one of the key assumptions made by HabNet when performing atmospheric pressure and composition calculations is that the atmospheric temperature remains constant. This assumption reduces the number of system equations that need to be solved, resulting in a corresponding reduction in model execution time. From a physical standpoint,

this assumption relies on the ability of the habitat thermal control system to maintain a constant ambient temperature within the cabin.

Within HabNet, all instantiated SimEnvironments (see Appendix B.1 for details) are assumed to remain at a constant ambient temperature of 23°C. To investigate the suitability of this assumption, data collected on the cabin temperature within the ISS Destiny Laboratory was examined. As can be seen in the cabin temperature histories shown in Figure 4-6, the cabin temperature within the Destiny Laboratory remained within ±0.4°C of 23°C from mid-July to early August 2015 (see Figure 4-6(a)), and mostly within ±0.5°C of 23°C from February 9th to 24th 2016 (hours 1000 to 1300 in Figure 4-6(b)). After this period, on the morning of February 26th 2016, the cabin temperature began to fluctuate about a value of 24°C, suggesting that the temperature set point within the module may have been modified.

In addition, a transient temperature spike of approximately 1.5°C was observed during the latter stages of both of the February time periods lasting 30 and 60 minutes, as indicated in Figures 4-6(c) and 4-6(d). The short duration of these spikes suggests that some additional thermal load was temporarily introduced to the cabin. Shortly thereafter, the thermal control system returned the cabin temperature to its nominal set point. A review of the major crew activities listed in Table 4.4 found that no clear heat source could be identified for either transient (occurring on February 22nd and February 29th). While the change of command ceremony conducted on February 29th may be a potential source of additional heat (due to the additional heat load of all six crew located within the same module), it was found that the temperature spike occurred approximately 7 hours prior to the moment at which the event took place [163]. Thus, based on the information available, it is not possible to precisely identify the cause of these temperature spikes. Regardless, the short duration of these temperature spikes relative to the overall cabin temperature trends within the Destiny Laboratory indicate that in general, the ISS cabin temperature remains largely constant, with fluctuations in the range of 23°C to 24°C. This observation validates the HabNet assumption of a constant cabin temperature.

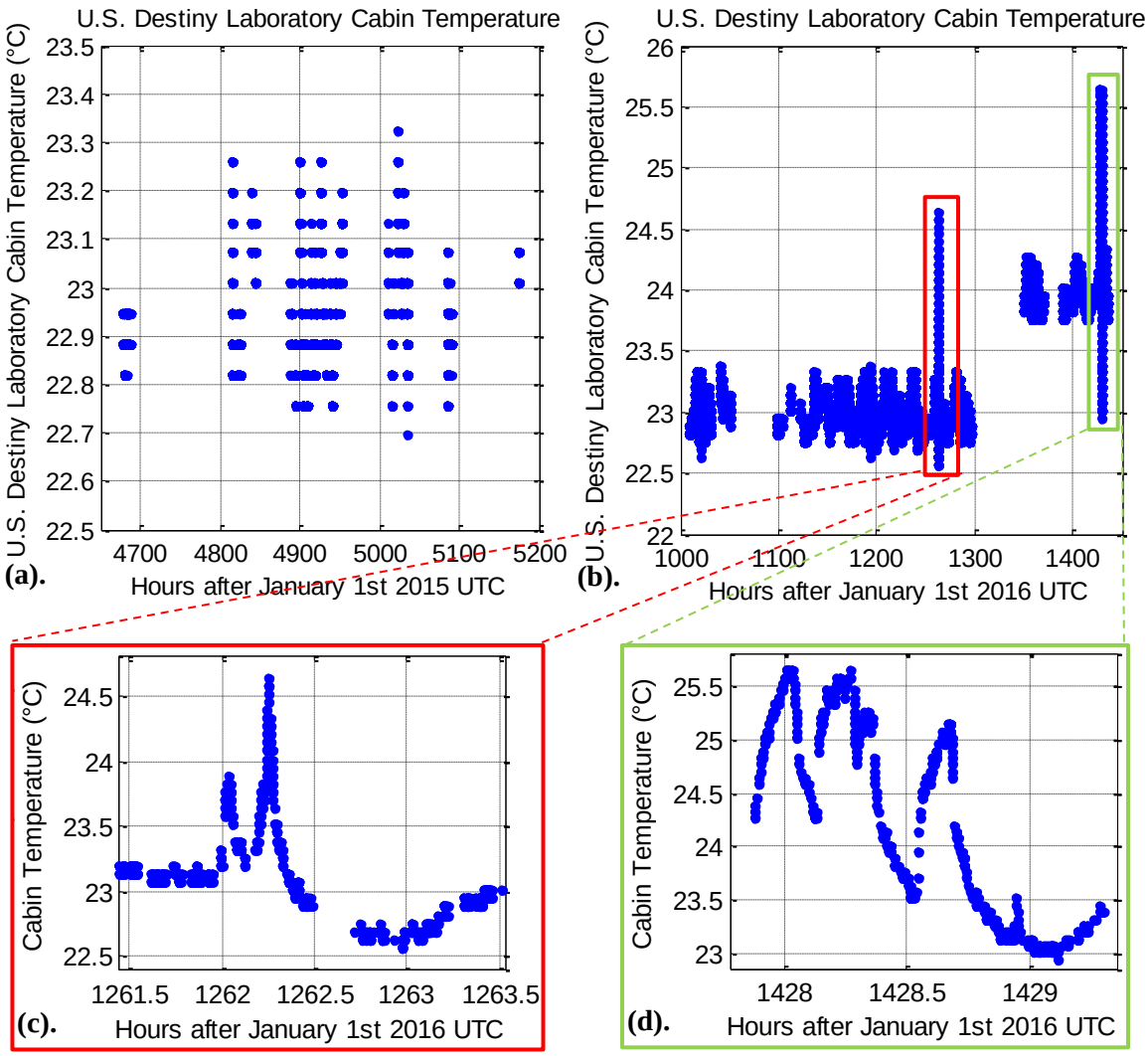

Figure 4-6: U.S. Destiny Laboratory Cabin Temperature (a). from July 14th, 2015 to August 4th, 2015 (b). from February 9th, 2016 to February 29th, 2016 (c) from 1:30pm to 3:30pm UTC February 22nd, 2016 (d) from 12:00pm to 1:30pm UTC February 29th, 2016

4.2.3 Urine Processor Assembly Model Validation

Within HabNet, the Urine Processor Assembly is modeled by the ISSWaterRSLinearImpl class, and involves the consumption of urine from a urine tank at a rate that is proportional to the amount of power available. Of this urine, 74% is recovered into urine distillate (based on published UPA performance data) and sent to the grey water tank, while the remainder is delivered as brine to a waste tank (see Appendix D.6.1 for details).

Thus, in order to validate this model, time history data on the fill level of the ISS urine and grey water tanks was examined and compared to the recorded operational status of the ISS

UPA. Figure 4-7 summarizes this data for the period spanning from 4:00pm UTC on February 16th, 2016 (hour 1120 of 2016) to 12:00am UTC on February 20th, 2016 (hour 1200 of 2016). Here, each of the colored bands represents the operational status of the UPA as indicated in the figure legend, while the urine tank level is measured by the purple markers, and the grey water tank level is measured by the grey markers.

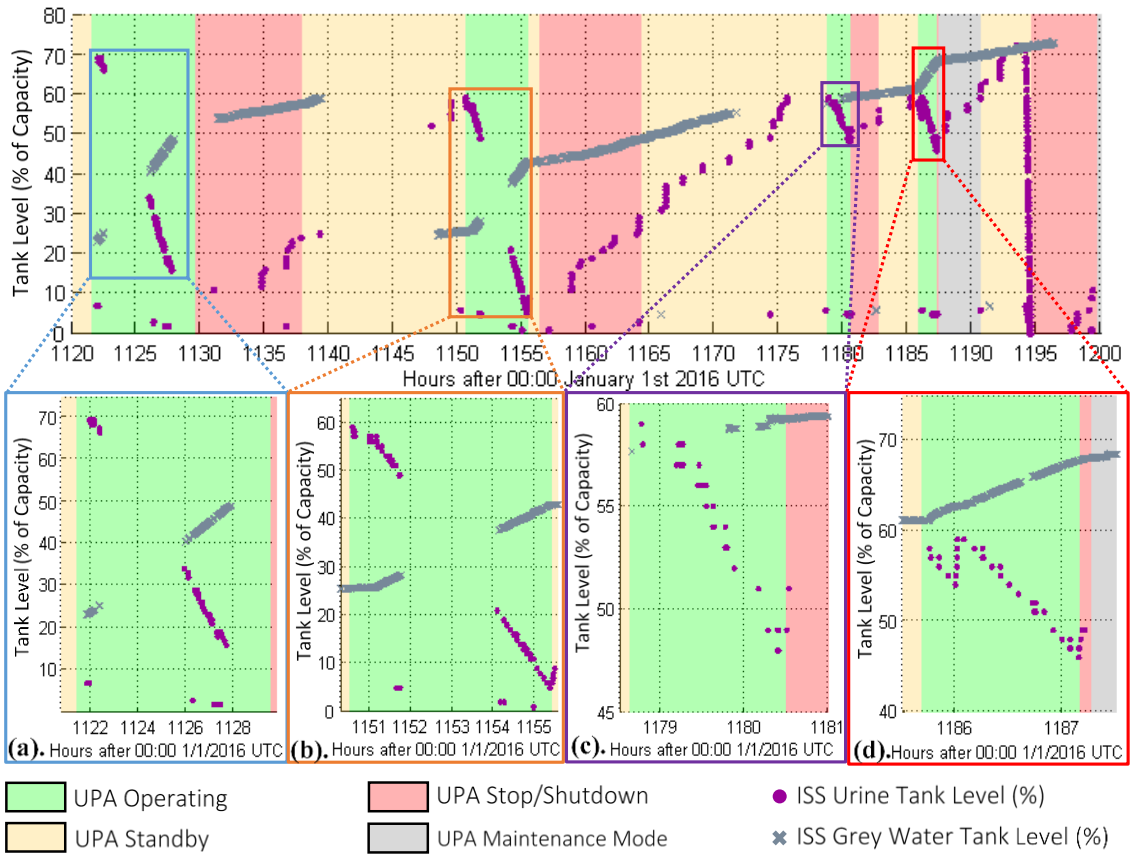

Figure 4-7: ISS Urine and Grey Water Tank Levels from 4:00pm UTC February 16th, 2016 to 12:00am UTC February 20th, 2016

It can be observed from Figure 4-7 that the UPA cycled through four operational runs of varying duration throughout the 80 hour period examined. After the final run, the UPA was put into a maintenance mode, before being ultimately shutdown. These four unique operational runs will form the basis of this model validation exercise, and have been extracted and zoomed-in upon in Figures 4-7(a) to 4-7(d).

Upon examination of these zoomed-in figures, it is apparent that significant gaps exist in both the urine and grey water tank capacity data. As mentioned earlier, this is likely due to

temporary interruptions in communications between either the ISS and the ground, and/or the MCC server and the data stream client application. Despite these data gaps, we can still infer operational trends in the data.

From Figure 4-7, we observe that whenever the UPA is in an operational state, the urine tank level decreases while the grey water tank increases, both in what appear to be a linear manner. This is particularly evident in the shorter duration UPA processing runs in Figures Figure 4-7(c) and Figure 4-7(d), where sufficient data points have been recorded to capture this linear trend. In the latter of these two runs, the urine tank level jumps at hour 1186 by approximately 400mL, likely due to a crewmember using the commode at this time.

In general, this observed linear behavior is well replicated by the HabNet ISSWaterRSLinearImpl class when simulated under the same initial conditions as those of the urine and grey water tanks at the beginning of the four ISS UPA processing cycles. Figures 4-8(a) to 4-8(d) present the results of these simulations, plotted over the same recorded ISS data as that presented in Figures 4-7(a) to 4-7(d). Here, it is important to note that because products other than urine are delivered to the grey water tank, an additional grey water tank fill rate was added to the HabNet simulation runs such that the aggregate increase in grey water level corresponded to that recorded in the ISS data. This additional fill rate is intended to correspond to the introduction of grey water products from other sources, such as humidity condensate from the cabin condensing heat exchangers, and product water from the Sabatier reactor, and is listed in the corresponding figure caption.

From Figure 4-8, we observe a very good fit between the ISSWaterRSLinearImpl prediction and the ISS UPA operational data for all UPA runs except for the second (see Figure 4-8(b)), where the rate of urine removal from the urine tank is greater than the maximum published UPA urine processing rate of 755mL/h [164]. This suggests that another source of urine removal is present during this second UPA run, contributing an additional urine removal rate of approximately 165mL/hr.

A review of the major ISS ECLS events listed in Table 4.4 found that the UPA Advanced Recycle Filter Tank Assembly (the ARFTA – (see Appendix D.6.1) is drained and filled on the same day as this urine process. While this process involves the transfer of urine from the urine tank to the ARFTA, it is typically not performed while the UPA is operating [75]. Thus, without further data on the operating characteristics of the UPA at this time, the source of this additional urine removal rate cannot be identified. However, even with this discrepancy, the consistent linear behavior of the UPA, along with the generally accurate prediction of urine tank depletion

rates (to within 8%), provides validation for the underlying assumptions made in the implementation of the urine processing portion of the ISSWaterRSLinearImpl HabNet class.

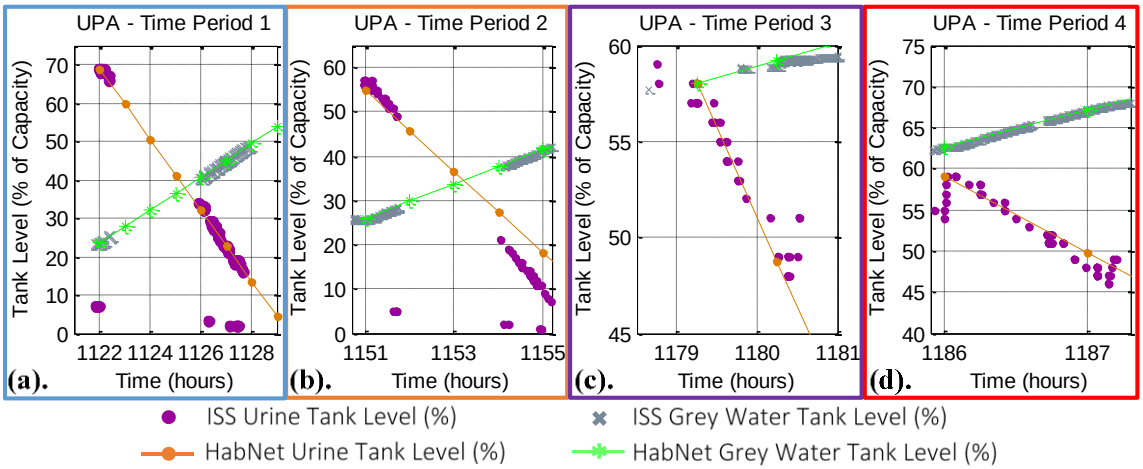

Figure 4-8: Comparison between ISS urine and grey water tank levels and the corresponding values predicted by the HabNet ISSWaterRSLinearImpl class (a) UPA operation with a condensate addition rate of 1.4L/h (b). UPA operation with a condensate addition rate of 0.85L per hour (c). Nominal UPA operation (zero grey water addition rate) (d). UPA operation with a condensate addition rate of 1.46L/h

4.2.4 Water Processor Assembly Model Validation

Like the Urine Processor Assembly, the Water Processor Assembly (WPA) is also modeled by the ISSWaterRSLinearImpl class within HabNet. Here, the WPA receives grey water from the grey water tank, and processes it to potable water at a nominal rate of 5.9L/h [164] whenever sufficient power is available. Product water from this process is then delivered to a potable water tank, where it is subsequently used by the crew or sent to the oxygen generation assembly to be electrolyzed into breathing oxygen.

Thus, to assess the accuracy of the water processor portion of the ISSWaterRSLinearImpl, time history data on the fill level of the ISS grey and potable water tanks was examined, along with the operational status of the WPA. Figure 4-9 presents this data for a two-day period spanning from 8:00pm UTC on February 10th, 2016 (hour 980 of 2016) to 10:00pm UTC on February 12th, 2016 (hour 1030 of 2016). Here, it can be seen that the ISS WPA was operational on two separate occasions throughout this period. During the first three to four hours of both WPA cycles during this period, the grey and potable water tank levels respectively decreased and increased in a linear manner, as can be seen in the zoom-in plots shown in Figures 4-9(a)

and 4-9(b). This suggests that the ISS WPA consumes grey water and produces potable water at near constant rates, as is assumed in the implementation of the HabNet ISSWaterRSLinearImpl class.

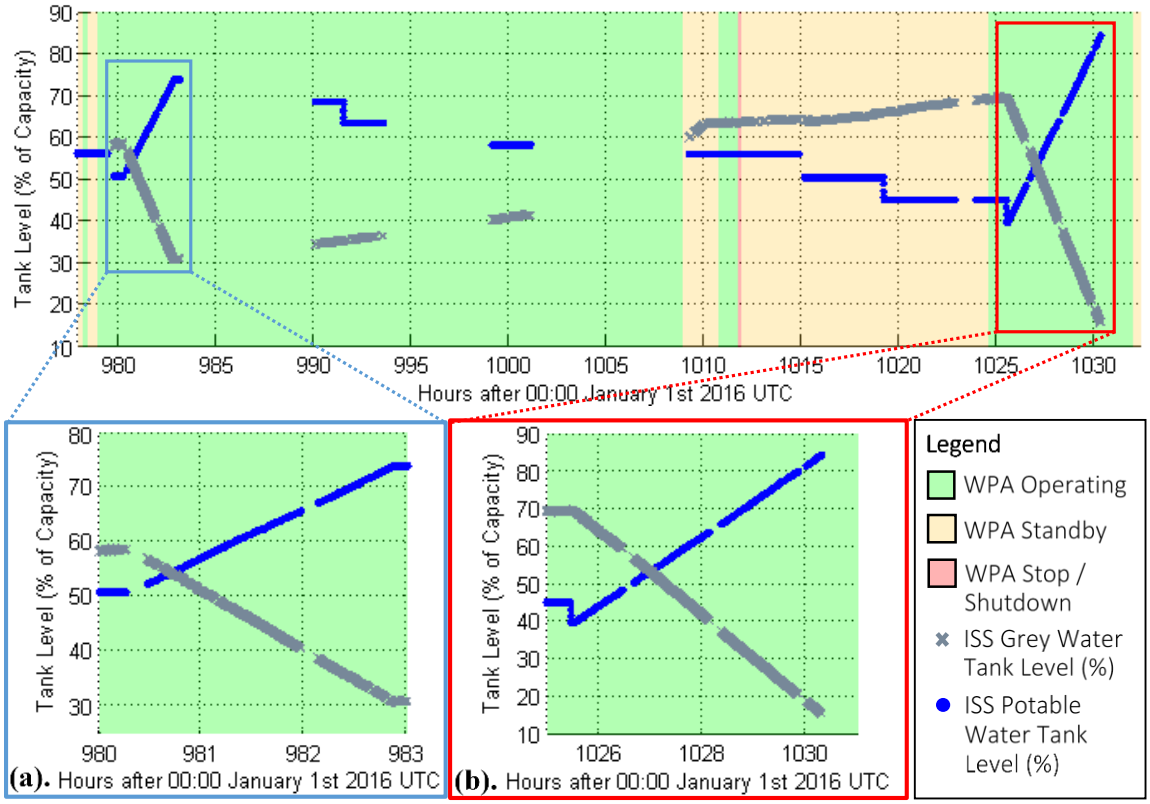

Figure 4-9: Summary of ISS data collected that is relevant to the operation of the WPA (a). WPA process starting at 8:30pm UTC, February 10th 2016 (b). WPA process starting shortly after 5:00pm UTC, February 12th 2016

As was performed for the UPA, we simulate the dynamic behavior of the water processor within HabNet with the same initial conditions as those recorded from the ISS operational data, and overplot the results to evaluate the validity of HabNet's water processor performance estimates. Figure 4-10 compares these simulation results for the two WPA operational cycles recorded in in Figures 4-9(a) and 4-9(b).

Here, two sets of simulations have been performed for each WPA operational cycle. The first corresponds to the HabNet-simulated WPA processing grey water under conditions where there are no other producers or consumers of grey or potable water that would act to modify the rates at which both tanks were respectively depleted or filled. These are indicated by the solid lines depicted in Figures 4-10(a) and 4-10(b), where the HabNet water processor exhibits

the general trend of over-consuming grey water and over-producing potable water relative to the corresponding tank depletion and fill rates recorded from the ISS.

Conversely, the second set of simulations reruns the first set, with additional grey water and potable water tank fill rates that have been modified to match those recorded from the ISS. Specifically, these additional fill rates are intended to represent additional sources of feed into the grey water tank (e.g. humidity condensate extracted by the Common Cabin Air Assembles and Sabatier product water, which are both delivered to the grey water tank on the ISS – see Appendices D.3 and D.7), as well as additional sources of depletion from the potable water tank (e.g. usage by the crew, experimental payloads, and feedwater for the Oxygen Generation Assembly). The results of this second set of simulations are represented by the dashed lines displayed in Figures 4-10(a) and 4-10(b), with the values of the supplementary fill rates used in these simulations described in the figure caption.

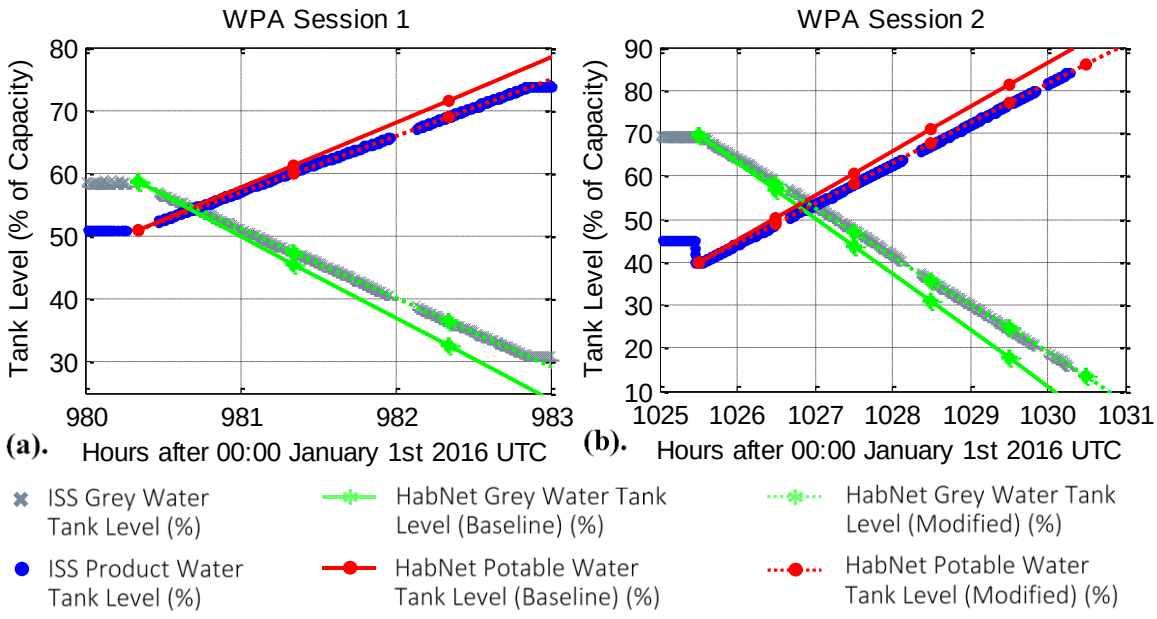

Figure 4-10: Comparison between ISS grey and potable water tank levels and the corresponding values predicted by the HabNet ISSWaterRSLinearImpl class (a) WPA operating with a grey water addition rate of 0.89L/h, consuming potable water at an additional rate of 0.72L/h (b).WPA operating with a grey water addition rate of 0.78L/h, consuming potable water at an additional rate of 0.64L/h

As can be seen in these figures, a very good match is obtained when these supplementary tank fill rates are included. This is to be expected since the original ISS data was used to inform the "modified" set of simulations. Although the actual additional grey water introduction and

potable water removal rates arising from the operation of other ISS ECLS systems are not explicitly recorded in the data, it was found that the values used in the modified set of simulations shown in Figure 4-10 are within the same order of magnitude as those expected on the ISS. Specifically, a maximum discrepancy in water production/consumption rate of 15% was computed based on the maximum supplementary rate of 0.89L/h assumed in the second set of simulations shown in Figure 4-10, and the nominal WPA processing rate of 5.7L/h [164].

Moreover, it was observed that over the two days that WPA data was recorded, the ISS OGA was set to a peak oxygen production rate of 3.2kg O_2/day (see Figure 4-11(a)). Based on the stoichiometry of the water electrolysis reaction, this corresponds to an average potable water consumption rate of approximately 0.15L/h – a value which is within the additional potable water consumption rates assumed in the modified simulations of Figure 4-10. Similarly, it was observed from preliminary cabin simulations of the HabNet condensing heat exchanger (CHX) model (the ISSDehumidifierImpl class described in Appendix D.2), that the typical amount of water vapor extracted from the cabin atmosphere and delivered to the grey water tank is approximately 0.25L/h per CHX (see Figure 4-11(b)). Again, this value is within the additional grey water tank fill rate values assumed in the modified simulations shown in Figure 4-10.

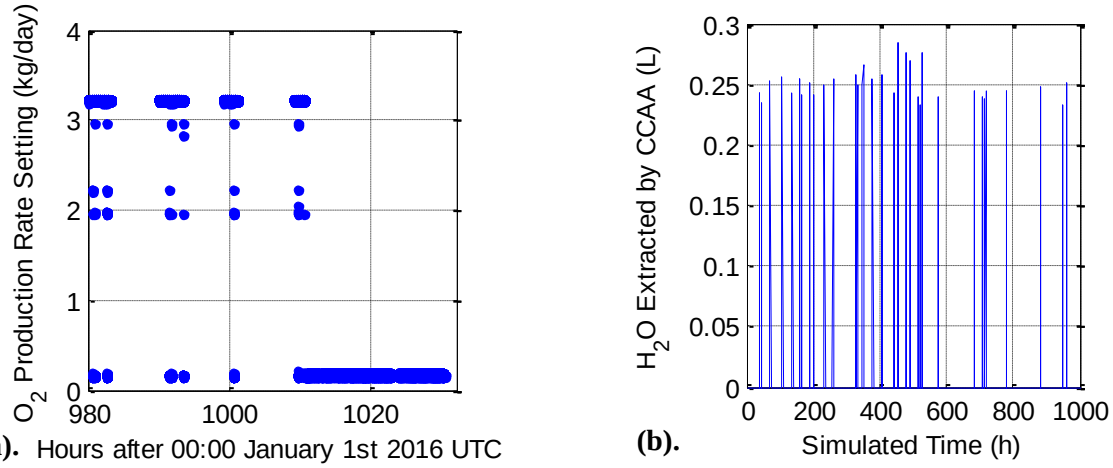

Figure 4-11: Comparison between OGA production rates recorded from the ISS and automatically selected with HabNet (a). OGA O_2 Production Rate Setting obtained from ISS Data (b). H_2O Extracted by the CCAA as simulated within HabNet

Thus, based on the consistent linear trends in grey and potable water tank fill levels arising from the operation of the ISS WPA, along with the fact that the predicted water usage and

production quantities are within the same order of magnitude as those observed on the ISS, we conclude that the implementation of the water processing portion of the HabNet ISSWaterRSLinearImpl class is valid for our purposes of predicting dynamic behavior and consumables requirements during the early stages of space habitation architecture development.

4.2.5 Oxygen Generation Assembly Model Tuning

As was described in Section 2.1.2, the Oxygen Generation Assembly provides breathing oxygen for the crew via the electrolysis of water. Within HabNet, this system is modeled by the ISSOGA class (see Appendix D.5 for details), where water is consumed from a potable water tank and product breathing oxygen is injected directly into the crew cabin, based on a commanded O_2 production rate setting. Unlike the previously evaluated ECLS technologies however, complete information on all attributes of the OGA was not available when it was first implemented within the ISSOGA class. To overcome this, OGA operational data recorded from the ISS was used to derive the missing parameter – namely the volume of the rotary separator / accumulator (RSA) that collects and stores water inside the OGA prior to delivering it to the electrolysis cell stack (see Appendix D.5). Thus, in contrast to the Urine and Water Processor Assemblies (the UPA and WPA) validated in the previous sections, the ISS operational data is used here to tune the OGA technology model (as implemented within the ISS OGA HabNet class).

The corresponding ISS OGA data that was obtained from the MCC server is summarized in Figure 4-12. This data represents a 10 day period from February 9th to 19th, 2016. Here, the partial pressure of oxygen within the ISS Node 3 (where the OGA is located) is displayed (Figure 4-12 (a)), along with the fill level of the potable water tank that supplies the OGA with electrolysis water (Figure 4-12(b)). In addition, both of these figures are overlaid with color bands representing the operational status of the OGA. For this particular data set, these bands indicate that the OGA was in operation for the majority of the ten day period being examined.

From Figure 4-12(b), we observe that the potable water tank fill level decreases in discrete steps during periods whenever the OGA is in an operational mode. As will be discussed below, these discrete drops correspond to the OGA RSA collecting water from the potable water tank to maintain a threshold water level required to feed the electrolysis stack. In addition, linear

increases in the potable water level can be seen interspersed throughout these discrete drops in water level. These correspond to the WPA potable water production trends examined in Section 4.2.4 (see Figures 4-9(a) and 4-9(b)).

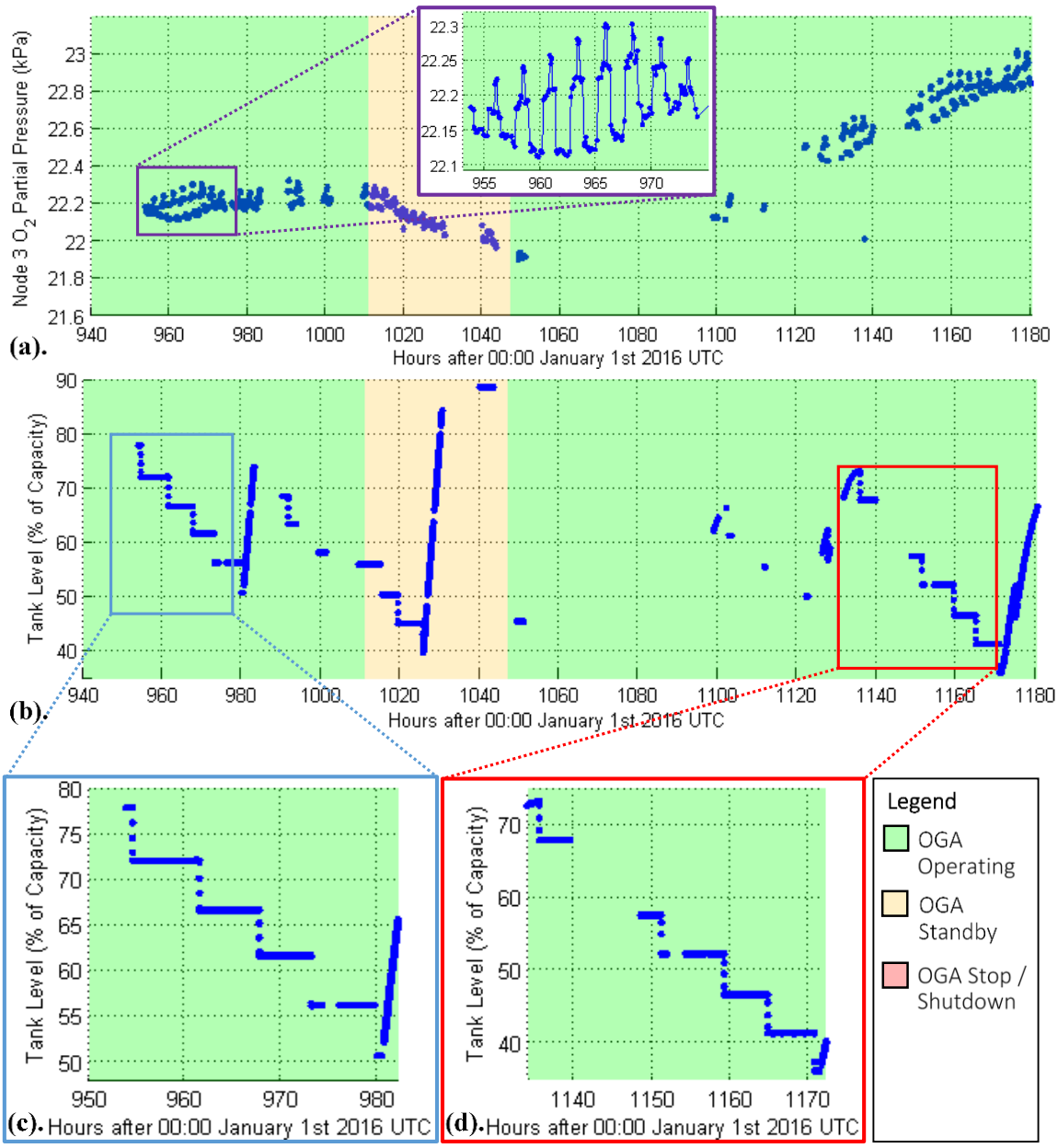

Figure 4-12: ISS Data related to the operation of the OGA obtained from February 9th to 19th, 2016 (a). Node 3 O_2 partial pressure level (b). Potable water tank level (c). Close up of ISS potable water store level from February 8-9th, 2016 (d). Close up of ISS potable water store level from February 17-18th, 2016

Contrastingly, no strong correlation between the cabin oxygen partial pressure trend (the destination of the products of the OGA) and the OGA operational state could be observed from the ISS data shown in Figure 4-12. As shown in the inset image in Figure 4-12(a), the trend in cabin oxygen partial pressure over the timescales at which the OGA is in an operational state is dominated by a periodic dynamic motion. The period of this pseudo-sinusoidal trend indicates that the dynamics of the cabin oxygen partial pressure are driven predominantly by the swing-bed operation of the Carbon Dioxide Removal Assembly (CDRA), which adsorbs and desorbs CO_2 from the cabin atmosphere at 155 minute cycles (see Section 4.2.6 for further details). Thus, from the perspective of evaluating the accuracy of the HabNet ISSOGA class, only the potable water tank data can be used.

The orange trend in Figure 4-13 presents the potable water consumption trends of the original instance of the HabNet ISSOGA class, prior to the analysis performed to derive the previously unknown OGA RSA volume. Here, an RSA volume of $58in^3$ was assumed, based on a lower bound value described in the literature [165]. In addition, the simulated OGA was set to operate at a continuous oxygen production rate of 3.2kg of oxygen per day, based on the production rate setting recorded from the ISS.

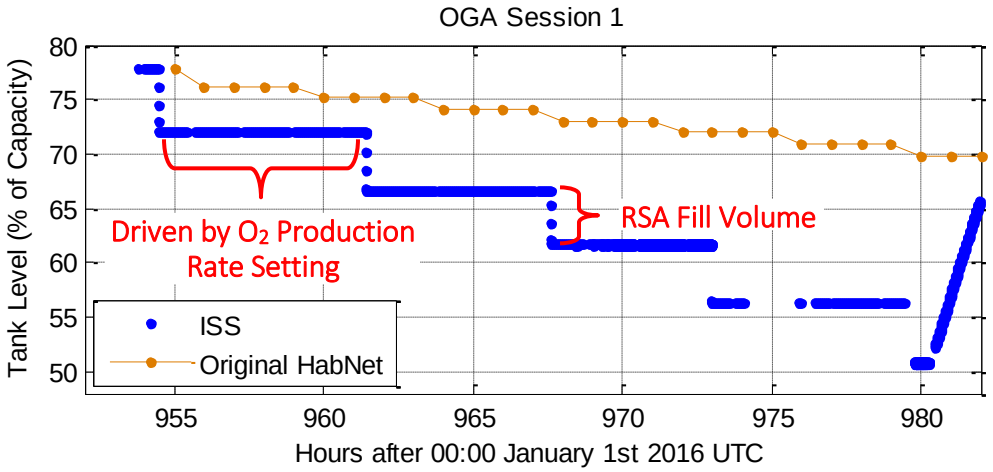

Figure 4-13: Comparison of potable water level predicted by the original HabNet ISSOGA class with corresponding ISS data

From Figure 4-13, we observe that the HabNet ISSOGA model predicts the same general discrete potable water level trend found in the ISS data (the blue trend shown in this figure). Here, the discrete drops in water level are much lower in magnitude and have a shorter duration than those observed in the ISS data. In addition, the drops are not instantaneous, as is exhibited

in the ISS data. This is due to the fixed hour-long simulation time steps assumed in the HabNet model (see Section 3.4.1 for a discussion on the selection of the simulation time step), which limits the minimum duration over which dynamic events can occur to one hour.

To further characterize this dynamic behavior, various initial conditions were perturbed one at a time and the HabNet ISSOGA resimulated. Through this, it was found that the magnitude of the discrete drop in water level corresponds to a discrete volume of water collected by the RSA – specifically, the difference between the capacity of the RSA and its lower threshold water fill level. Moreover, it was observed that the length of each step in the water fill level trend corresponded to the average oxygen production rate over the operational period of the OGA. These correlations are depicted above in Figure 4-13.

From this, it was found that a simulated RSA volume of 2.65L greater than the threshold fill level of 0.5L ($30in^3$) resulted in the same level of water consumption as the ISS data, and an average production rate of 3.5 times the commanded 3.2kg O_2/day setting resulted in the same water level step length. This latter finding indicates that the ISS OGA does not generate oxygen in a continuous manner throughout a 24 hour day, as is the case with its implementation within the HabNet ISSOGA class, where a continuous production rate of 3.2/24 = 0.133kg O_2/h is assumed. Rather, the ISS OGA generates larger amounts of oxygen over shorter discrete intervals, such that the total daily oxygen produced is equivalent to the production rate setting (3.2kg in this case). On the ISS, these intervals are driven by the day/night orbital cycles, where operations are typically preferred during the day side of each orbit, when more power is available [166]. The 3.5 multiplier value therefore implies that the over a 24 hour period, the ISS OGA typically generates oxygen over 24/3.5 = 6.85 hours. For the remaining time that the OGA is set to an operational state (the green band in Figure 4-12(a) and 4-12(b)), other operations in addition to the generation of oxygen also take place. These include the collection of water, the activation of heaters, the sensing of bubbles in feedwater, the detection of hydrogen in output oxygen, and the purging of the system gas lines with nitrogen [165].

With a volume for the RSA and an equivalent continuous O_2 production rate calculated, the HabNet ISSOGA class was updated and simulated with the same initial potable water fill levels as the two OGA process cycles shown in Figures 4-12(c) and 4-12(d). This volume value was adopted within this class for all the case studies performed within this thesis. Figure 4-14 compares the results of these simulations with the recorded ISS data.

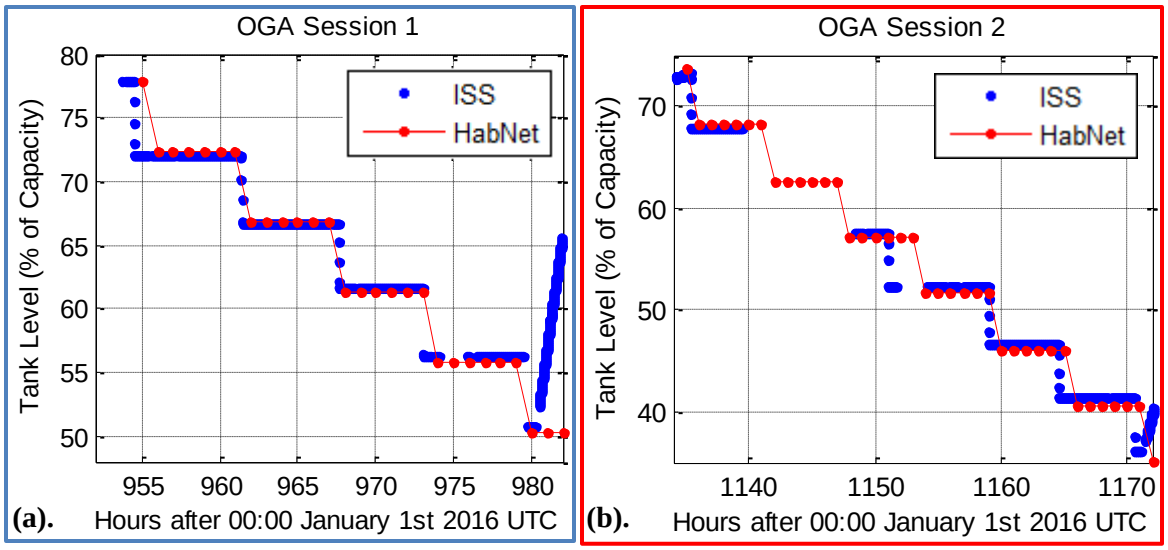

Figure 4-14: Comparison between potable water store level predicted by the HabNet ISSOGA class with the ISS potable water level obtained from the MCC server (a). From February 8th to 9th, 2016 (b). From February 17th to 18th, 2016

Here, the updates to the HabNet ISSOGA class have resulted in a significant improvement in its potable water fill level predictions, in both the discrete amount of water consumed by the ISS RSA, and the period of time between successive collections of feedwater samples. In both of these simulation cases, the discrepancy in water fill level was found to be less than 1%, thus signifying the correct tuning of the updated HabNet ISSOGA model.

4.2.6 Carbon Dioxide Removal Assembly Model Validation

In contrast to the previously discussed ISS technologies, no data on the operational status of the Carbon Dioxide Removal Assembly (CDRA) is available from the MCC server. Instead, the only available measure of the CDRA performance is data on the CO_2 partial pressure within the ISS Node 3, where one of the two USOS CDRAs is located. Thus, to evaluate the performance of the HabNet model of the CDRA (as implemented within the HabNet ISSVCCRLinearImpl class – see Appendix D.4), we compare the cabin CO_2 partial pressure levels observed within Node 3 of the ISS with those predicted by a HabNet simulation of the same mission scenario.

We begin this comparison by first examining the ISS CO_2 partial pressure data that was obtained from the MCC server. As shown in Figure 4-15, this data was collected for the ISS Node 3 over a two week period spanning from February 9th to 24th, 2016.

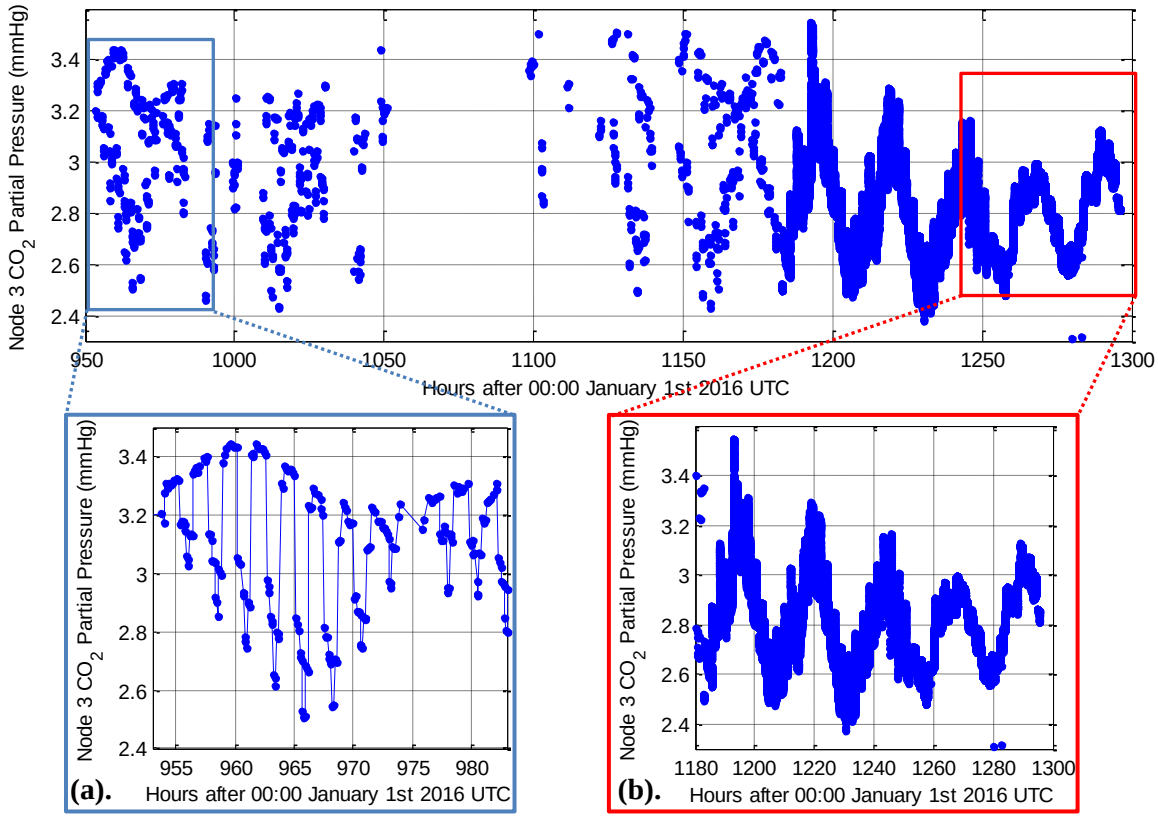

Figure 4-15: ISS Node 3 CO_2 Partial Pressure from February 9th to 24th, 2016

Here, we examine two distinct clusters of partial pressure data that were recorded. One spanning a 30 hour period from February 9th to 11th (hours 950 to 980 of 2016), as shown in Figure 4-15(a), and one from February 19th to 24th (hours 1180 to 1300 of 2016), as shown in Figure 4-15(b). As can be seen in these zoomed-in figures, the first cluster is characterized by a dominant short period dynamic trend, while the second cluster is governed by a longer period oscillatory trend. As was mentioned in Section 4.2.5, the short period trend within the first cluster is driven by the 155 minute cycle of each CDRA swing bed, as is summarized in Figure 4-16(a) below.

These two distinct pressure trends were used as the basis for evaluating the accuracy of the HabNet implementation of the CDRA, and by extension, the ability of HabNet to simulate crew members living and working in a simulated habitat, and exchanging metabolic resources with the surrounding atmosphere.

ISS CDRA Cyclic Operational Schedule (see Appendix D.4 for description of components)

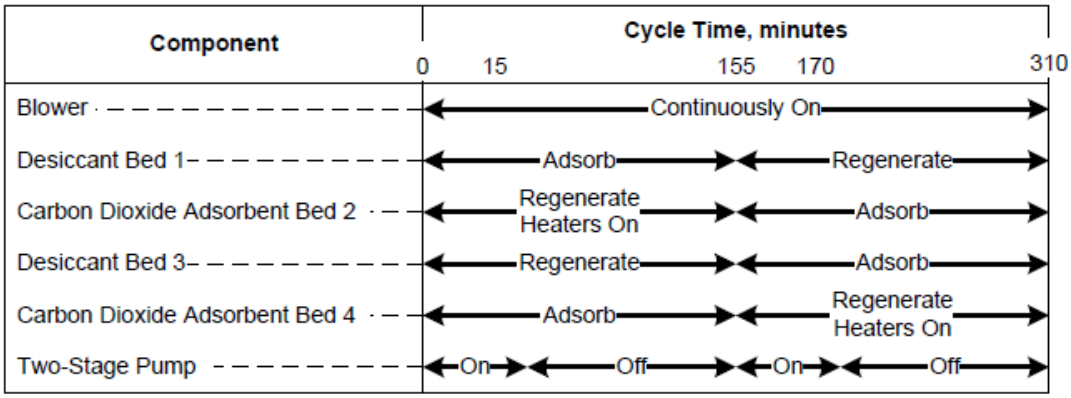

(a).

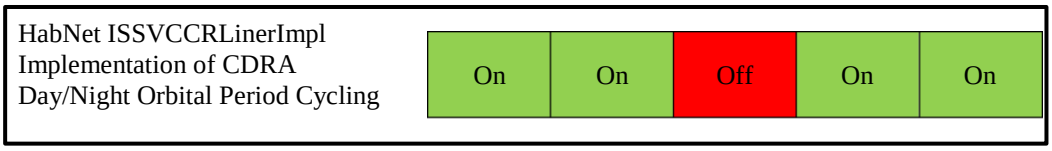

(b).

Figure 4-16: Comparison of the ISS CDRA cyclic operational schedule (labeled (a)) with HabNet implementation of the same schedule (labeled (b)). Since HabNet operates on one hour time steps, the five hour total cycle time of the ISS CDRA is discretized into five hour-long blocks, with the middle block switched off to simulate the switching of CDRA desiccant/adsorbent beds

In order to simulate an equivalent mission scenario within HabNet, a crew activity schedule was first estimated. In this analysis, the crew schedule is a particularly important parameter due to the fact that the intensity and duration of each activity performed by each crewmember influences their respiration rate, and hence the amount of CO_2 they expend into the cabin. Since no hourly crew schedule data is publicly available for the period over which the ISS data was collected, we assume a standard ISS daily crew schedule of 9 hours of combined pre-sleep, sleep and post-sleep, followed by 5 hours of low intensity IVA activities during a morning session, 2 hours of exercise, and 8 hours of afternoon and evening low intensity IVA. This is based on a 24-hour ISS crew schedule published online during ISS Expedition 40, shown below, in Figure 4-17.

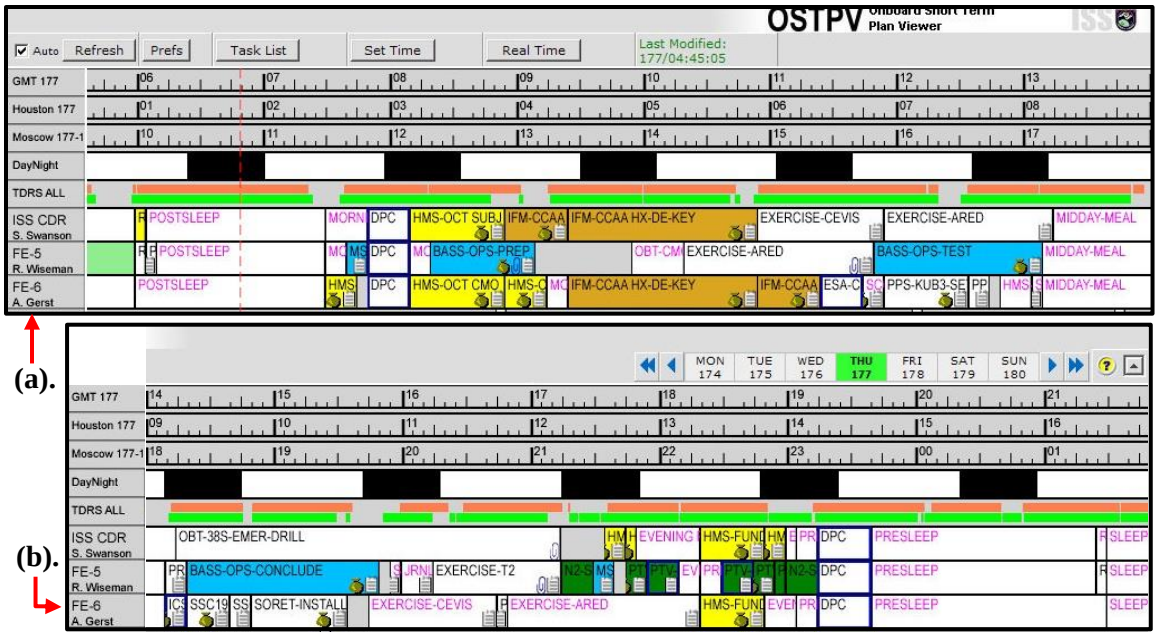

Figure 4-17: Typical ISS Daily Schedule [167] (a). First half of working day (b). Second half of working day

In addition, since only CO_2 partial pressure data within Node 3 was recorded, we simulate only the atmosphere within Node 3, rather than the entire ISS. Here, two simulated astronauts are placed within a virtual Node 3, each with the schedule described above, and both supported by the ISS ECLS systems listed in Table 4.2. Furthermore, in order to simulate the day/night orbital period cycling behavior of the CDRA, the HabNet ISSVCCRLinearImpl class was commanded to switch off in the third hour of every five hour block of time, to replicate the CDRA operational schedule shown in Figure 4-16(b). This differs from the baseline ISSVCCRLinearImpl mode of being continuously operational. Figure 4-18 summarizes the layout of this habitation scenario, while Figure 4-19 presents the atmospheric CO_2 partial pressure obtained from this simulation, over-plotted with the corresponding data from the second cluster of ISS data shown in Figure 4-15(b).

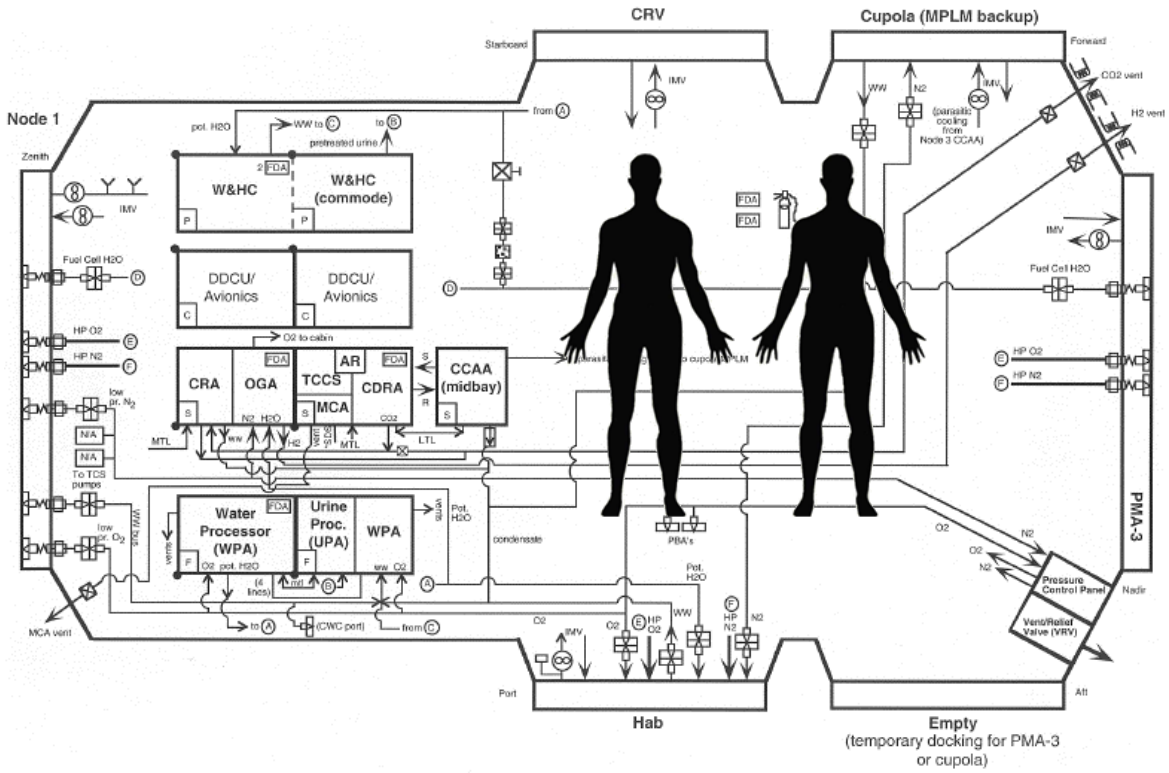

Figure 4-18: CDRA Validation Simulated Habitation Scenario

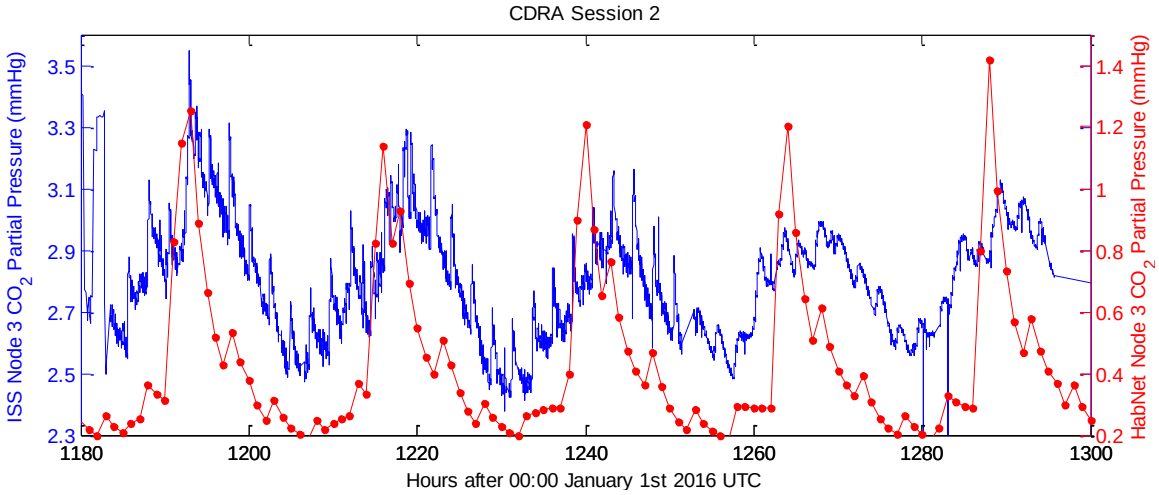

Figure 4-19: Comparison of Node 3 CO_2 partial pressure measured on the ISS (blue) with that predicted by HabNet (red) over the second time period highlighted in Figure 4-15(b).

From the comparison of the ISS- and HabNet-generated datasets shown in Figure 4-19, we observe that while HabNet under-predicts the ambient cabin CO_2 partial pressure levels by a constant value of approximately 2mmHg (0.27kPa), its predictions of the temporal variations in cabin CO_2 partial pressure track reasonably well with that of the ISS data.

One likely cause of HabNet's lower total CO_2 partial pressure prediction is the fact that the simulation scenario assumed two crewmembers located within a simulated Node 3 that was atmospherically isolated from the remainder of the ISS and its crew. On the ISS however, intermodule ventilation occurs between Node 3 and its adjacent modules. Since the CDRA is located in Node 3, the CO_2 load of all six crewmembers is eventually transferred into Node 3 for subsequent removal, thereby leading to a higher ambient CO_2 concentration than the isolated case assumed within the HabNet simulation. Here, a full simulation of the ISS was not performed since the Russian Vozdukh CO_2 removal system that shares the CO_2 removal function with the CDRA is not currently modeled within HabNet.

Conversely, the similarity in dynamic behavior between the ISS data and the HabNet simulation results can be attributed to the dominant effects of the crew schedule on cabin CO_2 partial pressure. Here, the synchronization of the peaks in the CO_2 partial pressure trend roughly correspond to the daily exercise routines of the crew members, while the extended troughs in these trends correspond to crew sleep periods. This correlation is especially apparent by the approximately 24 hour period between peaks in the ISS data. This exercise-sleep cycle in the crew schedule causes the dominant long-periodic dynamic behavior observed in the ISS data shown here and observed earlier in Figure 4-15(b), where this second cluster of data points was originally identified.

Interestingly, this long-periodic dynamic behavior was not observed in the first cluster of CO_2 partial pressure data points plotted in Figure 4-15(a). The lack of CO_2 peaks suggests that the crew did not exercise within Node 3 over this first 30 hour period. In light of this, another HabNet simulation was performed and compared to the first cluster of ISS data points. In this second simulation, exercise was removed from the crew schedule, with all other initial conditions remaining the same. Figure 4-20 compares the results of this second HabNet simulation with the CO_2 partial pressure over the first time period identified in Figure 4-15.

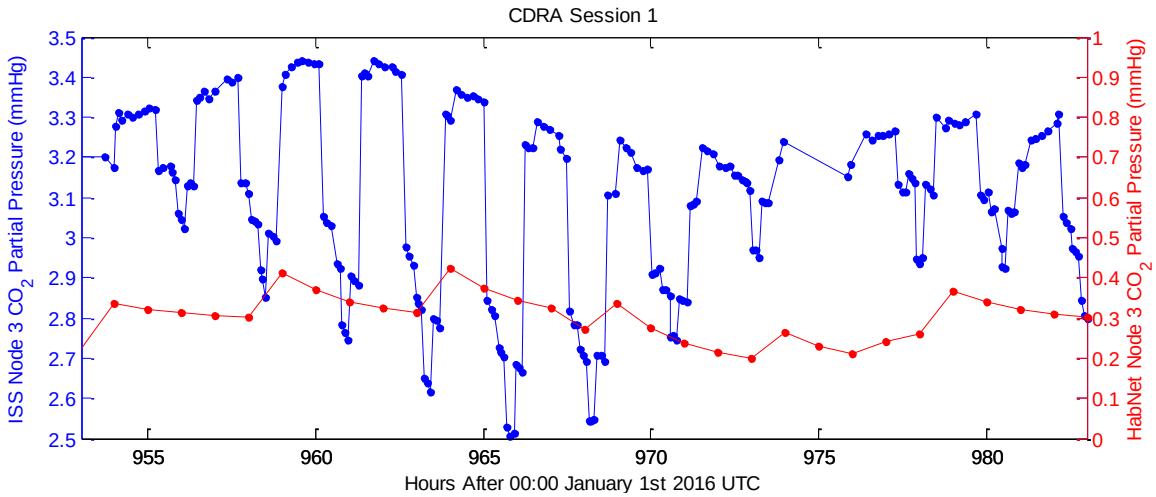

Figure 4-20: Comparison of Node 3 CO_2 partial pressure measured on the ISS (blue) with that predicted by HabNet (red) over the first time period highlighted in Figure 4-15(b).

From Figure 4-20, we observe that once again, the HabNet model under-predicts the total cabin CO_2 partial pressure. This suggests that the ISSVCCRLinearImpl model within HabNet is performing at a higher relative CO_2 removal rate than that of the ISS, likely due to the same reasons discussed earlier. With respect to the temporal variations in CO_2 partial pressure, we observe that the longer-period behavior of the HabNet prediction tracks reasonably well with that of the ISS data, as indicated by the similar 24-hour period between peak values in both data sets (from approximately hour 958 to hour 982). As was the case with the first set of simulations, this behavior is driven by the sleep cycles of the crew. During sleep periods, the ambient CO_2 level drops due to the lower metabolic activity of the crew.

With regards to the shorter period behavior in Figure 4-20, we find that the HabNet model is not able to predict the drops in CO_2 partial pressure that occur approximately every 155 minutes in the ISS data, due to the insufficient temporal resolution in the HabNet simulation, along with the fact that the complexity of adsorbent bed cycling dynamics is not modeled within the HabNet ISSVCCRLinearImpl class. Instead, the periodic powering down of the ISSVCCRLinearImpl object (see Figure 4-16(b)) results in a momentary increase in cabin CO_2 partial pressure every 5 hours, as shown in the red trend in Figure 4-20.

Thus, based on the two comparative analyses performed above, we conclude that the HabNet CDRA model, as implemented within the ISSVCCRLinearImpl class, produces generally accurate predictions of the temporal variations in cabin CO_2 partial pressure, but may be susceptible to over-predicting the CO_2 removal capability of the ISS CDRA. It is important to note that this latter observation is not conclusive due to the uncertainties in the U.S. CDRA

and Russian Vozdukh operating conditions, described earlier. With regards to the mission architecting analysis applications of HabNet, we expect this difference to have a minimal impact on the predictions of resource requirements, since the CDRA does not require consumable resources that need to be resupplied or produced in-situ in order for it to function.

4.2.7 Carbon Dioxide Reduction System Model Validation

The ISS Carbon Dioxide Reduction System (CRS) was one of the final life support technologies installed on the ISS. Unlike the other technologies examined throughout this chapter, no data on the operation of the CRS is available from the MCC server. This is likely due to the unique contractual structure that governed the CRS development and sustainment program, whereby NASA purchased water as a service provided by Hamilton Sundstrand – the company responsible for the development and operations of the ISS CRS [168].

As was discussed in Appendix D.7, the ISS CRS revolves around a Sabatier reactor, which produces water and methane by reacting CO_2 extracted from the cabin atmosphere by the CDRA with product hydrogen gas from the ISS OGA. Within HabNet, this system is modeled by the ISSCRS class.

Since raw data is not available on the ISS CRS, we refer to published test and simulation data generated during the development of the flight Sabatier reactor to validate the HabNet ISSCRS class. Specifically, we base our truth dataset on the output of a dynamic simulation of the CO_2 accumulator that interfaces between the CDRA and the Sabatier reactor, as shown in Figure 4-21 (see Appendix D.7 for further details about the CO_2 accumulator). Shown by the pink trend in Figure 4-22, this dataset was chosen as it was one of the few CRS-specific datasets that could be found in the literature.

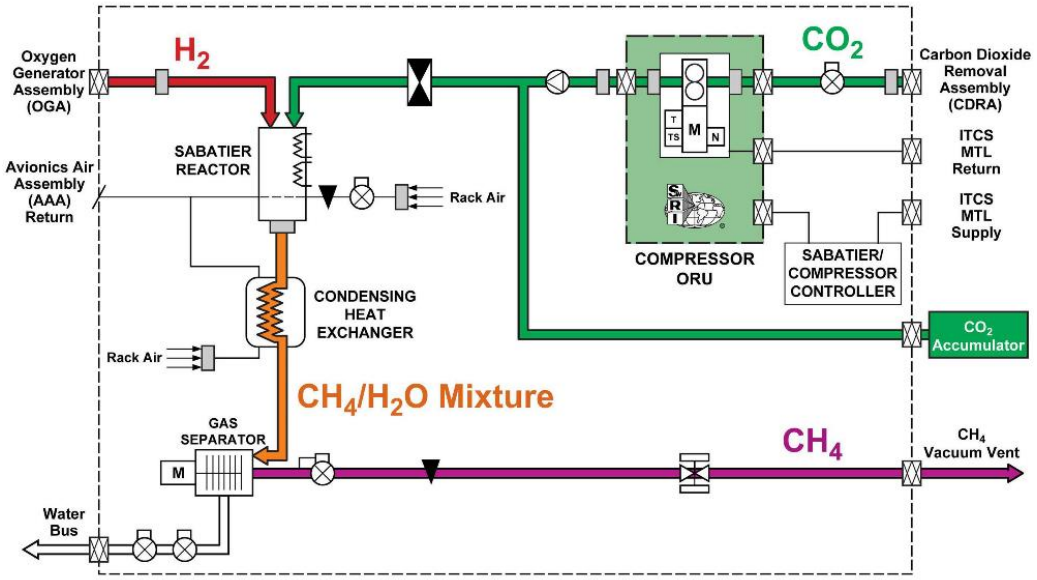

Figure 4-21: The major subassemblies of the ISS Carbon Dioxide Reduction System (CRS) [168]

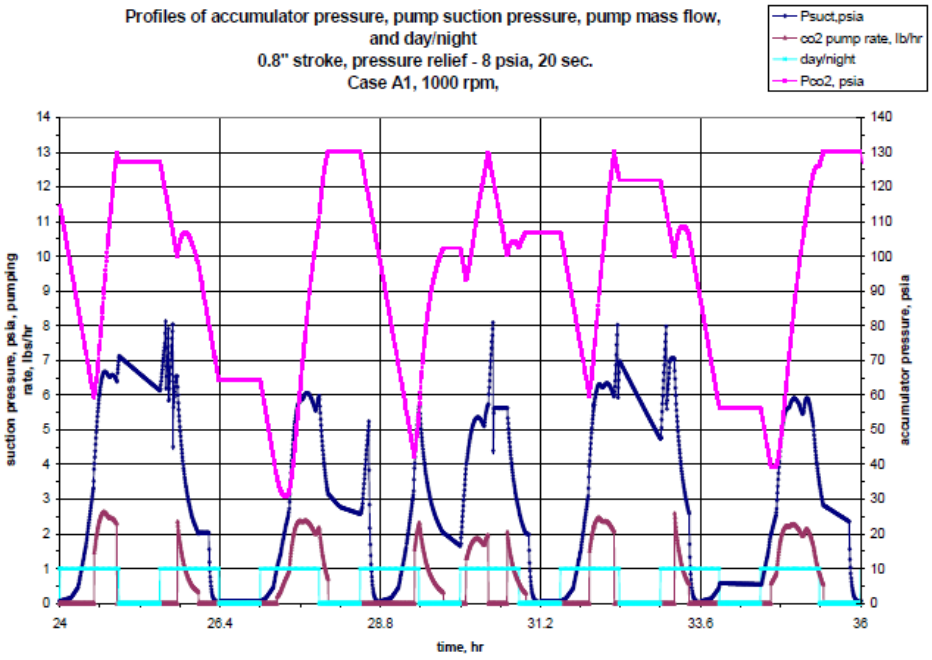

Figure 4-22: Test and simulation data generated during the development of the ISS CRS [169] (The CO_2 accumulator trend is represented by the pink curve)

The CO_2 accumulator pressure data shown in Figure 4-22 was generated from an integrated carbon dioxide reduction system model that was developed by Jeng et al. [169] to analyze and optimize the integration of a Sabatier Reactor into the ISS Oxygen Generation System (OGS)

Rack [169]. This model was ultimately validated with data from the CDRA testbed at NASA Marshall Space Flight Center (MSFC) [169], but not with a Sabatier reactor, since this latter system was still in its pre-development stage at the time.

In order to evaluate the fidelity of the HabNet ISSCRS class model, the same initial modeling conditions as those used to generate the CO_2 accumulator pressure trend shown in Figure 4-22 were used in HabNet. Specifically, these included six crewmembers operating within the ISS with the CDRA and OGA operating in day-night orbital cycling mode in the same manner as that implemented in Section 4.2.5. Here, the crew schedules for each of the six simulated crewmembers was randomly generated using the CrewScheduler function (see Appendix C.2 for details) since this data was not provided by Jeng et al. [169].

The CRS CO_2 accumulator level predictions made by HabNet for the same mission simulation scenario simulated by Jeng et al. [169] are presented in Figure 4-23. Here, a zoomed-in version of a 12-hour block of time corresponding to that of the Jeng et al. dataset has been highlighted for comparative purposes. In addition, the vertical axis of this HabNet-generated data has also been scaled to be equivalent to that of the Jeng et al. baseline dataset.

In the HabNet generated CO_2 accumulator level prediction shown in Figure 4-23, a linearly rising and decreasing trend similar to that found in the Jeng et al. dataset (see Figure 4-22) can be observed. In addition, we find that the HabNet version of the CRS CO_2 accumulator tends to have a lower level of CO_2 over longer periods of time than that of the CRS modeled by Jeng et al. [169].

In general, the linear rise in CO_2 accumulator level results from the CRS compressor periodically activating to transfer CO_2 from the CDRA into the accumulator when the accumulator pressure drops beneath a threshold level. Conversely, the linear reduction in CO_2 accumulator level occurs due to the consumption of CO_2 from the accumulator whenever hydrogen gas is available to support the Sabatier reaction. In the HabNet simulation, the magnitude of the CO_2 accumulator level is a function of the CO_2 removed by the CDRA, which is dependent on the aggregate intensity of the activities performed by each crewmember at each timestep. This accumulator level is also influenced by the amount of hydrogen and oxygen generated by the OGA, which is dependent on the crew's metabolic oxygen demand – a value that is also driven by the crew's activities. Consequently, differences in assumed crew activity levels are a likely cause of the discrepancies in magnitude and time-scale of the fluctuations in CO_2 accumulator level observed when comparing the two datasets.

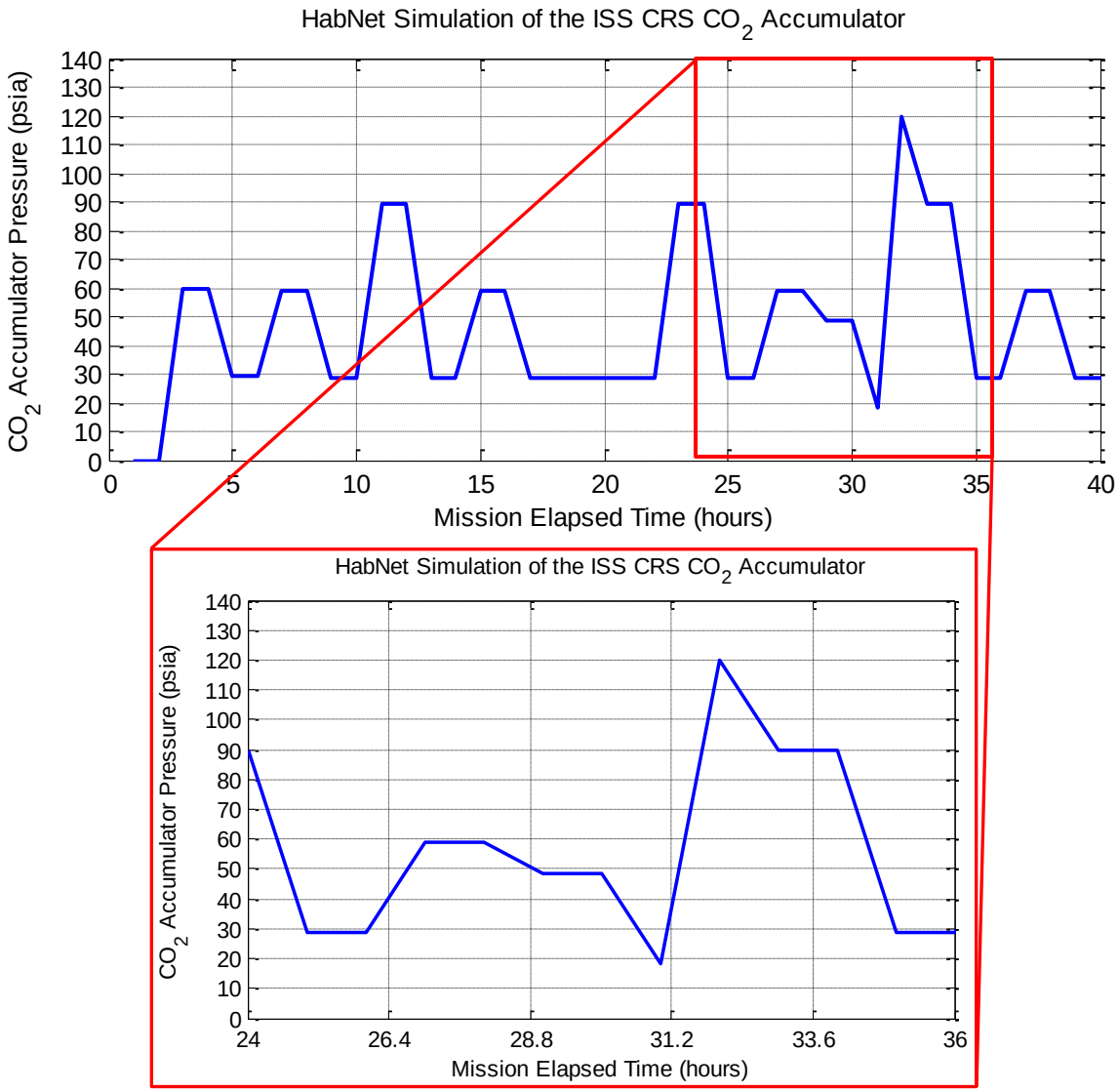

Figure 4-23: CO_2 Accumulator Level predicted by HabNet. (Inset) a close-up of the same 12 hour period as that of the published CO_2 accumulator level data shown in Figure 4-22

Even with these discrepancies however, the fact that the predictions of the HabNet ISSCRS class exhibit the same general linear behavior as that of the higher fidelity simulations of Jeng et al. [169], indicates that the HabNet implementation correctly captures the underlying dynamics of the operation of the ISS CRS. Under the initial simulation conditions assumed in this analysis, it was found that the HabNet ISSCRS class tends to have a lower average CO_2 accumulator level due to some combination of less CO_2 being delivered from the CDRA, or more CO_2 being consumed by the Sabatier reactor due to the higher availability of hydrogen gas from the OGA. Since data on the simulated performance of these two supporting systems

was not described by Jeng et al. in their analyses [169], it is not possible to precisely identify the root cause of this discrepancy. However, it is expected that with the combination of a validated HabNet OGA model (see Section 4.2.5), a HabNet CDRA model that accurately predicts temporal fluctuations in cabin CO_2 concentration, and a HabNet CRS model that correctly captures the control actions of the flight CRS, generally accurate predictions for system level resource consumption and production rates will be obtained. This will be tested further in Section 4.4.5, where an aggregate analysis of the total consumables requirements of different ECLS architectures will be performed and compared against baselined results published in the literature.

4.3 HabNet Crop Model Validation

In addition to ISS-based life support technologies, higher plant growth has also been modeled within the HabNet ECLS Technology Library. As is discussed in Appendix D.8, the Modified Energy Cascade (MEC) models have been implemented within HabNet via the ShelfImpl class. Here, two modifications have been implemented to enable the prediction of crop growth behavior at CO_2 concentration levels outside the 330-1300ppm bounds of the MEC models. The first of these modifications includes the imposition of a linear decrease in crop CO_2 exchange rate from ambient CO_2 concentrations of 330ppm (the lower bound of the MEC valid range) towards 150 ppm – the assumed lower limit for crop survival. Conversely, the second modification involves the enforcement of CO_2 exchange rates to remain at a constant level above ambient CO_2 concentrations of 1300ppm (the upper bound of the MEC valid range). Here, the imposed 150ppm lower CO_2 concentration limit corresponds to experimental observations made by Gerhart et al. [141], and Dippery et al. [142], while the crop insensitivity to high CO_2 concentration values (above 1300ppm) is supported by analyses performed by Wheeler et al. [170–172]. These modifications are depicted in Figure 4-25.

To evaluate the accuracy of the HabNet implementation of the MEC models, simulation results of the HabNet ShelfImpl class were compared with experimental data obtained from controlled crop growth experiments within the Biomass Production Chamber (BPC) located at NASA Kennedy Space Center (see Figure 4-24). Specifically, CO_2 exchange rate data recorded during a CO_2 drawdown test of $20m^2$ of Yecora Rojo wheat (*Triticum aestivum*) after 36 days of growth under $550\mu mol/m^2/s$ of photosynthetic photon flux (PPF) was used as the baseline

for this validation study [171]. In a CO_2 drawdown test, the ambient CO_2 concentration is typically raised to above 1500ppm and then allowed to be entirely drawn down by the test crop, until the crop reaches its compensation point [171] – the point at which the rate of plant photosynthesis equals the rate of plant respiration, resulting in a net zero rate of carbon assimilation [173].

Figure 4-24: The NASA KSC Biomass Production Chamber (BPC) (a) Front View (b) Rear View [174] (c) Wheat growth experiment within the NASA BPC [175]

Figure 4-25 compares the CO_2 exchange rate calculated from the crop Daily Carbon Gain (DCG) of wheat simulated by the HabNet ShelfImpl class (see Appendix D.8) with the corresponding experimental data obtained from drawdown tests performed at the NASA KSC BPC.

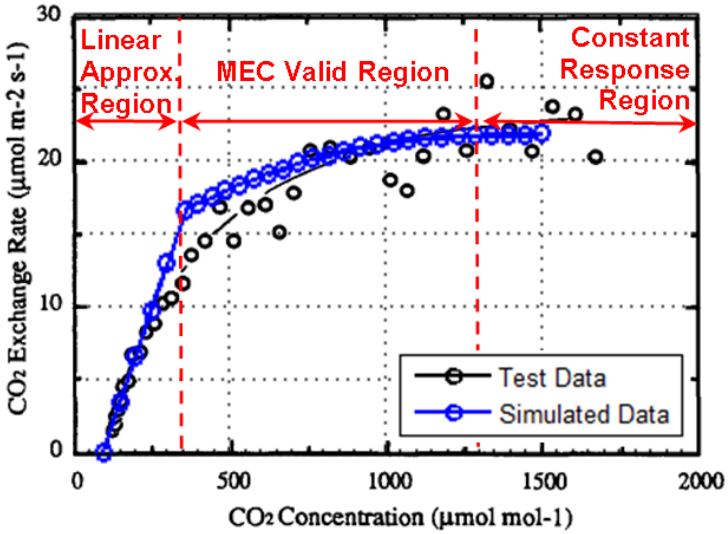

Figure 4-25: Comparison between test data from a CO_2 Drawdown Test of 20 m^2 of Wheat under PPF =550 µmol/m^2/s lighting conditions at 36 days of growth (black [171]) and data obtained from the MEC models simulated within HabNet under the same conditions (blue).

From Figure 4-25, we observe a good correlation between the wheat drawdown test data and the CO_2 exchange rate predicted by HabNet over the range of ambient CO_2 concentration levels examined. In general, the HabNet ShelfImpl performs very well at CO_2 concentration levels above approximately 700ppm, and over-predicts the rate of crop photosynthesis by a maximum of 40% at CO_2 concentration values approaching 330ppm. Given that spacecraft cabin atmospheres typically exhibit higher CO_2 levels ranging from between 3000 to 4000ppm (see Figures 4-19 and 4-20, as well as Wheeler et al. [172]), we conclude that the HabNet ShelfImpl class is valid for the purposes of modeling crop growth and resource exchanges within crewed space habitation systems. This conclusion is further supported by the fact that typical implementations of biomass production chambers attempt to maintain ambient CO_2 levels at above 1200ppm to facilitate the maximum crop growth rates required to sustain the crew's caloric demands [176]. The interactions between the atmospheric demands of crops and the crew they are intended to sustain will be further examined in Chapter 5 and Section 6.3.

4.4 Integrated Validation Case Study – One Year Deep Space Mission

Throughout this chapter thus far, the dynamic modeling capability of the HabNet Habitation Module has been evaluated at the individual technology level against sources ranging from simulation data, to experimental data, and finally to flight data. In this section, the sizing capability of the integrated HabNet modules will be evaluated via the comparison of the results of an end-to-end case study with those previously published within the literature. Specifically, this case study will investigate the impacts of increasing levels of ECLS architecture closure on the total ECLS system, consumables, and spare parts mass required to sustain a one year deep space mission. This case study is based on the analysis performed by Lange and Anderson [101] that is described in Section 2.3.2. As such, the results published by Lange and Anderson [101] will form the baseline dataset from which the integrated performance of HabNet will be evaluated. In the following sections, we provide an overview of the mission scenario investigated, describe the initial conditions that are fed into the HabNet framework, and present, analyze, and compare the results obtained with those of Lange and Anderson [101]. Through this, we demonstrate the key steps involved in performing integrated space habitation analyses with HabNet.

4.4.1 Overview of Mission Scenario

As mentioned earlier, the validation case study performed here will revolve around a one year deep space mission based on the Deep Space Habitat (DSH) concept developed in 2011 during the NASA Human Exploration Framework Team (HEFT) Phase 2 activities [40]. This habitat design was adopted by Lange and Anderson, and consists of a single cylindrical module with a pressurized volume of 115m^3, as shown in Figure 4-26(a). In their study, Lange and Anderson investigated the impact of spare parts requirements on the total system mass of ten different ECLS architectures of increasing resource loop closure [101]. From this study, they observed that for a fixed reliability level, a partially closed ECLS system consisting of water and urine processing technologies and an open loop oxygen supply was the most mass efficient. Figure 4-26(b) summarizes the results for five of the ECLS architectures examined in this study.

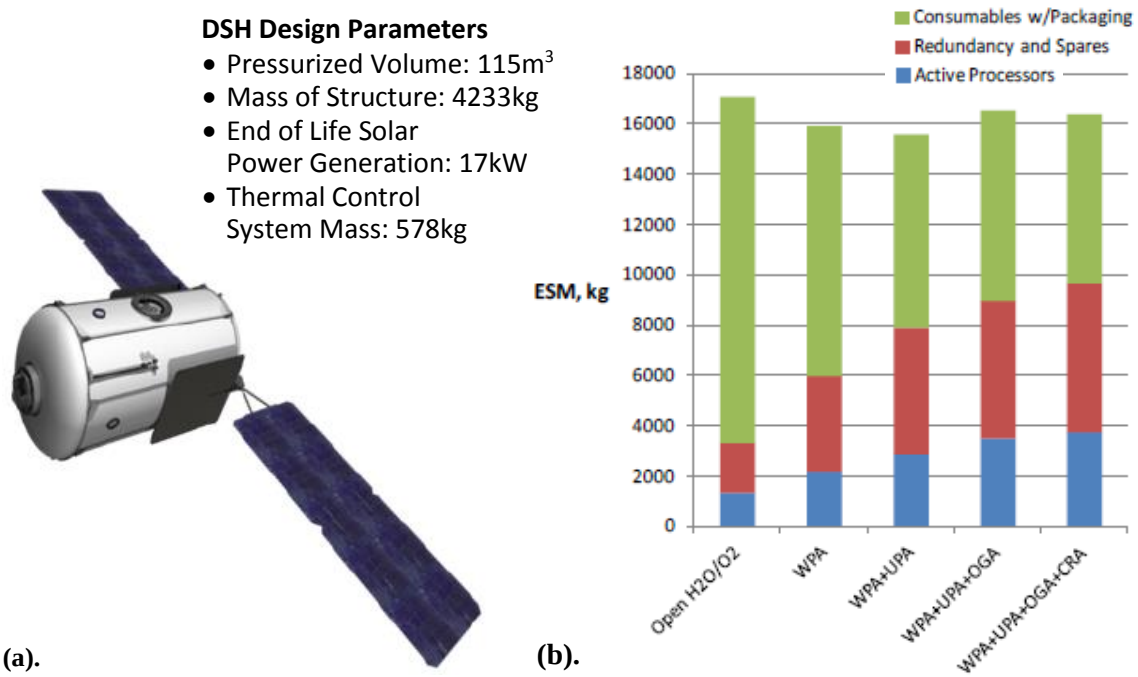

Figure 4-26: (a). One Year Deep Space Mission Scenario Analyzed by Lange and Anderson [40] (b). Aggregate ECLS hardware, consumables, and spare parts mass calculated by Lange and Anderson [101]

In the analysis performed here, we aim to demonstrate HabNet's capabilities in performing this type of comparative architectural analysis using five of the ECLS architectures examined by Lange and Anderson [101]. These architectures use some combination of ISS-derived regenerative ECLS technologies, including the Water Processor Assembly (WPA), the Urine

Processor Assembly (UPA), the Oxygen Generation Assembly (OGA), and the Carbon Dioxide Reduction System (CRS). In order of increasing resource closure, these architectures are:

- Case 1 – Open Loop Water and Oxygen
- Case 2 – WPA
- Case 3 – WPA + UPA
- Case 4 – WPA + UPA + OGA
- Case 5 – WPA + UPA + OGA + CRS

For all of these architectural cases, a Carbon Dioxide Removal Assembly (CDRA) is assumed to perform the CO_2 removal function, all water is assumed to be contained and transported in ISS Contingency Water Containers (CWCs), and all gases are assumed to be transported in high pressure tanks integrated into the structure of the DSH. Finally, a Common Cabin Air Assembly (CCAA) and Pressure Control Assembly (PCA) are installed within the DSH and spared for accordingly. Figure 4-27 depicts the ECLS architecture corresponding to Case 5 – the architecture with the highest level of resource closure.

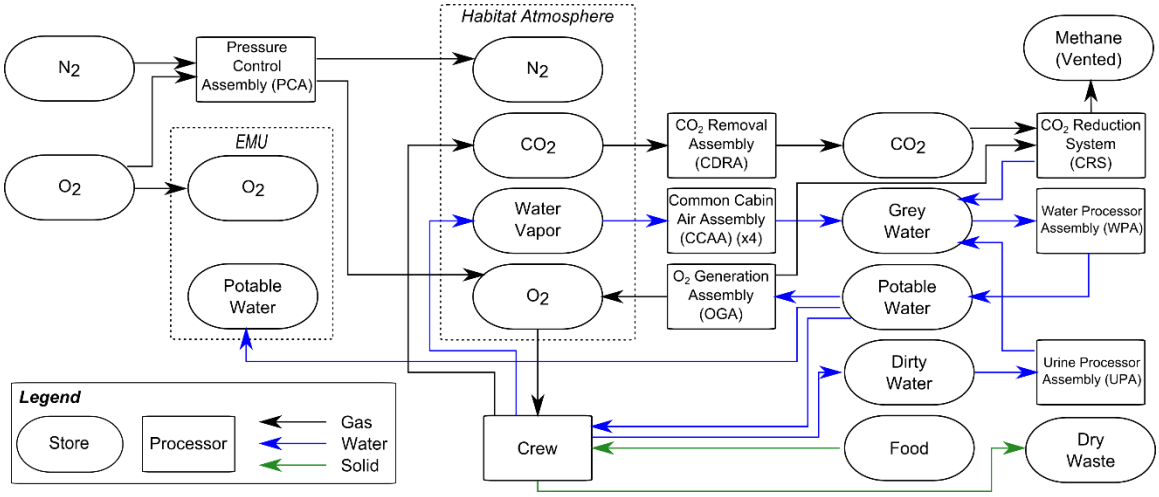

Figure 4-27. Case 5 ECLS Architecture based on that of the ISS (see Appendix H.1 for flowsheets of the other ECLS architecture cases evaluated in this validation case study)

To commence this analysis, we first define the input parameters for each of the HabNet modules. As was discussed throughout Sections 3.2 and 3.4, these input parameters correspond to a set of choices for each of the major decisions that govern the architecture of a space habitation system. These input parameters are summarized below, in Table 4.5.

Table 4.5: List of One Year Deep Space Mission Scenario HabNet Input Parameters

Input Parameter	Selected Option
Habitation Module Inputs	
Crew CONOPS • Number of Crew • Crew Activities • EVA Frequency	Crew Composition: Assumed to be a four person crew consisting of two males and two females, all aged 35 years old. Both males have a mass of 75kg and both females have a mass of 55kg. These figures are typical of the astronaut population [177] Crew Schedule: No extravehicular activities (EVA) are performed, based on the assumptions made by Lange and Anderson [101]. The crew daily schedule is assumed to be ISS-like. For each crewmember, 8 hours of sleep and 2 hours of exercise are budgeted per day, with the remaining time allocated to Intravehicular Activities (IVA). IVA can include activities such as performing scientific experiments or preparing meals. For the purposes of this simulation, all non-sleep and non-exercise activities are classified as IVA, where they are assumed to require the same level of crew energy expenditure.
Mission Duration	A one year deep space mission
Habitat Layout	A single module 115m^3 Deep Space Habitat (see Figure 4-26(a)) with an Earth-like cabin atmosphere
ECLS Architecture	ISS-based. Various options for the ECLS architecture at increasing levels of resource loop closure are explored in this case study. Figure 4-27 depicts the most complex architecture explored. Prepackaged food is supplied from Earth and all dry waste is stored and disposed of. Consequently, these do not vary with ECLS architecture for this analysis.
ISRU Module Inputs	
ISRU Strategy	None for this analysis, based on the assumptions made by Lange and Anderson [101]
Supportability Module Inputs	
Supportability Strategy	Spares and consumables are brought from Earth and stored on the spacecraft for this sortie mission. Sparing is performed at the lowest level at which reliability figures are available, such that the probability of having sufficient spares to perform all maintenance and repair tasks is 0.999. Consumable gases are assumed to be transported in high pressure tanks integrated into the habitat structure. Fluids are assumed to be transported in the Contingency Water Containers (CWCs) used on the ISS (container capacity of 44L, with each container weighing 1.27kg) [178]

With the basic habitation architecture for this case study established, we set up a virtual model of the deep space habitat in HabNet to analyze its lifecycle requirements under the various ECLS architectures described above. We perform this analysis by first running the Habitation Module to determine the consumables mass required for each of the five ECLS

architectural cases described above, as well as the operational times for each component. This latter set of information is then fed into the Supportability Module to determine the corresponding spares requirements. Finally we combine the results from the two modules to investigate the impact of ECLS architectural decisions on the combined ECLS system, consumables, and spare parts requirements of a one year crewed deep space mission. The results of these analyses are presented in the following sections.

4.4.2 ECLS Consumables Requirements

The consumables resupply requirements for each of the five ECLS architecture cases investigated in this case study are summarized in Figure 4-28 and Table 4.6. These values were obtained by running the Habitation Module with the baseline habitation architecture and crew schedule described in Table 4.5 over the simulated one year mission period. Here, we compute the raw amount of oxygen, nitrogen and water required to sustain the crew using each of the different architectural options, then calculate the storage mass required for each type of consumable. High pressure storage of gases is calculated as a function of the mass of gas stored, using mass factors described in the NASA Baseline Values and Assumptions Document (BVAD) [179] (0.556 kg of tankage/kg of gaseous N_2 and 0.364 kg of tankage/kg of gaseous O_2). Conversely, for water, the number of required CWCs is calculated, based on the assumption that each CWC can hold up to 44L of water [178].

From Figure 4-28, we observe that in general, the total consumables requirement decreases as system loop closure increases. This is in line with the conventional motivation behind pushing ECLS architectures towards increased system closure discussed in Section 2.1.2. In addition, Table 4.6 indicates that when the OGA is introduced from Case 4 onwards, the requirement for stored oxygen reduces to zero while the demand for water increases by a factor of 1.5 to 2. This is the result of the OGA removing the need for pre-stored oxygen by the electrolysis of water. Thus, the OGA has transferred the demand for oxygen into a demand for additional water.

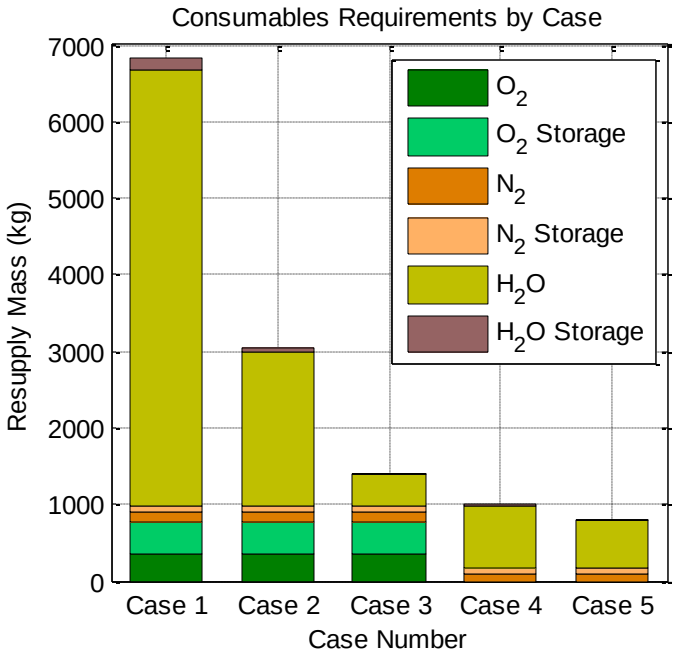

Figure 4-28: Consumables Requirements for each ECLS Architectural Case

Table 4.6: Consumables Requirements computed by the HabNet Habitation Module for each ECLS Architecture Case. Cells with the same values are colored for the purposes of clarity

	O_2 (kg)	**O_2 Storage (kg)**	**N_2 (kg)**	**N_2 Storage (kg)**	**H_2O (kg)**	**H_2O Storage (kg)**
Case 1 - Open Loop O2 + H2O	365	133	138	77	5687	166
Case 2 - WPA	365	133	138	77	2006	59
Case 3 - WPA + UPA	365	133	138	77	415	13
Case 4 - WPA + UPA + OGA	0	0	101	57	812	25
Case 5 - WPA + UPA + OGA + CRS	0	0	101	57	630	20

Moreover, from Table 4.6, we find that the demand for nitrogen remains relatively constant at a low value across all architectural cases. Specifically, nitrogen demands remain consistent at 138kg for the first three cases and drops to 101kg from Case 4 onwards. This reduction is due to the increased atmospheric control authority associated with the introduction of the OGA. Prior to the inclusion of the OGA, the only means of total atmospheric pressure control arises from the Pressure Control Assembly (PCA), which injects nitrogen and oxygen and vents air from the cabin atmosphere to maintain a predefined set point for atmospheric total pressure and composition. The introduction of an OGA provides an additional avenue for total pressure control via the direct injection of electrolysis-produced oxygen into the cabin atmosphere. This

in turn, reduces the reliance on PCA-injected nitrogen for total pressure control, resulting in a lower overall demand for nitrogen gas.

Finally, Figure 4-28 indicates that the addition of regenerative ECLS technologies beyond Case 3 appears to have a relatively minor impact on total consumables requirements as compared to the addition of the WPA and UPA. In absolute terms, the introduction of the OGA in Case 4 yields a total savings of 360kg of consumables mass as compared to Case 3, while the introduction of the CRS in Case 5 results in a saving in water resupply requirements of approximately 182kg as compared to Case 4. This trend indicates a diminishing savings in consumables requirements as the ECLS architecture approaches higher levels of resource closure and system complexity. We further investigate the implications of this observation in the following sections.

4.4.3 ECLS Technology Run Times

In addition to predicting ECLS consumables requirements, the HabNet Habitation Module was also used to determine the period of time over which each ECLS technology was operational in each architectural case. This is possible since the Habitation Module dynamically simulates each mission scenario, including the periods over which each technology element is switched on and off according to its control laws (see Appendix D for details on how each ECLS technology is operated). Not only does this information provide insight into the operation of each ECLS technology, it is a critical input parameter to the HabNet Supportability Module in the determination of spare parts requirements, since it is an indicator of system wear and tear. Table 4.7 summarizes the periods over which each technology was operated in each of the five ECLS architecture cases. This period is referred to as the "runtime". In addition to these runtime values, the number of on-off cycles experienced by each technology in each ECLS case is also listed. While this value is not currently used in the computation of spare parts requirements, the number of on-off cycles is a driver of fatigue life, which can in turn impact the operating life of each component, and hence the spare parts demands. Quantifying the contribution of on-off cycling on spare parts demands is the subject of future work on the HabNet Supportability Module.

Table 4.7: System Runtimes for each ECLS Architecture Case, as calculated by the HabNet Habitation Module. Grey cells indicate that the highlighted technology was not included within the corresponding ECLS architecture case. Where applicable, bracketed values list the number of on-off cycles experienced by the given technology

	CDRA Run Time (h)	**CCAA Run Time (h)**	**WPA Run Time (h)**	**UPA Run Time (h)**	**OGA Run Time (h)**	**CRS Run Time (h)**
Case 1 - Open Loop O2 + H2O	8760	8760	N/A	N/A	N/A	N/A
Case 2 - WPA	8760	8760	648 [81]	N/A	N/A	N/A
Case 3 - WPA + UPA	8760	8760	928 [116]	3097 [258]	N/A	N/A
Case 4 - WPA + UPA + OGA	8760	8760	928 [116]	3097 [258]	8634 [127]	N/A
Case 5 - WPA + UPA + OGA + CRS	8760	8760	960 [120]	3097 [258]	8635 [127]	1318 [126]

From Table 4.7, we observe that the CDRA and CCAA remain consistently on over the duration of the one year (or 8760 hour) mission. These systems constantly monitor and remove water vapor and CO_2 from the cabin atmosphere to ensure a comfortable and safe breathing environment for the crew. Contrastingly, the WPA run time increases with increasing ECLS system resource loop closure. The introduction of the UPA in Case 3 introduces urine condensate into the ECLS system, while the inclusion of the CRS in Case 5 introduces Sabatier reaction product water that needs to be managed. In both cases, these additional products are delivered to the WPA, where they are processed into potable water. This results in more wastewater batches that need to be processed and hence a corresponding increase in WPA runtime.

As for the remaining ECLS technologies, we find that they have virtually constant runtimes across the ECLS architecture cases that they are incorporated within. For the UPA and the OGA, this arises from the fact that their operation is initiated by data that is independent of other ECLS technologies – the UPA begins processing once the urine wastewater tank is filled to a threshold level by the crew, and the OGA commences processing once the crew's metabolic activity reduces the cabin oxygen level beneath some threshold level. Moreover, because these remaining technologies all operate in batch mode, they all have run times that are less than the total mission duration. This contrasts to the runtimes of the CDRA and the CCAA discussed above.

4.4.4 ECLS Spare Parts Requirements

To determine the number of spare parts required for each ECLS architecture case, the system runtimes estimated by the HabNet Habitation Module along with data on the mass, mean time between failure (MTBF) and life limit of each technology within each ECLS architecture were input into the HabNet Supportability Module. Figure 4-29 summarizes the output of this module, showing the mass of spare parts required by ECLS technology for each of the five ECLS architectures investigated, such that the probability of having sufficient spare parts is at least 0.999 (as listed in Table 4.5). We note that this analysis assumes that all required spare parts can be carried within the DSH on its mission. Mass and volume constraints of the DSH on the amount of spares that can be carried are not accounted for here.

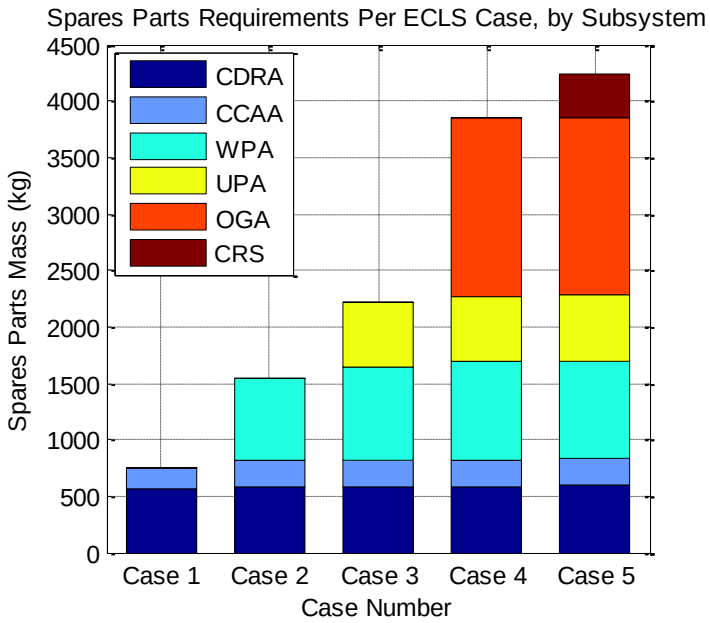

Figure 4-29: Spare Parts Requirements for each of the five ECLS Architectural Cases

Here, we find that as more technologies are included in the ECLS architecture, the spare parts requirements increase – a trend that is the reverse of that observed with the consumables resupply requirements studied in the previous analysis. This result is similar to the observations made in the studies of both Lange et al. [101] and Jones [102] that were discussed in Section 2.3.2, and can be attributed to the generally lower reliability of regenerable ECLS technologies as compared to their open-loop counterparts, and the fact that more technologies generally leads to a larger total spares requirement.

Furthermore, we find that the variations in spare parts requirements for each ECLS subsystem across the five ECLS cases correlate reasonably well with the runtime values presented in Table 4.7. With the exception of the CCAA and the WPA, spare parts requirements for all ECLS technologies remain constant across all ECLS cases, in the same manner that their runtimes remain constant across these same cases. Here, the variations in WPA spare parts requirements can be attributed to variations in runtimes across the ECLS architectural cases, while the slight fluctuations in the CCAA spare parts requirements are the result of the SMP algorithm in the Supportability Module preferably choosing one type of spare over another to achieve the same 0.999 probability of having sufficient spares for a lower total spares mass.

Finally, we observe that of all the systems accounted for within this spare parts analysis, the OGA has the largest spare parts demand. For the mission scenario being investigated here, this demand is driven by the Hydrogen ORU and the Water ORU, which have a mass of 162kg and 61kg respectively, and a relatively low MTBF of 27156 and 33288 hours respectively. In order to achieve the predefined threshold probability of sufficient spare parts of 0.999, three of each of these systems are required to be carried onboard the DSH. As is discussed in Appendix D.5, the Water ORU is responsible for managing the delivery of water from the potable water bus to the OGA, while the Hydrogen ORU consists of a dome that contains the electrolysis cell stack and the rotary separator accumulator used to ensure a constant water level within the system. It should be noted that this spare parts demand may be reduced if a lower level of repair than the ORU level assumed here is adopted. The potential savings attained from a lower level of repair would have to be traded against the additional crew time, crew training, and diagnosis and repair equipment required to facilitate this lower level of repair. Exploring this trade is the subject of future work.

4.4.5 Comparison of Aggregate ECLS Architecture Mass

In this section, we aggregate the mass of the emplaced systems for each ECLS architectural case with the previously computed consumables and spare parts requirements and compare the results with those published by Lange and Anderson [101]. Here, it is important to note that Lange and Anderson [101] use the Equivalent System Mass (ESM) metric to evaluate each of the ECLS architecture cases. This contrasts to the raw masses that have been calculated throughout the analysis conducted with HabNet thus far. As a result, we present our results using both the raw mass and ESM metric.

Here, we calculate the ESM using the same approach described by Lange and Anderson [101]. The ESM metric accounts for the "equivalent mass" contributions of system requirements other than mass, such as the additional structure required to support a system's volume, and the mass of the additional power and cooling systems needed to support a system's operation [180]. ESM is calculated as the sum of the requirements of each technology weighted by an equivalency factor that converts this requirement into an "equivalent mass" value, using the following equation:

$$ESM = M + (M_{PI} \cdot E_{M_{PI}}) + (V_{PS} \cdot E_{V_{PS}}) + (V_U \cdot E_{V_U}) + (P_E \cdot E_{P_E}) + (C \cdot E_C) \quad (4.1)$$

Where:

M = total mass of life support equipment, consumables, and spares (the raw mass calculated thus far in this analysis) (kg)

M_{PI} = total mass of active ECLS systems installed within spacecraft racks (kg)

V_{PS} = total pressurized volume of stored consumables, spares, and active ECLS systems (m^3)

V_U = total unpressurized volume of equipment, consumables, and spares (m^3)

P_E = total average system electrical power requirement (kW)

C = total average system cooling requirement (kW)

E_i = mass equivalencies associated with providing primary and secondary structure (based on volume), electrical power, and cooling via thermal control

For this analysis, the mass equivalencies were calculated from a combination of data based on the DSH design used by Lange and Anderson [101] (see Figure 4-26(a)) and values listed in the NASA Baseline Values and Assumptions Document (BVAD) [179]. These are summarized in Table 4.8 below:

Table 4.8: Mass Equivalency Values used in the calculation of ESM for a One Year Deep Space Mission Scenario

Mass Equivalency	**Systems and System Attributes Applied To:**	**Calculated From:**
$E_{M_{PI}}$	The mass of all active ECLS technologies – represents mass of spacecraft secondary structure	0.8kg per kg of active ECLS technology (assumed to be installed within trays of a stowage rack within the DSH), based on the NASA BVAD [179]
$E_{V_{PS}}$	The volume of all emplaced ECLS hardware, spare parts, and stored water – represents mass of spacecraft pressure vessel	Deep Space Habitat (DSH) structural mass (4233kg) and pressurized volume (115m^3) (see Figure 4-26): $E_{V_{PS}} = 4233/115 = 36.8\text{kg/m}^3$
E_{V_U}	None for this analysis since all hardware, spares, and consumables are assumed to be stored in a pressurized environment	
E_{P_E}	The average power demand of all ECLS technologies, as calculated by the Habitation Module (see Appendix D for details)	Deep Space Habitat (DSH) power system mass (1108kg) and end-of-life (EOL) power generation capacity (17kW) (see Figure 4-26): $E_{P_E} = 1108/17 = 65.2\text{kg/kW}$
E_C	The average cooling requirement of all ECLS technologies, assumed be equal to their average power demand	Deep Space Habitat (DSH) thermal control system mass (578kg) and heat removal capacity (assumed to equal the power generation capacity 17kW) (see Figure 4-26): $E_C = 578/17 = 34\text{kg/kW}$

Using the mass equivalency values from Table 4.8, the ESM of the five ECLS architectural cases was calculated. The results of this calculation are plotted in Figure 4-30, alongside the aggregated raw masses of each ECLS architecture.

Here, we find that based on the assumptions made in this analysis, the third architectural case (WPA+UPA) is the most efficient in terms of both aggregate ECLS system mass and ESM. Interestingly, the lower resource recycling architecture represented by Case 2 (the WPA only case) is the second most mass- and ESM-efficient, followed by the cases that include the OGA (Cases 4 and 5). As can be seen in Figure 4-30, these relative ECLS architecture rankings remain consistent across the two metrics evaluated. In addition, it is important to note that this trend contradicts the traditional ECLS heuristic discussed earlier in Section 2.1.2 and 4.4.2 – that increased levels of resource recycling result in more efficient ECLS architectures for long duration missions (considered to be greater than approximately 10 months [179]).

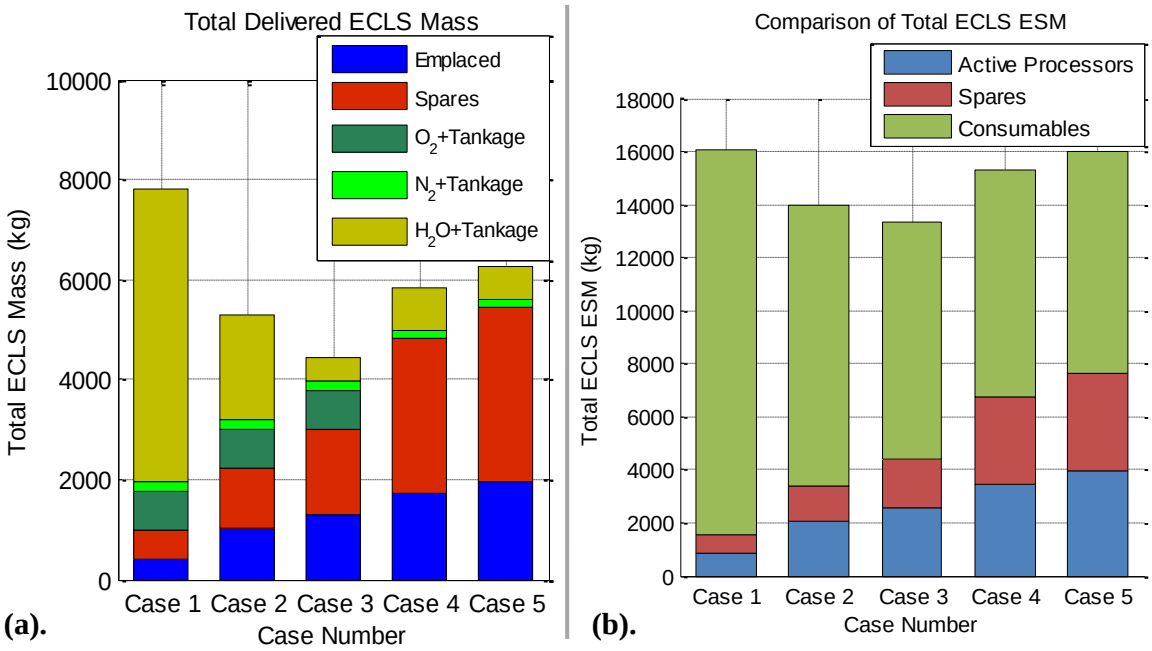

Figure 4-30: (a). Aggregate Masses for each of the five ECLS Architectural Cases examined, as predicted by HabNet (b). Aggregate ESM for each of the five ECLS Architectural Cases examined, as predicted by HabNet

In general, this trend can be explained by the fact that over the one year duration studied, technologies that process and recycle liquid water result in a larger consumables savings for a lower additional required mass, as compared to technologies that generate and/or recover oxygen gas. For instance, the addition of the WPA from Case 1 to Case 2 resulted in a consumables savings of 3788kg at the cost of an additional 1252kg of WPA hardware and spare parts. Conversely, the addition of the OGA from Case 3 to Case 4 resulted in a consumables savings of 414kg at the cost of 1824kg of OGA hardware and spare parts. Table 4.9 summarizes this calculation for all the technologies investigated in this analysis. Here, a value great than one indicates that total mass is saved through the addition of a given ECLS technology.

Table 4.9: Calculated Efficiencies for each ECLS Technology, based on data predicted by HabNet

	WPA	**UPA**	**OGA**	**CRS**
Consumables savings achieved (kg)	3788	1637	414	187
Cost of additional hardware (systems + spare parts) (kg)	1252	781	1824	626
Efficiency (Savings/Cost)	**3.03**	**2.10**	**0.27**	**0.30**

From Table 4.9, it is evident that at least for a one year mission, water processing technologies are generally more mass efficient than oxygen generation and recovery systems. In fact, this general trend was also found in the analysis performed by Lange and Anderson [101], where an ECLS system consisting of only a WPA and a UPA (ECLS Case 3) was observed to be the mass optimal architecture. This can be seen in the Figure 4-31 below, which compares the ESM of each ECLS architecture predicted by HabNet with that published by Lange and Anderson [101].

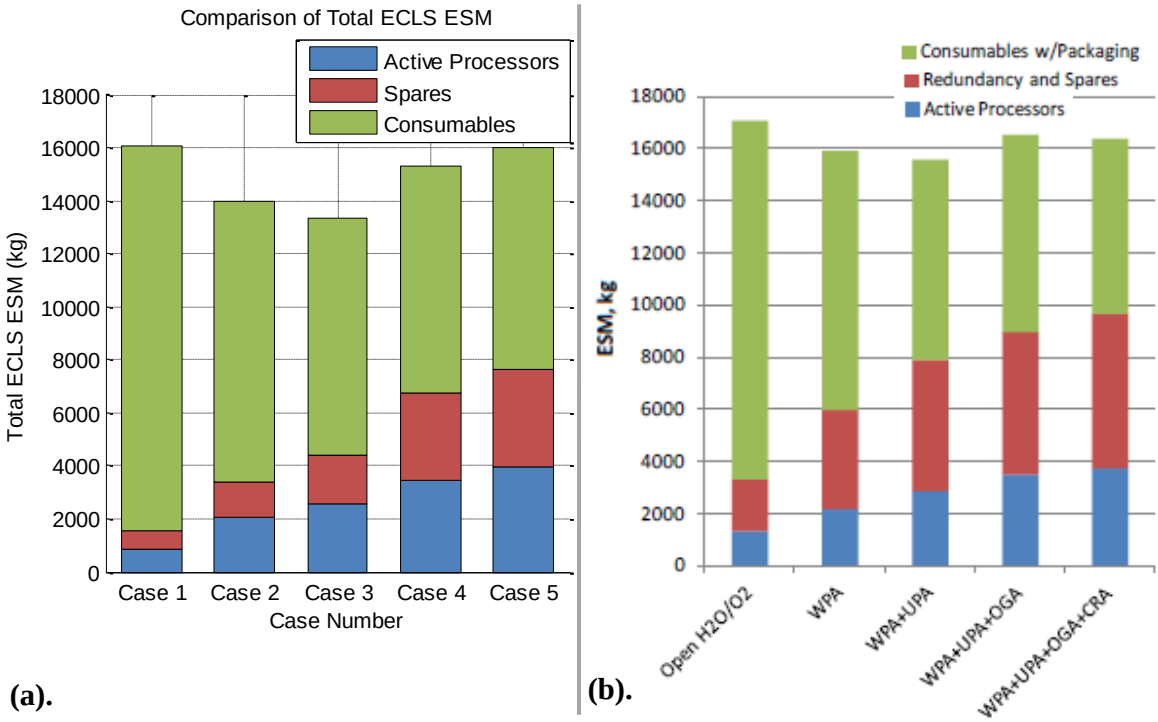

Figure 4-31: Comparison between ECLS ESM results obtained with HabNet and those derived by Lange and Anderson (a). HabNet (b). Lange and Anderson [101]

In this figure, we observe that Lange and Anderson also found that ECLS architectures with oxygen generation and/or recovery systems (Cases 4 and 5) have a larger equivalent mass than those that contain only water processing technologies (Cases 2 and 3), thus validating the HabNet-derived observations described above.

Moreover, we find that with the exception of the relative ordering of Cases 4 and 5, the overall ranking of ECLS architectures remains the same across both our analysis and that of Lange and Anderson. In our study, we found that the introduction of the OGA in Case 4 leads to an architecture that has a lower total mass and ESM than that of Case 5, whereas Lange and Anderson find the opposite result. Figure 4-31(b) indicates that this difference is the result of

Lange and Anderson's finding that Case 5 has a slightly lower total mass ESM than Case 4, which is the opposite of that found in our analysis. Under constant hardware masses and relative consumables requirements across the two analyses, this suggests that the mass efficiency of the CRS analyzed by Lange and Anderson is higher than that of the CRS used in our analysis. This, in turn suggests that the CRS analyzed by Lange and Anderson requires less spare parts and hence has a higher MTBF than that employed in our analysis. Because this value was not published with the Lange and Anderson's analysis, this hypothesis cannot be verified.

Finally, it is important to note that a difference of approximately 1000kg to 2000kg in ESM (5-10%) was observed between the predictions of HabNet and those made by Lange and Anderson [101]. This is most likely due to differences in values assumed for non-architecturally distinguishing elements within the two analyses, such as the ESM of food and hygiene items, both of which are non-recyclable commodities that can have a large mass contribution over a one year period.

Regardless, the fact that HabNet was able to predict the same mass-optimal solution as that of Lange and Anderson, as well as produce almost identical overall architectural rankings, provides validation for HabNet's use in comparing the lifecycle impacts of various space habitation architectures.

4.5 Chapter Summary

In this chapter, we performed a series of studies to validate both the dynamic simulation and sizing capabilities of HabNet. We first baselined the performance of the HabNet Habitation Module against the open-source BioSim ECLS simulator developed for NASA Johnson Space Center. After obtaining identical results with BioSim for seven simulation cases of increasing complexity, the regenerative ECLS technology models within the HabNet Habitation Module were tuned to match the performance of those onboard the International Space Station, and were then individually compared against operational data downlinked from the ISS flight server located at NASA's Mission Control Center. Through this comparative analysis, the HabNet ECLS technology models were observed to produce generally accurate predictions of the dynamic behavior of their ISS counterparts, with typical HabNet estimates of transient water store levels lying within 0% to 15% of the levels observed on the ISS depending on the ECLS technology. In addition, it was found that HabNet was able to predict all major dynamic

phenomena observed in the ISS data, thereby adding further validity to its dynamic simulation capabilities.

Following this initial benchmarking analysis, the HabNet sizing capability was evaluated via an end-to-end comparative study on the impacts of increasing levels of ECLS architecture resource recycling on total mission mass. This study was based on a previous study performed by analysts at NASA Johnson Space Center (JSC) for a four person, one year deep space mission. From this analysis, HabNet was able to identify the same mass-optimal ECLS architecture as that of the JSC analysts, as well as a nearly identical overall relative ranking of aggregate mass requirements for the five ECLS architectures examined. In addition to providing validation for HabNet's architecture sizing capability, the similarity in results obtained here further reinforces the findings of contemporary ECLS analyses that contradict traditional ECLS design heuristics – that increasing the level of resource recycling in long duration ECLS systems does not necessarily lead to a mass optimal solution, especially when the additional mass of spare parts requirements is accounted for.

Thus, with HabNet's dynamic simulation and sizing capability now benchmarked and validated against external data sources and analysis, we proceed with further exploring the impact of system architectural decisions on the lifecycle impacts of long-duration, continuously crewed, Mars surface mission scenarios. This is performed in the next two chapters, where we perform analyses on campaigns of missions under varying programmatic boundary conditions.

Chapter 5

Case Study 1 – The Mars One Mission Plan

Having developed and validated the HabNet framework throughout the previous chapters, we now apply HabNet to a series of long-duration "permanent presence" Mars mission scenarios, commencing with the examination of the lifecycle costs of the recently popularized one-way class of Mars mission plans. In particular, this chapter focuses on using HabNet to assess the feasibility of the Mars One mission plan – a highly publicized and somewhat controversial proposal to accelerate the first landing of humans on Mars via a series of four-person one-way missions to the red planet commencing in 2025. While this plan is not the first to propose the use of one-way missions, it is by far the most documented, and is therefore a suitable reference mission scenario from which we can investigate the sustainability and lifecycle requirements of one-way mission architectures in general.

In order to provide a historical context for this case study, this chapter commences with a brief review of the major one-way mission plans that have been proposed since the Apollo era. Following this, we summarize the background and architectural constraints governing the Mars One mission plan, and use this information to define the baseline input parameters required by HabNet. With this, we adopt an iterative analysis approach to evaluate the lifecycle costs, sustainability, and hence feasibility of the Mars One mission plan. This allows us to study both the baseline Mars One mission architecture, as well as variations in its architecture that abide by the same overarching constraint of relying on a series of one-way missions. Using the insights gathered from this analysis, we conclude this chapter with a discussion of the architectural requirements of one-way mission plans in general.

This case study was performed in collaboration with Andrew Owens, Koki Ho, and Sam Schreiner - all graduate researchers at MIT at the time of this study. The description and analysis provided in this chapter has been adapted from a journal article that was co-authored and published by this research team [143]. This author would like to acknowledge the invaluable contributions of these researchers to this analysis.

5.1 A Historical Overview of One-Way Mission Plans

Since the beginning of human spaceflight in the early 1960s, one-way mission concepts to celestial locations within the inner solar system have been occasionally proposed and strongly advocated for by members within the wider spaceflight community. In all cases, these have been motivated by the desire to accelerate the time at which the first visit of a human to a celestial body would occur. Consequently, they have always been promoted as a lower cost alternative to traditional round-trip mission plans due to the mass savings achieved in avoiding the need to deliver a fueled return vehicle to the exploration destination. Figure 5-1 summarizes the major one-way mission concepts that have been proposed over the past 60 years.

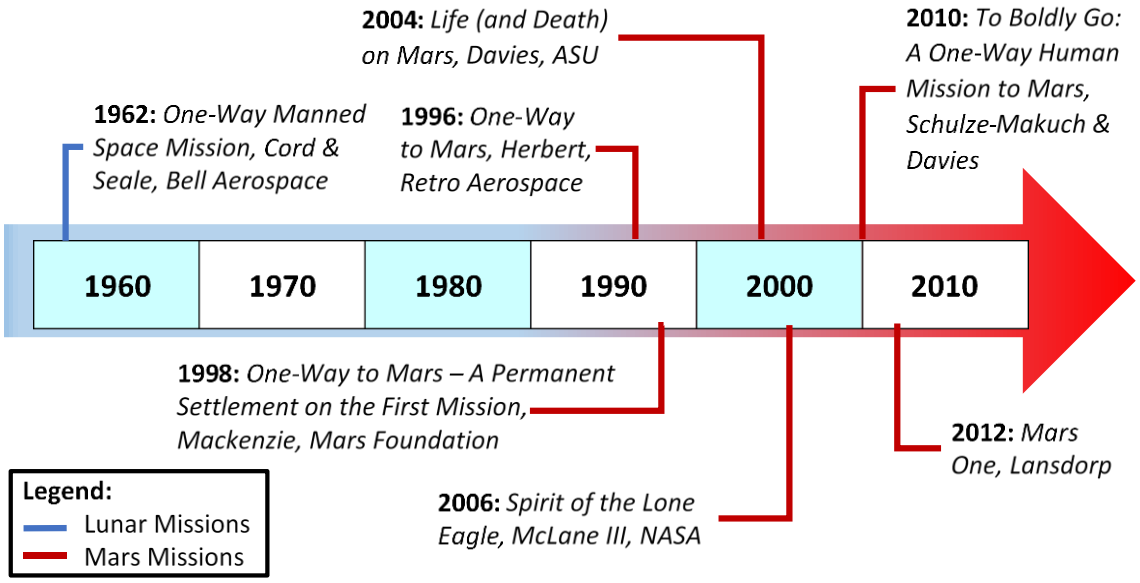

Figure 5-1: Summary of the Major One-Way Mars Mission Proposals Since 1960 (see text for references)

5.1.1 A "One-Way Manned Space Mission"

As can be seen in Figure 5-1, one-way mission architectures can be traced back to 1962, during the height of the Space Race. At the time, President Kennedy's mandate for NASA's Apollo Program had recently been announced, and fears of continued Soviet technological domination in the domain of spaceflight were at their peak. Motivated by concerns of losing the "race to the Moon", engineers at Bell Aerosystems Company proposed a "One-Way Manned Space Mission" in July 1962 as a means of ensuring that the United States would land a person on the moon before the Soviet Union [41].

This mission plan involved sending a single astronaut in a one-person lunar lander on a one-way direct-ascent trajectory to the Moon. It was argued that the savings in launch mass arising from the smaller single-person spacecraft coupled with the elimination of the mass of the ascent and return vehicle required to return the astronaut to Earth, enabled the use of less powerful launch vehicles that could be developed in a shorter period of time. Altogether, this would enable the first landing of a human on the Moon by as early as 1964 or 1965. Approximately three years later, when more powerful rocket technology was expected to become available, a dedicated mission would be undertaken to retrieve the astronaut from the Moon and return him to Earth. This recovery mission would become the first of the Apollo Program's lunar surface missions.

To sustain the lone lunar astronaut, four unmanned cargo landers were planned to land at the preselected site in the years prior to the human landing. Each lander would weigh 2190lb and carry 910lb of equipment and supplies. Immediately after landing, the single astronaut would begin setting up his lunar base by combining two of these cargo landers to form a lunar base. These landers would each come with pre-installed life support systems and would be designed to be easily tipped over and winched together by a single crewperson. As part of the habitat assembly process, the astronaut would also install micrometeorite and radiation shields around the habitat, as well as route a power cable from the habitat to a nuclear reactor delivered on one of the predeployed cargo landers.

To sustain the astronaut over the longer term, the mission designers estimated that 13 cargo landers would be required each year to deliver the necessary life support supplies. Over time, additional cargo landers could deliver a multi-purpose rover and construction equipment to facilitate the expansion of the lunar base.

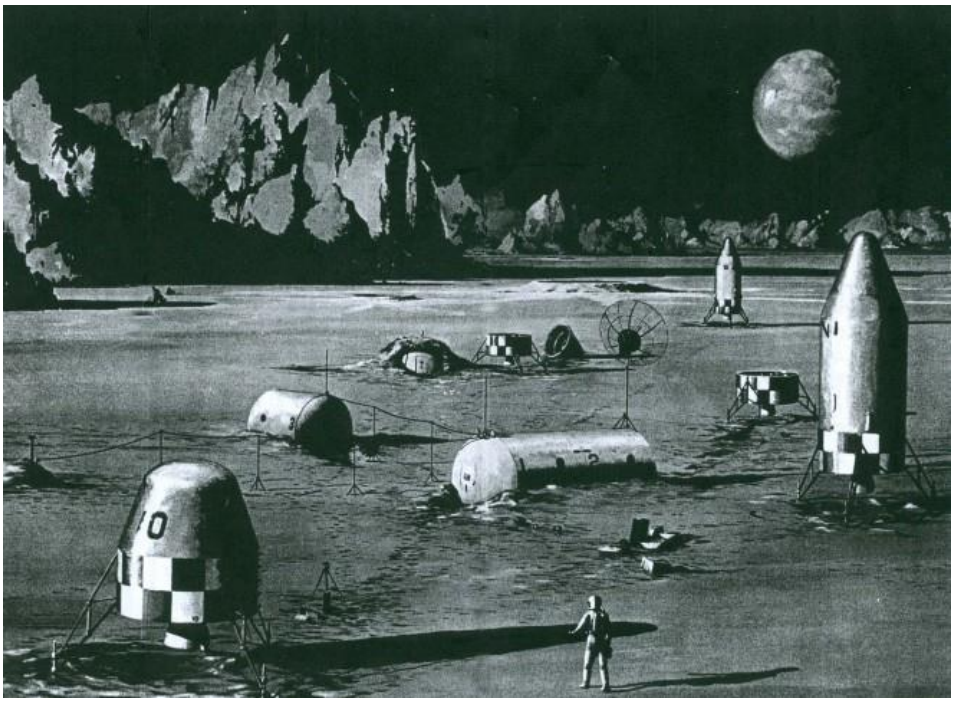

Figure 5-2: Artistic Rendering of the Single Person Lunar Base and its Cargo Landers [41]

While this plan was never seriously considered, it generated significant interest. The concept formed the basis of a 1964 science fiction novel entitled "The Pilgrim Project", which subsequently led to the 1968 Robert Altman film entitled "Countdown" [41].

5.1.2 "Mars to Stay" Mission Concepts

In the years following the Apollo Program, as the Space Race approached an end and President Nixon redirected NASA to focus its attention towards developing regular human access to low-Earth orbit, human space exploration planning activities experienced a significant decline [17,181]. It was not until the mid-1980s that interest reemerged in this area. This was catalyzed by the steady stream of data returning from the Viking orbiters and landers, the growing interest in the concept of ISRU pioneered by Ash et al.'s 1977 publication [16], and the beginning of the "Case for Mars" series of conferences that provided a public forum for the discussion and debate of Mars mission planning concepts [17]. This gap in mission planning activities beyond Earth orbit is evident in Figure 5-1.

Over a decade later in July 1996, as U.S. space policy shifted from the ambitious Space Exploration Initiative of President Bush Sr. towards the formation of the current International

Space Station Program and the era of "Faster, Better, Cheaper" robotic planetary exploration under the Clinton Administration [182,183], the concept of one-way missions was introduced by George Herbert of Retro Aerospace at the sixth Case for Mars conference [184]. This concept became the first of what has since been referred to as the "Mars to Stay" class of mission concepts. These are based on the notion that the first landing of humans on Mars should be a one-way mission with the goal of immediate settlement of the planet. In addition to the aforementioned arguments related to mass savings inherent in avoiding the need to return the crew, these types of mission have frequently been justified by references to the journey of the Pilgrims to the New World, the movement of families to the Wild West, and other mass migration events [185]. As such, "Mars to Stay" plans typically project the gradual addition of crewmembers and expansion of infrastructure over time towards some level of self-sufficiency. Interestingly, in almost all cases, these expansion plans involve repeating the originally proposed one-way plan multiple times. Specific details regarding the transition to self-sufficiency are left mostly undefined.

Herbert's proposal is perhaps the first to articulate the governing principals of the "Mars to Stay" class of mission. In his plan, a total of six people would be sent on a one-way, direct entry trajectory to Mars over two launch campaigns occurring 26 months apart. This would be enabled by a launch campaign consisting of five launches of a heavy lift launch vehicle capable of injecting 100 metric tons into a Mars transfer orbit. Each launch would carry three capsules that would eventually be delivered directly to the Martian surface. These capsules would serve as both the crew's transit and Mars surface habitat, and would contain ISRU systems, ECLS systems, and supplies that would last the crew for approximately 35 years. It was claimed that this plan would result in a saving of 25-35% in system development costs due to the relative maturity of the systems chosen, and would cost approximately $11 billion to land the first crew of six on Mars, and $8 billion for each optional two-person expansion of the surface crew thereafter [184].

As can be observed in Figure 5-1, plans of this type have been published at a steady cadence of approximately every two to six years since the publication of Herbert's one-way mission plan. In 1998, Brian Mackenzie of the Mars Foundation proposed a one-way mission to Mars at the 1998 International Space Development Conference that later evolved into the Mars Homestead project, aimed at permanently sustaining 12 people on the surface of Mars [186]. In 2004, Paul Davies, a renowned physicist and science communicator wrote an opinion piece in the New York Times that advocated for sending a four person crew on a one-way journey

to Mars instead of pursuing the "Moon-first" approach planned articulated in President Bush Jr.'s "Vision for Space Exploration". After landing, this crew would deploy ISRU systems to extract water and oxygen from the Martian environment for life support, and would be resupplied every two years with food, medical supplies, and spare parts and equipment delivered from Earth [187].

This opinion piece was followed two years later by a mission concept developed by Jim McLane III, a retired NASA engineer who in 2006, proposed a one astronaut, one-way Mars mission plan entitled "The Spirit of the Lone Eagle". Similar to the arguments made for the one-way lunar plan described in Section 5.1.1, McLane claimed that the reductions in system mass resulting from sending a single person to Mars, along with the removal of the need for a return capability, reduces the technological demand of the mission to a level that is within that of current capabilities. Altogether, this would enable the first launch of the mission to occur by 2017 – a time period that was near enough in the future to avoid the political obstacles that face tradition Mars mission concepts [188,189]. Instead of waiting to be retrieved sometime in the future, as was the case with the Bell Aerospace lunar plan, this lone astronaut would be supported by periodic resupply missions and in time, would be joined by other astronauts to eventually form a colony.

Shortly thereafter in 2010, Professor Dirk Schulze-Makuch of Washington State University along with Paul Davies co-authored an article in the Journal of Cosmology entitled: "To Boldly Go: A One-Way Human Mission to Mars" [190]. Like the previously discussed mission plans, the authors claimed that a one-way mission when compared to traditional return-trip mission concepts, would result in cost savings of several fold. Once more, a four person one-way expedition was to be sent to Mars and supported by pre-emplaced power generation system, food supplies and ISRU systems. This crew would be resupplied every two years with resources and equipment that could not be produced locally, and over time, as the level of technology matured, more crewmembers would be added to the growing colony.

More recently in 2012, the Mars One mission program was announced, with the aim of building the first human settlement on the surface of Mars. Following a series of precursor missions to demonstrate and deploy key technologies, the first crewed mission would depart Earth in 2024, sending four people on a one-way journey to the surface of Mars. After this initial mission, additional four-person crews would be sent to Mars at every subsequent launch opportunity to expand the extraterrestrial colony. Unlike the previously described proposals, the Mars One plan also included a funding model for raising the $6 billion claimed to be

required to fund the first crewed landing of the mission. This involved selling production rights and related merchandise for a television series that would follow the crew selection process, crew training, and each major stage of the mission plan. In 2013, the organization announced the opening of their astronaut selection program [11], which resulted in widespread media attention far greater than any of the previously proposed "Mars to Stay" mission plans. Similar to the previous plans however, the mass and technology development savings claimed to be achieved through the use of a one-way missions have been frequently used as an argument for the mission's feasibility. Also similar to these past proposals, little technical analysis beyond initial estimates have been performed on the mission requirements.

Thus, the Mars One mission plan can be viewed as the latest in a series of "Mars to Stay" plans that have been proposed over the past three decades. While its widespread exposure has popularized the general concept of one-way expeditions to Mars, the review performed here finds that the common justifications for the attractiveness of one-way mission architectures have not been supported by quantitative lifecycle analyses, particularly for the requirements of emplacing and sustaining the infrastructure required to support and grow a one-way crew.

5.2 Analysis Objectives and Approach

In light of the observations made in the previous section, this chapter aims to use HabNet and the lessons learned from the ongoing operations of the International Space Station to examine the lifecycle requirements, sustainability, and hence overall feasibility of the Mars One mission plan. The Mars One mission plan is considered to be representative of the "Mars to Stay" class of mission architectures and thus by extension, this analysis is also intended to gather insights on one-way Mars mission plans in general.

Specifically, the analysis performed in this chapter aims to:

(1) Objectively assess the feasibility of the Mars One mission plan based on statements made by Mars One and the technical information that the organization has made publicly available.

(2) When applicable, provide recommendations for the stated Mars One mission architecture and operational strategy. Here, it is important to note that in some instances, the implementation of a recommendation requires the relaxation of one or more of the constraints imposed by statements and assumptions made by Mars One. When this is the

case, recommendations are made with the intent of improving the Mars One mission architecture while minimizing the number of Mars One-specified constraints that are violated; and

(3) Highlight areas in which focused technology development can better enable future "Mars to Stay" mission plans and Mars settlement efforts in general

With regards to items (2) and (3) listed above, we emphasize that this analysis does not attempt to design the Mars One mission architecture. Rather, recommendations are suggested and analyzed to extend the scope of this feasibility analysis to less-constrained variants of the Mars One architecture.

This analysis is performed by first compiling statements and assumptions publicly made by Mars One to model and simulate their baseline mission plan within HabNet. Since no information regarding the Mars One mission was found in the technical literature, mission architecture details are primarily derived from the Mars One website [191], as well as the publicly-released request for proposals and proposal information package for a 2018 Mars Lander [192]. This analysis was performed from April to December 2014 and as such, all data used was taken from the Mars One website at this time. It is possible that at the time at which the reader reviews this analysis, the corresponding data described at the Mars One website would have been changed from the dataset used here. As a result, all website URLs cited in this analysis present both the current URL and a URL linking to an archived version of the webpage referenced at the time of this study. In addition, when insufficient data is available from Mars One sources, we use data from standard aerospace handbooks and data sources, such as the NASA Human Integration Design Handbook [139] and the NASA Baseline Values and Assumptions Document (BVAD) [179].

After simulating the baseline Mars One mission within HabNet, we use the obtained results to assess its feasibility, and if applicable, make recommendations to the mission architecture based on the results of the analysis. These recommendations are then implemented into a modified system architecture and the process of simulating, analyzing, providing recommendations based on an intermediate feasibility assessment, and performing an updated analysis with an updated architecture is repeated. We continue to iterate through this analysis cycle until we find that either: (1) the mission requires the development of new technologies whose capabilities are so uncertain that their performance and lifecycle properties cannot yet be confidently predicted; and/or (2) the lifecycle cost of the program does not reach a steady state and is hence unsustainable.

5.3 Problem Background

In this section, we summarize the Mars One mission plan, along with the underlying assumptions made in this analysis. In addition, we define our interpretation of the terminology used in statements made by Mars One, in order to enable the objective evaluation of their claims.

5.3.1 Summary of the Mars One Mission Plan

As is representative of the previously discussed "Mars to Stay" class of Mars mission architectures, the Mars One mission plan consists of a series of unmanned precursor missions to demonstrate and deploy key technologies, followed by one-way crewed missions to Mars at every subsequent launch opportunity (26-month intervals [193]). These missions are accomplished with a set of common mission elements, summarized in Table 5.1.

Table 5.1: Summary of the Mars One mission plan [191]

Mission Phase	Time-frame	Elements deployed	Image
Precursor	2018	Technology demonstration lander on Martian surface and communications satellite deployment in Mars orbit (not shown)	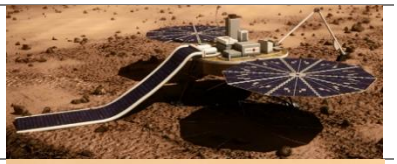
Pre-deployment	2020	Multipurpose rover used for site prospecting and clearing, habitat set up, crew transportation, and regolith collection for local processing	
Pre-deployment	2022-2023	Crew habitat: this consists of three variants of a core unit based on the SpaceX Dragon [194] module, as well as a 500m^3 Inflatable Unit. The initial habitat will consist of six modified Dragon modules connected with two inflatable units. Refer to Section 5.5 for additional details. (Image from Business Insider [195])	
First Crew Transit	2024	Mars Transit Vehicle: this consists of a Transit Habitat and a Mars Lander and functions as the means of crew transport from Earth to the Martian surface	
Colony Expansion	2025 onwards	Additional crew habitat units are launched during the same launch window as every crew launch. These are integrated into the Mars One habitat, enabling the infrastructure to grow over time	

The campaign commences with a precursor mission launching in 2018, involving a Mars surface lander based on the design of the NASA Phoenix Lander. The goal of this mission is to demonstrate key technologies required to sustain a human settlement on the Martian surface, including thin-film solar arrays and an oven to extract water from Martian regolith. A Mars orbiting communications satellite will also be launched on this mission to support both the precursor and subsequent missions [191].

Pending the success of this first mission, a follow up mission is planned for launch in 2020, transporting a multi-purpose rover to a predetermined site, likely in the northern hemisphere near 45° latitude [192]. The rover will survey the region for a suitable settlement site and prepare the selected site for the subsequent arrival of the habitation modules.

On the following launch opportunity in 2022, six scaled-up versions of the SpaceX Dragon [194] spacecraft will be launched and upon arrival in 2023, will be connected together using the previously deployed rover to form a contiguous habitat. These habitation units come in three variants:

- **Living Units**, which each contain a $500m^3$ inflatable structure, an airlock for crew extravehicular activity (EVA), and the wet areas of the habitat, such as the waste and hygiene compartment [196]. Within the inflatable units, $50m^2$ of crop growth area is allocated to provide food to sustain three crews of four people [197]
- **Life Support Units**, which each contain air revitalization, water processing and waste management technologies and stores. In addition, these units contain an ISRU system, as well as the thin-film solar arrays that will supply power to the habitat. The systems within the Life Support Units "will be very similar to" the ECLS technology currently flying on the International Space Station [198]
- **Supply Units**, which stores supplies and spare equipment for the habitat [193]

For the purposes of redundancy, each complete habitat contains two copies of each unit. More detail regarding the Mars One habitat layout is described in Section 5.5. In addition, a separate human lander unit, also based on the Dragon capsule, is used to deliver each crew to the surface from the year 2025 onwards.

After the initial emplacement of the habitation units, the thin-film solar arrays are deployed along with the ISRU system. Over the subsequent 500-day period, the rover delivers regolith to the ISRU oven, where it is baked to extract water. A portion of this water is then electrolyzed to generate oxygen. At the same time, an atmospheric processor extracts and stores nitrogen

from the Martian atmosphere. By the time the first crew departs Earth, the ISRU system will have produced 3000L ($3m^3$) of contingency water, 120kg of contingency oxygen, and sufficient oxygen and nitrogen to generate a breathable atmosphere of 70kPa within the habitat [191,197].

This first crew will nominally depart Earth in 2024 in a Mars Transit Vehicle (MTV) that will primarily employ an open-loop life support system. Within the same launch window, another six habitation units will be sent to provide the equipment and surface habitation required for the second four-person crew.

After landing in 2025, the first crew will enter the habitat, activate the food production system, and integrate the six habitation units that were launched with them into the initial habitation system. These newly added units will support a second four-person crew, who will depart Earth in 2026, along with another set of equipment to support the subsequent third crew. This cycle of sending four person crews along with the habitation equipment to support follow-on four-person crews continues every 26 months, thereby allowing the settlement to expand over time [191].

5.3.2 Currently "Existing, Validated and Available" Technologies

The Mars One mission plan is built upon a philosophy of exploiting existing technology [193]. The claim that currently available technology is capable of supporting the mission has often been used as an argument to justify the mission's feasibility, and is stated clearly on the Mars One website:

"No new major developments or inventions are needed to make the mission plan a reality. Each stage of the Mars One mission plan employs existing, validated and available technology" [193]

Given the potential for numerous interpretations of this statement, it is important to clearly define our interpretation of this statement in order to provide an unambiguous basis for this analysis. As a result of the lack of available clarifying data, we use the industry-standard Technology Readiness Level (TRL) metric, as specified in the NASA Systems Engineering Handbook [199], to define our interpretation. We note that the following TRL-based

interpretations of the above statement are our own, and may not necessarily align with those of Mars One.

The claim that "No new major developments or inventions are needed" implies that all technologies are at TRL 5-6, where they have been demonstrated in a relevant operating environment at either the component or system level [199]. The use of the term "validated" further supports this interpretation, based on the widely accepted definition that a validated technology has been proven to accomplish "the intended purpose in the intended environment… as shown through performance of a test, analysis, inspection, or demonstration" [199].

Finally, an "existing" technology can be considered as one that is at least at TRL 3, where an "analytical and experimental proof-of-concept" has been demonstrated [199]. Anything beneath this readiness level is within its early formulation phase, has not yet been built, and is therefore considered as nonexistent.

Given these definitions, we survey the current state of the art in spaceflight technology and find that in many cases, the technologies required for the Mars One mission plan either do not yet exist, or have not been demonstrated in a relevant operating environment. Some relevant technologies and operational approaches have had significant use in spaceflight but they were not designed for the Martian environment, while other relevant technologies are still in the early stages of development, where they are still being tested at small scales in laboratory or analog environment conditions. This technology survey is presented in Section 5.6.1.1, where we perform the first iteration of our analysis.

However, given the possibility for successful technology development and validation efforts for all required systems prior to the launch of the first Mars One crew, we make the optimistic assumption that all technologies specified by Mars One will be available when required, and continue our analysis based on the statements made on Mars One's website. It is important to highlight, however, that the development effort required to mature the required technologies to their necessary levels will contribute significantly to the cost of the Mars One program. Due to the high uncertainty in predicting this development cost, we do not capture it within this analysis.

We further note that because of the lack of relevant data and operational experience for many of the technologies included in Mars One's mission plan, we have been forced to make several assumptions. These have been based on extrapolations of the current state of the art (as discussed throughout Section 5.5), and on the fundamental design philosophies discussed

earlier. In cases where the analysis has necessitated architectural modifications, these have been implemented with the goal of increasing the feasibility of the system architecture while remaining as much as possible within the constraints set forth by statements and assumptions made by Mars One.

5.4 Analysis Scope

The analysis performed here concentrates on the habitat pre-deployment and crewed phases of the Mars One mission profile. Specifically, we treat the period between the pre-deployment of a complete surface habitat (consisting of 6 modified SpaceX Dragon capsules) and 26 months after the crew arrives (one launch cycle) as a repeating unit of resource demands over time. Applying HabNet to this time period allows us to quantify the resource demands of the settlement as it expands beyond the arrival of the first four-person crew. The only exception to this assumption is the spare parts requirement, for which it is assumed that crews can share spare parts for identical items. As will be discussed in Section 5.5.3, this commonality means that each crew can benefit from the spares that were brought by any mission before them. Modeling this spare parts strategy requires an analysis of the full mission campaign.

Furthermore, since a number and sequence of launches has been specified by Mars One, we extend the capabilities of the Evaluation Module in this analysis to calculate the number of launch vehicles required to deliver the total equipment manifests predicted by the Habitation, ISRU, and Supportability modules from Earth to Mars. This enables the evaluation of the Mars One plan along an additional dimension that can be converted into a dollar value, based on published launch cost estimates. The implementation and assumptions used throughout this analysis are described in the next section.

5.5 Problem Setup

To evaluate the feasibility of the Mars One mission plan, we first define the required input parameters for each of the HabNet modules, based on statements published by Mars One. Table 5.2 summarizes these input parameters, while Sections 5.5.1 to 5.5.4 provide further details on the assumptions behind each of these parameters.

Table 5.2: Summary of input parameters used to model the Mars One mission plan within HabNet

Input Parameter	Selected Option
Habitation Module Inputs	
Crew CONOPS • Number of Crew • Crew Activities • EVA Frequency	Crew Composition: Assumed to be a four person crew consisting of two males and two females, all aged 35 years old. One of the males has a mass of 72kg while the other has a mass of 75kg. Both females have a mass of 55kg. These figures are typical of the astronaut population [177] Crew Schedule: Based on the standard Mars mission schedule listed in the NASA BVAD [179] and on the frequent number of EVAs implied by the description on the Mars One website [200], it is assumed that five two-person EVAs will occur each week. For each crewmember, 8 hours of sleep and 2 hours of exercise are budgeted each day. (Note that this exercise requirement will be examined further in Section 5.7.5). On EVA days, exercise is not performed. Rather, 8 hours of EVA are scheduled, with the remainder being allocated to Intravehicular Activities (IVA) such as performing science experiments, preparing meals, or harvesting and replanting crops. All activities that are not EVA, sleep, or exercise are classified as IVA, and are assumed to require the same level of crew energy expenditure. As a result, on non-EVA days, crewmembers are assigned with IVA tasks during their non-exercising waking hours, in a manner similar to that adopted on the ISS and in the case study performed in Section 4.4.
Mission Duration	26 months (approximately 19000h) between resupply. This corresponds to the period between launch windows from Earth to Mars – that is, the period between resource and hardware resupply opportunities. This is the minimum continuous period over which the habitat must remain self-sufficient.
Habitat Layout	Layout: An eight module habitat consisting of six scaled up SpaceX Dragon capsules (each 25m^3) and two Inflatable Units (each 500m^3) based on the description provided by Mars One [201]. See Figure 5-4 for a schematic of the habitat, along with the allocation of ECLS technologies to physical locations within the habitat. This allocation is based on both images rendered by Mars One (see Figure 5-3) and heuristics derived from the allocation of ECLS technologies onboard the ISS United States Orbital Segment (USOS) (see Appendix B.2 for details) Internal Atmosphere: Assumed to be 70.3kPa total pressure with a nominal O_2 concentration of 26.5%, based on Mars One's statements that the habitat atmosphere will be 0.7bar [191]. The equivalent atmosphere recommended by the NASA Exploration Atmospheres Working Group (EAWG) consists of a 26.5% O_2 mixture [112]. The diluent gas is nitrogen.
ECLS Architecture	Assumed to be similar to those used on the ISS USOS based on the Mars One statement that their life support units will "*be very similar to those units which are fully functional on-board the International Space Station"* [198]. This system will be augmented with a Biomass Production System (BPS), which according to Mars One, will produce all food required by the crew [197]. See Sections 5.5.1 and 5.5.1.4 for further details on the selected ECLS architecture and the sizing of the BPS. A full listing of all ECLS technologies is provided in Appendix D. See Figure 5-4 for a flowsheet of the baseline combined ECLS and ISRU architecture.
ISRU Module Inputs	

ISRU Strategy	Water Extraction: A soil processor containing a specialized oven is used to extract water ice from Martian regolith. This is based on the design by Interbartolo *et al.*[202] described in Section 2.2.4 and sized using the equations in Appendix F. Oxygen Generation: To generate oxygen, a portion of the ISRU-derived water is electrolyzed with a water electrolysis unit. For this analysis, this electrolysis unit is assumed to be common with that of the Oxygen Generation Assembly (OGA) used in the ECLS system. See Figure 5-5 for details. Inert Gas Extraction: An atmospheric processor is used to extract inert gases (nitrogen and argon) from the Martian atmosphere. These inert gases are used to maintain cabin pressure within the habitat modules. To size this system a first order sizing model was developed by Schreiner [143]. This system is further discussed in Section 5.5.2.
Supportability Module Inputs	
Supportability Strategy	Spare parts are manifested to accommodate random failure and planned maintenance such that the probability of having sufficient spares is 0.99. These are delivered from Earth. Failure rates of ISS ECLS technologies are assumed, as per Mars One's statement that their life support units will "*be very similar to those units which are fully functional on-board the International Space Station"*[198]. For ISRU systems, failure rates are adopted from analogous ECLS hardware due to the lack of system maturity. (See Appendix D for a full list of assumed reliability data) Spare parts commonality is assumed between crews – that is, each arriving crew's system is identical to those that already emplaced and thus spare parts can be shared among the systems of each crew. See Section 5.5.3 for further details. All consumables resupply requirements are generated by local ISRU.

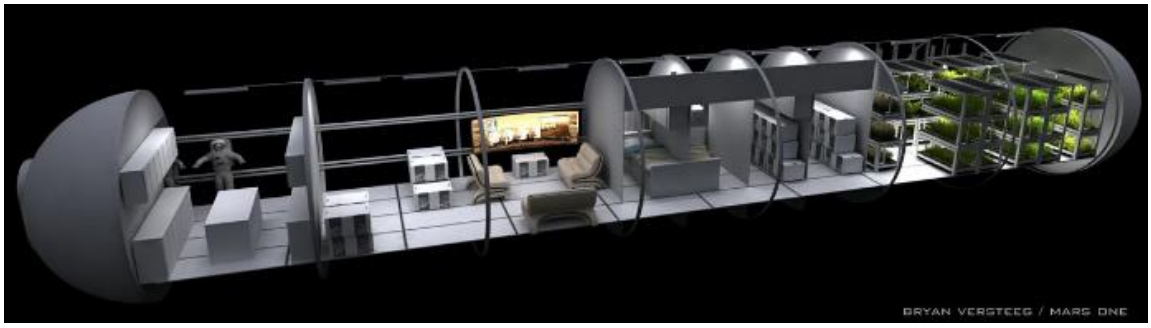

Figure 5-3: Artist's Rendering of the Mars One Inflatable Unit [203]

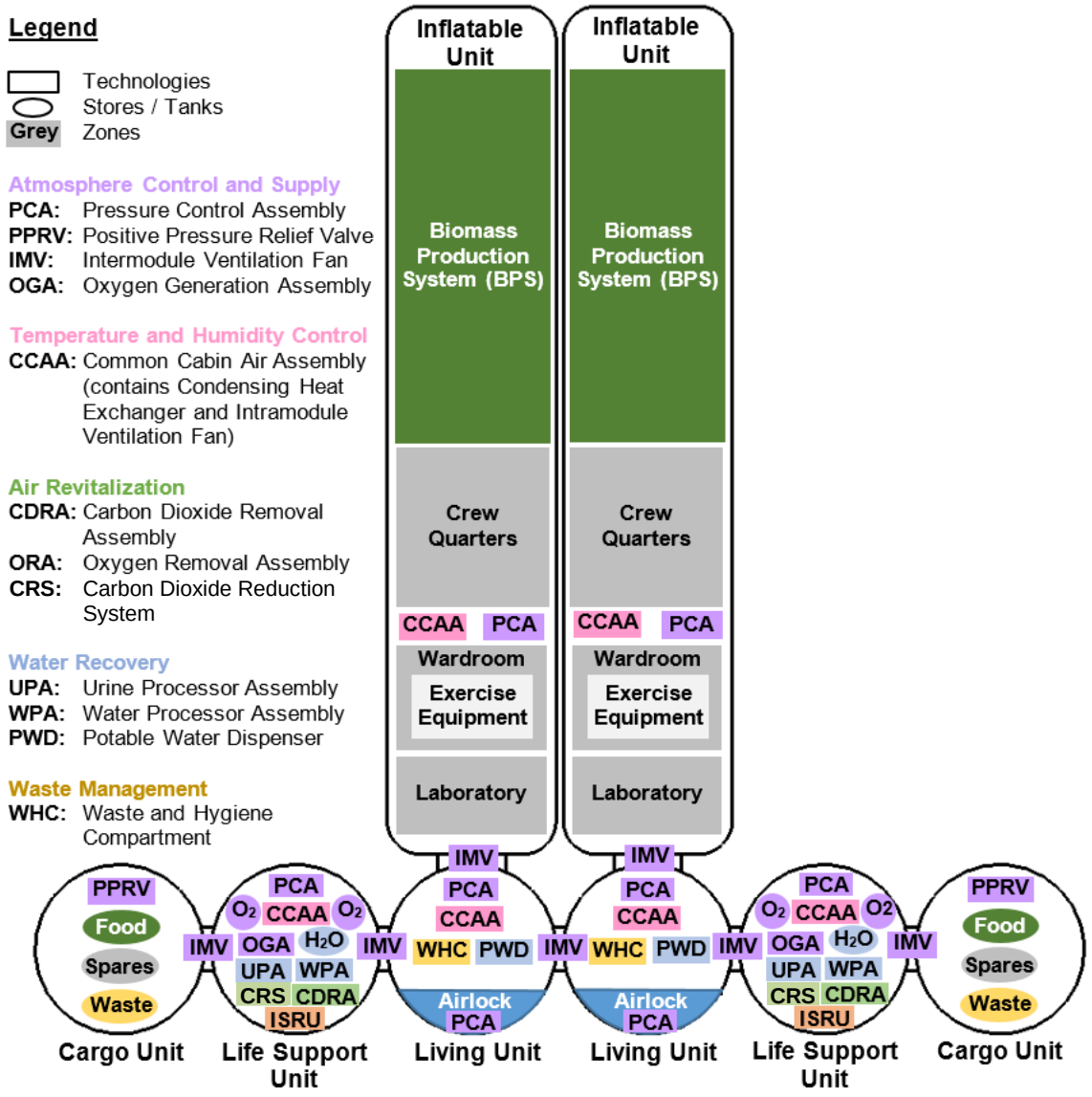

Figure 5-4: The Baseline Mars One Habitat Architecture with assumed ECLS Technology Location Allocation and the BPS area modified according to the results of the sizing analysis performed in Section 5.5.1.4.1

5.5.1 Habitation Module Inputs

As is described in Table 5.2, Mars One plans to use an ISS-based ECLS architecture augmented with a biomass production systems. Given the uncertainties in the implementation of these systems on the Martian surface, we further expand upon the assumptions made in the analysis of these systems in the sections below.

5.5.1.1 ECLS Architecture

Based on the claim that the Mars One life support units will "*be very similar to those units which are fully functional on-board the International Space Station"*[198], we assume that technologies similar to those onboard the International Space Station (ISS) United States Orbital Segment (USOS) will be used. We note that while there are currently ongoing development efforts for European [204] and Japanese [205,206] ECLS capabilities, the performance of these technologies in-flight has yet to be completely evaluated, and the operational data required for a sparing analysis is therefore unavailable (see Section 5.5.3). Similarly, while there has been substantial operational experience with Russian ECLS systems onboard the ISS, little information is publicly available regarding their mass and reliability properties, thus limiting the extent to which a quantitative analysis can be performed. Additionally, we observe that the current NASA baseline Mars surface habitat ECLS architecture [58] is also based on that of the ISS USOS. This observation provides additional confidence on the suitability of our ECLS technology assumption.

The one modification to our assumed ECLS architecture, however, is the food production system, which according to Mars One, will come predominantly from locally grown crops [197]. We assume this to be accomplished via the Nutrient Film Technique (NFT) described by Wheeler [170], and adopted as the baseline horticultural approach for crop growth within the NASA Kennedy Space Center (KSC) Biomass Production Chamber, due to its flexibility across plant species and its water efficiency [174]. The NFT is also implemented within the HabNet ShelfImpl class (see Appendix D.8 for details).

Further, we note that the ECLS technologies onboard the ISS were originally developed specifically for use in microgravity and have not been validated for use on the Martian surface. The introduction of a partial gravity environment will inevitably lead to different ECLS technologies that will likely be less complex than those onboard the ISS, due to the simplification in chemical separations that a gravity environment affords. Thus, in the absence of data for Mars-specific ECLS technologies, the assumption of ISS-based ECLS mass and volume properties for similar-functioning Mars-based ECLS systems can be considered to be conservative. However, in light of Mars One's existing technology constraint, the assumption of similar reliability characteristics between ISS-based and Mars-based ECLS systems can be considered reasonable, as increasing the reliability of flight-rated ECLS systems beyond that of the ISS remains an ongoing challenge within the ECLS community [29].

Moreover, as will be discussed in Section 5.6.1.1, the lack of currently available Mars-based ECLS technologies and the lack of experience in growing food crops on the Martian surface necessitates the adoption of the assumption stated in Section 5.3.2: that all technologies required by Mars One will be available when needed. These technologies are summarized in Appendix D.

Figure 5-5 depicts the baseline ECLS and ISRU system assumed for this analysis. In this figure, white elements represent technologies currently on the ISS, green elements represent the BPS and orange elements represent ISRU technologies. From this figure it is apparent that the baseline Mars One ECLS architecture is a version of the ISS ECLS architecture augmented with BPS and ISRU systems. Because there is currently no flight experience with these two systems, first order engineering estimates on their performance and sizing were performed for this analysis. Details of the BPS sizing process are described in Section 5.5.1.4, while Section 5.5.2 discusses the approach taken to size the ISRU system.

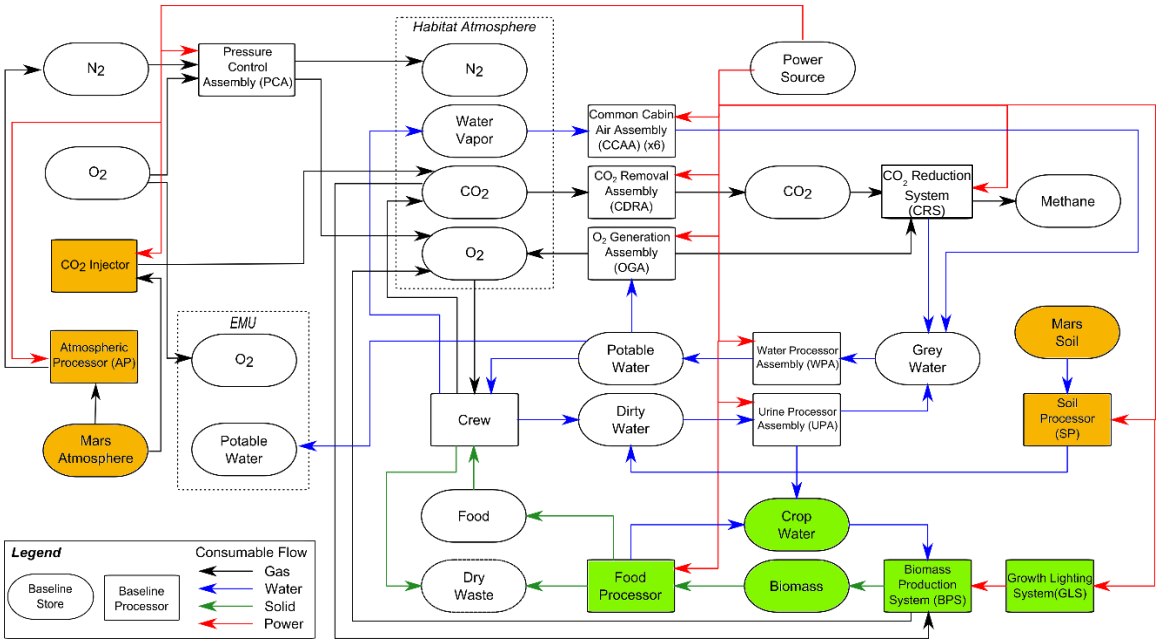

Figure 5-5: Baseline Mars One ECLS and ISRU system assumed for this study. Orange elements correspond to ISRU technologies and resources, and green elements represent plant growth technologies

5.5.1.2 Solid Waste Management

The ISS currently employs a solid waste management strategy of transferring all solid waste into the various single-use logistics vehicles that visit the station for subsequent burn up in the Earth's atmosphere. For a Mars settlement, the increasing storage requirement for solid waste over time makes this approach unsustainable, and necessitates the adoption of alternative solid waste management practices. Past approaches adopted within closed environments have included incineration (as part of NASA's Lunar Mars Life Support Test Project (LMLSTP)[207]), and biological means such as anaerobic digestion (see Section 5.5.1.4.8.1). Although these approaches have been shown to work within closed environments, several problems were experienced during their operation, and further research and development is needed to increase the reliability of these systems, and to scale their performance to the level required for the Mars One mission. Moreover, a review of publicly available Mars One literature found that no information regarding the solid waste management strategy has been specified, other than the statement that their life support system will be ISS-like.

Given these observations, along with the fact that information related to the expected waste streams is required to specify and size a notional solid waste management system (information that has not been made available), we have chosen to exclude solid waste management considerations from the scope of this analysis.

5.5.1.3 Crew Systems and Habitat Structures

The crew system and habitat structures considered in this analysis are based on first-order estimates provided in Stilwell et al. [208]. The commodities in this category include a galley and food system, a metabolic waste collection system, personal hygiene equipment, a clothing and laundry system, recreational equipment and personal stowage, housekeeping, operational supplies and crew restraints, photography, sleep accommodations, and crew health care. The mass of the inflatable habitats is calculated using the NASA BVAD estimate of 9.16kg/m^3 for an unshielded inflatable module on the surface of Mars [209]. The stowed volume of these inflatable modules is calculated by assuming a 15:1 packing ratio based on that of the Expandable Habitat Demonstration System deployed at McMurdo Station in Antarctica in 2008 [210]. A detailed mass and volume breakdown of these systems can be found in Appendix I.5.

5.5.1.4 Biomass Production System Architecture

Since an extraterrestrial crew-scale biomass production system (BPS) has yet to be developed, a dedicated BPS sizing analysis was performed to size a system capable of providing the caloric needs required by the Mars One mission plan. Architecting a BPS involves the selection of several decisions, including the types of crops grown and their growth area, the horticultural strategy, the crop shelf arrangement, and the water and nutrient management strategy. The assumptions behind each of these decisions are described in the following sections.

5.5.1.4.1 Biomass Production System Crop Selection

The lack of BPS flight experience introduces significant uncertainty to the integrated behavior of the habitat. Such a system can demand significant resources, depending on the number and type of crops grown. The quantity of crops ultimately depends on the proportion of the crew diet sourced from plant growth, as well as the daily caloric demand of the crew, which is in turn driven by each crewmember's gender, age, weight, and activity level.

For the purposes of this analysis, we use the approach described in Jones [211] to determine the crew daily macronutrient demand, and introduce our own optimization scheme around the HabNet ShelfImpl class (see Appendix D.8) to determine the appropriate crop mix to meet this demand. An initial simulation of the baselined crew composition and crew schedule (see

Table 5.2) using the Habitation Module found that on average, each crewmember had a daily caloric demand of 3040 kilocalories. According to Mars One, 100% of these calories will be provided every day by a biomass production system with a growth area of $50 m^2$. This area is claimed to be sufficient to feed three crews of four people [197].

For a typical diet consisting of a caloric macronutrient makeup of 68% carbohydrates, 12% protein, and 20% fat [211], this equates to a biomass production requirement of 2067.2 grams of carbohydrates, 364.8 grams of protein, and 270.2 grams of fat per day per crew of four with a daily caloric demand of 3040 kilocalories. Using these values, the required crop growth areas were determined by formulating and solving the following multi-objective optimization problem:

$$\min w_1 \sum_{i=1}^{i=9} x_i + w_2 \sigma(\mathbf{x}) \qquad (5.1)$$

$$\text{s.t.} \quad \sum_{i=1}^{i=9} c_i r_i x_i \geq 2067.2 \qquad (5.2)$$

$$\sum_{i=1}^{i=9} p_i r_i x_i \geq 364.8 \qquad (5.3)$$

$$\sum_{i=1}^{i=9} f_i r_i x_i \geq 270.2 \qquad (5.4)$$

$$x_i \geq 0 \quad \text{for} \, i = 1,...,9 \qquad (5.5)$$

where **x** is a nine element vector representing the growth area allocation for each of the nine candidate crops; **c**, **p**, and **f** correspond to vectors representing carbohydrate, protein, and fat fractions of dry mass of the nine candidate crops; **r** corresponds to a vector of static growth rates, measured in grams of crop growth per square meters of growth area per day. These values are listed in Appendix I.4. Furthermore, σ represents the standard deviation function; and w_1 and w_2 are weighting factors.

Here, the chosen objective function is the weighted sum of the total allocated crop growth area, and the standard deviation of the individual areas of each of the crops. The first component of this objective function is based on the goal of minimizing biomass production system mass and volume, since these parameters typically grow with increasing crop growth area [209]. Conversely, the second component of the objective function corresponds to maximizing the variety of crops grown. Reducing the standard deviation across the set of selected areas effectively drives the optimizer towards introducing more crop species into the solution. Finally, the constraints imposed ensure that the daily crew requirement for carbohydrates, proteins, and fats is met by the BPS. To solve this optimization problem, differing values for the weighting factors w_1 and w_2 were applied to the objective function and a non-linear constrained optimization solver was employed. Table 5.3 summarizes the results obtained for different weighting value combinations.

As we vary the relative magnitudes of the weighting values in the objective function, we move across Table 5.3 from left to right, causing the optimizer to gradually introduce more variety into the crew diet, at the cost of increased growth area. Moreover, we observe crops being added in a sequential manner with increasing variety, indicating that there is a priority towards selecting plants that have both a high growth rate and a large nutrient content. Peanut

and wheat crops are always included in the crop mix because peanuts have the highest fat content of all the crop options, while wheat has a high carbohydrate content.

Table 5.3: Optimized growth areas for various objective function weightings

Crop	Option 1 w_1=1, w_2=0	Option 2 w_1=0.4, w_2=0.6	Option 3 w_1=0.3, w_2=0.7	Option 4 w_1=0.27, w_2=0.73	Option 5 w_1=0, w_2=1
Dry Bean					52
Lettuce					52
Peanut	98	82	75	73	52
Rice					52
Soybean		23	35	40	52
Sweet Potato			4	10	52
Tomato					52
Wheat	87	85	81	73	52
White Potato				5	52
Total Growth Area	185	190	195	201	468

From Table 5.3, we observe a maximum crop growth area of 468m^2 (Option 5) and a minimum crop growth area requirement of 185m^2 (Option 1) to support one crew of four – a range of areas that is significantly greater than the 50m^2 per three crews of four claimed by Mars One [197]. We therefore conclude that the stated Mars One food production plan is calorically insufficient. To overcome this, we select Option 4 in Table 5.3 in order to continue our analysis, as it represents a reasonable balance between the two competing objectives. This profile achieves three more crop species over the minimum growth area option for the relatively low cost of an added 16m^2 of growth area.

5.5.1.4.2 Biomass Production System Layout

While the 201m^2 area required for Option 4 of Table 5.3 is four times larger than that originally stated by Mars One, a dimensional analysis indicates that it may still be possible to fit this into a portion of the Inflatable Unit if a high density packing and lighting scheme is employed, such as that originally planned for NASA's BIO-Plex [212] - a proposed integrated habitation-BPS test facility that was in development in the late 1990s.

Figure 5-6 shows a potential layout for the BPS based on the BIO-Plex [212] architecture, consisting of densely packed plant shelves, each with a dedicated lighting system and

hydroponic root zone. The root zones contain a nutrient solution supplied by a tank installed into the floor of the chamber. This particular BPS design requires about 40% of the pressurized volume of a single Inflatable Unit, as compared to the 17% volume estimated from renderings of the system as provided by Mars One (Figure 5-3). Furthermore, while the BIO-Plex was designed with a dedicated chamber for its BPS, rendered images of the baseline Mars One BPS indicate that it shares the same space and atmosphere with the crew inside each Inflatable Unit [203] (see Figure 5-3). The following subsections further expand on the various technologies required to grow the selected crop mix, while Section 5.6.1.3 explores the operational implications of including a BPS of this scale on the system-wide behavior of the habitat.

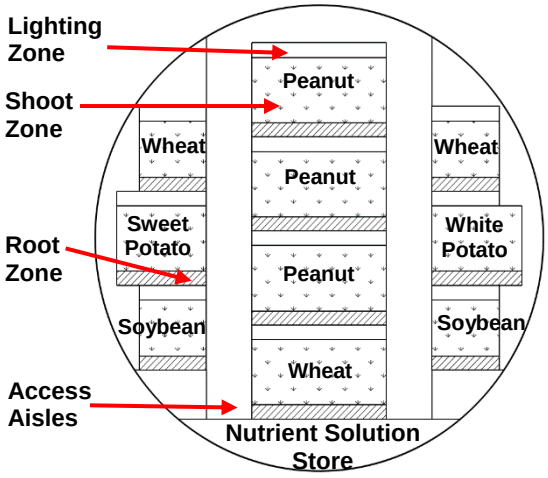

Figure 5-6: Potential shelf layout for the selected crop growth areas

5.5.1.4.3 Biomass Production System Lighting

We assume the use of LED lights in the Growth Lighting System (GLS) similar to the Heliospectra LX601 grow light [213], a current state of the art commercially available option. Using the performance data of this lighting system, it was calculated that at least 137 LED units, each weighing 8kg, would be required to provide full coverage of the 201m^2 growth area. This calculation was based on comparing the photosynthetic photon flux (PPF) requirements of the various crops selected for the BPS, with the published PPF density values of the selected grow light. This calculation is summarized in Table 5.4, as follows:

Table 5.4: Grow Light System Requirements Calculation

Crop	Assigned Area (m^2)	Ideal PPF Density (µmol/s/m^2)*	Equivalent PPF (Area × PPF Density) (µmol/s)
Peanut	73	313	22849
Soybean	40	325	13000
Sweet Potato	10	325	3250
Wheat	73	1332	97236
White Potato	5	325	1625
Total Equivalent PPF			137960
Minimum Number of Grow Lights^			137

*Calculated from data listed in the NASA BVAD [209]
^Based on a PPF density performance value [213] of 1011 µmol/s

5.5.1.4.4 Biomass Production System Water Management

For the selected crop profile, the MEC models implemented within the HabNet ShelfImpl class estimate that up to 150L of water will be consumed per hour, a quantity significantly beyond the capacity of the nominal ISS-derived water recovery and management system described by Mars One [198]. As a result, a dedicated crop water system was implemented, based on that of the NASA KSC Biomass Production Chamber mentioned earlier.

Here, a nutrient solution layer 0.5-1cm deep is maintained at the crop root zone. This solution flows in a circuit at a rate of 3.2-4.8L/min/m^2, and is recharged on a daily basis to make up for nutrients lost through crop uptake. To support this flow rate and nutrient recharge frequency, the KSC system maintains a nutrient solution reservoir of 185L to support the approximately 40L of solution required for each 5m^2 of crop growth area [214]. Assuming a linear relationship between nutrient solution buffer capacity and crop growth area, this equates to 9045L of nutrient solution required to sustain the 201m^2 of crop growth area required for the Mars One BPS.

Based on Mars One's reliance on ISRU technologies (see Section 5.3.1), we assume that this solution will be produced by dissolving raw nutrients into ISRU-derived water. Thus, to ensure that sufficient water is available to activate the BPS upon the arrival of the first Mars One crew, the predeployed ISRU system is required to generate at least 9045L of water (see Section 5.5.2 for ISRU system sizing assumptions). This requirement is in addition to the 3000L of contingency water budgeted by Mars One for the entire habitat [11]. We further make

the optimistic assumptions that all water used within the BPS can be completely recycled for reuse by the growing crops and that all nutrients are available when required without needing to be transported from Earth (as per the assumptions of the MEC models implemented within the ShelfImpl class – see Appendix D.8 [209]). Previous plant growth experiments at KSC have indicated that daily water makeup requirements can range from 0.7-10L/m^2/day depending on the type of crop grown, and the level of maturity of the crops [214].

5.5.1.4.5 Biomass Production System Horticultural Strategy

We select a continuous growing scheme as recommended by Gitelson, et al.[215], where the total growth area of each crop is divided into smaller batches that are staggered in time, such that after the first harvest, a batch of crops reaches maturity on every subsequent day. While increasing the crew time dedicated to horticulture, this growth scheme reduces food storage requirements and ensures that food will be available when required by the crew.

5.5.1.4.6 Biomass Production Water Carbon Dioxide Management

A commonly quoted heuristic in biological life support system analysis is that if approximately 50% of a crew's food requirements are sourced from a biomass production system, this same system can regenerate all of the air required for crew respiration [209]. Since the Mars One plan involves feeding the crew primarily with locally grown crops, this gas exchange will be imbalanced, with the CO_2 expired by the crew being insufficient to sustain the planned level of crop growth.

This phenomenon can be observed in Figure 5-7, where a preliminary simulation of the BPS finds that without additional CO_2 sources, crop death occurs after 12 to 19 days into the mission, even when the Carbon Dioxide Removal Assembly (CDRA) is operated in a reduced mode, where it is initially switched on to maintain atmospheric CO_2 to within crew safety levels, and switched off as the crops grow and are capable of managing the CO_2 load of the crew. These values are based on an assumed initial atmospheric CO_2 concentration of 3000ppm – a value commensurate with levels observed on the ISS [170]. In Figure 5-7, the increased CO_2 concentration occurring at every 7-8 day period corresponds to weekend days when all four crew are within the habitat. On every weekday, two crewmembers each perform eight hour EVAs.

In addition, we find that because this time of crop death is well before the time of harvest of the first crop (62 days for the wheat crop in this case), initially employing oxidation techniques such as incineration or aerobic digestion to recover CO_2 from inedible biomass[216] would be ineffective, since this biomass would not yet be available.

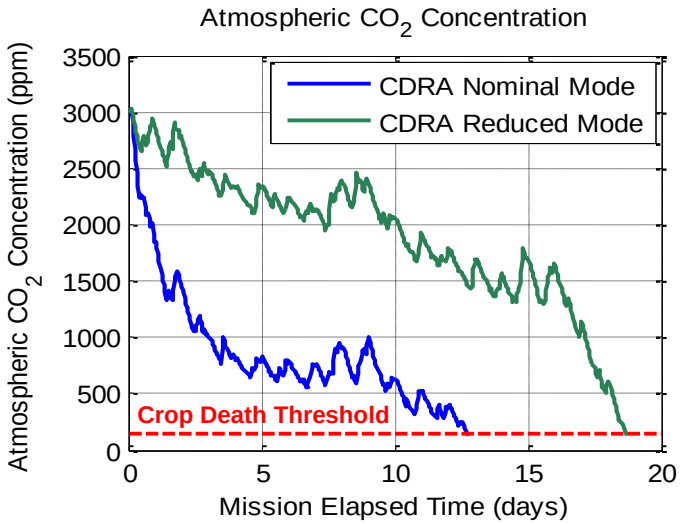

Figure 5-7: Atmospheric CO_2 concentration time histories for simulations of the baseline Mars One habitat configuration with the CDRA in both nominal (blue) and reduced (green) operating modes. The reduced mode involves switching the CDRA off as the crops grow and become capable of managing the CO_2 load of the crew. As the crops continue to grow, crew-exhaled CO_2 becomes insufficient for the crops as they demand increasing levels of CO_2, eventually resulting in crop death.

Mars One plans to address this imbalance by introducing CO_2 from the Martian atmosphere into the Martian cabin [197]. In this analysis, we model this system as an idealized CO2 injector that selectively separates and compresses CO_2 from the Martian atmosphere. A controller introduces CO_2 into the habitat to maintain a CO_2 concentration level of 1200 parts per million (ppm) – a value within the region of maximum growth for most C3 type plants [170–172]. This system is based on the cryocooler-based CO_2 capture concept modeled in Appendix F.2. A cryocooler-based concept was chosen over one based on mechanical compression due to its approximately 9 times lower mass and 3 times lower power consumption [217].

5.5.1.4.7 Food Production

To convert raw biomass into edible food and to recover water consumed by mature crops for reuse back into the BPS water management system, a notional food processor is included in the system architecture. Like many of the other technologies previously discussed, no space-rated version of this technology has yet been developed.

Regardless, we can still infer what such a system might contain. To process raw wheat, a mill will likely be required to convert wheat seeds into flour. From this form, multiple additional processing options are available, including an extruder to produce cereals and pasta, a breadmaker to produce bread, or a starch/gluten separator to extract wheat gluten, which can then be used to make seitan [218].

To process soy, a multifunctional processing system has been proposed by NASA JSC to produce soymilk, tofu, okara, and whey from raw soybeans [219]. The soaking and boiling functions contained within this system are likely sufficient to process the remaining crops chosen for this study.

5.5.1.4.8 Additional BPS Design Considerations

In the preceding sections, we sized a BPS based on Mars One's stated objective of developing a life support system that: (1) is based on existing technology [193]; and (2) provides all food using locally-grown crops [197]. As a result, the objective function used in developing the BPS was formulated with the primary goal of providing sufficient and varied calories for the crew. This represents a simplified, first order analysis that omits a number of additional considerations that are introduced as a result of including a BPS within a life support architecture. These can be broadly categorized as additional ECLS options that accompany the inclusion of a BPS, and additional requirements that need to be accommodated to support a BPS. The following sections discuss how these considerations are considered in this analysis.

5.5.1.4.8.1 Additional ECLS Options

The inclusion of a BPS system introduces additional ECLS options beyond those that can be served by physiochemical ECLS systems alone. These include biological options for water processing, urine pretreatment, air revitalization, nutrient recovery, and solid waste processing.

As discussed in Section III.I.H-4, we assume an independent BPS water management system for this analysis, due to the high water demand of the BPS. This system is assumed to

be decoupled from the portion of the ECLS system that provides potable water to the crew, based on Mars One's assumption of ISS-like ECLS systems [198]. While biological options do exist for both urine pretreatment and water processing, these typically come in the form of microorganisms (such as the thermophilic anaerobic bacteria used in the ESA MELiSSA project [220]), or aquatic plants (such as the duckweed, water hyacinth, and aquatic reeds used in the Biosphere 2 experiment [221]) – systems that have not been specified by Mars One and are hence not included within the scope of this study. Food crops on the other hand, are generally not considered for water processing due to concerns related to toxin accumulation and food safety. Rather, a minimal threshold for recycled water quality is required before it can be fed to food crops [222]. As a result, this study assumes physicochemical water and urine processing technologies for all water recycling functions.

Similarly, biological means for processing solid waste and recovering nutrients for plant growth are not considered in this analysis as they also have not been specified by Mars One. Approaches such as those adopted by the Biosphere 2 and MELiSSA projects (see above) are potential candidates, but require further research and development before they can be reliably operated in the Martian environment.

Conversely, the potential for crops to serve air revitalization functions will be explored in this analysis (see Section 5.6.2.1). Unlike the biological life support functions discussed earlier, air revitalization based on food crops has been previously demonstrated in the laboratory setting at relevant scales. Specific examples include NASA's LMLSTP [207] and the Japanese Closed Ecology Experiment Facilities (CEEF) [223]

5.5.1.4.8.2 Additional BPS-Derived Requirements

In addition to providing further options for ECLS, plant growth systems also impose additional requirements that would otherwise not be present. These primarily come in the form of additional power and thermal management requirements that arise from the need for dedicated lighting systems to support plant growth, and storage and processing requirements for inedible biomass produced by the BPS. For this study, we will consider power and thermal system requirements only in the context of comparing the lifecycle resupply requirements of a BPS-based ECLS architecture to one that is dependent on the periodic resupply of Stored Food (SF) (see Section 5.6.2.3). Power assumptions will be based on Mars One's stated power architecture consisting of flexible thin-film solar arrays and batteries for energy storage [224].

Conversely, inedible biomass storage and processing requirements will not be incorporated within this analysis. We note that these requirements impose mass and volume penalties on the system architecture and should be quantified when performing a detailed design of a flight system.

5.5.2 ISRU Module Inputs

The Mars One architecture leverages resources from both the Martian soil and atmosphere to support the habitat. To produce water, a soil processor utilizes a specialized oven to extract water from Martian regolith. This water is condensed and a fraction is electrolyzed to produce oxygen. The second system, an atmospheric processing module, utilizes the local atmosphere to produce nitrogen and argon to resupply the habitat atmosphere. These two technologies represent the lowest-TRL systems in the Mars One architecture, as neither has spaceflight experience. Thus, in order to size these technologies, designs from existing hardware and literature were employed in order to remain true to the Mars One constraint of utilizing existing technology. The assumptions made in the sizing of each of these systems is described in the following sections.

5.5.2.1 Soil Processor Sizing Model

The soil processor assumed in this analysis is based on the design of Interbartolo et al. [202] (see Section 2.2.4), and is sized based on the corresponding equations summarized in the ISRU Technology Model Library described in Appendix F.1. To size the soil processor, a soil water concentration of 3% by mass is assumed, based on values detected by the Curiosity rover. It should be noted however, that higher concentrations at levels closer to 10% may potentially be found in localized regions [225,226]. In addition, we assume that water can be readily extracted by heating and stirring the soil with an auger, and that this water will not require further processing to remove contaminants. Although Martian soil-derived water will likely include perchlorates [202], a water cleanup module was left out of the ISRU system design for simplicity.

5.5.2.2 Atmospheric Processor Sizing Model

In contrast to the soil processor, a first order design had to be created for the atmospheric processor, since the bulk of Martian atmospheric processing research has focused on obtaining CO_2 for the purpose of producing oxygen [227–229], rather than capturing inert gases for the purpose of maintaining habitat atmosphere against leakage and EVA losses. The design of a gaseous processing system for capturing nitrogen and argon from a CO_2-rich atmosphere is somewhat different from existing techniques developed for CO_2 acquisition from the Martian atmosphere. Thus, the design detailed herein is strongly conceptual in nature and will require further development prior to flight. This design was developed by Schreiner [143], and is summarized in Figure 5-8. This design was based on processing a standard Martian atmosphere (95.3% CO_2, 2.7% N_2, and 1.6% Argon by volume) [202] with a density of 0.02 kg/m^3 and a pressure of approximately 0.6kPa[54].

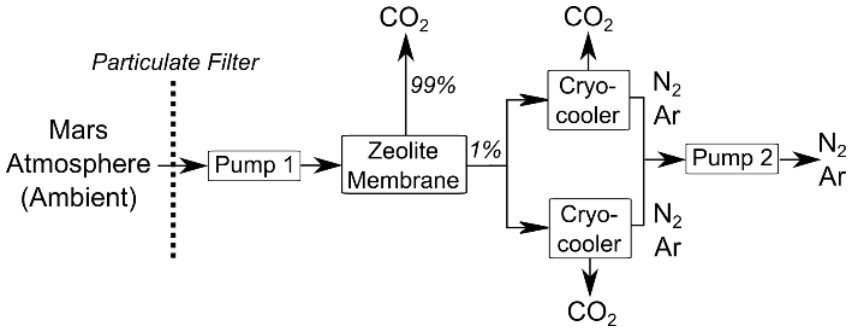

Figure 5-8: Block Diagram of Atmospheric Processor

The first challenge of Martian atmospheric processing is compressing the low ambient pressure of 0.6kPa to a nominal value of 101.3kPa for typical processing technologies. Although vacuum pumps are ideal for such a requirement, they are typically too large for space missions. Regression data from the DVJ family of blowers by Dresser Roots was used to generate the estimated mass, volume, and power of the inlet compressor as a function of flowrate [230]. Future work may analyze the effectiveness of alternative compression techniques.

The compressed gas is then directed through a cylindrical zeolite membrane filter that selectively allows CO_2 to permeate to the atmosphere while retaining nitrogen and argon [231,232]. To determine the required area of the zeolite membrane, a permeation simulation of the membrane was developed to calculate the required membrane area to achieve a certain cut fraction (the fraction of permeated gas flow over initial gas flow). The results from this model,

shown in Figure 5-9, were used to determine the surface area required to achieve a cut fraction of 0.99 (as indicated in the middle of Figure 5-8). A cut fraction of 0.99 was chosen to eliminate as much CO_2 as possible from the inlet stream while also avoiding too significant of a pressure drop. As the flow pressure approaches the ambient atmospheric pressure, the effectiveness of the membrane filter drops dramatically. From Figure 5-9, we can observe that even with such a dramatic filtering of the atmosphere, the retained flow still contains approximately 30% CO_2, with nitrogen and argon comprising the rest of the flow.

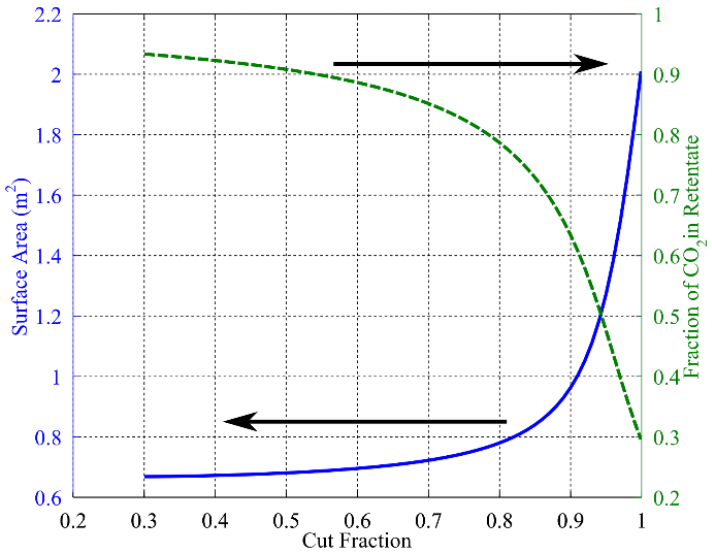

Figure 5-9: The design of the Atmospheric Processor. A larger zeolite membrane surface area results in a larger cut fraction (ratio of retained to permeated gas) and decreases the fraction of CO_2 in the retentate (retained gas). A cut fraction of 0.99 was chosen for the atmospheric processor design.

Once a cut fraction was chosen, the required surface area was used to generate a membrane design with a cylindrical diameter of 5 cm. A zeolite membrane with a density of 2.1 g/cm^3, a void fraction of 0.45 and a CO_2 permeance of 5×10^{-7} was used for this particular design [232]. A thin aluminum supporting frame was designed around the zeolite membrane. This frame was assumed to cover 33% of the zeolite surface area, so the length of the membrane was increased by 50% to achieve the required surface area. After passing through the zeolite membrane filter, the gas is compressed to tank pressure and directed to one of two cryocoolers (operating out of phase in parallel, similar to a pressure-swing system) which freeze the remaining CO_2 out of the flow before venting the remaining nitrogen to the storage tank (see Figure 5-8). These cryocoolers were modelled after the 16W CryoTel GT cryocooler [233].

It should be noted that it was assumed that two cryocoolers would be able to process enough gas, as simulating the performance of the cryocoolers was beyond the scope of this study. All other components in the atmospheric processor were parametrically sized to produce enough inert gas to supply the average demand predicted by the ECLS simulations. It was also assumed that the zeolite membrane would be sufficient to yield high purity N_2 after utilizing the cryocooler to remove additional CO_2. Additional components may be necessary to ensure that the trace amounts of carbon monoxide and nitric oxide do not contaminant the product gases, as their melting points are significantly lower than that of CO_2.

5.5.2.3 ISRU Systems for the Predeployment and Crewed Mission Phases

ISRU systems corresponding to two distinct mission phases were sized for each case examined in this study. A Pre-Deployed ISRU (PDISRU) was designed to produce enough O_2, N_2, and water to inflate the habitat and fill the reservoir tanks prior to human arrival. After the arrival of the first crew, this system was assumed to continue operations to prepare for the next crew's arrival. In addition, a second ISRU system was sized as a "support" system to resupply resources to counteract ECLS system inefficiencies, atmospheric leakage, and makeup for EVA losses during the crewed phase of the mission.

To appropriately combine the mass estimates from the ISRU system with those from the ECLS system, both a margin and contingency was added to the ISRU system mass estimate. This is because the mass and volume estimates for the ECLS system are based on ISS hardware data while the ISRU system mass estimate comes from conceptual designs of low-TRL technology. The atmospheric processing module is at a low TRL; all of the technology has undergone a proof-of-concept demonstration, but, to the authors' knowledge, no integrated test of such a system has been conducted. There has been significant development of technology for capturing and processing CO_2 from the atmosphere [227,234], but no such development has occurred for a system to capture N_2 and Argon [226]. Thus, we estimate the atmospheric processor to be TRL-3, indicating the need for continued technology development. The soil processing module is at a slightly higher TRL, as oven technology has been demonstrated on Martian soil in a relevant environment [225], but not at the scale of a full ISRU production system. We estimate soil processing technology to be TRL 4-5 [225]. Given the low TRL and conceptual nature of the system design, a mass and volume contingency of 30% along with a

margin of 25% was included in the design [235]. A complete listing of mass and volume estimates for the components of the ISRU system is presented in Appendix I.5.

5.5.3 Supportability Module Inputs

For this analysis, the HabNet Supportability Module developed by Owens [143] was used to estimate the spare parts required to ensure the continued operation of the Mars One ECLS and ISRU systems over the 26 month period between resupply missions. Here, the number of spares was calculated such that the probability of having sufficient spare parts is 0.99. To perform this analysis, a number of assumptions are required for the input parameters provided to the Supportability Module. These assumptions range from the failure rates of each of the components themselves, the level at which repair tasks are expected to be performed, to the overall supportability and maintenance strategy adopted by the system. Each of these input parameters is described in further detail in the sections below.

5.5.3.1 System Level of Repair and Reliability Data

As was discussed in Section 3.4.3, the Supportability Module estimates the number of spare parts required to accommodate both random failure and scheduled maintenance. In accordance with Mars One's statement that their life support units will "*be very similar to those units which are fully functional on-board the International Space Station"*[198], the ECLS system is assumed to be spared and repaired at a level comparable to that of the ISS Orbital Replacement Unit (ORU) architecture. In general, this consists of sub-assembly sparing and can include components at the level of electronics boards, sensors and valves.

In addition, based on the Mars One constraint of hardware similarity to ISS systems, reliability values of ISS ECLS technologies were assumed for the same ECLS technologies employed within the Mars One habitat. For ISRU components, failure rates are adopted from analogous ECLS hardware due to the lack of available data (see Section 2.3.3 for further details). In the scenario that a suitable analog system was not available, a Mean Time Between Failure (MTBF) value of 500,000h is assumed – a value that is higher than the MTBF values of most ECLS components and as such, is considered to be optimistic.

5.5.3.2 Maintenance Strategy

As an extension of Mars One's statements that their systems will be based on those of the ISS, the concept of operations for component replacement is assumed to follow the ISS paradigm of remove-and-replace maintenance. When a component failure occurs, the portion of the system containing that component is shut down and the backup system (in this case, the redundant Life Support Unit) is brought online to support the system during maintenance. The failed component is replaced with an identical spare, and the primary system is brought back online once maintenance is complete [236]. For simplicity, the Mean Time To Repair (MTTR) for any component is assumed to be 12h (with a standard deviation of 1h), and repairs are assumed to bring the system back to good-as-new condition.

Here, the inclusion of a redundant ECLS system is based on the architecture published by Mars One, which includes including two identical Life Support Units for each crew – one primary and one redundant secondary system [237]. For the purposes of this analysis, it is assumed that when a component failure occurs in the primary system, the redundant system is brought online to provide life support functions until a repair can be implemented. Calculations using the SMP approach implemented within the HabNet Supportability Module found the expected primary system downtime (and therefore redundant system operational time) to be less than 1% of the 26 months between resupply opportunities from Earth for each major subsystem. Therefore, the amount of operational time required for the secondary system is assumed to be negligible for the purposes of this analysis. It is assumed that the secondary unit does not fail while the primary unit is offline, and that the operation of the secondary unit does not significantly increase the total number of spares required by the system.

In addition, the storage tanks and buffers within the system are assumed to be large enough to isolate failures while they are repaired; that is, the failure of a given processor does not cause downstream processors to go offline due to a lack of resource supply. The mass of stored ECLS consumables is given in Appendix I.2. Since the objective of this analysis is not to examine the probability of failure but rather to determine the spares logistics demand, the probability that stored consumables will run out before a repair is implemented is not calculated. Rather, the redundant Life Support Unit is assumed to be sufficient to maintain the system during maintenance operations, as mentioned above. Furthermore, failures of different components are assumed to occur independently. As a result, failure of a particular component only causes

downtime for the assembly including that component and requires the replacement of only that component.

5.5.3.3 Resupply Strategy

Given that the Mars One surface base will be expanded and restocked every 26 months, we assume that the spare parts of incoming crews can be shared with the spare parts and systems that are already emplaced and operating on the Martian surface. For this to be valid, the systems deployed between each crew must be common. To perform this calculation, the Supportability Module is run over multiple missions of increasing durations and crew sizes according to the Mars One expansion strategy – that is, analyses are performed for increasing mission durations in integer multiples of 26 months and increasing crew sizes in integer multiples of 4 crewmembers. This allows for the cumulative spare parts that need to be delivered to the Martian surface up to a given point along the expansion pathway to be determined (such that the probability of having sufficient spares is 0.99). The required spare parts to be delivered on each mission while maintaining commonality between missions is then calculated from the difference between cumulative spare parts requirements of consecutive expansion phases (ie. missions) of the campaign. For instance, the number of spare parts required to be delivered by the third crew is calculated by the difference between the total number of spare parts required to sustain three crews on the Martian surface, and the total number of spare parts required to sustain two crews on the Martian surface.

It is important to note here that the imposition of commonality between different crews would place heavy constraints on Mars One's ability to upgrade systems over time, since any changes to the system design would have to ensure that the resulting spares remain common with previous systems in order to maintain the benefits of commonality. If a design change is implemented due to system upgrades, loss of a component supplier, or any other reason, this commonality is eliminated and the spare parts mass required to sustain the Mars One plan will increase beyond the amount calculated here.

5.5.4 Evaluation Module

As was mentioned in Section 5.4, the HabNet Evaluation Module has been expanded in this analysis to calculate the number of launch vehicles required to deliver the calculated habitation,

ECLS, and ISRU systems along with their spare parts to the surface of Mars for each mission of the Mars One campaign. This allows for the calculation of launch costs, and hence a comparison with the programmatic cost estimates stated by Mars One.

To determine the number of launch vehicles required, a launch manifest optimization routine was developed by Ho [143]. This routine provides a solution to the launch vehicle "packing problem" under mass and volume constraints – that is, it determines how all items that need to be delivered to Mars are packed into the various lander vehicles such that the total number of required launch vehicles is minimized. In order to perform this analysis, a number of assumptions related to the transportation vehicles and their payload masses were made. These are described in Sections 5.5.4.1 and 5.5.4.2, while details on the launch manifest optimization scheme are presented in Section 5.5.4.3.

5.5.4.1 Transportation System Assumptions

Based on the statements made by Mars One, this analysis is based on the use of the SpaceX Falcon Heavy rocket as the main launch vehicle, and a scaled-up version of the Dragon capsule as the primary landing vehicle [238]. Here, values listed in Table 5.5 are assumed for payload masses of these vehicles. We note that since the scaled up lander has not yet been developed, the numbers listed here have been acquired from an unofficial source [239], but compares well to scaled up values from the Red Dragon study performed by NASA and SpaceX. In addition, the recurring cost ($300M) used here is estimated by scaling values used in the Red Dragon analysis [240].

Table 5.5: Parameters related to the Delivery of Cargo to the Martian Surface assumed in this Analysis

Falcon Heavy [241]**:** - Payload to Low-Earth Orbit: 53,000 kg - Payload to Trans-Martian Orbit: 13,200 kg
Lander (a 5m-diameter variant of Dragon) [194,240,242]: - One lander is delivered by one Falcon Heavy launch - Lander Mass: 14,400 kg - Payload Mass: 2,500 kg - Payload Volume: 25 m^3 (pressurized) - Recurring Cost: $300M per launch vehicle and lander - Propulsive Entry, Descent, and Landing (EDL)

In addition to those listed in Table 5.5, assumptions were also required on entry, descent, and landing capabilities, as well as the sizing of some of the non-ECLS and ISRU components that need to be delivered to the Martian surface. These are listed below as follows:

- The Red Dragon study selected propulsive landing as the baseline option for its Martian Entry, Descent, and Landing system [240]. This paper assumes that the same technology will become available; therefore no detailed EDL feasibility analysis is performed; and
- All cargo except for the Inflatable Units is assumed to fit within the pressurized volume of the lander. This exception arises because the predicted mass of 4,580kg for each Inflatable Unit (based on equivalency coefficients provided within the NASA BVAD [179]) is heavier than the stated pressurized payload capacity of the assumed Dragon vehicle. It is important to note that this assumption effectively expands the payload mass capacity of two of the Dragon landers out of each mission to the value required to deliver the inflatable habitats, creating two specialized landers. Effectively, 9,160kg of inflatable habitat is assumed to be delivered to the surface by two vehicles with a nominal combined payload capacity of 5,000kg. This is a very optimistic assumption, but is adopted in recognition of the requirement to deliver the inflatable habitats to the surface in one landing. This requirement arises from Mars One's stated plan to have a completely integrated and functioning habitat prior to the departure of the first crew [11], and the need to avoid autonomous manufacture and integration of inflatable structures on the Martian surface due to significant limitations in current technology.

In addition to launch requirements for lander capsules, a series of launches are required to assemble a Mars Transit Vehicle (MTV), to support their journey to Mars. The MTV and the crew lander are launched with an additional crew on-board to assist with the assembly of the crew lander and MTV. Two propulsion stages for trans-Mars injection are also launched separately. After the integration of the MTV and lander, the Mars crew is launched and the assembly crew returns to the Earth. Therefore, transporting a single crew to Mars requires a total of four Falcon Heavy launches. Before entry into the Martian atmosphere, the crew moves to the lander and the MTV is discarded.

5.5.4.2 Launch Vehicle Feasibility Analysis

Using the values listed in Table 5.5, a preliminary analysis was performed to assess the feasibility of delivering a loaded lander directly to the Martian surface using a single launch

vehicle, as is the assumption made by Mars One [11]. Based on the values listed in the Red Dragon study, the lander is delivered to Trans-Martian Orbit using the upper stage of the launch vehicle and directly enters the Martian atmosphere prior to landing on the Martian surface [240]. The predicted Falcon Heavy launch capability is 13200 kg into Trans-Martian Orbit [241] and the estimated gross lander mass including the payload is 14400 kg (Living, Life Support, or Supply Units; not including the Crew Lander). Therefore, based on these values, a single Falcon Heavy launch cannot deliver a loaded lander module to Trans-Martian Orbit (ΔV = 3.8 km/s). Thus, a design change appears to be required for either the lander or to the Falcon Heavy rocket. To continue with this analysis, however, we make the optimistic assumption that one cargo lander can be delivered by one Falcon Heavy launch.

5.5.4.3 Manifest Optimization

To determine the minimum number of landers required to land a given list of components and spares, a manifest optimization [243] was developed and performed by Ho [143]. In this analysis, a geometric optimization is not performed due to the lack of component dimension data. Instead, only mass and volume constraints are considered. The resulting formulation is similar to a classical optimization problem known as a bin packing problem, and is described as follows:

Objective:
J: number of vehicles used

Variables:
x_{ij} = 1, if item i is accommodated in vehicle j;
0, otherwise
y_j =1, if vehicle j is used;
0, otherwise

Parameters/Constants:
N: number of items (including packaging)
m_i: mass of item i
v_i: volume of item i
M: mass of vehicle
V: volume of vehicle

Bin Packing Problem Formulation:

$$\min J = \sum_{j=1}^{N} y_j$$

$$\text{s.t.} \sum_{i=1}^{N} m_i x_{ij} \le M y_j \quad \forall j \in \{1,...,N\}$$

$$\sum_{i=1}^{N} v_i x_{ij} \le V y_j \quad \forall j \in \{1,...,N\}$$

$$\sum_{j=1}^{N} x_{ij} = 1 \quad \forall i \in \{1,...,N\}$$

$$x_{ij}, y_j \in \{0,1\} \quad \forall i \in \{1,...,N\}, \forall j \in \{1,...,N\}$$

Although the above classical bin packing problem assumes that all commodities are discrete, we make an exception for food storage, as well as power and thermal system mass. These masses are assumed to be continuous for the purposes of the bin packing problem, able to fill any remaining mass capacity of already packaged landers. Any remaining food, power, or thermal system mass that cannot be fit into landers that have already been packaged with the discrete bin packing problem is allocated to additional landers. Furthermore, as described earlier, the inflatable habitats are assumed to each take up a single lander even though their individual mass is larger than the lander capacity.

This optimization problem was solved using the commercial software IBM ILOG CPLEX, yielding the optimal number of launches and logistics cost results presented in Section 5.6.2.5.

5.6 Case Study Results

This section presents the results of our analysis of the feasibility of the Mars One mission plan using HabNet. We apply the iterative analysis process described in Section 5.2, wherein we first assess the baseline mission plan under the assumptions and constraints stated by Mars One. This assessment then informs whether or not modifications to the architecture and subsequent analysis iterations are required. We reiterate that any modifications implemented to the baseline Mars One architecture throughout this process are made with the goal of achieving a feasible architecture while conforming as much as possible Mars One's statements and assumptions. When exploring alternative architectures, it was found that typically one or more of Mars One's assumptions was, by necessity, violated in order to move the architecture

towards feasibility. This usually comes in the form of new technology development or the relaxation of a payload mass limit on a transportation stage.

The feasibility assessments performed here can be broadly categorized as either architectural or programmatic feasibility assessments. Assessments of architectural feasibility evaluate whether or not a system can sustain the Mars One crew for the 26 month period between resupply missions within the landed mass limits imposed by Mars One. Contrastingly, assessments of programmatic feasibility evaluate the lifecycle cost of the entire program. Architectures that lead to programs that exhibit resupply costs that grow indefinitely over time are deemed to be programmatically infeasible.

In order for the mission plan to be deemed feasible, it must be both architecturally and programmatically feasible. That is, it must not only sustain every crew for the 26-month period between resupply missions, but it must also have a sustainable resupply requirement that can be met for the rest of the crew's lives.

In total, four analysis iterations were performed. These yielded two architecturally feasible architectures that are capable of sustaining the crew over the 26 month period between resupply. Further analysis of these architectures, however, found them to be programmatically infeasible due to a significant rise in cost as the settlement grows over time. Potential solutions to this programmatic infeasibility are discussed in Section 5.7, but the immense technology development effort required to reach a point where the Mars One mission plan is programmatically feasible make it difficult to quantitatively examine how these solutions would be implemented. As a result, we qualitatively describe technology that could potentially be used and note that an architecturally and programmatically feasible mission plan would by necessity differ significantly from the stated plan of Mars One. The procession of analysis iterations is presented below.

5.6.1 Assessment of Architectural Feasibility

5.6.1.1 Iteration 1: Mars One Baseline

In Section 5.3.2, unambiguous definitions used in the Technology Readiness Level (TRL) metric were adopted and defined as the basis for our interpretation of the Mars One assertion that their mission plan can be accomplished exclusively with existing technology [193]. As a first step in our feasibility assessment, we test this claim by surveying the current state of the

art in spaceflight technology. Through this, we observe that in many cases, the technologies required for the Mars One mission plan either do not yet exist, or have not yet been validated. Specific examples relevant to the scope of this analysis include:

- ISRU technologies which, as discussed throughout Section 2.2, are currently at a low TRL, with most of their past operational experience coming from lunar-focused field analog tests conducted by NASA between 2008 and 2012 [202] (see Section 2.2.3).
- Unofficial sources have stated that the Mars One habitat will be based on a 5m diameter, 25m^3 variant of the SpaceX Dragon capsule [239]. The current Dragon [244] capsule has a diameter of 3.6m and a pressurized volume of 11m^3 and as of this writing, there has been no announcement from SpaceX regarding the development of a scaled-up version. Furthermore, the proposed Falcon Heavy launch vehicle does not appear to be capable of putting the lander module with payload on a transfer orbit to Mars, as discussed in Section 5.5.4.2.
- Plant growth for space applications is still in the early stages of development. Only a handful of small-scale plant experiments have been flown in space [245]. As a result, there is much uncertainty in the performance and reliability of flight-rated crop growth systems. Moreover, as discussed in Section 5.5.1.4, systems required to compactly support plant growth and efficiently process raw biomass into edible food at the scales required are still very much in development.
- As discussed in Section 2.1.3, the current operational paradigm for the International Space Station (ISS) relies on regular resupply from the ground. This has in turn affected its system design and operations, especially from the perspective of consumables use. No operational experience has been gained for long-duration human spaceflight missions beyond low Earth orbit [246,247]. Such missions will require crew and life support systems that have lower consumables and spare parts resupply requirements [29]. Thus, dedicated technology development is required to better mature these technologies
- Approaches for mitigating the adverse impacts of long-duration exposure of humans and crops to galactic cosmic radiation and solar particle events while in space and on the Martian surface are still very much in development. In fact, this challenge was highlighted in a 2012 National Research Council report as being one of the most important technology areas to address in order to enable sustained human spaceflight beyond Earth orbit [248].

- Manufacturing spare parts in space and on the Martian surface using additive manufacturing, or "3D printing," has been frequently proposed. While additive manufacturing is a new development with the potential to reduce resupply mass [249], the technology is still very much in its infancy. Limitations in materials selection as well as the quality, precision, reliability, and reproducibility of parts produced using 3D printing, as well as limited understanding of the impact of a partial gravity environment on the thermal and fluid processes involved in 3D printing mean that significant technology development and validation efforts are required before 3D printing can be deployed in support of critical functions on Mars [250].

Thus, based on the observations made in this first analysis iteration, we conclude that because the baseline Mars One architecture requires extensive use of technologies that are not "existing, validated, and available," the capability to sustain the Mars One crew for the 26 month period between resupply periods is not currently available. Therefore the baseline Mars One mission plan, as publicly presented, is architecturally infeasible.

5.6.1.2 Iteration 2: ISRU, Lander, and Plant Growth Technology Development

The second analysis iteration addresses the conclusion of the first analysis iteration by making the optimistic assumption that all required ISRU, lander, and plant growth technologies will be developed in time for the mission. The cost of this development effort is expected to be significant, but the estimation of that cost is outside the scope of this study so we simply assume that the required technology exists and proceed with the analysis.

Here, we revisit the analysis performed in Section 5.5.1.4.1, where Mars One's claim that $50m^2$ of crop growth area will provide "sufficient plant production capacity to feed about three crews of four" [193] was investigated. It was found from this analysis that at least $185m^2$ was required to sustain a single crew of four. A sensitivity analysis of this result found that increasing this area to $201m^2$ would allow for the introduction of more variety to the crew's diet, for the relatively low additional crop growth area of $16m^2$. We note however, that this analysis is based on idealized crop growth rates under optimal lighting and nutrient conditions. A higher fidelity analysis under conditions more similar to that experienced on the surface of Mars will likely result in a substantially larger crop growth area requirement. As a reference, Cassidy et al. [251] estimated that it currently takes on average $1667m^2$ of plant growth area to

feed a single person on Earth on a typical diet, accounting for the inefficiencies of feed-to-animal product conversion. If all crops currently grown on Earth were fed directly to people, this value would reduce to 1000m^2 per person. This leads us to conclude that despite the assumption of technology availability resulting from the first design iteration, the Mars One architecture is still architecturally infeasible due to the insufficiency of their planned 50m^2 crop growth area to sustain their stated crew population.

5.6.1.3 Iteration 3: Increased Crop Growth Area

In the third analysis iteration, we increase the plant growth area to 201m^2 based on the analysis performed in Section 5.5.1.4.1. This is intended to enable Mars One's plan to provide all food from locally-grown crops [197]. With this adjustment, we run an end-to-end simulation of this modified Mars One architecture.

As described in Section 3.2, the first step of this analysis is to run the Habitation module to determine requirements for the ISRU Module. This is accomplished by simulating the habitat with the baseline crew schedule and ECLS architecture, but without the periodic introduction of ISRU-derived consumables. Since the Mars One mission plan relies on all consumables resupply requirements being served by ISRU [193], the resulting rate of consumables depletion is set as the ISRU resupply requirement. This value is then fed to the ISRU Module, where the mass and volume of the corresponding ISRU system is calculated.

This first simulation revealed that increasing the crop growth area to sustain the caloric intake of the crew, while growing crops within the same atmospheric environment as that of the crew (see Figure 5-3), would introduce atmospheric imbalances that would lead to a nitrogen depletion rate that would require a prohibitively large atmospheric processor system.

Specifically, this imbalance arises from a mismatch between the respiration rate of the crew and the combined photosynthetic rate of the crops, and is related to the initial simulations performed in Section 5.5.1.4.6 where the need for a CO_2 injector was discussed. As the various crop batches (see Section 5.5.1.4.5) of the BPS are planted and grown, the rate of crop photosynthesis enabled by injected CO_2 quickly outpaces the rate of crew respiration. This causes the continual buildup of O_2 within the cabin over time, resulting in the fire safety threshold of 30% O_2 concentration (see Table 3.5) being exceeded on mission day 36 (see Figure 5-10). To address this issue, an ISS-based approach is adopted, based on Mars One's specification that their system will "be very similar to those units which are fully functional

on-board the International Space Station" [198]. This involves using Pressure Control Assemblies (PCAs) to vent a portion of the habitat atmosphere before introducing N_2 to dilute the O_2 concentration within the atmosphere, reducing it to below fire safety limits.

Within this simulation, this process occurs between mission days 36 and 49, reducing the O_2 concentration and maintaining it at the set value of 0.265 (see Figure 5-10) and rapidly consuming N_2 (see Figure 5-11) until day 49, when the N_2 tank is depleted.

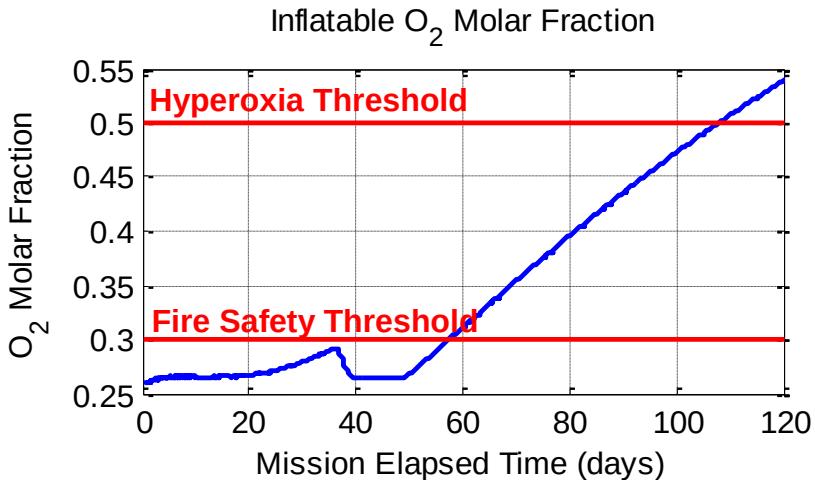

Figure 5-10: O_2 Molar Fraction within the habitat atmosphere

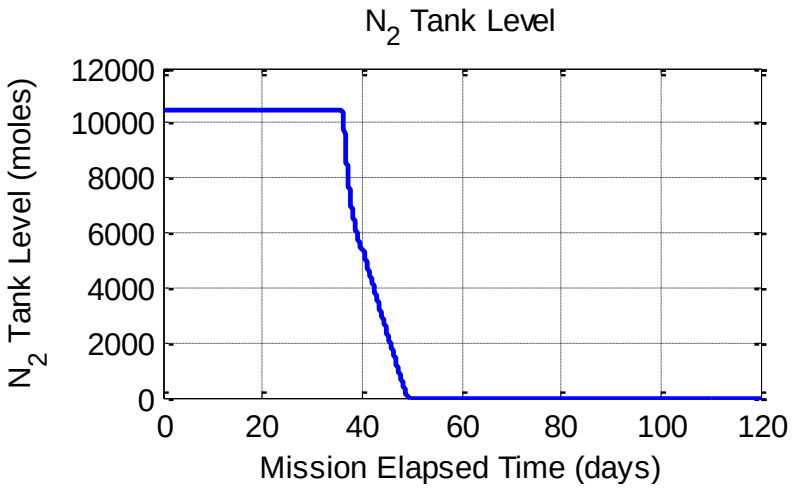

Figure 5-11: N_2 Tank Level for the nominal Mars One Habitat

Once the N_2 tank is depleted, the ISS-based O_2 concentration control strategy is no longer viable, since there is no more N_2 available to dilute the atmosphere. Without introducing further N_2 into the system, the O_2 molar fraction rises rapidly after day 49, as shown in Figure 5-10.

The fire safety threshold – O_2 concentration in excess of 30%[140] – is quickly violated on day 57, triggering one of the mission failure conditions described in Table 3.5. If this failure condition is ignored, the O_2 concentration continues to increase beyond the hyperoxia threshold of 50% on day 108, as shown in Figure 5-10.

As discussed earlier, these initial simulations were run to determine requirements for the ISRU system. Here, it was found that the assumed ISS-based O_2 concentration control scheme consumed N_2 at a rate of approximately 795 moles per day (22.26kg/day) at its peak. To sustain this demand, the ISRU Sizing module found that an Atmospheric Processor (AP) system with a mass of approximately 31,105kg is required. Table 5.6 presents a breakdown of this mass estimate. Here, we observe that the total mass of the required atmospheric processor is dominated by the mass of the pumps. This is due to a combination of: (1) the low pressure of the Martian atmosphere (600Pa); (2) the low nitrogen content of the Martian atmosphere (2.7% by volume); (3) the fact that the system is solar powered and hence can only operate during daylight (thereby increasing the required production rate during operation to compensate for its downtime during the night); (4) losses in flow through the zeolite membrane filter used to separate N_2 from the incoming flow (the cut-fraction described in Section 5.5.2); and (5) pressure losses downstream of the zeolite membrane filter. This combination of factors results in a requirement for 11.9m^3/s of Martian atmosphere to flow through the system, which in turn leads to the requirement for a large pump mass and support structure mass.

Table 5.6: Estimated Mass Breakdown for the Atmospheric Processor as predicted by the ISRU Sizing module

AP Component	**Estimated Mass (kg)**
Zeolite Bed	824
Pump 1	12,462
Pump 2	12,462
Cryocooler 1	5
Cryocooler 2	5
Support Structure	5,347
Total	**31,105**

The estimated 31,105kg mass of the required Atmospheric Processor far exceeds the 2,500kg payload mass of the SpaceX Dragon-derived Life Support Unit (described in Section

5.5.4.1), and is therefore considered to be prohibitively large. We thus conclude from this third iteration that **the assumed baseline Mars One architecture augmented with a 201m^2 BPS remains architecturally infeasible** due to inherent atmospheric imbalances that under Mars One's constraints, can only be managed with a prohibitively large ISRU system that exceeds their specified landed mass capabilities.

5.6.2 Iteration 4: Assessment of Architectural and Programmatic Feasibility for Two Habitation Cases

In light of the observations made in the third analysis iteration, we further relax Mars One's constraints and develop and compare two alternative habitat options. The first of these options attempts to develop an architecturally feasible solution based on Mars One's plan to produce all food locally with a BPS. Here, a BPS is retained, and an architecture that supports and takes advantage of the presence of this BPS is developed such that it can sustain the four person Mars One crew for 26 months. Subsequent expansion missions are assumed to repeat this architecture.

Contrastingly, the second habitat option is based on removing the BPS from the architecture altogether, and sustaining the crew's caloric needs entirely with prepackaged and stored food that is delivered from Earth. This architecture aims to eliminate the atmospheric imbalances observed in Analysis Iteration 3 by completely modifying Mars One's food system design. These two options, from here on referred to as the "Biomass Production System (BPS) Case" and the "Stored Food (SF) Case", can be considered as representative of the extremes of the range of food supply options. The following subsections describe these two architectures in greater detail, and present the results of their architectural and programmatic feasibility assessments.

5.6.2.1 The Biomass Production System (BPS) Habitation Case

This habitation option attempts to transform the baseline architecture explored in Iteration 3 into one that is architecturally feasible. This is accomplished by relaxing Mars One's constraint of using only technologies that are both "existing, validated, and available" [193] and "very similar to" those used on the ISS [198], to address the issues with atmospheric imbalances observed in Analysis Iteration 3. Specifically, we introduce a notional "Oxygen Removal

Assembly (ORA)" that selectively removes oxygen from the atmosphere, and transports it to an oxygen tank for later use by the crew, thereby mitigating the possibility of the cabin oxygen concentration exceeding the fire safety threshold. This ORA system will likely consist of a combination of a CDRA, an adsorption-based nitrogen scrubber, and a photocatalytic ethylene scrubber [252] to separate CO_2, water vapor, nitrogen, ethylene, and other BPS gas, such that a highly concentrated oxygen mixture remains.

In addition, we move the BPS to a dedicated plant growth chamber to decouple the effects of plant photosynthesis and transpiration from the atmospheric requirements of the crew. This modification enables the separate control of atmospheres for the crew and crops to levels that best suit their respective respiration rates. Implementing this requires dedicating one of the Inflatable Units entirely to plant growth, which in turn removes the dual redundancy originally envisioned by Mars One (see Section 5.5.1.4).

Finally, we attempt to minimize system mass and complexity by taking advantage of the excess O_2 provided by the BPS. As discussed in Section 5.5.1.4.8.1 and depicted by the dashed lines in Figure 5-12, we rearrange the ECLS system such that the BPS provides both food producing and air revitalization functions[1]. Specifically, we redirect the outlet of the CDRA so that it delivers CO_2 directly to the dedicated BPS chamber. Within this chamber, this CO_2 is supplemented with additional CO_2 introduced by the CO_2 injector to support crop photosynthesis[2]. The resulting oxygen is removed from the BPS chamber by the ORA, and delivered to the habitat's oxygen tanks, where it is used to support crew respiration and EVA. Figure 5-12 depicts the flowsheet for BPS case while Figure 5-13 shows the corresponding floor layout.

[1]Note that as discussed in Section 5.5.1.4.8.1, we do not consider using the BPS for potable water recovery functions due to food safety concerns and the high water demand of the BPS

[2]We note that in the later phases of the mission, as the rate of biomass production reaches a steady state, oxidation techniques such as incineration and aerobic digestion can be used to recover CO_2 from inedible biomass, thereby reducing the dependency on CO_2 introduced from the Martian atmosphere. Assessing the impact of this approach on the system architecture is beyond the scope of this analysis, and is left for future work. It should be noted however, that these techniques are inadequate during the start-up phase of the BPS due to the early lack of available inedible biomass (see Section 5.5.1.4.6). Thus, the approach adopted here for the BPS case is appropriate for supporting the start-up of the BPS.

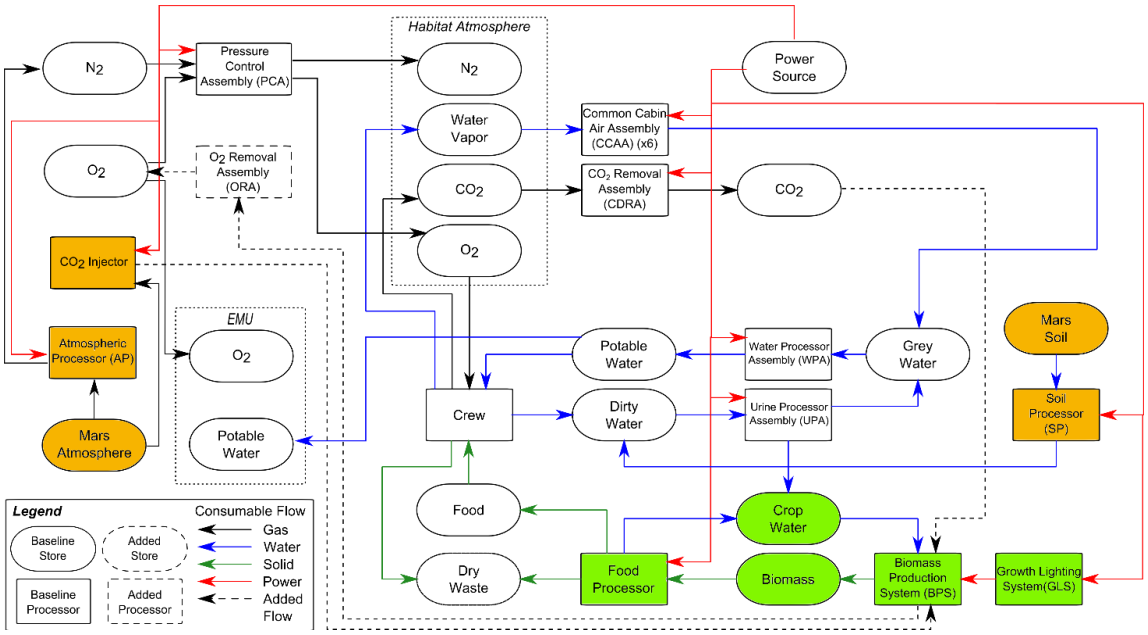

Figure 5-12: The Biomass Production System (BPS) Habitation Case ECLS and ISRU Flowsheet

Preliminary simulations of this modified architecture revealed that oxygen generated by the ORA is sufficient to support all crew respiration and EVA needs without the need for supplementary oxygen. Under nominal operating conditions, this means that the Oxygen Generation Assembly (OGA) and CO_2 Reduction System (CRS) are never operated and can hence be removed from the ECLS system of this habitation case for the purposes of assessing architectural and programmatic feasibility. We note, however, that during the predeployment phase of the BPS case, an OGA is still required to generate oxygen for initial inflation of the Inflatable Units, as per the Mars One plan (see Section 5.5.2.3). Thus, in the BPS case, the OGA is moved from the ECLS system to the ISRU system.

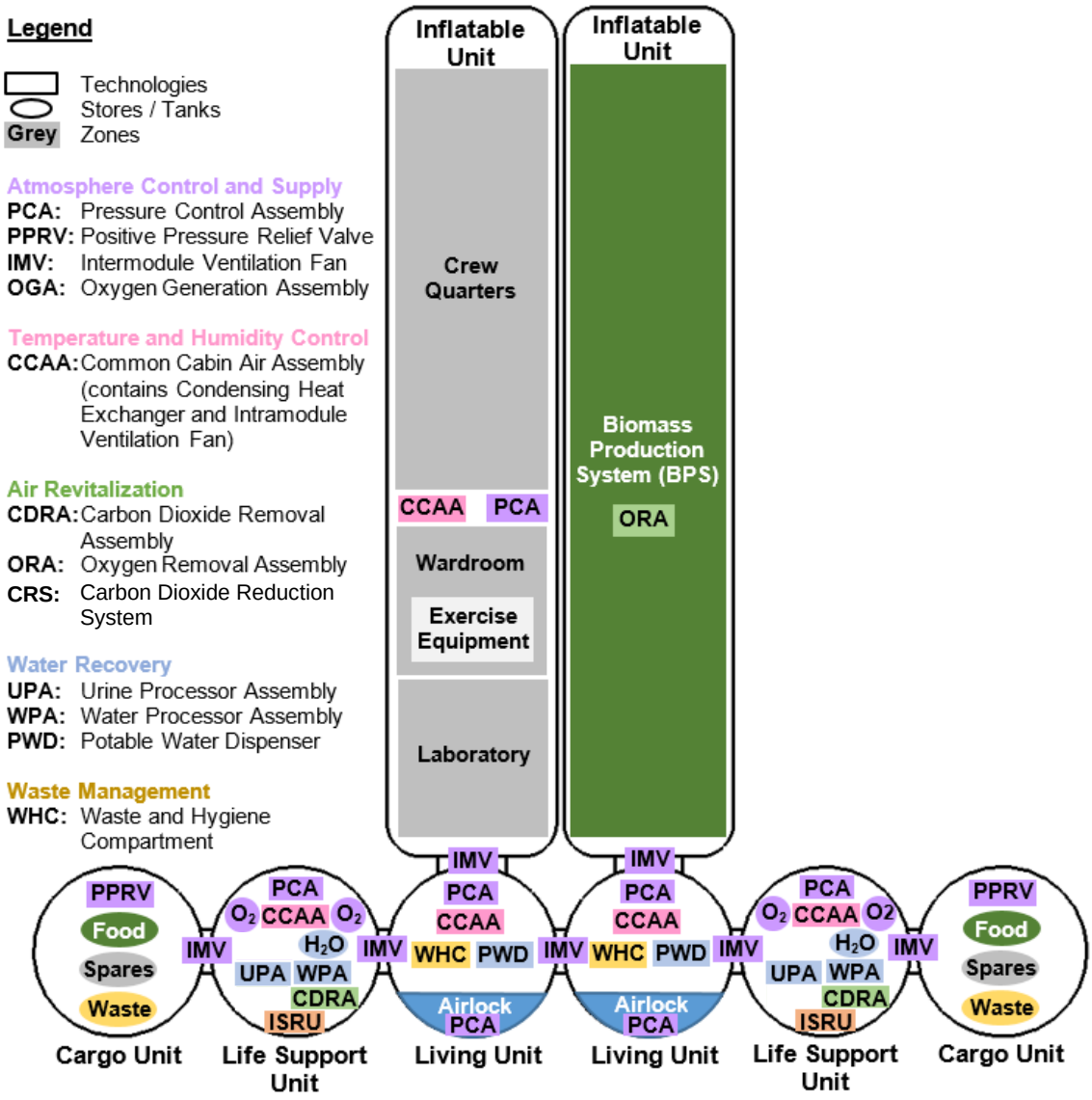

Figure 5-13: The Biomass Production System (BPS) Habitation Case Habitat Layout

5.6.2.2 The Stored Food (SF) Habitation Case

Contrasting to the BPS case, the Stored Food (SF) architecture attempts to address the atmospheric imbalance issues described in Section 5.6.1.3 by removing the BPS altogether and using stored food to meet the crew's nutritional needs. This results in a much less complex system, as can be seen in the system flowsheet and habitat layouts shown in Figures 5-14 and 5-15. Without crops creating excess oxygen, the notional ORA described in the BPS case is no longer needed. This system does, however, require regular resupply of food, which violates the Mars One plan to grow all food on site. For this architecture, it was calculated that each crew

of four would require 5152kg of food (including food packaging) to sustain them over the 26-month period between resupply. This value is based on NASA estimates for a Mars transit food system and assumes primarily thermostabilized food supplemented with a lower proportion of natural form and freeze-dried food [218]. This distribution of food type is driven by the shelf-life properties of the various forms of packaging [218].

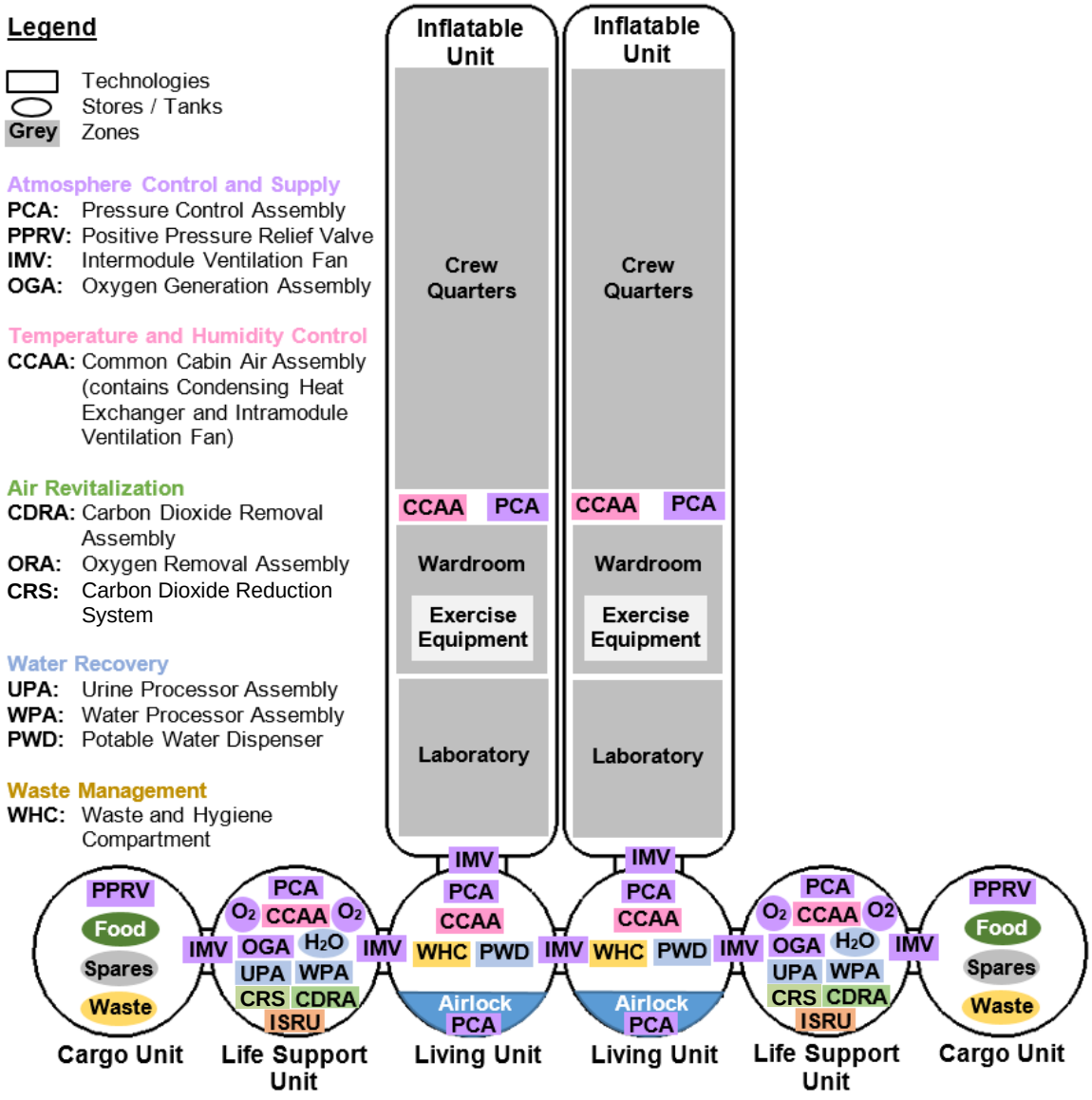

Figure 5-14: The Stored Food (SF) Habitation Case Habitat Layout

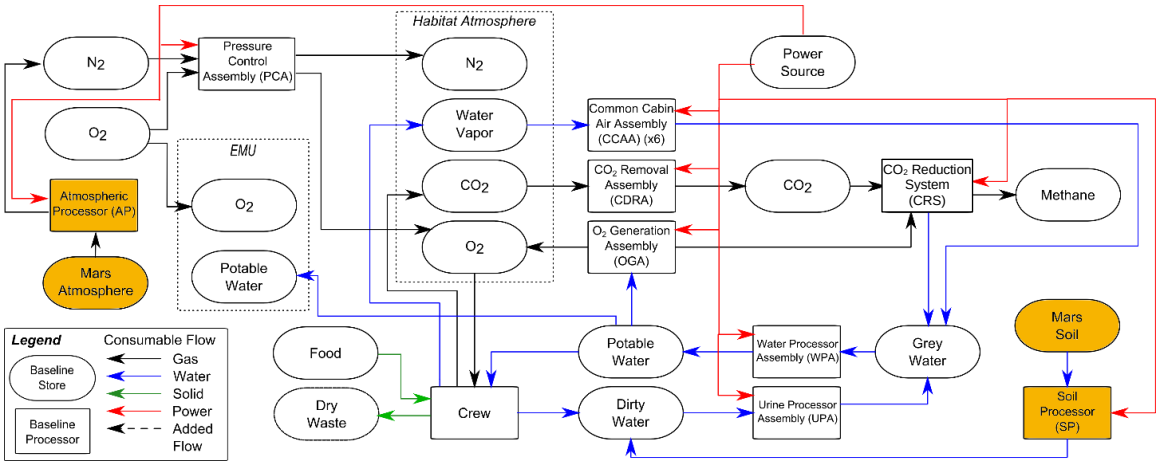

Figure 5-15: The Stored Food (SF) Habitation Case ECLS and ISRU Flowsheet

5.6.2.3 Comparative Power and Thermal System Analysis

In order to ensure a fair comparison between the lifecycle costs of the BPS and SF architectures, an analysis of the required power and thermal management systems is performed. This is particularly important because these two architectures have avenues for mass savings and mass penalties – both of which have significant implications on lifecycle cost. The BPS case for instance, provides additional ECLS functions that remove the total number of technologies needed over the baseline, while requiring additional supporting systems, such as lighting and crop water management. Moreover, a survey of previous studies of bioregenerative life support systems found that power, cooling, and volumetric requirements typically account for 70% of the equivalent system mass [253].

Contrastingly, the SF case leads to a significantly less complex architecture at the cost of needing to deliver an additional 5152kg of food mass for each crew of four on the surface of Mars at each resupply opportunity. As the crew population grows, the requirement to deliver food grows accordingly.

Rather than performing a full power and thermal system estimate for all systems in both habitation cases, we examine the power and thermal demands of only the systems that differentiate these two habitation cases. That is, the power and thermal demands of systems that are common to both the BPS and SF habitation cases, such as CDRA and the PCAs, are not considered. Adopting this approach allows us to instead focus our analysis on comparing the lifecycle impacts of both architectures.

Table 5.7 lists the key systems that differentiate the BPS and SF cases, along with their power demands. Systems listed under each habitation case are present within that particular architecture, but not in the other.

Table 5.7: Power demands for systems that differentiate the BPS and SF habitation cases

BPS Architecture		**SF Architecture**		
Differentiating System	**Power Demand (W)**	**Differentiating System**	**Power Demand (W)**	**Comments**
Predeployment Phase Soil Processor Module	22500	Predeployment Phase Soil Processor Module	5400	Although both architectures contain a predeployment phase soil processor module, their requirements are significantly different due to the high water demand of the BPS (which requires 25L/day as compared to the 6L/day required by the SF case - see Table 5.9). This results in vastly differently power requirements. These power estimates are based on the energy required to heat 3% water content (by mass) Martian regolith from an ambient temperature [254] of 192K to oven operating temperatures of 603K (330°C), as per the ISRU oven operational strategy described by Sanders [255] and Interbartolo et al. [202]
Total for Predeployment Phase	**22500**	**Total for Predeployment Phase**	**5400**	
Crewed Phase Soil Processor Module	4500	Crewed Phase Soil Processor Module	5900	For the crewed phase, supplemental oxygen is required for the SF Case but not the BPS Case (see Table 5.9). In addition, ISRU-derived water is required in both cases. Since oxygen is derived from electrolyzed water, which is in turn obtained from the soil processor, this leads to different power demands for the same system when operated in the two different cases. The crew requirement for oxygen listed in Table 5.9 is equivalent to a requirement of approximately 1.5L of additional water required to be processed by the soil processor per day.
BPS Lighting	86310	OGA	1720	BPS Lighting: Based on peak power demand for all 137 lighting units (the minimum number of lights required) operating simultaneously at 630W (based on the Heliospectra LX601 – see Section 5.5.1.4.3).

				OGA: Based on the ISS OGA operating at half its maximum oxygen production capacity (based on oxygen production rates obtained from simulation). This specific power demand is computed from data published by Bagdigian et al. [164] – also see Appendix D.5)
ORA	860	CRS	686	ORA: Power demand is assumed to be equivalent to the CDRA. This is a lower bound since an ORA will likely be composed of a CDRA, sorbent-based nitrogen scrubber, and photocatalytic ethylene scrubber (see Section 5.6.2.1). Here, we have only budgeted for the power demand of one component of this system CRS: Based on the combined power demands of the ISS CRS reactor heater, CO_2 compressor and separator listed by Jeng & Lin[256] and Murdoch et al.[257] – see Appendix D.7)
CO_2 Injector	1300			Power demand based on estimates made by scaling CO_2 extraction rates to the performance of the commercially available Sunpower Inc. CT-F flight-rated cryocooler [258]
Total for Crewed Phase	**92970**	**Total for Crewed Phase**	**8306**	

To determine the power and thermal system requirements of these differentiating systems, the following assumptions were made:

- All power will be generated using flexible thin-film solar arrays, as specified by Mars One [198]. For this analysis, we assume the performance characteristics of the MiaSole thin-film array [259] – the highest efficiency commercially available flexible thin-film solar array [260]. This particular model [261] has an efficiency of 15.5% and an areal mass density of 2.7kg/m^2
- Power storage will be provided by batteries, as per statements made by Mars One [224]. For this analysis, we assume next generation Lithium-Solid Polymer Electrolyte batteries listed in the NASA BVAD [179] with listed a cell specific energy of 200W·h/kg (assumed to be at 100% depth of discharge). These batteries are sized to store energy throughout the longest expected night (16.5 hours during the winter solstice at mid-Northern latitudes based on Mars One's stated landing location[192]. This 16.5h duration is based on dates listed by the Planetary Society [262] and simulated in the Mars 24 Sunclock program developed by the NASA Goddard Institute of Space Studies [263]

- No losses occur in the transmission of electricity through the various pathways within the power system
- In order to minimize power storage requirements, ISRU systems are assumed to only operate during daylight [198]
- The solar array area is sized to support the operation of all differentiating systems (Table 5.7) during daylight on the shortest expected day (winter solstice) and to charge batteries for continued operation of the non-ISRU systems listed in Table 5.7 during the night. In this analysis, the following equation is used to determine the power requirement for the solar arrays during daylight (P_{SA}):

$$P_{SA} = \frac{P_D T_D + P_E T_E}{T_D} \tag{5.6}$$

  Where P_D and P_E are the power demands during daylight and nighttime (eclipse) respectively, and T_D and T_E are the durations spent in daylight and nighttime respectively. For winter solstice, T_D is taken to be 8.1 hours, and T_E is taken to be 16.5 hours.
- An insolation value of 588.6W/m^2 is assumed. This corresponds to the mean solar irradiance in Martian orbit [264]. The effects of atmospheric attenuation, non-zero incidence angles, attenuation due to dust storms, and solar array degradation are ignored in this analysis. The estimated solar array area can therefore be considered to be an optimistic lower bound.
- Thermal management systems are sized only for non-ISRU systems listed in Table 5.7. These systems correspond to those that are contained within the habitable volume
- Thermal loads for each system assessed are assumed to equal their corresponding power requirements
- The internal thermal control system is assumed to consist of a combination of a flow loop and cold plates. A mass factor of 25kg/kW is assumed, based on the values listed in the NASA BVAD [179]
- The external thermal control system is assumed to be lightweight, flow-through radiators with a mass efficiency of 121kg/kW, based on values listed in the NASA BVAD [179]

Table 5.8 summarizes the mass of the power and thermal system contributions of the BPS and SF architectures over the predeployment and crewed phases of their missions.

Table 5.8: Power and Thermal System Contributions of the systems that differentiate the BPS and SF architectures

	BPS Case	**SF Case**
Predeployment Phase Power System Contribution		
Power requirement for solar array during daylight (W)	22500	5400
Solar Array Area (m^2)	247	60
Solar Array Mass (kg)	666	160
Battery Mass (kg)	1856	446
Total Mass Contribution (kg)	**2522**	**606**
Crewed Phase Power System Contribution		
Power requirement for solar array during daylight (W)	274705	13208
Solar Array Area (m^2)	3011	139
Solar Array Mass (kg)	8130	374
Battery Mass (kg)	7340	199
Total Mass Contribution (kg)	**15470**	**573**
Crewed Phase Thermal System Contribution		
Thermal Load (W)	88970	2406
Internal Thermal Control System Mass (kg)	2225	61
External Thermal Control System Mass (kg)	10765	292
Total Mass Contribution (kg)	**12990**	**352**

From Table 5.8, it can be observed that the BPS architecture has a significantly larger power and thermal system mass requirement than the SF. This is driven by a combination of the high power demand of the predeployment phase soil processor, which is driven by the high water demand required to sustain the BPS; and the high power demand of the lighting system required to sustain crop photosynthesis.

Finally, we note that Mars One plans to power their surface habitat with a $3000m^2$ array of thin-film solar panels [193]. Based on the results presented in Table 5.8, this planned value appears to be insufficient to sustain the combined power demand of the differentiating systems for the BPS case during its crewed phase, even under the optimistic conditions assumed for this analysis.

When accounting for less-than-optimal real-world operating conditions, the required solar array area will increase further beyond the power generation capacity budgeted by Mars One. This suggests that either more power generation capacity is required, and/or changes to the food system architecture are required.

5.6.2.4 Comparative Assessment of Architectural Feasibility

In this section, we present the results of our assessments of the architectural and programmatic feasibility of the two habitation cases described in Sections 5.6.2.1 and 5.6.2.2. These assessments were performed by firstly using the Habitation and ISRU modules to simulate both architectures and to size their required ISRU systems. From this analysis, it was found that both the BPS and SF habitation cases are architecturally feasible, as they are capable of sustaining a four person crew for the 26-month period between resupply with ISRU systems that are within range of the assumed payload mass limits of the lander vehicles.

Table 5.9 summarizes the ISRU resource requirements derived by the Habitation Module, and the corresponding ISRU system masses determined by the ISRU Module. From this table, we observe that the atmospheric processors required by the BPS and SF cases during the crewed phase are significantly lower in mass than that required by the baseline Mars One architecture. This is because the atmospheric imbalances observed within the baseline architecture are no longer present within the proposed BPS and SF cases.

Table 5.9: Summary of ISRU Resource Requirements and Corresponding ISRU System Mass for the Baseline Mars One habitat and two alternative architectural cases investigated in Section IV.II. BPS: Biomass Production System Architecture and SF: Stored Food Architecture. See Table 5.6 for a mass breakdown of the Baseline Mars One Atmospheric Processor, and Appendix I.5 for mass breakdowns of the ISRU systems sized for the BPS and SF Cases

		Baseline Mars One		**BPS Case**		**SF Case**	
		Pre-Deploy	**Crewed**	**Pre-Deploy**	**Crewed**	**Pre-Deploy**	**Crewed**
ISRU Resource Requirement	**H2O [L/d]**	25	5	25	5	6	5
	O2 [mol/d]	25	27	25	0	25	39
	N2 [mol/d]	69	795	69	12	69	12
ISRU System Mass [kg]	**Soil Processor**	822	292	822	263	326	305
	Atmosphere Processor	2,709	31,105	2,709	481	2,709	481

Furthermore, we observe that the BPS case requires a significantly larger soil processor than the SF case during the predeployment phase, due to its need to produce a significantly greater amount of initial water to support crop growth. During the crewed phase however, the BPS architecture has a lower ISRU requirement than the SF case, primarily due to the fact that the O_2 captured by the ORA is sufficient to sustain the crew, thereby eliminating the need for ISRU-generated O_2.

With these results established, the master equipment list (MEL) for the ECLS and ISRU systems for both habitation cases was updated with the required number of spares determined by the HabNet Supportability Module. These results were combined with the power and thermal system mass estimates computed in 5.6.2.3 (see Table 5.8) and input into the Evaluation Module (see Section 5.5.4) to determine the total number of landers and launches required over the lifecycle of each architecture, thus allowing for an assessment of their programmatic feasibility to be performed. The MEL for the BPS and SF cases are presented in Appendix I.5.

5.6.2.5 Comparative Assessment of Programmatic Feasibility

Figure 5-16 shows the distribution of total mass (for the systems described in this case study) that must be delivered to the surface of Mars for the BPS and SF architectures over the first 11 missions, including the predeployment mission. This chart shows the breakdown of mass between the Habitation, Crew and Storage Systems, ECLS, ISRU, and Food systems, as well as the spares required for those systems and the power and thermal systems required to support the differentiating systems between these architectures; thus giving insight into the mass cost of the various elements of the habitat. In this graph, the left bar in each cluster corresponds to the delivered mass requirements of the BPS case, while the right bar of each cluster corresponds to the delivery requirements of the SF case. Further, we note that the mass shown in this figure only includes the mass of components related to ISRU and habitation systems, including the BPS. Therefore, the actual mass requirements will be higher than the amount shown here when all subsystems necessary for a complete mission are included in the analysis.

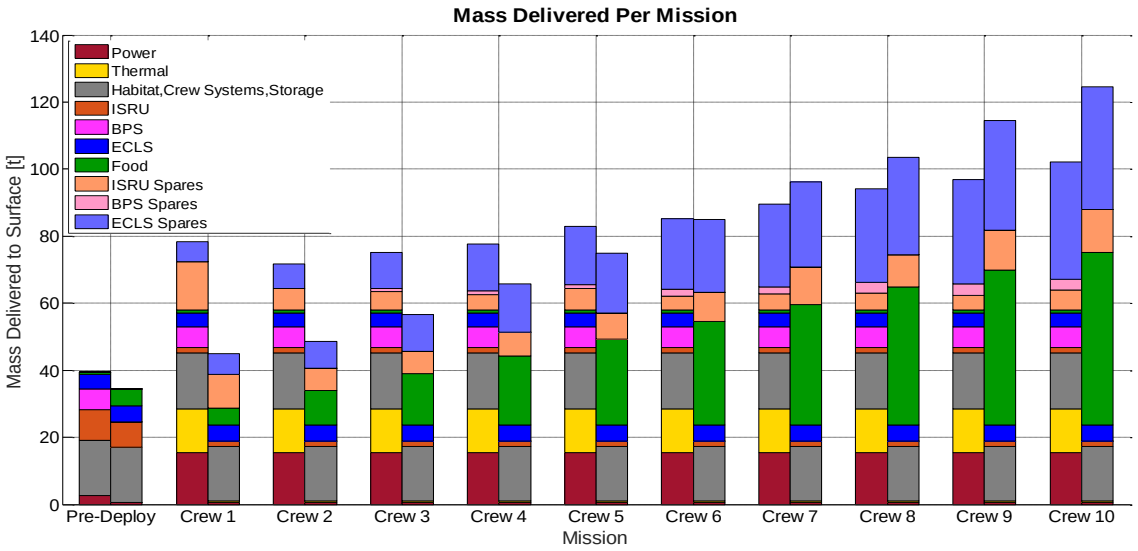

Figure 5-16: Mass breakdown of the cargo mass required for the pre-deploy and first 10 crewed missions. The left column of each cluster corresponds to the BPS case, while the right column corresponds to the SF case.

It is important to note that Figure 5-16 is not a plot of cumulative mass, but rather, a plot of mass required per mission. This figure indicates that in both habitation cases, the required mass increases significantly over time as the colony grows.

For the BPS case, the largest driver of this increase in mass over time is the demand for ECLS and ISRU spare parts, calculated by the Supportability Module. Here, we find that the first crew has a larger spares mass requirement than the other crews, since it must initialize the spares stockpile. When the second crew arrives, it must bring enough spares to replenish the stockpile to that same level of confidence for two crews. The third crew must replenish it to the level required for three crews, and so on. As more crews arrive, more Life Support Units are required to sustain them, and therefore more spare parts are required to maintain those Life Support Units. The mass of spares required for the second crew is lower than the mass of spares required for the first due to the large stockpile that was brought by the first crew and the use of commonality between different crews. However, starting with the third crew, the effect of increasing demand for spares overwhelms the benefits of commonality between crews. From this point on, the mass of spares required at each resupply opportunity increases over time, due to the increasing number of people delivered to the Martian surface. By the tenth crewed mission, 44t of spares are required to support the settlement, compared to the 14t of spares required at the second crewed mission.

Conversely, for the SF case, we find that the resupply mass growth is driven by a combination of an increasing requirement for food and spare parts. Since no BPS is included, the only food available to the colony is food shipped from Earth. As such, each crew must bring not only enough food to sustain themselves until the next resupply, but also a resupply of food for each crew that is already on the Martian surface. The food resupply requirement grows linearly with the number of crews on the surface.

Contributing to this mass growth is the growing demand for ECLS and ISRU spares at each resupply opportunity, for the same reasons observed in the BPS case. Once again, starting with the third crew, each resupply mission must carry more spares than the mission before it. As a result of the combination of these two growth factors, the resupply mass growth is more rapid in the SF case than in the BPS case.

The fact that both architectural cases experience increasing resupply requirements over time means that the number of required launches grows over time, and hence the operational cost grows over time. This cost growth is particularly evident in Figure 5-17, which shows the number and cost of launches required to deliver the manifests predicted for the BPS and SF cases to the Martian surface, as predicted by the Evaluation Module.

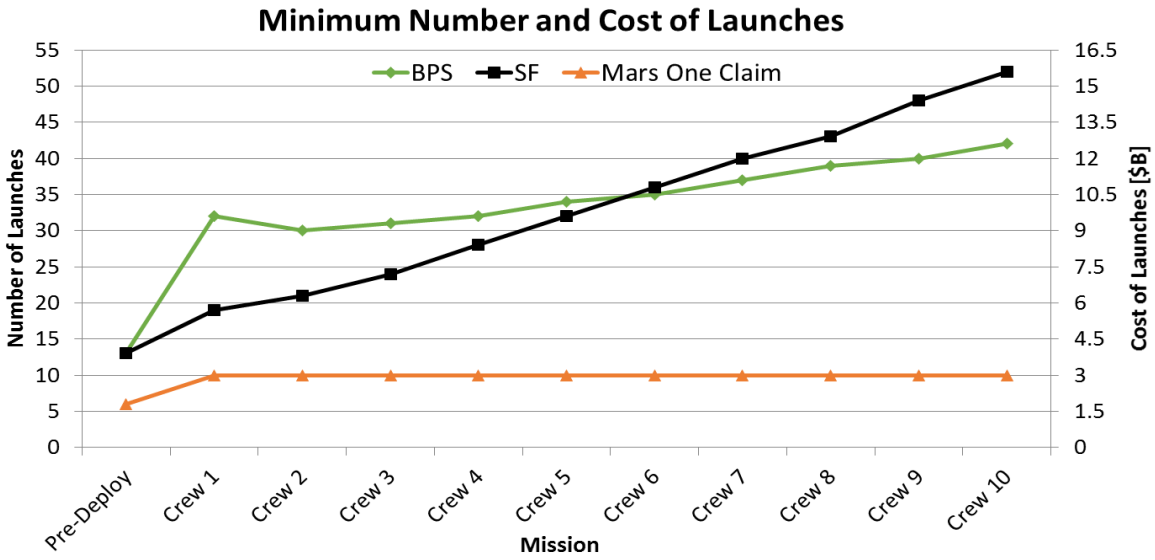

Figure 5-17: Minimum number and cost of launches required for the BPS and SF cases, compared to the number of launches estimated for Mars One

In both habitation cases, regardless of their significant differences in food growth strategy, ECLS architecture, and ISRU demands, this cost growth arises from the two defining characteristics of the Mars One plan:

(1). The one-way nature of the Mars One plan means that based on existing capabilities, system reliability, and spaceflight experience, a continual supply of spare parts is required to indefinitely sustain crews on the Martian surface

(2). Mars One's plan to continually increase their Mars surface crew size leads to corresponding increases in resupply requirements. This growth in resupply requirements and hence launch and operations costs will continue as long as the surface crew size grows.

These two characteristics - one-way trips and a continuous buildup of surface infrastructure - are inherent to the Mars One goal and strategy to develop a settlement on Mars while minimizing the development of new technologies. However, this analysis has illuminated the fact that the resupply costs associated with a growing colony on Mars will continue to increase as long as that colony relies on resupply from Earth to maintain critical functions. This continuous growth in cost is programmatically infeasible. Since this cost growth is dominated by the high cost of interplanetary transportation, an appropriate strategy to mitigate this programmatic infeasibility will likely be a balance between aggressive logistics mass reduction strategies and in-situ manufacturing capability. Both of these options will likely require a very significant technology development effort. As a result, we find that the constraints specified by Mars One – specifically, the concept of one-way missions to grow a settlement and the use of only existing technology – do not result in a feasible mission plan. A very significant technology development effort is required to allow the Mars One plan to be architecturally feasible, and an even more significant technology development effort is required to allow for programmatic feasibility. We therefore conclude that the Mars One mission plan is not feasible under the constraints that **have been stated publicly and specified on the Mars One website.**

5.7 Discussion of Results

In this section, we further explore the architectural and technology development implications of the results derived in Section 5.6. These are summarized in the following sections.

5.7.1 Mass Growth

A key finding of this analysis is that the amount of mass that must be sent to Mars at each resupply opportunity increases with the number of crews on the surface. As described in Section 5.6.2.5, this is largely due to the increasing demand for spare parts (see Figure 5-16), which cannot be produced on Mars without very significant technology development. Thus, as additional Life Support Units are put into operation on the surface of Mars, additional spare parts are required to sustain them. The first crew must bring enough spares to sustain themselves for 26 months. The second crew must bring enough for themselves and the first crew, the third crew must bring enough for themselves, the second crew, and the first crew, and so on. The only system for which spares do not need to be replenished in this way is the pre-deployed ISRU system, which is assumed to be reused every time. In the SF case, the growing mass is exacerbated by the need to also resupply food.

The use of commonality between crews helps to simplify the system and reduce the number of spares required, since crews can share spare parts. However, to achieve this level of spares requirement, the design of the habitation systems for each crew must be fixed for each crew – the spare parts must remain common. Any equipment updates for future crews that results in non-common spare parts would increase the spares requirement above this baseline. To avoid this, either the new system would need to be designed so that an old system could still accept the new spare parts (reverse compatibility), or all old habitats on Mars would need to be replaced with new ones in order to maintain commonality (upgrading). Otherwise the growth in resupply requirements would increase significantly due to a loss of commonality between crews.

The spares mass numbers presented here are an estimate of mass requirements based on the need to provide the same level of assurance to each crew, and could potentially be somewhat reduced by informing spares manifesting based on the performance of the surface systems up until the resupply mission launch date. Due to the long flight times between Earth and Mars, however, it is impossible to manifest resupply missions to only account for failures that have already occurred; resupply requirements will always be a stochastic value and that uncertainty will always drive up the number of spares that need to be manifested to provide confidence in the system.

As more systems are deployed and operated on the surface of Mars, more spares will be required to maintain them. This is true regardless of what level sparing is implemented at –

whether at the ORU level utilized on the ISS or the component/subassembly level implemented in this study. The Mars One website notes this challenge, stating that "for a long time, the supply requests from the outpost will be for complex spare parts, which cannot be readily reproduced with the limited technology on Mars" [193]. Without an advanced resource mining, processing, and manufacturing capability on Mars – which would involve both significant technology development efforts as well as (most likely) a very large initial mass transported to Mars from Earth – this demand for spare parts can only be met with supplies from Earth, and indicates that the mass required to resupply the Mars One colony will increase significantly and unsustainably as the colony grows.

Additive manufacturing (3D printing) technology, while promising, still requires significant technology development before it can be implemented in a Mars settlement [250]. However, even if 3D printers could be used to manufacture every component in the system the resupply mass would still grow over time due to the need for feedstock material. With significant technology development, this material could be obtained through ISRU processing of Martian soil, or perhaps old parts could be recycled into material for new parts. However, both of these options require significant technology development and validation efforts. Until the entire spare parts supply chain is located on Mars and uses Mars-derived resources – a capability that does not currently exist – the cost of maintaining a growing colony on Mars will continue to increase over time, thereby reaffirming the conclusions made in Section 5.6.2.5.

5.7.2 Lifecycle Launch Requirements

A comparison between the launch requirements estimated by Mars One with those calculated for the BPS and SF architectures is shown in Figure 5-17. The Mars One mission plan calls for 6 launches to transport the pre-deployment system to Mars in the first mission, then 10 launches (6 for cargo and 4 for crew transport) at each subsequent launch opportunity [265]. This analysis finds that – even when only considering the mass of the habitation and ISRU systems – Mars One significantly underestimates the number and cost of launches that will be required to place and sustain a colony on Mars.

This is true even for the predeployment missions, where the landed mass requirement for the predeployment mission requires at least 13 launches in both habitation cases - more than double the 6 launches estimated by Mars One. The cost of the 13 pre-deployment launches

(estimated at $300 million per capsule and launch vehicle without adjusting for inflation for future launches) is approximately $3.9 billion. As the settlement grows, the mass growth discussed in Section 5.7.1 causes an increase in the number of launches required at each resupply opportunity. Our analysis finds that for both architecture cases examined, the launch costs associated with the fifth crewed mission are approximately equal to half of the entire NASA FY2015 budget [266] (see Figure 5-17). By the tenth mission, the launch cost in the BPS case is approximately $12.6 billion, and the cumulative cost of launches to grow and sustain the colony is approximately $109.5 billion. For the SF case, the cost of the tenth mission is approximately $15.6 billion, and the cumulative launch cost is approximately $106.8 billion. It is important to emphasize that these estimates account for only the launch costs associated with transporting hardware required for the habitation and ISRU systems from Earth to Mars. They do not include development costs, nor do they include the costs associated with launching other systems such as communications and surface transportation. The actual number of launches required – and therefore the actual launch costs – of the Mars One plan is higher than the estimates presented here.

5.7.3 Biomass Production System versus Stored Food

This analysis examined two options for an architecturally feasible system: one using a Biomass Production System (BPS) for all food production (Section 5.6.2.1) and one using stored food (SF) (Section 5.6.2.2). Figure 5-18 shows the cumulative mass delivered to the surface of Mars between these two options. Based on these results, it appears that employing a BPS for food production does not pay off in terms of system mass over the time horizon chosen for this analysis.

In this figure, we observe that the use of a BPS increases the initial mass of the system with the goal of reducing resupply requirements by producing food locally. The power and thermal requirements resulting from the increased infrastructure (GLS, ORA, CO_2 Injector) required to support the BPS, as well as changes in the size of the ISRU systems, results in an increase in the total landed mass requirement when a BPS is used to grow food. In fact, as shown in Figure 5-18, the mass of equipment required to support the BPS case remains higher than the mass of spares required for the stored food case, and the gap between the two grows over the first six crewed missions. However, the mass of food required by the growing colony grows at a faster

rate, and after the sixth crewed mission, this gap begins to decrease again. Based on the trends observed in Figure 5-18, it is expected that a crossover point will occur during the 11th or 12th missions, where the BPS case becomes the lower-mass option. This result suggests that at least for the first ten crewed missions, it may be more efficient to carry food along rather than grow it in-situ. This finding agrees with those made by other researchers [253].

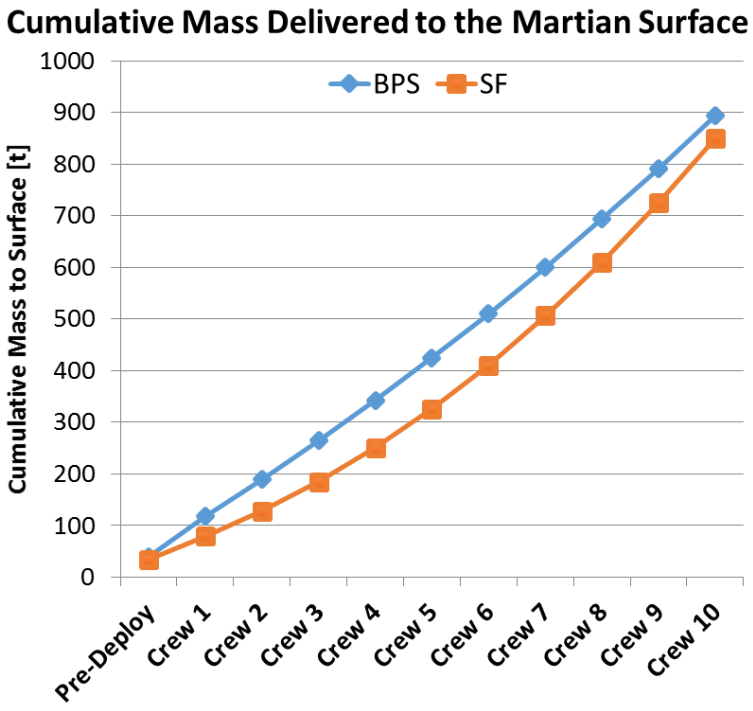

Figure 5-18: Cumulative Mass of ECLS, ISRU, and their supporting systems delivered to the Martian Surface for the first 10 crews for both the BPS and SF cases.

Further, we note that these two cases represent the two extremes of the food supply spectrum, where either all of the food is produced on-site or none of it is. It is possible that a more optimal architecture could be developed, balancing between food shipped from Earth and food grown on Mars. For example, early crews could supplement their diet with stored food while gradually building up plant growth capability. In addition, a balance could be found that enables the use of plants to grow food without requiring a notional ORA and CO_2 injector system to manage the resulting atmospheric imbalance. The elimination of spares mass for these two technologies may also somewhat reduce the overall resupply requirements. These alternative crop growth levels are further explored throughout Chapter 6.

5.7.4 Sensitivity to Component Reliability

The MTBF values used in this analysis are based, to the largest extent possible, on current state of the art ECLS technology with flight heritage on the ISS[209]. It is reasonable to expect, however, that the reliability of these components may increase before the start of the Mars One surface campaign. In order to investigate the potential benefits of more reliable components, the sparing analysis was repeated for an additional case where the MTBF of each individual component was doubled from the baseline value. The results are shown in Figure 5-19.

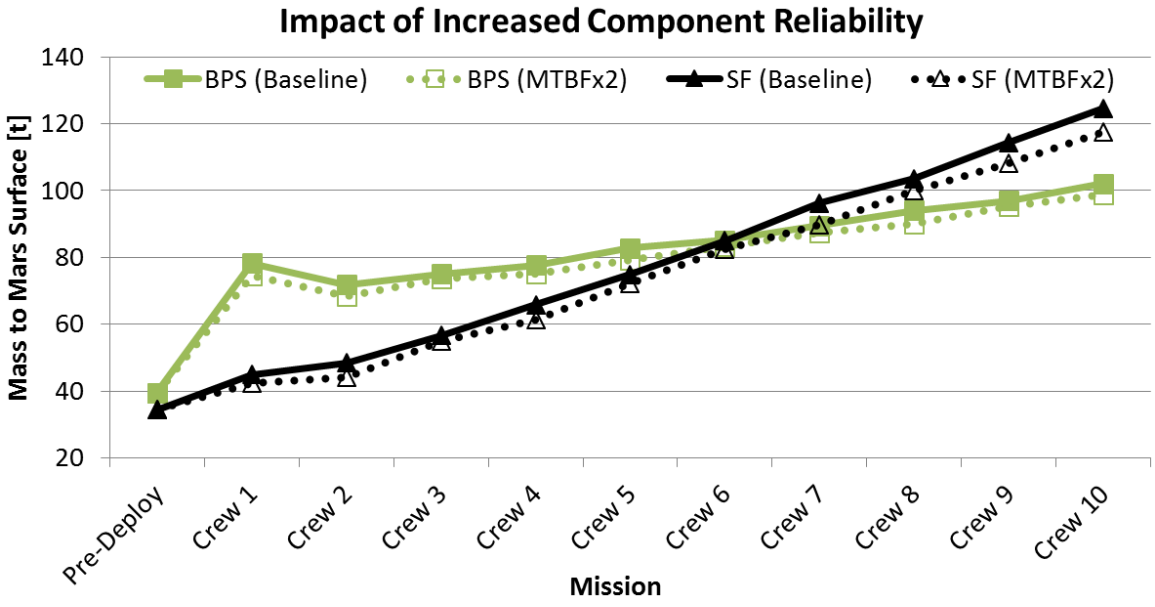

Figure 5-19: Impact of increased component MTBF on the mass required for the first 10 crewed missions. The total ECLS/ ISRU/crew systems mass (including spares and resupplied food) is shown for both the BPS and SF case (green and black lines, respectively), where the reliability of each individual component is either at the baseline MTBF value (solid line) or double that value (dotted line).

As expected, increased component reliability reduces the mass of spares required for both architectures. For the BPS case, doubling the MTBF reduces the total mass of spares required for the first crew by 3.7t. For the SF case, the reduction in spares mass is approximately 2.5t. The cumulative mass saved over the first 10 crewed missions is 27.5t for the BPS case and 41.9t for the stored food case, or about 3.1% and 4.9% from the baseline, respectively. The reduction in mass is slightly higher for the BPS case since the resupply mass is nearly all spare parts – in the SF case, there is a fixed resupply mass of food that cannot be reduced through increased reliability.

In both cases, several of the repairable components in the system, particularly filters, have spares demands dominated by scheduled rather than random repairs. Increased component reliability has little impact on the number of spares required for these components.

Thus, while increasing the reliability of individual components can have an impact on the number of spares required, it is a relatively small one. In addition, even at double the current component reliability levels, the resupply requirements still increase with the number of crews on the surface and the mass that must be delivered in order to sustain the colony after the first few crews becomes unsustainably high.

5.7.5 Sensitivity to Crew Schedule

This analysis assumed an intensive crew schedule that involved each crewmember exercising for two hours a day in addition to the planned EVA schedule of five EVAs per week, each consisting of two crewmembers and lasting 8 hours (see Section 5.5). Given the increase in ECLS resource demands, and the energy expenditure required for exercise activities, it may be possible to reduce total system performance and landed mass demands by removing exercise entirely from the crew schedule. To gain insight into the impacts of crew activities on system demands, we first quantify the reduction in caloric demands obtained when the crew maintains their EVA schedule but does not perform any exercise, and investigate the effect of this caloric saving on the SF and BPS architectures. Here, we maintain the existing aggressive EVA schedule in order to support Mars One's objectives of rapid expansion of their surface base through the frequent integration of new systems and modules to their surface habitat [191].

A simulation of this modified crew schedule found that without exercise, the average caloric requirement reduces from 3,040 to 2,940 kilocalories per crewperson per day, equating to a reduction of 3.3% - a value that is within the variation between individual dietary needs and day to day caloric intake. This indicates that the caloric requirements of the crew are dominated by the large energy expenditure needed to support the heavy EVA schedule. As a result, changes in the crew exercise schedule are not expected to have a major impact on the total landed-mass requirements.

To further explore this, we propagate this caloric difference into the system designs for the SF and BPS cases. For the SF architecture, we expect that this 100 kilocalorie per person per day difference can easily be accommodated by sending more calorically dense food. Moreover, since the ECLS systems are based on ISS technologies that are sized for more than four people,

we expect minimal changes to the mass of the systems delivered. The major mass saving resulting from the removal of exercise from the crew's schedule for the SF case is expected to come from the exercise equipment itself. The total mass of all exercise equipment assumed to be delivered with every crewed mission is estimated to be 1,343kg, based on the mass of current ISS hardware (see Appendix I.5). This value is approximately equivalent to half the payload mass of a Mars One lander, and equates to a mass saving of 3.9% for the first predeployment mission. Over time, as the demand for resupply increases with the increasing crew, this mass saving has a diminishing effect. By the tenth crew, the removal of crew exercise from the SF case results in a mass saving of only 1.1% from the total delivered mass.

For the BPS case, caloric savings can lead to reductions in BPS requirements, which can result in greater mass savings in supporting systems. Using the same weighting values as Option 4 in Table 5.3, the plant growth area optimizer (see Section 5.5.1.4.1) found that a 2,940 kilocalorie diet could be supported by 193m^2 of crops – 8m^2 less than the 201m^2. This equates to a reduction in predeployment water demand of 360L (see Section 5.5.1.4.4 for calculation assumptions) which leads to a predeployment soil processor system and power mass saving of 270kg (as predicted by the ISRU Module). Moreover, the reduction in plant growth area leads to a reduction in lighting demands to 132 grow lights (see Section 5.5.1.4.3 for analysis details), which equates to a combined lighting, power, and thermal mass saving of 1,244kg (see Section 5.6.2.3 for calculation assumptions). This relatively large mass saving is the result of significant mass factors that arise from the large power storage and thermal control mass required to manage each watt of solar power generated on the surface of Mars. Table 5.10 summarizes the total mass savings obtained for the BPS case.

Aside from the exercise equipment itself, no other systems are expected to be significantly affected by removing exercise activities from the BPS case. This is because during the crewed phase, N_2 demand and hence the size of the atmospheric processor is driven by the leakage rate of the habitat, and the ISRU demand for O_2 is zero, due to the presence of the ORA. Moreover, as was discussed with the SF case, the ISS-based ECLS technologies adopted here are oversized for sustaining a four person crew, and are hence not expected to be affected by minor reductions in crew activity.

Thus, the combined mass savings obtained from eliminating exercise from the BPS case are expected to be approximately 2,590kg during the crewed phase – a value that is a little greater than the payload capacity of a single lander. For the first crewed mission, this equates to a mass saving of 6.5%, and by the tenth mission, the effect of this saving reduces to 2.5%

due to the increasing demand for spare parts resupply. Therefore, we find that while removing exercise from the crew schedule can lead to reductions in resupply mass by values up to 2,590kg, these savings are minor compared to the total mass of equipment needed to be delivered to the Martian surface at each launch opportunity.

Table 5.10: System level impacts of removing exercise from the crew schedule for the BPS architecture

System	Mass for Baseline Schedule	Mass for Exercise-Free Schedule	Mass Saving (kg)
Predeployment Phase			
Predeployment Soil Processor	822	719	102
Predeployment Soil Processor Solar Array	666	622	44
Predeployment Soil Processor Batteries	1857	1733	124
Crewed Phase			
Grow Lights*	1096	1056	40
Grow Light Solar Array*	8130	7790	340
Grow Light Batteries*	7340	7029	311
Grow Light Internal Thermal Control*	2225	2130	95
Grow Light External Thermal Control*	10766	10308	458
Exercise Equipment	1343	0	1343

*Includes power and thermal demands of all non-ISRU systems listed in Table 6

5.7.6 Other Systems

It is important to reiterate that the mass breakdown presented in this analysis includes only the habitation and ISRU systems. Several key systems, including the Mars surface transportation and communications systems, were beyond the scope of this analysis and would need to be investigated to provide a holistic estimate for the cost of the Mars One program. As a result, the anticipated mass of a Martian settlement is expected to be larger than the estimates presented here. Therefore, the number of launches as well as the cost of those launches will also be higher than the numbers shown here.

5.8 Chapter Summary

In this chapter, we investigated the technical feasibility of the Mars One mission plan, focusing primarily on aspects related to ECLS and ISRU systems, their spare parts requirements, a portion of their power and thermal management demands, and the logistics supply chain required to deliver and deploy these on the Martian surface. Following a historical review of the major one-way class of mission plans that have been proposed since the 1960s, we applied HabNet to the latest, and most well-known instance of this type of mission to gather insights into the challenges associated with sending crews on one-way missions to Mars.

To accomplish this, we adopted an iterative analysis approach, where we modeled and simulated the Mars One mission plan within HabNet to assess its architectural and programmatic feasibility, implemented any necessary corrective changes to the architecture, and restarted the iterative design process with the updated architecture.

On several occasions throughout this analysis process, we found that the Mars One mission plan, as described on the Mars One website and in other sources, is infeasible. This conclusion primarily arises from the claim that "each stage of the Mars One mission plan employs existing, validated and available technology" [193], and the fact that Mars One plans to establish a growing colony on Mars – one that will incur a corresponding growing resupply requirement.

These conclusions are drawn from Section 5.6, where a series of analysis iterations were performed to assess the feasibility of the Mars One mission plan under various architectural assumptions. In each case, either architectural and/or programmatic infeasibilities were found, and corresponding recommendations were made. Table 5.11 summarizes these results.

Table 5.11: Summary of findings from the analysis iterations performed in Section 5.6, resulting recommendations, and key sections in this paper describing these results in greater detail.

Analysis Iteration	**Finding**	**Recommendation**	**Section**
1	Mars One claims that their plan utilizes only "existing, validated, and available technology," [193] but many of the technologies described in the mission plan are either nonexistent or at very low levels of technology readiness.	Eliminate the assumption that the Mars One plan can be executed with existing technology, carry out technology development and validation efforts required to produce the technology described in the mission plan, and update mission cost and schedule estimates to account for this technology development and validation effort.	5.6.1.1, 5.3.2

2	The 50m^2 crop growth area described in the Mars One mission plan is too small to provide sufficient food for a single crew of four, much less three crews of four as described by Mars One[197]	Increase the crop growth area to the 201m^2 required to provide enough food to support a crew of four, and scale accordingly for increased crew sizes. Alternatively, use prepackaged food to supply crew nutritional needs.	5.6.1.2, 5.5.1.4. 1, 5.7.3
3	If the crop growth area is increased to the level required to provide enough food for the crew, atmospheric processing imbalances result in a buildup of excess oxygen in the atmosphere, leading to a fire risk state that requires a peak N_2 rate of approximately 795 moles per day (22.26kg/day) to manage. To generate this level of N_2 under Mars One's ISRU strategy, a prohibitively large atmospheric processor system weighing an estimated 31,105kg is required	Modify the system architecture. Potential solutions include: (1) moving the BPS into its own atmospheric chamber to enable the separate control of atmospheres for the crew and crops to their preferred respiration rates, and developing and validating technology that selectively removes oxygen from the atmosphere; or (2) using stored food to supply crew nutritional needs.	5.6.1.3, 5.6.2.4
4	Even when only considering the mass of habitation and ISRU equipment, the number (and therefore cost) of launches required to land the required systems on the Martian surface is significantly higher than that estimated in the Mars One plan[267].	Increase the estimated number of launches to a value that is capable of transporting all required equipment to Mars and update mission cost estimates to reflect this increase.	5.6.2.5, 5.7.2
	The amount of spare parts required to sustain a growing colony increases as more and more crews are landed on Mars. By the launch of the fifth crew, the cost of the required launches of a portion of all equipment and spares needed is estimated to be approximately equal to half of the entire NASA FY2015 budget [266]. Without the capability to implement a full supply chain on Mars – a capability that does not currently exist – the cost of resupply missions grows unsustainably over time.	Develop and validate technology to mine, process, and refine raw manufacturing materials from Martian sources, develop and validate 3D printing technology to the level required to produce all spare parts and components from local resources in order to support the growing colony with an entirely Martian supply chain, improve reliability and life limits of mission hardware, and update mission cost and schedule estimates to account for this technology development and validation effort.	5.6.2.5, 5.7.1, 5.7.2

While the challenges described in Table 5.11 are by no means insurmountable, their solution requires a change in the assumptions behind the Mars One plan – specifically, the acceptance of the need for significant technology development, and the corresponding change in timeline and funding requirements for the project. The analysis performed here identified specific areas in which technology development could move the Mars One plan towards feasibility. These include the need to advance the reliability of ECLS systems, the TRL of

ISRU systems, the capability of Mars in-situ manufacturing, as well as the need to reduce in launch costs.

In addition to improving the general performance and reliability of the required technologies, these recommendations are also intended to address the challenge of growing spare parts requirements (and hence growing programmatic costs) that are inherent in the expansion phase of any "Mars to Stay" mission architecture. A key observation made from the results of this analysis is that without a local mining and manufacturing capability, any one-way mission architecture incurs indefinite resupply costs, due to the continual need for the spare parts required to sustain the continued operation of the habitation system. Thus, the acquisition of these capabilities should be a minimum condition prior to the commitment for a one-way mission. The initiation of a one-way mission without the satisfaction of this condition equates to the irreversible commitment of funding the resupply missions for the one-way crew for the remainder of their lives.

The analysis performed in this chapter focused on one type of Mars mission architecture: the one-way, or "Mars to Stay" class of mission plan. These types of mission plans are typically considered as nonconventional, as compared to the traditional opposition and conjunction class return trip mission plans. Even though this is the case, their inherent long-term nature forces mission designers to consider the long-term implications of the architectural decisions that govern these one-way types of mission plans, even if only at a conceptual level. Traditionally, these long-term considerations have not been applied to return trip mission scenarios. It is precisely this type of campaign of missions: one that consists of the string of return trip mission scenarios that lead towards a permanent human presence on Mars; that will be investigated in the case study performed in the next chapter.

Chapter 6

Case Study 2 – Return Trip Mission Scenarios

Having explored the lifecycle costs of "Mars to Stay" type mission scenarios in the previous chapter, this chapter now focuses on more traditional mission concepts that revolve around campaigns of return trip missions. Specifically, this chapter uses HabNet to explore the lifecycle impacts of different life support and food growth architectures on mission scenarios that involve sending multiple crews on 540 day conjunction class sorties to the same surface location, as well as scenarios that involve sustaining a continuous presence of a fixed number of crew at the same Mars habitat. In the latter scenario, surface crews are replaced after a minimum of 44 months spent on the Martian surface in order to satisfy the continuous crewed presence requirement. In this chapter, these two scenarios are respectively referred to as the "String of Sorties", and the "Minimum Continuous Presence" mission scenarios.

As was the case with the previous chapter, this chapter commences with a brief review of the major return-trip Mars mission campaigns that have been previously developed, in order to provide a historical context for the case study performed here. Following this review, an analysis is performed to understand the impact of varying levels of in-situ crop growth on habitat architecture. This analysis serves as a further investigation of the atmospheric imbalance findings observed in the baseline Mars One habitation scenario evaluated in the previous chapter. Based on the insights obtained from this analysis, additional habitat architecture options are derived and compared in the second major analysis performed in this chapter, where the coupled impact of varying levels of ECLS resource recycling and food growth on ISRU requirements and spare parts resupply are evaluated within a large-scale architectural tradespace exploration.

This second major analysis can be considered as the combination of the analyses performed in Chapters 4 and 5. In Chapter 4, the impact of varying levels of water and oxygen recycling

on aggregate ECLS mass for a single mission was assessed, while in Chapter 5 the lifecycle impacts of resupplying three variants of an integrated ECLS and ISRU architecture were analyzed. This chapter explores the effects of the coupled interaction between varying levels of ECLS resource recycling and food growth on ISRU and lifecycle resupply requirements for the two major return-trip mission scenarios discussed above. Based on the insights gathered from the integrated analysis of these two Mars mission scenarios, we conclude this chapter with a discussion of the main drivers of lifecycle cost, and how these drivers are reflected in the general trends that appear in the habitation architecture versus lifecycle cost tradespace.

6.1 A Brief Historical Overview of Mars Mission Campaigns Involving Return Trips

As was discussed in Section 1.1, the vast majority of Mars mission plans proposed since the early- to mid-1950s have been based on sortie-class missions, where crews are sent to the Martian surface for either a short stay (30-90 days) or a long stay (480-540 days) prior to returning to the Earth. As Mars mission planning activities became formalized within NASA throughout the era of President Bush Sr.'s Space Exploration Initiative (SEI) throughout the late 1980s and early 1990s [17], the long-stay, or conjunction class mission became the preferred mission type. This was due to the longer crew surface stay times and shorter transit times that it enabled, as compared to the short-stay, or opposition class mission (see Figure 1-9).

The development of the first Mars Design Reference Mission (DRM) in 1993 established the baseline approach of using ISRU together with the "split mission" concept to both minimize overall system mass while reducing overall mission risk. Based on Baker and Zubrin's Mars Direct concept [18], this concept involved pre-deploying an ISRU system along with an empty ascent vehicle on the mission opportunity prior to the first crewed launch (see Figures 6-1 and 6-2). In the period leading up to the first crewed launch, the ISRU system would generate the fuel and oxidizer required to launch the ascent vehicle from the Martian surface into low Martian orbit for the return leg of the first crew's mission. The successful operation of the ISRU system would become a key criterion by which the decision to launch the crew would occur. If, by the time the first crew was ready to launch to Mars, the ISRU system had not generated sufficient propellant to power their ascent vehicle, the mission would either be

delayed until a functioning ISRU system was deployed to the surface, or a new ISRU system would be launched with the departing crew. This single-fault tolerant approach established during the DRM 1.0 [19] activities has since become the baseline NASA strategy for delivering crew and cargo to the Martian surface, and has been repeatedly adopted in the NASA Design Reference Mission 3.0 [268] and Design Reference Architecture 5.0 mission concepts [20]. Figure 6-1 summarizes the generic mission timeline envisioned for this approach.

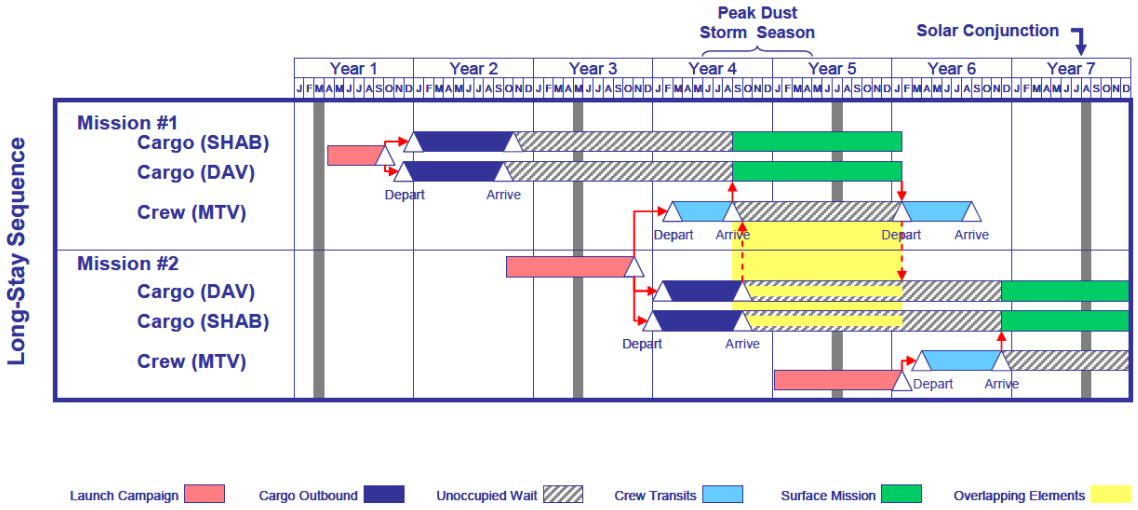

Figure 6-1: Split mission concept adopted in the NASA Design Reference Missions, consisting of a cargo and ISRU pre-deployment mission being launched on the mission opportunity before the launch of the first crew. The decision to launch the first crew is contingent upon the successful generation of sufficient ISRU-derived ascent vehicle propellant [83]

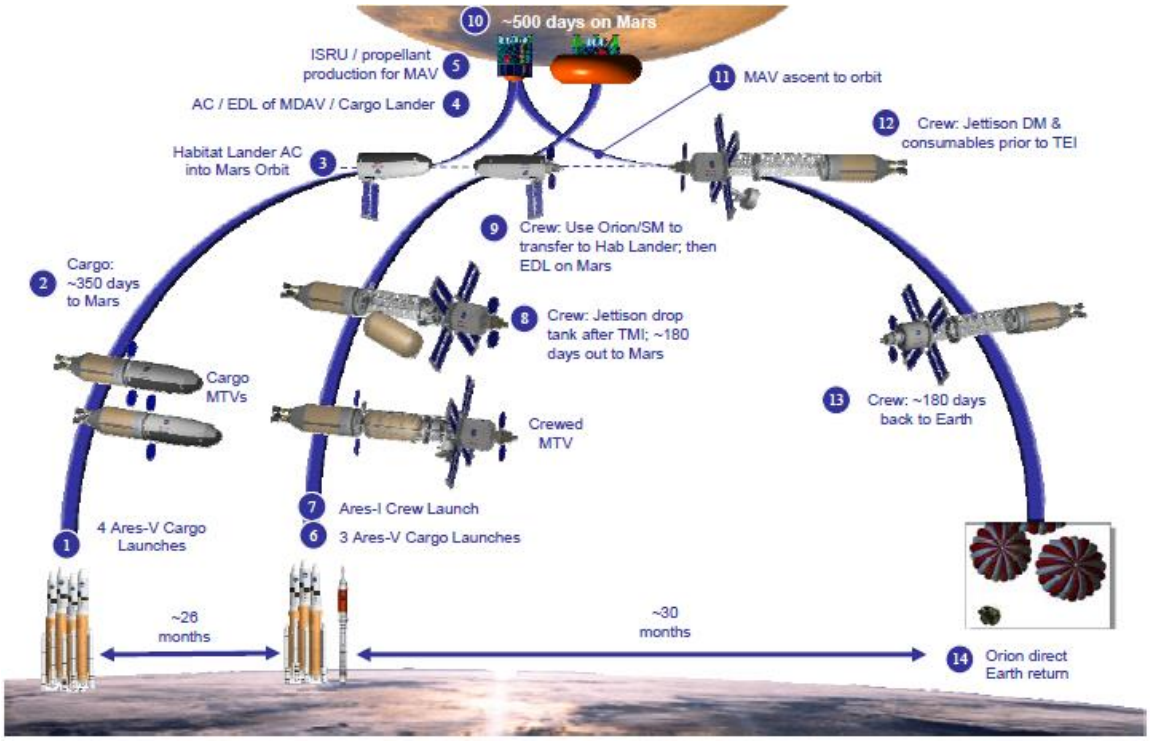

Figure 6-2: A bat chart of the Mars DRA5.0 Split Mission Concept, where cargo and ISRU systems are pre-deployed to the Martian surface on the mission opportunity prior to the launch of the first crew [20]

In addition to adopting the common baseline conjunction-class split-mission architecture, the NASA Design Reference Missions also assumed an initial campaign of three sortie missions, launching at consecutive launch opportunities from Earth to the Martian system. Initially, during the DRM 1.0 (1993) [19] and DRM 3.0 (1998) [268] activities, these missions were planned to visit the same location on Mars in order to enable the gradual buildup of capabilities. For NASA Design Reference Architecture 5.0 (2009) [20] however, this approach was modified such that each of the three sortie crews visited a different location on Mars, in order to facilitate broad coverage of the planet, thereby resulting in the maximum scientific return.

However, with the recent shift in overall programmatic goals towards developing a permanent extraterrestrial human presence arising from the signing of the 2010 and 2015 NASA Authorization Acts (see Section 1.1), the baseline NASA Mars mission strategy has reverted back to that adopted during DRM 1.0 and DRM 3.0 – where crews revisit the same surface location on Mars and continue to invest infrastructure at the same site over time [42,269].

In concert with the adoption of this mission strategy has been the development of the concept of the Mars Surface Field Station – a research laboratory with access to the Mars surface environment. Based on the field stations that have been operated in Antarctica since the early 1900s, the Mars Surface Field Station would be a location where surface crews would learn how to live within the Martian environment over some period of time before gradually transitioning towards an "Earth Independent" mode of operations [42,269].

This surface field station would be located at a site called an Exploration Zone (EZ) – a recently developed concept for a 100km diameter exploration site that contains a diverse set of regions of scientific interest, an abundance of resource regions of interest that can support ISRU operations, and that satisfies environmental constraints for human exploration [269,270]. Figure 6-3 depicts an example of a notional Exploration Zone centered on Jezero Crater, located within the Syrtis Major quadrangle on the surface of Mars.

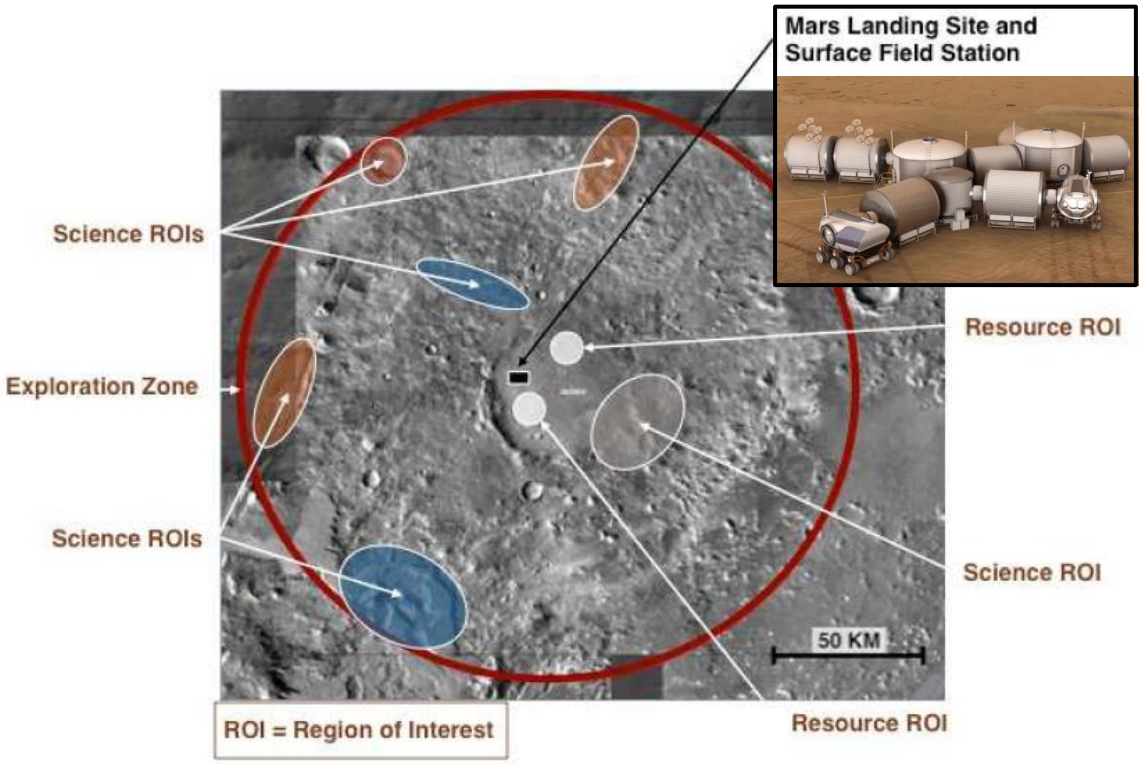

Figure 6-3: Summary of an Exploration Zone, consisting of a Habitation area in the center surrounded by Resource Regions of Interest and Science Regions of Interest [270]

In October 2015, the first Exploration Zones workshop was held by the NASA Human Landing Sites Study Steering Committee to identify potential EZs based on the aforementioned

criteria. During this workshop, 45 different Mars surface locations were proposed by representatives from across the scientific community as candidate locations for the first Exploration Zone. In addition, a list of specific in-situ measurement targets was developed for the Mars Reconnaissance Orbiter (MRO) spacecraft to gather further data to inform the EZ development process. Currently, as of this writing, the results of this workshop are being processed and an MRO imaging campaign has been initiated to gather data in support of further refinement of the list of candidate EZs.

Thus, in light of these recent developments, and the overarching evolution in Mars surface mission planning that has occurred since it became a formal activity at NASA in the late 1980s, this chapter explores the resource requirements and resupply demands needed to sustain the first two phases of the Mars Surface Field Station, where crews initially visit the field station in a "String of Sorties", and ultimately transition into a "Minimum Continuous Presence" mode, where expeditions each consisting of four crew members and lasting for approximately 44 months are conducted at the field station. Here, the expedition size of four was chosen based on recent studies performed as part of the Evolvable Mars Campaign [42]. These two mission profiles are depicted in the crew population profile figure below:

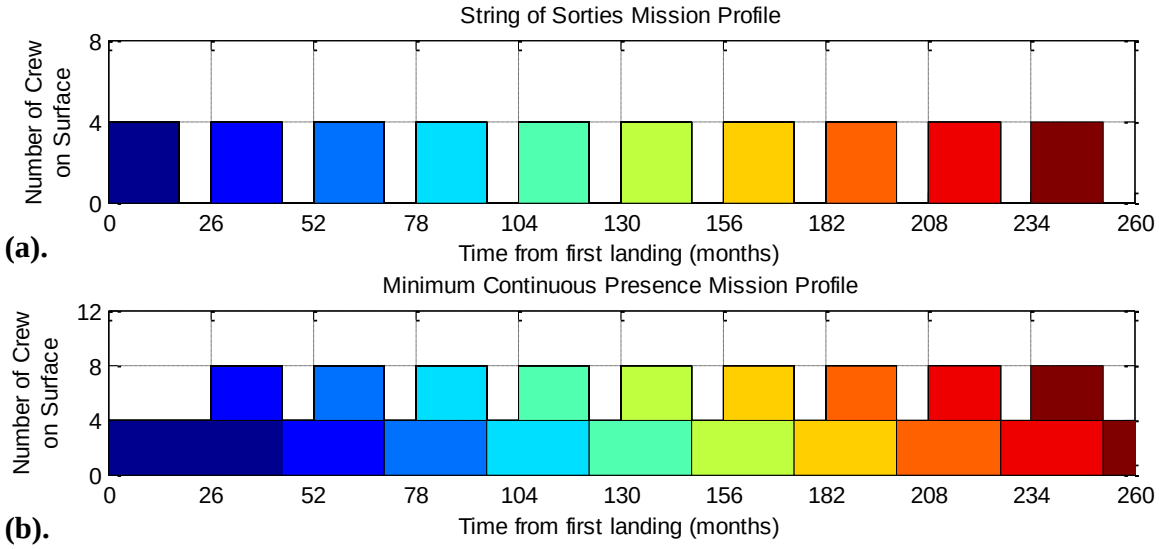

Figure 6-4: Summary of the crew profiles of the for the return-trip mission scenarios considered within this chapter (a). The String of Sorties Mission Scenario (b). The Minimum Continuous Presence Mission Scenario

6.2 Baseline Habitation Architecture

To investigate the lifecycle resupply requirements of the "String of Sorties" and the "Minimum Continuous Presence" mission scenarios discussed earlier, we assume a baseline habitation architecture based on a combination of the Scenario 12.1 lunar outpost concept developed during the Constellation Program [271], and the NASA Habitat Demonstration Unit (HDU) that was field-tested during the Desert Research and Technology Studies (D-RATS) campaigns that occurred between 2010 and 2012 (see Figure 6-5) [272]. As shown in Figure 6-6, this baseline habitat consists of five main modules, with an optional sixth Biomass Production Chamber (BPC) module included when local food production is included within the system architecture. The main characteristics of each of these modules is described in Table 3.

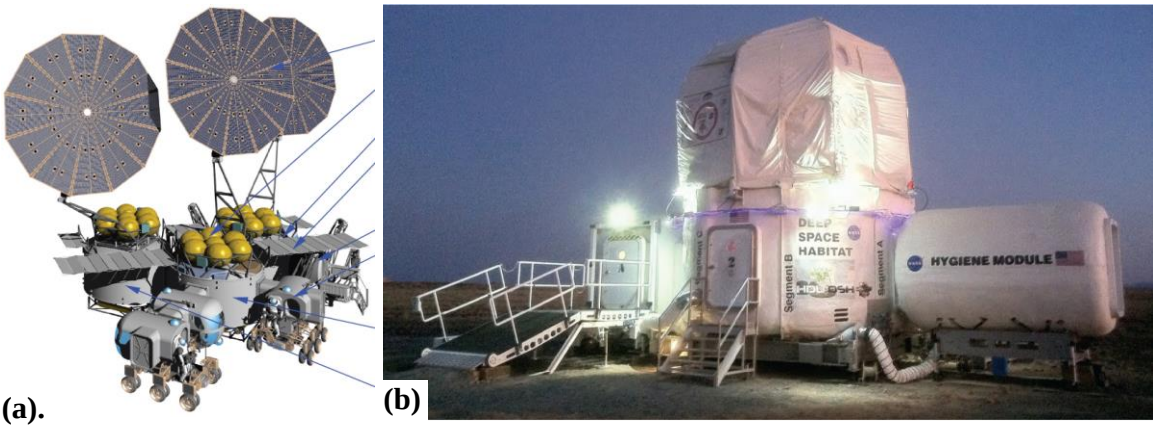

(a). **(b)**

Figure 6-5: Habitation Architectures that influenced the baseline habitation architecture assumed in the case studies performed in this chapter (a). Constellation Program Habitation Scenario 12.1 [271] (b). NASA Habitat Demonstration Unit (HDU) [272]

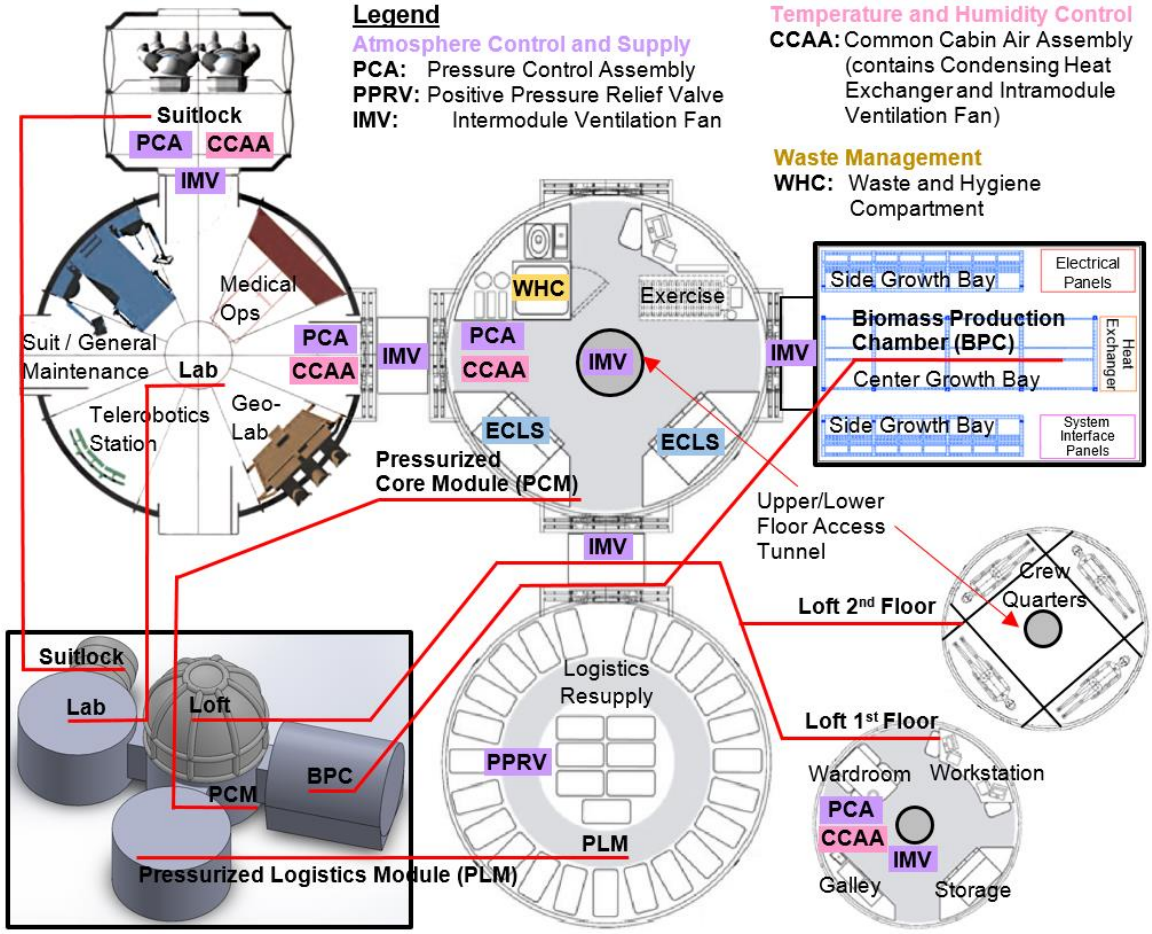

Figure 6-6: Floor plan of the baseline version of the Mars Surface Field Station assessed in this case study. Note that the first and second floor of the Loft are depicted at a smaller scale than the other modules shown here

Table 6.1: Summary of the main characteristics of each habitat module

Module	Habitation Functions Supported	Volume (m^3)	Comments
Baseline Modules			
Lab	Supports scientific activities, medical operations, telerobotics, and general maintenance	56	The layout of this module is based on the Pressurized Core Module of the HDU that was tested during the 2012 D-RATS campaign [272]
Pressurized Core Module (PCM)	Contains crew and life support systems	56	Slightly modified from the PCM architecture described in Constellation Scenario 12.1 [271]
Loft	Contains two floors. The first floor houses living areas and the second floor contains the crew quarters.	60	Based on the redesigned loft for the Human Exploration Research Analog (HERA) program [272].

Pressurized Logistics Module (PLM)	Storage location for supplies and spare parts	56	Based on the same PLM as that described in Constellation Scenario 12.1[271]
Suitlock	An alternative to an airlock - provides a quick EVA access	7.4	Based on the inflatable suitlock baselined for Constellation Scenario 12.1[271,273]
Total Baseline Habitat Volume		**235.4**	**Baseline habitat volume without food production**
Optional Additional Modules (depending on ECLS architecture)			
Biomass Production Chamber (BPC)	Optional module dedicated to local food production based on hydroponically growing crops based on the nutrient film technique	Variable – based on fraction of calories grown in-situ	Based on the Biomass Production Chamber design developed for the NASA BIO-Plex project [274]

With a high level description of the habitation architecture established, we now complete the specification of the input parameters required for a lifecycle analysis with HabNet. These are summarized below, in Table 6.2.

Table 6.2: Summary of main HabNet input parameters for the architectural tradespace exploration analyses performed in this chapter

Input Parameter	**Selected Option**
Habitation Module Inputs	
Crew CONOPS • Number of Crew • Crew Activities • EVA Frequency	Crew Composition: (Same as Validation Case Study performed in Section 4.4) Assumed to be a four person crew consisting of two males and two females, all aged 35 years old. Both males have a mass of 75kg and both females have a mass of 55kg. These figures are typical of the astronaut population [177] Crew Schedule: Based on the standard Mars mission schedule listed in the NASA BVAD [275], where five two-person EVAs occur each week. For each crewmember, 8 hours of sleep and 2 hours of exercise are budgeted each day. On EVA days, exercise is not performed. Rather, 8 hours of EVA are scheduled, with the remainder being allocated to Intravehicular Activities (IVA) such as performing science experiments, preparing meals, or harvesting and replanting crops. All activities that are not EVA, sleep, or exercise are classified as IVA, and are assumed to require the same level of crew energy expenditure. As a result, on non-EVA days, crewmembers are assigned with IVA tasks during their non-exercising waking hours, in a manner similar to that adopted on the ISS and in the case studies performed in Section 4.4 and Chapter 5. The above crew population and EVA frequency is doubled (to eight crew and five four-person EVAs per week) during periods of crew overlap in the "Minimum Continuous Presence" mission scenario explored in Section 6.5.
Mission Duration	Individual crew surface stay fixed at either 540 days (a conjunction-class sortie mission) or 1330 days (44 months) depending on the mission scenario being evaluated (see Figure 6-4) Resupply missions will occur every 26 months, corresponding to the Earth-Mars synodic period. For the "String of Sorties" mission scenario, each resupply mission is required to support a four person crew over a period of 540 days. For the "Minimum Continuous Presence" scenario, each resupply

	mission is required to support an eight person crew for the first 540 day period of the 26 months between resupply, and a four person crew for the remaining 250 days prior to the arrival of the next resupply mission.
Habitat Layout	Layout: Five main modules connected to each other with an optional sixth added in habitation scenarios involving local food production. The size of this sixth module is scaled according to the quantity of food grown based on the analysis performed in Section 5.5.1.4, where 500m^3 of volume was required to support 200m^2 of crops. This ratio is commensurate with those derived for the design of the BIO-Plex BPC [274]. Internal Atmosphere: Assumed to be 55kPa (8.0psia), 32% O_2 atmosphere with N_2 as the diluent gas. This corresponds to the baseline long-duration Mars surface habitat atmosphere recommended by the NASA Exploration Atmospheres Working Group [140]. Here a 50% O_2 concentration fire-risk threshold has been assumed. This threshold also corresponds to the crew hyperoxia threshold, based on the NASA HIDH [139]
ECLS Architecture	Will be varied to explore the impacts of different levels of resource recycling and in-situ food production on ISRU requirements and lifecycle resupply requirements. The ECLS architectural cases will be the same as those explored in the validation case study performed in Section 4.4, supplemented with additional architectures utilizing various levels of food production that are developed in Section 6.3. These architectures are listed below as follows: - Case 1 – Open Loop Water and Oxygen + Stored Food - Case 2 – WPA + Stored Food - Case 3 – WPA + UPA + Stored Food - Case 4 – WPA + UPA + OGA + Stored Food - Case 5 – WPA + UPA + OGA + CRS + Stored Food - Case 6 – WPA + UPA + 4.5% Locally Grown Food - Case 7 – WPA + UPA + 50% Locally Grown Food - Case 8 – WPA + UPA + 100% Locally Grown Food All prepackaged food delivered from Earth is assumed to have a caloric density equivalent to wheat (at 3600 kilocalories/kg). All values listed for prepackaged food do not include the associated mass of food packaging. See Appendix J.1 for flowsheets of each of these ECLS architectures
ISRU Module Inputs	
Surface Location	Assumed to be Jezero Crater (18.855°N, 77.519°E) based on one of the landing sites proposed during the Exploration Zones workshop (see Figure 6-3)
ISRU Strategy	Automatically sized using Schrenk's ISRU architecture optimizer [144] (see Section 3.4.2) based on the ECLS resource demands computed by the Habitation Module and the propellant requirements of the Mars Ascent Vehicle (see discussion below). Here, the ISRU architecture is automatically synthesized from a set of ISRU technologies consisting of a soil processor, Sabatier reactor, reverse water gas shift reactor, cryogenic CO_2 compressor, inert gas atmospheric processor (based on that developed in Section 5.5.2.2), water electrolyzer, and solid oxide CO_2 electrolyzer. These technologies are discussed in greater detail in Section 3.4.2 and Appendix F.
Supportability Module Inputs	

Supportability Strategy	Spare parts are manifested to accommodate random failure and planned maintenance such that the probability of having sufficient spares is 0.999. These spare parts are delivered from Earth. Failure rates of ISS ECLS technologies are assumed for all ECLS hardware. For ISRU systems, failure rates are adopted from analogous ECLS hardware due to the lack of system maturity. (See Appendices J.2 and J.3 for a full list of assumed reliability data) Spare parts commonality is assumed between crews – that is, each arriving crew's system is identical to those that are already emplaced and thus spare parts can be shared among the systems of each crew. All consumables resupply requirements are generated by local ISRU.

Finally, given the requirement to return crews from the Martian surface along with the prevalence of the split-mission concept of generating all Mars ascent vehicle propellant using ISRU (see Section 6.1), we assume a baseline propellant requirement for launching crews from the Martian surface, and factor this propellant demand into the sizing of the required ISRU systems. Here, we assume that the Mars Ascent Vehicle (MAV) concept recently developed as part of the Evolvable Mars Campaign analyses will be used on all Mars surface missions [276]. Shown in Figure 6-7, the assumed MAV is a two-stage vehicle designed to transport four astronauts from the Martian surface to a Mars parking orbit. To accomplish this, the MAV requires a total of 6978kg of liquid methane and 22728kg of liquid oxygen – all of which is produced locally by the ISRU system.

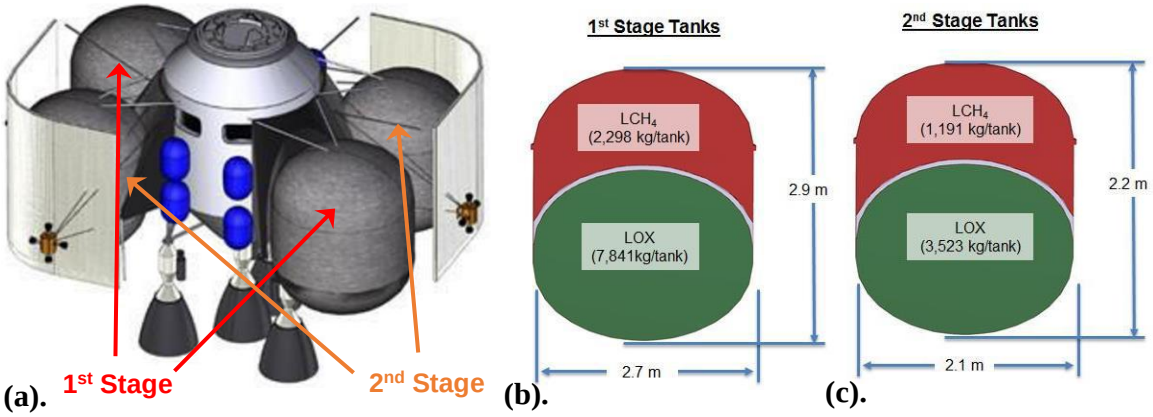

Figure 6-7: Mars Ascent Vehicle design adopted in the case studies performed in this chapter (a). Isometric View showing the 1st and 2nd stage ascent propulsion systems (b). 1st Stage Tank Fuel and Oxidizer Distribution (c). 2nd Stage Tank Fuel and Oxidizer Distribution

In the analyses conducted here, the ISRU system required to produce this propellant demand will be sized both independently from the ECLS system, as well as in an integrated manner with the ECLS system. This will enable any mass savings arising from the integration

of the demands of the MAV and the ECLS system into a single ISRU system to be quantified and evaluated.

6.3 Impacts of Food Growth on Habitation Architecture

In Section 5.6.1.3, upon analyzing the resource requirements of the baseline Mars One habitat, it was observed that growing 100% of the crew's caloric requirements within the same atmospheric volume as that of the crew cabin resulted in atmospheric imbalances that required either a large amount of nitrogen to manage, or a separate dedicated plant growth volume and a notional "oxygen removal assembly" to control. In response to this finding, we implemented two habitation architectures based on the extremes of the spectrum of delivering prepackaged food directly from Earth versus growing all food locally on the surface of Mars.

In this section, we investigate intermediate food growth options in order to generate additional architectures to evaluate in the analyses performed later in this chapter. Here, we are primarily interested in understanding how the quantity of food grown locally affects the habitat architecture, and more specifically, in quantifying the maximum amount of food that can be grown without creating atmospheric imbalances that would necessitate a dedicated plant growth chamber and the introduction of supplementary CO_2 through the use of a CO_2 injector.

This analysis is of particular interest as the collocation of crops and crewmembers within the same habitable volume has become an increasingly prevalent component of Mars surface habitat concepts depicted in both popular media and technical proposals since the early- to mid-1980s, when the general interest in human Mars exploration missions reemerged. Figure 6-8 summarizes some of these concepts:

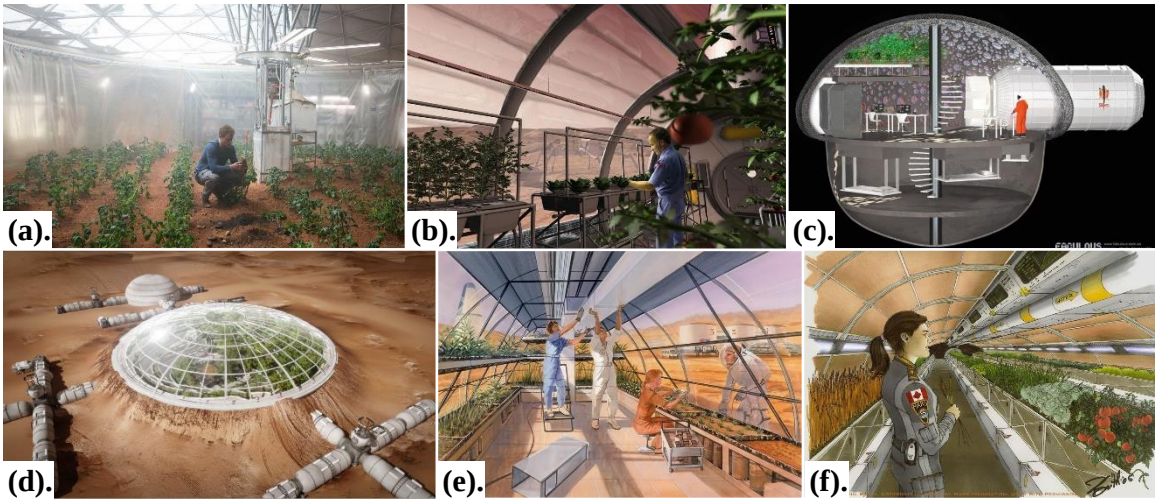

Figure 6-8: Habitation concepts involving the sharing of an atmospheric volume between crew and crops depicted in popular media and technical proposals (a). Matt Damon playing Mark Watney in the 2015 movie "The Martian" [277] (b). A NASA concept for a Mars greenhouse [278] (c). A submission for the 2015 NASA 3D Printed Habitat Challenge consisting of a plant growth area on the top floor [279] (d). A concept for a recreation park located within a crater developed by Versteeg [280] (e). Mars Society concept for a Martian greenhouse [281] (f). Mars Foundation concept for a Martian greenhouse [282]

To commence this analysis, we first revisit the analyses of the atmospheric exchanges within the baseline Mars One habitat presented in Section 5.6.1.3. Here, we further investigate the underlying mechanisms that result in the atmospheric imbalances previously observed. Based on the insights gathered from this analysis, we synthesize, test, and evaluate different plant growth architectures to understand the impact of different levels of crop growth on habitat architecture. This allows us to then propose a subset of food-based ECLS architectures for further evaluation within the campaign analyses performed later in this chapter. The following sections summarize each of the major steps conducted as part of this analysis.

6.3.1 Interaction between Crew Expired CO_2 and Crop Growth within a Dynamic Mission Environment

In Section 5.5.1.4.6, we mentioned that a commonly adopted heuristic used in the analysis of biological life support systems is that if 50% of a crew's food requirements are produced locally with a biomass production system, this same system can regenerate all of the air required for crew respiration [275]. This result arises from steady state stoichiometric analyses that are typically performed in the conceptual phase of biological life support system design to

determine the total crop growth area required, as well as the supporting systems required to facilitate this crop growth [216,253,283]. In such analyses, constant plant respiration and growth rates are assumed to balance with constant crew metabolic rates, as depicted in the representative molar balance analysis shown below, in Figure 6-9.

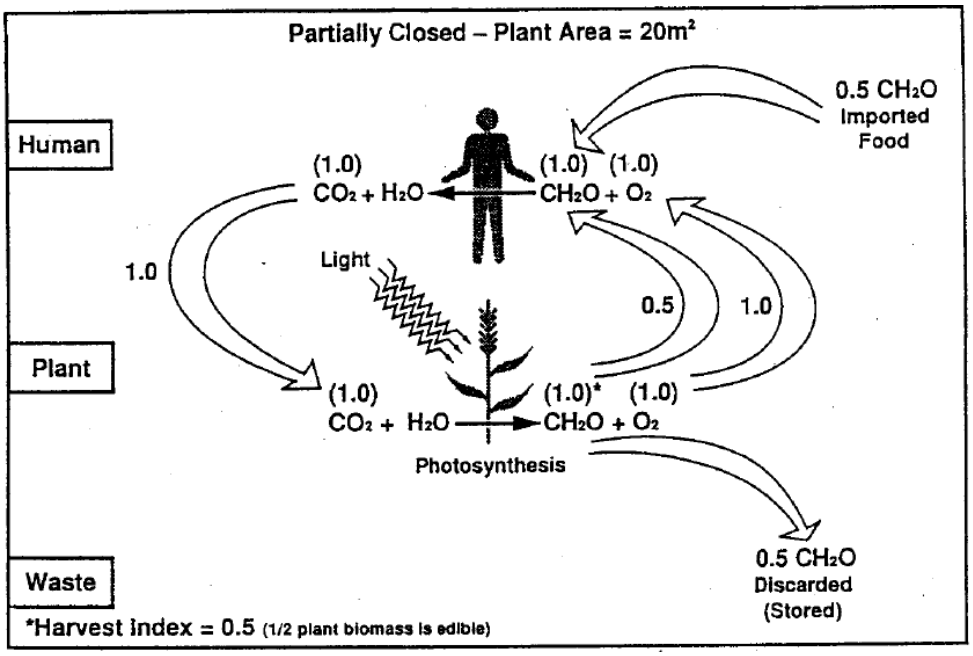

Figure 6-9: Typical Steady State Stoichiometric Analysis performed in the preliminary design of Biological Life Support Systems [216]

To test this heuristic, the HabNet Habitation Module was used to simulate the habitation scenario described in Section 6.2 with a biomass production system sized to grow 50% of the crew's caloric requirement. Here, the same crop mix that was derived in Section 5.5.1.4.1 was assumed, with half of the calculated plant growth areas used, in order to coincide with the requirement for 50% locally grown calories specified above. In addition, a 250m^3 volume was assumed for the BPC based on the assumptions listed in Table 6.2, and the free exchange of atmosphere between the BPC and the remainder of the habitat was enabled. Figure 6-10 compares the oxygen levels within the BPC obtained for this simulation (where 50% of calories was grown) with the oxygen levels observed within the Mars One habitat that were computed in Section 5.6.1.3 (where 100% of calories was grown).

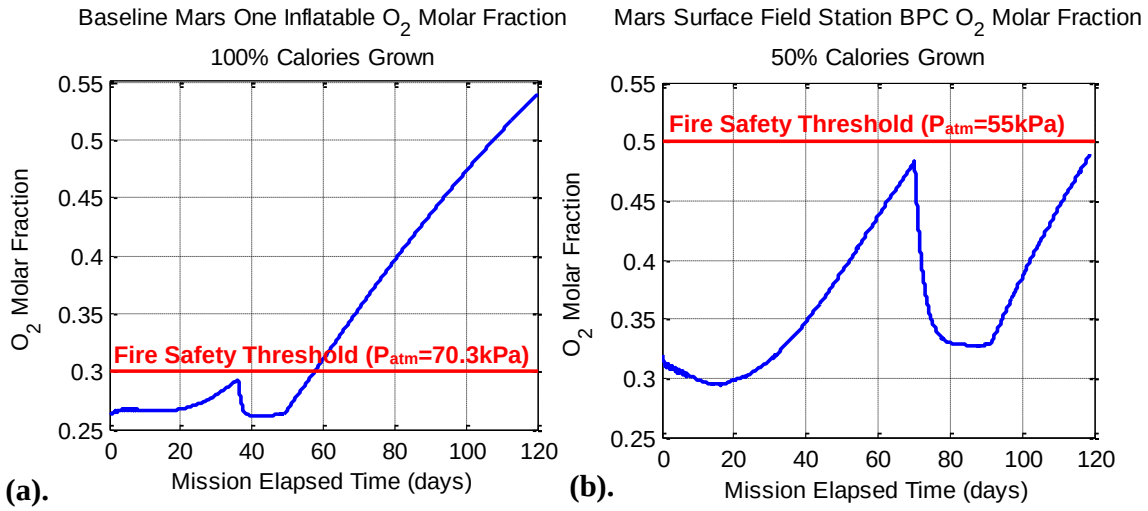

Figure 6-10: Cabin Oxygen Concentrations at different levels of food growth (a). 100% food growth within the baseline Mars One Inflatable Unit (with a volume of 500m^3) (b). 50% good growth within the Mars Surface Field Station Biomass Production Chamber (with a volume of 250m^3)

From Figure 6-10, we observe the same trend in the 50% plant growth case in the Mars Surface Field Station BPC as that of the 100% plant growth case within the baseline Mars One habitat. This trend can be explained by examining the various stages of growth of a single crop as it transitions through its lifecycle. This can be seen in Figure 6-11, which depicts the rate of CO_2 fixation (equivalent to the rate of photosynthesis) for a white potato plant over its three main phases of growth. These phases are representative of all C3-type plants, and are:

1. The period from seed emergence to canopy closure, where the crop's canopy emerges and grows to its full size
2. The period from canopy closure to initial grain setting, where the organ of the plant is initially formed; and
3. The period from initial grain setting to crop maturity, where the organ grows to its full size prior to being harvested

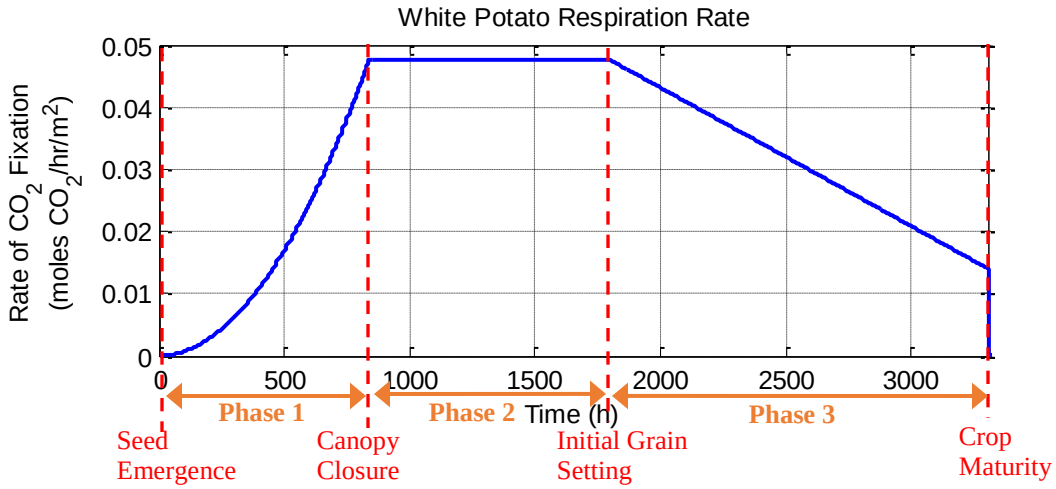

Figure 6-11: The three main phases with the lifecycle of a C3-type plant

As can be seen from Figure 6-11, the rate of CO_2 fixation (or photosynthesis) increases at an increasing rate during its first phase of growth. This occurs due to the increasing size of the plant canopy, which in turn results in an increasing rate of photosynthesis, In addition, the continuous growing scheme adopted here (see Section 5.5.1.4.5) means that new seeds are planted every day, to ensure a continuous supply of food once the first batch of crops reaches maturity. Thus, as the seeds of successive plant batches emerge initially, the collective rate of photosynthesis further increases, to a level where additional CO_2 is required to be injected into the cabin. This is because at these levels of crop growth, the CO_2 expired by the crew is insufficient to sustain the photosynthetic rate of the crops. This was observed in Section 5.5.1.4.6 for the Mars One case (see Figure 5-7) and again in the 50% food growth case here, as indicated by the CO_2 injection rate plotted below.

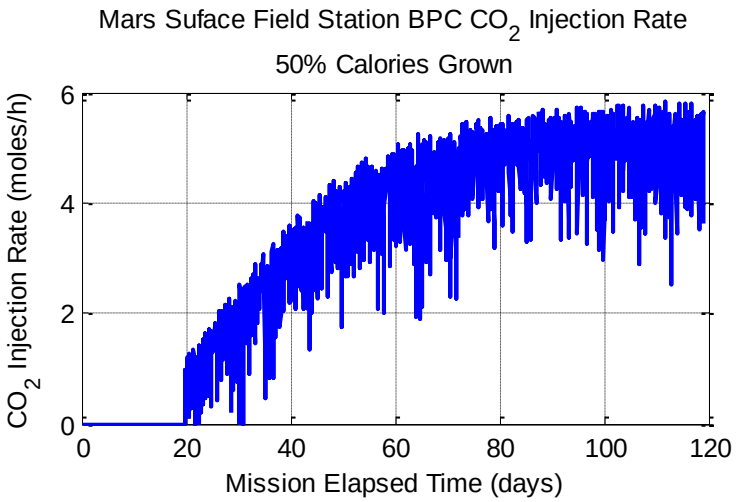

Figure 6-12: Mars Surface Field Station BPC CO_2 Injection Rate when 50% of Calories are grown in the same habitable volume as the crew

As the rate of photosynthesis increases, the rate of conversion of CO_2 to oxygen also increases, thereby increasing the cabin oxygen concentration. This trend can be observed in the initial phases of Figure 6-10 (a) and (b), where the oxygen concentration approaches the fire safety threshold after mission days 36 and 70 respectively. In both cases, nitrogen is introduced into the cabin shortly thereafter to bring the oxygen concentration back down to its predefined set point. Once this nitrogen is depleted however, the same increasing oxygen trend reemerges, causing the cabin oxygen concentration to again increase.

A further investigation into the cause of this trend found that the key mechanism for this system response is the fact that crop growth, and hence crop survival, is dependent on the ambient CO_2 concentration. When the rate of crop CO_2 consumption is higher than the CO_2 expiration rate of the crew, the net result is a reduction in CO_2 over time, which can ultimately lead to crop death. As was mentioned in Section 4.3, this can be demonstrated with a CO_2 drawdown test, where a plant is left in an atmospheric environment devoid of additional CO_2 injection sources. Over time, as it photosynthesizes CO_2 into O_2, the ambient CO_2 concentration decreases, thereby lowering the rate of photosynthesis. If left in this state, the CO_2 concentration eventually decreases to a level beneath 150ppm, resulting in crop death. This behavior was illustrated by the validation analysis performed in Section 4.3, and is shown again below, in Figure 6-13.

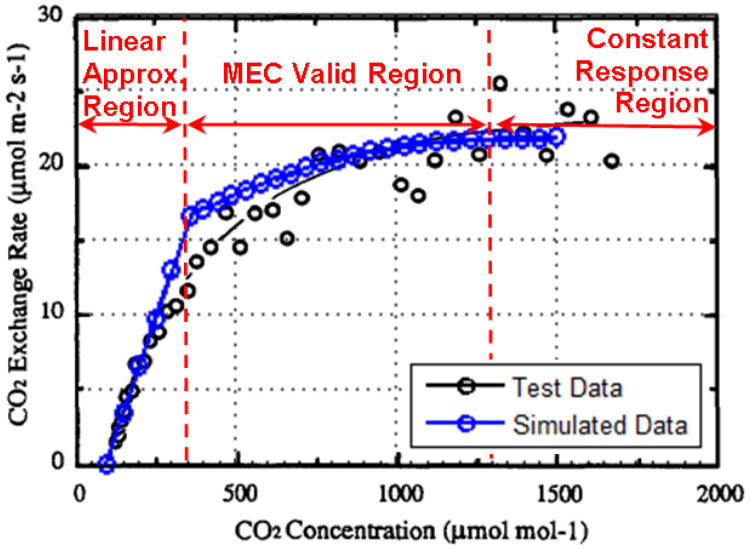

Figure 6-13: Comparison between test data from a CO_2 Drawdown Test of 20 m^2 of Wheat under PPF =550 µmol/m2/s lighting conditions at 36 days of growth (black [39]) and data obtained from the MEC models simulated within HabNet under the same conditions (blue).

To avoid this scenario, a CO_2 injector is installed within the plant growth chamber to maintain the ambient CO_2 concentration at a predetermined set point. For the simulations performed here, a set point CO_2 concentration of 1200ppm was chosen to ensure a maximum crop growth and hence food production rate. When a CO_2 injector is activated however, each mole of CO_2 ultimately becomes a mole of oxygen through photosynthesis. This in turn dilutes the amount of CO_2 within the cabin, thereby resulting in a lower CO_2 concentration, thus necessitating further CO_2 to be injected within the cabin to sustain crop photosynthesis. This phenomenon is particularly apparent during the first phase of crop growth, where the rate of photosynthesis increases with the size of the plant canopy, thereby increasing the requirement for injected CO_2, which is all eventually photosynthesized into oxygen that accumulates within the cabin. This sequence of events is explained mathematically below, by observing the set of equations that characterize the system dynamics over the first few time steps:

Let:

- $[CO_2]_t$ represent the ambient cabin CO_2 concentration at time *t*, and $[CO_2]_{Target}$ represent the target CO_2 concentration required for optimal plant growth (set at 1200ppm, as discussed above)
- $n_{CO2}(t)$ represent the number of CO_2 moles in the cabin atmosphere at time *t*
- $n_{Total}(t)$ represent the total number of moles in the cabin atmosphere at time *t*

- $\Delta CO2_{CREW}(t)$ represent the net number of moles of CO_2 introduced by crew respiration to the cabin atmosphere at time *t*
- $\Delta CO2_{CROPS}(t)$ represent the net number of moles of CO_2 consumed from the cabin atmosphere by the crops at time *t*; and
- $\Delta CO2_{INJECTED}(t)$ represent the number of moles of CO_2 injected into the cabin atmosphere by the CO_2 injector at time *t*

Initially, the CO_2 concentration within the cabin atmosphere is set to the target CO_2 concentration to ensure optimal crop growth:

$$[CO_2]_0 = \frac{n_{CO2}(0)}{n_{Total}(0)} = [CO_2]_{Target} = 1200\text{ppm} = 0.0012 \tag{6.1}$$

After the first time step, the crew has expired CO_2 and the crops have consumed CO_2, causing the ambient cabin CO_2 concentration to equal:

$$[CO_2]_1 = \frac{n_{CO2}(0) + \Delta CO2_{CREW}(1) - \Delta CO2_{CROPS}(1)}{n_{Total}(0)} = \frac{n_{CO2}(1)}{n_{Total}(0)} \tag{6.2}$$

If the amount of CO_2 generated by the crew is less than that consumed by the crops (as has been the case in the simulations observed above), then:

$$\Delta CO2_{CREW}(1) < \Delta CO2_{CROPS}(1) \tag{6.3}$$

This means that the amount of CO_2 at $t = 1$ is less than that at $t = 0$, and hence the CO_2 concentration at $t = 1$ is less than the target CO_2 concentration set at $t = 0$:

$$[CO_2]_1 = \frac{n_{CO2}(1)}{n_{Total}(0)} < \frac{n_{CO2}(0)}{n_{Total}(0)} = [CO_2]_{Target} = 1200\text{ppm} = 0.0012 \tag{6.4}$$

In this scenario, a CO_2 injector is programmed to inject an amount of CO_2 ($\Delta CO2_{INJECTED}(1)$) such that the ambient CO_2 concentration is increased back to the target value of 1200ppm to support optimal crop growth.

$$[CO_2]_1 = \frac{n_{CO2}(1) + \Delta CO2_{INJECTED}(1)}{n_{Total}(0) + \Delta CO2_{INJECTED}(1)} = [CO_2]_{target} = 1200\text{ppm} = 0.0012 \tag{6.5}$$

In the next time step, after the crew expires CO_2 and crops perform photosynthesis, the ambient cabin CO_2 concentration becomes:

$$\begin{aligned}[CO_2]_2 &= \frac{n_{CO2}(1) + \Delta CO2_{INJECTED}(1) + \Delta CO2_{CREW}(2) - \Delta CO2_{CROPS}(2)}{n_{Total}(0) + \Delta CO2_{INJECTED}(1)} \\ &= \frac{n_{CO2}(2)}{n_{Total}(0) + \Delta CO2_{INJECTED}(1)}\end{aligned} \tag{6.6}$$

Here, if the sum of the injected CO_2 and the CO_2 expired by the crew is insufficient to support crop photosynthesis during this second time step (as is likely to occur as the rate of photosynthesis increases during the first phase of crop growth), then:

$$\Delta CO2_{INJECTED}(1) + \Delta CO2_{CREW}(2) < \Delta CO2_{CROPS}(2) \tag{6.7}$$

This results in the cabin CO_2 concentration at t = 2 being less than the corrected CO_2 concentration at t = 1:

$$[CO_2]_2 = \frac{n_{CO2}(1)}{n_{Total}(0) + \Delta CO2_{INJECTED}(1)} < \frac{n_{CO2}(2)}{n_{Total}(0) + \Delta CO2_{INJECTED}(1)} = [CO_2]_{Target} \tag{6.8}$$

Which again necessitates the further injection of CO_2 into the cabin to maintain the set point value for CO_2 concentration. This CO_2 injection process continues to occur until the sum of the CO_2 injected in the current time step and the CO_2 expired by the crew is greater than the CO_2 demand of the crops. Here, it is important to note that when Equation (6.3) is satisfied, all injected CO_2 is converted into oxygen via crop photosynthesis, thus lowering the subsequent

cabin CO_2 concentration and negating the original purpose of introducing CO_2 into the cabin. Consequent simulation runs with HabNet have indicated that an initial CO_2 deficit typically results in a reinforcing demand for additional CO_2 injection to support crop photosynthesis. Without further intervention, this results in substantial increases in cabin oxygen concentration and cabin total pressure over time as the system attempts to find an equilibrium state where the condition represented in Equation (6.6) is satisfied. This trend was indeed observed with the plant growth scenarios simulated in this section and in Section 5.6.1.3. In the second of these two analyses, this CO_2 deficit was managed by moving the biomass production system into its own dedicated chamber to decouple the respiration rates of the crew and the crops, and by installing a notional Oxygen Removal Assembly within the same dedicated crop growth chamber. While this architectural modification did not reduce the need for CO_2 injection, it acted to control ambient cabin oxygen concentration and total pressure while also generating useful oxygen for use by the crew.

In the next section, we explore an alternative approach to overcoming this oxygen buildup problem. Here we attempt to quantify the maximum amount of crops that can be grown in a volume that is shared with the crew, such that additional CO_2 is not required to be introduced into the environment. As was observed with the simulation results presented in Figure 6-10, this quantity will likely be significantly less than 50% of the crew's caloric requirements, due to the need to lower the crop CO_2 demand to a level that is commensurate with the CO_2 production rate of the crew. Once this value is computed, the resulting habitation concept will be added to the list of architectures that are evaluated in the architectural exploration analyses presented in Sections 6.4 and 6.5.

6.3.2 Quantifying the Maximum Proportion of Crops that can be Grown in a Shared Volume with the Crew

In the previous section, we found that the key mechanism that influenced whether or not crop-derived excess oxygen occurred within a shared crew and plant growth volume was the relative difference between the CO_2 expired by the crew, and the CO_2 demands of the crops as they transition through their various phases of growth. In this section, we quantify these CO_2 production and consumption rates in order to calculate the maximum proportion of crops that can be produced without causing a CO_2 imbalance.

Rather than performing a full simulation of the MEC models to predict aggregate CO_2 demands for different levels of crop growth, we instead develop a surrogate model to derive a relationship between the proportion of calories grown (based on a fraction of the crew diet derived in Section 5.5.1.4.1) and the total crop CO_2 demand. As shown in Figure 6-14, this is based on integrating the CO_2 fixation curves (see Figure 6-11 for an example) of each of the selected crop batches to estimate the total crop CO_2 requirement over time.

From Figure 6-14(d), we observe that at a crop growth level of 100%, the aggregate steady state crop CO_2 demand is approximately 12.2moles/hr. This steady state behavior occurs after mission day 138 – the period corresponding to the duration of the growth cycle of white potato, the crop with the longest growth period of all the crops that are included within the biomass production system. A further analysis of this surrogate model found that the relationship between the level of food grown and the amount of aggregate CO_2 demanded by the crops is linear. This can be observed from the basic photosynthetic reaction listed below, where each mole of biomass requires six moles of CO_2.

$$6CO_2 + 6H_2O \xrightarrow{\text{Light}} 6O_2 + C_6H_{12}O_6 \tag{6.9}$$

Thus, for the crop profile assumed here, the following relationship can be derived for the total crop CO_2 demand as a function of the fraction of total calories grown locally:

$$\begin{gathered}\Delta CO2_{CROPS}(\text{Steady State}) = 12.2[\text{mol/h}]\cdot x \\ \text{Where: } x \in [0,1] \quad \text{the fraction of calories grown}\end{gathered} \tag{6.10}$$

In contrast to the crop CO_2 demand, the total rate of crew CO_2 expiration was derived by tracking the activities and locations of each crewmember (based on the schedule described in Table 6.2), determining the corresponding individual crew CO_2 productions, and combining the results. Figure 6-15 summarizes the crew CO_2 production rate profile over the first 180 days of the mission.

From this figure, we observe a fluctuating trend in the aggregate crew CO_2 exhalation rate. This arises from the fact that each crewmember's schedule fluctuates throughout a mission, ranging from low intensity activities such as sleep, to high intensity activities, such as exercise.

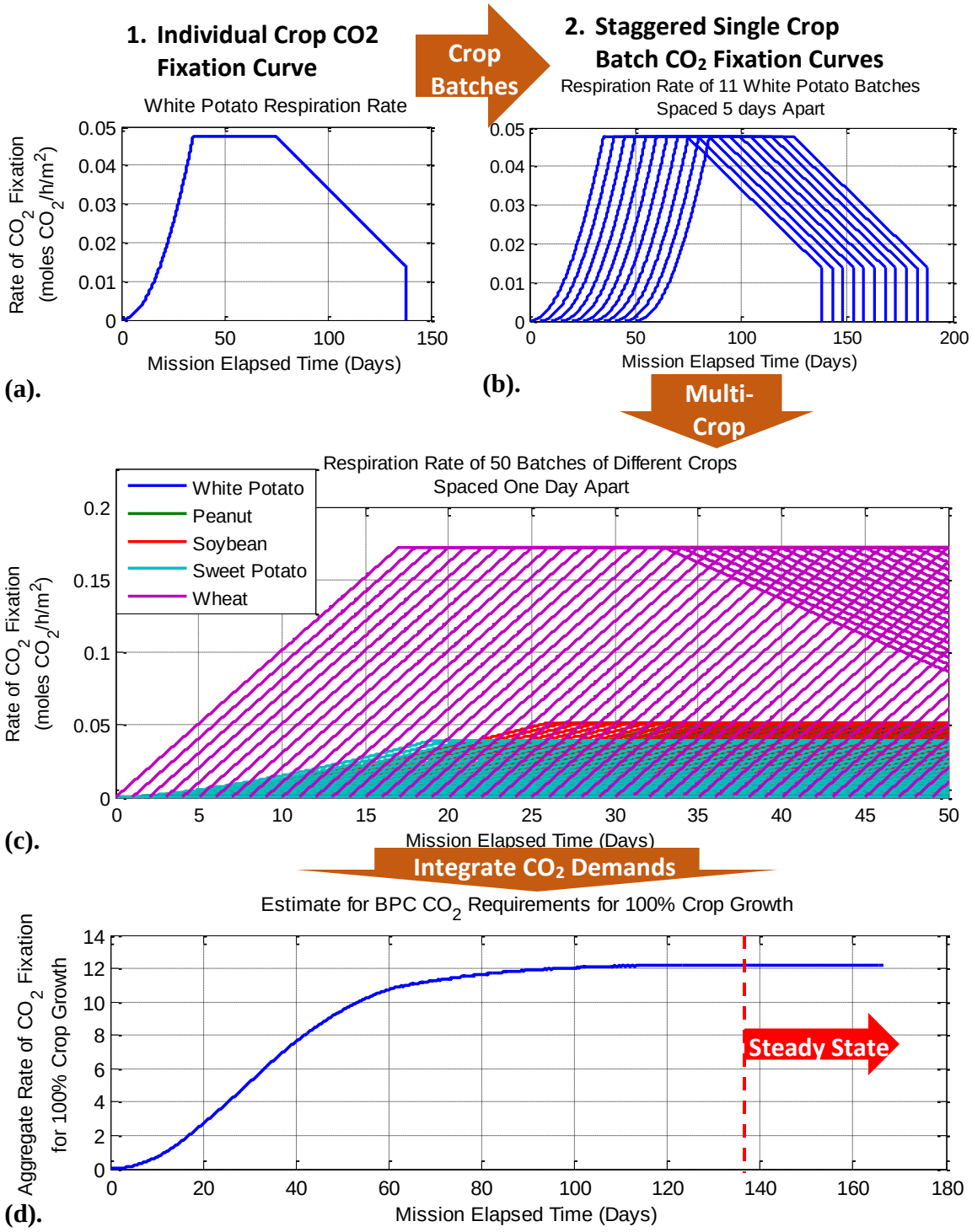

Figure 6-14: Process for developing a surrogate model of the MEC models to predict CO_2 demands for different levels of crop growth (a). Individual crop CO_2 fixation curve (b). Staggered single crop batch CO_2 fixation curves (c). Multi-crop batch staggered CO_2 fixation curves (d). Integral of multi-crop batch staggered CO_2 fixation curves, yielding the aggregate crop batch rate of CO_2 fixation

In addition, the fact that half the crew are on eight-hour EVAs for five days a week significantly reduces the amount of CO_2 generated within the habitat, since half the crew are not present within the habitat over these extended periods of time. Under the current spacesuit Portable Life Support System (PLSS) architecture, this CO_2 is essentially lost to the environment through the cycling of the Rapid Amine Swingbed, as it removes CO_2 from the EVA crew's spacesuits (see Appendix E.2). Thus, it is apparent that the total amount of CO_2 available, and hence the maximum proportion of calories that can be locally grown, is strongly dependent on the composition of the crew, the intensity and location of their activities, and the architecture of their spacesuit PLSS. Table 6.3 summarizes the range of aggregate CO_2 exhalation rates resulting from the crew schedules adopted in this analysis (see Table 6.2 for more details on the assumed crew schedule).

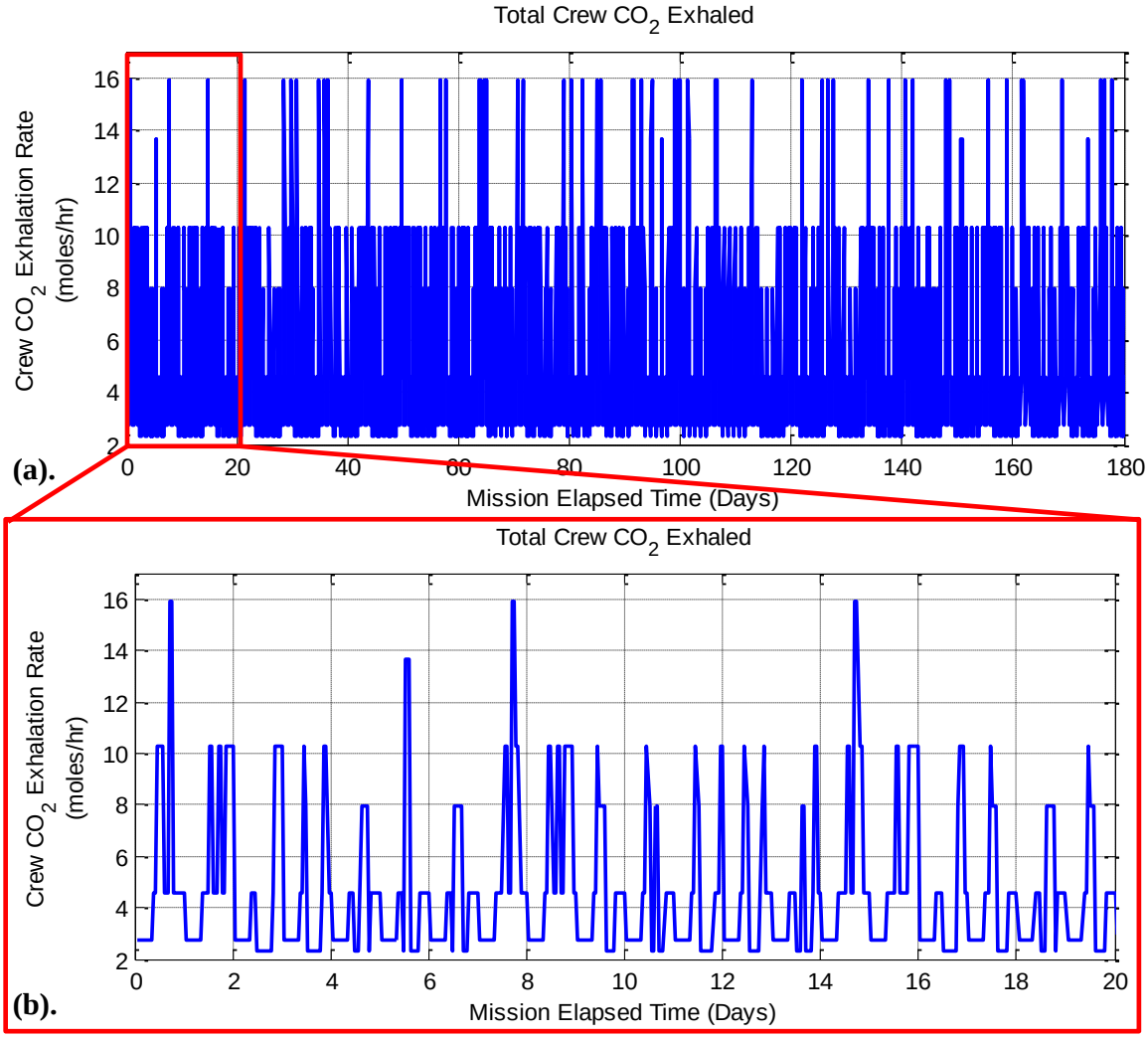

Figure 6-15: Aggregate Crew CO_2 Exhalation Profile for the first 180 days of the missions examined (Inset: Exhalation Profile over the first 20 mission days)

Table 6.3: Range of Aggregate Crew CO_2 Exhalation Rates for the crew schedules assumed in the case study performed in this chapter

	Aggregate Crew CO_2 Exhalation Rate (moles/hour)
Minimum	2.3
Mean	4.6
Maximum	15.9

The values listed in Table 6.3 suggest that at all periods throughout a mission, the combined CO_2 generation rate of the crew is at least 2.3moles/hour and at most 15.9moles/hour. Here, the minimum value corresponds to periods when half the crew is on EVA and the remaining IVA crew are doing low intensity activities, while the maximum value corresponds to periods when two crewmembers are exercising simultaneously. Since a constant CO_2 production rate of at least 2.3moles/hour is expected, we calculate the fraction of crop production with the equivalent CO_2 demand, and perform a simulation of the corresponding habitation scenario to verify the results.

Using Equation (6.10), we find that the proportion of the crew diet required to be grown such that the minimum crew CO_2 production rate is theoretically always sufficient is 2.3/12.2 = 18.8%, a value significantly lower than the 50% value typically assumed in biological life support system analyses (see Section 6.3.1). Figure 6-16 presents the resulting atmospheric trends from simulating the Mars Surface Field Station habitat with a BPC sized for 18.8% food production.

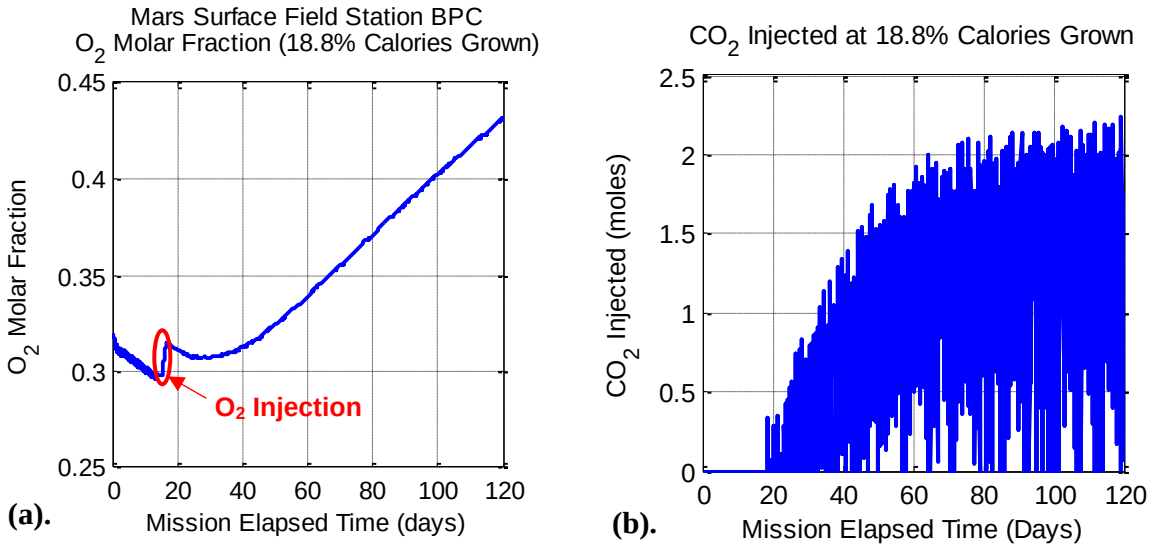

Figure 6-16: HabNet Simulation of a Mars Surface Field Station with a Food Production Level of 18.8% of Calories Grown (a). O_2 Molar Fraction (b). Supplementary CO_2 injection rate

From Figure 6-16, we can immediately observe that a CO_2 balance has not been achieved, causing the CO_2 injector to introduce CO_2 into the cabin atmosphere on mission day 19 onwards, and resulting in the increase in cabin oxygen concentration over time. Here, the CO_2 injection rate is approximately a third of that required for the 50% crop case (see Figure 6-12), indicating that the transition to an 18.8% crop growth profile has reduced the magnitude of the CO_2 deficit. This reduction has also resulted in a slightly different oxygen concentration trend in Figure 6-16(a). Here, the cabin oxygen level actually decreases initially, indicating that at least for the first 19 days of the mission, the CO_2 expended by the crew was sufficient to sustain the early rates of crop photosynthesis. In fact, the oxygen level decreases so much over the first 18 days that additional oxygen is required to be injected to maintain the cabin oxygen level above the hypoxic limit. This is indicated by the red oval in Figure 6-16(a). Shortly after this period, the rate of crop photosynthesis increases to a point where the CO_2 demand overtakes the rate of crew CO_2 production, causing the cycle of CO_2 injection and cabin oxygen accumulation to initiate.

These results suggest that the CO_2 demand of the 18.8% crop complement is still too high relative to the fluctuating CO_2 production rate of the crew, even though the previous CO_2 supply-demand analysis indicated that this should not be the case. A further analysis revealed that the likely cause of this discrepancy is the difference in location between the crew's activities and the location of the crops. When a crewmember exhales CO_2 on the opposite end of the habitat to the crops, some period of time is required for those moles of CO_2 to be distributed throughout the habitat (via intermodule ventilation fans) and to eventually impact the CO_2 concentration in the immediate vicinity of the crops. During this period, a momentary CO_2 deficit may occur, thereby causing the injection of CO_2 into the cabin.

Given the dynamic complexity of crew CO_2 generation and distribution about the habitat, an empirical approach was next adopted to determine the crop growth level at which the CO_2 demand would be accommodated by the CO_2 exhalation rate of the crew. This involved performing a series of dynamic simulations of the Mars Surface Field Station architecture at varying levels of crop growth to identify the point at which a CO_2 balance was achieved. Through this process, it was found that a crop growth level of 4.5% resulted in the desired CO_2 balance. Figure 6-17 presents the atmospheric dynamics observed within the habitat at various crop growth levels approaching 4.5%.

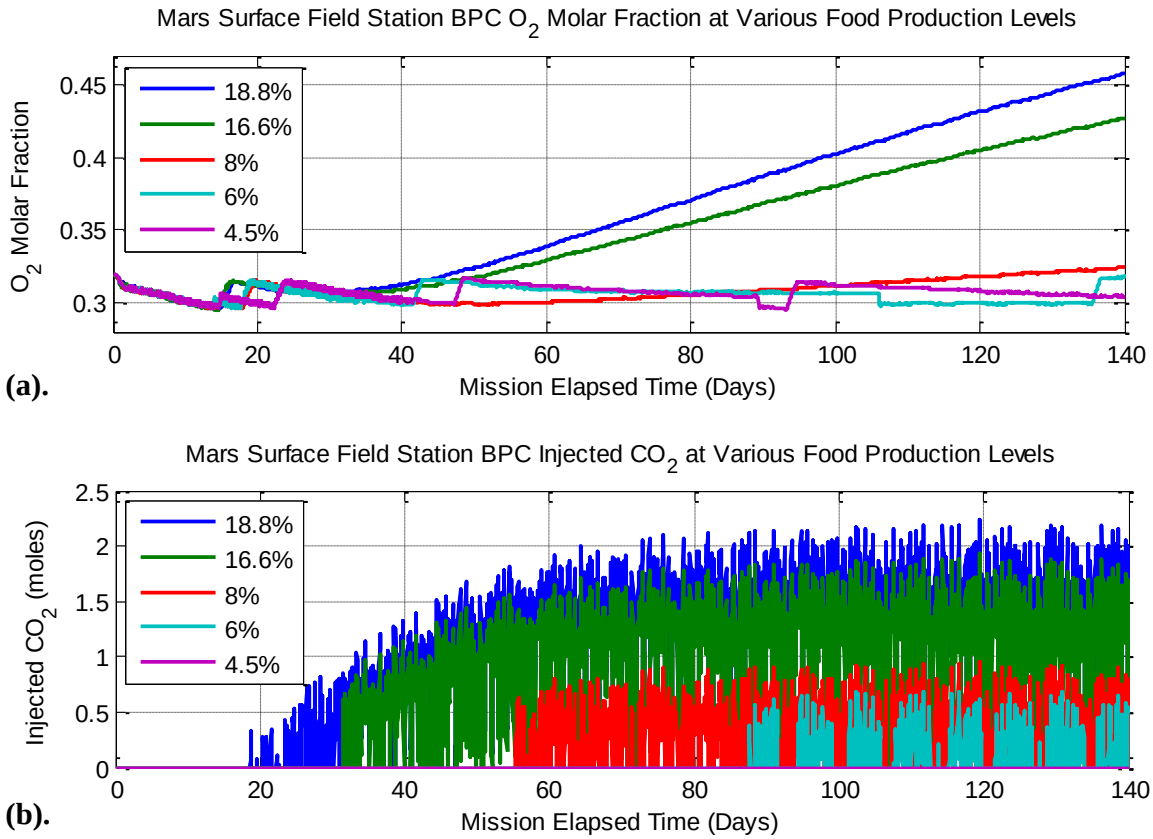

Figure 6-17: Cabin atmospheric dynamics at various crop growth levels approaching 4.5% and within a 250m^3 biomass production chamber (a). O_2 Molar Fraction (b). Injected CO_2

Upon examination of Figure 6-17(b), we observe that as the required food production level is decreased towards a value of 4.5%, the requirement for supplementary CO_2 to be injected into the cabin is both reduced, and delayed further into the future. Moreover, as the food production level is reduced from 6% to 4.5%, the requirement for CO_2 injection is eliminated, indicating that at this 4.5% level of food growth, the quantity of CO_2 exhaled by the crew is always sufficient to sustain the crops.

This transition in CO_2 injection trends maps to the reduction in the rate of oxygen concentration accumulation shown in Figure 6-17(a). Here, we observe that as the level of food growth decreases towards the 4.5% transition point, the slope of the O_2 molar fraction trend decreases towards zero, thereby reducing and ultimately eliminating the excess oxygen generation trend observed earlier.

Here, it is important to note that the simulation cases presented in Figure 6-17 all assumed a constant BPC volume of 250m^3. Thus, in order to verify the hypothesis that the key driver of atmospheric dynamics is the relative CO_2 generation and consumption rates of the crew and

crops (Equation (6.3)), we repeat the simulation of the 4.5% food growth habitat scenario at different BPC volumes. Figure 6-18 compares these results for volumes ranging between one order of magnitude less and greater than the baseline BPC volume of 250m^3.

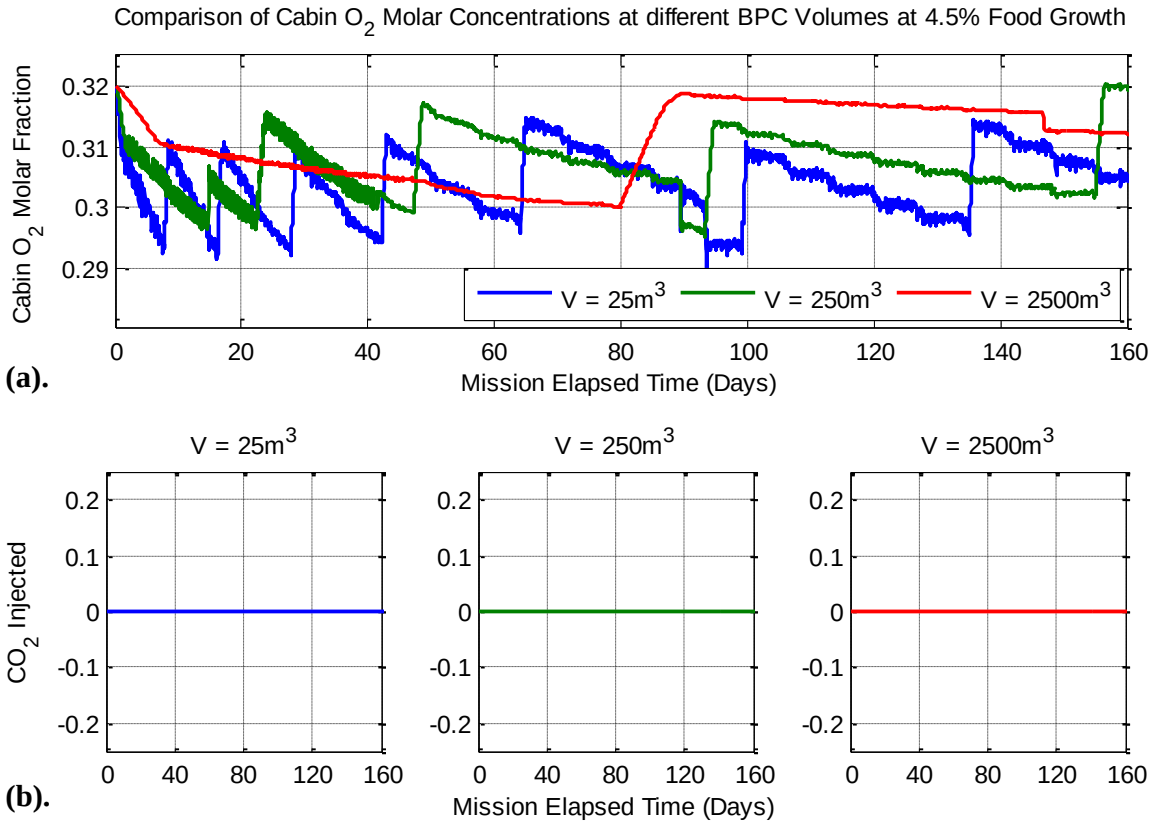

Figure 6-18: Comparison of dynamic atmospheric behavior with 4.5% food growth in various BPC volumes (a). Oxygen Molar Fraction (b). Injected CO_2

Here, we find that regardless of the BPC volume, the food growth level of 4.5% maintains a stable atmospheric behavior, thus verifying the analyses performed in Section 6.3.1. This is indicated by the fact that no additional CO_2 was required in any of the simulation cases performed in Figure 6-18, and that the cabin oxygen concentration remained relatively constant, fluctuating between a value of 0.29 and 0.32. For this latter trend, the major impact of varying BPC volume observed was that the frequency of the fluctuations in oxygen concentration decreased with increasing BPC volume. This is due to the fact that larger BPC volumes result in larger atmospheric buffers, which effectively dampen out short-period dynamics in a cabin atmosphere. The result of this is that a longer period of time is required before a control action is required to maintain the atmospheric composition – which in this

case, is the injection of oxygen from a PCA due to the gradual decline in cabin oxygen levels resulting from crew respiration and habitat leakage.

Thus, based on the results of the analyses conducted in this section, we introduce the following additional food-based habitation architectures into our analyses of the "String of Sorties" and "Minimum Continuous Presence" mission scenarios studied in the remainder of this chapter. These are:

- A 4.5% food growth case contained within $25m^3$ Biomass Production Chamber (BPC) module. Here, the BPC chamber atmosphere is shared with the rest of the habitat. The volume selected here is based on the packing densities described in Section 5.5.1.4.2 and Table 6.2. To facilitate the remainder of the crew's metabolic needs, a WPA and UPA are included, as well as an open-loop oxygen supply supplemented by ISRU-derived oxygen. Here, an OGA and CRS are not included based on the analysis performed in Section 5.6.2.1 and the results of the preliminary simulations performed here, where it was found that these two systems are seldomly used when crop production is included within a habitation architecture. This is because the crops serve the basic role of CO_2 reduction through the process of photosynthesis.
- A 50% food growth case based on the same BPS architecture developed in Section 5.6.2.1. Here, the crops are grown in a dedicated BPC with a volume of $250m^3$. To facilitate this growth, a CO_2 injector is installed to supplement any additional CO_2 required for photosynthesis. Product oxygen generated from the growing crops is removed from the BPC atmosphere via an oxygen removal assembly (ORA) and directed to oxygen tanks for later use by the crew. Similar to the 4.5% food growth case, a WPA and UPA are included but not an OGA or CRS. In addition, a separate crop-specific water recycling system is installed that recycles crop-transpired water back into a crop water tank that supports nutrient delivery to the roots of the crops
- A 100% food growth case that is a scaled up version of the 50% food growth case. Here, a $500m^3$ volume BPC supported by a CO_2 injector and ORA is used to facilitate crop growth. Again, a WPA, UPA, and dedicated crop transpired water collection and recycling system is used. This system architecture is largely the same as the BPS architecture developed in Section 5.6.2.1. Here, the main difference is that the food growth system is attached to the Mars Surface Field Station habitat, rather than the Mars One habitat.

6.3.3 Sizing Architectures with a Biomass Production Capability

As was observed in the analysis of the BPS architecture in Section 5.6.2, the implementation of a food production capability into a habitation system introduces additional systems that need to be accounted for, especially when computing its emplacement and lifecycle resupply requirements. These systems include the BPC structure itself, as well the required grow lights, and shelf structure to support crop growth. In addition, these systems incur additional power and thermal management demands that can have a significant impact on the systems required to support them, as was noted in Sections 5.6.2.3 and 5.6.2.5.

This section summarizes the assumptions used in calculating the impacts of these additional food-production-related systems on the total mission emplacement and resupply mass. Here, an equivalent system mass (ESM) approach is used (see Section 4.4.5), where the impacts of technology mass, power, and thermal management requirements are factored into an "equivalent mass" of delivering a given food production capability to the surface of Mars. The equivalent system mass is calculated by the following equation:

$$ESM = M + (P_E \cdot E_{P_E}) + (C \cdot E_C) \tag{6.11}$$

Where:

M = total mass of life support equipment, consumables, and spares (the raw mass calculated thus far in this analysis) (kg)

P_E = total average system electrical power requirement (kW)

C = total average system cooling requirement (kW)

E_i = mass equivalencies associated with providing primary and secondary structure (based on volume), electrical power, and cooling via thermal control

Here, we note that the volume contributions to ESM have not been included in Equation (6.11) as they have been factored into the mass of the BPC structure. The estimate of this mass, as well as the mass equivalencies used to calculate other contributions to the ESM, are summarized in Table 6.4.

Table 6.4: Summary of Equivalent System Mass Calculations for Systems involved in Food Production

System	Approach used to calculate Equivalent System Mass	Comments
BPC Structure	Mass[kg] = 13.40[kg/m^3] ×BPC Volume[m^3] BPC Volume[m^3] = Plant Growth Area [m^2] × 500/201[m^3/m^2] Or BPC Volume[m^3] = Fraction of Calories Grown [%] × 500 [m^3]	Assumed to be an inflatable structure, outfitted with avionics and power distribution lines. Mass factor is taken from BVAD [275] BPC Volume calculation is based on the analysis of the Mars One BPS performed in Section 5.5.1.4.2
Secondary Structure	Mass[kg] = 5.7[kg/m^2] × Plant Growth Area [m^2] No power demand	Includes shelving and other structure required to support hydroponic crop growth. Mass factor taken from BVAD [275]
Mechanization Systems	Mass[kg] = 4.1[kg/m^2] × Plant Growth Area [m^2] No power demand	Includes mechanical systems needed to support hydroponic crop growth. Mass factor taken from BVAD [275]
Grow Lights	Number of required lighting systems = $\left\lceil \frac{\text{Fraction of Calories Grown [\%]}}{137} \right\rceil$ Mass of lighting system [kg] = 8[kg/light] × Number of grow lights Power demand of lighting system [kW] = 0.63[kW/light] × Number of grow lights	Number of required lighting systems is based on the calculation performed in Section 5.5.1.4.3 for the Heliospectra LX601 grow light. Mass and power values for each grow light are based on the Heliospectra LX grow light [213]
Food Processor	Consists of the following components with a fixed mass: Hand Mixer: 2kg Food Processor / Blender: 8kg Grinder / Mill: 4.1kg Bread Machine: 7.4kg Griddle / Grill: 5.8kg Juice Extractor: 7.7kg	Based on the same food processing system assumed for the Mars One mission plan (see Section 5.5.1.4.7) [284]. The power demands of these systems are assumed to be negligible compared to those of other systems, and have hence been ignored
ORA	Mass = 262.8kg Power = 860kg	Assumed to have the same characteristics as the CDRA
ESM Mass Equivalencies		
E_{P_E}	Power Equivalent System Mass Contribution [kg] = 75[kg/kW] × Power demand [kW]	Based on a nuclear power source with static thermoelectric power production. Mass equivalency value taken from BVAD [275]

E_C	Thermal Management Equivalent System Mass Contribution [kg] = (25 + 121)[kg/kW] × Thermal load [kW]	System thermal loads are assumed to equal their corresponding power requirements The 25kg/kW mass equivalency corresponds to an internal thermal control system consisting of a flow loop with cold plates. The 121kg/kW mass equivalency corresponds to an external thermal control system consisting of light-weight flow-through radiators. The equivalency values are taken from BVAD [275]

In addition to the technologies listed in Table 6.4, the additional water and CO_2 demands of food production will be captured within the sizing of the ISRU systems required to satisfy these demands. As mentioned in Table 6.2, these ISRU systems will be automatically sized using Schrenk's ISRU architecture optimization code [144].

6.4 Lifecycle Impacts of Mission Campaign Scenario 1: The String of Sorties

In this section, we perform the first of the two mission campaign analyses presented in this chapter. Entitled the "String of Sorties", this campaign consists of repeated conjunction class missions to the same surface location on Mars, in a manner similar to the initial campaign strategies adopted in the NASA Design Reference Architectures developed since the early 1990s (see Section 6.1). Figure 6-19 summarizes the crew population profile at the Martian surface over time, where each color represents a different crew.

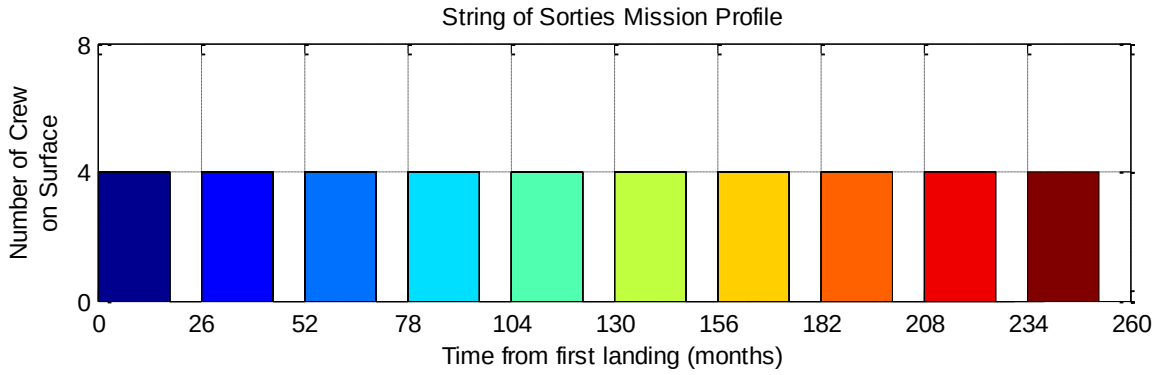

Figure 6-19: The String of Sorties Mission Profile. Each colored block represents a different crew on the Martian surface

As summarized in Table 6.2, this analysis assumes four person crews making 540 day expeditions to a Mars Surface Research Station located at Jezero Crater. Here, we are interested in quantifying the emplacement and lifecycle resupply costs of sustaining this campaign under different habitation scenarios consisting of different ECLS and food growth architectures. As was described in Table 6.2, these architectures include:

- Case 1: Open Loop Water and Oxygen + Stored Food
- Case 2: WPA + Stored Food
- Case 3: WPA + UPA + Stored Food
- Case 4: WPA + UPA + OGA + Stored Food
- Case 5: WPA + UPA + OGA + CRS + Stored Food
- Case 6: WPA + UPA + 4.5% Locally Grown Food (in a 25m^3 BPC)
- Case 7: WPA + UPA + 50% Locally Grown Food (in a 250m^3 BPC with a CO_2 injector and ORA)
- Case 8: WPA + UPA + 100% Locally Grown Food (in a 250m^3 BPC with a CO_2 injector and ORA)

For each of these architectures, ISRU systems are sized to provide all remaining consumables requirements, using Schrenk's ISRU architecture optimizer [144]. In addition, spare parts are assumed to be delivered at every launch opportunity (every 26 months), and are assumed to be capable of being shared amongst successive surface crews.

To analyze this mission scenario, we adopt the same approach used in the validation case study performed in Section 4.4, where we run each ECLS architectural case through each of the HabNet modules, prior to aggregating the results and performing a campaign-level comparative analysis. This process is described in the following sections.

6.4.1 Habitation Module Results

To initiate this analysis, the HabNet Habitation Module was first used to simulate the dynamic behavior of each of the eight architectural cases described above. Through this, the resource requirements and system runtimes of each of the technologies within each of the candidate architectures was computed. These results are then used to determine the corresponding ISRU system requirements, as well as the spare parts resupply requirements over time.

Figure 6-20 summarizes the consumables requirements for each of the eight ECLS architecture candidates throughout the 540 day surface mission duration, with and without the

propellant requirement for the Mars Ascent Vehicle (MAV). In addition, Table 6.5 summarizes the corresponding consumables requirements values graphed in Figure 6-20.

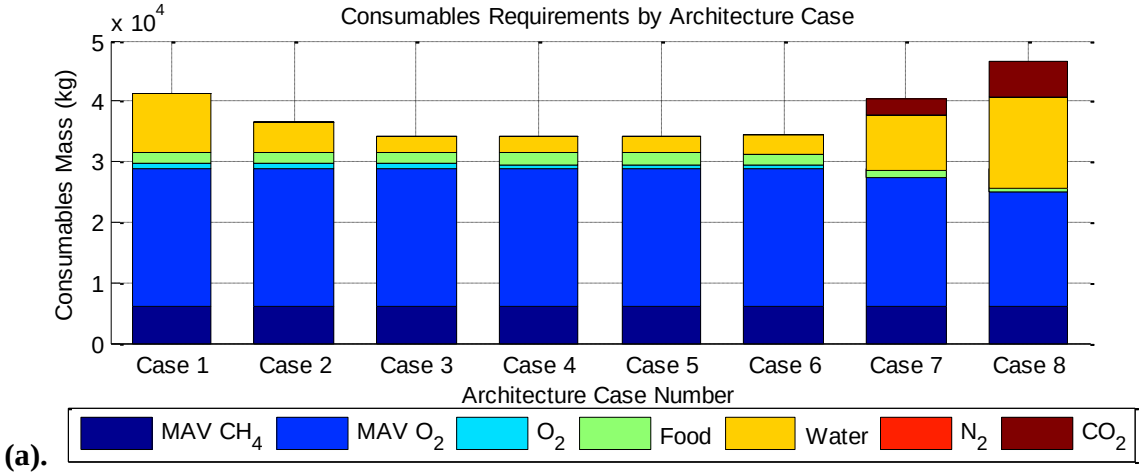

(a).

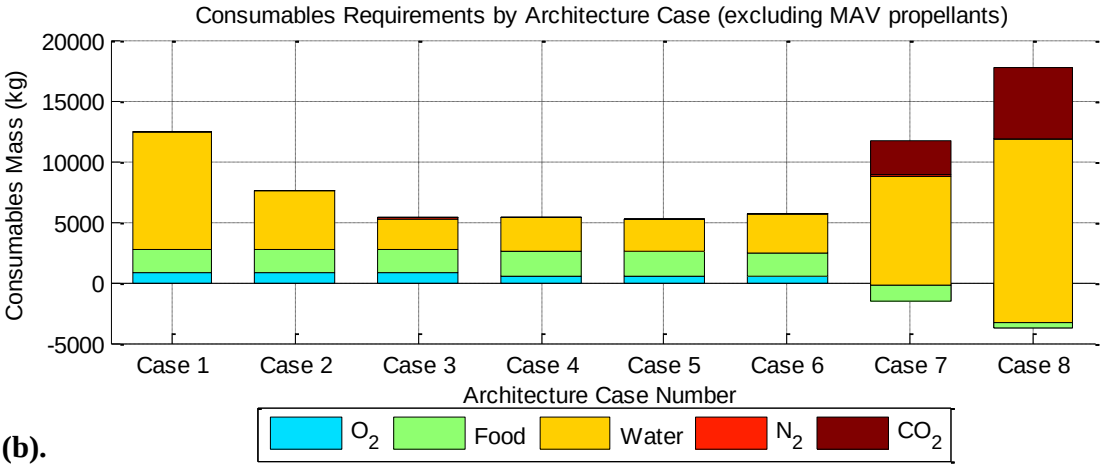

(b).

Figure 6-20: Consumables requirements over 540 days for each of the eight architecture cases examined (a). All ECLS and MAV Consumables (b). Only ECLS Consumables

From Figure 6-20(a), it can be immediately observed that the propellant demand for the Mars Ascent Vehicle dominates the consumables demands for all architectures. As will be seen in the next section, this demand drives the optimal ISRU system of all cases towards an archetypical architecture.

To better distinguish between the resource demands of each ECLS case, we remove the MAV propellant contribution and replot the results in Figure 6-20 (b). In this second figure, we observe that ECLS Cases 7 and 8 exhibit a negative mass contribution. These architecture cases correspond to those that incorporate local food production at levels of 50% and 100%

respectively. As was observed in Section 6.3.2, architectures that include food production at these levels tend to generate excess levels of oxygen through photosynthesis supplemented with Martian atmospheric CO_2. The incorporation of an ORA in these architectures allows this excess oxygen to be collected and used for other purposes. In the scenarios analyzed here, this excess oxygen offsets the oxygen demand of the MAV, thereby resulting in a negative oxygen demand and hence the negative contribution depicted in Figure 6-20(b). This phenomenon of offsetting total oxygen demand via the production of food is a new concept that emerges from the coupled architectural analysis of ECLS and ISRU systems. The implications of this architecture will be further revisited in Section 6.5.5.

In addition to this negative oxygen demand, these two architectures also require some level of food to be delivered from Earth to support them. This is the case even for Case 8, where 100% of the calories required by the crew are locally grown. As listed in Table 6.5, at least 427kg of food are required for architecture Case 8 to sustain the crew during the first phases of crop growth (see Figure 6-11), where the initial crop batches are growing and have yet to produce edible biomass. As successive crop batches reach maturity and crops are harvested, the crew's dependency on prepackaged food diminishes towards zero. As was observed in Figure 6-14, this period occurs after 138 days, when the first full complement of crops has reached maturity.

Table 6.5: Consumables Requirements computed by the HabNet Habitation Module for each ECLS Architecture Case. Cells with the same values are colored for the purposes of clarity. The consistency in values across these colored cells is similar to the observations made in the case study performed in Section 4.4 (see Table 4.6)

	O_2 (kg)	**N_2 (kg)**	**H_2O (kg)**	**CO_2 (kg)**	**Food (kg)**
Case 1 - Open Loop O2 + H2O	765	26	9633	0	1983
Case 2 - WPA	765	26	4815	0	1983
Case 3 - WPA + UPA	765	26	2542	0	1983
Case 4 - WPA + UPA + OGA	550	28	2794	0	1983
Case 5 - WPA + UPA + OGA + CRS	550	28	2703	0	1983
Case 6 – WPA + UPA + 4.5% Food	555	25	3172	0	1911
Case 7 – WPA + UPA + ORA + 50% Food	-1484	51	9093	2771	1205
Case 8 – WPA + UPA + ORA+ 100% Food	-3734	65	15076	5887	427

With regards to the remaining architectural cases, we observe a similar trend to that found in the validation case study performed in Section 4.4 – that increasing the level of resource

recycling generally leads to lower total consumables demands. A closer inspection of Cases 3 to 6, however, reveals that the addition of the OGA from Case 3 to Case 4 has in fact resulted in an increase in overall consumables requirements. This can be seen in both Table 6.5 and in Figure 6-21 below, and is the result of an increasing water requirement arising from the need for feedwater to support the operation of an OGA. This additional requirement offsets the savings gained in oxygen demand with the introduction of the OGA – a result that differs from that observed in the case study performed in Section 4.4. This difference is likely due to the fact that the Mars surface crew is performing a large number of EVAs compared to the crew of a Deep Space Habitat. Every time an EVA is performed, oxygen is used to recharge the crew's Portable Life Support Systems (PLSSs), which is then consumed and ultimately lost to the Martian environment via the Rapid Cycle Amine (RCA) system on the PLSS. This RCA system removes CO_2 from the spacesuit atmosphere and dumps it to the surrounding environment. In addition, every time a crew leaves the habitat to go on EVA, they cycle the suitlock (see Appendix E.1), which in turn leads to a small loss of cabin atmosphere. Over several EVAs, these accumulated atmospheric losses can lead to noticeable differences between the oxygen demands of a Mars surface habitat where EVA is a regular occurrence, versus a Deep Space Habitat, where EVAs are only budgeted for emergency situations.

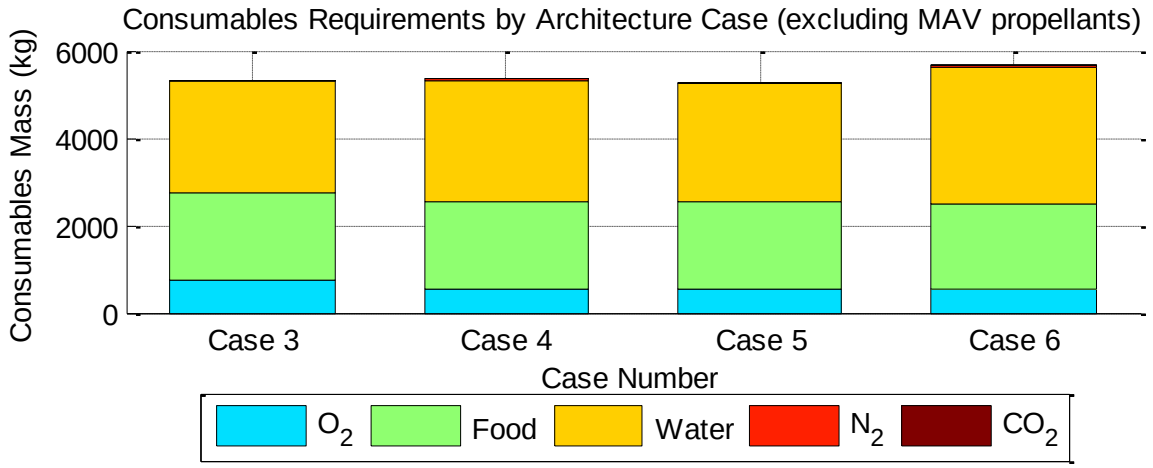

Figure 6-21: Close up of the consumables requirements predicted by the HabNet Habitation Module for Architecture Cases 3 to 6.

Moreover, it is interesting to note that the introduction of the 4.5% amount of food production in Case 6 results in only an increase of approximately 350kg in consumables mass as compared to Case 3, which is the equivalent architecture without an integrated BPC. While

this additional 350kg only results in a savings in food demand of approximately 72kg (see Table 6.5), the fact that the consumables requirements of Case 6 are only slightly (≈6.5%) greater than that of Case 3 indicates that this might be an attractive path towards transitioning from a completely prepackaged based ECLS architecture, to one that includes some level of local food production.

Finally, in order to size the ISRU systems required to satisfy the consumables demands listed in Table 6.5, the maximum required production rates were derived for each ECLS case, based on the maximum resource usage rates. The resulting values are summarized in Table 6.6, below.

Table 6.6: Resource production rates required for each ECLS architecture case, based on peak resource usage rate. Cells with the same values are colored for the purposes of clarity.

	O_2 (mol/h)	**N_2 (mol/h)**	**H_2O (L/h)**	**CO_2 (mol/h)**	**CH_4 (mol/h)**
Case 1 - Open Loop O2 + H2O	56.7	0.07	0.75	0	33.7
Case 2 - WPA	56.7	0.07	0.38	0	33.7
Case 3 - WPA + UPA	56.7	0.07	0.20	0	33.7
Case 4 - WPA + UPA + OGA	56.2	0.08	0.22	0	33.7
Case 5 - WPA + UPA + OGA + CRS	56.2	0.08	0.21	0	33.7
Case 6 – WPA + UPA + 4.5% Food	56.2	0.07	0.25	0	33.7
Case 7 – WPA + UPA + ORA + 50% Food	51.3	0.14	0.71	5.85	33.7
Case 8 – WPA + UPA + ORA+ 100% Food	45.8	0.18	1.17	11.8	33.7

6.4.2 ISRU Module Results

With the required ISRU production rates now derived for each ECLS architecture case, the ISRU architecture optimization tool within the HabNet ISRU module was run to size the corresponding ISRU technologies. Through this process, it was found that a dominant ISRU architecture emerged from the set of seven ISRU technologies currently modeled within HabNet (see Table 6.2). This architecture is depicted below in Figure 6-22, and consists of a soil processor based on the MARCO-POLO system (see Section 2.2.4) that extracts water from Martian regolith, a water electrolyzer that electrolyzes this water into oxygen and hydrogen gas, a CO_2 cryocooler that extracts CO_2 from the Martian atmosphere, a Sabatier reactor that produces methane and water by reacting CO_2 with hydrogen gas, and an atmospheric processor that uses zeolite sorbents to extract nitrogen from the Martian atmosphere.

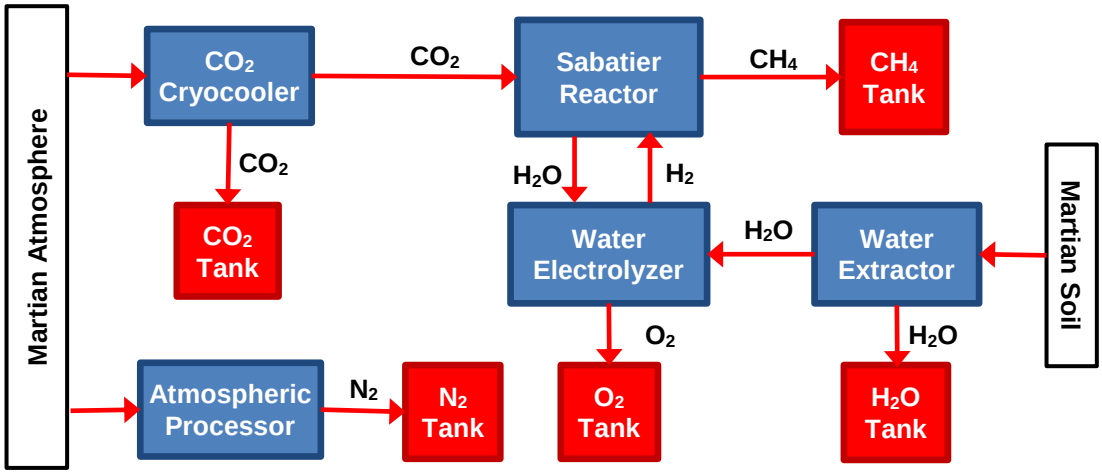

Figure 6-22: Archetypical ISRU Architecture predicted by the HabNet ISRU Module for all ECLS Architectural Cases examined

Table 6.7: ISRU system mass for each ECLS architecture case. Cells with the same values are colored for the purposes of clarity.

	Water Extractor (kg)	**CO_2 Cryo-cooler (kg)**	**Water Electro-lyzer (kg)**	**Sabatier Reactor (kg)**	**Atm. Process-or (kg)**
Case 1 - Open Loop O2 + H2O	431	153	70	22	27
Case 2 - WPA	351	153	70	22	27
Case 3 - WPA + UPA	314	153	70	22	27
Case 4 - WPA + UPA + OGA	318	153	70	22	29
Case 5 - WPA + UPA + OGA + CRS	316	153	70	22	29
Case 6 – WPA + UPA + 4.5% Food	324	153	70	22	26
Case 7 – WPA + UPA + ORA + 50% Food	422	179	70	22	47
Case 8 – WPA + UPA + ORA+ 100% Food	522	206	70	22	58

The emergence of this archetypical ISRU architecture can be explained by examining the ISRU production requirements listed in Table 6.6. From this table, we observe that the production rates required for the ISRU system are largely similar across all ECLS architectures for all resources. For methane and oxygen, this similar demand is driven by the dominant propellant demands of the MAV, while the similarities in nitrogen and CO_2 demand for the first 6 architecture cases arise from the lack of significant crop growth. Here, it is observed that the major source of variation in ISRU production rates is water, whose demand fluctuates

significantly with the ECLS architecture chosen. This general trend is reflected in the results of the ISRU system sizing analysis summarized in Table 6.7 and Figure 6-23.

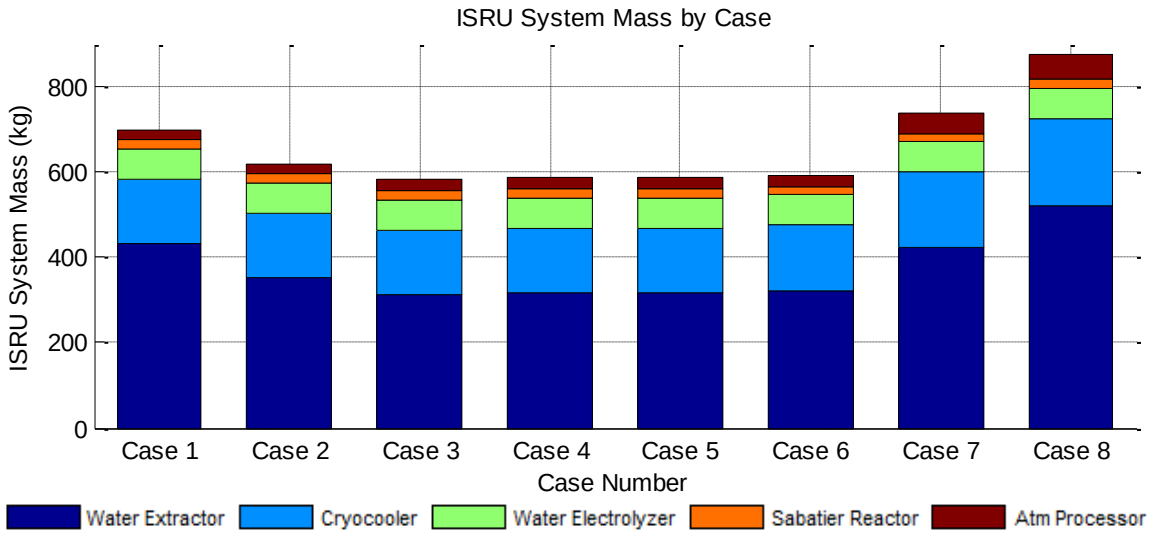

Figure 6-23: Comparison of ISRU system masses across the eight ECLS architecture cases

From Figure 6-23, we observe that as water recycling capabilities are added from Case 2 to Case 3, the total mass of the ISRU system decreases to a relatively constant value until large fractions of food production are included in Cases 7 and 8. The increased water demand of these latter two cases drives up the mass of the required water extractor by at least 100kg. In addition, the increased CO_2 requirements of these latter two cases further adds to their total ISRU system mass, due to the need for a correspondingly larger CO_2 cryocooler.

This trend can be observed in Table 6.7, where all architectures (Cases 1 to 6) that do not adopt large scale food production share the same CO_2 cryocooler design. This commonality is the result of the driving needs of the MAV for oxygen and methane propellants that were observed in Figure 6-20(a).

Since the only technology that can generate in-situ methane is the Sabatier reactor, its size is constant across all architectures. To generate methane, the Sabatier reactor requires CO_2 and hydrogen gas, which are obtained from the CO_2 cryocooler and the water electrolyzer, respectfully. Since the demand for methane is constant across all architectures, the corresponding demand for hydrogen is also the same, which leads to the constant water electrolyzer mass observed in Table 6.7. Similarly, the constant methane demand also results in a constant CO_2 demand for propellant production. The fact that Cases 1 to 6 only require

CO_2 for MAV propellant production, means that the required CO_2 cryocooler system is the same across these architectures.

The consistency in these system masses results in a relatively constant ISRU architecture across Cases 3 to 6. Within this set of architectures, the largest pairwise difference in total ISRU system mass is between Cases 3 and 6, where the addition of the 4.5% level of crop growth requires an additional 10kg of ISRU system mass.

6.4.3 Supportability Module Results

With the ECLS and ISRU system architectures of each habitation scenario established by the HabNet Habitation and ISRU Modules, Master Equipment Lists (MELs) for each of the eight architecture cases were developed and input into the Supportability Module. From this, demands for spare parts for each component within each architecture case were computed, such that the probability of having sufficient spares to manage both random failure and scheduled maintenance in each mission is 0.999.

The MELs developed for each architecture case are summarized in Appendix J.2. In most cases, system mean time between failure (MTBF) and life limit (LL) values are based on those listed in the 2004 version of the NASA Baseline Values and Assumptions Document (BVAD). This is particularly the case for ECLS technologies, which are based on those currently being operated on the ISS. For ISRU technologies, the failure rates of analogous ECLS hardware were adopted, due to the lack of maturity and operational data on the required ISRU systems. In cases where a suitable analogy could not be found, an MTBF value of 500,000h was assumed – the same value as that adopted in the case study performed in Chapter 5. In addition, as was described in Table 6.2, spare parts commonality is assumed to exist between successive crews, where the spare parts of a prior crew can be used by subsequent crews. As a result, the Supportability Module outputs distributions of spare parts requirements across the campaign of missions. For the ten sortie mission scenario examined here, this results in a set of ten spare parts profiles for each architecture case. Figure 6-24 presents the ECLS and ISRU spare parts resupply requirements predicted for each architecture case.

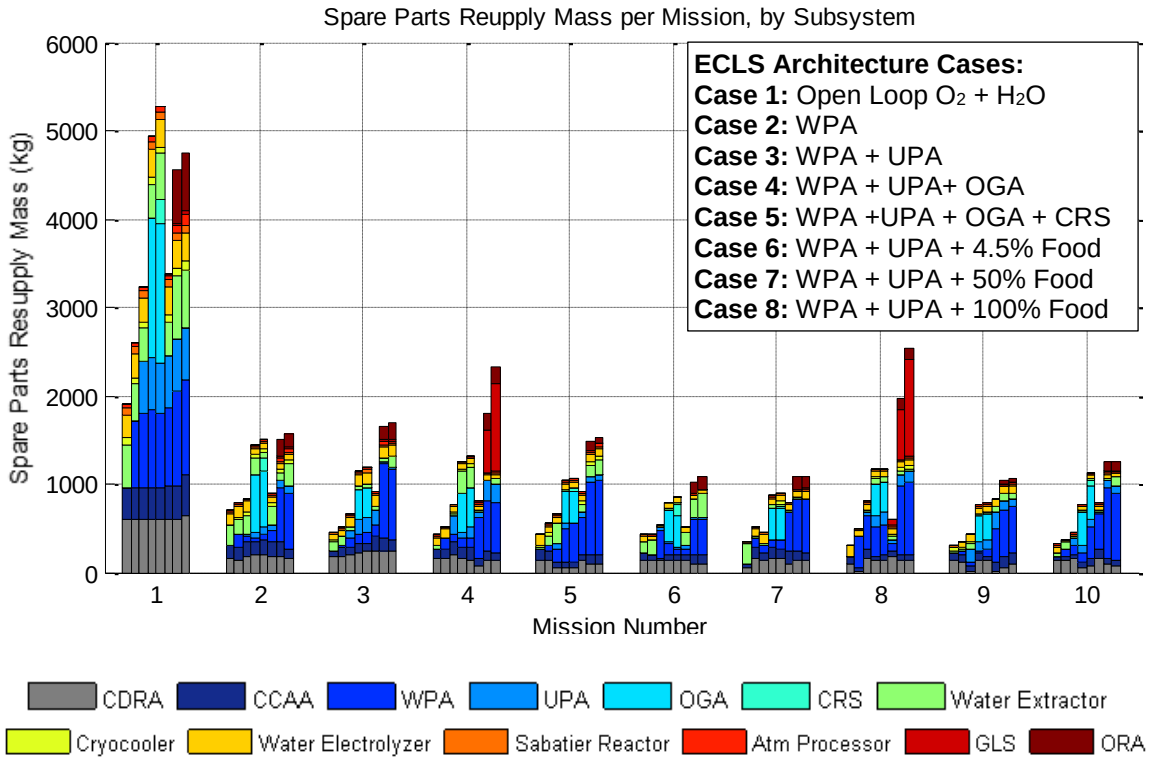

Figure 6-24: Spare Parts Resupply Requirements per Mission for each ECLS Architectural Case for the String of Sorties mission scenario (each bar within each eight-bar cluster corresponds to an individual ECLS case)

From Figure 6-24, we observe that across all missions for all architecture cases, an initial spike in spare parts is required for the first mission, followed by a relatively constant resupply demand with intermittent spikes thereafter. This trend is the result of the fact that in the first mission, when all equipment is deployed to the surface, a pool of spare parts needs to be established to ensure the continuous operation of all critical systems. In all subsequent missions, spare parts are delivered to maintain this spare parts pool, by replacing any parts that have been used during the 26 month period between resupply opportunities.

The intermittent spikes observed in the second mission onwards are most prevalent for architectures with high levels of food growth, and correspond to the periodic demand for all BPC growth lighting units to be simultaneously replaced. This requirement occurs due to the fact that crop growth is strongly dependent on the photosynthetic photon flux (PPF) generated by the near-continuous operation of grow lights. Furthermore, it should be noted that the sparing of these lights in this case study was performed at the level of individual lighting units, due to the nature of the reliability data used. It is likely that this resupply mass contribution could be reduced if sparing were performed at a lower level of repair (e.g. the individual light

emitting diode level), but this would require reliability data at this level and would need to be traded against the crew time required to perform this task.

With regards to the relative trends amongst the eight architecture cases, we make similar observations to those found in the validation case study performed in Section 4.4. These include the fact that spare parts requirements generally increase with the number of technologies included within a system architecture, and that the OGA is the largest driver of spare parts requirements. The first of these observations is the result of the increase in failure modes that accompanies systems with greater components and increasing complexity, as well as the fact that systems with greater levels of resource recycling tend to exhibit lower levels of reliability.

Contrastingly, the second of these observations arises from the relatively large mass and low to medium reliability level of the Hydrogen and Water ORUs (see Appendix D.5) incorporated into the OGA architecture. It is interesting to note that the spare parts demands of the ISRU water electrolyzer are significantly lower than those of the OGA, even though both technologies are based on the same fundamental process. This difference is mainly due to the fact that the OGA is designed to operate within a pressurized spacecraft cabin, thus necessitating a high-mass evacuated dome to mitigate the explosion risk arising from leaking hydrogen reacting with oxygen within the cabin atmosphere. A similar system operating within the ambient Martian atmosphere can avoid this requirement due to the high atmospheric concentration of CO_2, which acts as a fire suppressant [285]. This, in turn, results in a lower corresponding system mass.

In addition to the OGA, Figure 6-24 indicates that components related to the WPA also make up a large proportion of the aggregate spare parts resupply requirements, especially for cases involving local food production. This resupply mass is primarily driven by the numerous high mass, life-limited filters present within the WPA. These include multifiltration beds that each weigh 150kg and have a life-limit of 3153h, ion exchange beds that each weigh 13kg and have a life-limit of approximately 1400h, and particulate filters that each weigh 32kg and have a life-limit of 1927h (see Appendix J.2 for the full set of MELs). The higher rate of water usage in architectures involving crop production results in higher levels of cabin humidity, due to the presence of crop transpiration. This in turn leads to an increased level of humidity condensate being collected by the common cabin air assemblies (CCAAs – see Appendix D.3 for details), which consequently requires an increased WPA runtime for processing to a quality that is suitable for downstream use by the crew. This increased WPA runtime results in a higher spare parts demand than would be needed for architectures that do not involve local food production.

This suggests that efforts towards reducing the mass and/or increasing the life-limit of the multiple filters within the WPA can lead to significant savings in resupply mass, especially in architectures involving local food production. One potential avenue for achieving this is through the development of regenerable or self-cleaning filters, as is the case with the regenerable sorbents commonly used in spacecraft CO_2 removal systems. Alternatively, savings in WPA processing time may be obtained by rearchitecting the water system architecture to take advantage of the partial water cleaning effects of crop transpiration. In this scenario, depending on the quality of water required and its intended application, humidity condensate derived from transpired water may be used directly without processing via a WPA. This could result in a lower WPA runtime and a corresponding reduction in spare parts requirements, but would require further research into the water cleaning characteristics of the selected crops and their susceptibility to toxin accumulation (as was discussed in Section 5.5.1.4.8.1 and observed with the challenges experienced with DMSD on the ISS described in Table 2.6).

6.4.4 Evaluation Module Results

In this section, we combine the results of the previous intermediate analyses with the equivalent system mass of the supporting infrastructure described in Section 6.3.3 to calculate the aggregate lifecycle emplacement and resupply requirements for each of the eight architecture cases examined. Figure 6-25 summarizes the total equivalent mass required to be delivered to the Martian surface for each architecture case over each of the ten missions.

From this figure, we immediately observe the large initial infrastructure requirements of Cases 7 and 8, where food production levels of 50% and 100% are respectively integrated into the system architecture. Here, we find that the major contributors to these large initial masses arise from the mass of the primary and secondary structure of the BPC itself, as well as the additional power and thermal management requirements imposed by the need to provide continuous levels of high intensity lighting in order to support crop growth. This finding agrees with those made in Section 5.7.3 as well as the general trends discussed in Section 5.6.2.3, where it was mentioned that previous studies of bioregenerative life support systems have found that power, cooling, and volumetric requirements typically account for 70% of the total equivalent system mass.

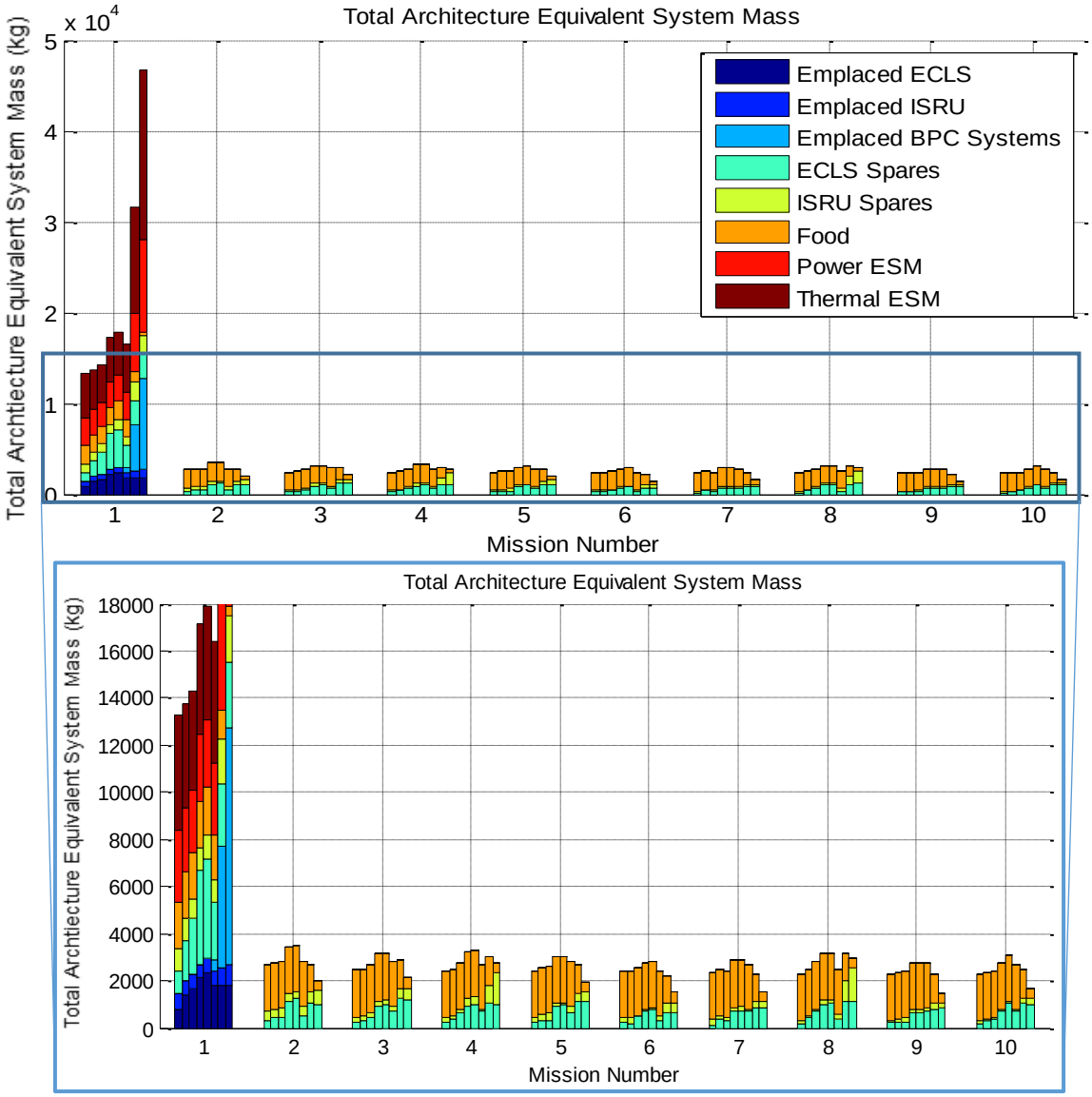

Figure 6-25: Total Equivalent System Mass required to be delivered to the Martian surface per Mission per Architecture for the String of Sorties Mission Scenario. Each cluster of bars represents a mission of the campaign, while each bar within a cluster represents an architectural case

This trend of requiring an initially high mass during the first deployment mission is consistent across all architecture cases examined here. This higher initial mass requirement arises from both the need to initially emplace the required ECLS systems, and the need to establish an initial pool of spare parts to support system maintenance and repair tasks. After this first deployment mission, significantly lower levels of resupply are required to sustain later sortie crews, with reductions in delivered mass relative to the first mission ranging from 68-83%. In these latter missions, the resupply requirement is composed entirely of items that cannot be produced locally on Mars at the necessary level of production. These include mainly

ECLS and ISRU spare parts, as well as food that is required to compensate for any gaps in local food production capability. This trend suggests that under the "String of Sorties" mission scenario, the cost of each mission after the first will be significantly lower than the cost of initial surface system deployment and setup.

With regards to the relative costs of the emplacement and sustainment of each architecture case, a closer inspection of the lower, inset image of Figure 6-25 suggests that increasing levels of ECLS resource recycling and food production result in increasing requirements for emplaced mass and lifecycle resupply. This observation is reaffirmed when comparing the cumulative equivalent system mass (ESM) requirements for each architecture case over the ten sortie campaign. Figure 6-26 summarizes these cumulative ESM trends, showing both the absolute cumulative ESM values per mission, as well as the difference in cumulative ESM between the top two ranked ECLS architectures.

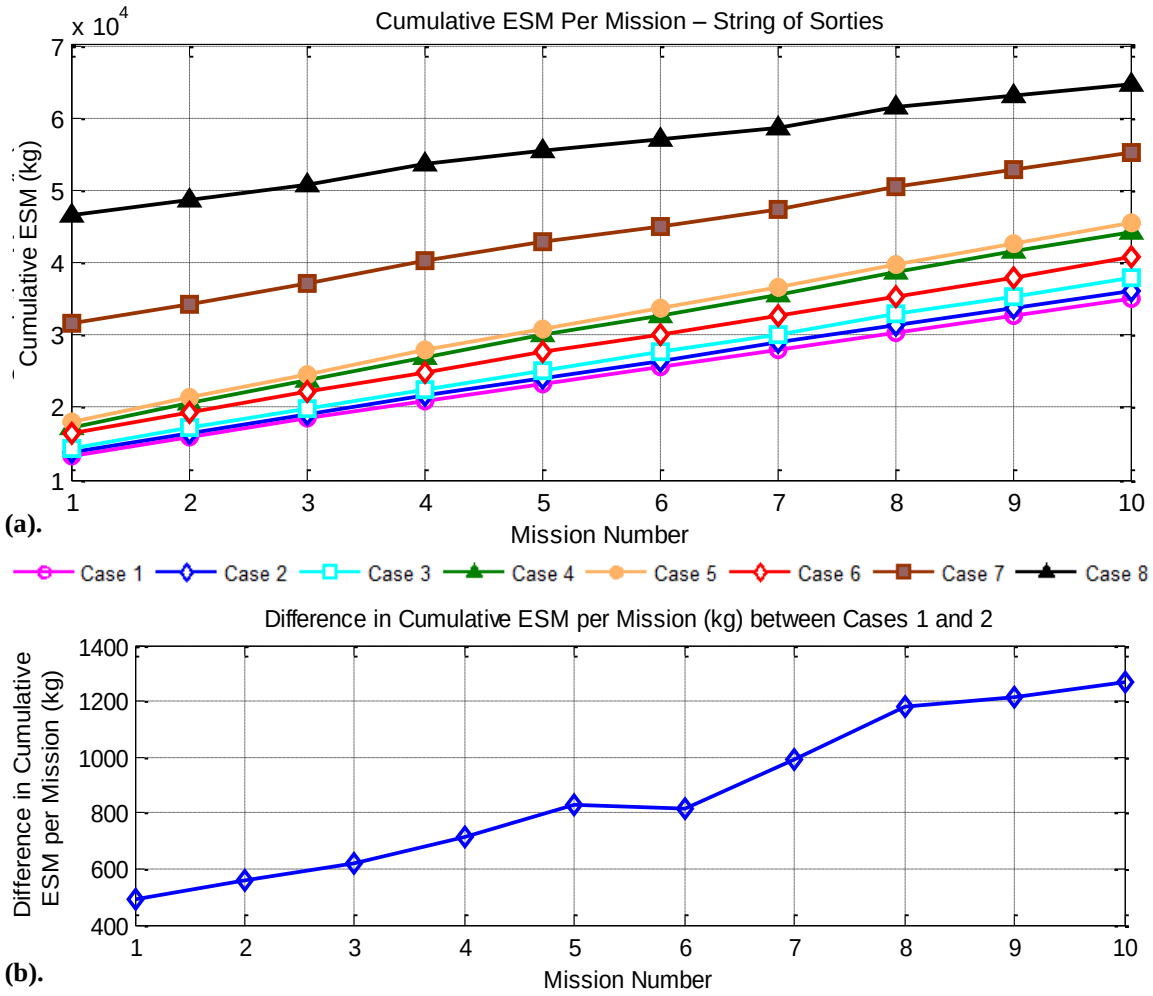

Figure 6-26: (a). Cumulative ESM per Mission per Architectural Case (b). Difference in ESM between the top two ranked ECLS architectures (Case 1 and Case 2)

From Figure 6-26(a), we find that Case 1 (open loop O_2 and water) marginally dominates all other architectures over the lifecycle of the campaign in terms of minimizing lifecycle resupply mass. Further, from Figure 6-26(b), we observe that at the first mission, Case 1 has a 490kg lower mass requirement compared to Case 2, the next most mass efficient architecture, as indicated in Figure 6-26(b). By the tenth mission, this mass saving grows to 1265kg.

A further investigation revealed that the primary reason for this result is the dominance of the MAV propellant demands observed in Figure 6-20(a). Here, it was found that the marginal increase in ECLS consumables requirements between Case 1 and Case 5 (the architecture with the highest level of resource recycling and the minimum level of consumables demand) is small relative to the total consumables demand across all architectures. Because the MAV demand for propellant is such a strong driver of total consumables requirements, and because ISRU systems are already required to satisfy this propellant demand, the marginal increase in ISRU system mass required to generate the additional ECLS consumables load of Case 1 is significantly lower than the additional ECLS mass required to recycle resources and lower its consumables demand. That is, on the surface of Mars, depending on the availability of local resources and the difficulty of its extraction, it may be more efficient to source consumables from ISRU systems, than by recycling consumables with additional ECLS technologies delivered from Earth. Table 6.8 summarizes the unit costs and efficiencies of consumables acquisition observed here.

This table is divided into two sections that describe the efficiencies and costs of additional ECLS and ISRU hardware required to generate a unit of ECLS consumable. The top half of this table summarizes the ECLS consumables demands of the first five of the architecture cases examined in this case study, as well as the effect of the addition of recycling systems on the cost of reducing this demand. Here, only the first five architecture cases were examined as Case 6 (4.5% food) shares the same ECLS architecture as Case 3, and Cases 7 (50% food) and 8 (100%) are strongly dominated due to the high infrastructure costs associated with large scale biomass production (see discussion above and Figure 6-25). In this section of Table 6.8, Row A corresponds to the total ECLS consumables demand as calculated by the HabNet Habitation Module, Row B lists the savings in ECLS consumables achieved through the progressive addition of ECLS resource recycling technologies, Row C lists the mass of the ECLS hardware and spares required to achieve the consumables savings listed in Row B, and Rows D and E summarize the efficiencies and costs of the addition of progressive levels of recycling (in a similar manner to the analysis performed in Section 4.4.5 and listed in Table 4.9).

Table 6.8: Summary of the Incremental Costs and Efficiencies of Adding ECLS and ISRU Systems to obtain required ECLS Consumables (with equations added in parentheses wherever applicable)

		Parameter	Case 1	Case 2	Case 3	Case 4	Case 5
ECLS Demands	**A**	**ECLS Consumables Demand** (excl. food) (kg)	12405	7587	5314	5353	5262
	B	**ECLS Consumables Savings from Recycling** (Row A of Case 1 – Row A of Case i) (kg)	0	4819	7091	7052	7143
	C	**Additional ECLS Hardware + Spares needed for Recycling*** (kg)	0	1360	2279	4392	4911
	D	**Efficiency of ECLS Recycling** (Row B / Row C) (kg consumables saved / kg ECLS Hardware)	N/A	**3.54**	**3.11**	**1.61**	**1.45**
	E	**Cost of ECLS Recycling** (Row C / Row B) (kg of ECLS Hardware Required / kg of ECLS consumables saved)	N/A	**0.28**	**0.32**	**0.62**	**0.69**
ISRU Demands	**F**	**Fixed MAV Propellant Demand** (kg)	29706	29706	29706	29706	29706
	G	**Fixed Mass of ISRU System Required for MAV Propellant Generation*** (kg)	1214	1214	1214	1214	1214
	H	**ECLS Consumables Demand Sourced from ISRU** (identical to the ECLS Consumables Demand – Row A) (kg)	12405	7587	5314	5353	5262
	I	**Total Mass of ISRU System Required for ECLS + MAV Propellant Generation*** (kg)	1662	1526	1439	1508	1644
	J	**Marginal ISRU Hardware + Spares Mass Required to Satisfy ECLS Demand** (Row I – Row G) (kg)	448	312	225	294	430
	K	**Efficiency of Marginal ISRU ECLS Consumables Generation** (Row H / Row J) (kg ECLS Consumables Generated / kg of additional ISRU needed)	**23.3**	**18.0**	**14.8**	**11.5**	**7.6**
	L	**Marginal Cost of ISRU Systems Required to Generate ECLS Consumables from ISRU** (Row J / Row H) (kg of additional ISRU Hardware Required / kg of ISRU-derived ECLS Consumable Generated)	**0.04**	**0.06**	**0.07**	**0.09**	**0.13**

*Includes emplaced hardware and spares required for the first mission only

Similarly, the second half of this table summarizes the masses of the ISRU systems required to generate both MAV propellant and ECLS consumables demands, as well as the costs and efficiencies of the systems required to generate these demands. Here, Rows F and G summarize the fixed propellant demands of the MAV, and the fixed mass of the ISRU system required to generate these demands (which was calculated separately using the HabNet ISRU Module). Row H lists the ECLS consumables demands over each 540 day sortie mission that need to be sourced from ISRU (the values in this row are identical to those listed in Row A, since all outstanding ECLS demands are expected to be satisfied by local ISRU – as specified in Table 6.2). Row I lists the total ISRU system mass required for each architecture case, as

was determined by the HabNet ISRU Module, while Row J summarizes the marginal mass of ISRU systems required to produce the required ECLS consumables. These values represent the ISRU mass required to be delivered to the Martian surface in addition to the mass that would have already been emplaced to support MAV propellant production operations. Finally, Rows K and L summarize the efficiencies and costs of generating ECLS consumables from these additional ISRU systems.

With regards to the lifecycle emplacement and resupply mass-optimality of architecture Case 1 discussed earlier, Rows E and L in Table 6.8 are of most interest. In Row E, we observe that for Cases 2 to 5, each kilogram of ECLS consumables saved through resource recycling costs between 0.28 and 0.69kg of additional ECLS hardware. Even with these savings in ECLS consumables however, additional costs are incurred in the form of the additional ISRU technologies that are needed to fill the deficit in ECLS consumables resulting from incomplete ECLS resource closure. These costs range from 0.06 to 0.13kg of additional ISRU hardware for every kilogram of ECLS consumables derived from ISRU.

Contrastingly, for the open loop architecture represented by Case 1, all ECLS consumables acquisition costs are attributed entirely to ISRU, for a lower unit cost of 0.04kg of additional ISRU hardware per kilogram of ISRU-derived ECLS consumable. The fact that Case 1 incurs a single resource acquisition cost at a lower rate than Cases 2 to 5, results in it having a lower emplacement and lifecycle resupply mass requirement.

Here, the approximately five-fold difference in the costs of ECLS recycling (Row E of Table 6.8) as compared to the costs of ISRU ECLS consumable production (Row L of Table 6.8) arise from the fact that the dominance of the MAV propellant demands on the total consumables budget means that the majority of the mass of the ISRU system is attributed to propellant production. Thus, any additional requirement for ECLS consumables production requires a relatively small addition in ISRU system mass (as can be seen by comparing Rows G and J in Table 6.8).

This phenomenon was observed earlier in Section 6.4.2, where it was found that the driving demand of MAV propellant production on ISRU system sizing meant that the only major influence of variations in ECLS demands across Cases 1 to 6 (those with zero to low levels of food production) was variations in the mass of the water extractor (see Table 6.7). As was discussed in Section 6.4.2, all other ISRU systems had a largely constant mass across all architecture cases due to the consistently high demand for methane. This constant high demand for methane in turn drives the mass of the supporting ISRU systems towards the same size.

6.4.5 Sensitivity of the Mass-Optimal Architecture to Variations in ISRU Hardware Mass and Reliability

One of the largest sources of data uncertainty in this case study is related to the reliability values assumed for the ISRU technologies modeled. As was described in Section 6.4.3 and mentioned in Table 6.2, the general infancy of ISRU technologies coupled with their low level of operational experience meant that failure rates of analogous ECLS hardware had to be adopted for the ISRU systems modeled. In scenarios where a suitable analogous system could not be found, an MTBF value of 500000h was assumed.

Given this uncertainty, coupled with the fact that hardware reliability has been known to degrade significantly when operated within dusty environments (see Section 2.3.3), we repeat the above architectural analysis with ISRU hardware reliabilities that are an order of magnitude less than those originally assumed. This supplementary analysis is intended to evaluate the robustness of the above finding that an open-loop ECLS architecture that is reliant on a surface ISRU system is the most mass-efficient architecture of the cases examined.

This analysis was performed by updating the ISRU reliability data in the MELs fed to the HabNet Supportability Module (see Appendix J.2), and rerunning the analyses performed in Sections 6.4.3 and 6.4.4. Figure 6-27 presents the cumulative ESM per mission data obtained from this analysis.

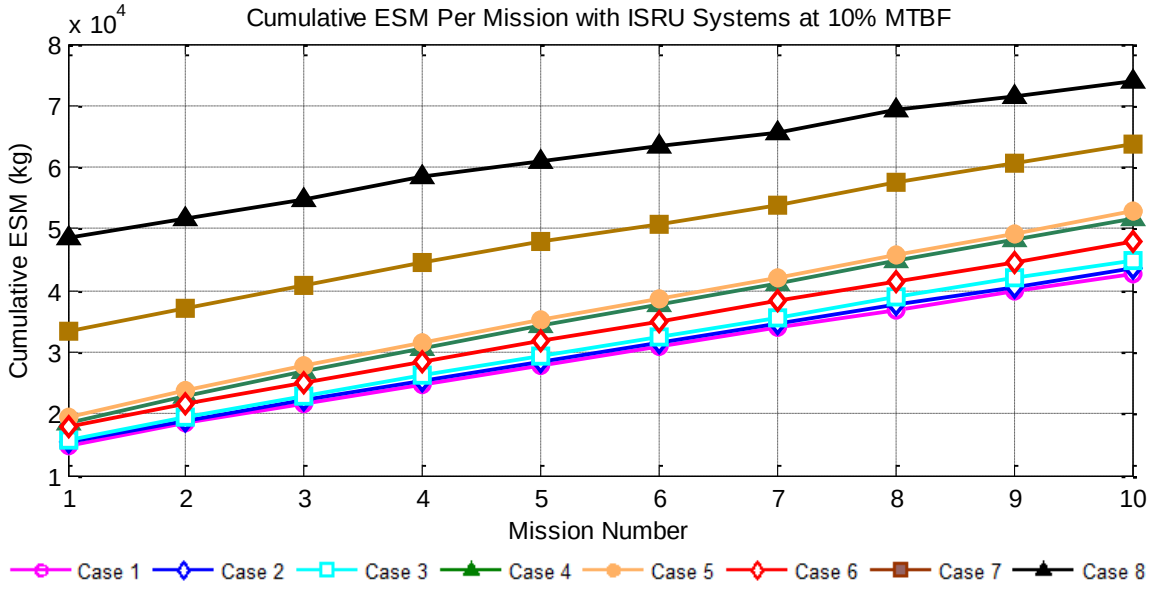

Figure 6-27: Cumulative ESM per Mission per Architectural Case with ISRU Technologies at 10% lower reliability levels

Here, we observe that even with an order of magnitude reduction in ISRU hardware reliability, the same relative ranking of architectures by mass is obtained, with the open loop ECLS architecture represented by Case 1 still remaining as the mass-optimal option. This indicates that even at this degraded level of reliability, the marginal cost of the ISRU systems required to produce the required ECLS consumables is still lower than the cost of additional ECLS technologies required to obtain substantial savings in ECLS consumables. Here, the main effect of reducing ISRU reliability was found to be the increase in emplaced and resupply mass for all architectures over all missions. In all cases, this is caused by the increase in ISRU spare parts required to compensate for lower hardware reliability.

In light of this observation, we further examine the robustness of our findings by examining its sensitivity to ISRU sizing predictions. As was discussed in Section 3.4.2 and Appendix F, the ISRU sizing models integrated into the HabNet ISRU module are based on a combination of physics-based equations and sizing by analogy to similar ISRU systems. To compensate for any discrepancies observed between the estimates made by the sizing models and those published in the literature, correction factors were derived and implemented. As can be seen in the model comparisons presented in Appendix F, the discrepancies in sizing estimates between those published in the literature and those made by HabNet can range from a few percentage points, to a factor of six or more. Of the ISRU technologies considered in this case study, the water electrolyzer, Sabatier reactor, and atmospheric processor were observed to have the highest level of uncertainty in their hardware mass. As a result, a second sensitivity analysis was performed where the original architecture analysis was rerun with these three ISRU systems having ten times their originally estimated mass, and all ISRU systems having 10% of their originally estimated reliability. This scenario is considered to be a significantly more challenging case from the perspective of ISRU efficiency, than the case performed above. As was performed above, we update the MELs of each architectural case with these updated constraints, and recalculate the corresponding cumulative mass per mission data. Figure 6-28 summarizes the results obtained from this second sensitivity analysis case.

From this figure, we observe that over the first 9 missions, the same relative architecture rankings remain, suggesting that even with the enforced increases in mass, the marginal cost of sourcing ECLS consumables from ISRU is lower than that of reducing consumables demands through ECLS recycling technologies. Interestingly, however, by the tenth mission of the campaign, the cumulative mass of Case 2 drops slightly beneath that of Case 1 (see Figure 6-28(b)). This result indicates that under the ISRU mass and reliability assumptions

made here, it takes ten sortie missions before the impact of the ECLS consumables savings obtained from the introduction of the WPA in Case 2 exceeds the efficiencies inherent in generating ECLS consumables with ISRU. Here, the decision to include a WPA within the habitat architecture would be driven by the duration of the campaign, and lifecycle mass savings that would be expected relative to the cost of the development and sustainment of the operations of the WPA.

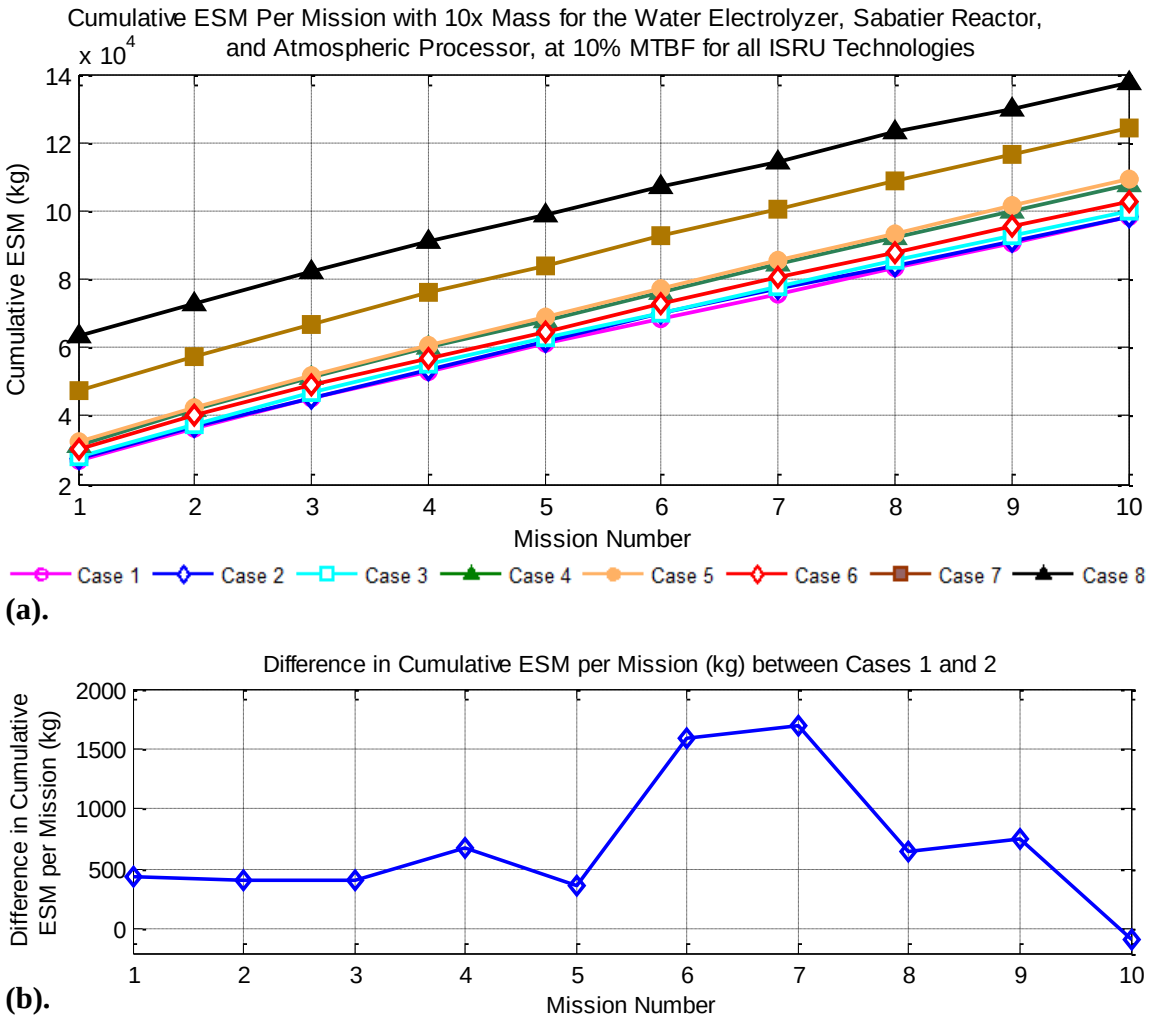

Figure 6-28: Cumulative ESM per Mission per Architectural Case with ISRU Technologies at 10% lower reliability levels and the Water Electrolyzer, Sabatier Reactor, and Atmospheric Processor at 10 times their originally estimated system mass (a). Comparison between all eight architecture cases (b). Difference in cumulative ESM per mission between Cases 1 and 2

The result of this analysis indicates that the relative rankings amongst the ECLS architecture cases examined here are likely to be highly sensitive to the masses of the ISRU systems. Thus, as a final test of the robustness of the lifecycle mass-optimality of Case 1, we

perform a final sensitivity analysis where we simultaneously increase the mass of all ISRU technologies by a factor of ten, and reduce their reliabilities by a factor of ten. Figure 6-29 presents the results of this final sensitivity analysis.

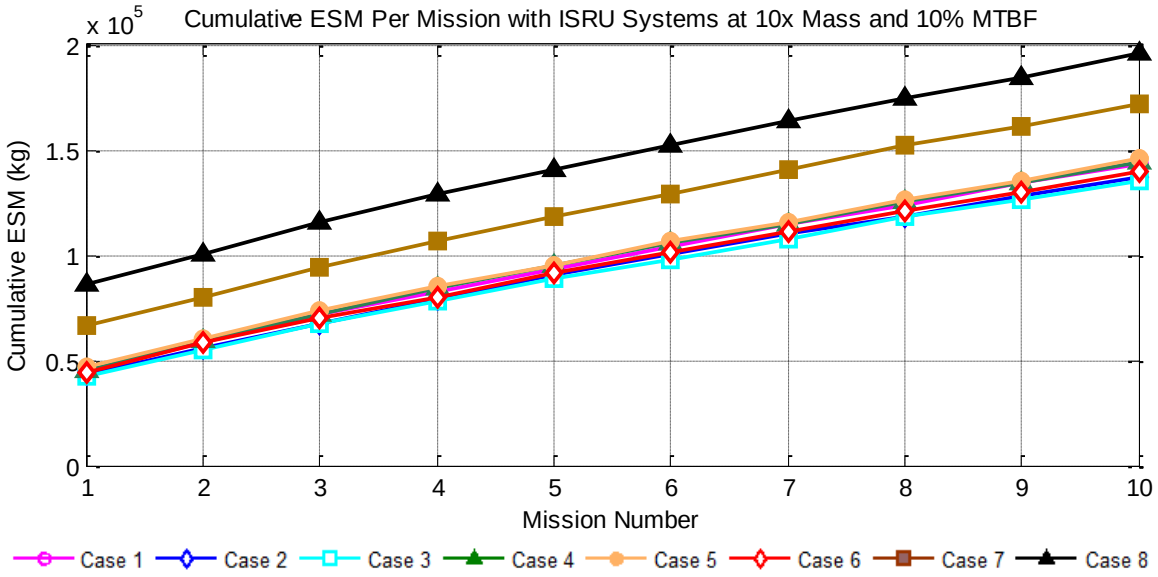

Figure 6-29: Cumulative ESM per Mission per Architectural Case with ISRU Technologies at 10% lower reliability levels and 10 times their originally estimated system mass

Contrasting to the previously observed trends, Figure 6-29 indicates that under the severely underperforming scenario where all ISRU technologies are 10 times heavier and have one tenth of their original reliabilities, the open loop ECLS architecture of Case 1 is no longer the mass optimal. Instead, the mass-optimal architecture is now Case 3 (WPA+UPA) followed by Case 2 (WPA). Interestingly, the next ranking architecture after Case 2 is Case 6, which includes the 4.5% level of crop growth combined with a Case 3-like ECLS architecture. These results imply that at these low levels of ISRU performance, ECLS recycling technologies become a better option for reducing lifecycle requirements, as compared to increasing the capacity of ISRU. We note however, that the progressive degradation of ISRU capabilities in these sensitivity analyses has resulted in the corresponding increase in total mission mass across all cases. In the original analysis, the minimum architecture exhibited an initial emplacement mass of 13280kg. As the ISRU reliability level was degraded and the ISRU system masses were progressively increased, this minimum mass increased first to 14930kg, then to 26900kg, and finally to 42080kg. This result indicates that the mass and reliability of ISRU systems are a

significant driver of architecture mass. This is primarily due to the dominance of MAV propellant demands over total consumables demands, which in turn dictates the majority of the minimum ISRU system mass that needs to be emplaced on the Martian surface.

6.5 Lifecycle Impacts of Mission Campaign Scenario 2: Minimum Continuous Presence

Having analyzed the impact of different ECLS architectures on the lifecycle cost of the "String of Sorties" Mission Scenario in the previous section, we now perform the same comparative architecture analysis on the "Minimum Continuous Presence" mission scenario, where each crew spends 44 months on the Martian surface such that a minimum overlap of 540 days (18 months) occurs between successive crews. This overlap enables a minimum level of continuous human presence to exist on the surface of Mars, thereby satisfying the goals set forth in the 2010 and 2015 NASA Authorization Acts (see Section 1.1).

As shown in Figure 6-30, this mission scenario results in the periodic doubling of the surface population, as handover occurs at the Mars surface base. In fact, after the first four person crew spends the first 26 months of the campaign on the Martian surface, the surface habitat is occupied by two crew increments for the majority of the time.

To perform this case study, we discretize this mission scenario into 26 month increments, simulate components of these increments based on their individual crew population profiles, and piece together the result to assess the system behavior over the mission campaign. Since a resupply mission and a new crew arrives at the surface base every 26 months, each 26-month increment can be considered as a period of time by which a stock of supplies delivered from Earth must sustain the crew.

As can be seen in Figure 6-30(a), the first of these increments corresponds to a 4-crew 26-month mission. After this first increment, all subsequent increments follow the same pattern of initially beginning with an 8-crew 540-day mission, and concluding with a 4-crew 240-day (8 month) mission, as shown in Figure 6-30(b). Here, this step decline in crew population in these subsequent 26-month increments corresponds to the departure of the previous crew from the Mars Surface Field Station.

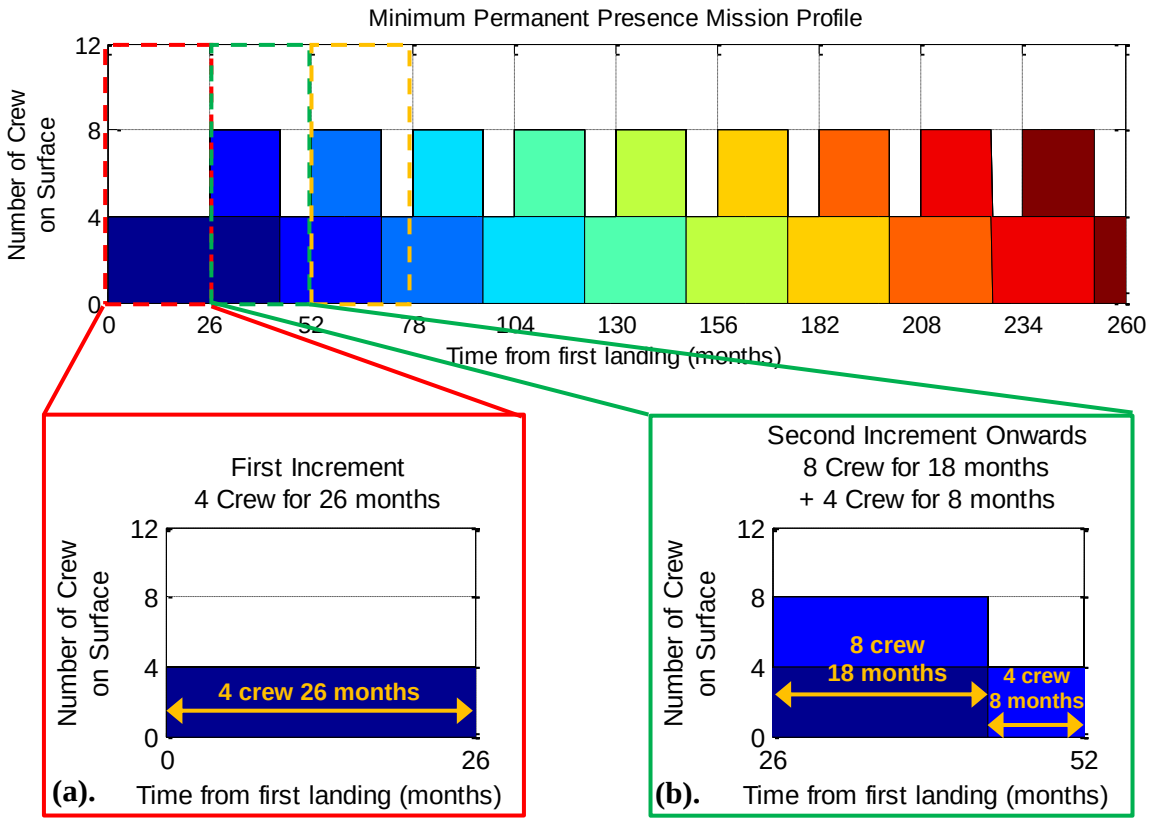

Figure 6-30: Crew Population profile for the Minimum Continuous Presence Mission Scenario (a). Crew profile for the first 26-month increment of the campaign, consisting of four crewmembers remaining on the surface for 26 months (b). 26-month increments that repeat continuously from the arrival of the second crew onwards. Here, a total of eight crewmembers are present at the surface habitat for the first 18 months, prior to the departure of the previous four-person crew. After this period, the population drops to 4 people until the next crew arrives, 8 months later

As was summarized in Table 6.2 and performed for the String of Sorties mission scenario in Section 6.4, this case study aims to evaluate and compare the emplacement and lifecycle resupply costs of different ECLS and food growth architectures when applied to this mission context. As has been previously described in Section 6.4, these architectures are:

- Case 1: Open Loop Water and Oxygen + Stored Food
- Case 2: WPA + Stored Food
- Case 3: WPA + UPA + Stored Food
- Case 4: WPA + UPA + OGA + Stored Food
- Case 5: WPA + UPA + OGA + CRS + Stored Food
- Case 6: WPA + UPA + 4.5% Locally Grown Food (in a 50m^3 BPC)

- Case 7: WPA + UPA + 50% Locally Grown Food (in a 500m^3 BPC with a CO_2 injector and ORA)
- Case 8: WPA + UPA + 100% Locally Grown Food (in a 1000m^3 BPC with a CO_2 injector and ORA)

To account for the transition from an initial four person crew to an eight person crew after the first 26 months of the campaign, we assume that the first crew lives in the same habitat as that described in Section 6.2 and analyzed in the String of Sorties case study performed in Section 6.4. At the beginning of the second 26-month increment, an additional four crewmembers land on the Martian surface, along with additional habitat modules to expand the living volume of the surface habitat. These modules are identical copies of the Lab, Loft, Suitlock, and Pressurized Logistics Modules described in Figure 6-6 and summarized in Table 6.1, and are added to the baseline habitat in the manner depicted in Figure 6-31. This transition from a four person habitat to an eight person habitat capable of sustaining continuous human presence can be considered as one avenue for transitioning from a String of Sorties mission scenario to one with Minimum Continuous Presence.

Here, we assume that with the exception of the additional Common Cabin Air Assemblies (CCAAs) and Pressure Control Assemblies (PCAs) installed for atmospheric pressure and composition control in each newly added module, the same life support system that sustains the first four-person crew is capable of sustaining eight-person crews on subsequent 26-month increments. This assumption was verified with the HabNet Habitation Module, via the successful simulation of eight crew living within the expanded habitat under different ECLS architectures.

For architectural cases consisting of food production, we assume that the first four-person crew grows food in a BPC sized to produce food at the levels specified for that crew. When the second four-person crew arrives, an additional identical BPC is installed to the first BPC, thereby doubling the total food production capacity. Since this event is accompanied by a doubling of the crew population, the addition of this second BPC to the habitat architecture effectively maintains the pre-specified level of food production. As a result, the steady state configuration of the habitat consists of BPCs that are double the volume of those analyzed in the String of Sorties case study. This is indicated by the BPC volume values listed above, for architecture Cases 6 to 8.

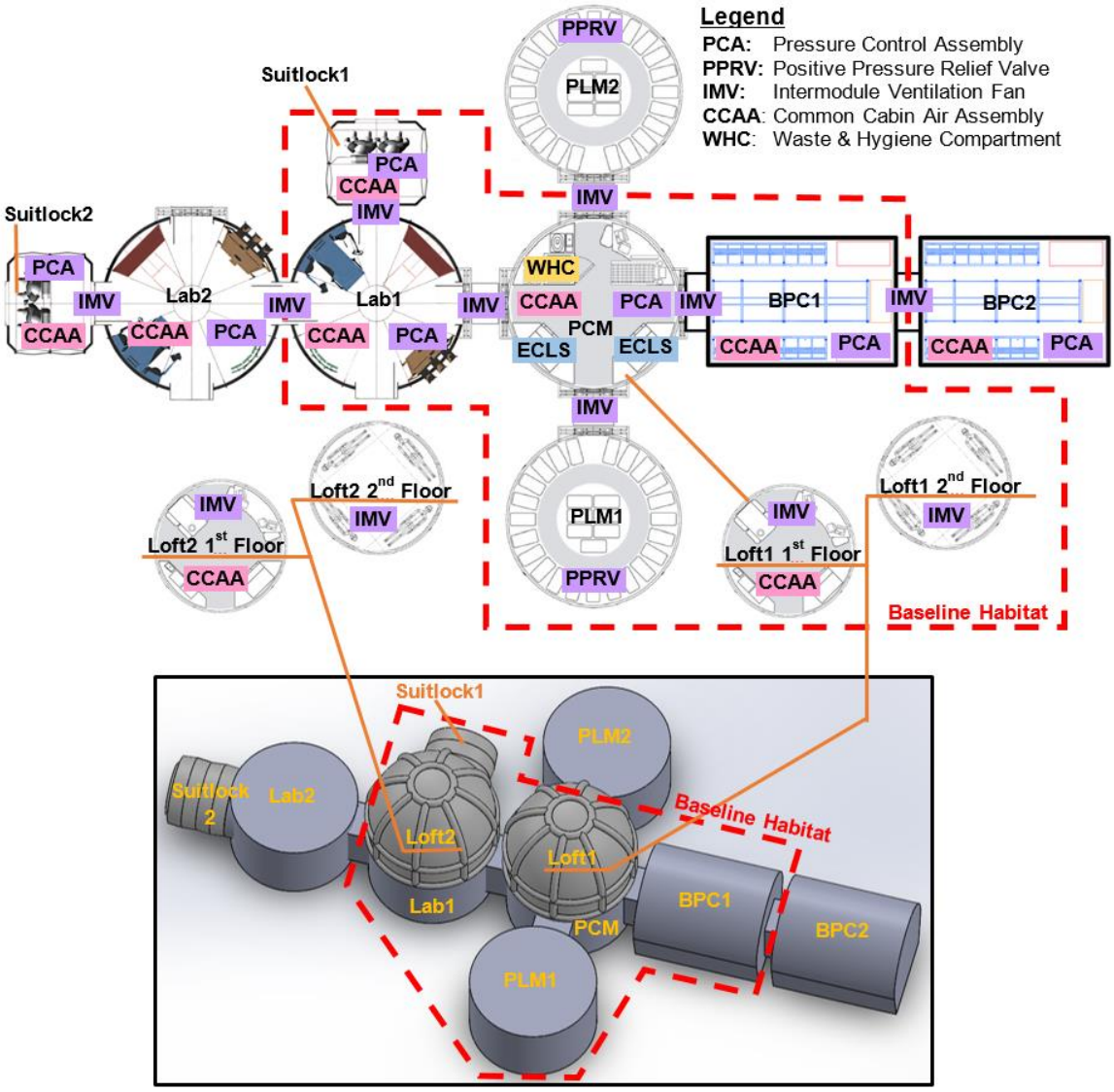

Figure 6-31: Floor plan of the 8-crew expanded version of the Mars Surface Field Station assessed in this case study. Note that the first and second floors of Loft1 and Loft2 are depicted at a smaller scale than the other modules shown here. Here, the acronyms used to describe the modules are the: Pressurized Core Module (PCM), Pressurized Logistics Module 1 and 2 (PLM1 and PLM2), and the Biomass Production Chamber 1 and 2 (BPC1 and BPC2)

With this habitation architecture now defined, we now analyze the emplacement and lifecycle impacts of each of the eight ECLS architectural cases listed above using the same approach employed in the String of Sorties case study performed earlier. This involves analyzing each architecture with each of the four modules of HabNet, and aggregating the results to perform a campaign level comparative analysis. The results of each of these analyses are presented in the following sections.

6.5.1 Habitation Module Results

As a first step in this comparative architecture analysis, the HabNet Habitation Module was used to dynamically simulate the behavior of each architecture case to derive both their resource requirements and their system runtimes. Because the mission profile changes from the first 26-month increment to the second (see Figure 6-30), two separate analyses were performed for each architectural case. These include an analysis of the resource demands for the first 4-person 26-month increment (see Figure 6-30(a)), and an analysis of the second repeating 26-month increment, where the surface population drops from eight crewmembers to four after 18-months (see Figure 6-30(b)).

To estimate the resource demands of the second 26-month increment, a first simulation was performed with eight crew living in the expanded version of the habitat (see Figure 6-31) for the 540 days (18 months) that they would inhabit the surface base. Following this, a second simulation was performed of a four-person crew living at the surface base for 240 days (8 months). The resource demands calculated from both of these simulations were then combined to yield the total crew resource demands for this second 26-month increment. These resource demands were assumed to remain the same for all 26-month periods following the second.

In architecture cases where food production is included, it is assumed that after the second crew arrives and activates the BPC that accompanies them, the total surface base will have food production capacity for eight crew by the end of the second 26-month increment. Because the population drops to four people in the last third of this 26-month increment, the proportion of locally grown food available to sustain the remaining surface crew essentially doubles during the last 8 months of the second and subsequent 26-month increments. This increase in effective calories per crewmember is factored into this analysis, and results in a food resupply requirement that is less than that required to support a full eight-person crew over a 26-month increment.

In addition, it should be noted that during the startup phase of biomass production, additional prepackaged food is required to sustain the crew for the first 138 days prior to the first full set of crops reaches maturity (see Section 6.3.2). This additional demand for prepackaged food is accounted for in the first two 26-month increments, where a BPC is delivered and activated with the arrival of the first and second crews. The result of this is that for architecture cases with local food production, the requirement for prepackaged food

delivered from Earth increases over the first two 26-month increments, prior to dropping to a steady-state value for the remainder of the campaign.

The specific values associated with these, and other consumables demands, are summarized for the first two 26-month increments in Figure 6-32 below. The corresponding values plotted in these figures are listed in Table 6.9.

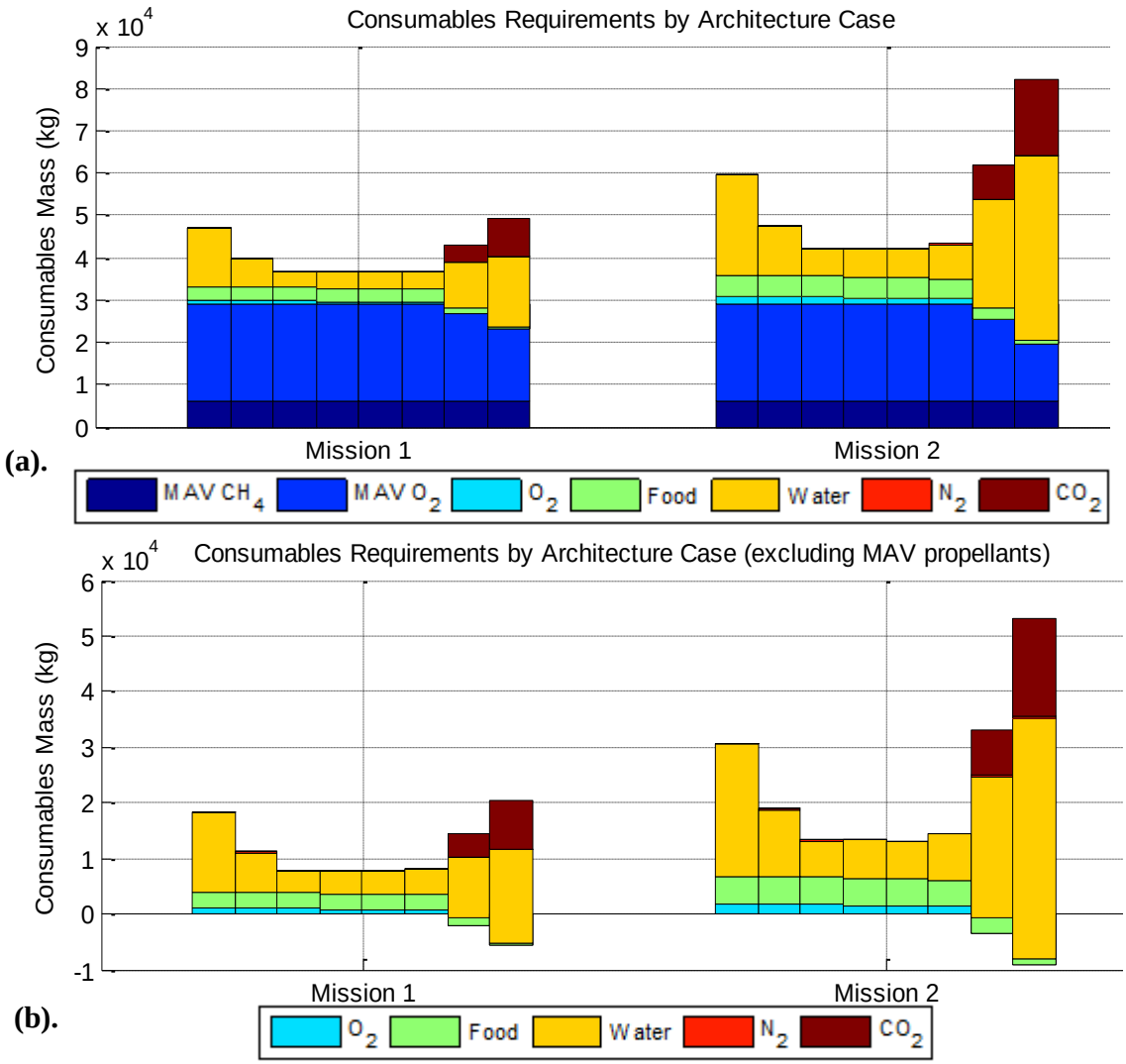

Figure 6-32: Consumables requirements for the first two 26-month increments (missions) for each of the eight architecture cases examined (a). All ECLS and MAV Consumables (b). Only ECLS Consumables

From Figure 6-32, we observe that the arrival of the second four-person crew causes the total consumables requirements of all architecture cases to increase from the first to the second mission. Within each of these missions, we observe similar trends to those found in the String

of Sorties case study described in Section 6.4.1. Specifically, we find that once again, the propellant demands for the MAV dominate the total consumables demands for all architecture cases (see Figure 6-32(a)). In addition, from Figure 6-32(b), we observe that the excess oxygen production resulting from high levels of food production in Cases 7 and 8 result in a negative oxygen demand, which offsets a portion of the MAV demand for oxygen.

With respect to the ECLS architectures that do not include food-production, a trend consistent with that found in the case studies performed in Sections 4.4 and 6.4.1 was found – that increasing levels of resource recycling result in lower overall consumables requirements, and that the largest impact on total system mass resulting from the introduction of recycling technology is the reduction in total water demand. This can be seen in the values listed in Table 6.9, where for the first five architectures, the largest variations occur in the column corresponding to total water demand.

Table 6.9: Consumables Requirements computed by the HabNet Habitation Module for the first two 26-month increments (indicated by the left and right sub-columns underneath each resource heading) for each ECLS Architecture Case. Cells with the same values are colored for the purposes of clarity. The consistency in values across these colored cells is similar to the observations made in the case studies performed in Sections 4.4 and 6.4.1

	O_2 (kg)		**N_2 (kg)**		**H_2O (kg)**		**CO_2 (kg)**		**Food (kg)**	
	1	**2**	**1**	**2**	**1**	**2**	**1**	**2**	**1**	**2**
Case 1 – Open Loop O_2 + H_2O	1121	1888	36	54	14123	23902	0	0	2907	4918
Case 2 – WPA	1121	1888	36	54	7078	12003	0	0	2907	4918
Case 3 – WPA + UPA	1121	1888	36	54	3714	6402	0	0	2907	4918
Case 4 – WPA + UPA + OGA	793	1399	43	60	4099	6967	0	0	2907	4918
Case 5 – WPA + UPA + OGA + CRS	793	1399	43	60	3962	6706	0	0	2907	4918
Case 6 – WPA + UPA + 4.5% Food	806	1381	39	53	4365	8275	0	0	2795	4706
Case 7 – WPA + UPA + ORA + 50% Food	-2252	-3603	73	111	10600	25499	4169	8343	1705	2910
Case 8 – WPA + UPA + ORA+ 100% Food	-5630	-9100	101	146	16622	43427	8844	17690	505	932

6.5.2 ISRU Module Results

In the previous section, we observed that the two initial missions of the Minimum Continuous Presence mission scenario result in two different sets of consumables demands, where the second set of demands grows by between 40 to 80% relative to the first. As can be seen in

Table 6.10, this results in two sets of resource generation requirements that need to be satisfied by the selected ISRU architecture. The fact that there are two sets of resource production requirements leads to the following key architectural question: should one ISRU system be emplaced to generate resources at the maximum productions rates expected to occur across all 26-month increments of the campaign? Or should a smaller ISRU system be initially deployed to support the first four-person crew over the first 26-month increment, and supplemented for the rest of the campaign with an additional ISRU system that is delivered with the second crew (in a similar manner to the BPC expansion strategy described above)?

To address this question, both sets of resource demands were input into the ISRU Module for each architectural case, so that the difference in mass between the systems required to support each phase of the mission could be computed and used to evaluate whether or not one or two systems should be deployed.

Table 6.10: Resource production rates required for each ECLS architecture case for the first two 26-month increments (indicated by the left and right sub-columns underneath each resource heading), based on peak resource usage rate. Here, the rates for MAV propellant production are selected such that all MAV propellant can be generated within 540 days. Cells with the same values are colored for the purposes of clarity.

	O_2 (mol/h)		**N_2 (mol/h)**		**H_2O (L/h)**		**CO_2 (molh/h)**		**CH_4 (mol/h)**	
	1	**2**	**1**	**2**	**1**	**2**	**1**	**2**	**1**	**2**
Case 1 – Open Loop O_2 + H_2O	56.6	58.5	0.07	0.11	0.74	1.49	0	0	33.7	33.7
Case 2 – WPA	56.6	58.5	0.07	0.11	0.37	0.75	0	0	33.7	33.7
Case 3 – WPA + UPA	56.6	58.5	0.07	0.11	0.20	0.40	0	0	33.7	33.7
Case 4 – WPA + UPA + OGA	56.1	57.5	0.08	0.13	0.22	0.43	0	0	33.7	33.7
Case 5 – WPA + UPA + OGA + CRS	56.1	57.5	0.08	0.13	0.21	0.42	0	0	33.7	33.7
Case 6 – WPA + UPA + 4.5% Food	56.1	57.5	0.07	0.12	0.23	0.50	0	0	33.7	33.7
Case 7 – WPA + UPA + ORA + 50% Food	51.1	47.6	0.14	0.24	0.56	1.39	5.84	11.6	33.7	33.7
Case 8 – WPA + UPA + ORA+ 100% Food	45.5	36.8	0.19	0.33	0.87	2.32	11.8	23.4	33.7	33.7

Through this analysis, the same archetypical ISRU architecture as that found in Section 6.4.2 emerged for all architectural cases. This architecture was presented in Figure 6-22, and is shown again below. As can be seen in this figure, the baseline ISRU architecture revolves around a Sabatier reactor that produces methane for the MAV. To generate the reactants required for the Sabatier reaction, this system is supported by a water electrolyzer, CO_2 cryocooler, and water extractor. In addition, an atmospheric processor is installed to generate nitrogen gas for cabin pressure makeup.

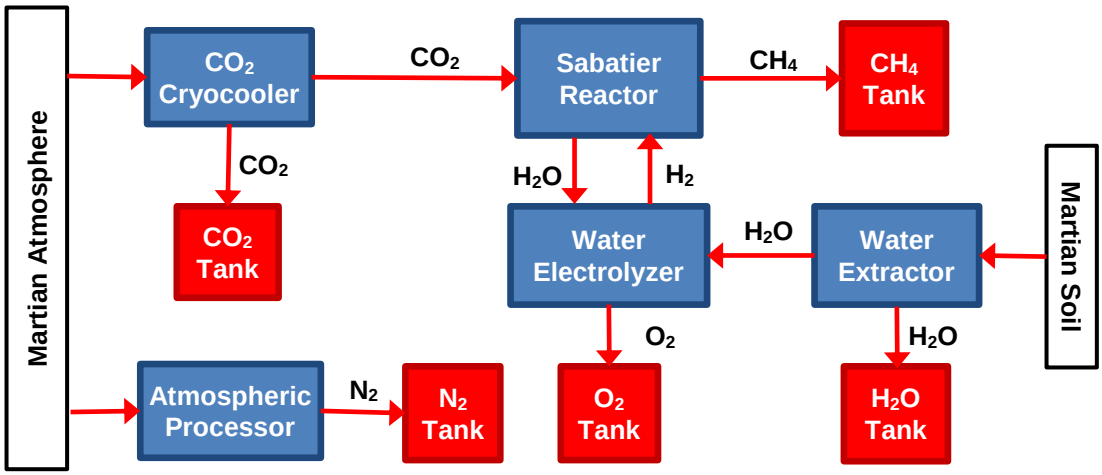

Figure 6-33: Archetypical ISRU Architecture predicted by the HabNet ISRU Module for all ECLS Architectural Cases examined

Table 6.11 summarizes the masses of the ISRU architectures sized to support the two sets of ISRU production rates listed in Table 6.10. Here, we observe that across both sets of requirements and across all architecture cases, the resultant ISRU architecture consists of largely the same CO_2 cryocooler, water electrolyzer, Sabatier reactor, and atmospheric processor technologies. As was discussed in Section 6.4.2, this commonality across the range of ECLS architectures and increment populations explored is due to the driving demand for MAV propellant that is consistent in all cases. More specifically, the dominant requirement for methane largely fixes the size of all of its required supporting systems, while the dominant requirement for MAV oxidizer directly drives the rate at which electrolysis feedwater needs to be extracted, and thus the minimum mass of the water electrolyzer and water extractor systems.

Summing the masses of each of the components listed in Table 6.11 for each ISRU architecture and for each of the two 26-month increments, we find that the total ISRU mass required for the second increment (consisting of eight crew for 18 months followed by four

crew for 8 months) ranges from being 9-25% larger than that required for the first increment of architecture Cases 1 to 6, and 33-50% larger than the first increment of Cases 7 and 8, where larger levels of local food production are involved.

Table 6.11: ISRU system mass for each ECLS architecture case for the first two 26-month increments (indicated by the left and right sub-columns underneath each resource heading). Cells with the same values are colored for the purposes of clarity.

	Water Extractor (kg)		**CO_2 Cryo-cooler (kg)**		**Water Electro-lyzer (kg)**		**Sabatier Reactor (kg)**		**Atm. Process-or (kg)**	
	1	**2**	**1**	**2**	**1**	**2**	**1**	**2**	**1**	**2**
Case 1 - Open Loop O2 + H2O	431	592	153	153	70	70	22	22	26	39
Case 2 - WPA	351	432	153	153	70	70	22	22	26	39
Case 3 - WPA + UPA	314	357	153	153	70	70	22	22	26	39
Case 4 - WPA + UPA + OGA	318	364	153	153	70	70	22	22	30	43
Case 5 - WPA + UPA + OGA + CRS	316	361	153	153	70	70	22	22	30	43
Case 6 – WPA + UPA + 4.5% Food	320	378	153	153	70	70	22	22	28	41
Case 7 – WPA + UPA + ORA + 50% Food	391	572	179	205	70	70	22	22	46	77
Case 8 – WPA + UPA + ORA+ 100% Food	459	775	206	259	70	70	22	22	61	101

These values indicate that for a relatively small increase in mass of the four-person 26-month ISRU system, an ISRU system capable of sustaining the larger population of the second 26-month increment can be obtained. This suggests that the most efficient ISRU deployment option is to deliver an ISRU system sized for the second increment with the first crew. This is true even for Cases 7 and 8, since the larger ISRU architecture essentially enables double the rate of food production for substantially less than double the ISRU system mass.

As a result of this finding, we select the ISRU architecture sized for the second increment of each ECLS case (the systems corresponding to the columns labeled “2” in Table 6.11) for the remainder of this analysis. Figure 6-34 graphically depicts the relative masses of this subset of ECLS architectures, along with the contributions of each individual technology. As was observed earlier, this figure shows that the water extractor is the source of the most mass, as well as fluctuations in total system mass, amongst all of the ISRU technologies examined. Interestingly, the trends observed here are also the same as those observed in the ISRU analysis for the String of Sorties mission scenario performed in Section 6.4.2.

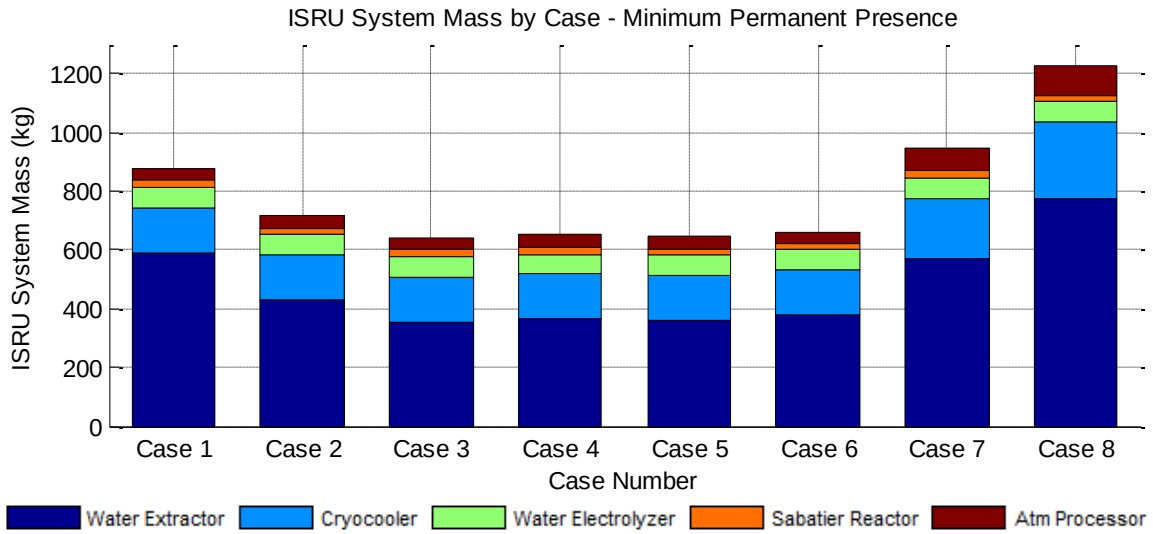

Figure 6-34: Comparison of ISRU system masses across the eight ECLS architecture cases examined in the Minimum Continuous Presence mission scenario

6.5.3 Supportability Module Results

With the ECLS and ISRU technologies and deployment sequences established for each architectural case in the previous analyses, we now compute the corresponding lifecycle spare parts requirements using the HabNet Supportability Module. Here, we adopt the same ECLS and ISRU component reliability and life limit assumptions as those employed in the String of Sorties case study (see Table 6.2) to predict the spare parts requirements over the first 11 missions of the campaign. This set of missions includes the first four-crew 26-month mission, followed by 10 copies of the second 26-month increment involving the reduction in the surface population from eight to four at month 18. Figure 6-35 presents the results of this analysis for each of the eight ECLS architectures evaluated.

Similar to the equivalent analysis performed for the String of Sorties case (see Section 6.4.3), we observe an initial spike in spare parts requirements in Figure 6-35, followed a pseudo-steady state demand in spare parts over subsequent missions of the campaign. As was previously mentioned, this initial spike is due to the requirement to establish an initial pool of spare parts in the first mission, in order to support operations over subsequent missions such that the probability of having sufficient spares meets the target probability threshold of 0.999. Here, the drop in spare parts requirements between the first and second missions is less distinct than that found in the String of Sorties scenario (see Figure 6-24 in Section 6.4.3) because new hardware is also being emplaced in the second mission (namely new CCAAs that accompany

the additional modules delivered to expand the surface habitat, and the additional crop lighting systems that accompany the expansion of the BPC in Cases 7 and 8). This means that a new pool of spare parts is also required in the second mission to support these newly installed components. After the second mission, sporadic spikes in spare parts requirements occur for Cases 7 and 8, as was also observed in the spare parts demand calculated for the String of Sorties mission scenario (see Figure 6-24). The frequency of these spikes is higher in this scenario however, due to the out-of-phase deployment of the first and second batch of plant lighting systems that enabled the expansion of the BPC capacity on the second mission. More specifically, after the life limit of the set of grow lights that was deployed with the first crew is exceeded, a new set are required (approximately two to three missions later). Because an additional set of lights was deployed with the second crew, these second set of lights exceed their life limits on the mission after the first set were replaced. As this trend cycles over time, the inherently high number of lights that need to be replaced for Cases 7 and 8 (approximately 69 at a time for Case 7 and approximately 137 at a time for Case 8) causes a higher frequency in spikes in spare parts requirements.

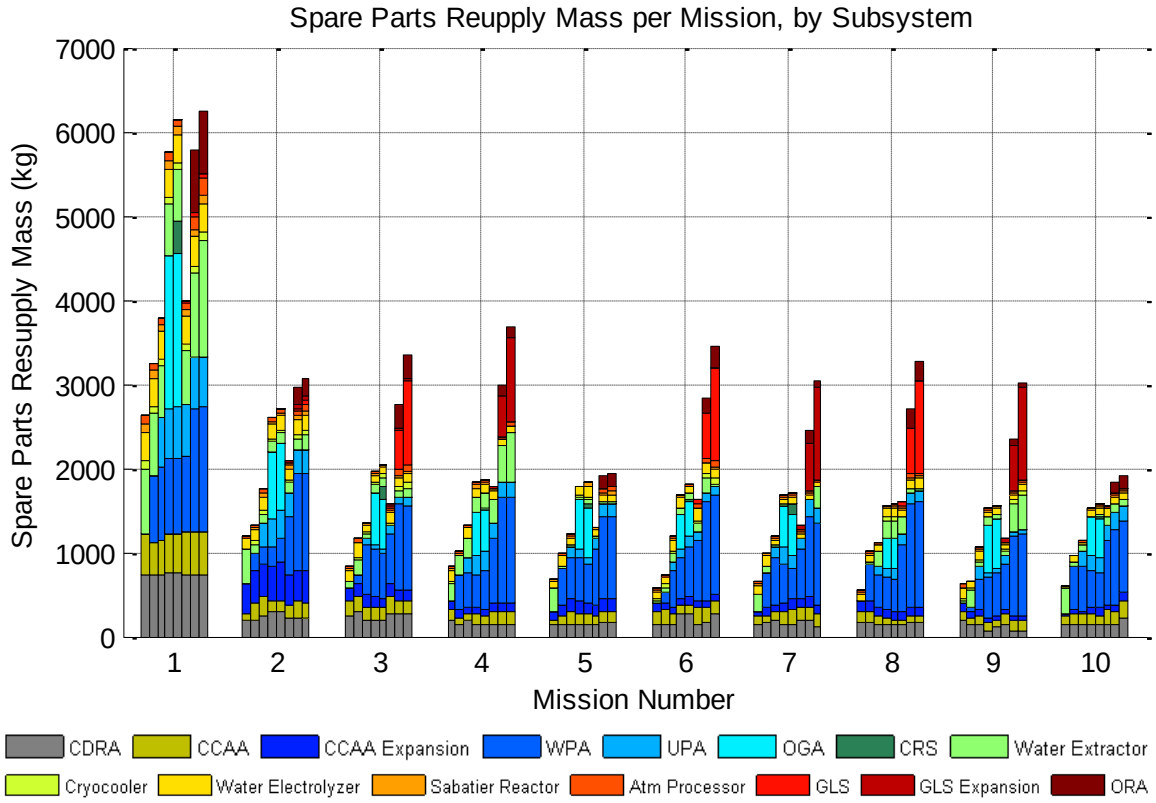

Figure 6-35: Spare Parts Resupply Requirements per Mission for each ECLS Architectural Case for the Minimum Continuous Presence mission scenario (each bar within each eight-bar cluster corresponds to an individual ECLS case)

With respect to the trends in spare parts demands amongst the individual architectural cases, we again find that increasing the level of recycling generally leads to a higher spare parts demand across the campaign. More specifically, the results of this analysis indicate that the introduction of the OGA leads to the highest spare parts demand, followed by the WPA and then the UPA. These spare parts demands are predominantly driven by heavy components with either short life limits and/or low reliabilities. For a further discussion on the specific components within these systems that exhibit these properties, see Sections 4.4.4 and 6.4.3.

6.5.4 Evaluation Module Results

Having quantified the mass of emplaced ECLS and ISRU hardware and their associated spare parts requirements in the previous three sections, we now integrate the impacts of the architecturally differentiating infrastructure requirements described in Section 6.3.3 to estimate the total lifecycle mass of the eight ECLS architectures examined for this Minimum Continuous Presence mission scenario. Figure 6-36 summarizes the results of this analysis, showing a more pronounced version of the trend observed in the spare parts analysis, where the first mission of the campaign exhibited a large peak in demand prior to this demand falling to a steady state value at a lower level.

Here, the inclusion of the impacts of power and thermal management systems have magnified the impacts of delivering a BPC to the surface of Mars, causing large spikes in equivalent system mass for the first two missions of Cases 7 and 8. In contrast to the String of Sorties mission scenario, spikes in mission mass occur in the first two missions in this campaign, due to the delivery of the BPC expansion module and its associated equipment in the second mission in order to support the doubling of the surface crew population. Interestingly however, these two architecture cases (Cases 7 and 8) have the lowest resupply requirements from the third mission onwards, since food becomes the largest driver of resupply after the first mission (see close-up in Figure 6-36).

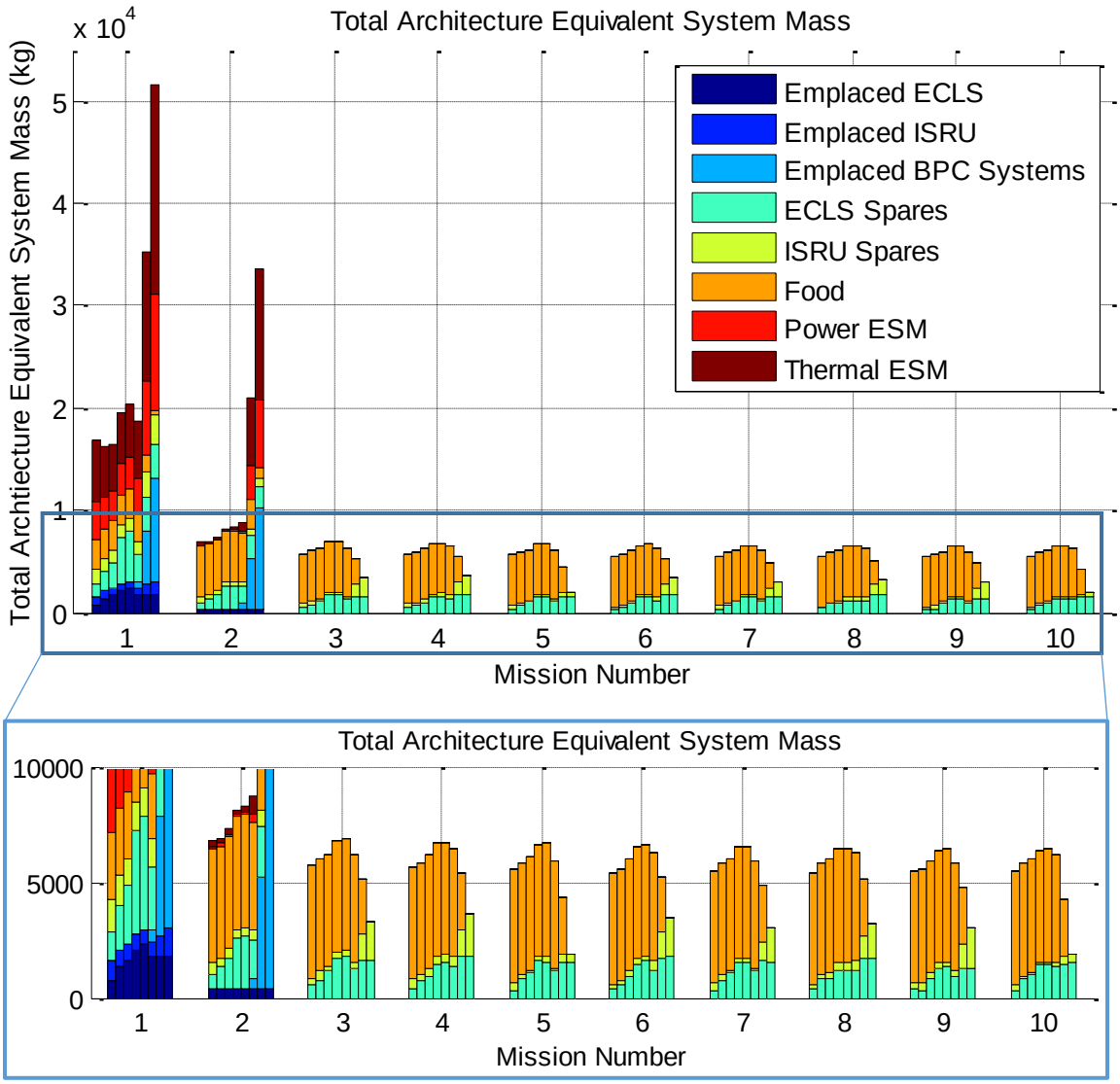

Figure 6-36: Total ESM required to be delivered to the Martian surface per mission per ECLS case for the Minimum Continuous Presence mission scenario. Each cluster of bars represents a mission of the campaign, while each bar within a cluster represents an architectural case

While this trend was also observed in the equivalent analysis for the String of Sorties mission scenario (see Figure 6-25 in Section 6.4.4), the requirement for the resupply of food in Case 8 (where 100% of food is grown) was never driven to zero in the steady state. This is because every time a new crew arrives in a String of Sorties scenario, they have to restart the BPC, which necessitates the addition of prepackaged food delivered from Earth to sustain them while the first batch of the reactivated crops grows to maturity. The only way to mitigate this additional food requirement is to develop a means of robotically tending to crops on Mars for the 8 month period between the departure of the previous crew, and the arrival of the new crew.

In addition to facilitating crop growth, mature plants would have to be harvested and autonomously placed in long-duration storage to ensure that they would be edible once the next crew arrives. The complexity of this task suggests that the most efficient use of a BPC rated to produce 100% of the crew's caloric requirements is when some level of continuous human presence can be achieved, such that there are always crewmembers available to tend to and consume the crops, thereby avoiding the need for robotic equipment and long term storage that may incur additional spare parts and maintenance costs.

In addition, from the first mission in Figure 6-36, we note that the total mass of initially emplaced ECLS and ISRU equipment is minor in comparison to the combined mass of food and spare parts resupply required over the campaign. These results indicate that it is more valuable to focus efforts on developing architectures that have minimum spare parts over their lifecycle, rather than minimizing the mass of specific processing technologies, as is typically the design goal in spaceflight hardware. Put another way, it is worthwhile to invest more mass in technology development upfront, in a manner that increases the operating life of the system.

With these general campaign level trends identified, we now compare the overall lifecycle costs of the eight ECLS architectures evaluated here, by comparing their cumulative equivalent system mass (ESM) requirements – that is, the cumulative ESM required to be delivered to the Martian surface to support each architecture over the first 11 missions of the campaign. Figure 6-37 presents the cumulative ESM data corresponding to the results shown in Figure 6-36.

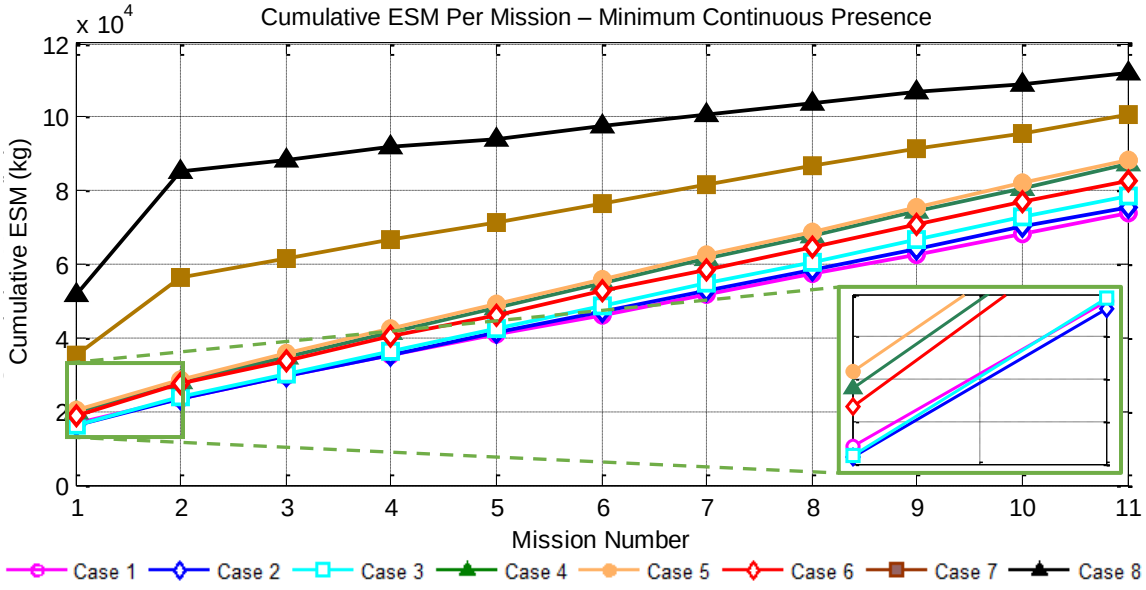

Figure 6-37: Cumulative ESM per Mission of each of the eight ECLS Architectures Cases examined for the Minimum Continuous Presence mission scenario - Inset: Close up of the cumulative trends between the first and second missions

From Figure 6-37, we observe that across the entire campaign, Cases 1 to 3 trend relatively closely with each other, with the largest difference among these three architectures beginning at approximately 490kg (3% of the minimum cumulative ESM) at the first mission, and increasing to 4835kg (7% of the minimum cumulative ESM) by the eleventh mission. Interestingly, a closer inspection of the inset image in Figure 6-37 reveals that while Case 2 is the initial minimum mass architecture, it is tracked closely by Case 1 until the fourth mission, where Case 1 becomes the mass-optimal architecture for the remainder of the campaign. This suggests that the savings in water achieved through the addition of the WPA in Case 2 allow it to overcome the cost of the additional ISRU systems needed to sustain Case 1's resource demands over the first four missions of the campaign.

This trend is different to that observed in the String of Sorties mission scenario (see Section 6.4.4), where Case 1 was found to be dominant over all missions within that campaign. Here, the higher resource demands resulting from the requirement to sustain more crew over longer durations means that an open loop architecture (Case 1) is initially at a mass disadvantage as compared to Cases 2 (WPA) and 3 (WPA+ UPA). Over time however, the efficiencies of deriving resources from ISRU relative to the cost of recycling resources using ECLS recycling technologies and their spare parts (see Table 6.8 and discussion in Section 6.4.4), allow Case 1 to ultimately become dominant. This pattern is particularly evident when viewing the difference in cumulative ESM between Case 1 and Case 2 (the next best performing mission architecture) over time, as is presented in Figure 6-38, below. In this figure, we observe that initially, the cumulative ESM of Case 2 is approximately 500kg lower than that of Case 1. Over time however, Case 1 becomes progressively lighter relative to Case 2, to the point that by the eleventh mission, it has a cumulative mission ESM that is 1877kg lower than that of Case 2.

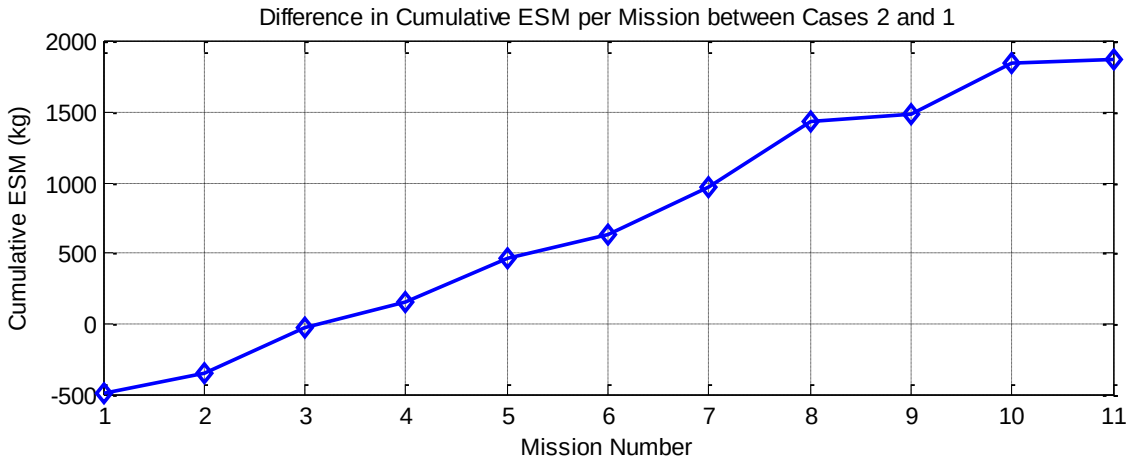

Figure 6-38: Difference in cumulative ESM per mission between ECLS Cases 2 and 1

In addition to the mass-optimality of Case 1 observed here, the shallower gradient of the cumulative ESM trend of Case 8 shown in Figure 6-37 indicates that the savings in lifecycle resupply mass obtained by growing all food locally (Case 8) may offset the high initial costs of BPC deployment, and lead to overall cumulative savings in mission ESM in the longer term. To further investigate this, the above comparative architecture analysis was extended to a 31 mission campaign. The resulting cumulative ESM trends from this analysis are presented below in Figure 6-39.

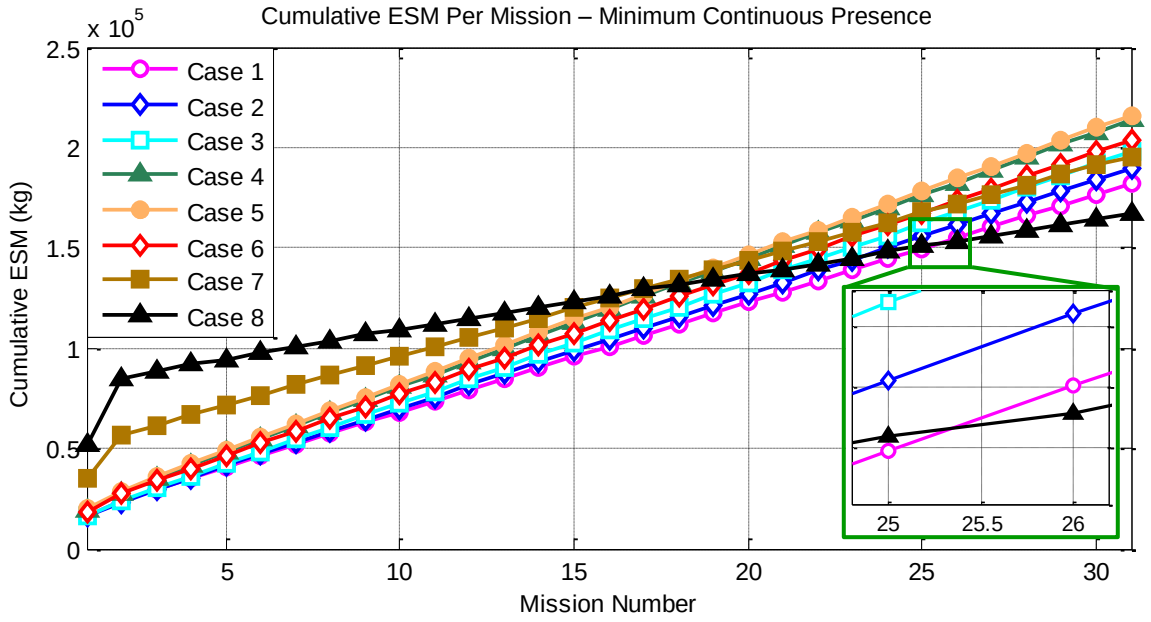

Figure 6-39: Cumulative Mass per Mission per Architectural Case over a 31 mission Minimum Continuous Presence campaign

From Figure 6-39, we observe that a point does indeed exist where the cumulative ESM trend of Case 8 crosses those of the other architecture cases, and the large upfront investment in BPC mass and infrastructure begins to pay-off. Here, this breakeven point occurs between Missions 25 and 26, as indicated by the inset image in Figure 6-39. This period corresponds to a period of approximately 55.5 years after the landing of the first mission.

This finding contrasts significantly to the corresponding results obtained in the String of Sorties campaign analysis performed in Section 6.4.4, where the gradient of the cumulative ESM trend for the 100% crop growth case was similar to that of the open loop ECLS architecture (Case 1) and no breakeven point appeared to emerge. In that analysis, the requirement for food resupply to supplement every new crew's diet as they waited for the first

batch of reactivated crops to reach maturity (see discussion earlier in this section) was comparable to the spare parts resupply requirements of the open loop ECLS case. In the analysis performed here however, the continuous presence of the crew eliminates the need for repeated reactivations of the crop growth system, thus eliminating the requirement for food resupply from Earth in the 100% crop growth case. This results in a resupply mass saving that over the very long term, offsets the large initial investment in BPC infrastructure required to facilitate crop growth.

These findings further imply that if the spare parts demands for Case 8 can be further reduced, this breakeven point may occur sooner. Based on the observation made in Section 6.4.4 that the cost of obtaining ECLS consumables from ISRU tends to be significantly lower than the cost of ECLS consumables recycling technologies, we develop a ninth architecture case that is the same as that of Case 8, with the exception that the WPA and UPA have been removed, and all crew and crop requirements for water are provided with ISRU. Here, the removal of these technologies is intended to eliminate the cost of their emplacement and lifecycle spare parts resupply. With this architecture defined, we repeat the above comparative architecture analysis to determine the impact of this modification.

Through this, it was found that the only major change in total consumables demands between Case 8 and the newly developed Case 9 was the amount of water required to be supplied by ISRU. Here, 24328L of water needs to be generated for the first 4-crew 26-month increment of Case 9, as compared to the 16623L required by Case 8. For the second 26-month increment, where eight crewmembers are initially on the surface until month 18, Case 9 requires a total of 56560L of water to sustain the increased level of biomass production, as compared to Case 8's requirement for 43428L. This increase in water demand was found to result in an increase in ISRU water extractor mass from 775kg in Case 8 to 957kg in Case 9. All other ISRU system technologies were found to remain the same as those required for Case 8.

Figures 6-40 and 6-41 plot the lifecycle equivalent system mass per mission and the cumulative equivalent system mass per mission results obtained from this analysis.

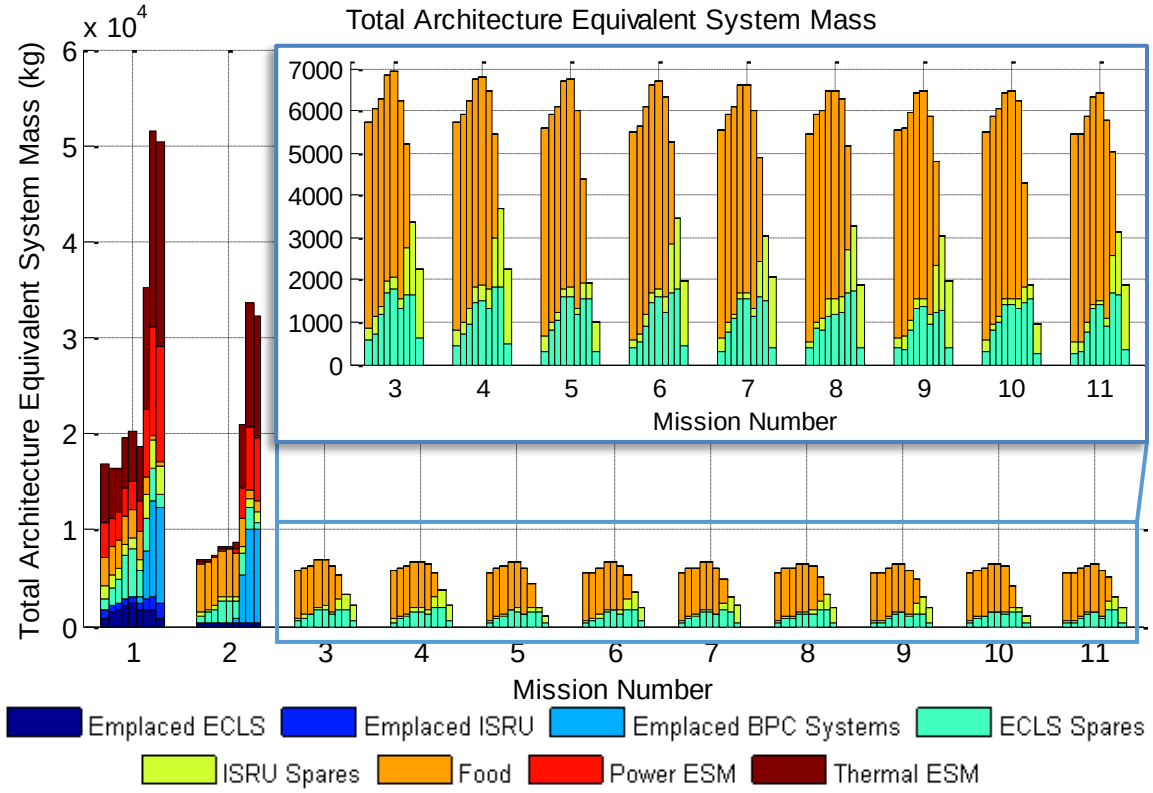

Figure 6-40: Total Architecture Lifecycle ESM including the newly developed ELCS Architecture Case 9. Here each cluster represents a mission within the campaign, and each bar within each cluster represents an ECLS architecture case

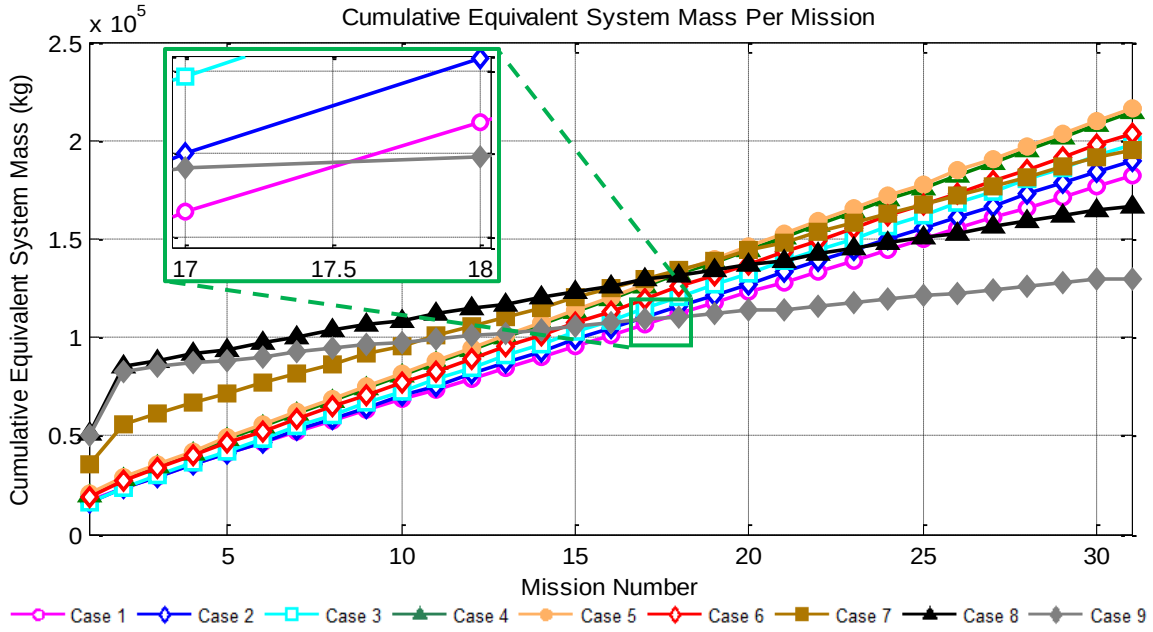

Figure 6-41: Cumulative ESM per Mission over 31 missions of the Minimum Continuous Presence campaign scenario, including Case 9 (100% food growth with open loop ECLS supplemented by ISRU)

From Figure 6-40, we observe that the removal of the WPA and UPA from architecture Case 8 has indeed reduced the spare parts resupply requirements for Case 9, to the point where only spare parts associated with the CDRA, CCAA, and ISRU systems are required. This reduction in total spare parts demands leads to a significant reduction in the period at which the savings derived from growing all food locally pay off for the cost of the infrastructure required to facilitate this food production. From the inset image in Figure 6-41, we observe that this breakeven point now occurs at about halfway through mission 17, or about 38 years after the beginning of the campaign. Prior to this mission, the open loop ECLS architecture (Case 1) still remains the mass-optimal choice, based on the assumptions made in this analysis.

In fact, relative to the ECLS architecture cases that do not incorporate 100% food growth, the dominance of architecture Case 1 appears to grow over time. This is indicated by the growing gap in cumulative mission mass that occurs between Case 1 and Cases 2 to 7 over time. As was discussed earlier, this result is driven by the dominant demand for MAV propellants, which drives the baseline mass of the required ISRU system, causing the marginal cost in ISRU systems required to support open loop ECLS consumables to be significantly lower than the cost of using additional technologies to recycle ECLS consumables. In the next section, we explore the sensitivity of this trend to the initial assumptions made for the ISRU system.

6.5.5 Sensitivity of Relative Architecture Rankings to Variations in ISRU Hardware Mass and Reliability

Given the significant uncertainties associated with predicting the mass and reliability of ISRU technologies that have yet to be developed and tested in relevant operating environments, this section investigates the impact of variations in the mass and reliability of individual ISRU technologies on the overall architectural ranking results obtained above. Here, we adopt the same approach as that used in the series of sensitivity analyses conducted in Section 6.4.5, where the integrated architectural analysis conducted in Section 6.5.4 is repeated at progressively degraded levels of ISRU system performance, and the change in the resulting cumulative equivalent system mass per mission trends are analyzed. For the sensitivity analyses performed here, we consider only ECLS architecture Cases 1 to 8 operating on the Martian surface for the first 11 missions of a Minimum Continuous Presence campaign, as was the case with the original comparative architecture analysis performed above.

We begin this analysis by lowering the MTBFs of all ISRU systems by an order of magnitude to investigate the sensitivity of the overall architecture rankings to degradations in system reliability – a phenomenon that has been observed to occur when operating equipment in dusty environments (as is the case with the Martian environment). Figure 6-42 summarizes the cumulative mass per mission results obtained from this analysis.

Here, we find that even with an order of magnitude reduction in the reliability of all ISRU technologies, the relative rankings between the original eight architecture cases remain virtually the same as that obtained in the original analysis. Again, we observe that Case 2 is initially dominant, but is later overtaken by Case 1 as the duration of the campaign increases over time (see Figure 6-43). The major difference here however, is that the point at which Case 1 becomes dominant in this degraded ISRU reliability scenario occurs between Missions 7 and 8 (see Figure 6-43), as compared to the earlier crossover between Missions 4 and 5 previously observed (see Figure 6-38). This indicates that the degradation in ISRU system reliability has caused a reduction in the overall efficiency of generating ECLS consumables with ISRU. This has consequently resulted in a longer period for the additional ISRU capacity required in the open loop ECLS architecture (Case 1) to recover from its large initial consumables demand relative to Case 2 (the next best performing ECLS architecture).

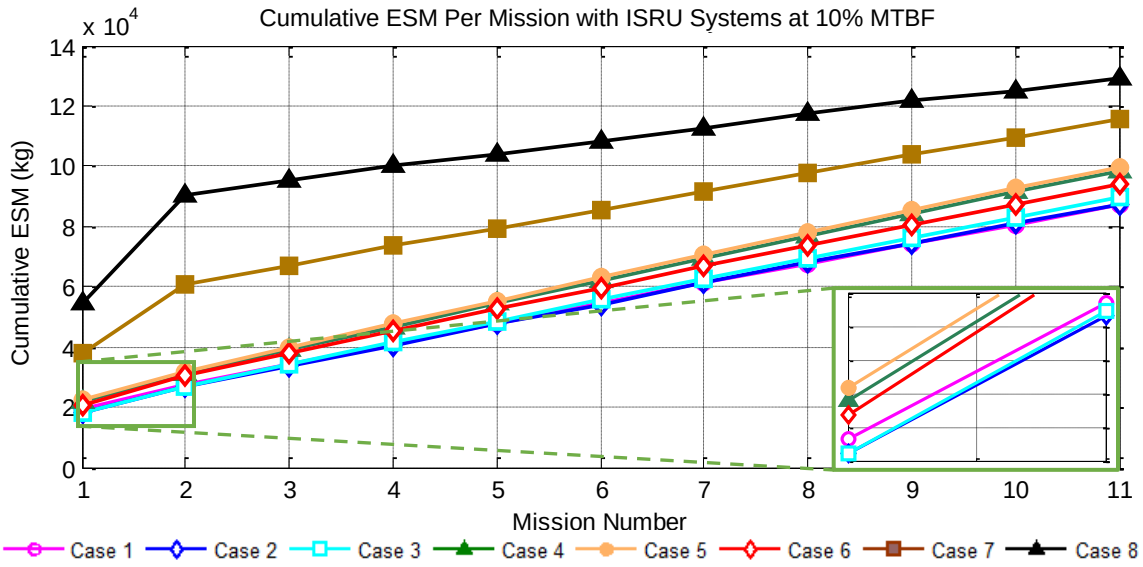

Figure 6-42: Cumulative ESM per mission per ECLS Architecture Case for the Minimum Continuous Presence mission scenario with all ISRU technologies at 10% lower reliability

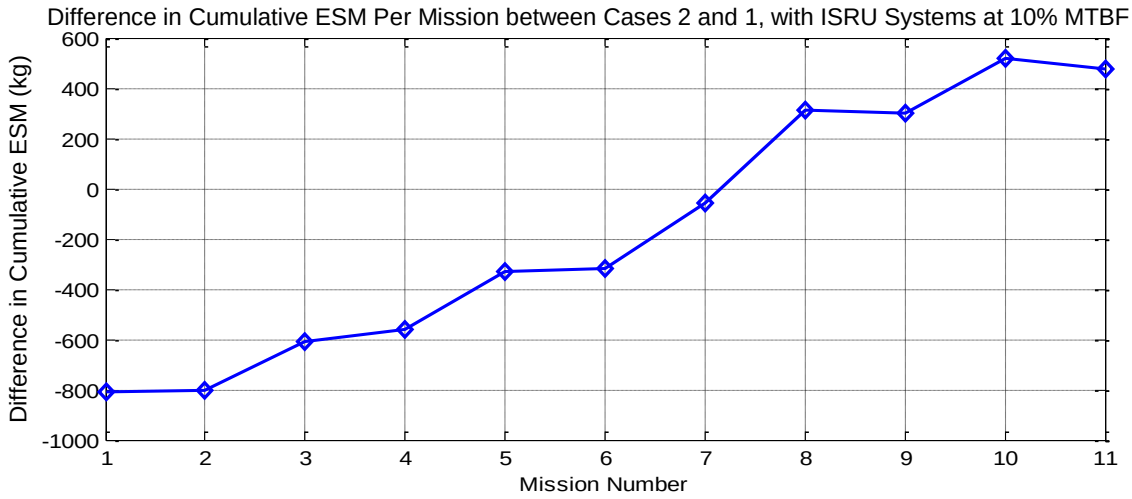

Figure 6-43: Difference in cumulative ESM per mission between ECLS architecture Cases 2 and 1 for the Minimum Continuous Presence mission scenario with all ISRU technologies at 10% lower reliability

To further investigate the limits of the mass-optimality of architecture Case 1, we perform an additional sensitivity analysis where we retain the MTBF degradation constraint imposed in the previous case study, while increasing the mass of the components of a subset of the set of ISRU technologies by an order of magnitude. These technologies are the water electrolyzer, the Sabatier reactor, and the atmospheric processor – technologies that have the most uncertainty regarding their sizing predictions (see Section 6.4.5 for a discussion). Figure 6-44 presents the cumulative ESM per mission results generated by this analysis.

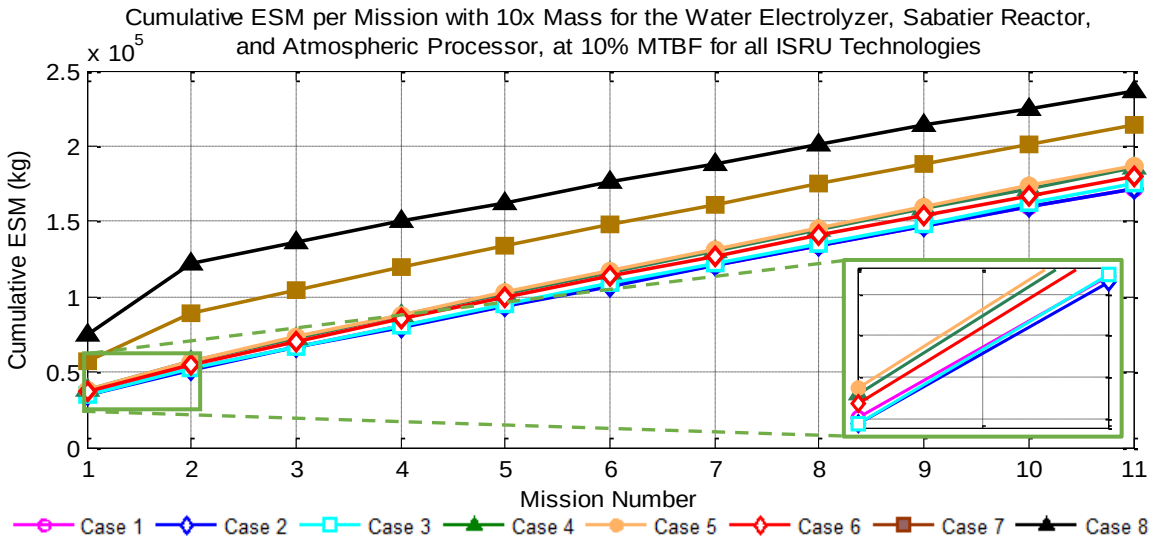

Figure 6-44: Cumulative ESM per Mission per Architectural Case for the Minimum Continuous Presence mission scenario with all ISRU Technologies at 10% lower reliability levels and the mass of the water electrolyzer, Sabatier reactor, and atmospheric processor increased by a factor of 10

Similar to the previous analysis, we again find that the cumulative ESM of Cases 1 and 2 trend closely with each other throughout the campaign. Under the ISRU mass values and reliability levels assumed here however, we find that neither of the cases emerges as a clear dominant architecture amongst all other architectural cases. Rather, the relative rankings in cumulative ESM of the two cases fluctuate about one another, as is evident in Figure 6-45, which graphs the difference in lifecycle cumulative ESM between Cases 2 and 1. This trend indicates that at the reliability levels observed here, the efficiency of deriving ECLS consumables from ISRU has been degraded to a level that is commensurate with the savings in ECLS consumables mass resulting from the addition of ECLS recycling technologies. The fluctuating trend depicted in Figure 6-45 is likely driven by the timing at which ECLS and ISRU spare parts are allocated to the resupply manifest of Cases 1 and 2. This is supported by the fact that the only types of commodities being resupplied are food and spare parts for ISRU and ECLS systems. Since the food resupply requirement for Cases 1 and 2 is the same (see Table 6.9 and Figure 6-32), the remaining differences in cumulative mass can only be attributed to differences in the allocation of ECLS and ISRU spare parts over time.

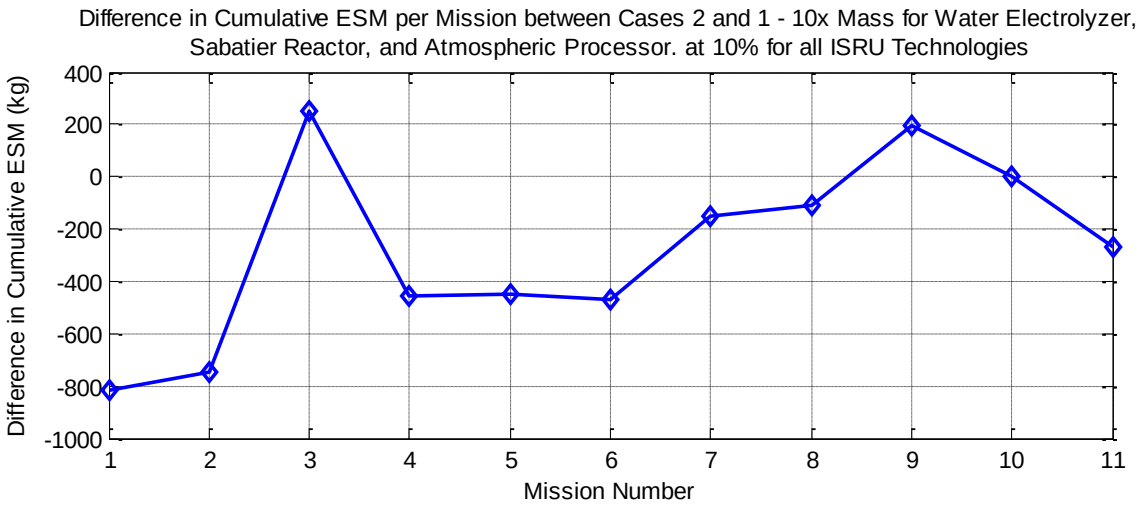

Figure 6-45: Difference in cumulative ESM per mission between Cases 2 and 1 for the scenario all ISRU technologies have 10% of their originally estimated MTBF, and mass of the water electrolyzer, Sabatier reactor, and atmospheric processor have been increased by a factor of 10.

The results of the previous sensitivity analysis indicate that the effects of an order of magnitude reduction in ISRU reliability, coupled with the order of magnitude increase in mass for a subset of the ISRU technologies, lead to what appears to be the boundary of mass-

optimality for the open loop ECLS architecture (Case 1). To verify that this is indeed the point at which Case 1 transitions from being the mass-optimal architecture to one that is dominated, we perform a final sensitivity analysis where we increase the mass of all ISRU technologies by an order of magnitude from their originally estimated values, while retaining the 10% reliability degradation enforced earlier. This scenario mirrors that of the worst-case ISRU performance modeled in the sensitivity analyses conducted in Section 6.4.5. The resulting cumulative ESM per mission estimates are presented below, in Figure 6-46.

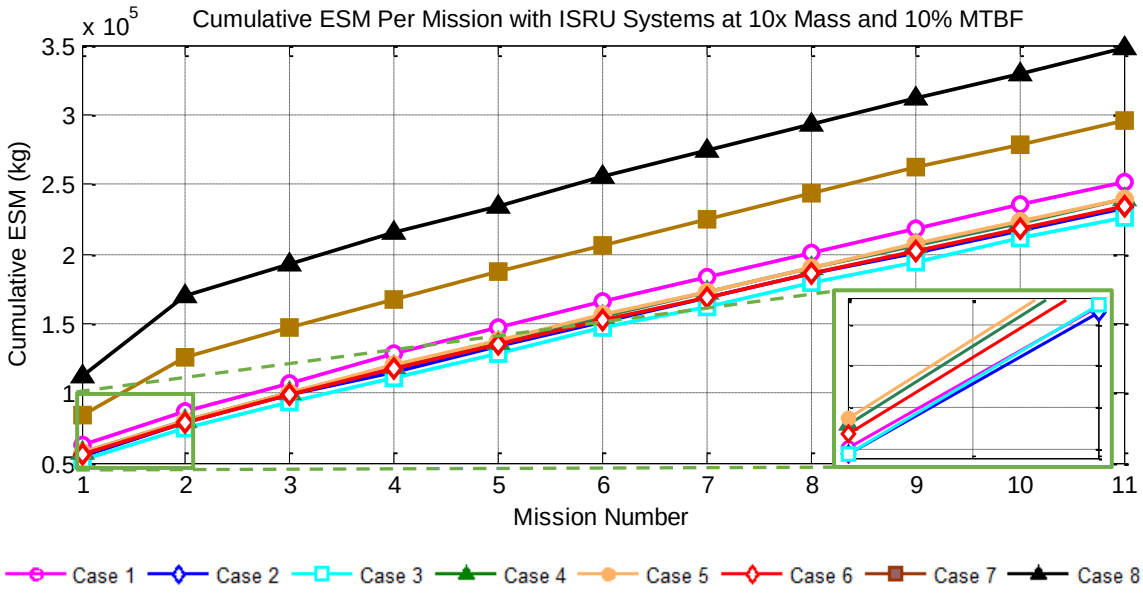

Figure 6-46: Cumulative ESM per Mission per Architectural Case for the Minimum Continuous Presence mission scenario with the masses of all ISRU Technologies increased by a factor of 10 and their reliabilities reduced by an order of magnitude

In this final set of sensitivity analysis results, we find that the imposition of ISRU technologies that are ten times heavier than their originally estimated values has caused the relative rankings of the ECLS architectures to fundamentally shift from the trends previously observed. Here, Case 3 (WPA+UPA) has emerged as the mass-optimal architecture, followed by Case 2 (WPA), Case 6 (5% food growth), Case 4 (WPA+UPA+OGA), Case 5 (WPA+UPA+OGA+CRS), and then by the open loop and food growth cases (Cases 1, 7, and 8).

When examining just the relative rankings between Cases 1 to 5 in this sensitivity analysis, we find that their ordering is identical to that of the deep space habitat case study performed in Section 4.4.5. This indicates that when the cost of ISRU is high, as is the case here and in an

orbital or deep space mission context (where there is no access to local resources), the relative ECLS architectural trends transition from those that prefer open loop architectures, towards the more traditional ECLS design philosophies that favor increased levels of recycling in long duration missions.

In addition to its effects on the relative rankings of ECLS Cases 1 to 5, the high cost of ISRU-derived water in this scenario has also made large scale crop growth a less attractive option, with the cumulative ESM trend of Case 8 in Figure 6-46 no longer appearing to have a foreseeable point at which it begins to dominate other architectures. This observation indicates that the main driver as to whether or not large scale biomass production will ever become a competitive architecture is strongly dependent on the mass and reliability of ISRU.

Finally, we note that in this final sensitivity analysis, Case 6 was ranked the third best architecture in terms of cumulative equivalent system mass (ESM), even though it included some level of food growth. Based on the dependency of relative ECLS architectural rankings on the cost of ISRU observed here, this suggests that for a deep space habitat, the maximum level of crop growth that can be implemented without imposing the requirement for additional infrastructure is in the order of 4.5%. Since the level of EVA in this mission scenario will likely be significantly lower than that assumed here (for the Mars surface context), this level of food growth is likely to slightly increase. While any level of food growth has been observed to result in sub-optimal architectures from a purely mass perspective, the added intangible psychological and habitability benefits of plant growth may offset this mass sub-optimality. The analysis performed here provides an upper bound to this level of plant growth, such that undesired propagations in supporting system requirements are avoided.

6.6 Discussion of Case Study Results

The lifecycle analyses performed in this chapter for the return trip class of Mars missions revealed a number of previously unidentified trends, some of which directly contradict the conventional thinking and design philosophies adopted in the design of spacecraft life support systems. A comparative ECLS architecture analysis for the two mission scenarios considered here – the String of Sorties, and the Minimum Continuous Presence scenarios – found and reaffirmed the finding that based on the ISRU system sizing assumptions currently implemented within the HabNet ISRU Module, an ECLS architecture consisting of open loop

oxygen and water provision supported by a local ISRU system appears to be the mass-optimal architecture. This result changes to a 100% food growth architecture, relying entirely on an open-loop ECLS architecture supported by ISRU, only in the scenario where a Minimum Continuous Presence campaign is adopted that lasts for 18 missions or more.

Through a series of sensitivity analyses, the mass optimality of the open loop ECLS architecture was found to be robust to order of magnitude reductions in ISRU system reliability, and order of magnitude increases in the mass of over half of the ISRU technologies required.

The consistent dominance of the open loop ECLS architecture was found to arise from a trend that is inherent in the two mission scenarios examined here – that the requirement for ISRU-derived MAV propellants dominates the mass of all consumables required on the surface of Mars, comprising 62-85% of the total consumables demand for the String of Sorties mission scenario, and 59-80% for the first mission of the Minimum Continuous Presence mission scenario. This dominant MAV propellant demand places a minimum requirement on the size of the total ISRU system required to be deployed on the surface. Any additional ECLS consumables generation requirements imposed on the ISRU system incurs a small marginal cost in ISRU equipment, relative to the cost of deploying and supporting additional ECLS technologies to reduce consumables demand through recycling. The analysis presented in Table 6.8 in Section 6.4.4 found that based on the system sizing and reliability assumptions adopted in this analysis, the cost of supplying ECLS consumables with ISRU was between 14-22% of the cost of reducing ECLS consumables demand with ECLS recycling systems. This significant cost difference results in architectures that rely more on ISRU rather than ECLS in generating consumables to become dominant in terms of minimizing system mass. As such, open loop ECLS architectures emerged as the mass-optimal solution in the two mission scenarios investigated.

Moreover, as mission durations and population sizes were increased between the String of Sorties and the Minimum Continuous Presence mission scenarios, the increased demand for water in the open loop architecture led to an initial mass advantage in recycling water with a WPA for the first few missions. Over time however, the lower cost of supplying ISRU-derived ECLS consumables compared to the cost of using ECLS technologies to recycle consumables eliminated this mass advantage, ultimately resulting in the open loop ECLS architecture becoming mass-optimal by the fourth mission of the campaign.

These findings are in direct opposition to the conventional thinking surrounding long-duration life support system architecting. As was mentioned in Section 2.1.2, the general

consensus across the ECLS community since the 1980s has been that as missions increase in duration, increasing levels of resource recycling should be incorporated to reduce the amount of consumables required, and hence lower the total system mass (see Figure 6-47).

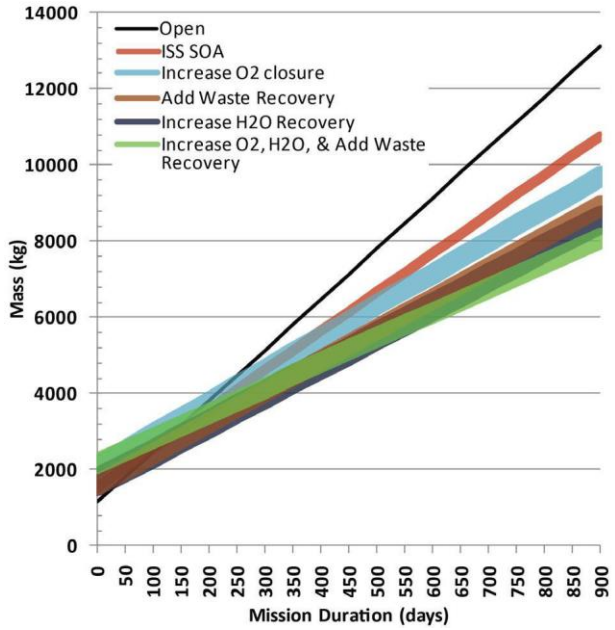

Figure 6-47: Notional Plot of total ECLS mass versus increasing mission duration printed in the NASA ECLS Integrated Roadmap [286], representing a trend whereby the total mass decreases with increasing levels of ECLS recycling over increasing mission durations

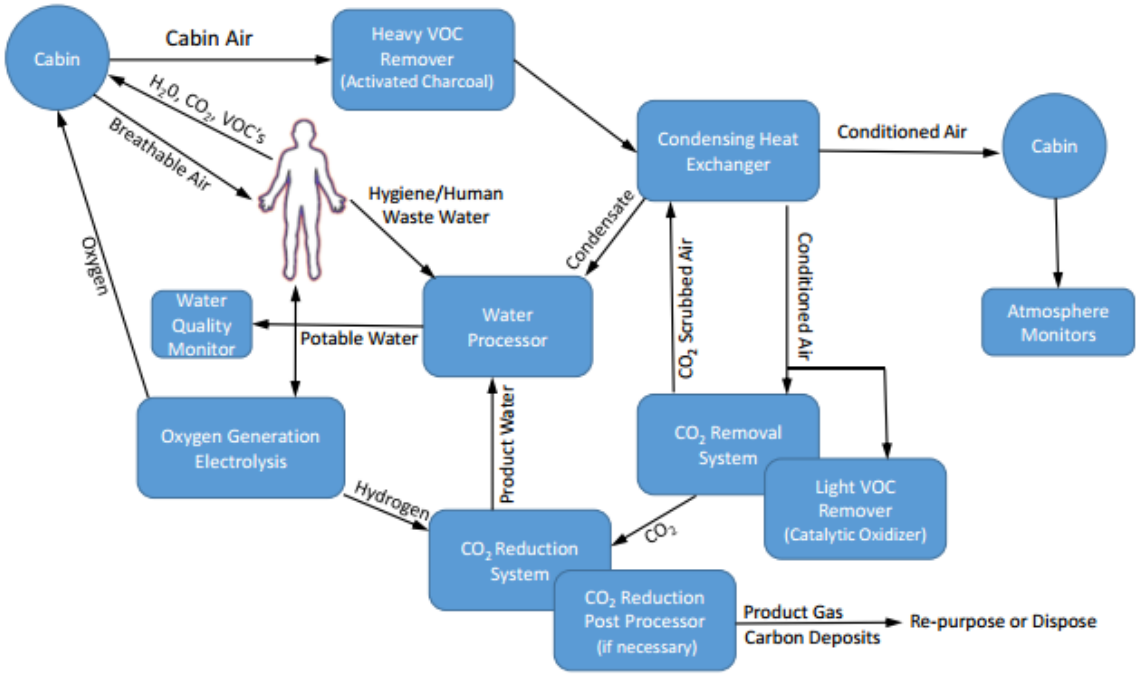

Figure 6-48: Baseline ECLS architecture currently being assessed as part of NASA's Evolvable Mars Campaign series of studies. [287]

This design heuristic has endured to today, where the goal of increased resource closure has been specified in NASA's current TA06 Human Health, Life Support, and Habitation Systems Technology Roadmap [29], NASA's internal ECLS Integrated Roadmap [286], NASA's latest addendum of the Mars Design Reference Architecture 5.0 [21], and other key documents. In fact, the ISS ECLS architecture (equivalent to Case 5) has been adopted as the baseline architecture within the ongoing Evolvable Mars Campaign series of studies [287], as is shown in Figure 6-48.

The analyses performed in this chapter revealed trends that are opposite to these traditionally held design philosophies. Here, it was found that on the surface of Mars, moving away from resource recycling towards open loop ECLS architectures supported by ISRU led to a minimum mass architecture. Even over longer mission durations with larger crew populations where the water demand was higher, open-loop ECLS architectures supplemented by ISRU emerged as the mass-optimal solution with increasing mission duration – a finding that is the opposite of that commonly assumed, as shown in the trends depicted in Figure 6-47. Moreover, the fact that an open-loop ECLS architecture is inherently less complex than the traditionally baselined high resource recycling ECLS architectures, suggests that the open-loop architecture identified here could potentially lead to lower programmatic costs, due to reductions in the number of technologies needed to be developed and supported over the duration of the Mars mission campaign.

A further sensitivity analysis performed in Section 6.5.5 revealed that the cause of the discrepancy in these trends is related to the cost of ISRU. In this analysis, it was found that when the cost of ISRU is low, open-loop ECLS architectures tend to emerge as those with the lowest cumulative mission mass, due to the mass savings achieved through avoiding the need to supply the spare parts required to sustain the continuous operations of ECLS resource recycling technologies. As the cost of ISRU increases above a certain threshold however, the relative ECLS architectural trends transition towards those that favor increased levels of resource recycling. This is especially the case in long-duration deep space transit vehicles or orbital space stations that do not have access to in-situ resources and can only source equipment and consumables from Earth.

Interestingly, the dependency of ECLS architecture mass-optimality on ISRU capability observed here is analogous to a metric that has recently gained prominence in the field of space logistics network architecting. Here, a threshold ISRU production rate (measured in mass of in-situ resources generated per year per unit mass of ISRU system) is used to determine

whether or not an ISRU plant should be emplaced at a particular celestial location to support an in-space transportation network [27]. This particular threshold captures only the performance of required ISRU capability, as measured by a resource production rate.

The findings made in this analysis suggest that for ECLS systems, the cost of ISRU is a function of performance and reliability, and as such, the ECLS-optimality ISRU threshold should be measured in terms of the mass of in-situ resources generated per year per unit mass of ISRU. Here, the mass of ISRU encompasses both the mass of the ISRU system itself, as well as the mass of the spare parts required to sustain its operation over a period of one year.

Further, this analysis found that the largest driver of ISRU system mass was the mass of the water extraction unit, as it scales directly with water and oxygen demand – the major forms of ECLS consumables, and elements that are necessary in the generation of MAV propellants. This suggests that the total lifecycle cost of a Mars mission architecture is strongly dependent on the performance efficiency and reliability of water extraction and processing systems. This is strongly dependent on the form in which water is locally available (eg. as water ice or as hydrated minerals), and has major implications on the selection of the surface location. The findings of this analysis reinforce current thinking surrounding the concept of an Exploration Zone (see Section 6.1), where a large and easily accessible supply of in-situ surface water is a necessary prerequisite to efficiently supporting future Mars exploration efforts [269].

6.7 Chapter Summary

In this chapter, a large-scale tradespace exploration was performed to evaluate the impact of different ECLS architectures on the emplacement and lifecycle resupply costs of two different types of return-trip Mars mission campaign scenarios – the String of Sorties mission scenario, and the Minimum Continuous Presence mission scenario. After a brief historical overview of the evolution of NASA's Mars mission planning activities, the baseline habitation architecture and Mars Ascent Vehicle assumed in these analyses was described. These are respectively based on an evolved version of NASA's Habitat Demonstration Unit, and the MAV design currently being developed as part of NASA's Evolvable Mars Campaign series of studies.

Following this, an analysis was performed to identify the underlying mechanisms that caused the atmospheric imbalances that were observed in the analysis of the baseline Mars One habitat architecture presented in Section 5.6.1. Here, it was found that an insufficient level of

CO_2 generated by the crew to sustain the crops necessitated the injection of additional CO_2 from the Martian environment, which was ultimately photosynthesized into oxygen that accumulated within the cabin atmosphere. Once this mechanism was identified, an additional analysis was performed to determine the maximum amount of crops that could be grown in a shared atmosphere as that of the crew, such that atmospheric imbalances would not be introduced. Through this, it was found that the peak level of crop growth such that these conditions were satisfied is approximately 4.5% of the crew's caloric requirements. With this value established, an architecture involving a 4.5% level of plant-based food production in a shared environment with the crew was developed, and appended to a list of seven other architectural cases, consisting of the five strictly physico-chemical ECLS architectures assessed in the validation case study performed in Section 4.4, along with two high capacity biomass-production cases, where food was produced locally at levels of 50% and 100% of the crew's total caloric requirements.

These eight architectures were then used as the basis of the architectural tradespace exploration analyses performed for both the String of Sorties and Minimum Continuous Presence mission campaigns. Through these analyses, it was found that for the String of Sorties scenario, an open-loop ECLS architecture supplemented by ISRU was the mass-optimal architecture across all missions, and even under conditions of degraded performance, where the reliability of all ISRU systems was reduced by an order of magnitude, and the mass of over half of the ISRU technologies was increased by a factor of ten. For the Minimum Continuous Presence mission scenarios, a similar result was found, where the open loop ECLS architecture was found to be competitive over time, even though it was marginally dominated over the first few missions. This initial sub-optimality was found to be the result of the large upfront resource demands of the open loop architecture relative to architectures that contain higher levels of recycling. Over time however, the lower cost of sourcing ECLS consumables from ISRU, relative to the cost of recycling ECLS consumables with ECLS technologies, resulted in the open loop ECLS architecture becoming more mass-efficient, such that it became the mass-optimal architecture after mission 4 of the campaign.

This series of tradespace exploration analyses also revealed that high levels of food growth only become attractive when some level of continuous human presence can be maintained, and when the cost of generating ISRU-derived water is low. Here, a continuous human presence enables the continuous tending of crops, eliminates the need for large scale biomass storage, and eliminates the need to send additional food to sustain the crew during the initial phases of

crop growth that occur with every reactivation of the biomass production system. This latter attribute becomes even more critical to the competitiveness of 100%+ food growth architectures, where the cost of resupplying food from Earth can be eliminated over time.

In addition, a low cost of ISRU-water allows the mass savings derived from the local production of food to offset the high initial costs of emplacing the infrastructure required to support crop growth over time. In the analysis performed here, it was found that based on the ISRU sizing equations implemented in the HabNet ISRU module, a 100% food growth architecture combined with an open loop ECLS and supported entirely by ISRU (Case 9 in Section 6.5.4) could potentially become mass-optimal by the eighteenth mission of a Minimum Continuous Presence campaign. This would occur after the savings in food resupply that it achieved over the first 17 missions of the campaign compensated for its initial biomass production infrastructure cost. Moreover, it was observed that this payback always occurred quicker for food-growth architectures that incorporated 100% food growth, as compared to those that generated lower levels of food. This suggests that if any level of food growth is planned for a 38+ year campaign, and if the cost of ISRU is low, the mass savings in food resupply over time are worth the mass of additional biomass production systems that need to be initially emplaced. That is, under these conditions, it is the most mass-efficient to begin immediately with 100%+ food growth so that the savings in food resupply mass can be achieved earlier.

To investigate the robustness of the mass-optimality of open loop ECLS architectures to variations in ISRU performance, a series of sensitivity analyses were performed, where the reliability of all ISRU technologies was first reduced by an order of magnitude, and the masses of subsets of ISRU technologies were progressively increased by a factor of ten. Through this, it was found that the mass-optimality of open loop ECLS architectures was robust up until a certain point of ISRU degradation, where the relative ECLS architectural trends transitioned to those that prefer higher levels of ECLS recycling, as is the case with traditional ECLS design philosophies. This finding provided a link between the traditional design heuristics adopted in the ECLS community, with the contradictory findings made here. The optimality of ECLS architectures can now be considered to exist on a continuum of ISRU performance, as measured by its production rate per unit system mass, and its spare parts requirements over time, as characterized by the reliability of its components. When the cost of ISRU is low, as is possible on the surface of a resource rich celestial body, open-loop ECLS architectures supplemented by ISRU emerge as the mass-optimal solution. Conversely, when the cost of

ISRU is high, as is the case in deep space or in a long-duration space station, where in-situ resources are not available, ECLS architectures that incorporate water recycling and recovery emerge as being mass optimal (as was found in Section 4.4, where spare parts requirements were also incorporated). This observation provides a more generalized framework by which human spaceflight systems can be architected.

Finally, we note that it was only through the integrated architectural analysis of ECLS and ISRU systems and their supportability requirements performed here, that a system synergy could be identified, where a simpler ECLS architecture was found to lead to a mass-optimal solution because of the presence of an already emplaced high capacity ISRU system. Traditionally, ECLS, ISRU, and supportability analyses have been performed separately from one another, thus preventing architectures such as the one derived here from being identified. The results of this analysis indicate that there is indeed merit to including higher levels of system integrality in mission architecting analyses, especially in light of their potential to identify previously unseen system interactions. This philosophy has been at the core of the development of HabNet, and will be a guiding principle as its capabilities continue to evolve.

Chapter 7

Summary and Conclusions

7.1 Thesis Summary

This thesis commenced with the recognition that although Mars mission studies have been performed since before the beginning of the Space Age, they have mostly focused on developing solutions to the challenge of *transporting* humans to and from the surface of Mars, and have largely ignored the challenges of *sustaining* human crews upon arrival. This trend is especially pertinent for the case of the "permanent presence" mission scenarios that have been the focus of the recent growing confluence of interest in the expansion of human presence beyond Earth orbit and in ultimately making humanity a multi-planetary species. In light of this fact, coupled with the numerous challenges that have been experienced in maintaining a continuous human presence on the International Space Station over the past 15+ years, this thesis develops, validates and applies an integrated habitation analysis tool to a range of "permanent presence" mission scenarios in order to characterize their lifecycle costs, and the variations in these costs to changing system architectures.

Following a historical review of the major milestones in Mars mission planning, and a survey of the evolution in the development of ECLS and ISRU capabilities and system supportability analyses, the development of this integrated habitation analysis tool, titled HabNet, was conducted throughout Chapter 3. Here, an Architecture Decision Graph was first developed to identify the key distinguishing decisions that shape the architecture of spaceflight systems. From this, the basic structure of the HabNet framework was derived, consisting of the Habitation Module, the ISRU Module, the Supportability Module, and the Evaluation Module.

After the development of the Habitation Module and its integration with the separately developed ISRU and Supportability Modules, a series of validation studies were performed to build confidence in HabNet's dynamic simulation and system sizing estimates. Through this

effort, HabNet was found to generate dynamic simulation results that generally correlated well with both ISS operational data and experimental crop growth data. Here, the majority of discrepancies observed were the result of either limitations in the temporal resolution of HabNet's dynamic simulation capability resulting from the choice of a fixed hour-long simulation time step, and/or uncertainties in the operational conditions (such as crew activities and locations) on the ISS at the time at which the ISS operational data was collected. The hour-long simulation time step adopted here was chosen as a compromise between being able to capture major system dynamic behaviors while minimizing computational cost.

In addition to this individual technology level validation, an integrated validation case study was also performed, investigating the impacts of increasing levels of ECLS recycling on the total mission mass of a deep space habitat mission. Through this, HabNet's integrated sizing and architecture predictions were found to largely agree with those previously published in the literature, thus providing confidence in its architecture sizing capabilities.

With the HabNet framework developed and validated, a series of "permanent presence" mission case studies was then conducted. The first of these was a lifecycle analysis of the Mars One mission plan – the most widely publicized instance of the "Mars to Stay" class of Mars mission architectures. These types of missions are based on the premise that the most cost-efficient and near-term approach to sending humans to Mars is via a series of one-way crewed missions that progressively lead to the buildup of a sustained human presence on the surface of Mars. Through four analysis iterations of three different variants of the Mars One mission architecture, this analysis found that based on current spaceflight capabilities both in development and in operation, the decision to commence a one-way Mars mission campaign equates to the commitment to the near-indefinite resupply costs associated with the continual need to resupply the crew with the spare parts required to sustain the continued operation of the habitation system. Moreover, the addition of more crewmembers to the surface base, as is the case with the majority of "Mars to Stay" type missions, results in the corresponding increase in spare parts demand and hence mission cost over time. These results imply that without shifting the entire spare parts supply chain to Mars (including raw materials mining, and in-situ parts manufacturing), one-way mission architectures will always require spare parts resupply from Earth, which over the lifespan of the one-way crew, will make these types of architectures inevitably more expensive than the traditional Mars conjunction class missions that they intend to replace.

Following this one-way mission case study, the lifecycle impacts of different ECLS architectures on two types of return-trip mission scenarios were investigated. These scenarios were the "String of Sorties" mission scenario, where multiple four person crews are sent on 540 day conjunction class sorties to the same Mars surface base; and the "Minimum Continuous Presence" mission scenario, where four-person crews are replaced after 44-month stays at a Mars surface base in order to satisfy the requirement for a continuous human presence. Through a large-scale architectural tradespace analysis for both these mission scenarios, an open loop ECLS architecture supplemented by local ISRU was consistently found to be an attractive, if not dominant architecture. A further analysis revealed that the primary reason for this trend is the fact that the demand for ISRU-derived Mars Ascent Vehicle (MAV) propellants dominates the total consumables demands of all architectures, to the point where the difference in ECLS consumables demands across different ECLS architectures is relatively minor in the context of ISRU production rates established by the demand for MAV propellant. This results in the cost of producing ECLS consumables with ISRU being 14-22% of the cost of reducing ECLS consumables demands with ECLS recycling technologies, as measured by the additional mass of hardware required to satisfy this ECLS consumables demand. The consistent mass-optimality observed for the ISRU-supplemented open-loop ECLS architecture directly contradicts the conventional design philosophies governing ECLS system design. The reason for this inconsistency was identified through a series of sensitivity analyses that evaluated the cumulative lifecycle equivalent system mass requirements of different ECLS architectures at different levels of ISRU performance. Through this, it was found that the relative rankings in ECLS architecture performance are dependent on the cost of ISRU, as measured by the mass and reliability of the systems required to generate the required resources. When the cost of ISRU is low, as is likely the case on the surface of Mars, open-loop ECLS architectures tend to be preferred, as they result in less complex systems that require less spare parts resupply over the lifetime of a campaign. In fact, at a low enough cost of ISRU, architectures involving in-situ food production at levels sufficient to sustain the entire crew were found to be competitive over multi-decadal campaigns. Conversely, if the cost of ISRU is high, as is the case in deep space or on long-duration space stations that do not have access to local resources, architectures with higher levels of resource recycling tend to become mass-optimal. The analyses conducted here found that in such scenarios, the implementation of water recycling technologies coupled with an open loop oxygen supply lead to a mass-optimal solution. Here, the optimal solution consists of only partial resource closure because the large

spare parts demand associated with recycling oxygen makes an open-loop oxygen supply a more mass-efficient option. While the specific ISRU cost-threshold at which relative ECLS architecture rankings change was not computed, the nature of its existence, as well as its dependency on ISRU system mass and reliability was identified.

7.2 Summary of Key Findings and Contributions

Through the development and application of HabNet to a series of "permanent presence" mission scenarios, this thesis made several contributions and findings that expand the current understanding of the Mars mission architecture tradespace. Specifically, these include:

- The **development of a generalized Architecture Decision Graph (ADG) of Human Spaceflight Systems** to provide a consistent, integrated representation of the key architecturally distinguishing decisions that shape the architecture of human spaceflight systems. This ADG allows the mapping of the multitude of engineering disciplines uniquely involved in developing a human spaceflight system to key decision variables that shape its architecture.
- The **development and validation of HabNet**, which was based on a subset of integrated decisions identified in the Human Spaceflight Systems ADG. Specifically, this work developed the HabNet software architecture and the Habitation Module, and incorporated the ISRU and Supportability Modules developed by other researchers into this framework. Here, the Habitation Module was developed by extending NASA JSC's BioSim software to incorporate validated ISS ECLS technology models. When combined with the ISRU and Supportability Modules, as was performed in the case studies described in Chapters 4 to 6, HabNet was found to enable the consistent and efficient analysis of integrated human spaceflight architectures, which in turn, allows for tradespace exploration and sensitivity analyses to be performed. To the best of our knowledge, HabNet is the first integrated space mission analysis environment to be validated both in its dynamic simulation and its sizing capabilities.
- What we believe to be **the first integrated and quantitative analysis of the emplacement and lifecycle resupply requirements of a "Mars to Stay" class of mission**. In addition, to the finding that traditional missions of this nature incur near-indefinite resupply costs and grow more expensive with increasing crew size, this study identified challenges with

atmospheric imbalances that occur when large quantities of crops are grown in the same cabin as the crew, as well as the critical role of in-situ resource mining and manufacturing in controlling the lifecycle costs of such mission plans.

- The **development and analysis of the Minimum Continuous Presence mission plan**, the first mission that we have seen that enables the transition from a series of conjunction class sortie missions to a continuous human presence on Mars, while at the same time enabling periodic crew return. Traditional Mars mission concepts are either specifically conjunction class sorties, or one-way missions. Concepts that consider the transition from sortie missions towards a more extended and ultimately continuous presence have not been as widely published.
- The finding that a **food production level of approximately 4.5% is the upper bound by which food can be grown in a shared volume with the crew** without incurring addition requirements for supplementary CO_2. This has implications on the level of food that can be grown in habitation systems that do not have access to ISRU resources, such as deep space habitats or long-duration space stations.
- The finding that an **archetypical Mars surface ISRU architecture emerges** as a result of the dominant demand for ISRU-derived MAV propellants relative to the mass of all consumables required. This architecture is based on the ISRU technologies currently modeled within the HabNet ISRU Model Library, and consists of a Sabatier Reactor supported by a water electrolyzer, water extraction unit, and a CO_2 cryocooler, as well as an atmospheric processor to extract nitrogen from the Martian atmosphere.
- The finding of the **consistent mass-optimality of an ISRU-supplemented open loop ECLS architecture**, which arises due to the dominant demand for MAV propellants causing the incremental cost of deriving ECLS consumables from ISRU to be significantly lower than the cost of emplacing additional ECLS hardware to recycle consumables (by a factor of 4 to 7).
- The finding of the **competitiveness of the 100% food production architecture integrated with an ISRU-supplemented open loop ECLS system**, under conditions where the cost of ISRU is low and some level of continuous human presence is sustained over multiple decades. Here, it was found that if food growth is desired at any level beyond the threshold value of 4.5%, and the above-listed conditions are satisfied, the food

production level should be set at 100% in order to more quickly attain the benefits associated with eliminating the requirement for the resupply of food from Earth.

- The finding of the **dependency of ECLS architecture mass-optimality on the cost of ISRU**, where open-loop ECLS architectures become mass-optimal when ISRU systems exhibit low mass and high reliability, and ECLS architectures that recycle water become mass-optimal when ISRU systems are either very costly to implement, or are not a feasible option due to the mission environment.
- The finding of the **existence of an ISRU cost-threshold** – an ISRU system mass and reliability level for a given resource production rate requirement where ECLS mass-optimality transitions from the preference towards open-loop architectures, to the preference towards higher levels of recycling. In this thesis, the existence and characteristics of this threshold were identified but not quantified. As will be seen in the next section, the precise calculation of this threshold under different mission scenarios has been identified as an area for future work.

7.3 Research Limitations and Opportunities for Future Work

In this thesis, every effort was made to gather and apply the most up to date publicly available data on habitation, ECLS, and ISRU systems in the architectural analysis of a range of Mars mission scenarios. While the implementation and application of this data within HabNet led to new insights on the challenges of human spaceflight mission architecting, a number of limitations were inevitably present. These come in the form of limitations in the scope of the case studies performed, as well as limitations in the fidelity and breadth of the current capabilities of HabNet. Each of these types of limitations provides opportunities for future work, in the form of additional case studies to be performed, as well as the further refinement and expansion of HabNet's capabilities. These are discussed further in the following subsections.

7.3.1 Limitations in the Scope of the Case Studies Performed and Options for Future Analyses within HabNet

This thesis established a consistent integrated campaign analysis methodology that was applied to a wide range of mission scenarios. While these analyses covered a broad swath of the space of potential mission options, a number of case studies and sensitivity analyses were not addressed, and are thus considered as limitations in the scope of case studies performed. These limitations, along with future analyses that could be performed to address them, are listed as follows:

- The **characterization of the ISRU cost-threshold** identified in Section 6.5.5. While this task was not performed within this thesis, the current capabilities of HabNet are well suited to computing this ISRU cost-threshold value under different mission scenarios. Performing this analysis would involve repeating the sensitivity analyses in Sections 6.4.5 and 6.5.5 with a series of ISRU mass and reliability values that are discretized to some high level of resolution. Developing a first order estimate for this ISRU cost-threshold would be an important contribution towards guiding future analyses that attempt to search for optimal architectures through the human spaceflight architecture tradespace. This threshold value could also be used to set performance targets for the development of future ISRU technologies.
- Limitations in the **surface habitation scenarios** whereby all crewmembers remained in the vicinity of the surface habitat for the duration of their mission (either by remaining within the habitat itself, or performing EVA in the immediate area surrounding the habitat). NASA's current Mars mission architecture anticipates the addition of a number of pressurized rovers that would enable surface exploration at larger distances from the surface habitat. These pressurized rovers are planned to be capable of sustaining two crewmembers for up to two weeks at a time, and are based on life support systems similar to the portable life support systems carried by the crew during EVA [21]. As such, future analyses should model the resource demands of these surface transportation systems in order to increase the overall scope and fidelity of the mission scenarios considered. Incorporating these considerations may lead to new insights and new trades not previously identified. One such example might be a trade in rover consumables requirements versus exploration time spent away from the main surface base.

- The fact that the analyses considered throughout this thesis did not account for **additional resources required to manage contingency scenarios**, such as fire, habitat pressure vessel damage, or chemical spills. Such conditions would require additional ECLS resources to aid in their recovery. An analysis performed whereby the system level impacts of the additional ECLS consumables required to manage different probabilities of the occurrence of different contingency scenarios would provide beneficial insights to mission architects. Based on the results obtained in this thesis, one potential architectural solution may be to add additional ISRU capability to generate a dedicated cache of consumables for use in such contingency scenarios.

7.3.2 Limitations of Current Analysis Capabilities and Opportunities for Further Refinement

In addition to the limitations in the scope of the case studies performed, limitations are also present in the current capabilities of HabNet, primarily due to **uncertainties in the attributes of the technologies modeled**. This section describes the sources of uncertainty in HabNet in greater detail, and proposes future work aimed at reducing this uncertainty. These are listed below, as follows:

- **Mass as a proxy for cost:** In the case studies conducted in this thesis, mass has been consistently used as the measure of effectiveness. On numerous occasions, the term "cost" has been used to describe a mass value, since mass has been adopted as a proxy for cost. This has been a necessary implementation due to the significant uncertainties associated with estimating the development and operational costs of systems that are at very low levels of technical maturity. Thus, a key step in advancing the capabilities of HabNet, and spaceflight mission architecting in general, would be the development and implementation of some means to estimate the development, emplacement, operations, and sustainment costs of the various architectures evaluated.
- **Adoption of ISS-based ECLS technologies:** While the characteristics of the ECLS technologies assumed in the case studies performed in this thesis were based on ECLS flight hardware currently operating onboard the International Space Station (ISS), the presence of a partial gravity environment on the surface of Mars will inevitably lead to different ECLS technologies. Currently, however, the baseline Mars surface ECLS architecture under development by NASA assumes an extension of the ISS ECLS architecture, and has not

been refined to a level where their mass and reliability characteristics have been quantified. Ideally, a capability would exist to size an optimal ECLS architecture based on the number and composition of the surface crew as well as their activities. This would require a bottom-up system sizing routine that would estimate the mass of systems required to perform each of the unit operations involved in each ECLS process. A first step in the development of such a routine may be to use the mass and reliability characteristics of analogous chemical processing hardware operating in comparable extreme environments (e.g. the Antarctic).

- **Uncertainty in the mass and reliability of ISRU systems:** As was mentioned in Sections 3.4.3 and 6.4.5, there is currently a significant level of uncertainty associated with the mass and reliability of ISRU systems, due to their low technology readiness level. A survey of sizing estimates published in the literature by Schrenk [144] found that in some cases, mass estimates of systems can vary by an order of magnitude or more. In addition, given the limited operational experience of experimental ISRU systems in analogous environments, data on the reliability of ISRU systems is extremely scarce. Thus to improve the campaign level predictions of HabNet, more data on ISRU system performance is necessary. As this data becomes available, the HabNet ISRU Module will be updated accordingly.

7.3.3 Expansion of Current Analysis Scope

While HabNet, in its current state, covers a broad range of architectural decisions within its framework, there are limitations in its analysis scope. As such, several opportunities exist for the expansion of its capabilities to enable the deeper exploration of a broader mission architecting tradespace. These include:

- The **incorporation of additional ECLS technologies** not currently operating on the ISS. For long-duration orbital habitats, the set of ECLS technologies that were traded off during the Space Station Freedom Comparative Test Program (see Section 2.1.2) may become competitive, especially given the fact that a key determining criteria in the selection of the ISS technologies was technical maturity, rather than performance and reliability. For planetary surface habitats, biological life support technologies such as algal photobioreactors [288] and biological air filters [52] may become attractive, especially if they result in reductions in resupply mass.

- The implementation of options for **solid waste management strategies** beyond basic storage, which was implemented in all of the case studies considered here. This would involve the expansion of the ECLS Technology Model Library to include waste processing technologies such as aerobic and anaerobic digestion to support nutrient recovery, heat melt compactors [289], and/or "Trash-to-Gas" technologies that convert solid waste into useful commodities [290].
- The implementation of **additive manufacturing and feedstock recycling** technologies to investigate the costs and benefits of reducing spare parts resupply demands via this new technology. Although this technology is currently in its infancy in the spaceflight context, its technical maturity is rapidly advancing, especially in light of the series of 3D printing experiments currently being performed on the International Space Station [291]. As more system data is acquired, representative technology models can be developed and implemented into HabNet to evaluate their impact on the lifecycle costs of long-duration human spaceflight mission campaigns.
- The addition of a means to **track crew time requirements** related to system repair and maintenance as a function of the architecture selected. This would allow for trade-offs in crew time versus system capability and total system mass to be performed. This is an especially important consideration given that minimizing the amount of crew time dedicated to system upkeep so that more time can be spent on performing science continues to be a challenge on the ISS [292–294].
- The addition of a means to **automatically synthesize habitat layouts** as a function of crew size, mission concepts of operation, and location. In all of the analyses conducted here, a habitat layout was assumed prior to the analysis of the habitation system with HabNet. The implementation of a means to automatically synthesize habitat layouts would enable the efficient analyses of spaceflight campaigns involving surface crew and infrastructure expansion.
- The **integration of the habitation architecting capabilities of HabNet with an in-space transportation network architecting capability**, such as the graph-theoretic approaches incorporated into space logistics architecting environments like SpaceNet [243] (see Section 1.2.1). This would enable larger scale system interactions and constraints to be modeled, leading to an overall advancement in our understanding of the human spaceflight systems architecting tradespace, and potentially uncovering previously unidentified dominant

architectures. Points of integration could include the co-optimization of destination surface systems and the transportation systems required to deliver them, while considering the trades associated with building long-duration surface infrastructure under mass- and volume- constrained crew and cargo transportation systems. This type of integrated analysis becomes particularly important in the context of deploying and evolving an interplanetary transportation network, where crew and cargo are delivered to different locations in a network to support both economic and exploration activities in space.

This thesis formed a first step towards codifying the human spaceflight mission architecting process. The avenues for future work discussed throughout this section were identified with the intention of advancing the scope of HabNet's analysis capability so that eventually, the entire human spaceflight system tradespace can be efficiently characterized. Through continued efforts towards the attainment of this capability, it is hoped that HabNet will continue to support and inform the architectural decisions that will shape the systems that will ultimately enable humanity's continued expansion into the cosmos.

Appendix A

Summary of Main Object Process Methodology (OPM) Constructs

Table A.1: OPM Basic Elements [124]

Name	OPD Example	OPL Example
Object 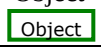	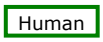	Human
Process 		Nourishing
State 		Human *can be* Hungry *or* Satiated

Table A.2: OPM Structural Links [124]. Terms in parentheses can be considered as descriptions of the class of items stemming from the given link

Name	OPD Example	OPL Example
Decomposition  (Sub-components)	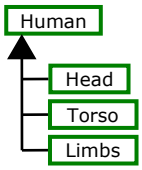	Human *consists of* Head, Torso, *and* Limbs
	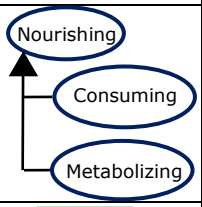	Nourishing *consists of* Consuming *and* Metabolizing
Exhibition  (Attributes)	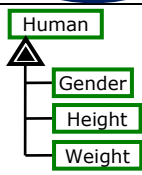	Human *exhibits* Gender, Height, *and* Weight
	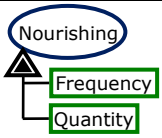	Nourishing *exhibits* Frequency *and* Quantity
Specialization  (is a Variant of)	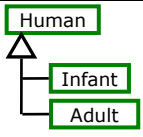	Infant *is a type of* Human Adult *is a type of* Human
	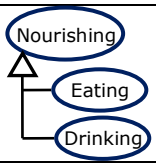	Eating *is a type of* Nourishing Drinking *is a type of* Nourishing
Instantiation  (is an Instance of)	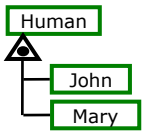	John *is an instance of* Human Mary *is an instance of* Human

Table A.3: OPM Procedural Links [124]

Name	OPD Example	OPL Example
Consumption 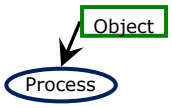	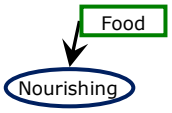	Nourishing *consumes* Food
Result 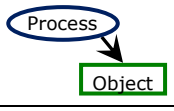	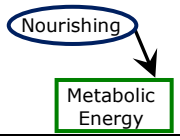	Nourishing *yields* Metabolic Energy
Affect 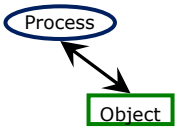	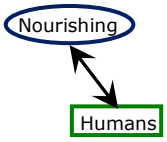	Nourishing *affects* Humans
Enabler 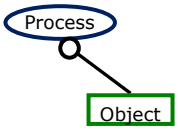	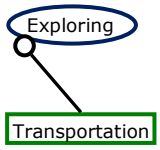	Exploring *requires* Transportation
Intelligent Enabler 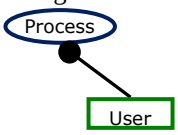	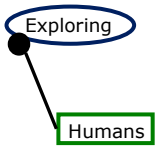	Exploring *is handled by* Humans

Table A.4: Equivalent Representations in OPM [124]

	OPD Example	OPL Example
Representing Function	Explicit Form 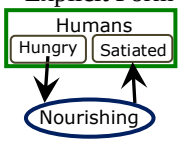	Nourishing *changes* Humans *from* Hungry *to* Satiated
	Affect Link 	Nourishing *affects* Humans
	Suppressed Representation 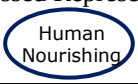	Human Nourishing (Noun + Verb + "ing")
Invocation	Explicit Form 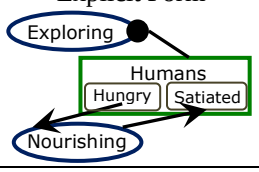	Exploring *is handled by* Humans. Nourishing *changes* Humans *from* Hungry *to* Satiated
	Invocation Link 	Exploring *invokes* Human Nourishing

Appendix B

Habitat Architecture Modeling within HabNet

B.1 The SimEnvironment HabNet Class

In Section 3.2, it was specified that one of the initial inputs required by the HabNet Habitation Module was a definition of a habitat layout. This appendix further expands on the procedure by which a habitat is defined and simulated within HabNet.

When a pressurized module is instantiated within HabNet, it calls a class referred to as a SimEnvironment. As shown in the SimEnvironment Technology Map depicted in Figure B-1, each SimEnvironment stores a range of data regarding its atmospheric pressure and composition, as well as levels of various grades of water, food and dry waste within it.

During initialization of a SimEnvironment, the Architecture attributes listed in the Technology Map in Figure B-1 are defined by the user. Here, the definition of the atmospheric composition initializes "stores" for each of the atmospheric species that are attributed to the SimEnvironment. Each of these "stores" initially holds a certain number of moles of the given atmospheric species, calculated as a function of the specified pressure, volume, temperature, and molar fraction of that species. The initialized atmospheric composition is typically chosen based on the recommendations of the NASA Exploration Atmospheres Working Group (EAWG) [112], and is dependent on the mission context in which the habitat is expected to function.

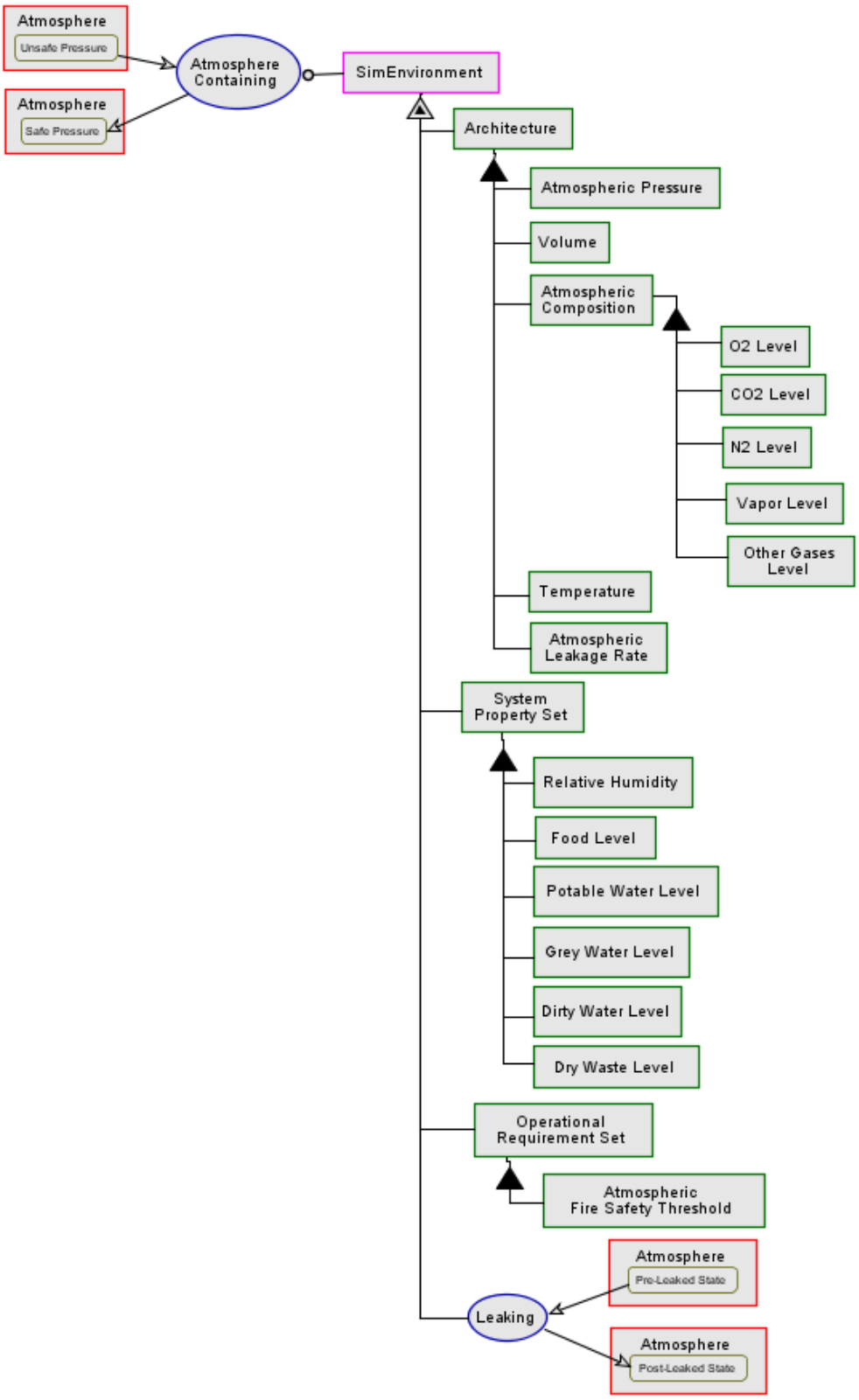

Figure B-1: The SimEnvironment Class Technology Map

In addition, the user can optionally initialize levels of potable, grey, and dirty water, as well as food and dry waste levels. This corresponds to assigning stores for each of these consumables within this particular habitat module.

During each simulated time step, the "tick" method is called for each SimEnvironment, causing an update in the global timestamp of the SimEnvironment, as well as the leakage of atmosphere based a user specified atmospheric leakage rate. If no leakage rate is specified, a default value of 0.05% of atmospheric loss by moles per day is used, based on values specified in the NASA Baseline Values and Assumptions Document (BVAD) [179].

B.2 Modeling Multi-Module Habitats

In the case of multi-module habitats, a SimEnvironment is required to be initialized for each module. In addition, an adjacency matrix is required to be defined in order to model pressure driven air flow between adjacent modules. Figure B-2 shows an example of an adjacency matrix for the Habitat Demonstration Unit multi-module habitat used in Chapter 6.

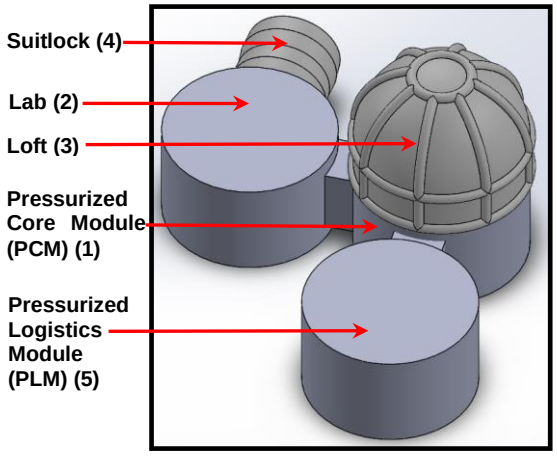

Adjacency Matrix:

	PCM (1)	Lab (2)	Loft (3)	Suitlock (4)	PLM (5)
PCM(1)		1	1		1
Lab (2)	1			1	
Loft (3)	1				
Suitlock (4)		1			
PLM (5)	1				

Figure B-2: A sample habitat and its adjacency matrix

The list of newly created SimEnvironments (representing each individual habitat module) along with the corresponding adjacency matrix are then input the HabNet function called "PressureDistribute", which in turn automatically generates a linear system of equations based on the information stored within the adjacency matrix. At every time step during the simulation, the average pressure across all modules is calculated via the Ideal Gas Law, and the number of moles needed to be transferred into or out of each module in order to reach this average target

pressure are then computed. This vector of molar differences ($\boldsymbol{\Delta n}$) is then used as the forcing function from which the linear system of equations is solved. The result of this computation is a vector containing the number of moles of gas that need to be transferred between adjacent modules in order to equalize pressure across all modules ($\dot{\boldsymbol{n}}$). An example of this linear system is presented below, for the multi-module habitat example depicted in Figure B-3.

$$\begin{bmatrix} 1 & 1 & 1 & 0 & 0 & 0 & 0 & 0 \\ 0 & 0 & 0 & 1 & 1 & 0 & 0 & 0 \\ 0 & 0 & 0 & 0 & 0 & 1 & 0 & 0 \\ 0 & 0 & 0 & 0 & 0 & 0 & 1 & 0 \\ 0 & 0 & 0 & 0 & 0 & 0 & 0 & 1 \\ 1 & 0 & 0 & 1 & 0 & 0 & 0 & 0 \\ 0 & 1 & 0 & 0 & 0 & 1 & 0 & 0 \\ 0 & 0 & 1 & 0 & 0 & 0 & 0 & 1 \\ 0 & 0 & 0 & 0 & 1 & 0 & 1 & 0 \end{bmatrix} \begin{bmatrix} \dot{n}_{12} \\ \dot{n}_{13} \\ \dot{n}_{15} \\ \dot{n}_{21} \\ \dot{n}_{24} \\ \dot{n}_{31} \\ \dot{n}_{42} \\ \dot{n}_{51} \end{bmatrix} = \begin{bmatrix} \Delta n_1 \\ \Delta n_2 \\ \Delta n_3 \\ \Delta n_4 \\ \Delta n_5 \\ 0 \\ 0 \\ 0 \\ 0 \end{bmatrix}$$

Flow equilibrium equations
The sum of all flows into and out of each module is equal to 0

Flow equality constraint
The flow from module A to B is the negative of the flow from module B to A: ($\dot{n}_{AB} = -\dot{n}_{BA}$)

Figure B-3: A Linear System of Equations built to solve for pressure-driven flow for the Habitation Demonstration Unit Case

Once the vector of molar gas flows ($\dot{\boldsymbol{n}}$) is solved for, the amount of gas listed in each element of the vector is transferred between the corresponding pairs of adjacent habitat modules. For example, in the linear system depicted in Figure B-3, $\dot{\mathbf{n}}_{\mathbf{12}}$ corresponds to the number of moles required to flow from the Pressured Core Module (Module 1 as listed in Figure B-2) to the Lab (Module 2 as listed in Figure B-2) in order for the modules to equalize pressures with the rest of the habitat. This process is repeated at every time step.

B.3 Intermodule Ventilation and the ISSFan Class

In addition to pressure driven air flow, fan driven air flow is also typically desired in multi-module habitat configurations, especially when air revitalization hardware is not installed in all modules. In such cases, local buildup of high CO_2 concentration and/or high humidity air can occur, thus providing a health and comfort risk to the crew. To mitigate this risk, forced atmospheric exchange between the module with and without CO_2 removal and dehumidifying

equipment is required to provide a flow path for revitalization of high CO_2 and/or humidity air. As shown in the ISS U.S. Node 1 and Laboratory ducting diagram below, this atmospheric exchange is typically facilitated by Intermodule Ventilation (IMV) Fans.

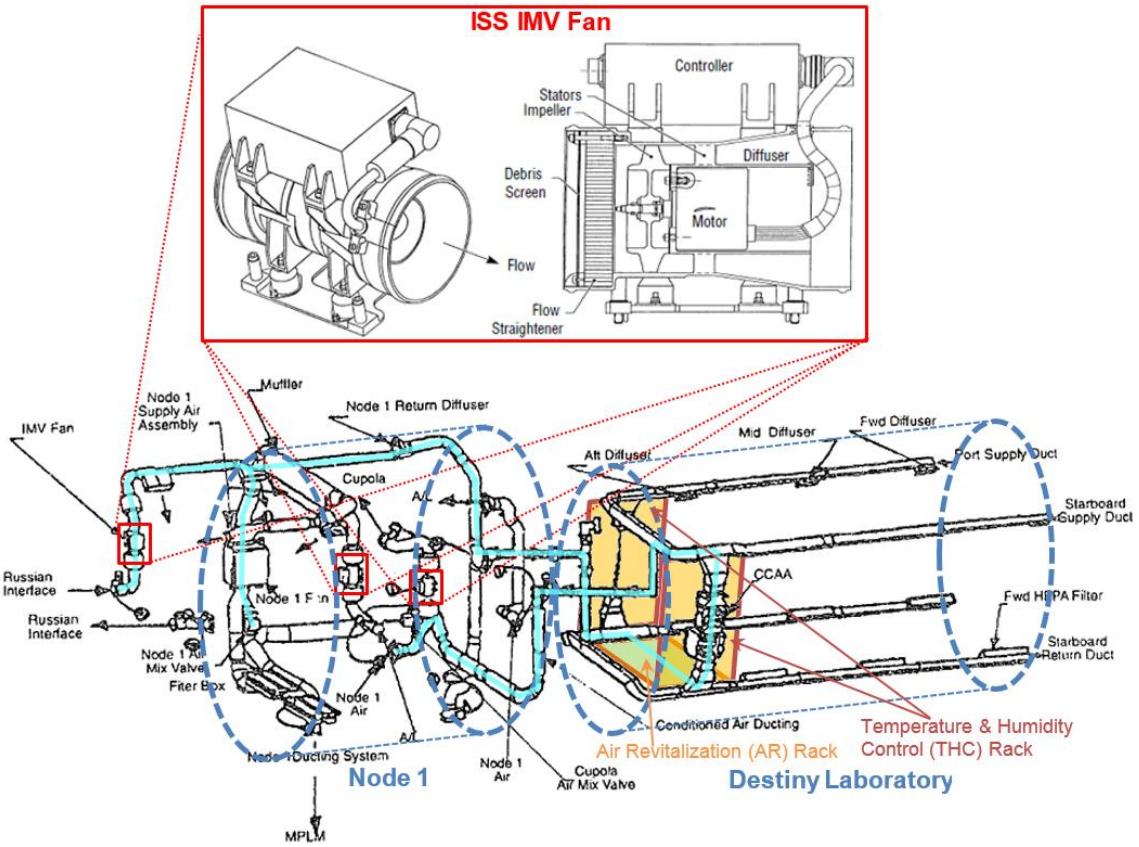

Figure B-4*:* The ISS Intermodule Ventilation (IMV) Fan and some of its locations onboard the ISS (as per ISS planning in 1997). Here, IMV Fans transport air from Node 1, the Cupola, the Airlock, and the ISS Russian Segment towards the Air Revitalization (AR) and Temperature and Humidity Control (THC) racks within the U.S. Destiny Laboratory, where CO_2 is removed and humidity is lowered. One of the several flow paths is highlighted in light blue (figures adapted from [44,295])

Within HabNet, IMV fans are modeled by the ISSFan Class. Specifically, the IMV currently used onboard the ISS is implemented within this class. As shown in the ISSFan Technology Map shown in Figure B-5, this fan has a nominal volumetric flow rate of 3964L/min, a nominal power consumption of 55W, and a mass of 4.7kg [44].

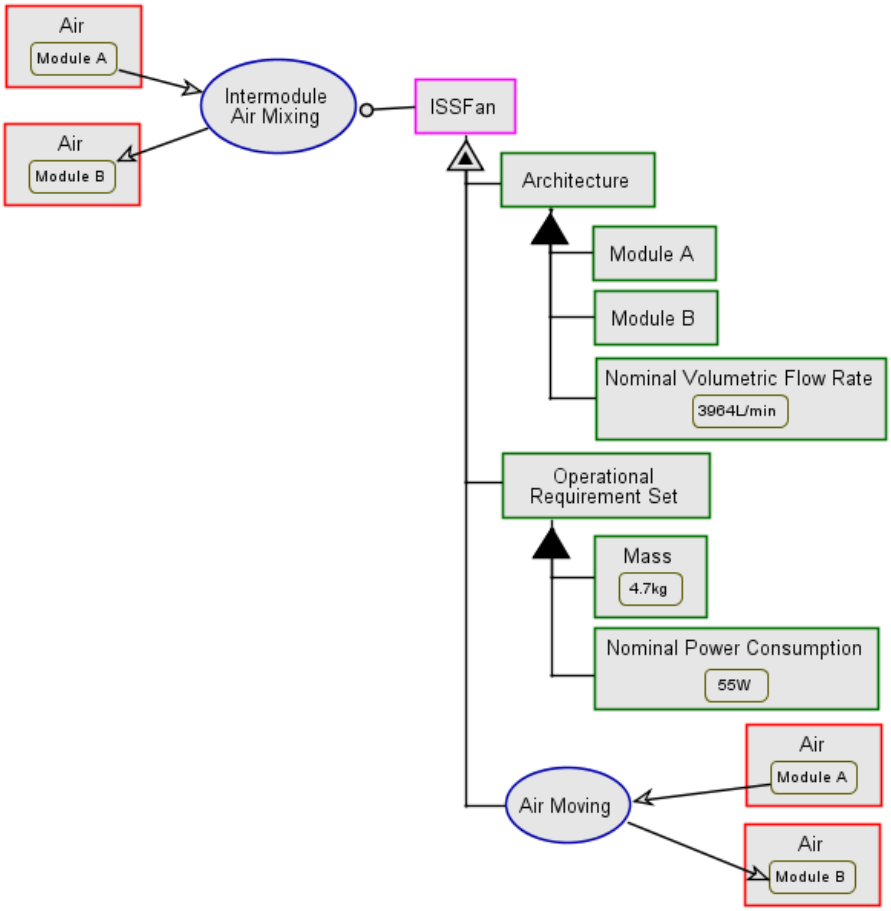

Figure B-5: ISSFan Technology Map (Data obtained from [44])

To initialize an instance of an ISSFan, the user inputs the two adjacent SimEnvironments representing the habitat modules that the IMV fan is intended to connect, along with the power source intended to supply the fan with power. During each time step, the fan attempts to consume 55W from the assigned power source, and exchanges an amount of air linearly proportional to the amount of power consumed (calibrated to the nominal flow of 3964L/min at 55W) between the two adjacent SimEnvironments.

Appendix C

Crew and Crew Activity Modeling

In Section 3.4.1, a high level description of the HabNet Habitation Module was described, consisting of the interaction between a simulated human crew, their individual schedules, and the habitation and life support systems that support them (see Figure C-1 below). In this appendix, we discuss the modeling implementation of the crew and schedule portions of this interrelationship. We begin by first introducing the ActivityImpl HabNet class, which represents a generic crew activity. After this, we describe how crew schedules are automatically created within HabNet using the CrewScheduler HabNet function. Following this, we conclude this appendix with a description of the crew model – the model used to dynamically simulate the consumption of resources and generation of metabolic wastes by the human crew as a function of their activities and their location within the simulated habitat.

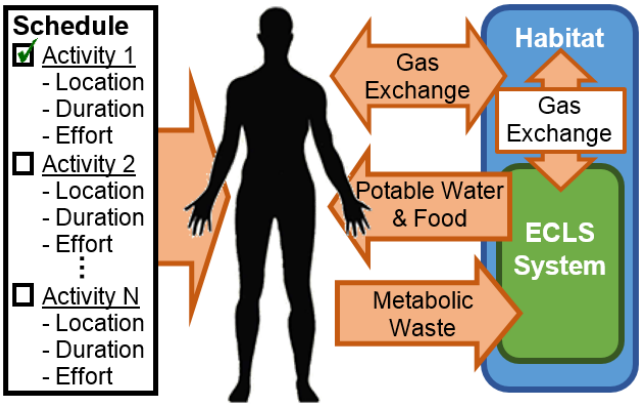

Figure C-1: Data Flow within the Habitation Module

C.1 The ActivityImpl Class

The ActivityImpl class within HabNet represents a generic crew activity – the fundamental building block of a crew schedule and their concept of operations (CONOPS). As shown in Figure C-2, an ActivityImpl object is defined by the declaration of its name, an intensity value, a duration, and a location.

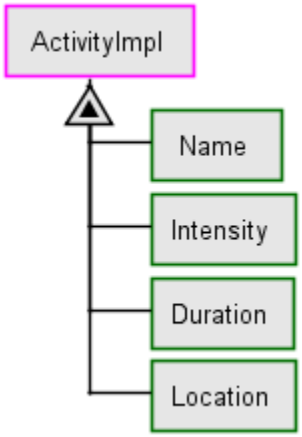

Figure C-2: ActivityImpl Technology Map

Here, the intensity value refers to an integer value between 1 and 5 that qualitatively represents the level of energy expended by the crew in performing a given activity. This implementation is based on the crew scheduling scheme adopted within BioSim and combined with the crew model of Goudarzi and Ting [138], where the intensity value is used to estimate a crewmember's heart rate and hence oxygen demand during a particular activity, as well as their caloric expenditure during an activity (see Appendix C.3 for details).

Table C.1 summarizes the intensity values assumed for the main activities expected to be performed in a mission simulation. This set of activities is based on those performed by crew members on the ISS (see Figure C-3), and is used in HabNet to form crew schedules.

Table C.1: Mapping Intensity Values used by the ActvityImpl class and Crew Activities

Activity	**Intensity Value**
Sleep	1
Standard (Sedentary) Intravehicular Activity (IVA) such as performing science experiments, eating, housekeeping, planning meetings, etc.	2
Light Exercise	3
EVA	3-4
Exercise	5

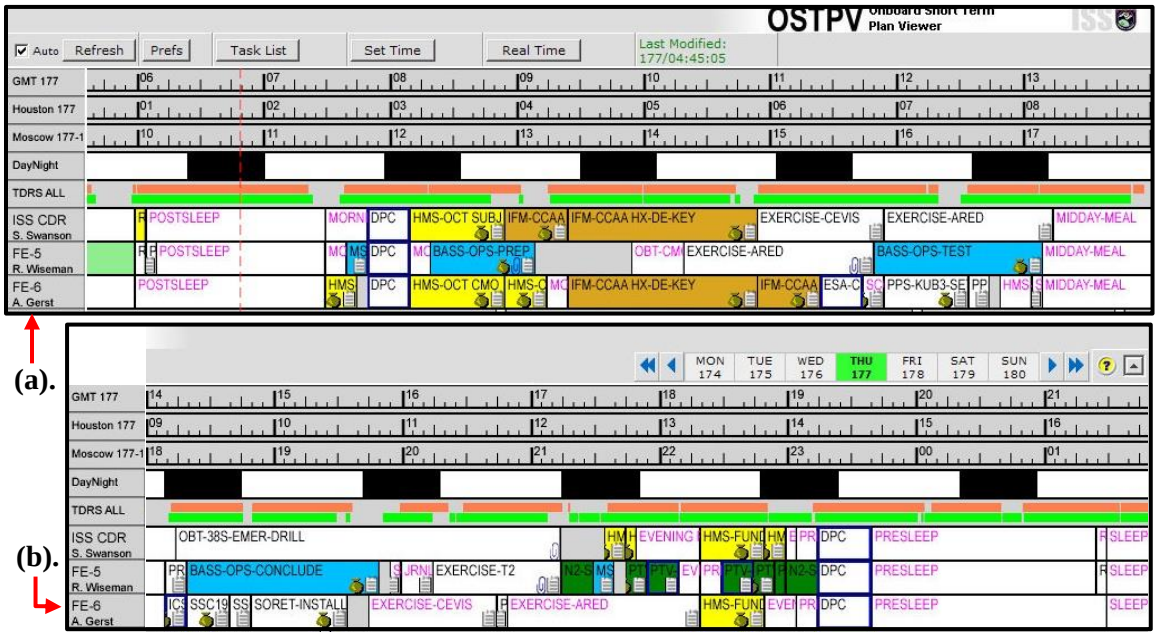

Figure C-3: Snapshot of a 24 hour schedule recorded on the Onboard Short Term Plan Viewer software used onboard the International Space Station [167]. This particular schedule was for ISS Expedition 40 on June 26th, 2014

In addition to the intensity value declared for each ActivityImpl object, a duration and location are also assigned, as depicted in Figure C-2. The location property assigned to the ActivityImpl object corresponds to a SimEnvironment (see Appendix B.1) where the activity takes place, while the duration property corresponds to the number of hours required to complete the activity.

C.2 Building a Crew Schedule with the Crew Scheduler Function

Within HabNet, a crew schedule is modeled as an array of activities that are assigned to each simulated crew member. During a simulation, the array of activities is parsed through at each time step, and the corresponding crew member is transported to the location of the activity, where they exert energy equivalent to the specified intensity level for a period of time equal to the pre-specified duration of the current activity.

This array of activities can either be built manually by the user, or generated automatically using the CrewScheduler function within HabNet. As can be seen in Figure C-4, this function

requires the user to define information regarding the number of extravehicular activities (EVAs) expected to be performed by the crew each week, the number of crew, the duration of the mission, and a list of the elemental crew activities.

Figure C-4: Inputs and Outputs of the CrewScheduler HabNet Function

Using this user-input information, the CrewScheduler function then generates a schedule for each crewmember based on the following assumptions:

- The minimum number of crewmembers required for an extravehicular activity (EVA) to occur is three, where two crewmembers are performing the EVA, while the third is located within the habitat in support of the EVA [179]
- Only two crewmembers are on EVA at any one time, regardless of the size of the crew
- No EVAs are performed on weekends [179], and a maximum of one EVA is performed per day. Thus the maximum number of EVAs per week is five
- EVAs occur in 8 hour continuous blocks of time
- The mission starts at the beginning of a weekend – that is, at midnight on a Saturday
- Crewmembers who perform an EVA do not exercise on the same day
- Two hours of exercise are performed by each crewmember every day
- The maximum number of people exercising simultaneously at any one time is two. This is due to exercise equipment availability constraints
- Each crewmember sleeps for eight hours every day
- On a non-EVA day, there is at least one hour of nominal intravehicular activity (IVA) (see Table C.1)

The process of automatically generating a crew schedule commences with the automatic allocation of EVA-days to all work weeks over the course of the mission. By default, this is performed by parsing through each mission week, and randomly selecting which days an EVA

will occur, as well as randomly assigning two crewmembers to each EVA. On an EVA day, the 24 hour schedule is fixed to the set of activities listed in Table C.2.

Table C.2: Assumed EVA-day schedule

Activity	Duration (hours)	Intensity Value
Sleep	8	1
IVA (Eating, EVA prep)	3	2
EVA	8	4
IVA (Post-EVA, Eating, Pre-sleep)	5	2

For non-EVA days, a two hour block of exercise is randomly assigned to some non-sleeping hour for each crewmember. All other non-sleeping hours are assumed to a standard intravehicular activity with an intensity value of 2.

C.3 The CrewPersonImpl HabNet Class

With a means for defining a schedule for each crew member established, we now describe the crew model implemented within HabNet. As mentioned in Section 3.4.1, each crewmember simulated within HabNet uses schedule information to simulate their resource consumption and metabolic waste production over time. This basic function of exchanging resources under required operational conditions maps to the Technology Concept Template formulation developed in Section 3.3.2. Thus the selection of a human crew can be considered to be the selection of some system to serve the high level function of performing exploration. Within HabNet, each crewmember is modeled as an instance of the CrewPersonImpl class. This class is summarized in the Technology Map depicted below, in Figure C-5.

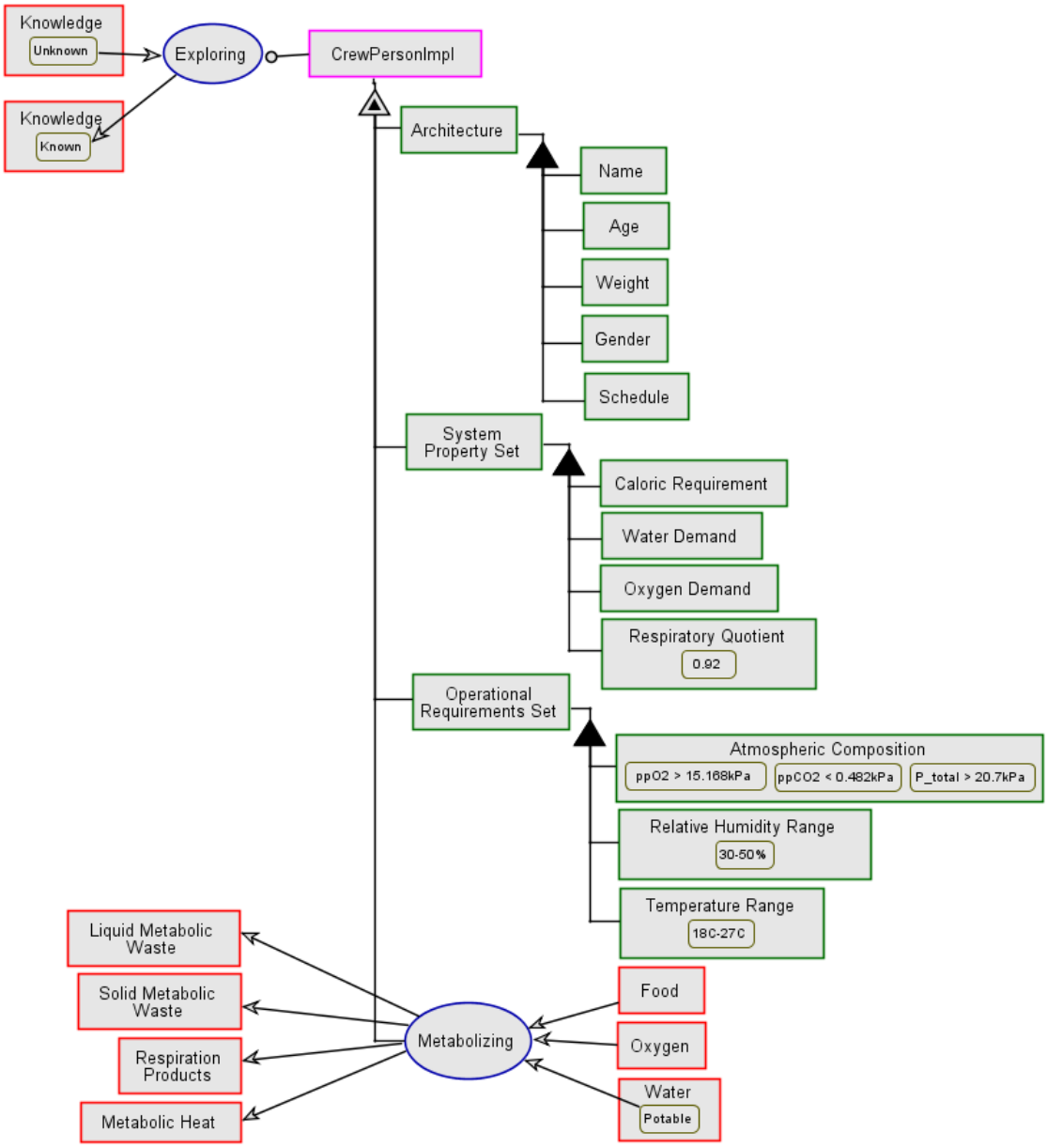

Figure C-5: Technology Map of the CrewPersonImpl HabNet Class (Data obtained from [139])

As can be seen in Figure C-5, the instantiation of a CrewPersonImpl object commences with a definition of the name, age, weight, gender, and schedule of each crewmember modeled. During each time step within a typical simulation, the current activity of each CrewPersonImpl object is identified, and the simulated crewmember is transported to the SimEnvironment declared for the activity. In addition, the intensity value of the activity is used to determine the heart rate of the crewmember and hence their oxygen demand (see Equation (C.1)), as well as their caloric requirement (see Equation (C.2)). These metabolic demands are based on the crew

model developed by Goudarzi and Ting [138]. With these values computed, the moles of CO_2 exhaled by the crewmember is calculated based on their respiratory quotient (the number of moles of CO_2 exhaled for every mole of O_2 consumed), and the required number of calories is taken from the food store located within the current SimEnvironment.

Hourly Oxygen Demand [138]:

$$\text{HeartRate} = \text{ActivityIntensity} \cdot 30 + 15$$
$$VO_2\,[\text{L/h}] = (a + b \cdot \text{HeartRate}^3) \cdot 60$$
Where: (C.1)
$a = 0.223804$ [L/min]
$b = 5.67 \times 10^{-7}$ [L/min (bpm^3)]

Hourly Caloric Requirement [138]:

Gender	Age [y]	Hourly Metabolic Rate [kJ/person/hr]	
Male	18-30	(160 · m + 5040 · ActivityCoefficient)/24	(C.2)
	30-60	(86 · m + 59900 · ActivityCoefficient)/24	
Female	18-30	(100 · m + 3200 · ActivityCoefficient)/24	
	30-60	(50 · m + 6066.7 · ActivityCoefficient)/24	
Where: *m* = mass of crewperson ActivityCoefficient = 0.5 · (ActivityIntensity - 1) + 1			

In addition, a simplified model is implemented to simulate potable water demand and liquid metabolic waste production, based on the approach adopted within BioSim [126]. Specifically, a constant total potable water consumption rate of 0.1667L/hr, including water in food consumed, is assumed (equating to a daily water intake of 4L). To determine the corresponding amount of water removed from the potable water store, the equivalent amount of water within the food consumed for the current time step is subtracted from this 0.1667L/hr value. Of the water consumed, it is assumed that 17.5% is converted into water vapor through respiration, 36.25% is converted into urine, and the remainder is converted to some form of grey water (such as perspiration or other liquid metabolic effluent) that may or may not be ultimately processed by a water processor assembly. This implementation is based on the models proposed by Goudarzi and Ting [138] and implemented within BioSim [126], and is intended

to maintain a water mass balance within the simulation. In addition, it is also assumed that 2.2% of all food mass consumed is converted to solid metabolic waste, as per the model of Goudarzi and Ting [138]. After these metabolic wastes are computed, they are distributed to the corresponding waste stores declared for the SimEnvironment in which the current activity is located.

In the scenario where insufficient resources are available to support the crew's metabolism during a particular time step (such as food, water, or oxygen), a warning is returned to the user to indicate that the crewmember has entered a degraded state. Warnings also appear when the atmospheric composition shifts outside the safe total pressure, or the oxygen and carbon dioxide partial pressure boundaries summarized in Figure C-5. Rather than immediately declaring a crew death in such events, internal stores are implemented for each CrewPersonImpl object to represent the period of time that a crewmember can be exposed to a degraded state before a fatality occurs.

Furthermore, a means of recovering from each of the aforementioned degraded states is also modeled for each simulated crewmember. This occurs if the conditions that originally led to the onset of the degraded state return to a nominal level before the crew's internal stores are depleted and a fatality can be invoked. This recovery is modeled as the refilling of the previously depleted internal stores of the CrewPersonImpl object at each time step that the crewmember is no longer exposed to the hazardous condition. Table C.3 summarizes the causes of each of the degraded states modeled, the conditions by which this degraded state leads to a crew fatality, and the manner in which a crewmember recovers from these degraded states. These values are largely based on the crew model originally developed within BioSim [126].

Table C.3: Causes, Effects, and Recovery Mechanisms from the Various Degraded States modeled within the CrewPersonImpl HabNet Object. Note that the default time step length within HabNet is assumed to be one hour

Degraded State	**Cause**	**Condition by which a fatality is invoked**	**Recovery Mechanism**
Starvation	Insufficient calories available for crewmember to consume	Cumulative caloric deficit reaches 180000 calories [126]	For every hour that sufficient calories are available after a starvation state has been entered, the cumulative caloric deficit is reduced by 0.01%
Dehydration	Insufficient potable water available for crewmember to consume	Cumulative potable water deficit reaches 5.3L [126]	For every hour that sufficient water is available after a dehydration state has been entered, the cumulative potable water deficit is reduced by 1%
Carbon dioxide poisoning	Partial pressure of CO_2 within the local atmosphere exceeds the high limit of 0.482kPa [139]	Cumulative exposure to CO_2 above the partial pressure limit of 0.482kPa reaches 4×0.482kPa = 1.928kPa [126]	For every hour that the ambient CO_2 partial pressure is within safe limits after a CO_2 poisoned state has been entered, the cumulative CO_2 exposure budget is reduced by 0.5%
Hypoxia	Partial pressure of oxygen within the local atmosphere is beneath the low limit of 15.168kPa [139]	Two consecutive hours in an oxygen-deprived state [126]	For every hour that the ambient oxygen pressure is above the low pressure limit after a hypoxia state has been entered, the time left before a fatality is invoked (initially 2 hours) is increased by 1%
Low Pressure Environment	Total local atmospheric pressure is beneath the low limit of 20.7kPa [139]	One hour spent in a low pressure environment [126]	No recovery mechanism exists for this degraded state. Once the pressure drops below the low limit, it is assumed that a crew fatality occurs immediately

As can be seen in Table C.3, the recovery rate is typically much lower than the depletion rate experienced once a degraded state has been entered. This difference is intended to represent the fact that recovering from a degraded state typically takes much longer than it takes a person already in a degraded state to deteriorate to the point of death.

Appendix D

ECLS Technology Model Library

In this appendix, we discuss each of the ECLS technologies modeled within the HabNet ECLS Technology Library. As will be seen in the subsequent discussion, most of the ECLS technologies modeled here are based on those currently used onboard the ISS United States Orbital Segment (USOS), mainly due to their technical maturity and the wide availability of their data relative to other ECLS systems. For each technology, we use the Technology Concept Template (see Section 3.3.2) to summarize its function, its architecture, its operational context onboard the ISS (if relevant), as well as its quantitative attributes. In cases where some form of control logic is required to properly model the function of an ECLS technology, this is also described.

D.1 The Store Class

In Section 2.1.1, the concept of ECLS loop closure was introduced. Here, it was observed that the simplest life support system was one that had a completely open level of closure, where life support resources like water and oxygen were consumed directly from storage containers, and the resulting wastes were likewise stored in containers. Thus, the concept of storing material, either useful resources for later consumption or waste materials that have been previously generated, is fundamental to the modeling of life support systems.

Within HabNet, this function is served by the Store class – a generic store that when instantiated, can simulate any type of material container. As shown in the Technology Map below, the Store class consists of four attributes, all of which are input by the user during its initial construction. These are the Resource Type, the Store Type, the Capacity of the store, and the Current Level within the store. Here, the Store Type refers to whether the capacity is

finite or infinite. In the former case, a fixed capacity, or a "Material" type of store, simulates a typical resource container which is capable of overflowing when material is added such that its current level exceeds its finite capacity. Conversely, a store with an infinite capacity is referred to as an "Environmental" Store. These types of stores are intended to simulate resource sinks within the system, such as the external environment, when waste products are disposed or dumped overboard. In such cases, the "Environmental" store functions as a means of tracking the amount that a particular resource is discarded over time.

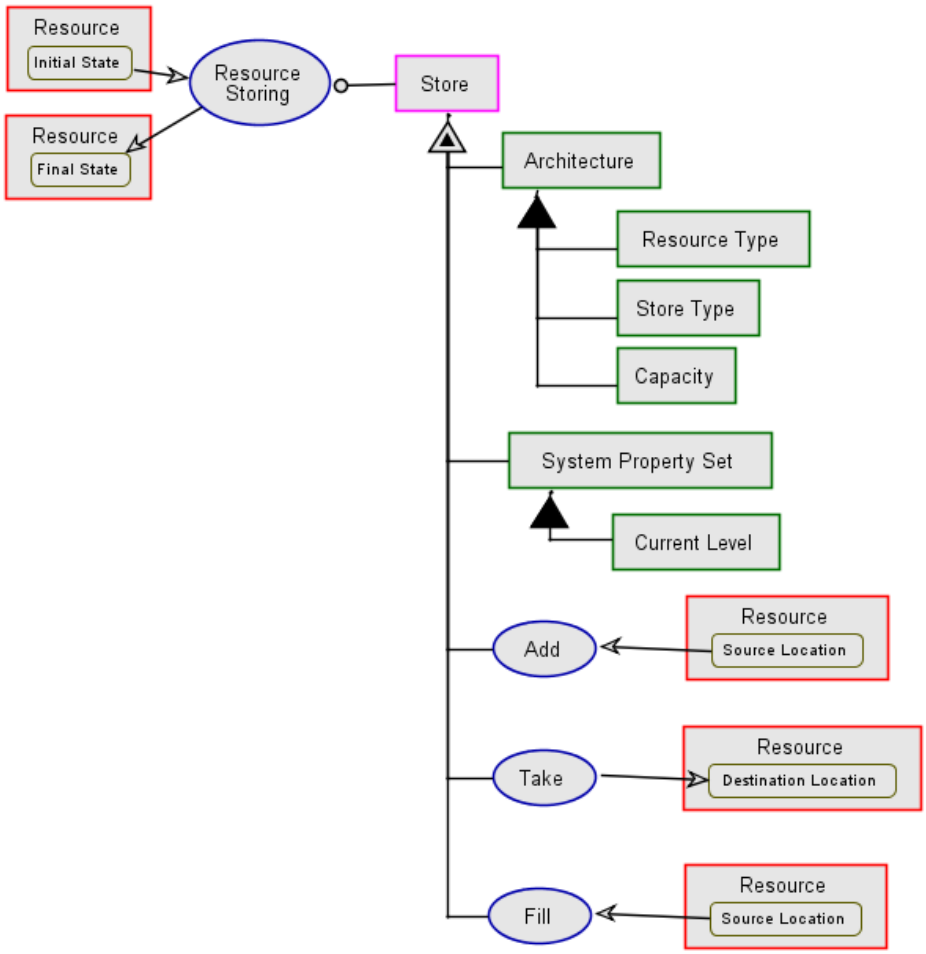

Figure D-1: Technology Map of the Store HabNet Class

In addition to the attributes described above, the Store class also contains a number of methods. These manipulate the manner in which resources are added to or removed from the Store, based on a source or destination for the resource (usually another instance of a HabNet Store) declared by the user. More specifically, the currently implemented methods are:

- the “Add” method, which adds resources to the current store from a declared source location
- the “Take” method, which transports material from the store to some declared destination; and
- the “Fill” method, which only applies to “Material” type stores and fills the store to its capacity using resources from some declared source location

Within HabNet, the Store class is used in a wide range of contexts at various levels within the system hierarchy. Instances where the Store class is used include:

- In SimEnvironments, where they are used to store each of the gaseous species that compose the atmosphere
- As major stores of life support consumables and wastes, such as oxygen, nitrogen, and potable and waste water tanks
- As the environment external to the habitat, where wet and dry waste might be disposed and gases might be vented
- As intermediate buffers within various technologies, such as the CO_2 accumulator that aggregates CO_2 extracted by a CO_2 removal system before being introduced into a Sabatier reactor for CO_2 reduction; and
- As internal food and water buffers within simulated crewmembers, in order to simulate the time delay between the onset of a hazardous condition (such as a hungry or dehydrated state), and the time at which a loss of crew event occurs

Currently, all stores instantiated within HabNet are assumed to be immune to failure and experience zero leakage. If desired, the user can remove this assumption by declaring a unique leakage rate for each store.

Finally, we note that no attributes related to the operational requirements of the Store class have been listed in the Technology Map depicted in Figure D-1. This is because in general, these requirements vary widely, depending on the type of material being contained by the store. For instance, a high pressure gas tank will have very different requirements to one that stores gases cryogenically. Furthermore, a rigid water tank will have different characteristics to one that is made of soft goods (as is the case with the water containers currently in use onboard the ISS). Within the case studies explored in this thesis, stores that have had operational experience onboard the ISS will be referenced by default. These stores and their attributes are summarized below, in Table D.1.

Table D.1: Summaries of Various Types of Stores used on the ISS and Modeled within HabNet

High Pressure Gas Tank (HPGT)	**Contingency Water Container (CWC)**	**Advanced Recycle Filter Tank Assembly (ARFTA)**
Stores high pressure O_2 or N_2 gas for EVA and for compensating for atmospheric leakage through the habitat structure	Stores water at various qualities on orbit, including potable, technical, condensate, and waste water [296,297]	Stores waste brine generated after urine is processed [298]
		
Empty Mass: 463kg [299]	Empty mass: 1.27kg [178]	Empty mass: ~50kg (based data listed in [300] and verified by calculations based on data in [301])
Capacity: 100kg of high pressure O_2 or N_2 gas (at 16.9MPa) [299]	Capacity: 44L [178]	Capacity: 21.7L [301] The ARFTA is emptied and reused every 11 days into a waste storage tank on a visiting logistics vehicle (e.g. Progress) after it reaches capacity [301]

D.2 The ISSInjector Class

With the concept of resource stores introduced in the previous section, we now introduce the ISSInjector HabNet class. This class represents technologies that manage and control the total atmospheric pressure and composition within a pressurized module. Within HabNet, the ISSInjector is based on the ISS Pressure Control Assembly, which serves these atmospheric pressure and control functions using high pressure oxygen and nitrogen gas supplied by high pressure gas tanks attached to the exterior of the Quest airlock (see Figure D-2).

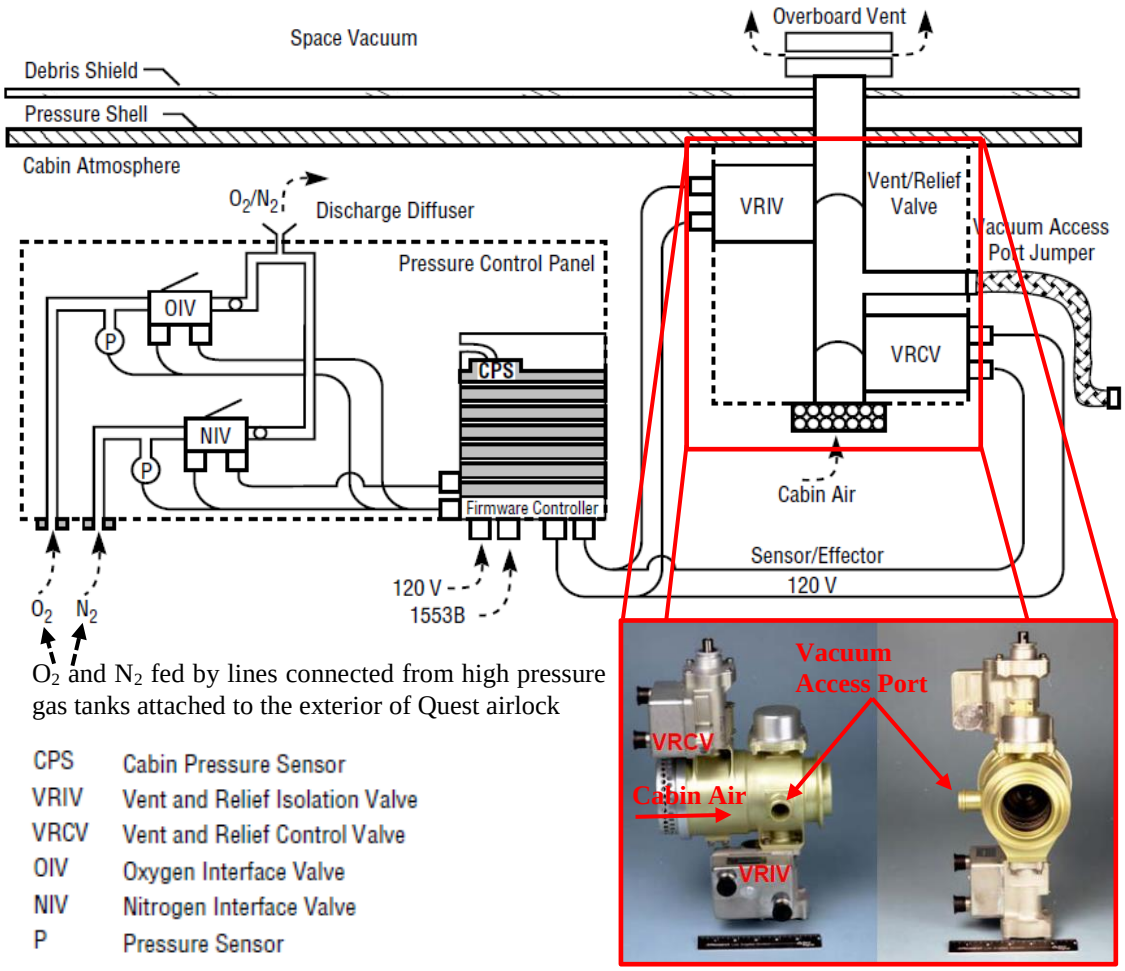

Figure D-2: Schematic of Pressure Control Assembly Interface with Habitat Shell on the ISS (Image adapted from [44] and [302])

As shown in the ISSInjector Technology Map depicted in Figure D-3, these functions include the:

- Reduction of oxygen concentration if it exceeds an upper threshold by introducing nitrogen from a predefined nitrogen gas source. By default, this upper threshold is set to 30% O_2 molar fraction, based on the fire safety threshold defined by NASA's Exploration Atmospheres Working Group (EAWG) [112]
- Reduction of total atmospheric pressure within the module when it exceeds the limits of the pressure control box defined by the user. This is accomplished by venting atmosphere from the habitat, as is the case with the current ISS Pressure Control Assembly (see Figure D-2). By default, the bounds of the pressure control box are set to ±0.2psia from the set pressure, based on recommendations of the NASA EAWG [112]
- Increasing the partial pressure of oxygen within the habitat if it decreases to a level outside of the pressure control box surrounding the oxygen partial pressure set point. Similar to the previous case, the pressure control box is set to ±0.2psia around the oxygen partial pressure set point based on recommendations of the NASA EAWG [112]
- Increasing the total atmospheric pressure within the habitat if it decreases to a level outside of the pressure control box surrounding the total pressure set point. Similar to the previous case, the pressure control box is set to ±0.2psia around the total pressure set point based on recommendations of the NASA EAWG [112]

Moreover, the ISSInjector can be set to operate in two different modes, being the "Pressure Control Assembly (PCA)" mode, where all of the above listed functions are made available; or the "Positive Pressure Relief Valve (PPRV)" mode, where only the overpressure relief function is available. If no operational mode is declared, the PCA mode is selected by default when instantiating an ISSInjector class.

During the setup of a typical habitation case within HabNet, an ISSInjector is usually assigned to each SimEnvironment to allow for local pressure control. As is the case with the distribution of pressure relief devices onboard the ISS, the PPRV mode is typically used only for SimEnvironments that represent logistics modules, while all other SimEnvironments are assigned ISSInjectors that operate in PCA mode.

Finally, we note that within the current version of HabNet, ISSInjectors are assumed not to fail, and are hence not spared for by the Supportability Module. This assumption may be modified in future releases of HabNet as more mass and reliability data becomes available for the operational PCAs.

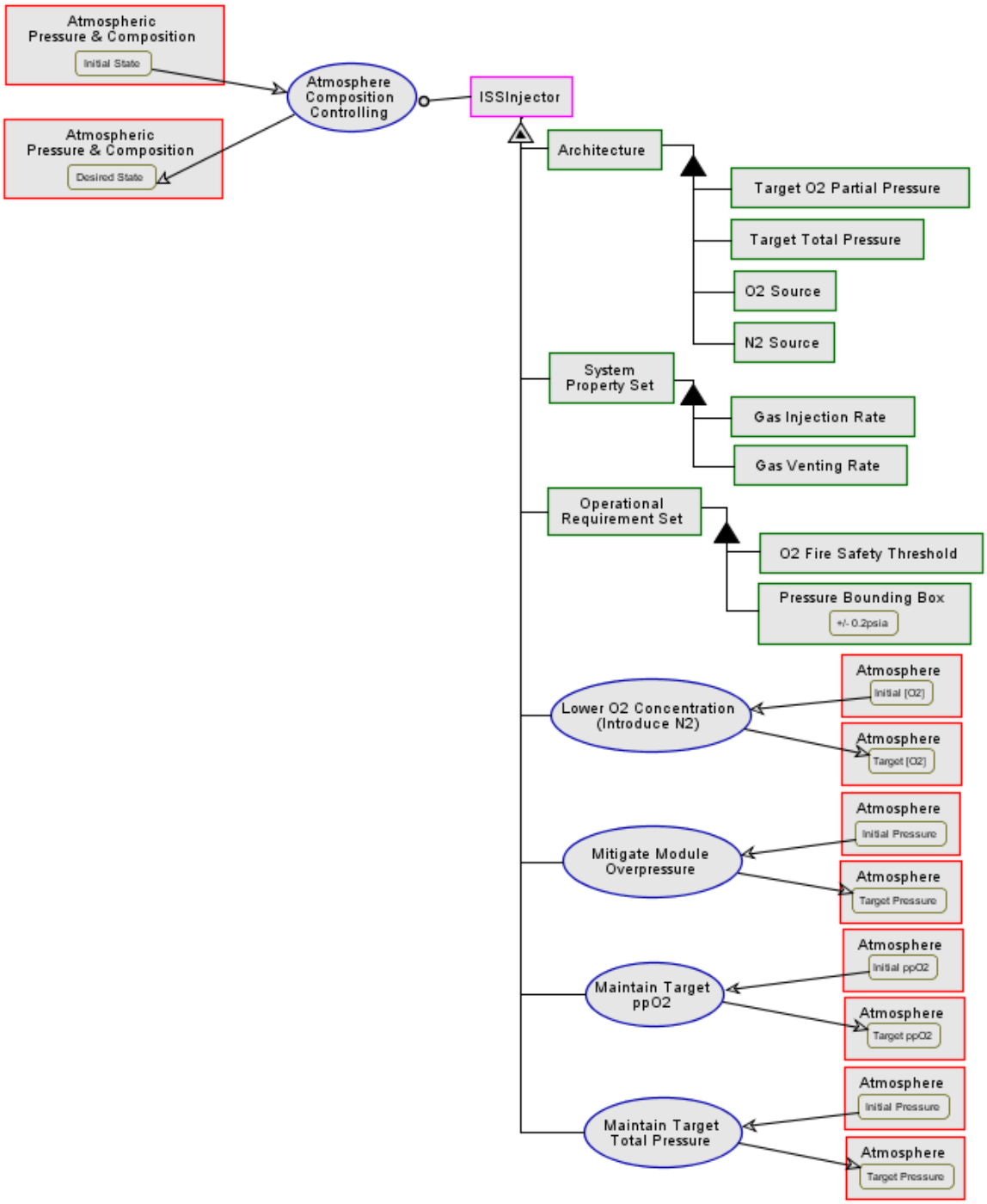

Figure D-3: Technology Map of the ISSInjector HabNet Class, Pressure Bounding Box based on EAWG [112]

D.3 The ISSDehumidifier Class

As its name suggests, the ISSDehumidifier class models the technologies used to control habitat temperature and humidity. Within HabNet, this class is modeled after the functions served by the Common Cabin Air Assembly (CCAA) used on the ISS. As can be seen in Figure D-4, the CCAA consists of three major components: the Inlet Orbital Replacement Unit (ORU), which contains a fan assembly that transports air into the CCAA and provides for intramodule ventilation; the Heat Exchanger (HX) ORU, which contains a Condensing Heat Exchanger (CHX) to lower air temperature through the removal of water vapor; and a Water Separator ORU to separate and deliver humidity condensate to the waste water bus for eventual recycling into potable water.

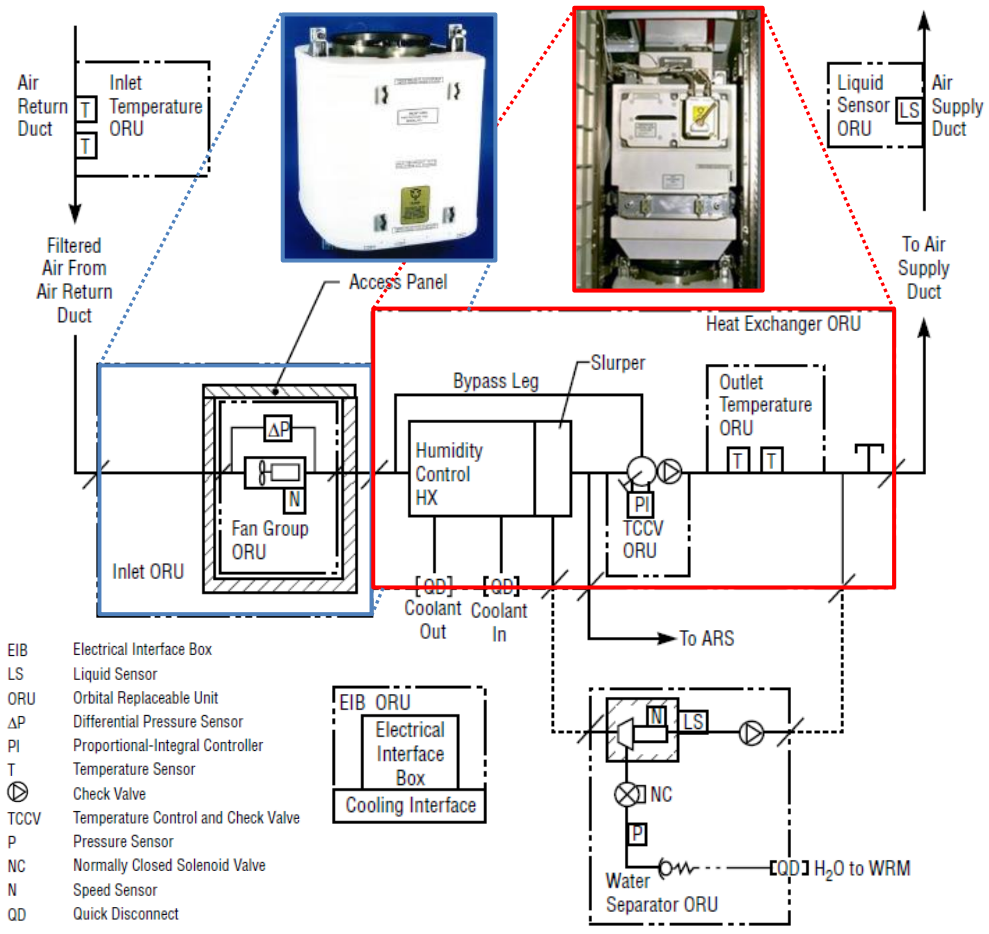

Figure D-4: Flowsheet for the ISS Common Cabin Air Assembly (Image adapted from [44,72,303])

Instead of modeling the function of each of these components separately and combining their result, the ISSDehumidifier class models these three components as if they were one integrated system. Specifically, a target relative humidity level, habitat module (represented by an instantiated SimEnvironment), power supply, and destination for extracted humidity condensate are declared by the user during instantiation of the ISSDehumidifier class. If no target relative humidity is specified, the ISSDehumidifier defaults to a value of 40% with a control box of ±10%, as per recommendations of the NASA Human Integration Design Handbook (HIDH) [139].

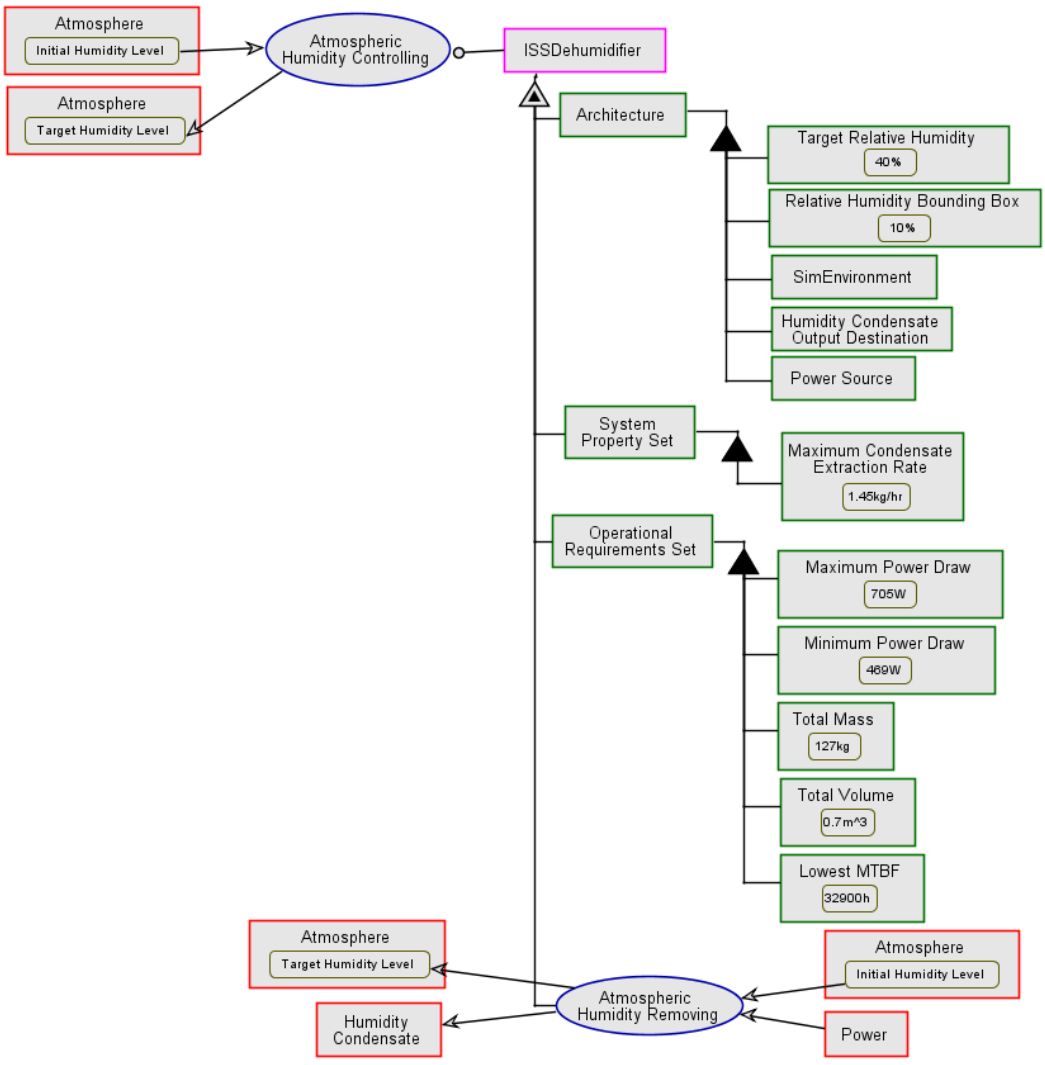

Figure D-5: Technology Map for the ISSDehumidifier HabNet class. (Data obtained from [44,139,209])

At each time step during a HabNet simulation, the ISSDehumidifier compares the current relative humidity of the atmosphere within the target habitat with the relative humidity control box defined by the user (see the ISSDehumidifier Technology Map in Figure D-5). If the current atmospheric relative humidity is beyond that of the control box, the required amount of water vapor moles to be removed to reduce the relative humidity towards the target value is calculated. This resulting value is then used to determine the power needed by the ISSDehumidifier, based on a linear scaling law derived from the maximum condensate extraction rate and the minimum and maximum power draws values of the ISS CCAA (see values in Figure D-5). If there is sufficient power available from the power supply, the ISSDehumidifier removes the previously calculated amount of water vapor moles from the atmosphere and delivers these to the humidity condensate output store declared by the user. In the scenario where insufficient power is available to the ISSDehumidifier, the system is shut down and an error message is returned to the user.

For all of the case studies performed in this thesis, an ISSDehumidifier object is instantiated within all habitat modules modeled, except for those that correspond to logistics modules. This convention is based on the design guidelines adopted for the ISS United States Orbital Segment ECLS architecture [304], where it was required that all long-duration habitation modules have a temperature and humidity control capability to ensure crew comfort and prevent the growth of mold and other undesired biomass.

Finally, to the estimate spare parts for the ISSDehumidifier, the Supportability Module accesses mass, volume, reliability, and part count data related to the ISS CCAA so that sparing can be performed at the lowest part level at which data is available. This implementation thus assumes that the ISSDehumidifier is composed of the same components and architecture as that of the ISS CCAA. We note that although the approach adopted for the spares analysis contrasts to the integrated manner in which the CCAA function is modeled, the component by component approach to spares analysis is analogous to how spare parts would be manifested in an operational mission. Table D.2 summarizes the component data accessed when performing a spares analysis on the ISSDehumidifier class.

Table D.2: Component Data Used to Model the ISSDehumidifier HabNet Class, based on values listed in the NASA BVAD 2004 [209] (unless otherwise noted)

ISSDehumidifier/CCAA Subassembly	Mass [kg]	Volume [m^3]	MTBF [h]	Life Limit [y]	Number per Unit
Condensing Heat Exchanger	49.71	0.39329	832600		1
Electronic Interface Box (EIB)	4.037	0.01728	2350000		2
Fan Delta Pressure Sensor	0.454	0.00016	1250000		1
Heat Exchanger Liquid Sensor	0.635	0.00057	1140000		2
Inlet ORU	25.31	0.13088	333000		1
Pressure Transducer	0.476	0	1250000	15	1
Temperature Control Check Valve (TCCV)	7.453	0.00708	32900		2
Temperature Sensor	0.263	0.00142	37600000		4
Water Separator	11.93	0.05829	131000	5	2
Water Separator Liquid Sensor	0.635	0.00057	1140000*		2

*Value based on analogy to the CCAA Heat Exchanger Liquid Sensor

D.4 The ISSVCCRLinear Class

The ISSVCCRLinear class models one of the most fundamental life support functions – the removal of carbon dioxide from a pressurized habitat environment. In HabNet, this class is based on the Carbon Dioxide Removal Assembly (CDRA) currently operating within the Atmosphere Revitalization (AR) racks installed in the ISS Destiny Laboratory and Node 3.

As shown by the blue path highlighted in Figure D-6, the CDRA consists of two Desiccant/Adsorbent Beds (DAB) that operate in a swing mode to facilitate the continuous removal of CO_2 from the incoming airstream. As CO_2 laden air enters the CDRA, it first passes through the desiccant side of the desorbing DAB where water is removed in order to increase the efficiency of the subsequent CO_2 adsorption process. Next, the dry air stream is further cooled as it passes through the blower/precooler unit, again in order to increase the efficiency of CO_2 adsorption. Following this step, the cold, dry air stream passes through the adsorbent side of the adsorbing DAB, where the zeolite 5A sorbent removes CO_2 gas from the airstream. After this phase, the air mixture passes through the desiccant side of the adsorbing DAB where previously separated water is added back to the airstream. From here, the now CO_2-lean air stream is returned to the cabin.

While this adsorption process is occurring on one of the CDRA DABs, the adsorbent side of the desorbing DAB is heated to desorb previously adsorbed CO_2, thereby regenerating the sorbent bed for future adsorption cycles (see the orange path depicted in Figure D-6). Prior to the commencement of this process, the Air Save pump is activated to recover residual gas within the air outlet line, thereby preventing loss of unnecessary atmosphere from the system. The high concentration CO_2 stream generated by the DAB desorption process is then sent to the CO_2 outlet, where it is either vented to space or directed to a downstream processor.

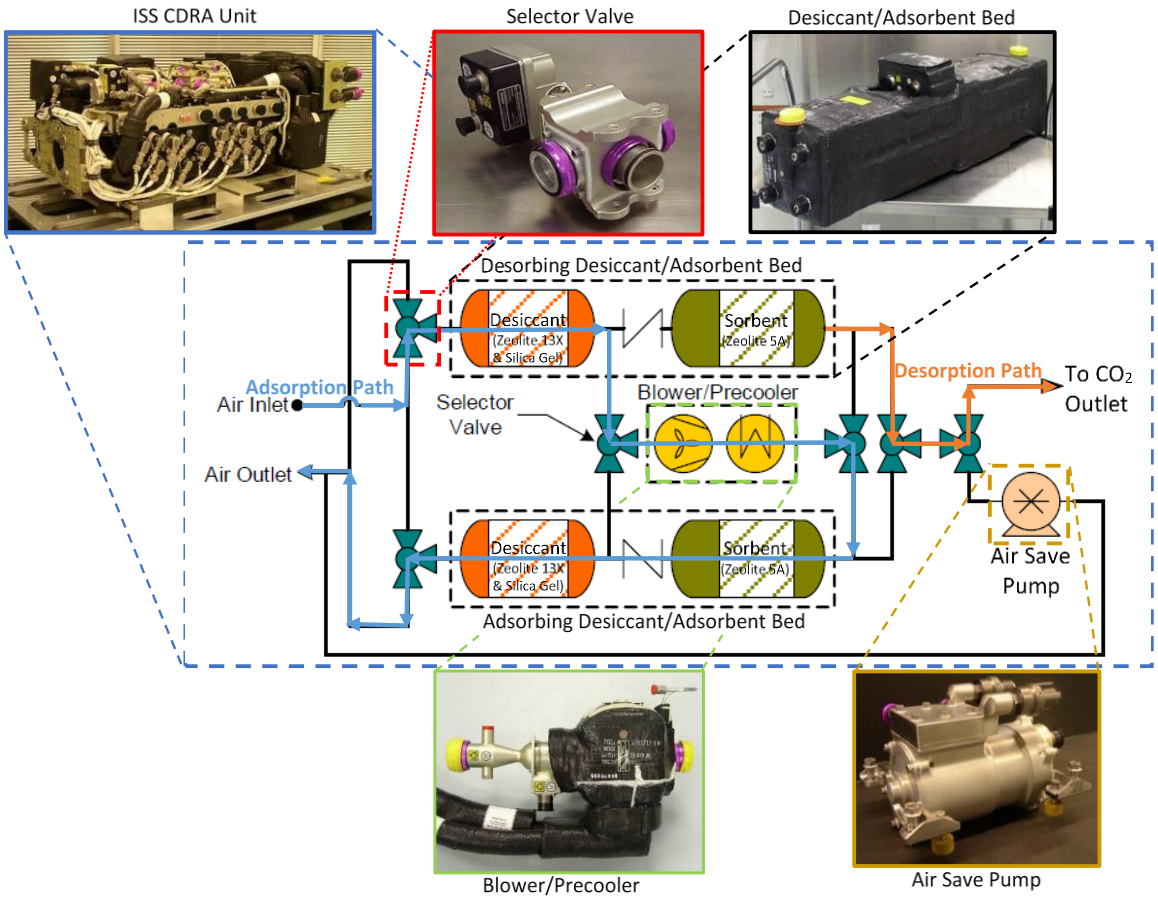

Figure D-6: Summary of the ISS Carbon Dioxide Removal Assembly and its Subassemblies (Image adapted from [305]

When the adsorbent side of the adsorbing DAB becomes saturated with CO_2, the six selector valves within the CDRA (see Figure D-6) are reconfigured such that the previously desorbing DAB switches to a CO_2 adsorbing mode and the previously adsorbing DAB enters a desorbing mode. This swing bed approach enables the continuous removal of CO_2 from the cabin air supply.

Within HabNet, the ISSVCCRLinear class (which stands for the ISS Variable Configuration CO_2 Removal system – Linear implementation) takes advantage of this pseudo-continuous CO_2 removal behavior by removing CO_2 in a single step at each time step, based on the amount of power available, the adsorption capacity of the DAB's zeolite sorption beds, and the system properties that are built into the ISSVCCRLinear class definition. During instantiation, the user specifies the input and output SimEnvironments that the ISSVCCRLinear object is connected to, as well as its power source and the output destination for extracted CO_2. Moreover, the user has the option of setting the operating mode to one of two options: the first being the nominal mode where the ISSVCCRLinear object attempts to remove as much CO_2 as possible at each time step, and the second "set point" mode, where the ISSVCCRLinear object removes CO_2 such that the CO_2 concentration within the cabin remains at some predefined set point. This latter operational mode is particularly useful when plants are being grown within a SimEnvironment and a steady, optimal CO_2 concentration is desired.

In addition, as shown in the Technology Map depicted in Figure D-7, this instantiation step also initializes property values that are inherent to the ISSVCCRLinear class, based on published performance values of the ISS CDRA. These include values for the nominal and maximum CO_2 removal rate, inlet air flow rate, and power consumption.

Under the default operating mode, the ISSVCCRLinear object attempts to consume as much CO_2 as possible from the incoming air stream during each time step within a simulation. Specifically, the ISSVCCRLinear object first attempts to draw its maximum power requirement of 1487W from the power store. If this amount of power is not available, the ISSVCCRLinear object consumes whatever amount of power is available. From here, the corresponding inlet air flow rate and CO_2 removal rate are calculated based on two linear scaling laws: one relating inlet air flow to available power, and the other relating CO_2 removal rate to available power.

The ISSVCCRLinear model then calculates the amount of CO_2 within the computed inlet air flow stream based on the CO_2 concentration within the cabin (this implementation assumes that real-time CO_2 concentration data is available to the CO_2 removal system). Subsequently, the ISSVCCRLinear object compares these two values: the CO_2 present within the incoming air stream, and the maximum CO_2 removal rate; and removes a number of CO_2 moles equivalent to the lower of these two from the habitat atmosphere. This calculation simulates the CO_2 adsorption limits of a CO_2 removal system in that the amount of CO_2 removed can never exceed the maximum CO_2 removal rate (which is a function of sorbent bed size, sorbent

type, and inlet airstream CO_2 concentration, temperature and humidity level). The removed CO_2 is then directed to the CO_2 output destination store previously declared by the user during instantiation.

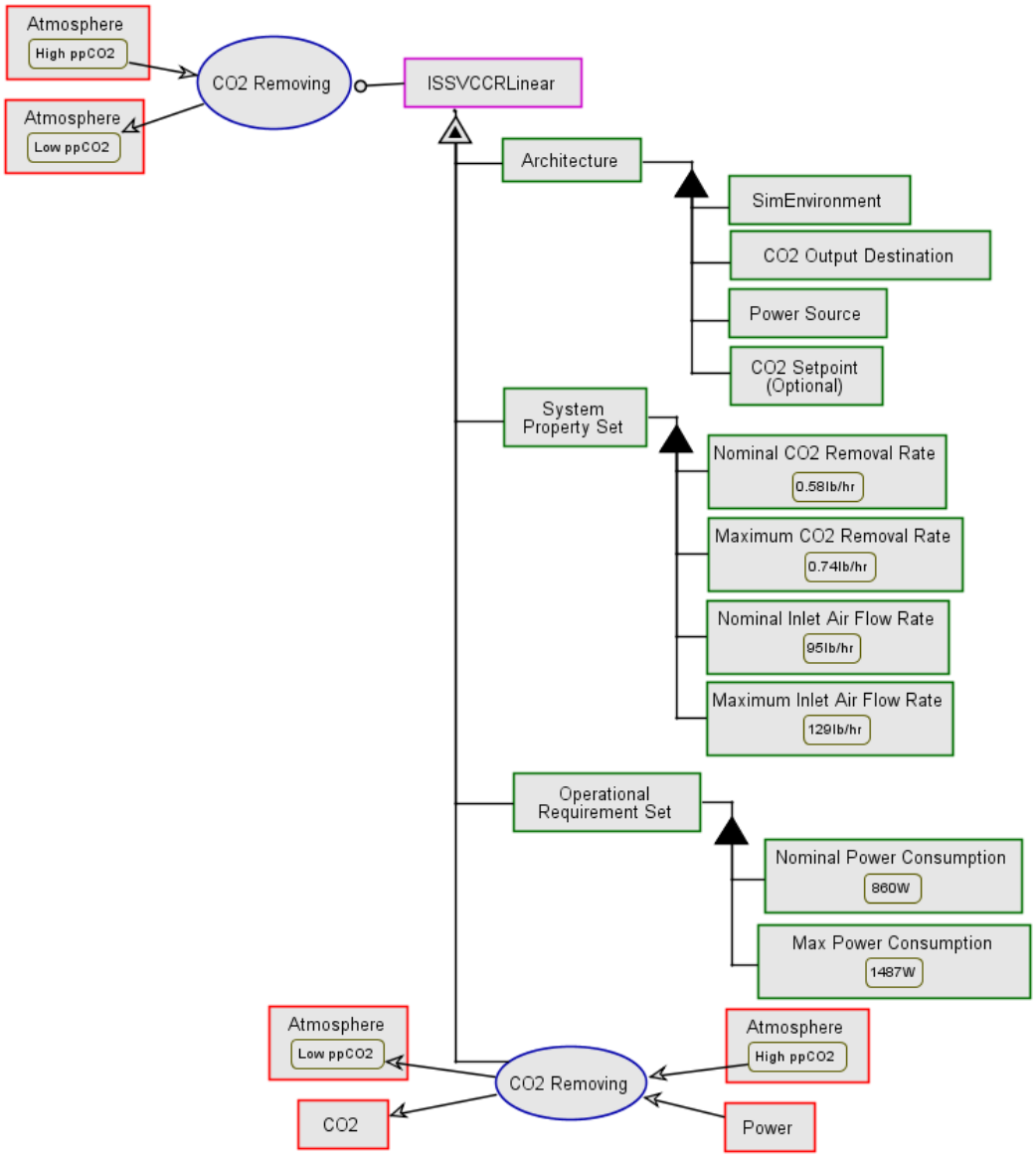

Figure D-7: Technology Map for the ISSVCCRLinear HabNet class (Data obtained from [44,209,305–307])

Conversely, in the "set point" operating mode, the ISSVCCRLinear object behaves more like the ISSDehumidifier class, in that the required number of moles of CO_2 to be removed from the habitat atmosphere to achieve the target CO_2 concentration is first calculated, and the corresponding power requirement is computed based on the abovementioned linear scaling law. This power requirement is then compared to the maximum power consumption of the

ISSVCCRLinear object (1487W listed in Figure D-7), and the lower of the two values is set as the power requirement in order to simulate a power constrained operation. From here, the sequence of simulation calculations is the same as that of the default ISSVCCRLinear operational mode. That is, the ISSVCCRLinear object next attempts to consume the calculated power requirement from the power store and if this is not available, it consumes whatever power is available. The corresponding moles of CO_2 entering the system and the available CO_2 removal rate are then calculated and compared to determine the final number of CO_2 moles removed from the habitat atmosphere for the current time step.

With regards to spare parts predictions, the HabNet Supportability module assumes that the ISSVCCRLinear object has the same component breakdown as that of the ISS CDRA. Spare parts requirements are calculated based on the lowest component level at which data is available. This data is summarized in Table D.3, below:

Table D.3: Component Data Used to Model the ISSVCCRLinear HabNet Class, based on values listed in the NASA BVAD 2004 [209] (unless otherwise noted)

ISSVCCRLinear/CDRA Subassembly	**Mass [kg]**	**Volume [m^3]**	**MTBF [h]**	**Life Limit [y]**	**No. per Unit**
Air Pump Two-Stage ORU	10.886	0.00453	156200	15.29	1
Blower	5.58	0.03	129700	10	1
Check Valves	39.916	0.17842	32900*		1
Dessicant Beds	42.638	0.08496	77100		2
Heat Controller	3.311	0.0085	242700		2
Precooler	5.579	0.02549	129700	10	1
Pump Fan Motor Controller	2.722	0.00566	2270000		2
Selector Valves	3.039	0.0017	117000	10.61	6
Sorbent Beds (Zeolite)	42.638	0.08496	77100		2

*Value based on analogy to that of the CCAA Temperature Control Check Valve (TCCV)

D.5 The ISSOGA Class

The ISSOGA class within HabNet models the ISS Oxygen Generation Assembly (OGA) – a technology that couples the water and atmosphere management functions within a life support system by electrolyzing liquid water to produce oxygen gas for crew consumption, and hydrogen gas that is either vented overboard or used by other downstream processors. As shown in the schematic in Figure D-8, the current operational OGA consists of an electrolysis cell stack, supplemented by other subsystems that monitor and control the electrolysis process to ensure its safe and reliable function.

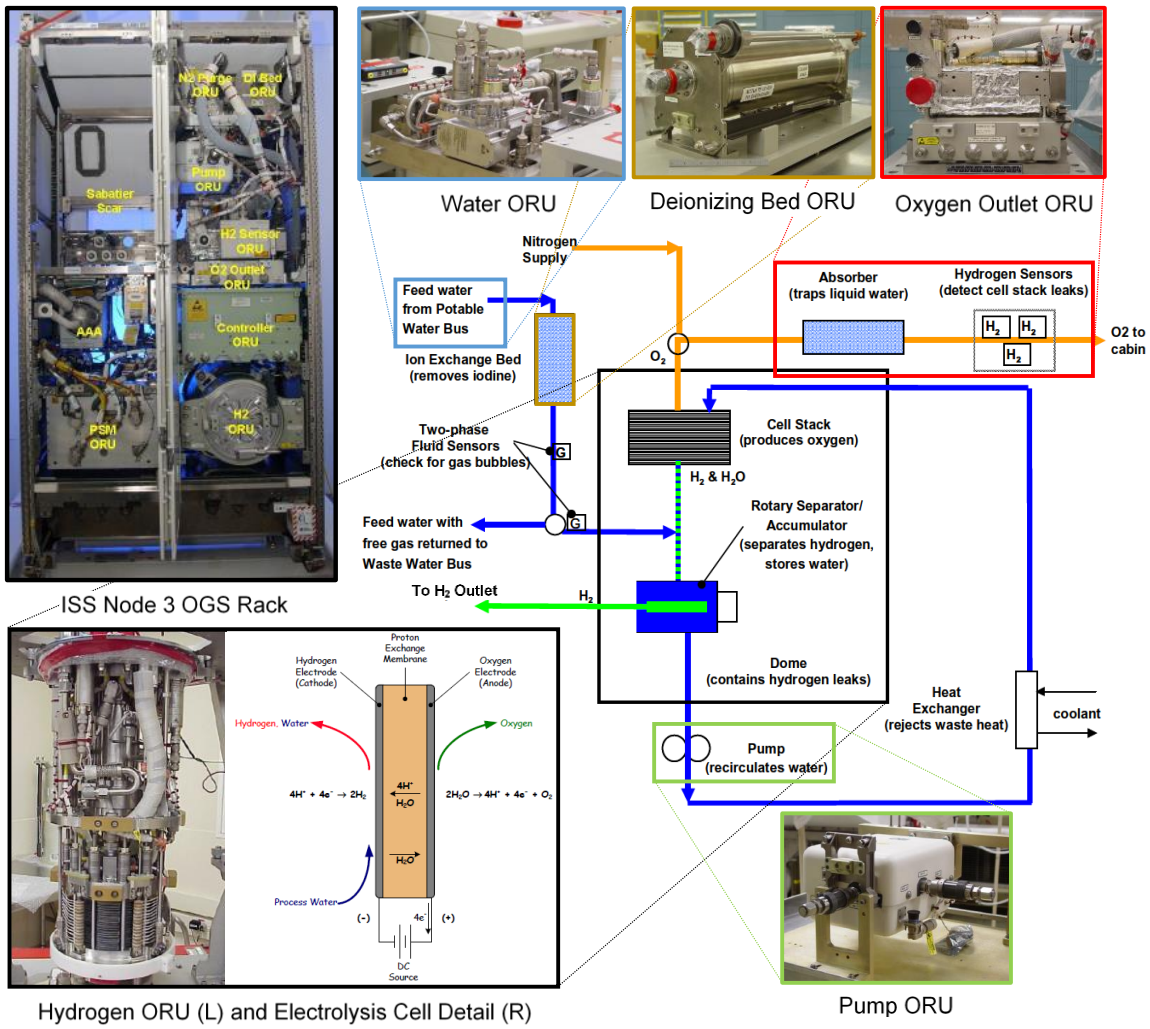

Figure D-8: Summary of the ISS Oxygen Generation Assembly and its Subassemblies (Data obtained from [74,164,165])

In the OGA, potable grade water first enters the system from the potable water bus through the Water Orbital Replacement Unit (ORU), which consists of a series of gas and pressure sensors and two normally closed solenoid valves that are commanded open when more water is needed within the system. Following this, the incoming water passes through an ion exchange bed, where iodine biocide that was previously mixed into the potable water during ISS water processing is removed. Next, the water passes through a gas detector, where it is monitored for gas bubbles prior to being permitted to entering the electrolysis cell stack. Here, any water containing gas bubbles is rejected from the system and sent for further processing. This gas detection step was implemented as a safety feature, due to concerns that free gas in water (usually in the form of oxygen) entering the electrolyzer could mix with hydrogen and create an explosion hazard [165].

The remaining bubble-free water then enters a rotary separator/accumulator, where it is subsequently pumped to an electrolysis cell stack. This stack, containing a stack of individual cells composed of Nafion membranes coated with catalyst layers, electrolyzes water to produce oxygen gas on one side of the stack, and a hydrogen gas/liquid water mixture on the other side [74]. Product oxygen on the oxygen side of the stack exits the electrolysis system, and passes through an absorber that removes residual water from the outlet stream. After this, the dry oxygen is passed through a set of hydrogen sensors prior to directly entering the cabin. Similar to the role of the gas detector, this final set of hydrogen sensors was implemented as a safety feature [166]. If any hydrogen is detected in the product oxygen from the OGA, the system is shut down as this is an indicator of improper cell stack operation. Moreover, hydrogen becomes an explosion hazard in air if local concentrations exceed 4%. Thus any leakage of hydrogen into the cabin is considered to be a safety risk [308].

On the other side of the stack, the hydrogen-water mixture is recycled through the rotary separator accumulator (RSA) that separates the gaseous hydrogen from the stream and delivers it to the hydrogen outlet. The remaining water is then recirculated back through the electrolysis stack by the Pump ORU to continue the electrolysis process [166].

To regulate the amount of oxygen being produced, the OGA has four linearly spaced operating set points ranging from 2.3kg O_2/day (equivalent to 25% production capacity) to 9.2 kg O_2/day (equivalent to 100% production capacity). This operating set point is usually set by mission controllers on the ground [166].

To model the functional behavior of the ISS OGA within HabNet, the user first instantiates an ISSOGA object by defining the SimEnvironment that it is located within, the target total

atmospheric pressure and oxygen concentration, the power source for the ISSOGA object, the input water source, and the destination stores for the product oxygen and hydrogen. When the ISSOGA object is instantiated, data regarding its oxygen production rate settings and its maximum and minimum power consumption is also initialized, as shown in the ISSOGA Technology Map in Figure D-9.

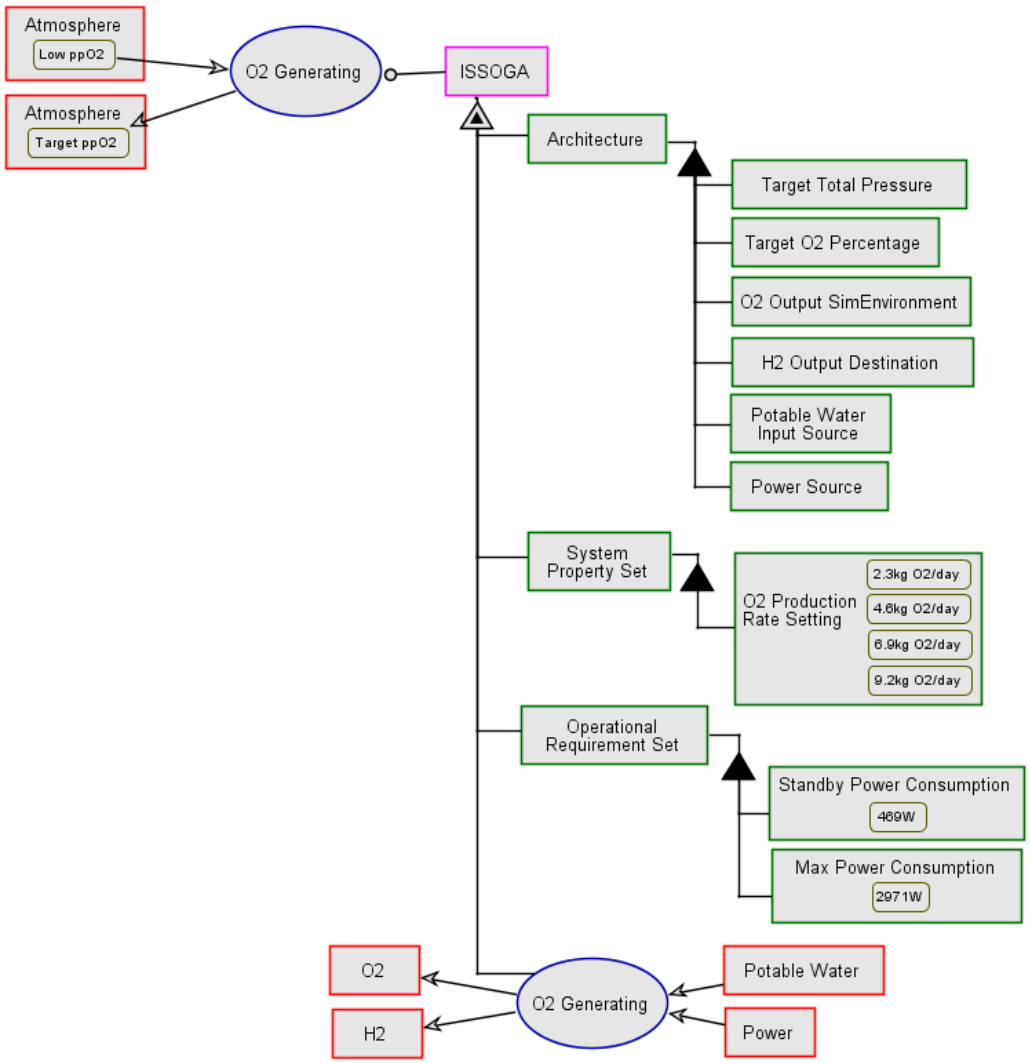

Figure D-9: Technology Map for the HabNet ISSOGA Class (Data obtained from [166])

At the beginning of each simulation time step, the ISSOGA object checks the level of water within its rotary separator/accumulator (modeled as an internal water store) to ensure that it is above a pre-specified minimum fill level. If this condition is not met, water is removed from the user-defined input water source to fill the accumulator such that it can later supply water

to the electrolysis cell stack. Next, the ISSOGA object compares the current cabin oxygen concentration with the user-defined target oxygen concentration. If additional oxygen is required to raise the current cabin oxygen concentration to the target level, the appropriate oxygen production rate setting is automatically determined, and the corresponding power requirement is calculated based on a linear scaling law derived from the power draw and oxygen production rate data listed in Figure D-9. Contrasting to the human-in-the-loop control strategy currently used for the ISS OGA, this implementation assumes that the ISSOGA object has full knowledge of the atmospheric composition of the habitat module and can automatically respond to fluctuations in this atmospheric composition.

The ISSOGA object then attempts to consume its required power from the user-defined power source. If there is insufficient power available, the ISSOGA object shuts down and raises an error. Otherwise, if sufficient power is available, the amount of water corresponding to the desired oxygen production rate is calculated, and is removed from the rotary accumulator/separator located within the ISSOGA object. If there is insufficient water available, the ISSOGA object removes as much water as is available, and electrolyzes it to oxygen and hydrogen gas, based on the following electrolysis reaction:

$$2H_2O + Energy \rightarrow 2H_2 + O_2 + Heat \tag{D.1}$$

Here, it is assumed that complete electrolysis occurs and that all water is converted to hydrogen and oxygen gas. The resulting product oxygen is vented directly into the SimEnvironment containing the ISSOGA object (as is the case with the ISS OGA), and the product hydrogen is sent to the output store defined by the user.

With regards to the estimation of spare parts requirements, the ISSOGA HabNet object is assumed to be composed of the same parts as the ISS OGA. Thus the Supportability Module spares the ISSOGA at the same level that is currently performed on the ISS. Table D.4 lists the component data used to support these sparing analyses.

Table D.4: Component Data Used to Model the ISSOGA HabNet Class, based on values listed in the NASA BVAD 2004 [209] (unless otherwise noted)

ISSOGA Subassembly	Mass [kg]	Volume [m^3]	MTBF [h]	Life Limit [y]	No. per Unit
Hydrogen ORU (Electrolysis Cell Stack)	161.6176	0.146697	27156	2.38	1
Hydrogen Sensor	4.355	0.0034	61845.6	0.25	1
Inlet Deionizing Bed	28.668	0.02945	296701.2	6	1
Nitrogen Purge ORU	34.247	0.03115*	138408		1
Oxygen Outlet	48.172	0.03115	98112	10	1
Power Supply Module	42.638	0.06485	47479.2	4.17	1
Process Controller	47.084	0.08383	103280.4	7.72	1
Pump	17.963	0.01015	144540	1	1
Water ORU	61.0545	0.075614	33288	2.92	1

*Value based on analogy to the OGA Oxygen Outlet

D.6 The ISSWaterRSLinear Class

The ISSWaterRSLinear class within HabNet models the combined function of the ISS Urine Processor Assembly (UPA) and the Water Processor Assembly (WPA) – the ECLS technologies that recover potable water from urine and humidity condensate. In this section, we first summarize the current operations of both of these systems on the ISS, before describing their implementation within the ISSWaterRSLinear HabNet class.

D.6.1 ISS UPA Description

As shown in Figure D-10, the processing of urine within the UPA commences with collection of urine in the UPA Wastewater Storage Tank Assembly (WSTA). Prior to entering the WSTA from the Waste and Hygiene Compartment (WHC) commode, the urine is pretreated with a mixture of chromium trioxide and sulfuric acid to prevent microbial growth and the formation of ammonia from urea. Once the WSTA fills to capacity, the pretreated urine is pumped into the UPA Distillation Assembly (DA) by a four-tube peristaltic pump called the Fluids Control and Pump Assembly (FCPA). Within the DA, the urine batch is evaporated at low pressure, and the resulting vapor is compressed and condensed by the DA's centrifugal action. During this process, another four-tube peristaltic pump referred to as the Pressure Control and Pump Assembly (PCPA) removes non-condensable gases and water vapor from the DA and sends it

to the Separator Plumbing Assembly, where the non-condensable gases are separated and vented to the cabin while the remaining water is recombined with the distillate generated by the UPA. The resulting product stream is then sent for further processing in the ISS WPA.

Moreover, waste brine produced from the distillation process is sent to the Advanced Recycle Filter Tank Assembly (ARFTA) – a bellows tank that is filled with DA-generated brine and emptied into the waste tanks of logistics vehicles that periodically visit the ISS (such as the Russian Progress vehicle).

Finally, any residual urine present in the waste brine after it enters the ARFTA is passed through a brine filter and redirected by the FCPA back into the DA for further distillation [76].

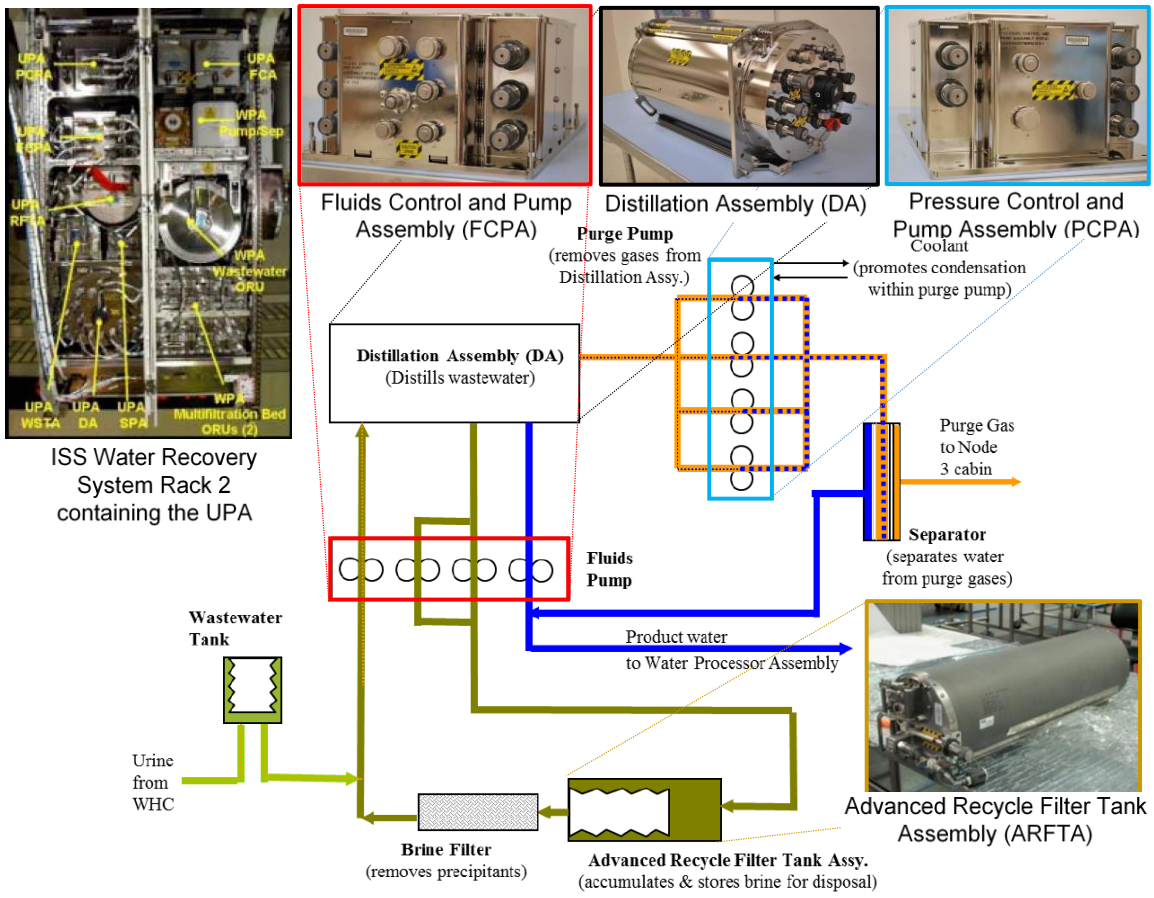

Figure D-10: Summary of the ISS Urine Processor Assembly and its Subassemblies (Image adapted from [76] and [309])

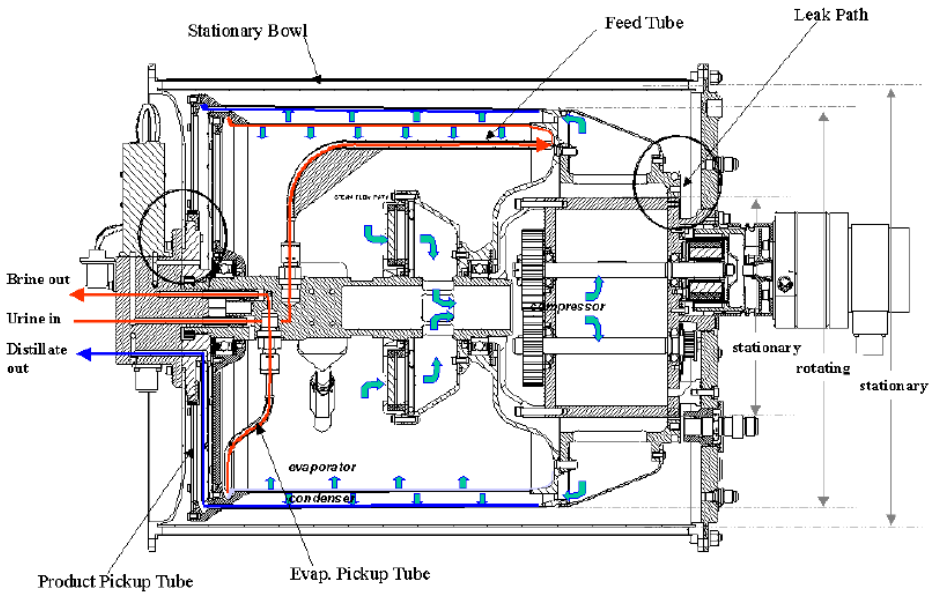

Figure D-11: Flow path of urine through the UPA Distillation Assembly [310]

D.6.2 ISS WPA Description

The ISS WPA processes urine distillate produced by the UPA, humidity condensate collected by the condensing heat exchangers within the CCAAs (see Appendix D.3), and product water from the Sabatier reactor (see Appendix D.7) to potable grade water for use by the crew. As can be seen in Figure D-12, the WPA water treatment process begins in much the same way as that of the UPA – water to be processed is first collected in a waste water tank and when this tank reaches capacity, it is transferred into the WPA processing circuit. During the beginning of a processing run, the input water first passes through a "Mostly Liquid Separator" which removes gas from the wastewater stream, returning it to the cabin. From here, a pump within the WPA processing circuit moves the wastewater through a series of filters and reactors that each remove targeted contaminants from the wastewater stream. This begins with the Particulate Filter which removes particulates, followed by a set of two Multifiltration (MF) Beds, which remove inorganic and non-volatile organic contaminants. After the MF Beds, the wastewater stream is preheated before being sent to a catalytic reactor, where it is oxidized in the presence of oxygen and a solid catalyst to remove any remaining low molecular weight organics not removed by the previous filtration systems. Next, the catalytic reactor product water passes through a regenerative heat exchanger to recover heat from the oxidation reaction, and then proceeds to a Gas/Liquid Separator, where excess oxygen and other gaseous by-

products from the oxidation reaction are separated and sent to the cabin. The product water stream then flows through a series of reactor health sensors that measure its conductivity (as a means of gauging reactor health) prior to passing through an Ion Exchange Bed, where dissolved products of oxidation are removed and iodine biocide is added for microbial control. The resulting product water is then delivered to a product water tank, where it is stored for future use by the crew [310].

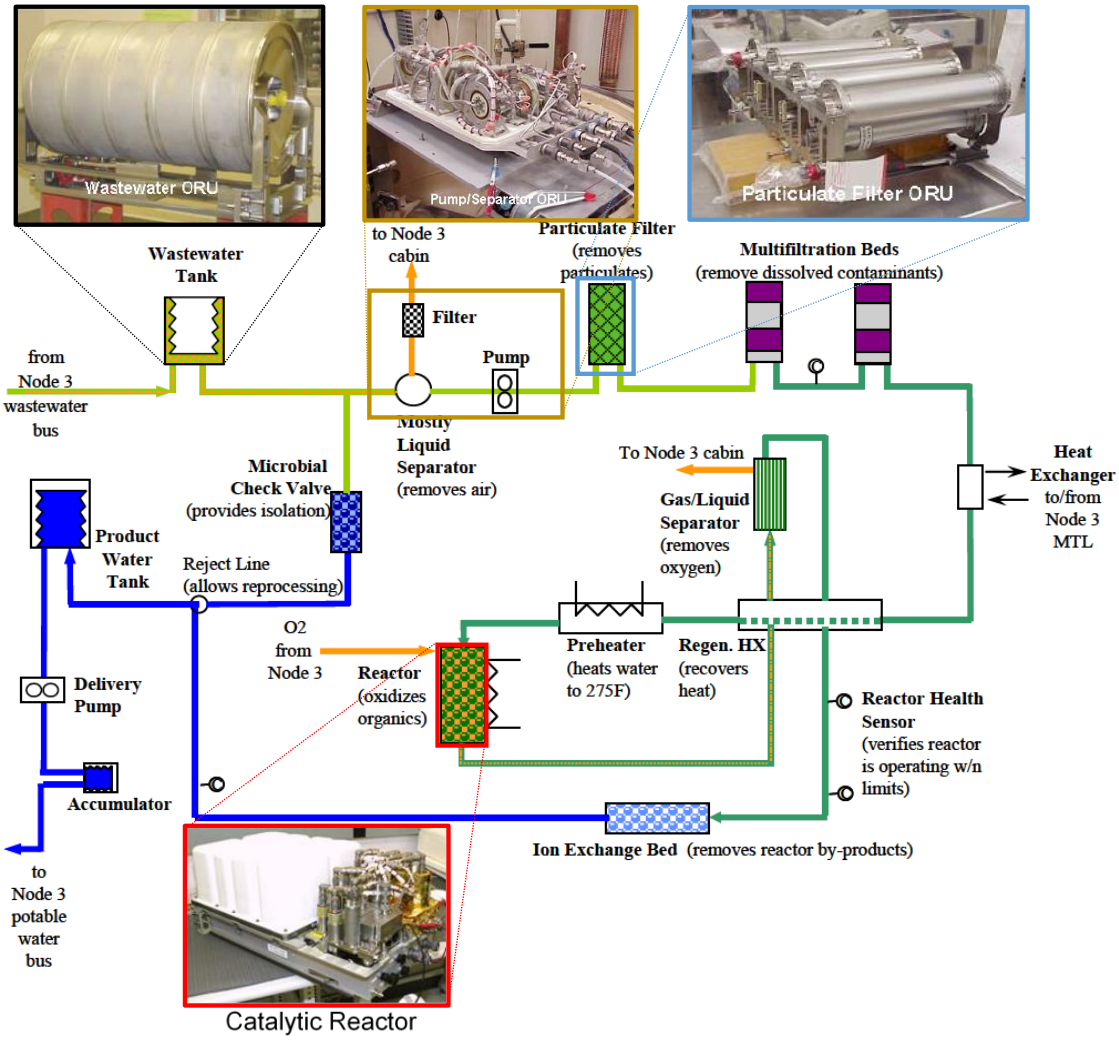

Figure D-12: Summary of the ISS Water Processor Assembly and its Subassemblies (Image adapted from [72] and [311])

D.6.3 Modeling the ISS UPA and WPA within the HabNet ISSWaterRSLinear Class

As mentioned earlier, the ISS UPA and WPA are modeled together in HabNet by the ISSWaterRSLinear class. Here, the name of this class stands for: "ISS Water Recovery System – Linear Implementation". During the initial instantiation of an ISSWaterRSLinear object, the user declares a number of input and output sources for water at different grades, as well as a power source for the system. Within HabNet, three grades of water are tracked, being potable water, grey water, and dirty water. Grey water corresponds to humidity condensate and product water from other reactors (such as urine distillate from the UPA and Sabatier reactor product water (see Appendix D.7), while dirty water corresponds to urine. Thus, during initialization, the user defines the following water sources and sinks in addition to a power source:

- an input source for dirty water to be fed to the modeled UPA
- a grey water and waste output destination for the urine condensate and brine produced by the UPA
- an input source for grey water to be fed to the modeled WPA
- a destination source for potable water produced by the WPA

Moreover, when the ISSWaterRSLinear case is initialized, the user can choose to instantiate either the UPA model, the WPA model, or both. By default, the ISSWaterRSLinear class definition activates both UPA and WPA models during instantiation. However, either one of the two can be deactivated by commanding an error using the UPAerror and WPAerror properties of the ISSWaterRSLinear class. These properties, as well as other properties related to the performance and power requirements of the ISS UPA and WPA that this class definition is based on, are summarized in the Technology Map depicted in Figure D-13.

With regards to the system properties listed in this figure, we note that:

- the 74% urine processing efficiency of the modeled UPA corresponds to the efficiency value published in 2013, after changes were made to the operations of the UPA in response to problems experienced with calcium sulfate precipitating within the DA (see Table 2.6 in Section 2.1.3)
- the 65lb water processing inlet tank capacity corresponds to the level at which a WPA process is commenced on the ISS. This level is lower than the 100lb capacity of this tank due to concerns with biomass accumulating with longer wastewater residence times leading to the biofouling of downstream components [297]

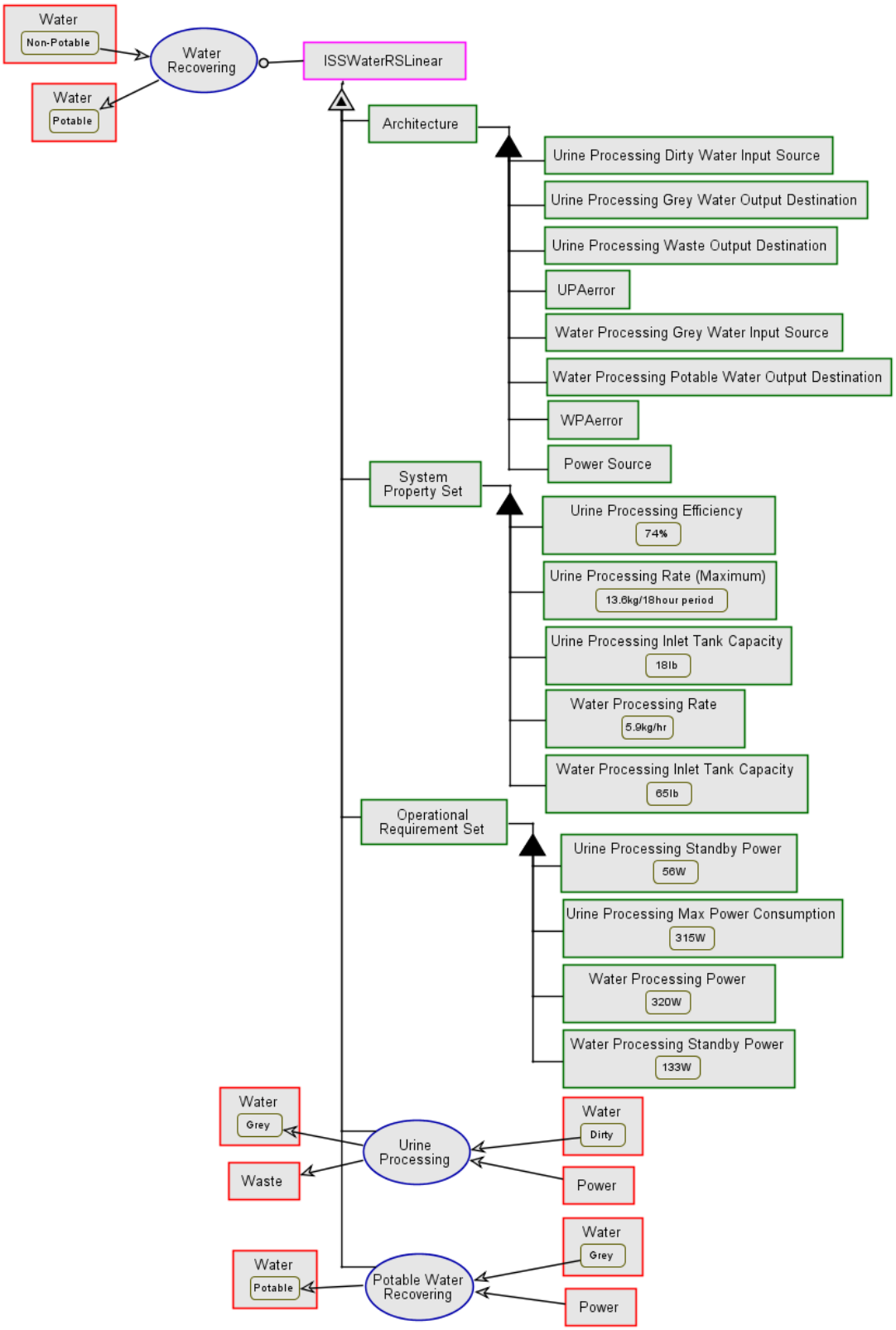

Figure D-13: Technology Map for the HabNet ISSWaterRSLinear Class (Data obtained from [164,297,312])

During each time step within a HabNet simulation, if both the UPA and WPA models within the ISSWaterRSLinear object are activated, the capacities of the user-defined dirty and grey water inlet sources are first tracked. If the levels within these inlet tanks reach their respective capacities, they are emptied into the corresponding processor and are processed. This batch mode of operation has been modeled to coincide with the operational approach utilized by the flight UPA and WPA systems.

Once a process begins within the ISSWaterRSLinear UPA object, the maximum processing power is attempted to be drawn from the power store declared by the user. If insufficient power is available, the ISSWaterRSLinear object consumes what power is available, and calculates a urine processing rate based on a linear scaling relationship derived from the urine processing and power consumption value listed in Figure D-13. Otherwise, if sufficient power is available, the maximum urine processing rate is assumed. Following this, the corresponding amount of product grey water is calculated based on the previously calculated urine processing rate and the urine processing efficiency. This product grey water is then sent to the urine processing grey water output destination initially declared by the user. The residual dry waste, calculated as the difference between the input dirty water and the product grey water, is then sent to the predefined dry waste store.

The WPA model within the ISSWaterRSLinear object operates in much the same way in that once a process is initiated, a water processing rate is calculated based on whatever power is available, and the corresponding volume of grey water is converted into potable water and sent to a predefined potable water output destination. For the case of the WPA, an efficiency of 100% is assumed for the processing of grey water into potable water – that is, all grey water is completely converted into potable water and no byproducts are produced.

In reality, any loss in greywater mass occurs in the accumulation of contaminants with the WPA particulate filters and multifiltration and ion exchange beds. Once these filtration systems become saturated, they are removed and replaced. This maintenance paradigm, along with data on the reliability of each of the components of the UPA and WPA, is used by the HabNet Supportability module to predict the spare parts requirements for the ISSWaterRSLinear object. Tables D.5 and D.6 summarize this reliability data.

Table D.5: Component Data Used to Model the UPA within the ISSWaterRSLinear HabNet Class, based on values listed in the NASA BVAD 2004 [209] (unless otherwise noted)

ISS UPA Subassembly	Mass [kg]	Volume [m^3]	MTBF [h]	Life Limit [y]	No. per Unit
Distillation Assembly	92.761	0.14217	142525.2	2	1
Firmware Controller Assembly	23.088	0.0286	27331.2	2.4	1
Fluids Control and Pump Assembly	47.583	0.07307	90140.4	4	1
Pressure Control and Pump Assembly	49.08	0.11583	181507.2	2	1
Advanced Recycle Filter Tank Assembly*	50	0.1011	199640.4		1
Separator Plumbing Assembly	16.783	0.02294	384651.6	1	1

*Mass is obtained from [300] and verified with calculations based on data from Link et al. [301]. All other data is assumed to be the same as the Recycle Filter Tank Assembly (RFTA) described in the NASA BVAD 2004 [209] – the original system from which the ARFTA was upgraded from. Here, the life limit of the ARFTA has been assumed to be zero, based on its development objective of facilitating the same function as the RFTA without the need for periodic replacement [301].

Table D.6: Component Data Used to Model the WPA within the ISSWaterRSLinear HabNet Class, based on values listed in the NASA BVAD 2004 [209] (unless otherwise noted)

ISS WPA Subassembly	Mass [kg]	Volume [m^3]	MTBF [h]	Life Limit [y]	No. per Unit
Catalytic Reactor	67.042	0.11555	25579.2	2.25	1
Gas Separator	39.146	0.06599	84008.4	1	1
Ion Exchange Bed	13.018	0.01728	296701.2	0.16	1
Microbial Check Valve	5.761	0.00651	143488.8	1	1
Multifiltration Bed #1	149.234	0.0657	296701.2	0.36	1
Multifiltration Bed #2	149.234	0.0657	296701.2	0.36	1
Particulate Filter	32.251	0.07165	717356.4	0.22	1
pH Adjuster	2.54	0.00255	137181.6	1	1
Process Controller	44.997	0.08383	87950.4	7.72	1
Pump Separator	31.344	0.08694	42398.4	2	1
Reactor Health Sensor	16.829	0.04248	56677.2	1	1
Sensor	4.808	0.0034	143664	10	1
Separator Filter	7.666	0.0102	359072.4	0.84	1
Start-up Filter	9.435	0.01841	226884	19.92	1
Water Delivery	47.537	0.09742	64561.2	5	1

D.7 The ISSCRS Class

The ISSCRS Class within HabNet models the Carbon Dioxide Reduction System (CRS) currently operating onboard the ISS. This system reacts hydrogen gas produced by the OGA with carbon dioxide extracted from the cabin by the CDRA to produce water and methane, based on the Sabatier reaction shown below:

$$CO_2 + 4H_2 \rightarrow CH_4 + 2H_2O + \text{Heat} \quad \text{(D.2)}$$

As shown in the flow diagram in Figure D-14, product water is obtained from this reaction by first directing the gaseous reaction products through a condensing heat exchanger, where the water is condensed to a liquid, before sending the two phase mixture through a gas separator to separate the gaseous reaction products from the liquid water [168]. This water is then sent to the WPA for further processing and eventual electrolysis to produce oxygen for crew consumption and further hydrogen for subsequent Sabatier reactions. The remaining gaseous mixture of methane, uncondensed water vapor, and unreacted reactants are vented to space [313].

Since hydrogen gas produced by the OGA is not stored, the CRS is configured such that as soon as hydrogen reactant becomes available, it is combined with CO_2 gas in the Sabatier reaction chamber to initiate the reaction. This on-demand reaction capability is enabled by the compressor and CO_2 accumulator depicted in Figure D-14. Specifically, CO_2 produced by the CDRA during its desorption cycles is compressed to 827kPa by the Compressor Orbital Replacement Unit (ORU) within the CRS, and used to fill the 19.8L CO_2 accumulator tank [314]. When hydrogen gas is sensed within the flow lines connecting the OGA outlet to the CRS, a flow control valve downstream of the CO_2 accumulator introduces CO_2 into the Sabatier reaction chamber at a rate corresponding to the desired reactant molar ratio [315]. Since CO_2 is always in excess of hydrogen in this setup, the Sabatier reaction is typically run with a molar ratio of 3.5 – that is, 3.5 moles of hydrogen for every mole of CO_2 introduced into the reaction chamber [316]. This non-stoichiometric molar ratio has been found to increase the efficiency of the reactor.

Finally, in the scenario that insufficient CO_2 is available within the CO_2 accumulator, the Sabatier reactor is put in a standby mode and all hydrogen gas produced by the OGA is vented

overboard. This low CO_2 state is flagged when the pressure within the CO_2 accumulator drops to a level beneath 18psia [169].

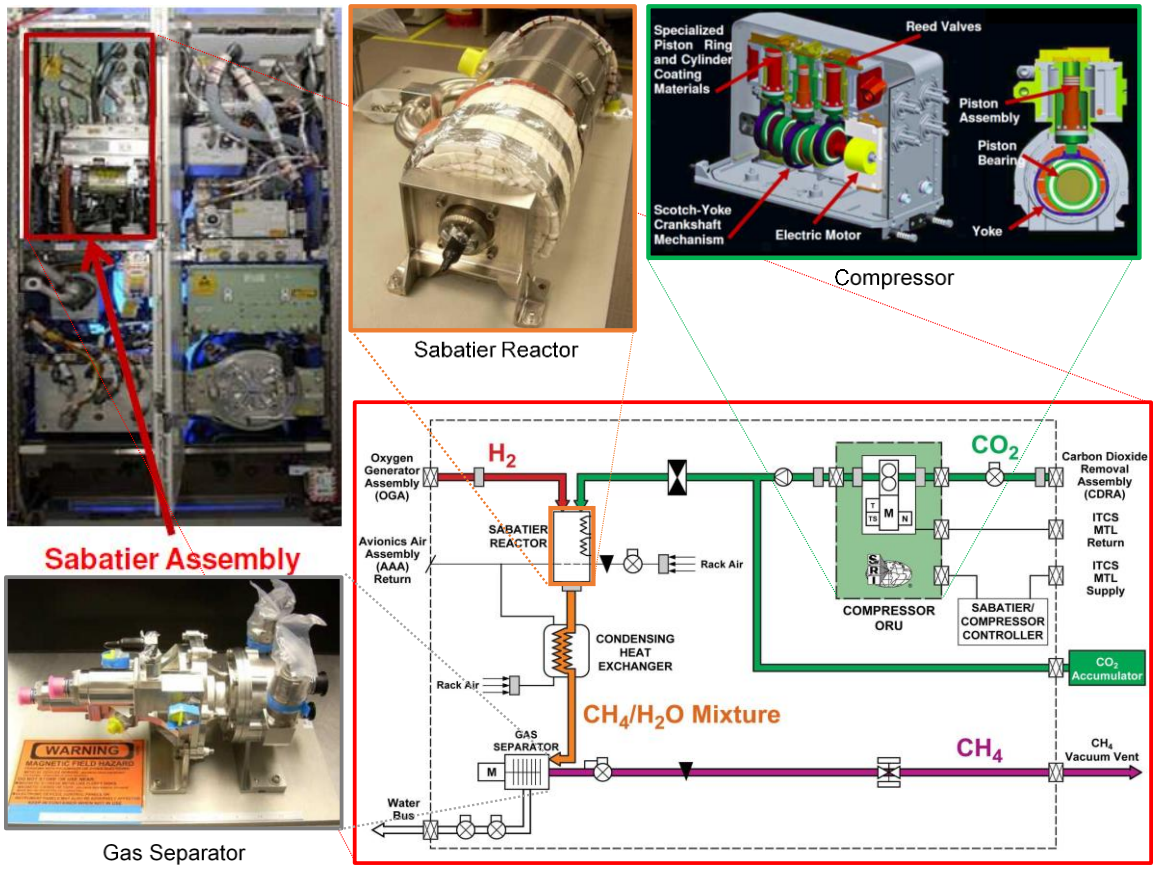

Figure D-14: Summary of the ISS Carbon Dioxide Reduction System and its Subassemblies (Image adapted from [168])

D.7.1 Modeling the ISS CRS within the HabNet ISSCRS Class

To model this technology within HabNet, the ISSCRS class is instantiated with a definition of the hydrogen and CO_2 input sources, the destinations for the grey water and methane output, and a power source for the system. When the ISSCRS object is created, additional properties are also initialized, including the reaction molar ratio, the reaction efficiency, and the power requirements of the individual components of the CRS system. These values are based on the characteristics of the ISS CRS, and are summarized in the Technology Map below:

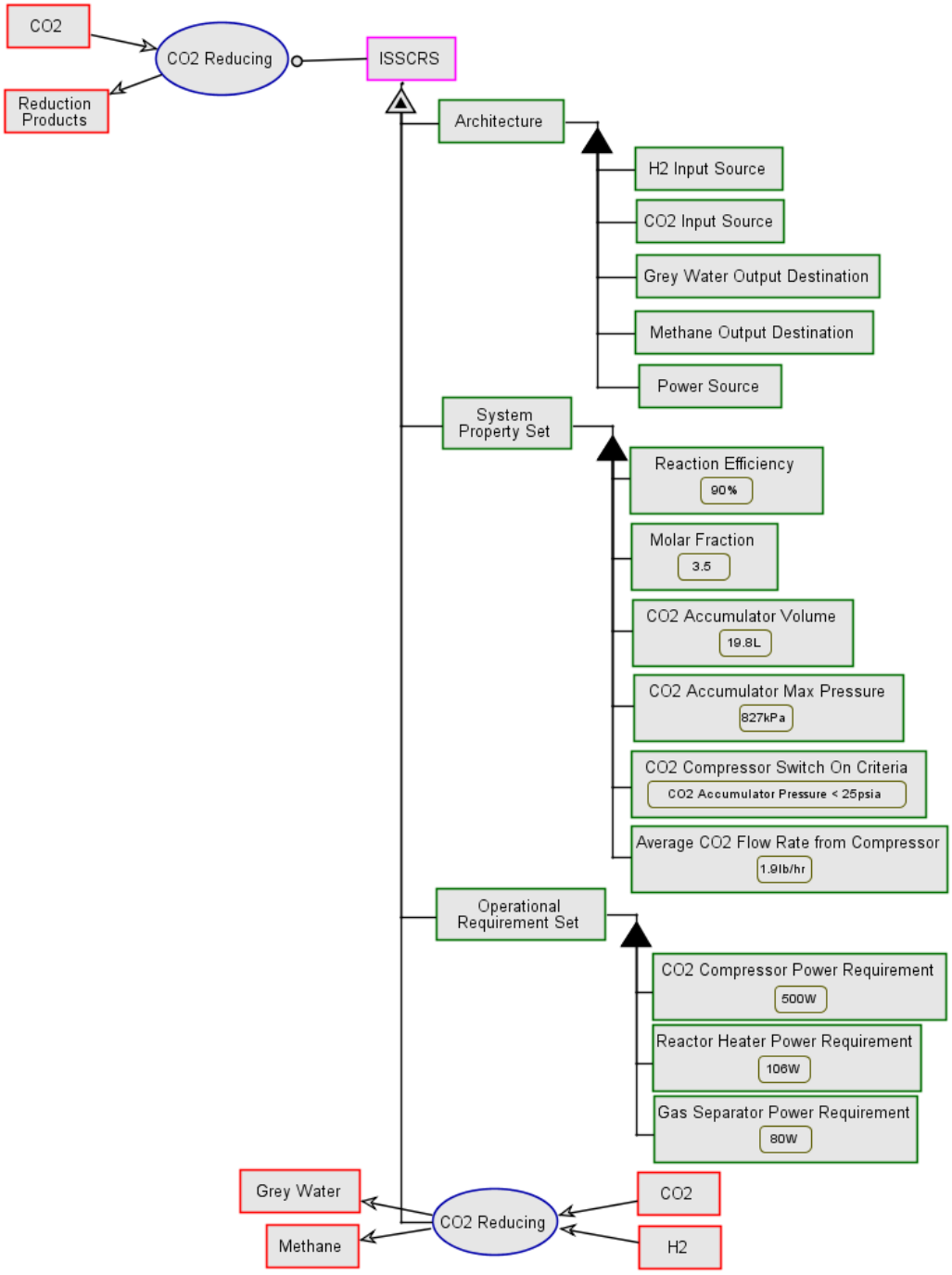

Figure D-15: Technology Map for the HabNet ISSCRS Class (Data obtained from [169,307,313,314,316,317])

The ISSCRS class models the high level function of the three main components of the ISS CRS system, being the CO_2 compressor, the Sabatier reactor, and the gas separator. At the beginning of each simulation time step, the CO_2 compressor model within the ISSCRS object

first compares the current level within the user-defined CO_2 input source with that of the CO_2 accumulator. If there is a sufficient amount of CO_2 available from the input source to fill the CO_2 accumulator, and the pressure within the CO_2 input source is greater than that of the accumulator; the CO_2 compressor is activated and 1.9lb/hr of CO_2 is introduced into the CO_2 accumulator. This value is equivalent to the average CO_2 compressor flow rate value listed in the Technology Map shown in Figure D-15. Moreover, this implementation ensures that the number of times that the CO_2 compressor is cycled on and off is minimized, thus minimizing the total power draw of the ISSCRS system (since the power requirement of the CO_2 compressor dominates the power requirements of all other CRS components). This corresponds to the operational objectives of the CRS operating onboard the ISS [169]. If insufficient power is available to power the CO_2 compressor, the compressor is shut down and an error flag is raised.

Next, the amount of hydrogen available within the user-defined hydrogen input source is measured to determine whether or not the ISSCRS Sabatier reactor model should be executed. If there is a non-zero amount of hydrogen available, 106W of power is consumed (corresponding to the Sabatier reactor power - see Figure D-15), and the number of CO_2 moles required to complete the Sabatier reaction at the desired molar fraction of 3.5 is calculated. If there is an insufficient amount of CO_2 moles available from within the CO_2 accumulator, the CO_2 compressor model is re-executed in the same manner as described above, and more CO_2 is attempted to be introduced into the reactor.

Next, the corresponding moles of product methane and water resulting from the Sabatier reaction are calculated based on the reaction molar ratio. Since this molar ratio is non-stoichiometric, the following reaction is instead modeled:

$$\overbrace{0.5/4CO_2}^{\text{Excess}CO_2} + \overbrace{3.5/4CO_2 + 3.5H_2 \rightarrow 3.5/4CH_4 + 2(3.5/4)H_2O}^{\text{Stoichiometric Reaction}} + \overbrace{0.5/4CO_2}^{\text{Excess}CO_2} \quad \text{(D.3)}$$

Following this step, the ISSCRS object attempts to collect power for the gas separator. If insufficient power is available, an error flag is raised and all reaction products are vented overboard. Otherwise, product water corresponding to the reaction water conversion efficiency is sent to the potable water output destination declared by the user, while unreacted CO_2 (see Equation (D.3) listed above), and uncondensed water (corresponding to [1-reaction water

conversion efficiency] of the product water) is vented overboard. In addition, product methane is directed to the predefined methane output destination.

To compute the spare parts requirements for the ISSCRS object, data corresponding to the components of the CRS operating onboard the ISS is used. This assumes that the architecture of the ISSCRS HabNet object is the same as that of the CRS on the ISS. Table D.7 summarizes the mass, power, reliability and parts count data assumed for the ISSCRS object.

Table D.7: Component Data Used to Model the ISS CRS within the ISSCRS HabNet Class, based on values listed in the NASA BVAD 2004 [209] (unless otherwise noted)

ISSCRS Subassembly	**Mass [kg]**	**Volume [m^3]**	**MTBF [h]**	**Life Limit [y]**	**No. per Unit**
Sabatier Methanation Reactor	120[1]	0.208[1]	50000[2]		1
Condensing Heat Exchanger[3]	49.71	0.39329	832600		1
Phase Separator[4]	11.93	0.05829	131000	5	1
Valves[5]	3.039	0.0017	117000	10.61	7[6]
Sensors[7]	4.808	0.0034	143664	10	1
Controller	3[1]	0.0053[8]	103280.4[9]	7.72[9]	1
CO_2 Compressor	27	0.01124[10]	66666.7[2]		1

[1]Data taken from Jeng and Lin [256]
[2]Data taken from Papale et al. [318]
[3]Analogy to CCAA Condensing Heat Exchanger
[4]Analogy to CCAA Water Separator
[5]Analogy to CDRA Selector Valves
[6]Data taken from Jones [319]
[7]Analogy to WPA Sensor
[8]Linear scaling (based on mass) from OGA Process Controller
[9]Analogy to OGA Process Controller
[10]Linear scaling (based on mass) from CDRA Air Pump

D.8 The ShelfImpl Class

The ShelfImpl class within HabNet models the dynamics of crop growth within a biomass production system using the Modified Energy Cascade (MEC) models described in the NASA Baseline Values and Assumptions Document [209]. These models were originally developed by Jones and Cavazonni to support the NASA BIO-Plex project that throughout the 1990s, aimed to evaluate the effectiveness of biological support systems in sustaining human crews within closed environments [320]. Initially, the MEC models were limited to predicting plant growth rates as a function of atmospheric CO_2 concentration, humidity level, and local lighting level. Over time, as more experimental data became available, these models were updated with plant transpiration and oxygen production models to predict crop water vapor and oxygen output [321]. The HabNet ShelfImpl class implements this latter version of the MEC models, and shares the same assumptions that the atmospheric temperature and photoperiod (the number of hours per day at which the crops are exposed to light) are held constant, and that plant growth rates are not limited by the availability of nutrients or water [209].

As shown in the Technology Map in Figure D-16, a ShelfImpl object is first initialized with the user definition of the type of crop to be grown, its crop growth area, the SimEnvironment that the plant growth shelf will exchange atmosphere with, the water and power sources for the plant growth shelf, and a destination for product biomass.

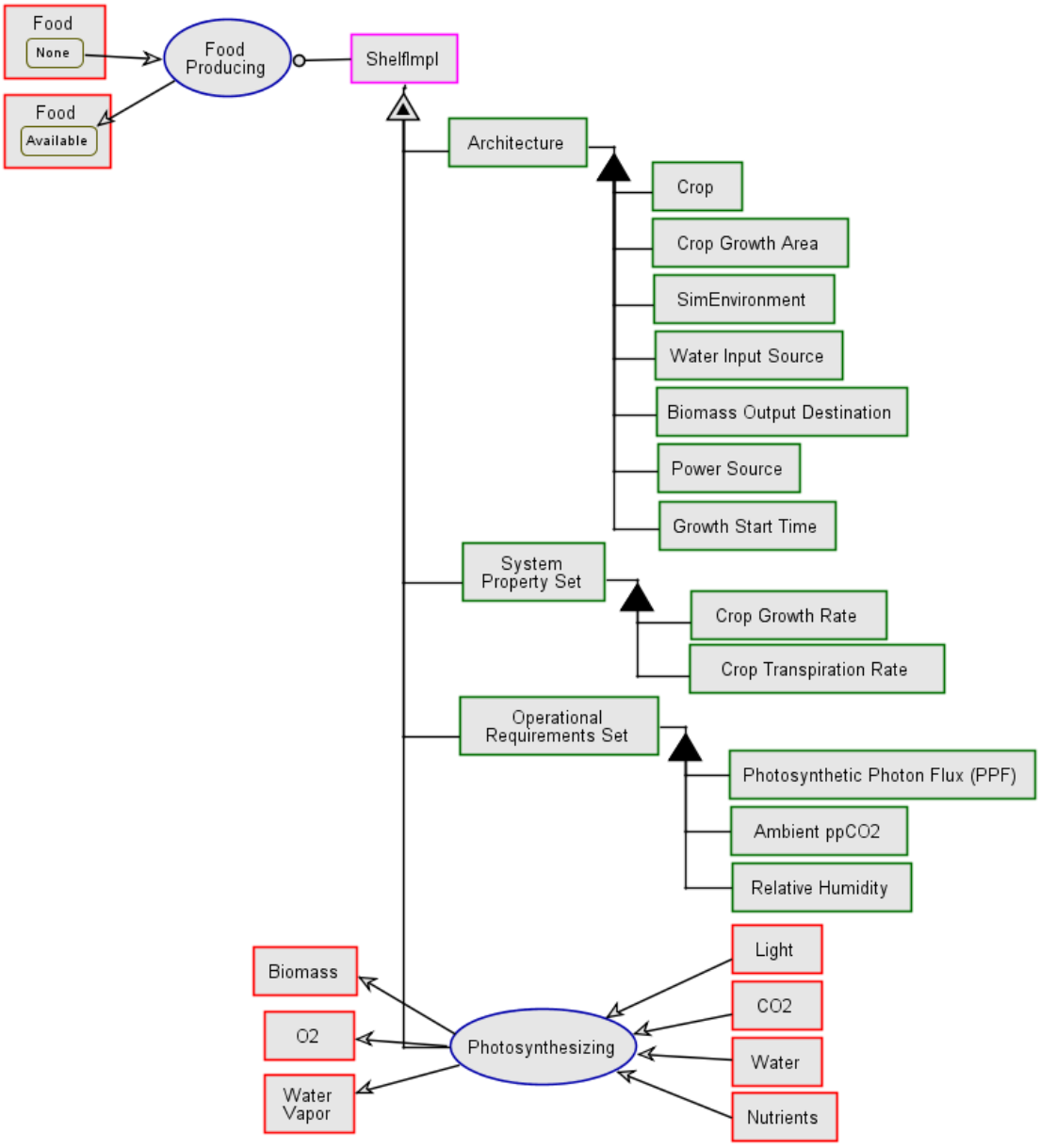

Figure D-16: Technology Map for the HabNet ShelfImpl Class

During each time step within a typical HabNet simulation, power is first taken from the user declared power source to power the grow lights within the shelf. The amount of power available is then used to calculate the photosynthetic photon flux (PPF) available for the crop growth. This value is combined with the CO_2 concentration level within the local SimEnvironment, as well as the water availability within the input water store, to predict the rate at which biomass and photosynthetic by-products are generated, according to the photosynthesis reaction below:

$$6CO_2 + 6H_2O \xrightarrow{\text{Light}} 6O_2 + C_6H_{12}O_6 \quad \text{(D.4)}$$

Here, the crop growth rate is calculated as a function of a number of crop-specific parameters that are initialized when a crop is assigned to the ShelfImpl. These parameters characterize crop photosynthetic and growth attributes such as [320]:

- the variations in the fraction of total PPF absorbed by the plant canopy throughout its growth cycle
- the Canopy Quantum Yield (CQY) of the crop, defined as the number of moles of carbon that are fixed in glucose for each mole of PPF absorbed (a measure of the PPF use efficiency); and
- the Carbon Use Efficiency (CUE) of the crop, defined as the fraction of glucose fixed carbon that is converted into biomass

These crop-specific parameters are stored in their own dedicated HabNet class definitions as architectural attributes. Figure D-17 summarizes the total list of crop-specific information stored in a typical HabNet crop class.

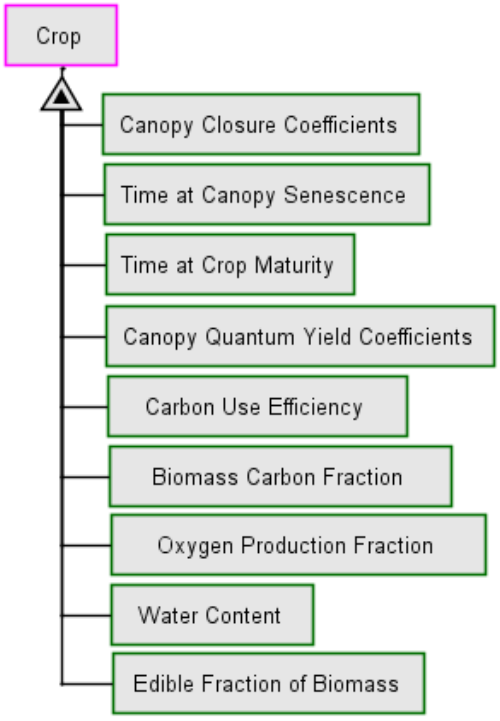

Figure D-17: Crop-specific attributes stored in a generic HabNet Crop Class

The MEC models use this crop-specific information to model the three main stages in the crop growth cycle. These are: (1) the period from seed emergence to canopy closure (2) the

period from canopy closure to initial grain setting (or the onset of senescence); and (3) the period from initial grain setting to crop maturity, when it is ultimately harvested [320]. These stages are summarized in Figure D-18.

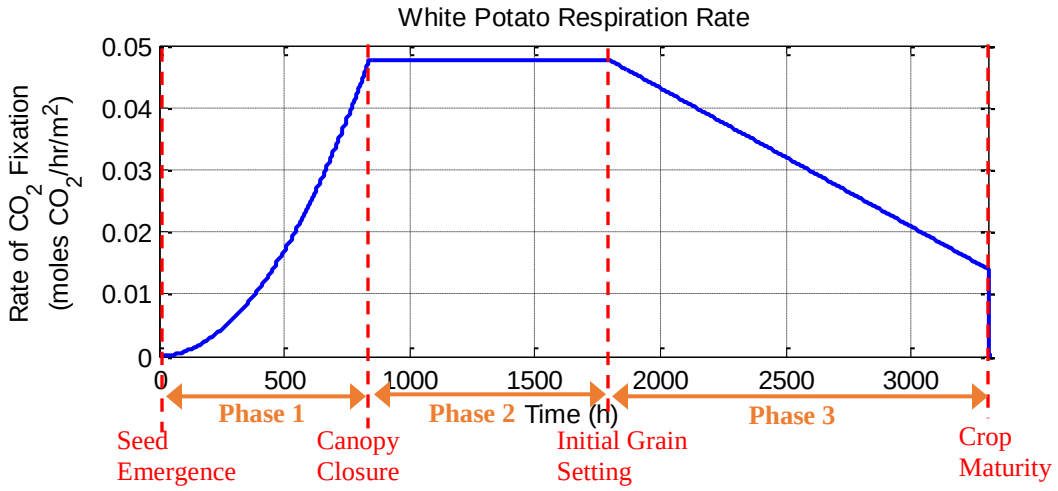

Figure D-18: Typical Stages of Crop Growth Modeled within the MEC Models (shown here for White Potato)

Within the ShelfImpl class, the time at canopy closure (ta) is calculated by using an experimentally derived 15-coefficient multivariate polynomial that is dependent on the current PPF and the ambient CO_2 concentration, while the time of initial grain setting (tq) and the time at crop maturity (tm) are fixed values that are stored within the crop-specific HabNet class.

This information is then used to calculate the fraction of light (or incident PPF) absorbed by the crop (measured in μmol of photons absorbed per m^2 of crop growth area per second) over time. The fraction of incident PPF absorbed (A) is initially low, but increases over time, towards a maximum value at ta, when the crop canopy has completely closed. This growth rate in PPF fraction absorbed (A) is approximated by a crop-specific power law that represents the rate at which leaves form in a plant's canopy and thus the rate at which incident PPF can be absorbed [209].

The determination of the fraction of PPF absorbed (A) enables for the calculation of the efficiency of the photosynthetic reaction listed in Equation (D.4) above. This efficiency is computed via two parameters:

- the canopy quantum yield (CQY), which as described above, is a measure of the efficiency of using energy from incident PPF to fix carbon from ambient CO_2 into glucose. Like the computation of ta, CQY is calculated using an experimentally derived 15-coefficient

multivariate polynomial that is a function of ambient CO_2 concentration and absorbed PPF [209]. The specific coefficient values are stored within the crop-specific HabNet crop class definition (see Figure D-17)

- the carbon use efficiency (CUE), which as noted earlier, is a measure of the efficiency of the conversion of glucose to biomass. Within the MEC models, this value is assumed to be constant for all crops except for legumes, where its value is at a fixed peak at the period of initial grain setting, and decreases linearly towards a minimum value when the crop reaches maturity [320].

These two efficiency values are then combined with the amount of incident PPF absorbed and the photoperiod (H – the number of hours per day that the crop is exposed to light) to determine the Daily Carbon Gain (DCG), defined as the moles of carbon gained per unit crop growth area per day. This is evaluated with the following equation:

$$\mathrm{DCG}\left[\mathrm{mol_{Carbon}/m^2 \cdot day}\right] = 0.0036\left[\frac{\mathrm{s}}{\mathrm{h}}\frac{\mathrm{mol}}{\mu\mathrm{mol}}\right] \times \mathrm{H}\left[\mathrm{hours\ of\ light/day}\right] \times \mathrm{CUE} \times \mathrm{CQY} \times \mathrm{A} \times \mathrm{PPF} \tag{D.5}$$

With this DCG value, the CO_2 consumed, as well as the amount of oxygen produced, can be determined, according to the stoichiometric ratios of the photosynthesis reaction shown in Equation (D.4). Once these values are determined, their corresponding quantities are respectively taken and added to the user-defined SimEnvironment in which the ShelfImpl object is located. In addition, the DCG value allows for the growth rate of dry biomass to be computed, based on the crop-specific Biomass Carbon Fraction (BCF) parameter stored within the corresponding HabNet crop class. This parameter represents the fraction of all crop biomass that is composed of carbon. This computation is evaluated with the following equation:

$$\mathrm{Dry\ Biomass\ Growth\ Rate}\left[\mathrm{grams\ dry\ biomass/m^2/day}\right] = \mathrm{Carbon\ Molecular\ Weight} \times \frac{\mathrm{DCG}}{\mathrm{BCF}} \tag{D.6}$$

From here, the total rate of biomass production can be determined by summing the dry biomass growth rate with the water content expected to be within the biomass. This latter value is based on the crop-specific water content parameter stored within the corresponding HabNet crop class (see Figure D-17).

To determine the amount of water consumed by the crops, the water transpiration equations incorporated within the MEC models are used, rather than the stoichiometric approach

employed for the computation of gaseous exchange. These transpiration equations predict the amount of water vapor transpired by the crops, based on the ambient relative humidity, temperature, and pressure, and the current photosynthetic rate of the crops (as measured by DCG). This is accomplished by calculating the stomatal conductance of the crops – a measure of the rate at which water vapor exits through the stomata of the leaves of a crop. The dependency on ambient atmospheric conditions is a consequence of the fact that stomatal conductance is directly proportional to the concentration gradient of water vapor from the leaf to the surrounding atmosphere [322].

The resulting water transpiration rate is then summed with the water content within the biomass produced (see above discussion after Equation (D.6)), to determine the total water uptake of the crops. This water demand is removed from the user-defined input water store, and the water vapor transpired from the crops is sent to the current SimEnvironment, in the same manner as the photosynthetic oxygen described earlier. In addition, the total wet biomass produced is delivered to the initially defined product biomass output destination.

Finally it is important to note that the MEC models are limited to a set of nine crops due to the lack of experimental data required to develop the multivariate polynomial functions used to estimate time to canopy closure and canopy quantum yield. As a result, the crops that can be modeled by the ShelfImpl class are limited to these same nine crops. These crops are: dry bean, lettuce, peanut, rice, soybean, sweet potato, tomato, white potato, and wheat.

Similarly, it is important to note that based on the available experimental data, the MEC models were developed to apply to photosynthetic photon flux (lighting) levels ranging from 200 to 1000μmol/m^2·s and a CO_2 concentration ranging from 330 to 1300ppm [209]. Beneath the 330ppm lower CO_2 concentration bound, a linear trend in crop responses has been assumed up until a CO_2 concentration value of 150 ppm – the assumed lower limit for crop survival. Ambient CO_2 concentrations beneath this limit are assumed to result in crop death. This is in line with experimental observations made by Gerhart et al. [141], and Dippery et al. [142]. Conversely, above ambient CO_2 concentration levels of 1300ppm, the crop response is enforced to equal to the corresponding value at 1300ppm. This insensitivity at high CO_2 concentration values is supported by observations made by Wheeler et al. [170–172] (see Section 4.3 for further details).

Appendix E

Extravehicular Activity Modeling

In addition to modeling the crew activity and their corresponding metabolic demands on habitat ECLS systems, crew extravehicular activity (EVA) is also modeled within HabNet. This requires the user to declare dedicated SimEnvironments representing airlocks/suitlocks and Extravehicular Mobility Units (EMUs or spacesuits) during the setup of a habitation simulation. In addition, EVA activities need to be assigned to the schedules of simulated spacewalking crewmembers. These EVA activities are typically given an activity intensity value of 4 (see Appendix C.2) and are designated to the user-defined EMU SimEnvironment in order to simulate metabolic exchange independent from the crew habitat during EVA.

When an EVA is scheduled within a HabNet simulation, oxygen is first taken from the habitat oxygen tanks to inflate the crew's spacesuits, to support their EVA prebreathe activities, and to fill their Portable Life Support System (PLSS) oxygen tanks. If insufficient oxygen is available from the habitat oxygen tanks, an error message is returned to the user, and the EVA is skipped. Conversely, if sufficient oxygen is available to support EVA, the PLSS feedwater tanks are filled to supply the spacesuit thermal control system with cooling water.

Once these PLSS resources have been collected, the habitat's depressurization pumps are activated to transfer the atmosphere within the airlock/suitlock back into the main habitat cabin to mitigate gaseous losses through airlock/suitlock cycling. After this process, the airlocks/suitlocks are cycled, with any remaining residual gases being lost to space. This atmospheric loss is typically the result of low pressure limits inherent in the design of airlock depressurization pumps, or the scenario where a depressurization pump is not installed. For instance, the depressurization pump installed on the Quest airlock on the International Space

Station can only be operated down to 13.8kPa [323], thus all remaining atmosphere is vented every time the airlock is cycled.

While the crew is on EVA, metabolic resource exchanges occur between the crew and their respective EMUs. This is simulated in the same manner as a typical crew habitat simulation, with the exception that the SimEnvironment selected for these EVA-hours corresponds to the volume and atmospheric composition of an EMU Pressure Garment Assembly (PGA), and the life support system used to sustain the EVA-crew corresponds to the EMU PLSS.

Once an EVA is completed, the EVA crew reenters the main habitat cabin, and remaining gases within the EMU SimEnvironments are reintroduced back into the Airlock/Suitlock SimEnvironment. Moreover, if a Metal Oxide–based (METOX) CO_2 removal system is selected for the EMU PLSS, the CO_2 removed during EVA is reintroduced into the Airlock/Suitlock cabin at the end of an EVA for eventual processing by the habitat life support system. This step is intended to replicate the METOX regeneration process that typically occurs at the conclusion of an ISS U.S. EVA [324]. Similarly, if a Urine Collection and Transfer Assembly (UCTA) based approach is adopted for waste management, urine expelled by the crew during EVA is transferred to the habitat's urine processor waste water tank for later recycling into potable water.

As can be seen in the above EVA simulation summary, several architectural decisions are required before an EVA can be simulated. These are primarily related to the selection of the habitat egress system (i.e. whether an airlock or a suitlock is selected), and the selection of the EMU and PLSS architecture. The following sections, describe these architectural decisions and the implementation of their options in further detail.

E.1 Habitat Egress Architecture – Airlocks versus Suitlocks

Traditionally, long-duration space habitats have employed airlocks to facilitate the movement of crew and equipment into and out of their pressurized environments. These consist of a dedicated volume within a spacecraft that is depressurized and repressurized to enable spacesuited crewmembers to move between the spacecraft pressure vessel and the external environment. While this concept has been successfully deployed over the past several decades in the microgravity environment, additional concerns related to the intrusion of potentially toxic surface dust into the habitat volume for planetary surface habitats have motivated the development of alternative egress concepts [110].

The most prominent of these alternative concepts is the suitlock, which was conceived during lunar surface outpost architectural studies performed in support of the NASA Constellation Program [325]. The suitlock concept is the result of combining the suitport concept developed for small roving vehicles, with a traditional airlock (see Figure E-1). Suitports allow for the quick donning and doffing of spacesuits, while nominally maintaining a constant barrier between surfaces exposed to dust, and the interior environment of the habitat. Conversely, airlocks protect spacesuits from constant exposure to the elements, and provide a means for access to the spacesuits by the crew for pre-EVA checkout and maintenance. Within HabNet, both airlocks and suitlocks are modeled as SimEnvironments with their own volumes and cycle losses. Table E.1 compares the implementation of both airlock and suitlock concepts.

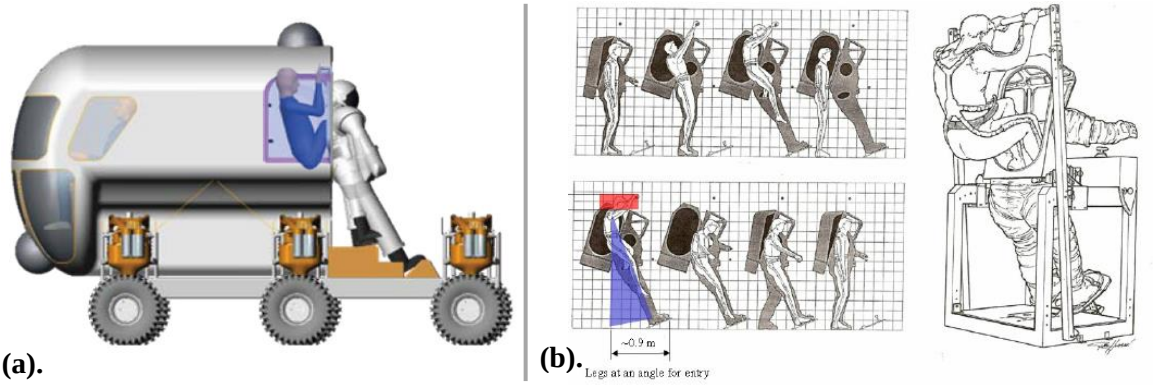

(a). **(b).**

Figure E-1: The Suitport concept developed for facilitating quick EVAs in small pressurized roving vehicles (a). Suitport integrated into a pressurized rover [110] (b). Anthropometrics of entering a suitport [325]

Table E.1: Comparison between Airlocks and Suitlocks (data from [110] and [273])

	Airlock	**Suitlock**
HabNet Implementation Based On	Legacy Airlock Design used on the Space Shuttle and ISS	Dual-Chamber Inflatable Suitlock [273]
Plan View	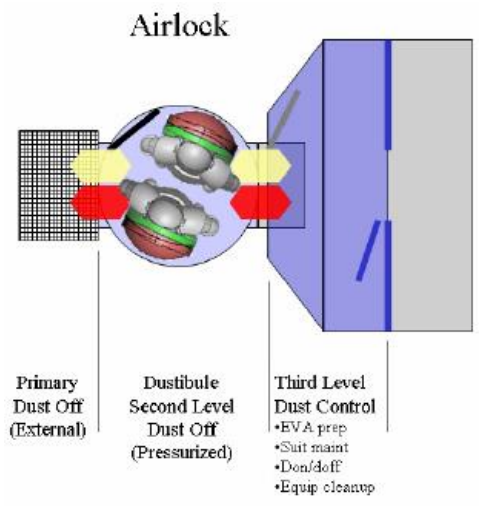	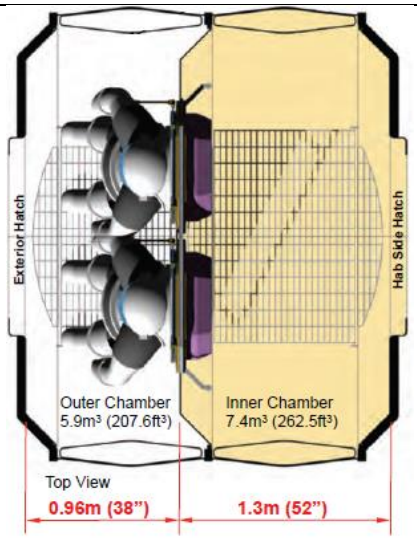
Isometric View		
Free Gas Volume (m^3)	3.7 (from [209])	7.4 (from [273])
Cycle Loss Conditions	The depressurization pump installed on the Quest airlock on the ISS can only be operated down to 13.8kPa [323], thus all remaining atmosphere is vented every time the airlock is cycled. This is equivalent to 3700L at 13.8kPa	Atmospheric losses arise from the air gap between EMU PLSS and outside surface of suitport hatch every time an EVA is performed. Assuming a 1 inch air gap, this is equivalent to the loss of 17.7L of air at a peak pressure of 57kPa (anticipated operating pressure of Mars surface space suits [112]) per crewmember per EVA (based on dimensions from Griffin [325])

E.2 Spacesuit and Portable Life Support System Architectural Decisions

As was mentioned earlier, one of the key drivers of crew consumables demand during EVA is the selection of the life support technologies included within the spacesuit Portable Life Support System (PLSS). In HabNet, two technology options are modeled for the CO_2 removal, heat rejection, and metabolic waste collection functions, while all other life support functions are assumed to be served by a fixed technology. For the most part, these technologies are based on those employed in the Extravehicular Mobility Unit (EMU) currently in use on the International Space Station, and the next generation Portable Life Support System 2.0 (PLSS2.0)[326,327] currently being developed at NASA Johnson Space Center (JSC). When a current technology is found to be unsuitable in serving a given life support function when on the Martian surface, the next generation technology is chosen by default. Similarly, when no new technology alternative is available, or when insufficient data is available for alternative technologies under development, the current state of the art is baselined if it is deemed suitable for use in the Martian environment. Finally, we note that constraints exist for some combinations of technologies due to the integrated design of the PLSS architectures that support them. These include the fact that when a Metal Oxide (METOX) contaminant control cartridge is selected for the CO_2 removal function, the sublimator must be selected to support the heat rejection function, due the tight integration of both of these components within the ISS EMU PLSS. Similarly, when a Rapid Cycle Amine (RCA) Swing Bed is selected for the CO_2 removal function, the Spacesuit Water Membrane Evaporator (SWME) technology must be chosen to serve the heat rejection function due to the tight integration of these two technologies within the PLSS2.0 system. Table E.2 summarizes the current implementation of these and other spacesuit and PLSS technologies within HabNet.

Table E.2: PLSS Technologies currently modeled within HabNet

Life Support Function	**Technology**	**Comments**
Atmos-phere and Pressure Contain-ment	ISS EMU Pressure Garment Assembly (PGA) [328] 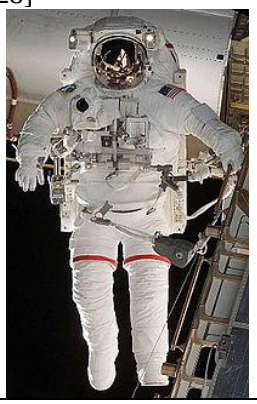	HabNet model based on the PGA of the current ISS EMU [324] Modeled as a SimEnvironment object within HabNet with a: - free gas volume of 2 cubic feet - a pressure of 29.6kPa; and - a peak leakage rate of 36.2cm^3/min
O_2 Storage and Supply	ISS EMU High Pressure Oxygen Tanks [329] 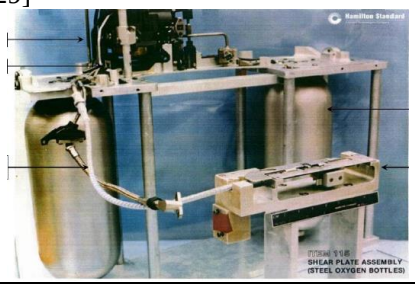	- HabNet model based on the O_2 tanks used in the current ISS EMU PLSS - Modeled as a StoreImpl object within HabNet with a total O_2 capacity of 1.217lb [324]
Thermal Control System Water Storage	ISS EMU PLSS Feedwater Tanks [330] 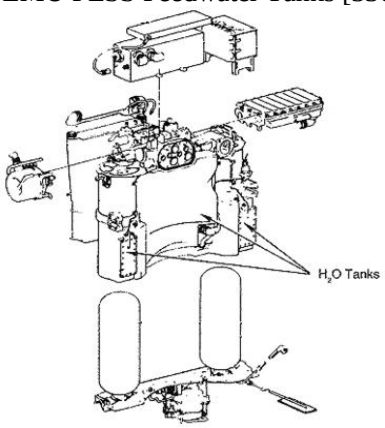	- HabNet model based on the feedwater tanks used in the current ISS EMU PLSS - Modeled as a StoreImpl object within HabNet with a total capacity of 10lb [324]
Heat Rejection	PLSS2.0 Spacesuit Water Membrane Evaporator (SWME) [331]	HabNet model is based on the PLSS2.0 SWME technology currently in development for operation within both the space vacuum and Martian atmospheric environments The SWME is designed to use less water but have a greater operational life as compared to current sublimator technologies used on the ISS EMU PLSS [326]. During an EVA within HabNet, the SWME is modeled as a constant source of water leakage to

	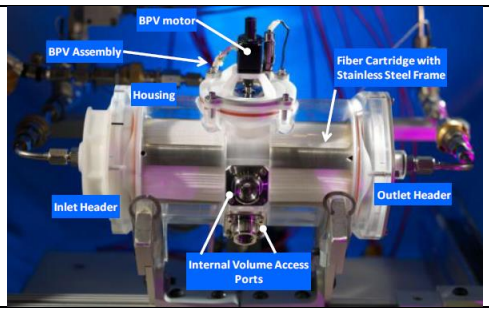	simulate the rejection of heat through membrane-based evaporation of water. This leakage rate is fixed to be 2.1kg of water per 7 hour EVA [332]
	ISS EMU PLSS Sublimator [324] 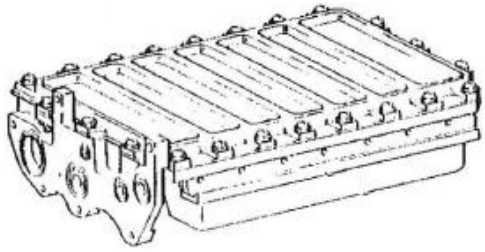	HabNet model based on the Sublimator used within the ISS EMU PLSS. During an EVA within HabNet, the SWME is modeled with a constant water leakage rate of 0.57L/h to simulate the sublimation of water during heat rejection [209]
Carbon Dioxide Removal	ISS EMU PLSS Metal Oxide (METOX) Contaminant Control Cartridge (CCC) [333] 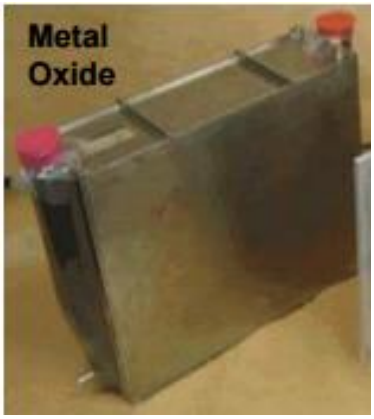	HabNet model based on the METOX cartridge used within the ISS EMU PLSS. Within HabNet, the METOX canister is modeled as a CO_2 store with a capacity of 1.48lb (equivalent to the capacity of the METOX canister [324]) that is a filled throughout an EVA. The maximum flow rate of air through the simulated METOX canister corresponds to 7 cubic feet per minute [324]. At the conclusion of each EVA, the CO_2-laden METOX cartridge is inserted into a regenerator assembly located within the airlock, and is heated to release previously METOX-adsorbed CO_2 into the spacecraft cabin for subsequent processing by the habitat air revitalization system. Within HabNet, this is modeled as the transfer of CO_2 from the METOX store into the atmosphere of the airlock.
	Rapid Cycle Amine (RCA) Swing Bed [334] 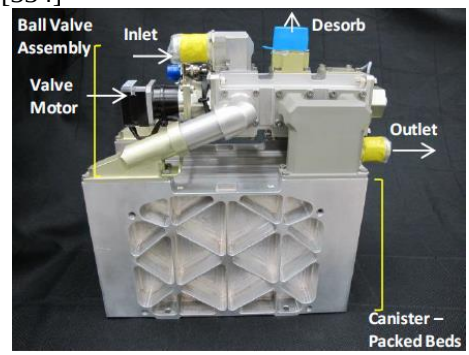	HabNet model based on the RCA Swing Bed technology currently being developed for the PLSS2.0 [334]. This system adsorbs CO_2 and water vapor from the EMU atmospheric loop and desorbs it to the space environment, thereby eliminating the limitations of CO_2 removal on EVA time. Within HabNet, the RCA Swing Bed is modeled as a system that removes CO_2 and water vapor from the EMU SimEnvironment such that the ambient CO_2 partial pressure is maintained at 2.18mmHg [335] and the relative humidity is maintained at 40%. Removed CO_2 and water vapor is then vented from the system
Liquid and Solid Metabolic	Maximum Absorbency Garment (MAG) [336]	HabNet model based on the MAG currently worn by spacewalking astronauts [324]. The MAG absorbs liquid and solid metabolic wastes during EVA and is disposed of afterwards. After a

Waste Collection		simulated EVA within HabNet, any metabolic waste produced by the crew is removed from the system to simulate the disposal of a MAG
	Urine Collection and Transfer Assembly (UCTA) [337] 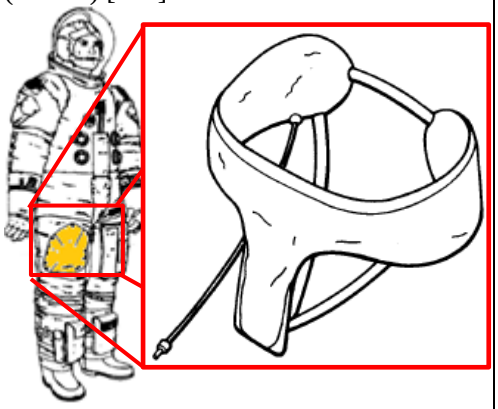	HabNet model based on the UCTA worn as part of Apollo A7L spacesuit used during the Apollo lunar missions. The UCTA collects and stores urine produced by the crew during EVA for later disposal into the spacecraft waste management system, after the EVA has been completed. Within HabNet, the UCTA is modeled as a StoreImpl with a 950 cubic centimeter capacity (corresponding to the volume of the UCTA [337]) that is filled during EVA, and emptied into the habitat urine wastewater tank at the conclusion of the EVA.

Appendix F

ISRU Technology Model Library

This appendix summarizes the models included in the ISRU technology sizing model library that is incorporated within the HabNet ISRU Module. This library was developed by Schrenk [144], who built upon initial model development work by Schreiner [143]. Table F.1 summarizes the technologies currently modeled within this library.

Table F.1: ISRU Technologies currently modeled within the HabNet ISRU Module

ISRU Function	**ISRU Technology**	**Governing Reaction**
Water Extraction / Production	Soil Processor	Hydrated Soil → H_2O + Dehydrated Soil
	Sabatier Reactor	$CO_2 + 4H_2 \rightarrow CH_4 + 2H_2O$
	Reverse Water Gas Shift Reactor	$CO_2 + H_2 \rightleftharpoons CO + H_2O$
CO_2 Extraction	CO_2 Cryocooler	Mars Atmosphere → CO_2 + N_2 + Ar + Unused Products
Inert Gas Extraction	Atmospheric Processor*	
Oxygen Production	Water Electrolyzer	$2H_2O \rightarrow 2H_2 + O_2$
	Solid Oxide CO_2 Electrolyzer	$2CO_2 \rightarrow 2CO + O_2$

*Sizing model is described in Section 5.5.2.2 rather than in this appendix

For each ISRU technology described in this appendix, we provide a high level description of the technology, present a flowsheet of its main components, and summarize the equations used to estimate its mass, power, and volume as a function of the desired resource production rate and operating location. Following this, a comparison is made between the predictions made by the developed equations with those published in the literature. For more details on the derivation of these equations, the reader is referred to Schrenk [144].

F.1 Soil Processor

The role of the soil processor modeled within the HabNet ISRU Module is to extract water from Martian regolith. The architecture adopted here was originally based on the soil processor module of the Mars Atmosphere and Regolith Collector/PrOcessor for Lander Operations (MARCO POLO) system developed at NASA JSC and KSC (see Section 2.2.4) and later updated with a sweep gas system to aid in the separation, transport, and filtration of water prior to its delivery to the product water tank..

As can be seen in the flowsheet depicted in Figure F-1, the soil processor consists of a feed hopper and a sieve that receives input soil from an excavator rover (not currently modeled within HabNet), and filters out larger fragments in order to prevent clogging of downstream components. From here, the filtered regolith is transported along a horizontal auger before being fed into a combination oven and mixing auger unit, which both agitates and heats the regolith with a pre-heated sweep gas to vaporize any water embedded within the feed mixture. As mentioned above, the sweep gas then transports the water vapor through a heat exchanger to recover energy for the heating of subsequent batches of regolith, and then to a Nafion filter, where a final water cleaning process is performed before the vapor is condensed and made available for downstream use. Table F.2 summarizes the assumptions and equations used to size each of the components within this system.

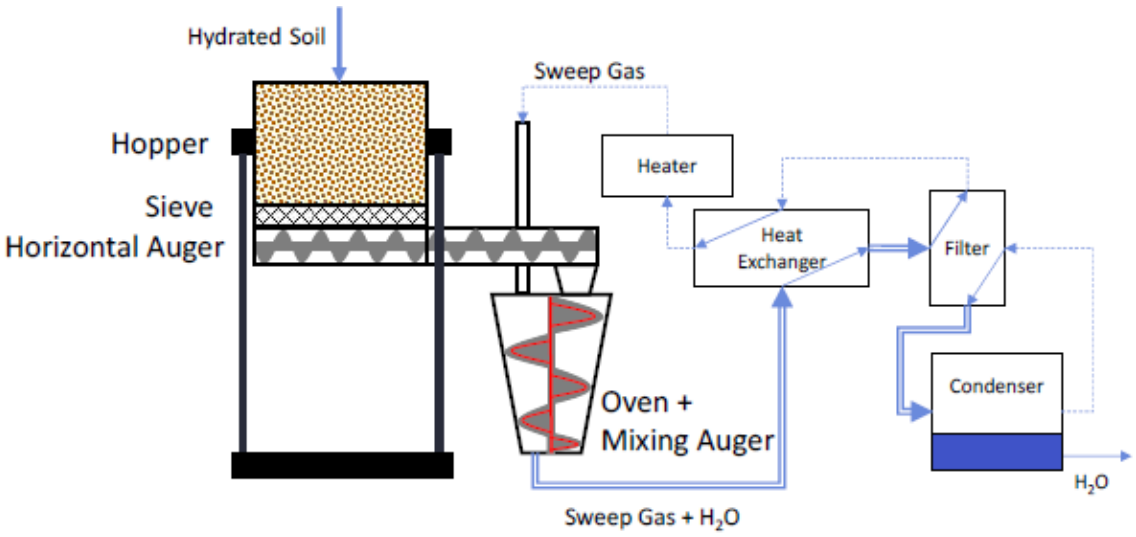

Figure F-1: Flowsheet of the Soil Processor modeled within HabNet. This architecture is based on the MARCO POLO system developed by Interbartolo et al. (see Section 2.2.4)

Table F.2: Summary of Soil Processor Sizing Equations developed by Schrenk [144]:

Component	Sizing Equations (Mass (m), Power (P), Volume (V))	Comments / Variables
Heater	$P[W] = \frac{1}{\eta} \times \frac{E_h + E_s}{T_B}$	• A resistive heater with negligible mass and power is assumed. • Variables: η = efficiency; E_h = energy required for heating [J]; E_s = energy required for sublimation [J]; T_B = batch time [s]
Oven	$V[m^3] = f \times \frac{100 \times R_W}{H_2O} \times T_B \times \frac{1}{\rho_s}$ $m[kg] = A \times t \times \rho$	• To facilitate continuous operation at approximately 500°C, an aluminum, conical-shaped oven is assumed (see Figure F-1) • Variables: f = oven fill factor [%]; R_W = commanded water production rate [kg/h]; H_2O = local water abundance [%]; T_B = batch time [h]; ρ_s = soil density [kg/m^3]; A = surface area [m^3]; t = wall thickness [mm]; ρ = material density (2700kg/m^3 for aluminum)
Hopper	$V[m^3] = (b+1) \times V_B \times \left(1 + \frac{S}{100}\right)$ $m[kg] = \left(a^2 + 4ah\right) \times t \times \rho$	• The hopper is assumed to have a quadratic cross-section in order to mitigate clogging in corners within its volume. It is sized to support two batches of soil to enable continuous operation, and is assumed to be made of aluminum • Variables: b = back up soil in hopper (assumed to be one batch); V_B = volume per batch [m^3]; S = margin (10% assumed); h = hopper height (0.5m assumed); a = base length [m]; t = wall thickness (5mm assumed); ρ = material density (2700kg/m^3 for aluminum)
Sieve	$m[kg] = a^2 \times t_s \times \rho \times 0.5$	• The sieve is sized to support the load of the soil. It is installed within the hopper and hence its volume is ignored • Variables: a = base side length [m] (determined by hopper dimensions); t_s = sieve thickness [m] (sized based on batch mass); ρ = material density (2700kg/m^3 for aluminum)
Augers	Geometry: Shaft diameter: $d_{shaft} = \frac{d_{auger}}{5}$ Pitch: $P = d_{auger}$ Blade Thickness: $t_{blade} = \frac{P}{15}$	• Auger diameter (d_{auger}), auger rotation rate (measured in revolutions per minute (RPM)), and bearing factor is based on graphical volumetric flow rate correlations derived by Couper et al. [338]

	Auger Container Volume: $V_{auger}[m^3] = \frac{2d_{auger}t_{auger} + t_{auger}^2}{4} \times \pi \times L_{auger}$ Auger Shaft Volume: $V_{shaft}[m^3] = \frac{\pi d_{shaft}^2}{4} \times L_{auger}$ Auger Blade Volume: $V_{blade}[m^3] = \frac{d_{auger} - d_{shaft}}{2} \times L_{blade} \times t_{blade}$ Auger Blade Length: $L_{blade}[m] = \left(2\pi \frac{L_{auger}}{P}\right)\sqrt{\left(\frac{d_{auger} - d_{shaft}}{4}\right)^2 + \left(\frac{P}{2\pi}\right)^2}$ Auger Mass, Power, and Volume: $m[kg] = (V_{auger} + V_{shaft} + V_{blade}) \times \rho$ $V[m^3] = \frac{\pi d_{auger}^2}{4} \times L_{auger}$ $P[W] = \frac{1.25(3.28L_{auger})\left(S \times RPM + 0.7(35.31)\left(\frac{2.2}{35.31}\rho_{soil}\right)\right)}{0.9 \times 10^6} \times 746$	• Auger blade length is derived from the helix equation • All components are assumed to be made of aluminum • Variables: t_{auger} = auger container wall thickness [mm]; L_{auger} = auger length;); ρ = material density (2700kg/m^3 for aluminum); ρ_{soil} = soil density, as determined by the location of the system
Sweep Gas Subsystem	Piping: $m_{pipe}[kg] = L\pi\rho \times (2Rt + t^2)$ $V_{pipe}[m^3] = L\pi \times (R + t^2)$ Mass of sweep gas: $m_{gas}[kg] = R^2\pi \times L \times \rho_{gas}$	• The sweep gas pipe length has been assumed to be six times the height of the oven. It is assumed to be made of steel • Variables: L = length of pipe [m]; ρ = material density (6800kg/m^3 for steel); t = pipe wall thickness [m]; R = pipe inner radius [m] based on the assumed sweep gas flow rate of $\dot{m}_{sg}[kg/h] = 2.37 \times R_W$ where R_W is the commanded water production rate [kg/h]; ρ_{gas} = mean sweep gas density [kg/m^3]
Water Filtration System	Filter Tube Assembly: $m_{TA}[kg] = 200 \times R_W \times 3.5 \times 10^{-4}$ Housing: $D[m] = 2 \times \sqrt{\frac{n \times r^2}{\eta}}$ $V[m^3] = 0.61 \times D^2$ $m[kg] = 1443 \times V$	• Filter design based on that of Kelsey et al. [339] which contains 200 Nafion tubes each weighing approximately 3.5×10^{-4}kg. Here, the volume is estimated by assuming that the Nafion tubes are packed within a cylindrical container. • The height of the housing has been estimated to be 0.61m based on a visual analysis of the images presented in Kelsey et al. [339]. • Variables: R_W = commanded water production rate [kg/h]; n = number of Nafion tubes; r = radius of Nafion tubes (0.00042m); η = packing density (assumed to be 0.0564)
Condenser	Radiator Geometry:	• The condenser is assumed to consist of a radiator and a water reservoir that

	Area: $A_{rad}[m^2] = \frac{P_{cond}}{\sigma\left(T_{gas}^4 - T_{env}^4\right)}$ Length: $L_{rad}[m] = \frac{A_{rad}}{2\pi R}$ Total Purge Length: $L_{pipe\_purge}[m] = 2.5 \times L_{rad}$ Radiator Mass and Volume $m_{rad}[kg] = L_{pipe\_purge} \times \pi\rho \times (2Rt + t^2)$ $V_{rad}[m^3] = L_{pipe\_purge} \times \pi \times (R + t)^2$ Water Reservoir: $V_{store}[m^3] = \frac{2 \times R_W \times T_{batch}}{1000}$ $m_{store}[kg] = \left(\frac{4}{3}\pi(R_{store} + t_{store})^3 - V_{store}\right)\rho$	stores product water. The condenser is shaped like a pipe-section and is sized based on the assumption that radiation is the primary source of heat rejection. • The water reservoir is assumed to have a capacity of double the maximum expected water content of one batch • Variables: P_{cond} = radiated power for condensing of water [W]; σ = Stefan-Boltzmann Constant; T_{gas} = purge gas temperature [373K]; T_{env} = ambient environmental temperature [K]; ρ= material density [kg/m^3]; t = pipe wall thickness [m]; R = pipe inner radius [m]; R_W = commanded water production rate [kg/h]; R_{store} = reservoir inner radius [m]; t_{store} = reservoir wall thickness

Due to the conceptual nature of published soil processor designs, wide discrepancies were observed when comparing the predictions of the soil processor sizing model developed here with those described in the literature. Table F.3 compares the predicted mass, power, and volume by the above formulated model with those of published soil processor designs operating at various production rates.

Table F.3: Soil Processor / Water Extraction system model comparison

Source	**H_2O (% in soil - kg/h)**	**Mass (kg per kg/h(H_2O))**	**Volume (m^3 per kg/h(H_2O))**	**Power (kW per kg/h(H_2O))**
Sanders 2010 [340]	3% - 2.3	267	7	13.9
HabNet Soil Processor Model [144]	3% - 2.3	162	0.61	12.2
Comparison		**60.7 %**	**8.7 %**	**87.8 %**
Sanders 2010 [340]	8% - 2.4	197	4	6.6
HabNet Soil Processor Model [144]	8% - 2.4	103	0.38	7
Comparison		**52.3 %**	**9.5 %**	**106.1 %**
Stoker 1993 [341]	1% - 1.0	-	-	10.3
HabNet Soil Processor Model [144]	1% - 1.0	-	-	13
Comparison		**-**	**-**	**126.2 %**

To compensate for these observed discrepancies, Schrenk included multiplicative factors to the mass and volume sizing equations for the soil processor. These are listed as follows:

Table F.4: Multiplicative factors derived for the soil processor sizing equations

Soil Processor Sizing Equation	**Adjusted Soil Processor Sizing Equation**
Mass	1.8 × calculated mass
Volume	11 × calculated volume

F.2 CO_2 Cryocooler

In most ISRU architectures, the primary role of the CO_2 cryocooler is to extract CO_2 from the Martian atmosphere for downstream use by other ISRU systems. As a first step in developing a sizing model, Schrenk [144] surveyed the literature and found three major classes of CO_2 extraction technologies that have been previously proposed for use within the Martian environment. These are:

- Thermal-swing adsorption compression, which relies on large capacity sorbents selectively adsorbing CO_2 from the Martian atmosphere and desorbing the product CO_2 into a tank for downstream use
- Mechanical compressors that force pressurized Martian atmosphere through specialized filters to separate CO_2 from the incoming flow stream; and
- Cryogenic compressors that freeze CO_2 out of the Martian atmosphere and reheat the collected CO_2 ice to generate high pressure pure CO_2 gas

Within the HabNet ISRU Module, the cryogenic CO_2 compressor concept has been selected for modeling due to its generally lower mass and lower complexity as compared to mechanical compressors [144], and its widespread use in published ISRU CO_2 acquisition concepts, such as the MARCO POLO system discussed in Section 2.2.4. As can be seen in the flowsheet in Figure F-2, the cryogenic compressor modeled here consists of two cryocoolers that operate in a swing-mode in order to facilitate the continuous extraction of CO_2. While one cryocooler is operating within a “cold” mode to collect CO_2 from the Martian atmosphere, the other cryocooler is operating in a “hot” mode, where an internal heater is activated to vaporize the previously accumulated pure CO_2 ice and deliver it to a downstream processor. Table F.5

summarizes the assumptions and equations used to size each of the components within this system.

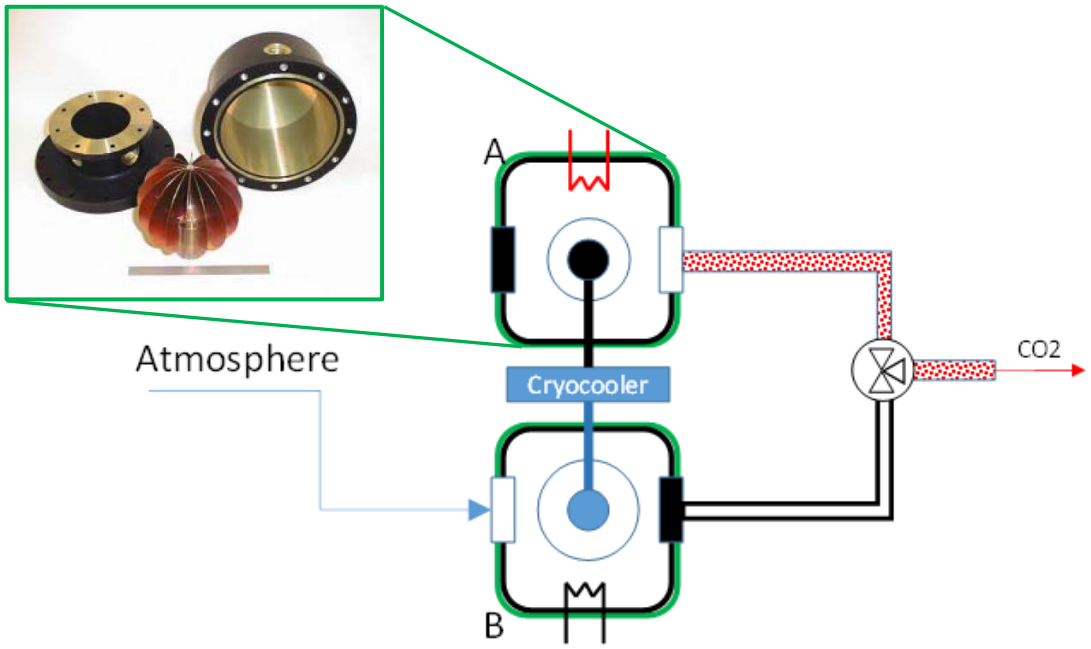

Figure F-2: Cryogenic CO_2 Compressor system model architecture (Inset – Freezer chamber and copper cold tip developed by Anderson and Curley [342])

Table F.5: Summary of Cryogenic CO_2 Compressor Sizing Equations developed by Schrenk [144]

Component	**Sizing Equations (Mass (m), Power (P), Volume (V))**	**Comments / Variables**
Freezing Chamber	Extracted CO_2 ice sphere: $V_{ice}[m^3] = \frac{R_{CO2} \times T}{\rho_{ice}}$ Radius: $R_{ice}[m] = \left(\frac{3V_{ice}}{4\pi}\right)^{1/3}$ Chamber Geometry: Height: $H[m] = 3 \times R_{ice}$ Radius: $R[m] = 1.5 \times R_{ice}$ Chamber Mass and Volume: $m[kg] = \rho\left(2\pi t(R+t)^2 + \pi H(2Rt+t^2)\right)$ $V[m^3] = \pi H(R+t)^2$	• Chamber geometry is dictated by extrapolation from the design of Anderson and Curley [342] (see Figure F-2) and the total amount of CO_2 extracted per batch, which is in turn a function of the commanded CO_2 production rate • Variables: R_{CO2} = commanded CO_2 production rate [mol/h]; T = batch time [h]; ρ_{ice} = density of CO_2 ice (assumed to be 1500kg/m^3); ρ = freezing chamber material density (assumed to be steel: 7800kg/m^3); t = freezing chamber wall thickness (sized for 2MPa internal pressure)
Cryocooler	Required Cooling Power: $P_{cool}[W] = R_{CO2} \times c_p \times (T_{atm} - T_{freeze})$ Required Resublimation Power:	• Sizing of the cryocooler was based on performance correlations with the commercially available SunPower CryTel

	$P_{resub}[W] = R_{CO2} \times L_{resub}$ Total Required Freezing Power: $P_{freeze}[W] = \frac{P_{cool} + P_{resub}}{0.8}$ Chamber Mass, Power and Volume: $M[kg] = 2.1 \times N$ $P[W] = 80 \times N$ $V[m^3] = 0.0013 \times N$ Where N = number of coolers, derived from manufacturer specified correlations for effective lift and required cooling power (see comments)	coolers [343] operating with an overall cooling efficiency of 80%. The required freezing power was first calculated, and the corresponding effective lift (L_{eff}) (the amount of power that the cooler can remove) and number of coolers (N) is estimated based on these correlations. See Schrenk [144] for further details • Variables: R_{CO2} = commanded CO_2 production rate [mol/h]; c_p = specific heat of CO_2 (estimated at 700J/kg·K at expected operating temperature); L_{resub} = latent heat of resublimation (598.6kJ); T_{atm} = ambient atmospheric temperature [K]; T_{freeze} = freezing pint of CO_2 (150K at Martian pressures)

A comparison of the predictions from this cryogenic CO_2 compressor sizing model with values published in the literature revealed that the model developed here slightly under predicts the mass and power requirements of comparable concepts. This can be seen in the comparison table below:

Table F.6: Cryogenic CO_2 Compressor sizing model comparison

Source	**Mass (kg per kg/h(CO_2))**	**Volume (m^3 per kg/h(CO_2))**	**Power (kW per kg/h(CO_2))**
Rapp et al. 2005 [344]	54	-	1.23
HabNet Cryogenic CO_2 Compressor Sizing Model [144]	45.7	0.043	1.1
Comparison	**84.6 %**	**-**	**89.4 %**

This mass difference can likely be attributed to flow control hardware not accounted for in the sizing calculation here, such as valves and piping. Consequently, Schrenk [144] derived the following corrective factors to this sizing model based on the results of this model comparison. These are summarized as follows:

Table F.7: Multiplicative factors derived for the CO_2 compressor sizing equations

Cryogenic CO_2 Compressor Sizing Equation	**Adjusted Cryogenic CO_2 Compressor Sizing Equation**
Mass	1.18 × calculated mass
Volume	4 × calculated volume

F.3 Solid Oxide CO_2 Electrolysis

As was discussed in Section 2.2.4, the Solid Oxide CO_2 Electrolysis (SOCE) process is currently being developed for the Mars Oxygen ISRU Experiment (MOXIE) payload to be flown on the Mars 2020 rover mission [94]. This system directly electrolyzes a pre-heated feed stream of CO_2 gas into oxygen and carbon monoxide gas. The oxygen is then delivered to a downstream product tank, while the carbon monoxide gas is vented from the system. This process is summarized in the flowsheet shown in Figure F-3. Also shown in this figure is a detailed view of the SOCE cell stack configuration assumed for this sizing analysis. Here, the yttrium-stabilized-zirconia (YSZ) cell configuration developed by Crow [345] is baselined. Each YSZ cell is surrounded by electrodes which are supported by a grill that directs the CO_2 feed stream. This combination is surrounded by a diaphragm, which physically separates and electrically insulates adjacent stack elements. The thicknesses of each of the components of this YSZ cell configuration are listed in Figure F-3.

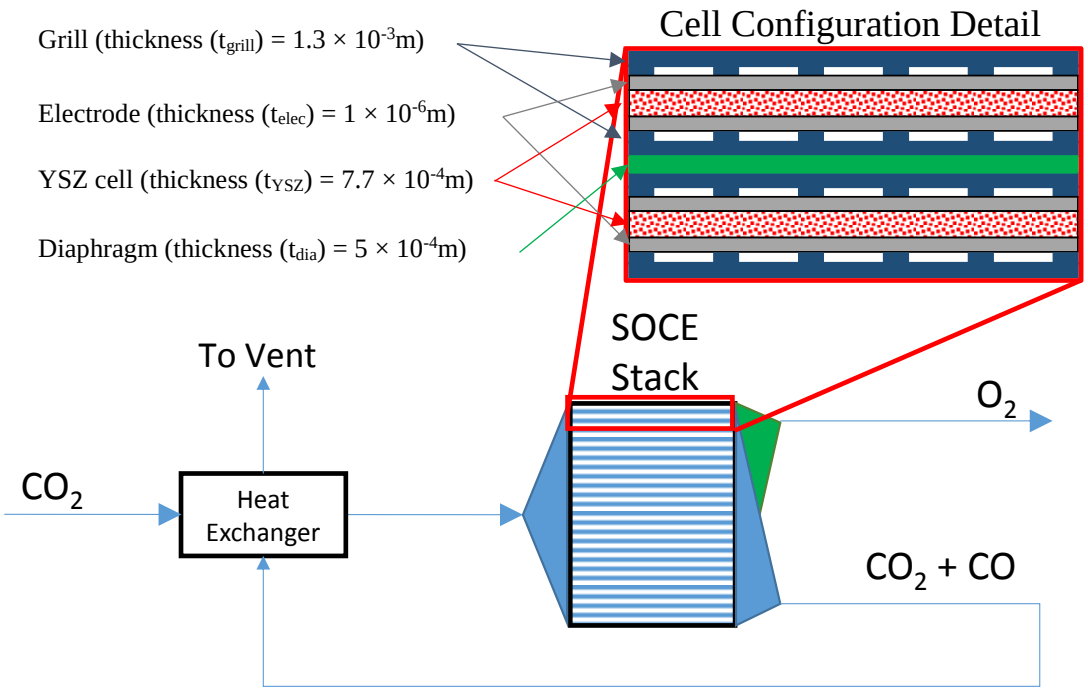

Figure F-3: Solid Oxide CO_2 electrolysis model architecture

Currently, the sizing model for the SOCE system accounts for only the solid oxide electrolysis cell stack. Table F.8 summarizes the assumptions and equations used to size these components.

Table F.8: Summary of Solid Oxide CO_2 Electrolysis System Sizing Equations developed by Schrenk [144]:

Component	Sizing Equations (Mass (m), Power (P), Volume (V))	Comments / Variables
Electrolysis Cell Stack	Flow rates: $R_{CO2} = \frac{2 \times R_{O2}}{\eta}$ $R_{CO} = 2 \times R_{O2}$ Power Requirement: Current: $I[A] = \frac{R_{O2}}{3.25 \times 10^{-4}}$ $P[W] = UI$ Number of Stack Elements: Electrode Area: $A[m^2] = \frac{I}{\rho_{current}}$ $N = \frac{A}{A_{\max}}$ Stack Height and Mass: $H[m] = N \times (2t_{grill} + 2t_{elec} + t_{YSZ} + t_{dia})$ $m[kg] = N \times A \times \begin{pmatrix} 2t_{grill}\rho_{grill} + 2t_{elec}\rho_{elec} \\ + t_{YSZ}\rho_{YSZ} + t_{dia}\rho_{dia} \end{pmatrix}$	• Variables: R_{O2} = commanded O_2 production rate [mol/h]; R_{CO2} = Required CO_2 inlet flow rate [mol/h]; R_{CO} = CO flow rate [mol/h]; η = electrolysis conversion efficiency (assumed to be 75% based on Sridhar et al. [346]); I = system current; U = cell voltage (set at 1.6V); $\rho_{current}$ = current density (assumed to be 5000A/m^2 based on Sridhar et al. [346]); A_{max} = surface area per cell (assumed to be 0.0079m^2 based on Crow [345]); N = number of cell stack elements; ρ_{grill} = grill material density (assumed to be steel at 7800kg/m^3); ρ_{elec} = electrode material density (assumed to be platinum at 21450kg/m^3); ρ_{YSZ} = ion conductor material density (assumed to be YSZ at 5690kg/m^3); ρ_{dia} = diaphragm material density (assumed to be platinum at 21450kg/m^3) • The electrolysis cell stack is contained within a container. Thus the container volume is used when sizing the SOCE system rather than the electrolysis cell stack volume
Cell Stack Container	$m_{cont}[kg] = \rho\pi \times \begin{pmatrix} 2t_{cont}(R + t_{cont})^2 + \\ H(2Rt_{cont} + t_{cont}^2 \end{pmatrix}$ $V_{cont}[m^3] = H\pi \times (R + t_{cont})^2$	• Variables: ρ = container material density (assumed to be a ceramic at 6500kg/m^3); t_{cont} = container wall thickness (Assumed to be 0.002m); R = stack radius [m] , sized from electrode area; H = assembled stack height [m] • The CO_2 transportation piping system is assumed to be integrated into the stack structure and are therefore assumed to have no additional mass or volume

As was the case with the previously modeled ISRU technologies, the predictions of the SOCE sizing equations developed here were compared with other SOCE concepts described in the literature. Table F.9 summarizes the results of this comparison.

Table F.9: Solid oxide CO_2 electrolysis model comparison

Source	**Mass (kg per kg/h(O_2))**	**Volume (m^3 per kg/h(O_2))**	**Power (kW per kg/h(O_2))**
Rapp et al. 2005 [344]	7.7	-	6.6
HabNet SOCE Sizing Model [144]	8.5	0.0012	5
Comparison	**110.4 %**	**-**	**75.8 %**
Sridhar et al. [346]	10.2	0.0056	6.2
HabNet SOCE Sizing Model [144]	8.5	0.0012	5
Comparison	**83.3 %**	**21.4 %**	**80.7 %**

As can be seen from Table F.9, the HabNet SOCE mass prediction lies between the mass values observed in the literature, and underestimates the volume and power demand. To correct for these, the following correction factors were implemented by Schrenk. Here, the mass was increased by a factor of 20% to account for the mass of additional flow control hardware such as valves and heat exchangers.

Table F.10: Multiplicative factors derived for the SOCE sizing equations

SOCE Sizing Equation	**Adjusted SOCE Sizing Equation**
Mass	1.2 × calculated mass
Volume	4.8 × calculated volume
Power	1.33 × calculated power

F.4 Water Electrolyzer

The water electrolyzer modeled within the HabNet ISRU Module generates oxygen and hydrogen from the electrolysis of water in the same manner as that of the Oxygen Generation Assembly (OGA) modeled within the HabNet Habitation Module (see Appendix D.5). Rather than modeling the function of a water electrolyzer, as is the case in the Habitation Module, the model developed here aims to size a water electrolyzer system based on a required demand for oxygen and/or hydrogen gas. This fluctuating demand between the two product gases consequently affects the rate at which reactant water is needed for the reaction, and thus the size of the electrolysis cell stack. This contrasts somewhat to the OGA used for ECLS applications, where the system is designed to primarily produce oxygen. Moreover, the fact

that the OGA is operated within the spacecraft cabin, imposes additional safety requirements on its design, which result in additional system mass. These include the need to operate the electrolysis cell stack within an explosion-proof pressurized dome and at near vacuum operating pressures to prevent the potential leakage of hydrogen gas into the cabin, where it can become explosive when exposed to ambient oxygen [165]. In comparison, an ISRU-based electrolyzer will likely operate outside of the habitable volume in the Martian atmosphere, where these safety features become less important.

Figure F-4 depicts the flowsheet assumed for the ISRU water electrolyzer sizing model developed for the ISRU Module. Here, a Proton Exchange Membrane (PEM) type of electrolyzer has been baselined due to its prevalence in ISRU water electrolyzers described in the literature [144]. To generate the desired products, feedwater is introduced into the system by a pump and directed to a combined buffer tank/water separator that stores a previously generated water/oxygen mixture. From here, the feedwater is directed through the electrolysis stack, where it is electrolyzed into oxygen and hydrogen. This results in an oxygen/water mixture being produced on the anode side of the stack, and a hydrogen/water vapor mixture on the cathode side. The oxygen/water mixture is recycled back into the buffer tank, where it is run through the water separator to liberate oxygen for downstream use. The remaining water is then recycled through the electrolysis stack. Conversely, the hydrogen/water vapor mixture on the hydrogen side of the stack is sent through a dryer to remove the relatively lower amount of water vapor from the hydrogen mixture. The resultant pure hydrogen is then either vented or delivered downstream for later use.

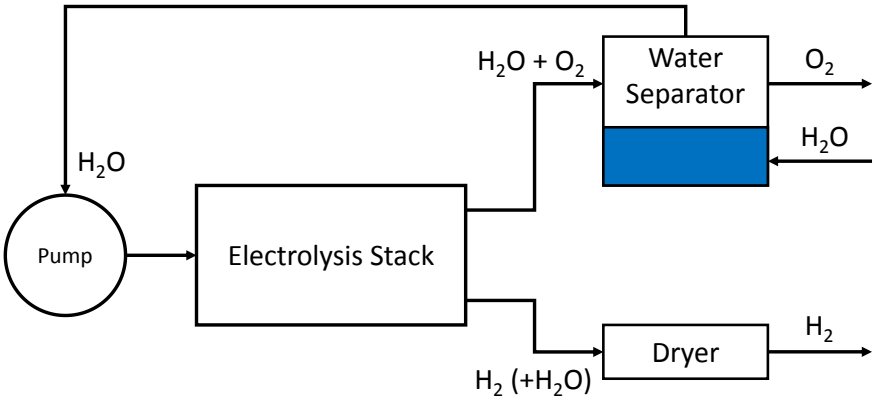

Figure F-4: Water electrolysis model architecture

To size the water electrolyzer, the driving production rate (i.e. O_2 or H_2 gas) is first determined based on the molar stoichiometric ratio of 2:1 (H_2:O_2) for the electrolysis process. With this driving rate computed, the electrolysis cell stack, the combined buffer tank/water separator, and the water pump are sized using the relationships listed below in Table F.11.

Table F.11: Summary of ISRU Water Electrolyzer Sizing Equations developed by Schrenk [144]:

Component	**Sizing Equations (Mass (m), Power (P), Volume (V))**	**Comments / Variables**
Electrolysis Cell Stack	Power Requirement: $P[W] = 45700 \times R_{H2}$ Number of Stack Elements: $N = \frac{P}{U\rho_c} \times \frac{1}{A_{cell}}$ Cell Mass: $m_{cell}[kg] = A_{cell}\begin{pmatrix} 0.004\rho_{Ti} \\ +0.0024 \times 0.6\rho_{Ti} \\ +\rho_{membrane} \end{pmatrix}$ Cell Stack Mass: $m_{stack}[kg] = N \times m_{cell}$ Container Mass and Volume: $m_c[kg] = \rho\left(2(r_s + t_c)^2 \pi t_c + (2r_s t_c + t_c^2)\pi H_s\right)$ $V_c[m^3] = (r_s + t_c)^2 \pi H_s$	• Sized using a similar approach to that used for the SOCE electrolysis cell stack (see Appendix F.3), but with different cell element materials • Power requirement is based on current industrial water electrolyzer units (Giner [347]) • Each cell is assumed to have a thickness of 6.7mm based on existing PEM electrolysis cell stack designs (Millet et al. [348]). It is assumed that 2.4mm of this 6.7mm is comprised of two 1.2mm 40% porosity titanium current collectors, a 0.3mm thick Nafion membrane coated with a noble catalyst, and two titanium separating plates with a total thickness of 4mm • Variables: R_{H2} = commanded H_2 production rate [mol/h]; U = cell voltage (set at 1.7V based on Giner [347]); ρ_c = current density (assumed to be 25kA/m^2 based on Giner [347]); A_{cell} = cell area (assumed to have a radius of 9cm based on Millet et al. [348]); ρ_{Ti} = density of titanium alloy (4000kg/m^3); $\rho_{membrane}$ = cell membrane material density (assumed to be 0.5kg/m^3 based on DuPont [349]); r_s = stack radius [m]; t_c = container wall thickness [m] (sized for an internal pressure of 3MPa); H_s = stack height [m]; ρ = container material density (assumed to be a ceramic at 2000kg/m^3)
Anode Side Buffer Tank / Water Separator	Volume: $V[m^3] = 3 \times R_{H2O}$ Tank Radius: $r[m] = \left(\frac{3V}{4\pi}\right)^{1/3}$	• It is assumed that the separator is also used as a buffer tank, with a capacity of three times the feedwater flow rate into the electrolysis cell stack • The tank is assumed to be spherical in shape, with a wall thickness of 5mm

	Mass: $m[kg] = \rho\left(\frac{4}{3}\pi(r+0.005)^3 - V\right)$	• Variables: R_{H2O} = rate of water flow into the electrolysis cell stack [L/hr]; ρ = tank material density, assumed to be steel at 7800kg/m^3
Cathode Side Hydrogen Separator / Dryer	Volume: $V[m^3] = R_{H2O}$ Tank Radius: $r[m] = \left(\frac{3V}{4\pi}\right)^{1/3}$ Mass: $m[kg] = \rho\left(\frac{4}{3}\pi(r+0.005)^3 - V\right)$	• The volume of the cathode side hydrogen separator / dryer is assumed to be equivalent to the feedwater flow rate into the electrolysis cell stack • The tank is assumed to be spherical in shape, with a wall thickness of 5mm • Variables: R_{H2O} = rate of water flow into the electrolysis cell stack [L/hr]; ρ = tank material density, assumed to be steel at 7800kg/m^3
Water Pump	$m[kg] = 0.54$ $V[m^3] = 0.0007$ $P[W] = 10$	• The pump mass, power, and volume are assumed to be fixed values based on an existing water pump described by Koolance [350] • The pump power is selected such that the output flow rate is 5L/min with a pressure head of 0.6bar to overcome pressure losses within the system

A comparison between the predictions of the water electrolyzer sizing model developed here with data published in the literature found that the system mass and volume tended to be underestimated, while the power requirement was largely accurate. Table F.12 summarizes the results of this comparison.

Table F.12: Water Electrolyzer Sizing model comparison

Source	**Mass (kg per kg/h(H_2))**	**Volume (m^3 per kg/h(H_2))**	**Power (kW per kg/h(H_2))**
Clark 1997 [351] and Rapp et al. 2005 [344]	100.8	-	47.5
HabNet ISRU Water Electrolyzer Sizing Model [144]	53.6	0.046	45.6
Comparison	**52.6 %**	**-**	**96 %**
Brooks et al. 2006 [352]	329	0.0752	40
HabNet ISRU Water Electrolyzer Sizing Model [144]	53.6	0.046	45.6
Comparison	**16.1 %**	**61.2 %**	**114 %**

The discrepancy in mass and volume estimates found in Table F.12 is likely due to uncertainties in the specific arrangement of flow control components within the system and the

piping arrangement used to connect them. To compensate for these discrepancies, Schrenk [144] incorporated the following corrective factors into the water electrolyzer sizing equations:

Table F.13: Multiplicative factors derived for the water electrolyzer sizing equations

ISRU Water Electrolyzer Sizing Equation	**Adjusted ISRU Water Electrolyzer Sizing Equation**
Mass	4 × calculated mass
Volume	1.64 × calculated volume

F.5 Sabatier Reactor Model

The Sabatier reaction has been a prevalent component of ISRU architectures since the concept of ISRU was first proposed by Ash et al. in 1978 [16] (see Section 2.2.1), where it has traditionally been proposed as a means of producing methane ascent vehicle fuel from the reaction of hydrogen with carbon dioxide, as shown in the reaction below:

$$CO_2 + 4H_2 \rightarrow CH_4 + 2H_2O + Heat \tag{F.1}$$

Moreover, as was discussed in Appendix D.7, a Sabatier reactor has also been operating onboard the International Space Station since October 2010 [49], where it has been used as the first step in the recovery of oxygen from CO_2 exhaled by the crew. In this application, all product methane is vented overboard, instead of being stored for use as a fuel, as is the case with the ISRU-based concepts referenced above.

For the ISRU Module, a set of equations have been developed to make first-order sizing estimates of a generic Sabatier reaction chamber, along with its supporting heat exchanger and gas/liquid separation equipment. This contrasts to the Sabatier reactor modeled in the ECLS Technology Model Library, where the function of a specific instance of a Sabatier Reactor (namely, the reactor operating onboard the ISS) is modeled. Figure F-5 summarizes the architecture of the generic Sabatier reactor system assumed here:

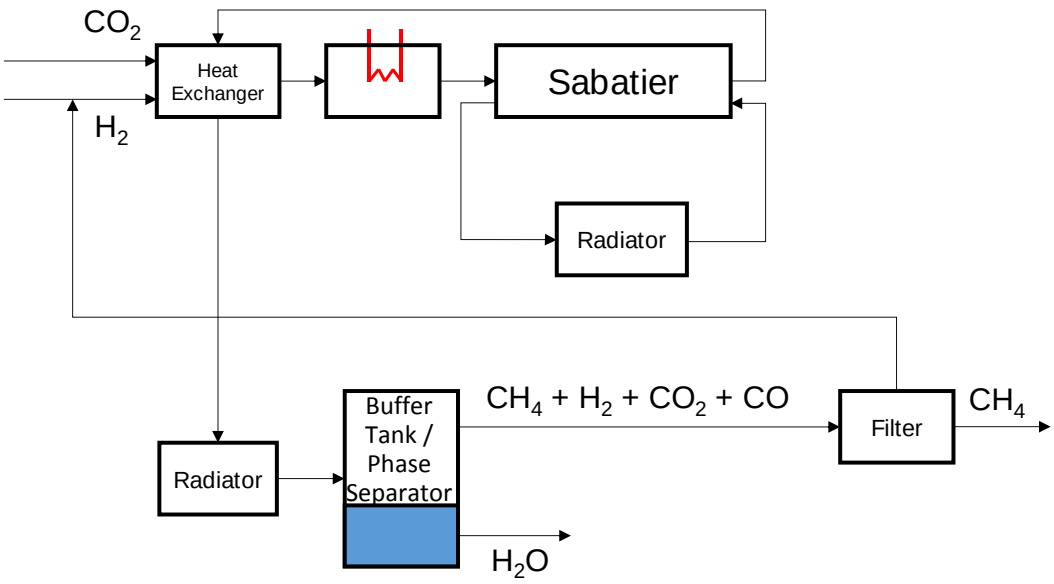

Figure F-5: Sabatier reactor modeling architecture

As can be seen in Figure F-5, hydrogen and CO_2 gas are first passed through a heat exchanger and a heater before being fed into the Sabatier reactor. This preheating process increases the efficiency of the reaction by reducing the amount of energy required to bring the reactants up to reaction temperatures within the reactor. Once in the reaction chamber, the Sabatier reaction takes place, producing a mixture of predominantly water and methane gas that is then fed through a radiator to be cooled before being directed to a product tank. Here, the radiator makes use of the cold ambient Martian temperature to cool the reaction products. Within the buffer tank, a phase separator is then used condense and separate water from the product stream. The remaining gaseous mixture is then sent to a filter that separates methane from the product stream for future use. At this point, the remaining product gases are either vented, or recycled back into the Sabatier reactor. This second option would require an additional compressor system that is not depicted here. Moreover, if water is not a desired product of the ISRU Sabatier reactor, a water electrolyzer unit may be installed to generate hydrogen for reuse within the Sabatier reactor. Table F.14 summarizes the equations developed to size this system.

Table F.14: Summary of Sabatier Reactor Sizing Equations developed by Schrenk [144]:

Component	Sizing Equations (Mass (m), Power (P), Volume (V))	Comments / Variables
Reaction Chamber	Number of Reactor Units Needed: $N = \frac{R_{H2O}}{0.102}$ Chamber Mass and Volume: $m[kg] = N \times 1.75$ $V[m^3] = N \times 0.0088$	• The reactor is sized based on multiples of the Sabatier reactor design by Jaunedi et al. 2014 [353–355]). This design uses a Microlith substrate catalyst to facilitate even heat distribution throughout the chamber, thereby improving reaction efficiency. This reactor weighs 1.75kg, has a specific volume of 0.0088m^2, a CO_2 conversion efficiency of 90%, and a nominal water production rate of 0.102kg/h. Each reactor unit consists of the reactor, the reactor housing, a resistive heater, and a heat exchanger. • Variables: R_{H2O} = commanded H_2O production rate [kg/h];
Piping	Cross Sectional Area: $A[m^2] = N \times 0.0002025$ Radius: $r[m] = \sqrt{\frac{A}{\pi}}$ Mass: $m[kg] = 0.7\rho\left(\pi(r+0.0005)^2 - A\right) \times 1.1$	• The piping is assumed to be a 0.7m long. Its cross-sectional area is scaled according to the number of equivalent Microlith-based reactors required (see above). Each reactor has piping with a cross-sectional area of 20.25mm^2 • The piping is assumed to be made of steel with a wall thickness of 0.5mm • An additional 10% factor is added to the piping mass estimate to account for other flow componnets such as valves and connectors • Variables: ρ = piping material density, assumed to be steel at 7800kg/m^3
Buffer Tank / Phase Separator	Volume: $V[m^3] = \frac{2R_{H2O}}{1000}$ Radius: $r[m] = \left(\frac{3V}{4\pi}\right)^{1/3}$ Mass: $m[kg] = \rho\left(4\pi(r+0.001)^3/3 - V\right)$	• The buffer tank volume is assumed to be twice that of the commanded water production rate • The buffer tank is assumed to be constructed of aluminum, be spherical in shape, and have a wall thickness of 1mm • Variables: R_{H2O} = commanded H_2O production rate [kg/h]; ρ = material density (2700kg/m^3 for aluminum)

Upon comparing the estimates of the Sabatier reactor sizing equations developed here with the corresponding values of similar systems described within the literature, it was observed that on average the mass estimate was reasonable. Conversely, insufficient data was available to perform comparisons on the volume and power predictions. Table F.15 summarizes the results of this comparison.

Table F.15: Sabatier reactor model comparison

Source	Mass (kg per kg/h(H_2O))	Volume (m^3 per kg/h(H_2O))	Power (kW per kg/h(H_2O))
Rapp et al. 2005 [344]	17	-	0.163
HabNet ISRU Sabatier Reactor Sizing Equation [144]	17.9	0.0883	-
Comparison	**105.3 %**	**-**	**-**
Junaedi et al. 2014 [355]	340	-	0.75
HabNet ISRU Sabatier Reactor Sizing Equation [144]	17.9	0.0883	-
Comparison	**5.3 %**	**-**	**-**
Brooks et al. 2006 [352]	6.4	0.00088	-
HabNet ISRU Sabatier Reactor Sizing Equation [144]	17.9	0.0883	-
Comparison	**280 %**	**10000 %**	**-**

To ensure a conservative estimate for the system volume, Schrenk included a correction factor of 4 to the volume estimate for the Sabatier reactor, based on the general volume discrepancies observed with the other developed ISRU sizing models. With regards to the power estimate, the performance of the system proposed by Rapp et al. [344] was adopted. Table F.16 summarizes the final correction factors incorporated into the Sabatier reactor sizing equations:

Table F.16: Multiplicative factors derived for the ISRU Sabatier Reactor sizing equations

ISRU Sabatier Reactor Sizing Equation	Adjusted ISRU Sabatier Reactor Sizing Equation
Mass	1 × calculated mass
Volume	4 × calculated volume
Power	0.163 × commanded water production rate (based on Rapp et al. 2005 [344])

F.6 Reverse Water Gas Shift Reactor

The Reverse Water Gas Shift (RWGS) reaction was first studied for Mars ISRU applications in the late 1990s at Pioneer Astronautics as an alternative approach to the Sabatier/Electrolysis and SOCE processes for obtaining oxygen from Martian atmospheric CO_2. Since then, improved versions of the RWGS reactor have been developed and tested at NASA Kennedy

Space Center (KSC) [356], as well as Pacific Northwest National Laboratory (PNNL) [357]. As can be seen in the equation below, the RWGS reaction combines hydrogen gas with Mars atmospheric CO_2 over an alumina catalyst to generate water and carbon monoxide [356].

$$CO_2 + H_2 \rightleftharpoons CO + H_2O \tag{F.2}$$

Under expected Mars surface operating temperatures of 500°C, the reaction equilibrium of this reversible reaction is limited, resulting in a lower conversion of CO_2 to water than a typical Sabatier reactor [356]. Thus, in order to increase overall conversion, an intermediate separation step is typically implemented, whereby water and carbon monoxide are removed from the product stream and the remaining unreacted CO_2/H_2 is recycled back into the reactor to push the reaction further to the right.

Figure F-6 summarizes the RWGS reactor architecture assumed for the sizing model developed here. In addition to the RWGS reaction chamber, a heat exchanger and resistive heater are included to preheat the reactants before they enter the reactor to increase the reaction efficiency. Here, the reactor is lined with ten 1/8 inch diameter heating rods in order to control the equilibrium point of the reaction. After the RWGS reaction takes place, the resulting product mixture is directed to a phase separator, where water is condensed into the liquid phase and collected in a buffer water tank. The remaining $H_2/CO_2/CO$ mixture is then fed through a hollow fiber polymeric membrane filter to preferentially remove H_2 and CO_2 [356], which is then recycled back into the reactor. The remaining carbon monoxide is then vented from the system. Table F.17 summarizes the equations developed by Schrenk [144] to size this system.

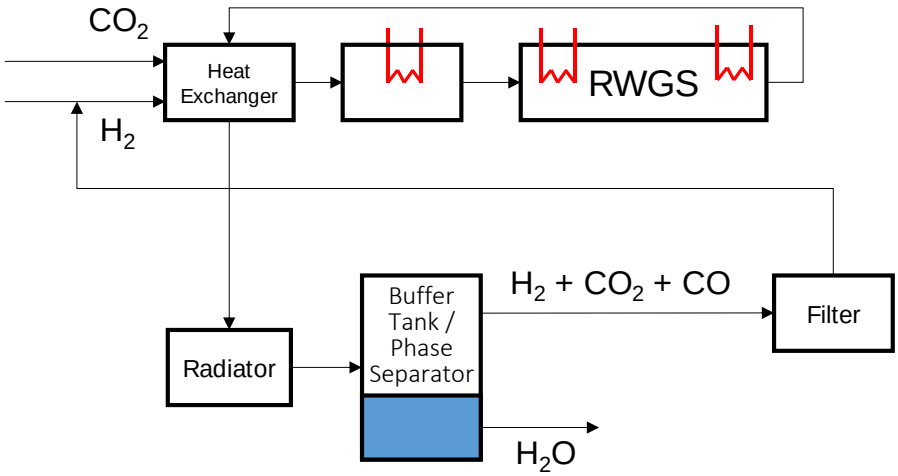

Figure F-6: Reverse water gas shift reactor modeling architecture

Table F.17: Summary of RWGS Reactor Sizing Equations developed by Schrenk [144]:

Component	Sizing Equations (Mass (m), Power (P), Volume (V))	Comments / Variables
Reaction Chamber	Number of Reactor Units Needed: $N = \frac{R_{H2O}}{0.1541}$ Chamber Mass, Volume, and Power: $m[kg] = N \times 0.05$ $V[m^3] = N \times 1.5 \times 10^{-5}$ $P[W] = \frac{R_{H2O} \times 41000}{3600 \times \eta}$ Heating Rod Mass: $m_h[kg] = N \times 10 \times A_h \times L_h \times \rho_h$	• As was the case with the Sabatier reactor, the RWGS reactor is sized based on multiples of an existing reactor design. Here, the reactor developed at PNNL [357] has been adopted. This miniaturized reactor has a mass of 50g, a volume of 15cm^3, a CO_2 conversion efficiency of 57.95% a peak water production rate of 154.1 g/h, and an energy requirement of 41kJ per moles of reacted CO_2 • Variables: R_{H2O} = commanded H_2O production rate [kg/h]; η = heater efficiency, assumed to be 80%; A_h = heating rod cross-sectional area (1/8 inch diameter); L_h = heating rod length, derived from the longest dimension of the reactor volume; ρ_h = heating rod material density, assumed to be Fe/Cr/Al alloy at 7200kg/m^3 [358]
Piping and Heat Exchanger	$m_p[kg] = N \times L_p \times \left(2 r_p t_p + t_p^2\right)\pi \times \rho_p$ $V_p[m^3] = N \times L_p \times r_p^2 \pi$	• The length of the piping is assumed to be 12 times the length of the reaction chamber heating rods, based on a visual analysis of the PNNL design [357] • Variables: N = number of equivalent PNNL RWGS reactors required; L_p = length of feed and product pipe [m]; r_p = feed and product pipe inner radius, assumed to be 2mm; t_p = feed and product pipe wall thickness, assumed to be 0.5mm; ρ = piping material density, assumed to be steel at 7800kg/m^3
Buffer Tank / Phase Separator	$V[m^3] = 2\frac{R_{H2O}}{1000}$ $m[kg] = \left(\frac{4}{3}\pi\left(r_c + t_c\right)^3 - V\right) \times \rho$	• The condenser/buffer tank is assumed to be passively cooled by the ambient Martian environment, to have a capacity equivalent to twice the hourly water production rate, and to be spherical in shape • Variables: R_{H2O} = commanded H_2O production rate [kg/h]; r_c = buffer tank inner radius [m], determined from estimated volume; t_c = buffer tank wall thickness, assumed to be 0.5mm; ρ = buffer tank material density, assumed to be aluminum at 2700kg/m^3

A comparison between the sizing estimates predicted by the equations summarized in Table F.17 with the corresponding values recorded in the literature revealed that while the volume estimates are within the correct order of magnitude, the power and the mass requirements are significantly underestimated. This is likely due to the fact that the PNNL RWGS reactor was optimized for a Mars sample return mission while the other concepts discussed in the literature are intended for larger scale production. Moreover, the low production requirements of the PNNL reactor design mean that it does not include H_2/CO_2 recycling, which results in it having a lower mass and power demand than the alternative concepts reviewed in this model comparison. Table F.18 summarizes the results of this model comparison, while Table F.19 summarizes the corrective factors derived by Schrenk [144] to compensate for the observed discrepancies in the sizing estimates.

Table F.18: RWGS model comparison

Source	**Mass (kg per kg/h(H_2O))**	**Volume (m^3 per kg/h(H_2O))**	**Power (kW per kg/h(H_2O))**
Rapp et al. 2005 [344]	66.2	-	2.77
HabNet RWGS Reactor Sizing Equations [144]	1.22	0.0022	0.8
Comparison	**1.8 %**	**-**	**28.9 %**
Brooks et al. 2006 [352]	18.8	0.0014	1.83
HabNet RWGS Reactor Sizing Equations [144]	1.22	0.0022	0.8
Comparison	**6.5 %**	**157 %**	**43.7 %**

Table F.19: HabNet RWGS Sizing Equations with Correction Factors

ISRU RWGS Reactor Sizing Equation	**Adjusted ISRU RWGS Reactor Sizing Equation**
Mass	35 × calculated mass* (based on a mean value between the discrepancies observed in Table F.18)
Volume	1 × calculated volume
Power	3 × calculated power

*Schrenk [144] recommends that this correction factor be reverted back to a value of 1 if a H_2/CO_2 recycling system is not included in the RWGS system design

Appendix G

BioSim Validation Results

This appendix catalogs the results obtained from the HabNet Habitation Module validation analysis performed in Section 4.1. Here, HabNet's dynamic simulation capability was compared against results generated by BioSim under the same simulation initial and boundary conditions. As was mentioned in Section 4.1, BioSim is a mid-fidelity ECLS simulation engine that was developed under a contract with NASA Johnson Space Center in order to evaluate different ECLS control strategies on system wide behavior.

In this appendix, comparative results are over-plotted on the same figure when only one simulation output variable is being compared. Otherwise, when multiple simulation output variables are being simultaneously compared, the BioSim result is plotted on the left, and the MATLAB result is plotted on the right.

G.1 Simulation Case 1 – Open Loop ECLS

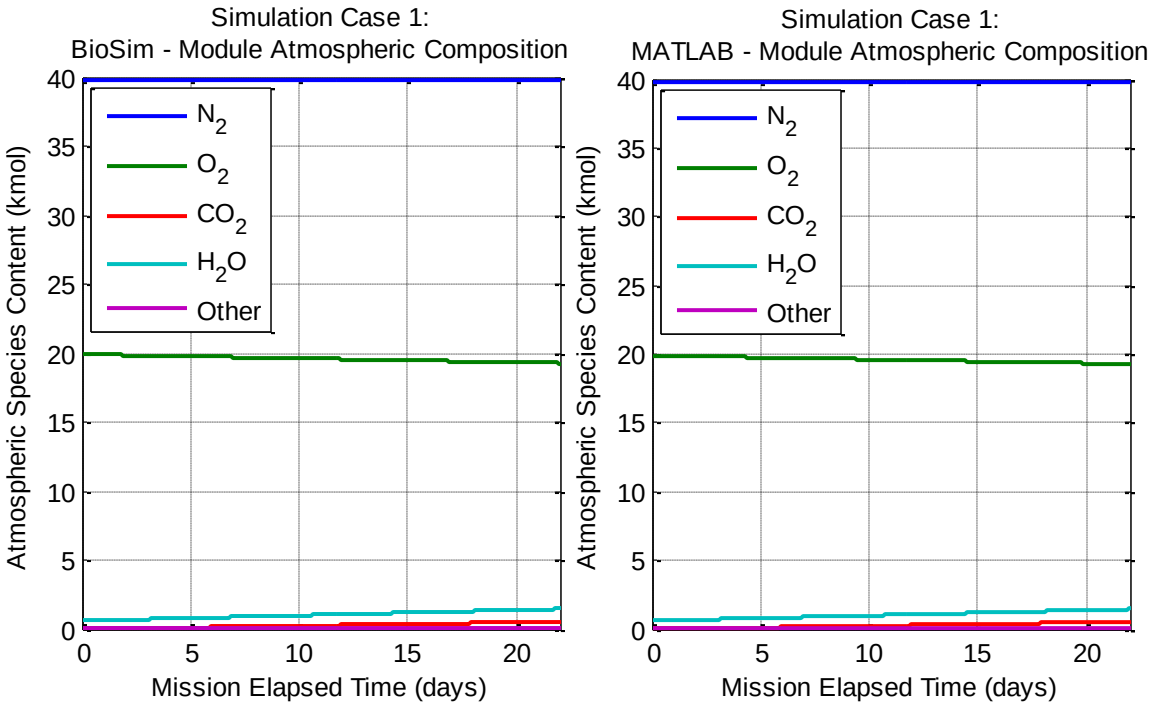

Figure G-1: Comparison of Atmospheric Composition for Simulation Case 1

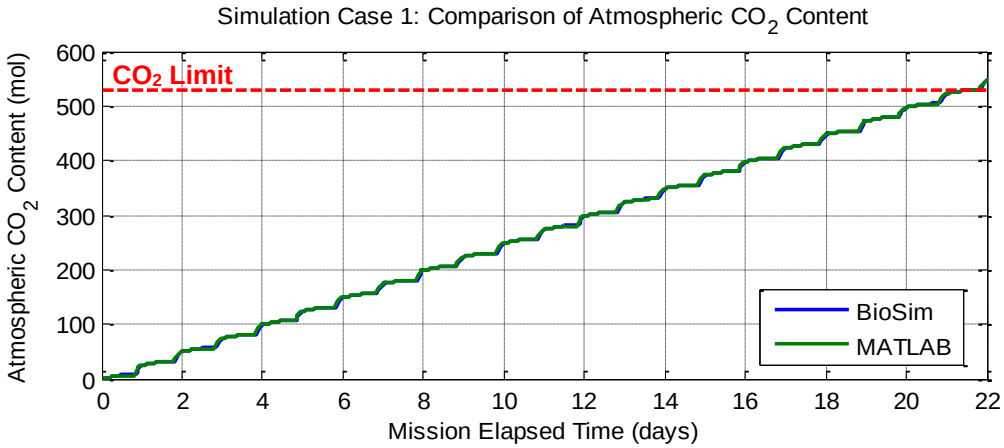

Figure G-2: Comparison of Atmospheric CO_2 for Simulation Case 1

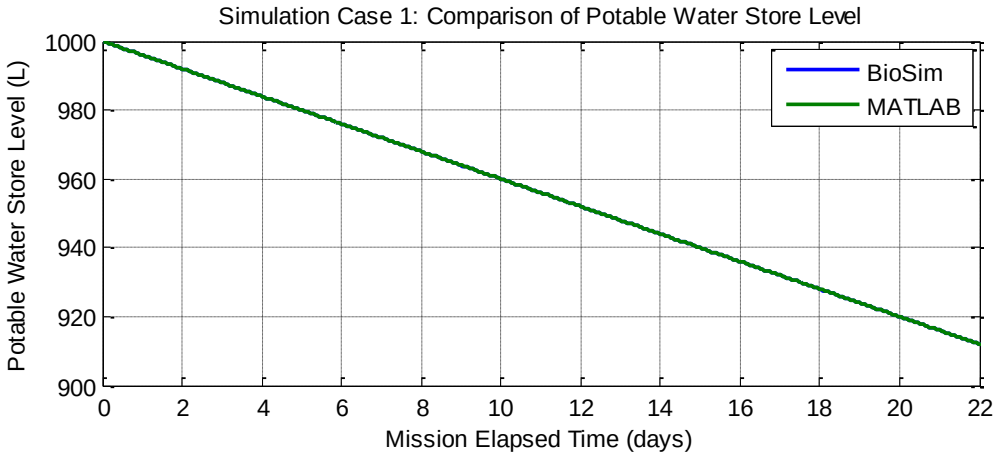

Figure G-3: Comparison of Potable Water Store Level for Simulation Case 1

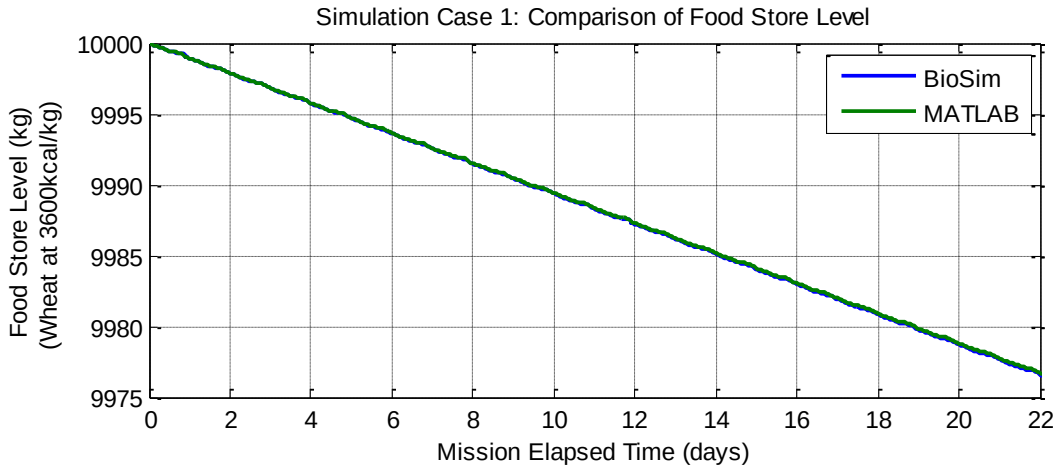

Figure G-4: Comparison of Food Store Level for Simulation Case 1

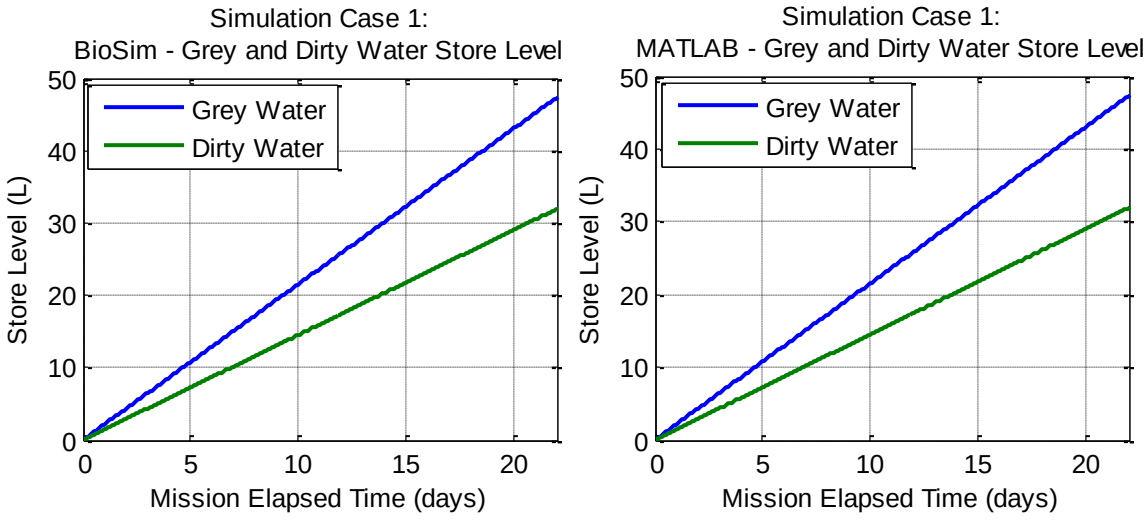

Figure G-5: Comparison of Grey and Dirty Water Store Levels for Simulation Case 1

G.2 Simulation Case 2 – Open Loop ECLS with CO_2 Removal Assembly

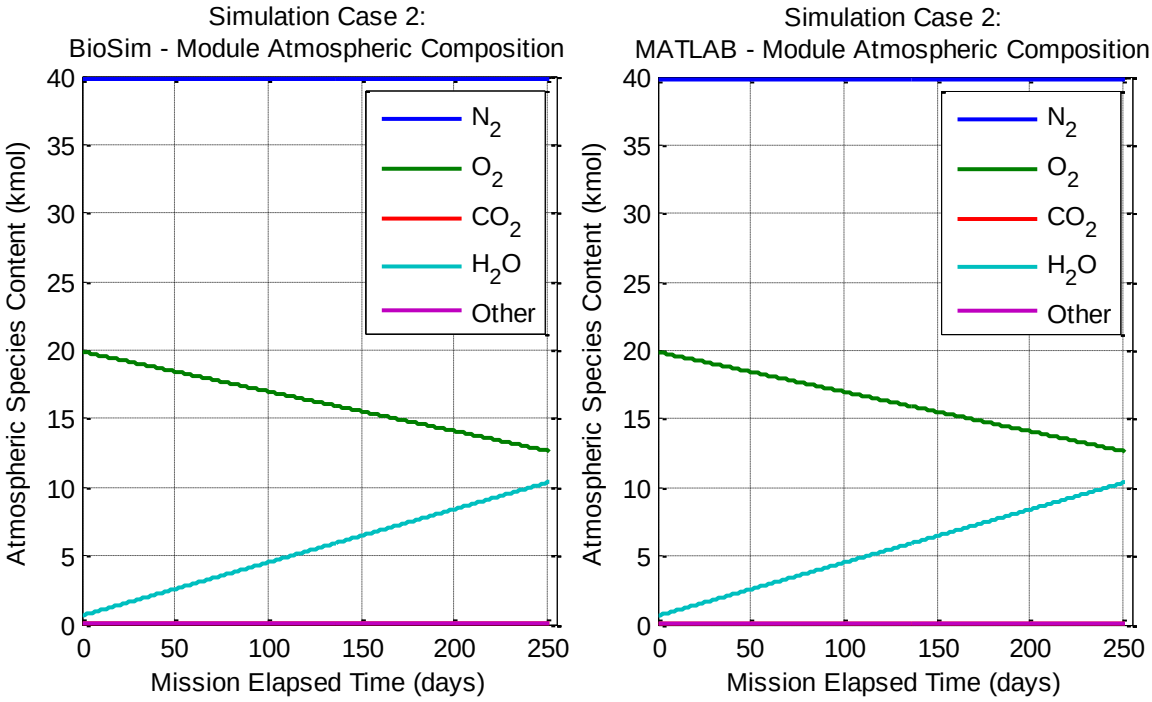

Figure G-6: Comparison of Atmospheric Composition for Simulation Case 2

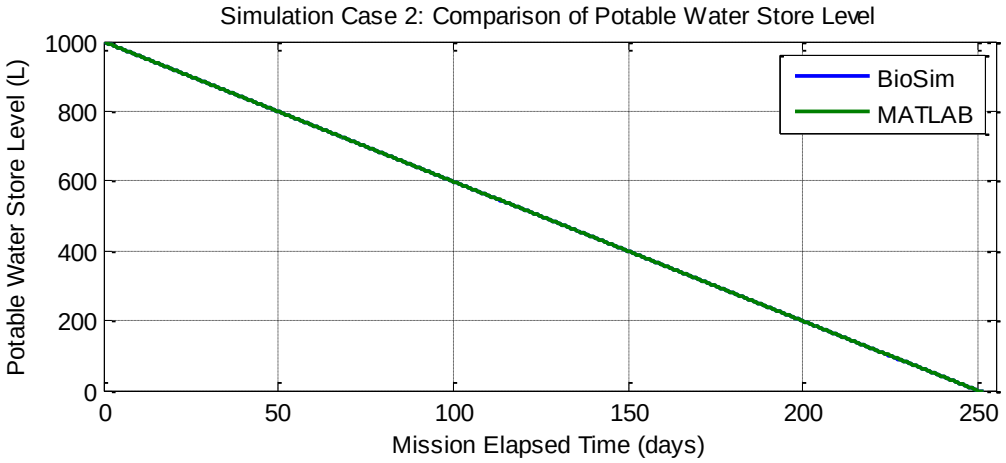

Figure G-7: Comparison of Potable Water Store Level for Simulation Case 2

Figure G-8: Comparison of Food Store Level for Simulation Case 2

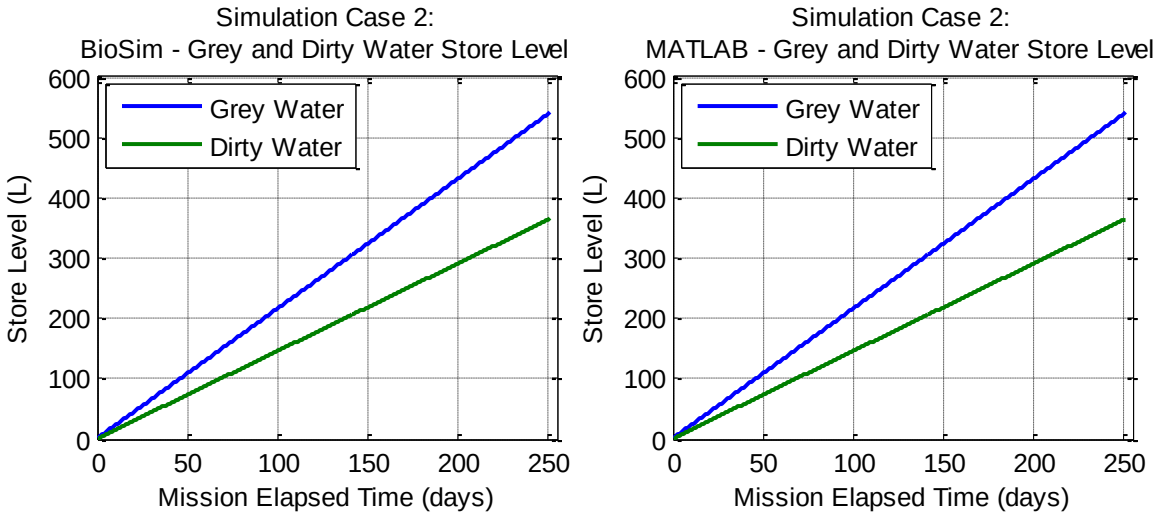

Figure G-9: Comparison of Grey and Dirty Water Store Levels for Simulation Case 2

G.3 Simulation Case 3 – Semi-Closed Water Loop with an Integrated Water Recovery System and a CO_2 Removal Assembly

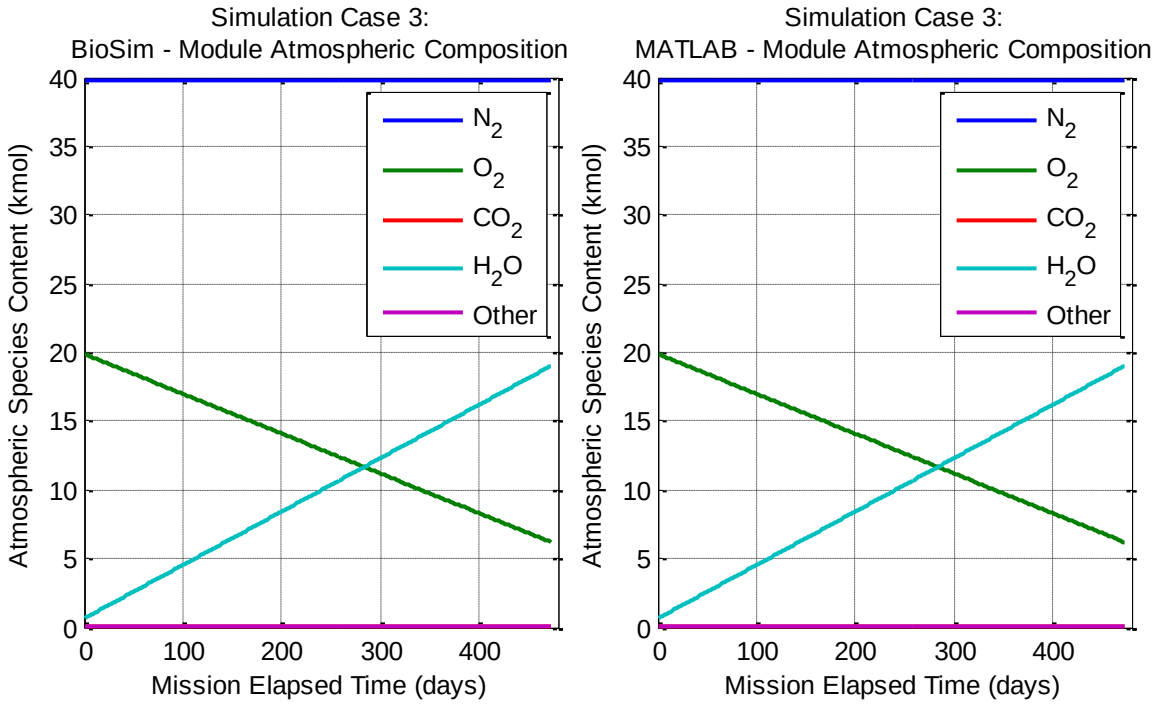

Figure G-10: Comparison of Atmospheric Composition for Simulation Case 3

The increase in water vapor content within the atmosphere arises from the fact that no condensing heat exchanger is incorporated within this habitation scenario, and thus no water vapor is removed from the habitat atmosphere.

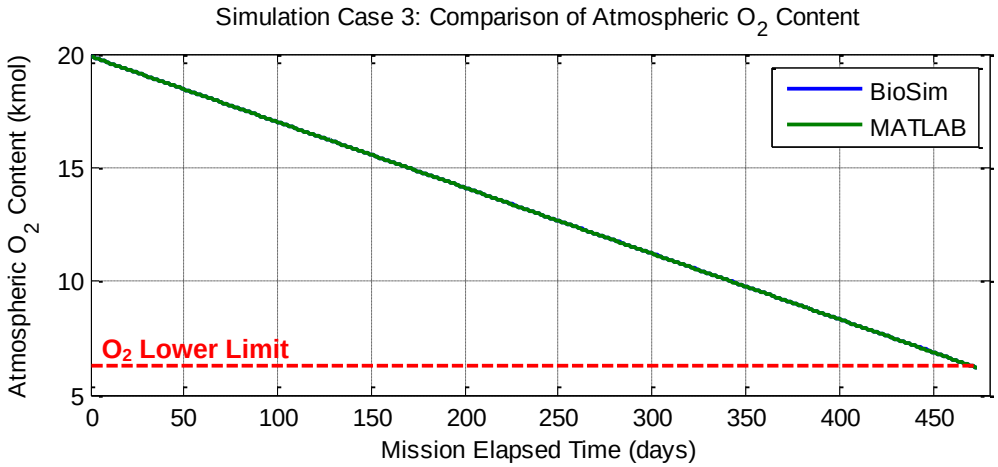

Figure G-11: Comparison of Atmospheric Oxygen Content for Simulation Case 3

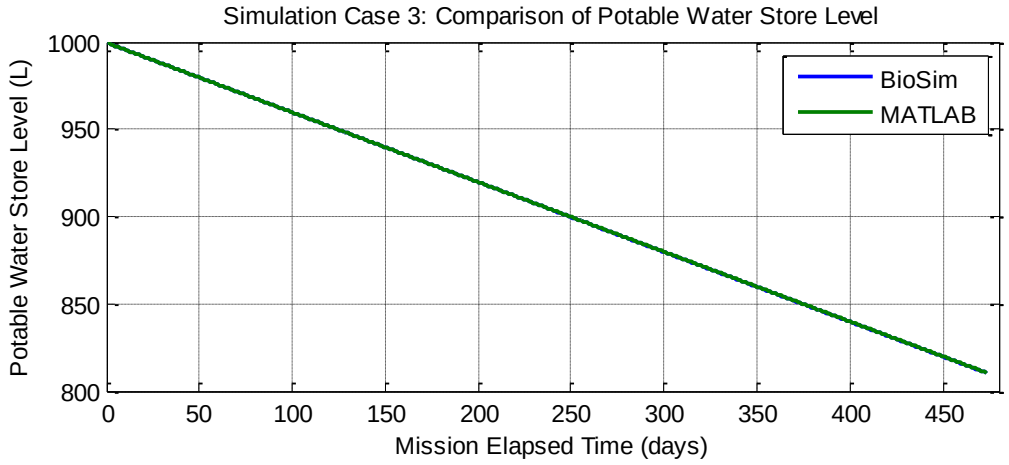

Figure G-12: Comparison of Potable Water Store Level for Simulation Case 3

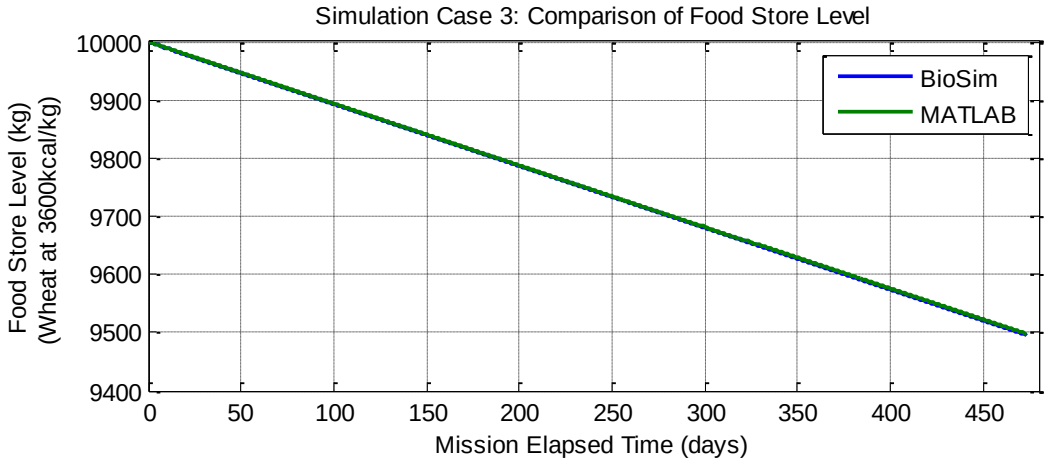

Figure G-13: Comparison of Food Store Level for Simulation Case 3

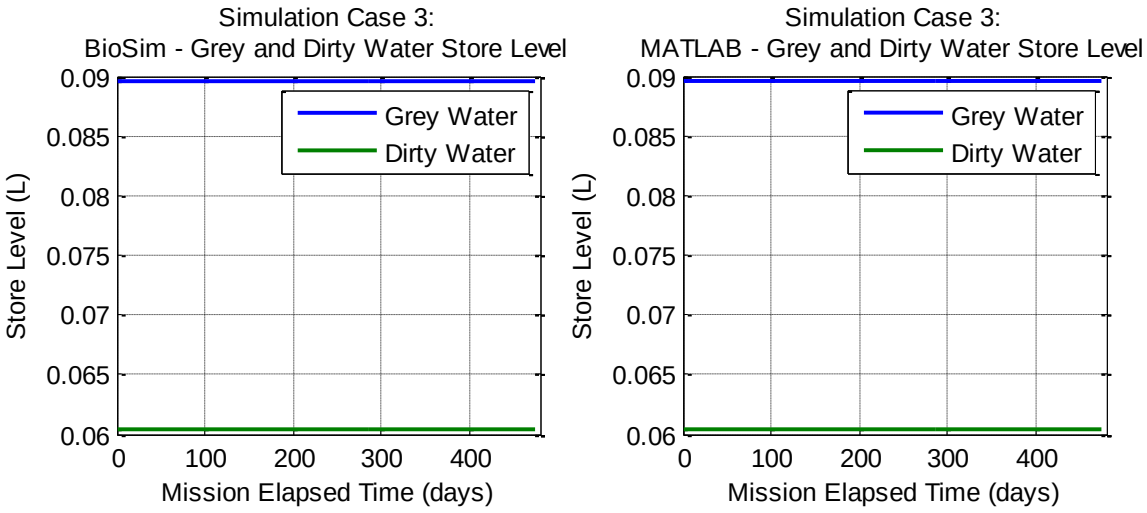

Figure G-14: Comparison of Grey and Dirty Water Store Levels for Simulation Case 3

Grey and dirty water stores reach a steady state as their contents are directed to the water recovery system for processing back into potable water for crew consumption.

G.4 Simulation Case 4 – Semi-Closed Water Loop with an Integrated Water Recovery System, CO_2 Removal Assembly, and Oxygen Generation Assembly

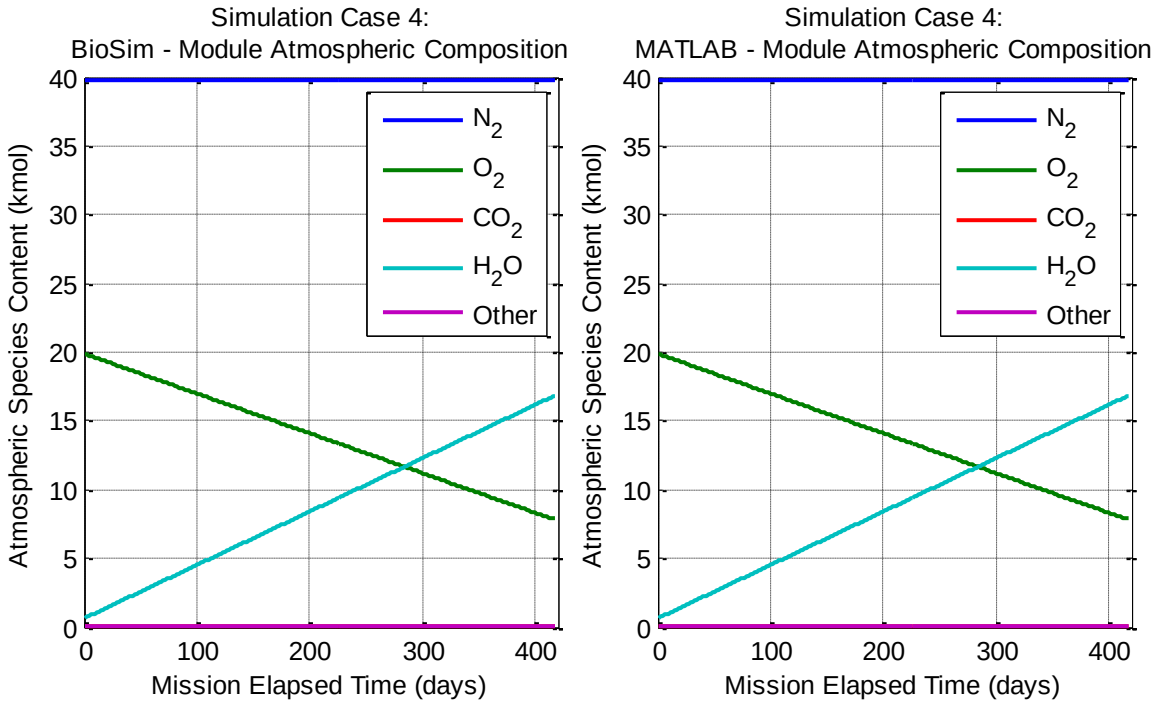

Figure G-15: Comparison of Atmospheric Composition for Simulation Case 4

As was the case with Simulation Case 3, the increase in water vapor content within the atmosphere arises from the fact that no condensing heat exchanger is incorporated within this habitation scenario, and thus no water vapor is removed from the habitat atmosphere.

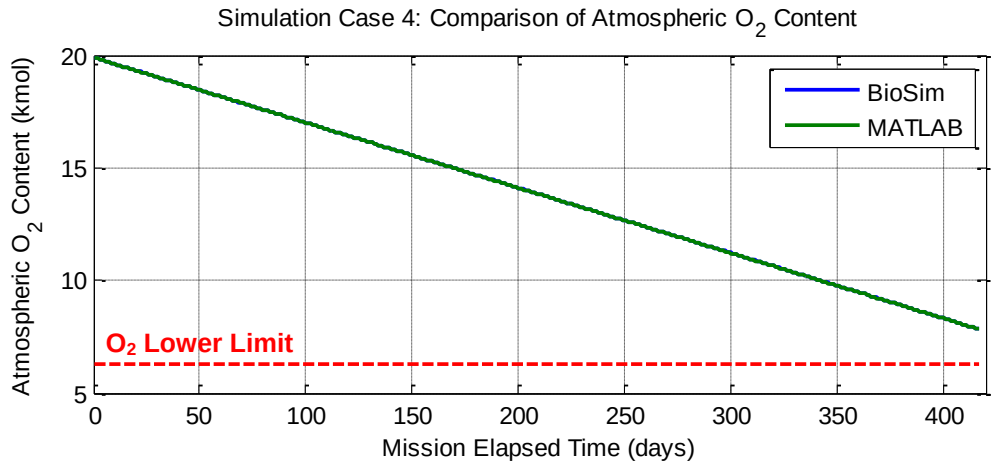

Figure G-16: Comparison of Atmospheric Oxygen Content for Simulation Case 4

The inclusion of an OGA has reduced the rate at which oxygen is consumed relative to Simulation Case 3.

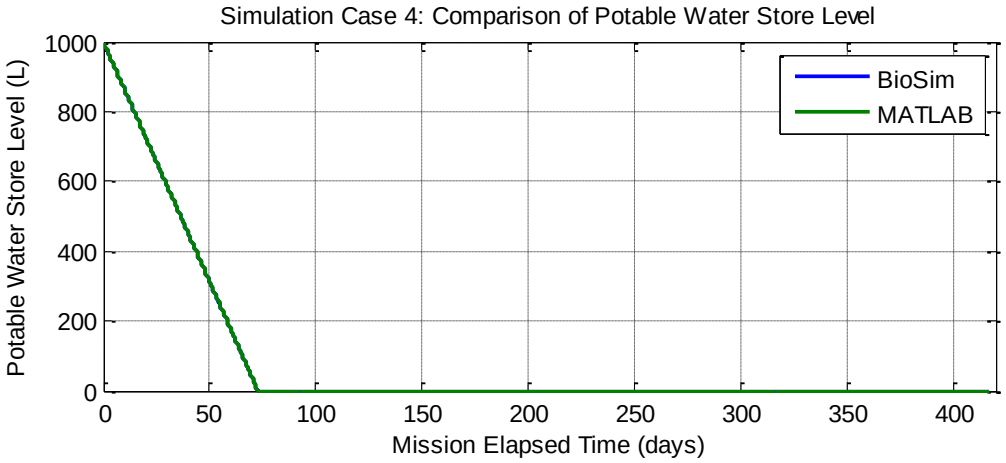

Figure G-17: Comparison of Potable Water Store Level for Simulation Case 4

The potable water store is emptied on mission day 72 due to the additional consumption of potable water by the OGA. Even though this store is empty after day 72, the crewmember manages to survive until the end of the mission due to the WRS producing potable water at a rate that is sufficient to sustain the crewmember.

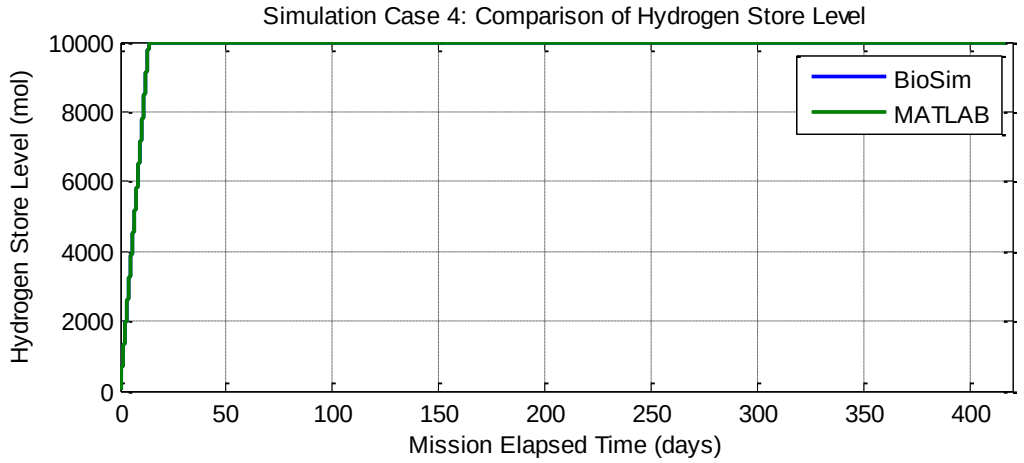

Figure G-18: Comparison of Hydrogen Store Level for Simulation Case 4

Hydrogen store becomes saturated with hydrogen gas product from the OGA at mission day 13, causing the store to overflow.

G.5 Simulation Case 5 – Mostly Closed Oxygen and Semi-Closed Water Loop ECLS Architecture

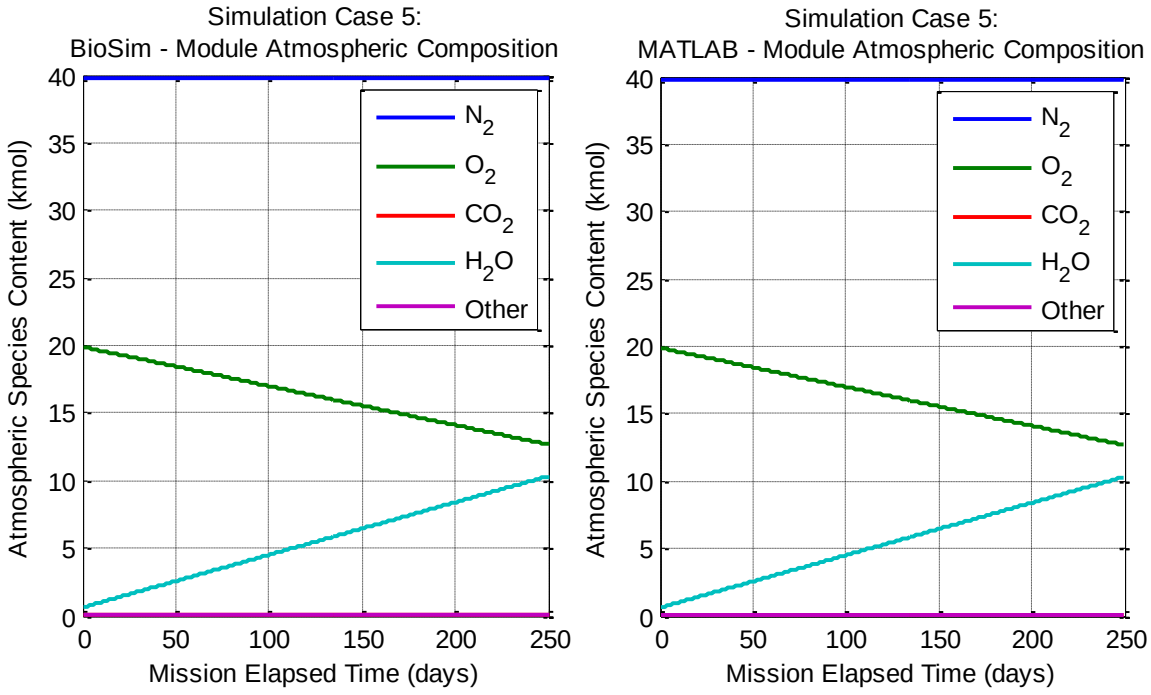

Figure G-19: Comparison of Atmospheric Composition for Simulation Case 5

As was the case with Simulation Cases 3 and 4, the increase in water vapor content within the atmosphere arises from the fact that no condensing heat exchanger is incorporated within this habitation scenario, and thus no water vapor is removed from the habitat atmosphere.

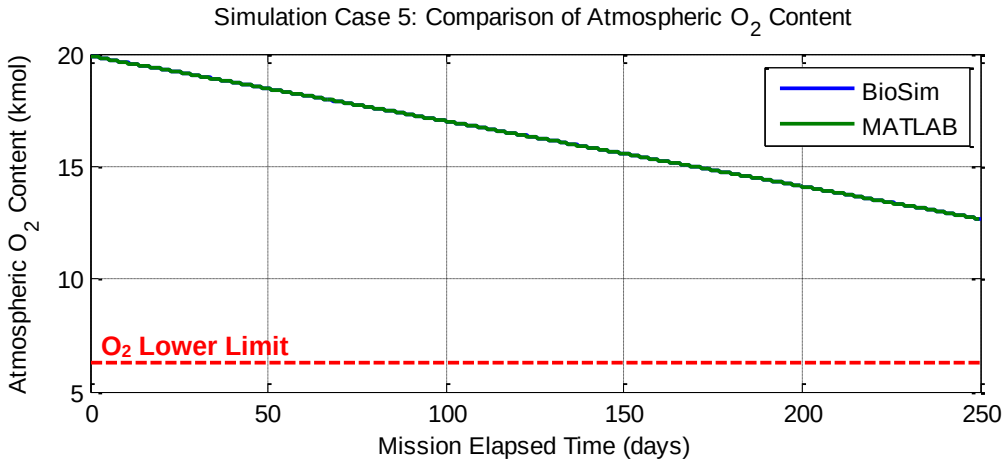

Figure G-20: Comparison of Atmospheric Oxygen Content for Simulation Case 5

The inclusion of a CRS has reduced the rate at which oxygen is consumed relative to Simulation Case 3.

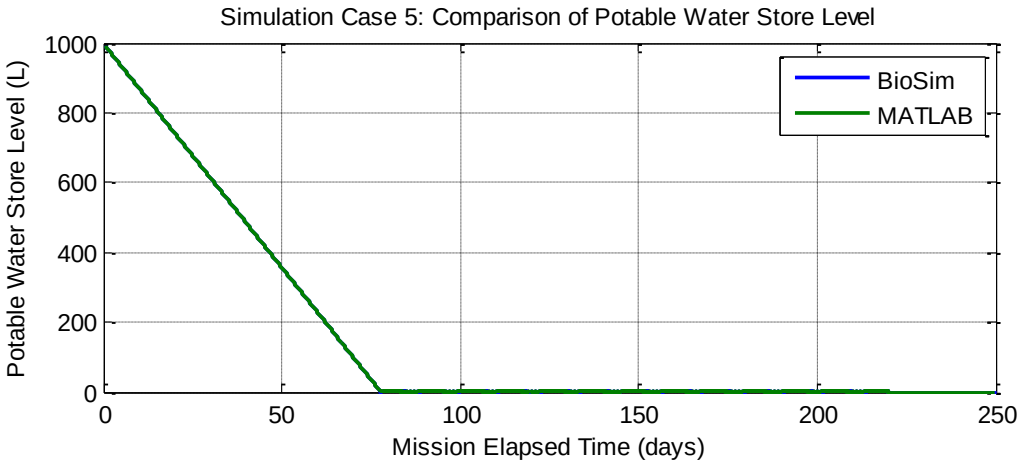

Figure G-21: Comparison of Potable Water Store Level for Simulation Case 5

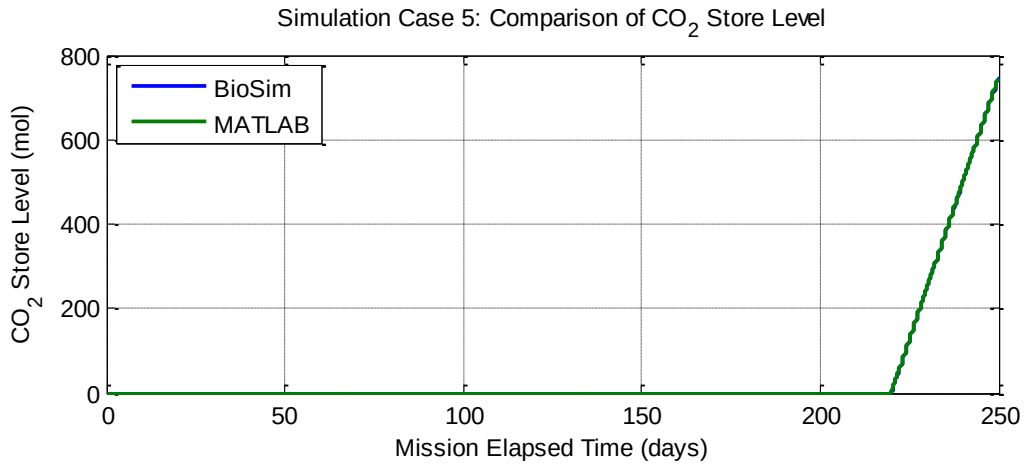

Figure G-22: Comparison of CO_2 Store Level for Simulation Case 5

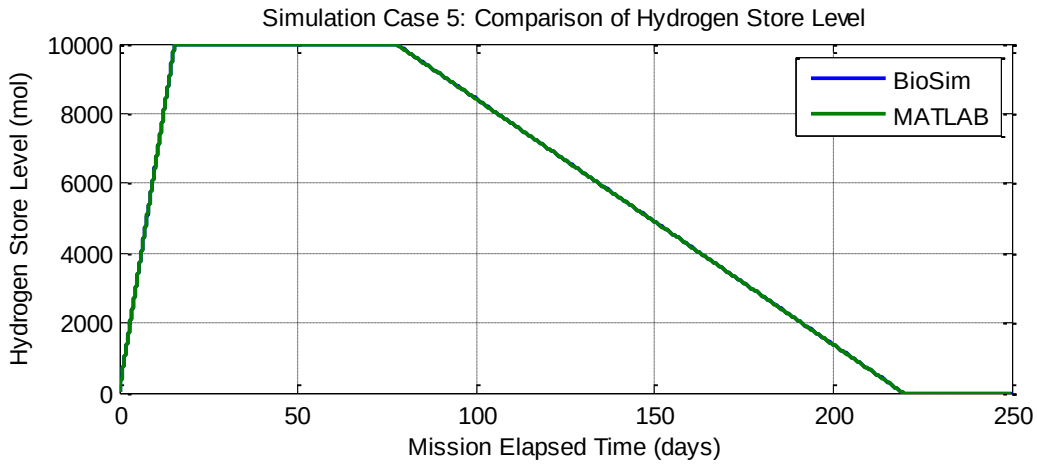

Figure G-23: Comparison of Hydrogen Store Level for Simulation Case 5

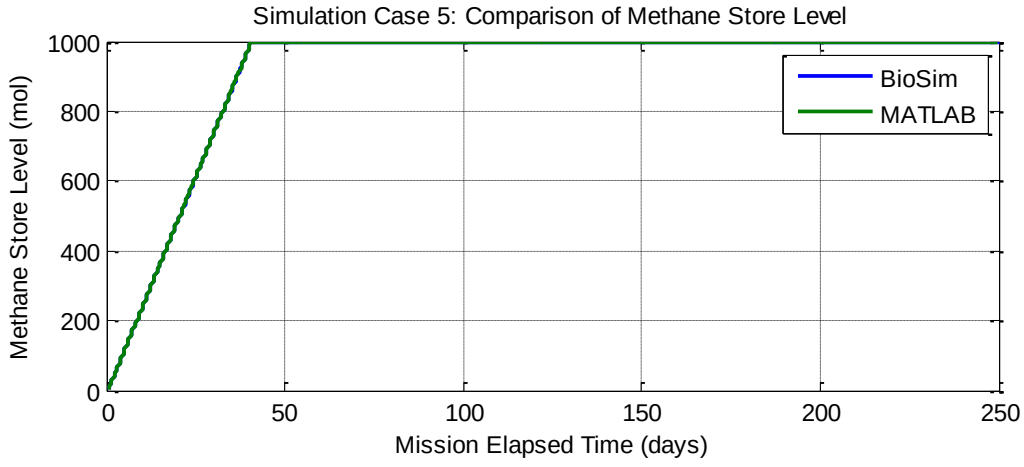

Figure G-24: Comparison of Methane Store Level for Simulation Case 5

G.6 Simulation Case 6 – Mostly Closed Oxygen and Water Loop ECLS Architecture

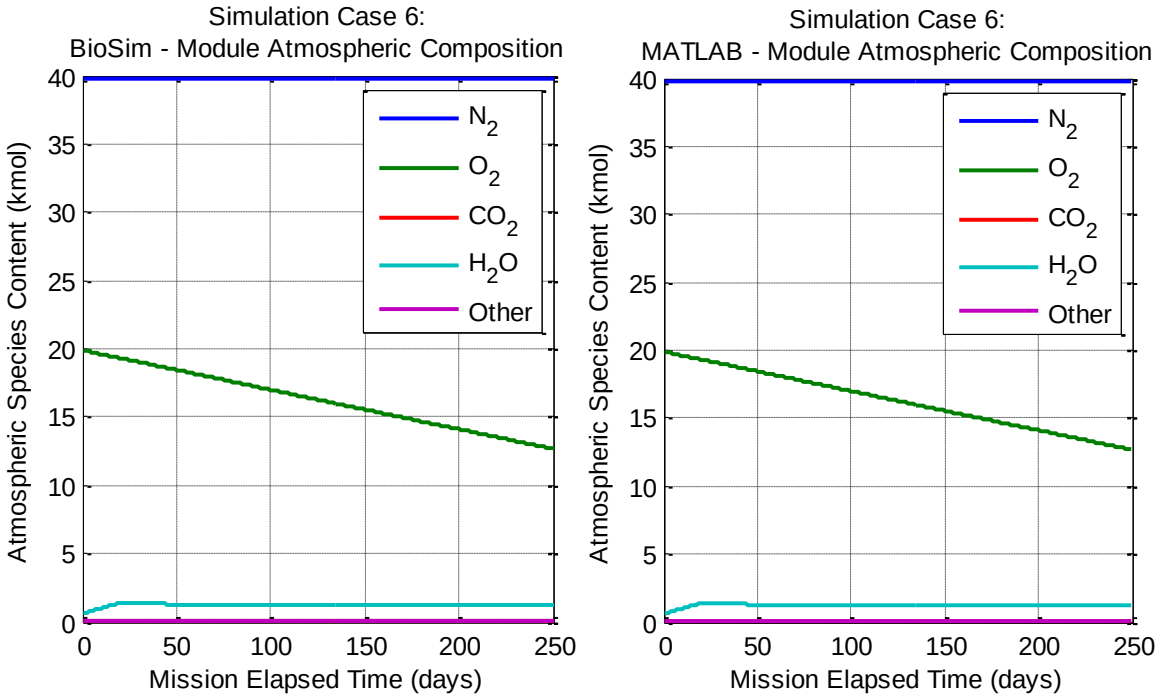

Figure G-25: Comparison of Atmospheric Composition for Simulation Case 6

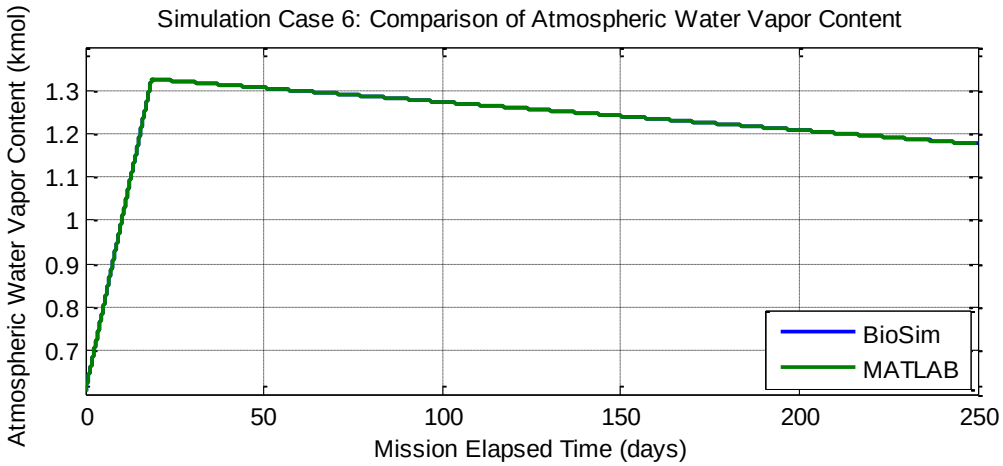

Figure G-26: Comparison of Atmospheric Water Vapor Content for Simulation Case 6

In the above figure, the decline in atmospheric vapor content occurs after the atmospheric water vapor reaches a predefined limit, when the condensing heat exchanger is switched on to remove water vapor from the atmosphere.

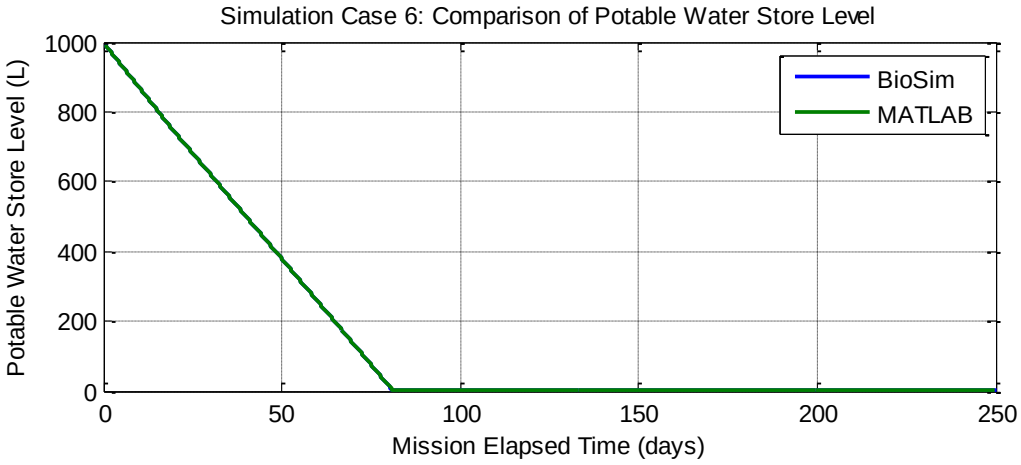

Figure G-27: Comparison of Potable Water Store Level for Simulation Case 6

G.7 Simulation Case 7 – Default Biosim Architecture – Four Crewmembers in a Four-Module Habitat

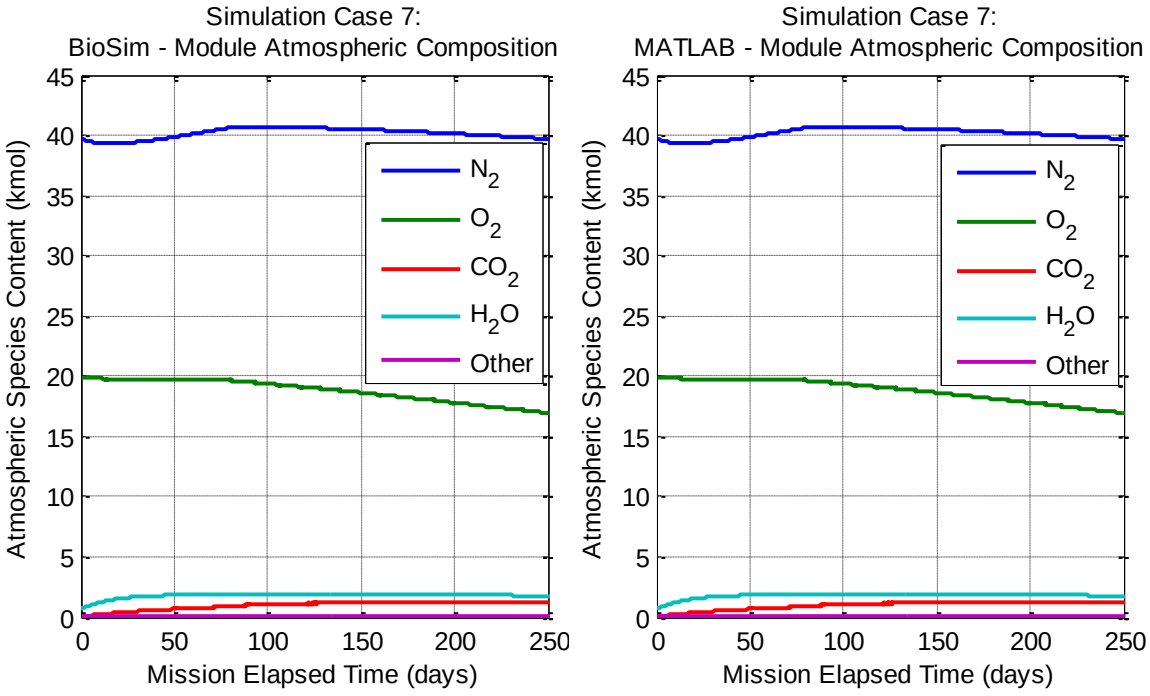

Figure G-28: Comparison of Atmospheric Composition for Simulation Case 7

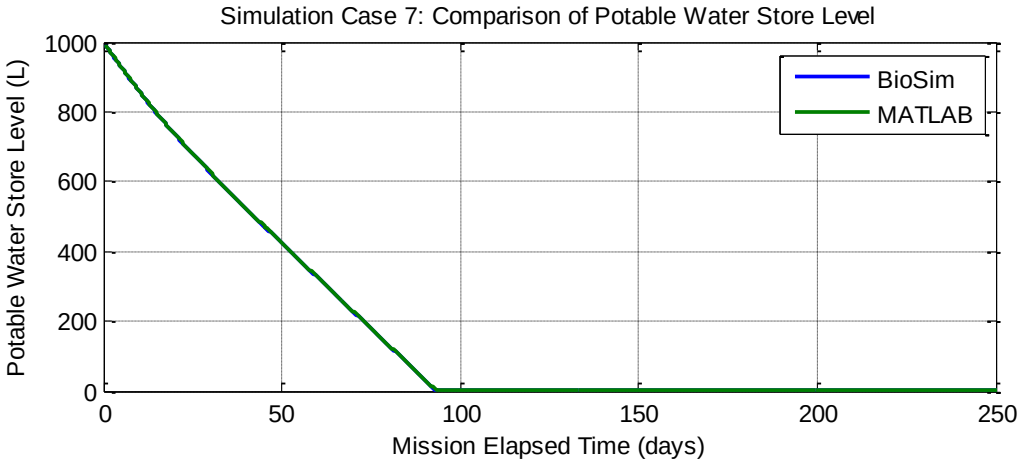

Figure G-29: Comparison of Potable Water Store Level for Simulation Case 7

Figure G-30: Comparison of Food Store Level for Simulation Case 7

Appendix H

Deep Space Habitat Validation Case Study Assumptions and Results

This appendix summarizes the data and assumptions used in the Deep Space Habitat validation case study performed in Section 4.4. In addition, the complete set of spare parts results obtained from this analysis is also presented. These are described in the following subsections.

H.1 ECLS Architecture Case Flowsheets

Cataloged below are flowsheets of the five ECLS architecture cases explored in this case study.

H.1.1 Architecture Case 1

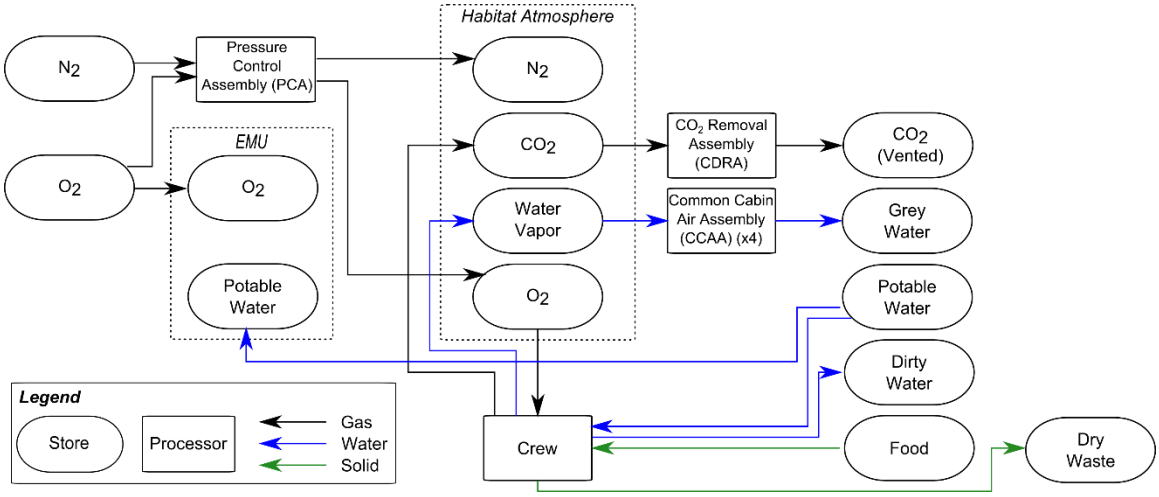

Figure H-1: ECLS Architecture Case 1, consisting of a completely open loop oxygen and water supply

H.1.2 Architecture Case 2

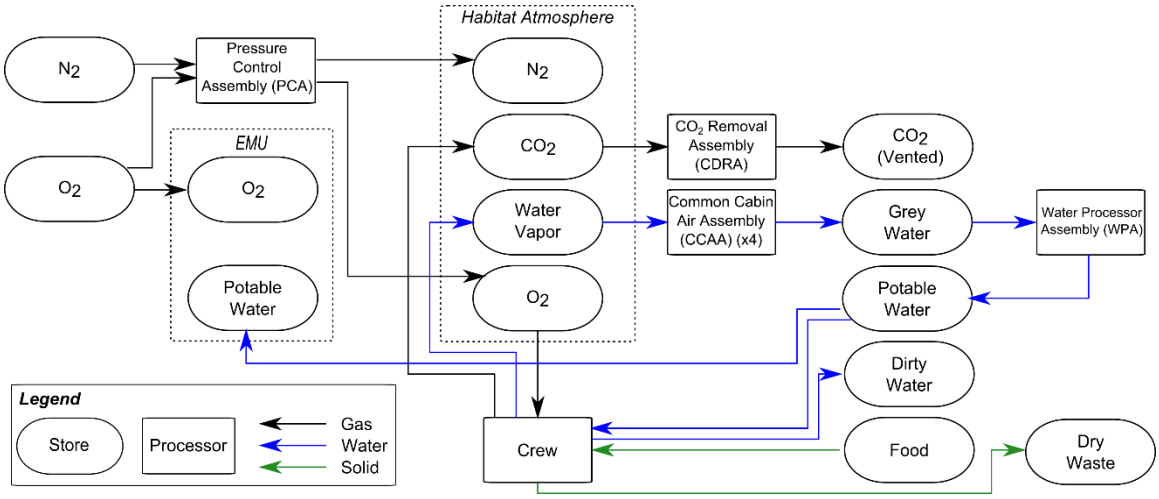

Figure H-2: ECLS Architecture Case 2, consisting of a CDRA, CCAA, and WPA. Here, all crew-expired CO_2 is vented and all dirty water is either stored in dirty water tanks or vented overboard.

H.1.3 Architecture Case 3

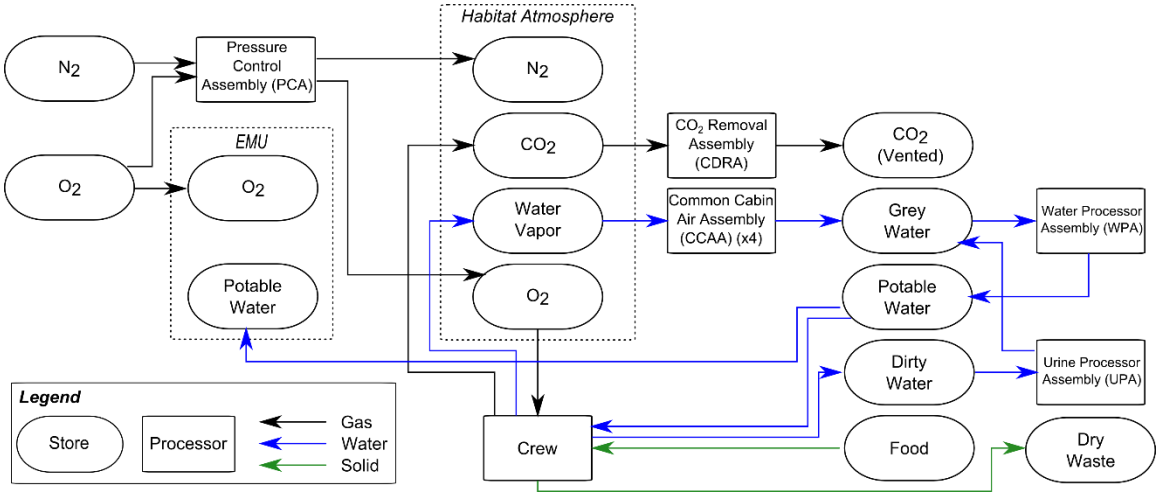

Figure H-3: ECLS Architecture Case 3, consisting of a CDRA, CCAA, WPA, and UPA. Here all crew expired CO_2 is vented. Thus the architecture consists of an open-loop oxygen supply.

H.1.4 Architecture Case 4

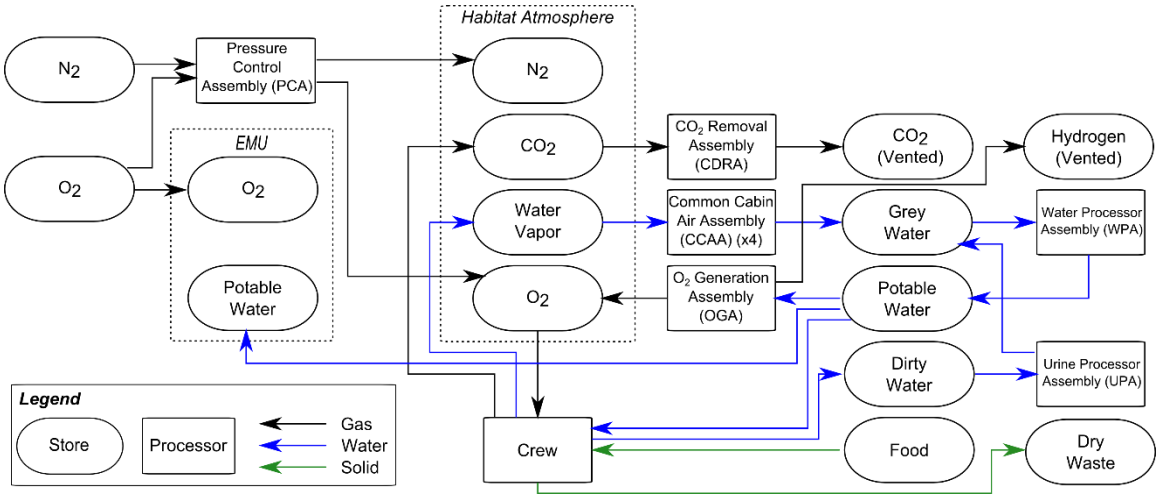

Figure H-4: ECLS Architecture Case 4, consisting of a CDRA, CCAA, WPA, UPA, and OGA

H.1.5 Architecture Case 5

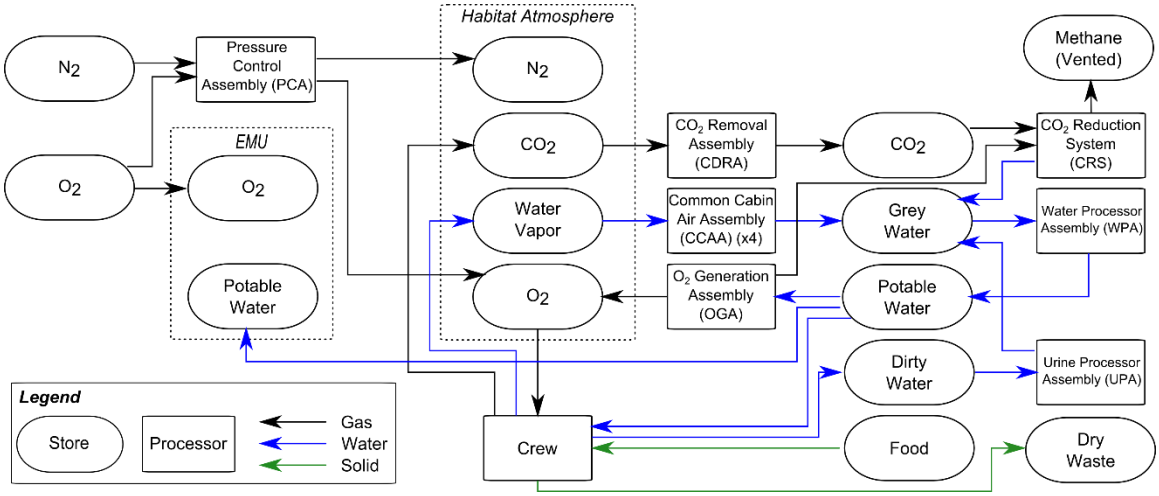

Figure H-5: ECLS Architecture Case 5, based on the ISS ECLS Architecture

H.2 Master Equipment Lists and Component Data for each ECLS Architecture Case

Cataloged below are the complete master equipment lists (MELs) derived for each of the five ECLS architecture cases explored in this case study. For each MEL, the mass, volume, meantime between failures (MTBF), and life limit (LL) of each element is listed. Unless

otherwise noted, values are from the NASA Baseline Values and Assumptions Document (BVAD) [209]. Assumptions and use of analogy to other components for data are indicated and described with endnotes. In addition, spare parts requirements predicted by the HabNet Supportability Module are listed. For this case study, these are calculated such that the probability of having sufficient spare parts is 0.999.

H.2.1 Architecture Case 1 Master Equipment List

Assembly	Subassembly	Mass [kg]	Vol. [m^3]	MTBF [h]	Run Time [h]	LL [y]	# in Pmry.	# of Spares
CDRA	Air Pump Two-Stage ORU	10.89	0.0045	156200.0	8760	15.29	1	1
	Blower	5.58	0.0300	129700.0	8760	10.00	1	1
	Check Valves	39.92	0.1784	32900.0[i]	8760		1	2
	Desiccant Beds	42.64	0.0850	77100.0	8760		2	2
	Heat Controller	3.31	0.0085	242700.0	8760		2	2
	Precooler	5.58	0.0255	129700.0	8760	10.00	1	2
	Pump Fan Motor Controller	2.72	0.0057	2270000.0	8760		2	1
	Selector Valves	3.04	0.0017	117000.0	8760	10.61	6	4
	Sorbent Beds (Zeolite)	42.64	0.0850	77100.0	8760	2.28	2	2
CCAA	Condensing Heat Exchanger	49.71	0.3933	832600.0	8760		1	1
	Electronic Interface Box (EIB)	4.04	0.0173	2350000.0	8760		2	1
	Fan Delta Pressure Sensor	0.45	0.0002	1250000.0	8760		1	1
	Heat Exchanger Liquid Sensor	0.64	0.0006	1140000.0	8760		2	2
	Inlet ORU	25.31	0.1308	333000.0	8760		1	1
	Pressure Transducer	0.48	0.0000	1250000.0	8760	15.00	1	1
	Temperature Control Check Valve (TCCV)	7.45	0.0071	32900.0	8760		2	3
	Temperature Sensor	0.26	0.0014	37600000.0	8760		4	1
	Water Separator	11.93	0.0583	131000.0	1750	5.00	2	2
	Water Separator Liquid Sensor	0.64	0.0006	1140000.0[ii]	1750		2	1

[i] Analogy to CCAA TCCV
[ii] Analogy to CCAA Heat Exchanger Liquid Sensor

H.2.2 Architecture Case 2 Master Equipment List

Assembly	Subassembly	Mass [kg]	Vol. [m^3]	MTBF [h]	Run Time [h]	LL [y]	# in Pmry.	# of Spares
CDRA	Air Pump Two-Stage ORU	10.89	0.0045	156200.0	8760	15.29	1	2
	Blower	5.58	0.0300	129700.0	8760	10.00	1	2
	Check Valves	39.92	0.1784	32900.0[i]	8760		1	2
	Desiccant Beds	42.64	0.0850	77100.0	8760		2	2
	Heat Controller	3.31	0.0085	242700.0	8760		2	2
	Precooler	5.58	0.0255	129700.0	8760	10.00	1	2
	Pump Fan Motor Controller	2.72	0.0057	2270000.0	8760		2	1
	Selector Valves	3.04	0.0017	117000.0	8760	10.61	6	4
	Sorbent Beds (Zeolite)	42.64	0.0850	77100.0	8760	2.28	2	2
CCAA	Condensing Heat Exchanger	49.71	0.3933	832600.0	8760		1	1
	Electronic Interface Box (EIB)	4.04	0.0173	2350000.0	8760		2	1
	Fan Delta Pressure Sensor	0.45	0.0002	1250000.0	8760		1	1
	Heat Exchanger Liquid Sensor	0.64	0.0006	1140000.0	8760		2	1
	Inlet ORU	25.31	0.1308	333000.0	8760		1	1
	Pressure Transducer	0.48	0.0000	1250000.0	8760	15.00	1	1
	Temperature Control Check Valve (TCCV)	7.45	0.0071	32900.0	8760		2	4
	Temperature Sensor	0.26	0.0014	37600000.0	8760		4	1
	Water Separator	11.93	0.0583	131000.0	1750	5.00	2	2
	Water Separator Liquid Sensor	0.64	0.0006	1140000.0[ii]	1750		2	1
WPA	Catalytic Reactor	67.04	0.1156	25579.2	648	2.25	1	1
	Gas Separator	39.15	0.0660	84008.4	648	1.00	1	1
	Ion Exchange Bed	13.02	0.0173	296701.2	648	0.16	1	1
	Microbial Check Valve	5.76	0.0065	143488.8	648	1.00	1	1
	Multifiltration Bed #1	149.23	0.0657	296701.2	648	0.36	1	0
	Multifiltration Bed #2	149.23	0.0657	296701.2	648	0.36	1	0
	Particulate Filter	32.25	0.0717	717356.4	648	0.22	1	1
	pH Adjuster	2.54	0.0026	137181.6	648	1.00	1	1
	Process Controller	45.00	0.0838	87950.4	648	7.72	1	1
	Pump Separator	31.34	0.0869	42398.4	648	2.00	1	1
	Reactor Health Sensor	16.83	0.0425	56677.2	648	1.00	1	1
	Sensor	4.81	0.0034	143664.0	648	10.00	1	1
	Separator Filter	7.67	0.0102	359072.4	648	0.84	1	1
	Start-up Filter	9.44	0.0184	226884.0	648	19.92	1	1
	Water Delivery	47.54	0.0974	64561.2	648	5.00	1	1

[i] Analogy to CCAA TCCV
[ii] Analogy to CCAA Heat Exchanger Liquid Sensor

H.2.3 Architecture Case 3 Master Equipment List

Assembly	Subassembly	Mass [kg]	Vol. [m^3]	MTBF [h]	Run Time [h]	LL [y]	# in Pmry.	# of Spares
CDRA	Air Pump Two-Stage ORU	10.89	0.0045	156200.0	8760	15.29	1	2
	Blower	5.58	0.0300	129700.0	8760	10.00	1	2
	Check Valves	39.92	0.1784	32900.0[i]	8760		1	3
	Desiccant Beds	42.64	0.0850	77100.0	8760		2	3
	Heat Controller	3.31	0.0085	242700.0	8760		2	2
	Precooler	5.58	0.0255	129700.0	8760	10.00	1	2
	Pump Fan Motor Controller	2.72	0.0057	2270000.0	8760		2	1
	Selector Valves	3.04	0.0017	117000.0	8760	10.61	6	4
	Sorbent Beds (Zeolite)	42.64	0.0850	77100.0	8760	2.28	2	2
CCAA	Condensing Heat Exchanger	49.71	0.3933	832600.0	8760		1	1
	Electronic Interface Box (EIB)	4.04	0.0173	2350000.0	8760		2	1
	Fan Delta Pressure Sensor	0.45	0.0002	1250000.0	8760		1	1
	Heat Exchanger Liquid Sensor	0.64	0.0006	1140000.0	8760		2	2
	Inlet ORU	25.31	0.1308	333000.0	8760		1	1
	Pressure Transducer	0.48	0.0000	1250000.0	8760	15.00	1	1
	Temperature Control Check Valve (TCCV)	7.45	0.0071	32900.0	8760		2	4
	Temperature Sensor	0.26	0.0014	37600000.0	8760		4	1
	Water Separator	11.93	0.0583	131000.0	1750	5.00	2	2
	Water Separator Liquid Sensor	0.64	0.0006	1140000.0[ii]	1750		2	2
WPA	Catalytic Reactor	67.04	0.1156	25579.2	928	2.25	1	1
	Gas Separator	39.15	0.0660	84008.4	928	1.00	1	1
	Ion Exchange Bed	13.02	0.0173	296701.2	928	0.16	1	1
	Microbial Check Valve	5.76	0.0065	143488.8	928	1.00	1	1
	Multifiltration Bed #1	149.23	0.0657	296701.2	928	0.36	1	0
	Multifiltration Bed #2	149.23	0.0657	296701.2	928	0.36	1	0
	Particulate Filter	32.25	0.0717	717356.4	928	0.22	1	1
	pH Adjuster	2.54	0.0026	137181.6	928	1.00	1	1
	Process Controller	45.00	0.0838	87950.4	928	7.72	1	1
	Pump Separator	31.34	0.0869	42398.4	928	2.00	1	1
	Reactor Health Sensor	16.83	0.0425	56677.2	928	1.00	1	1
	Sensor	4.81	0.0034	143664.0	928	10.00	1	1
	Separator Filter	7.67	0.0102	359072.4	928	0.84	1	1
	Start-up Filter	9.44	0.0184	226884.0	928	19.92	1	1
	Water Delivery	47.54	0.0974	64561.2	928	5.00	1	1
UPA	Distillation Assembly	92.76	0.1422	142525.2	2838	2.00	1	1
	Firmware Controller Assembly	23.09	0.0286	27331.2	3097	2.40	1	2
	Fluids Control and Pump Assembly	47.58	0.0731	90140.4	3097	4.00	1	1
	Pressure Control and Pump Assembly	49.08	0.1158	181507.2	2838	2.00	1	1
	Advanced Recycle Filter Tank Assembly[iii]	50.00	0.1011	199640.4	2838		1	1
	Separator Plumbing Assembly	16.78	0.0229	384651.6	2838	1.00	1	1

[i] Analogy to CCAA TCCV
[ii] Analogy to CCAA Heat Exchanger Liquid Sensor
[iii] Mass is obtained from [300] and verified with calculations based on data from Link et al. [301]. All other data is assumed to be the same as the Recycle Filter Tank Assembly (RFTA) described in the NASA BVAD 2004 [209] – the original system from which the ARFTA was upgraded from. Here, the life limit of the ARFTA has been assumed to be zero, based on its development objective of facilitating the same function as the RFTA without the need for periodic replacement [301].

H.2.4 Architecture Case 4 Master Equipment List

Assembly	Subassembly	Mass [kg]	Vol. [m^3]	MTBF [h]	Run Time [h]	LL [y]	# in Pmry.	# of Spares
CDRA	Air Pump Two-Stage ORU	10.89	0.0045	156200.0	8760	15.29	1	2
	Blower	5.58	0.0300	129700.0	8760	10.00	1	2
	Check Valves	39.92	0.1784	32900.0[i]	8760		1	3
	Desiccant Beds	42.64	0.0850	77100.0	8760		2	3
	Heat Controller	3.31	0.0085	242700.0	8760		2	2
	Precooler	5.58	0.0255	129700.0	8760	10.00	1	2
	Pump Fan Motor Controller	2.72	0.0057	2270000.0	8760		2	1
	Selector Valves	3.04	0.0017	117000.0	8760	10.61	6	5
	Sorbent Beds (Zeolite)	42.64	0.0850	77100.0	8760	2.28	2	3
CCAA	Condensing Heat Exchanger	49.71	0.3933	832600.0	8760		1	1
	Electronic Interface Box (EIB)	4.04	0.0173	2350000.0	8760		2	1
	Fan Delta Pressure Sensor	0.45	0.0002	1250000.0	8760		1	2
	Heat Exchanger Liquid Sensor	0.64	0.0006	1140000.0	8760		2	2
	Inlet ORU	25.31	0.1308	333000.0	8760		1	1
	Pressure Transducer	0.48	0.0000	1250000.0	8760	15.00	1	2
	Temperature Control Check Valve (TCCV)	7.45	0.0071	32900.0	8760		2	4
	Temperature Sensor	0.26	0.0014	37600000.0	8760		4	1
	Water Separator	11.93	0.0583	131000.0	1750	5.00	2	3
	Water Separator Liquid Sensor	0.64	0.0006	1140000.0[ii]	1750		2	2
WPA	Catalytic Reactor	67.04	0.1156	25579.2	928	2.25	1	1
	Gas Separator	39.15	0.0660	84008.4	928	1.00	1	1
	Ion Exchange Bed	13.02	0.0173	296701.2	928	0.16	1	1
	Microbial Check Valve	5.76	0.0065	143488.8	928	1.00	1	1
	Multifiltration Bed #1	149.23	0.0657	296701.2	928	0.36	1	1
	Multifiltration Bed #2	149.23	0.0657	296701.2	928	0.36	1	0
	Particulate Filter	32.25	0.0717	717356.4	928	0.22	1	1
	pH Adjuster	2.54	0.0026	137181.6	928	1.00	1	1
	Process Controller	45.00	0.0838	87950.4	928	7.72	1	1
	Pump Separator	31.34	0.0869	42398.4	928	2.00	1	1
	Reactor Health Sensor	16.83	0.0425	56677.2	928	1.00	1	1
	Sensor	4.81	0.0034	143664.0	928	10.00	1	1
	Separator Filter	7.67	0.0102	359072.4	928	0.84	1	1
	Start-up Filter	9.44	0.0184	226884.0	928	19.92	1	1
	Water Delivery	47.54	0.0974	64561.2	928	5.00	1	1
UPA	Distillation Assembly	92.76	0.1422	142525.2	2838	2.00	1	1
	Firmware Controller Assembly	23.09	0.0286	27331.2	3097	2.40	1	2
	Fluids Control and Pump Assembly	47.58	0.0731	90140.4	3097	4.00	1	1
	Pressure Control and Pump Assembly	49.08	0.1158	181507.2	2838	2.00	1	1
	Advanced Recycle Filter Tank Assembly[iii]	50.00	0.1011	199640.4	2838		1	1
	Separator Plumbing Assembly	16.78	0.0229	384651.6	2838	1.00	1	1
OGA	Hydrogen ORU	161.62	0.14670	27156.0	1309	2.38	1	2
	Hydrogen Sensor	4.36	0.0034	61845.6	1309	0.25	1	3
	Inlet Deionizing Bed	28.67	0.0295	296701.2	1319	6.00	1	1
	Nitrogen Purge ORU	34.25	0.0312[iv]	138408.0	241		1	2
	Oxygen Outlet	48.17	0.0312	98112.0	1309	10.00	1	2
	Power Supply Module	42.64	0.0649	47479.2	8634	4.17	1	2
	Process Controller	47.08	0.0838	103280.4	8634	7.72	1	2
	Pump	17.96	0.0102	144540.0	1309	1.00	1	2
	Water ORU	61.055	0.07561	33288.0	1319	2.92	1	3

[i] Analogy to CCAA TCCV
[ii] Analogy to CCAA Heat Exchanger Liquid Sensor
[iii] Mass is obtained from [300] and verified with calculations based on data from Link et al. [301]. All other data is assumed to be the same as the Recycle Filter Tank Assembly (RFTA) described in the NASA BVAD 2004 [209] – the original system from which the ARFTA was upgraded from. Here, the life limit of the ARFTA has been assumed to be zero, based on its development objective of facilitating the same function as the RFTA without the need for periodic replacement [301].
[iv] Analogy to OGA Oxygen Outlet

H.2.5 Architecture Case 5 Master Equipment List

Assembly	Subassembly	Mass [kg]	Vol. [m^3]	MTBF [h]	Run Time [h]	LL [y]	# in Pmry.	# of Spares
CDRA	Air Pump Two-Stage ORU	10.89	0.0045	156200.0	8760	15.29	1	2
	Blower	5.58	0.0300	129700.0	8760	10.00	1	2
	Check Valves	39.92	0.1784	32900.0[i]	8760		1	3
	Desiccant Beds	42.64	0.0850	77100.0	8760		2	3
	Heat Controller	3.31	0.0085	242700.0	8760		2	2
	Precooler	5.58	0.0255	129700.0	8760	10.00	1	2
	Pump Fan Motor Controller	2.72	0.0057	2270000.0	8760		2	1
	Selector Valves	3.04	0.0017	117000.0	8760	10.61	6	4
	Sorbent Beds (Zeolite)	42.64	0.0850	77100.0	8760	2.28	2	3
CCAA	Condensing Heat Exchanger	49.71	0.3933	832600.0	8760		1	1
	Electronic Interface Box (EIB)	4.04	0.0173	2350000.0	8760		2	1
	Fan Delta Pressure Sensor	0.45	0.0002	1250000.0	8760		1	2
	Heat Exchanger Liquid Sensor	0.64	0.0006	1140000.0	8760		2	2
	Inlet ORU	25.31	0.1308	333000.0	8760		1	1
	Pressure Transducer	0.48	0.0000	1250000.0	8760	15.00	1	2
	Temperature Control Check Valve (TCCV)	7.45	0.0071	32900.0	8760		2	4
	Temperature Sensor	0.26	0.0014	37600000.0	8760		4	1
	Water Separator	11.93	0.0583	131000.0	1750	5.00	2	3
	Water Separator Liquid Sensor	0.64	0.0006	1140000.0[ii]	1750		2	2
WPA	Catalytic Reactor	67.04	0.1156	25579.2	960	2.25	1	1
	Gas Separator	39.15	0.0660	84008.4	960	1.00	1	1
	Ion Exchange Bed	13.02	0.0173	296701.2	960	0.16	1	1
	Microbial Check Valve	5.76	0.0065	143488.8	960	1.00	1	1
	Multifiltration Bed #1	149.23	0.0657	296701.2	960	0.36	1	1
	Multifiltration Bed #2	149.23	0.0657	296701.2	960	0.36	1	0
	Particulate Filter	32.25	0.0717	717356.4	960	0.22	1	1
	pH Adjuster	2.54	0.0026	137181.6	960	1.00	1	1
	Process Controller	45.00	0.0838	87950.4	960	7.72	1	1
	Pump Separator	31.34	0.0869	42398.4	960	2.00	1	1
	Reactor Health Sensor	16.83	0.0425	56677.2	960	1.00	1	1
	Sensor	4.81	0.0034	143664.0	960	10.00	1	1
	Separator Filter	7.67	0.0102	359072.4	960	0.84	1	1
	Start-up Filter	9.44	0.0184	226884.0	960	19.92	1	1
	Water Delivery	47.54	0.0974	64561.2	960	5.00	1	1
UPA	Distillation Assembly	92.76	0.1422	142525.2	2838	2.00	1	1
	Firmware Controller Assembly	23.09	0.0286	27331.2	3097	2.40	1	2
	Fluids Control and Pump Assembly	47.58	0.0731	90140.4	3097	4.00	1	1
	Pressure Control and Pump Assembly	49.08	0.1158	181507.2	2838	2.00	1	1
	Advanced Recycle Filter Tank Assembly[iii]	50.00	0.1011	199640.4	2838		1	1
	Separator Plumbing Assembly	16.78	0.0229	384651.6	2838	1.00	1	1
OGA	Hydrogen ORU	161.62	0.14670	27156.0	1318	2.38	1	2
	Hydrogen Sensor	4.36	0.0034	61845.6	1318	0.25	1	3
	Inlet Deionizing Bed	28.67	0.0295	296701.2	1326	6.00	1	1
	Nitrogen Purge ORU	34.25	0.0312[iv]	138408.0	240		1	2
	Oxygen Outlet	48.17	0.0312	98112.0	1318	10.00	1	2
	Power Supply Module	42.64	0.0649	47479.2	8635	4.17	1	3
	Process Controller	47.08	0.0838	103280.4	8635	7.72	1	2
	Pump	17.96	0.0102	144540.0	1318	1.00	1	2
	Water ORU	61.055	0.07561	33288.0	1326	2.92	1	3
CRS	Sabatier Methanation Reactor	120[v]	0.208[v]	50000.0[vi]	1318		1	1
	Condensing Heat Exchanger[vii]	49.71	0.3933	832600.0	1318		1	1
	Phase Separator[viii]	11.93	0.0583	131000.0	1318	5.00	1	1
	Valves[ix]	3.04	0.0017	117000.0	1272	10.61	7[x]	2
	Sensors[xi]	4.81	0.0034	143664.0	1318	10.00	1	1
	Controller	3.00[v]	0.0053[xii]	103280.4[xiii]	1318	7.72[xiii]	1	1
	Compressor	27.00[v]	0.0112[xiv]	66666.7[vi]	1272		1	1

[i]Analogy to CCAA TCCV
[ii]Analogy to CCAA Heat Exchanger Liquid Sensor
[iii]Mass is obtained from [300] and verified with calculations based on data from Link et al. [301]. All other data is assumed to be the same as the Recycle Filter Tank Assembly (RFTA) described in the NASA BVAD 2004 [209] – the original system from which the ARFTA was upgraded from. Here, the life limit of the ARFTA has been assumed to be zero, based on its development objective of facilitating the same function as the RFTA without the need for periodic replacement [301].
[iv]Analogy to OGA Oxygen Outlet
[v]Data taken from Jeng and Lin [256]
[vi]Data taken from Papale et al. [318]
[vii]Analogy to CCAA Condensing Heat Exchanger
[viii]Analogy to CCAA Water Separator
[ix]Analogy to CDRA Selector Valves
[x]Data taken from Jones [319]
[xi]Analogy to WPA Sensor
[xii]Linear scaling (based on mass) from OGA Process Controller
[xiii]Analogy to OGA Process Controller
[xiv]Linear scaling (based on mass) from CDRA Air Pump

Appendix I

Case Study 1: The Mars One Mission Plan – Assumptions and Results

This appendix summarizes the data and assumptions used in the Mars One Mission plan feasibility analysis performed in Chapter 5. In addition, the complete set of spare parts results obtained from this analysis is also presented. The data and results presented here were generated in collaboration with Andrew Owens, Koki Ho, and Sam Schreiner – all graduate researchers at MIT at the time at which this analysis was performed. This author would like to acknowledge the invaluable contributions of these researchers to this analysis.

I.1 Habitation Module Assumptions

Listed below are the assumptions made in the modeling of the baseline Mars One habitat within the HabNet Habitation Module. As was mentioned in Section 5.5, these assumptions are based on a combination of public statements made by the organization, as well as values listed in various NASA design handbooks.

Table I.1: Habitation Module Assumptions used to model the baseline Mars One habitat

Parameter	Value	Reference / Comments
Time Horizon (Mission Duration)	26 months (19000hours)	This corresponds to the period between launch windows to Mars from Earth – that is, the period between resource and hardware resupply opportunities. This is the minimum continuous period over which the habitat must be self-sufficient.
Number of Crew	4	Specified by Mars One [193]
Habitat Atmosphere	70.3kPa, 26.5% O_2 Diluent gas: N_2	Mars One states that the habitat atmosphere will be 0.7bar [11]. The equivalent atmosphere studied by the NASA Exploration Atmospheres Working Group (EAWG) is a 26.5% O_2 mixture. This corresponds to the Space Shuttle atmosphere employed prior to and during extravehicular activity (EVA) operations [140]

Habitat Volume	6x scaled up Dragon capsules (each $25m^3$) and 2x Inflatable modules (each $500m^3$)	See Section 5.5.4.1 for a discussion on the assumed SpaceX Dragon modules volume. The inflatable module is specified on the Mars One website [201]
Habitat Leakage Rate	0.05% lost by mass per day	Value taken from Table 4.1.1 of BVAD [209]
ECLS Architecture	Based on that of the International Space Station	Explicit claim made by Mars One regarding the life support unit: *"This system will be very similar to those units which are fully functional on-board the International Space Station."* [198]
Food System	Entirely locally grown	Mars One plans for $50m^2$ dedicated to plant growth. Moreover, they claim that this: *"will be sufficient plant production capacity to feed about three crews of four"* [197]
EVA Frequency	5 EVAs/week, 2 crewmembers per EVA, 8 hours per EVA	Although not explicitly specified, the description on the Mars One website[200] implies that EVAs will occur frequently. The NASA Baseline Values and Assumptions (BVAD) document suggests a nominal EVA duration of 8 hours and a maximum EVA frequency of 5 two-person EVAs per week [209]
Spacesuit pressure	29.6kPa (4.3 psi), at 100% O_2	EAWG recommended suit pressure for EVAs requiring dexterous tasks. This suit pressure also limits the oxygen in-suit prebreathe time from the 70.3kPa habitat atmosphere to about 40 minutes [140]
Spacesuit Portable Life Support System (PLSS)	NASA PLSS2.0 Architecture	Currently in development, the PLSS2.0 architecture is the current state of the art in spacesuit life support systems [327]. Unlike the spacesuits currently used on the International Space Station, the PLSS2.0 is capable of supporting a crewmember on the Martian surface.
Spacesuit Urine Management	Urine Collection and Transfer Assembly (UCTA)	Astronauts currently performing EVA on the ISS wear Maximum Absorbency Garments (MAGs) to collect their urine. These are then discarded at the end of the EVA. The large number of EVAs anticipated for Mars One means that choosing to discard urine expelled during EVA can become a major source of water loss to the system over time. To overcome this, we have assumed an Apollo like system, where urine is collected in a bag attached to the astronaut's thigh [337]. The collected urine can then be emptied back into the habitat's urine processor for water recovery.
Airlock cycle losses	Equivalent to 13.8kPa within an assumed $3.7m^3$ airlock	The discussion on the Mars One website [237] implies that airlocks will be used rather than other means of habitat entry (such as suitports). Here we assume an airlock volume of $3.7m^3$, which corresponds to the minimum volume that can accommodate 2 crewmembers at a time[209]. The gaseous loss of 13.8kPa corresponds to the minimum pressure that the current ISS Quest Airlock depressurization pump can be operated down to [323]
Potable Water Tanks	2x 1500L capacity tanks	Mars One states that 3000L of water will be produced and stored locally prior to the arrival of the first crew [11]. This water will act as contingency water to sustain the crew in the event that the ISRU system goes offline. Water usage is budgeted for 50L per person per day [197]
Oxygen Tanks	120kg capacity	Mars One states that 120kg of oxygen will be produced and stored locally prior to the arrival of the first crew [11]
Nitrogen Tanks	292kg capacity	Corresponds to the amount of nitrogen required to mix with 120kg of oxygen to produce a 26.5% oxygen (molar percentage) atmosphere

I.2 Assumed ECLS Technologies Employed within the Mars One Habitat

The ECLS technologies assumed for the baseline Mars One habitat are assumed to be based on those currently operating on the Internatioal Space Station. This is based on Mars One's statement that their Life Support Unit *"will be very similar to those units which are fully functional on-board the International Space Station."*[198]

Table I.2: Assumed ECLS technologies employed within the baseline Mars One habitat

ECLS Function	ECLS Technology	Corresponding ISS USOS Technology	Location of Technology on ISS
Gas Storage	High Pressure Tanks	High pressure N_2 and O_2 tanks	Installed on the exterior of the Quest airlock[236]
O_2 Generation	Solid Polymer Water Electrolysis	Oxygen Generation Assembly (OGA)	Installed in the Oxygen Generation System (OGS) rack in Node 3[359]
CO_2 Removal	Molecular Sieve (Zeolite5A)	Carbon Dioxide Removal Assembly (CDRA)	One is installed in the Air Revitalization (AR) rack within Node 3, and another is installed in the AR rack in the Destiny Laboratory[360]
CO_2 Reduction	Sabatier Reactor	CO_2 Reduction System (CRS)	Installed in the Oxygen Generation System (OGS) rack in Node 3[360]
Humidity Control	Condensing Heat Exchanger	Common Cabin Air Assembly (CCAA)	Located in all USOS modules except for Node 1 and the PMM[361]
Water Storage	Bellows Tanks and Soft Containers	WPA Product Water Tank and Contingency Water Containers (CWCs)	Located throughout the ISS[362]
Water Processing	Vapor Compression Distillation & Multifiltration	Urine Processor Assembly (UPA) and Water Processor Assembly (WPA)	Installed in the Water Recovery System (WRS) Racks 1 and 2 in Node 3[360]
Waste Processing	Water recovered from urine via VCD. Feces and brine disposed in logistics resupply vehicles	The Advanced Recycle Filter Tank Assembly (ARFTA) collects brine and sends it to Rodnik tanks on the Progress vehicle, or one of the water tanks on the ATV. Feces is collected in a waste canister and disposed of in one of the resupply vehicles	One of the several logistics resupply vehicles that visit the ISS[363]

I.3 Heuristics used for ECLS Technology Location Allocation

Mars One Habitation Module	Life Support Functions supported by Habitation Module	Analogous ISS Module	Comments
Inflatable	Main living area of the habitat. Supports recreation and houses food production units (See Figure 5-3)[203]	Node 3 and Destiny Laboratory	The exercise equipment on the ISS USOS is distributed across the Destiny Laboratory and Node 3
Living Unit	Contains airlock and habitat "'wet areas', such as the shower and kitchen"[196]	Quest Airlock and Node 3	Node 3 contains the Waste and Hygiene Compartment[364], while the Quest airlock serves all airlock functions on the U.S. Segment
Life Support Unit	Contains ECLS and ISRU technologies, as well as solar arrays[198]	Node 3	The majority of ECLS technologies are located within Node 3[364]
Cargo / Supply Unit	Storage volume for hardware, spare parts and consumables[238]	Permanent Multipurpose Module (PMM)	The PMM was added to the ISS primarily to increase on-orbit storage volume[365]

I.4 Crop Static Growth Parameters

Crop	Carbohydrate Fraction of Dry Mass (c)[i]	Protein Fraction of Dry Mass (p)[i]	Fat Fraction of Dry Mass (f)[i]	Average Growth Rate ($g/m^2/day$) (r)[ii]	Time to Crop Maturity (days)[iii]	Mature Plant Height (m)[iii]
Dry (Kidney) Bean	0.711	0.279	0.010	9.064	63	0.5
Lettuce	0.655	0.311	0.034	7.433	30	0.25
Peanut	0.173	0.286	0.542	4.131	110	0.65
Rice	0.919	0.075	0.006	11.86	88	0.8
Soybean	0.348	0.421	0.230	6.867	86	0.55
Sweet Potato	0.925	0.072	0.002	18.29	120	0.65
Tomato	0.783	0.177	0.040	6.609	80	0.4
Wheat	0.866	0.112	0.023	26.74	62	0.5
White Potato	0.898	0.096	0.006	16.82	138	0.65

[i]Data obtained from the United States Department of Agriculture National Nutrient Database for Standard Reference – Release 27. Available at: http://ndb.nal.usda.gov/ndb/, Accessed: August 30th 2014
[ii]Determined through simulation of the Modified Energy Cascade crop models under nominal conditions
[iii]Data obtained from the NASA Baseline Values and Assumptions Document NASA CR-2004-208941

I.5 Component Data

I.5.1 Biomass Production System (BPS) Architecture Component Data

Tabulated below are component data for the BPS architecture developed in Section 5.6.2.1. The mass, volume, mean time between failures (MTBF), and life limit (LL) of each element considered in this analysis is shown, along with the number of each element in the primary and secondary (redundant backup) systems. Elements without an entry for MTBF and/or LL are assumed to not fail randomly and/or require scheduled replacement, respectively. Unless otherwise noted, values are from the NASA Advanced Life Support Baseline Values and Assumptions Document [209]. Assumptions and use of analogy to other components for data are indicated and described with endnotes.

Sub-system	Assembly	Subassembly	Mass [kg]	Vol. [m^3]	MTBF [h]	LL [y]	# in Pmry.	# in Scdry.
ECLSS	CDRA	Air Pump Two-Stage ORU	10.87	0.0045	156200.0	15.29	1	1
		Blower	5.58	0.0300	129700.0	10.00	1	1
		Check Valves	39.92	0.1784	32900.0[i]		1	1
		Desiccant Beds	42.64	0.0850	77100.0		2	2
		Heat Controller	3.31	0.0085	242700.0		2	2
		Precooler	5.58	0.0255	129700.0	10.00	1	1
		Pump Fan Motor Controller	2.72	0.0057	2270000.0		2	2
		Selector Valves	3.04	0.0017	117000.0	10.61	6	6
		Sorbent Beds (Zeolite)	42.64	0.0850	77100.0		2	2
	ORA[ii]	Air Pump Two-Stage ORU	10.89	0.0045	156200.0	15.29	1	1
		Blower	5.58	0.0300	129700.0	10.00	1	1
		Check Valves	39.92	0.1784	32900.0[i]		1	1
		Desiccant Beds	42.64	0.0850	77100.0		2	2
		Heat Controller	3.31	0.0085	242700.0		2	2
		Precooler	5.58	0.0255	129700.0	10.00	1	1
		Pump Fan Motor Controller	2.72	0.0057	2270000.0		2	2
		Selector Valves	3.04	0.0017	117000.0	10.61	6	6
		Sorbent Beds (Zeolite)	42.64	0.0850	77100.0		2	2
	CCAA (x6)	Condensing Heat Exchanger	49.71	0.3933	832600.0		6	6
		Electronic Interface Box (EIB)	4.04	0.0173	2350000.0		12	12
		Fan Delta Pressure Sensor	0.45	0.0002	1250000.0		6	6
		Heat Exchanger Liquid Sensor	0.64	0.0006	1140000.0		12	12
		Inlet ORU	25.31	0.1309	333000.0		6	6
		Pressure Transducer	0.48	0.0000	1250000.0	15.00	6	6
		Temperature Control Check Valve (TCCV)	7.45	0.0071	32900.0		12	12
		Temperature Sensor	0.26	0.0014	37600000.0		24	24
		Water Separator	11.93	0.0583	131000.0	5.00	12	12
		Water Separator Liquid Sensor	0.64	0.0006	1140000.0[iii]		12	12
	UPA	Distillation Assembly	92.76	0.1422	142525.2	2.00	1	1
		Firmware Controller Assembly	23.09	0.0286	27331.2	2.40	1	1
		Fluids Control and Pump Assembly	47.58	0.0731	90140.4	4.00	1	1
		Pressure Control and Pump Assembly	49.08	0.1158	181507.2	2.00	1	1
		Recycle Filter Tank Assembly	15.38	0.1011	199640.4	0.08	1	1
		Separator Plumbing Assembly	16.78	0.0229	384651.6	1.00	1	1
	WPA	Catalytic Reactor	67.04	0.1156	25579.2	2.25	1	1
		Gas Separator	39.15	0.0660	84008.4	1.00	1	1
		Ion Exchange Bed	13.02	0.0173	296701.2	0.16	1	1
		Microbial Check Valve	5.76	0.0065	143488.8	1.00	1	1
		Multifiltration Bed #1	149.23	0.0657	296701.2	0.36	1	1
		Multifiltration Bed #2	149.23	0.0657	296701.2	0.36	1	1
		Particulate Filter	32.25	0.0717	717356.4	0.22	1	1
		pH Adjuster	2.54	0.0026	137181.6	1.00	1	1

		Process Controller	45.00	0.0838	87950.4	7.72	1	1
		Pump Separator	31.34	0.0869	42398.4	2.00	1	1
		Reactor Health Sensor	16.83	0.0423	56677.2	1.00	1	1
		Sensor	4.81	0.0034	143664.0	10.00	1	1
		Separator Filter	7.67	0.0102	359072.4	0.84	1	1
		Start-up Filter	9.44	0.0184	226884.0	19.92	1	1
		Water Delivery	47.54	0.0974	64561.2	5.00	1	1
	BPS	Mechanization Systems and Secondary Structure	1960.00	14.2649[iv]			1	0
	GLS	LED Growth Light ORU [366]	8.00	0.0185	1743216.0[v]	5.71	137	0
ISRU[vi]	AP	Zeolite and Support Structure	94.58	0.1495	77100.0[vii]		1	1
		Compressor	188.11	1.0878	66666.7[viii]		2	2
		Cryocooler	5.04	0.0024	500000.0[ix]		2	2
	SP	Mixing Auger	95.13	0.0000[x]	500000.0[ix]		1	1
		Feed Cone	59.36	0.2103	500000.0[ix]		1	1
		Hopper	20.35	0.1225			1	1
		Horizontal Feed Auger	1.31	0.0044	500000.0[ix]		1	1
		Condensing Heat Exchanger	80.78	0.6391	832600.0		1	1
		Oven Heater	6.26	0.0138	242700.0		1	1
	CO2 Injection System	Cryocooler	22.00	0.0500	200000.0		2	2
		Blower	5.58	0.0300	129700.0	10.00	1	1
		Valves	3.04	0.0017	117000.0	10.61	5	5
PDISRU[vi]	AP	Zeolite and Support Structure	535.59	0.8595	77100.0[vii]		1	1
		Compressor 1 (Mars to 1atm)	1081.60	6.2549	66666.7[viii]		2	2
		Cryocooler	5.04	0.0024	500000.0[ix]		2	2
	SP	Mixing Auger	498.02	0.0000[x]	500000.0[ix]		1	1
		Feed Cone	178.97	1.1008	500000.0[ix]		1	1
		Hopper	56.32	0.6417			1	1
		Horizontal Feed Auger	1.31	0.0044	500000.0[ix]		1	1
		Condensing Heat Exchanger	80.78	0.6391	832600.0		1	1
		Oven Heater	6.26	0.0138	242700.0		1	1
	OGA	Hydrogen Sensor	4.36	0.0034	2576.9	0.25	1	1
		Inlet Deionizing Bed	28.67	0.0295	12362.6	6.00	1	1
		Nitrogen Purge ORU	34.25	0.0312	5767.0		1	1
		Oxygen Outlet	48.17	0.0312	4088.0	10.00	1	1
		Power Supply Module	42.64	0.0649	1978.3	4.17	1	1
		Process Controller	47.08	0.0838	4303.4	7.72	1	1
		Pump	17.96	0.0102	6022.5	1.00	1	1
Storage	O2 Tank		21.84	0.2802[xi]			1	1
	N2 Tank		80.95	0.6868[xi]			1	1
	CO2 Accumulator[xii]		0.06	0.0207			1	1
	Potable Water Tank		100.21[xiii]	0.0500[xiv]			1	1
	Dirty Water Tank		10.50[xv]	0.0090			1	1
	Grey Water Tank		53.05[xv]	0.0455			1	1
	Crop Water Tank		261.07[xiii]	0.3015[xiv]			1	0
	Biomass Storage		0.00	0.0000			1	0
	Food Storage[xvi]		775.00	0.0007			1	0
Habitat	Inflatable Hab.		4580.00	33.3333[xvii]			1	1
Crew Systems [367]	Galley and Food System	Freezers	400.00	2.0000			1	0
		Conventional oven	50.00	0.2500			1	0
		Microwave ovens (2 ea.)	70.00	0.3000			1	0
		Kitchen/oven cleaning supplies (fluids, sponges, etc.)	197.92	1.4250			1	0
		Sink, spigot for hydration of food and drinking water	15.00	0.0135			1	0
		Dishwasher	40.00	0.5600			1	0
		Cooking/eating supplies	20.00	0.0056			1	0
	BPS Food Processor	Hand Mixer	2.00	0.0050			1	0
		Food Processor / Blender	8.00	0.0230			1	0
		Grinder / Mill	4.10	0.0120			1	0
		Bread Machine	7.40	0.0310			1	0
		Griddle / Grill	5.80	0.0270			1	0
		Juice Extractor	7.70	0.0390			1	0
	Waste Collection System	Waste Collection System (2 toilets)	90.00	4.3600			1	0
		WCS supplies	158.33	4.1167			1	0
		Contingency fecal/urine collection mittens/bags	728.33	2.5333			1	0
	Personal Hygiene	Shower	75.00	1.4100			1	0
		Handwash/mouthwash faucet	8.00	0.0100			1	0
		Personal hygiene kit	7.20	0.0750			1	0
		Hygiene supplies	237.50	4.7500			1	0
	Clothing	Clothing	396.00	1.3440			1	0
		Washing machine	100.00	0.7500			1	0
		Clothes dryer	60.00	0.7500			1	0
	Recreational	Personal Stowage/Closet Space	200.00	3.0000			1	0
	Housekeeping	Vacuum	13.00	0.0700			1	0
		Trash compactor/trash lock	150.00	0.3000			1	0
		Trash bags	158.33	3.1667			1	0

Operational	Operational Supplies and Restraints	80.00	0.0080		1	0
Supplies and	Restraints and mobility aids	100.00	0.5400		1	0
Photography	Equipment	120.00	0.5000		1	0
Sleep	Sleep Provisions	36.00	0.4000		1	0
Crew Healthcare	Medical/Surgical/Dental suite	1000.00	4.0000		1	0
	Medical/Surgical/Dental consumables	500.00	2.5000		1	0
Exercise Equipment	ARED [368]	317.51	1.3592[xviii]		1	0
	COLBERT [369]	997.90	0.3398[xviii]		1	0
	CEVIS [370]	26.76	0.0850[xviii]		1	0
EVA	Battery[xix]	6.33	0.0048[xx]	0.12[xxi]	2	2
	Misc. Hardware	78.04[xxii]	0.6680[xxiii]		2	2

I.5.2 Stored Food (SF) Architecture Component Data

Tabulated below are component data for the SF architecture developed in Section 5.6.2.2. The mass, volume, mean time between failures (MTBF), and life limit (LL) of each element considered in this analysis is shown, along with the number of each element in the primary and secondary (redundant backup) systems. Elements without an entry for MTBF and/or LL are assumed to not fail randomly and/or require scheduled replacement, respectively. Unless otherwise noted, values are from the NASA Advanced Life Support Baseline Values and Assumptions Document [209]. Assumptions and use of analogy to other components for data are indicated and described with endnotes.

Sub-system	Assembly	Subassembly	Mass [kg]	Vol. [m^3]	MTBF [h]	LL [y]	# in Pmry	# in Scdry
ECLSS	OGA	Hydrogen Sensor	4.36	0.0034	61845.6	0.25	1	1
		Inlet Deionizing Bed	28.67	0.0295	296701.2	6.00	1	1
		Nitrogen Purge ORU	34.25	0.0312[xxiv]	138408.0		1	1
		Oxygen Outlet	48.17	0.0312	98112.0	10.00	1	1
		Power Supply Module	42.64	0.0649	47479.2	4.17	1	1
		Process Controller	47.08	0.0838	103280.4	7.72	1	1
		Pump	17.96	0.0102	144540.0	1.00	1	1
	CDRA	Air Pump Two-Stage ORU	10.89	0.0045	156200.0	15.29	1	1
		Blower	5.58	0.0300	129700.0	10.00	1	1
		Check Valves	39.92	0.1784	32900.0[i]		1	1
		Desiccant Beds	42.64	0.0850	77100.0		2	2
		Heat Controller	3.31	0.0085	242700.0		2	2
		Precooler	5.58	0.0255	129700.0	10.00	1	1
		Pump Fan Motor Controller	2.72	0.0057	2270000.0		2	2
		Selector Valves	3.04	0.0017	117000.0	10.61	6	6
		Sorbent Beds (Zeolite)	42.64	0.0850	77100.0	2.28	2	2
	CCAA (x6)	Condensing Heat Exchanger	49.71	0.3933	832600.0		6	6
		Electronic Interface Box (EIB)	4.04	0.0173	2350000.0		12	12
		Fan Delta Pressure Sensor	0.45	0.0002	1250000.0		6	6
		Heat Exchanger Liquid Sensor	0.64	0.0006	1140000.0		12	12
		Inlet ORU	25.31	0.1308	333000.0		6	6
		Pressure Transducer	0.48	0.0000	1250000.0	15.00	6	6
		Temperature Control Check Valve (TCCV)	7.45	0.0071	32900.0		12	12
		Temperature Sensor	0.26	0.0014	37600000.0		24	24
		Water Separator	11.93	0.0583	131000.0	5.00	12	12
		Water Separator Liquid Sensor	0.64	0.0006	1140000.0[iii]		12	12
	UPA	Distillation Assembly	92.76	0.1422	142525.2	2.00	1	1
		Firmware Controller Assembly	23.09	0.0286	27331.2	2.40	1	1
		Fluids Control and Pump Assembly	47.58	0.0731	90140.4	4.00	1	1
		Pressure Control and Pump Assembly	49.08	0.1158	181507.2	2.00	1	1
		Recycle Filter Tank Assembly	15.38	0.1011	199640.4	0.08	1	1

		Separator Plumbing Assembly	16.78	0.0229	384651.6	1.00	1	1
	WPA	Catalytic Reactor	67.04	0.1156	25579.2	2.25	1	1
		Gas Separator	39.15	0.0660	84008.4	1.00	1	1
		Ion Exchange Bed	13.02	0.0173	296701.2	0.16	1	1
		Microbial Check Valve	5.76	0.0065	143488.8	1.00	1	1
		Multifiltration Bed #1	149.23	0.0657	296701.2	0.36	1	1
		Multifiltration Bed #2	149.23	0.0657	296701.2	0.36	1	1
		Particulate Filter	32.25	0.0717	717356.4	0.22	1	1
		pH Adjuster	2.54	0.0026	137181.6	1.00	1	1
		Process Controller	45.00	0.0838	87950.4	7.72	1	1
		Pump Separator	31.34	0.0869	42398.4	2.00	1	1
		Reactor Health Sensor	16.83	0.0425	56677.2	1.00	1	1
		Sensor	4.81	0.0034	143664.0	10.00	1	1
		Separator Filter	7.67	0.0102	359072.4	0.84	1	1
		Start-up Filter	9.44	0.0184	226884.0	19.92	1	1
		Water Delivery	47.54	0.0974	64561.2	5.00	1	1
	CRS	Sabatier Methanation Reactor	120.0[xxv]	0.208[xxv]	50000.0[xxvi]		1	1
		Condensing Heat Exchanger[xxvii]	49.71	0.3933	832600.0		1	1
		Phase Separator[xxviii]	11.93	0.0583	131000.0	5.00	1	1
		Valves[xxix]	3.04	0.0017	117000.0	10.61	7[xxx]	7[xxx]
		Sensors[xxxi]	4.81	0.0034	143664.0	10.00	1	1
		Controller	3.00[xxv]	0.0053[xxxii]	103280[xxxiii]	7.7[xxxiii]	1	1
		Compressor	27.00[xxv]	0.0112[xxxi]	66666.7[xxvi]		1	1
ISRU[vi]	AP	Zeolite and Support Structure	94.58	0.1495	77100.0[vii]		1	1
		Compressor	188.11	1.0878	66666.7[viii]		2	2
		Cryocooler	5.04	0.0024	500000.0[ix]		2	2
	SP	Mixing Auger	122.86	0.0000[x]	500000.0[ix]		1	1
		Feed Cone	70.40	0.2715	500000.0[ix]		1	1
		Hopper	23.64	0.1583			1	1
		Horizontal Feed Auger	1.31	0.0044	500000.0[ix]		1	1
		Condensing Heat Exchanger	80.78	0.6391	832600.0		1	1
		Oven Heater	6.26	0.0138	242700.0		1	1
PD-ISRU[vi]	AP	Zeolite and Support Structure	535.59	0.8595	77100.0[vii]		1	1
		Compressor 1 (Mars to 1atm)	1081.60	6.2549	66666.7[viii]		2	2
		Cryocooler	5.04	0.0024	500000.0[ix]		2	2
	SP	Mixing Auger	136.54	0.0000[x]	500000.0[ix]		1	1
		Feed Cone	75.53	0.3018	500000.0[ix]		1	1
		Hopper	25.17	0.1760			1	1
		Horizontal Feed Auger	1.31	0.0044	500000.0[ix]		1	1
		Condensing Heat Exchanger	80.78	0.6391	832600.0		1	1
		Oven Heater	6.26	0.0138	242700.0		1	1
Storage	O2 Tank		21.84	0.2802[xi]			1	1
	N2 Tank		80.95	0.6868[xi]			1	1
	CO2		0.06	0.0207			1	1
	Potable Water		100.21[xii]	0.0500[xiv]			1	1
	Dirty Water Tank		10.50[xv]	0.0090			1	1
	Gray Water Tank		53.05[xv]	0.0455			1	1
	Food Storage[xvi]		5152.00	0.0046			1	0
Habitat	Inflatable Hab.		4580.00	33.3333[xvi]			1	1
Crew Systems [367]	Galley and Food System	Freezers	400.00	2.0000			1	0
		Conventional oven	50.00	0.2500			1	0
		Microwave ovens (2 ea.)	70.00	0.3000			1	0
		Kitchen/oven cleaning supplies	197.92	1.4250			1	0
		Sink, spigot for hydration of food and drinking	15.00	0.0135			1	0
		Dishwasher	40.00	0.5600			1	0
		Cooking/eating supplies	20.00	0.0056			1	0
	Waste Collection System	Waste Collection System (2 toilets)	90.00	4.3600			1	0
		WCS supplies	158.33	4.1167			1	0
		Contingency fecal/urine collection mittens/bags	728.33	2.5333			1	0
	Personal Hygiene	Shower	75.00	1.4100			1	0
		Handwash/mouthwash faucet	8.00	0.0100			1	0
		Personal hygiene kit	7.20	0.0750			1	0
		Hygiene supplies	237.50	4.7500			1	0
	Clothing	Clothing	396.00	1.3440			1	0
		Washing machine	100.00	0.7500			1	0
		Clothes dryer	60.00	0.7500			1	0
	Recreational	Personal Stowage/Closet Space	200.00	3.0000			1	0
	Housekeeping	Vacuum	13.00	0.0700			1	0
		Trash compactor/trash lock	150.00	0.3000			1	0
		Trash bags	158.33	3.1667			1	0
	Operational Supplies and Photography	Operational Supplies and Restraints	80.00	0.0080			1	0
		Restraints and mobility aids	100.00	0.5400			1	0
		Equipment	120.00	0.5000			1	0
	Sleep	Sleep Provisions	36.00	0.4000			1	0

Crew Healthcare	Medical/Surgical/Dental suite	1000.00	4.0000		1	0
	Medical/Surgical/Dental consumables	500.00	2.5000		1	0
Exercise	ARED[368]	317.51	1.3592[xviii]		1	0
Equipment	COLBERT[369]	997.90	0.3398[xviii]		1	0
	CEVIS[370]	26.76	0.0850[xviii]		1	0
EVA	Battery	6.33	0.0048[xx]	0.12[xxi]	2	2
	Misc. Hardware	78.04[xxii]	0.6680[xxiii]		2	2

[i]Analogy to CCAA TCCV
[ii]Analogy to CDRA
[iii]Analogy to CCAA Heat Exchanger Liquid Sensor
[iv]Assumed to have same packed density as inflatable habitat
[v]Assuming 2yr warranty accounts for 1% failures during that time
[vi]Based on sizing calculations; see Section 5.5.2 for more detail
[vii]Analogy to CDRA Sorbent Beds
[viii]Analogy to Sabatier Compressor [318]
[ix]Optimistic assumption; no data were available
[x]Assumed to be stored inside feed cone for transport
[xi]Linear scaling from ISS O2/N2 tanks [236]
[xii]Based on hoop stress calculations for a 0.73ft^3 spherical tank at 130psia (factor of safety 2; A517 steel) [371–373]
[xiii]Linear scaling from ISS Contingency Water Container
[xiv]Assumes 30:1 packing efficiency (twice that of inflatable habitat)
[xv]Linear scaling from UPA Wastewater Storage Tank
[xvi]Includes food and packaging, assuming ISS Phase III packaging
[xvii]Assuming 15:1 packing efficiency [210]
[xviii]Estimated based on imagery
[xix]Analogy to EMU Series 2000 Battery [324]
[xx]Assumed to be ½ volume of METOX canister based on drawings [324]
[xxi]Life limit of 32 EVAs at a rate of 5 EVAs/wk [324]
[xxii]Based on Apollo A7LB Suit mass, minus battery mass [324,337]
[xxiii]Estimated from images of EMU HUT and PLSS (other components assumed to fit within that volume)[324]
[xxiv]Analogy to OGA Oxygen Outlet
[xxv]Data taken from Jeng and Lin [256]
[xxvi]Data taken from Papale et al. [318]
[xxvii]Analogy to CCAA Condensing Heat Exchanger
[xxviii]Analogy to CCAA Water Separator
[xxix]Analogy to CDRA Selector Valves
[xxx]Data taken from Jones [319]
[xxxi]Analogy to WPA Sensor
[xxxii]Linear scaling (based on mass) from OGA Process Controller
[xxxiii]Analogy to OGA Process Controller
[xxxiv]Linear scaling (based on mass) from CDRA Air Pump

I.6 HabNet Supportability Module Results

I.6.1 Biomass Production System (BPS) Architecture Spare Parts Requirements

Tabulated below are the results of the sparing analysis for the first 10 crews in the BPS case, giving the number of spares delivered to the surface at each crewed mission for each component.

Group	Subgroup	Subassembly	Crew									
			1	**2**	**3**	**4**	**5**	**6**	**7**	**8**	**9**	**10**
ECLSS	CDRA	Air Pump Two-Stage ORU	3	2	1	2	1	2	2	2	2	2
		Blower	3	2	2	1	2	2	2	3	2	3
		Check Valves	6	3	4	5	5	5	7	6	8	8
		Dessicant Beds	5	3	4	4	5	4	6	6	6	7
		Heat Controller	3	2	2	2	2	2	2	2	3	3
		Precooler	3	2	2	1	2	2	2	3	2	3
		Pump Fan Motor Controller	2	0	1	0	1	1	0	1	0	1
		Selector Valves	7	5	6	6	8	9	9	11	12	12
		Sorbent Beds (Zeolite)	5	3	4	4	5	4	6	6	6	7
	ORA	Air Pump Two-Stage ORU	3	1	1	1	1	1	1	1	1	1
		Blower	3	1	1	1	1	1	2	1	1	2
		Check Valves	4	2	3	3	2	4	3	4	4	4
		Dessicant Beds	4	2	2	3	2	3	3	3	4	4
		Heat Controller	3	1	1	1	1	2	1	1	2	1
		Precooler	3	1	1	1	1	1	2	1	1	2
		Pump Fan Motor Controller	2	0	0	1	0	0	1	0	1	0
		Selector Valves	5	3	4	3	5	4	6	5	6	7

		Sorbent Beds (Zeolite)	4	2	2	3	2	3	3	3	4	4
	CCAA (x6)	Condensing Heat Exchanger	3	2	1	2	2	2	2	2	2	3
		Electronic Interface Box (EIB)	3	1	2	1	1	2	1	2	2	2
		Fan Delta Pressure Sensor	3	1	1	2	1	2	1	2	1	2
		Heat Exchanger Liquid Sensor	4	2	2	2	2	3	2	3	3	4
		Inlet ORU	4	3	3	3	3	4	4	5	4	6
		Pressure Transducer	3	1	1	2	1	2	1	2	5	6
		Temperature Control Check Valve (TCCV)	20	21	29	35	42	49	56	63	70	76
		Temperature Sensor	2	0	1	0	1	0	0	1	0	1
		Water Separator	9	8	9	10	13	23	36	36	36	48
		Water Separator Liquid Sensor	4	2	2	2	2	3	2	3	3	4
	UPA	Distillation Assembly	3	1	2	4	5	6	7	8	9	10
		Firmware Controller Assembly	4	3	2	3	4	3	4	5	8	9
		Fluids Control and Pump Assembly	3	1	1	2	1	2	2	4	4	5
		Pressure Control and Pump Assembly	2	1	3	4	5	6	7	8	9	10
		Recycle Filter Tank Assembly	27	54	81	108	135	162	189	216	244	271
		Separator Plumbing Assembly	2	4	6	8	10	13	15	17	19	21
	WPA	Catalytic Reactor	3	1	1	1	4	5	6	7	8	9
		Gas Separator	2	4	6	8	10	13	15	17	19	21
		Ion Exchange Bed	13	27	40	54	67	81	94	108	122	135
		Microbial Check Valve	2	4	6	8	10	13	15	17	19	21
		Multifiltration Bed #1	6	12	18	24	30	36	42	48	54	60
		Multifiltration Bed #2	6	12	18	24	30	36	42	48	54	60
		Particulate Filter	9	19	29	39	49	59	69	78	88	98
		pH Adjuster	2	4	6	8	10	13	15	17	19	21
		Process Controller	2	1	0	1	1	0	1	1	1	2
		Pump Separator	2	1	3	4	5	6	7	8	9	10
		Reactor Health Sensor	2	4	6	8	10	13	15	17	19	21
		Sensor	2	0	1	0	1	0	1	0	1	1
		Separator Filter	2	5	7	10	12	15	18	20	23	25
		Start-up Filter	2	0	1	0	0	1	0	1	0	0
		Water Delivery	2	1	1	0	1	1	3	3	3	4
	BPS	Mechanization Systems and Secondary Structure										
	GLS	LED Growth Light ORU	8	7	122	137	137	274	274	411	411	411
ISRU (Crew System)	AP	Zeolite and Support Structure	4	2	2	3	3	3	3	3	4	4
		Compressor	5	4	4	4	6	5	6	7	7	8
		Cryocooler	3	1	1	1	1	2	1	1	2	2
	SP	Mixing Auger	2	1	1	1	0	1	1	1	1	1
		Feed Cone	2	1	1	1	0	1	1	1	1	1
		Hopper										
		Horizontal Feed Auger	2	1	1	1	0	1	1	1	1	1
		Condensing Heat Exchanger	2	1	0	1	0	1	1	0	1	1
		Oven Heater	3	1	1	1	2	1	1	2	1	2
	CO2 Injection System	Cryocooler	4	1	2	3	2	2	3	3	3	3
		Blower	3	2	2	1	2	2	2	3	2	3
		Valves	6	5	5	6	6	8	8	9	10	11
ISRU (Pre-Deployed)	AP	Zeolite and Support Structure	4	1	1	1	1	0	1	1	0	1
		Compressor 1 (Mars to 1atm)	5	2	2	1	2	1	1	1	1	1
		Cryocooler	3	0	1	0	1	0	0	1	0	0
	SP	Mixing Auger	2	1	0	0	1	0	0	0	0	1
		Feed Cone	2	1	0	0	1	0	0	0	0	1
		Horizontal Feed Auger										
		Condensing Heat Exchanger	2	1	0	0	1	0	0	0	0	1
		Oven Heater	2	0	1	0	0	0	0	1	0	0
	OGA	Hydrogen Sensor	20	12	10	10	10	9	9	9	9	9
		Inlet Deionizing Bed	8	4	3	3	3	2	2	3	2	2
		Nitrogen Purge ORU	13	6	5	5	5	5	4	5	4	4
		Oxygen Outlet	15	8	7	7	7	6	6	6	6	6
		Power Supply Module	24	14	13	13	12	12	12	11	11	12
		Process Controller	15	8	6	7	6	6	6	6	5	6
		Pump	12	6	6	4	5	5	4	4	4	5
Crew Systems	EVA	Battery	34	70	104	140	176	210	246	280	316	352

I.6.2 Stored Food (SF) Architecture Spare Parts Requirements

Tabulated below are results of the sparing analysis for the first 10 crews for the stored food case, giving the number of spares delivered to the surface at each crewed mission for each component.

Group	Subgroup	Subassembly	Crew									
			1	**2**	**3**	**4**	**5**	**6**	**7**	**8**	**9**	**10**
ECLSS	OGA	Hydrogen Sensor	8	17	26	34	43	52	60	69	78	86
		Inlet Deionizing Bed	2	1	0	1	0	1	2	2	3	3
		Nitrogen Purge ORU	2	1	1	1	1	1	1	1	1	1
		Oxygen Outlet	3	1	1	1	1	1	1	2	1	2
		Power Supply Module	3	2	1	2	2	2	2	2	4	5
		Process Controller	2	2	1	1	1	1	1	2	1	1
		Pump	2	4	6	8	10	13	15	17	19	21
	CDRA	Air Pump Two-Stage ORU	3	1	2	1	2	2	2	1	3	2
		Blower	3	2	1	2	2	2	2	2	3	2
		Check Valves	5	4	4	4	5	6	6	7	7	8
		Desiccant Beds	5	3	4	4	4	5	5	6	6	7
		Heat Controller	3	2	2	1	2	2	2	3	2	3
		Precooler	3	2	1	2	2	2	2	2	3	2
		Pump Fan Motor Controller	2	0	1	0	1	0	1	0	1	0
		Selector Valves	7	5	5	7	7	9	10	10	12	12
		Sorbent Beds (Zeolite)	5	3	4	4	4	10	12	14	16	18
	CCAA (x6)	Condensing Heat Exchanger	3	2	1	2	2	1	2	3	2	2
		Electronic Interface Box (EIB)	3	1	1	2	1	1	2	2	1	2
		Fan Delta Pressure Sensor	3	1	1	1	2	1	2	1	2	2
		Heat Exchanger Liquid Sensor	4	1	2	2	3	2	3	3	3	3
		Inlet ORU	4	3	3	3	3	4	4	4	5	5
		Pressure Transducer	3	1	1	1	2	1	2	1	6	6
		Temperature Control Check Valve (TCCV)	19	22	28	35	42	48	56	63	69	76
		Temperature Sensor	2	0	1	0	0	1	0	1	0	1
		Water Separator	9	7	9	11	12	24	36	36	36	48
		Water Separator Liquid Sensor	4	1	2	2	3	2	3	3	3	3
	UPA	Distillation Assembly	2	1	3	4	5	6	7	8	9	10
		Firmware Controller Assembly	4	3	2	3	3	4	4	5	8	9
		Fluids Control and Pump Assembly	3	1	1	2	1	1	3	4	4	5
		Pressure Control and Pump Assembly	2	1	3	4	5	6	7	8	9	10
		Recycle Filter Tank Assembly	27	54	81	108	135	162	189	216	244	271
		Separator Plumbing Assembly	2	4	6	8	10	13	15	17	19	21
	WPA	Catalytic Reactor	3	1	1	1	4	5	6	7	8	9
		Gas Separator	2	4	6	8	10	13	15	17	19	21
		Ion Exchange Bed	13	27	40	54	67	81	94	108	122	135
		Microbial Check Valve	2	4	6	8	10	13	15	17	19	21
		Multifiltration Bed #1	6	12	18	24	30	36	42	48	54	60
		Multifiltration Bed #2	6	12	18	24	30	36	42	48	54	60
		Particulate Filter	9	19	29	39	49	59	69	78	88	98
		pH Adjuster	2	4	6	8	10	13	15	17	19	21
		Process Controller	2	1	0	1	0	1	1	0	2	2
		Pump Separator	2	1	3	4	5	6	7	8	9	10
		Reactor Health Sensor	2	4	6	8	10	13	15	17	19	21
		Sensor	2	0	1	0	1	0	1	0	1	1
		Separator Filter	2	5	7	10	12	15	18	20	23	25
		Start-up Filter	1	1	0	1	0	1	0	0	1	0
		Water Delivery	2	1	1	0	1	1	3	3	3	4
	CRS	Sabatier Methanation Reactor	3	2	1	2	2	2	2	2	2	3
		Condensing Heat Exchanger	1	1	0	1	0	0	1	0	0	1
		Phase Separator	2	1	1	1	1	1	2	3	3	4
		Valves	5	3	3	3	4	5	4	6	5	11
		Sensors	2	1	1	1	1	1	1	1	1	1
		Controller	2	2	1	1	1	1	1	2	1	1
		Compressor	3	1	2	1	1	2	2	1	2	2
ISRU (Crew System)	AP	Zeolite and Support Structure	4	2	2	3	2	3	3	3	4	4
		Compressor	5	4	4	4	5	5	7	6	7	8
		Cryocooler	3	1	1	1	1	1	2	1	2	1
	SP	Mixing Auger	2	1	1	0	1	1	1	1	1	1
		Feed Cone	2	1	1	0	1	1	1	1	1	1
		Horizontal Feed Auger										
		Condensing Heat Exchanger	2	1	1	0	1	1	1	1	1	1
		Oven Heater	2	0	1	1	0	1	1	0	1	0

ISRU (Pre-Deployed)	AP	Zeolite and Support Structure	4	2	2	3	2	3	3	3	4	4
		Compressor 1 (Mars to 1atm)	5	4	4	4	5	5	7	6	7	8
		Cryocooler	3	1	1	1	1	1	2	1	2	1
	SP	Mixing Auger	2	1	0	0	0	1	0	0	0	0
		Feed Cone	2	1	0	0	0	1	0	0	0	0
		Hopper										
		Horizontal Feed Auger	2	1	0	0	0	1	0	0	0	0
		Condensing Heat Exchanger	2	0	0	1	0	0	0	0	1	0
		Oven Heater	3	0	1	0	1	0	0	0	1	0
Crew Systems	Food	5152kg Units of Thermostabilized Food	0	1	2	3	4	5	6	7	8	9
	EVA	Battery	34	70	104	140	176	210	246	280	316	352

Appendix J

Case Study 2: Return Trip Mission Scenarios – Catalog of Results

This appendix summarizes the results obtained for the "String of Sorties" and "Minimum Continuous Presence" mission scenarios investigated in Chapter 6. Here, integrated ECLS and ISRU flowsheets are first presented for each of the nine different architectures evaluated. Following this, master equipment lists developed for each architecture case are presented, along with their individual component data. Finally, tables summarizing the spare parts requirements of each architecture case over the "String of Sorties" and "Minimum Continuous Presence" campaigns are provided. This data is summarized in the following subsections.

J.1 ECLS Architecture Case Flowsheets

Cataloged below are flowsheets of the five ECLS architecture cases explored in this case study.

J.1.1 Architecture Case 1

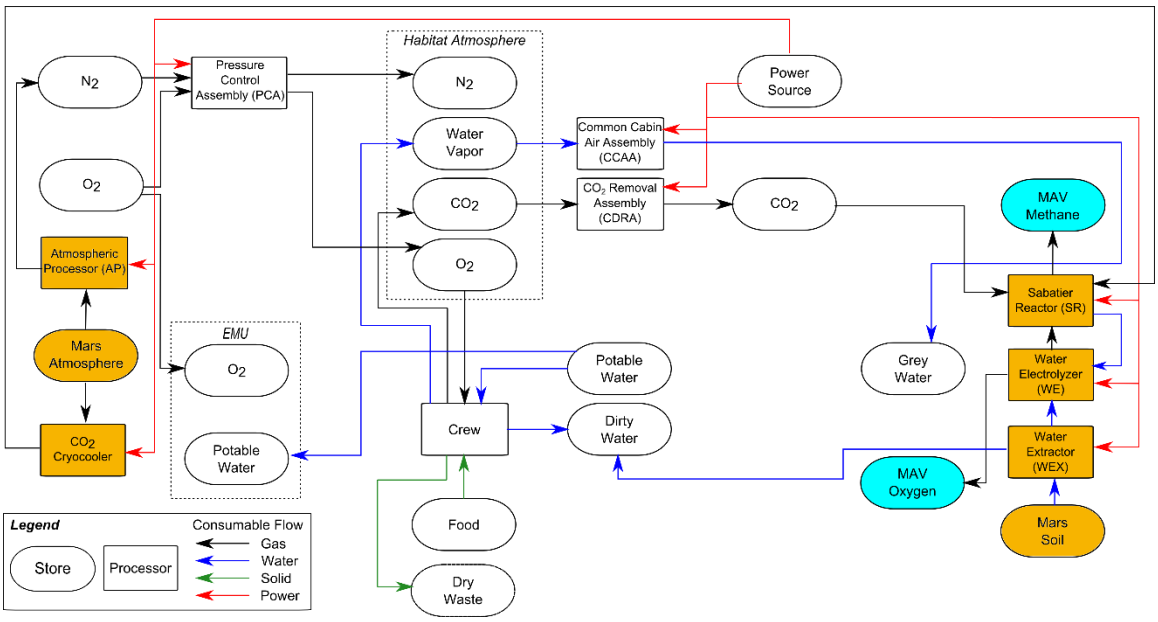

Figure J-1: ECLS Architecture Case 1, consisting of a completely open loop oxygen and water supply (ECLS Elements in White, ISRU Elements in Orange, MAV Propellant Tanks in Blue).

J.1.2 Architecture Case 2

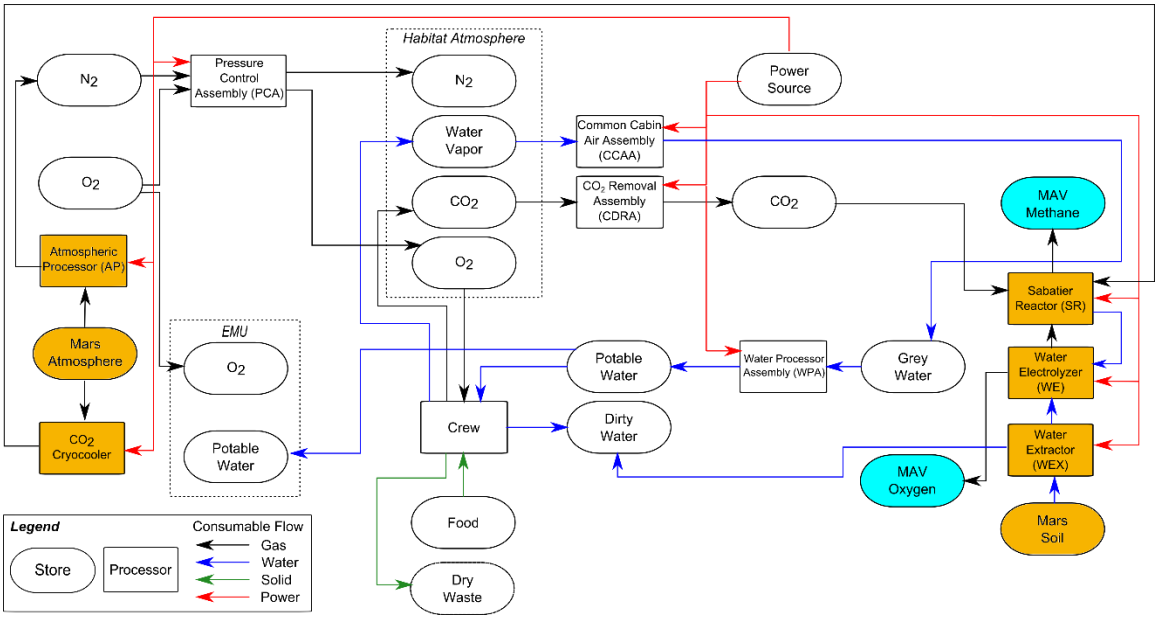

Figure J-2: ECLS Architecture Case 2, consisting of a CDRA, CCAA, and WPA. Here, all dirty water is either stored in dirty water tanks or vented overboard (ECLS Elements in White, ISRU Elements in Orange, MAV Propellant Tanks in Blue).

J.1.3 Architecture Case 3

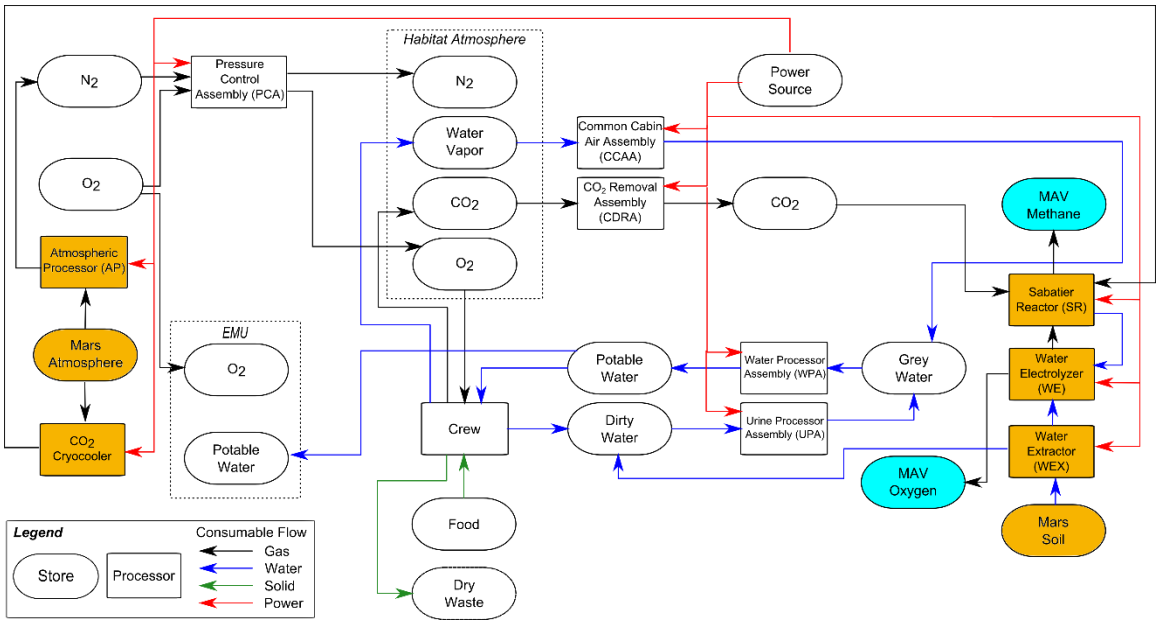

Figure J-3: ECLS Architecture Case 3, consisting of a CDRA, CCAA, WPA, and UPA (ECLS Elements in White, ISRU Elements in Orange, MAV Propellant Tanks in Blue).

J.1.4 Architecture Case 4

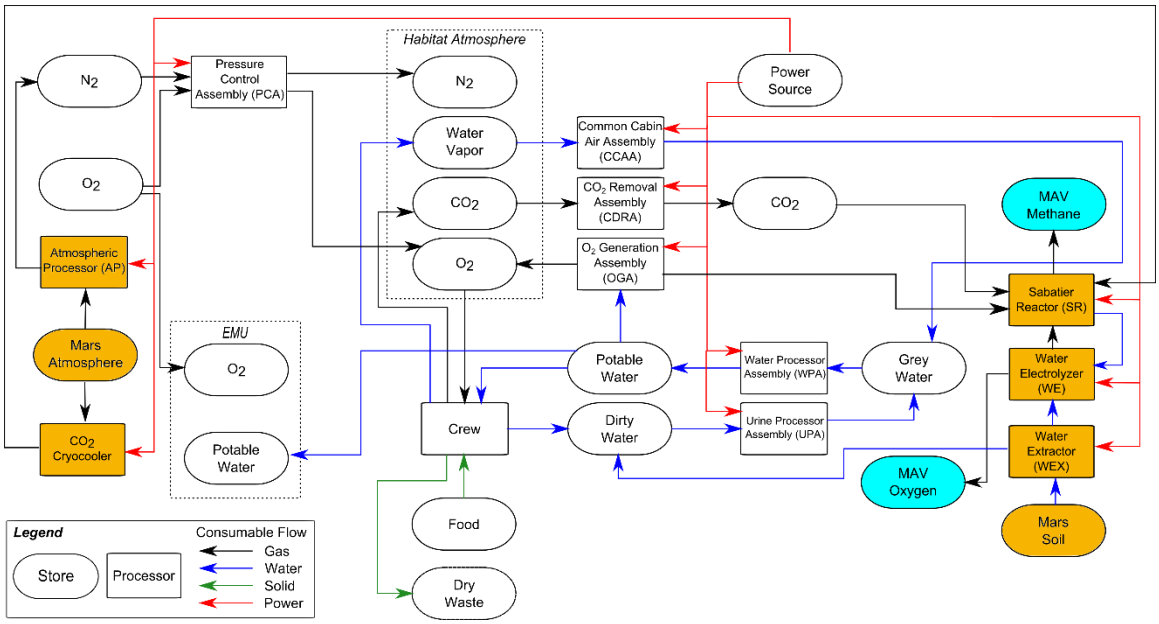

Figure J-4: ECLS Architecture Case 4, consisting of a CDRA, CCAA, WPA, UPA, and OGA (ECLS Elements in White, ISRU Elements in Orange, MAV Propellant Tanks in Blue).

J.1.5 Architecture Case 5

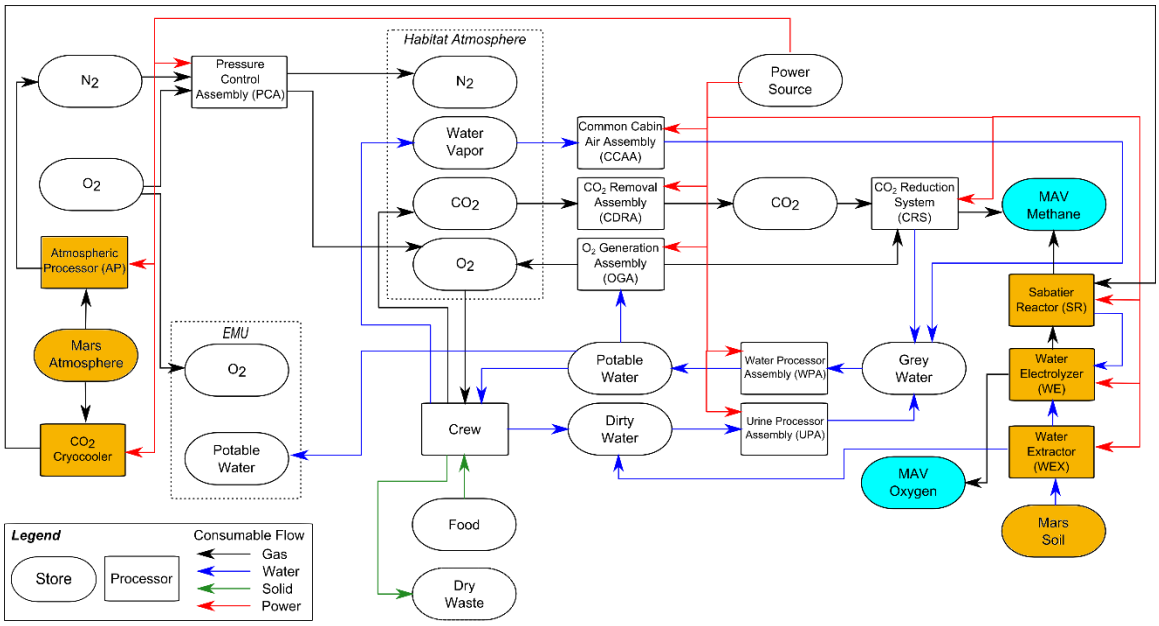

Figure J-5: ECLS Architecture Case 5, based on the ISS ECLS Architecture supplemented with ISRU (ECLS Elements in White, ISRU Elements in Orange, MAV Propellant Tanks in Blue).

J.1.6 Architecture Case 6

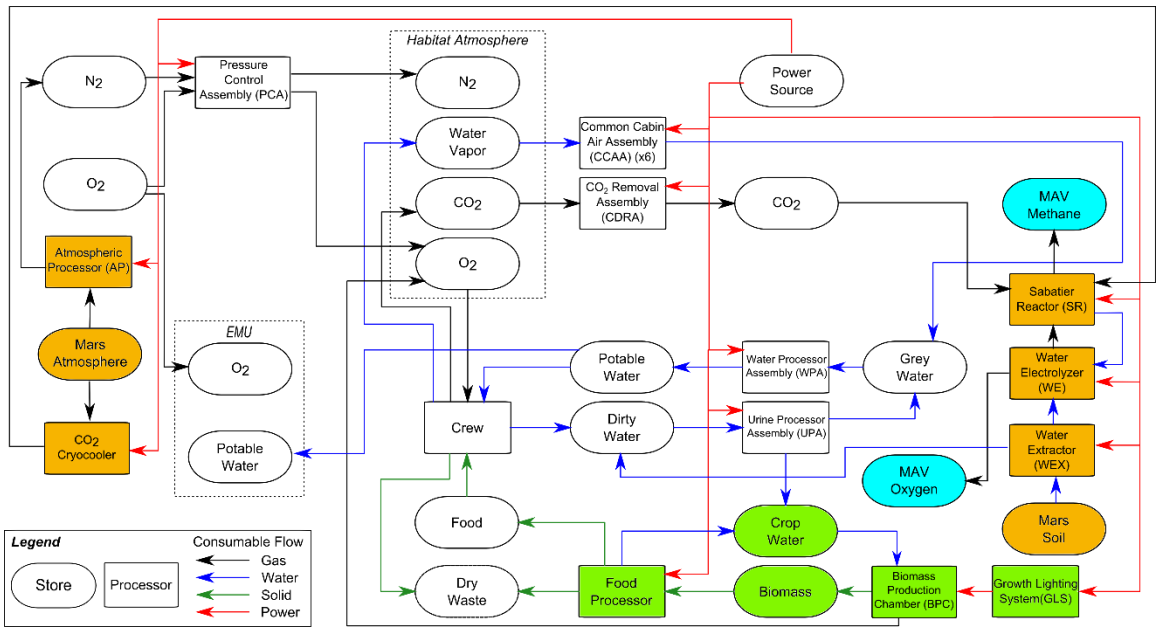

Figure J-6: ECLS Architecture Case 6, consisting of a Biomass Production Chamber with a food production level of 4.5% of the total caloric needs of the crew. This system is supplemented by a growth lighting system, and ISRU-derived water. All crop CO_2 demand is derived from crew CO_2 expiration. ECLS water is recycled with a WPA and a UPA (ECLS Elements in White, ISRU Elements in Orange, MAV Propellant Tanks in Blue, BPC Elements in Green).

J.1.7 Architecture Case 7

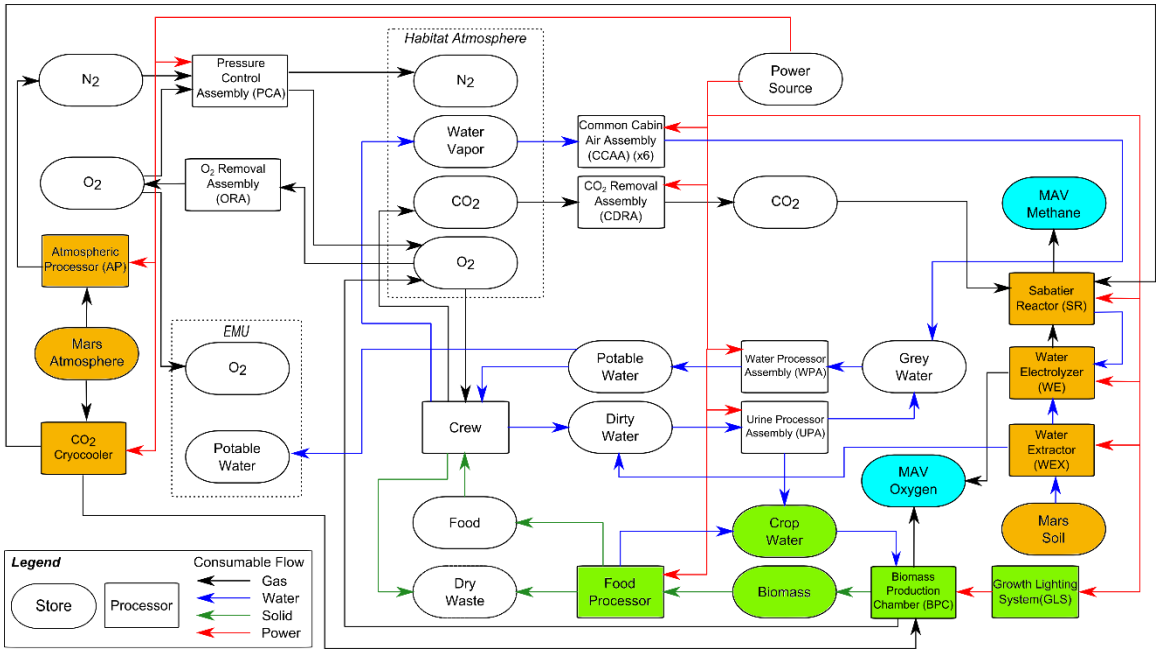

Figure J-7: ECLS Architecture Case 7, consisting of a Biomass Production Chamber (BPC) with a food production level of 50% of the total caloric needs of the crew. Here, additional CO_2 is injected into the BPC to support crop growth. Resulting oxygen is removed with an Oxygen Removal Assembly (ORA) and directed to both EVA and MAV oxygen tanks. ECLS water is recycled with a WPA and a UPA (ECLS Elements in White, ISRU Elements in Orange, MAV Propellant Tanks in Blue, BPC Elements in Green).

J.1.8 Architecture Case 8

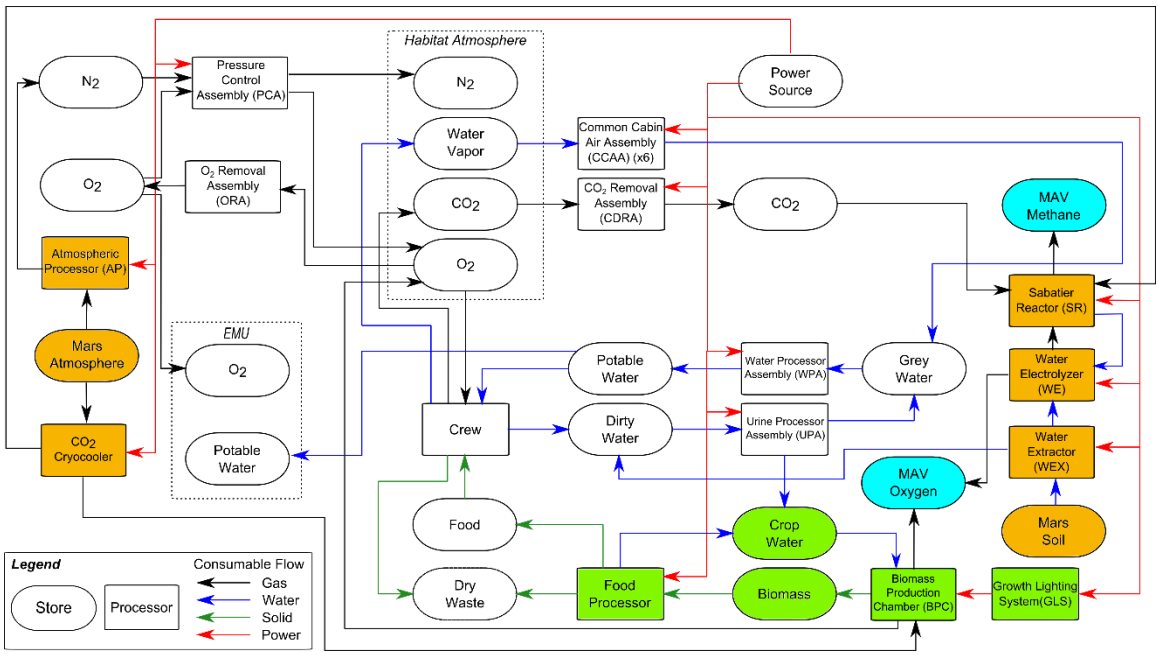

Figure J-8: ECLS Architecture Case 8. This is the same architecture as Case 7 with the exception that the BPC is sized to produce 100% of the crew's caloric needs (ECLS Elements in White, ISRU Elements in Orange, MAV Propellant Tanks in Blue, BPC Elements in Green).

J.1.9 Architecture Case 9

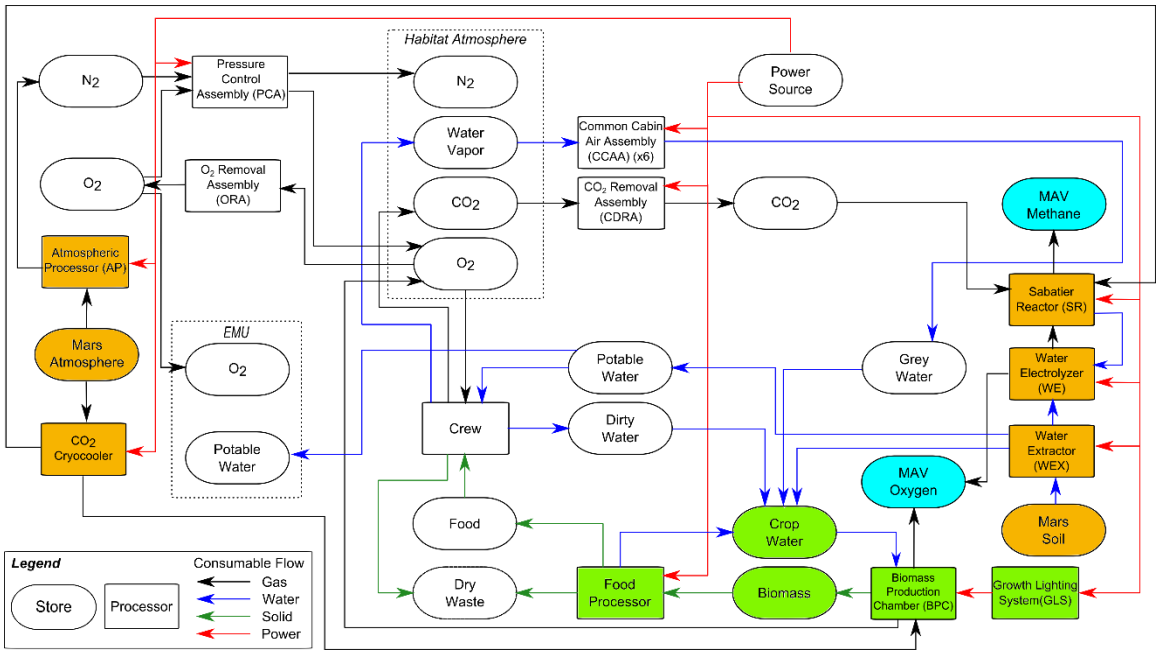

Figure J-9: ECLS Architecture Case 9, examined only for the Minimum Continuous Presence mission scenario. This architecture is based on a combination of Cases 1 and 8, where a 100% food production level BPC is supported entirely with ISRU-derived resources (ECLS Elements in White, ISRU Elements in Orange, MAV Propellant Tanks in Blue, BPC Elements in Green).

J.2 String of Sorties Mission Scenario Analysis - Master Equipment Lists and Component Data for each ECLS Architecture Case

Cataloged below are the complete master equipment lists (MELs) derived for each of the eight ECLS architecture cases explored in the String of Sorties mission scenario analysis. For each architecture case, a MEL is presented with the mass, volume, meantime between failures (MTBF), and life limit (LL) of each element within the architecture. Unless otherwise noted, values are taken from the NASA Baseline Values and Assumptions Document (BVAD) [209]. Assumptions and use of analogy to other components for data are indicated and described with endnotes. In addition, spare parts requirements predicted by the HabNet Supportability Module for each architecture case over the ten missions of the campaign are also listed, under both nominal ISRU reliability levels, and reliability levels that have been degraded by an order of magnitude. This latter set of data corresponds to the sensitivity analyses performed in Section

6.4.5. For this case study, the spare parts requirements are calculated such that the probability of having sufficient spare parts is 0.999.

J.2.1 Architecture Case 1

Table J.1: Architecture Case 1 Master Equipment List, containing component mass, volume and reliability data, as well as run times and power demands. Power is listed here on a per unit basis. ISRU technologies displayed here were sized by the HabNet ISRU Module.

Sys.	Assembly	Subassembly	Mass [kg]	Vol. [m^3]	MTBF [h]	Run Time [h]	LL [y]	# in Pmry.	Power [kW]
ECLS	CDRA	Air Pump Two-Stage ORU	10.89	0.0045	156200.0	12960	15.29	1	0.860
		Blower	5.58	0.0300	129700.0	12960	10.00	1	
		Check Valves	39.92	0.1784	32900.0[i]	12960		1	
		Desiccant Beds	42.64	0.0850	77100.0	12960		2	
		Heat Controller	3.31	0.0085	242700.0	12960		2	
		Precooler	5.58	0.0255	129700.0	12960	10.00	1	
		Pump Fan Motor Controller	2.72	0.0057	2270000.0	12960		2	
		Selector Valves	3.04	0.0017	117000.0	12960	10.61	6	
		Sorbent Beds (Zeolite)	42.64	0.0850	77100.0	12960		2	
	CCAA (x4)	Condensing Heat Exchanger	49.71	0.3933	832600.0	12960		4	0.532
		Electronic Interface Box (EIB)	4.04	0.0173	2350000.0	12960		8	
		Fan Delta Pressure Sensor	0.45	0.0002	1250000.0	12960		4	
		Heat Exchanger Liquid Sensor	0.64	0.0006	1140000.0	12960		8	
		Inlet ORU	25.31	0.1308	333000.0	12960		4	
		Pressure Transducer	0.48	0.0000	1250000.0	12960	15.00	4	
		Temperature Control Check Valve (TCCV)	7.45	0.0071	32900.0	12960		8	
		Temperature Sensor	0.26	0.0014	37600000.0	12960		16	
		Water Separator	11.93	0.0583	131000.0	12960	5.00	8	
		Water Separator Liquid Sensor	0.64	0.0006	1140000.0[ii]	12960		8	
ISRU	Water Extractor	Oven + Insulating Cone	78.05	3.3808	242700[iii]	12960		1	21.90
		Hopper	58.56	3.9420		12960		1	
		Sieve	36.52	0.0000	500000[iv]	12960		1	
		Augers (vertical)	200.07	0.0000	500000[iv]	12960		1	0.053
		Horizontal Auger	11.38	0.1463	500000[iv]	12960		1	
		Sweep Gas System	0.02	0.0000	138408[v]	12960		1	
		Sweep Gas Piping	6.03	0.1186		12960		1	
		Condensing Heat Exchanger	37.81	0.8551	832600[vi]	12960		1	
		Water Filtration System	2.18	0.0082	296701.2[vii]	12960	0.36	1	
	CO2 Cryocooler	Cryocooler	34.61	0.0726	500000[iv]	12960		2	1.474
		Container	83.02	0.4906		12960		1	
	Water Electrolyzer	Electrolysis Cell Stack	47.43	0.0045	27156[viii]	12960	2.38	1	12.28
		O2 Separator / Water Reservoir	5.71	0.0119	27156[viii]	12960	2.38	1	
		H2 Separator and Dryer	14.44	0.0040	98112[ix]	12960	10	1	
		Water Pump	2.16	0.0007	144540[x]	12960	1	1	8×10^{-5}
	Sabatier Reactor	Reactor	20.78	0.4181	50000[xi]	12960		1	0.198
		Water / Methane Separator	0.24	0.0097	131000[xii]	12960		1	
		Heat Exchanger	0.53	0.0000	832600[xiii]	12960		1	
	Atmospheric Processor	Zeolite	0.53	0.0064	77100[xiv]	12960		1	
		Compressor	8.04	0.0465	66666.7	12960		2	0.733
		Cryocoolers	3.10	0.0015	500000[iv]	12960		2	0.480
		Support Structure	3.45			12960		1	

[i] Analogy to CCAA TCCV
[ii] Analogy to CCAA Heat Exchanger Liquid Sensor
[iii] Analogy to CDRA Heater Controller
[iv] Optimistic assumption; no data were available
[v] Analogy to OGA Nitrogen Purge ORU
[ix] Analogy to OGA Oxygen Outlet
[x] Analogy to OGA Pump
[xi] Analogy to CRS Sabatier Methanation Reactor
[xii] Analogy to CRS Phase Separator
[xiii] Analogy to CRS Condensing Heat Exchanger

[vi]Analogy CCAA Condensing Heat Exchanger
[vii]Analogy to WPA Multifiltration Bed
[viii]Analogy to OGA Hydrogen ORU (contains Electrolysis Cell Stack and Rotary Separator / Accumulator)
[xiv]Analogy to CDRA Dessicant-Adsorbent Bed
[xv]Analogy to CRS Compressor

Table J.2: Architecture Case 1 Spare Parts Requirements for each Component over a 10 Mission String of Sorties Campaign. Empty rows correspond to components assumed to have 100% reliability, and hence do not require spare parts

Group	Assembly	Subassembly	Mission									
			1	2	3	4	5	6	7	8	9	10
ECLSS	CDRA	Air Pump Two-Stage ORU	3	0	1	1	0	0	1	0	0	0
		Blower	3	1	0	1	1	0	0	0	1	0
		Check Valves	4	1	2	1	1	1	0	1	1	1
		Desiccant Beds	4	1	1	1	1	1	0	1	1	1
		Heat Controller	3	1	1	1	0	1	0	0	0	1
		Precooler	3	1	0	1	1	0	0	0	1	0
		Pump Fan Motor Controller	2	0	0	1	0	0	0	0	0	0
		Selector Valves	6	3	1	2	1	2	1	1	2	1
		Sorbent Beds (Zeolite)	4	1	1	1	1	1	1	0	1	1
	CCAA	Condensing Heat Exchanger	2	1	0	0	1	0	0	1	0	0
		Electronic Interface Box (EIB)	2	1	0	1	0	1	0	0	0	0
		Fan Delta Pressure Sensor	3	1	0	0	1	0	0	0	1	0
		Heat Exchanger Liquid Sensor	3	1	1	1	0	1	0	0	0	1
		Inlet ORU	3	1	0	1	1	1	0	0	1	0
		Pressure Transducer	3	1	0	0	1	0	0	0	1	0
		Temperature Control Check Valve (TCCV)	12	6	5	7	4	5	4	4	5	4
		Temperature Sensor	2	1	0	0	0	0	0	0	0	0
		Water Separator	6	2	2	2	2	2	1	1	2	1
		Water Separator Liquid Sensor	3	1	1	1	0	0	1	0	1	0
ISRU	Water Extractor	Oven + Insulating Cone	2	0	1	0	0	1	0	0	0	0
		Hopper										
		Sieve	2	0	0	1	0	0	0	0	0	1
		Augers (vertical)	1	1	0	0	0	0	1	0	0	0
		Horizontal Auger	2	0	1	0	0	0	1	0	0	0
		Sweep Gas System	4	2	0	0	0	1	0	0	1	1
		Sweep Gas Piping										
		Condensing Heat Exchanger	1	1	0	0	0	1	0	0	0	0
		Water Filtration System	4	4	4	4	4	4	4	4	4	5
	CO2 Cryocooler	Cryocooler	2	0	1	0	1	0	0	0	1	0
		Container										
	Water Electrolyzer	Electrolysis Cell Stack	4	2	1	1	2	1	0	2	0	1
		O2 Separator / Water Reservoir	5	2	1	2	1	1	1	1	1	1
		H2 Separator and Dryer	3	1	0	1	1	0	0	1	0	1
		Water Pump	3	1	0	1	2	1	2	1	2	1
	Sabatier Reactor	Reactor	4	1	1	1	0	1	1	0	1	1
		Water / Methane Separator	4	1	0	1	0	1	0	0	2	0
		Heat Exchanger	2	1	0	0	0	1	0	0	0	0
	Atmospheric Processor	Zeolite	4	1	1	1	1	0	1	0	1	0
		Compressor	4	2	1	2	1	1	0	1	1	1
		Cryocoolers	2	1	1	0	0	1	0	0	0	1
		Support Structure										

Table J.3: Architecture Case 1 Spare Parts Requirements for each Component over a 10 Mission String of Sorties Campaign with all ISRU technologies at 10% of their originally estimated values. Empty rows correspond to components assumed to have 100% reliability, and hence do not require spare parts

Group	Assembly	Subassembly	Mission									
			1	2	3	4	5	6	7	8	9	10
ECLSS	CDRA	Air Pump Two-Stage ORU	3	0	1	1	0	0	1	0	0	1
		Blower	3	1	0	1	1	0	0	1	0	1
		Check Valves	4	2	1	1	1	1	1	1	0	1
		Desiccant Beds	4	1	1	1	1	1	1	1	0	1
		Heat Controller	3	1	1	0	1	1	0	0	1	0

		Precooler	3	1	0	1	1	0	0	1	0	1
		Pump Fan Motor Controller	2	0	0	1	0	0	0	0	0	1
		Selector Valves	6	2	2	2	2	1	1	2	1	2
		Sorbent Beds (Zeolite)	4	1	1	1	1	1	1	1	0	1
	CCAA	Condensing Heat Exchanger	2	1	0	1	0	0	0	1	0	0
		Electronic Interface Box (EIB)	2	1	1	0	0	1	0	0	0	1
		Fan Delta Pressure Sensor	3	0	1	1	0	0	0	1	0	0
		Heat Exchanger Liquid Sensor	4	0	1	1	0	1	0	0	1	0
		Inlet ORU	3	1	1	0	1	0	1	1	0	1
		Pressure Transducer	3	0	1	0	1	0	0	1	0	0
		Temperature Control Check Valve (TCCV)	12	6	6	5	6	4	4	5	5	4
		Temperature Sensor	2	0	0	1	0	0	0	0	0	1
		Water Separator	6	2	3	1	3	1	1	2	1	2
		Water Separator Liquid Sensor	4	0	1	1	0	1	0	1	0	0
ISRU	Water Extractor	Oven + Insulating Cone	4	2	2	1	1	1	1	1	1	1
		Hopper										
		Sieve	4	1	1	0	1	1	1	0	1	1
		Augers (vertical)	3	1	1	1	0	1	1	0	1	0
		Horizontal Auger	4	1	1	1	1	1	0	1	1	1
		Sweep Gas System	9	2	3	3	2	1	3	1	3	3
		Sweep Gas Piping										
		Condensing Heat Exchanger	3	1	0	1	1	0	1	0	1	0
		Water Filtration System	5	3	4	4	4	4	4	4	4	5
	CO2 Cryocooler	Cryocooler	5	1	2	1	2	1	0	2	1	1
		Container										
	Water Electrolyzer	Electrolysis Cell Stack	14	8	7	7	7	6	6	6	6	7
		O2 Separator / Water Reservoir	15	9	8	7	7	6	6	8	5	8
		H2 Separator and Dryer	7	4	3	2	3	2	2	2	2	3
		Water Pump	7	3	2	3	2	1	1	3	1	2
	Sabatier Reactor	Reactor	10	6	4	4	5	3	4	4	4	4
		Water / Methane Separator	9	2	3	3	3	1	2	2	2	2
		Heat Exchanger	4	1	1	1	1	0	1	1	0	1
	Atmospheric Processor	Zeolite	10	4	4	4	3	3	3	3	3	2
		Compressor	14	7	6	6	7	5	5	6	5	5
		Cryocoolers	5	3	1	2	1	1	1	2	1	1
		Support Structure										

J.2.2 Architecture Case 2

Table J.4: Architecture Case 2 Master Equipment List, containing component mass, volume and reliability data, as well as run times and power demands. Power is listed here on a per unit basis. ISRU technologies displayed here were sized by the HabNet ISRU Module.

Sys.	Assembly	Subassembly	Mass [kg]	Vol. [m^3]	MTBF [h]	Run Time [h]	LL [y]	# in Pmry.	Power [kW]
ECLS	CDRA	Air Pump Two-Stage ORU	10.89	0.0045	156200.0	12960	15.29	1	0.860
		Blower	5.58	0.0300	129700.0	12960	10.00	1	
		Check Valves	39.92	0.1784	32900.0[i]	12960		1	
		Desiccant Beds	42.64	0.0850	77100.0	12960		2	
		Heat Controller	3.31	0.0085	242700.0	12960		2	
		Precooler	5.58	0.0255	129700.0	12960	10.00	1	
		Pump Fan Motor Controller	2.72	0.0057	2270000.0	12960		2	
		Selector Valves	3.04	0.0017	117000.0	12960	10.61	6	
		Sorbent Beds (Zeolite)	42.64	0.0850	77100.0	12960		2	
	CCAA (x4)	Condensing Heat Exchanger	49.71	0.3933	832600.0	12960		4	0.532
		Electronic Interface Box (EIB)	4.04	0.0173	2350000.0	12960		8	
		Fan Delta Pressure Sensor	0.45	0.0002	1250000.0	12960		4	
		Heat Exchanger Liquid Sensor	0.64	0.0006	1140000.0	12960		8	
		Inlet ORU	25.31	0.1308	333000.0	12960		4	
		Pressure Transducer	0.48	0.0000	1250000.0	12960	15.00	4	
		Temperature Control Check Valve (TCCV)	7.45	0.0071	32900.0	12960		8	
		Temperature Sensor	0.26	0.0014	37600000.0	12960		16	

		Water Separator	11.93	0.0583	131000.0	12960	5.00	8	
		Water Separator Liquid Sensor	0.64	0.0006	1140000.0[ii]	12960		8	
	WPA	Catalytic Reactor	67.04	0.1156	25579.2	848	2.25	1	0.320
		Gas Separator	39.15	0.0660	84008.4	848	1	1	
		Ion Exchange Bed	13.02	0.0173	296701.2	848	0.16	1	
		Microbial Check Valve	5.76	0.0065	143488.8	848	1	1	
		Multifiltration Bed #1	149.23	0.0657	296701.2	848	0.36	1	
		Multifiltration Bed #2	149.23	0.0657	296701.2	848	0.36	1	
		Particulate Filter	32.25	0.0717	717356.4	848	0.22	1	
		pH Adjuster	2.54	0.0026	137181.6	848	1	1	
		Process Controller	45.00	0.0838	87950.4	848	7.72	1	
		Pump Separator	31.34	0.0869	42398.4	848	2	1	
		Reactor Health Sensor	16.83	0.0425	56677.2	848	1	1	
		Sensor	4.81	0.0034	143664	848	10	1	
		Separator Filter	7.67	0.0102	359072.4	848	0.84	1	
		Start-up Filter	9.44	0.0184	226884	848	19.92	1	
		Water Delivery	47.54	0.0974	64561.2	848	5	1	
ISRU	Water Extractor	Oven + Insulating Cone	63.20	2.7378	242700[iii]	12960		1	17.74
		Hopper	51.13	3.1923		12960		1	
		Sieve	26.61	0.0000	500000[iv]	12960		1	
		Augers (vertical)	162.02	0.0000	500000[iv]	12960		1	0.047
		Horizontal Auger	10.24	0.1316	500000[iv]	12960		1	
		Sweep Gas System	0.01	0.0000	138408[v]	12960		1	
		Sweep Gas Piping	5.06	0.0900		12960		1	
		Condensing Heat Exchanger	30.71	0.6293	832600[vi]	12960		1	
		Water Filtration System	1.77	0.0066	296701.2[vii]	12960	0.36	1	
	CO2 Cryocooler	Cryocooler	34.61	0.0726	500000[iv]	12960		2	1.474
		Container	83.02	0.4906		12960		1	
	Water Electrolyzer	Electrolysis Cell Stack	47.43	0.0045	27156[viii]	12960	2.38	1	12.28
		O2 Separator / Water Reservoir	5.71	0.0119	27156[viii]	12960	2.38	1	
		H2 Separator and Dryer	14.44	0.0040	98112[ix]	12960	10	1	
		Water Pump	2.16	0.0007	144540[x]	12960	1	1	8×10^{-5}
	Sabatier Reactor	Reactor	20.78	0.4181	50000[xi]	12960		1	0.198
		Water / Methane Separator	0.24	0.0097	131000[xii]	12960		1	
		Heat Exchanger	0.53	0.0000	832600[xiii]	12960		1	
	Atmospheric Processor	Zeolite	0.53	0.0064	77100[xiv]	12960		1	
		Compressor	8.04	0.0465	66666.7	12960		2	0.733
		Cryocoolers	3.10	0.0015	500000[iv]	12960		2	0.480
		Support Structure	3.45			12960		1	

[i] Analogy to CCAA TCCV
[ii] Analogy to CCAA Heat Exchanger Liquid Sensor
[iii] Analogy to CDRA Heater Controller
[iv] Optimistic assumption; no data were available
[v] Analogy to OGA Nitrogen Purge ORU
[vi] Analogy CCAA Condensing Heat Exchanger
[vii] Analogy to WPA Multifiltration Bed
[viii] Analogy to OGA Hydrogen ORU (contains Electrolysis Cell Stack and Rotary Separator / Accumulator)
[ix] Analogy to OGA Oxygen Outlet
[x] Analogy to OGA Pump
[xi] Analogy to CRS Sabatier Methanation Reactor
[xii] Analogy to CRS Phase Separator
[xiii] Analogy to CRS Condensing Heat Exchanger
[xiv] Analogy to CDRA Dessicant-Adsorbent Bed
[xv] Analogy to CRS Compressor

Table J.5: Architecture Case 2 Spare Parts Requirements for each Component over a 10 Mission String of Sorties Campaign. Empty rows correspond to components assumed to have 100% reliability, and hence do not require spare parts

Group	Assembly	Subassembly	Mission									
			1	**2**	**3**	**4**	**5**	**6**	**7**	**8**	**9**	**10**
ECLSS	CDRA	Air Pump Two-Stage ORU	3	0	1	1	0	0	1	0	0	0
		Blower	3	1	0	1	1	0	1	0	0	0
		Check Valves	4	1	2	1	1	1	1	0	1	1
		Desiccant Beds	4	1	1	1	1	1	1	0	1	1
		Heat Controller	3	1	1	0	1	1	0	0	0	0

		Precooler	3	1	0	1	1	0	1	0	0	0
		Pump Fan Motor Controller	2	0	0	1	0	0	0	0	0	1
		Selector Valves	6	2	2	2	2	1	2	1	0	2
		Sorbent Beds (Zeolite)	4	1	1	1	1	1	1	0	1	1
	CCAA	Condensing Heat Exchanger	2	1	0	1	0	0	1	0	0	0
		Electronic Interface Box (EIB)	3	0	0	1	0	1	0	0	0	0
		Fan Delta Pressure Sensor	3	0	1	0	1	0	1	0	0	0
		Heat Exchanger Liquid Sensor	3	1	1	0	1	1	0	1	0	0
		Inlet ORU	3	1	1	0	1	0	1	0	1	0
		Pressure Transducer	3	0	1	0	1	0	1	0	0	0
		Temperature Control Check Valve (TCCV)	12	6	6	5	6	4	5	4	3	5
		Temperature Sensor	2	0	0	0	1	0	0	0	0	0
		Water Separator	6	2	2	2	2	2	1	1	2	1
		Water Separator Liquid Sensor	3	1	1	0	1	0	1	0	1	0
	WPA	Catalytic Reactor	2	0	0	1	0	0	0	1	0	0
		Gas Separator	1	1	0	0	0	0	0	0	1	0
		Ion Exchange Bed	1	0	0	1	1	0	1	0	1	1
		Microbial Check Valve	2	0	0	0	0	0	1	0	0	0
		Multifiltration Bed #1	1	0	0	0	0	0	0	1	0	0
		Multifiltration Bed #2	1	0	0	0	0	0	0	1	0	0
		Particulate Filter	1	0	0	0	1	0	1	0	0	1
		pH Adjuster	2	0	0	0	1	0	0	0	0	0
		Process Controller	1	1	0	0	0	0	0	0	0	1
		Pump Separator	2	0	0	1	0	0	0	0	0	0
		Reactor Health Sensor	2	0	0	0	1	0	0	0	0	0
		Sensor	2	0	0	0	0	0	1	0	0	0
		Separator Filter	1	0	1	0	0	0	0	0	0	0
		Start-up Filter	1	0	1	0	0	0	0	0	0	0
		Water Delivery	1	1	0	0	0	0	1	0	0	0
ISRU	Water Extractor	Oven + Insulating Cone	2	0	1	0	1	0	0	0	0	1
		Hopper										
		Sieve	2	0	1	0	0	0	1	0	0	0
		Augers (vertical)	1	1	0	0	0	1	0	0	0	0
		Horizontal Auger	2	0	1	0	0	1	0	0	0	0
		Sweep Gas System	4	1	1	0	1	1	0	1	0	0
		Sweep Gas Piping										
		Condensing Heat Exchanger	2	0	0	0	1	0	0	0	0	0
		Water Filtration System	4	4	4	4	4	4	4	4	4	5
	CO2 Cryocooler	Cryocooler	2	1	0	0	1	0	0	0	1	0
		Container										
	Water Electrolyzer	Electrolysis Cell Stack	4	2	1	2	1	1	1	1	1	0
		O2 Separator / Water Reservoir	5	2	2	1	2	0	2	0	1	1
		H2 Separator and Dryer	3	1	1	0	1	0	1	0	0	1
		Water Pump	3	1	1	0	2	1	2	1	2	1
	Sabatier Reactor	Reactor	4	1	1	1	1	0	1	1	0	0
		Water / Methane Separator	4	1	0	1	0	1	1	0	0	0
		Heat Exchanger	2	1	0	0	1	0	0	0	0	0
	Atmospheric Processor	Zeolite	4	1	1	1	1	0	1	1	0	0
		Compressor	5	1	2	1	1	1	1	1	0	1
		Cryocoolers	3	0	1	0	1	0	0	1	0	0
		Support Structure										

Table J.6: Architecture Case 2 Spare Parts Requirements for each Component over a 10 Mission String of Sorties Campaign with all ISRU technologies at 10% of their originally estimated values. Empty rows correspond to components assumed to have 100% reliability, and hence do not require spare parts

Group	**Assembly**	**Subassembly**	**Mission**									
			1	**2**	**3**	**4**	**5**	**6**	**7**	**8**	**9**	**10**
ECLSS	CDRA	Air Pump Two-Stage ORU	3	0	1	1	0	1	0	0	0	1
		Blower	3	1	1	0	1	0	1	0	0	1
		Check Valves	4	2	1	1	1	1	1	1	0	1
		Desiccant Beds	4	1	1	1	1	2	0	1	0	1
		Heat Controller	3	1	1	0	1	1	0	0	1	0
		Precooler	3	1	1	0	1	0	1	0	0	1

		Pump Fan Motor Controller	2	0	1	0	0	0	0	0	0	1
		Selector Valves	6	2	2	2	2	2	1	1	1	1
		Sorbent Beds (Zeolite)	4	1	1	1	1	1	1	1	0	1
	CCAA	Condensing Heat Exchanger	2	1	0	1	0	0	1	0	0	0
		Electronic Interface Box (EIB)	2	1	1	0	0	1	0	0	0	1
		Fan Delta Pressure Sensor	3	1	0	1	0	0	1	0	0	0
		Heat Exchanger Liquid Sensor	3	1	1	1	0	1	0	0	1	0
		Inlet ORU	3	1	1	1	0	1	0	1	0	0
		Pressure Transducer	3	1	0	0	1	0	0	1	0	0
		Temperature Control Check Valve (TCCV)	12	7	5	6	4	6	4	4	4	5
		Temperature Sensor	2	0	0	1	0	0	0	0	0	0
		Water Separator	6	3	2	1	2	2	1	2	1	1
		Water Separator Liquid Sensor	3	1	1	1	0	1	0	0	1	0
	WPA	Catalytic Reactor	2	0	1	0	0	0	1	0	0	0
		Gas Separator	1	1	0	0	0	0	1	0	0	0
		Ion Exchange Bed	1	0	1	0	1	0	1	0	1	1
		Microbial Check Valve	1	1	0	0	0	1	0	0	0	0
		Multifiltration Bed #1	1	0	0	0	0	0	0	1	0	0
		Multifiltration Bed #2	1	0	0	0	0	0	0	1	0	0
		Particulate Filter	1	0	0	0	1	0	1	0	0	1
		pH Adjuster	2	0	0	0	1	0	0	0	0	0
		Process Controller	1	1	0	0	0	0	0	0	1	0
		Pump Separator	2	0	0	1	0	0	0	0	0	1
		Reactor Health Sensor	2	0	0	1	0	0	0	0	0	0
		Sensor	1	1	0	0	0	1	0	0	0	0
		Separator Filter	1	0	1	0	0	0	0	0	0	0
		Start-up Filter	1	0	1	0	0	0	0	0	0	0
		Water Delivery	1	1	0	0	0	1	0	0	0	0
ISRU	Water Extractor	Oven + Insulating Cone	5	1	2	1	1	2	1	1	1	0
		Hopper										
		Sieve	4	1	1	1	1	1	0	1	0	1
		Augers (vertical)	3	1	1	1	1	0	1	0	1	1
		Horizontal Auger	4	1	1	1	1	1	1	0	1	0
		Sweep Gas System	8	4	2	3	2	2	2	1	3	3
		Sweep Gas Piping										
		Condensing Heat Exchanger	3	1	1	0	1	1	0	0	1	0
		Water Filtration System	5	3	4	4	4	4	4	4	4	5
	CO2 Cryocooler	Cryocooler	5	2	1	1	2	1	1	1	1	1
		Container										
	Water Electrolyzer	Electrolysis Cell Stack	14	8	7	7	7	7	6	5	6	6
		O2 Separator / Water Reservoir	16	8	8	7	6	8	7	5	6	6
		H2 Separator and Dryer	7	4	3	2	3	3	2	1	2	2
		Water Pump	7	3	2	2	2	3	1	1	2	2
	Sabatier Reactor	Reactor	10	6	4	5	4	4	4	3	4	3
		Water / Methane Separator	9	2	4	2	1	3	2	2	3	1
		Heat Exchanger	4	1	1	1	1	0	1	0	1	0
	Atmospheric Processor	Zeolite	10	5	3	4	2	4	3	3	2	3
		Compressor	14	7	6	7	5	7	5	4	6	5
		Cryocoolers	6	2	1	2	1	2	1	1	1	1
		Support Structure										

J.2.3 Architecture Case 3

Table J.7: Architecture Case 3 Master Equipment List, containing component mass, volume and reliability data, as well as run times and power demands. Power is listed here on a per unit basis. ISRU technologies displayed here were sized by the HabNet ISRU Module.

Sys.	Assembly	Subassembly	Mass [kg]	Vol. [m^3]	MTBF [h]	Run Time [h]	LL [y]	# in Pmry.	Power [kW]
ECLS	CDRA	Air Pump Two-Stage ORU	10.89	0.0045	156200.0	12960	15.29	1	0.860
		Blower	5.58	0.0300	129700.0	12960	10.00	1	
		Check Valves	39.92	0.1784	32900.0[i]	12960		1	

		Desiccant Beds	42.64	0.0850	77100.0	12960		2	
		Heat Controller	3.31	0.0085	242700.0	12960		2	
		Precooler	5.58	0.0255	129700.0	12960	10.00	1	
		Pump Fan Motor Controller	2.72	0.0057	2270000.0	12960		2	
		Selector Valves	3.04	0.0017	117000.0	12960	10.61	6	
		Sorbent Beds (Zeolite)	42.64	0.0850	77100.0	12960		2	
	CCAA (x4)	Condensing Heat Exchanger	49.71	0.3933	832600.0	12960		4	0.532
		Electronic Interface Box (EIB)	4.04	0.0173	2350000.0	12960		8	
		Fan Delta Pressure Sensor	0.45	0.0002	1250000.0	12960		4	
		Heat Exchanger Liquid Sensor	0.64	0.0006	1140000.0	12960		8	
		Inlet ORU	25.31	0.1308	333000.0	12960		4	
		Pressure Transducer	0.48	0.0000	1250000.0	12960	15.00	4	
		Temperature Control Check Valve (TCCV)	7.45	0.0071	32900.0	12960		8	
		Temperature Sensor	0.26	0.0014	37600000.0	12960		16	
		Water Separator	11.93	0.0583	131000.0	12960	5.00	8	
		Water Separator Liquid Sensor	0.64	0.0006	1140000.0[ii]	12960		8	
	WPA	Catalytic Reactor	67.04	0.1156	25579.2	1248	2.25	1	0.320
		Gas Separator	39.15	0.0660	84008.4	1248	1	1	
		Ion Exchange Bed	13.02	0.0173	296701.2	1248	0.16	1	
		Microbial Check Valve	5.76	0.0065	143488.8	1248	1	1	
		Multifiltration Bed #1	149.23	0.0657	296701.2	1248	0.36	1	
		Multifiltration Bed #2	149.23	0.0657	296701.2	1248	0.36	1	
		Particulate Filter	32.25	0.0717	717356.4	1248	0.22	1	
		pH Adjuster	2.54	0.0026	137181.6	1248	1	1	
		Process Controller	45.00	0.0838	87950.4	1248	7.72	1	
		Pump Separator	31.34	0.0869	42398.4	1248	2	1	
		Reactor Health Sensor	16.83	0.0425	56677.2	1248	1	1	
		Sensor	4.81	0.0034	143664	1248	10	1	
		Separator Filter	7.67	0.0102	359072.4	1248	0.84	1	
		Start-up Filter	9.44	0.0184	226884	1248	19.92	1	
		Water Delivery	47.54	0.0974	64561.2	1248	5	1	
	UPA	Distillation Assembly	92.76	0.1422	142525.2	4580	2	1	0.315
		Firmware Controller Assembly	23.09	0.0286	27331.2	4580	2.4	1	
		Fluids Control and Pump Assembly	47.58	0.0731	90140.4	4580	4	1	
		Pressure Control and Pump Assembly	49.08	0.1158	181507.2	4580	2	1	
		Advanced Recycle Filter Tank Assembly[xvi]	50.00	0.1011	199640.4	4580		1	
		Separator Plumbing Assembly	16.78	0.0229	384651.6	4580	1	1	
ISRU	Water Extractor	Oven + Insulating Cone	56.20	2.4345	242700[iii]	12960		1	15.77
		Hopper	47.46	2.8386		12960		1	
		Sieve	22.31	0.0000	500000[iv]	12960		1	
		Augers (vertical)	144.07	0.0000	500000[iv]	12960		1	0.045
		Horizontal Auger	9.66	0.1241	500000[iv]	12960		1	
		Sweep Gas System	0.01	0.0000	138408[v]	12960		1	
		Sweep Gas Piping	4.59	0.0772		12960		1	
		Condensing Heat Exchanger	27.34	0.5308	832600[vi]	12960		1	
		Water Filtration System	1.57	0.0059	296701.2[vii]	12960	0.36	1	
	CO2 Cryocooler	Cryocooler	34.61	0.0726	500000[iv]	12960		2	1.474
		Container	83.02	0.4906		12960		1	
	Water Electrolyzer	Electrolysis Cell Stack	47.43	0.0045	27156[viii]	12960	2.38	1	12.28
		O2 Separator / Water Reservoir	5.71	0.0119	27156[viii]	12960	2.38	1	
		H2 Separator and Dryer	14.44	0.0040	98112[ix]	12960	10	1	
		Water Pump	2.16	0.0007	144540[x]	12960	1	1	8×10^{-5}
	Sabatier Reactor	Reactor	20.78	0.4181	50000[xi]	12960		1	0.198
		Water / Methane Separator	0.24	0.0097	131000[xii]	12960		1	
		Heat Exchanger	0.53	0.0000	832600[xiii]	12960		1	
	Atmospheric Processor	Zeolite	0.53	0.0064	77100[xiv]	12960		1	
		Compressor	8.04	0.0465	66666.7	12960		2	0.733
		Cryocoolers	3.10	0.0015	500000[iv]	12960		2	0.480
		Support Structure	3.45			12960		1	

[i] Analogy to CCAA TCCV

[xi] Analogy to CRS Sabatier Methanation Reactor

[ii] Analogy to CCAA Heat Exchanger Liquid Sensor
[iii] Analogy to CDRA Heater Controller
[iv] Optimistic assumption; no data were available
[v] Analogy to OGA Nitrogen Purge ORU
[vi] Analogy CCAA Condensing Heat Exchanger
[vii] Analogy to WPA Multifiltration Bed
[viii] Analogy to OGA Hydrogen ORU (contains Electrolysis Cell Stack and Rotary Separator / Accumulator)
[ix] Analogy to OGA Oxygen Outlet
[x] Analogy to OGA Pump
[xii] Analogy to CRS Phase Separator
[xiii] Analogy to CRS Condensing Heat Exchanger
[xiv] Analogy to CDRA Dessicant-Adsorbent Bed
[xv] Analogy to CRS Compressor
[xvi] Mass is obtained from [300] and verified with calculations based on data from Link et al. [301]. All other data is assumed to be the same as the Recycle Filter Tank Assembly (RFTA) described in the NASA BVAD 2004 [209] – the original system from which the ARFTA was upgraded from. Here, the life limit of the ARFTA has been assumed to be zero, based on its development objective of facilitating the same function as the RFTA without the need for periodic replacement [301].

Table J.8: Architecture Case 3 Spare Parts Requirements for each Component over a 10 Mission String of Sorties Campaign. Empty rows correspond to components assumed to have 100% reliability, and hence do not require spare parts

Group	Assembly	Subassembly	Mission									
			1	**2**	**3**	**4**	**5**	**6**	**7**	**8**	**9**	**10**
ECLSS	CDRA	Air Pump Two-Stage ORU	3	0	1	1	0	0	0	1	0	1
		Blower	3	1	0	1	1	0	0	1	0	0
		Check Valves	4	2	1	1	1	1	1	1	0	1
		Desiccant Beds	4	1	2	1	0	1	1	1	0	1
		Heat Controller	3	1	1	0	1	0	1	0	1	0
		Precooler	3	1	1	0	1	0	0	1	0	1
		Pump Fan Motor Controller	2	0	0	1	0	0	0	0	1	0
		Selector Valves	6	2	2	2	2	1	1	2	1	2
		Sorbent Beds (Zeolite)	4	1	1	2	0	1	1	1	0	1
	CCAA	Condensing Heat Exchanger	2	1	0	1	0	0	0	1	0	0
		Electronic Interface Box (EIB)	3	0	0	1	0	1	0	0	0	1
		Fan Delta Pressure Sensor	3	1	0	0	1	0	0	1	0	0
		Heat Exchanger Liquid Sensor	3	1	1	1	0	0	1	1	0	0
		Inlet ORU	3	1	1	1	0	0	1	0	1	0
		Pressure Transducer	3	1	0	0	1	0	0	1	0	0
		Temperature Control Check Valve (TCCV)	13	6	5	6	5	3	4	5	5	5
		Temperature Sensor	2	0	0	1	0	0	0	0	0	0
		Water Separator	6	3	2	2	1	1	2	2	1	1
		Water Separator Liquid Sensor	4	0	1	1	0	0	0	2	0	0
	WPA	Catalytic Reactor	2	0	1	0	1	0	0	0	0	1
		Gas Separator	2	0	0	0	1	0	0	0	0	0
		Ion Exchange Bed	1	1	0	1	1	1	1	1	1	0
		Microbial Check Valve	2	0	0	0	1	0	0	0	0	0
		Multifiltration Bed #1	1	0	0	0	0	1	0	1	0	0
		Multifiltration Bed #2	1	0	0	0	0	1	0	1	0	0
		Particulate Filter	1	0	0	1	1	0	1	1	0	1
		pH Adjuster	2	0	0	1	0	0	0	0	0	0
		Process Controller	1	1	0	0	0	0	1	0	0	0
		Pump Separator	2	0	1	0	0	0	0	1	0	0
		Reactor Health Sensor	2	0	1	0	0	0	0	0	1	0
		Sensor	2	0	0	0	1	0	0	0	0	0
		Separator Filter	1	1	0	0	0	0	0	0	0	0
		Start-up Filter	1	1	0	0	0	0	0	0	0	1
		Water Delivery	2	0	0	1	0	0	0	0	0	0
	UPA	Distillation Assembly	2	0	0	1	0	0	0	0	1	0
		Firmware Controller Assembly	3	1	1	1	0	1	0	1	0	1
		Fluids Control and Pump Assembly	2	0	1	0	1	0	0	0	1	0
		Pressure Control and Pump Assembly	2	0	0	1	0	0	0	0	0	1
		Advanced Recycle Filter Tank Assembly[xvi]	2	0	0	1	0	0	0	0	0	0
		Separator Plumbing Assembly	2	0	0	0	0	1	0	1	0	1
ISRU	Water Extractor	Oven + Insulating Cone	2	1	0	0	1	0	0	0	1	0
		Hopper										
		Sieve	2	0	1	0	0	0	0	1	0	0
		Augers (vertical)	1	1	0	0	1	0	0	0	0	0
		Horizontal Auger	2	0	1	0	0	0	1	0	0	0
		Sweep Gas System	4	1	1	0	1	0	0	1	0	1
		Sweep Gas Piping										

		Condensing Heat Exchanger	2	0	0	0	1	0	0	0	0	0
		Water Filtration System	4	4	4	4	4	4	4	4	4	5
	CO2 Cryocooler	Cryocooler	2	1	0	1	0	0	0	0	1	0
		Container										
	Water Electrolyzer	Electrolysis Cell Stack	4	2	2	1	1	0	2	1	1	0
		O2 Separator / Water Reservoir	5	2	2	1	1	1	1	1	1	1
		H2 Separator and Dryer	3	1	1	0	1	0	1	0	1	0
		Water Pump	3	1	1	0	2	1	2	1	2	1
	Sabatier Reactor	Reactor	4	1	1	1	1	0	1	1	0	1
		Water / Methane Separator	4	1	0	1	0	1	0	1	0	2
		Heat Exchanger	3	0	0	0	0	1	0	0	0	0
	Atmospheric Processor	Zeolite	4	2	0	1	1	0	1	1	0	1
		Compressor	5	1	2	1	1	1	0	2	0	1
		Cryocoolers	3	0	1	0	1	0	0	0	1	0
		Support Structure										

Table J.9: Architecture Case 3 Spare Parts Requirements for each Component over a 10 Mission String of Sorties Campaign with all ISRU technologies at 10% of their originally estimated values. Empty rows correspond to components assumed to have 100% reliability, and hence do not require spare parts

Group	**Assembly**	**Subassembly**	**Mission**									
			1	**2**	**3**	**4**	**5**	**6**	**7**	**8**	**9**	**10**
ECLSS	CDRA	Air Pump Two-Stage ORU	3	0	1	1	0	0	1	0	0	1
		Blower	3	1	1	0	1	0	0	1	0	1
		Check Valves	4	2	1	1	1	1	1	1	1	0
		Desiccant Beds	4	1	2	1	0	1	1	1	1	0
		Heat Controller	3	1	1	1	0	1	0	0	1	0
		Precooler	3	1	1	0	1	0	0	1	0	1
		Pump Fan Motor Controller	2	0	1	0	0	0	0	0	1	0
		Selector Valves	6	2	3	2	1	1	2	1	1	2
		Sorbent Beds (Zeolite)	4	1	2	1	0	1	1	1	1	0
	CCAA	Condensing Heat Exchanger	2	1	0	1	0	0	1	0	0	0
		Electronic Interface Box (EIB)	3	0	1	0	0	1	0	0	0	1
		Fan Delta Pressure Sensor	3	0	1	0	1	0	0	1	0	0
		Heat Exchanger Liquid Sensor	4	0	1	1	0	1	0	0	1	0
		Inlet ORU	3	1	1	1	0	1	0	1	0	0
		Pressure Transducer	3	0	1	0	1	0	0	1	0	0
		Temperature Control Check Valve (TCCV)	13	6	6	5	5	4	4	5	5	4
		Temperature Sensor	2	0	1	0	0	0	0	0	1	0
		Water Separator	6	3	2	2	1	2	1	2	1	1
		Water Separator Liquid Sensor	3	1	1	1	0	1	0	0	1	0
	WPA	Catalytic Reactor	2	1	0	0	1	0	0	0	0	1
		Gas Separator	1	1	0	0	0	1	0	0	0	0
		Ion Exchange Bed	1	1	0	1	1	1	1	1	1	0
		Microbial Check Valve	2	0	0	0	1	0	0	0	0	0
		Multifiltration Bed #1	1	0	0	0	1	0	0	1	0	0
		Multifiltration Bed #2	1	0	0	0	0	1	0	1	0	0
		Particulate Filter	1	0	0	1	1	0	1	1	0	1
		pH Adjuster	2	0	0	1	0	0	0	0	0	0
		Process Controller	1	1	0	0	0	1	0	0	0	0
		Pump Separator	2	0	1	0	0	0	1	0	0	0
		Reactor Health Sensor	2	0	1	0	0	0	0	1	0	0
		Sensor	2	0	0	1	0	0	0	0	0	0
		Separator Filter	1	1	0	0	0	0	0	0	0	0
		Start-up Filter	1	1	0	0	0	0	0	1	0	0
		Water Delivery	2	0	0	1	0	0	0	0	0	0
	UPA	Distillation Assembly	2	0	0	1	0	0	0	0	1	0
		Firmware Controller Assembly	3	1	1	1	0	1	0	1	0	1
		Fluids Control and Pump Assembly	2	1	0	0	1	0	0	0	1	0
		Pressure Control and Pump Assembly	2	0	1	0	0	0	0	0	1	0
		Advanced Recycle Filter Tank Assembly[xvi]	2	0	0	1	0	0	0	0	0	1
		Separator Plumbing Assembly	2	0	0	0	1	0	0	1	0	1
ISRU	Water Extractor	Oven + Insulating Cone	5	2	1	1	2	1	1	1	1	1

	Hopper										
	Sieve	4	1	1	1	1	0	1	1	0	1
	Augers (vertical)	3	1	1	1	1	0	1	1	0	1
	Horizontal Auger	4	1	2	0	1	1	1	0	1	0
	Sweep Gas System	9	2	5	1	2	3	0	4	3	1
	Sweep Gas Piping										
	Condensing Heat Exchanger	3	1	1	1	0	0	1	1	0	0
	Water Filtration System	6	2	4	4	4	4	4	4	4	5
CO2 Cryocooler	Cryocooler	5	2	1	1	2	1	1	1	1	1
	Container										
Water Electrolyzer	Electrolysis Cell Stack	14	8	8	7	6	6	6	6	6	6
	O2 Separator / Water Reservoir	16	8	9	7	6	7	6	6	6	6
	H2 Separator and Dryer	8	3	3	3	2	2	2	2	2	2
	Water Pump	7	3	3	2	2	1	2	2	1	2
Sabatier Reactor	Reactor	10	6	5	4	4	4	3	4	4	3
	Water / Methane Separator	8	4	3	2	3	2	1	3	2	2
	Heat Exchanger	4	1	1	1	1	1	0	0	1	1
Atmospheric Processor	Zeolite	10	4	4	4	4	3	1	4	4	1
	Compressor	14	7	7	6	6	5	5	6	5	5
	Cryocoolers	6	2	2	1	1	1	2	1	1	1
	Support Structure										

J.2.4 Architecture Case 4

Table J.10: Architecture Case 4 Master Equipment List, containing component mass, volume and reliability data, as well as run times and power demands. Power is listed here on a per unit basis. ISRU technologies displayed here were sized by the HabNet ISRU Module.

Sys.	Assembly	Subassembly	Mass [kg]	Vol. [m^3]	MTBF [h]	Run Time [h]	LL [y]	# in Pmry.	Power [kW]
ECLS	CDRA	Air Pump Two-Stage ORU	10.89	0.0045	156200.0	12960	15.29	1	0.860
		Blower	5.58	0.0300	129700.0	12960	10.00	1	
		Check Valves	39.92	0.1784	32900.0[i]	12960		1	
		Desiccant Beds	42.64	0.0850	77100.0	12960		2	
		Heat Controller	3.31	0.0085	242700.0	12960		2	
		Precooler	5.58	0.0255	129700.0	12960	10.00	1	
		Pump Fan Motor Controller	2.72	0.0057	2270000.0	12960		2	
		Selector Valves	3.04	0.0017	117000.0	12960	10.61	6	
		Sorbent Beds (Zeolite)	42.64	0.0850	77100.0	12960		2	
	CCAA (x4)	Condensing Heat Exchanger	49.71	0.3933	832600.0	12960		4	0.532
		Electronic Interface Box (EIB)	4.04	0.0173	2350000.0	12960		8	
		Fan Delta Pressure Sensor	0.45	0.0002	1250000.0	12960		4	
		Heat Exchanger Liquid Sensor	0.64	0.0006	1140000.0	12960		8	
		Inlet ORU	25.31	0.1308	333000.0	12960		4	
		Pressure Transducer	0.48	0.0000	1250000.0	12960	15.00	4	
		Temperature Control Check Valve (TCCV)	7.45	0.0071	32900.0	12960		8	
		Temperature Sensor	0.26	0.0014	37600000.0	12960		16	
		Water Separator	11.93	0.0583	131000.0	12960	5.00	8	
		Water Separator Liquid Sensor	0.64	0.0006	1140000.0[ii]	12960		8	
	WPA	Catalytic Reactor	67.04	0.1156	25579.2	1248	2.25	1	0.320
		Gas Separator	39.15	0.0660	84008.4	1248	1	1	
		Ion Exchange Bed	13.02	0.0173	296701.2	1248	0.16	1	
		Microbial Check Valve	5.76	0.0065	143488.8	1248	1	1	
		Multifiltration Bed #1	149.23	0.0657	296701.2	1248	0.36	1	
		Multifiltration Bed #2	149.23	0.0657	296701.2	1248	0.36	1	
		Particulate Filter	32.25	0.0717	717356.4	1248	0.22	1	
		pH Adjuster	2.54	0.0026	137181.6	1248	1	1	
		Process Controller	45.00	0.0838	87950.4	1248	7.72	1	
		Pump Separator	31.34	0.0869	42398.4	1248	2	1	

		Reactor Health Sensor	16.83	0.0425	56677.2	1248	1	1	
		Sensor	4.81	0.0034	143664	1248	10	1	
		Separator Filter	7.67	0.0102	359072.4	1248	0.84	1	
		Start-up Filter	9.44	0.0184	226884	1248	19.92	1	
		Water Delivery	47.54	0.0974	64561.2	1248	5	1	
	UPA	Distillation Assembly	92.76	0.1422	142525.2	4577	2	1	0.315
		Firmware Controller Assembly	23.09	0.0286	27331.2	4577	2.4	1	
		Fluids Control and Pump Assembly	47.58	0.0731	90140.4	4577	4	1	
		Pressure Control and Pump Assembly	49.08	0.1158	181507.2	4577	2	1	
		Advanced Recycle Filter Tank Assembly[xvi]	50.00	0.1011	199640.4	4577		1	
		Separator Plumbing Assembly	16.78	0.0229	384651.6	4577	1	1	
	OGA	Hydrogen ORU	161.62	0.1467	27156	12909	2.38	1	2.971
		Hydrogen Sensor	4.36	0.0034	61845.6	12909	0.25	1	
		Inlet Deionizing Bed	28.67	0.0295	296701.2	12909	6	1	
		Nitrogen Purge ORU	34.25	0.0312	138408	12909		1	
		Oxygen Outlet	48.17	0.0312	98112	12909	10	1	
		Power Supply Module	42.64	0.0649	47479.2	12909	4.17	1	
		Process Controller	47.08	0.0838	103280.4	12909	7.72	1	
		Pump	17.96	0.0102	144540	12909	1	1	
		Water ORU	61.05	0.0756	33288	12909	2.92	1	
ISRU	Water Extractor	Oven + Insulating Cone	56.98	2.4680	242700[iii]	12960		1	15.99
		Hopper	47.87	2.8777		12960		1	
		Sieve	22.78	0.0000	500000[iv]	12960		1	
		Augers (vertical)	146.06	0.0000	500000[iv]	12960		1	0.045
		Horizontal Auger	9.73	0.1250	500000[iv]	12960		1	
		Sweep Gas System	0.01	0.0000	138408[v]	12960		1	
		Sweep Gas Piping	4.64	0.0786		12960		1	
		Condensing Heat Exchanger	27.73	0.5414	832600[vi]	12960		1	
		Water Filtration System	1.59	0.0060	296701.2[vii]	12960	0.36	1	
	CO2 Cryocooler	Cryocooler	34.61	0.0726	500000[iv]	12960		2	1.474
		Container	83.02	0.4906		12960		1	
	Water Electrolyzer	Electrolysis Cell Stack	47.43	0.0045	27156[viii]	12960	2.38	1	12.28
		O2 Separator / Water Reservoir	5.71	0.0119	27156[viii]	12960	2.38	1	
		H2 Separator and Dryer	14.44	0.0040	98112[ix]	12960	10	1	
		Water Pump	2.16	0.0007	144540[x]	12960	1	1	8×10^{-5}
	Sabatier Reactor	Reactor	20.78	0.4181	50000[xi]	12960		1	0.198
		Water / Methane Separator	0.24	0.0097	131000[xii]	12960		1	
		Heat Exchanger	0.53	0.0000	832600[xiii]	12960		1	
	Atmospheric Processor	Zeolite	0.58	0.0070	77100[xiv]	12960		1	
		Compressor	8.81	0.0509	66666.7	12960		2	0.803
		Cryocoolers	3.10	0.0015	500000[iv]	12960		2	0.480
		Support Structure	3.78			12960		1	

[i] Analogy to CCAA TCCV
[ii] Analogy to CCAA Heat Exchanger Liquid Sensor
[iii] Analogy to CDRA Heater Controller
[iv] Optimistic assumption; no data were available
[v] Analogy to OGA Nitrogen Purge ORU
[vi] Analogy CCAA Condensing Heat Exchanger
[vii] Analogy to WPA Multifiltration Bed
[viii] Analogy to OGA Hydrogen ORU (contains Electrolysis Cell Stack and Rotary Separator / Accumulator)
[ix] Analogy to OGA Oxygen Outlet
[x] Analogy to OGA Pump
[xi] Analogy to CRS Sabatier Methanation Reactor
[xii] Analogy to CRS Phase Separator
[xiii] Analogy to CRS Condensing Heat Exchanger
[xiv] Analogy to CDRA Dessicant-Adsorbent Bed
[xv] Analogy to CRS Compressor
[xvi] Mass is obtained from [300] and verified with calculations based on data from Link et al. [301]. All other data is assumed to be the same as the Recycle Filter Tank Assembly (RFTA) described in the NASA BVAD 2004 [209] – the original system from which the ARFTA was upgraded from. Here, the life limit of the ARFTA has been assumed to be zero, based on its development objective of facilitating the same function as the RFTA without the need for periodic replacement [301].

Table J.11: Architecture Case 4 Spare Parts Requirements for each Component over a 10 Mission String of Sorties Campaign. Empty rows correspond to components assumed to have 100% reliability, and hence do not require spare parts

Group	Assembly	Subassembly	Mission									
			1	2	3	4	5	6	7	8	9	10
ECLSS	CDRA	Air Pump Two-Stage ORU	3	1	0	1	0	0	1	0	1	0
		Blower	3	1	1	0	1	0	1	0	0	1
		Check Valves	4	2	1	1	1	1	1	1	1	1
		Desiccant Beds	4	1	2	1	0	1	1	1	1	0
		Heat Controller	3	1	1	1	0	0	1	0	1	0
		Precooler	3	1	1	0	1	0	1	0	0	1
		Pump Fan Motor Controller	2	0	0	1	0	0	0	0	0	1
		Selector Valves	6	3	1	2	2	1	2	1	1	2
		Sorbent Beds (Zeolite)	4	1	2	1	0	1	1	1	1	0
	CCAA	Condensing Heat Exchanger	2	1	0	1	0	0	1	0	0	0
		Electronic Interface Box (EIB)	3	0	1	0	0	0	1	0	0	1
		Fan Delta Pressure Sensor	3	1	0	1	0	0	1	0	0	0
		Heat Exchanger Liquid Sensor	4	1	0	1	1	0	0	0	1	0
		Inlet ORU	3	1	1	1	0	1	0	0	1	0
		Pressure Transducer	3	1	0	1	0	0	1	0	0	0
		Temperature Control Check Valve (TCCV)	13	6	5	6	5	3	6	4	5	4
		Temperature Sensor	2	0	0	1	0	0	0	0	1	0
		Water Separator	6	3	2	2	1	2	2	1	1	2
		Water Separator Liquid Sensor	4	0	1	1	0	1	0	0	1	0
	WPA	Catalytic Reactor	2	0	1	0	0	1	0	0	0	1
		Gas Separator	2	0	0	0	1	0	0	0	0	0
		Ion Exchange Bed	1	1	0	1	1	1	1	1	1	0
		Microbial Check Valve	2	0	0	0	1	0	0	0	0	0
		Multifiltration Bed #1	1	0	0	0	1	0	0	1	0	0
		Multifiltration Bed #2	1	0	0	0	1	0	0	1	0	0
		Particulate Filter	1	0	0	1	1	0	1	1	0	1
		pH Adjuster	2	0	0	1	0	0	0	0	0	0
		Process Controller	2	0	0	0	0	1	0	0	0	0
		Pump Separator	2	0	1	0	0	0	1	0	0	0
		Reactor Health Sensor	2	0	1	0	0	0	1	0	0	0
		Sensor	2	0	0	0	1	0	0	0	0	0
		Separator Filter	1	1	0	0	0	0	0	0	0	0
		Start-up Filter	1	1	0	0	0	0	0	0	1	0
		Water Delivery	2	0	0	1	0	0	0	0	0	0
	UPA	Distillation Assembly	2	0	1	0	0	0	0	1	0	0
		Firmware Controller Assembly	3	1	1	1	0	1	0	1	0	1
		Fluids Control and Pump Assembly	2	1	0	0	1	0	0	0	1	0
		Pressure Control and Pump Assembly	2	0	1	0	0	0	0	0	1	0
		Advanced Recycle Filter Tank Assembly[xvi]	2	0	0	1	0	0	0	0	0	1
		Separator Plumbing Assembly	2	0	0	0	1	0	0	1	0	1
	OGA	Hydrogen ORU	4	2	1	1	1	1	1	1	1	1
		Hydrogen Sensor	5	6	6	6	6	6	6	6	6	5
		Inlet Deionizing Bed	2	1	0	0	1	0	0	0	1	0
		Nitrogen Purge ORU	3	0	1	1	0	0	1	0	0	1
		Oxygen Outlet	3	1	0	1	0	1	0	1	0	1
		Power Supply Module	4	1	1	1	1	0	1	1	0	1
		Process Controller	3	1	0	1	0	1	0	1	0	0
		Pump	3	0	1	1	2	1	2	1	2	1
		Water ORU	4	2	1	1	1	1	1	0	1	1
ISRU	Water Extractor	Oven + Insulating Cone	2	1	0	1	0	0	0	1	0	0
		Hopper										
		Sieve	2	0	1	0	0	0	1	0	0	0
		Augers (vertical)	1	1	0	1	0	0	0	0	0	0
		Horizontal Auger	2	0	1	0	0	1	0	0	0	0
		Sweep Gas System	4	1	1	0	1	0	1	0	1	0
		Sweep Gas Piping										
		Condensing Heat Exchanger	2	0	0	1	0	0	0	0	0	0
		Water Filtration System	4	4	4	4	4	4	4	4	4	5
	CO2 Cryocooler	Cryocooler	2	1	0	1	0	0	0	1	0	0
		Container										
	Water Electrolyzer	Electrolysis Cell Stack	5	1	2	1	1	1	1	1	1	1
		O2 Separator / Water Reservoir	6	1	2	1	1	1	2	1	1	1

		H2 Separator and Dryer	3	1	1	0	1	0	1	0	1	0
		Water Pump	3	1	1	0	2	1	2	1	2	1
	Sabatier Reactor	Reactor	4	1	1	1	1	0	1	1	1	0
		Water / Methane Separator	4	1	0	1	1	0	1	0	1	0
		Heat Exchanger	2	1	0	1	0	0	0	0	1	0
	Atmospheric Processor	Zeolite	4	2	0	2	0	1	0	1	1	0
		Compressor	5	1	2	1	1	1	1	1	1	1
		Cryocoolers	3	0	1	0	1	0	0	1	0	0
		Support Structure										

Table J.12: Architecture Case 4 Spare Parts Requirements for each Component over a 10 Mission String of Sorties Campaign with all ISRU technologies at 10% of their originally estimated values. Empty rows correspond to components assumed to have 100% reliability, and hence do not require spare parts

Group	Assembly	Subassembly	Mission									
			1	2	3	4	5	6	7	8	9	10
ECLSS	CDRA	Air Pump Two-Stage ORU	3	1	0	1	0	1	0	0	1	0
		Blower	3	1	1	0	1	0	1	0	0	1
		Check Valves	4	2	1	1	1	1	1	1	1	1
		Desiccant Beds	4	1	2	1	1	0	1	1	1	0
		Heat Controller	3	1	1	1	0	1	0	0	1	0
		Precooler	3	1	1	0	1	0	1	0	0	1
		Pump Fan Motor Controller	2	0	1	0	0	0	0	0	1	0
		Selector Valves	6	3	2	2	1	2	1	1	2	1
		Sorbent Beds (Zeolite)	4	1	2	1	0	1	1	1	1	0
	CCAA	Condensing Heat Exchanger	2	1	0	1	0	0	1	0	0	0
		Electronic Interface Box (EIB)	2	1	1	0	1	0	0	0	0	1
		Fan Delta Pressure Sensor	3	1	0	1	0	0	0	1	0	0
		Heat Exchanger Liquid Sensor	4	1	0	1	0	1	0	0	1	0
		Inlet ORU	3	1	1	1	0	1	0	1	0	1
		Pressure Transducer	3	1	0	1	0	0	0	1	0	0
		Temperature Control Check Valve (TCCV)	12	7	6	6	4	5	4	4	5	5
		Temperature Sensor	2	0	1	0	0	0	0	0	1	0
		Water Separator	6	3	2	2	2	1	2	1	2	1
		Water Separator Liquid Sensor	4	1	0	1	0	1	0	0	1	0
	WPA	Catalytic Reactor	2	1	0	0	1	0	0	0	1	0
		Gas Separator	2	0	0	1	0	0	0	0	0	0
		Ion Exchange Bed	1	1	0	1	1	1	1	1	1	0
		Microbial Check Valve	2	0	0	1	0	0	0	0	0	0
		Multifiltration Bed #1	1	0	0	0	1	0	0	1	0	0
		Multifiltration Bed #2	1	0	0	0	1	0	0	1	0	0
		Particulate Filter	1	0	0	1	1	0	1	1	0	1
		pH Adjuster	2	0	1	0	0	0	0	0	0	1
		Process Controller	2	0	0	0	0	1	0	0	0	0
		Pump Separator	2	0	1	0	0	0	1	0	0	0
		Reactor Health Sensor	2	0	1	0	0	0	1	0	0	0
		Sensor	2	0	0	1	0	0	0	0	0	0
		Separator Filter	1	1	0	0	0	0	0	0	0	0
		Start-up Filter	1	1	0	0	0	0	0	0	1	0
		Water Delivery	2	0	0	1	0	0	0	0	0	0
	UPA	Distillation Assembly	2	0	1	0	0	0	1	0	0	0
		Firmware Controller Assembly	3	1	1	1	0	1	1	0	1	0
		Fluids Control and Pump Assembly	2	1	0	1	0	0	0	1	0	0
		Pressure Control and Pump Assembly	2	0	1	0	0	0	0	0	1	0
		Advanced Recycle Filter Tank Assembly[xvi]	2	0	1	0	0	0	0	0	1	0
		Separator Plumbing Assembly	2	0	0	1	0	0	0	1	0	1
	OGA	Hydrogen ORU	4	2	1	1	1	1	1	1	1	1
		Hydrogen Sensor	5	6	6	6	6	6	6	6	6	5
		Inlet Deionizing Bed	2	1	0	1	0	0	0	0	1	0
		Nitrogen Purge ORU	3	0	1	1	0	0	1	0	0	1
		Oxygen Outlet	3	1	1	0	0	1	1	0	0	1
		Power Supply Module	4	1	1	1	1	0	1	1	1	0
		Process Controller	3	1	1	0	0	1	0	1	0	0

		Pump	3	1	0	1	2	1	2	1	2	1
		Water ORU	4	2	1	1	1	1	1	1	0	1
ISRU	Water Extractor	Oven + Insulating Cone	5	2	1	2	1	1	1	1	1	1
		Hopper										
		Sieve	4	1	1	1	1	1	0	1	1	0
		Augers (vertical)	3	1	1	1	1	1	0	1	0	1
		Horizontal Auger	4	2	1	1	0	1	1	0	1	1
		Sweep Gas System	9	4	1	4	3	1	1	3	2	2
		Sweep Gas Piping										
		Condensing Heat Exchanger	3	1	1	1	0	1	0	1	0	1
		Water Filtration System	6	2	4	4	4	4	4	4	4	5
	CO2 Cryocooler	Cryocooler	5	2	1	2	1	1	1	1	1	1
		Container										
	Water Electrolyzer	Electrolysis Cell Stack	14	9	7	7	6	7	6	6	6	6
		O2 Separator / Water Reservoir	16	9	8	7	7	6	6	6	7	7
		H2 Separator and Dryer	8	3	4	2	2	2	3	2	2	2
		Water Pump	7	4	2	2	2	2	1	2	1	2
	Sabatier Reactor	Reactor	11	5	5	4	4	4	4	3	4	4
		Water / Methane Separator	8	4	3	2	4	0	2	2	2	1
		Heat Exchanger	4	1	1	1	1	1	0	1	0	0
	Atmospheric Processor	Zeolite	10	5	4	4	2	3	2	4	2	3
		Compressor	14	8	7	6	5	5	6	5	5	6
		Cryocoolers	6	2	2	1	1	1	2	1	1	1
		Support Structure										

J.2.5 Architecture Case 5

Table J.13: Architecture Case 5 Master Equipment List, containing component mass, volume and reliability data, as well as run times and power demands. Power is listed here on a per unit basis. ISRU technologies displayed here were sized by the HabNet ISRU Module.

Sys.	Assembly	Subassembly	Mass [kg]	Vol. [m^3]	MTBF [h]	Run Time [h]	LL [y]	# in Pmry.	Power [kW]
ECLS	CDRA	Air Pump Two-Stage ORU	10.89	0.0045	156200.0	12960	15.29	1	0.860
		Blower	5.58	0.0300	129700.0	12960	10.00	1	
		Check Valves	39.92	0.1784	32900.0[i]	12960		1	
		Desiccant Beds	42.64	0.0850	77100.0	12960		2	
		Heat Controller	3.31	0.0085	242700.0	12960		2	
		Precooler	5.58	0.0255	129700.0	12960	10.00	1	
		Pump Fan Motor Controller	2.72	0.0057	2270000.0	12960		2	
		Selector Valves	3.04	0.0017	117000.0	12960	10.61	6	
		Sorbent Beds (Zeolite)	42.64	0.0850	77100.0	12960		2	
	CCAA (x4)	Condensing Heat Exchanger	49.71	0.3933	832600.0	12960		4	0.532
		Electronic Interface Box (EIB)	4.04	0.0173	2350000.0	12960		8	
		Fan Delta Pressure Sensor	0.45	0.0002	1250000.0	12960		4	
		Heat Exchanger Liquid Sensor	0.64	0.0006	1140000.0	12960		8	
		Inlet ORU	25.31	0.1308	333000.0	12960		4	
		Pressure Transducer	0.48	0.0000	1250000.0	12960	15.00	4	
		Temperature Control Check Valve (TCCV)	7.45	0.0071	32900.0	12960		8	
		Temperature Sensor	0.26	0.0014	37600000.0	12960		16	
		Water Separator	11.93	0.0583	131000.0	12960	5.00	8	
		Water Separator Liquid Sensor	0.64	0.0006	1140000.0[ii]	12960		8	
	WPA	Catalytic Reactor	67.04	0.1156	25579.2	1264	2.25	1	0.320
		Gas Separator	39.15	0.0660	84008.4	1264	1	1	
		Ion Exchange Bed	13.02	0.0173	296701.2	1264	0.16	1	
		Microbial Check Valve	5.76	0.0065	143488.8	1264	1	1	
		Multifiltration Bed #1	149.23	0.0657	296701.2	1264	0.36	1	
		Multifiltration Bed #2	149.23	0.0657	296701.2	1264	0.36	1	

		Particulate Filter	32.25	0.0717	717356.4	1264	0.22	1	
		pH Adjuster	2.54	0.0026	137181.6	1264	1	1	
		Process Controller	45.00	0.0838	87950.4	1264	7.72	1	
		Pump Separator	31.34	0.0869	42398.4	1264	2	1	
		Reactor Health Sensor	16.83	0.0425	56677.2	1264	1	1	
		Sensor	4.81	0.0034	143664	1264	10	1	
		Separator Filter	7.67	0.0102	359072.4	1264	0.84	1	
		Start-up Filter	9.44	0.0184	226884	1264	19.92	1	
		Water Delivery	47.54	0.0974	64561.2	1264	5	1	
	UPA	Distillation Assembly	92.76	0.1422	142525.2	4578	2	1	0.315
		Firmware Controller Assembly	23.09	0.0286	27331.2	4578	2.4	1	
		Fluids Control and Pump Assembly	47.58	0.0731	90140.4	4578	4	1	
		Pressure Control and Pump Assembly	49.08	0.1158	181507.2	4578	2	1	
		Advanced Recycle Filter Tank Assembly[xvi]	50.00	0.1011	199640.4	4578		1	
		Separator Plumbing Assembly	16.78	0.0229	384651.6	4578	1	1	
	OGA	Hydrogen ORU	161.62	0.1467	27156	12906	2.38	1	2.971
		Hydrogen Sensor	4.36	0.0034	61845.6	12906	0.25	1	
		Inlet Deionizing Bed	28.67	0.0295	296701.2	12906	6	1	
		Nitrogen Purge ORU	34.25	0.0312	138408	12906		1	
		Oxygen Outlet	48.17	0.0312	98112	12906	10	1	
		Power Supply Module	42.64	0.0649	47479.2	12906	4.17	1	
		Process Controller	47.08	0.0838	103280.4	12906	7.72	1	
		Pump	17.96	0.0102	144540	12906	1	1	
		Water ORU	61.05	0.0756	33288	12906	2.92	1	
	CRS	Sabatier Methanation Reactor	120[xvii]	0.21[xvii]	50000[xviii]	883		1	0.106
		Condensing Heat Exchanger[xix]	49.71	0.3933	832600	883		1	0.08
		Phase Separator[xx]	11.93	0.0583	131000	883	5	1	
		Valves[xxi]	3.04	0.0017	117000	883	10.61	7[xxii]	
		Sensors[xxiii]	4.81	0.0034	143664	883	10	1	
		Controller	3.00[xvii]	0.0053[xxiv]	103280[xxv]	883	7.72[xxv]	1	
		Compressor	27.0[xvii]	0.0112[xxvi]	66666.7[xviii]	883		1	0.5
ISRU	Water Extractor	Oven + Insulating Cone	56.70	2.4559	242700[iii]	12960		1	15.91
		Hopper	47.72	2.8636		12960		1	
		Sieve	22.61	0.0000	500000[iv]	12960		1	
		Augers (vertical)	145.34	0.0000	500000[iv]	12960		1	0.045
		Horizontal Auger	9.70	0.1247	500000[iv]	12960		1	
		Sweep Gas System	0.01	0.0000	138408[v]	12960		1	
		Sweep Gas Piping	4.63	0.0781		12960		1	
		Condensing Heat Exchanger	27.60	0.5376	832600[vi]	12960		1	
		Water Filtration System	1.59	0.0060	296701.2[vii]	12960	0.36	1	
	CO2 Cryocooler	Cryocooler	34.61	0.0726	500000[iv]	12960		2	1.474
		Container	83.02	0.4906		12960		1	
	Water Electrolyzer	Electrolysis Cell Stack	47.43	0.0045	27156[viii]	12960	2.38	1	12.28
		O2 Separator / Water Reservoir	5.71	0.0119	27156[viii]	12960	2.38	1	
		H2 Separator and Dryer	14.44	0.0040	98112[ix]	12960	10	1	
		Water Pump	2.16	0.0007	144540[x]	12960	1	1	8×10^{-5}
	Sabatier Reactor	Reactor	20.78	0.4181	50000[xi]	12960		1	0.198
		Water / Methane Separator	0.24	0.0097	131000[xii]	12960		1	
		Heat Exchanger	0.53	0.0000	832600[xiii]	12960		1	
	Atmospheric Processor	Zeolite	0.58	0.0070	77100[xiv]	12960		1	
		Compressor	8.81	0.0509	66666.7	12960		2	0.803
		Cryocoolers	3.10	0.0015	500000[iv]	12960		2	0.480
		Support Structure	3.78			12960		1	

[i]Analogy to CCAA TCCV
[ii]Analogy to CCAA Heat Exchanger Liquid Sensor
[iii]Analogy to CDRA Heater Controller
[iv]Optimistic assumption; no data were available
[v]Analogy to OGA Nitrogen Purge ORU
[vi]Analogy CCAA Condensing Heat Exchanger
[vii]Analogy to WPA Multifiltration Bed

[xvi]Mass is obtained from [300] and verified with calculations based on data from Link et al. [301]. All other data is assumed to be the same as the Recycle Filter Tank Assembly (RFTA) described in the NASA BVAD 2004 [209] – the original system from which the ARFTA was upgraded from. Here, the life limit of the ARFTA has been assumed to be zero, based on its development objective of facilitating the same function as the RFTA without the need for periodic replacement [301].

[viii]Analogy to OGA Hydrogen ORU (contains Electrolysis Cell Stack and Rotary Separator / Accumulator)
[ix]Analogy to OGA Oxygen Outlet
[x]Analogy to OGA Pump
[xi]Analogy to CRS Sabatier Methanation Reactor
[xii]Analogy to CRS Phase Separator
[xiii]Analogy to CRS Condensing Heat Exchanger
[xiv]Analogy to CDRA Dessicant-Adsorbent Bed
[xv]Analogy to CRS Compressor
[xvii]Data taken from Jeng and Lin [256]
[xviii]Data taken from Papale et al. [318]
[xix]Analogy to CCAA Condensing Heat Exchanger
[xx]Analogy to CCAA Water Separator
[xxi]Analogy to CDRA Selector Valves
[xxii]Data taken from Jones [319]
[xxiii]Analogy to WPA Sensor
[xxiv]Linear scaling (based on mass) from OGA Process Controller
[xxv]Analogy to OGA Process Controller
[xxvi]Linear scaling (based on mass) from CDRA Air Pump

Table J.14: Architecture Case 5 Spare Parts Requirements for each Component over a 10 Mission String of Sorties Campaign. Empty rows correspond to components assumed to have 100% reliability, and hence do not require spare parts

Group	Assembly	Subassembly	Mission 1	2	3	4	5	6	7	8	9	10
ECLSS	CDRA	Air Pump Two-Stage ORU	3	1	0	1	0	0	1	0	0	1
		Blower	3	1	1	0	1	0	1	0	0	1
		Check Valves	4	2	1	1	1	1	1	1	1	1
		Desiccant Beds	4	1	2	1	0	1	1	1	1	0
		Heat Controller	3	1	1	1	0	1	0	0	1	0
		Precooler	3	1	1	0	1	0	1	0	0	1
		Pump Fan Motor Controller	2	0	1	0	0	0	0	0	1	0
		Selector Valves	6	3	2	2	1	2	1	1	2	1
		Sorbent Beds (Zeolite)	4	1	2	1	0	1	1	1	1	0
	CCAA	Condensing Heat Exchanger	2	1	0	1	0	0	1	0	0	0
		Electronic Interface Box (EIB)	3	0	1	0	0	1	0	0	0	1
		Fan Delta Pressure Sensor	3	1	0	1	0	0	1	0	0	1
		Heat Exchanger Liquid Sensor	3	2	0	1	0	1	0	0	1	1
		Inlet ORU	3	1	1	1	0	1	0	1	0	1
		Pressure Transducer	3	1	0	0	1	0	0	1	0	0
		Temperature Control Check Valve (TCCV)	12	7	6	5	5	4	5	5	4	5
		Temperature Sensor	2	0	0	1	0	0	0	0	1	0
		Water Separator	6	3	2	2	2	1	2	1	1	2
		Water Separator Liquid Sensor	3	2	0	1	0	1	0	0	1	0
	WPA	Catalytic Reactor	2	0	1	0	1	0	0	0	1	0
		Gas Separator	2	0	0	0	1	0	0	0	0	0
		Ion Exchange Bed	1	1	0	1	1	1	1	1	1	1
		Microbial Check Valve	2	0	0	1	0	0	0	0	0	0
		Multifiltration Bed #1	1	0	0	0	1	0	0	1	0	1
		Multifiltration Bed #2	1	0	0	0	1	0	0	1	0	1
		Particulate Filter	1	0	0	1	1	0	1	1	0	1
		pH Adjuster	2	0	1	0	0	0	0	0	1	0
		Process Controller	1	1	0	0	0	1	0	0	0	0
		Pump Separator	2	0	1	0	0	0	1	0	0	0
		Reactor Health Sensor	2	0	1	0	0	0	1	0	0	0
		Sensor	2	0	1	0	0	0	0	0	0	0
		Separator Filter	1	1	0	0	0	0	0	0	0	1
		Start-up Filter	1	1	0	0	0	0	1	0	0	0
		Water Delivery	2	0	0	1	0	0	0	0	0	0
	UPA	Distillation Assembly	2	0	1	0	0	0	0	1	0	0
		Firmware Controller Assembly	3	1	1	1	0	1	0	1	0	1
		Fluids Control and Pump Assembly	2	1	0	1	0	0	0	0	1	0
		Pressure Control and Pump Assembly	2	0	1	0	0	0	0	0	1	0
		Advanced Recycle Filter Tank Assembly[xvi]	2	0	0	1	0	0	0	0	0	1
		Separator Plumbing Assembly	2	0	0	1	0	0	0	1	0	1
	OGA	Hydrogen ORU	4	2	1	1	1	1	1	1	1	1
		Hydrogen Sensor	5	6	6	6	6	6	6	6	6	5
		Inlet Deionizing Bed	2	1	0	0	1	0	0	0	1	0
		Nitrogen Purge ORU	3	0	1	1	0	0	1	0	0	1
		Oxygen Outlet	3	1	0	1	0	1	0	1	0	1
		Power Supply Module	4	1	1	1	1	0	1	1	0	1
		Process Controller	3	1	0	1	0	1	0	1	0	0
		Pump	3	0	1	1	2	1	2	1	2	1
		Water ORU	4	2	1	1	1	1	1	0	1	1

	CRS	Sabatier Methanation Reactor	1	1	0	0	0	1	0	0	0	0
		Condensing Heat Exchanger	1	0	0	0	0	0	0	0	0	1
		Phase Separator	1	1	0	0	0	0	1	0	0	0
		Valves	3	1	0	0	1	0	0	1	0	0
		Sensors	1	1	0	0	0	1	0	0	0	0
		Controller	2	0	1	0	0	0	0	0	0	0
		Compressor	2	0	0	0	1	0	0	0	0	0
ISRU	Water Extractor	Oven + Insulating Cone	2	1	0	1	0	0	0	1	0	0
		Hopper										
		Sieve	2	0	1	0	0	0	1	0	0	0
		Augers (vertical)	2	0	0	1	0	0	0	0	0	0
		Horizontal Auger	2	1	0	0	1	0	0	0	0	1
		Sweep Gas System	4	1	1	1	0	0	1	1	0	0
		Sweep Gas Piping										
		Condensing Heat Exchanger	2	0	0	1	0	0	0	0	0	0
		Water Filtration System	4	4	4	4	4	4	4	4	4	5
	CO2 Cryocooler	Cryocooler	2	1	0	1	0	0	1	0	0	0
		Container										
	Water Electrolyzer	Electrolysis Cell Stack	5	1	2	1	1	1	1	1	1	1
		O2 Separator / Water Reservoir	5	2	2	1	1	2	1	1	1	1
		H2 Separator and Dryer	3	1	1	1	0	0	1	0	1	0
		Water Pump	3	1	1	0	2	1	2	1	2	1
	Sabatier Reactor	Reactor	4	1	2	0	1	0	1	1	1	0
		Water / Methane Separator	4	1	1	1	0	0	1	0	1	0
		Heat Exchanger	2	1	0	0	1	0	0	0	0	1
	Atmospheric Processor	Zeolite	4	2	1	0	1	1	0	0	1	1
		Compressor	5	1	2	1	1	1	1	1	1	1
		Cryocoolers	3	0	1	0	1	0	0	1	0	0
		Support Structure										

Table J.15: Architecture Case 5 Spare Parts Requirements for each Component over a 10 Mission String of Sorties Campaign with all ISRU technologies at 10% of their originally estimated values. Empty rows correspond to components assumed to have 100% reliability, and hence do not require spare parts

Group	**Assembly**	**Subassembly**	**Mission**									
			1	**2**	**3**	**4**	**5**	**6**	**7**	**8**	**9**	**10**
ECLSS	CDRA	Air Pump Two-Stage ORU	3	1	0	1	0	1	0	0	1	0
		Blower	3	1	1	0	1	0	1	0	0	1
		Check Valves	4	2	1	1	1	1	1	1	1	1
		Desiccant Beds	4	2	1	1	1	0	1	1	1	0
		Heat Controller	3	1	1	1	0	1	0	1	0	0
		Precooler	3	1	1	0	1	0	1	0	0	1
		Pump Fan Motor Controller	2	0	1	0	0	0	0	1	0	0
		Selector Valves	7	2	2	2	1	1	2	1	2	1
		Sorbent Beds (Zeolite)	4	1	2	1	1	0	1	1	1	0
	CCAA	Condensing Heat Exchanger	2	1	0	1	0	0	1	0	0	0
		Electronic Interface Box (EIB)	3	0	1	0	0	1	0	0	1	0
		Fan Delta Pressure Sensor	3	1	0	1	0	0	1	0	0	0
		Heat Exchanger Liquid Sensor	4	0	1	1	0	1	0	1	0	0
		Inlet ORU	3	1	1	1	0	1	0	1	0	1
		Pressure Transducer	3	1	0	1	0	0	1	0	0	0
		Temperature Control Check Valve (TCCV)	13	6	6	5	4	6	5	4	4	5
		Temperature Sensor	2	0	1	0	0	0	0	0	1	0
		Water Separator	7	2	2	2	1	2	2	1	2	1
		Water Separator Liquid Sensor	4	1	0	1	1	0	0	1	0	0
	WPA	Catalytic Reactor	2	1	0	0	1	0	0	0	1	0
		Gas Separator	2	0	0	0	1	0	0	0	0	0
		Ion Exchange Bed	1	1	0	1	1	1	1	1	1	1
		Microbial Check Valve	2	0	0	1	0	0	0	0	0	0
		Multifiltration Bed #1	1	0	0	0	1	0	0	1	0	1
		Multifiltration Bed #2	1	0	0	1	0	0	0	1	0	1
		Particulate Filter	1	0	0	1	1	0	1	1	0	1
		pH Adjuster	2	0	1	0	0	0	0	0	0	1

		Process Controller	2	0	0	0	1	0	0	0	0	0
		Pump Separator	2	0	1	0	0	1	0	0	0	0
		Reactor Health Sensor	2	0	1	0	0	0	1	0	0	0
		Sensor	2	0	0	1	0	0	0	0	0	0
		Separator Filter	1	1	0	0	0	0	0	0	0	1
		Start-up Filter	2	0	0	0	0	0	1	0	0	0
		Water Delivery	2	0	0	1	0	0	0	0	0	1
	UPA	Distillation Assembly	2	0	1	0	0	0	1	0	0	0
		Firmware Controller Assembly	3	1	1	1	0	1	1	0	1	0
		Fluids Control and Pump Assembly	2	1	0	1	0	0	0	1	0	0
		Pressure Control and Pump Assembly	2	0	1	0	0	0	0	0	1	0
		Advanced Recycle Filter Tank Assembly[xvi]	2	0	0	1	0	0	0	0	1	0
		Separator Plumbing Assembly	2	0	0	1	0	0	0	1	0	1
	OGA	Hydrogen ORU	4	2	1	1	1	1	1	1	1	1
		Hydrogen Sensor	5	6	6	6	6	6	6	6	6	5
		Inlet Deionizing Bed	2	1	0	1	0	0	0	0	1	0
		Nitrogen Purge ORU	3	0	1	1	0	0	1	0	0	1
		Oxygen Outlet	3	1	1	0	1	0	1	0	0	1
		Power Supply Module	4	1	1	1	1	0	1	1	1	0
		Process Controller	3	1	0	1	0	1	0	1	0	0
		Pump	3	1	0	1	2	1	2	1	2	1
		Water ORU	4	2	1	1	1	1	1	1	0	1
	CRS	Sabatier Methanation Reactor	1	1	0	0	0	1	0	0	0	0
		Condensing Heat Exchanger	1	0	0	0	0	0	0	0	1	0
		Phase Separator	2	0	0	0	0	0	1	0	0	0
		Valves	3	0	1	1	0	0	1	0	0	0
		Sensors	2	0	0	0	0	1	0	0	0	0
		Controller	2	0	0	1	0	0	0	0	0	0
		Compressor	2	0	0	0	1	0	0	0	0	0
ISRU	Water Extractor	Oven + Insulating Cone	5	2	1	2	1	1	1	1	1	1
		Hopper										
		Sieve	4	1	1	1	1	1	1	0	1	0
		Augers (vertical)	3	1	2	0	1	1	0	1	0	1
		Horizontal Auger	4	1	2	1	0	1	1	0	1	1
		Sweep Gas System	9	3	2	4	2	2	2	1	3	0
		Sweep Gas Piping										
		Condensing Heat Exchanger	3	1	1	1	0	1	0	1	0	1
		Water Filtration System	6	2	4	4	4	4	4	4	4	5
	CO2 Cryocooler	Cryocooler	5	2	2	1	1	1	1	1	1	1
		Container										
	Water Electrolyzer	Electrolysis Cell Stack	15	8	7	7	6	7	6	6	6	6
		O2 Separator / Water Reservoir	16	8	8	8	6	7	7	6	7	6
		H2 Separator and Dryer	8	3	3	3	2	2	3	2	2	2
		Water Pump	7	3	3	2	2	1	3	1	1	2
	Sabatier Reactor	Reactor	11	5	5	4	4	4	4	4	4	3
		Water / Methane Separator	9	3	3	3	3	0	2	2	2	2
		Heat Exchanger	5	1	0	2	0	1	0	1	0	0
	Atmospheric Processor	Zeolite	10	5	4	4	3	2	3	3	4	1
		Compressor	14	7	7	7	5	6	5	5	6	5
		Cryocoolers	6	2	2	1	1	2	1	1	1	1
		Support Structure										

J.2.6 Architecture Case 6

Table J.16: Architecture Case 6 Master Equipment List, containing component mass, volume and reliability data, as well as run times and power demands. Power is listed here on a per unit basis. ISRU technologies displayed here were sized by the HabNet ISRU Module.

Sys.	Assembly	Subassembly	Mass [kg]	Vol. [m^3]	MTBF [h]	Run Time [h]	LL [y]	# in Pmry.	Power [kW]
ECLS	CDRA	Air Pump Two-Stage ORU	10.89	0.0045	156200.0	12960	15.29	1	0.860
		Blower	5.58	0.0300	129700.0	12960	10.00	1	
		Check Valves	39.92	0.1784	32900.0[i]	12960		1	
		Desiccant Beds	42.64	0.0850	77100.0	12960		2	
		Heat Controller	3.31	0.0085	242700.0	12960		2	
		Precooler	5.58	0.0255	129700.0	12960	10.00	1	
		Pump Fan Motor Controller	2.72	0.0057	2270000.0	12960		2	
		Selector Valves	3.04	0.0017	117000.0	12960	10.61	6	
		Sorbent Beds (Zeolite)	42.64	0.0850	77100.0	12960		2	
	CCAA (x5)	Condensing Heat Exchanger	49.71	0.3933	832600.0	12960		5	0.553
		Electronic Interface Box (EIB)	4.04	0.0173	2350000.0	12960		10	
		Fan Delta Pressure Sensor	0.45	0.0002	1250000.0	12960		5	
		Heat Exchanger Liquid Sensor	0.64	0.0006	1140000.0	12960		10	
		Inlet ORU	25.31	0.1308	333000.0	12960		5	
		Pressure Transducer	0.48	0.0000	1250000.0	12960	15.00	5	
		Temperature Control Check Valve (TCCV)	7.45	0.0071	32900.0	12960		10	
		Temperature Sensor	0.26	0.0014	37600000.0	12960		20	
		Water Separator	11.93	0.0583	131000.0	12960	5.00	10	
		Water Separator Liquid Sensor	0.64	0.0006	1140000.0[ii]	12960		10	
	WPA	Catalytic Reactor	67.04	0.1156	25579.2	1912	2.25	1	0.320
		Gas Separator	39.15	0.0660	84008.4	1912	1	1	
		Ion Exchange Bed	13.02	0.0173	296701.2	1912	0.16	1	
		Microbial Check Valve	5.76	0.0065	143488.8	1912	1	1	
		Multifiltration Bed #1	149.23	0.0657	296701.2	1912	0.36	1	
		Multifiltration Bed #2	149.23	0.0657	296701.2	1912	0.36	1	
		Particulate Filter	32.25	0.0717	717356.4	1912	0.22	1	
		pH Adjuster	2.54	0.0026	137181.6	1912	1	1	
		Process Controller	45.00	0.0838	87950.4	1912	7.72	1	
		Pump Separator	31.34	0.0869	42398.4	1912	2	1	
		Reactor Health Sensor	16.83	0.0425	56677.2	1912	1	1	
		Sensor	4.81	0.0034	143664	1912	10	1	
		Separator Filter	7.67	0.0102	359072.4	1912	0.84	1	
		Start-up Filter	9.44	0.0184	226884	1912	19.92	1	
		Water Delivery	47.54	0.0974	64561.2	1912	5	1	
	UPA	Distillation Assembly	92.76	0.1422	142525.2	4577	2	1	0.315
		Firmware Controller Assembly	23.09	0.0286	27331.2	4577	2.4	1	
		Fluids Control and Pump Assembly	47.58	0.0731	90140.4	4577	4	1	
		Pressure Control and Pump Assembly	49.08	0.1158	181507.2	4577	2	1	
		Advanced Recycle Filter Tank Assembly[xvi]	50.00	0.1011	199640.4	4577		1	
		Separator Plumbing Assembly	16.78	0.0229	384651.6	4577	1	1	
ISRU	Water Extractor	Oven + Insulating Cone	58.14	2.5186	242700[iii]	12960		1	16.32
		Hopper	48.49	2.9367		12960		1	
		Sieve	23.48	0.0000	500000[iv]	12960		1	
		Augers (vertical)	149.05	0.0000	500000[iv]	12960		1	0.045
		Horizontal Auger	9.82	0.1263	500000[iv]	12960		1	
		Sweep Gas System	0.01	0.0000	138408[v]	12960		1	
		Sweep Gas Piping	4.72	0.0807		12960		1	
		Condensing Heat Exchanger	28.29	0.5576	832600[vi]	12960		1	
		Water Filtration System	1.63	0.0061	296701.2[vii]	12960	0.36	1	
	CO2 Cryocooler	Cryocooler	34.61	0.0726	500000[iv]	12960		2	1.474
		Container	83.02	0.4906		12960		1	
	Water Electrolyzer	Electrolysis Cell Stack	47.43	0.0045	27156[viii]	12960	2.38	1	12.28
		O2 Separator / Water Reservoir	5.71	0.0119	27156[viii]	12960	2.38	1	

		H2 Separator and Dryer	14.44	0.0040	98112[ix]	12960	10	1	
		Water Pump	2.16	0.0007	144540[x]	12960	1	1	8×10^{-5}
	Sabatier Reactor	Reactor	20.78	0.4181	50000[xi]	12960		1	0.198
		Water / Methane Separator	0.24	0.0097	131000[xii]	12960		1	
		Heat Exchanger	0.53		832600[xiii]	12960		1	
	Atmospheric Processor	Zeolite	0.52	0.0062	77100[xiv]	12960		1	
		Compressor	7.80	0.0451	66666.7	12960		2	0.711
		Cryocoolers	3.10	0.0015	500000[iv]	12960		2	0.480
		Support Structure	3.35			12960		1	
BPC	Crop Lighting	Lighting System Unit[xvii]	8.00	0.0185	1743216	12960		7	4.41
	BPC Structure[xviii]	Primary Structure (Inflatable)	335.00					1	
		Secondary Structure (Shelving)	51.56					1	
		Mechanization Systems	37.08					1	
	Food Processor[xix]	Hand Mixer	2.00	0.0050				1	
		Food Processor / Blender	8.00	0.0230				1	
		Grinder / Mill	4.10	0.0120				1	
		Bread Machine	7.40	0.0310				1	
		Griddle / Grill	5.80	0.0270				1	
		Juice Extractor	7.70	0.0390				1	

[i]Analogy to CCAA TCCV
[ii]Analogy to CCAA Heat Exchanger Liquid Sensor
[iii]Analogy to CDRA Heater Controller
[iv]Optimistic assumption; no data were available
[v]Analogy to OGA Nitrogen Purge ORU
[vi]Analogy CCAA Condensing Heat Exchanger
[vii]Analogy to WPA Multifiltration Bed
[viii]Analogy to OGA Hydrogen ORU (contains Electrolysis Cell Stack and Rotary Separator / Accumulator)
[ix]Analogy to OGA Oxygen Outlet
[x]Analogy to OGA Pump
[xi]Analogy to CRS Sabatier Methanation Reactor
[xii]Analogy to CRS Phase Separator
[xiii]Analogy to CRS Condensing Heat Exchanger
[xiv]Analogy to CDRA Dessicant-Adsorbent Bed
[xv]Analogy to CRS Compressor
[xvi]Mass is obtained from [300] and verified with calculations based on data from Link et al. [301]. All other data is assumed to be the same as the Recycle Filter Tank Assembly (RFTA) described in the NASA BVAD 2004 [209] – the original system from which the ARFTA was upgraded from. Here, the life limit of the ARFTA has been assumed to be zero, based on its development objective of facilitating the same function as the RFTA without the need for periodic replacement [301].
[xvii]Based on the Heliospectra LX601 grow light [213]. MTBF value is based on the assumption that a 2 year warranty accounts for 1% failures during that time
[xviii]Based on assumptions listed in Section 6.3.3
[xix]Based on sizing estimates from Stilwell et al. [367]

Table J.17: Architecture Case 6 Spare Parts Requirements for each Component over a 10 Mission String of Sorties Campaign. Empty rows correspond to components assumed to have 100% reliability, and hence do not require spare parts

Group	Assembly	Subassembly	Mission									
			1	**2**	**3**	**4**	**5**	**6**	**7**	**8**	**9**	**10**
ECLSS	CDRA	Air Pump Two-Stage ORU	3	0	1	1	0	0	1	0	0	1
		Blower	3	1	1	0	0	1	0	1	0	0
		Check Valves	4	2	1	1	1	1	0	2	0	1
		Desiccant Beds	4	1	2	0	1	1	1	1	0	1
		Heat Controller	3	1	1	1	0	0	1	0	1	0
		Precooler	3	1	1	0	0	1	0	1	0	1
		Pump Fan Motor Controller	2	0	1	0	0	0	0	0	1	0
		Selector Valves	6	2	2	3	1	1	1	2	1	2
		Sorbent Beds (Zeolite)	4	1	2	0	1	1	1	1	0	1
	CCAA	Condensing Heat Exchanger	2	1	1	0	0	0	1	0	0	1
		Electronic Interface Box (EIB)	3	0	1	0	0	1	0	0	1	0
		Fan Delta Pressure Sensor	3	1	1	0	0	0	1	0	0	1
		Heat Exchanger Liquid Sensor	4	0	2	0	1	0	0	1	1	0
		Inlet ORU	3	1	1	1	1	0	1	0	1	0
		Pressure Transducer	3	1	0	1	0	0	1	0	0	1
		Temperature Control Check Valve (TCCV)	14	7	7	7	4	6	5	6	6	5
		Temperature Sensor	2	0	1	0	0	0	0	1	0	0
		Water Separator	7	2	3	2	2	1	3	1	2	2
		Water Separator Liquid Sensor	4	0	2	0	1	0	0	1	0	1
	WPA	Catalytic Reactor	2	1	0	1	0	0	1	0	0	0
		Gas Separator	2	0	0	1	0	0	0	0	0	1

		Ion Exchange Bed	1	1	2	1	1	2	1	1	2	1
		Microbial Check Valve	2	0	0	1	0	0	0	0	0	1
		Multifiltration Bed #1	1	0	0	1	1	0	1	0	1	1
		Multifiltration Bed #2	1	0	0	1	1	0	1	0	1	1
		Particulate Filter	1	0	1	1	1	1	1	1	1	1
		pH Adjuster	2	0	1	0	0	0	0	1	0	0
		Process Controller	2	0	0	0	1	0	0	0	0	0
		Pump Separator	2	1	0	0	1	0	0	0	1	0
		Reactor Health Sensor	2	0	1	0	0	0	1	0	0	0
		Sensor	2	0	1	0	0	0	0	0	0	1
		Separator Filter	1	1	0	0	0	0	0	0	1	0
		Start-up Filter	1	1	0	0	0	0	1	0	0	0
		Water Delivery	2	0	1	0	0	0	0	1	0	0
	UPA	Distillation Assembly	2	0	1	0	0	0	0	0	1	0
		Firmware Controller Assembly	3	1	1	1	0	1	0	1	0	1
		Fluids Control and Pump Assembly	2	1	0	0	1	0	0	0	1	0
		Pressure Control and Pump Assembly	2	0	1	0	0	0	0	0	1	0
		Advanced Recycle Filter Tank Assembly[xvi]	2	0	0	1	0	0	0	0	0	0
		Separator Plumbing Assembly	2	0	0	0	0	1	0	1	0	1
ISRU	Water Extractor	Oven + Insulating Cone	2	1	0	0	1	0	0	0	1	0
		Hopper										
		Sieve	2	0	1	0	0	0	0	1	0	0
		Augers (vertical)	1	1	0	0	0	1	0	0	0	0
		Horizontal Auger	2	0	1	0	0	0	1	0	0	0
		Sweep Gas System	4	1	1	2	0	0	0	1	0	1
		Sweep Gas Piping										
		Condensing Heat Exchanger	2	0	0	0	1	0	0	0	0	0
		Water Filtration System	4	4	4	4	4	4	4	4	4	5
	CO2 Cryocooler	Cryocooler	2	1	0	0	1	0	0	1	0	0
		Container										
	Water Electrolyzer	Electrolysis Cell Stack	5	1	2	1	1	1	1	1	1	1
		O2 Separator / Water Reservoir	5	2	2	1	1	1	1	2	0	1
		H2 Separator and Dryer	3	1	1	0	1	0	1	0	1	0
		Water Pump	3	1	1	0	2	1	2	1	2	1
	Sabatier Reactor	Reactor	4	1	1	1	1	0	1	1	0	1
		Water / Methane Separator	3	1	2	0	0	0	1	1	0	1
		Heat Exchanger	2	0	1	0	1	0	0	0	0	1
	Atmospheric Processor	Zeolite	4	1	2	0	1	0	1	0	1	1
		Compressor	5	1	2	1	1	1	0	2	1	0
		Cryocoolers	3	0	1	0	1	0	0	0	1	0
		Support Structure										
BPC	Crop Lighting	Lighting System Unit	2	1	1	3	0	0	0	7	0	0

Table J.18: Architecture Case 6 Spare Parts Requirements for each Component over a 10 Mission String of Sorties Campaign with all ISRU technologies at 10% of their originally estimated values. Empty rows correspond to components assumed to have 100% reliability, and hence do not require spare parts

Group	**Assembly**	**Subassembly**	**Mission**									
			1	**2**	**3**	**4**	**5**	**6**	**7**	**8**	**9**	**10**
ECLSS	CDRA	Air Pump Two-Stage ORU	3	1	0	1	0	1	0	0	0	1
		Blower	3	1	1	0	1	0	1	0	0	0
		Check Valves	4	2	1	1	1	1	1	1	1	0
		Desiccant Beds	4	1	2	0	1	1	1	1	0	1
		Heat Controller	3	1	1	1	0	1	0	0	1	0
		Precooler	3	1	1	0	1	0	1	0	0	1
		Pump Fan Motor Controller	2	0	1	0	0	0	0	0	1	0
		Selector Valves	6	3	2	1	2	1	2	1	1	1
		Sorbent Beds (Zeolite)	4	1	2	0	1	1	1	1	0	1
	CCAA	Condensing Heat Exchanger	2	1	1	0	0	1	0	0	1	0
		Electronic Interface Box (EIB)	3	0	1	0	1	0	0	1	0	0
		Fan Delta Pressure Sensor	3	1	1	0	0	1	0	0	1	0
		Heat Exchanger Liquid Sensor	4	1	1	1	0	0	1	0	1	0
		Inlet ORU	3	2	0	1	1	0	1	0	1	0
		Pressure Transducer	3	1	0	1	0	1	0	0	1	0

		Temperature Control Check Valve (TCCV)	14	8	7	6	5	6	6	5	5	5
		Temperature Sensor	2	1	0	0	0	0	0	1	0	0
		Water Separator	7	3	2	2	2	2	2	2	1	2
		Water Separator Liquid Sensor	4	1	1	0	1	0	1	0	1	0
	WPA	Catalytic Reactor	2	1	0	1	0	0	1	0	0	1
		Gas Separator	2	0	0	1	0	0	0	0	1	0
		Ion Exchange Bed	1	1	2	1	1	2	1	1	2	1
		Microbial Check Valve	2	0	1	0	0	0	0	0	1	0
		Multifiltration Bed #1	1	0	1	0	1	0	1	0	1	1
		Multifiltration Bed #2	1	0	0	1	1	0	1	0	1	1
		Particulate Filter	1	0	1	1	1	1	1	1	1	1
		pH Adjuster	2	0	1	0	0	0	1	0	0	0
		Process Controller	2	0	0	1	0	0	0	0	0	0
		Pump Separator	2	1	0	0	1	0	0	0	1	0
		Reactor Health Sensor	2	1	0	0	0	1	0	0	0	0
		Sensor	2	0	1	0	0	0	0	0	1	0
		Separator Filter	1	1	0	0	0	0	0	1	0	0
		Start-up Filter	2	0	0	0	0	1	0	0	0	0
		Water Delivery	2	0	1	0	0	0	0	1	0	0
	UPA	Distillation Assembly	2	0	1	0	0	0	0	1	0	0
		Firmware Controller Assembly	3	1	1	1	0	1	0	1	0	1
		Fluids Control and Pump Assembly	2	1	0	0	1	0	0	0	1	0
		Pressure Control and Pump Assembly	2	0	1	0	0	0	0	0	1	0
		Advanced Recycle Filter Tank Assembly[xvi]	2	0	0	1	0	0	0	0	0	1
		Separator Plumbing Assembly	2	0	0	0	0	1	0	1	0	1
ISRU	Water Extractor	Oven + Insulating Cone	5	2	1	1	1	2	1	1	1	1
		Hopper										
		Sieve	4	1	1	1	1	1	0	1	0	1
		Augers (vertical)	3	1	1	1	1	0	1	1	0	1
		Horizontal Auger	4	1	2	0	1	1	1	0	1	0
		Sweep Gas System	9	3	3	2	2	3	2	1	2	2
		Sweep Gas Piping										
		Condensing Heat Exchanger	3	1	1	0	1	1	0	0	1	0
		Water Filtration System	5	3	4	4	4	4	4	4	4	5
	CO2 Cryocooler	Cryocooler	5	2	1	1	2	1	1	1	1	1
		Container										
	Water Electrolyzer	Electrolysis Cell Stack	14	9	7	6	6	7	6	6	7	5
		O2 Separator / Water Reservoir	16	9	7	7	7	7	6	7	6	5
		H2 Separator and Dryer	8	3	3	2	3	2	2	3	2	1
		Water Pump	7	3	2	2	3	1	2	2	1	2
	Sabatier Reactor	Reactor	10	6	5	4	4	4	4	3	4	3
		Water / Methane Separator	9	3	3	2	1	4	1	2	2	1
		Heat Exchanger	4	2	0	1	1	1	0	1	0	0
	Atmospheric Processor	Zeolite	10	6	3	4	2	4	1	4	2	3
		Compressor	14	7	7	6	5	6	6	5	5	5
		Cryocoolers	5	3	1	2	1	2	1	1	1	1
		Support Structure										
BPC	Crop Lighting	Lighting System Unit	2	1	1	3	0	0	0	7	0	0

J.2.7 Architecture Case 7

Table J.19: Architecture Case 7 Master Equipment List, containing component mass, volume and reliability data, as well as run times and power demands. Power is listed here on a per unit basis. ISRU technologies displayed here were sized by the HabNet ISRU Module.

Sys.	Assembly	Subassembly	Mass [kg]	Vol. [m^3]	MTBF [h]	Run Time [h]	LL [y]	# in Pmry.	Power [kW]
ECLS	CDRA	Air Pump Two-Stage ORU	10.89	0.0045	156200.0	12960	15.29	1	0.860
		Blower	5.58	0.0300	129700.0	12960	10.00	1	
		Check Valves	39.92	0.1784	32900.0[i]	12960		1	

		Desiccant Beds	42.64	0.0850	77100.0	12960		2	
		Heat Controller	3.31	0.0085	242700.0	12960		2	
		Precooler	5.58	0.0255	129700.0	12960	10.00	1	
		Pump Fan Motor Controller	2.72	0.0057	2270000.0	12960		2	
		Selector Valves	3.04	0.0017	117000.0	12960	10.61	6	
		Sorbent Beds (Zeolite)	42.64	0.0850	77100.0	12960		2	
	CCAA (x5)	Condensing Heat Exchanger	49.71	0.3933	832600.0	12960		5	0.705
		Electronic Interface Box (EIB)	4.04	0.0173	2350000.0	12960		10	
		Fan Delta Pressure Sensor	0.45	0.0002	1250000.0	12960		5	
		Heat Exchanger Liquid Sensor	0.64	0.0006	1140000.0	12960		10	
		Inlet ORU	25.31	0.1308	333000.0	12960		5	
		Pressure Transducer	0.48	0.0000	1250000.0	12960	15.00	5	
		Temperature Control Check Valve (TCCV)	7.45	0.0071	32900.0	12960		10	
		Temperature Sensor	0.26	0.0014	37600000.0	12960		20	
		Water Separator	11.93	0.0583	131000.0	12960	5.00	10	
		Water Separator Liquid Sensor	0.64	0.0006	1140000.0[ii]	12960		10	
	WPA	Catalytic Reactor	67.04	0.1156	25579.2	4416	2.25	1	0.320
		Gas Separator	39.15	0.0660	84008.4	4416	1	1	
		Ion Exchange Bed	13.02	0.0173	296701.2	4416	0.16	1	
		Microbial Check Valve	5.76	0.0065	143488.8	4416	1	1	
		Multifiltration Bed #1	149.23	0.0657	296701.2	4416	0.36	1	
		Multifiltration Bed #2	149.23	0.0657	296701.2	4416	0.36	1	
		Particulate Filter	32.25	0.0717	717356.4	4416	0.22	1	
		pH Adjuster	2.54	0.0026	137181.6	4416	1	1	
		Process Controller	45.00	0.0838	87950.4	4416	7.72	1	
		Pump Separator	31.34	0.0869	42398.4	4416	2	1	
		Reactor Health Sensor	16.83	0.0425	56677.2	4416	1	1	
		Sensor	4.81	0.0034	143664	4416	10	1	
		Separator Filter	7.67	0.0102	359072.4	4416	0.84	1	
		Start-up Filter	9.44	0.0184	226884	4416	19.92	1	
		Water Delivery	47.54	0.0974	64561.2	4416	5	1	
	UPA	Distillation Assembly	92.76	0.1422	142525.2	4566	2	1	0.315
		Firmware Controller Assembly	23.09	0.0286	27331.2	4566	2.4	1	
		Fluids Control and Pump Assembly	47.58	0.0731	90140.4	4566	4	1	
		Pressure Control and Pump Assembly	49.08	0.1158	181507.2	4566	2	1	
		Advanced Recycle Filter Tank Assembly[xvi]	50.00	0.1011	199640.4	4566		1	
		Separator Plumbing Assembly	16.78	0.0229	384651.6	4566	1	1	
ISRU	Water Extractor	Oven + Insulating Cone	76.38	3.3087	242700[iii]	12960		1	21.43
		Hopper	57.75	3.8579		12960		1	
		Sieve	35.35	0.0000	500000[iv]	12960		1	
		Augers (vertical)	195.80	0.0000	500000[iv]	12960		1	0.053
		Horizontal Auger	11.26	0.1447	500000[iv]	12960		1	
		Sweep Gas System	0.02	0.0000	138408[v]	12960		1	
		Sweep Gas Piping	5.92	0.1153		12960		1	
		Condensing Heat Exchanger	37.02	0.8287	832600[vi]	12960		1	
		Water Filtration System	2.14	0.0080	296701.2[vii]	12960	0.36	1	
	CO2 Cryocooler	Cryocooler	40.62	0.0852	500000[iv]	12960		2	1.730
		Container	97.43	0.5758		12960		1	
	Water Electrolyzer	Electrolysis Cell Stack	47.43	0.0045	27156[viii]	12960	2.38	1	12.28
		O2 Separator / Water Reservoir	5.71	0.0119	27156[viii]	12960	2.38	1	
		H2 Separator and Dryer	14.44	0.0040	98112[ix]	12960	10	1	
		Water Pump	2.16	0.0007	144540[x]	12960	1	1	8×10^{-5}
	Sabatier Reactor	Reactor	20.78	0.4181	50000[xi]	12960		1	0.198
		Water / Methane Separator	0.24	0.0097	131000[xii]	12960		1	
		Heat Exchanger	0.53		832600[xiii]	12960		1	
	Atmospheric Processor	Zeolite	1.06	0.0128	77100[xiv]	12960		1	
		Compressor	16.09	0.0930	66666.7	12960		2	1.466
		Cryocoolers	3.10	0.0015	500000[iv]	12960		2	0.480
		Support Structure	6.90			12960		1	
BPC	Crop Lighting	Lighting System Unit[xvii]	8.00	0.0185	1743216	12960		69	43.47
	ORA[xx]	Air Pump Two-Stage ORU	10.89	0.0045	156200.0	12960	15.29	1	0.860
		Blower	5.58	0.0300	129700.0	12960	10.00	1	

	Check Valves	39.92	0.1784	32900.0[i]	12960		1
	Desiccant Beds	42.64	0.0850	77100.0	12960		2
	Heat Controller	3.31	0.0085	242700.0	12960		2
	Precooler	5.58	0.0255	129700.0	12960	10.00	1
	Pump Fan Motor Controller	2.72	0.0057	2270000.0	12960		2
	Selector Valves	3.04	0.0017	117000.0	12960	10.61	6
	Sorbent Beds (Zeolite)	42.64	0.0850	77100.0	12960		2
BPC Structure[xviii]	Primary Structure (Inflatable)	335.00					1
	Secondary Structure (Shelving)	51.56					1
	Mechanization Systems	37.08					1
Food Processor[xix]	Hand Mixer	2.00	0.0050				1
	Food Processor / Blender	8.00	0.0230				1
	Grinder / Mill	4.10	0.0120				1
	Bread Machine	7.40	0.0310				1
	Griddle / Grill	5.80	0.0270				1
	Juice Extractor	7.70	0.0390				1

[i]Analogy to CCAA TCCV
[ii]Analogy to CCAA Heat Exchanger Liquid Sensor
[iii]Analogy to CDRA Heater Controller
[iv]Optimistic assumption; no data were available
[v]Analogy to OGA Nitrogen Purge ORU
[vi]Analogy CCAA Condensing Heat Exchanger
[vii]Analogy to WPA Multifiltration Bed
[viii]Analogy to OGA Hydrogen ORU (contains Electrolysis Cell Stack and Rotary Separator / Accumulator)
[ix]Analogy to OGA Oxygen Outlet
[x]Analogy to OGA Pump
[xi]Analogy to CRS Sabatier Methanation Reactor
[xii]Analogy to CRS Phase Separator
[xiii]Analogy to CRS Condensing Heat Exchanger
[xiv]Analogy to CDRA Dessicant-Adsorbent Bed
[xv]Analogy to CRS Compressor
[xvi]Mass is obtained from [300] and verified with calculations based on data from Link et al. [301]. All other data is assumed to be the same as the Recycle Filter Tank Assembly (RFTA) described in the NASA BVAD 2004 [209] – the original system from which the ARFTA was upgraded from. Here, the life limit of the ARFTA has been assumed to be zero, based on its development objective of facilitating the same function as the RFTA without the need for periodic replacement [301].
[xvii]Based on the Heliospectra LX601 grow light [213]. MTBF value is based on the assumption that a 2 year warranty accounts for 1% failures during that time
[xviii]Based on assumptions listed in Section 6.3.3
[xix]Based on sizing estimates from Stilwell et al. [367]
[xx]Analogy to CDRA

Table J.20: Architecture Case 7 Spare Parts Requirements for each Component over a 10 Mission String of Sorties Campaign. Empty rows correspond to components assumed to have 100% reliability, and hence do not require spare parts

Group	Assembly	Subassembly	Mission									
			1	**2**	**3**	**4**	**5**	**6**	**7**	**8**	**9**	**10**
ECLSS	CDRA	Air Pump Two-Stage ORU	3	0	1	1	0	0	1	0	0	1
		Blower	3	1	1	0	1	0	0	1	0	0
		Check Valves	4	2	1	1	1	1	1	1	1	0
		Desiccant Beds	4	1	2	1	0	1	1	1	0	1
		Heat Controller	3	1	1	1	0	0	1	0	1	0
		Precooler	3	1	1	0	1	0	0	1	0	1
		Pump Fan Motor Controller	2	0	1	0	0	0	0	0	1	0
		Selector Valves	6	3	2	1	2	1	2	1	1	1
		Sorbent Beds (Zeolite)	4	1	2	1	1	0	1	1	0	1
	CCAA	Condensing Heat Exchanger	2	1	1	0	0	1	0	0	1	0
		Electronic Interface Box (EIB)	3	0	1	0	1	0	0	1	0	0
		Fan Delta Pressure Sensor	3	1	0	1	0	1	0	0	0	1
		Heat Exchanger Liquid Sensor	4	1	0	1	1	1	0	0	1	1
		Inlet ORU	3	1	1	1	1	0	1	0	1	0
		Pressure Transducer	3	1	0	1	0	1	0	0	0	1
		Temperature Control Check Valve (TCCV)	14	7	7	7	6	4	6	5	6	5
		Temperature Sensor	2	0	0	1	0	0	0	0	1	0
		Water Separator	7	3	2	2	2	2	2	2	1	2
		Water Separator Liquid Sensor	4	1	0	1	1	0	0	1	1	0
	WPA	Catalytic Reactor	3	1	1	0	1	0	1	0	1	0
		Gas Separator	2	1	0	1	0	0	0	1	0	0
		Ion Exchange Bed	3	3	3	3	3	3	4	3	3	3
		Microbial Check Valve	2	1	0	1	0	0	0	0	1	0
		Multifiltration Bed #1	1	1	2	1	2	1	1	2	1	2

		Multifiltration Bed #2	1	1	2	1	2	1	1	2	1	2
		Particulate Filter	2	2	2	3	2	2	3	2	2	2
		pH Adjuster	2	1	0	1	0	0	0	1	0	0
		Process Controller	2	1	0	0	1	0	0	0	1	0
		Pump Separator	3	0	1	1	0	0	1	0	0	1
		Reactor Health Sensor	3	0	1	0	1	0	0	1	0	0
		Sensor	2	1	0	1	0	0	0	0	1	0
		Separator Filter	2	0	0	1	0	0	1	0	1	1
		Start-up Filter	2	0	1	0	0	0	0	1	0	0
		Water Delivery	2	1	0	1	0	0	1	0	0	1
	UPA	Distillation Assembly	2	0	0	1	0	0	0	1	0	0
		Firmware Controller Assembly	3	1	1	1	0	1	0	1	0	1
		Fluids Control and Pump Assembly	2	1	0	0	1	0	0	0	1	0
		Pressure Control and Pump Assembly	2	0	0	1	0	0	0	0	1	0
		Advanced Recycle Filter Tank Assembly[xvi]	2	0	0	1	0	0	0	0	0	1
		Separator Plumbing Assembly	2	0	0	0	1	0	0	1	0	1
ISRU	Water Extractor	Oven + Insulating Cone	2	1	0	0	1	0	0	0	1	0
		Hopper										
		Sieve	2	0	1	0	0	0	0	1	0	0
		Augers (vertical)	2	0	0	0	0	1	0	0	0	0
		Horizontal Auger	2	0	1	0	0	1	0	0	0	0
		Sweep Gas System	4	1	1	0	1	1	0	0	1	1
		Sweep Gas Piping										
		Condensing Heat Exchanger	2	0	0	0	1	0	0	0	0	0
		Water Filtration System	4	4	4	4	4	4	4	4	4	5
	CO2 Cryocooler	Cryocooler	2	1	0	0	1	0	0	1	0	0
		Container										
	Water Electrolyzer	Electrolysis Cell Stack	5	1	2	1	1	1	1	1	1	1
		O2 Separator / Water Reservoir	5	2	2	1	2	0	1	1	2	0
		H2 Separator and Dryer	3	1	1	0	1	0	1	0	1	0
		Water Pump	3	1	1	0	2	1	2	1	2	1
	Sabatier Reactor	Reactor	4	1	1	1	1	0	1	1	0	1
		Water / Methane Separator	4	0	2	0	1	0	1	0	1	0
		Heat Exchanger	2	1	0	0	1	0	0	0	0	1
	Atmospheric Processor	Zeolite	4	1	1	1	1	0	1	0	1	1
		Compressor	4	2	2	1	1	1	0	1	1	1
		Cryocoolers	3	0	1	0	1	0	0	0	0	1
		Support Structure										
BPC	Crop Lighting	Lighting System Unit	5	2	2	60	0	0	0	69	0	0
	ORA	Air Pump Two-Stage ORU	3	0	1	1	0	0	1	0	0	1
		Blower	3	1	1	0	1	0	0	1	0	0
		Check Valves	4	2	1	1	1	1	1	1	1	0
		Desiccant Beds	4	1	1	1	1	1	1	1	0	1
		Heat Controller	3	1	1	1	0	0	1	0	1	0
		Precooler	3	1	1	0	1	0	0	1	0	0
		Pump Fan Motor Controller	2	0	1	0	0	0	0	0	1	0
		Selector Valves	6	2	3	1	2	1	2	1	1	1
		Sorbent Beds (Zeolite)	4	1	1	2	0	1	1	1	0	1

Table J.21: Architecture Case 7 Spare Parts Requirements for each Component over a 10 Mission String of Sorties Campaign with all ISRU technologies at 10% of their originally estimated values. Empty rows correspond to components assumed to have 100% reliability, and hence do not require spare parts

Group	**Assembly**	**Subassembly**	**Mission**									
			1	**2**	**3**	**4**	**5**	**6**	**7**	**8**	**9**	**10**
ECLSS	CDRA	Air Pump Two-Stage ORU	3	1	0	1	0	1	0	0	0	1
		Blower	3	1	1	0	1	0	1	0	0	1
		Check Valves	4	2	1	1	1	1	1	1	1	1
		Desiccant Beds	4	2	1	1	1	0	1	1	1	0
		Heat Controller	3	1	1	0	1	1	0	0	1	0
		Precooler	3	1	1	0	1	0	1	0	0	1
		Pump Fan Motor Controller	2	0	1	0	0	0	0	0	1	0
		Selector Valves	7	2	2	1	2	2	1	1	2	1

		Sorbent Beds (Zeolite)	4	2	1	1	0	1	1	1	1	0
	CCAA	Condensing Heat Exchanger	3	0	1	0	0	1	0	0	1	0
		Electronic Interface Box (EIB)	3	1	0	0	1	0	0	0	1	0
		Fan Delta Pressure Sensor	3	1	1	0	0	1	0	0	1	0
		Heat Exchanger Liquid Sensor	4	1	1	0	1	0	0	2	0	0
		Inlet ORU	4	1	0	1	1	0	1	0	1	0
		Pressure Transducer	3	1	1	0	0	1	0	0	0	1
		Temperature Control Check Valve (TCCV)	14	8	6	6	7	5	6	5	5	6
		Temperature Sensor	2	1	0	0	0	0	0	1	0	0
		Water Separator	7	3	2	2	2	2	2	2	1	2
		Water Separator Liquid Sensor	4	1	1	0	1	0	1	0	1	0
	WPA	Catalytic Reactor	3	1	1	0	1	1	0	0	1	0
		Gas Separator	2	1	0	1	0	0	0	1	0	0
		Ion Exchange Bed	3	3	3	3	3	3	4	3	3	3
		Microbial Check Valve	2	1	0	0	1	0	0	0	1	0
		Multifiltration Bed #1	1	1	2	1	2	1	1	2	1	2
		Multifiltration Bed #2	1	1	2	1	2	1	1	2	1	2
		Particulate Filter	2	2	2	3	2	2	3	2	2	2
		pH Adjuster	3	0	0	1	0	0	0	1	0	0
		Process Controller	2	1	0	0	1	0	0	1	0	0
		Pump Separator	3	1	0	1	0	1	0	0	1	0
		Reactor Health Sensor	3	0	1	0	1	0	1	0	0	0
		Sensor	2	1	0	1	0	0	0	0	1	0
		Separator Filter	2	0	0	1	0	0	1	0	1	1
		Start-up Filter	2	0	1	0	0	0	1	0	0	0
		Water Delivery	2	1	0	1	0	1	0	0	0	1
	UPA	Distillation Assembly	2	0	0	1	0	0	0	1	0	0
		Firmware Controller Assembly	3	1	1	1	0	1	1	0	0	1
		Fluids Control and Pump Assembly	2	1	0	0	1	0	0	1	0	0
		Pressure Control and Pump Assembly	2	0	1	0	0	0	0	0	1	0
		Advanced Recycle Filter Tank Assembly[xvi]	2	0	0	1	0	0	0	0	0	1
		Separator Plumbing Assembly	2	0	0	0	1	0	0	1	0	1
ISRU	Water Extractor	Oven + Insulating Cone	5	1	2	1	1	2	1	1	1	1
		Hopper										
		Sieve	4	1	1	1	1	0	1	1	0	1
		Augers (vertical)	3	1	1	1	1	0	1	1	0	1
		Horizontal Auger	4	1	2	0	1	1	1	0	1	1
		Sweep Gas System	9	4	1	3	2	2	2	3	1	3
		Sweep Gas Piping										
		Condensing Heat Exchanger	3	1	1	0	1	1	0	0	1	0
		Water Filtration System	6	2	4	4	4	4	4	4	4	5
	CO2 Cryocooler	Cryocooler	5	2	1	1	2	1	1	1	1	1
		Container										
	Water Electrolyzer	Electrolysis Cell Stack	15	8	7	7	6	7	6	6	6	6
		O2 Separator / Water Reservoir	16	8	8	7	7	7	6	6	7	6
		H2 Separator and Dryer	8	3	3	2	3	3	2	2	2	2
		Water Pump	7	3	3	2	2	1	2	2	1	2
	Sabatier Reactor	Reactor	11	5	5	4	4	4	4	3	4	4
		Water / Methane Separator	9	3	3	2	2	2	3	1	3	3
		Heat Exchanger	4	1	1	1	1	1	0	1	0	1
	Atmospheric Processor	Zeolite	10	5	4	2	3	4	2	3	3	3
		Compressor	14	7	6	6	5	7	5	5	5	5
		Cryocoolers	6	1	2	2	1	1	1	1	1	1
		Support Structure										
BPC	Crop Lighting	Lighting System Unit	6	1	2	60	0	0	0	69	0	0
	ORA	Air Pump Two-Stage ORU	3	1	0	1	0	1	0	0	0	1
		Blower	3	1	1	0	1	0	1	0	0	1
		Check Valves	4	2	1	1	1	1	1	1	1	0
		Desiccant Beds	4	1	2	1	0	1	1	1	0	1
		Heat Controller	3	1	1	1	0	1	0	0	1	0
		Precooler	3	1	1	0	1	0	1	0	0	1
		Pump Fan Motor Controller	2	0	1	0	0	0	0	0	1	0
		Selector Valves	7	2	2	1	2	1	2	1	1	1
		Sorbent Beds (Zeolite)	4	1	2	1	0	1	1	1	1	0

J.2.8 Architecture Case 8

Table J.22: Architecture Case 8 Master Equipment List, containing component mass, volume and reliability data, as well as run times and power demands. Power is listed here on a per unit basis. ISRU technologies displayed here were sized by the HabNet ISRU Module.

Sys.	Assembly	Subassembly	Mass [kg]	Vol. [m^3]	MTBF [h]	Run Time [h]	LL [y]	# in Pmry.	Power [kW]
ECLS	CDRA	Air Pump Two-Stage ORU	10.89	0.0045	156200.0	12960	15.29	1	0.860
		Blower	5.58	0.0300	129700.0	12960	10.00	1	
		Check Valves	39.92	0.1784	32900.0[i]	12960		1	
		Desiccant Beds	42.64	0.0850	77100.0	12960		2	
		Heat Controller	3.31	0.0085	242700.0	12960		2	
		Precooler	5.58	0.0255	129700.0	12960	10.00	1	
		Pump Fan Motor Controller	2.72	0.0057	2270000.0	12960		2	
		Selector Valves	3.04	0.0017	117000.0	12960	10.61	6	
		Sorbent Beds (Zeolite)	42.64	0.0850	77100.0	12960		2	
	CCAA (x5)	Condensing Heat Exchanger	49.71	0.3933	832600.0	12960		5	0.705
		Electronic Interface Box (EIB)	4.04	0.0173	2350000.0	12960		10	
		Fan Delta Pressure Sensor	0.45	0.0002	1250000.0	12960		5	
		Heat Exchanger Liquid Sensor	0.64	0.0006	1140000.0	12960		10	
		Inlet ORU	25.31	0.1308	333000.0	12960		5	
		Pressure Transducer	0.48	0.0000	1250000.0	12960	15.00	5	
		Temperature Control Check Valve (TCCV)	7.45	0.0071	32900.0	12960		10	
		Temperature Sensor	0.26	0.0014	37600000.0	12960		20	
		Water Separator	11.93	0.0583	131000.0	12960	5.00	10	
		Water Separator Liquid Sensor	0.64	0.0006	1140000.0[ii]	12960		10	
	WPA	Catalytic Reactor	67.04	0.1156	25579.2	4432	2.25	1	0.320
		Gas Separator	39.15	0.0660	84008.4	4432	1	1	
		Ion Exchange Bed	13.02	0.0173	296701.2	4432	0.16	1	
		Microbial Check Valve	5.76	0.0065	143488.8	4432	1	1	
		Multifiltration Bed #1	149.23	0.0657	296701.2	4432	0.36	1	
		Multifiltration Bed #2	149.23	0.0657	296701.2	4432	0.36	1	
		Particulate Filter	32.25	0.0717	717356.4	4432	0.22	1	
		pH Adjuster	2.54	0.0026	137181.6	4432	1	1	
		Process Controller	45.00	0.0838	87950.4	4432	7.72	1	
		Pump Separator	31.34	0.0869	42398.4	4432	2	1	
		Reactor Health Sensor	16.83	0.0425	56677.2	4432	1	1	
		Sensor	4.81	0.0034	143664	4432	10	1	
		Separator Filter	7.67	0.0102	359072.4	4432	0.84	1	
		Start-up Filter	9.44	0.0184	226884	4432	19.92	1	
		Water Delivery	47.54	0.0974	64561.2	4432	5	1	
	UPA	Distillation Assembly	92.76	0.1422	142525.2	4561	2	1	0.315
		Firmware Controller Assembly	23.09	0.0286	27331.2	4561	2.4	1	
		Fluids Control and Pump Assembly	47.58	0.0731	90140.4	4561	4	1	
		Pressure Control and Pump Assembly	49.08	0.1158	181507.2	4561	2	1	
		Advanced Recycle Filter Tank Assembly[xvi]	50.00	0.1011	199640.4	4561		1	
		Separator Plumbing Assembly	16.78	0.0229	384651.6	4561	1	1	
ISRU	Water Extractor	Oven + Insulating Cone	94.82	4.1072	242700[iii]	12960		1	26.60
		Hopper	66.51	4.7890		12960		1	
		Sieve	48.90	0.0000	500000[iv]	12960		1	
		Augers (vertical)	243.06	0.0000	500000[iv]	12960		1	0.060
		Horizontal Auger	12.55	0.1612	500000[iv]	12960		1	
		Sweep Gas System	0.02	0.0000	138408[v]	12960		1	
		Sweep Gas Piping	7.08	0.1531		12960		1	
		Condensing Heat Exchanger	45.83	1.1356	832600[vi]	12960		1	
		Water Filtration System	2.65	0.0100	296701.2[vii]	12960	0.36	1	
	CO2 Cryocooler	Cryocooler	46.69	0.0980	500000[iv]	12960		2	1.999
		Container	112.00	0.6619		12960		1	
	Water Electrolyzer	Electrolysis Cell Stack	47.43	0.0045	27156[viii]	12960	2.38	1	12.28
		O2 Separator / Water Reservoir	5.71	0.0119	27156[viii]	12960	2.38	1	

		H2 Separator and Dryer	14.44	0.0040	98112[ix]	12960	10	1	
		Water Pump	2.16	0.0007	144540[x]	12960	1	1	8×10^{-5}
	Sabatier Reactor	Reactor	20.78	0.4181	50000[xi]	12960		1	0.198
		Water / Methane Separator	0.24	0.0097	131000[xii]	12960		1	
		Heat Exchanger	0.53		832600[xiii]	12960		1	
	Atmospheric Processor	Zeolite	1.36	0.0163	77100[xiv]	12960		1	
		Compressor	20.54	0.1188	66666.7	12960		2	1.872
		Cryocoolers	3.10	0.0015	500000[iv]	12960		2	0.480
		Support Structure	8.81			12960		1	
BPC	Crop Lighting ORA[xx]	Lighting System Unit[xvii]	8.00	0.0185	1743216	12960		137	86.31
		Air Pump Two-Stage ORU	10.89	0.0045	156200.0	12960	15.29	1	0.860
		Blower	5.58	0.0300	129700.0	12960	10.00	1	
		Check Valves	39.92	0.1784	32900.0[i]	12960		1	
		Desiccant Beds	42.64	0.0850	77100.0	12960		2	
		Heat Controller	3.31	0.0085	242700.0	12960		2	
		Precooler	5.58	0.0255	129700.0	12960	10.00	1	
		Pump Fan Motor Controller	2.72	0.0057	2270000.0	12960		2	
		Selector Valves	3.04	0.0017	117000.0	12960	10.61	6	
		Sorbent Beds (Zeolite)	42.64	0.0850	77100.0	12960		2	
	BPC Structure[xviii]	Primary Structure (Inflatable)	335.00					1	
		Secondary Structure (Shelving)	51.56					1	
		Mechanization Systems	37.08					1	
	Food Processor[xix]	Hand Mixer	2.00	0.0050				1	
		Food Processor / Blender	8.00	0.0230				1	
		Grinder / Mill	4.10	0.0120				1	
		Bread Machine	7.40	0.0310				1	
		Griddle / Grill	5.80	0.0270				1	
		Juice Extractor	7.70	0.0390				1	

[i] Analogy to CCAA TCCV
[ii] Analogy to CCAA Heat Exchanger Liquid Sensor
[iii] Analogy to CDRA Heater Controller
[iv] Optimistic assumption; no data were available
[v] Analogy to OGA Nitrogen Purge ORU
[vi] Analogy CCAA Condensing Heat Exchanger
[vii] Analogy to WPA Multifiltration Bed
[viii] Analogy to OGA Hydrogen ORU (contains Electrolysis Cell Stack and Rotary Separator / Accumulator)
[ix] Analogy to OGA Oxygen Outlet
[x] Analogy to OGA Pump
[xi] Analogy to CRS Sabatier Methanation Reactor
[xii] Analogy to CRS Phase Separator
[xiii] Analogy to CRS Condensing Heat Exchanger
[xiv] Analogy to CDRA Dessicant-Adsorbent Bed
[xv] Analogy to CRS Compressor
[xvi] Mass is obtained from [300] and verified with calculations based on data from Link et al. [301]. All other data is assumed to be the same as the Recycle Filter Tank Assembly (RFTA) described in the NASA BVAD 2004 [209] – the original system from which the ARFTA was upgraded from. Here, the life limit of the ARFTA has been assumed to be zero, based on its development objective of facilitating the same function as the RFTA without the need for periodic replacement [301].
[xvii] Based on the Heliospectra LX601 grow light [213]. MTBF value is based on the assumption that a 2 year warranty accounts for 1% failures during that time
[xviii] Based on assumptions listed in Section 6.3.3
[xix] Based on sizing estimates from Stilwell et al. [367]
[xx] Analogy to CDRA

Table J.23: Architecture Case 8 Spare Parts Requirements for each Component over a 10 Mission String of Sorties Campaign. Empty rows correspond to components assumed to have 100% reliability, and hence do not require spare parts

Group	Assembly	Subassembly	Mission									
			1	**2**	**3**	**4**	**5**	**6**	**7**	**8**	**9**	**10**
ECLSS	CDRA	Air Pump Two-Stage ORU	3	1	0	1	0	0	1	0	0	1
		Blower	3	1	1	0	1	0	0	1	0	0
		Check Valves	5	1	1	1	1	1	1	1	1	0
		Desiccant Beds	4	1	2	1	0	1	1	1	0	1
		Heat Controller	4	0	1	0	1	1	0	0	1	0
		Precooler	3	1	1	0	1	0	0	1	0	1
		Pump Fan Motor Controller	2	0	1	0	0	0	0	0	0	1
		Selector Valves	7	2	2	2	2	0	2	1	1	2
		Sorbent Beds (Zeolite)	4	1	2	1	1	0	1	1	1	0
	CCAA	Condensing Heat Exchanger	3	0	1	0	0	1	0	0	1	0
		Electronic Interface Box (EIB)	3	0	1	0	1	0	0	0	1	0

		Fan Delta Pressure Sensor	3	1	1	0	0	1	0	0	0	1
		Heat Exchanger Liquid Sensor	4	1	1	0	1	1	0	0	1	0
		Inlet ORU	4	1	0	1	1	0	1	0	1	0
		Pressure Transducer	3	1	1	0	0	1	0	0	0	1
		Temperature Control Check Valve (TCCV)	15	6	8	5	7	5	5	6	5	5
		Temperature Sensor	2	0	1	0	0	0	1	0	0	0
		Water Separator	7	3	2	2	2	2	2	2	1	2
		Water Separator Liquid Sensor	4	1	1	0	1	0	1	0	1	0
	WPA	Catalytic Reactor	3	1	1	0	1	0	1	0	1	0
		Gas Separator	2	1	0	1	0	0	0	1	0	0
		Ion Exchange Bed	3	3	3	3	3	3	4	3	3	3
		Microbial Check Valve	2	1	0	0	1	0	0	0	1	0
		Multifiltration Bed #1	1	1	2	1	2	1	1	2	1	2
		Multifiltration Bed #2	1	1	2	1	2	1	1	2	1	2
		Particulate Filter	2	2	2	3	2	2	3	2	2	2
		pH Adjuster	3	0	0	1	0	0	0	1	0	0
		Process Controller	2	1	0	0	1	0	0	1	0	0
		Pump Separator	3	1	0	1	0	0	1	0	1	0
		Reactor Health Sensor	3	0	1	0	1	0	0	1	0	0
		Sensor	2	1	0	0	1	0	0	0	1	0
		Separator Filter	2	0	1	0	0	0	1	0	1	1
		Start-up Filter	2	0	1	0	0	0	0	1	0	0
		Water Delivery	2	1	0	1	0	0	1	0	0	1
	UPA	Distillation Assembly	2	0	0	1	0	0	0	1	0	0
		Firmware Controller Assembly	3	1	1	1	0	1	0	1	0	1
		Fluids Control and Pump Assembly	2	1	0	0	1	0	0	0	1	0
		Pressure Control and Pump Assembly	2	0	0	1	0	0	0	0	1	0
		Advanced Recycle Filter Tank Assembly[xvi]	2	0	0	1	0	0	0	0	0	1
		Separator Plumbing Assembly	2	0	0	0	1	0	0	1	0	1
ISRU	Water Extractor	Oven + Insulating Cone	2	0	1	0	1	0	0	0	0	1
		Hopper										
		Sieve	2	0	0	1	0	0	0	0	1	0
		Augers (vertical)	1	1	0	0	0	1	0	0	0	0
		Horizontal Auger	2	0	1	0	0	1	0	0	0	0
		Sweep Gas System	4	1	0	1	1	1	0	0	1	0
		Sweep Gas Piping										
		Condensing Heat Exchanger	2	0	0	0	1	0	0	0	0	0
		Water Filtration System	4	4	4	4	4	4	4	4	4	5
	CO2 Cryocooler	Cryocooler	2	1	0	0	1	0	0	1	0	0
		Container										
	Water Electrolyzer	Electrolysis Cell Stack	5	1	2	1	1	1	1	1	1	1
		O2 Separator / Water Reservoir	6	1	2	1	2	1	0	1	2	0
		H2 Separator and Dryer	3	1	1	0	1	0	1	0	1	0
		Water Pump	3	1	1	0	2	1	2	1	2	1
	Sabatier Reactor	Reactor	4	1	1	1	1	0	1	1	1	0
		Water / Methane Separator	4	1	1	0	1	1	1	0	0	0
		Heat Exchanger	2	1	0	0	1	0	0	0	0	0
	Atmospheric Processor	Zeolite	4	1	1	1	1	0	2	0	0	1
		Compressor	5	1	1	1	2	0	1	1	1	1
		Cryocoolers	3	1	0	0	1	0	0	0	1	0
		Support Structure										
BPC	Crop Lighting	Lighting System Unit	7	3	3	124	0	0	0	137	0	0
	ORA	Air Pump Two-Stage ORU	3	1	0	1	0	0	1	0	0	1
		Blower	3	1	1	0	1	0	0	1	0	0
		Check Valves	5	1	1	1	1	1	1	1	1	0
		Desiccant Beds	4	1	1	2	0	1	1	1	0	1
		Heat Controller	4	0	1	0	1	1	0	0	1	0
		Precooler	3	1	1	0	1	0	0	1	0	0
		Pump Fan Motor Controller	2	0	1	0	0	0	0	0	0	1
		Selector Valves	7	2	2	1	2	1	2	1	1	1
		Sorbent Beds (Zeolite)	4	1	2	1	0	1	1	1	0	1

Table J.24: Architecture Case 8 Spare Parts Requirements for each Component over a 10 Mission String of Sorties Campaign with all ISRU technologies at 10% of their originally estimated values. Empty rows correspond to components assumed to have 100% reliability, and hence do not require spare parts

Group	Assembly	Subassembly	Mission									
			1	2	3	4	5	6	7	8	9	10
ECLSS	CDRA	Air Pump Two-Stage ORU	3	1	0	1	0	1	0	0	0	1
		Blower	3	1	1	0	1	0	1	0	0	1
		Check Valves	4	2	1	1	1	1	1	1	1	1
		Desiccant Beds	4	2	1	1	1	0	1	1	1	0
		Heat Controller	3	1	1	1	0	1	0	1	0	0
		Precooler	3	1	1	0	1	0	1	0	0	1
		Pump Fan Motor Controller	2	0	1	0	0	0	0	1	0	0
		Selector Valves	7	2	2	1	2	2	1	1	2	1
		Sorbent Beds (Zeolite)	4	2	1	1	1	0	1	1	1	0
	CCAA	Condensing Heat Exchanger	3	0	1	0	0	1	0	0	1	0
		Electronic Interface Box (EIB)	3	1	0	0	1	0	0	1	0	0
		Fan Delta Pressure Sensor	4	0	0	1	1	0	0	0	1	0
		Heat Exchanger Liquid Sensor	4	1	1	0	1	0	1	0	1	0
		Inlet ORU	4	1	0	1	1	1	0	1	0	1
		Pressure Transducer	3	1	0	1	0	1	0	0	0	0
		Temperature Control Check Valve (TCCV)	15	7	7	5	7	5	6	6	4	6
		Temperature Sensor	2	0	1	0	0	0	0	1	0	0
		Water Separator	7	3	2	2	2	2	2	2	1	2
		Water Separator Liquid Sensor	4	1	1	0	1	0	1	0	1	0
	WPA	Catalytic Reactor	3	1	1	0	1	1	0	1	0	0
		Gas Separator	2	1	0	1	0	0	0	1	0	0
		Ion Exchange Bed	3	3	3	3	3	3	4	3	3	3
		Microbial Check Valve	2	1	0	0	1	0	0	1	0	0
		Multifiltration Bed #1	1	1	2	1	2	1	1	2	1	2
		Multifiltration Bed #2	1	1	2	1	2	1	1	2	1	2
		Particulate Filter	2	2	2	3	2	2	3	2	2	2
		pH Adjuster	3	0	1	0	0	0	1	0	0	0
		Process Controller	2	1	0	0	1	0	0	1	0	0
		Pump Separator	3	1	0	1	0	1	0	0	1	0
		Reactor Health Sensor	3	0	1	0	1	0	1	0	0	1
		Sensor	2	1	0	1	0	0	0	1	0	0
		Separator Filter	2	0	0	1	0	0	1	0	1	1
		Start-up Filter	2	0	1	0	0	0	1	0	0	0
		Water Delivery	2	1	0	1	0	1	0	0	0	1
	UPA	Distillation Assembly	2	0	0	1	0	0	0	1	0	0
		Firmware Controller Assembly	3	1	1	1	0	1	1	0	0	1
		Fluids Control and Pump Assembly	2	1	0	0	1	0	0	1	0	0
		Pressure Control and Pump Assembly	2	0	1	0	0	0	0	1	0	0
		Advanced Recycle Filter Tank Assembly[xvi]	2	0	0	1	0	0	0	0	1	0
		Separator Plumbing Assembly	2	0	0	0	1	0	0	1	0	1
ISRU	Water Extractor	Oven + Insulating Cone	5	1	2	1	1	2	1	1	0	1
		Hopper										
		Sieve	4	1	1	1	0	1	1	1	0	1
		Augers (vertical)	3	1	1	1	1	0	1	0	1	1
		Horizontal Auger	4	1	1	1	1	1	1	0	1	1
		Sweep Gas System	9	3	3	3	1	2	3	1	2	1
		Sweep Gas Piping										
		Condensing Heat Exchanger	3	1	1	0	1	1	0	0	1	0
		Water Filtration System	6	2	4	4	4	4	4	4	4	5
	CO2 Cryocooler	Cryocooler	5	2	1	1	2	1	1	1	1	1
		Container										
	Water Electrolyzer	Electrolysis Cell Stack	15	7	8	7	6	7	6	6	6	6
		O2 Separator / Water Reservoir	16	8	8	7	7	7	6	7	6	6
		H2 Separator and Dryer	8	3	3	2	3	2	3	2	2	2
		Water Pump	7	3	3	1	3	2	1	2	2	1
	Sabatier Reactor	Reactor	11	5	5	4	4	4	4	4	3	4
		Water / Methane Separator	9	3	3	1	4	2	1	2	3	0
		Heat Exchanger	4	1	1	1	1	0	1	1	0	0
	Atmospheric	Zeolite	10	4	4	4	2	3	3	3	3	2
	Processor	Compressor	14	7	6	6	5	6	6	5	4	6

		Cryocoolers	6	2	2	1	1	2	1	1	1	1
		Support Structure										
BPC	Crop Lighting	Lighting System Unit	7	3	3	124	0	0	0	137	0	0
	ORA	Air Pump Two-Stage ORU	3	1	0	1	0	1	0	0	0	1
		Blower	3	1	1	0	1	0	1	0	0	1
		Check Valves	4	2	1	1	1	1	1	1	1	1
		Desiccant Beds	4	2	1	1	0	1	1	1	1	0
		Heat Controller	3	1	1	1	0	1	0	1	0	0
		Precooler	3	1	1	0	1	0	0	1	0	1
		Pump Fan Motor Controller	2	0	1	0	0	0	0	1	0	0
		Selector Valves	7	2	2	1	2	2	1	1	2	1
		Sorbent Beds (Zeolite)	4	1	2	1	0	1	1	1	1	0

J.3 Minimum Continuous Presence Mission Scenario Analysis - Master Equipment Lists and Component Data for each ECLS Architecture Case

Cataloged below are the complete master equipment lists (MELs) derived for each of the nine ECLS architecture cases explored in the Minimum Continuous Presence mission scenario analysis. For each architecture case, a MEL is presented with the mass, volume, meantime between failures (MTBF), and life limit (LL) of each element within the architecture. Unless otherwise noted, values are taken from the NASA Baseline Values and Assumptions Document (BVAD) [209]. Assumptions and use of analogy to other components for data are indicated and described with endnotes. In addition, spare parts requirements predicted by the HabNet Supportability Module for each architecture case over the first ten missions of the campaign are also listed, under both nominal ISRU reliability levels, and reliability levels that have been degraded by an order of magnitude. This latter set of data corresponds to the sensitivity analyses performed in Section 6.5.5. For this case study, the spare parts requirements are calculated such that the probability of having sufficient spare parts is 0.999. Finally, in contrast to the results presented in Appendix J.2, the MELs in this appendix include an additional runtime column, to represent the variations in system runtime between the first two missions of the campaign. Here, the first non-zero entry across the two runtime columns for a particular component represents the first mission at which that component was delivered, integrated, and operated during the campaign. As a result, in cases where additional instances of the same type of component are added during the second surface habitat expansion mission, these components are listed twice in the MEL so that their different deployment periods can be represented within the appropriate runtime columns.

J.3.1 Architecture Case 1

Table J.25: Architecture Case 1 Master Equipment List, containing component mass, volume and reliability data, as well as run times and power demands. Power is listed here on a per unit basis. ISRU technologies displayed here were sized by the HabNet ISRU Module.

Sys.	Assembly	Subassembly	Mass [kg]	Vol. [m^3]	MTBF [h]	Run Time Miss. 1 [h]	Run Time Miss. 2 [h]	LL [y]	# in Pmry.	Power [kW]
ECLS	CDRA	Air Pump Two-Stage ORU	10.89	0.0045	156200.0	19000	19000	15.29	1	0.860

		Blower	5.58	0.0300	129700.0	19000	19000	10.00	1	
		Check Valves	39.92	0.1784	32900.0[i]	19000	19000		1	
		Desiccant Beds	42.64	0.0850	77100.0	19000	19000		2	
		Heat Controller	3.31	0.0085	242700.0	19000	19000		2	
		Precooler	5.58	0.0255	129700.0	19000	19000	10.00	1	
		Pump Fan Motor Controller	2.72	0.0057	2270000.0	19000	19000		2	
		Selector Valves	3.04	0.0017	117000.0	19000	19000	10.61	6	
		Sorbent Beds (Zeolite)	42.64	0.0850	77100.0	19000	19000		2	
	CCAA Mission 1 (x4)	Condensing Heat Exchanger	49.71	0.3933	832600.0	19000	19000		4	0.544
		Electronic Interface Box (EIB)	4.04	0.0173	2350000.0	19000	19000		8	
		Fan Delta Pressure Sensor	0.45	0.0002	1250000.0	19000	19000		4	
		Heat Exchanger Liquid Sensor	0.64	0.0006	1140000.0	19000	19000		8	
		Inlet ORU	25.31	0.1308	333000.0	19000	19000		4	
		Pressure Transducer	0.48	0.0000	1250000.0	19000	19000	15.00	4	
		Temperature Control Check Valve	7.45	0.0071	32900.0	19000	19000		8	
		Temperature Sensor	0.26	0.0014	37600000.0	19000	19000		16	
		Water Separator	11.93	0.0583	131000.0	19000	19000	5.00	8	
		Water Separator Liquid Sensor	0.64	0.0006	1140000.0[ii]	19000	19000		8	
	CCAA Mission 2 (x3)	Condensing Heat Exchanger	49.71	0.3933	832600.0	0	19000		3	0.528
		Electronic Interface Box (EIB)	4.04	0.0173	2350000.0	0	19000		6	
		Fan Delta Pressure Sensor	0.45	0.0002	1250000.0	0	19000		3	
		Heat Exchanger Liquid Sensor	0.64	0.0006	1140000.0	0	19000		6	
		Inlet ORU	25.31	0.1308	333000.0	0	19000		3	
		Pressure Transducer	0.48	0.0000	1250000.0	0	19000	15.00	3	
		Temperature Control Check Valve	7.45	0.0071	32900.0	0	19000		6	
		Temperature Sensor	0.26	0.0014	37600000.0	0	19000		12	
		Water Separator	11.93	0.0583	131000.0	0	19000	5.00	6	
		Water Separator Liquid Sensor	0.64	0.0006	1140000.0[ii]	0	19000		6	
ISRU	Water Extractor	Oven + Insulating Cone	107.72	4.6663	242700[iii]	19000	19000		1	30.23
		Hopper	72.38	5.4409		19000	19000		1	
		Sieve	59.21	0.0000	500000[iv]	19000	19000		1	
		Augers (vertical)	276.14	0.0000	500000[iv]	19000	19000		1	0.064
		Horizontal Auger	13.37	0.1719	500000[iv]	19000	19000		1	
		Sweep Gas System	0.03	0.0000	138408[v]	19000	19000		1	
		Sweep Gas Piping	7.87	0.1810		19000	19000		1	
		Condensing Heat Exchanger	51.99	1.3682	832600[vi]	19000	19000		1	
		Water Filtration System	3.01	0.0113	296701.2[vii]	19000	19000	0.36	1	
	CO2 Cryocooler	Cryocooler	34.61	0.0726	500000[iv]	19000	19000		2	1.474
		Container	83.02	0.4906		19000	19000		1	
	Water Electrolyzer	Electrolysis Cell Stack	47.43	0.0045	27156[viii]	19000	19000	2.38	1	12.28
		O2 Separator / Water Reservoir	5.71	0.0119	27156[viii]	19000	19000	2.38	1	
		H2 Separator and Dryer	14.44	0.0040	98112[ix]	19000	19000	10	1	
		Water Pump	2.16	0.0007	144540[x]	19000	19000	1	1	8×10^{-5}
	Sabatier Reactor	Reactor	20.78	0.4181	50000[xi]	19000	19000		1	0.198
		Water / Methane Separator	0.24	0.0097	131000[xii]	19000	19000		1	
		Heat Exchanger	0.53	0.0000	832600[xiii]	19000	19000		1	
	Atmospheric Processor	Zeolite	0.866	0.0104	77100[xiv]	19000	19000		1	
		Compressor	13.101	0.0758	66666.7	19000	19000		2	1.194
		Cryocoolers	3.100	0.0015	500000[iv]	19000	19000		2	0.480
		Support Structure	5.622			19000	19000		1	
Food	First Mission	Prepackaged Food Supply	2907			19000	0		1	
	Subsequent Missions	Prepackaged Food Supply	4919			0	19000		1	

[i] Analogy to CCAA TCCV
[ii] Analogy to CCAA Heat Exchanger Liquid Sensor
[iii] Analogy to CDRA Heater Controller
[iv] Optimistic assumption; no data were available
[v] Analogy to OGA Nitrogen Purge ORU
[vi] Analogy CCAA Condensing Heat Exchanger
[vii] Analogy to WPA Multifiltration Bed
[viii] Analogy to OGA Hydrogen ORU (contains Electrolysis Cell Stack and Rotary Separator / Accumulator)
[ix] Analogy to OGA Oxygen Outlet
[x] Analogy to OGA Pump
[xi] Analogy to CRS Sabatier Methanation Reactor
[xii] Analogy to CRS Phase Separator
[xiii] Analogy to CRS Condensing Heat Exchanger
[xiv] Analogy to CDRA Dessicant-Adsorbent Bed
[xv] Analogy to CRS Compressor

Table J.26: Architecture Case 1 Spare Parts Requirements for each Component over a 10 Mission Minimum Continuous Presence Campaign. Empty rows correspond to components assumed to have 100% reliability, and hence do not require spare parts

Group	Assembly	Subassembly	Mission									
			1	2	3	4	5	6	7	8	9	10
ECLSS	CDRA	Air Pump Two-Stage ORU	3	1	1	0	0	1	0	1	1	0
		Blower	4	0	1	1	0	1	0	1	1	0
		Check Valves	5	2	1	2	1	1	1	1	2	1
		Desiccant Beds	5	1	2	1	1	1	1	1	1	1
		Heat Controller	4	1	1	0	1	0	1	0	1	0
		Precooler	4	0	1	1	0	1	0	1	1	0
		Pump Fan Motor Controller	2	0	1	0	0	0	0	1	0	0
		Selector Valves	7	3	3	2	1	2	2	2	3	1
		Sorbent Beds (Zeolite)	5	1	2	1	1	1	1	1	1	1
	CCAA Mission 1	Condensing Heat Exchanger	3	0	1	0	0	1	0	1	0	0
		Electronic Interface Box (EIB)	3	0	1	1	0	0	0	1	0	0
		Fan Delta Pressure Sensor	3	1	0	1	0	1	0	0	1	0
		Heat Exchanger Liquid Sensor	4	1	1	1	0	0	1	1	1	0
		Inlet ORU	4	0	1	2	0	1	0	1	1	0
		Pressure Transducer	3	1	0	1	0	0	1	0	1	0
		Temperature Control Check Valve (TCCV)	16	7	8	7	6	7	5	8	6	5
		Temperature Sensor	2	0	1	0	0	0	0	0	1	0
		Water Separator	8	2	3	3	1	2	5	0	2	6
		Water Separator Liquid Sensor	4	1	1	1	0	0	1	0	1	1
	CCAA Mission 2	Condensing Heat Exchanger	0	2	1	0	1	0	0	1	0	0
		Electronic Interface Box (EIB)	0	3	0	1	0	0	1	0	0	0
		Fan Delta Pressure Sensor	0	3	1	0	0	1	0	0	1	0
		Heat Exchanger Liquid Sensor	0	4	1	1	0	0	1	0	1	0
		Inlet ORU	0	3	1	1	0	1	1	0	1	0
		Pressure Transducer	0	3	1	0	0	1	0	0	1	0
		Temperature Control Check Valve	0	13	7	6	4	6	4	6	6	4
		Temperature Sensor	0	2	0	1	0	0	0	0	0	0
		Water Separator	0	6	3	2	2	2	1	2	2	1
		Water Separator Liquid Sensor	0	4	0	1	0	1	1	0	1	0
ISRU	Water Extractor	Oven + Insulating Cone	2	1	0	1	0	0	1	0	0	0
		Hopper										
		Sieve	2	0	1	0	0	0	1	0	0	0
		Augers (vertical)	1	1	0	0	1	0	0	0	0	1
		Horizontal Auger	2	1	0	1	0	0	0	0	1	0
		Sweep Gas System	4	1	1	2	0	1	0	2	0	1
		Sweep Gas Piping										
		Condensing Heat Exchanger	2	0	0	1	0	0	0	0	0	0
		Water Filtration System	6	6	6	6	6	6	6	6	6	6
	CO2 Cryocooler	Cryocooler	3	0	0	1	0	1	0	0	1	0
		Container										
	Water Electrolyzer	Electrolysis Cell Stack	5	2	2	2	1	1	2	1	2	0
		O2 Separator / Water Reservoir	6	2	2	2	1	2	1	2	2	1
		H2 Separator and Dryer	4	0	1	1	1	0	1	1	0	1
		Water Pump	4	1	1	2	2	3	2	2	2	2
	Sabatier Reactor	Reactor	5	1	1	1	1	1	1	1	1	0
		Water / Methane Separator	4	1	1	1	0	1	1	0	1	0
		Heat Exchanger	3	0	0	1	0	0	0	1	0	0
	Atmospheric Processor	Zeolite	5	1	1	1	0	2	0	1	1	0
		Compressor	6	1	2	2	0	2	1	1	2	0
		Cryocoolers	3	1	0	1	0	0	1	0	1	0
		Support Structure										

Table J.27: Architecture Case 1 Spare Parts Requirements for each Component over a 10 Mission Minimum Continuous Presence Campaign with all ISRU technologies at 10% of their originally estimated values. Empty rows correspond to components assumed to have 100% reliability, and hence do not require spare parts

Group	Assembly	Subassembly	Mission									
			1	2	3	4	5	6	7	8	9	10
ECLSS	CDRA	Air Pump Two-Stage ORU	3	1	1	0	1	0	1	0	1	0
		Blower	3	2	0	1	1	0	1	0	1	0
		Check Valves	5	2	1	2	1	1	2	1	1	1
		Desiccant Beds	5	1	2	1	1	1	1	1	2	0
		Heat Controller	4	1	1	0	1	1	0	1	0	1
		Precooler	3	2	0	1	1	0	1	0	1	0
		Pump Fan Motor Controller	2	0	1	0	0	0	1	0	0	0
		Selector Valves	7	3	3	2	2	2	2	2	1	2
		Sorbent Beds (Zeolite)	5	1	2	1	1	1	1	2	0	1
	CCAA Mission 1	Condensing Heat Exchanger	2	1	1	0	1	0	0	1	0	0
		Electronic Interface Box (EIB)	3	0	1	1	0	0	1	0	0	1
		Fan Delta Pressure Sensor	3	1	1	0	0	1	0	1	0	0
		Heat Exchanger Liquid Sensor	4	1	1	1	0	1	0	1	0	1
		Inlet ORU	3	2	1	0	1	1	1	0	1	0
		Pressure Transducer	3	1	1	0	0	1	0	1	0	0
		Temperature Control Check Valve (TCCV)	15	9	8	6	7	7	6	6	7	5
		Temperature Sensor	2	0	1	0	0	1	0	0	0	0
		Water Separator	7	4	2	3	2	2	4	0	2	6
		Water Separator Liquid Sensor	4	1	1	1	0	1	0	1	0	1
	CCAA Mission 2	Condensing Heat Exchanger	0	2	1	0	1	0	0	1	0	0
		Electronic Interface Box (EIB)	0	3	0	1	0	1	0	0	0	1
		Fan Delta Pressure Sensor	0	3	1	0	1	0	0	1	0	0
		Heat Exchanger Liquid Sensor	0	4	1	1	0	1	0	1	0	0
		Inlet ORU	0	3	1	1	1	0	1	1	0	1
		Pressure Transducer	0	3	1	0	1	0	0	1	0	0
		Temperature Control Check Valve	0	13	7	6	6	5	5	5	5	5
		Temperature Sensor	0	2	1	0	0	0	0	0	0	1
		Water Separator	0	7	2	2	2	2	2	1	2	2
		Water Separator Liquid Sensor	0	4	1	1	0	1	0	0	1	0
ISRU	Water Extractor	Oven + Insulating Cone	5	2	2	2	1	2	1	2	1	1
		Hopper										
		Sieve	4	2	1	1	1	1	1	0	1	1
		Augers (vertical)	4	1	1	1	1	1	1	0	1	1
		Horizontal Auger	4	2	1	2	1	1	1	0	1	1
		Sweep Gas System	10	4	4	4	3	2	1	3	3	2
		Sweep Gas Piping										
		Condensing Heat Exchanger	3	2	0	1	1	0	1	1	0	1
		Water Filtration System	6	6	6	6	6	6	6	6	6	6
	CO2 Cryocooler	Cryocooler	6	2	2	2	1	2	1	2	1	1
		Container										
	Water Electrolyzer	Electrolysis Cell Stack	18	11	10	9	9	9	9	9	8	9
		O2 Separator / Water Reservoir	20	11	11	10	9	9	9	9	9	9
		H2 Separator and Dryer	9	5	3	4	3	3	3	3	3	3
		Water Pump	9	3	3	3	2	3	2	3	2	2
	Sabatier Reactor	Reactor	13	7	6	6	6	5	5	6	5	5
		Water / Methane Separator	10	4	4	4	2	3	1	4	2	3
		Heat Exchanger	5	1	2	0	1	1	0	1	1	1
	Atmospheric Processor	Zeolite	13	5	5	5	3	5	2	5	3	5
		Compressor	17	10	8	8	9	8	7	7	8	7
		Cryocoolers	7	2	3	1	2	2	1	2	1	1
		Support Structure										

J.3.2 Architecture Case 2

Table J.28: Architecture Case 2 Master Equipment List, containing component mass, volume and reliability data, as well as run times and power demands. Power is listed here on a per unit basis. ISRU technologies displayed here were sized by the HabNet ISRU Module.

Sys.	Assembly	Subassembly	Mass [kg]	Vol. [m^3]	MTBF [h]	Run Time Miss. 1 [h]	Run Time Miss. 2 [h]	LL [y]	# in Pmry.	Power [kW]
ECLS	CDRA	Air Pump Two-Stage ORU	10.89	0.0045	156200.0	19000	19000	15.29	1	0.860
		Blower	5.58	0.0300	129700.0	19000	19000	10.00	1	
		Check Valves	39.92	0.1784	32900.0[i]	19000	19000		1	
		Desiccant Beds	42.64	0.0850	77100.0	19000	19000		2	
		Heat Controller	3.31	0.0085	242700.0	19000	19000		2	
		Precooler	5.58	0.0255	129700.0	19000	19000	10.00	1	
		Pump Fan Motor Controller	2.72	0.0057	2270000.0	19000	19000		2	
		Selector Valves	3.04	0.0017	117000.0	19000	19000	10.61	6	
		Sorbent Beds (Zeolite)	42.64	0.0850	77100.0	19000	19000		2	
	CCAA Mission 1 (x4)	Condensing Heat Exchanger	49.71	0.3933	832600.0	19000	19000		4	0.544
		Electronic Interface Box (EIB)	4.04	0.0173	2350000.0	19000	19000		8	
		Fan Delta Pressure Sensor	0.45	0.0002	1250000.0	19000	19000		4	
		Heat Exchanger Liquid Sensor	0.64	0.0006	1140000.0	19000	19000		8	
		Inlet ORU	25.31	0.1308	333000.0	19000	19000		4	
		Pressure Transducer	0.48	0.0000	1250000.0	19000	19000	15.00	4	
		Temperature Control Check Valve	7.45	0.0071	32900.0	19000	19000		8	
		Temperature Sensor	0.26	0.0014	37600000.0	19000	19000		16	
		Water Separator	11.93	0.0583	131000.0	19000	19000	5.00	8	
		Water Separator Liquid Sensor	0.64	0.0006	1140000.0[ii]	19000	19000		8	
	CCAA Mission 2 (x3)	Condensing Heat Exchanger	49.71	0.3933	832600.0	0	19000		3	0.528
		Electronic Interface Box (EIB)	4.04	0.0173	2350000.0	0	19000		6	
		Fan Delta Pressure Sensor	0.45	0.0002	1250000.0	0	19000		3	
		Heat Exchanger Liquid Sensor	0.64	0.0006	1140000.0	0	19000		6	
		Inlet ORU	25.31	0.1308	333000.0	0	19000		3	
		Pressure Transducer	0.48	0.0000	1250000.0	0	19000	15.00	3	
		Temperature Control Check Valve	7.45	0.0071	32900.0	0	19000		6	
		Temperature Sensor	0.26	0.0014	37600000.0	0	19000		12	
		Water Separator	11.93	0.0583	131000.0	0	19000	5.00	6	
		Water Separator Liquid Sensor	0.64	0.0006	1140000.0[ii]	0	19000		6	
	WPA	Catalytic Reactor	67.04	0.1156	25579.2	1240	2080	2.25	1	0.320
		Gas Separator	39.15	0.0660	84008.4	1240	2080	1	1	
		Ion Exchange Bed	13.02	0.0173	296701.2	1240	2080	0.16	1	
		Microbial Check Valve	5.76	0.0065	143488.8	1240	2080	1	1	
		Multifiltration Bed #1	149.23	0.0657	296701.2	1240	2080	0.36	1	
		Multifiltration Bed #2	149.23	0.0657	296701.2	1240	2080	0.36	1	
		Particulate Filter	32.25	0.0717	717356.4	1240	2080	0.22	1	
		pH Adjuster	2.54	0.0026	137181.6	1240	2080	1	1	
		Process Controller	45.00	0.0838	87950.4	1240	2080	7.72	1	
		Pump Separator	31.34	0.0869	42398.4	1240	2080	2	1	
		Reactor Health Sensor	16.83	0.0425	56677.2	1240	2080	1	1	
		Sensor	4.81	0.0034	143664	1240	2080	10	1	
		Separator Filter	7.67	0.0102	359072.4	1240	2080	0.84	1	
		Start-up Filter	9.44	0.0184	226884	1240	2080	19.92	1	
		Water Delivery	47.54	0.0974	64561.2	1240	2080	5	1	
ISRU	Water Extractor	Oven + Insulating Cone	78.17	3.3863	242700[iii]	19000	19000		1	21.94
		Hopper	58.62	3.9485		19000	19000		1	
		Sieve	36.61	0.0000	500000[iv]	19000	19000		1	
		Augers (vertical)	200.40	0.0000	500000[iv]	19000	19000		1	0.053
		Horizontal Auger	11.39	0.1464	500000[iv]	19000	19000		1	
		Sweep Gas System	0.02	0.0000	138408[v]	19000	19000		1	
		Sweep Gas Piping	6.03	0.1188		19000	19000		1	

		Condensing Heat Exchanger	37.87	0.8571	832600[vi]	19000	19000		1	
		Water Filtration System	2.19	0.0082	296701.2[vii]	19000	19000	0.36	1	
	CO2 Cryocooler	Cryocooler	34.61	0.0726	500000[iv]	19000	19000		2	1.474
		Container	83.02	0.4906		19000	19000		1	
	Water Electrolyzer	Electrolysis Cell Stack	47.43	0.0045	27156[viii]	19000	19000	2.38	1	12.28
		O2 Separator / Water Reservoir	5.71	0.0119	27156[viii]	19000	19000	2.38	1	
		H2 Separator and Dryer	14.44	0.0040	98112[ix]	19000	19000	10	1	
		Water Pump	2.16	0.0007	144540[x]	19000	19000	1	1	8×10^{-5}
	Sabatier Reactor	Reactor	20.78	0.4181	50000[xi]	19000	19000		1	0.198
		Water / Methane Separator	0.24	0.0097	131000[xii]	19000	19000		1	
		Heat Exchanger	0.53	0.0000	832600[xiii]	19000	19000		1	
	Atmospheric Processor	Zeolite	0.866	0.0104	77100[xiv]	19000	19000		1	
		Compressor	13.101	0.0758	66666.7	19000	19000		2	1.194
		Cryocoolers	3.100	0.0015	500000[iv]	19000	19000		2	0.480
		Support Structure	5.622			19000	19000		1	
Food	First Mission	Prepackaged Food Supply	2907			19000	0		1	
	Subsequent Missions	Prepackaged Food Supply	4919			0	19000		1	

[i]Analogy to CCAA TCCV
[ii]Analogy to CCAA Heat Exchanger Liquid Sensor
[iii]Analogy to CDRA Heater Controller
[iv]Optimistic assumption; no data were available
[v]Analogy to OGA Nitrogen Purge ORU
[vi]Analogy CCAA Condensing Heat Exchanger
[vii]Analogy to WPA Multifiltration Bed
[viii]Analogy to OGA Hydrogen ORU (contains Electrolysis Cell Stack and Rotary Separator / Accumulator)
[ix]Analogy to OGA Oxygen Outlet
[x]Analogy to OGA Pump
[xi]Analogy to CRS Sabatier Methanation Reactor
[xii]Analogy to CRS Phase Separator
[xiii]Analogy to CRS Condensing Heat Exchanger
[xiv]Analogy to CDRA Dessicant-Adsorbent Bed
[xv]Analogy to CRS Compressor

Table J.29: Architecture Case 2 Spare Parts Requirements for each Component over a 10 Mission Minimum Continuous Presence Campaign. Empty rows correspond to components assumed to have 100% reliability, and hence do not require spare parts

Group	Assembly	Subassembly	Mission									
			1	2	3	4	5	6	7	8	9	10
ECLSS	CDRA	Air Pump Two-Stage ORU	3	1	1	0	1	0	1	0	0	1
		Blower	3	1	1	1	0	1	1	0	0	1
		Check Valves	5	2	2	1	1	1	1	2	1	1
		Desiccant Beds	5	1	2	1	1	1	1	1	1	1
		Heat Controller	4	1	1	0	1	1	0	1	0	0
		Precooler	3	1	1	1	0	1	1	0	0	1
		Pump Fan Motor Controller	2	0	1	0	0	0	1	0	0	0
		Selector Valves	7	3	3	2	2	2	2	2	2	1
		Sorbent Beds (Zeolite)	5	1	2	1	1	1	1	1	1	1
	CCAA Mission 1	Condensing Heat Exchanger	2	1	1	0	0	1	0	1	0	0
		Electronic Interface Box (EIB)	3	0	1	0	1	0	0	1	0	0
		Fan Delta Pressure Sensor	3	1	1	0	0	1	0	1	0	0
		Heat Exchanger Liquid Sensor	4	1	1	0	1	1	0	1	0	0
		Inlet ORU	3	2	1	0	1	1	0	1	1	0
		Pressure Transducer	3	1	1	0	0	1	0	1	0	0
		Temperature Control Check Valve (TCCV)	15	9	8	6	6	8	6	6	6	5
		Temperature Sensor	2	1	0	0	0	1	0	0	0	0
		Water Separator	7	3	3	2	2	3	4	0	2	6
		Water Separator Liquid Sensor	4	1	1	0	1	0	1	1	0	1
	CCAA Mission 2	Condensing Heat Exchanger	0	2	1	0	1	0	0	1	0	0
		Electronic Interface Box (EIB)	0	3	0	1	0	0	1	0	0	0
		Fan Delta Pressure Sensor	0	3	1	0	1	0	1	0	0	0
		Heat Exchanger Liquid Sensor	0	4	1	0	1	0	1	1	0	0
		Inlet ORU	0	3	1	1	1	0	1	0	1	0
		Pressure Transducer	0	3	1	0	0	1	0	1	0	0
		Temperature Control Check Valve	0	13	7	6	5	6	5	5	4	5
		Temperature Sensor	0	2	0	0	1	0	0	0	1	0
		Water Separator	0	7	2	2	2	2	2	2	1	1
		Water Separator Liquid Sensor	0	4	1	0	1	0	1	1	0	0

	WPA	Catalytic Reactor	2	1	0	1	0	0	1	0	0	1
		Gas Separator	1	1	0	0	1	0	0	0	0	1
		Ion Exchange Bed	1	1	1	2	1	2	1	2	1	2
		Microbial Check Valve	2	0	0	1	0	0	0	0	0	1
		Multifiltration Bed #1	1	0	0	1	1	0	1	1	0	1
		Multifiltration Bed #2	1	0	0	1	1	0	1	1	0	1
		Particulate Filter	1	0	1	1	1	2	1	1	1	1
		pH Adjuster	2	0	1	0	0	0	1	0	0	0
		Process Controller	1	1	0	0	1	0	0	0	0	1
		Pump Separator	2	1	0	0	0	1	0	1	0	0
		Reactor Health Sensor	2	0	1	0	0	1	0	0	0	0
		Sensor	2	0	1	0	0	0	0	1	0	0
		Separator Filter	1	1	0	0	0	0	0	1	0	0
		Start-up Filter	1	1	0	0	0	1	0	0	0	0
		Water Delivery	2	0	1	0	0	0	0	1	0	0
ISRU	Water Extractor	Oven + Insulating Cone	2	1	1	0	0	0	1	0	0	0
		Hopper										
		Sieve	2	0	1	0	0	1	0	0	0	0
		Augers (vertical)	2	0	0	1	0	0	0	0	1	0
		Horizontal Auger	2	1	0	1	0	0	0	1	0	0
		Sweep Gas System	4	2	0	1	1	1	1	1	0	0
		Sweep Gas Piping										
		Condensing Heat Exchanger	2	0	1	0	0	0	0	0	0	1
		Water Filtration System	6	6	6	6	6	6	6	6	6	6
	CO2 Cryocooler	Cryocooler	2	1	1	0	0	1	0	0	1	0
		Container										
	Water Electrolyzer	Electrolysis Cell Stack	5	2	3	0	2	1	2	1	1	1
		O2 Separator / Water Reservoir	6	3	2	1	2	1	2	1	1	2
		H2 Separator and Dryer	4	1	1	0	1	1	0	1	0	1
		Water Pump	4	1	1	2	2	3	2	2	2	2
	Sabatier Reactor	Reactor	4	2	1	1	1	1	1	1	1	0
		Water / Methane Separator	4	1	2	0	1	1	0	0	2	0
		Heat Exchanger	3	0	1	0	0	0	0	1	0	0
	Atmospheric Processor	Zeolite	5	1	2	0	1	1	1	1	0	1
		Compressor	5	2	2	1	2	1	1	2	0	1
		Cryocoolers	3	1	1	0	0	1	0	1	0	0
		Support Structure										

Table J.30: Architecture Case 2 Spare Parts Requirements for each Component over a 10 Mission Minimum Continuous Presence Campaign with all ISRU technologies at 10% of their originally estimated values. Empty rows correspond to components assumed to have 100% reliability, and hence do not require spare parts

Group	**Assembly**	**Subassembly**	**Mission**									
			1	**2**	**3**	**4**	**5**	**6**	**7**	**8**	**9**	**10**
ECLSS	CDRA	Air Pump Two-Stage ORU	3	1	1	0	1	0	1	0	1	0
		Blower	3	2	1	0	1	0	1	0	1	0
		Check Valves	5	2	2	1	1	2	1	1	1	1
		Desiccant Beds	5	1	2	1	1	1	1	1	1	1
		Heat Controller	4	1	1	0	1	0	1	1	0	1
		Precooler	4	1	1	0	1	0	1	0	1	0
		Pump Fan Motor Controller	2	1	0	0	0	0	1	0	0	0
		Selector Valves	7	3	3	2	2	2	2	2	1	2
		Sorbent Beds (Zeolite)	5	1	2	1	1	1	1	1	1	1
	CCAA Mission 1	Condensing Heat Exchanger	2	1	1	0	1	0	0	1	0	0
		Electronic Interface Box (EIB)	3	1	0	1	0	0	1	0	0	1
		Fan Delta Pressure Sensor	3	1	1	0	0	1	0	1	0	0
		Heat Exchanger Liquid Sensor	4	1	1	0	1	1	1	0	0	1
		Inlet ORU	4	1	1	1	0	1	1	0	1	0
		Pressure Transducer	3	1	1	0	0	1	0	0	1	0
		Temperature Control Check Valve (TCCV)	16	8	8	7	6	7	6	6	7	6
		Temperature Sensor	2	1	0	0	0	0	1	0	0	0
		Water Separator	7	4	3	2	2	2	4	0	2	6
		Water Separator Liquid Sensor	4	1	1	0	1	1	0	1	0	1

	CCAA Mission 2	Condensing Heat Exchanger	0	2	1	0	1	0	0	1	0	0
		Electronic Interface Box (EIB)	0	3	0	1	0	0	1	0	0	1
		Fan Delta Pressure Sensor	0	3	1	0	0	1	0	1	0	0
		Heat Exchanger Liquid Sensor	0	4	1	0	1	0	1	0	1	0
		Inlet ORU	0	3	2	0	1	0	1	0	1	1
		Pressure Transducer	0	3	1	0	0	1	0	1	0	0
		Temperature Control Check Valve	0	14	7	5	5	6	5	5	5	5
		Temperature Sensor	0	2	0	0	1	0	0	0	1	0
		Water Separator	0	7	3	2	1	2	2	1	2	2
		Water Separator Liquid Sensor	0	4	1	0	1	1	0	0	1	0
	WPA	Catalytic Reactor	2	1	0	1	0	1	0	0	1	0
		Gas Separator	2	0	0	1	0	0	0	0	1	0
		Ion Exchange Bed	1	1	1	2	1	2	1	2	1	2
		Microbial Check Valve	2	0	1	0	0	0	0	0	1	0
		Multifiltration Bed #1	1	0	0	1	1	0	1	1	0	1
		Multifiltration Bed #2	1	0	0	1	1	0	1	1	0	1
		Particulate Filter	1	0	1	1	1	2	1	1	1	1
		pH Adjuster	2	0	1	0	0	0	1	0	0	0
		Process Controller	1	1	0	1	0	0	0	0	1	0
		Pump Separator	2	1	0	0	1	0	0	1	0	0
		Reactor Health Sensor	2	0	1	0	0	1	0	0	1	0
		Sensor	2	0	1	0	0	0	0	0	1	0
		Separator Filter	1	1	0	0	0	0	0	1	0	0
		Start-up Filter	1	1	0	0	0	1	0	0	0	0
		Water Delivery	2	0	1	0	0	0	1	0	0	0
ISRU	Water Extractor	Oven + Insulating Cone	5	3	2	1	2	1	2	1	1	2
		Hopper										
		Sieve	4	2	1	1	1	1	1	1	1	0
		Augers (vertical)	4	1	1	1	1	1	1	1	0	1
		Horizontal Auger	5	1	2	1	1	1	1	0	1	1
		Sweep Gas System	10	5	4	2	2	3	4	2	3	1
		Sweep Gas Piping										
		Condensing Heat Exchanger	3	2	1	0	1	1	0	1	1	0
		Water Filtration System	6	6	6	6	6	6	6	6	6	6
	CO2 Cryocooler	Cryocooler	6	2	2	2	1	2	1	2	1	1
		Container										
	Water Electrolyzer	Electrolysis Cell Stack	18	11	11	8	9	9	9	8	9	8
		O2 Separator / Water Reservoir	20	12	10	10	9	9	9	9	9	9
		H2 Separator and Dryer	9	5	4	3	3	3	3	3	3	3
		Water Pump	9	3	3	3	2	3	2	3	2	2
	Sabatier Reactor	Reactor	13	7	7	5	6	5	5	6	5	5
		Water / Methane Separator	10	6	2	3	3	3	3	2	3	2
		Heat Exchanger	5	1	2	0	1	1	1	0	1	1
	Atmospheric Processor	Zeolite	12	6	5	4	4	4	5	3	4	4
		Compressor	17	10	9	8	7	8	7	8	7	7
		Cryocoolers	7	2	3	1	2	1	2	2	1	2
		Support Structure										

J.3.3 Architecture Case 3

Table J.31: Architecture Case 3 Master Equipment List, containing component mass, volume and reliability data, as well as run times and power demands. Power is listed here on a per unit basis. ISRU technologies displayed here were sized by the HabNet ISRU Module.

Sys.	Assembly	Subassembly	Mass [kg]	Vol. [m^3]	MTBF [h]	Run Time Miss. 1 [h]	Run Time Miss. 2 [h]	LL [y]	# in Pmry.	Power [kW]
ECLS	CDRA	Air Pump Two-Stage ORU	10.89	0.0045	156200.0	19000	19000	15.29	1	0.860
		Blower	5.58	0.0300	129700.0	19000	19000	10.00	1	
		Check Valves	39.92	0.1784	32900.0[i]	19000	19000		1	
		Desiccant Beds	42.64	0.0850	77100.0	19000	19000		2	

		Heat Controller	3.31	0.0085	242700.0	19000	19000		2	
		Precooler	5.58	0.0255	129700.0	19000	19000	10.00	1	
		Pump Fan Motor Controller	2.72	0.0057	2270000.0	19000	19000		2	
		Selector Valves	3.04	0.0017	117000.0	19000	19000	10.61	6	
		Sorbent Beds (Zeolite)	42.64	0.0850	77100.0	19000	19000		2	
	CCAA Mission 1 (x4)	Condensing Heat Exchanger	49.71	0.3933	832600.0	19000	19000		4	0.544
		Electronic Interface Box (EIB)	4.04	0.0173	2350000.0	19000	19000		8	
		Fan Delta Pressure Sensor	0.45	0.0002	1250000.0	19000	19000		4	
		Heat Exchanger Liquid Sensor	0.64	0.0006	1140000.0	19000	19000		8	
		Inlet ORU	25.31	0.1308	333000.0	19000	19000		4	
		Pressure Transducer	0.48	0.0000	1250000.0	19000	19000	15.00	4	
		Temperature Control Check Valve	7.45	0.0071	32900.0	19000	19000		8	
		Temperature Sensor	0.26	0.0014	37600000.0	19000	19000		16	
		Water Separator	11.93	0.0583	131000.0	19000	19000	5.00	8	
		Water Separator Liquid Sensor	0.64	0.0006	1140000.0[ii]	19000	19000		8	
	CCAA Mission 2 (x3)	Condensing Heat Exchanger	49.71	0.3933	832600.0	0	19000		3	0.528
		Electronic Interface Box (EIB)	4.04	0.0173	2350000.0	0	19000		6	
		Fan Delta Pressure Sensor	0.45	0.0002	1250000.0	0	19000		3	
		Heat Exchanger Liquid Sensor	0.64	0.0006	1140000.0	0	19000		6	
		Inlet ORU	25.31	0.1308	333000.0	0	19000		3	
		Pressure Transducer	0.48	0.0000	1250000.0	0	19000	15.00	3	
		Temperature Control Check Valve	7.45	0.0071	32900.0	0	19000		6	
		Temperature Sensor	0.26	0.0014	37600000.0	0	19000		12	
		Water Separator	11.93	0.0583	131000.0	0	19000	5.00	6	
		Water Separator Liquid Sensor	0.64	0.0006	1140000.0[ii]	0	19000		6	
	WPA	Catalytic Reactor	67.04	0.1156	25579.2	1832	3064	2.25	1	0.320
		Gas Separator	39.15	0.0660	84008.4	1832	3064	1	1	
		Ion Exchange Bed	13.02	0.0173	296701.2	1832	3064	0.16	1	
		Microbial Check Valve	5.76	0.0065	143488.8	1832	3064	1	1	
		Multifiltration Bed #1	149.23	0.0657	296701.2	1832	3064	0.36	1	
		Multifiltration Bed #2	149.23	0.0657	296701.2	1832	3064	0.36	1	
		Particulate Filter	32.25	0.0717	717356.4	1832	3064	0.22	1	
		pH Adjuster	2.54	0.0026	137181.6	1832	3064	1	1	
		Process Controller	45.00	0.0838	87950.4	1832	3064	7.72	1	
		Pump Separator	31.34	0.0869	42398.4	1832	3064	2	1	
		Reactor Health Sensor	16.83	0.0425	56677.2	1832	3064	1	1	
		Sensor	4.81	0.0034	143664	1832	3064	10	1	
		Separator Filter	7.67	0.0102	359072.4	1832	3064	0.84	1	
		Start-up Filter	9.44	0.0184	226884	1832	3064	19.92	1	
		Water Delivery	47.54	0.0974	64561.2	1832	3064	5	1	
	UPA	Distillation Assembly	92.76	0.1422	142525.2	6716	11283	2	1	0.315
		Firmware Controller Assembly	23.09	0.0286	27331.2	6716	11283	2.4	1	
		Fluids Control and Pump Assembly	47.58	0.0731	90140.4	6716	11283	4	1	
		Pressure Control and Pump Assembly	49.08	0.1158	181507.2	6716	11283	2	1	
		Advanced Recycle Filter Tank Assembly[xvi]	50.00	0.1011	199640.4	6716	11283		1	
		Separator Plumbing Assembly	16.78	0.0229	384651.6	6716	11283	1	1	
ISRU	Water Extractor	Oven + Insulating Cone	64.31	2.7858	242700[iii]	19000	19000		1	18.05
		Hopper	51.70	3.2483		19000	19000		1	
		Sieve	27.31	0.0000	500000[iv]	19000	19000		1	
		Augers (vertical)	164.86	0.0000	500000[iv]	19000	19000		1	0.045
		Horizontal Auger	10.33	0.1328	500000[iv]	19000	19000		1	
		Sweep Gas System	0.01	0.0000	138408[v]	19000	19000		1	
		Sweep Gas Piping	5.13	0.0920		19000	19000		1	
		Condensing Heat Exchanger	31.24	0.6454	832600[vi]	19000	19000		1	
		Water Filtration System	1.80	0.0068	296701.2[vii]	19000	19000	0.36	1	
	CO2 Cryocooler	Cryocooler	34.61	0.0726	500000[iv]	19000	19000		2	1.474
		Container	83.02	0.4906		19000	19000		1	
	Water Electrolyzer	Electrolysis Cell Stack	47.43	0.0045	27156[viii]	19000	19000	2.38	1	12.28
		O2 Separator / Water Reservoir	5.71	0.0119	27156[viii]	19000	19000	2.38	1	
		H2 Separator and Dryer	14.44	0.0040	98112[ix]	19000	19000	10	1	
		Water Pump	2.16	0.0007	144540[x]	19000	19000	1	1	8×10^{-5}

	Sabatier Reactor	Reactor	20.78	0.4181	50000[xi]	19000	19000	1	0.198
		Water / Methane Separator	0.24	0.0097	131000[xii]	19000	19000	1	
		Heat Exchanger	0.53	0.0000	832600[xiii]	19000	19000	1	
	Atmospheric Processor	Zeolite	0.866	0.0104	77100[xiv]	19000	19000	1	
		Compressor	13.101	0.0758	66666.7	19000	19000	2	1.194
		Cryocoolers	3.100	0.0015	500000[iv]	19000	19000	2	0.480
		Support Structure	5.622			19000	19000	1	
Food	First Mission	Prepackaged Food Supply	2907			19000	0	1	
	Subsequent Missions	Prepackaged Food Supply	4919			0	19000	1	

[i]Analogy to CCAA TCCV
[ii]Analogy to CCAA Heat Exchanger Liquid Sensor
[iii]Analogy to CDRA Heater Controller
[iv]Optimistic assumption; no data were available
[v]Analogy to OGA Nitrogen Purge ORU
[vi]Analogy CCAA Condensing Heat Exchanger
[vii]Analogy to WPA Multifiltration Bed
[viii]Analogy to OGA Hydrogen ORU (contains Electrolysis Cell Stack and Rotary Separator / Accumulator)
[ix]Analogy to OGA Oxygen Outlet
[x]Analogy to OGA Pump
[xi]Analogy to CRS Sabatier Methanation Reactor
[xii]Analogy to CRS Phase Separator
[xiii]Analogy to CRS Condensing Heat Exchanger
[xiv]Analogy to CDRA Dessicant-Adsorbent Bed
[xv]Analogy to CRS Compressor
[xvi]Mass is obtained from [300] and verified with calculations based on data from Link et al. [301]. All other data is assumed to be the same as the Recycle Filter Tank Assembly (RFTA) described in the NASA BVAD 2004 [209] – the original system from which the ARFTA was upgraded from. Here, the life limit of the ARFTA has been assumed to be zero, based on its development objective of facilitating the same function as the RFTA without the need for periodic replacement [301].

Table J.32: Architecture Case 3 Spare Parts Requirements for each Component over a 10 Mission Minimum Continuous Presence Campaign. Empty rows correspond to components assumed to have 100% reliability, and hence do not require spare parts

Group	Assembly	Subassembly	Mission									
			1	**2**	**3**	**4**	**5**	**6**	**7**	**8**	**9**	**10**
ECLSS	CDRA	Air Pump Two-Stage ORU	3	1	1	0	1	0	1	0	0	1
		Blower	3	2	0	1	0	1	1	0	0	1
		Check Valves	5	2	1	2	1	1	2	1	1	1
		Desiccant Beds	5	1	2	1	1	1	1	1	1	1
		Heat Controller	4	1	1	0	1	1	0	1	0	0
		Precooler	4	1	0	1	0	1	1	0	1	0
		Pump Fan Motor Controller	2	1	0	0	0	1	0	0	0	0
		Selector Valves	7	4	2	2	2	2	2	1	3	0
		Sorbent Beds (Zeolite)	5	2	1	1	1	1	1	1	1	1
	CCAA Mission 1	Condensing Heat Exchanger	2	1	1	0	1	0	0	1	0	0
		Electronic Interface Box (EIB)	3	1	0	0	1	0	1	0	0	0
		Fan Delta Pressure Sensor	3	1	1	0	0	1	0	1	0	0
		Heat Exchanger Liquid Sensor	4	1	1	0	1	1	0	1	0	1
		Inlet ORU	3	2	1	0	1	1	0	1	1	0
		Pressure Transducer	3	1	1	0	0	1	0	1	0	0
		Temperature Control Check Valve (TCCV)	15	9	7	7	7	7	6	6	6	6
		Temperature Sensor	2	0	1	0	0	0	0	1	0	0
		Water Separator	7	4	2	2	2	3	4	0	2	6
		Water Separator Liquid Sensor	4	1	1	0	1	1	0	1	0	1
	CCAA Mission 2	Condensing Heat Exchanger	0	2	1	0	1	0	0	1	0	0
		Electronic Interface Box (EIB)	0	3	0	1	0	0	1	0	0	0
		Fan Delta Pressure Sensor	0	3	1	0	0	1	0	1	0	0
		Heat Exchanger Liquid Sensor	0	4	1	0	1	0	1	0	1	0
		Inlet ORU	0	3	1	1	1	0	1	0	1	0
		Pressure Transducer	0	3	1	0	0	1	0	1	0	0
		Temperature Control Check Valve	0	14	6	5	6	6	5	5	5	4
		Temperature Sensor	0	2	0	0	1	0	0	0	0	0
		Water Separator	0	7	2	2	2	2	2	1	2	1
		Water Separator Liquid Sensor	0	4	1	0	1	0	1	0	1	0
	WPA	Catalytic Reactor	2	1	1	0	1	0	1	0	0	1
		Gas Separator	2	0	1	0	0	0	1	0	0	0
		Ion Exchange Bed	1	2	2	2	3	2	2	2	2	2
		Microbial Check Valve	2	0	1	0	0	0	1	0	0	0

		Multifiltration Bed #1	1	0	1	1	1	1	1	1	1	1
		Multifiltration Bed #2	1	0	1	1	1	1	1	1	1	1
		Particulate Filter	1	1	2	1	2	1	2	2	1	2
		pH Adjuster	2	1	0	0	0	1	0	0	0	0
		Process Controller	2	0	1	0	0	0	1	0	0	0
		Pump Separator	2	1	0	1	0	1	0	0	0	1
		Reactor Health Sensor	2	1	0	1	0	0	1	0	0	0
		Sensor	2	1	0	0	0	1	0	0	0	0
		Separator Filter	1	1	0	0	0	1	0	0	0	0
		Start-up Filter	1	1	0	0	1	0	0	0	0	0
		Water Delivery	2	0	1	0	0	1	0	0	0	1
	UPA	Distillation Assembly	2	1	0	1	0	0	1	0	0	1
		Firmware Controller Assembly	4	2	1	1	1	1	1	1	1	1
		Fluids Control and Pump Assembly	2	1	1	1	0	1	0	0	1	0
		Pressure Control and Pump Assembly	2	1	0	0	1	0	0	1	0	1
		Advanced Recycle Filter Tank Assembly	2	1	0	0	1	0	0	0	1	0
		Separator Plumbing Assembly	2	0	1	1	1	2	1	1	2	1
ISRU	Water Extractor	Oven + Insulating Cone	2	1	0	1	0	1	0	0	0	1
		Hopper										
		Sieve	2	1	0	0	0	1	0	0	0	0
		Augers (vertical)	2	0	0	1	0	0	0	1	0	0
		Horizontal Auger	2	1	0	0	1	0	0	0	1	0
		Sweep Gas System	4	1	2	0	1	0	2	0	1	0
		Sweep Gas Piping										
		Condensing Heat Exchanger	2	0	1	0	0	0	0	0	1	0
		Water Filtration System	6	6	6	6	6	6	6	6	6	6
	CO2 Cryocooler	Cryocooler	2	1	1	0	0	1	0	0	1	0
		Container										
	Water Electrolyzer	Electrolysis Cell Stack	5	3	1	2	1	2	1	1	2	0
		O2 Separator / Water Reservoir	6	3	1	2	2	1	2	1	1	1
		H2 Separator and Dryer	4	1	1	0	1	1	0	1	0	1
		Water Pump	4	1	1	2	2	3	2	2	2	2
	Sabatier Reactor	Reactor	4	2	1	1	1	1	1	1	1	0
		Water / Methane Separator	4	1	1	0	1	1	2	0	0	0
		Heat Exchanger	2	1	1	0	0	0	0	1	0	0
	Atmospheric Processor	Zeolite	5	1	1	1	1	1	0	1	1	0
		Compressor	5	3	1	1	2	1	1	1	1	1
		Cryocoolers	3	1	1	0	0	1	0	0	1	0
		Support Structure										

Table J.33: Architecture Case 3 Spare Parts Requirements for each Component over a 10 Mission Minimum Continuous Presence Campaign with all ISRU technologies at 10% of their originally estimated values. Empty rows correspond to components assumed to have 100% reliability, and hence do not require spare parts

Group	**Assembly**	**Subassembly**	**Mission**									
			1	**2**	**3**	**4**	**5**	**6**	**7**	**8**	**9**	**10**
ECLSS	CDRA	Air Pump Two-Stage ORU	3	1	1	0	1	0	1	0	1	0
		Blower	4	1	0	1	1	0	1	0	1	0
		Check Valves	5	2	1	2	1	2	1	1	1	1
		Desiccant Beds	5	2	1	1	1	2	0	1	2	1
		Heat Controller	4	1	1	0	1	1	0	1	0	1
		Precooler	4	1	0	1	1	0	1	0	1	0
		Pump Fan Motor Controller	2	1	0	0	0	1	0	0	0	0
		Selector Valves	7	4	2	2	2	2	2	2	2	2
		Sorbent Beds (Zeolite)	5	2	1	1	1	1	1	1	2	0
	CCAA Mission 1	Condensing Heat Exchanger	2	1	1	0	1	0	0	1	0	0
		Electronic Interface Box (EIB)	3	1	0	1	0	0	1	0	0	1
		Fan Delta Pressure Sensor	3	1	1	0	1	0	0	1	0	0
		Heat Exchanger Liquid Sensor	4	1	1	1	0	1	0	1	0	1
		Inlet ORU	4	1	1	1	0	1	1	0	1	0
		Pressure Transducer	3	1	1	0	1	0	0	1	0	0
		Temperature Control Check Valve (TCCV)	15	9	8	7	7	6	6	6	7	6
		Temperature Sensor	2	1	0	0	0	0	1	0	0	0

		Water Separator	7	4	2	3	2	2	4	0	2	6
		Water Separator Liquid Sensor	4	1	1	1	0	1	0	1	0	1
	CCAA Mission 2	Condensing Heat Exchanger	0	2	1	1	0	0	1	0	0	0
		Electronic Interface Box (EIB)	0	3	0	1	0	1	0	0	0	1
		Fan Delta Pressure Sensor	0	3	1	0	1	0	1	0	0	0
		Heat Exchanger Liquid Sensor	0	4	1	1	0	1	0	1	0	1
		Inlet ORU	0	4	0	1	1	0	1	1	0	1
		Pressure Transducer	0	3	1	0	1	0	0	1	0	0
		Temperature Control Check Valve	0	14	6	6	6	5	5	5	5	5
		Temperature Sensor	0	2	1	0	0	0	0	0	1	0
		Water Separator	0	7	2	2	2	2	2	2	1	2
		Water Separator Liquid Sensor	0	4	1	0	1	0	1	0	1	0
	WPA	Catalytic Reactor	2	1	1	0	1	0	1	0	1	0
		Gas Separator	2	0	1	0	0	1	0	0	0	0
		Ion Exchange Bed	1	2	2	2	3	2	2	2	2	2
		Microbial Check Valve	2	0	1	0	0	1	0	0	0	0
		Multifiltration Bed #1	1	0	1	1	1	1	1	1	1	1
		Multifiltration Bed #2	1	0	1	1	1	1	1	1	1	1
		Particulate Filter	1	1	2	1	2	1	2	2	1	2
		pH Adjuster	2	1	0	0	1	0	0	0	0	1
		Process Controller	2	0	1	0	0	0	1	0	0	0
		Pump Separator	2	1	0	1	0	1	0	0	1	0
		Reactor Health Sensor	2	1	0	1	0	0	1	0	0	1
		Sensor	2	0	1	0	0	1	0	0	0	0
		Separator Filter	1	1	0	0	1	0	0	0	0	0
		Start-up Filter	2	0	0	1	0	0	0	0	0	1
		Water Delivery	2	1	0	0	1	0	0	0	1	0
	UPA	Distillation Assembly	2	1	0	1	0	0	1	0	0	1
		Firmware Controller Assembly	4	2	1	1	1	1	1	1	1	1
		Fluids Control and Pump Assembly	2	1	1	1	0	1	0	0	1	0
		Pressure Control and Pump Assembly	2	1	0	1	0	0	1	0	0	1
		Advanced Recycle Filter Tank Assembly	2	1	0	0	1	0	0	1	0	0
		Separator Plumbing Assembly	2	0	1	1	1	2	1	1	2	1
ISRU	Water Extractor	Oven + Insulating Cone	5	3	2	1	2	2	1	1	2	1
		Hopper										
		Sieve	4	2	1	1	1	1	1	1	1	1
		Augers (vertical)	4	1	1	1	1	1	1	1	0	1
		Horizontal Auger	5	2	1	1	1	1	1	1	1	0
		Sweep Gas System	10	6	2	3	3	2	3	5	2	3
		Sweep Gas Piping										
		Condensing Heat Exchanger	4	1	1	1	0	1	0	1	1	0
		Water Filtration System	6	6	6	6	6	6	6	6	6	6
	CO2 Cryocooler	Cryocooler	6	2	2	2	1	2	1	2	1	1
		Container										
	Water Electrolyzer	Electrolysis Cell Stack	18	12	9	10	9	9	8	9	8	9
		O2 Separator / Water Reservoir	20	12	10	10	10	9	9	8	9	9
		H2 Separator and Dryer	9	5	3	4	3	3	3	3	3	3
		Water Pump	9	4	2	3	2	3	2	2	3	2
	Sabatier Reactor	Reactor	13	8	6	6	5	6	4	6	5	5
		Water / Methane Separator	10	4	5	2	2	3	3	3	3	3
		Heat Exchanger	5	2	1	0	1	1	1	1	0	1
	Atmospheric Processor	Zeolite	13	6	4	4	5	3	4	4	4	4
		Compressor	17	10	8	9	8	8	6	8	7	8
		Cryocoolers	7	2	2	2	2	2	1	2	1	2
		Support Structure										

J.3.4 Architecture Case 4

Table J.34: Architecture Case 4 Master Equipment List, containing component mass, volume and reliability data, as well as run times and power demands. Power is listed here on a per unit basis. ISRU technologies displayed here were sized by the HabNet ISRU Module.

Sys.	Assembly	Subassembly	Mass [kg]	Vol. [m^3]	MTBF [h]	Run Time Miss. 1 [h]	Run Time Miss. 2 [h]	LL [y]	# in Pmry.	Power [kW]
ECLS	CDRA	Air Pump Two-Stage ORU	10.89	0.0045	156200.0	19000	19000	15.29	1	0.860
		Blower	5.58	0.0300	129700.0	19000	19000	10.00	1	
		Check Valves	39.92	0.1784	32900.0[i]	19000	19000		1	
		Desiccant Beds	42.64	0.0850	77100.0	19000	19000		2	
		Heat Controller	3.31	0.0085	242700.0	19000	19000		2	
		Precooler	5.58	0.0255	129700.0	19000	19000	10.00	1	
		Pump Fan Motor Controller	2.72	0.0057	2270000.0	19000	19000		2	
		Selector Valves	3.04	0.0017	117000.0	19000	19000	10.61	6	
		Sorbent Beds (Zeolite)	42.64	0.0850	77100.0	19000	19000		2	
	CCAA Mission 1 (x4)	Condensing Heat Exchanger	49.71	0.3933	832600.0	19000	19000		4	0.544
		Electronic Interface Box (EIB)	4.04	0.0173	2350000.0	19000	19000		8	
		Fan Delta Pressure Sensor	0.45	0.0002	1250000.0	19000	19000		4	
		Heat Exchanger Liquid Sensor	0.64	0.0006	1140000.0	19000	19000		8	
		Inlet ORU	25.31	0.1308	333000.0	19000	19000		4	
		Pressure Transducer	0.48	0.0000	1250000.0	19000	19000	15.00	4	
		Temperature Control Check Valve	7.45	0.0071	32900.0	19000	19000		8	
		Temperature Sensor	0.26	0.0014	37600000.0	19000	19000		16	
		Water Separator	11.93	0.0583	131000.0	19000	19000	5.00	8	
		Water Separator Liquid Sensor	0.64	0.0006	1140000.0[ii]	19000	19000		8	
	CCAA Mission 2 (x3)	Condensing Heat Exchanger	49.71	0.3933	832600.0	0	19000		3	0.528
		Electronic Interface Box (EIB)	4.04	0.0173	2350000.0	0	19000		6	
		Fan Delta Pressure Sensor	0.45	0.0002	1250000.0	0	19000		3	
		Heat Exchanger Liquid Sensor	0.64	0.0006	1140000.0	0	19000		6	
		Inlet ORU	25.31	0.1308	333000.0	0	19000		3	
		Pressure Transducer	0.48	0.0000	1250000.0	0	19000	15.00	3	
		Temperature Control Check Valve	7.45	0.0071	32900.0	0	19000		6	
		Temperature Sensor	0.26	0.0014	37600000.0	0	19000		12	
		Water Separator	11.93	0.0583	131000.0	0	19000	5.00	6	
		Water Separator Liquid Sensor	0.64	0.0006	1140000.0[ii]	0	19000		6	
	WPA	Catalytic Reactor	67.04	0.1156	25579.2	1832	3067	2.25	1	0.320
		Gas Separator	39.15	0.0660	84008.4	1832	3067	1	1	
		Ion Exchange Bed	13.02	0.0173	296701.2	1832	3067	0.16	1	
		Microbial Check Valve	5.76	0.0065	143488.8	1832	3067	1	1	
		Multifiltration Bed #1	149.23	0.0657	296701.2	1832	3067	0.36	1	
		Multifiltration Bed #2	149.23	0.0657	296701.2	1832	3067	0.36	1	
		Particulate Filter	32.25	0.0717	717356.4	1832	3067	0.22	1	
		pH Adjuster	2.54	0.0026	137181.6	1832	3067	1	1	
		Process Controller	45.00	0.0838	87950.4	1832	3067	7.72	1	
		Pump Separator	31.34	0.0869	42398.4	1832	3067	2	1	
		Reactor Health Sensor	16.83	0.0425	56677.2	1832	3067	1	1	
		Sensor	4.81	0.0034	143664	1832	3067	10	1	
		Separator Filter	7.67	0.0102	359072.4	1832	3067	0.84	1	
		Start-up Filter	9.44	0.0184	226884	1832	3067	19.92	1	
		Water Delivery	47.54	0.0974	64561.2	1832	3067	5	1	
	UPA	Distillation Assembly	92.76	0.1422	142525.2	6713	11291	2	1	0.315
		Firmware Controller Assembly	23.09	0.0286	27331.2	6713	11291	2.4	1	
		Fluids Control and Pump Assembly	47.58	0.0731	90140.4	6713	11291	4	1	
		Pressure Control and Pump Assembly	49.08	0.1158	181507.2	6713	11291	2	1	
		Advanced Recycle Filter Tank Assembly[xvi]	50.00	0.1011	199640.4	6713	11291		1	
		Separator Plumbing Assembly	16.78	0.0229	384651.6	6713	11291	1	1	

	OGA	Hydrogen ORU	161.62	0.1467	27156	18922	18919	2.38	1	2.971
		Hydrogen Sensor	4.36	0.0034	61845.6	18922	18919	0.25	1	
		Inlet Deionizing Bed	28.67	0.0295	296701.2	18922	18919	6	1	
		Nitrogen Purge ORU	34.25	0.0312	138408	18922	18919		1	
		Oxygen Outlet	48.17	0.0312	98112	18922	18919	10	1	
		Power Supply Module	42.64	0.0649	47479.2	18922	18919	4.17	1	
		Process Controller	47.08	0.0838	103280.4	18922	18919	7.72	1	
		Pump	17.96	0.0102	144540	18922	18919	1	1	
		Water ORU	61.05	0.0756	33288	18922	18919	2.92	1	
ISRU	Water Extractor	Oven + Insulating Cone	65.68	2.8450	242700[iii]	19000	19000		1	18.43
		Hopper	52.40	3.3173		19000	19000		1	
		Sieve	28.19	0.0000	500000[iv]	19000	19000		1	
		Augers (vertical)	168.36	0.0000	500000[iv]	19000	19000		1	0.048
		Horizontal Auger	10.44	0.1342	500000[iv]	19000	19000		1	
		Sweep Gas System	0.01	0.0000	138408[v]	19000	19000		1	
		Sweep Gas Piping	5.22	0.0946		19000	19000		1	
		Condensing Heat Exchanger	31.90	0.6654	832600[vi]	19000	19000		1	
		Water Filtration System	1.84	0.0069	296701.2[vii]	19000	19000	0.36	1	
	CO2 Cryocooler	Cryocooler	34.61	0.0726	500000[iv]	19000	19000		2	1.474
		Container	83.02	0.4906		19000	19000		1	
	Water Electrolyzer	Electrolysis Cell Stack	47.43	0.0045	27156[viii]	19000	19000	2.38	1	12.28
		O2 Separator / Water Reservoir	5.71	0.0119	27156[viii]	19000	19000	2.38	1	
		H2 Separator and Dryer	14.44	0.0040	98112[ix]	19000	19000	10	1	
		Water Pump	2.16	0.0007	144540[x]	19000	19000	1	1	8×10^{-5}
	Sabatier Reactor	Reactor	20.78	0.4181	50000[xi]	19000	19000		1	0.198
		Water / Methane Separator	0.24	0.0097	131000[xii]	19000	19000		1	
		Heat Exchanger	0.53	0.0000	832600[xiii]	19000	19000		1	
	Atmospheric Processor	Zeolite	0.97	0.0116	77100[xiv]	19000	19000		1	
		Compressor	14.65	0.0847	66666.7	19000	19000		2	1.335
		Cryocoolers	3.10	0.0015	500000[iv]	19000	19000		2	0.480
		Support Structure	6.29			19000	19000		1	
Food	First Mission	Prepackaged Food Supply	2907			19000	0		1	
	Subsequent Missions	Prepackaged Food Supply	4919			0	19000		1	

[i] Analogy to CCAA TCCV
[ii] Analogy to CCAA Heat Exchanger Liquid Sensor
[iii] Analogy to CDRA Heater Controller
[iv] Optimistic assumption; no data were available
[v] Analogy to OGA Nitrogen Purge ORU
[vi] Analogy CCAA Condensing Heat Exchanger
[vii] Analogy to WPA Multifiltration Bed
[viii] Analogy to OGA Hydrogen ORU (contains Electrolysis Cell Stack and Rotary Separator / Accumulator)
[ix] Analogy to OGA Oxygen Outlet
[x] Analogy to OGA Pump
[xi] Analogy to CRS Sabatier Methanation Reactor
[xii] Analogy to CRS Phase Separator
[xiii] Analogy to CRS Condensing Heat Exchanger
[xiv] Analogy to CDRA Dessicant-Adsorbent Bed
[xv] Analogy to CRS Compressor
[xvi] Mass is obtained from [300] and verified with calculations based on data from Link et al. [301]. All other data is assumed to be the same as the Recycle Filter Tank Assembly (RFTA) described in the NASA BVAD 2004 [209] – the original system from which the ARFTA was upgraded from. Here, the life limit of the ARFTA has been assumed to be zero, based on its development objective of facilitating the same function as the RFTA without the need for periodic replacement [301].

Table J.35: Architecture Case 4 Spare Parts Requirements for each Component over a 10 Mission Minimum Continuous Presence Campaign. Empty rows correspond to components assumed to have 100% reliability, and hence do not require spare parts

Group	Assembly	Subassembly	Mission									
			1	**2**	**3**	**4**	**5**	**6**	**7**	**8**	**9**	**10**
ECLSS	CDRA	Air Pump Two-Stage ORU	3	1	1	0	1	0	1	0	1	0
		Blower	4	1	0	1	1	0	1	0	1	0
		Check Valves	5	2	2	1	1	2	1	1	1	1
		Desiccant Beds	5	2	1	1	1	2	1	1	0	1
		Heat Controller	4	1	1	1	0	1	0	1	0	1
		Precooler	4	1	1	0	1	0	1	0	1	0

		Pump Fan Motor Controller	2	1	0	0	0	1	0	0	0	0
		Selector Valves	8	3	2	2	2	2	2	2	1	2
		Sorbent Beds (Zeolite)	5	2	1	1	1	2	1	1	0	1
	CCAA Mission 1	Condensing Heat Exchanger	3	0	1	0	1	0	0	1	0	0
		Electronic Interface Box (EIB)	3	1	0	1	0	0	1	0	0	1
		Fan Delta Pressure Sensor	3	1	1	0	1	0	0	1	0	0
		Heat Exchanger Liquid Sensor	4	1	1	1	0	1	0	1	0	1
		Inlet ORU	4	1	1	1	0	1	1	0	1	0
		Pressure Transducer	3	1	1	0	0	1	0	1	0	0
		Temperature Control Check Valve (TCCV)	16	8	8	7	6	7	7	5	6	7
		Temperature Sensor	2	0	1	0	0	0	1	0	0	0
		Water Separator	7	4	2	3	2	2	4	0	2	6
		Water Separator Liquid Sensor	4	1	1	1	0	1	0	1	0	1
	CCAA Mission 2	Condensing Heat Exchanger	0	2	1	0	1	0	1	0	0	0
		Electronic Interface Box (EIB)	0	3	0	1	0	0	1	0	0	1
		Fan Delta Pressure Sensor	0	3	1	0	1	0	1	0	0	0
		Heat Exchanger Liquid Sensor	0	4	1	1	0	1	0	1	0	1
		Inlet ORU	0	4	0	1	1	1	0	1	0	1
		Pressure Transducer	0	3	1	0	0	1	0	1	0	0
		Temperature Control Check Valve	0	14	6	6	6	5	5	5	5	5
		Temperature Sensor	0	2	0	1	0	0	0	0	1	0
		Water Separator	0	7	2	2	2	2	2	2	1	2
		Water Separator Liquid Sensor	0	4	1	0	1	1	0	1	0	1
	WPA	Catalytic Reactor	2	1	1	0	1	0	1	0	1	0
		Gas Separator	2	0	1	0	0	1	0	0	0	0
		Ion Exchange Bed	1	2	2	2	3	2	2	2	2	3
		Microbial Check Valve	2	0	1	0	0	1	0	0	0	0
		Multifiltration Bed #1	1	0	1	1	1	1	1	1	1	1
		Multifiltration Bed #2	1	0	1	1	1	1	1	1	1	1
		Particulate Filter	1	1	2	1	2	1	2	2	1	2
		pH Adjuster	2	1	0	0	1	0	0	0	0	1
		Process Controller	2	0	1	0	0	1	0	0	0	0
		Pump Separator	2	1	1	0	0	1	0	0	1	0
		Reactor Health Sensor	2	1	0	1	0	0	1	0	0	1
		Sensor	2	1	0	0	0	1	0	0	0	0
		Separator Filter	1	1	0	0	1	0	0	0	0	1
		Start-up Filter	2	0	0	1	0	0	0	0	0	0
		Water Delivery	2	1	0	0	1	0	0	0	1	0
	UPA	Distillation Assembly	2	1	0	1	0	0	1	0	0	1
		Firmware Controller Assembly	4	2	1	1	1	1	2	0	1	1
		Fluids Control and Pump Assembly	2	2	0	1	0	1	0	1	0	0
		Pressure Control and Pump Assembly	2	1	0	1	0	0	1	0	0	1
		Advanced Recycle Filter Tank Assembly	2	1	0	0	1	0	0	1	0	0
		Separator Plumbing Assembly	2	0	1	1	1	2	1	1	2	1
	OGA	Hydrogen ORU	5	2	2	1	2	1	1	1	2	1
		Hydrogen Sensor	8	9	8	9	9	8	9	9	8	9
		Inlet Deionizing Bed	2	1	1	0	0	1	0	0	0	1
		Nitrogen Purge ORU	3	1	1	0	1	0	1	0	0	1
		Oxygen Outlet	3	2	0	1	1	0	1	0	1	0
		Power Supply Module	4	2	1	1	1	1	1	1	1	1
		Process Controller	3	1	1	1	0	1	1	0	0	1
		Pump	3	1	2	2	2	2	3	2	2	2
		Water ORU	5	2	1	2	1	1	1	1	1	1
ISRU	Water Extractor	Oven + Insulating Cone	2	1	1	0	0	1	0	0	1	0
		Hopper										
		Sieve	2	1	0	0	1	0	0	0	1	0
		Augers (vertical)	2	0	0	1	0	0	0	1	0	0
		Horizontal Auger	2	1	0	1	0	0	0	1	0	0
		Sweep Gas System	5	1	1	1	0	2	0	0	1	0
		Sweep Gas Piping										
		Condensing Heat Exchanger	2	0	1	0	0	0	0	1	0	0
		Water Filtration System	6	6	6	6	6	6	6	6	6	6
	CO2 Cryocooler	Cryocooler	2	1	1	0	1	0	0	1	0	0
		Container										
	Water Electrolyzer	Electrolysis Cell Stack	5	3	1	2	1	2	1	2	1	1
		O2 Separator / Water Reservoir	6	3	2	1	2	1	2	1	2	1
		H2 Separator and Dryer	4	1	1	0	1	1	0	1	0	1
		Water Pump	4	1	1	2	2	3	2	2	2	2
	Sabatier Reactor	Reactor	5	1	1	2	0	1	1	1	1	1

		Water / Methane Separator	4	1	1	2	0	1	0	1	0	1
		Heat Exchanger	2	1	1	0	0	0	1	0	0	0
	Atmospheric	Zeolite	5	1	1	1	1	1	1	1	0	1
	Processor	Compressor	5	3	1	2	1	1	2	0	2	1
		Cryocoolers	3	1	0	1	0	1	0	0	1	0
		Support Structure										

Table J.36: Architecture Case 4 Spare Parts Requirements for each Component over a 10 Mission Minimum Continuous Presence Campaign with all ISRU technologies at 10% of their originally estimated values. Empty rows correspond to components assumed to have 100% reliability, and hence do not require spare parts

Group	Assembly	Subassembly	Mission									
			1	**2**	**3**	**4**	**5**	**6**	**7**	**8**	**9**	**10**
ECLSS	CDRA	Air Pump Two-Stage ORU	3	1	1	1	0	1	0	0	1	0
		Blower	4	1	1	0	1	0	1	0	1	0
		Check Valves	5	2	2	1	2	1	1	1	1	1
		Desiccant Beds	5	2	1	1	2	1	1	1	1	1
		Heat Controller	4	1	1	1	0	1	0	1	0	1
		Precooler	4	1	1	0	1	0	1	0	1	0
		Pump Fan Motor Controller	2	1	0	0	0	1	0	0	0	0
		Selector Valves	8	3	2	2	3	1	2	2	2	2
		Sorbent Beds (Zeolite)	5	2	1	1	2	1	1	1	1	1
	CCAA Mission 1	Condensing Heat Exchanger	3	0	1	0	1	0	1	0	0	1
		Electronic Interface Box (EIB)	3	1	0	1	0	0	1	0	0	1
		Fan Delta Pressure Sensor	4	0	1	0	1	0	0	1	0	0
		Heat Exchanger Liquid Sensor	4	1	1	1	0	1	1	0	0	1
		Inlet ORU	4	1	1	1	0	1	1	0	1	1
		Pressure Transducer	3	1	1	0	1	0	0	1	0	0
		Temperature Control Check Valve (TCCV)	16	9	7	7	7	6	7	5	7	6
		Temperature Sensor	2	1	0	0	0	0	1	0	0	0
		Water Separator	8	3	3	2	2	2	4	0	2	6
		Water Separator Liquid Sensor	4	1	1	1	0	1	0	1	0	1
	CCAA Mission 2	Condensing Heat Exchanger	0	3	0	1	0	0	1	0	0	1
		Electronic Interface Box (EIB)	0	3	0	1	0	1	0	0	0	1
		Fan Delta Pressure Sensor	0	3	1	0	1	0	0	1	0	0
		Heat Exchanger Liquid Sensor	0	4	1	1	0	1	0	0	1	0
		Inlet ORU	0	4	0	1	1	1	0	1	0	1
		Pressure Transducer	0	3	1	0	1	0	0	1	0	0
		Temperature Control Check Valve	0	14	6	7	5	6	4	5	5	6
		Temperature Sensor	0	2	1	0	0	0	0	0	0	0
		Water Separator	0	7	2	3	2	1	2	2	1	2
		Water Separator Liquid Sensor	0	4	1	1	0	1	0	0	1	0
	WPA	Catalytic Reactor	2	1	1	1	0	0	1	0	1	0
		Gas Separator	2	0	1	0	0	1	0	0	0	1
		Ion Exchange Bed	1	2	2	2	3	2	2	2	2	3
		Microbial Check Valve	2	1	0	0	0	1	0	0	0	0
		Multifiltration Bed #1	1	1	0	1	1	1	1	1	1	1
		Multifiltration Bed #2	1	0	1	1	1	1	1	1	1	1
		Particulate Filter	1	1	2	1	2	1	2	2	1	2
		pH Adjuster	2	1	0	0	1	0	0	0	0	1
		Process Controller	2	0	1	0	0	1	0	0	0	0
		Pump Separator	2	1	1	0	0	1	0	0	1	0
		Reactor Health Sensor	2	1	0	1	0	1	0	0	0	1
		Sensor	2	1	0	0	0	1	0	0	0	0
		Separator Filter	2	0	0	0	1	0	0	0	0	1
		Start-up Filter	2	0	0	1	0	0	0	0	0	1
		Water Delivery	2	1	0	0	1	0	0	0	1	0
	UPA	Distillation Assembly	2	1	0	1	0	1	0	0	0	1
		Firmware Controller Assembly	4	2	1	2	1	1	1	0	1	1
		Fluids Control and Pump Assembly	2	2	0	1	0	1	0	1	0	0
		Pressure Control and Pump Assembly	2	1	0	1	0	0	1	0	0	1
		Advanced Recycle Filter Tank Assembly	2	1	0	1	0	0	0	1	0	0
		Separator Plumbing Assembly	2	0	1	1	1	2	1	1	2	1

	OGA	Hydrogen ORU	5	2	2	1	2	1	1	2	1	1
		Hydrogen Sensor	8	9	8	9	9	8	9	9	8	9
		Inlet Deionizing Bed	2	1	1	0	0	1	0	0	0	1
		Nitrogen Purge ORU	3	1	1	0	1	0	1	0	1	0
		Oxygen Outlet	3	1	1	1	1	0	1	0	1	0
		Power Supply Module	4	2	1	1	1	1	1	1	1	1
		Process Controller	3	1	1	1	1	0	1	0	1	0
		Pump	3	1	2	2	2	2	3	2	2	2
		Water ORU	5	2	1	2	1	1	1	2	1	1
ISRU	Water Extractor	Oven + Insulating Cone	6	2	2	2	1	2	1	2	1	1
		Hopper										
		Sieve	4	2	1	1	1	1	1	1	1	1
		Augers (vertical)	4	1	1	1	1	1	1	1	1	0
		Horizontal Auger	5	2	1	1	1	1	1	1	0	2
		Sweep Gas System	11	3	4	5	1	5	1	1	4	2
		Sweep Gas Piping										
		Condensing Heat Exchanger	4	1	1	1	0	1	1	0	1	0
		Water Filtration System	7	5	6	6	6	6	6	6	6	6
	CO2 Cryocooler	Cryocooler	6	2	2	2	2	1	1	2	1	2
		Container										
	Water Electrolyzer	Electrolysis Cell Stack	18	12	10	9	9	9	9	8	9	8
		O2 Separator / Water Reservoir	20	13	9	11	9	9	9	9	8	10
		H2 Separator and Dryer	9	5	4	3	3	4	2	3	3	3
		Water Pump	9	4	3	2	3	3	2	1	3	2
	Sabatier Reactor	Reactor	13	8	6	6	5	6	5	5	5	6
		Water / Methane Separator	11	4	3	4	2	2	4	2	3	3
		Heat Exchanger	5	2	1	0	1	1	1	0	1	1
	Atmospheric Processor	Zeolite	12	6	5	5	3	5	4	3	3	4
		Compressor	17	10	9	8	8	8	7	7	7	8
		Cryocoolers	7	3	2	1	2	2	1	2	1	2
		Support Structure										

J.3.5 Architecture Case 5

Table J.37: Architecture Case 5 Master Equipment List, containing component mass, volume and reliability data, as well as run times and power demands. Power is listed here on a per unit basis. ISRU technologies displayed here were sized by the HabNet ISRU Module.

Sys.	Assembly	Subassembly	Mass [kg]	Vol. [m^3]	MTBF [h]	Run Time Miss. 1 [h]	Run Time Miss. 2 [h]	LL [y]	# in Pmry.	Power [kW]
ECLS	CDRA	Air Pump Two-Stage ORU	10.89	0.0045	156200.0	19000	19000	15.29	1	0.860
		Blower	5.58	0.0300	129700.0	19000	19000	10.00	1	
		Check Valves	39.92	0.1784	32900.0[i]	19000	19000		1	
		Desiccant Beds	42.64	0.0850	77100.0	19000	19000		2	
		Heat Controller	3.31	0.0085	242700.0	19000	19000		2	
		Precooler	5.58	0.0255	129700.0	19000	19000	10.00	1	
		Pump Fan Motor Controller	2.72	0.0057	2270000.0	19000	19000		2	
		Selector Valves	3.04	0.0017	117000.0	19000	19000	10.61	6	
		Sorbent Beds (Zeolite)	42.64	0.0850	77100.0	19000	19000		2	
	CCAA Mission 1 (x4)	Condensing Heat Exchanger	49.71	0.3933	832600.0	19000	19000		4	0.544
		Electronic Interface Box (EIB)	4.04	0.0173	2350000.0	19000	19000		8	
		Fan Delta Pressure Sensor	0.45	0.0002	1250000.0	19000	19000		4	
		Heat Exchanger Liquid Sensor	0.64	0.0006	1140000.0	19000	19000		8	
		Inlet ORU	25.31	0.1308	333000.0	19000	19000		4	
		Pressure Transducer	0.48	0.0000	1250000.0	19000	19000	15.00	4	
		Temperature Control Check Valve	7.45	0.0071	32900.0	19000	19000		8	
		Temperature Sensor	0.26	0.0014	37600000.0	19000	19000		16	
		Water Separator	11.93	0.0583	131000.0	19000	19000	5.00	8	
		Water Separator Liquid Sensor	0.64	0.0006	1140000.0[ii]	19000	19000		8	

	CCAA Mission 2 (x3)	Condensing Heat Exchanger	49.71	0.3933	832600.0	0	19000		3	0.528
		Electronic Interface Box (EIB)	4.04	0.0173	2350000.0	0	19000		6	
		Fan Delta Pressure Sensor	0.45	0.0002	1250000.0	0	19000		3	
		Heat Exchanger Liquid Sensor	0.64	0.0006	1140000.0	0	19000		6	
		Inlet ORU	25.31	0.1308	333000.0	0	19000		3	
		Pressure Transducer	0.48	0.0000	1250000.0	0	19000	15.00	3	
		Temperature Control Check Valve	7.45	0.0071	32900.0	0	19000		6	
		Temperature Sensor	0.26	0.0014	37600000.0	0	19000		12	
		Water Separator	11.93	0.0583	131000.0	0	19000	5.00	6	
		Water Separator Liquid Sensor	0.64	0.0006	1140000.0[ii]	0	19000		6	
	WPA	Catalytic Reactor	67.04	0.1156	25579.2	1856	3112	2.25	1	0.320
		Gas Separator	39.15	0.0660	84008.4	1856	3112	1	1	
		Ion Exchange Bed	13.02	0.0173	296701.2	1856	3112	0.16	1	
		Microbial Check Valve	5.76	0.0065	143488.8	1856	3112	1	1	
		Multifiltration Bed #1	149.23	0.0657	296701.2	1856	3112	0.36	1	
		Multifiltration Bed #2	149.23	0.0657	296701.2	1856	3112	0.36	1	
		Particulate Filter	32.25	0.0717	717356.4	1856	3112	0.22	1	
		pH Adjuster	2.54	0.0026	137181.6	1856	3112	1	1	
		Process Controller	45.00	0.0838	87950.4	1856	3112	7.72	1	
		Pump Separator	31.34	0.0869	42398.4	1856	3112	2	1	
		Reactor Health Sensor	16.83	0.0425	56677.2	1856	3112	1	1	
		Sensor	4.81	0.0034	143664	1856	3112	10	1	
		Separator Filter	7.67	0.0102	359072.4	1856	3112	0.84	1	
		Start-up Filter	9.44	0.0184	226884	1856	3112	19.92	1	
		Water Delivery	47.54	0.0974	64561.2	1856	3112	5	1	
	UPA	Distillation Assembly	92.76	0.1422	142525.2	6716	11288	2	1	0.315
		Firmware Controller Assembly	23.09	0.0286	27331.2	6716	11288	2.4	1	
		Fluids Control and Pump Assembly	47.58	0.0731	90140.4	6716	11288	4	1	
		Pressure Control and Pump Assembly	49.08	0.1158	181507.2	6716	11288	2	1	
		Advanced Recycle Filter Tank Assembly[xvi]	50.00	0.1011	199640.4	6716	11288		1	
		Separator Plumbing Assembly	16.78	0.0229	384651.6	6716	11288	1	1	
	OGA	Hydrogen ORU	161.62	0.1467	27156	18922	18918	2.38	1	2.971
		Hydrogen Sensor	4.36	0.0034	61845.6	18922	18918	0.25	1	
		Inlet Deionizing Bed	28.67	0.0295	296701.2	18922	18918	6	1	
		Nitrogen Purge ORU	34.25	0.0312	138408	18922	18918		1	
		Oxygen Outlet	48.17	0.0312	98112	18922	18918	10	1	
		Power Supply Module	42.64	0.0649	47479.2	18922	18918	4.17	1	
		Process Controller	47.08	0.0838	103280.4	18922	18918	7.72	1	
		Pump	17.96	0.0102	144540	18922	18918	1	1	
		Water ORU	61.05	0.0756	33288	18922	18918	2.92	1	
	CRS	Sabatier Methanation Reactor	120[xvii]	0.21[xvii]	50000[xviii]	1354	2032		1	0.106
		Condensing Heat Exchanger[xix]	49.71	0.3933	832600	1354	2032		1	0.08
		Phase Separator[xx]	11.93	0.0583	131000	1354	2032	5	1	
		Valves[xxi]	3.04	0.0017	117000	1354	2032	10.61	7[xxii]	
		Sensors[xxiii]	4.81	0.0034	143664	1354	2032	10	1	
		Controller	3.00[xvii]	0.0053[xxiv]	103280[xxv]	1354	2032	7.72[xxv]	1	
		Compressor	27.0[xvii]	0.0112[xxvi]	66666.7[xviii]	1354	2032		1	0.5
ISRU	Water Extractor	Oven + Insulating Cone	65.01	2.8163	242700[iii]	19000	19000		1	18.24
		Hopper	52.06	3.2837		19000	19000		1	
		Sieve	27.76	0.0000	500000[iv]	19000	19000		1	
		Augers (vertical)	166.66	0.0000	500000[iv]	19000	19000		1	0.048
		Horizontal Auger	10.39	0.1335	500000[iv]	19000	19000		1	
		Sweep Gas System	0.01	0.0000	138408[v]	19000	19000		1	
		Sweep Gas Piping	5.18	0.0934		19000	19000		1	
		Condensing Heat Exchanger	31.58	0.6557	832600[vi]	19000	19000		1	
		Water Filtration System	1.82	0.0068	296701.2[vii]	19000	19000	0.36	1	
	CO2 Cryocooler	Cryocooler	34.61	0.0726	500000[iv]	19000	19000		2	1.474
		Container	83.02	0.4906		19000	19000		1	
	Water Electrolyzer	Electrolysis Cell Stack	47.43	0.0045	27156[viii]	19000	19000	2.38	1	12.28
		O2 Separator / Water Reservoir	5.71	0.0119	27156[viii]	19000	19000	2.38	1	
		H2 Separator and Dryer	14.44	0.0040	98112[ix]	19000	19000	10	1	

		Water Pump	2.16	0.0007	144540[x]	19000	19000	1	1	8×10^{-5}
	Sabatier Reactor	Reactor	20.78	0.4181	50000[xi]	19000	19000		1	0.198
		Water / Methane Separator	0.24	0.0097	131000[xii]	19000	19000		1	
		Heat Exchanger	0.53	0.0000	832600[xiii]	19000	19000		1	
	Atmospheric Processor	Zeolite	0.97	0.0116	77100[xiv]	19000	19000		1	
		Compressor	14.65	0.0847	66666.7	19000	19000		2	1.335
		Cryocoolers	3.10	0.0015	500000[iv]	19000	19000		2	0.480
		Support Structure	6.29			19000	19000		1	
Food	First Mission	Prepackaged Food Supply	2907			19000	0		1	
	Subsequent Missions	Prepackaged Food Supply	4919			0	19000		1	

[i]Analogy to CCAA TCCV
[ii]Analogy to CCAA Heat Exchanger Liquid Sensor
[iii]Analogy to CDRA Heater Controller
[iv]Optimistic assumption; no data were available
[v]Analogy to OGA Nitrogen Purge ORU
[vi]Analogy CCAA Condensing Heat Exchanger
[vii]Analogy to WPA Multifiltration Bed
[viii]Analogy to OGA Hydrogen ORU (contains Electrolysis Cell Stack and Rotary Separator / Accumulator)
[ix]Analogy to OGA Oxygen Outlet
[x]Analogy to OGA Pump
[xi]Analogy to CRS Sabatier Methanation Reactor
[xii]Analogy to CRS Phase Separator
[xiii]Analogy to CRS Condensing Heat Exchanger
[xiv]Analogy to CDRA Dessicant-Adsorbent Bed
[xv]Analogy to CRS Compressor
[xvi]Mass is obtained from [300] and verified with calculations based on data from Link et al. [301]. All other data is assumed to be the same as the Recycle Filter Tank Assembly (RFTA) described in the NASA BVAD 2004 [209] – the original system from which the ARFTA was upgraded from. Here, the life limit of the ARFTA has been assumed to be zero, based on its development objective of facilitating the same function as the RFTA without the need for periodic replacement [301].
[xvii]Data taken from Jeng and Lin [256]
[xviii]Data taken from Papale et al. [318]
[xix]Analogy to CCAA Condensing Heat Exchanger
[xx]Analogy to CCAA Water Separator
[xxi]Analogy to CDRA Selector Valves
[xxii]Data taken from Jones [319]
[xxiii]Analogy to WPA Sensor
[xxiv]Linear scaling (based on mass) from OGA Process Controller
[xxv]Analogy to OGA Process Controller
[xxvi]Linear scaling (based on mass) from CDRA Air Pump

Table J.38: Architecture Case 5 Spare Parts Requirements for each Component over a 10 Mission Minimum Continuous Presence Campaign. Empty rows correspond to components assumed to have 100% reliability, and hence do not require spare parts

Group	Assembly	Subassembly	Mission									
			1	**2**	**3**	**4**	**5**	**6**	**7**	**8**	**9**	**10**
ECLSS	CDRA	Air Pump Two-Stage ORU	3	1	1	0	1	0	1	0	1	0
		Blower	4	1	1	0	1	0	1	0	1	0
		Check Valves	5	2	2	1	1	2	1	1	1	1
		Desiccant Beds	5	2	1	1	1	2	1	1	1	1
		Heat Controller	4	1	1	1	0	1	0	1	0	1
		Precooler	4	1	1	0	1	0	1	0	1	0
		Pump Fan Motor Controller	2	1	0	0	0	1	0	0	0	0
		Selector Valves	8	3	2	2	2	2	2	2	1	2
		Sorbent Beds (Zeolite)	5	2	1	1	1	2	1	1	0	1
	CCAA Mission 1	Condensing Heat Exchanger	3	0	1	0	1	0	1	0	0	0
		Electronic Interface Box (EIB)	3	1	0	1	0	0	1	0	0	1
		Fan Delta Pressure Sensor	3	1	1	0	1	0	0	1	0	0
		Heat Exchanger Liquid Sensor	4	1	1	1	0	1	1	0	1	0
		Inlet ORU	4	1	1	1	0	1	1	0	1	0
		Pressure Transducer	3	1	1	0	0	1	0	1	0	0
		Temperature Control Check Valve (TCCV)	16	9	7	7	6	7	7	6	6	5
		Temperature Sensor	2	1	0	0	0	0	1	0	0	0
		Water Separator	7	4	2	3	2	2	4	1	1	6
		Water Separator Liquid Sensor	4	1	1	1	0	1	0	1	1	0
	CCAA Mission 2	Condensing Heat Exchanger	0	3	0	0	1	0	1	0	0	0
		Electronic Interface Box (EIB)	0	3	0	1	0	1	0	0	0	1
		Fan Delta Pressure Sensor	0	3	1	1	0	0	0	1	0	1
		Heat Exchanger Liquid Sensor	0	4	1	1	0	1	0	1	0	0
		Inlet ORU	0	4	1	0	1	1	0	1	0	1
		Pressure Transducer	0	3	1	0	1	0	0	1	0	0
		Temperature Control Check Valve	0	14	7	5	6	6	4	6	4	5
		Temperature Sensor	0	2	1	0	0	0	0	0	1	0
		Water Separator	0	7	2	3	1	2	2	2	1	2
		Water Separator Liquid Sensor	0	4	1	1	0	0	1	1	0	0

	WPA	Catalytic Reactor	2	1	1	1	0	1	0	0	1	0
		Gas Separator	2	1	0	0	0	1	0	0	0	0
		Ion Exchange Bed	1	2	2	2	3	2	2	2	3	2
		Microbial Check Valve	2	1	0	0	0	1	0	0	0	0
		Multifiltration Bed #1	1	0	1	1	1	1	1	1	1	1
		Multifiltration Bed #2	1	0	1	1	1	1	1	1	1	1
		Particulate Filter	1	1	2	1	2	2	1	2	1	2
		pH Adjuster	2	1	0	0	1	0	0	0	0	1
		Process Controller	2	0	1	0	0	1	0	0	0	0
		Pump Separator	2	1	1	0	0	1	0	0	1	0
		Reactor Health Sensor	2	1	0	1	0	0	1	0	0	0
		Sensor	2	1	0	0	0	1	0	0	0	0
		Separator Filter	2	0	0	0	0	1	0	0	0	1
		Start-up Filter	2	0	0	1	0	0	0	0	0	1
		Water Delivery	2	1	0	0	1	0	0	0	1	0
	UPA	Distillation Assembly	2	1	0	1	0	0	1	0	0	1
		Firmware Controller Assembly	4	2	1	1	1	2	0	1	1	1
		Fluids Control and Pump Assembly	2	2	0	1	0	1	0	1	0	0
		Pressure Control and Pump Assembly	2	1	0	1	0	0	1	0	0	1
		Advanced Recycle Filter Tank Assembly	2	1	0	0	1	0	0	1	0	0
		Separator Plumbing Assembly	2	0	1	1	1	2	1	1	2	1
	OGA	Hydrogen ORU	5	2	2	1	2	1	1	1	2	1
		Hydrogen Sensor	8	9	8	9	9	8	9	9	8	9
		Inlet Deionizing Bed	2	1	1	0	0	1	0	0	0	1
		Nitrogen Purge ORU	3	1	1	0	1	0	1	0	1	0
		Oxygen Outlet	3	2	0	1	1	0	1	0	1	0
		Power Supply Module	4	2	1	1	1	1	1	1	1	1
		Process Controller	3	1	1	1	0	1	1	0	0	1
		Pump	3	1	2	2	2	2	3	2	2	2
		Water ORU	5	2	1	2	1	1	1	1	1	2
	CRS	Sabatier Methanation Reactor	2	0	1	0	0	0	1	0	0	0
		Condensing Heat Exchanger	1	0	0	0	1	0	0	0	0	0
		Phase Separator	2	0	0	1	0	0	0	0	0	1
		Valves	3	1	1	1	0	1	0	1	0	0
		Sensors	2	0	1	0	0	0	0	1	0	0
		Controller	2	1	0	0	1	0	0	0	0	0
		Compressor	2	0	1	0	0	1	0	0	0	0
ISRU	Water Extractor	Oven + Insulating Cone	2	1	1	0	0	1	0	0	1	0
		Hopper										
		Sieve	2	1	0	0	1	0	0	0	0	1
		Augers (vertical)	2	0	0	1	0	0	0	1	0	0
		Horizontal Auger	2	1	0	1	0	0	0	1	0	0
		Sweep Gas System	5	1	1	1	0	1	1	0	1	0
		Sweep Gas Piping										
		Condensing Heat Exchanger	2	0	1	0	0	0	0	1	0	0
		Water Filtration System	6	6	6	6	6	6	6	6	6	6
	CO2 Cryocooler	Cryocooler	2	1	1	0	1	0	0	1	0	0
		Container										
	Water Electrolyzer	Electrolysis Cell Stack	5	3	1	2	2	1	1	2	1	1
		O2 Separator / Water Reservoir	6	3	2	1	2	2	1	1	2	1
		H2 Separator and Dryer	4	1	1	0	1	1	0	1	0	1
		Water Pump	4	1	1	2	2	3	2	2	2	2
	Sabatier Reactor	Reactor	5	1	1	1	2	0	1	1	1	1
		Water / Methane Separator	4	1	2	0	1	1	0	1	1	0
		Heat Exchanger	2	1	1	0	0	0	1	0	0	0
	Atmospheric Processor	Zeolite	5	1	2	1	0	1	1	0	1	1
		Compressor	5	3	1	2	1	1	2	1	1	1
		Cryocoolers	3	1	0	1	0	1	0	1	0	0
		Support Structure										

Table J.39: Architecture Case 5 Spare Parts Requirements for each Component over a 10 Mission Minimum Continuous Presence Campaign with all ISRU technologies at 10% of their originally estimated values. Empty rows correspond to components assumed to have 100% reliability, and hence do not require spare parts

Group	Assembly	Subassembly	Mission									
			1	2	3	4	5	6	7	8	9	10
ECLSS	CDRA	Air Pump Two-Stage ORU	3	1	1	1	0	1	0	0	1	0
		Blower	4	1	1	0	1	0	1	0	1	0
		Check Valves	5	2	2	1	2	1	1	1	1	1
		Desiccant Beds	5	2	1	1	2	1	1	1	1	1
		Heat Controller	4	1	1	1	0	1	0	1	0	1
		Precooler	4	1	1	0	1	0	1	0	1	0
		Pump Fan Motor Controller	2	1	0	0	0	1	0	0	0	0
		Selector Valves	8	3	2	3	1	2	2	2	2	2
		Sorbent Beds (Zeolite)	5	2	1	1	2	1	1	1	1	1
	CCAA Mission 1	Condensing Heat Exchanger	3	0	1	0	1	0	1	0	0	1
		Electronic Interface Box (EIB)	3	1	0	1	0	1	0	0	0	1
		Fan Delta Pressure Sensor	4	1	0	0	1	0	1	0	0	0
		Heat Exchanger Liquid Sensor	4	2	0	1	0	1	1	0	0	1
		Inlet ORU	4	1	1	1	1	0	1	0	1	1
		Pressure Transducer	4	0	1	0	0	1	1	0	0	0
		Temperature Control Check Valve (TCCV)	16	9	7	7	7	7	6	6	6	6
		Temperature Sensor	2	1	0	0	0	0	1	0	0	0
		Water Separator	8	3	3	2	2	2	4	0	2	6
		Water Separator Liquid Sensor	4	2	0	1	0	1	1	0	0	1
	CCAA Mission 2	Condensing Heat Exchanger	0	3	0	1	0	0	1	0	0	1
		Electronic Interface Box (EIB)	0	3	0	1	0	1	0	0	0	1
		Fan Delta Pressure Sensor	0	3	1	1	0	0	1	0	0	1
		Heat Exchanger Liquid Sensor	0	4	1	1	0	1	0	0	1	0
		Inlet ORU	0	4	1	0	1	1	0	1	0	1
		Pressure Transducer	0	3	1	1	0	0	1	0	0	0
		Temperature Control Check Valve	0	14	7	6	5	6	5	5	4	5
		Temperature Sensor	0	2	0	1	0	0	0	0	0	1
		Water Separator	0	7	3	2	2	2	1	2	1	2
		Water Separator Liquid Sensor	0	4	1	1	0	1	0	0	1	0
	WPA	Catalytic Reactor	2	1	1	1	0	1	0	0	1	0
		Gas Separator	2	1	0	0	0	1	0	0	0	1
		Ion Exchange Bed	1	2	2	2	3	2	2	2	3	2
		Microbial Check Valve	2	1	0	0	0	1	0	0	0	0
		Multifiltration Bed #1	1	1	0	1	1	1	1	1	1	1
		Multifiltration Bed #2	1	0	1	1	1	1	1	1	1	1
		Particulate Filter	1	1	2	1	2	2	1	2	1	2
		pH Adjuster	2	1	0	0	1	0	0	0	0	1
		Process Controller	2	0	1	0	0	1	0	0	0	0
		Pump Separator	2	1	1	0	0	1	0	0	1	0
		Reactor Health Sensor	2	1	0	1	0	1	0	0	0	1
		Sensor	2	1	0	0	0	1	0	0	0	0
		Separator Filter	1	1	0	0	1	0	0	0	0	1
		Start-up Filter	2	0	0	1	0	0	0	0	0	1
		Water Delivery	2	1	0	0	1	0	0	0	1	0
	UPA	Distillation Assembly	2	1	0	1	0	1	0	0	0	1
		Firmware Controller Assembly	4	2	1	2	1	1	1	0	1	1
		Fluids Control and Pump Assembly	2	2	0	1	0	1	0	1	0	1
		Pressure Control and Pump Assembly	2	1	0	1	0	0	1	0	0	1
		Advanced Recycle Filter Tank Assembly	2	1	0	1	0	0	0	1	0	0
		Separator Plumbing Assembly	2	1	0	1	1	2	1	1	2	1
	OGA	Hydrogen ORU	5	2	2	1	2	1	1	2	1	1
		Hydrogen Sensor	8	9	8	9	9	8	9	9	8	9
		Inlet Deionizing Bed	2	1	1	0	0	1	0	0	1	0
		Nitrogen Purge ORU	3	1	1	0	1	0	1	0	1	0
		Oxygen Outlet	3	2	0	1	1	0	1	0	1	0
		Power Supply Module	4	2	1	2	0	1	1	1	1	1
		Process Controller	3	1	1	1	1	0	1	0	1	0
		Pump	3	1	2	2	2	2	3	2	2	2
		Water ORU	5	2	1	2	1	1	1	2	1	1
	CRS	Sabatier Methanation Reactor	2	0	1	0	0	0	1	0	0	0

		Condensing Heat Exchanger	1	0	0	0	1	0	0	0	0	0
		Phase Separator	2	0	0	1	0	0	0	0	1	0
		Valves	3	1	1	1	0	1	0	1	0	1
		Sensors	2	0	1	0	0	0	0	1	0	0
		Controller	2	1	0	0	0	1	0	0	0	0
		Compressor	2	0	1	0	0	1	0	0	0	0
ISRU	Water Extractor	Oven + Insulating Cone	6	2	2	2	1	2	1	2	1	1
		Hopper										
		Sieve	4	2	1	2	1	1	0	1	1	1
		Augers (vertical)	4	1	1	1	1	1	1	1	1	0
		Horizontal Auger	5	2	1	1	1	1	1	1	1	1
		Sweep Gas System	11	4	3	5	1	3	4	2	1	4
		Sweep Gas Piping										
		Condensing Heat Exchanger	4	1	1	1	0	1	1	0	1	1
		Water Filtration System	7	5	6	6	6	6	6	6	6	6
	CO2 Cryocooler	Cryocooler	6	2	2	2	2	1	1	2	1	2
		Container										
	Water Electrolyzer	Electrolysis Cell Stack	18	12	10	9	9	9	9	8	9	9
		O2 Separator / Water Reservoir	20	12	10	11	9	9	10	8	8	9
		H2 Separator and Dryer	10	4	4	3	4	3	3	3	2	3
		Water Pump	9	4	3	3	2	3	2	2	2	2
	Sabatier Reactor	Reactor	13	8	6	6	6	5	5	5	5	6
		Water / Methane Separator	10	5	3	3	3	3	4	1	2	3
		Heat Exchanger	5	2	1	1	0	1	1	1	0	1
	Atmospheric Processor	Zeolite	12	7	4	5	3	5	4	3	3	5
		Compressor	17	10	9	8	8	8	7	8	7	7
		Cryocoolers	7	3	1	3	1	2	1	2	1	2
		Support Structure										

J.3.6 Architecture Case 6

Table J.40: Architecture Case 6 Master Equipment List, containing component mass, volume and reliability data, as well as run times and power demands. Power is listed here on a per unit basis. ISRU technologies displayed here were sized by the HabNet ISRU Module.

Sys.	Assembly	Subassembly	Mass [kg]	Vol. [m^3]	MTBF [h]	Run Time Miss. 1 [h]	Run Time Miss. 2 [h]	LL [y]	# in Pmry.	Power [kW]
ECLS	CDRA	Air Pump Two-Stage ORU	10.89	0.0045	156200.0	19000	19000	15.29	1	0.860
		Blower	5.58	0.0300	129700.0	19000	19000	10.00	1	
		Check Valves	39.92	0.1784	32900.0[i]	19000	19000		1	
		Desiccant Beds	42.64	0.0850	77100.0	19000	19000		2	
		Heat Controller	3.31	0.0085	242700.0	19000	19000		2	
		Precooler	5.58	0.0255	129700.0	19000	19000	10.00	1	
		Pump Fan Motor Controller	2.72	0.0057	2270000.0	19000	19000		2	
		Selector Valves	3.04	0.0017	117000.0	19000	19000	10.61	6	
		Sorbent Beds (Zeolite)	42.64	0.0850	77100.0	19000	19000		2	
	CCAA Mission 1 (x5)	Condensing Heat Exchanger	49.71	0.3933	832600.0	19000	19000		5	0.602
		Electronic Interface Box (EIB)	4.04	0.0173	2350000.0	19000	19000		10	
		Fan Delta Pressure Sensor	0.45	0.0002	1250000.0	19000	19000		5	
		Heat Exchanger Liquid Sensor	0.64	0.0006	1140000.0	19000	19000		10	
		Inlet ORU	25.31	0.1308	333000.0	19000	19000		5	
		Pressure Transducer	0.48	0.0000	1250000.0	19000	19000	15.00	5	
		Temperature Control Check Valve	7.45	0.0071	32900.0	19000	19000		10	
		Temperature Sensor	0.26	0.0014	37600000.0	19000	19000		20	
		Water Separator	11.93	0.0583	131000.0	19000	19000	5.00	10	
		Water Separator Liquid Sensor	0.64	0.0006	1140000.0[ii]	19000	19000		10	
		Condensing Heat Exchanger	49.71	0.3933	832600.0	0	19000		3	0.515

	CCAA Mission 2 (x3)	Electronic Interface Box (EIB)	4.04	0.0173	2350000.0	0	19000		6	
		Fan Delta Pressure Sensor	0.45	0.0002	1250000.0	0	19000		3	
		Heat Exchanger Liquid Sensor	0.64	0.0006	1140000.0	0	19000		6	
		Inlet ORU	25.31	0.1308	333000.0	0	19000		3	
		Pressure Transducer	0.48	0.0000	1250000.0	0	19000	15.00	3	
		Temperature Control Check Valve	7.45	0.0071	32900.0	0	19000		6	
		Temperature Sensor	0.26	0.0014	37600000.0	0	19000		12	
		Water Separator	11.93	0.0583	131000.0	0	19000	5.00	6	
		Water Separator Liquid Sensor	0.64	0.0006	1140000.0[ii]	0	19000		6	
	WPA	Catalytic Reactor	67.04	0.1156	25579.2	2816	4664	2.25	1	0.320
		Gas Separator	39.15	0.0660	84008.4	2816	4664	1	1	
		Ion Exchange Bed	13.02	0.0173	296701.2	2816	4664	0.16	1	
		Microbial Check Valve	5.76	0.0065	143488.8	2816	4664	1	1	
		Multifiltration Bed #1	149.23	0.0657	296701.2	2816	4664	0.36	1	
		Multifiltration Bed #2	149.23	0.0657	296701.2	2816	4664	0.36	1	
		Particulate Filter	32.25	0.0717	717356.4	2816	4664	0.22	1	
		pH Adjuster	2.54	0.0026	137181.6	2816	4664	1	1	
		Process Controller	45.00	0.0838	87950.4	2816	4664	7.72	1	
		Pump Separator	31.34	0.0869	42398.4	2816	4664	2	1	
		Reactor Health Sensor	16.83	0.0425	56677.2	2816	4664	1	1	
		Sensor	4.81	0.0034	143664	2816	4664	10	1	
		Separator Filter	7.67	0.0102	359072.4	2816	4664	0.84	1	
		Start-up Filter	9.44	0.0184	226884	2816	4664	19.92	1	
		Water Delivery	47.54	0.0974	64561.2	2816	4664	5	1	
	UPA	Distillation Assembly	92.76	0.1422	142525.2	6713	11271	2	1	0.315
		Firmware Controller Assembly	23.09	0.0286	27331.2	6713	11271	2.4	1	
		Fluids Control and Pump Assembly	47.58	0.0731	90140.4	6713	11271	4	1	
		Pressure Control and Pump Assembly	49.08	0.1158	181507.2	6713	11271	2	1	
		Advanced Recycle Filter Tank Assembly[xvi]	50.00	0.1011	199640.4	6713	11271		1	
		Separator Plumbing Assembly	16.78	0.0229	384651.6	6713	11271	1	1	
ISRU	Water Extractor	Oven + Insulating Cone	68.28	2.9575	242700[iii]	19000	19000		1	19.16
		Hopper	53.72	3.4485		19000	19000		1	
		Sieve	29.88	0.0000	500000[iv]	19000	19000		1	
		Augers (vertical)	175.02	0.0000	500000[iv]	19000	19000		1	0.050
		Horizontal Auger	10.65	0.1368	500000[iv]	19000	19000		1	
		Sweep Gas System	0.01	0.0000	138408[v]	19000	19000		1	
		Sweep Gas Piping	5.39	0.0995		19000	19000		1	
		Condensing Heat Exchanger	33.14	0.7040	832600[vi]	19000	19000		1	
		Water Filtration System	1.91	0.0072	296701.2[vii]	19000	19000	0.36	1	
	CO2 Cryocooler	Cryocooler	34.61	0.0726	500000[iv]	19000	19000		2	1.474
		Container	83.02	0.4906		19000	19000		1	
	Water Electrolyzer	Electrolysis Cell Stack	47.43	0.0045	27156[viii]	19000	19000	2.38	1	12.28
		O2 Separator / Water Reservoir	5.71	0.0119	27156[viii]	19000	19000	2.38	1	
		H2 Separator and Dryer	14.44	0.0040	98112[ix]	19000	19000	10	1	
		Water Pump	2.16	0.0007	144540[x]	19000	19000	1	1	8×10^{-5}
	Sabatier Reactor	Reactor	20.78	0.4181	50000[xi]	19000	19000		1	0.198
		Water / Methane Separator	0.24	0.0097	131000[xii]	19000	19000		1	
		Heat Exchanger	0.53	0.0000	832600[xiii]	19000	19000		1	
	Atmospheric Processor	Zeolite	0.90	0.0109	77100[xiv]	19000	19000		1	
		Compressor	13.67	0.0790	66666.7	19000	19000		2	1.335
		Cryocoolers	3.10	0.0015	500000[iv]	19000	19000		2	0.480
		Support Structure	5.86			19000	19000		1	
BPC	Crop Lighting 1	Lighting System Unit[xvii]	8.00	0.0185	1743216	19000	19000	5.71	7	4.41
	Crop Lighting 2	Lighting System Unit[xvii]	8.00	0.0185	1743216	0	19000	5.71	6	3.78
	BPC Structure 1[xviii]	Primary Structure (Inflatable)	335.00	25		19000	19000		1	
		Secondary Structure (Shelving)	51.56			19000	19000		1	
		Mechanization Systems	37.08			19000	19000		1	
	BPC Structure 2[xviii]	Primary Structure (Inflatable)	335.00	25		0	19000		1	
		Secondary Structure (Shelving)	51.56			0	19000		1	
		Mechanization Systems	37.08			0	19000		1	
		Hand Mixer	2.00	0.0050		19000	19000		1	

	Food Processor[xix]	Food Processor / Blender	8.00	0.0230	19000	19000	1
		Grinder / Mill	4.10	0.0120	19000	19000	1
		Bread Machine	7.40	0.0310	19000	19000	1
		Griddle / Grill	5.80	0.0270	19000	19000	1
		Juice Extractor	7.70	0.0390	19000	19000	1
Food	First Mission	Prepackaged Food Supply	2796		19000	0	1
	Second Mission	Prepackaged Food Supply	4706		0	19000	1
	Subsequent Missions	Prepackaged Food Supply	4698		0	0	1

[i]Analogy to CCAA TCCV
[ii]Analogy to CCAA Heat Exchanger Liquid Sensor
[iii]Analogy to CDRA Heater Controller
[iv]Optimistic assumption; no data were available
[v]Analogy to OGA Nitrogen Purge ORU
[vi]Analogy CCAA Condensing Heat Exchanger
[vii]Analogy to WPA Multifiltration Bed
[viii]Analogy to OGA Hydrogen ORU (contains Electrolysis Cell Stack and Rotary Separator / Accumulator)
[ix]Analogy to OGA Oxygen Outlet
[x]Analogy to OGA Pump
[xi]Analogy to CRS Sabatier Methanation Reactor
[xii]Analogy to CRS Phase Separator
[xiii]Analogy to CRS Condensing Heat Exchanger
[xiv]Analogy to CDRA Dessicant-Adsorbent Bed
[xv]Analogy to CRS Compressor
[xvi]Mass is obtained from [300] and verified with calculations based on data from Link et al. [301]. All other data is assumed to be the same as the Recycle Filter Tank Assembly (RFTA) described in the NASA BVAD 2004 [209] – the original system from which the ARFTA was upgraded from. Here, the life limit of the ARFTA has been assumed to be zero, based on its development objective of facilitating the same function as the RFTA without the need for periodic replacement [301].
[xvii]Based on the Heliospectra LX601 grow light [213]. MTBF value is based on the assumption that a 2 year warranty accounts for 1% failures during that time
[xviii]Based on assumptions listed in Section 6.3.3
[xix]Based on sizing estimates from Stilwell et al. [367]

Table J.41: Architecture Case 6 Spare Parts Requirements for each Component over a 10 Mission Minimum Continuous Presence Campaign. Empty rows correspond to components assumed to have 100% reliability, and hence do not require spare parts

Group	Assembly	Subassembly	Mission									
			1	**2**	**3**	**4**	**5**	**6**	**7**	**8**	**9**	**10**
ECLSS	CDRA	Air Pump Two-Stage ORU	3	1	1	0	1	0	1	0	0	1
		Blower	3	2	0	1	0	1	1	0	0	1
		Check Valves	5	2	2	1	1	1	2	1	1	1
		Desiccant Beds	5	1	2	1	1	1	1	1	1	1
		Heat Controller	4	1	1	0	1	1	0	1	0	0
		Precooler	3	2	1	0	0	1	1	0	0	1
		Pump Fan Motor Controller	2	0	1	0	0	1	0	0	0	0
		Selector Valves	7	3	3	2	1	3	2	2	1	2
		Sorbent Beds (Zeolite)	5	1	2	1	1	1	1	1	1	1
	CCAA Mission 1	Condensing Heat Exchanger	3	0	1	1	0	1	0	0	1	0
		Electronic Interface Box (EIB)	3	1	1	0	0	1	0	0	1	0
		Fan Delta Pressure Sensor	4	0	1	0	1	1	0	0	1	0
		Heat Exchanger Liquid Sensor	4	1	2	0	1	1	0	1	0	1
		Inlet ORU	4	1	1	1	1	1	1	0	1	0
		Pressure Transducer	4	0	1	0	1	0	1	0	0	1
		Temperature Control Check Valve (TCCV)	18	10	9	8	7	10	7	7	7	7
		Temperature Sensor	2	1	0	0	0	1	0	0	0	0
		Water Separator	8	4	3	3	2	3	7	0	0	10
		Water Separator Liquid Sensor	4	1	2	0	1	1	0	1	0	1
	CCAA Mission 2	Condensing Heat Exchanger	0	2	1	0	1	0	0	1	0	0
		Electronic Interface Box (EIB)	0	3	0	1	0	1	0	0	0	1
		Fan Delta Pressure Sensor	0	3	1	0	1	0	0	1	0	0
		Heat Exchanger Liquid Sensor	0	4	1	0	1	1	0	0	1	0
		Inlet ORU	0	3	1	1	1	0	1	0	1	0
		Pressure Transducer	0	3	1	0	1	0	0	0	1	0
		Temperature Control Check Valve	0	13	7	6	5	6	5	5	4	5
		Temperature Sensor	0	2	0	0	1	0	0	0	1	0
		Water Separator	0	7	2	2	2	2	2	2	1	1
		Water Separator Liquid Sensor	0	4	1	0	1	0	1	0	1	0
	WPA	Catalytic Reactor	2	2	1	0	1	0	1	0	1	0
		Gas Separator	2	1	0	0	1	0	0	1	0	0

		Ion Exchange Bed	2	3	3	3	4	3	3	4	3	3
		Microbial Check Valve	2	1	0	0	1	0	0	0	1	0
		Multifiltration Bed #1	1	1	1	2	1	2	1	2	1	2
		Multifiltration Bed #2	1	1	1	2	1	2	1	2	1	2
		Particulate Filter	1	2	3	2	3	2	2	3	2	3
		pH Adjuster	2	1	0	1	0	0	1	0	0	0
		Process Controller	2	0	1	0	1	0	0	0	1	0
		Pump Separator	2	1	1	0	1	0	1	0	0	1
		Reactor Health Sensor	2	1	1	0	0	1	1	0	0	0
		Sensor	2	1	0	0	1	0	0	0	1	0
		Separator Filter	2	0	0	0	1	0	1	0	1	1
		Start-up Filter	2	0	1	0	0	0	1	0	0	0
		Water Delivery	2	1	0	1	0	0	1	0	0	0
	UPA	Distillation Assembly	2	1	0	1	0	0	1	0	0	1
		Firmware Controller Assembly	4	2	1	1	1	1	1	1	1	1
		Fluids Control and Pump Assembly	2	1	1	1	0	1	0	0	1	0
		Pressure Control and Pump Assembly	2	1	0	0	1	0	0	1	0	1
		Advanced Recycle Filter Tank Assembly	2	1	0	0	1	0	0	1	0	0
		Separator Plumbing Assembly	2	0	1	1	1	2	1	1	2	1
ISRU	Water Extractor	Oven + Insulating Cone	2	1	0	1	0	1	0	0	0	1
		Hopper										
		Sieve	2	1	0	0	0	1	0	0	0	0
		Augers (vertical)	2	0	0	1	0	0	0	1	0	0
		Horizontal Auger	2	1	0	0	1	0	0	1	0	0
		Sweep Gas System	5	1	0	1	0	2	1	0	0	1
		Sweep Gas Piping										
		Condensing Heat Exchanger	2	0	0	1	0	0	0	0	1	0
		Water Filtration System	6	6	6	6	6	6	6	6	6	6
	CO2 Cryocooler	Cryocooler	2	1	1	0	0	1	0	0	1	0
		Container										
	Water Electrolyzer	Electrolysis Cell Stack	5	2	2	2	1	2	1	1	1	2
		O2 Separator / Water Reservoir	6	3	2	1	1	3	1	1	1	2
		H2 Separator and Dryer	4	1	1	0	1	1	0	1	0	1
		Water Pump	4	1	1	2	2	3	2	2	2	2
	Sabatier Reactor	Reactor	4	2	1	1	1	1	1	1	1	0
		Water / Methane Separator	5	0	2	0	1	0	2	0	0	0
		Heat Exchanger	3	0	1	0	0	0	0	1	0	0
	Atmospheric Processor	Zeolite	5	1	1	1	1	1	1	0	1	1
		Compressor	5	2	2	1	1	2	1	2	0	1
		Cryocoolers	3	1	1	0	0	1	0	0	1	0
		Support Structure										
BPC	Crop Lighting 1	Lighting System Unit	3	1	3	0	0	7	0	7	0	0
	Crop Lighting 2	Lighting System Unit	0	3	1	2	0	0	6	0	6	0

Table J.42: Architecture Case 6 Spare Parts Requirements for each Component over a 10 Mission Minimum Continuous Presence Campaign with all ISRU technologies at 10% of their originally estimated values. Empty rows correspond to components assumed to have 100% reliability, and hence do not require spare parts

Group	**Assembly**	**Subassembly**	**Mission**									
			1	**2**	**3**	**4**	**5**	**6**	**7**	**8**	**9**	**10**
ECLSS	CDRA	Air Pump Two-Stage ORU	3	1	1	0	1	0	1	0	1	0
		Blower	4	1	0	1	1	0	1	0	1	0
		Check Valves	5	2	2	1	1	2	1	1	1	1
		Desiccant Beds	5	1	2	1	1	1	1	1	2	0
		Heat Controller	4	1	1	1	0	1	0	1	0	1
		Precooler	4	1	0	1	1	0	1	0	1	0
		Pump Fan Motor Controller	2	1	0	0	0	1	0	0	0	0
		Selector Valves	7	3	3	2	2	2	2	2	1	2
		Sorbent Beds (Zeolite)	5	1	2	1	1	1	1	1	2	0
	CCAA Mission 1	Condensing Heat Exchanger	3	1	0	1	0	1	0	0	1	0
		Electronic Interface Box (EIB)	3	1	0	1	0	1	0	0	1	0
		Fan Delta Pressure Sensor	4	1	0	1	0	1	0	0	1	0
		Heat Exchanger Liquid Sensor	5	0	1	1	1	1	0	1	0	1

		Inlet ORU	4	1	1	1	1	1	1	0	1	1
		Pressure Transducer	4	0	1	1	0	0	1	0	1	0
		Temperature Control Check Valve (TCCV)	18	10	9	8	8	8	8	7	8	7
		Temperature Sensor	2	1	0	0	0	1	0	0	0	0
		Water Separator	8	4	3	3	3	2	7	0	0	10
		Water Separator Liquid Sensor	4	1	1	1	1	1	0	1	0	1
	CCAA Mission 2	Condensing Heat Exchanger	0	2	1	1	0	0	1	0	0	0
		Electronic Interface Box (EIB)	0	3	0	1	0	1	0	0	0	1
		Fan Delta Pressure Sensor	0	3	1	0	1	0	1	0	0	0
		Heat Exchanger Liquid Sensor	0	4	1	1	0	1	0	0	1	0
		Inlet ORU	0	3	1	1	1	0	1	1	0	1
		Pressure Transducer	0	3	1	0	1	0	1	0	0	0
		Temperature Control Check Valve	0	13	7	6	6	5	5	5	5	5
		Temperature Sensor	0	2	0	1	0	0	0	0	1	0
		Water Separator	0	7	2	3	1	2	2	1	2	2
		Water Separator Liquid Sensor	0	4	1	0	1	1	0	0	1	0
	WPA	Catalytic Reactor	3	1	1	0	1	1	0	1	0	1
		Gas Separator	2	1	0	1	0	0	0	1	0	0
		Ion Exchange Bed	2	3	3	3	4	3	3	4	3	3
		Microbial Check Valve	2	1	0	0	1	0	0	0	1	0
		Multifiltration Bed #1	1	1	1	2	1	2	1	2	1	2
		Multifiltration Bed #2	1	1	1	2	1	2	1	2	1	2
		Particulate Filter	1	2	3	2	3	2	2	3	2	3
		pH Adjuster	2	1	0	1	0	0	1	0	0	0
		Process Controller	2	1	0	0	1	0	0	1	0	0
		Pump Separator	2	1	1	1	0	1	0	0	1	0
		Reactor Health Sensor	2	1	1	0	1	0	1	0	0	0
		Sensor	2	1	0	1	0	0	0	1	0	0
		Separator Filter	2	0	0	1	0	0	1	0	1	1
		Start-up Filter	2	0	1	0	0	0	1	0	0	0
		Water Delivery	2	1	0	1	0	1	0	0	0	1
	UPA	Distillation Assembly	2	1	0	1	0	0	1	0	0	1
		Firmware Controller Assembly	4	2	1	1	1	1	1	1	1	1
		Fluids Control and Pump Assembly	2	1	1	1	0	1	0	0	1	0
		Pressure Control and Pump Assembly	2	1	0	1	0	0	1	0	0	1
		Advanced Recycle Filter Tank Assembly	2	1	0	0	1	0	0	1	0	0
		Separator Plumbing Assembly	2	0	1	1	1	2	1	1	2	1
ISRU	Water Extractor	Oven + Insulating Cone	5	3	2	1	2	2	1	1	2	1
		Hopper										
		Sieve	4	2	1	1	1	1	1	1	1	1
		Augers (vertical)	4	1	1	1	1	1	1	1	0	1
		Horizontal Auger	5	1	2	1	1	1	1	1	1	0
		Sweep Gas System	10	5	3	3	2	4	2	4	2	2
		Sweep Gas Piping										
		Condensing Heat Exchanger	3	2	1	1	0	1	0	1	1	0
		Water Filtration System	7	5	6	6	6	6	6	6	6	6
	CO2 Cryocooler	Cryocooler	6	2	2	2	1	2	1	2	1	1
		Container										
	Water Electrolyzer	Electrolysis Cell Stack	18	11	10	10	9	9	8	9	9	8
		O2 Separator / Water Reservoir	20	11	11	10	9	9	9	9	9	9
		H2 Separator and Dryer	9	5	3	4	3	3	3	3	3	3
		Water Pump	9	3	3	3	2	3	2	2	3	2
	Sabatier Reactor	Reactor	13	7	7	5	6	5	6	5	5	5
		Water / Methane Separator	10	4	5	2	2	3	4	1	4	2
		Heat Exchanger	5	1	1	1	1	1	1	0	1	1
	Atmospheric Processor	Zeolite	12	6	4	5	5	4	4	3	4	4
		Compressor	17	9	9	9	8	7	8	7	7	8
		Cryocoolers	7	2	2	2	2	1	2	2	1	2
		Support Structure										
BPC	Crop Lighting 1	Lighting System Unit	3	1	3	0	0	7	0	7	0	0
	Crop Lighting 2	Lighting System Unit	0	3	0	3	0	0	6	0	6	0

J.3.7 Architecture Case 7

Table J.43: Architecture Case 7 Master Equipment List, containing component mass, volume and reliability data, as well as run times and power demands. Power is listed here on a per unit basis. ISRU technologies displayed here were sized by the HabNet ISRU Module.

Sys.	Assembly	Subassembly	Mass [kg]	Vol. [m^3]	MTBF [h]	Run Time Miss. 1 [h]	Run Time Miss. 2 [h]	LL [y]	# in Pmry.	Power [kW]
ECLS	CDRA	Air Pump Two-Stage ORU	10.89	0.0045	156200.0	19000	19000	15.29	1	0.860
		Blower	5.58	0.0300	129700.0	19000	19000	10.00	1	
		Check Valves	39.92	0.1784	32900.0[i]	19000	19000		1	
		Desiccant Beds	42.64	0.0850	77100.0	19000	19000		2	
		Heat Controller	3.31	0.0085	242700.0	19000	19000		2	
		Precooler	5.58	0.0255	129700.0	19000	19000	10.00	1	
		Pump Fan Motor Controller	2.72	0.0057	2270000.0	19000	19000		2	
		Selector Valves	3.04	0.0017	117000.0	19000	19000	10.61	6	
		Sorbent Beds (Zeolite)	42.64	0.0850	77100.0	19000	19000		2	
	CCAA Mission 1 (x5)	Condensing Heat Exchanger	49.71	0.3933	832600.0	19000	19000		5	0.705
		Electronic Interface Box (EIB)	4.04	0.0173	2350000.0	19000	19000		10	
		Fan Delta Pressure Sensor	0.45	0.0002	1250000.0	19000	19000		5	
		Heat Exchanger Liquid Sensor	0.64	0.0006	1140000.0	19000	19000		10	
		Inlet ORU	25.31	0.1308	333000.0	19000	19000		5	
		Pressure Transducer	0.48	0.0000	1250000.0	19000	19000	15.00	5	
		Temperature Control Check Valve	7.45	0.0071	32900.0	19000	19000		10	
		Temperature Sensor	0.26	0.0014	37600000.0	19000	19000		20	
		Water Separator	11.93	0.0583	131000.0	19000	19000	5.00	10	
		Water Separator Liquid Sensor	0.64	0.0006	1140000.0[ii]	19000	19000		10	
	CCAA Mission 2 (x3)	Condensing Heat Exchanger	49.71	0.3933	832600.0	0	19000		3	0.532
		Electronic Interface Box (EIB)	4.04	0.0173	2350000.0	0	19000		6	
		Fan Delta Pressure Sensor	0.45	0.0002	1250000.0	0	19000		3	
		Heat Exchanger Liquid Sensor	0.64	0.0006	1140000.0	0	19000		6	
		Inlet ORU	25.31	0.1308	333000.0	0	19000		3	
		Pressure Transducer	0.48	0.0000	1250000.0	0	19000	15.00	3	
		Temperature Control Check Valve	7.45	0.0071	32900.0	0	19000		6	
		Temperature Sensor	0.26	0.0014	37600000.0	0	19000		12	
		Water Separator	11.93	0.0583	131000.0	0	19000	5.00	6	
		Water Separator Liquid Sensor	0.64	0.0006	1140000.0[ii]	0	19000		6	
	WPA	Catalytic Reactor	67.04	0.1156	25579.2	6481	7665	2.25	1	0.320
		Gas Separator	39.15	0.0660	84008.4	6481	7665	1	1	
		Ion Exchange Bed	13.02	0.0173	296701.2	6481	7665	0.16	1	
		Microbial Check Valve	5.76	0.0065	143488.8	6481	7665	1	1	
		Multifiltration Bed #1	149.23	0.0657	296701.2	6481	7665	0.36	1	
		Multifiltration Bed #2	149.23	0.0657	296701.2	6481	7665	0.36	1	
		Particulate Filter	32.25	0.0717	717356.4	6481	7665	0.22	1	
		pH Adjuster	2.54	0.0026	137181.6	6481	7665	1	1	
		Process Controller	45.00	0.0838	87950.4	6481	7665	7.72	1	
		Pump Separator	31.34	0.0869	42398.4	6481	7665	2	1	
		Reactor Health Sensor	16.83	0.0425	56677.2	6481	7665	1	1	
		Sensor	4.81	0.0034	143664	6481	7665	10	1	
		Separator Filter	7.67	0.0102	359072.4	6481	7665	0.84	1	
		Start-up Filter	9.44	0.0184	226884	6481	7665	19.92	1	
		Water Delivery	47.54	0.0974	64561.2	6481	7665	5	1	
	UPA	Distillation Assembly	92.76	0.1422	142525.2	6697	11229	2	1	0.315
		Firmware Controller Assembly	23.09	0.0286	27331.2	6697	11229	2.4	1	
		Fluids Control and Pump Assembly	47.58	0.0731	90140.4	6697	11229	4	1	
		Pressure Control and Pump Assembly	49.08	0.1158	181507.2	6697	11229	2	1	
		Advanced Recycle Filter Tank Assembly[xvi]	50.00	0.1011	199640.4	6697	11229		1	
		Separator Plumbing Assembly	16.78	0.0229	384651.6	6697	11229	1	1	

ISRU	Water Extractor	Oven + Insulating Cone	103.96	4.5033	242700[iii]	19000	19000		1	29.17
		Hopper	70.69	5.2509		19000	19000		1	
		Sieve	56.14	0.0000	500000[iv]	19000	19000		1	
		Augers (vertical)	266.50	0.0000	500000[iv]	19000	19000		1	0.063
		Horizontal Auger	13.14	0.1688	500000[iv]	19000	19000		1	
		Sweep Gas System	0.02	0.0000	138408[v]	19000	19000		1	
		Sweep Gas Piping	7.64	0.1727		19000	19000		1	
		Condensing Heat Exchanger	50.19	1.2990	832600[vi]	19000	19000		1	
		Water Filtration System	2.91	0.0109	296701.2[vii]	19000	19000	0.36	1	
	CO2 Cryocooler	Cryocooler	46.52	0.0976	500000[iv]	19000	19000		2	1.982
		Container	111.59	0.6595		19000	19000		1	
	Water Electrolyzer	Electrolysis Cell Stack	47.43	0.0045	27156[viii]	19000	19000	2.38	1	12.28
		O2 Separator / Water Reservoir	5.71	0.0119	27156[viii]	19000	19000	2.38	1	
		H2 Separator and Dryer	14.44	0.0040	98112[ix]	19000	19000	10	1	
		Water Pump	2.16	0.0007	144540[x]	19000	19000	1	1	8×10^{-5}
	Sabatier Reactor	Reactor	20.78	0.4181	50000[xi]	19000	19000		1	0.198
		Water / Methane Separator	0.24	0.0097	131000[xii]	19000	19000		1	
		Heat Exchanger	0.53	0.0000	832600[xiii]	19000	19000		1	
	Atmospheric Processor	Zeolite	1.86	0.0224	77100[xiv]	19000	19000		1	
		Compressor	28.13	0.1627	66666.7	19000	19000		2	2.564
		Cryocoolers	3.10	0.0015	500000[iv]	19000	19000		2	0.480
		Support Structure	12.07			19000	19000		1	
BPC	Crop Lighting 1	Lighting System Unit[xvii]	8.00	0.0185	1743216	19000	19000	5.71	69	43.47
	Crop Lighting 2	Lighting System Unit[xvii]	8.00	0.0185	1743216	0	19000	5.71	68	42.84
	ORA[xx]	Air Pump Two-Stage ORU	10.89	0.0045	156200.0	19000	19000	15.29	1	0.860
		Blower	5.58	0.0300	129700.0	19000	19000	10.00	1	
		Check Valves	39.92	0.1784	32900.0[i]	19000	19000		1	
		Desiccant Beds	42.64	0.0850	77100.0	19000	19000		2	
		Heat Controller	3.31	0.0085	242700.0	19000	19000		2	
		Precooler	5.58	0.0255	129700.0	19000	19000	10.00	1	
		Pump Fan Motor Controller	2.72	0.0057	2270000.0	19000	19000		2	
		Selector Valves	3.04	0.0017	117000.0	19000	19000	10.61	6	
		Sorbent Beds (Zeolite)	42.64	0.0850	77100.0	19000	19000		2	
	BPC Structure 1[xviii]	Primary Structure (Inflatable)	3350	250		19000	19000		1	
		Secondary Structure (Shelving)	572.85			19000	19000		1	
		Mechanization Systems	412.05			19000	19000		1	
	BPC Structure 2[xviii]	Primary Structure (Inflatable)	3350	250		0	19000		1	
		Secondary Structure (Shelving)	572.85			0	19000		1	
		Mechanization Systems	412.05			0	19000		1	
	Food Processor[xix]	Hand Mixer	2.00	0.0050		19000	19000		1	
		Food Processor / Blender	8.00	0.0230		19000	19000		1	
		Grinder / Mill	4.10	0.0120		19000	19000		1	
		Bread Machine	7.40	0.0310		19000	19000		1	
		Griddle / Grill	5.80	0.0270		19000	19000		1	
		Juice Extractor	7.70	0.0390		19000	19000		1	
Food	First Mission	Prepackaged Food Supply	1706			19000	0		1	
	Second Mission	Prepackaged Food Supply	2910			0	19000		1	
	Subsequent Missions	Prepackaged Food Supply	2460			0	0		1	

[i] Analogy to CCAA TCCV
[ii] Analogy to CCAA Heat Exchanger Liquid Sensor
[iii] Analogy to CDRA Heater Controller
[iv] Optimistic assumption; no data were available
[v] Analogy to OGA Nitrogen Purge ORU
[vi] Analogy CCAA Condensing Heat Exchanger
[vii] Analogy to WPA Multifiltration Bed
[viii] Analogy to OGA Hydrogen ORU (contains Electrolysis Cell Stack and Rotary Separator / Accumulator)
[ix] Analogy to OGA Oxygen Outlet
[x] Analogy to OGA Pump
[xi] Analogy to CRS Sabatier Methanation Reactor
[xii] Analogy to CRS Phase Separator
[xiii] Analogy to CRS Condensing Heat Exchanger
[xiv] Analogy to CDRA Dessicant-Adsorbent Bed
[xv] Analogy to CRS Compressor
[xvi] Mass is obtained from [300] and verified with calculations based on data from Link et al. [301]. All other data is assumed to be the same as the Recycle Filter Tank Assembly (RFTA) described in the NASA BVAD 2004 [209] – the original system from which the ARFTA was upgraded from. Here, the life limit of the ARFTA has been assumed to be zero, based on its development objective of facilitating the same function as the RFTA without the need for periodic replacement [301].
[xvii] Based on the Heliospectra LX601 grow light [213]. MTBF value is based on the assumption that a 2 year warranty accounts for 1% failures during that time
[xviii] Based on assumptions listed in Section 6.3.3
[xix] Based on sizing estimates from Stilwell et al. [367]
[xx] Analogy to CDRA

Table J.44: Architecture Case 7 Spare Parts Requirements for each Component over a 10 Mission Minimum Continuous Presence Campaign. Empty rows correspond to components assumed to have 100% reliability, and hence do not require spare parts

Group	Assembly	Subassembly	Mission									
			1	**2**	**3**	**4**	**5**	**6**	**7**	**8**	**9**	**10**
ECLSS	CDRA	Air Pump Two-Stage ORU	3	1	1	0	1	0	1	0	1	0
		Blower	4	1	1	0	1	0	1	0	1	0
		Check Valves	5	2	2	1	1	2	1	1	1	1
		Desiccant Beds	5	1	2	1	1	1	1	2	0	1
		Heat Controller	4	1	1	0	1	1	0	1	0	0
		Precooler	4	1	1	0	1	0	1	0	1	0
		Pump Fan Motor Controller	2	1	0	0	0	1	0	0	0	0
		Selector Valves	7	4	2	2	2	2	2	2	2	1
		Sorbent Beds (Zeolite)	5	1	2	1	1	1	2	1	0	1
	CCAA Mission 1	Condensing Heat Exchanger	3	1	0	1	0	1	0	0	1	0
		Electronic Interface Box (EIB)	3	1	1	0	0	1	0	1	0	0
		Fan Delta Pressure Sensor	3	1	1	1	0	1	0	0	0	1
		Heat Exchanger Liquid Sensor	4	2	1	0	1	1	0	1	0	1
		Inlet ORU	4	1	1	1	1	1	1	0	1	0
		Pressure Transducer	3	1	1	1	0	0	0	1	0	1
		Temperature Control Check Valve (TCCV)	18	10	9	8	9	7	7	9	7	7
		Temperature Sensor	2	1	0	0	0	1	0	0	0	0
		Water Separator	8	4	3	3	3	2	7	0	0	10
		Water Separator Liquid Sensor	4	2	0	1	1	1	0	1	0	1
	CCAA Mission 2	Condensing Heat Exchanger	0	2	1	0	1	0	1	0	0	0
		Electronic Interface Box (EIB)	0	3	0	1	0	1	0	0	0	1
		Fan Delta Pressure Sensor	0	3	1	0	1	0	1	0	0	0
		Heat Exchanger Liquid Sensor	0	4	1	0	1	1	0	1	0	0
		Inlet ORU	0	3	1	1	1	1	0	1	0	0
		Pressure Transducer	0	3	1	0	1	0	0	1	0	0
		Temperature Control Check Valve	0	14	6	6	6	5	5	6	4	5
		Temperature Sensor	0	2	0	1	0	0	0	0	0	0
		Water Separator	0	7	2	2	3	1	2	2	1	2
		Water Separator Liquid Sensor	0	4	1	0	1	1	0	1	0	0
	WPA	Catalytic Reactor	3	2	1	1	1	0	1	1	0	1
		Gas Separator	2	1	1	0	1	0	1	0	1	1
		Ion Exchange Bed	4	6	5	6	5	5	6	5	6	5
		Microbial Check Valve	2	1	1	0	0	1	0	1	1	1
		Multifiltration Bed #1	2	2	2	3	2	3	2	3	2	2
		Multifiltration Bed #2	2	2	2	3	2	3	2	3	2	2
		Particulate Filter	3	4	4	4	4	4	4	4	4	4
		pH Adjuster	3	0	1	0	1	0	0	1	1	1
		Process Controller	2	1	1	0	1	0	0	1	0	0
		Pump Separator	3	1	1	1	0	1	1	0	1	0
		Reactor Health Sensor	3	1	1	0	1	0	1	0	1	0
		Sensor	3	0	1	0	1	0	0	1	0	0
		Separator Filter	2	1	0	1	1	1	1	1	1	1
		Start-up Filter	2	1	0	0	1	0	0	1	0	0
		Water Delivery	3	1	0	1	0	1	0	0	1	0
	UPA	Distillation Assembly	2	1	0	1	0	0	1	0	0	1
		Firmware Controller Assembly	4	2	1	1	1	1	1	1	1	1
		Fluids Control and Pump Assembly	2	1	1	1	0	1	0	1	0	0
		Pressure Control and Pump Assembly	2	1	0	0	1	0	1	0	0	1
		Advanced Recycle Filter Tank Assembly	2	1	0	0	1	0	0	1	0	0
		Separator Plumbing Assembly	2	0	1	1	1	2	1	1	2	1
ISRU	Water Extractor	Oven + Insulating Cone	2	1	0	1	0	1	0	0	0	1
		Hopper										
		Sieve	2	0	1	0	0	1	0	0	0	0
		Augers (vertical)	2	0	0	1	0	0	0	0	1	0
		Horizontal Auger	2	1	0	0	1	0	0	1	0	0
		Sweep Gas System	4	2	1	0	1	1	0	0	1	0
		Sweep Gas Piping										
		Condensing Heat Exchanger	2	0	0	1	0	0	0	0	1	0
		Water Filtration System	6	6	6	6	6	6	6	6	6	6

	CO2 Cryocooler	Cryocooler	2	1	1	0	0	1	0	0	1	0
		Container										
	Water Electrolyzer	Electrolysis Cell Stack	5	3	2	1	1	2	1	2	1	1
		O2 Separator / Water Reservoir	6	3	2	1	2	2	1	2	1	1
		H2 Separator and Dryer	4	1	1	0	1	1	0	1	0	1
		Water Pump	4	1	1	2	2	3	2	2	2	2
	Sabatier Reactor	Reactor	4	2	1	1	1	1	1	1	1	1
		Water / Methane Separator	4	1	1	1	1	1	0	1	0	0
		Heat Exchanger	2	1	1	0	0	0	0	1	0	0
	Atmospheric Processor	Zeolite	4	2	1	0	2	1	0	1	1	0
		Compressor	5	2	2	1	2	1	1	1	1	1
		Cryocoolers	3	1	1	0	0	1	0	1	0	0
		Support Structure										
BPC	Crop Lighting 1	Lighting System Unit	6	3	60	0	0	69	0	69	0	0
	Crop Lighting 2	Lighting System Unit	0	7	2	59	0	0	68	0	68	0
	ORA	Air Pump Two-Stage ORU	3	1	1	0	1	0	1	0	1	0
		Blower	4	1	1	0	1	0	1	0	1	0
		Check Valves	5	2	2	1	1	2	1	1	1	1
		Desiccant Beds	5	1	2	1	1	1	1	2	0	1
		Heat Controller	4	1	1	0	1	1	0	1	0	1
		Precooler	4	1	0	1	1	0	1	0	1	0
		Pump Fan Motor Controller	2	1	0	0	0	1	0	0	0	0
		Selector Valves	7	4	2	2	2	2	2	2	1	2
		Sorbent Beds (Zeolite)	5	1	2	1	1	1	1	2	0	1

Table J.45: Architecture Case 7 Spare Parts Requirements for each Component over a 10 Mission Minimum Continuous Presence Campaign with all ISRU technologies at 10% of their originally estimated values. Empty rows correspond to components assumed to have 100% reliability, and hence do not require spare parts

Group	**Assembly**	**Subassembly**	**Mission**									
			1	**2**	**3**	**4**	**5**	**6**	**7**	**8**	**9**	**10**
ECLSS	CDRA	Air Pump Two-Stage ORU	3	1	1	1	0	1	0	0	1	0
		Blower	4	1	0	1	1	0	1	0	1	0
		Check Valves	5	2	2	1	1	2	1	1	1	1
		Desiccant Beds	5	2	1	1	2	1	1	1	1	1
		Heat Controller	4	1	1	1	0	1	0	1	0	1
		Precooler	4	1	1	0	1	0	1	0	1	0
		Pump Fan Motor Controller	2	1	0	0	0	1	0	0	0	0
		Selector Valves	8	3	2	3	2	1	2	2	2	2
		Sorbent Beds (Zeolite)	5	2	1	1	2	1	1	1	1	1
	CCAA Mission 1	Condensing Heat Exchanger	3	1	0	1	0	1	0	0	1	0
		Electronic Interface Box (EIB)	3	1	1	0	1	0	0	1	0	0
		Fan Delta Pressure Sensor	4	1	0	1	0	1	0	0	1	0
		Heat Exchanger Liquid Sensor	4	2	1	0	1	1	0	1	1	0
		Inlet ORU	4	1	1	2	0	1	1	0	1	1
		Pressure Transducer	3	2	0	1	0	1	0	0	1	0
		Temperature Control Check Valve (TCCV)	18	10	9	9	8	8	7	8	8	7
		Temperature Sensor	2	1	0	0	1	0	0	0	0	0
		Water Separator	8	4	3	3	3	2	7	0	0	10
		Water Separator Liquid Sensor	4	2	1	0	1	1	0	1	1	0
	CCAA Mission 2	Condensing Heat Exchanger	0	2	1	1	0	0	1	0	0	1
		Electronic Interface Box (EIB)	0	3	0	1	0	1	0	0	0	1
		Fan Delta Pressure Sensor	0	3	1	0	1	0	1	0	0	0
		Heat Exchanger Liquid Sensor	0	4	1	1	0	1	0	0	1	1
		Inlet ORU	0	3	1	1	1	1	0	1	0	1
		Pressure Transducer	0	3	1	0	1	0	1	0	0	0
		Temperature Control Check Valve	0	14	6	7	5	5	6	4	5	5
		Temperature Sensor	0	2	0	1	0	0	0	0	0	1
		Water Separator	0	7	2	3	2	1	2	2	1	2
		Water Separator Liquid Sensor	0	4	1	1	0	1	0	0	1	0
	WPA	Catalytic Reactor	4	1	1	1	1	1	0	1	1	0
		Gas Separator	3	0	1	0	1	0	1	0	1	1
		Ion Exchange Bed	4	6	5	6	5	5	6	5	6	5

		Microbial Check Valve	3	0	1	0	1	0	0	1	1	1
		Multifiltration Bed #1	2	2	2	3	2	3	2	3	2	2
		Multifiltration Bed #2	2	2	2	3	2	3	2	3	2	2
		Particulate Filter	3	4	4	4	4	4	4	4	4	4
		pH Adjuster	3	1	0	1	0	0	1	0	1	1
		Process Controller	2	1	1	0	1	0	0	1	0	0
		Pump Separator	3	1	1	1	1	0	1	0	1	0
		Reactor Health Sensor	3	1	1	1	0	1	0	0	1	0
		Sensor	3	0	1	0	1	0	0	0	1	0
		Separator Filter	2	0	1	1	1	1	1	1	1	1
		Start-up Filter	2	1	0	1	0	0	0	0	1	0
		Water Delivery	3	1	0	1	0	1	0	1	0	0
	UPA	Distillation Assembly	2	1	0	1	0	0	1	0	0	1
		Firmware Controller Assembly	4	2	1	1	1	1	1	1	1	1
		Fluids Control and Pump Assembly	2	1	1	1	0	1	0	1	0	0
		Pressure Control and Pump Assembly	2	1	0	1	0	0	1	0	0	1
		Advanced Recycle Filter Tank Assembly	2	1	0	1	0	0	0	1	0	0
		Separator Plumbing Assembly	2	0	1	1	1	2	1	1	2	1
ISRU	Water Extractor	Oven + Insulating Cone	5	3	2	1	2	1	2	1	2	1
		Hopper										
		Sieve	4	2	1	1	1	1	1	1	1	0
		Augers (vertical)	4	1	1	1	1	1	1	1	0	1
		Horizontal Auger	5	1	2	1	1	1	1	0	2	0
		Sweep Gas System	10	6	2	4	2	3	3	1	3	4
		Sweep Gas Piping										
		Condensing Heat Exchanger	3	2	1	0	1	1	0	1	1	0
		Water Filtration System	6	6	6	6	6	6	6	6	6	6
	CO2 Cryocooler	Cryocooler	6	2	2	2	1	2	1	1	2	1
		Container										
	Water Electrolyzer	Electrolysis Cell Stack	18	11	10	10	9	9	8	9	9	9
		O2 Separator / Water Reservoir	20	12	10	11	9	9	9	8	10	8
		H2 Separator and Dryer	9	5	4	3	3	3	3	3	3	3
		Water Pump	9	4	3	2	3	2	3	2	2	2
	Sabatier Reactor	Reactor	13	7	7	6	5	6	5	5	5	6
		Water / Methane Separator	11	5	2	3	3	3	2	3	3	2
		Heat Exchanger	5	1	1	2	0	1	1	0	1	1
	Atmospheric	Zeolite	12	6	5	4	4	4	4	3	4	4
	Processor	Compressor	17	9	9	8	8	7	7	8	8	7
		Cryocoolers	7	3	2	2	1	2	1	2	1	2
		Support Structure										
BPC	Crop Lighting 1	Lighting System Unit	6	3	60	0	0	69	0	69	0	0
	Crop Lighting 2	Lighting System Unit	0	7	2	59	0	0	68	0	68	0
	ORA	Air Pump Two-Stage ORU	3	1	1	1	0	0	1	0	1	0
		Blower	4	1	1	0	1	0	1	0	1	0
		Check Valves	5	2	2	1	1	2	1	1	1	1
		Desiccant Beds	5	2	1	1	2	1	1	1	1	1
		Heat Controller	4	1	1	1	0	1	0	1	0	1
		Precooler	4	1	1	0	1	0	1	0	1	0
		Pump Fan Motor Controller	2	1	0	0	1	0	0	0	0	0
		Selector Valves	7	4	2	2	3	1	2	2	2	1
		Sorbent Beds (Zeolite)	5	1	2	1	1	2	1	1	1	1

J.3.8 Architecture Case 8

Table J.46: Architecture Case 8 Master Equipment List, containing component mass, volume and reliability data, as well as run times and power demands. Power is listed here on a per unit basis. ISRU technologies displayed here were sized by the HabNet ISRU Module.

Sys.	Assembly	Subassembly	Mass [kg]	Vol. [m^3]	MTBF [h]	Run Time Miss. 1 [h]	Run Time Miss. 2 [h]	LL [y]	# in Pmry	Power [kW]
ECLS	CDRA	Air Pump Two-Stage ORU	10.89	0.0045	156200.0	19000	19000	15.29	1	0.860
		Blower	5.58	0.0300	129700.0	19000	19000	10.00	1	
		Check Valves	39.92	0.1784	32900.0[i]	19000	19000		1	
		Desiccant Beds	42.64	0.0850	77100.0	19000	19000		2	
		Heat Controller	3.31	0.0085	242700.0	19000	19000		2	
		Precooler	5.58	0.0255	129700.0	19000	19000	10.00	1	
		Pump Fan Motor Controller	2.72	0.0057	2270000.0	19000	19000		2	
		Selector Valves	3.04	0.0017	117000.0	19000	19000	10.61	6	
		Sorbent Beds (Zeolite)	42.64	0.0850	77100.0	19000	19000		2	
	CCAA Mission 1 (x5)	Condensing Heat Exchanger	49.71	0.3933	832600.0	19000	19000		5	0.705
		Electronic Interface Box (EIB)	4.04	0.0173	2350000.0	19000	19000		10	
		Fan Delta Pressure Sensor	0.45	0.0002	1250000.0	19000	19000		5	
		Heat Exchanger Liquid Sensor	0.64	0.0006	1140000.0	19000	19000		10	
		Inlet ORU	25.31	0.1308	333000.0	19000	19000		5	
		Pressure Transducer	0.48	0.0000	1250000.0	19000	19000	15.00	5	
		Temperature Control Check Valve	7.45	0.0071	32900.0	19000	19000		10	
		Temperature Sensor	0.26	0.0014	37600000.0	19000	19000		20	
		Water Separator	11.93	0.0583	131000.0	19000	19000	5.00	10	
		Water Separator Liquid Sensor	0.64	0.0006	1140000.0[ii]	19000	19000		10	
	CCAA Mission 2 (x3)	Condensing Heat Exchanger	49.71	0.3933	832600.0	0	19000		3	0.532
		Electronic Interface Box (EIB)	4.04	0.0173	2350000.0	0	19000		6	
		Fan Delta Pressure Sensor	0.45	0.0002	1250000.0	0	19000		3	
		Heat Exchanger Liquid Sensor	0.64	0.0006	1140000.0	0	19000		6	
		Inlet ORU	25.31	0.1308	333000.0	0	19000		3	
		Pressure Transducer	0.48	0.0000	1250000.0	0	19000	15.00	3	
		Temperature Control Check Valve	7.45	0.0071	32900.0	0	19000		6	
		Temperature Sensor	0.26	0.0014	37600000.0	0	19000		12	
		Water Separator	11.93	0.0583	131000.0	0	19000	5.00	6	
		Water Separator Liquid Sensor	0.64	0.0006	1140000.0[ii]	0	19000		6	
	WPA	Catalytic Reactor	67.04	0.1156	25579.2	6499	7675	2.25	1	0.320
		Gas Separator	39.15	0.0660	84008.4	6499	7675	1	1	
		Ion Exchange Bed	13.02	0.0173	296701.2	6499	7675	0.16	1	
		Microbial Check Valve	5.76	0.0065	143488.8	6499	7675	1	1	
		Multifiltration Bed #1	149.23	0.0657	296701.2	6499	7675	0.36	1	
		Multifiltration Bed #2	149.23	0.0657	296701.2	6499	7675	0.36	1	
		Particulate Filter	32.25	0.0717	717356.4	6499	7675	0.22	1	
		pH Adjuster	2.54	0.0026	137181.6	6499	7675	1	1	
		Process Controller	45.00	0.0838	87950.4	6499	7675	7.72	1	
		Pump Separator	31.34	0.0869	42398.4	6499	7675	2	1	
		Reactor Health Sensor	16.83	0.0425	56677.2	6499	7675	1	1	
		Sensor	4.81	0.0034	143664	6499	7675	10	1	
		Separator Filter	7.67	0.0102	359072.4	6499	7675	0.84	1	
		Start-up Filter	9.44	0.0184	226884	6499	7675	19.92	1	
		Water Delivery	47.54	0.0974	64561.2	6499	7675	5	1	
	UPA	Distillation Assembly	92.76	0.1422	142525.2	6689	11231	2	1	0.315
		Firmware Controller Assembly	23.09	0.0286	27331.2	6689	11231	2.4	1	
		Fluids Control and Pump Assembly	47.58	0.0731	90140.4	6689	11231	4	1	
		Pressure Control and Pump Assembly	49.08	0.1158	181507.2	6689	11231	2	1	
		Advanced Recycle Filter Tank Assembly[xvi]	50.00	0.1011	199640.4	6689	11231		1	
		Separator Plumbing Assembly	16.78	0.0229	384651.6	6689	11231	1	1	

ISRU	Water Extractor	Oven + Insulating Cone	140.96	6.1058	242700[iii]	19000	19000		1	39.55
		Hopper	86.75	7.1194		19000	19000		1	
		Sieve	88.63	0.0000	500000[iv]	19000	19000		1	
		Augers (vertical)	361.34	0.0000	500000[iv]	19000	19000		1	0.075
		Horizontal Auger	15.30	0.1966	500000[iv]	19000	19000		1	
		Sweep Gas System	0.04	0.0000	138408[v]	19000	19000		1	
		Sweep Gas Piping	9.83	0.2578		19000	19000		1	
		Condensing Heat Exchanger	67.84	2.0282	832600[vi]	19000	19000		1	
		Water Filtration System	3.94	0.0148	296701.2[vii]	19000	19000	0.36	1	
	CO2 Cryocooler	Cryocooler	58.68	0.1231	500000[iv]	19000	19000		2	2.499
		Container	140.76	0.8318		19000	19000		1	
	Water Electrolyzer	Electrolysis Cell Stack	47.43	0.0045	27156[viii]	19000	19000	2.38	1	12.28
		O2 Separator / Water Reservoir	5.71	0.0119	27156[viii]	19000	19000	2.38	1	
		H2 Separator and Dryer	14.44	0.0040	98112[ix]	19000	19000	10	1	
		Water Pump	2.16	0.0007	144540[x]	19000	19000	1	1	8×10^{-5}
	Sabatier Reactor	Reactor	20.78	0.4181	50000[xi]	19000	19000		1	0.198
		Water / Methane Separator	0.24	0.0097	131000[xii]	19000	19000		1	
		Heat Exchanger	0.53	0.0000	832600[xiii]	19000	19000		1	
	Atmospheric Processor	Zeolite	2.50	0.0300	77100[xiv]	19000	19000		1	
		Compressor	37.76	0.2184	66666.7	19000	19000		2	3.441
		Cryocoolers	3.10	0.0015	500000[iv]	19000	19000		2	0.480
		Support Structure	16.20			19000	19000		1	
BPC	Crop Lighting 1	Lighting System Unit[xvii]	8.00	0.0185	1743216	19000	19000	5.71	137	86.31
	Crop Lighting 2	Lighting System Unit[xvii]	8.00	0.0185	1743216	0	19000	5.71	137	86.31
	ORA[xx]	Air Pump Two-Stage ORU	10.89	0.0045	156200.0	19000	19000	15.29	1	0.860
		Blower	5.58	0.0300	129700.0	19000	19000	10.00	1	
		Check Valves	39.92	0.1784	32900.0[i]	19000	19000		1	
		Desiccant Beds	42.64	0.0850	77100.0	19000	19000		2	
		Heat Controller	3.31	0.0085	242700.0	19000	19000		2	
		Precooler	5.58	0.0255	129700.0	19000	19000	10.00	1	
		Pump Fan Motor Controller	2.72	0.0057	2270000.0	19000	19000		2	
		Selector Valves	3.04	0.0017	117000.0	19000	19000	10.61	6	
		Sorbent Beds (Zeolite)	42.64	0.0850	77100.0	19000	19000		2	
	BPC Structure 1[xviii]	Primary Structure (Inflatable)	6700	500		19000	19000		1	
		Secondary Structure (Shelving)	1145.7			19000	19000		1	
		Mechanization Systems	824.1			19000	19000		1	
	BPC Structure 2[xviii]	Primary Structure (Inflatable)	6700	500		0	19000		1	
		Secondary Structure (Shelving)	1145.7			0	19000		1	
		Mechanization Systems	824.1			0	19000		1	
	Food Processor[xix]	Hand Mixer	2.00	0.0050		19000	19000		1	
		Food Processor / Blender	8.00	0.0230		19000	19000		1	
		Grinder / Mill	4.10	0.0120		19000	19000		1	
		Bread Machine	7.40	0.0310		19000	19000		1	
		Griddle / Grill	5.80	0.0270		19000	19000		1	
		Juice Extractor	7.70	0.0390		19000	19000		1	
Food	First Mission	Prepackaged Food Supply	505			19000	0		1	
	Second Mission	Prepackaged Food Supply	932			0	19000		1	
	Subsequent Missions	Prepackaged Food Supply	0			0	0		1	

[i]Analogy to CCAA TCCV
[ii]Analogy to CCAA Heat Exchanger Liquid Sensor
[iii]Analogy to CDRA Heater Controller
[iv]Optimistic assumption; no data were available
[v]Analogy to OGA Nitrogen Purge ORU
[vi]Analogy CCAA Condensing Heat Exchanger
[vii]Analogy to WPA Multifiltration Bed
[viii]Analogy to OGA Hydrogen ORU (contains Electrolysis Cell Stack and Rotary Separator / Accumulator)
[ix]Analogy to OGA Oxygen Outlet
[x]Analogy to OGA Pump
[xi]Analogy to CRS Sabatier Methanation Reactor
[xii]Analogy to CRS Phase Separator
[xiii]Analogy to CRS Condensing Heat Exchanger
[xiv]Analogy to CDRA Dessicant-Adsorbent Bed
[xv]Analogy to CRS Compressor
[xvi]Mass is obtained from [300] and verified with calculations based on data from Link et al. [301]. All other data is assumed to be the same as the Recycle Filter Tank Assembly (RFTA) described in the NASA BVAD 2004 [209] – the original system from which the ARFTA was upgraded from. Here, the life limit of the ARFTA has been assumed to be zero, based on its development objective of facilitating the same function as the RFTA without the need for periodic replacement [301].
[xvii]Based on the Heliospectra LX601 grow light [213]. MTBF value is based on the assumption that a 2 year warranty accounts for 1% failures during that time
[xviii]Based on assumptions listed in Section 6.3.3
[xix]Based on sizing estimates from Stilwell et al. [367]
[xx]Analogy to CDRA

Table J.47: Architecture Case 8 Spare Parts Requirements for each Component over a 10 Mission Minimum Continuous Presence Campaign. Empty rows correspond to components assumed to have 100% reliability, and hence do not require spare parts

Group	Assembly	Subassembly	Mission									
			1	2	3	4	5	6	7	8	9	10
ECLSS	CDRA	Air Pump Two-Stage ORU	3	1	1	0	1	0	1	0	1	0
		Blower	4	1	1	0	1	0	1	0	1	0
		Check Valves	5	2	2	1	1	2	1	1	1	1
		Desiccant Beds	5	1	2	1	1	2	1	1	0	2
		Heat Controller	4	1	1	0	1	1	0	1	0	1
		Precooler	4	1	1	0	1	0	1	0	1	0
		Pump Fan Motor Controller	2	1	0	0	0	1	0	0	0	0
		Selector Valves	7	4	2	2	3	1	2	2	1	2
		Sorbent Beds (Zeolite)	5	1	2	1	1	2	0	2	0	2
	CCAA Mission 1	Condensing Heat Exchanger	3	1	0	1	0	1	0	0	1	0
		Electronic Interface Box (EIB)	3	1	1	0	0	1	0	1	0	0
		Fan Delta Pressure Sensor	3	1	1	1	0	1	0	0	0	1
		Heat Exchanger Liquid Sensor	4	2	1	0	1	1	0	1	0	0
		Inlet ORU	4	1	1	1	1	1	1	0	1	1
		Pressure Transducer	3	1	1	1	0	0	1	0	0	1
		Temperature Control Check Valve (TCCV)	18	10	9	8	9	7	7	9	6	8
		Temperature Sensor	2	1	0	0	0	1	0	0	0	0
		Water Separator	8	4	3	3	3	2	7	0	0	10
		Water Separator Liquid Sensor	4	1	1	1	1	1	0	1	0	1
	CCAA Mission 2	Condensing Heat Exchanger	0	2	1	0	1	0	1	0	0	0
		Electronic Interface Box (EIB)	0	3	0	1	0	1	0	0	0	1
		Fan Delta Pressure Sensor	0	3	1	0	1	0	1	0	0	0
		Heat Exchanger Liquid Sensor	0	4	1	1	0	1	0	0	1	0
		Inlet ORU	0	3	1	1	1	1	0	1	0	1
		Pressure Transducer	0	3	1	0	1	0	0	1	0	0
		Temperature Control Check Valve	0	14	6	6	6	5	5	5	5	5
		Temperature Sensor	0	2	0	1	0	0	0	0	0	0
		Water Separator	0	7	2	2	3	1	2	2	1	2
		Water Separator Liquid Sensor	0	4	1	0	1	1	0	0	1	0
	WPA	Catalytic Reactor	3	2	1	1	1	0	1	1	1	0
		Gas Separator	2	1	1	0	1	0	1	0	1	1
		Ion Exchange Bed	4	6	5	6	5	6	5	5	6	5
		Microbial Check Valve	3	0	1	0	1	0	0	1	1	1
		Multifiltration Bed #1	2	2	2	3	2	3	2	3	2	2
		Multifiltration Bed #2	2	2	2	3	2	3	2	3	2	2
		Particulate Filter	3	4	4	4	4	4	4	4	4	4
		pH Adjuster	3	1	0	0	1	0	0	1	1	1
		Process Controller	2	1	1	0	1	0	0	1	0	0
		Pump Separator	3	1	1	1	0	1	1	0	1	0
		Reactor Health Sensor	3	1	1	0	1	0	1	0	1	0
		Sensor	3	0	1	0	1	0	0	0	1	0
		Separator Filter	2	1	0	1	1	1	1	1	1	1
		Start-up Filter	2	1	0	0	1	0	0	0	1	0
		Water Delivery	3	1	0	1	0	1	0	1	0	0
	UPA	Distillation Assembly	2	1	0	1	0	0	1	0	0	1
		Firmware Controller Assembly	4	2	1	1	1	1	1	1	1	1
		Fluids Control and Pump Assembly	2	1	1	1	0	1	0	1	0	0
		Pressure Control and Pump Assembly	2	1	0	0	1	0	1	0	0	1
		Advanced Recycle Filter Tank Assembly	2	1	0	0	1	0	0	1	0	0
		Separator Plumbing Assembly	2	0	1	1	1	2	1	1	2	1
ISRU	Water Extractor	Oven + Insulating Cone	2	1	0	1	0	0	1	0	0	0
		Hopper										
		Sieve	2	0	1	0	0	0	1	0	0	0
		Augers (vertical)	2	0	0	1	0	0	0	0	1	0
		Horizontal Auger	2	1	0	0	1	0	0	0	1	0
		Sweep Gas System	4	1	2	0	1	1	1	0	0	0
		Sweep Gas Piping										
		Condensing Heat Exchanger	2	0	0	1	0	0	0	0	0	1

		Water Filtration System	6	6	6	6	6	6	6	6	6	6
	CO2 Cryocooler	Cryocooler	2	1	1	0	0	1	0	0	1	0
		Container										
	Water Electrolyzer	Electrolysis Cell Stack	5	3	2	1	1	2	1	2	1	1
		O2 Separator / Water Reservoir	6	3	2	1	2	2	1	1	2	1
		H2 Separator and Dryer	4	1	1	0	1	1	0	1	0	1
		Water Pump	4	1	1	2	2	3	2	2	2	2
	Sabatier Reactor	Reactor	4	2	1	1	2	1	0	1	1	1
		Water / Methane Separator	4	1	2	1	0	0	1	0	1	0
		Heat Exchanger	2	1	1	0	0	0	0	1	0	0
	Atmospheric Processor	Zeolite	4	2	1	0	2	1	0	1	0	1
		Compressor	5	2	2	1	1	2	1	1	1	1
		Cryocoolers	3	1	1	0	0	1	0	0	1	0
		Support Structure										
BPC	Crop Lighting 1	Lighting System Unit	8	5	124	0	0	137	0	137	0	0
	Crop Lighting 2	Lighting System Unit	0	9	4	124	0	0	137	0	137	0
	ORA	Air Pump Two-Stage ORU	3	1	1	0	1	0	1	0	1	0
		Blower	4	1	1	0	1	0	1	0	1	0
		Check Valves	5	2	2	1	1	2	1	1	1	1
		Desiccant Beds	5	1	2	1	1	2	0	2	0	1
		Heat Controller	4	1	1	0	1	1	0	1	0	1
		Precooler	4	1	0	1	1	0	1	0	1	0
		Pump Fan Motor Controller	2	1	0	0	0	1	0	0	0	0
		Selector Valves	7	4	2	2	2	2	2	2	1	2
		Sorbent Beds (Zeolite)	5	1	2	1	1	2	0	2	0	1

Table J.48: Architecture Case 8 Spare Parts Requirements for each Component over a 10 Mission Minimum Continuous Presence Campaign with all ISRU technologies at 10% of their originally estimated values. Empty rows correspond to components assumed to have 100% reliability, and hence do not require spare parts

Group	**Assembly**	**Subassembly**	**Mission**									
			1	**2**	**3**	**4**	**5**	**6**	**7**	**8**	**9**	**10**
ECLSS	CDRA	Air Pump Two-Stage ORU	3	1	1	1	0	0	1	0	1	0
		Blower	4	1	1	0	1	0	1	0	1	0
		Check Valves	5	2	2	1	1	2	1	1	1	1
		Desiccant Beds	5	2	1	1	2	1	1	1	1	1
		Heat Controller	4	1	1	1	0	1	0	1	0	1
		Precooler	4	1	1	0	1	0	1	0	1	0
		Pump Fan Motor Controller	2	1	0	0	0	1	0	0	0	0
		Selector Valves	8	3	2	3	1	2	2	2	2	2
		Sorbent Beds (Zeolite)	5	2	1	1	2	1	1	1	1	1
	CCAA Mission 1	Condensing Heat Exchanger	3	1	0	1	0	1	0	1	0	0
		Electronic Interface Box (EIB)	3	1	1	0	1	0	0	1	0	0
		Fan Delta Pressure Sensor	3	1	1	1	0	1	0	1	0	0
		Heat Exchanger Liquid Sensor	4	2	1	0	1	1	0	1	1	0
		Inlet ORU	4	1	2	0	1	1	1	1	0	1
		Pressure Transducer	3	1	1	1	0	0	1	0	1	0
		Temperature Control Check Valve (TCCV)	18	10	9	9	8	8	7	8	8	8
		Temperature Sensor	2	1	0	0	1	0	0	0	0	0
		Water Separator	9	3	3	3	3	2	7	0	1	9
		Water Separator Liquid Sensor	4	2	1	0	1	1	0	1	1	0
	CCAA Mission 2	Condensing Heat Exchanger	0	2	1	1	0	0	1	0	0	1
		Electronic Interface Box (EIB)	0	3	0	1	0	1	0	0	1	0
		Fan Delta Pressure Sensor	0	3	1	1	0	0	1	0	0	0
		Heat Exchanger Liquid Sensor	0	4	1	1	0	1	0	1	0	0
		Inlet ORU	0	4	1	0	1	1	0	1	0	1
		Pressure Transducer	0	3	1	1	0	0	1	0	0	0
		Temperature Control Check Valve	0	14	7	6	5	5	6	5	5	5
		Temperature Sensor	0	2	1	0	0	0	0	0	0	1
		Water Separator	0	7	3	2	2	1	2	2	2	1
		Water Separator Liquid Sensor	0	4	1	1	0	1	0	1	0	0
	WPA	Catalytic Reactor	4	1	1	1	1	1	0	1	1	0
		Gas Separator	3	0	1	0	1	0	1	0	1	1

		Ion Exchange Bed	4	6	5	6	5	6	5	5	6	5
		Microbial Check Valve	3	0	1	0	1	0	0	1	1	1
		Multifiltration Bed #1	2	2	2	3	2	3	2	3	2	2
		Multifiltration Bed #2	2	2	2	3	2	3	2	3	2	2
		Particulate Filter	3	4	4	4	4	4	4	4	4	4
		pH Adjuster	3	1	0	1	0	0	1	0	1	1
		Process Controller	2	1	1	0	1	0	0	1	0	0
		Pump Separator	3	1	1	1	1	0	1	0	1	0
		Reactor Health Sensor	3	1	1	1	0	1	0	1	0	0
		Sensor	3	0	1	0	1	0	0	1	0	0
		Separator Filter	2	1	0	1	1	1	1	1	1	1
		Start-up Filter	2	1	0	1	0	0	0	1	0	0
		Water Delivery	3	1	0	1	0	1	0	1	0	0
	UPA	Distillation Assembly	2	1	0	1	0	0	1	0	1	0
		Firmware Controller Assembly	4	2	1	2	0	1	2	1	0	1
		Fluids Control and Pump Assembly	2	1	1	1	0	1	0	1	0	0
		Pressure Control and Pump Assembly	2	1	0	1	0	0	1	0	0	1
		Advanced Recycle Filter Tank Assembly	2	1	0	1	0	0	0	1	0	0
		Separator Plumbing Assembly	2	0	1	1	1	2	1	1	2	1
ISRU	Water Extractor	Oven + Insulating Cone	5	2	2	2	2	1	2	1	1	2
		Hopper										
		Sieve	4	2	1	1	1	1	0	2	0	1
		Augers (vertical)	4	1	1	1	1	1	1	0	1	1
		Horizontal Auger	5	1	2	1	1	1	1	1	1	0
		Sweep Gas System	10	4	5	3	2	2	3	3	4	3
		Sweep Gas Piping										
		Condensing Heat Exchanger	3	2	1	0	1	1	0	1	1	0
		Water Filtration System	6	6	6	6	6	6	6	6	6	6
	CO2 Cryocooler	Cryocooler	6	2	2	2	1	2	1	2	1	1
		Container										
	Water Electrolyzer	Electrolysis Cell Stack	18	12	10	9	9	9	9	9	9	8
		O2 Separator / Water Reservoir	20	12	10	11	9	9	9	10	8	9
		H2 Separator and Dryer	10	4	4	3	3	4	3	3	3	3
		Water Pump	9	4	2	3	3	2	3	2	2	2
	Sabatier Reactor	Reactor	13	8	6	6	5	6	5	5	6	5
		Water / Methane Separator	10	5	4	2	3	3	2	3	3	1
		Heat Exchanger	5	1	2	0	2	0	1	0	1	1
	Atmospheric Processor	Zeolite	12	6	4	5	4	3	4	4	4	4
		Compressor	16	10	9	8	7	8	7	8	7	7
		Cryocoolers	7	2	3	2	1	2	1	2	2	1
		Support Structure										
BPC	Crop Lighting 1	Lighting System Unit	9	4	124	0	0	137	0	137	0	0
	Crop Lighting 2	Lighting System Unit	0	9	4	124	0	0	137	0	137	0
	ORA	Air Pump Two-Stage ORU	3	1	1	1	0	0	1	0	1	0
		Blower	4	1	1	0	1	0	1	0	1	0
		Check Valves	5	2	2	1	1	2	1	1	1	1
		Desiccant Beds	5	2	1	1	2	1	1	1	1	1
		Heat Controller	4	1	1	1	0	1	0	1	0	1
		Precooler	4	1	1	0	1	0	1	0	1	0
		Pump Fan Motor Controller	2	1	0	0	0	1	0	0	0	0
		Selector Valves	8	3	2	3	1	2	2	2	2	2
		Sorbent Beds (Zeolite)	5	2	1	1	2	1	1	1	1	1

J.3.9 Architecture Case 9

Table J.49: Architecture Case 9 Master Equipment List, containing component mass, volume and reliability data, as well as run times and power demands. Power is listed here on a per unit basis. ISRU technologies displayed here were sized by the HabNet ISRU Module.

Sys.	Assembly	Subassembly	Mass [kg]	Vol. [m^3]	MTBF [h]	Run Time Miss. 1 [h]	Run Time Miss. 2 [h]	LL [y]	# in Pmry.	Power [kW]
ECLS	CDRA	Air Pump Two-Stage ORU	10.89	0.0045	156200.0	19000	19000	15.29	1	0.860
		Blower	5.58	0.0300	129700.0	19000	19000	10.00	1	
		Check Valves	39.92	0.1784	32900.0[i]	19000	19000		1	
		Desiccant Beds	42.64	0.0850	77100.0	19000	19000		2	
		Heat Controller	3.31	0.0085	242700.0	19000	19000		2	
		Precooler	5.58	0.0255	129700.0	19000	19000	10.00	1	
		Pump Fan Motor Controller	2.72	0.0057	2270000.0	19000	19000		2	
		Selector Valves	3.04	0.0017	117000.0	19000	19000	10.61	6	
		Sorbent Beds (Zeolite)	42.64	0.0850	77100.0	19000	19000		2	
	CCAA Mission 1 (x5)	Condensing Heat Exchanger	49.71	0.3933	832600.0	19000	19000		5	0.705
		Electronic Interface Box (EIB)	4.04	0.0173	2350000.0	19000	19000		10	
		Fan Delta Pressure Sensor	0.45	0.0002	1250000.0	19000	19000		5	
		Heat Exchanger Liquid Sensor	0.64	0.0006	1140000.0	19000	19000		10	
		Inlet ORU	25.31	0.1308	333000.0	19000	19000		5	
		Pressure Transducer	0.48	0.0000	1250000.0	19000	19000	15.00	5	
		Temperature Control Check Valve	7.45	0.0071	32900.0	19000	19000		10	
		Temperature Sensor	0.26	0.0014	37600000.0	19000	19000		20	
		Water Separator	11.93	0.0583	131000.0	19000	19000	5.00	10	
		Water Separator Liquid Sensor	0.64	0.0006	1140000.0[ii]	19000	19000		10	
	CCAA Mission 2 (x3)	Condensing Heat Exchanger	49.71	0.3933	832600.0	0	19000		3	0.532
		Electronic Interface Box (EIB)	4.04	0.0173	2350000.0	0	19000		6	
		Fan Delta Pressure Sensor	0.45	0.0002	1250000.0	0	19000		3	
		Heat Exchanger Liquid Sensor	0.64	0.0006	1140000.0	0	19000		6	
		Inlet ORU	25.31	0.1308	333000.0	0	19000		3	
		Pressure Transducer	0.48	0.0000	1250000.0	0	19000	15.00	3	
		Temperature Control Check Valve	7.45	0.0071	32900.0	0	19000		6	
		Temperature Sensor	0.26	0.0014	37600000.0	0	19000		12	
		Water Separator	11.93	0.0583	131000.0	0	19000	5.00	6	
		Water Separator Liquid Sensor	0.64	0.0006	1140000.0[ii]	0	19000		6	
ISRU	Water Extractor	Oven + Insulating Cone	173.63	7.5214	242700[iii]	19000	19000		1	48.72
		Hopper	100.12	8.7699		19000	19000		1	
		Sieve	121.17	0.0000	500000[iv]	19000	19000		1	
		Augers (vertical)	445.10	0.0000	500000[iv]	19000	19000		1	0.086
		Horizontal Auger	16.98	0.2182	500000[iv]	19000	19000		1	
		Sweep Gas System	0.05	0.0000	138408[v]	19000	19000		1	
		Sweep Gas Piping	11.69	0.3392		19000	19000		1	
		Condensing Heat Exchanger	83.42	2.7544	832600[vi]	19000	19000		1	
		Water Filtration System	4.86	0.0183	296701.2[vii]	19000	19000	0.36	1	
	CO2 Cryocooler	Cryocooler	58.68	0.1231	500000[iv]	19000	19000		2	2.499
		Container	140.76	0.8318		19000	19000		1	
	Water Electrolyzer	Electrolysis Cell Stack	47.43	0.0045	27156[viii]	19000	19000	2.38	1	12.28
		O2 Separator / Water Reservoir	5.71	0.0119	27156[viii]	19000	19000	2.38	1	
		H2 Separator and Dryer	14.44	0.0040	98112[ix]	19000	19000	10	1	
		Water Pump	2.16	0.0007	144540[x]	19000	19000	1	1	8×10^{-5}
	Sabatier Reactor	Reactor	20.78	0.4181	50000[xi]	19000	19000		1	0.198
		Water / Methane Separator	0.24	0.0097	131000[xii]	19000	19000		1	
		Heat Exchanger	0.53	0.0000	832600[xiii]	19000	19000		1	
	Atmospheric Processor	Zeolite	2.50	0.0300	77100[xiv]	19000	19000		1	
		Compressor	37.76	0.2184	66666.7	19000	19000		2	3.441
		Cryocoolers	3.10	0.0015	500000[iv]	19000	19000		2	0.480
		Support Structure	16.20			19000	19000		1	

BPC	Crop Lighting 1	Lighting System Unit[xvii]	8.00	0.0185	1743216	19000	19000	5.71	137	86.31
	Crop Lighting 2	Lighting System Unit[xvii]	8.00	0.0185	1743216	0	19000	5.71	137	86.31
	ORA[xx]	Air Pump Two-Stage ORU	10.89	0.0045	156200.0	19000	19000	15.29	1	0.860
		Blower	5.58	0.0300	129700.0	19000	19000	10.00	1	
		Check Valves	39.92	0.1784	32900.0[i]	19000	19000		1	
		Desiccant Beds	42.64	0.0850	77100.0	19000	19000		2	
		Heat Controller	3.31	0.0085	242700.0	19000	19000		2	
		Precooler	5.58	0.0255	129700.0	19000	19000	10.00	1	
		Pump Fan Motor Controller	2.72	0.0057	2270000.0	19000	19000		2	
		Selector Valves	3.04	0.0017	117000.0	19000	19000	10.61	6	
		Sorbent Beds (Zeolite)	42.64	0.0850	77100.0	19000	19000		2	
	BPC Structure 1[xviii]	Primary Structure (Inflatable)	6700	500		19000	19000		1	
		Secondary Structure (Shelving)	1145.7			19000	19000		1	
		Mechanization Systems	824.1			19000	19000		1	
	BPC Structure 2[xviii]	Primary Structure (Inflatable)	6700	500		0	19000		1	
		Secondary Structure (Shelving)	1145.7			0	19000		1	
		Mechanization Systems	824.1			0	19000		1	
	Food Processor[xix]	Hand Mixer	2.00	0.0050		19000	19000		1	
		Food Processor / Blender	8.00	0.0230		19000	19000		1	
		Grinder / Mill	4.10	0.0120		19000	19000		1	
		Bread Machine	7.40	0.0310		19000	19000		1	
		Griddle / Grill	5.80	0.0270		19000	19000		1	
		Juice Extractor	7.70	0.0390		19000	19000		1	
Food	First Mission	Prepackaged Food Supply	505			19000	0		1	
	Second Mission	Prepackaged Food Supply	932			0	19000		1	
	Subsequent Missions	Prepackaged Food Supply	0			0	0		1	

[i]Analogy to CCAA TCCV
[ii]Analogy to CCAA Heat Exchanger Liquid Sensor
[iii]Analogy to CDRA Heater Controller
[iv]Optimistic assumption; no data were available
[v]Analogy to OGA Nitrogen Purge ORU
[vi]Analogy CCAA Condensing Heat Exchanger
[vii]Analogy to WPA Multifiltration Bed
[viii]Analogy to OGA Hydrogen ORU (contains Electrolysis Cell Stack and Rotary Separator / Accumulator)
[ix]Analogy to OGA Oxygen Outlet
[x]Analogy to OGA Pump
[xi]Analogy to CRS Sabatier Methanation Reactor
[xii]Analogy to CRS Phase Separator
[xiii]Analogy to CRS Condensing Heat Exchanger
[xiv]Analogy to CDRA Dessicant-Adsorbent Bed
[xv]Analogy to CRS Compressor
[xvi]Mass is obtained from [300] and verified with calculations based on data from Link et al. [301]. All other data is assumed to be the same as the Recycle Filter Tank Assembly (RFTA) described in the NASA BVAD 2004 [209] – the original system from which the ARFTA was upgraded from. Here, the life limit of the ARFTA has been assumed to be zero, based on its development objective of facilitating the same function as the RFTA without the need for periodic replacement [301].
[xvii]Based on the Heliospectra LX601 grow light [213]. MTBF value is based on the assumption that a 2 year warranty accounts for 1% failures during that time
[xviii]Based on assumptions listed in Section 6.3.3
[xix]Based on sizing estimates from Stilwell et al. [367]
[xx]Analogy to CDRA

Table J.50: Architecture Case 9 Spare Parts Requirements for each Component over a 10 Mission Minimum Continuous Presence Campaign. Empty rows correspond to components assumed to have 100% reliability, and hence do not require spare parts. Further, we note that because the sensitivity analysis performed in Section 6.5.5 did not include Case 9, a separate listing of spare parts requirements at degraded ISRU reliability levels is not shown.

Group	**Assembly**	**Subassembly**	**Mission**									
			1	**2**	**3**	**4**	**5**	**6**	**7**	**8**	**9**	**10**
ECLSS	CDRA	Air Pump Two-Stage ORU	4	0	1	0	1	0	1	0	1	0
		Blower	4	1	0	1	0	1	1	0	1	0
		Check Valves	5	2	2	1	1	2	1	1	1	1
		Desiccant Beds	5	1	2	1	1	1	1	2	1	0
		Heat Controller	4	1	1	1	0	1	0	1	0	1
		Precooler	4	1	0	1	0	1	1	0	1	0
		Pump Fan Motor Controller	2	1	0	0	0	0	1	0	0	0
		Selector Valves	8	2	3	2	2	2	2	2	2	1

		Sorbent Beds (Zeolite)	5	1	2	1	1	1	1	1	2	0
	CCAA Mission 1	Condensing Heat Exchanger	3	0	1	1	0	1	0	0	1	0
		Electronic Interface Box (EIB)	3	1	1	0	0	1	0	1	0	0
		Fan Delta Pressure Sensor	4	0	1	1	0	0	1	0	0	1
		Heat Exchanger Liquid Sensor	5	0	1	2	0	1	0	1	0	0
		Inlet ORU	4	1	1	1	1	1	1	0	1	0
		Pressure Transducer	4	0	1	1	0	0	1	0	0	1
		Temperature Control Check Valve (TCCV)	19	9	9	9	6	9	8	8	7	7
		Temperature Sensor	2	1	0	0	0	1	0	0	0	0
		Water Separator	9	3	3	3	2	3	7	0	0	10
		Water Separator Liquid Sensor	5	0	1	1	1	1	0	1	0	0
	CCAA Mission 2	Condensing Heat Exchanger	0	2	1	1	0	0	0	1	0	0
		Electronic Interface Box (EIB)	0	3	0	1	0	0	1	0	0	1
		Fan Delta Pressure Sensor	0	3	1	0	1	0	1	0	0	0
		Heat Exchanger Liquid Sensor	0	4	1	1	0	1	0	0	1	0
		Inlet ORU	0	3	1	1	0	1	1	1	0	0
		Pressure Transducer	0	3	1	0	0	1	0	1	0	0
		Temperature Control Check Valve	0	13	7	7	4	6	5	5	5	4
		Temperature Sensor	0	2	0	1	0	0	0	1	0	0
		Water Separator	0	7	2	3	1	2	2	2	1	2
		Water Separator Liquid Sensor	0	4	1	1	0	0	1	0	1	0
ISRU	Water Extractor	Oven + Insulating Cone	2	1	0	1	0	0	1	0	0	0
		Hopper										
		Sieve	2	0	1	0	0	0	0	1	0	0
		Augers (vertical)	1	1	0	0	1	0	0	0	0	1
		Horizontal Auger	2	1	0	1	0	0	0	0	1	0
		Sweep Gas System	5	1	1	1	0	0	1	1	0	0
		Sweep Gas Piping										
		Condensing Heat Exchanger	2	0	0	1	0	0	0	0	0	0
		Water Filtration System	6	6	6	6	6	6	6	6	6	6
	CO2 Cryocooler	Cryocooler	3	0	0	1	0	1	0	0	1	0
		Container										
	Water Electrolyzer	Electrolysis Cell Stack	6	1	2	2	1	2	1	1	2	1
		O2 Separator / Water Reservoir	7	2	2	2	0	2	2	1	2	1
		H2 Separator and Dryer	4	1	1	1	0	1	0	1	0	1
		Water Pump	4	1	1	2	2	3	2	2	2	2
	Sabatier Reactor	Reactor	5	1	1	2	0	1	1	1	1	1
		Water / Methane Separator	5	0	1	2	0	0	1	1	0	0
		Heat Exchanger	3	0	0	1	0	0	1	0	0	0
	Atmospheric Processor	Zeolite	5	1	1	1	1	0	1	1	1	0
		Compressor	5	2	1	2	1	1	2	1	1	1
		Cryocoolers	3	1	1	0	0	1	0	1	0	0
		Support Structure										
BPC	Crop Lighting 1	Lighting System Unit	9	3	125	0	0	137	0	137	0	0
	Crop Lighting 2	Lighting System Unit	0	9	3	125	0	0	137	0	137	0
	ORA	Air Pump Two-Stage ORU	3	1	1	0	1	0	1	0	1	0
		Blower	4	1	0	1	0	1	1	0	1	0
		Check Valves	5	2	2	1	1	1	2	1	1	1
		Desiccant Beds	5	1	2	1	1	1	1	1	2	0
		Heat Controller	4	1	1	1	0	1	0	1	0	1
		Precooler	4	1	0	1	0	1	1	0	1	0
		Pump Fan Motor Controller	3	0	0	0	0	1	0	0	0	0
		Selector Valves	8	2	3	2	2	2	2	2	1	2
		Sorbent Beds (Zeolite)	5	1	2	1	1	1	1	1	2	0

Appendix K

Glossary of Terms

Carrying Capacity	A term used in the field of ecology to describe the maximum population of a biological species that an environment or habitation system can sustain indefinitely
Conjunction Class Mission	Same as a Long Stay Mission – a type of Mars mission characterized by an approximately 500 day stay on the surface of Mars and minimum energy transfers to and from Mars
Continuous Presence	The capability to sustain human presence at an exploration destination on a continuous basis – in a similar manner to how the International Space Station has supported a continuous human presence in low Earth orbit since November 2000.
Crew Profile	Same as a Population Profile – the profile by which people arrive and depart from an exploration destination (in this case, the surface of Mars). Graphically, the population profile is depicted by the trend in the surface habitat population over time
CRS	CO_2 Reduction System – ISS ECLS technology that when combined with the OGA, recovers oxygen from crew expired CO_2. This system relies on the Sabatier reaction that reacts hydrogen (from the OGA) with CO_2 to produce water and methane. Product water is then electrolyzed with the OGA to recover oxygen
Duty Cycle	The proportion of the total mission time in which a system is actively operating
Earth Independence	A type of space habitation architecture that operates in a manner that is entirely independent of the resupply of resources from Earth
Earth Reliant	A type of space habitation architecture that relies on the periodic resupply of resources from Earth

ESM	Equivalent System Mass (a measure of the mass of a system + the mass of the systems required to support its operation – eg. additional power and cooling systems required to support the addition of a life support technology)
Endurance	The maximum time that a habitat can sustain a given number of crew before needing to be resupplied with resources derived from Earth
ISRU	In-Situ Resource Utilization – the concept of "living off the land", or using technologies to extract local resources to support human activities at an exploration destination
K-Factor	Uncertainty factors used to estimate the reliability of a system in a state other than its originally intended operational state (e.g. to account for the impact of environmental factors on system reliability)
Loop closure rate	The extent of resource reclamation within an environmental control and life support system
Long Stay Mission	Same as a Conjunction Class Mission – a type of Mars mission characterized by an approximately 500 day stay on the surface of Mars and minimum energy transfers to and from Mars
Mass loop closure	Equivalent to the loop closure rate
MAV	Mars Ascent Vehicle (note that a dedicated ISRU system is always emplaced to generate propellant for this vehicle)
MTBF	Mean Time Between Failure – a measure of system reliability; the average time between successive failures of a system (assuming that any failure is repaired immediately)
OGA	Oxygen Generation Assembly – ISS ECLS technology used to generate oxygen and hydrogen through the electrolysis of water
Opposition Class Mission	Same as a Short Stay Mission – a type of Mars mission characterized by a 30 to 60 day stay on the surface of Mars, and a fly-by of Venus on the outbound journey towards or return journey from Mars
Outpost (–type, –class, or –development) Mission	A campaign of missions consisting of repeated visits to the same exploration site with the intent of expanding infrastructure at that location over time.
Permanent Presence	Similar to Continuous Presence, with the additional requirement that there is no foreseeable conclusion to the end of a mission campaign (thus making human presence "permanent")

Population Profile	Same as a Crew Profile – the profile by which people arrive and depart from an exploration destination (in this case, the surface of Mars). Graphically, the population profile is depicted by the trend in the surface habitat population over time
Short Stay Mission	Same as an Opposition Class Mission – a type of Mars mission characterized by a 30 to 60 day stay on the surface of Mars, and a fly-by of Venus on the outbound journey towards or return journey from Mars
Sortie (–type or –class) Mission	A mission are characterized by a single visit to a predefined location, as was the case with the Apollo lunar missions
Space Logistics	Defined by the AIAA Space Logistics Technical Committee as "the theory and practice of driving space system design for operability, and of managing the flow of materiel, services, and information needed throughout the space system lifecycle" [26]
Split Mission	A type of Mars transportation strategy whereby a Mars Ascent Vehicle and ISRU system are deployed to the surface of Mars on the flight opportunity before the launch of the crew (equal to about 26 months prior to the launch of the crew). Here, the ISRU system is intended to generate ascent propellant for the MAV prior to the departure of the crew. In this manner, the ISRU production of sufficient ascent propellant for the MAV becomes a criterion for the launch of the crew – they never depart Earth without the assurance of a means to return to Mars orbit at the completion of their stay on the Mars surface.
Supportability	The collection of considerations related to the reliability, maintainability, reparability, redundancy, and sparing philosophy of a system – attributes that influence the lifecycle operating and sustainment costs of a system
Sustainability	The capability of a system to be sustained over long-durations, typically characterized by a stable cost of operations and a minimal adverse impact on its surrounding environment
Synodic Period	The amount of time needed for a planet or celestial body to return to the same point in its orbit relative to the Earth. For Mars, the synodic period is approximately 26 months.
System Architecture	The definition of the functions performed by a system, its mapping to elements of form, and its interfaces, both internal to itself and with the surrounding context (e.g. physical environment, users, regulations, etc.)
Systems Architecting Problem	A type of problem that involves defining a set of technologies, supporting systems, and operational strategies to accomplish a set of functions that together, deliver value to a set of stakeholders

Technology Map	An Object Process Diagram of a technology, depicting its major function, its architectural attributes (attributes that the designer has control over), its properties, and its operational requirements
UPA	Urine Processor Assembly – ISS ECLS technology used to recover greywater from urine
WPA	Water Processor Assembly – ISS ECLS technology used to process greywater (from cabin humidity, processed urine, or Sabatier reaction product water) into potable water

References

[1] Committee on Human Spaceflight, Aeronautics and Space Engineering Board, National Research Council of the National Academies, 2014, Pathways to Exploration: Rationales and Approaches for a U.S. Program of Human Space Exploration, Washington D.C., The National Academies Press, Available at: http://www.nap.edu/catalog/18801/pathways-to-exploration-rationales-and-approaches-for-a-us-program

[2] Augustine, N. R. (Chair), 2009, Seeking a Human Spaceflight Program Worthy of a Great Nation, Review of U.S. Human Spaceflight Plans Committee, National Aeronautics and Space Administration, Washington, D.C.

[3] 111th Congress of the United States of America, 2010, NASA Authorization Act 2010, 111th Congress of the United States of America, Washington D.C., Available at: http://www.nasa.gov/pdf/649377main_PL_111-267.pdf

[4] Griffin, B., Thomas, B., Vaughan, D., Drake, B., and Woodcock, G., 2004, A Comparison of Transportation Systems for Human Missions to Mars, AIAA 2004-3834, 40th AIAA/ASME/SAE/ASEE Joint Propulsion Conference and Exhibit, 11-14 July 2004, Fort Lauderdale, FL.

[5] Rep. Palazzo, S. M., 2015, H.R. 810 - NASA Authorization Act 2015, 114th Congress of the United States of America, Washington D.C., Available at: https://www.congress.gov/bill/114th-congress/house-bill/810/text

[6] Crusan, J., 2014, An Evolvable Mars Campaign, NASA Advanced Exploration Systems Division, NASA Headquarters, Washington, D.C., Available at: https://www.nasa.gov/sites/default/files/files/20140429-Crusan-Evolvable-Mars-Campaign.pdf

[7] NASA, 2015, NASA's Journey to Mars - Pioneering Next Steps in Space Exploration, NASA Headquarters, Washington D.C., http://www.nasa.gov/sites/default/files/atoms/files/journey-to-mars-next-steps-20151008_508.pdf

[8] Craig, D., Evolvable Mars Campaign Overview to FISO Telecon, NASA Advanced Exploration Systems Division, NASA Headquarters, Washington, D.C., Available at: http://images.spaceref.com/fiso/2015/061015_doug_craig_nasa_hq/Craig_6-10-15.pdf, Visited: October 14, 2015

[9] Berger, E., "Elon Musk to unveil Mars plans this year, wants to go to space by 2020," Ars Technica [Online]. Available at: http://arstechnica.com/science/2016/01/elon-musk-to-unveil-mars-plans-this-year-wants-to-go-to-space-by-2020/ [Accessed: 05-Apr-2016]

[10] Aldrin, B., Saikia, S., and Longuski, J., 2015, A Proposed Architecture to Establish a Permanent Human Presence on Mars, IAC-15-A5.2.6, 66th International Astronautical Congress, 12-16 October 2015, Jerusalem, Israel.

[11] Mars One, 2014, Mars One: Roadmap 2023, Original URL: http://www.mars-one.com/mission/roadmap/2023, Date accessed: July 16th, 2014, Archived URL: http://web.archive.org/web/20140716210617/http://www.mars-one.com/mission/roadmap/2023

[12] Cirillo, W., Goodliff, K., Ames, N., and Field, M., 2011, "Supportability for Beyond Low Earth Orbit Missions," (September), pp. 1–12.

[13] Lee, G., Jordan, E., Shishko, R., de Weck, O. L., Armar, N., and Siddiqi, A., 2008, SpaceNet: Modeling and Simulating Space Logistics, AIAA 2008-7747, AIAA Space 2008 Conference and Exposition, 9-11 September 2008, San Diego, CA, Available online at: <http://www.aric.or.kr/treatise/journal/content.asp?idx=110367>.

[14] Mindell, D. A., 2008, Digital Apollo, MIT Press, Cambridge, MA.
[15] Brooks, C. G., Grimwood, J. M., and Swenson Jr., L. S., 1979, Chariots for Apollo: A History of Manned Lunar Spacecraft, Scientific and Technical Information Office, National Aeronautics and Space Administration, Washington, D.C., Available online at: <http://history.nasa.gov/SP-4205/cover.html>.
[16] Ash, R. L., Dowler, W. L., and Varsi, G., 1978, "Feasibility of rocket propellant production on Mars," Acta Astronaut., **5**(9), pp. 705–724.
[17] Portree, D. S. F., 2001, Humans to Mars: Fifty Years of Mission Planning, 1950-2000, NASA SP-2001-4521, Monographs in Aerospace History #21, NASA History Division, NASA Headquarters, Washington D.C.
[18] Baker, D., and Zubrin, R., 1990, "Mars Direct: Combining Near-Term Technologies to Achieve a Two-Launch Manned Mars Mission," J. Br. Interplanet. Soc., **43**(11), pp. 519–525.
[19] Hoffman, S. J., and Kaplan, D. I., 1998, "Human Exploration of Mars: The Reference Mission of the NASA Mars Exploration Study Team," NASA Spec. Publ., **6107**(July), pp. 98–036 Available online at: <http://www.nss.org/settlement/mars/1997-NASA-HumanExplorationOfMarsReferenceMission.pdf>.
[20] Drake, B. G. (ed)., 2009, Human Exploration of Mars Design Reference Architecture 5.0, National Aeronautics and Space Administration, Mars Architecture Steering Group, July 2009, NASA-SP-2009-566, Mars Architecture Steering Group, NASA Headquarters, Washington, D.C., Available from: https://www.nasa.gov/pdf/373665main_NASA-SP-2009-566.pdf.
[21] Drake, B. G. (ed. ., and Watts, K. D. (ed. ., 2014, Human Exploration of Mars Design Reference Architecture 5.0 Addendum #2, NASA/SP-2009-566-ADD2, March 2014, Mars Architecture Steering Group, NASA Headquarters.
[22] Simmons, W. L., 2008, "A Framework for Decision Support in Systems Architecting," Ph.D. Dissertation, Department of Aeronautics and Astronautics, Massachusetts Institute of Technology.
[23] Simmons, W. L., Koo, B. H. Y., and Crawley, E. F., 2005, "Space Systems Architecting Using Meta-Languages", IAC-05-D1.P-03, 56th International Astronautical Congress, 16-21 October 2005, Fukuoka, Japan
[24] Aliakbargolkar, A., Crawley, E. F., Wicht, A. C., Battat, J. A., and Calandrelli, E. D., 2013, "Systems Architecting Methodology for Space Transportation Infrastructure," J. Spacecr. Rockets, Vol . 50, No/ 3 (2013), pp. 579-590, doi: 10.2514/1.A32320
[25] Rudat, A., Battat, J., and Cameron, B., 2013, The Modeling and Evaluation of Interplanetary Manned Missions Using System Architecting Techniques, IEEE, 2013 IEEE Aerospace Conference, 2-9 March 2013, Big Sky, Montana.
[26] AIAA Space Logistics Technical Committee, "Space Logistics Definitions" [Online]. Available online at: https://info.aiaa.org/tac/SMG/SLTC/Web Pages/Definitions.aspx. [Accessed: 02-Dec-2015],
[27] Ishimatsu, T., de Weck, O. L., Hoffman, J. A., Ohkami, Y., and Shishko, R., 2015, "Generalized Multicommodity Network Flow Model for the Earth–Moon–Mars Logistics System," J. Spacecr. Rockets, **53**(1), pp. 25–38, Available online at: <http://arc.aiaa.org/doi/10.2514/1.A33235>.
[28] Ho, K., 2015, "Dynamic Network Modeling for Spaceflight Logistics with Time-Expanded Networks," Ph.D. Dissertation, Department of Aeronautics and Astronautics, Massachusetts Institute of Technology.
[29] NASA Office of the Chief Technologist, 2015, NASA Technology Roadmaps - TA 6: Human Health, Life Support, and Habitation Systems, NASA Headquarters, Washington D.C. Available at: http://www.nasa.gov/sites/default/files/atoms/files/2015_nasa_technology_roadmaps_ta_6_human_health_life_support_habitation.pdf.
[30] Nield, G. C., and Vorobiev, P. M., 1999, Phase 1 Program Joint Report, January 1999, NASA-SP-1999-6108/(In English), NASA Headquarters, Washington D.C.
[31] NASA, "Shuttle-Mir" [Online]. Available online at: http://grin.hq.nasa.gov/IMAGES/LARGE/GPN-2000-001315.jpg. [Accessed: 18-Dec-2015]

[32] NASA, "Shuttle-ISS" [Online]. Available online at: http://www.nasa.gov/images/content/557365main_iss027e036712_1600_946-710.jpg. [Accessed: 08-Dec-2015]
[33] Wikipedia, 2012, "List of Unmanned Spaceflights to the International Space Station" [Online]. Available online at: https://en.wikipedia.org/wiki/List_of_unmanned_spaceflights_to_the_International_Space_Station. [Accessed: 13-Mar-2012]
[34] Malik, T., 2009, "Population in Space at Historic High: 13," Space.com [Online]. Available: http://www.space.com/6503-population-space-historic-high-13.html. [Accessed: 04-Nov-2015],
[35] Moskowitz, C., 2009, "Space Station Population Hits Record High," Space.com [Online]. Available: http://www.space.com/7003-space-station-population-hits-record-high.html. [Accessed: 04-Nov-2015]
[36] NASA, Space Shuttle Mission STS-127 - A Porch in Space - Press Kit, June 2009, Available from: https://www.nasa.gov/pdf/358018main_sts127_press_kit.pdf.
[37] NASA, 2010, Space Shuttle Mission STS-131: Experiment Express - Press Kit, April 2010, Available from: https://www.nasa.gov/pdf/440897main_sts_131_press_kit.pdf.
[38] World Health Organization, 2015, "Global Health Observatory data repository - Life expectancy data by country" [Online]. Available online at: http://apps.who.int/gho/data/node.main.688?lang=en. [Accessed: 04-Oct-2015]
[39] Hui, C., 2006, "Carrying capacity, population equilibrium, and environment's maximal load," Ecol. Modell., **192**(1-2), pp. 317–320.
[40] Toups, L., Smitherman, D., Shyface, H., Simon, M., Bobskill, M., Komar, D. R., Guirgis, P., Bagdigian, R., and Spexarth, G., 2011, Deep Space Habitat Team: HEFT Phase 2 Efforts, NASA Human Exploration Framework Team, NASA/ESA Bilateral Meeting, January 2011, Available from: http://ntrs.nasa.gov/archive/nasa/casi.ntrs.nasa.gov/20110006982_2011003312.pdf [cited 22 March 2012].
[41] Portree, D. S. F., 2012, "One-Way Space Man (1962)," Wired [Online]. Available: http://www.wired.com/2012/04/one-way-space-man-1962/. [Accessed: 14-Nov-2014],
[42] Toups, L., and Hoffman, S. J., 2015, Pioneering Objectives and Activities on the Surface of Mars, AIAA 2015-4410, AIAA Space 2015 Conference and Exposition, August 31 - Septemeber 2, 2015, Pasadena, CA.
[43] Wieland, P. O., 1994, Designing for Human Presence in Space: An Introduction to Environmental Control and Life Support Systems, NASA-RP-1324, National Aeronautics and Space Administration, Office of Management, Scientific and Technical Information Program.
[44] Wieland, P. O., 1998, Living Together in Space: The Design and Operation of the Life Support Systems on the International Space Station, National Aeronautics and Space Administration, NASA/TM-1998-206956/VOL1, NASA Marshall Space Flight Center, Huntsville, AL.
[45] Wieland, P. O., 2005, Designing for Human Presence in Space: An Introduction to Environmental Control and Life Support Systems (ECLSS) -Appendix I, Update - Historical ECLSS for U.S. and U.S.S.R./Russian Space Habitats, NASA, NASA Marshall Space Flight Center, Alabama.
[46] Hacker, B. C., and Grimwood, J. M., 1977, On the Shoulders of Titans - A History of Project Gemini, Scientific and Technical Information Office, National Aeronautics and Space Administration, Washington, D.C.
[47] Johnston, R. S., Dietlein, L. F., and Berry, C. A., 1975, Biomedical Results of Apollo, Scientific and Technical Information Office, National Aeronautics and Space Administration, Washington, D.C., Available online at: <http://history.nasa.gov/SP-368/sp368.htm>.
[48] Belew, L. F., and Stuhlinger, E., 1973, SKYLAB: A Guidebook, National Aeronautics and Space Administration, George C. Marshall Space Flight Center, Huntsville, AL, Available online at: <http://history.nasa.gov/EP-107/contents.htm>.
[49] Williams, D. E., Dake, J. R., and Gentry, G. J., 2012, International Space Station Environmental Control and Life Support System Status for the Prior Year: 2010 - 2011, AIAA, AIAA 2012-3612, 42nd International Conference on Environmental Systems 15 - 19 July 2012, San Diego, CA.

[50] Portree, D. S. F., Mir Hardware Heritage, National Aeronautics and Space Administration, Lyndon B. Johnson Space Center, Houston, Texas, Available online at: <http://history.nasa.gov/SP-4225/documentation/mhh/mhh.htm>.
[51] Diamant, B. L., and Humphries, W. R., 1990, Past and Present Environmental Control and Life Support Systems on Manned Spacecraft, Society of Automotive Engineers, SAE International Conference On Environmental Systems, July 9, 1990, Williamsburg, Virginia, United States.
[52] Eckart, P., 1994, Spaceflight Life Support and Biospherics, Microcosm Press, Torrance, CA.
[53] Newkirk, R. W., Ertel, I. D., and Brooks, C. G., 1977, Skylab - A Chronology, Scientific and Technical Information Office, National Aeronautics and Space Administration, Washington, D.C., Available online at: <http://history.nasa.gov/SP-4011/cover.htm>.
[54] Compton, W. D., and Benson, C. D., 1983, Living and Working in Space - A History of Skylab, Scientific and Technical Information Branch, National Aeronautics and Space Administration, Washington, D.C.
[55] Kitmacher, G., and Maxwell, T. G., 2006, Furthering Exploration - International Space Station Operational Experience, AIAA, AIAA SpaceOps 2006, 19-23 June 2006, Rome, Italy.
[56] DallBaumann, L. A., and Finn, F. E., 1999, "Adsorption processes in spacecraft environmental control and life support systems," Stud. Surf. Sci. Catal., **120**(Part B), pp. 455–471.
[57] Kitmacher, G. H., Gerstenmaier, W. H., and Rosenberg, A., 2004, Space Stations, AIAA 2004-5980, AIAA Space 2004 Conference and Exhibit, 28 - 30 September 2004, San Diego, CA.
[58] Hanford, A. J., Advanced Life Support Research and Technology Development Metric – Fiscal Year 2005, NASA/CR-2006-213694, NASA Johnson Space Center, Houston, TX.
[59] Carrasquillo, R. L., Carter, D. L., Holder, D. W., McGriff, C. F., and Ogle, K. Y., 1991, ECLSS Regenerative Systems Comparative Testing and Subsystem Selection, SAE Technical Paper 911415, 1991, doi: 10.4271/911415, Available online at: <http://www.sae.org/technical/papers/911415>.
[60] Jones, H., and Kliss, M., 2005, Air and Water System (AWS) Design and Technology Selection for the Vision for Space Exploration, SAE 2005-01-2810, 35th International Conference on Environmental Systems, Rome, Italy, July 11-14, 2005.
[61] Lin, C. H., and Meyer, M. S., 1983, "Systems Engineering Aspects of a Preliminary Conceptual Design of the Space Station Environmental Control and Life Support System," SAE Technical Paper 831109, 1983, doi: 10.4271/831109, Available online at: <http://papers.sae.org/831109/>.
[62] NASA Space Station Task Force, 1986, Space Station Program Description Document, System Requirements and Characteristics, Book 3, TM-86652, Available at: http://hdl.handle.net/2060/19840025366.
[63] Wydeven, T., 1988, A Survey of Some Regenerative Physico-Chemical Life Support Technology, NASA Technical Memorandum 101004, NASA Ames Research Center, Moffett Field, CA, 94035.
[64] Mitchell, K., 2004, Past , Present and Future Advanced ECLS Systems for Human Exploration of Space, NASA/CP-2004-213205/VOL1, Strategic Research to Enable NASA's Exploration Mission Conference and Workshop, June 22-23 2004, Cleveland OH, Available from: http://ntrs.nasa.gov/archive/nasa/casi.ntrs.nasa.gov/20040142383.pdf.
[65] United States General Accounting Office, 1994, Space Station - Impact of the Expanded Russian Role on Funding md Research, June 21, 1994, Report to the Ranking Minority Member, Subcommittee on Oversight of Government Management, Committee on Governmental Affairs, U.S. Senate, Available from: http://www.gao.gov/assets/220/219830.pdf.
[66] Carrasquillo, R. L., Wieland, P. O., and Reuter, J. L., 1996, International Space Station Environmental Control and Life Support System Technology Evolution, SAE Paper 961475, 26th International Conference On Environmental Systems, July 8, 1996, Monterey, CA
[67] Cloud, D., Devin, M., Schneider, S., Roy, R., Bagdigian, R., and Erickson, R., 1999, ISS Oxygen Generation Design Status, SAE 1999-01-2116, 29th International Conference on Environmental Systems, July 12-15, 1999, Denver, Colorado.
[68] NASA, 1998, Space Shuttle Mission STS-89 Press Kit, January 1998, Available from: https://spacepresskit.files.wordpress.com/2012/08/sts-89.pdf

[69] Matty, C. M., 2010, Overview of Carbon Dioxide Control Issues During International Space Station/Space Shuttle Joint Docked Operations, American Institute of Aeronautics and Astronautics, AIAA 2010-6251, 40th International Conference on Environmental Systems, 11-15 July 2010, Barcelona, Spain.
[70] Reuter, J. L., and Reysa, R., 2001, "International Space Station Environmental Control and Life Support System Status: 2000–2001," SAE 2001-01-2386, 31st International Conference on Environmental Systems, Orlando, FL, July 9-12, 2001, Available online at: <http://papers.sae.org/2001-01-2386/>.
[71] Reysa, R. P., Lumpkin, J. P., Sherif, D. E., Kay, R., and Williams, D. E., 2007, International Space Station (ISS) Carbon Dioxide Removal Assembly (CDRA) Desiccant/Adsorbent Bed (DAB) Orbital Replacement Unit (ORU) Redesign, SAE 2007-01-3181, 37th International Conference on Environmental Systems (ICES), July 9-12, 2007, Chicago, Illinois.
[72] Gentry, G. J., and Cover, J., 2015, International Space Station (ISS) Environmental Control and Life Support (ECLS) System Overview of Events: 2010 - 2014, ICES-2015-155, 45th International Conference on Environmental Systems, 12-16 July 2015, Bellevue, WA.
[73] Takada, K. C., Ghariani, A. E., and Van Keuren, S., 2015, Advancing the Oxygen Generation Assembly Design to Increase Reliability and Reduce Costs for a Future Long Duration Mission, ICES-2015-115, 45th International Conference on Environmental Systems, 12-16 July 2015, Bellevue, WA.
[74] Carpenter, J. E., Gentry, G. J., Diderich, G. S., Roy, R. J., Golden, J. L., VanKeuren, S. P., Steele, J. W., Rector, T. J., Varsik, J. D., Montefusco, D. J., Cole, H. E., Wilson, M. E., and Worthy, E. S., 2012, Investigation into the High-Voltage Shutdown of the Oxygen Generation System Aboard the International Space Station, AIAA 2012-3613, 42nd International Conference on Environmental Systems, 15 - 19 July 2012, San Diego, CA.
[75] Bagdigian, R. M., Dake, J. R., Gentry, G. J., and Gault, M., 2015, International Space Station Environmental Control and Life Support System Mass and Crewtime Utilization In Comparison to a Long Duration Human Space Exploration Mission, ICES-2015-094, 45th International Conference on Environmental Systems, 12-16 July 2015, Bellevue, WA.
[76] Carter, L., Pruitt, J., Brown, C., Schaezler, R., and Bankers, L., 2015, Status of ISS Water Management and Recovery, ICES-2015-073, 45th International Conference on Environmental Systems, 12-16 July 2015, Bellevue, WA.
[77] Carter, L., Bowman, E. M., Wilson, M., Gentry, G. J., and Rector, T. J., 2013, Investigation of DMSD Trend in the ISS Water Processor Assembly, AIAA 2013-3510, 43rd International Conference on Environmental Systems, July 14-18 2013, Vail, CO.
[78] Carter, L., Perry, J., Kayatin, M. J., Wilson, M., Gentry, G. J., Bowman, E., Monje, O., Rector, T., and Steele, J., 2015, Process Development for Removal of Siloxanes from ISS Atmosphere, ICES-2015-074, 45th International Conference on Environmental Systems, 12-16 July 2015, Bellevue, WA.
[79] Carter, L., 2010, Status of the Regenerative ECLS Water Recovery System, AIAA 2010-6216, 40th International Conference on Environmental Systems, 11-15 July 2010, Barcelona, Spain.
[80] Cirillo, W., Goodliff, K., Aaseng, G., Stromgren, C., and Maxwell, A., 2011, Supportability for Beyond Low Earth Orbit Missions, AIAA 2011-7231, AIAA Space 2011 Conference and Exposition, September 27-29, 2011, Long Beach, CA, Available online at: <http://arc.aiaa.org/doi/abs/10.2514/6.2011-7231>.
[81] NASA, 2009, "STS-129: Stocking the Station," nasa.gov [Online]. Available online at: http://www.nasa.gov/mission_pages/shuttle/shuttlemissions/sts129/overview.html. [Accessed: 27-Apr-2016]
[82] NASA, 1969, Proceedings of the Seventh Annual Working Group on Extraterrestrial Resources, NASA SP-229, Office of Technology Utilization, NASA Headquarters, Washington D.C., Available from: http://ntrs.nasa.gov/archive/nasa/casi.ntrs.nasa.gov/19700029960.pdf
[83] Drake, B. G., 2009, Human Exploration of Mars Design Reference Architecture 5.0 Addendum, NASA/SP-2009-566-ADD, July 2009, Mars Architecture Steering Group, NASA Headquarters, Available from: http://www.nasa.gov/pdf/373667main_NASA-SP-2009-566-ADD.pdf

[84] Sanders, G., Trevathan, J., Peters, T., Baird, R., Larson, W., Lueck, D., and Parrish, C., 2000, Preparing For Robotic & Human Exploration Missions Which Incorporate In-Situ Resource Utilization, AIAA 2000-5317, Space 2000 Conference and Exhibit, 19-21 September 2000, Long Beach, CA, Available online at: <http://arc.aiaa.org/doi/10.2514/6.2000-5317>.

[85] Kaplan, D. I., Ratliff, J. E., Baird, R. S., Sanders, G. B., Johnson, K. R., Karlmann, P. B., Baraona, C. R., Landis, G. A., Jenkins, P. P., and Scheiman, D. A., 2001, The Mars In-Situ-Propellant-Production Precursor (MIP) Flight Demonstration, Paper 2503, Workshop on Mars 2001: Integrated Science in Preparation for Sample Return and Human Exploration, October 2-4, 1999, Houston, TX, Available from: http://www.lpi.usra.edu/meetings/marsmiss99/pdf/2503.pdf

[86] Sanders, G. B., and Larson, W. E., 2015, "Final review of analog field campaigns for In Situ Resource Utilization technology and capability maturation," Adv. Sp. Res., **55**(10), pp. 2381–2404.

[87] Clark, D. L., Patterson, R. R., and Wurts, D. W., 2009, A Novel Approach to Planetary Regolith Collection: the Bucket Drum Soil Excavator, AIAA 2009-6430, AIAA Space 2009 Conference & Exposition, 14-17 September 2009, Pasadena, CA, Available online at: <http://arc.aiaa.org/doi/pdf/10.2514/6.2009-6430>.

[88] Greer, L. C., Krasowski, M. J., Prokop, N. F., and Spina, D. C., 2013, Cratos : The Evolution of a Robotic Vehicle, February 2013, NASA/TM-2013-216491, Available from: http://ntrs.nasa.gov/archive/nasa/casi.ntrs.nasa.gov/20130010983.pdf.

[89] Boucher, D. S., Atwell, J. T., Theiss, R., Armsotrong, R., and Benigni, S., 2011, Development and Testing Of An Autonomous Regolith Excavation and Delivery System, AIAA 2011-431, 49th AIAA Aerospace Sciences Meeting including the New Horizons Forum and Aerospace Exposition, 4-7 January 2011, Orlando, FL.

[90] Gustafson, R. J., White, B. C., and Fidler, M. J., 2011, 2010 Field Demonstration of the Solar Carbothermal Regolith Reduction Process to Produce Oxygen, AIAA 2011-431, 49th AIAA Aerospace Sciences Meeting including the New Horizons Forum and Aerospace Exposition, 4-7 January 2011, Orlando, FL.

[91] Loftin, K., Captain, J., Griffin, T., Kidd, R., Niedholdt, E., Kibelka, G., and Wright, K., 2013, Integration and Ruggedization of a Commercially Available Gas Chromatograph and Mass Spectrometer (GCMS) for the Resource Prospector Mission (RPM), 9th Workshop on Harsh-Environment Mass Spectrometry (HEMS), September 15-18 2013, St. Pete Beach, FL.

[92] NASA Advanced Exploration Systems, 2015, "Resource Prospector" [Online]. Available online at: https://www.nasa.gov/resource-prospector. [Accessed: 21-Nov-2015]

[93] Shiro, B., 2012, "Roving for resources on an analog Moon," astronautsforhire.com [Online]. Available online at: http://www.astronautforhire.com/2012/07/roving-for-resources-on-analog-moon.html. [Accessed: 29-Apr-2016]

[94] Sanders, G. B., Paz, A., Oryshchyn, L., Araghi, K., Muscatello, A. C., Linne, D. L., Kleinhenz, J. E., and Peters, T., 2015, Mars ISRU for Production of Mission Critical Consumables – Options, Recent Studies, and Current State of the Art, AIAA 2015-4458, AIAA Space 2015 Conference and Exposition, August 31 - Septemeber 2, 2015, Pasadena, CA.

[95] Interbartolo III, M. A., Sanders, G. B., Oryshchyn, L., Lee, K., Vaccaro, H., Santiago-Maldonado, E., and Muscatello, A. C., 2013, "Prototype Development of an Integrated Mars Atmosphere and Soil-Processing System," J. Aerosp. Eng., **26**(January), pp. 57–66.

[96] Rapp, D., Hoffman, J. A., Meyen, F., and Hecht, M. H., 2015, The Mars Oxygen ISRU Experiment (MOXIE) on the Mars 2020 Rover, AIAA 2015-4561, AIAA Space 2015 Conference and Exposition, August 31 - Septemeber 2, 2015, Pasadena, CA.

[97] NASA Headquarters, The Vision for Space Exploration, NASA Headquarters, February 2004, Washington DC, Available from: http://www.nasa.gov/pdf/55583main_vision_space_exploration2.pdf.

[98] Green, J. L., and Watson, J. K., 2008, Supportability and Operability Planning for Lunar Missions, AIAA 2008-7779, AIAA Space 2008 Conference and Exposition, 9-11 September 2008, San Diego, CA.

[99] Cirillo, W., Earle, K., Goodliff, K., Reeves, J. D., Andraschko, M., Merrill, R. G., and Stromgren,

C., Analysis of Logistics in Support of a Human Lunar Outpost, The Internatioal Workshop on Modeling and Applied Simulation, September 2008, Available from: http://ntrs.nasa.gov/archive/nasa/casi.ntrs.nasa.gov/20080042297.pdf
[100] Stromgren, C., Terry, M., Mattfield, B., Cirillo, W., Goodliff, K., Shyface, H., and Maxwell, A., Assessment of Maintainability for Future Human Asteroid and Mars Missions, AIAA 2013-5328, AIAA Space 2013 Conference and Exposition, September 10-12, 2013, San Diego, CA.
[101] Lange, K. E., and Anderson, M. S., 2012, Reliability Impacts in Life Support Architecture and Technology Selection, AIAA, AIAA 2012-3491, 42nd International Conference on Environmental Systems 15 - 19 July 2012, San Diego, CA.
[102] Jones, H. W., 2012, Design and Analysis of a Flexible, Reliable Deep Space Life Support System, AIAA, AIAA 2012-3418, 42nd International Conference on Environmental Systems, 15-19 July 2012, San Diego, CA.
[103] Agte, J., Borer, N., and de Weck, O., 2012, "Design of Long-Endurance Systems with Inherent Robustness to Partial Failures During Operations," J. Mech. Des., **134**(100903).
[104] Mettas, A., 2000, Reliability Allocation and Optimization for Complex Systems, 2000 Proceedings of the Annual Reliability and Maintainability Symposium.
[105] Woldman, M., Tinga, T., Heide, E. Van Der, and Masen, M. A., 2015, "Abrasive wear based predictive maintenance for systems operating in sandy conditions," Wear, **338-339**, pp. 316–324, Available online at: <http://dx.doi.org/10.1016/j.wear.2015.07.004>.
[106] Treichel, T. H., and Gustafson, R. J., 2009, Environmental Testing for the Reliability Effects of Lunar Dust, SAE Technical Paper 2009-01-2378, doi: 10.4271/2009-01-2378.
[107] Wagner, S., 2008, An Assessment of Dust Effects on Planetary Surface Systems to Support Exploration Requirements, NASA/TM-2008-213722, NASA Johnson Space Center, Houston, TX.
[108] Logsdon, J., 2013, John F. Kennedy and the Race to the Moon, Palgrave Macmillan.
[109] Seamans, Jr., R. C., 2007, Project Apollo - The Tough Decisions, Monographs in Aerosapce History No. 37, NASA SP2007-4537, NASA Office of External Relations, History Divisoin, Washington, DC.
[110] Howe, A. S., and Sherwood, B., 2009, Out Of This World : The New Field of Space Architecture, American Institute of Aeronautics and Astronautics, Reston, VA.
[111] Simon, M., Whitmire, A., Otto, C., and Neubek, D., 2011, Factors Impacting Habitable Volume Requirements: Results from the 2011 Habitable Volume Workshop, NASA Scientific and Technical Information Program Office, April 18-21, 2011, Center for Advanced Space Studies - Universities Space Research Association, Houston, TX, NASA/TM-2011-217352.
[112] Campbell, P. D., 2006, Recommendations for Exploration Spacecraft Internal Atmospheres - The Final Report of the NASA Exploration Atmospheres Working Group, JSC-63309, NASA Lyndon B. Johnson Space Center, Houston, Texas 77058.
[113] Tullis, T. S., 1988, Space Station Functional Relationships Analsysis Final Report, NASA_CR-177497, Contract NAS2-11723, NASA Ames Research Center, Moffett Field, CA.
[114] Tito, D. A., Anderson, G., Carrico, J. P., Clark, J., Finger, B., Lantz, G. A., Loucks, M. E., MacCallum, T., Poynter, J., Squire, T. H., and Worden, S. P., 2013, "Feasibility analysis for a manned mars free-return mission in 2018," 2013 IEEE Aerospace Conference, IEEE, pp. 1–18, Available online at: <http://ieeexplore.ieee.org/lpdocs/epic03/wrapper.htm?arnumber=6497413>.
[115] Gibson, D. C., Wildsmith, E., Schneller, A., Garcia, K., and Sawadya, J., 2009, The Significance of Outer Space Hotels in Development of the Space Tourism Industry, AIAA 2009-6579, AIAA Space 2009 Conference & Exposition, 14-17 September 2009, Pasadena, CA.
[116] Taylor, T. C., Overman, A., Gimarc, A., Pittman, B., Spencer, J., and Meyers, G., 2005, Affordable Commercial Space Tourism Infrastructure, AIAA 2005-3621, 41st AIAA/ASME/SAE/ASEE Joint Propulsion Conference & Exhibit, 10-13 July 2005, Tucson, AZ.
[117] Bigelow Aerospace, 2015, "Bigelow Aerospace" [Online]. Available online at: http://www.bigelowaerospace.com. [Accessed: 28-Jul-2015]
[118] Filburn, T., Malla, R. B., Smith, J. K., Brown, K., Clark, A., and Genovese, J., 2011, "An

Investigation into Life Support Systems for a Lunar Habitat," AIAA 2011-5040, 41st International Conference on Environmental Systems, 17-21 July 2011, Portland, Oregon
[119] Do, S., Weck, O. De, Pellicciotti, J., Brady, T., Introduction, I., Station, I. S., Student, U., Systems, M., and Engineering, S., 2009, "An Airbag-Based Crew Impact Attenuation System Concept for the Orion CEV – First Generation System Development," AIAA 2009-6438, AIAA Space 2009 Conference & Exposition, 14-17 Sept. 2009, Pasadena, CA.
[120] Metcalf, J., Motil, B., and Bagdigian, B., 2011, NASA Environmental Control and Life Support (ECLS) Integrated Roadmap Development, NASA, NASA Johnson Space Center, Houston, TX, 77058.
[121] Callahan, M., Patel, V., and Pickering, K., 2010, "Cascade Distillation Subsystem Development: Early Results From the Exploration Life Support Distillation Technology Comparison Test," AIAA 2010-6149, 40th International Conference on Environmental Systems, Available online at: <http://arc.aiaa.org/doi/abs/10.2514/6.2010-6149>.
[122] Suh, E. S., Furst, M. R., Mihalyov, K. J., and Weck, O. De, 2010, "Technology infusion for complex systems: A framework and case study," Syst. Eng., **13**(2), pp. 186–203, Available online at: <http://doi.wiley.com/10.1002/sys.20142>.
[123] Drysdale, A., 2006, "Recommendations for Clothing Systems for Advanced Missions Environmental Systems (ICES)," SAE 2006-01-2248, 36th International Conference on Environmental Systems, July 17-20, 2006, Norfolk, VA
[124] Dori, D., 2002, Object-Process Methodology, Springer, New York.
[125] De Weck, O. L., Roos, D., and Magee, C. L., 2011, Engineering Systems - Meeting Human Needs in a Complex Technological World, MIT Press, Cambridge, MA, Available online at: <http://www.knovel.com.libproxy.mit.edu/web/portal/browse/display?_EXT_KNOVEL_DISPLA_bookid=4611>.
[126] Kortenkamp, D., and Bell, S., 2003, BioSim: An Integrated Simulation of an Advanced Life Support System for Intelligent Control Research Users Manual (draft), Metrica Inc. and S&K Technologies, NASA Johnson Space Center/ER2, Houston, TX 77058, Obtained from: http://svn.traclabs.com/biosim/documentation.html>
[127] McGlothlin, E. P., Yeh, H. Y., and Lin, C. H., 1999, Development of the ECLSS Sizing Analysis Tool and ARS Mass Balance Model Using Microsoft Excel, SAE 1999-01-2080, 29th International Conference on Environmental Systems Denver, Colorado July 12-15, 1999.
[128] Swickrath, M. J., Anderson, M. S., and Bagdigian, B. M., 2011, Parametric Analysis of Life Support Systems for Future Space Exploration Missions, AIAA 2011-5039, 41st International Conference on Environmental Systems, 17 - 21 July 2011, Portland, OR.
[129] Pérez-vara, R., Mannu, S., Müller, R., and Gmbh, A., 2003, Overview of European Applications of EcosimPro to ECLSS, CELSS, and ATCS, SAE 2003-01-2439, 33rd International Conference on Environmental Systems (ICES), July 7-10, 2003, Vancouver, B.C., Canada.
[130] Cobas-Herrero, P., Garcia-Gutierrez, B., Perez-Vara, R., Avezuela-Rodriguez, R., and Gregoi-de la Malla, C., 2006, An ESA State-of-the-Art Simulation Tool for Space Applications, 9th International Workshop on Simulation for European Space Programmes, SESP 2006, 6-8 November 2006, ESTEC, Noordwijk, the Netherlands, Available online at: <http://www.ecosimpro.com/download/articles/SESP_2006_01_en.pdf>.
[131] Kortenkamp, D., and Bell, S., 2003, Simulating Advanced Life Support Systems for Integrated Controls Research, Society of Automotive Engineers International, SAE 2003-01-2546, 33rd International Conference on Environmental Systems, July 7 - 10, 2003, Vancouver, B.C., Canada.
[132] Czupalla, M., Zhukov, A., Schnaitmann, J., Bickel, T., and Walter, U., 2010, The Virtual Habitat – A Tool for Dynamic Life Support System Simulations, AIAA 2010-6016, 40th International Conference on Environmental Systems, 11-15 July 2010, Barcelona, Spain.
[133] Personal Communication with Class Olthoff of the Technical University of Munich - April 16, 2013.
[134] Osburg, J., 2002, "An Interdisciplinary Approach to the Conceptual Design of Inhabited Space Systems", PhD Dissertation, Institute of Space Systems, University of Stuttgart
[135] Detrell, G., Ganzer, B., and Messerschmid, E., 2011, "Adaptation of the ELISSA Simulation Tool

for Reliability Analysis", AIAA 2011-5279, 41st International Conference on Environmental Systems, 17-21 July 2011, Portland, Oregon.
[136] Osburg, J., Bertrand, R., and Messerschmid, E., 1998, "MELISSA - A Graphical Environment for Life-Support Systems Simulation", SAE 981754, 28th International Conference on Environmental Systems, July 13-16, 1998, Danvers, MA.
[137] Personal Communication with Emil Nathanson of the University of Stuttgart - March 25, 2013.
[138] Goudarzi, S., and Ting, K. C., 1999, "Top Level Modeling of Crew Component of ALSS", SAE 1999-01-2042, 29th International Conference on Environmental Systems Denver, Colorado July 12-15, 1999.
[139] NASA HQ, 2010, NASA Human Integration Design Handbook (HIDH) - NASA/SP-2010-3407, Washington D.C.
[140] NASA JSC, 2006, Recommendations for Exploration Spacecraft Internal Atmospheres - The Final Report of the NASA Exploration Atmospheres Working Group (EAWG) - JSC-63309, Houston, TX.
[141] Gerhart, L. M., and Ward, J. K., 2010, "Tansley Reviews: Plant responses to low [CO2] of the past," New Phytol., **188**, pp. 674–695.
[142] Dippery, J. K., Tissue, D. T., Thomas, R. B., and Strain, B. R., 1995, "Effects of low and elevated CO2 on C3 and C4 annuals - I. Growth and biomass allocation," Oecologia, (101), pp. 13–20.
[143] Do, S., Owens, A., Ho, K., Schreiner, S., and De Weck, O., 2016, "An independent assessment of the technical feasibility of the Mars One mission plan - Updated analysis," Acta Astronaut., **120**, pp. 192–228.
[144] Schrenk, L., 2015, "Development of an In-Situ Resource Utilization (ISRU) Module for the Mission Analysis Environment HabNet", Master's Dissertation, Technical University of Munich.
[145] NASA, "The Topography of Mars by the Mars Orbiter Laser Altimeter (MOLA)" [Online]. Available at: http://mola.gsfc.nasa.gov/images/mercat_med.jpg [Accessed: 26-Nov-2015]
[146] Mellon, M. T., Feldman, W. C., and Prettyman, T. H., 2004, "The presence and stability of ground ice in the southern hemisphere of Mars," Icarus, **169**(2), pp. 324–340.
[147] Grott, M., Helbert, J., and Nadalini, R., 2007, "Thermal structure of Martian soil and the measurability of the planetary heat flow," J. Geophys. Res., **112**(9), pp. 1–10.
[148] Mitrofanov, I., Boynton, W., Demidov, N., Hamara, D., Kozyrev, A., Litvak, M., Sanin, A., and Shinohara, C., 2009, Distribution of standard regolith and water at moderate latitudes of Mars: data analysis from GRS and HEND instruments on Mars Odyssey, European Planetary Science Conference (EPSC) 2009, 13-18 September 2009, Potsdam, Germany, Available online at: <http://adsabs.harvard.edu/abs/2010LPI....41.2174M>.
[149] Maurice, S., Feldman, W., Diez, B., Gasnault, O., Lawrence, D. J., Pathare, A., and Prettyman, T., 2011, "Mars Odyssey neutron data: 1. Data processing and models of water-equivalent-hydrogen distribution," J. Geophys. Res. E Planets, **116**(11), pp. 1–41.
[150] Feldman, W. C., Pathare, A., Maurice, S., Prettyman, T. H., Lawrence, D. J., Milliken, R. E., and Travis, B. J., 2011, "Mars Odyssey neutron data: 2. Search for buried excess water ice deposits at nonpolar latitudes on Mars," J. Geophys. Res. E Planets, **116**(11), pp. 1–17.
[151] Muscatello, A. C., and Santiago-Maldonado, E., 2012, "Mars In Situ Resource Utilization technology evaluation", AIAA 2012-0360, 50th AIAA Aerospace Sciences Meeting Including the New Horizons Forum and Aerospace Exposition, 9-12 January 2012, Nashville, TN, Available online at: <http://www.scopus.com/inward/record.url?eid=2-s2.0-84872833348&partnerID=40&md5=79487955a964122bd5dc3f38b1b857fe>.
[152] Owens, A. C., 2014, "Quantitative Probabilistic Modeling of Environmental Control and Life Support System Resilience for Long-Duration Human Spaceflight", Master's Dissertation, Department of Aeronautics and Astronautics, Massachusetts Institute of Technology.
[153] Owens, A. C., de Weck, O. L., Mattfield, B., Stromgren, C., and Cirillo, W., 2015, Comparison of Spares Logistics Analysis Techniques for Long Duration Human Spaceflight, ICES-2015-288, 45th International Conference on Environmental Systems, 12-16 July 2015, Bellevue, Washington.
[154] Kline, M., 1984, "Suitability of the lognormal distribution for corrective maintenance repair

times," Reliab. Eng., **9** (July 1983), pp. 65–80, Available online at: <http://www.sciencedirect.com/science/article/pii/0143817484900416>.
[155] Jones, H., 2010, "Life Support Dependability for Distant Space Missions", AIAA 2010-6287, 40th International Conference on Environmental Systems, July 11-15 2010, Barcelona, Spain, Available online at: <http://arc.aiaa.org/doi/abs/10.2514/6.2010-6287>.
[156] Kortenkamp, D., Bell, S., and Rodriguez, L., 2005, Simulating Lunar Habitats and Activities to Derive System Requirements, AIAA 2005-2708, 1st Space Exploration Conference: Continuing the Voyage of Discovery, January 30 - February 1, 2005, Orlando, FL, Available online at: <http://dx.doi.org/10.2514/6.2005-2708>.
[157] Jiang, H., Rodriguez, L. F., Bell, S., Kortenkamp, D., and Capristan, F. M., 2011, "Prediction of Reliability for Environmental Control and Life Support Systems," J. Spacecr. Rockets, **48**(2), pp. 336–345, Available online at: <http://arc.aiaa.org/doi/abs/10.2514/1.44792>.
[158] Diep, V., 2015, ISS Live! Data Stream Client, ISS Live! Data Stream Client developed by Vivian Diep (MIT Media Lab) in support of Sydney Do's HabNet Validation Analyses.
[159] Gebhardt, C., 2011, "ISS Live to integrate public with orbital ops and science" [Online]. Available online at: http://www.nasaspaceflight.com/2011/10/iss-liveintegrate-public-orbital-ops-science/. [Accessed: 05-Mar-2016]
[160] NASA, 2016, "ISS Live! Console Displays" [Online]. Available online at: http://isslive.com/displays/ [Accessed: 29-Feb-2016]
[161] syntelos, 2015, "Github - syntelos/iss-live-meta" [Online]. Available online at: https://github.com/syntelos/iss-live-meta [Accessed: 19-Jul-2015]
[162] Cosbourn and NASA, 2016, "ISS On-Orbit Status Report" [Online]. Available online at: https://blogs.nasa.gov/stationreport/ [Accessed: 03-Mar-2016]
[163] Garcia, M., 2016, "Scott Kelly Hands Over Station Command to Tim Kopra" [Online]. Available online at: https://blogs.nasa.gov/spacestation/2016/02/29/scott-kelly-hands-over-station-command-to-tim-kopra/ [Accessed: 03-Mar-2016]
[164] Bagdigian, R. M., Cloud, D., and Bedard, J., 2005, Status of the International Space Station Regenerative ECLSS Water Recovery and Oxygen Generation Systems, SAE 2006-01-2057, 36th International Conference on Environmental Systems (ICES) Norfolk, Virginia July 17-20, 2006, Available online at: <http://www.sae.org/technical/papers/2005-01-2779>.
[165] Bonadies, M., 2007, OGS Console Handbook, Hamilton Sundstrand Space Systems International, Report Number PPS WP/OGA-807, Draft Rev B, May 11 2007, Prepared for NASA Marshall Space Flight Center, Huntsville, AL under contract No. NAS8-98053.
[166] Erickson, R. J., Jr, J. H., Kulp, G. W., and Keuren, S. P. Van, 2008, International Space Station United States Orbital Segment Oxygen Generation System On-orbit Operational Experience, SAE 2008-01-1962, 38th International Conference on Environmental Systems, 30 June - 3 July 2008, San Francisco, CA.
[167] ESA blogteam, "Planning Down to the Minute," ESA [Online]. Available online at: http://blogs.esa.int/alexander-gerst/2014/07/02/planning-down-to-the-minute/ [Accessed: 24-Jul-2015]
[168] Samplatsky, D.J.; Grohs, K.; Edeen, M.; Crusan, J.; Burkey, R., 2011, Development and Integration of the Flight Sabatier Assembly on the ISS, AIAA 2011-5151, 41st International Conference on Environmental Systems 17 - 21 July 2011, Portland, Oregon.
[169] Jeng, F. F., Lafuse, S., Smith, F. D., Lu, S., Knox, J. C., Campbell, M. L., Scull, T. D., and Green, S., 2004, Analyses of the Integration of Carbon Dioxide Removal Assembly , Compressor , Accumulator and Sabatier Carbon Dioxide Reduction Assembly, SAE 2004-01-2946, 34th International Conference on Environmental Systems (ICES), July 19-22 2004, Colorado Springs, CO.
[170] Wheeler, R. M., 2006, "Potato and Human Exploration of Space : Some Observations from NASA-Sponsored Controlled Environment Studies," Potato Res., **49**, pp. 67–90.
[171] Wheeler, R. M., Corey, K. A., Sager, J. C., and Knott, W. M., 1993, "Gas Exchange Characteristics of Wheat Stands Grown in a Closed, Controlled Environment," Crop Sci., (33), pp. 161–168.

[172] Wheeler, R. M., Mackowiak, C. L., Sager, J. C., and Knott, W. M., 1994, "Growth of Soybean and Potato at High CO2 Partial Pressures," Adv. Sp. Res., **14**(11), pp. 251–255.
[173] Farquhar, G. D., and von Caemmerer, S., 1982, "Modelling of Photosynthetic Response to Environmental Conditions," Physiological Plant Ecology II, O.L. Lange, P.S. Nobel, C.B. Osmond, and H. Ziegler, eds., Springer-Verlag, New York, pp. 549–587, Available online at: <http://link.springer.com/chapter/10.1007/978-3-642-68150-9_17>.
[174] Wheeler, R. M., Sager, J. C., Prince, R. P., Knott, W. M., Mackowiak, G. W., Stutte, G. W., Yorio, N. C., Ruffe, L. M., Peterson, B. V., Goins, G. D., Hinkle, C. R., and Berry, W. L., 2006, Crop Production for Advanced Life Support Systems - Observations From the Kennedy Space Center Breadboard Project, NASA/TM-2003-211184, NASA Kennedy Space Center, FL.
[175] Nichols, M., "Issue 58: The Next Step... Mars or Bust," Pract. Hydroponics Greenhouses [Online]. Available online at: http://www.hydroponics.com.au/issue-58-the-next-step-mars-or-bust/ [Accessed: 04-Mar-2016]
[176] NASA Johnson Space Center Crew and Thermal Systems Division, 2000, Lunar-Mars Life Support Test Project Phase III Final Report, February 23, 2000, JSC-39144, Report Number: CTSD-ADV-341.
[177] Rajulu, L., and Klute, G. K., 1993, "Anthropometric Survey of the Astronaut Applicants and Astronauts From 1985 to 1991", NASA RP-1304, NASA Johnson Space Center, Houston, TX.
[178] Mudgett, P. D., Schultz, J. R., Cyrus, K. K., Chhipwadia, K. S., and Packham, N. J., 2003, Fluid Containers for Life Support Systems and Payloads, SAE 2003-01-2532, 33rd International Conference on Environmental Systems (ICES), Vancouver, B.C., Canada July 7-10, 2003.
[179] Anderson, M. S., Ewert, M. K., Keener, J. F., and Wagner, S. A., 2015, NASA Life Support Baseline Values and Assumptions Document, NASA/TP-2015-218570, NASA Lyndon B. Johnson Space Center, Houston, TX, Available online at: http://ston.jsc.nasa.gov/collections/TRS/_techrep/TP-2015-218570.pdf
[180] Levri, J. A., Fishel, J. W., Jones, H. W., Ewert, M. K., Drysdale, A. E., Hanford, A. J., Hogan, J. A., Joshi, J. A., and Vaccari, D. A., 2003, Advanced Life Support Equivalent System Mass Guidelines Document, NASA/TM-2003-212278, NASA Ames Research Center, Moffett Field, CA 94035.
[181] Logsdon, J., 2015, After Apollo? Richard Nixon and the American Space Program, Palgrave Macmillan, New York, NY.
[182] The White House National Science and Technology Council, 1993, Fact Sheet - National Space Policy 1996, September 19th 1996, Washington, DC, Available online at: http://history.nasa.gov/appf2.pdf
[183] Spear, T., 2000, NASA Faster Better Cheaper Task Final Report, NASA Headquarters, Washington D.C., Available online at: http://mars.nasa.gov/msp98/misc/fbctask.pdf
[184] Herbert, G. W., 1996, One-Way to Mars, AAS-96-322, The Case for Mars VI: Making Mars an Affordable Destination, Kelly R. McMillen (editor); Proceedings of the Sixth Case for Mars Conference, 17-20 July 1996, Boulder, CO.
[185] Durfee, R., "Purchase a lovely new home on... Mars?," Pop. Sci. [Online]. Available online at: http://www.popsci.com/military-aviation-amp-space/article/2008-10/purchase-lovely-new-home-onmars [Accessed: 14-Mar-2016]
[186] Petrov, G. I., Mackenzie, B., Homnick, M., and Palaia, J., 2005, A Permanent Settlement on Mars: The Architecture of the Mars Homestead Project, SAE 2005-01-2853, 35th International Conference on Environmental Systems, Rome, Italy, July 11-14, 2005, Available online at: <http://papers.sae.org/2005-01-2853/>.
[187] Davies, P., 2004, "Life (and Death) on Mars," New York Times, Available online at: <http://www.nytimes.com/2004/01/15/opinion/life-and-death-on-mars.html>, Date accessed: March 28th, 2016
[188] McLane III, J. C., "'Spirit of the Lone Eagle': An Audacious Program for a Manned Mars Landing," Sp. Rev. [Online]. Available online at: http://www.thespacereview.com/article/669/1. [Accessed: 12-Mar-2016]
[189] Atkinson, N., "A One-Way, One-Person Mission to Mars," Universe Today [Online]. Available

online at: http://www.universetoday.com/13037/a-one-way-one-person-mission-to-mars/ [Accessed: 12-Mar-2016]
[190] Schulze-Makuch, D., and Davies, P., 2010, "To Boldly Go: A One Way Human Mission to Mars," J. Cosmol., **Vol 12**, pp. 3619–3626, Available online at: <http://philpapers.org/rec/MAKTBG>.
[191] Mars One, 2014, Mars One: Roadmap, Original URL: http://www.mars-one.com/mission/roadmap, Date accessed: July 14th, 2014, Archived URL: http://web.archive.org/web/20140714142348/http://www.mars-one.com/mission/roadmap
[192] Lockheed Martin, 2014, Proposal Information Package Mars One 2018 Lander Payload, Denver, CO, Available online at: <http://www.mars-one.com/images/uploads/MarsOne_PIP.pdf>, Date accessed: July 13th, 2014
[193] Mars One, 2014, Mars One: Technical Feasibility, Original URL: http://www.mars-one.com/mission/technical-feasibility, Date accessed: August 6th, 2014, Archived URL: http://web.archive.org/web/20140806004257/http://www.mars-one.com/mission/technical-feasibility
[194] 2013, "Dragon," Space Exploration Technologies Corporation [Online]. Available online at: <http://www.spacex.com/dragon>, Date accessed: June 4th 2014
[195] Taylor, A., "This Incredible Plan For A Mission To Mars In 2023 Is No Hoax," Bus. Insid. [Online]. Available online at: <http://www.businessinsider.com/mars-one-hoax-bas-landorp-2023-2012-6>, Date accessed: June 4th 2014
[196] Mars One, 2014, Mars One Living Unit, Original URL: http://www.mars-one.com/technology/living-unit, Date accessed: July 15th, 2014, Archived URL: http://web.archive.org/web/20140715052304/http://www.mars-one.com/technology/living-unit,
[197] Mars One, 2014, Mars One - Will the astronauts have enough water, food and oxygen?, Original URL: http://www.mars-one.com/faq/health-and-ethics/will-the-astronauts-have-enough-water-food-and-oxygen, Date accessed: July 8th, 2014, Archived URL: http://web.archive.org/web/20140708053539/http://www.mars-one.com/faq/health-and-ethics/will-the-astronauts-have-enough-water-food-and-oxygen
[198] Mars One, 2014, Mars One: Life Support Unit, Original URL: http://www.mars-one.com/technology/life-support-unit, Date accessed: July 16th, 2014, Archived URL: http://web.archive.org/web/20140716152758/http://www.mars-one.com/technology/life-support-unit
[199] NASA, 2007, NASA Systems Engineering Handbook, National Aeronautics and Space Administration, NASA/SP-2007-6105 Rev1, NASA Headquarters, Washington, D.C.
[200] Mars One, 2014, Mars One - What will the astronauts do on Mars?, Original URL: http://www.mars-one.com/faq/mission-to-mars/what-will-the-astronauts-do-on-mars, Date accessed: July 8th, 2014, Archived URL: http://web.archive.org/web/20140708062415/http://www.mars-one.com/faq/mission-to-mars/what-will-the-astronauts-do-on-mars
[201] Mars One, 2014, Mars One - How much living space will the astronauts have?, Original URL: http://www.mars-one.com/faq/health-and-ethics/how-much-living-space-will-the-astronauts-have, Date accessed: July 14th, 2014, Archived URL: http://web.archive.org/web/20140714125817/http://www.mars-one.com/faq/health-and-ethics/how-much-living-space-will-the-astronauts-have
[202] Interbartolo III, M. A., Sanders, G. B., Oryshchyn, L., Lee, K., Vaccaro, H., Santiago-Maldonado, E., and Muscatello, A. C., 2012, "Prototype Development of an Integrated Mars Atmosphere and Soil-Processing System," J. Aerosp. Eng., **26**(1), pp. 57–66.
[203] de zeen magazine, 2013, "Over 200,000 people apply to live on Mars" [Online]. Available online at: <http://www.dezeen.com/2013/09/11/over-200000-people-apply-to-live-on-mars/>. Date accessed: June 4th 2014
[204] Witt, J., Bockstahler, K., Matthias, C., Lucas, J., Laurini, D., and Hovland, S., 2015, Status of the Advanced Closed Loop System ACLS, ICES-2015-93, 45th International Conference on Environmental Systems, 12-16 July 2015, Bellevue, Washington.

[205] Sakurai, M., Shima, A., Sone, Y., Ohnishi, M., Tachihara, S., and Ito, T., 2014, Development of Oxygen Generation Demonstration on JEM (KIBO) for Manned Space Exploration, ICES-2014-125, 44th International Conference on Environmental Systems, 13-17 July 2014, Tucson, Arizona.
[206] Shima, A., Sakurai, M., Sone, Y., Ohnishi, M., and Abe, T., 2012, Development of a CO2 Reduction Catalyst for the Sabatier Reaction, AIAA 2012-3552, 42nd International Conference on Environmental Systems 15 - 19 July 2012, San Diego, California.
[207] Lane, H. W., Sauer, R. L., and Feeback, D. L., "Isolation: NASA Experiments in Closed-Environment Living - Advanced Human Life Support Enclosed System," Am. Astronaut. Soc. - Sci. Technol. Ser., **104**, Available online at: <https://lsda.jsc.nasa.gov/books/ground/chambers.pdf>.
[208] Stilwell, D., Boutros, R., and Connolly, J. H., 2000, "Crew Accommodations," Human Spaceflight Mission Analysis and Design, W.J. Larson, and L.K. Pranke, eds., McGraw-Hill Higher Education.
[209] Hanford, A. J., 2004, Advanced Life Support Baseline Values and Assumptions Document (CTSD-ADV-484A), JSC 47804, NASA Lyndon B. Johnson Space Center, Houston, TX, Available online at: http://ston.jsc.nasa.gov/collections/trs/_techrep/CR-2004-208941.pdf
[210] Cadogan, D., and Scheir, C., 2008, "Expandable Habitat Technology Demonstration for Lunar and Antarctic Applications," (724), pp. 776–790, Available online at: <http://papers.sae.org/2008-01-2024/>.
[211] Jones, H., 2000, Matching Crew Diet and Crop Food Production in BIO-Plex, SAE 2000-01-2397, 30th International Conference on Environmental Systems Toulouse, France July 10-13, 2000.
[212] Tri, T. O., 1999, "Bioregenerative Planetary Life Support Systems Test Complex (BIO-Plex): Test Mission Objectives and Facility Development," SAE 1999-01-2186, 29th International Conference on Environmental Systems, July 12-15 1999, Denver, CO
[213] Heliospectra, 2014, "LX Series Tech Specs" [Online]. Available online at: <http://www.heliospectra.com/led_grow_light_products#lx-techspecs>. Date accessed: June 15th 2014
[214] Wheeler, R. M., Mackowiak, C. L., Peterson, B. V, Sager, J. C., Knott, W. M., Berry, W. l., and Sharifi, M. R., 1998, A Data Base of Nutrient Use, Water Use , CO2 Exchange, and Ethylene Production by Soybeans in a Controlled Environment, NASA/TM-1998-270903, NASA Biomedical Office and Dynamac Corporation, Kennedy Space Center, FL 32899, Available online at: <http://hdl.handle.net/2060/19980137405>.
[215] Gitelson, I. I., Lisovsky, G. M., and MacElroy, R. D., 2003, Manmade Closed Ecological Systems, Taylor & Francis, London ; New York;
[216] Wheeler, R. M., 2003, "Carbon Balance in Bioregenerative Life Support Systems: Some Effects of System Closure, Waste Management, and Crop Harvest Index," Adv. Sp. Res., **31**(1), pp. 169–175.
[217] Rapp, D., Andringa, J., Easter, R., Smith, J. H., Wilson, T. J., Clark, D. L., and Payne, K., 2005, "Preliminary system analysis of in situ resource utilization for Mars human exploration," 2005 IEEE Aerosp. Conf.
[218] Perchonok, M., 2008, "The Challenges of Developing a Food System for a Mars Mission," NASA Tech. Reports Serv. [Online]. Available online at: <http://hdl.handle.net/2060/20080012587>.
[219] Toerne, M., Swango, B., Byford, I., and Perchonok, M., 2001, Food Processing Systems For Long-Term Planetary Missions: The Design of A Prototype for Soy Processing, SAE 2001-01-2322, 31st International Conference on Environmental Systems, Orlando, FL, July 9-12, 2001, Available online at: <http://www.sae.org/technical/papers/2001-01-2322>.
[220] Hendrickx, L., De Wever, H., Hermans, V., Mastroleo, F., Morin, N., Wilmotte, A., Janssen, P., and Mergeay, M., 2006, "Microbial ecology of the closed artificial ecosystem MELiSSA (Micro-Ecological Life Support System Alternative): Reinventing and compartmentalizing the Earth's food and oxygen regeneration system for long-haul space exploration missions," Res. Microbiol., **157**(1), pp. 77–86.
[221] Nelson, M., Finn, M., Wilson, C., Zabel, B., Van Thillo, M., Hawes, P., and Fernandez, R., 1999,

"Bioregenerative recycling of wastewater in Biosphere 2 using a constructed wetland: 2-Year results," Ecol. Eng., **13**(1-4), pp. 189–197.
[222] National Water Research Institute, 2012, Review of California's Water Recycling Criteria for Agricultural Irrigation, Prepared for: California Department of Public Health, Available at: http://nwri-usa.org/cdph.ag.htm, Date Accessed: August 3rd, 2015.
[223] Tako, Y., Arai, R., Tsuga, S., Komatsubara, O., Masuda, T., Nozoe, S., and Nitta, K., 2010, "CEEF: Closed Ecology Experiment Facilities," Gravitational Sp. Biol., **23**(2), pp. 13–24, Available online at: <http://gravitationalandspacebiology.org/index.php/journal/article/view/489/483>.
[224] Mars One, What are the risks of dust and sand on Mars?, Original URL: http://www.mars-one.com/faq/mission-to-mars/what-are-the-risks-of-dust-and-sand-on-mars, Date Accessed: July 16th, 2014, Archived URL: http://web.archive.org/web/20140716161002/http://www.mars-one.com/faq/mission-to-mars/what-are-the-risks-of-dust-and-sand-on-mars
[225] Leshin, L. A., Mahaffy, P. R., Webster, C. R., Cabane, M., Coll, P., Conrad, P. G., Archer, P. D., Atreya, S. K., Brunner, A. E., Buch, A., and others, 2013, "Volatile, isotope, and organic analysis of martian fines with the Mars Curiosity rover," Science, 27 September 2013, Vol. 341, Issue 6153, DOI: 10.1126/science.1238937
[226] Rapp, D., 2013, "Mars ISRU Technology" in "Use of Extraterrestrial Resources for Human Space Missions to Moon or Mars", Springer, pp. 31–90.
[227] Sanders, G. B., and Kaplan, D. I., 1998, Mars ISPP Precursor (MIP): The First Flight Demonstration of In-Situ Propellant Production, AIAA 1998-3306, 34th AIAA/ASME/SAE/ASEE Joint Propulsion Conference and Exhibit, 13-15 July 1998, Cleveland OH, http://dx.doi.org/10.2514/6.1998-3306
[228] Muscatello, A. C., 2012, Mars In Situ Resource Utilization Technology Evaluation, AIAA 2012-360, 50th AIAA Aerospace Sciences Meeting including the New Horizons Forum and Aerospace Exposition, 9-12 January 2012, Nashville, TN, http://dx.doi.org/10.2514/6.2012-360
[229] Landis, G. A., Cunio, P., Ishimatsu, T., Keller, J., Khan, Z., and Odegard, R., 2007, Mars Sample Return with ISRU, 7th International Conference on Mars, Pasadena CA, July 9-13 2007.
[230] PP&S Inc., 2002, "DVJ Dimension Table," Roots Dresser Rotary Posit. Blowers Exhausters [Online]. Available online at: <http://www.pp-s.com/Files/Dresser Roots/All about Roots.pdf>, Date Accessed: May 19th 2014
[231] Henley, E. J., Seader, J. D., and Roper, D. K., 2011, Separation Process Principles, Wiley, ISBN-13: 978-0470481837.
[232] Shekhawat, D., Luebke, D. R., and Pennline, H. W., 2003, "A review of carbon dioxide selective membranes," US Dep. Energy. Report Number: DOE/NETL-2003/1200, Available online at: http://www.osti.gov/scitech/servlets/purl/819990
[233] CryoTel 2014, "CryoTel GT Specification Sheet," SunPower - CryoTel GT 16W Cryocooler, Available online at: http://sunpowerinc.com/cryocoolers/cryotel-family/gt/, Data Accessed: July 21st 2014
[234] Holladay, J. D., Brooks, K. P., Humble, P., Hu, J., and Simon, T. M., 2008, "Compact Reverse Water-Gas-Shift Reactor for Extraterrestrial ISRU," J. Propuls. Power, **24**(3), pp. 578–582.
[235] Wertz, J. R., Everett, D. F., and Puschell, J. J., eds., 2011, Space Mission Engineering: The New SMAD, Microcosm, Hawthorne.
[236] Wieland, P. O., 1998, "Living Together in Space : The Design and Operation of the Life Support Systems on the International Space Station,", NASA/TM-1998-206956/VOL1, NASA Marschall Space Flight Center, Huntsville, AL
[237] Mars One, 2014, Mars One Roadmap 2025, Original URL: http://www.mars-one.com/mission/roadmap/2025, Date accessed: July 16th 2014, Archived URL: http://web.archive.org/web/20140716210623/http://www.mars-one.com/mission/roadmap/2025
[238] Mars One: The Technology, Original URL: http://www.mars-one.com/mission/the-technology, Date accessed: July 14th, 2014, Archived URL: http://web.archive.org/web/20140714224447/http://www.mars-one.com/mission/the-technology
[239] Christiansen, B., 2014, Handbook of Research on Global Business Opportunities, IGI Global.

[240] Karcz, A. R. C. J., Allen, G., Davila, A., Heldmann, J., Lemke, L., Marinova, M., Stoker, C., and Trumble, K., 2011, "Red Dragon: Feasibility of a Dragon-derived Mars lander for scientific and human-precursor investigations," pp. 1–14, Available online at: <http://digitalvideo.8m.net/SpaceX/RedDragon/karcz-red_dragon-nac-2011-10-29-1.pdf>.
[241] Space Exploration Technologies Corporation 2013, "Falcon Heavy," Available online at: <http://www.spacex.com/falcon-heavy>, Date Accessed: May 22nd 2014
[242] World-Mysteries Blog 2014, "Would you Sign up for One-way trip to Mars?," [Online]. Available online at: <http://blog.world-mysteries.com/science/would-you-sign-up-for-one-way-trip-to-mars/>. Date accessed: April 22nd 2014
[243] de Weck, O. L., Simchi-Levi, D., Shishko, R., Ahn, J., Gralla, E. L., Klabjan, D., Mellein, J., Shull, S. A., Siddiqi, A., Bairstow, B. K., and Lee, G. Y., 2007, "SpaceNet v1.3 User's Guide (NASA/TP-2007-214725)," (January), Available online at: <http://strategic.mit.edu/spacelogistics/pdf/SpaceNet_UserGuide_1_3_final.pdf>.
[244] Space Exploration Technologies Corporation 2014, "SpaceX Dragon" [Online]. Available online at: <http://www.spacex.com/dragon>. Date Accessed: May 22nd 2014
[245] Morrow, R. C., Crabb, T. M., and Lee, M. C., 2004, Evolution of Space-Based Plant Growth Systems from Research to Life Support, AIAA 2004-6022, AIAA Space 2004 Conference and Exhibit, 28-30 September 2004, San Diego, CA.
[246] Cirillo, W., Aaseng, G., Goodliff, K., Stromgren, C., and Maxwell, A., 2011, "Supportability for Beyond Low Earth Orbit Missions," AIAA 2011-7231, AIAA Space 2011 Conference and Exhibit, 27-29 September 2011, Long Beach, CA, Available online at: <http://arc.aiaa.org/doi/abs/10.2514/6.2011-7231>.
[247] Jones, H. W., Hodgson, E. W., and Kliss, M. H., 2014, "Life Support for Deep Space and Mars", ICES-2014-74, 44th International Conference on Environmental Systems, July 13-17 2014, Tucson, AZ
[248] Steering Committee for NASA Technology Roadmaps - Aeronautics and Space Engineering Board - National Research Council of the National Academies, 2012, "NASA Space Technology Roadmaps and Priorities - Restoring NASA's Technological Edge and Paving the Way for a New Era in Space", The National Academies Press, Washington D.C., Available online at: <http://www.nap.edu/catalog/13354/nasa-space-technology-roadmaps-and-priorities-restoring-nasas-technological-edge>.
[249] Owens, A., Do, S., Kurtz, A., and de Weck, O., 2015, "Benefits of Additive Manufacturing for Human Exploration of Mars", ICES-2015-287, 45th International Conference on Environmental Systems, 12-16 July 2015, Bellevue, WA.
[250] Committee on Space-Based Additive Manufacturing, 2014, 3D Printing in Space, National Research Council of the National Academies, Washington D.C., Available online at: <http://www.nap.edu/catalog/18871/3d-printing-in-space>.
[251] Cassidy, E. S., West, P. C., Gerber, J. S., and Foley, J. a, 2013, "Redefining agricultural yields: from tonnes to people nourished per hectare," Environ. Res. Lett., **8**, p. 034015, Available online at: <http://iopscience.iop.org/1748-9326/8/3/034015/article/>.
[252] Zhou, W., 2005, "Advanced ASTROCULTURE Plant Growth Unit : Capabilities and Performances", SAE 2005-01-2840, 35th International Conference on Environmental Systems, July 11-14, 2005, Rome, Italy.
[253] Jones, H., 2006, Comparison of Bioregenerative and Physical/Chemical Life Support Systems Environmental Systems, SAE 2006-01-2082, 36th International Conference on Environmental Systems (ICES), July 17-20, 2006, Norfolk, Virginia.
[254] Rapp, D., 2006, Accessible Water on Mars, NASA JPL Report Number D-31343-Rev.7, Available at: https://www.researchgate.net/publication/228806019_Accessible_Water_on_Mars
[255] Sanders, G. B., 2010, In-Situ Resource Utilization on Mars – Update from DRA 5.0 Study, AIAA 2010-799, 48th AIAA Aerospace Sciences Meeting Including the New Horizons Forum and Aerospace Exposition, 4 - 7 January 2010, Orlando, Florida.
[256] Jeng, F. F., and Lin, C. H., 2001, "A Trade Study on Sabatier CO2 Reduction Subsystem for Advanced Missions," 31st International Conference on Environmental Systems, SAE

International, Orlando, Available online at: <http://www.sae.org/technical/papers/2001-01-2293>.
[257] Murdoch, K., Fort, J., Barone, M., and Holder, D., 2005, Rotary Drum Separator and Pump for the Sabatier Carbon Dioxide Reduction System, SAE 2005-01-2863, 35th International Conference on Environmental Systems, Rome, Italy, July 11-14, 2005, Available online at: <http://www.sae.org/technical/papers/2001-01-2293>.
[258] Sunpower 2015, "Sunpower Flight Cryocoolers", [Online]. Available online at: <http://sunpowerinc.com/cryocoolers/cryotel-family/flight/>; Date accessed: August 18, 2015.
[259] MiaSole, 2014, "MiaSole Flex Series", [Online]. Available online at: <http://miasole.com/en/product/modules0/>, Date accessed: August 30th, 2015.
[260] Shahan, Z., 2015, "Which Solar Panels Are Most Efficient?", CleanTechnica, [Online]. Available online at: <http://cleantechnica.com/2014/02/02/which-solar-panels-most-efficient/>, Date accessed: August 30th, 2015.
[261] MiaSole, "MiaSole Flex Series -02W", [Online]. Available online at: <http://miasole.com/uploads/media/FLEX-02W_Datasheet_1.pdf>; Date accessed: August 30, 2015.
[262] Planetary Society, "Mars' Calendar", [Online]. Available online at: <http://www.planetary.org/explore/space-topics/mars/mars-calendar.html>, Date Accessed: August 30th, 2015.
[263] NASA Goddard Institute of Space Studies, 2015, "Mars24 Sunclock - Time on Mars", [Online]. Available online at: <http://www.giss.nasa.gov/tools/mars24/>, Date Accessed: July 15th, 2015.
[264] National Renewable Energy Laboratory, "Solar Spectra: Standard Air Mass Zero" [Online]. Available at: http://rredc.nrel.gov/solar/spectra/am0/ASTM2000.html. [Accessed: 20-Mar-2015]
[265] Mars One, 2014, Mars One Roadmap 2026, Original URL: http://www.mars-one.com/mission/roadmap/2026, Date accessed: July 16th, 2014, Archived URL: http://web.archive.org/web/20140716211319/http://www.mars-one.com/mission/roadmap/2026,
[266] National Aeronautics and Space Administration, 2015, "National Aeronautics and Space Administration FY 2016 Budget Request" [Online]. Available online at: http://www.nasa.gov/sites/default/files/files/Agency_Fact_Sheet_FY_2016.pdf. [Accessed: 11-Sep-2015]
[267] Mars One, 2014, Mars One Roadmap 2022, Available at: http://www.mars-one.com/mission/roadmap/2022, Date accessed: July 16th, 2014, Archived URL: http://web.archive.org/web/20140716205728/http://www.mars-one.com/mission/roadmap/2022.
[268] Drake, B. G., 1998, "Reference Mission Version 3.0 Addendum to the Human Exploration of Mars : The Reference Mission of the NASA Mars Exploration Study Team," NASA/SP-6107-ADD, NASA Lyndon B. Johnson Space Center, Houston TX
[269] Bussey, B., 2016, "Selecting a Landing Site for Humans on Mars, Future In-Space Operations (FISO) Presentation - March 16, 2016", Presentation materials available online at: http://spirit.as.utexas.edu/~fiso/telecon/Davis-Bussey_3-16-16/Davis-Bussey_3-16-16.pptx and http://spirit.as.utexas.edu/~fiso/telecon/Davis-Buss.
[270] NASA Human Landing Sites Study Steering Committee, 2016, First Landing Site/Exploration Zone Workshop for Human Missions to the Surface of Mars - Second Announcement, Announcement dated: October 27-30, 2015, Available online at: http://www.nasa.gov/sites/default/files/atoms/files/hls2-2nd-announcement-7-8.pdf.
[271] Howe, A. S., Spexarth, G., Toups, L., Howard, R., Rudisill, M., and Dorsey, J., 2010, "Constellation Architecture Team: Lunar Outpost 'Scenario 12.1' Habitation Concept," Earth Sp. 2010, pp. 966–988, Available online at: <http://dx.doi.org/10.1061/41096(366)91>.
[272] Howe, A. S., Kennedy, K. J., and Gill, T., 2013, NASA Habitat Demonstration Unit (HDU) Deep Space Habitat Analog, AIAA 2013-5436, AIAA Space 2013 Conference and Exposition, September 10-12, 2013, San Diego, CA.
[273] Howe, A. S., Kennedy, K., Guirgis, P., Trevino, R., Boyle, R., Lynch, A., Toups, L., Tri, T., Gill, T., Walsh, E., Smitherman, D., and Liolios, S., 2011, A Dual-Chamber Hybrid Inflatable Suitlock (DCIS) for Planetary Surfaces or Deep Space, AIAA 2011-5064, 41st International Conference

on Environmental Systems, 17-21 July 2011, Portland, OR, Available online at: <http://dx.doi.org/10.2514/6.2011-5064>.
[274] Barta, D. J., and Castillo, J. M., 2001, Preliminary Designs of the Biomass Production System for the Bioregenerative Planetary Life Support Systems Test Complex on Environmental Systems, SAE 2001-01-2319, 31st International Conference on Environmental Systems, July 9-12, 2001, Orlando, FL.
[275] Anderson, M. S., Ewert, M. K., Keener, J. F., and Wagner, S. A., 2015, Life Support Baseline Values and Assumptions Document 2015, NASA/TP-2015-218570, NASA Lyndon B. Johnson Space Center, Houston, TX, Available at: http://ston.jsc.nasa.gov/collections/TRS/_techrep/TP-2015-218570.pdf.
[276] Polsgrove, T., Thomas, H. D., Stephens, W., and Rucker, M. A., 2015, Mars Ascent Vehicle Design for Human Exploration, AIAA 2015-4416, AIAA Space 2015 Conference and Exposition, August 31 - Septemeber 2, 2015, Pasadena, CA, Available online at: <http://arc.aiaa.org/doi/10.2514/6.2015-4416>.
[277] Shamsian, J., 2015, "Fact-Checking 'The Martian': Can You Really Grow Plants on Mars?," Modern Farmer [Online]. Available: http://modernfarmer.com/2015/10/can-you-grow-plants-on-mars/. [Accessed: 13-Apr-2016], Available online at: <http://modernfarmer.com/2015/10/can-you-grow-plants-on-mars/>.
[278] Fecht, S., 2014, "Crops Grow on Fake Moon and Mars Soil," Pop. Sci. [Online]. Available online at: http://www.popsci.com/article/technology/crops-grow-fake-moon-and-mars-soil. [Accessed: 13-Apr-2016]
[279] Williams, A., 2015, "3D-printed Mars shelter concept is out of this world," gizmag [Online]. Available online at: http://www.gizmag.com/3d-printed-shelter-mars-fabulous/39392/. [Accessed: 13-Apr-2016]
[280] Versteeg, B., "Crater Dome Interior," spacehabs.com [Online]. Available online at: http://www.spacehabs.com/wp-content/themes/emona/content-portfolio.php?ajax=true&id=925. [Accessed: 13-Apr-2016]
[281] Murray, R., 2015, "Mars Greenhouse," humanmars.net [Online]. Available online at: http://www.humanmars.net/2015_04_01_archive.html. [Accessed: 13-Apr-2016]
[282] Smith, P., "Mars Greenshouse," Mars Found. [Online]. Available online at: http://www.philsmith.us/files/QuickSiteImages/MarsGreenhouse.jpg. [Accessed: 13-Apr-2016],
[283] Drysdale, A. E., 2001, Life Support Trade Studies Involving Plants, SAE 2001-01-2362, 31st International Conference on Environmental Systems, July 9-12, 2001, Orlando, FL.
[284] Perchonok, M. "The Challenges of Developing a Food System for a Mars Mission.", Available online at: http://ntrs.nasa.gov/archive/nasa/casi.ntrs.nasa.gov/20070008092.pdf, Date accessed: November 12th 2014
[285] Thyer, A. M., Kay, J., Gant, S. E., and Connolly, S., 2009, Investigations into the effects of carbon dioxide and nitrogen on the flammability limits of gas mixtures, IChemE Symposium Series No. 155, Hazards XXI, Available from: https://www.icheme.org/~/media/Documents/Subject%20Groups/Safety_Loss_Prevention/Hazards%20Archive/XXI/XXI-Paper-060.pdf
[286] Metcalf, J., Peterson, L., Carrasquillo, R., and Bagdigian, B., 2012, National Aeronautics and Space Administration (NASA) Environmental Control and Life Support (ECLS) Integrated Roadmap Development, American Institute of Aeronautics and Astronautics, AIAA 42nd International Conference on Environmental Systems, 15 - 19 July 2012, San Diego, California.
[287] Sargusingh, M., Perry, J., Howard, D., and Toomarian, N., 2015, Notional Environmental Control and Life Support System Architectures for Human Exploration beyond Low-Earth Orbit, AIAA 2015-4456, AIAA Space 2015 Conference and Exposition, August 31 - Septemeber 2, 2015, Pasadena, CA, Available online at: <http://arc.aiaa.org/doi/10.2514/6.2015-4456>.
[288] Ganzer, B., and Messerschmid, E., 2009, "Integration of an algal photobioreactor into an environmental control and life support system of a space station," Acta Astronaut., **65**(1-2), pp. 248–261, Available online at: <http://linkinghub.elsevier.com/retrieve/pii/S0094576509000769>.

[289] Turner, M. F., Fisher, J. W., Broyan, J. L., and Pace, G., 2014, Generation 2 Heat Melt Compactor Development, ICES-2014-024, 44th International Conference on Environmental Systems, 13-17 July 2014, Tucson, Arizona.
[290] Caraccio, A. J., Hintze, P., Anthony, S. M., Devor, R. W., Captain, J. G., and Muscatello, A. C., 2013, Trash-to-Gas: Converting Space Trash into Useful Products, AIAA 2013-3440, 43rd International Conference on Environmental Systems, July 14-18 2013, Vail, CO, Available online at: <http://arc.aiaa.org/doi/abs/10.2514/6.2013-3440>.
[291] NASA International Space Station Program, 2016, "3D Printing in Zero-G Technology demonstration 93d Printing in Zero-G)," nasa.gov [Online]. Available online at: http://www.nasa.gov/mission_pages/station/research/experiments/1115.html. [Accessed: 24-Apr-2016]
[292] Russell, J. F., Klaus, D. M., and Mosher, T. J., 2006, "Applying Analysis of International Space Station Crew-Time Utilization to Mission Design," J. Spacecr. Rockets, **43**(1), pp. 130–136.
[293] Mattfeld, B., Stromgren, C., Shyface, H., Cirillo, W., and Goodliff, K., 2015, Developing a Crew Time Model for Human Exploration Missions to Mars, 2015 IEEE Aerospace Conference, 7-14 March 2015, Big Sky, MT.
[294] Bertels, C., 2006, Crew Maintenance Lessons Learned from ISS and Considerations for Future Manned Missions, AIAA 2006-5952, SpaceOps 2006 Conference, June 19th-23rd 2006, Rome , Italy.
[295] Barker, R. S., and von Jouanne, R. G., 1997, "Space Station THC/IMV Development Test/Analysis Correlations and Flight Predictions," SAE Technical Paper 972565, doi:10.4271/972565, Available online at: <http://papers.sae.org/972565/>.
[296] Shkedi, B., International Space Station (ISS) Water Transfer Hardware Logistics, SAE 2006-01-2093, 36th International Conference on Environmental Systems (ICES) Norfolk, Virginia July 17-20, 2006.
[297] Tobias, B., Garr II, J. D., and Erne, M., 2011, International Space Station Water Balance Operations, AIAA 2011-5150, 41st International Conference on Environmental Systems 17 - 21 July 2011, Portland, Oregon.
[298] NASA, 2011, STS-135: The Final Mission - Press Kit/July 2011, NASA Headquarters, Washington D.C., Available at: https://www.nasa.gov/pdf/566071main_135_press_kit2.pdf.
[299] NASA, 2009, Space Shuttle Mission STS-129 - Stocking the Station - Press Kit - November 2009, NASA Headquarters, Washington D.C., Available online at: <http://www.nasa.gov/pdf/397216main_sts129_presskit.pdf>.
[300] NASA Human Research Program Education and Outreach, Recycling Urine In Space - Exploring Space Through MATH - Educator Edition, NASA Johnson Space Center, Houston, TX, Available online at: https://nctm.confex.com/nctm/2014AM/webprogram/Handout/Session23535/Alg2-ED_Nspire_RecUrine.pdf; Date accessed: March 12th 2016.
[301] Link, D. E., Carter, D. L., and Higbie, S., 2010, Development of an Advanced Recycle Filter Tank Assembly for the ISS Urine Processor Assembly, AIAA 2010-6249, 40th International Conference on Environmental Systems, 11-15 July 2010, Barcelona, Spain.
[302] Simmons, J. L., and Reeves, D. R., 2004, ISS Pressure Control Assembly, SAE 2004-01-2547, 34th International Conference on Environmental Systems (ICES), Colorado Springs, Colorado, July 19-22, 2004.
[303] NASA, 2011, The Final Flight of Discovery - Space Shuttle Mission STS-133 Press Kit - February 2011, NASA Headquarters, Washington D.C., Available online at: https://www.nasa.gov/sites/default/files/files/491387main_STS-133.pdf.
[304] Mitchell, K. L., Bagdigian, R. M., Carrasquillo, R. L., Carter, D. L., Franks, G. D., Holder, D. W., Hutchens, C. F., Ogle, K. Y., Perry, J. L., and Ray, C. D., 1994, Technical Assessment of Mir-1 Life Support Hardware for the International Space Station, NASA TM-108441, NASA George C. Marshall Space Flight Center, Huntsville, AL.
[305] Yates, S. F., and Kay, R. J., 2010, High Capacity Adsorbent Development for Carbon Dioxide Removal System Efficiency Improvements, AIAA 2010-8673, AIAA Space 2010 Conference &

Exposition, 30 August - 2 September 2010, Anaheim CA.
[306] Prokhorov, K., and Shkedi, B., 2006, Methodology and Assumptions of Contingency Shuttle Crew Support (CSCS) Calculations Using ISS Environmental Control and Life Support Systems, SAE 2006-01-2061, 36th International Conference on Environmental Systems (ICES) Norfolk, Virginia July 17-20, 2006.
[307] Knox, J. C., Campbell, M., Murdoch, K., Miller, L. A., Jeng, F., and Sverdrup, J. E., 2005, Integrated Test and Evaluation of a 4-Bed Molecular Sieve (4BMS) Carbon Dioxide Removal System (CDRA), Mechanical Compressor Engineering Development Unit (EDU), and Sabatier Engineering Development Unit (EDU), SAE 2005-01-2864, 35th International Conference on Environmental Systems, Rome, Italy, July 11-14, 2005.
[308] Cloud, D., and Kundrotas, R. E., 2001, Development Status and Maintainability Features of ISS Oxygen Generation and Water Processor Assemblies, SAE 2001-01-2314, 31st International Conference on Environmental Systems, Orlando, FL, July 9-12, 2001.
[309] NASA Human Exploration and Operations Mission Directorate, 2015, "International Space Station Urine Processor Assembly Hardware Improvements (UPA) - 11.25.15" [Online]. Available online at: http://www.nasa.gov/mission_pages/station/research/experiments/1796.html, Date accessed: March 3rd 2016
[310] Holder, D. W., and Hutchens, C. F., 2003, Development Status of the International Space Station Urine Processor Assembly, SAE 2003-01-2690, 33rd International Conference on Environmental Systems (ICES), Vancouver, B.C., Canada July 7-10, 2003.
[311] Carrasquillo, R. L., Cloud, D., and Bedard, J., 2003, Status of the Node 3 Regenerative ECLSS Water Recovery and Oxygen Generation Systems, SAE 2003-01-2590, 33rd International Conference on Environmental Systems (ICES), Vancouver, B.C., Canada July 7-10, 2003.
[312] Carter, L.; Brown, C.; Orozco, N., 2013, Status of ISS Water Management and Recovery, AIAA 2013-3509, 43rd International Conference on Environmental Systems, July 14-18 2013, Vail, CO.
[313] Jeng, F. F., and Lin, C. H., 2001, A Trade Study on Sabatier CO2 Reduction Subsystem for Advanced Missions, SAE International, SAE 2001-01-2293, 31st International Conference on Environmental Systems, Orlando, FL, July 9-12, 2001, Available online at: <http://www.sae.org/technical/papers/2001-01-2293>.
[314] Perry, J., Abney, M., Frederick, K., Greenwood, Z., Kayatin, M., Newton, R., Parrish, K., Roman, M., Takada, K., Marshall, N., Flight, S., Miller, L., Technologies, E., Scott, J., Engineering, J., Stanley, C., and Corporation, Q., 2013, Functional Performance of an Enabling Atmosphere Revitalization Subsystem Architecture for Deep Space Exploration Missions, AIAA 2013-3421, 43rd International Conference on Environmental Systems, July 14-18 2013, Vail, CO.
[315] Murdoch, K., Goldblatt, L., Carrasquillo, R., and Harris, D., 2005, Sabatier Methanation Reactor for Space Exploration, AIAA 2005-2706, 1st Space Exploration Conference: Continuing the Voyage of Discovery, January 30 - February 1, 2005, Orlando, FL, Available online at: <http://www.scopus.com/inward/record.url?eid=2-s2.0-28744443151&partnerID=tZOtx3y1>.
[316] Murdock, K., 2010, Integrated Evaluation of Closed Loop Air Revitalization System Components, NASA/CR-2010-216451, Contractor report prepared for NASA Marshall Space Flight Center under Contract NNM10AB15P.
[317] Murdoch, K., Fort, J., Barone, M., and Holder, D., 2005, Rotary Drum Separator and Pump for the Sabatier Carbon Dioxide Reduction System, SAE 2005-01-2863, 35th International Conference on Environmental Systems, Rome, Italy, July 11-14, 2005, Available online at: <http://www.sae.org/technical/papers/2001-01-2293>.
[318] Jones, H., 2011, "Reliability Analysis of Carbon Dioxide Reduction Systems," AIAA 2011-5271, 41st International Conference on Environmental Systems, July 17-21 2011, Portland, Oregon, Available online at: <http://arc.aiaa.org/doi/pdf/10.2514/6.2011-5271>.
[319] Jones, H., 2012, "Design and Analysis of a Flexible, Reliable Deep Space Life Support System", AIAA 2012-3418, 42nd International Conference on Environmental Systems, July 15-19 2012, San Diego, California
[320] Jones, H., and Cavazzoni, J., 2000, Top-Level Crop Models for Advanced Life Support Analysis,

SAE 2000-01-2261, 30th International Conference on Environmental Systems, July 10-13, 2000, Toulouse, France.
[321] Boscheri, G., Kacira, M., Patterson, L., Giacomelli, G., Sadler, P., Furfaro, R., Lobascio, C., Lamantea, M., and Grizzaffi, L., 2012, "Modified energy cascade model adapted for a multicrop Lunar greenhouse prototype," Adv. Sp. Res., **50**(7), pp. 941–951, Available online at: <http://dx.doi.org/10.1016/j.asr.2012.05.025>.
[322] Taiz, L., and Zeiger, E., 2010, "Plant Physiology", Sinauer Associates, Sunderland, MA.
[323] Schaezler, R. N., Cook, A. J., Leonard, D. J., and Company, T. B., 2011, Trending of Overboard Leakage of ISS Cabin Atmosphere, AIAA 2011-5149, 41st International Conference on Environmental Systems 17 - 21 July 2011, Portland, Oregon.
[324] Hamilton Sundstrand Corporation, 2002, "NASA Extravehicular Mobility Unit (EMU) LSS/SSA Data Book (Rev. H)," (September).
[325] Griffin, B. N., 2008, Lunar Habitat Airlock/Suitlock, ASCE Earth and Space Conference 2008, 11th International Conference on Engineering, Science, Construction, and Operations in Challenging Environments, 3-5 Mar 2008, Long Beach, CA, Available from: http://hdl.handle.net/2060/20080018968.
[326] Chullen, C., and Westheimer, D. T., 2011, Extravehicular Activity and Technology Development Status and Forecast, AIAA 2011-5179, 41st International Conference on Environmental Systems, 17 - 21 July 2011, Portland, OR.
[327] Papale, W., and Chullen, Cinda; Campbell, Colin; Conger, Bruce; McMillin, S., 2014, Continued Development of the Rapid Cycle Amine System for Advanced Extravehicular Activity Systems, 44th International Conference on Environmental Systems, 13-17 July 2014, Tucson, Arizona.
[328] NASA JSC Public Affairs Office, 2007, "STS-118 Shuttle Mission Imagery" [Online]. Available online at: http://www.spaceflight.nasa.gov/gallery/images/shuttle/sts-118/html/s118e06304.html. [Accessed: 08-Mar-2016].
[329] Campbell, C., 2015, Shuttle / ISS EMU Failure History and the Impact on Advanced EMU Portable Life Support System (PLSS) Design, ICES-2015-327, 45th International Conference on Environmental Systems, 12-16 July 2015, Bellevue, WA.
[330] NASA Quest, "The Primary and Secondary Life-Support System" [Online]. Available online at: http://quest.nasa.gov/space/teachers/suited/5emu4.html. [Accessed: 08-Mar-2016]
[331] Bue, G. C., Makinen, J., Cox, M., Watts, C., Campbell, C., Vogel, M., Colunga, A., and Conger, B., 2012, Long-Duration Testing of a Spacesuit Water Membrane Evaporator Prototype, AIAA 2012-3459, 42nd International Conference on Environmental Systems, 15-19 July 2012, San Diego, CA.
[332] Fisher, J., Hogan, J., Pace, G., and Wignarajah, K., 2010, Impact of Water Recovery from Wastes on the Lunar Surface Mission Water Balance, AIAA 2010-6008, 40th International Conference on Environmental Systems, 11-15 July 2010, Barcelona, Spain, Available online at: <http://arc.aiaa.org/doi/abs/10.2514/6.2010-6008>.
[333] Papale, W., Paul, H., and Thomas, G., 2006, Development of Pressure Swing Adsorption Technology for Spacesuit Carbon Dioxide and Humidity Removal, SAE 2006-01-2023, 36th International Conference on Environmental Systems (ICES), Norfolk, Virginia July 17-20, 2006.
[334] Papale, W., and Chullen, Cinda; Campbell, Colin; Conger, Bruce; McMillin, S., 2014, Continued Development of the Rapid Cycle Amine System for Advanced Extravehicular Activity Systems, ICES-2014-196, 44th International Conference on Environmental Systems, 13-17 July 2014, Tucson, Arizona.
[335] Swickrath, M., Watts, C., Anderson, M., Vogel, M., Colunga, A., McMillin, S., and Broerman, C., 2012, Performance Characterization and Simulation of Amine-Based Vacuum Swing Sorption Units for Spacesuit Carbon Dioxide and Humidity Control, AIAA 2012-3461, 42nd International Conference on Environmental Systems, 15-19 July 2012, San Diego, CA, Available online at: <http://arc.aiaa.org/doi/abs/10.2514/6.2012-3461>.
[336] Baptist, J., 2013, "MAG - Maximum Absorbency Garment," flickr [Online]. Available online at: https://www.flickr.com/photos/justbe74/10311866835. [Accessed: 12-Mar-2016]
[337] NASA JSC, 1971, Apollo Operations Handbook Extravehicular Mobility Unit, Houston, TX,

Available online at: <http://www.lpi.usra.edu/lunar/documents/NASA TM-X-69516.pdf>.
[338] Couper, J. R., Penney, W. R., Fair, J. R., and Walas, S. M., 2012, Chemical Process Equipment: Selection and Design (3rd Edition), Elsevier Science and Technology Books, Available online at: <http://dx.doi.org/10.1016/B978-0-12-396959-0.00025-2>.
[339] Kelsey, L., Straus, J., and Zuniga, D., 2012, Contaminant Robust Water Extraction from Lunar and Martian Soil for In Situ Resource Utilization - System Architecture Development, American Institute of Aeronautics and Astronautics, AIAA 2012-3502, 42nd International Conference on Environmental Systems, 15-19 July 2012, San Diego, CA, Available online at: <http://arc.aiaa.org/doi/abs/10.2514/6.2012-3502>.
[340] Sanders, G. B., 2010, In-Situ Resource Utilization on Mars – Update from DRA 5.0 Study, AIAA2010-799, 48th AIAA Aerospace Sciences Meeting Including the New Horizons Forum and Aerospace Exposition, 4-7 January 2010, Orlando, Florida.
[341] Stoker, C. R., Gooding, J. L., Roush, T., Banin, A., Burt, D., Clark, B. C., Flynn, G., and Gwynne, O., 1993, "The Physical and Chemical Properties and Resource Potential of Martian Surface Soils," Resources of Near-Earth Space, J.S. Lewis, M.S. Matthews, and M.L. Guerrieri, eds., The University of Arizona Press, p. 977, Available online at: <http://www.uapress.arizona.edu/onlinebks/ResourcesNearEarthSpace/contents.php>.
[342] Anderson, M., and Curley, S., 2005, Evaluation of Cryofreezer Technology Through Simulation and Testing, SAE 2005-01-2869, 35th International Conference on Environmental Systems, Rome, Italy, July 11-14, 2005, Available online at: <http://papers.sae.org/2005-01-2869/>.
[343] Sunpower Inc., 2015, "Space Cryocoolers" [Online]. Available online at: http://sunpowerinc.com/cryocoolers/cryotel-family/flight/. [Accessed: 27-Nov-2015]
[344] Rapp, D., Andringa, J., Easter, R., Smith, J. H., Wilson, T. J., Clark, D. L., and Payne, K., 2005, "Preliminary system analysis of in situ resource utilization for Mars human exploration," 2005 IEEE Aerospace Conference, IEEE, pp. 319–338, Available online at: <http://ieeexplore.ieee.org/lpdocs/epic03/wrapper.htm?arnumber=1559325>.
[345] Crow, S., 1997, The MOXCE Project - New cells for producing oxygen on Mars, AIAA 1997-2766, 33rd Joint Propulsion Conferene and Exhibit, 6-9 July 1997, Seattle, WA, Available online at: <http://arc.aiaa.org/doi/abs/10.2514/6.1997-2766>.
[346] Sridhar, K. R., Iacomini, C. S., and Finn, J. E., 2004, "Combined H2O/CO2 Solid Oxide Electrolysis for Mars In Situ Resource Utilization," J. Propuls. Power, **20**(5), pp. 892–901, Available online at: <http://arc.aiaa.org/doi/abs/10.2514/1.3480>.
[347] Giner Inc., 2015, "High Pressure Hydrogen Generators" [Online]. Available online at: http://www.ginerinc.com/products.php?a=HPH2 [Accessed: 27-Nov-2015]
[348] Millet, P., Ngameni, R., Grigoriev, S. A., Mbemba, N., Brisset, F., Ranjbari, A., and Etiévant, C., 2010, "PEM water electrolyzers: From electrocatalysis to stack development," Int. J. Hydrogen Energy, **35**(10), pp. 5043–5052, Available online at: <http://linkinghub.elsevier.com/retrieve/pii/S036031990901386X>.
[349] DuPont, 2015, "Nafion PFSA Membranes" [Online]. Available online at: http://www.quintech.de/img/technischeinformationen/. [Accessed: 27-Nov-2015]
[350] Koolance, 2015, "PMP-500 Pump" [Online]. Available online at: http://koolance.com/pmp-500-pump-g-1-4-bsp. [Accessed: 27-Nov-2015]
[351] Clark, D., 1997, "In-situ propellant production on Mars - A Sabatier/electrolysis demonstration plant," 33rd Joint Propulsion Conference and Exhibit, AIAA 1997-2764, 33rd Joint Propulsion Conference and Exhibit, 6-9 July 1997, Seattle, WA, Available online at: <http://arc.aiaa.org/doi/abs/10.2514/6.1997-2764>.
[352] Brooks, K., 2006, "Development of a Microchannel In Situ Propellant Production System," AIP Conference Proceedings, pp. 1111–1121, Available online at: <http://scitation.aip.org/content/aip/proceeding/aipcp/10.1063/1.2169292>.
[353] Junaedi, C., Hawley, K., Walsh, D., Roychoudhury, S., Abney, M., and Perry, J., 2011, Compact and Lightweight Sabatier Reactor for Carbon Dioxide Reduction, AIAA 2011-5033, 41st International Conference on Environmental Systems, 17 - 21 July 2011, Portland, OR, Available online at: <http://arc.aiaa.org/doi/abs/10.2514/6.2011-5033>.

[354] Junaedi, C., Hawley, K., Walsh, D., Roychoudhury, S., Busby, S., Abney, M., Perry, J., and Knox, J., 2012, Compact, Lightweight Adsorber and Sabatier Reactor for CO2 Capture and Reduction for Consumable and Propellant Production, AIAA 2012-3482, 42nd International Conference on Environmental Systems, 15-19 July 2012, San Diego, CA, Available online at: <http://arc.aiaa.org/doi/abs/10.2514/6.2012-3482>.

[355] Junaedi, C., Hawley, K., Walsh, D., Roychoudhury, S., Abney, M. B., and Perry, J. L., 2014, CO2 Reduction Assembly Prototype Using Microlith-Based Sabatier Reactor for Ground Demonstration, ICES-2014-090, 44th International Conference on Environmental Systems, 13-17 July 2014, Tucson, Arizona.

[356] Whitlow, J. E., and Parrish, C. F., 2003, "Operation, Modeling and Analysis of the Reverse Water Gas Shift Process," AIP Conf. Proc., **654**(1), pp. 1116–1123, Available online at: <http://scitation.aip.org/content/aip/proceeding/aipcp/10.1063/1.1541409>.

[357] Holladay, J. D., Brooks, K. P., Humble, P. H., Hu, J., and Simon, T. M., 2008, "Compact Reverse Water-Gas-Shift Reactor for Extraterrestrial In Situ Resource Utilization," J. Propuls. Power, **24**(3), pp. 578–582.

[358] Riken Environment System Co., 2015, "Pyromax - Heating materials, Electrical resistance materials, Heat-resistant construction materials" [Online]. Available online at: http://www.riken-kankyo.com/en/pdf/PYROMAX_Catalog_en.pdf. [Accessed: 27-Nov-2015]

[359] Erickson, R. J., Jr, J. H., Kulp, G. W., and Keuren, S. P. Van, 2008, "International Space Station United States Orbital Segment Oxygen Generation System On-orbit Operational Experience," 08-ICES-0035, 38th International Conference on Environmental Systems, 30 June - 3 July 2008, San Francisco, CA

[360] Bagdigian, R. M., Cloud, D., and Bedard, J., 2006, Status of the Regenerative ECLSS Water Recovery and Oxygen Generation Systems Environmental Systems, SAE 2006-01-2057, 36th International Conference on Environmental Systems (ICES) Norfolk, Virginia July 17-20, 2006.

[361] Barker, R. S., and von Jouanne, R., 1997, Space Station THC/IMV Development Test / Analysis Correlations and Flight Predictions, SAE Technical Paper 972565, doi: 10.4271/972565

[362] Carter, L., Tobias, B., and Orozco, N., 2012, "Status of ISS Water Management and Recovery", AIAA 2012-3594, 42nd International Conference on Environmental Systems, 15-19 July 2012, San Diego, CA

[363] Wieland, P. O., 2005, Designing for Human Presence in Space: An Introduction to Environmental Control and Life Support Systems (ECLSS) -Appendix I, Update - Historical ECLSS for U.S. and U.S.S.R./Russian Space Habitats, NASA/TM-2005-214007, NASA Marshall Space Flight Center, Huntsville AL.

[364] Williams, D. E., and Dake, J. R., 2012, International Space Station Environmental Control and Life Support System Status for the Prior Year : 2010 - 2011, AIAA 2012-3612, 42nd International Conference on Environmental Systems, 15 - 19 July 2012, San Diego, California.

[365] Wright, J., 2013, "Permanent Multipurpose Module," NASA International Space Station Program [Online]. Available online at: <http://www.nasa.gov/mission_pages/station/structure/elements/pmm.html#.VA772PldV8E>. Date accessed: June 14th 2014

[366] Heliospectra, 2014, "LX60 Tech Specs," LX Ser. [Online]. Available online at: http://www.heliospectra.com/led_grow_light_products#lx-techspecs. [Accessed: 11-Sep-2015],

[367] Stilwell, D., Boutros, R., and Connolly, J. H., 2000, "Crew Accommodations," Human Spaceflight: Mission Analysis and Design, W.J. Larson, and L.K. Pranke, eds., McGraw-Hill Higher Education.

[368] Lien, R., 2014, "Advanced Resistive Exercise Device (ARED)," ISS Science for Everyone [Online]. Available online at: <http://www.nasa.gov/mission_pages/station/research/experiments/1001.html>. Date accessed: August 7th 2014

[369] NASA 2009, "Do Tread On Me," International Space Station Feature [Online]. Available online at: <http://www.nasa.gov/mission_pages/station/behindscenes/colbert_feature.html>. Date accessed: August 7th 2014

[370] NASA 2014, “Cycle Ergometer with Vibration Isolation and Stabilization System (CEVIS),” ISS Science for Everyone [Online]. Available online at: <http://www.nasa.gov/mission_pages/station/research/experiments/841.html>. Date accessed: August 7th 2014

[371] ASTM 2014, “Standard Specification for Pressure Vessel Plates, Alloy Steel, High-Strength, Quenched and Tempered (A517/A517M-10),” pp. 10–13., Available online at: <http://www.astm.org/Standards/A517.htm>. Date accessed: May 18th 2014

[372] MatWeb 2014, “ASTM A517 Low Alloy Steel, Grade A,” MatWeb Material Property Data [Online]. Available online at: < http://www.matweb.com/search/datasheettext.aspx?matguid=e494a6884b9f4f1dbe66fb0376b0ce1f >. Date accessed: August 4th 2014

[373] Murdock, K., 2010, “Integrated Evaluation of Closed Loop Air Revitalization System Components,” NASA/CR-2010-216451, Contractor report prepared for NASA Marshall Space Flight Center under Contract NNM10AB15P